Vol. II

LUNAR FLIGHT HANDBOOK

for the

NATIONAL AERONAUTICS AND SPACE ADMINISTRATION

George C. Marshall Space Flight Center
Huntsville, Alabama

REPRODUCTION RESTRICTIONS OVERRIDDEN
NASA Scientific and Technical Information Facility

MARTIN MARTIN MARIETTA
SPACE SYSTEMS DIVISION Baltimore 3, Maryland

REPRODUCTION RESTRICTIONS OVERRIDDEN
NASA Scientific and Technical Information Facility

REPRODUCTION RESTRICTIONS OVERRIDDEN
NASA Scientific and Technical Information Facility

REPRODUCTION RESTRICTIONS OVERRIDDEN
NASA Scientific and Technical Information Facility

© Copyright by Martin Company
1963

FOREWORD

This handbook has been produced by the Space Systems Division of the Martin Company under contract NAS 8-5031 with the George C. Marshall Space Flight Center of the National Aeronautics and Space Administration. The Lunar Flight Handbook is considered the second in a series of volumes by various contractors, sponsored by MSFC, treating the dynamics of space flight in a variety of aspects of interest to the mission designer and evaluator. The primary purpose of these books is to serve as a basic tool in preliminary mission planning. In condensed form they provide background data and material collected through several years of intensive studies in each space mission area, such as earth orbital flight, lunar flight and interplanetary flight. Volume II, the present volume, is concerned with lunar missions. The Martin Company Program Manager for this project has been Jorgen Jensen; George Townsend has been Technical Director. Fred Martikan has had the direct responsibility for the coordination of this volume; he has shared the responsibility for the generation of material with Frank Santora.

Additional contributors were Robert Salinger, Donald Kraft, Thomas Garceau, Andrew Jazwinski and Lloyd Emery. The graphical work has been prepared by Dieter Kuhn and Elsie M. Smith. John Magnus has assisted in preparing the handbook for publication. William Pragluski, Don Novak, James Porter, Edward Markson, Sidney Roedel, Wade Foy and James Tyler have made helpful suggestions during the writing of this book.

The assistance given by the Future Projects Office at MSFC and by the MSFC contract management panel, directed by Conrad D. Swanson is gratefully acknowledged.

CONTENTS

		Page
I	Introduction	I-1
II	Physical Data	II-1
III	The Earth-Moon System	III-1
IV	Trajectories in the Earth-Moon System	IV-1
V	Earth Departure	V-1
VI	Earth-to-Moon Transfer	VI-1
VII	Lunar Orbit	VII-1
VIII	Descent to and Ascent from the Lunar Surface	VIII-1
IX	Moon-to-Earth Transfer	IX-1
X	Earth Return	X-1
XI	Mission Planning	XI-1
XII	Bibliography	XII-1
	Appendix A--Glossary	A-1
	Appendix B--Symbols	B-1

INTRODUCTION

I. INTRODUCTION

The primary intent of the Lunar Flight Handbook is to introduce the engineer to the flight mechanics aspects of lunar missions. In addition, the handbook material is designed to enable the user to design a lunar mission for any date in this decade.

To fulfill this double purpose while presenting new material in compact form, several guidelines were established and followed in the selection and arrangement of the material.

The format selected for the Lunar Flight Handbook is somewhere between textbooks of celestial mechanics and observational astronomy, and the recent literature in journals and reports. The material presented in the Handbook is intended to provide the link between these two types of publications and to provide a framework for the published articles and reports covering specialized aspects of lunar flight.

The order of the presentation progresses from relatively simple physical concepts to a derivation, or the outline of the derivation, of more detailed results and concepts. More important and useful results are presented analytically, and if possible graphically, while results which depend on the vehicle configuration and operational concepts, such as the use of tracking and communication equipment, have been described in narrative form only. A large number of sketches are included in the text in order to permit a quick grasp and easy visualization of the concepts and techniques of lunar flight.

Frequent reference to outside material is provided to enable the reader to trace numerical values to their source and find references to further material. Frequent reference is made to material in the Orbital Flight Handbook, the companion volume to this Handbook, since the technical material overlaps to some extent. It was attempted to keep the technical level and notation uniform throughout the Handbook. This was no small task if one considers that a number of people were contributing to the Handbook directly and much outside material was reviewed, checked and integrated into the text.

The technical material of the Handbook is arranged into three groups:

(1) Background material. This group, consisting of Chapters II, III and IV, gives the results of astronomy, describes the geometry, the environment, the force models for trajectory calculation, and classifies lunar trajectories and missions. In addition, since all material in the Lunar Flight Handbook is in the metric system of units, conversions to the commonly used English system of units is given.

(2) Lunar mission phases. This group, consisting of Chapters V to X, discusses all possible phases of lunar flight chronologically from earth departure to re-entry into the earth's atmosphere upon return from the moon. Of special interest is the attempt to catalogue a major portion of circumlunar and approach trajectories to the moon and return trajectories to a degree of accuracy which has not so far been achieved in the published literature.

(3) Mission planning. In the final technical chapter of the Handbook, the previous material is applied to the design of two specific lunar missions to illustrate its use in preliminary design.

The subject material of each technical chapter and some general guidelines for use of the data presented in the Lunar Flight Handbook follow.

Chapter II. PHYSICAL DATA

Chapter II describes the environment of the space vehicles, gives conversion factors between the various systems of units and describes the lunar exploration programs. In the first section, the astronautical constants, or constants describing the gravitational force acting on the space vehicle and the geometry of the celestial bodies, have been discussed. The recently published data on astronautical constants has been summarized, and the best values of these constants, together with a confidence interval determined with the Student's t distribution, have been used for all trajectory calculations in the Handbook. Thus, a standard and nearly consistent set of constants based on recent data has been adopted. Future, more accurate determinations of these astronautical constants will not change any of the graphical trajectory data significantly. Thus, the Handbook will retain its value for preliminary design purposes.

The atmospheric, meteoritic, radiative and thermal environment of the space vehicle and the effect of this environment on the vehicle and its occupants are then discussed. The data on the near-earth environment and earth-moon space environment has been classified and summarized with frequent reference to the Orbital Flight Handbook for details, while the near-moon and lunar surface environment, as deduced from observations and as it is known at the present, has been discussed in much more detail.

Since handbook data is given in the absolute MKS system of units, the various systems of mechanical and thermal units employed for trajectory calculations as well as conversion factors between metric, English and astronomical systems of units are given. Much of the data is in tabular form, but basic definitions and fundamental units with common multiples and submultiples have been listed in the text to provide for convenient conversions between the various systems of units.

The chapter continues with a review of the current status of the U. S. lunar exploration

program to familiarize the reader with the project terminology and with the immense scope of the lunar exploration task. A list of announced space vehicle launches with lunar missions, their trajectories, results and attempted experiments completes the material of Chapter II.

Chapter III. THE EARTH-MOON SYSTEM

Chapter III provides some astronomical background for lunar flight. The various coordinate systems centered at the earth or the moon and used for describing the position of space vehicles are introduced, and transformations between the various moon-centered and trajectory coordinate systems are given. A list of available lunar maps is also included.

The motion of a space vehicle in earth-moon space as interpreted in the three-body and restricted three-body problems of astronomy is discussed. Conclusions that can be drawn from these astronomical results in their application to ballistic space-vehicle trajectories in earth-moon space have been presented in some detail.

Since knowledge of lunar position and orientation is also required for lunar flight, brief descriptions of Delaunay's Hansen's and the Hill-Brown lunar theories are followed by a listing of the available lunar ephemerides and by a method for including lunar librations in trajectory digital computer programs.

Chapter IV. TRAJECTORIES IN THE EARTH-MOON SYSTEM

This chapter introduces, in descriptive form, the nomenclature and classification of lunar missions and trajectories as well as the determination of the trajectories. The restricted three-body problem permits the use of many types of ballistic trajectories for lunar flights. If thrust is available to modify these ballistic trajectories at predetermined points, a wide variety of lunar missions are possible. The most common missions have been described and illustrated by sketches in the text.

The force models, or the physical assumptions, underlying trajectory calculations, have been described in considerable detail in order to show the assumptions involved in the use of particular equations of motion for lunar trajectory calculations. The description starts from simple two-body equations permitting closed-form solutions; it progresses through the "patching" of two-body trajectories around the earth and moon in order to obtain a complete ballistic lunar trajectory; the restricted three-body force model is discussed as a tool to determine trajectories; the n-body force model with earth oblateness and lunar triaxiality is presented in detail; and the chapter concludes with a discussion of the effects of non-gravitational forces, such as rocket thrust, atmospheric drag, meteoritic drag, solar radiation pressure, electromagnetic forces, special and general relativistic effects. In most cases the form of the equations of motion has been given or derived and the effect of including the non-gravitational forces in lunar trajectories is evaluated. The description of methods for numerical integration of these trajectories on the digital computer round out this section.

The Voice (volume-of-influence calculated envelopes) computation technique, which uses a patched conic force model, and the geometry and nomenclature peculiar to the Voice technique have been introduced in the final section of Chapter IV. This special treatment is necessary since the particular trajectory geometry enables the efficient cataloguing of lunar trajectories to be discussed in the summary of Chapter VI.

Chapter V. EARTH DEPARTURE

This is the first chapter in the chronological description of the separate phases of a lunar mission. The fixed translunar trajectory technique, in which the translunar trajectory has a specified inclination to the moon's orbital plane at injection, the variable translunar trajectory technique, in which the inclination of the translunar trajectory varies with the time of injection, and the translunar injection itself are discussed.

It is demonstrated how the use of parking orbits during earth departure increases the period in which space vehicle launch can take place (i.e., the launch tolerance) and hence provides additional flexibility for the planning of lunar missions. During the injection phase, abort requirements, or the requirements to return the space vehicle to earth as quickly as possible in the event of a malfunction, have been discussed. Abort requirements are mentioned for each phase of lunar flight in the Handbook since they are important for the selection of trajectories and vehicle hardware for manned lunar missions and since many published articles disregard this aspect of lunar missions.

All graphical data for specific numerical examples in the Lunar Flight Handbook reflects launches from Cape Canaveral, Florida, under appropriate launch azimuth restrictions. At present, NASA has announced plans to use this launch site for lunar flights, and in view of the long-range planning and expense of the launch support equipment, these plans are likely to be carried out. Launch from other sites with different launch azimuth restrictions requires a different set of graphs since trajectories have a strong dependence on launch site location.

Chapter VI. EARTH-TO-MOON TRANSFER

Of special note in this chapter is the catalogue of a large portion of circumlunar trajectories to an accuracy which permits the preliminary selection of lunar mission parameters--a level of accuracy which is unique among presentations of this type. Use of the Voice patched-conic trajectory program, use of trajectory symmetry about the moon's orbital plane as well as a plane perpendicular to it, and use of two equations for extending injection parameters, enables the presentation of a major portion of the circumlunar trajectories launched from Cape

Canaveral in only 83 figures. Typical comparisons of trajectories calculated by use of the Voice technique, the restricted three-body force model, and the n-body force model have been given frequently throughout the Handbook in order to illustrate the remarkable accuracy achievable with the Voice technique.

Navigation during lunar missions has been discussed qualitatively and quantitatively, with examples given for a particularly useful navigation technique for position determination in cislunar space. Tracking and communications, on the other hand, have been described qualitatively, since the actual procedures depend to a great degree on the available equipment as well as on the trajectory. Several techniques for determining midcourse guidance corrections have been discussed and some typical fuel requirements are also given.

Abort requirements and possible abort procedures during the translunar trajectory phase together with abort maneuver graphs for a typical circumlunar mission conclude the material of Chapter VI.

Chapter VII. LUNAR ORBIT

Artificial satellites in orbits around the moon behave in the same fashion as artificial satellites in earth orbits. Only the astronautical constants appearing in the equations and the magnitude of the perturbing forces of the other celestial bodies are different. Hence, satellite data most commonly used in preliminary design such as period, velocity, lunar oblateness effects on the orbit, as well as reconnaissance aspects of lunar orbits, are given analytically and graphically, and the relative magnitude of the various perturbing effects is presented.

The effect of finite rocket burning time on fuel requirements for entry to and exit from lunar orbits has been discussed, and a comparison with Voice trajectory data is made. This supplements the fuel requirements for orbit entry and exit given in the trajectory catalogues of Chapters VI and IX, which is based on an impulsive change of velocity (infinite thrust-to-weight ratio). Finally, lunar orbit determination schemes are described briefly.

Chapter VIII. DESCENT TO AND ASCENT FROM THE LUNAR SURFACE

In this chapter, the vehicle trajectory near the lunar surface has been described: the need to reduce the lunar approach velocity of the space vehicle for most landing missions, the descent burning and ballistic flight phases, any required hovering or translation, landing safety boundaries and abort during each descent or ascent phase are covered. In each case the equations of motion, some methods of trajectory optimization and guidance as well as typical results describe the trajectory phase.

Chapter IX. MOON-TO-EARTH TRANSFER

This chapter gives a catalogue of trajectories from the vicinity of the moon to the vicinity of the earth in 90 figures. Use of symmetry and reinterpretation of moon-to-earth trajectories as earth-to-moon trajectories again enables a significant extension of the catalogued data. The catalogues of Chapters VI and IX thus include a major portion of feasible circumlunar and approach trajectories. Impact as well as specialized periodic trajectories have not been catalogued since they most probably will not be used for lunar exploration in the 1965 to 1970 time period; however, they are described and classified in Chapter IV.

Midcourse guidance and energy requirements during the moon-to-earth transfer phase have been briefly discussed. The description of guidance techniques, navigational techniques and tracking requirements of Chapter VI applies directly to moon-to-earth trajectories.

Chapter X. EARTH RETURN

A description of re-entry into the earth's atmosphere and landing at a specific site completes the chronological description of the lunar mission phases. The problem of timing earth return provides the introduction to the chapter which considers two methods for re-entering the atmosphere and landing.

The first method considers a direct entry of the space vehicle into the earth's atmosphere from the transearth trajectory at speeds near the parabolic speed for earth (or earth escape speed). Equations of motion, characteristics of re-entry trajectories, maneuverability by use of aerodynamic forces and various guidance techniques during this supercircular re-entry are considered.

The second method of re-entry employs a combination of atmospheric and rocket or pure rocket deceleration to establish a circular earth satellite orbit prior to re-entering and landing from circular orbital speed. The requirements on the guidance system and the materials are thus reduced, but a significant amount of fuel is required for the deceleration and deorbit maneuvers.

Chapter XI. MISSION PLANNING

Chapter XI, provides the link between the background and trajectory material presented in Chapters II to X and the planning of a lunar mission on a specific date in the period of 1965 to 1970.

The following material is necessary for the conversion from generalized trajectory data to specific mission dates: transformations from the Voice coordinate system to the selenographic coordinate system, the illumination of the moon by the sun, lunar declination and distance from the earth, and some useful empirical relationships for extending catalogued

trajectory data. Also included are mission planning envelopes, or graphs which give several geometrical trajectory parameters as a function of mission constraints in summary form, thus enabling a ready patching of the translunar, lunar orbit, and transearth trajectories into a complete and continuous trajectory for the mission.

The use of the material in the Handbook and the procedure of planning lunar missions has been illustrated by two sample missions in the final section of the chapter. One mission is a manned lunar exploration mission with a stay of three days on the lunar surface, while the other is an unmanned photographic reconnaissance mission of the moon lasting one month. In addition to illustrating the use of the Handbook material for mission planning, these missions are representative of the type of lunar missions planned for the end of this decade.

CHAPTER II

PHYSICAL DATA

Prepared by:

F. Martikan and R. Salinger
Martin Company (Baltimore)
Aerospace Mechanics Department
March 1963

Page

A. Astronautical Constants II-1

B. Environmental Data II-10

C. Systems of Units and Conversion Tables II-20

D. Summary of Lunar Exploration Programs and Results II-26

E. References II-32

Illustrations II-35

II. PHYSICAL DATA

The purpose of this chapter is to present background data for the discussion of lunar missions--to be more specific, the astrodynamical constants needed for lunar trajectories, a discussion of the space vehicle environment, and of the absolute MKS system of units used in the handbook, together with conversion factors to English units. The astrodynamical constants and near-earth environment have been discussed in the companion volume (Chapter II, Ref. 1), and data from that reference is given in summary form for the convenience of the user. Additional data needed specifically for lunar missions has been included in more detail in Sections A and B. A list of space vehicle launches with lunar missions, their objectives, and the present lunar exploration program of the United States is given at the end of the chapter, in Section D.

A. ASTRONAUTICAL CONSTANTS

The constants of the solar system determined from astronomical observations are accurate enough for the prediction of the positions of celestial bodies. However, for a successful lunar or interplanetary mission, better values for the astronomical unit (AU), the distances, diameters, figures, masses, and other data concerning the earth, moon, sun, and planets are required. As these values should be internally consistent, they depend on the physical model used for the trajectory calculation. In addition, some indication of the uncertainty in the values is necessary since these constants define the ballistic trajectory, and uncertainties in the constants are reflected in trajectory "errors" and "miss distances."

In recent years, several articles on astronautical constants have appeared in the literature (Refs. 2, 3, 4, 5 to name but a few). Of these, Refs. 2 and 3 have aimed at a standardization of the constants for astronautical calculations (although there seem to be small inconsistencies in the data, and no indication of a "standard deviation" or other "confidence interval" is given in the data). Reference 4 is restricted to a statistical analysis of geocentric constants, and the constants in Ref. 5, even though internally consistent, appeared too late for their evaluation and inclusion in the handbook. Reference 5 is reproduced in its entirety as Appendix B of Ref. 1. In addition, the calculation of the lunar ephemeris is based on a different set of constants, which is given in the American Ephemeris (Ref. 6). Since more accurate values of constants will become available in the future from observations of space vehicles, radar echoes, and by other means, most of these constants will be superseded by more accurate values and smaller tolerances. In any case, the best values available should be used in trajectory calculations.

For the trajectories in this handbook and its companion volume, Ref. 1, the recently published data has been summarized, and the best values of the constants have been used. The procedure used for determining the means of the various constants is as follows:

(1) Collect all recent values of a particular constant.

(2) Assume that the various values of the particular constant are of roughly the same accuracy.

(3) Obtain the mean ($\bar{x}$) and variance (σ^2) of this sample,

$$\bar{x} = \frac{1}{n}\sum_{i=1}^{n} x_i, \quad \sigma_{\bar{x}}^2 = \frac{1}{n}\sum_{i=1}^{n} (x_i - \bar{x})^2, \quad \sigma^2 = \frac{n-1}{n}\,\sigma_{\bar{x}}^2$$

, where n is the number of values for the constant.

(4) Throw out all values deviating from the mean by more than one standard deviation (1σ).

(5) Recompute the mean and use this value as the "adjusted mean" for the constant.

The "confidence interval" of a constant is used here to indicate that the sample interval brackets the true mean or adjusted mean, as computed by the procedure above, some prescribed percentage of the time. For these small samples, the confidence interval has been obtained from the Student's t-distribution. As this procedure has been fully discussed in Chapter II of Ref. 1, no further details will be given here.

In the remainder of this section, the astronautical constants are defined (and discussed, when necessary), and at the end of the section, their values and confidence levels as used in the handbook are summarized. Since, in the broadest sense, all celestial bodies influence the trajectory to some degree, heliocentric and planetocentric constants will be given, together with the geocentric and selenocentric constants which are of primary interest for lunar trajectories.

1. Heliocentric Constants

Planetary observations and theories of planetary motion permit precise computation of the angular position of the planets. Although angular measurements are quite accurate, no distance scale is readily available. Attempts to resolve this problem have led to the comparison of large, unknown interplanetary distances to the largest of the known distances available to man, the equatorial radius R_e of the earth. In the process, solar parallax was defined as the ratio of the earth's equatorial radius to the mean distance to the sun from a fictitious unperturbed planet whose mass and sidereal period are those utilized by Gauss in his computation of the solar gravitation constant (i.e., one astronomical unit, AU). This definition renders unnecessary the revisions in planetary tables as more accurate fundamental constants are made available, since the length (in kilometers) of the astronomical unit can be modified.

In the broadest sense, the solar parallax is the ratio between two sets of units: (1) the astronomical set utilizing the solar mass, the astronomical unit and the mean solar day (which has recently been replaced by the ephemeris day), and (2) the laboratory set, for which the absolute MKS system of units has been adopted in this handbook.

Another important heliocentric quantity is the value of the solar gravitational constant, $\mu_\odot = GM_\odot$, where G is the universal gravitational constant and $M_\odot$ is the mass of the sun. This constant can be determined in both the astronomical and the laboratory units; results from both determinations are given in this subsection.

In 1938 it was internationally agreed (IAU 1938) that to maintain the Gaussian value of the solar gravitational constant or Gaussian constant $K_\odot^2 = GM_\odot$ as determined by Gauss from Kepler's third law in astronomical units.

$$K_\odot = \frac{2\pi}{\tau} \sqrt{\frac{\bar{r}_{\odot\oplus}^{-3}}{M_\odot + \frac{M_\oplus}{M_\odot}}} = 0.017,202,098,95 \frac{AU^{3/2}}{\text{solar day}} \qquad (1)$$

where

$\bar{r}_{\odot\oplus}$ = 1 AU

τ = 365.256,383,5 mean solar days

$M_\odot$ = solar mass = 1

$\frac{M_\oplus}{M_\odot}$ = ratio of earth and solar masses = 0.000,002,819

The value of $K_\odot$ has nine significant figures by this definition.

The value of $\mu_\odot = GM_\odot$ (as $K_\odot^2$ is usually denoted when measured in laboratory units) can be determined directly by use of the best values for G and $M_\odot$. This yields, if we refer to Ref. 2,

$$\mu_\odot = 1.3251\ (1 \pm 0.0010) \times 10^{20}\ [m^3/sec^2]$$
$$\mu_\odot^{1/2} = 1.1511\ (1 \pm 0.0005) \times 10^{10}\ [m^3/sec^2]^{1/2}$$

The latter value, which corresponds to $K_\odot$ measured in laboratory units, is accurate only to the three significant figures as compared to the nine significant figures of the determination of $K_\odot$ in astronomical units.

It is thus advantageous to compute in the astronomical system of units, converting only when necessary. This procedure assures that the results will become more accurate as better values for the astronomical unit are obtained and produces a much lower end figure error due to round-off.

The sun's orbit and such auxiliary constants as the mean obliquity of the ecliptic, its rate of rotation, and lengths of the various years can be found in the American Ephemeris (Ref. 6).

2. Planetocentric Constants

The mass of a planet is its most important property from the standpoint of trajectory analysis; only in the vicinity of a planet will its actual shape influence the trajectory to some degree. From the mass and its shape, some auxiliary quantities such as the radius of a sphere having the equivalent volume can be derived.

Planetary and some lunar data is summarized in tabular form at the end of this subsection. Table 1 presents the gravitational properties of the sun and planets--their masses and gravitational constants $\mu = GM$ in absolute MKS, gravitational FPS, and astronomical units. In addition, the radius of action of the particular planet with respect to the sun is given in the same units. The radius of action

$$r^* = r_{\odot p} \left(\frac{M_p}{M_\odot}\right)^{2/5} \qquad (2)$$

where $r_{\odot p}$ = distance from sun to planet

defines a spherical region around the planet p which approximates the sphere of influence of the planet in the dynamical system of the planet and the sun. (For more detail, see Subsection B-1b of Chapter IV.) The main significance of the radius of action lies in its use in the "patching" of conic trajectories; inside the sphere of influence, the gravitational attraction of the planet may be neglected as a first approximation to the trajectory, while outside the sphere of influence the gravitational attraction of the planet may be neglected. In the case of the moon, the tabulated radius of action is centered at the moon and defined with respect to the earth, while in the case of the earth-moon system it is centered at the earth-moon barycenter, and the combined masses of the earth and moon are used in its definition with respect to the sun. The last three columns of Table 1 present the sidereal period of revolution, its mean distance from the sun, and the true distance of the planet from the earth on a given date to illustrate the scale of planetary distances and for typical calculations of planetary gravitational attractions near the earth. The data is taken from Refs. 7 and 6, respectively.

Table 2 presents the geometry of the planets. Most celestial bodies are very nearly spherical in shape. However, an oblate ellipsoid can be assumed as a second approximation to the planetary shape, while, for the shape of the moon, a triaxial ellipsoid has been deduced from observations. The oblate ellipsoid is defined by its equatorial radius R_e, its polar radius R_p, or, alternatively, by R_e and its flattening, f, with

$$f = \frac{R_e - R_p}{R_e} \qquad (3)$$

TABLE 1

Gravitational Properties of the Planets

Planet	Mass M: 10^{24} kg	Mass M: 10^{24} slugs	$M_\odot / M_p$	Gravitational Constant μ: 10^6 km^3/sec^2	Gravitational Constant μ: 10^{16} ft^3/sec^2	Gravitational Constant μ: 10^{-9} AU^3/solar day^2	Radius of Action r*: 10^6 km	Radius of Action r*: 10^9 ft	Radius of Action r*: AU	Sidereal Period of Revolution (yr)	Mean Distance from the Sun to the Planet (AU)	True Distance from Earth (AU) Epoch: December 25.0, 1963
Mercury	0.3257	0.02232	6,100,000 ±65,000	0.021,725	0.076,721	0.048,509	0.11178	0.36674	0.000,747,6	0.2411	0.387	0.8407
Venus	4.8811	0.3345	407,000 ±1300	0.325,581	1.149,78	0.726,987	0.61696	2.0241	0.004,126	0.6156	0.724	1.4076
Earth	5.9758	0.40947	332,440 ±50	0.398,601,5	1.407,648	0.890,033	0.92482	3.03429	0.006,185,0	1.0000	1.0000	0
Earth-Moon	6.0484	0.41444	328,400 ±25	0.403,444	1.424,75	0.900,847	0.92933	3.04898	0.006,215,1	--	--	--
Moon	0.073451	0.0050330	$\frac{M_\oplus}{M_\mathbb{C}}$ = 81.357 ± 0.010	0.004,899,4	0.017,302,1	0.010,939,8	0.066282	0.217460	0.000,443,3	0.0748**	--	0.0025
Mars	0.6429	0.04405	3,090,000 ±12,000	0.042,883,0	0.151,440	0.095,753,1	0.57763	1.8951	0.003,863	1.8822	1.53	2.3554
Jupiter	1896.7	129.97	1,047.4 ±0.1	126.515	446.783	282.493	48.141	157.943	0.321,96	11.86	5.20	4.7246
Saturn	567.60	38.89	3500 ±1.7	37.860,4	133.703	84.538,3	54.774	179.70	0.366,31	29.46	9.54	10.4871
Uranus	87.132	5.970	22,800 ±100	5.811,91	20.524,6	12.977,4	51.755	169.80	0.346,13	84.0	19.2	17.9031
Neptune	101.88	6.981	19,500 ±200	6.795,75	23.999,0	15.174,2	86.952	285.28	0.581,51	164.8	30.1	31.0049
Pluto	5.676	0.3889	350,000 ±27,000	0.378,596	1.337,0	0.845,364	35,812	117.49	0.239,5	247.7	39.4	32.5967
Sun	1.9866×10^6	0.13613×10^6	1.00000	132,511	467,960	295,912.208,3*	--	--	--	--	--	0.9835

Underlined digits are questionable.
* Solar gravitational constant is Gaussian value.
** Period of revolution is around earth.

Table 2 also presents the radius of the sphere having the same volume as the oblate ellipsoid,

$$R = \left(R_e^2 R_p\right)^{1/3} \tag{4}$$

to facilitate Keplerian orbit calculations and to illustrate the small planetary asphericities.

Table 3 presents the circular velocity, escape velocity and gravity at the surface of the equivalent sphere (called "sea level") in metric, English and astronomical units, as computed from the following equations:

$$V_{circular} = \sqrt{\frac{\mu}{R}}$$

$$V_{parabolic} = V_{escape} = \sqrt{\frac{2\mu}{R}} \tag{5}$$

$$g_0 = \frac{\mu}{R^2}$$

Preliminary trajectory calculations use the spherical body assumption (i.e., that the celestial body is spherically symmetric in concentric layers) with the radius R given by Eq (4) and the gravitational potential by $U = \frac{\mu}{r}$, where r is the distance from its center. The gravitational attraction is given by $g = \frac{\partial U}{\partial r} = -\frac{\mu}{r^2}$, where the negative sign denotes an attractive force. Orbital data for the planets and auxiliary quantities can be obtained from Ref. 6. Since the orbits of planets (with the exception of Mercury and Pluto) are very nearly circular and are near the ecliptic plane, another common assumption for preliminary calculations is that planetary orbits are circular and in the ecliptic. Further data on planets and their orbits, together with the sources of this information, has been presented in Chapter III of Kuiper (Ref. 8) and in the references listed in the Bibliography of background material of the Lunar Flight Handbook.

3. Geocentric Constants

The approximation of the earth's shape by a rotating oblate ellipsoid which in the interior is symmetric in ellipsoidal layers is quite good for ascent and descent trajectories as well as short-time orbits around the earth. The further assumption is made that the surface of the oblate ellipsoid is an equipotential surface of the geopotential which consists of the gravitational potential of the earth, $U_\oplus$, and the potential of the centrifugal force due to the rotation, $\frac{1}{2}\omega_\oplus^2 R_\phi^2 \cos^2 \phi'$, where $\omega_\oplus$ is the rotational rate of the earth around its axis, R_ϕ is the local radius of the earth, and ϕ' is the geocentric latitude.

The local radius of the oblate ellipsoid R_ϕ as a function of geocentric latitude is given by

$$\frac{R_\phi^2 \cos^2 \phi'}{R_e^2} + \frac{R_\phi^2 \sin^2 \phi'}{R_e^2 (1-f)^2} = 1$$

which can be expressed to order f^2 as

$$R_\phi \simeq R_e \left[1 - f \sin^2 \phi + \frac{5}{8} f^2 \sin^2 2\phi\right]$$

$$\simeq R_e \left[1 - f \sin^2 \phi' - \frac{3}{8} f^2 \sin^2 2\phi'\right] \tag{6}$$

where the flattening f is defined by Eq (3), R_e is the earth's equatorial radius, ϕ is the geodetic latitude (as given on maps), and ϕ' is the geocentric latitude. These latter two quantities are related by

$$\tan \phi' = (1-f)^2 \tan \phi. \tag{7}$$

A consistent expression for $U_\oplus$ is given by

$$U_\oplus = \frac{GM_\oplus}{r_G}\left[1 - \frac{1}{2} J_2 \left(\frac{R_e}{r_G}\right)^2 (3 \sin^2 \phi' - 1) - \frac{1}{8} J_4 \left(\frac{R_e}{r_G}\right)^4 (35 \sin^4 \phi' - 30 \sin^2 \phi' + 3)\right] \tag{8}$$

where r_G is the distance from the center of the earth (the radius in the geographic coordinate system) $GM_\oplus = \mu_\oplus$ is the gravitational constant of the earth, and J_2 and J_4 are numerical coefficients which can be expressed in terms of f, R_e, $\mu_\oplus$, and $\omega_\oplus$. Equations (6) through (8) can be applied to any oblate planet.

The earth's gravitational potential, $U_\oplus$, at a point exterior to the earth must satisfy Laplace's equation.

$$\nabla^2 U_\oplus \equiv \frac{\partial^2 U_\oplus}{\partial x_\oplus^2} + \frac{\partial^2 U_\oplus}{\partial y_\oplus^2} + \frac{\partial^2 U_\oplus}{\partial z_\oplus^2} = 0 \tag{9}$$

A solution of this partial differential equation by separation of variables suggests an expansion of $U_\oplus$ in terms of spherical harmonics which can be written in the form

$$U_\oplus = \frac{\mu_\oplus}{r_G}\left\{1 + \sum_{n=1}^{\infty} \sum_{m=0}^{n} \left(\frac{R_e}{r_G}\right)^n P_n^m (\sin \phi') \cdot \left[C_{n,m} \cos m\lambda + S_{n,m} \sin m\lambda\right]\right\} \tag{10}$$

where R_e now becomes the earth's mean equatorial radius, λ is the longitude (counted positive to the east through 360°), $C_{n,m}$, $S_{n,m}$ are numerical coefficients, and P_n^m is the associated Legendre polynomial, defined in terms of the Legendre polynomial P_n by

$$P_n^m (x) = (1-x^2)^{\frac{m}{2}} \frac{d^m}{dx^m}\left[P_n (x)\right] \tag{11}$$

TABLE 2

Geometry of the Planets

Planet	Equatorial Radius, R_e (km)	(stat mi)	(naut mi)	(ft x 10^7)	1/f	Polar Radius, R_p (km)	(stat mi)	(naut mi)	(ft x 10^7)	Radius of Sphere of Equivalent Volume, R ($R^3 = R_e^2 R_p$) (km)	(stat mi)	(naut mi)	(ft x 10^7)
Mercury	2330 ±10	1448 ±6	1258 ±5	0.7644 ±0.0032	∞*	2330 ±10	1448 ±6	1258 ±5	0.7644 ±0.0032	2330 ±10	1488 ±6	1258 ±5	0.7644 ±0.0032
Venus	6100 ±50	3790 ±30	3290 ±25	2.001 ±0.016	∞*	6100 ±50	3790 ±30	3290 ±25	2.001 ±0.016	6100 ±50	3790 ±30	3290 ±25	2.001 ±0.016
Earth	6378.16 ±0.02	3963.20 ±0.03	3443.93 ±0.02	2.09257 ±164 x 10^{-7}	298.24 ±0.01	6356.77 ±0.05	3949.77 ±0.03	3432.38 ±0.02	2.08555 ±164 x 10^{-7}	6371.02 ±0.05	3958.77 ±0.03	3440.08 ±0.02	2.09023 ±164 x 10^{-7}
Earth-Moon	--	--	--	--	--	--	--	--	--	--	--	--	--
Moon** a	1738.57 ±0.07	1080.30 ±0.04	938.75 ±0.03	0.57040 ±0.00002	--	--	--	--	--	--	--	--	--
b	1738.31 ±0.07	1080.14 ±0.04	938.61 ±0.03	0.57031 ±0.00002	--	1737.58 ±0.07	1079.68 ±0.07	938.22 ±0.03	0.57007 ±0.00002	1738.16 ±0.07	1080.04 ±0.04	938.53 ±0.03	0.57026 ±0.00002
c	1737.58 ±0.07	1079.68 ±0.04	938.22 ±0.03	0.57007 ±0.00002	--	--	--	--	--	--	--	--	--
Mars	3415 ±5	2122 ±3	1844 ±2	1.1204 ±0.0016	75 ±12	3369 ±5	2094 ±3	1819 ±2	1.1055 ±0.0016	3400 ±5	2113 ±3	1836 ±2	1.1155 ±0.0016
Jupiter	71,375 ±50	44,350 ±30	38,539 ±25	23.417 ±0.016	15.2 ±0.1	66,679 ±50	41,432 ±30	36,004 ±25	21.876 ±0.016	69,774 ±50	43,356 ±30	37,675 ±25	22,892 ±0.016
Saturn	60,500 ±50	37,590 ±30	32,670 ±25	19.849 ±0.016	10.2 ± ?	54,560 ±50	33,900 ±30	29,470 ±25	17.990 ±0.016	58,450 ±50	36,320 ±30	31,560 ±25	19.176 ±0.016
Uranus	24,850 ±50	15,440 ±30	13,420 ±25	8.153 ±0.016	14* ± ?	23,070 ±50	14,340 ±30	12,460 ±25	7.571 ±0.016	24,240 ±50	15,060 ±30	13,090 ±25	7.953 ±0.016
Neptune	25,000 ±250	15,530 ±150	13,500 ±130	8.202 ±0.080	58.5 ± ?	24,600 ±250	15,260 ±150	13,270 ±130	8.062 ±0.080	24,870 ±250	15,450 ±150	13,430 ±130	8.159 ±0.080
Pluto	3000 ±500	1860 ±300	1620 ±250	0.984 ±0.16	--	--	--	--	--	3000 ±500	1860 ±300	1620 ±250	0.984 ±0.16
Sun	696,500 ±500	432,800 ±300	376,100 ±250	228.51 ±0.16	--	--	--	--	--	696,500 ±500	432,800 ±300	376,100 ±250	228.51 ±0.16

*Taken from K. A. Ehricke **(Ref. 7)**

**Moon is best presented by triaxial ellipsoid--a: toward earth
b: orthogonal to "a" and "c"
c: along axis of rotation.

TABLE 3

Planetary Circular and Escape Velocities and Planetary Gravity

Planet	Circular Velocity at Sea Level				Escape Velocity at Sea Level				Gravity at Sea Level			
	(km/sec)	(ft/sec)	(stat mi/hr)	(AU/solar day)	(km/sec)	(ft/sec)	(stat mi/hr)	(AU/solar day)	(cm/sec^2)	(ft/sec^2)	($stat\ mi/hr^2$)	($AU/solar\ day^2$)
Mercury	3.05361	10,018.4	6,830.73	0.00176444	4.31846	14,168.2	9,660.13	0.00249530	400.212	13.1303	32,228.9	0.199801
Venus	7.30630	23,970.8	16,343.7	0.00422174	10.33266	33,899.8	23,113.5	0.00597043	875.261	28.7159	70,484.5	0.436964
Earth	7.909773	25,950.7	17,693.7	0.00457044	11.18610	36,699.8	25,022.6	0.00646357	982.0214	32.21855	79,081.88	0.4902632
Earth-Moon	--	--	--	--	--	--	--	--	--	--	--	--
Moon	1.678900	5,508.2	3,755.59	0.00097010	2.374831	7,789.8	5,311.23	0.00137194	162.169	5.32049	13,059.38	0.0809608
Mars	3.55141	11,651.6	7,944.27	0.00205208	5.02243	16,477.8	11,234.9	0.00290207	370.951	12.1703	29,872.5	0.185193
Jupiter	42.5818	139,704	95,252.7	0.0246047	60.2196	197,571	134,707	0.0347962	2598.63	85.2569	209,267	1.29734
Saturn	25.4511	83,500.9	56,932.4	0.0147062	35.9932	118,088	80,514.5	0.0207977	1108.26	36.3601	89,247.5	0.553284
Uranus	15.4841	50,800.9	34,637.0	0.00894705	21.8978	71,843.3	48,984.1	0.0126530	989.073	32.4499	79,649.7	0.493784
Neptune	16.5308	54,234.8	36,978.3	0.00955183	23.3780	76,699.6	52,295.2	0.0135083	1098.84	36.0512	88,489.3	0.548584
Pluto	11.23(?)	36,860(?)	25,130(?)	0.00649(?)	15.89(?)	52,130(?)	35,540(?)	0.00918(?)	4209(?)	138.1(?)	338,900(?)	2.101(?)
Sun	436.181	1,431,040	975,709	0.252035	616.853	2,023,795	1,379,860	0.356431	27,315.7	896,186	2,199,730	13.6371

____ Underlined digits are questionable.

A frequent variant of the form (10) is

$$U_\oplus = \frac{\mu_\oplus}{r_G}\left\{1 + \sum_{n=1}^{\infty}\sum_{m=0}^{n}\left(\frac{R_e}{r_G}\right)^n P_{n,m}(\sin\phi')\cdot \left[A_{n,m}\cos m\lambda + B_{n,m}\sin m\lambda\right]\right\} \quad (12)$$

where

$$P_{n,m}(x) = \left[\frac{(n-m)!}{(n+m)!}\right]^{1/2} P_n^m(x).$$

A simplification of the expressions (10) or (11) to axially symmetric cases removes the bothersome time-dependence of $U_\oplus$ by eliminating the longitude λ, which is defined on the rotating earth. The inclusion of λ in $U_\oplus$ requires a transformation of the potential to inertial coordinates before it can be used in most trajectory programs. For the axially symmetric earth, $U_\oplus$ can be written (in expression which holds to inertial as well as in rotating coordinates):

$$U_\oplus = \frac{\mu_\oplus}{r_G}\left[1 - \sum_{n=1}^{\infty} J_n\left(\frac{R_e}{r_G}\right)^n P_n(\sin\phi')\right], \quad (13)$$

where $J_n = -C_{n,0}$, $S_{n,0} = 0$. Equation (8), giving $U_\oplus$ for an oblate ellipsoidal earth, is a special case of Eq (13) restricted to n = 2 and n = 4. The expressions (10), (12) and (13) were adopted as standard notation by the IAU in 1961. Other expressions used in the literature for $U_\oplus$, as well as the equivalent constants in terms of J_n, have been catalogued in Chapter II of Ref. 1.

An analytic expression for the local radius of the earth, R_ϕ, which is consistent with the general forms (10) and (12) of $U_\oplus$, is too complex to derive. It is customary to give R_ϕ--describing the radius of the geoid, or mean sea level surface of the earth (which is also an equipotential surface of the geopotential)--in graphical form by superimposing the deviations of the geoid from the oblate ellipsoid characterized by R_e and f on a world map. Since these deviations are less than ±50 meters at any point of the earth, many trajectory calculations retain the simple form (6) for R_ϕ, while using a form for $U_\oplus$ which is adequate for the approximation of the trajectory. This is done with the knowledge that R_ϕ and $U_\oplus$ are not strictly consistent.

From long-term observations of earth satellites, the values of J_n, n = 2, 3, 4, 5, 6, have been determined relatively well, where $J_1 = 0$ if the center of mass and the origin of the coordinate system coincide, and the oblateness coefficient J_2 is much larger than J_n, $n \geq 3$. Values of $C_{m,n}$ and $S_{m,n}$ together with standard deviations have been obtained up to m, n = 8 from gravity measurements in Ref. 4 and elsewhere. Values for $\mu_\oplus$, J_2 through J_6, R_e and 1/f are given in the table of adopted constants at the end of Section A. The oblateness coefficient J_2 is, numerically, by far the largest coefficient of J_n.

The value of $\omega_\oplus$ is extremely accurately known from astronomical observations. For the handbooks, the constant value

$$\omega_\oplus = 7.292\ 115\ 146 \times 10^{-5} \text{ rad/sec} \quad (14)$$

has been taken, which in turn determines the period of the earth's rotation with respect to a fixed equinox or the sidereal day at 86164.0989 sec. The mean solar day, or period of the earth's rotation with respect to the mean sun, is 24 hr, or 86,400 sec.

4. Selenocentric Constants

Selenocentric constants can be conveniently divided into two categories--those of primary interest in determining the moon's motion, and those determining its shape and gravitational potential.

In the first category, the constants $\bar{r}_\mathbb{C}$, the lunar distance, L', the lunar inequality as defined by W. de Sitter (Ref. 8) and the mass ratio $\frac{M_\oplus}{M_\mathbb{C}} = \frac{\mu_\oplus}{\mu_\mathbb{C}}$ have been discussed in Chapter II of Ref. 1, and the numerical values are given in the table of adopted constants at the end of this subsection.

The moon has been captured rotationally by the earth, which means that the relatively strong gravitational attraction of the earth has aligned the longest axis of the moon toward the earth in an effect similar to the action of the earth's gravitational torque on a dumbbell-shaped satellite. This has the immediate consequence that the rotational rate of the moon about its axis, $\omega_\mathbb{C}$, equals the sidereal mean motion of the moon around the earth. For the Lunar Flight Handbook, the constant value

$$\omega_\mathbb{C} = \omega_{\oplus\mathbb{C}} = 2.661\ 699\ 484 \times 10^{-6} \text{ rad/sec} \quad (15)$$

has been adopted, fixing the length of the sidereal lunar month and the sidereal period of revolution of the moon about its axis at $27^d\ 7^h\ 43^m\ 11.^s55$, or 27.321 661 4 days. The eccentricity and inclination of the lunar orbit as well as gravitational torques of the sun and other planets cause the moon to perform a "wobble motion" or librations in its orientation with respect to the earth at a given time in its orbit. These lunar librations are discussed further in Chapter III, Section C. Other examples of rotational capture in the solar system include Mercury, which has been captured by the sun, and possibly Venus, as determined by the recent findings of the Mariner II space vehicle.

Values of $\bar{r}_\mathbb{C}$, $\frac{\mu_\oplus}{\mu_\mathbb{C}}$, and $\omega_{\oplus\mathbb{C}}$ have been determined for the n-body problem (i.e., the motion

of the moon under the attraction of the sun and planets). If the simpler restricted three-body problem is used for trajectory calculations (spherical earth, spherical moon in a circular orbit around the earth, massless space vehicle), then the value of one constant must be changed for consistency with Kepler's third law for this force model, as mentioned in Subsection B-2 of Chapter IV. It is customary to retain the values of $\mu_\oplus$, $\mu_\leftmoon$ and $\omega_{\oplus\leftmoon}$ and use a mean earth-moon distance of

$$\bar{r}_{\oplus\leftmoon} = 384,747.2 \text{ km} \qquad (16)$$

instead of the lunar distance $\bar{r}_\leftmoon = 384,402$ km. The distance $\bar{r}_{\oplus\leftmoon}$ is also called the lunar unit (LU) and is analogous to the astronomical unit (AU) on the planetary scale of distances. The value of $\bar{r}_{\oplus\leftmoon}$ is 0.09% larger than $\bar{r}_\leftmoon$, but the restricted three-body force model constants cannot be expected to match observed quantities exactly, as the force model doesn't include all the forces acting on the moon.

Another item of interest in connection with the motion of the moon are the lengths of the lunar months, which have been obtained from Ref. 6 (data is for the epoch 1900.0):

Synodic month	$29^d.530589$	$29^d12^h44^m02^s.9$
Tropical month	$27^d.321582$	$27^d07^h43^m04^s.7$
Sidereal month	$27^d.321661$	$27^d07^h43^m11^s.5$
Anomalistic month	$27^d.554551$	$27^d13^h18^m33^s.2$
Draconitic month	$27^d.212220$	$27^d05^h05^m35^s.8$

Any variation of these values since 1900 from lunar theory and any observed difference can safely be neglected for most astronautical calculations.

Accurate orbital data for the moon, which involves several additional constants, can be found in Ref. 6. The lunar theory which has been used in obtaining the data, the comparison of theory with observation, and the variables given are discussed in detail in Section C of Chapter III. Some orbital elements--important spherical position coordinates as well as the illumination of the moon by the sun--have been given in Chapter XI up to the year 1970 to enable the planning of lunar missions.

The second category of constants deals with the figure of the moon and its gravitational potential. The asphericity of the moon can be deduced from photographic measurements as well as from physical librations (the small wobble-motion of the moon due to gravitational torques of the sun and planets other than earth), and the data indicates that the moon may best be represented by a triaxial ellipsoid with semiaxes a, b and c. The c axis is assumed to coincide with the rotational axis of the moon, the a axis is directed to the mean center point of the moon (see Subsection A-2 of Chapter III for a definition), and the b axis completes the right-handed Cartesian coordinate system. Thus, the a, b, and c axes coincide with the selenographic x_S, y_S and z_S axes, respectively. Define moments of inertia of the moon I_a, I_b and I_c about the a, b, and c axes, and assume that the moon is symmetric in concentric ellipsoidal shells. From observation it has been determined that $a > b > c$. Consequently, $I_a < I_b < I_c$.

Very little data is available on the lunar shape. For the manual, the data given by Alexandrov (Ref. 9), which is based on Yakovkin's observations, Jeffreys' calculations, and the assumptions given in the previous paragraph, has been adopted.

The lengths of the lunar semiaxes depend on the rigid-body motion of the moon and have been calculated as:

	Forced Libration	Free Libration
Semiaxis a (km)	1738.67 ± 0.07	1738.57 ± 0.07
Semiaxis b (km)	1738.21 ± 0.07	1738.31 ± 0.07
Semiaxis c (km)	1737.58 ± 0.07	1737.58 ± 0.07

Values for free libration, adopted by Baker, have also been adopted for the Lunar Flight Handbook. These values are based on the dimensionless moment-of-inertia parameters:

$$\frac{I_c - I_a}{I_b} = 0.000,626,6 \pm 0.000,002,7 \text{ (standard error)}$$

$$\frac{I_a - I_b}{I_c} = 0.000,204.9 \pm 0.000,000,9 \text{ for a forced libration}$$

$$= 0.000,209,8 \pm 0.000,002,2 \text{ for a free libration.}$$

These were calculated by Jeffreys (Ref. 10) from the observational data of Yakovkin. The moments of inertia are given by

$$I_a = \lambda M \quad (b^2 + c^2)$$

$$I_b = \lambda M \quad (c^2 + a^2) \qquad (17)$$

$$I_c = \lambda M \quad (a^2 + b^2)$$

where λ is the inhomogeneity factor, which has the value $\lambda = 0.2$ for a constant density model of the moon and $\lambda = 0.199$ for a modified compressional model of the moon having a density gradient caused by the pressure of the outer layers on the interior (Ref. 9). For $\lambda = 0.199$ (exact value) the moments of inertia are:

Moment of Inertia	Forced Libration	Free Libration
I_a (10^{34} kg-m^2)	8.8293 ± 0.0018	8.8298 ± 0.0018
I_b (10^{34} kg-m^2)	8.8317 ± 0.0018	8.8312 ± 0.0018
I_c (10^{34} kg-m^2)	8.8349 ± 0.0018	8.8349 ± 0.0018

Again, the values for free libration have been adopted in this handbook.

The surface of the lunar ellipsoid is given by

$$\frac{x_S^2}{a^2} + \frac{y_S^2}{b^2} + \frac{z_S^2}{c^2} = 1 \tag{18}$$

This expression will be transformed to spherical coordinates $R_{\phi\lambda}$, the selenocentric radius of a surface point, ϕ_ℓ, the selenographic latitude, and λ_ℓ, the selenographic longitude in order to obtain an expression for $R_{\phi\lambda}$. Define the flattening of the lunar equator as

$$f' = \frac{a - b}{a} = 0.00015 \tag{19}$$

and the flattening of the lunar prime meridian as

$$f^* = \frac{a - c}{a} = 0.00057. \tag{20}$$

The equation of the lunar ellipsoid becomes, in spherical coordinates,

$$\left(\frac{R_{\phi\lambda}}{a}\right)^2 \cdot \left[\cos^2\phi_\ell \cos^2\lambda_\ell + \frac{\cos^2\phi_\ell \sin^2\lambda_\ell}{(1 - f')^2} + \frac{\sin^2\phi_\ell}{(1 - f^*)^2}\right] = 1 \tag{21}$$

Since both f' and f* are very small, it is sufficiently accurate to solve for $R_{\phi\lambda}$ and subsequently expand by use of the binomial theorem, retaining only first-order terms in f' and f*. The resulting expression for $R_{\phi\lambda}$ is

$$R_{\phi\lambda}(\phi_\ell, \lambda_\ell) \simeq a\left[1 - f' \cos^2\phi_\ell \ (1 - \cos^2\lambda_\ell) - f^* \sin^2\phi_\ell\right] \tag{22}$$

The expression for the local radius of the oblate earth--R_ϕ to first order--can be obtained from Eq (22) if $f' \to 0$, $f^* \to f$, as can be verified by comparison with Eq (6). Altitude on lunar maps is not given with respect to the ellipsoidal surface, which is defined to first order by Eq (22), and it is not given with respect to a spherical moon, but it is given with respect to an arbitrary spherical lunar datum which is well below the lunar surface and results in positive altitudes for all lunar surface features.

It remains to obtain an expression for the lunar gravitational potential U_ℓ corresponding to its triaxially ellipsoidal shape and for the modified compressional lunar model. Alexandrov (Ref. 9) and Baker, Makemson (Ref. 10) give the lunar potential in the following widely used form:

$$U_\ell = \frac{\mu_\ell}{r_S}\left\{1 + \frac{1}{2}\left(\frac{a}{r_S}\right)^2\left[\frac{I_b - I_a}{I_c}\left(1 - 3\frac{y_S^2}{r_S^2}\right) + \frac{I_c - I_a}{I_c}\left(1 - 3\frac{z_S^2}{r_S^2}\right)\right]\right\} =$$

$$\frac{\mu_\ell}{r_S}\left\{1 + \frac{1}{2}\left(\frac{a}{r_S}\right)^2\left[\frac{I_b - I_a}{I_c}(1 - 3\cos^2\beta_\ell) + \frac{I_c - I_a}{I_c}(1 - 3\sin^2\phi_\ell)\right]\right\} \tag{23}$$

where r_S is the distance from the center of the moon (the radius in the selenographic coordinate system), y_S and z_S denote components of r_S in selenographic coordinates and β_ℓ is the angle between the y_S axis and r_S. Since the y_S axis rotates with the moon, the expression for U_ℓ is in a non-inertial rotating coordinate system.

The transformation from the selenographic coordinate system $x_S\ y_S\ z_S$ to the lunar equatorial system $x_\ell\ y_\ell\ z_\ell$ is given in Subsection A-2b of Chapter III, from where:

$$y_S = -\sin(\Lambda_S + \omega_\ell t)\, x_\ell + \cos(\Lambda_S + \omega_\ell t)\, y_\ell$$

$$z_S = z_\ell \tag{24}$$

where Λ_S is an arbitrary initial phase angle between the x_ℓ and x_S axes. The expression for U_ℓ in non-rotating lunar equatorial coordinates becomes, after substitution of Eq (24) into Eq (23) and some mathematical operations

$$U_\ell = \frac{\mu_\ell}{r_\ell}\left\{1 - \frac{1}{2}\left(\frac{a}{r_\ell}\right)^2\left[\frac{I_b - I_a}{I_c}\left(-\frac{1}{2} + \frac{3}{2}\frac{z_\ell^2}{r_\ell^2} + 3\left(\frac{1}{2} - \frac{z_\ell^2}{2r_\ell^2} - \frac{y_\ell^2}{r_\ell^2}\right)\cos 2(\Lambda_S + \omega_\ell t) + \frac{3x_\ell y_\ell}{r_\ell^2}\sin 2(\Lambda_S + \omega_\ell t)\right) + \frac{I_c - I_a}{I_c}\left(1 - 3\frac{z_\ell^2}{r_\ell^2}\right)\right]\right\} \tag{25}$$

where $r_\ell \equiv r_S$. (The change in subscript has been introduced in order to emphasize that the radius has components in the lunar equatorial coordinate system.)

Another form of the lunar gravitational potential has been given by Jeffreys (Ref. 11, p 140). It is more useful than the forms (23) and (25) because it allows the expression of the lunar potential in a form analogous to Eq (10) for the earth's potential, with the polar flattening of the moon described by the numerical coefficient

$J_2 = -C_{2,0}$ and the lunar equatorial ellipticity by the coefficient $C_{2,2}$. This form is given in the selenographic coordinate system, and, with a slight change in notation for compatibility with Eq (10), it is:

$$U_{\mathbb{C}} = \frac{\mu_{\mathbb{C}}}{r_S}\left\{1 + \frac{1}{2}\left(\frac{a}{r_S}\right)^2\left[J_2\ (1 - 3\sin^2\phi_{\mathbb{C}}) + 3\,C_{2,2}\cos^2\phi_{\mathbb{C}}\cos 2\lambda_{\mathbb{C}}\right]\right\} \quad (26)$$

where the values of the coefficients are:

$$J_2 = \frac{I_c - \frac{1}{2}(I_a + I_b)}{M_{\mathbb{C}}\,a^2} = 200 \times 10^{-6}$$

$$C_{2,2} = \frac{I_b - I_a}{4M_{\mathbb{C}}\,a^2} = 27 \times 10^{-6} \quad (27)$$

The semiaxis used in Eqs (26) and (27) should be the largest semiaxis, or a, in order to ensure that $U_{\mathbb{C}}$ represents the potential external to the moon. Further forms of the lunar potential useful for determining the magnitudes of the earth's perturbation on a lunar satellite orbit are given in Chapter VII.

For the compressional and constant density lunar models, the origin of the selenographic coordinate system is at the mass center of the moon, so that $J_1 = 0$. As in the case of the earth, the oblateness coefficient J_2 is numerically the largest for the moon, with $(J_2)_{\mathbb{C}} \simeq \frac{1}{8}(J_2)_{\oplus}$. Oblateness effects on lunar satellite orbits will be discussed further in Chapter VII.

The values for J_2 and $C_{2,2}$ given in Eq (27) are rather crude, so no uncertainties will be given. For calculations in the lunar handbook, the values given by Krause (Ref. 5), together with his uncertainty, will be adopted, even though his values are slightly inconsistent with the values for a, b, c, I_a, I_b, I_c adopted for the handbook. Krause obtains:

$$J_2 = 212.5 \times 10^{-6} \pm 2.9 \times 10^{-6}$$

$$C_{2,2} = 18.8 \times 10^{-6} \pm 1.3 \times 10^{-6} \quad (28)$$

5. Summary of Adopted Constants

The constants needed for trajectory calculations which were given in this section are summarized in Table 4. Note is made of the source of each number. The values given, together with the uncertainty and the confidence level have been calculated by Townsend (Ref. 12); they reflect our present knowledge regarding such observations and measurements. The values have been adopted for uniformity in trajectory calculations and in the presentation of results for the handbooks. Better values, with smaller uncertainties and a higher confidence level will appear in the future and should be used in trajectory calculations as soon as they become available. The data in the handbook will remain valid, as any anticipated future changes in the constants will be too small to be reflected in the graphical data, which is for relatively short-term trajectories. A significant improvement in the values for selenocentric constants is expected, however, as soon as long-term satellite orbits around the moon can be established and observed.

B. ENVIRONMENTAL DATA

Section A discussed and summarized the astronautical constants which in effect determine the gravitational environment of the space vehicle. Section B gives some background on other forces and the atmospheric, radiation, meteoroid, and thermal environment in which the space vehicle finds itself during lunar missions.

Environmental data may be subdivided into (1) data pertaining directly to the celestial body, which includes the near-satellite environment of this body, and (2) data pertaining to space between the celestial bodies, such as cislunar space data, interplanetary, interstellar and intergalactic space data. The dividing line between the two types of environment is not very well defined, especially for celestial bodies without a dense gaseous atmosphere, but the delineation will help in the discussion of environmental data.

For lunar missions near earth, cislunar space and near-moon environmental data is required. As near-earth data has been discussed extensively in Chapter II of Ref. 1, this environment will only be summarized and its applicability to lunar flight discussed. Near-earth data has been accumulated rapidly by earth satellites so a clearer picture of the environment is rapidly becoming available. Much less is known about the cislunar environment (the region beyond the earth's atmosphere) and the effect of its magnetic field, due to the small number of space probes and the relatively short time that these probes are in cislunar space. The effects of radiation and micrometeoroids have been discussed quite generally in Chapter II of Ref. 1 and are also applicable to cislunar space. The bulk of the data in this section is on the near-moon environment--the lunar surface, its appearance and approximate thermal characteristics, together with a brief discussion of the tenuous lunar atmosphere.

Much of the environmental data is of a qualitative nature and intended to provide a classification and framework into which the numerous sources and articles in this field can be placed. References giving a comprehensive survey and providing a link between the material in this section and the actual sources have been indicated in order to enable the tracing of data required for lunar flight to its source.

The primary concern in this section is to describe the space environment with very slight mention of its effect on the trajectory, people and materials. The modification of the force model (and hence of the trajectory) by the environment has been discussed in Section B of Chapter IV. A recent survey article by Jaffe and Rittenhouse

TABLE 4

Adopted Constants

Quantity	Best Value	Uncertainty	Approximate Confidence Level[b] (%)
General Constants			
Speed of light	[f] 299792.5 km/sec	[f] 0.1 km/sec	--
Universal grav constant G	6.670×10^{-11} $\frac{m^3}{kg\ sec^2}$	0.005×10^{11} $\frac{nt - m^2}{kg^2}$	--
Heliocentric Constants			--
Solar parallax	[a] 8".798	[b] ±0.001	90
Astronomical unit	[a] 149.53×10^6 km	[a] ±0.03	90
$K_\odot^2$	[c] 0.2959122083 AU^3/solar day^2	[a] $\pm 0.010^{-10}$	99+
Planetocentric Constants			
Mercury			
Solar mass/mass Mercury	[a] 6,100,000	[b] ±65,000	70
Equatorial radius	[a] 2330 km	[b] ±11	70
1/f	?	?	?
Venus			
Solar mass/mass Venus	[a] 407,000	[b] ±1300	90
Equatorial radius	[a] 6100 km (incl. atmosphere)	[b] ±12	70
1/f	?	?	?
Earth-Moon			
Solar mass/earth-moon mass	[a] 328,450	[b] ±25	81
Equatorial radius	--	--	--
1/f	--	--	--
Mars			
Solar mass/mass Mars	[a] 3,090,000	[b] ±12,000	81
Equatorial radius	[a] 3415	[b] ±12	88
1/f	[b] 75	[b] ±12	80
Jupiter			
Solar mass/mass Jupiter	[a] 1047.4	[b] ±0.1	81
Equatorial radius	[a] 71,875 km	[b] ±20	50
1/f	[a] 15.2	[b] ±0.1	50
Saturn			
Solar mass/mass Saturn	[a] 3500	[b] ±2.0	70
Equatorial radius	[a] 60,500 km	[b] ±480	50
1/f	[a] 10.2	± ?	?

(continued)

NOTE:

[a] Baker's value (Ref. 3)

[b] Townsend's value (Ref. 12)

[c] Gaussian value

[d] Ehricke's value (Ref. 7)

[e] Kaula's value (Ref. 4)

[f] Krause's value (Ref. 5)

TABLE 4 (continued)

Quantity	Best Value	Uncertainty	Approximate Confidence Level[b] (%)
Uranus			
Solar mass/mass Uranus	[a] 22,800	[b] ±60	50
Equatorial radius	[a] 24,850	[b] ±50	?
1/f	[a] 14.0	± ?	?
Neptune			
Solar mass/mass Neptune	[a] 19,500	[b] ±200	70
Equatorial radius	[a] 25,000 km	[b] ±2100	50
1/f	[a] 58.5	± ?	?
Pluto			
Solar mass/mass Pluto	[a] 350,000	[b] ±27,000	70
Equatorial radius	[a] 3000 km	[b] ±500	20
1/f	?	?	?
Geocentric Constants			
$\omega_{\oplus}$ (rad/sec)	[f] $7.292115146 \times 10^{-5}$	(exact)	--
μ (km^3/sec^2)	[e] 398601.5	±9.9	88
J_2	[a] 1082.28×10^{-6}	[a] $\pm 0.2 \times 10^{-6}$	95
J_3	[a] -2.30×10^{-6}	[a] $\pm 0.2 \times 10^{-6}$	90
J_4	[a] -2.12×10^{-6}	[a] $\pm 0.5 \times 10^{-6}$	92
J_5	[a] -0.20×10^{-6}	[a] $\pm 0.1 \times 10^{-6}$	88
J_6	[a] -1.0×10^{-6}	[a] $\pm 0.8 \times 10^{-6}$	70
Equatorial radius (km)	[e] 6378.163	[e] ±0.021	95
1/f	[e] 298.24	[e] ±0.01	95
Selenocentric Constants			
$\omega_{\leftmoon} = \omega_{\oplus\leftmoon}$ (rad/sec)	[f] $2.661699484 \times 10^{-6}$	(exact)	--
Lunar distance (km)	[a] 384,402 km	[a] ±1 km	88
L'	[a] 6.4385	[a] ±0.0015	92
$M_{\oplus} / M_{\leftmoon}$	[b] 81.357	[b] ±0.01	90
Semiaxis a (km)	[a] 1738.57 km	[a] ±0.07 km	50
b (km)	[a] 1738.31 km	[a] ±0.07 km	50
c (km)	[a] 1737.58 km	[a] ±0.07 km	50
J_2	[f] 212.5×10^{-6}	[f] $\pm 2.9 \times 10^{-6}$	50
$C_{2,2}$	[f] 18.8×10^{-6}	[f] $\pm 1.3 \times 10^{-6}$	50

(Ref. 13) discusses the behavior of materials in space environments; the 330 references at the end of this article may be consulted for more detailed information.

1. Near-Earth Environment

a. Atmospheric environment

Three types of near-earth environment can be distinguished--the atmospheric, the radiation, and the meteoroid environment. Due to the many large-scale and local variations in the earth's atmosphere, most trajectory calculations are based on a model atmosphere which is assumed to describe average properties of the actual atmosphere and to obey the perfect gas law

$$\rho = \frac{p\bar{M}}{R^*T} \tag{29}$$

and the hydrostatic differential equation

$$dp = -g\rho\, dh, \tag{30}$$

where

ρ = the density in kg/m^3

p = the pressure in newtons $/m^2$

T = the temperature in °K

$\bar{M}$ = the molecular weight of air

R^* = 8.31439×10^3 joules $/kg\,°K$ is the universal gas constant

g = the acceleration due to gravity in m/sec^2

h = the geometric altitude in meters.

The physical properties for the model atmosphere have been calculated under additional assumptions and by use of satellite observations. They are tabulated as a function of altitude up to 700 km as the 1961 U. S. Standard atmosphere. This tabulation, the history of model atmospheres, and additional background have been presented in Chapter II of Ref. 1 and in the listed references of that chapter. Atmospheric effects on space vehicles with lunar mission objectives at altitudes in excess of 700 km are negligible over the short periods of time the vehicle is at these altitudes, and hence no atmosphere need be assumed for altitudes in excess of 700 km. However, if density data at extreme altitudes is required, Nicolet (Ref. 14) can be used as a guide. The atmosphere up to 700 km can be assumed to rotate with the same angular velocity as the earth to a good degree of accuracy.

The 1961 U. S. Standard model atmosphere represents average atmospheric conditions between the maximum and minimum of the sunspot cycle. The actual atmospheric properties that the space vehicle encounters may differ quite considerably from the model atmosphere. This variability is due primarily to solar radiation and heating, gravitational effects of the sun and moon or tidal motions, as well as viscous and turbulent effects, which have been discussed in Chapter II of Ref. 1. To approximate variability for preliminary engineering design, it is sufficient, in most cases, to introduce a certain percentage dispersion in density about the 1961 U. S. Standard atmosphere.

The main effects of the earth's atmosphere on a space vehicle's trajectory are the aerodynamic forces, and the aerodynamic heating it produces. The parameter relating these two effects is the atmospheric density. Expressions for aerodynamic forces have been given in Subsection B-4b of Chapter IV; they are important in designing parking orbits and waiting orbits (see Chapter V and Chapter V of Ref. 1). Aerodynamic forces and heating define a safe re-entry corridor for earth return, or a region of possible re-entry trajectories within the design limits of the lunar vehicle. This aspect is discussed in Chapters IX of Ref. 1 and briefly mentioned in Chapter X.

b. Radiation environment

Contrary to the atmospheric effects on the space vehicle, the effect of radiation is damage to man, electronic equipment, and structural components of the space vehicle. Of all the elements in a space vehicle, man and semiconductors have the lowest threshold of damage from ionizing radiation. The radiation dosage to be expected in a near-earth orbit, radiation damage thresholds, and the shielding (which is defined as additional structural material in the vehicle to absorb radiation before it can reach man and electronic equipment) have been discussed extensively in Chapter II of Ref. 1.

Most of the data on penetrating radiation in the near-earth environment has been acquired since 1958, when the first earth satellites and space probes carried radiation-measurement equipment aloft. Little penetrating radiation reaches the surface of the earth, as the atmosphere represents shielding material of approximately 1 kg/cm^2, and, hence, much of the radiation was not detected until satellite experiments could be performed. In fact, many parameters are still poorly known. The space radiation can be classified into five general types:

(1) Van Allen radiation, consisting of high-energy charged particles which have been trapped in the earth's magnetic field. An inner and an outer belt have been distinguished; the outer belt may extend out as far as 10 ER (earth radii). The particle flux of these two belts is affected by geomagnetic storms.

(2) Solar flare radiation, consisting of high-energy protons and electrons which are ejected at certain times from the sun. Half an hour or more after a large chromospheric flare, high-energy protons (and possibly electrons) can be detected on the earth (p 62, Ref. 15).

(3) Cosmic radiation, consisting of atomic nuclei (mostly of hydrogen, but atomic numbers in excess of 30 have been observed) which move with velocities near the speed of light.

(4) Auroral radiation, consisting of electrons and protons emitted by the sun and concentrated near the geomagnetic poles. The electrons supply the energy for the auroral light.

(5) Penetrating electromagnetic radiation of the sun, consisting mostly of X-rays and γ-rays with energies as high as 500 kilo-electron volts and wavelengths as short as 0.02 Å (1Å = 10^{-10} meter) having been observed.

More detailed descriptions of these radiations and recent data can be found in Ref. 15, while Chapter II of Ref. 1 includes data on radiation, the type of damage, as well as shielding requirements from these radiations. Table 5 summarizes the space radiations which penetrate at least 10^{-6} kg material per square centimeter. This table has been taken from Ref. 15, pp 70 to 71; additional remarks and sources of the data can be found in this reference. Tabulated are the types of radiation, the particle energy and an indication of the integral spectrum (the slope of the particle flux per energy versus energy curve as a function of energy), or differential spectrum (the distribution of particles as a function of the energy of the particle flux in an increment of energy) as well as the particle flux itself.

In the near-earth environment, radiation hazards occur mainly in the parking and/or waiting orbit phase, in any orbital phase on earth return, and in the near-earth portions of lunar flight, when the vehicle velocity relative to earth is about 10 km/sec. Radiation dosages and shielding requirements during that portion have been given in Chapter II of Ref. 1. The parking and waiting orbit altitudes in Chapter V as well as the orbital phase during earth return in Chapter X can be selected so as to be below the inner Van Allen belt.

Figure 1 illustrates the early phases of a typical lunar mission launched from Cape Canaveral. The doughnut-shaped inner Van Allen belt is shown, with the proton flux indicated by eight cross sections and the geomagnetic equator shown on the earth. The shading indicates the proton flux--the darker the appearance of the shaded area, the higher the flux. The illustrated trajectory (with a relatively high parking orbit altitude) intersects the fringes of the inner Van Allen belt after injection, but the time spent in the region of high proton flux is very small due to the high initial space vehicle velocities.

Solar flare radiation occurs sporadically, especially during sunspot maxima. The only protection against this type of radiation and against cosmic and solar electromagnetic radiation is the shielding of the space vehicle and the layout of the equipment so as to provide maximum protection to the vulnerable men and electronic equipment. For launches from Cape Canaveral, the auroral radiation can be neglected, since the parking and waiting orbits will not reach the regions near the geomagnetic poles.

c. Meteoroid environment

Meteoroids are small astronomical bodies which are generally in highly eccentric orbits around the sun. They range in dimension from several meters (extremely rare) to dust particles or micrometeorites as small as one micron in diameter. Beyond the earth's atmosphere, meteoroids may present a hazard to space vehicles. As pointed out by a sample calculation in Subsection B-4d of Chapter IV, the force on the space vehicle due to meteoroids is relatively small and can be neglected in all but the most precise trajectory calculations. However, of major concern is the possibility of a meteoroid collision with the space vehicle resulting in penetration or even puncture of the skin of the vehicle or fuel tank. Puncture of the skin causes a loss of pressurization or fuel, which may require an abort of the mission.

Data concerning average meteoroid fluxes, encounter probabilities and penetration has been given in Chapter II of Ref. 1. Also listed there are the more common meteoroid penetration models and a typical model for evaluating meteoroid effects on propellant storage vessel design.

Meteoroid showers are phenomena which are observed on earth and tend to recur annually. They result from swarms of meteoroids which are roughly in the same solar orbit. When a meteoroid shower is observed on earth, all meteoroids seem to come from the same area in the sky, known as its "quadrant." Data on meteor showers observed on earth has been given on page 99 of Ref. 15. It can be assumed that many other showers may be expected in space and that the value of the micrometeorite flux is enhanced in and near the meteoroid shower.

2. Cislunar Space Environment

In cislunar space, the solar flare radiation, cosmic radiation, the penetrating electromagnetic radiation from the sun, and the meteoroid environment must be considered. The qualitative description and summary of Subsection B-1 regarding these areas apply, as does the referenced quantitative material in Chapter II of Ref. 1 and in Ref. 15. In general, increasingly less reliable data is available than for the near-earth environment. In the list of lunar probes in Section D, some of the vehicle-borne experiments and results have been listed.

3. Lunar Environment

The figure of the moon has been discussed in some detail in Subsection A-4 of Chapter II and its motion in space in Section C of Chapter III. Still to be discussed are lunar topography as deduced by observation of the moon with telescopes, the photographs and maps which have resulted from these observations, the thermal environment on the lunar surface, the type of surface, and the lunar atmosphere. Since many lunar observations have been made by telescopes, Table 6, showing the smallest lunar features visible from earth with perfect optics and under excellent viewing conditions (see Wilkins and Moore, Ref. 16, p 349) gives an idea of the finest lunar surface detail that can be observed.

TABLE 5

Penetrating Radiations in Space

Radiation	Particle Energy or Photon Energy	Flux
Protons		(protons/cm^2-sec)
Auroral--altitudes > 100 km	Integral spectrum, 100 kev < E < 800 kev, varies between E^{-1} and E^{-4}	Normally 10^4 to 10^6 with E > 100 Mev
Van Allen--±40° from integral-invariant equator, altitudes from 10^3 to 8 x 10^3 km	$E^{-0.8}$ integral spectrum above 40 Mev; no radiation observed with E > 700 Mev	Up to ~10^4
Solar-flare--relativistic	E > 1 Bev and usually < 10 Bev	Usually 10 to 10^2; occasionally to ~10^4
Solar-flare--nonrelativistic	From 30 to 300 Mev, E^{-1} to E^{-6} integral spectrum; for typical large solar-flare event, max-intensity integral spectrum might be represented by 3 x 10^{10} E^{-4} protons/cm^2 sec, where E is proton energy in Mev; should not be applied below 30 Mev	Usually 10^2 but occasionally to ~10^4
Cosmic rays--interplanetary space	$E^{-1.5}$ integral spectrum for E > 10 Bev	2 ± 0.3 for E > 40 Mev near max of sunspot cycle; probably increases to ~5 near sunspot min
Cosmic-ray ("splash") albedo-- <10 Earth radii	1 to 10 Mev	~1 near top of atmosphere
Electrons		(electrons/cm^2-sec)
Auroral--from 100 to 1000 km altitudes	<50 kev; spectrum highly variable; integral spectrum >4 kev between E^{-1} and $E^{-2.5}$; 1 observation showed nearly mono-energetic 6-kev stream	Up to 10^{11} to 10^{13} average ~10^5 to 10^7
Van Allen radiation	Integral spectrum ranges from E^{-3} to E^{-6}	Up to ~10^8 for E > 20 kev
Solar-flare--magnetic latitudes > 60°	~100 Mev	Probably < 10^2
Neutrons		(neutrons/cm^2-sec)
Cosmic-ray albedo	$E^{-0.9}$ differential spectrum for 0.1 ev < E < 100 kev, E^{-2} differential spectrum for 1 Mev < E < 1 Bev	~1
X- and γ-Rays		(photons/cm^2-sec)
Electron bremsstrahlung		
Auroral zone	~E^{-4} integral spectrum for E > 30 kev	10 to 10^3 above absorbing atmosphere
Low-latitude visible aurora	$E^{-2.5}$ integral spectrum, ~100 kev	10^3 to 10^5
Atmosphere below radiation belt near 100 km, usually between magnetic latitudes 50 and 60°	10 to 500 kev; theoretical spectrum,	~10^4
Van Allen belt	20 to 50 kev with an energy flux of 10^{-7} erg/cm^2-sec	
Nuclear γ-rays from atmosphere above polar caps	E > 100 kev	~10^3 initially
Solar flares Above 100 km on sunlit hemisphere	5 to 80 kev with an energy flux of 10^{-2} to 10^{-5} erg/cm^2-sec) ~500 kev with an energy flux of 10^{-4} erg/cm^2-sec	

TABLE 6

Smallest Lunar Features Visible from Earth Assuming Perfect Optics and Excellent Viewing Conditions

Aperture of Telescope (cm)	Diameter of Smallest Crater (km)	Smallest Cleft	
		Minimum Width (km)	Minimum Length (km)
15.2	2.4	0.13	1.1
30.5	1.2	0.06	0.5
91.4 (Lick Observatory)	0.4	0.02	0.18
508 (Mt. Palomar Observatory)	0.07	0.005	0.03

However, the necessary excellence of the viewing conditions can be illustrated by the fact that photographs have not shown craters less than 1 km in diameter on the moon,and hence visual observations are the primary source for small details on the lunar surface.

a. Lunar topography

About 100,000 formations on the surface of the moon have been described. In order to discuss these formations, the nomenclature in general use for lunar features is introduced in this subsection. The problem of classification has been taken up by Blagg and Saunders (Ref. 17) and Blagg and Müller (Ref. 18) for those wishing more detail, and another system has been proposed by Bobrovnikoff (Ref. 19), which is claimed to be more detailed than those of Refs. 17 and 18.

The moon as viewed from earth is characterized by light and dark areas. In general, the lighter the appearance of the lunar surface, the higher its elevation.

The dark areas are called "maria," or seas. They are, in general, low plains with some small irregularities (compare the surface elevation contours as given on the USAF lunar aeronautical charts, one of which is reproduced as Fig. 2 in the present chapter). The term "maria" is restricted to larger areas. The terms "lacus" (lake) and "sinus" (bay) are applied to smaller dark features on the lunar surface, while the term "palus" (marsh) describes regions of intermediate coloration.

The boundaries between the dark maria and the lighter-colored "continents" and "mountains" are generally quite sharp. The continents have not been given names, except for a few "capes" which jut out into the maria.

Mountains on the moon usually are named after terrestrial mountains or after scientists; smaller mountains are designated by suffixing a small Greek letter to the name of a large mountain in their vicinity, i.e., Stadius Y. They occur as "chain mountains" in mountain ranges, "ridges," "cellular ring formations" or "domes," which are small, rounded mountains. The vertical relief of the lunar surface can be determined in two steps:

(1) Determine the relative height by measuring the length of a mountain's shadow (a technique which is quite accurate as long as there are mountains in the particular region of the moon by determining the altitudes by scanning the photographic negative of the moon with a photometer and noting the brightness (photometric method), by making direct measurement at or near the limb, or by other methods.

(2) Determine absolute heights by measuring the selenographic locations of these points very accurately and correcting for the projection and the refraction of the earth's atmosphere.

For more detail, Fielder (Ref. 20) can be consulted. From these observations, the vertical relief of the lunar surface has been found to be high.

Some peaks near the lunar south pole exceed an altitude of 9000 meters above the neighboring valleys. This compares with an elevation of 12,000 meters of the Island of Mindanao above the Philippine trench on earth, which has almost four times the radius of the moon. The slopes are usually gentle, with angles less than those on earth. However, in the Jura mountains, slopes average as much as 45°. The maximum elevation in this region is about 6000 meters above Sinus Iridum (Ref. 21).

Very characteristic features of the lunar surface are the "walled enclosures", the larger of which have been referred to as "walled plains" and the smaller of which are called "craters" by Bobrovnikoff. Walled enclosures consist of a plain surrounded by mountains which slope relatively steeply inward (up to a 20° slope, which locally may exceed 45°, as for Copernicus, Ref. 21) and somewhat more gently outward (5° to 10° overall for Copernicus, Ref. 21). They are named primarily after scientists and philosophers, but smaller craters are named after a larger one in the vicinity by suffixing a capital Latin letter, i.e., "Mösting A." Walled enclosures may have one or more central peaks, or they may be without one. The walled plains are quite irregular in shape--hexagonal, quadrangular, triangular, or oval--with the maximum linear dimension from about 300-60 km. Craters are much more circular in shape, and range in diameter from 60 km down to the limit of the present optical resolution, which is of the order of 1 km. The craters may be large and submerged, as is Stadius, large and partially filled, or small craterlets ranging in size down to blowholes or "pits," which are the smallest observed craters. There are also such features as confluent craters and crater chains.

Associated with some craters, and named after them, are "fractures," which range in size from large valleys to fault lines (caused when part of the lunar surface has subsided relative to the surrounding), clefts or rills, and cracks, which consist of a large number of small craters joined together in a chain.

At the time of full moon, "rays", or white streaks which seem to originate from a crater can be observed on the moon, their brightness depending on the phase of the moon. The most prominent is the system of rays associated with the crater Tycho. These ray systems can be classified as radial ray systems, tangential ray systems, ray systems in certain directions, or as "bright spots."

Lunar surface features may merge into one another, as in the following sequences of features

listed by Bobrovnikoff (Ref. 19), for example:

Maria, walled plains, craters, craterlets, crater chains, valleys;

Mountain ranges, isolated peaks, mounds, domes, pits.

In a similar fashion, mountain ranges on the moon are connected with maria, while isolated peaks occur in or near walled plains and craters, as mentioned previously.

During the history of observing the moon (since Galileo's time), no clear-cut changes of the lunar surface have been observed. Changes in small lunar surface features (those several km in extension) depend on such conditions of visibility as the phase of the moon, the libration, the resolving power of the telescope, atmospheric refraction, cloud cover, and the subjective interpretation of the observer. These changes are mostly observed as variations in the brightness and color of small craters, the observation of something looking like a mist, and the appearance of flashes, i.e., any apparent changes in physical relief. Real changes of physical relief must occur due to the impact of meteorites, but no such observation can be safely attributed to that cause (Ref. 19, p 62). The lunar surface must also change due to the pressure of tidal motions inside the moon (Ref. 20, p 127).

Much more material on lunar topography and the nature of the lunar surface can be found in Bobrovnikoff (Ref. 19), Fielder (Ref. 20), Firsoff (Ref. 21), and the bibliography listed in each of these references. In addition, the present theories on the origin of the lunar features, and questions of selenology (which form the lunar counterpart of geology on earth), such as the composition of the interior, the type of surface, the pattern of tectonic grids, and the divisions of selenological time are discussed in Refs. 19 through 21. Our knowledge of the moon's topography and interior will increase vastly in the near future as the planned lunar missions of Ranger, Surveyor, and Apollo spacecraft return scientific data to earth. Until such time, many of the present theories should be regarded as provisional. An illustration of the actual photographically observed lunar topography can be found in the Lunar Aeronautical Chart, which has been reproduced as Fig. 2. Other lunar maps and series of lunar maps prepared in the same fashion are listed in Subsection A-2g of Chapter III.

b. Lunar photometry

In integrated photometry, the total emission of a celestial body is measured. The brightness of the full moon under standard conditions is usually given in stellar magnitudes (mag). In the visual region (average wavelength 5280 Å), the latest determination is by Nikonova (1949) who finds -12.67 mag, and in the photographic region (average wavelength 4250 Å) Bobrovnikoff gives an average value of -11.55 mag, ±0.09 mag; the color index of the moon, or the difference between the two, is +1.12 mag. The amount of light from the full moon under standard conditions is 0.342 ± 0.011 lux (Bobrovnikoff, p 66). Integrated phase curves of the moon, or the variation of the lunar brightness with the phase, have been given by Bobrovnikoff on p 67. The albedo, or reflecting power of the lunar surface, can be defined in two ways: (1) the spherical albedo of the moon or the ratio of the light of the sun scattered in all directions by the lunar hemisphere to the total light, is 0.073; (2) the average geometric albedo of the moon, or ratio between the average brightness of the disk at full moon and the brightness of a white screen of the same size normal to the incident solar rays, is 0.105 (Bobrovnikoff).

In detailed photometry, the emission of light from a small area is measured. Actually, this is to be regarded as the average emission of light over the various surface materials, slopes and the microfeatures or unevenness of the surface in that small area. The moon can be studied in detail due to its nearness to earth, and many photometric studies of lunar details have been made. Of course, the brightness of the lunar feature depends on the directions to the sun and to the observer on earth. If one defines photometric coordinates (α_P, ϵ_P, i_P) of a point P whose brightness is measured by reference to the following sketch:

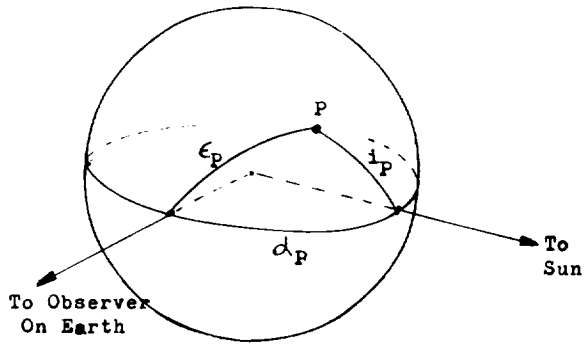

where i_P is the angle of incidence of the solar rays, ϵ_P is the angle of reflection of these rays to the observer on earth, and α_P is the phase angle of the sun with respect to earth, then the brightness of P can be expressed in the form

$$\rho^* = \rho^*_0 f(i_P, \epsilon_P, \alpha_P). \quad (31)$$

In Eq (31), ρ^* is called the "brightness factor," or the ratio of the brightness of the diffusing surface at point P to the brightness of a white screen of the same size placed normally to the sun, and it can be directly compared with the brightness of terrestrial objects. The normalized factor f depends on the photometric coordinates of P such that f = 1 when $i_P = 0°$, $\epsilon_P = 0°$ and $\alpha_P = 0°$. Hence ρ^*_0, or the normal albedo, is the value of ρ for an object near the center of the full moon. It should be remarked that the brightness of every detail of the moon reaches its maximum at full moon, and at that time the brightness of structurally similar details does not depend on the solar position with respect to them, i.e., f = 1 when i = ϵ

(see Bobrovnikoff, Ref. 19, p 68). The following table of normal albedos ρ_0^* of lunar features has been taken from Kuiper (Ref. 8, p 236) and was obtained from a catalogue of 104 normal visual albedos which were reduced to absolute values:

Location	ρ_0^*
Darkest spot (inside Oceanus Procellarum $\lambda_{\leftmoon} = 60°$, $\phi_{\leftmoon} = +27°$)	0.051
Maria (seas)	0.065
Paludes (marshes)	0.091
Mountain regions	0.105
Crater bottoms	0.112
Bright rays	0.131
Brightest spot (Aristarchus)	0.176

The ratio of brightness between the brightest and darkest points is 3.45, which corresponds to 1.34 stellar magnitudes.

One can observe the ashen light on the moon; this is sunlight which reaches the observer from the dark hemisphere of the moon after having been reflected from the earth. It is about 4000 times fainter than moonlight. Seasonal and diurnal variation has been detected in the brightness (see Fielder, Ref. 20, p 55). In addition, there is observational evidence from spectroscopic data that there are luminescent substances on the moon.

The surface of the moon seems to be quite varied in color. These colors range from the greenish tint of the maria to yellow and orange hues on the continents and mountains. These shades have also been photographed and are represented on many of the lunar maps listed in Subsection A-2g of Chapter III. However, measurements of lunar color by photography through filters yield a surprisingly small coloration range (see Bobrovnikoff, Ref. 19, p 71).

c. Temperature of the lunar surface

If the moon is assumed to be a black body in thermal equilibrium, its temperature is given by the Stefan-Boltzmann law:

$$W_{\leftmoon} = \sigma T^4 \tag{32}$$

where $W_{\leftmoon}$ watts/m^2 is the total amount of radiated power by unit area of the lunar area whose temperature is to be calculated, T is the absolute temperature in °K, and $\sigma = 5.67 \times 10^{-8}$ watts/m^2-$(°K)^4$ is the Stefan-Boltzmann constant. Let $r_{\odot\leftmoon}$ be the distance of the moon from the sun. The total radiated solar power crossing a sphere of radius $r_{\odot\leftmoon}$ is $4\pi r_{\odot\leftmoon}^2 W_{\leftmoon}$, and, by definition of the solar constant S, the total radiated power crossing a sphere of radius $\bar{r}_{\odot\oplus} = 1$ AU is $4\pi \bar{r}_{\odot\oplus}^2 S$. From conservation of energy,

$$W_{\leftmoon} = \left(\frac{\bar{r}_{\odot\oplus}}{r_{\odot\leftmoon}}\right)^2 S \tag{33}$$

and the temperature of the lunar surface area becomes

$$T = \left(\frac{\bar{r}_{\odot\oplus}}{r_{\odot\leftmoon}}\right)^{1/2} \left(\frac{S}{\sigma}\right)^{1/4} \tag{34}$$

For $S = 1379$ watts/m^2 (Allen, Ref. 22) and $r_{\odot\leftmoon} = \bar{r}_{\odot\oplus}$ it follows that $T \simeq 394.5°$ K $= 121.5°$ C. This value should be regarded as the maximum temperature that the lunar surface can attain, since in practice some energy can flow to the interior of the moon, and some energy is reflected.

The temperature of the moon is a very difficult quantity to measure. Lunar temperatures have been determined by investigating the emitted light of the moon at various wavelengths (radiometric measurements). Problems arise with the resolution of the measuring instrument and the penetration of the radiation into the lunar surface as well. Thus one can at best obtain an average temperature over some area at some estimated depth below the lunar surface, and the temperature of certain lunar rocks, i.e., a specific local temperature, cannot be determined.

Variations of the lunar surface temperature depend on the thermal inertia constant,

$$K = (\lambda \rho c)^{-1/2} \tag{35}$$

where λ (cal/cm^2-sec) is the thermal conductivity of the surface material, ρ (grams/cm^3) is its density, and c (cal/gram) is the specific heat per unit mass, all measured in cgs units. Optical lunar observations indicate that $K \simeq 1000$. However, Muncey (Ref. 23) has postulated that λ and c vary with the absolute temperature in vacuo, and K for 300° K $\simeq$ 27° C should be between 200 and 300.

Radiometric observations of lunar surface temperatures indicate a maximum temperature of about 130° C and a very unreliable minimum of -153° C depending on the phase of the moon. Some recent measurements by Mezger and Strassl (Ref. 29) indicate a subsurface equilibrium temperature which is independent of the phases. Lunar surface isotherms which were obtained by Geoffrion, et al. (Ref. 25) have been given as a function of phase in Space and Planetary Environments (Ref. 26). A rough estimate of average lunar surface temperatures as a function of the lunar day (1 lunar day = 1 synodic month = $29^d\ 12^h\ 44^m\ 2.^s9$) has been given in Fig. 3. The data in Fig. 3 is based on Pettit and Nicholson's data (Ref. 27) under the assumptions that the temperature variations in latitude and longitude

are identical (i.e., the surface isotherms are circular) and that the ecliptic and lunar equatorial planes coincide; the solar irradiation at the subsolar point has been taken as given by the solar constant, S = 1396.4 watts/m^2.

d. Lunar magnetic field

The instrumentation on the Soviet Lunik II space vehicle did not detect a lunar magnetic field. These measurements put an upper limit on the lunar magnetic field of 3×10^{-4} gauss, which compares to a field strength of 0.6 gauss in the polar region of the earth. Thus the lunar field is very weak compared to the earth's. However, one can still assume that the magnetic field on the lunar surface is of the order of 2.5×10^{-5} gauss, due to the general interplanetary magnetic field, rising to a maximum of 4×10^{-4} gauss at periods of high solar activity (Ref. 26, p 102).

e. Lunar surface characteristics

The structure of the surface and the subsurface layers of the maria, continents, and mountains varies according to different theories about the origin of the major surface features. One theory postulates the volcanic origin of these features, while another postulates meteoritic origin. The spectroscopic, radiometric, radar and radio data on the moon suggest a surface cover of dust or finely ground powder, but there is disagreement on the thickness of the dust layer. It is assumed to vary in thickness from a few millimeters to several meters, although some small areas on the moon seem to be substantially free from dust cover (Bobrovnikoff, Ref. 19, p 106). Both the meteoritic and volcanic theories predict a layer of dust.

The behavior of the dust is also open to question. Theories range from an extremely loose top layer held in suspension by electrostatic forces and subject to migration (Gold, Ref. 28) to a layer of dust grains cemented together (Whipple, Ref. 29). The vacuum welding effect found by Roche (Ref. 30) predicts a strong tendency of particles to adhere to each other when disturbed by seismic quakes. In Ref. 26, p 111, it is stated that theoretical considerations suggest "dust on the lunar surface which is cemented into a porous, low-density matrix, weak compared to sedimentary rocks on earth but strong compared to earth dust and not subject to migration."

The microfeatures (i.e., unobservably small features) of the lunar surface are also open to question. Radar measurements seem to indicate both a smooth and rough surface on the decimeter scale (see Ref. 26, p 112), while the photometric interpretations of Sytinskaya (Ref. 31) indicate a mean dimension of these microfeatures of the order of several millimeters to several centimeters.

f. Natural resources on the moon

A good reference on lunar natural resources is Ref. 26, pp 114 to 121 and the listed sources. The conclusion in that reference is that limited amounts of useful materials may be present on the lunar surface. One of these useful materials could be water. Due to the low vapor pressure of water at -150° C, it could remain in the solid state at zero pressure for millions of years. Such surface conditions exist in some lunar areas which remain in perpetual shadow. There might also be large ice deposits sealed off beneath the lunar surface. It has been predicted that the volatile materials associated with earth volcanism such as H_2O, H_2S, CO_2 and SO_2 have been concentrated near the margins of the circular maria.

g. Lunar atmosphere

The lunar atmosphere must be extremely rarefied, as determined from such observational evidence as sharp surface shadows, sudden star occultation and the absence of refraction phenomena during solar eclipses. Jeans (Ref. 32) was able to show from considerations of kinetic theory that, under certain assumptions, if the root-mean-square velocity $\sqrt{(\bar{V}^2)}$ of the individual molecules of a planet's atmosphere is 0.2 V_p, where V_p is the parabolic or escape velocity of the planet, then atmospheric dissipation periods of 100 million years can be expected. The low value of V_p = 2.375 km/sec for the moon as compared to the earth's value of V_p = 11.186 km/sec would then suggest that only molecules with a high molecular weight such as SO_2, CO_2, H_2S can be retained by the moon for long periods of time. Some radiogenic krypton, xenon, argon, radon and helium should be continually released from the lunar interior, and some gases may be released during the vaporization of ice deposits. However, the latter would escape rather rapidly due to the low value of V_p. Hence, the composition of the lunar atmosphere is open to question. The following table, taken essentially from Fielder (Ref. 20 , p 115), gives maximum densities of the lunar atmosphere as established by various methods:

Observation	Method	Source	Maximum Density of the Lunar Atmosphere (atmospheres)
1	Absence of twilight	Russel, Dugan and Stewart (Ref. 33)	$< 10^{-4}$
2	Photography of twilight in green light with a polarimeter	Lipski (Ref. 34)	$< 10^{-4}$
3	Photography of twilight in yellow light with a 20-cm coronograph	Lyot and Dollfus (Ref. 35)	$< 10^{-8}$
4	Photography of twilight in orange light, with a 20-cm coronograph and a polariscope	Dollfus (Ref. 36)	$< 10^{-9}$
5	Refraction of radio waves in the lunar ionosphere	Elsmore and Whitfield (Ref. 37)	$< 10^{-12}$
6	Refraction of radio waves in the lunar ionosphere	Costain, Elsmore and Whitfield (Ref. 38)	$< 10^{-13}$

In general, the minimum density on the lunar surface is assumed to be the same as that of the interplanetary medium. However, Öpik and Singer (Ref. 39) have postulated zero pressure due to the repulsion of ionized gas molecules by the positively changed lunar surface. Under these circumstances a maximum lunar atmospheric density of 10^{-12} atmospheres can be assumed (Bobrovnikoff), compared to 10^{-13} atmospheres assumed in Ref. 26.

Locally the atmospheric density may exceed these values due to very rare gaseous discharges. There have been observations of haziness near some features, notably of a "volcanic eruption" in the crater Alphonsus observed by Kozyrev (Ref. 40). Again, from kinetic theory considerations, most of these gases quickly escape from the moon.

Due to the absence of a lunar atmosphere, the surface of the moon is bombarded much more frequently by meteorites, micrometeorites, cosmic rays and high-energy solar radiation (such as X-rays and γ-rays) than the earth. The radiation and meteoritic environment near the lunar surface is probably not much different from that in cislunar space, since such an atmosphere can provide no shielding.

h. Summary

The lunar environmental data has been discussed in narrative form for this handbook because of its importance for lunar flight. The major references used for this discussion have been Refs. 8, 19, 20, 21 and 26, and the sources indicated in these references. If it is desired to trace the lunar environmental information to the source, the major references which give the source should be consulted. All numerical data on the lunar environment has been either referenced to the major reference or to the source itself to allow further checking of numerical data.

Our present ideas about surface conditions on the moon can be summarized as follows (see also Bobrovnikoff, Ref. 19, p 108):

(1) The lunar surface has a rough microrelief with many small pits, depressions and elevations.

(2) The vertical relief (macrorelief) is high, but the slopes are generally gentle.

(3) The lunar surface consists of dust (probably radioactive) which is cemented into a porous, low-density matrix not subject to migration.

(4) There is no appreciable atmosphere, the upper limit on atmospheric density being 10^{-12} atmospheres.

(5) Locally, gases must be escaping, and seismic quakes must be rather common.

(6) The temperature variations are extremely great, from a maximum of about +130° C near the subsolar point to a minimum of about -150° C.

(7) There is no appreciable lunar magnetic field.

(8) There is no shielding of the lunar surface from the bombardment of meteorites, micrometeorites, particles and radiation which affect the structure, texture and composition of the surface.

Some lunar environmental data, as it was acquired by the space vehicles listed in Section D of this chapter, has already been incorporated in the present writeup. It should be mentioned again that planned space vehicle flights into the vicinity of the moon and exploration of the lunar surface will yield much more data and may modify our present ideas on the near-moon environment.

C. SYSTEMS OF UNITS AND CONVERSION TABLES

Throughout the Lunar Flight Handbook the absolute MKS system of units, which is based on the meter as the basic unit of length, the kilogram as the basic unit of mass, and the second as the basic unit of time, has been used. In order to be able to compare the handbook data with that presented elsewhere, the systems of units in common use and conversion factors between the units are presented in summary form in this section. More information on units and conversions can be found in Judson (Ref. 41). It is important that this or later references be consulted, since the metric equivalents of the U.S. foot, and U.S. pound (avoirdupois) have recently been changed slightly by act of Congress. Another good reference on units of measurement is Green (Ref. 42), who also discusses electrical systems of units. Astronomical units have been discussed to some extent by Herrick, Baker, and Hilton (Ref. 2) and in the standard textbooks of astronomy.

1. Systems of Mechanical and Astronomical Units.

The unit force in an absolute system of units gives unit acceleration to unit mass, while the unit force in a gravitational system of units gives the acceleration of g_0 to a unit mass (see Table 7).

There are two types of gravitational units; choice of either depends on whether the unit of mass is numerically equal to the unit mass in the absolute system (Type 2) or differs from it by a factor g_0 (Type 1).

TABLE 7

Systems of Mechanical Units

	Metric				English		
	1	2	3	4	5	6	7
Property	Absolute MKS $F = Ma$	Absolute CGS $F = Ma$	*** Gravitational MKS Type 1 $F = Ma$	*** Gravitational MKS Type 2 $F = \frac{M}{g_0} a$	Absolute FPS $F = Ma$	*** Gravitational FPS Type 1 $F = Ma$	*** Gravitational FPS Type 2 $F = \frac{M}{g_0} a$
Length	meter (m)	centimeter (cm)	meter (m)	meter (m)	foot (ft)	foot (ft)	foot (ft)
Mass	kilogram (kg)	gram (g)	*kgf sec^2/m	kilogram (kg)	pound (lb)	**slug $= \frac{lbf\ sec^2}{ft}$	pound (lb)
Time	second (sec)	sec	sec	sec	sec	sec	sec
Force	newton (nt) $= \frac{kg\ m}{sec^2}$	dyne $= \frac{g\ cm}{sec^2}$	*kilogram force (kgf)	*kilogram force (kgf)	poundal (pdl) $= \frac{lbf}{sec^2}$	**pound force (lbf)	**pound force (lbf)
Energy	joule = nt-m	erg = dyne-cm	*kgf-m	*kgf-m	pdl-ft	**lbf-ft	**lbf-ft
Power	watt $= \frac{joule}{sec} = \frac{nt\text{-}m}{sec}$	$\frac{erg}{sec} = \frac{dyne\text{-}cm}{sec}$	$\frac{*kgf\text{-}m}{sec}$	$\frac{*kgf\text{-}m}{sec}$	$\frac{pdl\text{-}ft}{sec}$	$\frac{**lbf\text{-}ft}{sec}$	$\frac{**lbf\text{-}ft}{sec}$
Pressure	10^{-2} millibar (mb) $= \frac{nt}{m^2}$	10^{-3} millibar (mb) $= \frac{dyne}{cm^2}$	$\frac{*kgf}{m^2}$	$\frac{*kgf}{m^2}$	$\frac{pdl}{ft^2}$	$\frac{**lbf}{ft^2}$	$\frac{**lbf}{ft^2}$

*The numbers associated with these units are only $\frac{1}{g_0} = \frac{1}{9.80665}$ (exact) as large as the numbers associated with corresponding units of system 1.

**The numbers associated with these units are only $\frac{1}{g_0} = \frac{1}{32.17404855}$ as large as the numbers associated with corresponding units of system 5.

***All gravitational units are based on the standard acceleration due to gravity, g_0, no matter where the force measurement takes place. This weight, thrust, etc., in the vicinity of the moon is given in terms of g_0, not the lunar acceleration of gravity.

(1) The absolute MKS system of units in column 1, which is used by physicists, has been employed throughout the Lunar Flight Handbook.

Auxiliary units, related to the basic units in the table by powers of 10, are defined by the following standard pre-prefixes and abbreviations

tera:	10^{12}	T
giga:	19^9	G
mega:	10^6	M
kilo:	10^3	k
hecto:	10^2	h
deka:	10^1	da
deci:	10^{-1}	d
centi:	10^{-2}	c
milli:	10^{-3}	m
micro:	10^{-6}	μ
nano:	10^{-9}	n
pico:	10^{-12}	p
femto:	10^{-15}	f
atto:	10^{-18}	a

Both basic and auxiliary units will be used in the Handbook, whichever are more convenient in describing the quantity in question.

(2) The gravitational MKS system of units in column 4 of the preceding table is in general use in Europe. The word "kilogram" is very often used as the unit of both mass and force. Consequently, the expression "kilogram" is ambiguous, although its meaning as a unit of mass or force is usually clear from the context. To avoid confusion, it is desirable to denote the basic unit of mass by "kilogram" and the basic unit of force by "kilogram force" as has been done in the table above. The same remark applies to derived units such as "gram," "metric ton," etc.

(3) The gravitational MKS system of units in column 3 of the preceding table is used by European aeronautical engineers.

(4) The gravitational FPS system of units in column 7 is in general use in the U.S. The word "pound" is very often used interchangeably as a unit of force and mass, and consequently its meaning is ambiguous. To avoid confusion, the basic unit of mass has been designated "pound" and the basic unit of force has been designated "pound force" in the preceding table. Again, the same remark applies to derived units such as "ounce" and "ton."

(5) The gravitational FPS system of units in column 6 is used by American aeronautical engineers. The basic unit of mass in this system of units is the slug. One slug corresponds to g_0 pounds (mass), so that the mass M expressed in slugs is M/g_0, where M is the mass expressed in pounds (mass).

Astronomers frequently use systems of units which are adapted to calculations in dynamical astronomy. A comparison of two common systems of astronomical units with the absolute MKS system is given in Table 8.

TABLE 8

Systems of Astronomical Units

Property	Absolute MKS $F = \frac{G M_1 M_2}{r^2}$	Astronomical	
		Type 1 $F = \frac{K_\odot^2 M_2}{r^2}$	Type 2 $F = \frac{K_\odot^2 M_2}{r^2}$
Length	Meter (m)	Astronomical unit (AU) *1 AU = 149.53×10^9 m	AU
Mass	Kilogram (kg)	Solar mass ($M_\odot$) *1 $M_\odot$ = 1.9866×10^{30} kg	**$M_\odot$
Time	Second (sec)	Mean solar day (MSD) 1 MSD = 86,400 sec	*$t_\odot$ = 58.13244087 MSD
Universal gravitational constant G or solar gravitational constant $K_\odot$	*$G = 6.670 \times 10^{-11}$ $m^3/kg\ sec^2$	*$K_\odot = 0.01720209895 \frac{(AU)^{3/2}}{MSD}$	$K_\odot = 1 \frac{(AU)^{3/2}}{t_\odot}$
Force	Newton = 1 kg · m/sec^2	$\frac{M_\odot (AU)}{(MSD)^2}$	** $\frac{M_\odot (AU)}{t_\odot^2}$
Angular velocity	Radian/sec	$\frac{radian}{MSD}$	$\frac{radian}{t_\odot}$

*Value adopted in the handbook. For further details see Section A.

**If the mass M_2 is an appreciable fraction of $M_\odot$, i.e., $\frac{M_2}{M_\odot} > 10^{-6}$, then quite frequently the unit of mass is chosen as $M = (M_\odot + M_2)$, and the unit of force becomes $\frac{M (AU)}{t_\odot^2}$.

The astronomical system of units, Type 1, has been defined because the angular motion of the planets and moons can be determined much more accurately by observation than their distances. As long as all calculations are performed in astronomical units, they are very accurate. At the end of the calculations one can make the transformation to the absolute MKS laboratory units (see Subsection A-1).

The astronomical system of units, Type 2, has been introduced in order that the mean motion (or average angular velocity) of the earth around the sun has magnitude 1.

In both systems of astronomical units, the dynamical system consists of a spherical earth in an elliptical orbit around a spherical sun, so that two-body results apply. It is also possible to construct other sets of astronomical units by use of other planets or comets and the sun, or of moons around planets. The earth case is of particular interest in lunar flight problems when applied to the dynamical system of a spherical moon in an elliptic orbit around the earth. For the earth-moon system, the unit of length becomes the lunar unit (*1 LU = 384,747.2 km) and unit of mass the earth's mass (*$M_\oplus$ = 5.9758×10^{24} kg). The unit of time in a Type 1 astronomical system is the mean solar day (MSD) and the gravitational constant of the earth becomes:

$$*K_\oplus = \frac{2\pi}{\tau} \sqrt{\frac{\bar{r}_{\oplus \leftmoon}}{M_\oplus + \frac{M_\leftmoon}{M_\oplus}}} = 0.228570389 \frac{(LU)^{3/2}}{MSD}$$

where

$\bar{r}_{\oplus \leftmoon}$ = 1 LU

*τ = 27.3216614 mean solar days

$M_\oplus$ = 1 earth mass

$\frac{*M_\leftmoon}{M_\oplus} = \frac{1}{81.357} = 0.012291505$ (exact).

The unit of time in a Type 2 astronomical system is $t_\oplus$ = 4.37501990 MSD, therefore, the gravitational constant of the earth becomes $K_\oplus = 1 \frac{(LU)^{3/2}}{t_\oplus}$

2. Length, Velocity, Acceleration and Volume/Capacity Unit Conversions

a. Defined relations

Meter (m) = 1,650,763.73 wavelengths of the orange-red radiation of Krypton-86: the fundamental metric unit of length.

Foot (ft) = 0.3048 m (exact): the fundamental U.S. unit of length.

Second (sec) = 1/86400 mean solar day: the fundamental unit of civil time.

Velocity units: length/time.

Acceleration units: length/$(time)^2$.

Volume (or capacity) units: $(length)^3$.

The fundamental unit of volume is one cubic meter (m^3) or the unit of volume equal to a cube with edges 1 m in length.

The fundamental metric unit of capacity is the liter (ℓ), which is equal to the volume of 1 kg of pure water at its maximum density near 4° C and under standard atmospheric pressure of 760 mm Hg. 1 ℓ = 1000.028 (cm^3).

The gallon is a unit of liquid capacity equal to 231 cubic inches (in^3).

*The values adopted in the lunar handbook have been used for the calculations.

b. Length conversions

Table 9 lists conversion factors for standard units of length.

TABLE 9

Length Conversions

	Astronomical Units	International Nautical Miles	Statute Miles	Meters	International Yards	International Feet	International Inches
1 Astronomical Unit =	1	$80.737,90 \times 10^{6}$	$92.911,52 \times 10^{6}$	149.5266×10^{9}	$163.524,3 \times 10^{9}$	490.5728×10^{9}	$588.687,4 \times 10^{10}$
1 International Nautical Mile =	$1.238,575 \times 10^{-8}$	1	1.150,779,447	1852*	2025,371,828	6076,115,485	72,913,385,826
1 Statute Mile =	$1.076,292 \times 10^{-8}$	0.868,976,242	1	1609,344*	1760*	5280*	63,360*
1 Meter =	$0.668,777,3 \times 10^{-11}$	$0.539,956,803 \times 10^{-3}$	$0.621,371,192 \times 10^{-3}$	1	1.093,613,298	3,280,839,895	39,370,078,740
1 International Yard =	$0.611,529,9 \times 10^{-11}$	$0.493,736,501 \times 10^{-3}$	$0.568,181,818 \times 10^{-3}$	0.9144*	1	3*	36*
1 International Foot =	$0.203,843,3 \times 10^{-11}$	$0.164,578,833 \times 10^{-3}$	$0.189,393,939 \times 10^{-3}$	0.3048*	0.333,333,333	1	12*
1 International Inch =	$0.169,869,4 \times 10^{-12}$	$0.137,149,028 \times 10^{-4}$	$0.157,828,282 \times 10^{-4}$	0.0254*	0.027,777,777	0.083,333,333	1

1 micron = 10^{-6} meter, 1 Angstrom unit = 10^{-10} meter

c. Velocity conversions

Table 10 lists conversion factors for standard units of velocity.

TABLE 10

Velocity Conversions

	Astronomical Units per Mean Solar Day	Astronomical Units per Sidereal Day	International Nautical Miles per Hour	Statute Miles per Hour	Kilometers per Hour	Meters per Second	Feet per Second
1 Astronomical Unit per Mean Solar Day =	1	1.002,737,90	$3.364,079 \times 10^{6}$	$3.871,313 \times 10^{6}$	$6.230,273 \times 10^{6}$	$1.730,632 \times 10^{6}$	$5.677,928 \times 10^{6}$
1 Astronomical Unit per Sidereal Day =	0.997,269,57	1	$3.354,892 \times 10^{6}$	$3.860,743 \times 10^{6}$	$6.213,260 \times 10^{6}$	$1.725,907 \times 10^{6}$	$5.662,424 \times 10^{6}$
1 International Nautical Mile per Hour =	$0.297,258,2 \times 10^{-6}$	$0.298,072,1 \times 10^{-6}$	1	1.150,779,447	1.852*	0.514,444,444	1.687,809,856
1 Statute Mile per Hour =	$0.258,310,3 \times 10^{-6}$	$0.259,017,5 \times 10^{-6}$	0.868,976,242,6	1	1.609,344*	0.447,040*	1.466,666,666
1 Kilometer per Hour =	$0.160,506,6 \times 10^{-6}$	$0.160,946,1 \times 10^{-6}$	0.539,956,803,4	0.621,371,192	1	0.277,777,777	0.911,344,415
1 Meter per Second =	$0.577,823,6 \times 10^{-6}$	$0.579,405,6 \times 10^{-6}$	1.943,844,491	2.236,936,288	3.600*	1	3.280,839,895
1 Foot per Second =	$0.176,210,6 \times 10^{-6}$	$0.176,602,8 \times 10^{-6}$	0.592,483,800	0.681,818,181	1.097,280*	0.3048*	1

—Underlined digits are questionable.

*Denotes exact conversion factor.

d. Acceleration conversions

Table 11 lists conversion factors for standard units of acceleration.

TABLE 11

Acceleration Conversions

	Astronomical Units per Mean Solar Day^2	Astronomical Units per Sidereal Day^2	International Nautical Miles per Hour^2	Statute Miles per Hour^2	Kilometers per Hour^2	Meters per Second^2	International Feet per Second^2
1 Astronomical Unit per Solar Day^2 =	1	1.005,483,30	$1.401,700 \times 10^{5}$	$1.613,047 \times 10^{5}$	$2.595,989 \times 10^{5}$	20.030,46	65.716,76
1 Astronomical Unit per Sidereal Day^2 =	0.994,546,60	1	$1.394,056 \times 10^{5}$	$1.604,250 \times 10^{5}$	$2.581,832 \times 10^{5}$	19.921,23	65.358,38
1 International Nautical Mile per Hour^2 =	$0.713,419,4 \times 10^{-5}$	$0.717,331,1 \times 10^{-5}$	1	1.150,779,447	1.852*	$1.429,012,345 \times 10^{-4}$	$4.688,360,711 \times 10^{-4}$
1 Statute Mile per Hour^2 =	$0.619,944,7 \times 10^{-5}$	$0.623,344,2 \times 10^{-5}$	0.868,976,242,6	1	1.609,344*	$1.241,777,778 \times 10^{-4}$	$4.074,074,074 \times 10^{-4}$
1 Kilometer per Hour^2 =	$0.385,209,6 \times 10^{-5}$	$0.387,321,9 \times 10^{-5}$	0.539,956,803,4	0.621,371,192	1	$0.771,604,938,2 \times 10^{-4}$	$2.531,512,264 \times 10^{-4}$
1 Meter per Second^2 =	0.049,923,97	0.050,197,70	$0.699,784,017,6 \times 10^{4}$	$0.805,297,064,9 \times 10^{4}$	12,960*	1	3.280,839,895
1 International Foot per Second^2 =	0.015,216,82	0.015,300,26	$0.213,294,168,6 \times 10^{4}$	$0.245,345,245,2 \times 10^{4}$	0.395,020,800	0.3048*	1

e. Volume and capacity conversions

Table 12 lists conversion factors for standard units of volume and capacity.

TABLE 12

Volume and Capacity Unit Conversions

	Cubic Inches	Cubic Feet	Cubic Meters	Liters	Gallons
1 Cubic Inch	1*	5.787037×10^{-4}	1.6387064×10^{-5}	0.01638661	0.004329004
1 Cubic Foot	1,728*	1	0.028316846592*	28.31605	7.480519
1 Cubic Meter	61,023.74*	35.31467*	1	999.972	264.172
1 Liter	61.02545	0.03531566	1.000028×10	1	0.2641794
1 Gallon (U.S.)	231*	0.1336806	3.7854118×10^{-3}	3.785306	1

*Denotes exact conversion factor

3. Angular conversions

Table 13 lists conversion factors for standard units of angular measurement.

TABLE 13

Angular Unit Conversions

	Revolutions	Radians	Degrees	Minutes of Arc	Seconds of Arc	Angular Mils
1 Revolution =	1	6.283,185,307	360.0*	21,600.0*	1,296,000.0*	6400*
1 Radian =	0.159,154,943	1	57.295,779,511	3,437.746,771	206,264.806,236	1018.591636
1 Degree =	$2.777,777,777 \times 10^{-3}$	$1.745,329,252 \times 10^{-2}$	1	60.0*	3,600.0*	17.777,777,77
1 Minute of Arc =	$4.629,629,629 \times 10^{-5}$	$2.908,882,086 \times 10^{-4}$	$1.666,666,666 \times 10^{-2}$	1	60.0*	0.296,296,296
1 Second of Arc =	$7.716,049,382 \times 10^{-7}$	$4.848,136,812 \times 10^{-6}$	$2.777,777,777 \times 10^{-4}$	0.016,666,666	1	$4.938,271,605 \times 10^{-3}$
**1 Angular Mil =	1.5625×10^{-4}*	$9.817,477,040 \times 10^{-4}$	5.6250×10^{-2}*	3.375*	202.5*	1

*Denotes exact conversion factor.

**The "angular mil" should be differentiated from the milliradian, which is often designated "mil" in targeting, and the "mil" which is a unit of length corresponding to 0.001 inch. From the table, 1 angular mil = 0.981,747,704 milliradian

4. Mass and Force Unit Conversions

a. Defined relations

Kilogram (kg) the mass of the international prototype kilogram: the fundamental metric unit of mass in the absolute MKS system of units.

Pound avoirdupois (lb) = 0.45359237 kg (exact): the fundamental U.S. unit of mass in the absolute FPS system of units.

Unit force in an absolute system of units is a unit which gives unit acceleration to unit mass:

1 newton (nt) = 1 kg-m/sec^2

1 poundal (pdl) = 1 lb-ft/sec^2

Unit force in a gravitational system of units is a mass unit multiplied by g_0, where g_0 = 9.80665 m/sec^2 (exact) is the standard acceleration due to gravity, the adopted sea level value for 45° latitude. In U.S. units

g_0 = 32.17404855 + ft/sec^2 (derived value).

1 kilogram force (kgf) = 9.80665 kg-m/sec^2 = 9.80665 nt

1 pound force (lbf) = 32.17404855 + lb-ft/sec^2 = 32.17404855 + pdl

b. Derived mass unit conversions

Table 14 lists conversion factors for mass units.

c. Derived force and mass unit conversions

1 kgf = 2.204622621 + lbf

1 lbf = 0.45359237 kgf = 4.448176256 + newtons

1 newton = 10^5 g-cm/sec^2 = 10^5 dynes

1 newton = 0.101972661 + kgf

1 newton = 0.224811235 + lbf

1 newton = 7.23301387 + pdl

1 pdl = 0.1382549543 + newtons

1 pdl = 0.31080950 + lbf

1 kg = 0.101972661 + kgf sec^2/m

1 lb = 0.0310809501 + lbf sec^2/ft = 0.0310809501 slugs.

TABLE 14

Derived Mass Conversions

	Solar Mass	Earth Mass	Moon Mass	Slugs	Kilograms	Pounds (avdp)	Ounces (avdp)
1 Solar Mass =	1	332,440	27,646,600	$1.361,25 \times 10^{29}$	$1.986,6 \times 10^{30}$	$4.379,70 \times 10^{30}$	$70.075,3 \times 10^{30}$
1 Earth Mass =	$3.088,062 \times 10^{6}$	1	81.358	$4.094,2 \times 10^{23}$	$5.975,0 \times 10^{24}$	$13.172,6 \times 10^{24}$	210.76×10^{24}
1 Moon Mass =	$3.697,320 \times 10^{-8}$	$1.229,14 \times 10^{-2}$	1	$5.032,3 \times 10^{21}$	$7.344,0 \times 10^{22}$	$16.191,0 \times 10^{22}$	259.06×10^{22}
1 Slug =	$7.346,18 \times 10^{-29}$	$0.244,25 \times 10^{-23}$	$0.198,72 \times 10^{-21}$	1	14.593,902,876	32.174,048,556	514,784,777,0
1 Kilogram =	$5.033,73 \times 10^{-31}$	$0.167,36 \times 10^{-24}$	$0.136,16 \times 10^{-22}$	$6.852,176,612 \times 10^{-2}$	1	2,204,622,621	35.273,961,94
1 Pound (avdp) =	$2.283,26 \times 10^{-31}$	$0.759,15 \times 10^{-25}$	$0.617,63 \times 10^{-23}$	$3.108,095,016 \times 10^{-2}$	0.453,592,37*	1	16.0*
1 Ounce (avdp) =	$1.427,04 \times 10^{-32}$	$0.474,47 \times 10^{-26}$	$0.386,01 \times 10^{-24}$	$1.942,559,385 \times 10^{-3}$	$0.283,495,231 \times 10^{-2}$	0.062,5*	1

—Underlined digits are questionable.

*Denotes exact conversion factor.

$g_0 = 9.80665^* \frac{meters}{sec} = 32.174,048,556\ ft/sec^2$

5. Energy Unit Conversions

a. Derived conversion factors between mechanical units of energy

1 joule = 1 nt - m = 1 kg - m^2/sec^2

1 joule = 10^7 erg = 10^7 g - cm^2/sec^2

1 joule = 0.101972661 + kgf m

1 joule = 0.7375621493 + lbf ft

1 erg = 10^{-7} joule = 10^{-7} kg - m^2/sec^2

1 pdl ft = 0.04214011007 + joule

1 pdl ft = 0.0310809501 + lbf ft

1 kgf m = 9.80665 joules

1 lbf ft = 32.17404855 + pdl ft

1 lbf ft = 1.35581794 + joules

b. Defined conversion factors from thermal to mechanical units of energy

1 kilocalorie or kilogram calorie (kg - cal) = $\frac{1}{860}$ kilowatt - hours (kw hr)

1 kg - cal = $\frac{1}{0.45359237}$ Btu = 3.98320719 + Btu

1 watt - sec = 1 joule

c. Derived conversion factors from thermal to mechanical units of energy

1 kwhr = 3.6×10^6 joules

1 kg - cal = 1000 calories

1 kg - cal = 4186.046511 + joules = 4186.046511 + kg m^2/sec^2

1 metric ton = 1000* kilogram

1 ton = 2000* pound (avdp) = 907.18474* kilograms

1 kg - cal = 426.8579495 + m - kgf

1 kg - cal = 3087.469937 + ft - lbf

1 Btu = 0.2519957611 + kg - cal

1 Btu = 778.0292165 + ft - lbf

1 Btu = 25032.34980 + lb - ft^2/sec^2

1 Btu = 1054.866068 + joules

1 joule = $2.388888888 + \times 10^{-4}$ kg - cal

1 joule = $9.479876444 + \times 10^{-4}$ Btu

d. Atomic energy units

The "electron volt" is defined as the amount of work done on one electron by a potential difference of 1 volt; the charge on the electron is taken as 4.80286×10^{-10} electrostatic units of charge.

1 electron volt (EV) = 1.60206×10^{-12} erg

1 kilo-electron volt (kEV) = 10^3 EV

1 mega-electron volt (MEV) = 10^6 EV

1 billion electron volt (BEV) = 10^9 EV

1 erg = 6.24196×10^{11} EV

1 lbf - ft = 8.46297×10^{18} EV

1 kg - cal = 2.6116×10^{22} EV

6. Pressure Unit Conversions

a. Defined units

One atmosphere is defined as the standard pressure (of the earth's atmosphere) at sea level and under $g_0 = 9.80665\ m/sec^2$. It corresponds

to the sea level pressure of the 1959 ARDC and the 1961 U.S. Standard Model Atmospheres.

One millimeter of mercury (mm Hg) is the pressure that a column of mercury 1 millimeter (10^{-3}m) in height exerts at 0° C and under g_0 = 9.80665 m/sec^2.

One inch of mercury (in. Hg) is the pressure that a column of mercury 1 inch in height exerts at 32° F and under g_0 = 32.17404855 + ft/sec^2.

One bar is a unit of pressure corresponding to a force of 10^6 dynes per square centimeter (or 10^5 nt/m^2). Usually, pressure is given in terms of millibars (mb), where 1 mb = 10^{-3} bar.

b. Conversion factors between pressure units

1 nt/m^2	=	10^{-4} nt/cm^2
1 nt/m^2	=	10^{-2} millibar (mb)
1 nt/m^2	=	0.101972661 + kgf/m^2
1 nt/m^2	=	0.67196908 - pdl/ft^2
1 nt/m^2	=	0.020885437 + lbf/ft^2
1 nt/m^2	=	1.4503776- x 10^{-4} lbf/in.^{2}
1 kgf/m^2	=	9.80665 (exact) nt/m^2
1 pdl/ft^2	=	1.48816371 + nt/m^2
1 lbf/ft^2	=	47.8802515 - nt/m^2
1 lbf/in.^{2}	=	6894.756 + nt/m^2
1 atmosphere	=	101,325.00 nt/m^2
1 atmosphere	=	10,332.275 kgf/m^2
1 atmosphere	=	68,087.267 pdl/ft^2
1 atmosphere	=	2116.2170 lbf/ft^2
1 atmosphere	=	14.695951 + lbf/in.^{2}
1 atmosphere	=	760 mm Hg
1 atmosphere	=	29.921260 in. Hg
1 atmosphere	=	1013.2500 mb

7. Temperature Unit Conversions

a. Defined relations

$$t(°C) = T(°K) - T_i(°K)$$

$$T(°R) = 1.8\,T(°K)$$

$$t(°F) - t_i(°F) = T(°R) - T_i(°R)$$

where

$$T_i(°K) = 273.16° K$$

$$t_i(°F) = 32° F$$

b. Derived relations

$$t_i(°C) = 0° C$$

$$T_i(°R) = 491.688° R$$

$$t(°C) = \frac{T(°R) - T_i(°R)}{1.8} = \frac{t(°F) - t_i(°F)}{1.8}$$

$$T(°R) = 1.8\ t(°C) + 273.16(°C)$$

$$= t(°F) - t_i(°F) + 491.688° R$$

$$t(°F) - 32° F = 1.8\,t(°C) = 1.8\ T(°K) - 273.16(°K)$$

where

°C = degrees in thermodynamic centigrade (Celsius) scale

°K = degrees in thermodynamic Kelvin scale

°R = degrees in thermodynamic Rankine scale

the subscript "i" denotes the freezing point of water.

D. SUMMARY OF LUNAR EXPLORATION PROGRAMS AND RESULTS

In the United States, the National Aeronautics and Space Administration has been established by Congress to direct the nation's civilian space program which up to the time of writing includes the entire announced U. S. lunar exploration program. Table 15 summarizes the current U. S. lunar spacecraft programs, while Table 16 lists all announced U. S. and Soviet space vehicle launches with lunar mission objectives. The data presented in the first table has been taken partially from Ref. 43, while the data for the second table has been obtained from Refs. 43, 44 and 45 and many lesser sources.

TABLE 15

Current U.S. Lunar Spacecraft Programs

Project	Contractors	Description	Status
Apollo, NASA	North American, command and mission modules, systems integration; MIT, guidance development; Collins Radio, telecommunications; Minneapolis-Honeywell, stabilization and control; AiResearch, environmental control; Radioplane, parachute recovery; Lockheed Propulsion Company, escape tower rocket; Marquardt, reaction controls; Grumman, lunar excursion module (LEM); Avco, heat shield, etc.	Three-man spacecraft for earth-orbital, lunar-orbital and landing missions. Boosters: Saturn for earth orbits, Saturn C-5 for lunar rendezvous, NOVA for direct flight. Spacecraft has three modules: command module, 4.5×10^4 newtons, 3.5 m high; service module, 20.5×10^4 newtons, 7 m high; lunar excursion vehicle, 13×10^4 newtons, 6 m high; total weight 38×10^4 newtons. An idea of the magnitude of this lunar program may be gained in that, by the first launch, about 20,000 companies and 150,000 to 200,000 scientists and engineers will have been involved. The total cost is estimated at $20 billion.	Earth orbital shots scheduled 1964 to 1965, lunar orbits 1966, lunar landing 1967 to 1968. Lunar orbit rendezvous mission profile has been selected.
Lunar Logistics Vehicle (LLV), NASA	Grumman, Northrop Space Technology Laboratories submitted feasibility studies, contract award expected early 1963; Pratt and Whitney, variable-thrust RL-10 liquid hydrogen engine.	3300-newton spacecraft "bus" to carry support payloads to the moon, initially boosted by Saturn C-1B; later 9×10^4-newton "bus" boosted by Saturn C-5. Seven specific payloads will be studied.	Development expected to begin in 1963 after congressional approval of fiscal year 1964 budget. Cost is expected to run to $500 million.
Ranger, NASA	JPL, prime contractor; Aeronutronic, capsule; Hercules, retrorocket.	1300-newton instrument capsule with seismometer will be hard-landed on the moon. Before impact, a TV camera tapes pictures of the lunar surface. The booster is an Atlas-Agena B combination.	Research and development stage. First two Rangers failed to launch from earth orbit; Ranger III launched January 26, 1962, but failed to impact the moon and is in solar orbit; Ranger IV impacted on the moon April 26, 1962; Ranger V, launched October 18, 1962, had a power failure after 8 hours and 44 minutes; it failed to impact the moon and is in solar orbit. A total of 9 more Rangers are planned for 1962 to 1963, and there may be as many as 15 additional Ranger shots. At the time of writing, the program has been temporarily halted for an extensive review of the many failures.
Surveyor, NASA	Hughes, prime contractor; Martin, SNAP II nuclear power generator.	3300-newton spacecraft lands 400 to 1300 newton instruments on the moon. Booster: Atlas-Centaur lunar orbiting vehicle is planned.	First lunar flights planned for 1964--seven soft landing vehicles and five lunar orbiting vehicles for transmitting pictures of the lunar surface.

TABLE 16

Data on U.S. and Soviet Space Vehicle Launches with Lunar Mission Objectives
(Chronological listing)

Definitions of success, partial success, failure are given below:

Success: major mission objective was achieved.

Partial success: yielded scientific information.

Failure: yielded no scientific information on major mission objective. No mission will be stated for failures.

1. Pioneer O (U.S.), 17 August 1958, failure. Propulsion failure of the first stage.

2. Pioneer I (U.S.), 11 October 1958, partial success..

   Pioneer I, a lunar probe, reached a distance of 113,000 km from earth. It carried an ionization chamber to measure cosmic radiation, and the returned data gave a qualitative peak of radiation in space.

3. Pioneer II (U.S.), 8 November 1958, failure.

4. Pioneer III (U.S.), 6 December 1958, partial success..

   The mission objective was to place a scientific payload on an earth escape trajectory into the vicinity of the moon. The space vehicle failed to achieve earth escape velocity; it achieved a maximum distance of about 100,000 km from earth.

   On-board instruments included two Geiger-Mueller counters. Cosmic ray data from Pioneer III revealed the existence of a second Van Allen radiation belt at a higher altitude than that discovered by the Explorer I earth satellite. The region of high-intensity radiation was found to consist of two concentric belts around the earth.

5. Lunik I (U.S.S.R.), 2 January 1959, success.

   This lunar probe was probably an attempt to impact. Pericynthion distance (closes approach to the moon) of 7500 km was achieved about 36 hr after launch. After lunar passage, the space vehicle went into a solar orbit between earth and Mars with the following characteristics:

Period	=	450^d
Eccentricity	=	0.148
Inclination	=	15.18°
Perihelion	=	146.4×10^6 km = 0.9791 AU
Aphelion	=	197.2×10^6 km = 1.319 AU

   On-board instruments included:

   Magnetometer
   Twin Geiger-Mueller counters
   Nitrium spectral analyzer
   Skin and chamber temperature thermocouples
   Micrometeorite erosion gauge
   Sodium vapor discharge device (which released, for tracking purposes, a sodium cloud 100 km in diameter at a distance of 115,000 km from earth).

   The total vehicle weight was 14,435 newtons.

   The purpose of the vehicle was to measure intensities of radiation and cosmic rays. Actual measurements of the moon included magnetic field strength, gravitational forces, cosmic ray intensity, sediment evaluation of the lunar craters, properties of the moon's inner strata and optical teletransmission of the moon's surface.

6. Pioneer IV (U.S.), 3 March 1959, success.

   This lunar probe passed the moon at a distance of approximately 60,000 km because the injection velocity was 84 m/sec below the planned velocity of 11,166 m/sec. The vehicle continued on to a solar orbit between earth and Mars with the following characteristics:

Period	=	$397^d.75$
Eccentricity	=	0.067
Inclination to the earth's equator	=	29.9°

Perihelion	=	147.6×10^6 km = 0.9871 AU
Aphelion	=	173.7×10^6 km = 1.162 AU
Inclination to ecliptic	=	1.5°

On-board instruments included:

2 Geiger-Mueller counters
A photoelectric sensor
A despin mechanism

The total space vehicle weight was 60 newtons.

Primary mission objectives were to:

Achieve an earth-moon trajectory
Determine the physical limits of the Van Allen radiation belts
Determine the extent of radiation in the vicinity of the moon
Test the operation of a photoelectric sensor

During the 8 hr of its battery life, this payload transmitted to earth new information on the extent and nature of cosmic radiation in space, indicating variations on both the extent and intensity of the high-altitude Van Allen radiation belt.

The first Van Allen radiation belt was found to consist of high energy protons and low energy electrons, while the second belt consists primarily of low energy protons after shielding.

Data was received to a range of 650,000 km.

7. Lunik II (U.S.S.R.), 12 September 1959, success.

Lunik II impacted on the moon in a triangular area bounded by the Mare Tranquillitatis, Mare Serenitatis, and Mare Vaporum after covering the earth-moon distance of $r_{\oplus \leftrightarrow} = 381,100$ km in $35^h 2^m 24^s$ from launch to impact. The selenocentric velocity of the space vehicle 5 hr before impact was 2317 m/sec, and at impact it was about 3315 m/sec. The last stage of the rocket also impacted on the moon.

The guidance system of Lunik II functioned only during the initial powered phase of flight.

The mission objectives of Lunik II were to investigate:

The magnetic fields of the earth and moon
Radiation belts around the earth
Intensity and variations in cosmic radiation
Heavy nuclei in cosmic radiation
Gas components of interplanetary substance
Meteoritic particles

The results of the flight included discovery that

(1) The moon has no magnetic field or radiation belt of charged particles.

(2) The moon is enveloped by a belt of low energy ionized gases which might resemble an ionosphere.

8. Lunik III (U.S.S.R.), 4 October 1959, success.

Lunik III carried scientific equipment, including both photographic and television systems to the vicinity of the moon. It passed close to it, so oriented as to photograph the part of the lunar surface that is hidden from the earth.

Photography continued for 40 minutes and images were later televised to earth. The plates and their interpretation were subsequently published by the U.S.S.R. Academy of Sciences as an Atlas of the Moon's Far Side.

Lunik III passed within 7000 km of the moon's south pole at its pericynthion on 6 October 1959.

Its initial orbital parameters were:

Nodal period	=	$16^d.2$
Eccentricity	=	0.8
Inclination	=	76.8°

Perigee distance = 40,671 km
Apogee distance = 469,306.4 km

9. Lunar Orbiter I (U.S.) 26 November 1959, failure.

The booster for all Lunar Orbiters was an Atlas-Able combination.

10. Pioneer V (U.S.), 11 March 1960, success.

The primary mission of Pioneer V was to record space data within approximately 80 x 10^6 km from the earth. It went into a solar orbit between Earth and Venus with the following characteristics:

Period	=	$311^d.6$
Eccentricity	=	0.104
Inclination to ecliptic	=	3.35°
Perihelion	=	120.5 x 10^6 km = 0.8059 AU
Aphelion	=	148.5 x 10^6 km = 0.9931 AU

On-board instruments included:

High energy radiation counter to measure high energy radiation, particularly from the sun
Ionization chamber and a Geiger-Mueller tube to measure the total radiation flux encountered
Micrometeorite counter
Search coil magnetometer
Photoelectric cell "aspect indicator" designed to send a signal when the device directly faced the sun
The total weight of the spacecraft was 100 newtons

Important experimental accomplishments of this cislunar and interplanetary space probe were:

(1) Discovery of large electrical current system in the outer atmosphere, namely, a "ring" current of 5 million amperes, 40,000 km in diameter, exists 65,000 km from earth.

(2) Discovery that the earth's magnetic field at times extends out as far as 100,000 km and oscillates with solar flare activity.

(3) Discovery of interplanetary magnetic field which fluctuates in intensity in relation to solar flare activity.

(4) Achievement of the first radio communication over interplanetary distances.

(5) Discovery that the planar angle of the interplanetary magnetic field forms a large angle with the plane of the ecliptic.

(6) Discovery that the Forbush decrease does not depend on presence of earth's magnetic field.

(7) Discovery of penetrating radiation beyond the Van Allen belts. The conclusion is that radiation will be a major hazard for manned flight between earth and Venus.

11. Lunar Orbiter II (U.S.), 25 September 1960, failure.

12. Lunar Orbiter III (U.S.), 15 December 1960, failure.

13. Ranger I (U.S.), 23 August 1961, failure.

The mission objective was to make highly elliptical earth orbits near minimum three-body velocity for earth escape. Ranger I was injected into a parking orbit around earth. It was planned to inject the space vehicle from parking orbit by a velocity impulse of about 3200 m/sec into the desired trajectory. However, the actual velocity impulse was only 73 m/sec, which resulted in a low altitude earth orbit and caused the vehicle to re-enter the atmosphere after one week. During this time, the on-board instruments functioned flawlessly.

The planned experiments and instruments for Rangers I and II are:

Subjects of Experiment	Instruments and Measurements
Fields, charged particles and solar X-rays	Electrostatic analyzer for solar plasma
	Semiconductor detectors and thin-walled Geiger-Mueller counter

Subjects of Experiment	Instruments and Measurements
	Ionization chamber
	Triple-coincidence telescopes
	Rn vapor magnetometer
	X-ray scintillation detectors
Hydrogen geocorona	Lyman-alpha telescope
Interplanetary dust	Micrometeorite composite detectors

14. Ranger II (U.S.), 18 November 1961, failure.

Ranger II had the same mission objectives and on-board instruments as Ranger I. Its injection rocket from earth parking orbit failed and it re-entered the earth's atmosphere after 9 hr.

15. Ranger III (U.S.), 26 January 1962, partial success.

The mission of Rangers III, IV and V was to impact the moon to land a scientific package.

Ranger III used an earth parking orbit. However, the injection velocity was too high. Pericynthion was reached 51 hr after launch. The lunar distance at that time was 36,785 km and the selenocentric velocity was 1872 m/sec. It continued into a solar orbit with the following characteristics:

Period	=	$406^{d}.4$
Perihelion distance	=	147.12×10^{6} km = 0.9839 AU
Aphelion distance	=	173.90×10^{6} km = 1.163 AU

The mission objectives and experiments planned for Rangers III, IV and V were to:

(1) Collect γ-ray data in flight and in the vicinity of the moon.

(2) Relay to earth, by a vidicon TV camera, photos of the lunar surface.

(3) Place an instrumented transmitting capsule containing a seismometer on the lunar surface to relay seismic data to earth.

(4) Determine the radar reflectivity of the moon by a radar altimeter.

(5) Develop spacecraft and space flight technology.

The weight of Rangers III, IV and V was in the vicinity of 3000 newtons.

16. Ranger IV (U.S.), 23 April 1962, partial success.

Ranger IV was launched at 2050 UT, 23 April 1962, and impacted on the moon at 1250 UT, 26 April 1962, after a flight time of 63 hr. It failed to perform any of its planned experiments.

17. Ranger V (U.S.), 18 October 1962, failure.

The space vehicle was launched at 1659 UT. Ranger V had a power failure $8^{h}46^{m}$ after launch, and it missed the moon by 725 km on 21 October, continuing into a solar orbit. The Ranger program was temporarily halted for a program review in view of the fact that 5 firings were either failures or, at best, partial successes.

E. REFERENCES

1. "Orbital Flight Handbook," ER 12684, Martin Company, Space Systems Division, (Baltimore), 1963.

2. Herrick, S., Baker, R.M.L., Jr. and Hilton, C. G., "Gravitational and Related Constants for Accurate Space Navigation," Eighth International Astronautical Congress, Barcelona, 1957 (Proceedings), Springer Verlag (Vienna), 1958, pp 197 to 235.

3. Makemson, M. W., Baker, R.M.L., Jr. and Westrom, G. B., "Analysis and Standardization of Astrodynamic Constants," Journal of Astronautical Sciences, Vol. 8, No. 1, Spring 1961, pp 1 to 13.

4. Kaula, W. M., "A Geoid and World Geodetic System Based on a Combination of Gravimetric, Astrogeodetic, and Satellite Data," Journal of Geophysics Res. Vol. 66, June 1961, pp 1799 to 1811; also NASA Technical Note TN D-702, May 1961.

5. Krause, H. G. L., "On a Consistent Set of Astrodynamic Constants," George C. Marshall Space Flight Center Report MTP-P & VE-F 62-12 (NASA) (Huntsville, Alabama), 1963.

6. "American Ephemeris and Nautical Almanac," published annually by the Nautical Almanac Office, United States Naval Observatory, Washington, D. C. (obtainable from the Superintendent of Documents, U. S. Government Printing Office, Washington 25, D. C.).

7. Ehricke, K. A., "Space Flight," Van Nostrand (Princeton, New Jersey), 1960.

8. deSitter, W. and Brouwer, D., "On the System of Astronomical Constants," Bulletin of the Astronomical Institutes of the Netherlands, Vol. VIII, No. 307, 8 July 1938, pp 213 to 231.

9. Alexandrov, I., "The Lunar Gravitational Potential," Advances in the Astronautical Sciences, Vol. 5, Plenum Press, New York, 1960, pp 320 to 324.

10. Baker, R.M.L., Jr. and Makemson, M. W., "An Introduction to Astrodynamics," Academic Press (New York), 1960.

11. Jeffreys, H., "The Earth, Its Origin, History, and Physical Constitution," Fourth ed., Cambridge University Press, 1959.

12. Townsend, G. E., "Analysis of Heliocentric, Planetocentric, Geocentric and Selenocentric Constants," ER 12201, Martin Company, Space Systems Division (Baltimore), June 1962.

13 Jaffe, L. D. and Rittenhouse, J. B., "Behavior of Materials in Space Environments," ARS Journal, Vol. 32, No. 3, March 1962, pp 320 to 345.

14. Nicolet, M., "Density of the Heterosphere Related to Temperature," SAO Special Report No. 75, Smithsonian Astrophysical Observatory (Cambridge, Massachusetts), 1961.

15. Johnson, F. S., editor, "Satellite Environment Handbook," Stanford University Press (Stanford, California), 1961.

16. Wilkins, H. P. and Moore, P., "The Moon," Macmillan (New York, 1955.

17. Blagg, M. A. and Saunder, S. A., "Collated List of Lunar Formations Named or Lettered in the Maps of Neison, Schmidt, Mädler," Lunar Nomenclature Committee of the International Association of Academies, 1913, p 196.

18. Blagg, M. A. and Müller, K., "Named Lunar Formations," International Astronomical Union, 1935.

19. Bobrovnikoff, N. T., "Natural Environment of the Moon," WADC Phase Technical Note 847-3, Wright Air Development Center (Dayton, Ohio), June 1959, ASTIA Document No. AD 242177.

20. Fielder, G., "Structure of the Moon's Surface," Pergamon Press (New York), 1961.

21. Firsoff, V. A., "Surface of the Moon, Its Structure and Origin," Hutchinson and Company, Ltd. (London), 1961.

22. Allen, C. W., "Astrophysical Quantities" (London), 1955.

23. Muncey, R. W., "Calculation of Lunar Temperature," Nature, Vol. 181, 24 May 1958, pp 1458 to 1459.

24. Mezger, P. S. and Strassl, H., "The Thermal Radiation of the Moon at 1420 MC/S," Planetary and Space Science, Vol. 1, 1959, pp 213 to 226.

25. Geoffrion, A. R., Korner M. and Sinton, W. M., "Isothermal Contours of the Moon," Lowell Observatory Bulletin No. 106, 1960.

26. Valley, S. L., editor, "Space and Planetary Environments," AFCRL-62-270, Air Force Surveys in Geophysics No. 139, GRD Air Force Cambridge Research Laboratories (Bedford, Massachusetts), January 1962.

27. Pettit, E. and Nicholson, S. B., "Lunar Radiation Temperatures," Astrophysical Journal, Vol. 71, 1930, p 102, and Astrophysical Journal, Vol. 91, 1940, p 408.

28. Gold, Q., "Dust on the Moon," Vistas in Astronautics, Vol. 2, 1959, pp 261 to 266.

29. Whipple, F. L., "On the Lunar Dust Layer," Vistas in Astronautics, Vol. 2, 1959, pp 267 to 272.

30. Roche, R. A., "The Importance of High Vacuum in Space Environment Simulation," Vistas in Astronautics, Vol. 2, 1959, pp 22 to 27.

31. Sytinskaya, N. N., "Probable Dimensions of Microfeatures of the Lunar Surface," ARS Journal (Russian Supplement), Vol. 32, No. 3, March 1962, pp 488 and 489.

32. Jeans, J., "Dynamical Theory of Gases," Dover Publications, Inc., 1954.

33. Russell, H. N., Dugan, R. S. and Stewart J. Q., "Astronomy," Ginn and Company, 1945.

34. Lipski, Y. N., "On the Existence of a Lunar Atmosphere," Dokl Akad. Nauk., Vol. 65, 1949, pp 465 to 468.

35. Lyot, B. and Dollfus, A., "Recherche d'une Atmosphére au Voisinage de la Lune," Comptes Rendus d'Academie de Science, Vol. 229, 1949, pp 1277 to 1280.

36. Dollfus, A., "Nouvelle, Recherche d'une Atmosphére au Voisinage de la Lune," Comptes Rendus d'Academie de Science, Vol. 234, 1952, pp 2046 to 2049.

37. Elsmore, B. and Whitfield, G. R., "Lunar Occultation of a Radio Star and the Derivation of an Upper Limit for the Density of the Lunar Atmosphere," Nature, Vol. 176, 1955, pp 457 to 458.

38. Costain, C. H., Elsmore, B. and Whitfield, G. R., "Radio Observations of a Lunar Occultation of the Crab Nebula," Monthly Notices of the Royal Astronomical Society, Vol. 116, 1956, pp 380 to 385.

39. Öpik, E. J. and Singer, S. F., "Escape of Gases from the Moon," Journal of Geophysical Research, Vol. 65, 1960, pp 3065 to 3070.

40. Kozyrev, N. A., "Observations of a Volcanic Process on the Moon," Sky and Telescope, Vol. 18, 1959, pp 184 to 186.

41. Judson, L. V., "Units of Weight and Measure (United States Customary and Metric), Definitions and Tables of Equivalents," National Bureau of Standards Miscellaneous Publications 233 (Washington), December 20, 1960.

42. Green, M. H., "International and Metric Units of Measurement," Chemical Publishing Company, Inc. (New York), 1961.

43. "Astrolog--Current Status of U.S. Missile and Space Programs Plus All Orbiting Satellites," Missiles and Rockets, Vol. 11, No. 10, 3 September 1962, pp 19 to 30.

44. Stafford, W. H. and Croft, R. M., "Artificial Earth Satellites and Successful Solar Probes, 1957 to 1960," NASA Technical Note TN D-601, March 1961.

45. Cummings, C. I., et al., "The Ranger Program," JPL Technical Report 32-141, Jet Propulsion Laboratory (Pasadena, California), September 1961.

46. Kuiper, G. and Middlehurst, B. M., editors, "Planets and Satellites," University of Chicago Press (Chicago), 1961.

ILLUSTRATIONS

LIST OF ILLUSTRATIONS

Figure	Title	Page
1	Inner Van Allen Belt Proton Flux and Initial Portions of a Typical Lunar Trajectory.	II-39
2	Lunar Chart of the Mare Humorum Region	II-40
3	Estimate of Average Lunar Surface Temperatures . .	II-41

Fig. 1. Inner Van Allen Belt Proton Flux and Initial Portions of a Typical Lunar Trajectory

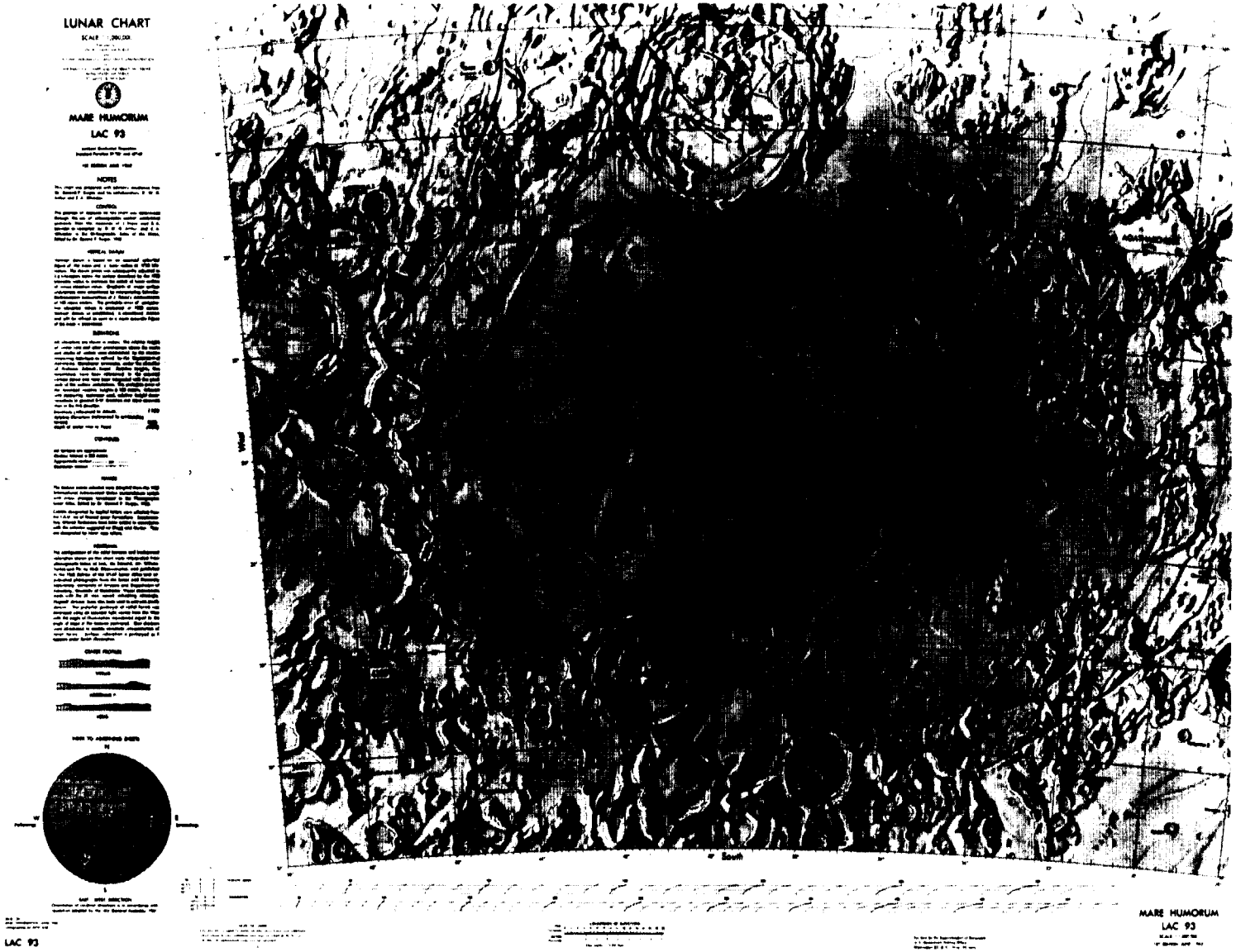

Fig. 2. Lunar Chart Of The Mare Humorum Region

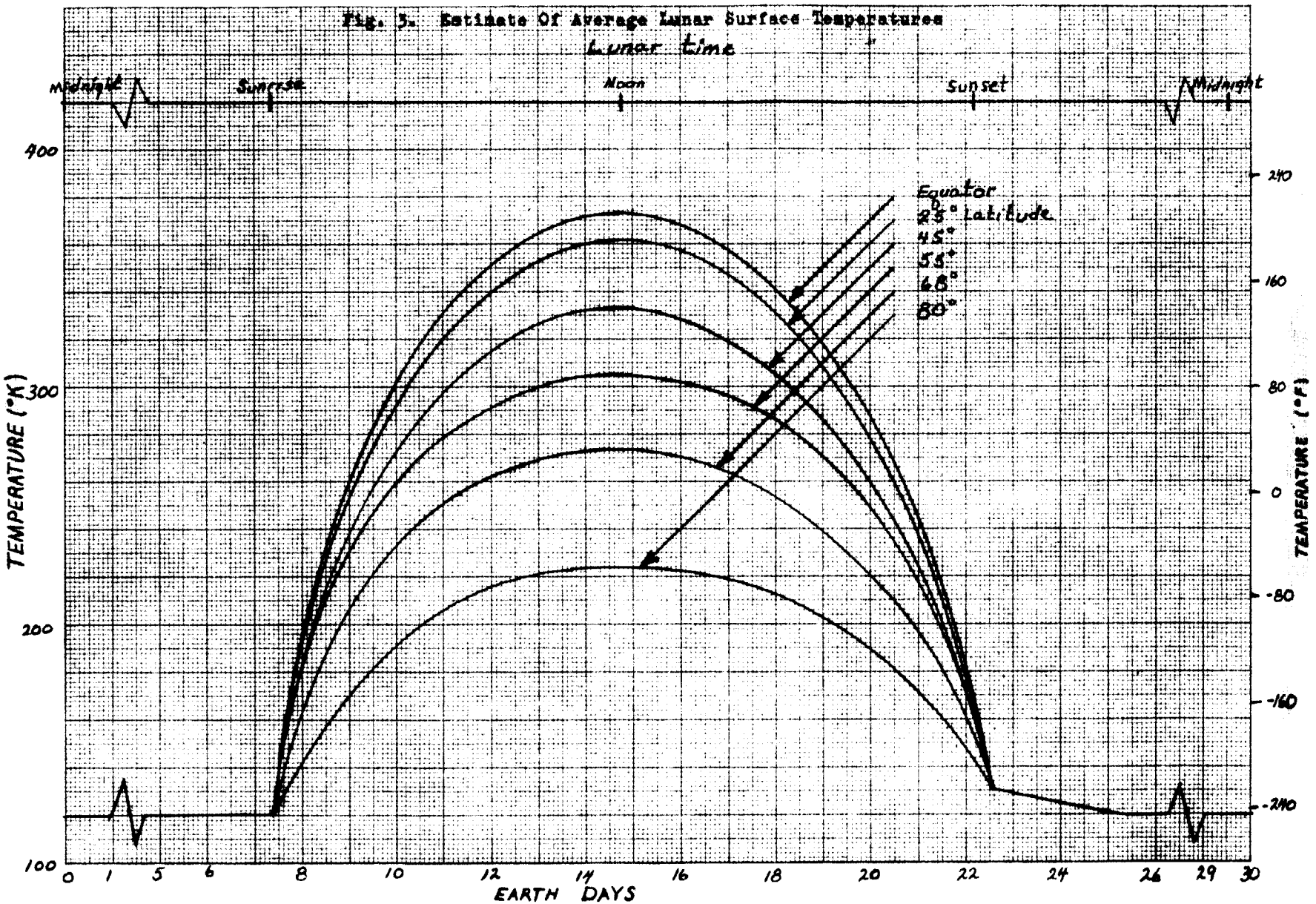

Fig. 5. Estimate Of Average Lunar Surface Temperatures

CHAPTER III

THE EARTH-MOON SYSTEM

Prepared by:

F. O. Martikan, F. Santora, and R. Salinger
Martin Company (Baltimore)
Aerospace Mechanics Department
March 1963

Page

A. Geometry and Coordinate Systems III-1

B. Motion in Earth-Moon Space III-14

C. Motion of the Moon III-22

D. References III-34

Tables and Illustrations III-37

III. THE EARTH-MOON SYSTEM

This chapter is an introduction to the kinematics and dynamics of the earth-moon system. This introduction is necessary before any actual trajectory programs or trajectories can be discussed, in order to present a clear understanding of the geometry, the various coordinate systems, the vocabulary and previous work in celestial mechanics peculiar to the earth-moon system.

Section A introduces coordinate systems useful for various aspects of earth to moon flight such as tracking, motion in space, guidance, lunar reconnaissance and attitude control. Emphasis is placed on the selenographic or moon-centered rotating coordinate system and transformation from geocentric or earth-centered inertial to selenographic coordinates. A list of current lunar maps is also given. Section B introduces the classical three-body and restricted three-body problems of astronomy and their application to the dynamical system of the earth, moon, and space vehicle. Valuable qualitative as well as quantitative trajectory information can be obtained from the restricted three-body problem. However, the application of the restricted three-body problem to the classification of lunar missions and its adaptation for trajectory calculations will be deferred to Chapter IV. Section C discusses the very complex motion of the moon, some theories used to find this motion, and the adaptation of these theories in generating lunar ephemerides for observations and simulation of the moon in accurate trajectory computer programs.

A. GEOMETRY AND COORDINATE SYSTEMS

In the description of the motion of the moon and of vehicles in the earth-moon space many different coordinate systems have been employed depending on the particular problem of motion to be solved. Several coordinate systems are used in lunar flight problems since several different disciplines such as geography, astronomy, aerodynamics, kinematics, dynamics, and numerical analysis enter into the problem with each discipline having evolved its own techniques and sets of coordinates. Some of the more commonly employed coordinate systems are described in the following pages according to their origin of coordinates, the principal directions and the fundamental plane; transformation equations between the major systems are given. The coordinate systems are further classified into (1) earth-centered coordinates, (2) selenographic coordinates, (3) trajectory coordinates, and (4) vehicle-centered coordinates.

Before a detailed discussion of the various coordinate systems is attempted, some basic definitions of the principal time systems will be given since time usually enters the description of motion or observation of celestrial bodies and space vehicles as the independent variable. The fundamental time unit is the sidereal day, or the period of revolution of the earth about its axis with respect to the stars. This time system is known as sidereal time (ST). Mean solar time (MST) or civil time is defined with respect to the position of a fictitious mean sun which moves uniformly along the equator and hence is a function of the earth's rotation and its orbital motion as well. The difference between mean solar time and apparent solar time, the latter being based on the apparent position of the sun, never exceeds 16 minutes. Universal time (UT), sometimes referred to as Greenwich mean time, is the mean solar time referred to the Greenwich (prime) meridian. However, the above listed clock times reflect the variability in the rotational rate of the earth due to tidal friction and irregularities from unknown sources. A uniform mathematical time which is defined by the apparent annual motion of the sun in true orbital longitude rather than the rotation of the earth, is the ephemeris time (ET) or Newtonian time. The mathematical theory of ephemeris time has been developed, and the values

$$\Delta T = ET - UT \qquad (1)$$

are given in the American Ephemeris (Ref. 1), which is published annually, or in the Explanatory Supplement (Ref. 2) up to the year of publication. The fundamental epoch from which ephemeris time is measured is 1900 January 0, Greenwich mean noon in UT which is simultaneously 1900 January 0, 12^h ET in ET. At that instant $\Delta T \equiv 0$. From past observations ΔT is approximately $+35^s$ in 1962 and the change in ΔT is generally less than 1^s between years (Ref. 1, page vii). A discussion of time systems is given in Ref. 3.

1. Earth-Centered Coordinates

a. Geographic system

The origin of the geographic coordinate system is the earth's center and the fundamental plane is the equatorial plane. Longitude λ is measured either east or west from the Greenwich (prime) meridian and the geocentric latitude ϕ' is the angle measured along a meridian from the equatorial plane, positive if north and negative if south of the equatorial plane. The local radius of the earth, R_ϕ, is the third spherical coordinate. (See following sketch.)

The latitude used on maps is the geodetic latitude ϕ which is defined as the angle between the equatorial plane and a normal to the reference ellipsoid which most nearly describes the mean sea level surface of the earth. The greatest difference between ϕ' and ϕ is approximately 0.19° at $\phi' = 45°$. In addition, there is an astronomical latitude ϕ^* which is the angle between the local vertical (as determined by the local gravitational field and affected by the centrifugal force) and the equatorial plane. The difference between ϕ and ϕ^* is called "station error" and is usually negligible. The geographic coordinate system is not an inertial one since it rotates around the earth's axis z_G at a constant angular velocity $\vec{\omega}_\oplus$. A

rectangular geographic coordinate system with origin at the center of the earth has its x_G-axis in the direction of $\lambda = 0$, $\phi = 0$, the z_G-axis toward the north pole, and the y_G-axis completing the right-handed coordinate system in the equatorial plane.

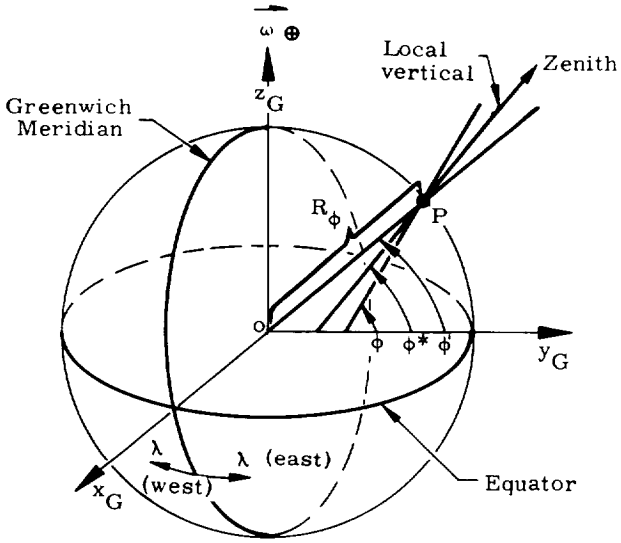

b. Topocentric system

Electronic and optical observations of space vehicles will be generally made from the surface of the earth. It is therefore advantageous to define a topocentric or local coordinate system with origin at the observer and the plane of the horizon as the fundamental plane. The x_h-axis of the rectangular topocentric system is directed to the south (unit vector $\hat{x}_h$), the y_h-axis is directed to the east (unit vector $\hat{y}_h$), and the z_h-axis is directed to the astronomical zenith (unit vector $\hat{z}_h$). The astronomical zenith $\hat{z}_h$ is in the direction of the local vertical and the horizon is a plane perpendicular to z_h. The azimuth, A, is defined as the angle from north measured positive clockwise in the horizon plane and the elevation, ϵ, as the angle measured from this plane toward the zenith. The range r_P, or distance from the observer to the vehicle, is the third spherical coordinate (see the following sketch). The topocentric system is not inertial since it rotates with the earth.

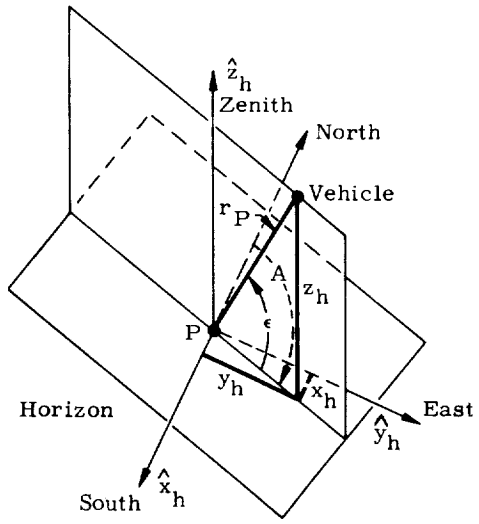

c. Equatorial system

The origin is generally taken at the earth's center and the fundamental plane is the true equatorial plane of the earth. The $x'_\oplus$-axis is directed toward the true vernal equinox (unit vector $\hat{x}'_\oplus$) the $z'_\oplus$-axis directed toward the north celestial pole (unit vector $\hat{z}'_\oplus$) and the $y'_\oplus$-axis directed so as to form a right-handed coordinate system (unit vector $\hat{y}'_\oplus$). Since the equator and the vernal equinox are not inertially fixed due to the precession and nutation of the earth's axis, the "equator and equinox" of a certain date should be specified in precision work. The true equinox takes into account the nutation and precession of the earth while the mean equinox ignores the nutation. Define a coordinate system $x_\oplus$, $y_\oplus$, $z_\oplus$ with the same origin as the $x'_\oplus$, $y'_\oplus$, $z'_\oplus$ system, except that the $x_\oplus$-axis points toward the mean equinox and $x_\oplus y_\oplus$-plane is the mean equatorial plane of the earth (see following sketch).

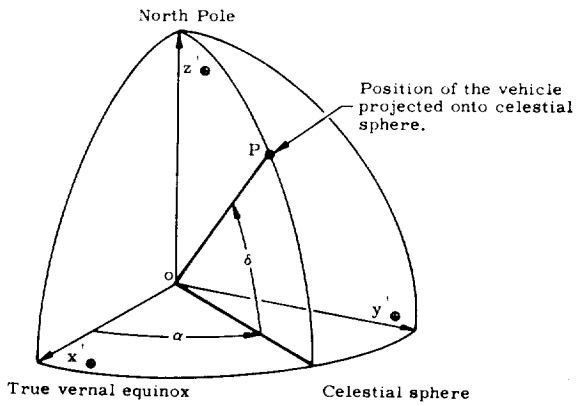

α = right ascension, measured east from the true vernal equinox along the celestial equator. The right ascension may be measured either in degrees or hours (1 hr = 15°).

δ = declination, measured from the true celestial equator to the radius vector of object, positive toward the north, negative toward the south.

In Ref. 1 the coordinates are usually referred to the mean equator and equinox of the beginning of the appropriate year. For the case of the sun, the celestial longitude referred to the true equator and equinox of a certain date is not given but is obtained by applying a reduction factor, which is tabulated in the Ephemeris, to the celestial longitude referred to the mean equinox and equator of the same date. This reduction is the sum of the precession in longitude from the beginning of the year to date, the nutation in longitude and the correction for aberration. For a definition of celestial longitude see the next coordinate system. A standard reference for the mean equator and equinox used for comparison of data from various sources is 1950.0.

d. Ecliptic system

The origin is generally taken as the earth's center and the fundamental plane is the ecliptic, or plane of the earth's orbit around the sun. The x_ϵ-axis is directed to the true vernal equinox (unit vector $\hat{x}_\epsilon$), the z_ϵ-axis is directed along the normal to the ecliptic plane (unit vector $\hat{z}_\epsilon$), and the y_ϵ-axis is directed so as to form a right-handed coordinate system (unit vector $\hat{y}_\epsilon$) (see the following sketch).

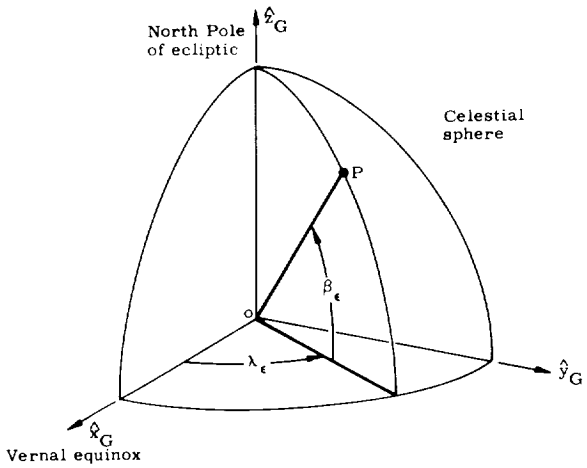

λ_ϵ = celestial longitude, measured positive east along the ecliptic from the true vernal equinox

β_ϵ = celestial latitude, measured from the ecliptic to the radius vector of the object

The equatorial and ecliptic coordinate systems are defined in terms of directions from a particular origin and not by the origin itself, which may be taken at the earth's center, the sun's center, the moon's center, or translated anywhere. We introduce a double subscript notation to define the coordinate system as well as the origin. If the origin of the ecliptic and equatorial coordinate systems is taken at the center of the earth, then there is a single subscript "$\oplus$" or "ϵ". However, if the origin is taken at the center of the moon, for instance, then we use two subscripts separated by a comma "$\oplus, \mathbb{C}$" or "$\epsilon, \mathbb{C}$", respectively. A double subscript without the comma indicates the position of the object denoted by the second subscript in the coordinate system of the first. If the origin of the coordinate system has been translated to another place, then a third subscript will denote the object whose position is given. Thus $r_{\oplus\Delta}$ is the distance of the vehicle from the center of the earth in a geocentric equatorial coordinate system while $r_{\oplus,\mathbb{C}\to\Delta}$ is the distance of the vehicle from the center of the moon in a selenocentric equatorial system.

Transformations between the various earth-centered coordinate systems will not be given here since this subject is treated more properly in Chapter XI of Ref. 3.

2. Selenographic Coordinate System

a. Definitions

The selenographic coordinate system is fixed with respect to the moon and rotates with it. The north pole of the moon is toward the direction of the lunar angular velocity vector $\vec{\omega}_\mathbb{C}$, and the lunar equatorial plane is perpendicular to $\vec{\omega}_\mathbb{C}$. Selenographic latitude $\phi_\mathbb{C}$ is measured from the lunar equator, positive toward the north, i.e., in the hemisphere containing Mare Serenitatis, and negative toward the south. Selenographic longitude $\lambda_\mathbb{C}$ is measured east and west from the lunar prime meridian $\lambda_\mathbb{C} = 0$ which passes through the mean center point of the moon. East, or the positive direction for $\lambda_\mathbb{C}$, is toward the hemisphere containing Mare Crisium. The mean center of the lunar disk is the point on the lunar surface intersected by the moon-earth line if the moon is at the mean ascending node when the node coincides either with the mean perigee or mean apogee. It is located in the Sinus Medii, a specified distance from the crater Mösting A (see Fig. 1). Orientation of these cardinal directions for astronautical calculations is in accordance with a resolution adopted by the International Astronomical Union general assembly, 1961. Sometimes, notably in the American Ephemeris (Ref. 1), $\lambda_\mathbb{C}$ is measured eastward from the prime meridian through 360°. For the primary purpose of astronomical observations, longitude on the moon is sometimes measured from the lunar prime meridian positive toward the west through 360°.

The axes in the selenographic coordinate system are designated by x_S, y_S, z_S with origin at the center of the moon. The z_S-axis points to the north pole of the moon's equatorial plane. The x_S- and y_S-axes lie in the moon's equatorial plane, the x_S-axis being directed to the lunar prime meridian and y_S completing the right-handed coordinate system. Unit vectors $\hat{x}_S$, $\hat{y}_S$, $\hat{z}_S$ are defined in the direction of the x_S-, y_S- and z_S axes.

b. Transformation from lunar equatorial to selenographic coordinates

In addition it is useful to define a selenocentric lunar equatorial coordinate system which does not rotate with the moon. The axes in this system are designated by $x_{\mathbb{C}}$, $y_{\mathbb{C}}$, $z_{\mathbb{C}}$ with origin at the center of the moon. The $z_{\mathbb{C}}$- and z_S-axes coincide. The $x_{\mathbb{C}}$-axis is in the moon's equatorial plane directed toward an inertial reference direction which will be specified each time this coordinate system is used, and the $y_{\mathbb{C}}$-axis completes the right-handed coordinate system. (See following sketch.)

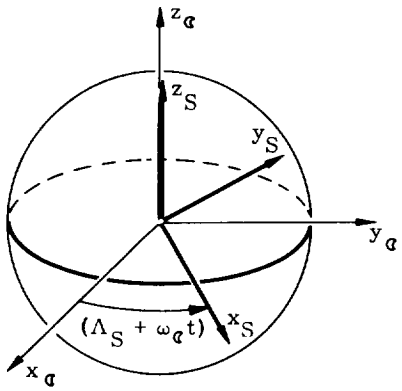

Inertial reference direction

If the angle between the $x_{\mathbb{C}}$- and x_S-axes at time $t = 0$ is Λ_S, then at any subsequent time t it will be $(\Lambda_S + \omega_{\mathbb{C}} t)$. Hence the transformation from selenocentric lunar equatorial to selenographic coordinates is given by

$$\begin{Bmatrix} x_S \\ y_S \\ z_S \end{Bmatrix} = \begin{bmatrix} \cos(\Lambda_S + \omega_{\mathbb{C}} t) & \sin(\Lambda_S + \omega_{\mathbb{C}} t) & 0 \\ -\sin(\Lambda_S + \omega_{\mathbb{C}} t) & \cos(\Lambda_S + \omega_{\mathbb{C}} t) & 0 \\ 0 & 0 & 1 \end{bmatrix} \begin{Bmatrix} x_{\mathbb{C}} \\ y_{\mathbb{C}} \\ z_{\mathbb{C}} \end{Bmatrix} \quad (2)$$

$$= \left[T(\Lambda_S + \omega_{\mathbb{C}} t)\right] \begin{Bmatrix} x_{\mathbb{C}} \\ y_{\mathbb{C}} \\ z_{\mathbb{C}} \end{Bmatrix}$$

and the inverse transformation is:

$$\begin{Bmatrix} x_{\mathbb{C}} \\ y_{\mathbb{C}} \\ z_{\mathbb{C}} \end{Bmatrix} = \begin{bmatrix} \cos(\Lambda_S + \omega_{\mathbb{C}} t) & -\sin(\Lambda_S + \omega_{\mathbb{C}} t) & 0 \\ \sin(\Lambda_S + \omega_{\mathbb{C}} t) & \cos(\Lambda_S + \omega_{\mathbb{C}} t) & 0 \\ 0 & 0 & 1 \end{bmatrix} \begin{Bmatrix} x_S \\ y_S \\ z_S \end{Bmatrix}$$

$$= \left[T(\Lambda_S + \omega_{\mathbb{C}} t)\right]^{-1} \begin{Bmatrix} x_S \\ y_S \\ z_S \end{Bmatrix} \quad (3)$$

The origin of the lunar equatorial system in the present case was taken at the center of the moon, but it may be translated anywhere just as in the equatorial and ecliptic coordinate systems (subsection 1c and 1d)

c. Rotation from equatorial to selenographic coordinates

The rotation from selenocentric equatorial coordinates $x'_{\oplus,\mathbb{C}}$, $y'_{\oplus,\mathbb{C}}$, $z'_{\oplus,\mathbb{C}}$, to selenographic coordinates x_S, y_S, z_S consists of a rotation about $z'_{\oplus,\mathbb{C}}$ through the angle Ω', a rotation about $\mathbb{C}N$ through the angle $i_{\mathbb{C}}$, and finally a rotation about $\hat{z}_S$ through the angle Λ_M (see following sketch). A further rotation to an inertial coordinate system $x_{\oplus,\mathbb{C}}$, $y_{\oplus,\mathbb{C}}$, $z_{\oplus,\mathbb{C}}$ with the x-axis directed to the mean equinox of date or to the mean equinox at epoch (a specified date) may be performed, but the difference between true equinox and mean equinox of date or of a recent epoch is small and can usually be neglected in preliminary design work.

The rotations are defined by the following matrix equation:

$$\begin{Bmatrix} x_S \\ y_S \\ z_S \end{Bmatrix} = \begin{bmatrix} \cos\Lambda_M & \sin\Lambda_M & 0 \\ -\sin\Lambda_M & \cos\Lambda_M & 0 \\ 0 & 0 & 1 \end{bmatrix} \cdot \begin{bmatrix} 1 & 0 & 0 \\ 0 & \cos i_{\mathbb{C}} & \sin i_{\mathbb{C}} \\ 0 & -\sin i_{\mathbb{C}} & \cos i_{\mathbb{C}} \end{bmatrix} \cdot \begin{bmatrix} \cos\Omega' & \sin\Omega' & 0 \\ -\sin\Omega' & \cos\Omega' & 0 \\ 0 & 0 & 1 \end{bmatrix} \begin{Bmatrix} x'_{\oplus,\mathbb{C}} \\ y'_{\oplus,\mathbb{C}} \\ z'_{\oplus,\mathbb{C}} \end{Bmatrix} \quad (4)$$

$$= \left[T(\Lambda_M)\right] \cdot \left[T(i_{\mathbb{C}})\right] \cdot \left[T(\Omega')\right] \cdot \begin{Bmatrix} x'_{\oplus,\mathbb{C}} \\ y'_{\oplus,\mathbb{C}} \\ z'_{\oplus,\mathbb{C}} \end{Bmatrix}$$

and the transformation to unit vectors in the selenographic coordinate system can be obtained by matrix multiplication and replacing the coordinates by unit vectors in the coordinate directions:

$$\begin{aligned} \hat{x}_S = {} & \hat{x}'_{\oplus,\mathbb{C}} (\cos\Lambda_M \cos\Omega' - \sin\Lambda_M \sin\Omega' \cos i_{\mathbb{C}} \\ & + \hat{y}'_{\oplus,\mathbb{C}} (\cos\Lambda_M \sin\Omega' + \sin\Lambda_M \cos\Omega' \cos i_{\mathbb{C}} \\ & + \hat{z}'_{\oplus,\mathbb{C}} (\sin\Lambda_M \sin i_{\mathbb{C}}) \end{aligned} \quad (5)$$

$$
\begin{aligned}
\hat{y}_S &= \hat{x}'_{\oplus,\mathbb{C}}(-\sin\Lambda_M\cos\Omega' \\
&\quad - \cos\Lambda_M \sin\Omega'\cos i_{\mathbb{C}}) \\
&\quad + \hat{y}'_{\oplus,\mathbb{C}}(-\sin\Lambda_M \sin\Omega' \\
&\quad + \cos\Lambda_M \cos\Omega'\cos i_{\mathbb{C}}) \\
&\quad + \hat{z}'_{\oplus,\mathbb{C}}(\cos\Lambda_M \sin i_{\mathbb{C}}) \\
\hat{z}_S &= \hat{x}'_{\oplus,\mathbb{C}}(\sin\Omega'\sin i_{\mathbb{C}}) \\
&\quad + \hat{y}'_{\oplus,\mathbb{C}}(-\cos\Omega'\sin i_{\mathbb{C}}) + \hat{z}'_{\oplus,\mathbb{C}}\cos i_{\mathbb{C}}
\end{aligned}
\qquad (5)
$$

The inverse rotation from x_S, y_S, z_S coordinates to $x'_{\oplus,\mathbb{C}}$, $y'_{\oplus,\mathbb{C}}$, $z'_{\oplus,\mathbb{C}}$ coordinates is given by the inverse of the product of the transformation matrices, which in turn is the product of the inverses of the individual matrices in reverse order:

$$
\begin{Bmatrix} x'_{\oplus,\mathbb{C}} \\ y'_{\oplus,\mathbb{C}} \\ z'_{\oplus,} \end{Bmatrix} = \left[T^{-1}(\Omega')\right]\cdot\left[T^{-1}(i_{\mathbb{C}})\right]\cdot\left[T^{-1}(\Lambda_M)\right]\begin{Bmatrix} x_S \\ y_S \\ z_S \end{Bmatrix} \qquad (6)
$$

$$
= \begin{bmatrix} \cos\Omega' & -\sin\Omega' & 0 \\ \sin\Omega' & \cos\Omega' & 0 \\ 0 & 0 & 1 \end{bmatrix}\cdot\begin{bmatrix} 1 & 0 & 0 \\ 0 & \cos i_{\mathbb{C}} & -\sin i_{\mathbb{C}} \\ 0 & \sin i_{\mathbb{C}} & \cos i_{\mathbb{C}} \end{bmatrix}\cdot\begin{bmatrix} \cos\Lambda_M & -\sin\Lambda_M & 0 \\ \sin\Lambda_M & \cos\Lambda_M & 0 \\ 0 & 0 & 1 \end{bmatrix}\begin{Bmatrix} x_S \\ y_S \\ z_S \end{Bmatrix} \qquad (6)
$$

The values of $i_{\mathbb{C}}$ and Ω' are tabulated to the nearest 0.001° in Ref. 1 for intervals of 10 days and referred to the true equator of the earth and equinox of date.

In order to carry out the transformations Eqs (4), (5) or (6), values of sin Λ_M and cos Λ_M are needed in terms of tabulated quantities. It is convenient to choose as the tabulated quantity the displacement of the earth-moon line from the mean center of the moon, or libration of the moon in longitude and latitude. This is given in Ref. 1 as the earth's selenographic longitude and latitude (ℓ, b) to the nearest 0°01, which represents 300 meters on the moon's surface. Librations will be discussed in detail in Section C-2 of the present chapter.

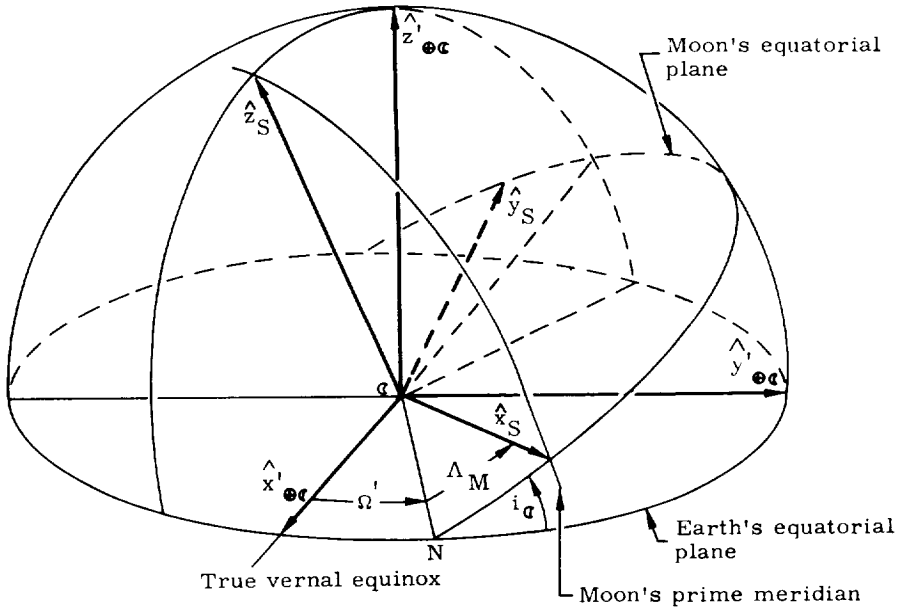

Ω' = right ascension of the moon's ascending node measured from the true equinox of date.

$i_{\mathbb{C}}$ = inclination of the lunar equator to the earth's equator.

Λ_M = angle in the lunar equatorial plane from the ascending node to the lunar prime meridian.

Let $\hat{L}$ be a unit vector along the earth-moon line. The components of $\hat{L}$ in the selenocentric equatorial coordinate system $x'_{\oplus,\mathbb{C}}$, $y'_{\oplus,\mathbb{C}}$, $z'_{\oplus,\mathbb{C}}$ are:

$$\left.\begin{aligned} L_x &= -\cos\delta\cos\alpha \\ L_y &= -\cos\delta\sin\alpha \\ L_z &= -\sin\delta \end{aligned}\right\} \qquad (7)$$

where α is the right ascension of the moon and δ the declination of the moon. If the librations in longitude are ℓ and latitude b (see following sketch), then we obtain, by applying the law of cosines to the spherical triangle with sides b, ℓ, d, cos d = cos b cos ℓ so that

$$\hat{x}_S \cdot \hat{L} = \cos d = \cos b \cos \ell \qquad (8)$$

$$\hat{y}_S \cdot \hat{L} = \cos b \sin \ell \qquad (9)$$

If we take the expression for $\hat{x}_S \cdot \hat{L}$ and $\hat{y}_S \cdot \hat{L}$ from Eqs (5) and (7), substitute it in Eqs (8) and (9) and simplify the results, then the following expressions for sin Λ_M and cos Λ_M in terms of tabulated quantities are obtained:

$$\sin\Lambda_M = \frac{\cos\ell}{\cos b}\left[\cos i_{\mathbb{C}}\cos\delta\sin(\Omega' - \alpha) - \sin i_{\mathbb{C}}\sin\delta\right] - \frac{\sin\ell}{\cos b}\left[\cos\delta\cos(\Omega' - \alpha)\right] \qquad (10)$$

$$\cos\Lambda_M = \frac{\sin\ell}{\cos b}\left[\cos i_{\mathbb{C}}\cos\delta\sin(\Omega' - \alpha) - \sin i_{\mathbb{C}}\sin\delta\right] - \frac{\cos\ell}{\cos b}\left[\cos\delta\cos(\Omega' - \alpha)\right] \qquad (11)$$

The right ascension α, declination δ and horizontal parallax, $\pi_{\mathbb{C}}$, of the moon are obtained from Ref. 1 and can be used to find the rectangular geocentric equatorial coordinates of the moon (see sketch on the following page).

Let the magnitude of $\vec{r}_{\oplus\mathbb{C}}$ be $r_{\oplus\mathbb{C}}$, then:

$$\left.\begin{aligned} x'_{\oplus\mathbb{C}} &= r_{\oplus\mathbb{C}}\cos\delta\cos\alpha \\ y'_{\oplus\mathbb{C}} &= r_{\oplus\mathbb{C}}\cos\delta\sin\alpha \\ z'_{\oplus\mathbb{C}} &= r_{\oplus\mathbb{C}}\sin\delta \end{aligned}\right\} \qquad (12)$$

and $r_{\oplus\mathbb{C}}$ is found from the tabulated lunar horizontal parallax $\pi_{\mathbb{C}}$ by: $r_{\oplus\mathbb{C}} = \frac{R_e}{\pi_{\mathbb{C}}}$ where R_e is

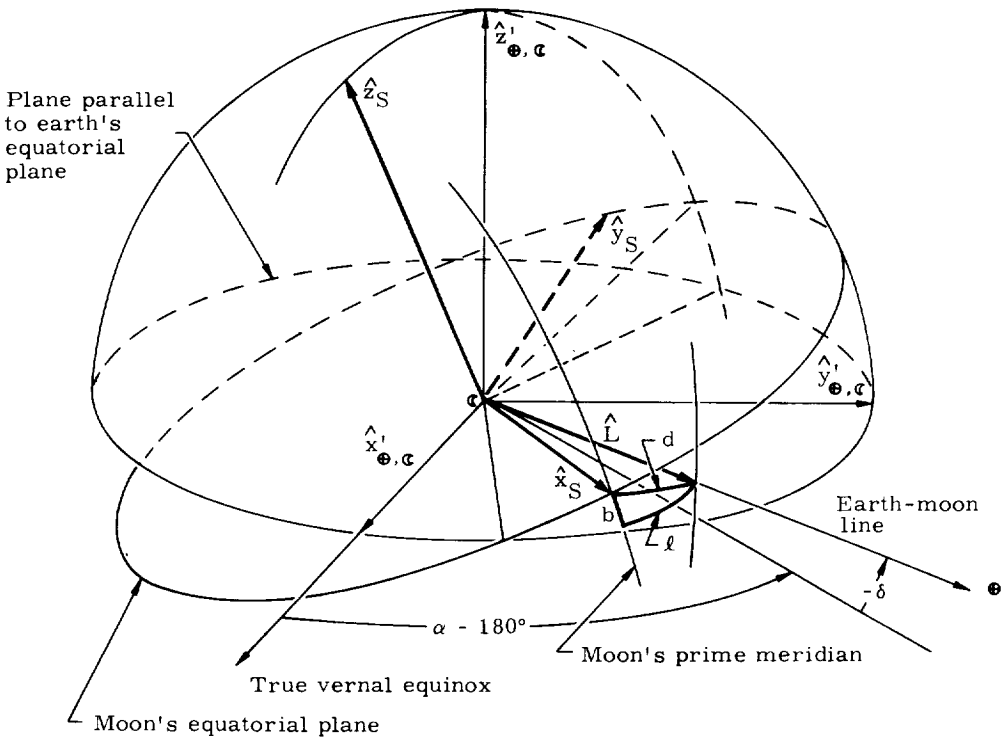

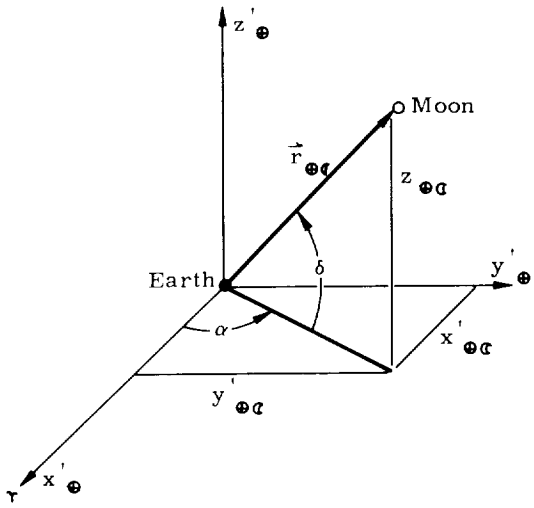

the earth's equatorial radius. By making the necessary substitutions for $\sin\alpha$, $\cos\alpha$, $\sin\delta$ and $\cos\delta$ Eqs (10) and (11) become:

$$\sin\Lambda_M = \frac{\cos\ell}{r_{\oplus\mathbb{C}}\cos b}\left[\cos i_{\mathbb{C}}\,(x'_{\oplus\mathbb{C}}\sin\Omega' - y'_{\oplus\mathbb{C}}\cos\Omega') - z'_{\oplus\mathbb{C}}\sin i_{\mathbb{C}}\right] + \frac{\sin\ell}{r_{\oplus\mathbb{C}}\cos b}\left[x'_{\oplus\mathbb{C}}\cos\Omega' + y'_{\oplus\mathbb{C}}\sin\Omega'\right] \quad (13)$$

$$\cos\Lambda_M = \frac{\sin\ell}{r_{\oplus\mathbb{C}}\cos b}\left[\cos i_{\mathbb{C}}\,(x'_{\oplus\mathbb{C}}\sin\Omega' - y'_{\oplus\mathbb{C}}\cos\Omega') - z'_{\oplus\mathbb{C}}\sin i_{\mathbb{C}}\right] - \frac{\cos\ell}{r_{\oplus\mathbb{C}}\cos b}\left[x'_{\oplus\mathbb{C}}\cos\Omega' + y'_{\oplus\mathbb{C}}\sin\Omega'\right] \quad (14)$$

With $\sin\Lambda_M$ and $\cos\Lambda_M$ known, the rotations indicated by Eqs (4), (5) and (6) can be carried out. This transformation has also been discussed in Koskela (Ref. 4), Baker (Ref. 5) and Kalensher (Ref. 6).

d. Vehicle position in selenographic coordinates

The selenographic coordinate system has a nearly constant angular velocity $\vec{\omega}_{\mathbb{C}}$ about the z_S axis and its origin is translated by the vector $\vec{r}_{\oplus\mathbb{C}}$ from the origin of the geocentric equatorial system. Before the vehicle position can be given in the selenographic coordinate system, the following quantities are defined by reference to the following sketch:

The position vector of the vehicle in the geocentric equatorial system,

$$\vec{r}_{\oplus\Delta} = x'_{\oplus\Delta}\hat{x}'_{\oplus} + y'_{\oplus\mathbb{C}}\hat{y}'_{\oplus} + z'_{\oplus\mathbb{C}}\hat{z}'_{\oplus} \quad (15)$$

The position vector of the center of the moon in the geocentric equatorial system,

$$\vec{r}_{\oplus\mathbb{C}} = x'_{\oplus\mathbb{C}}\hat{x}'_{\oplus} + y'_{\oplus\mathbb{C}}\hat{y}'_{\oplus} + z'_{\oplus\mathbb{C}}\hat{z}'_{\oplus} \quad (16)$$

The position vector of the vehicle referred to the selenocentric equatorial coordinates, i.e., in equatorial coordinates translated to the center of the moon,

$$\vec{r}_{\oplus,\mathbb{C}\to\Delta} = x'_{\oplus,\mathbb{C}\to\Delta}\hat{x}'_{\oplus} + y'_{\oplus,\mathbb{C}\to\Delta}\hat{y}'_{\oplus} + z'_{\oplus,\mathbb{C}\to\Delta}\hat{z}'_{\oplus} \quad (17)$$

The position vector of the vehicle in selenographic coordinates,

$$\vec{r}_{S\Delta} = x_{S\Delta}\hat{x}_S + y_{S\Delta}\hat{y}_S + z_{S\Delta}\hat{z}_S \quad (18)$$

Note from the sketch below that

$$\vec{r}_{\oplus,\mathbb{C}\to\Delta} = \vec{r}_{\oplus\Delta} - \vec{r}_{\oplus\mathbb{C}} \quad (19)$$

and

$$\vec{r}_{S\Delta} = \vec{r}_{\oplus,\mathbb{C}\to\Delta}. \quad (20)$$

The position of the vehicle in selenographic coordinates, $(x_{S\Delta}, y_{S\Delta}, z_{S\Delta})$, in terms of selenocentric equatorial coordinates, $(x'_{\oplus,\mathbb{C}\to\Delta}, y'_{\oplus,\mathbb{C}\to\Delta}, z'_{\oplus,\mathbb{C}\to\Delta})$, can be found by the rotation given in Eq (4)

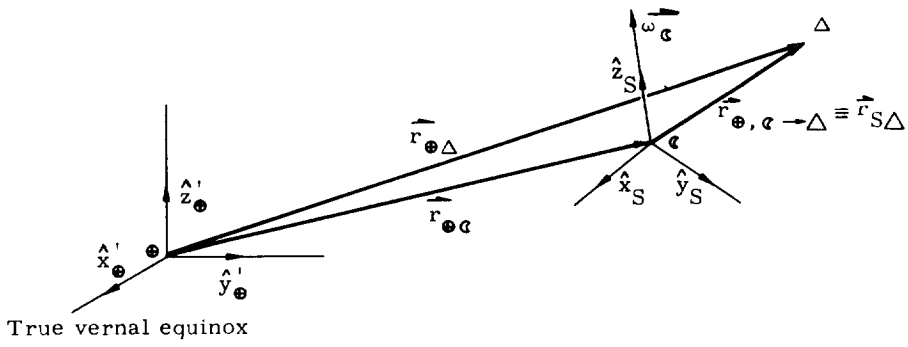

$$\begin{Bmatrix} x_{S\Delta} \\ y_{S\Delta} \\ z_{S\Delta} \end{Bmatrix} = \left[T(\Lambda_M)\right] \cdot \left[T(i_{\mathbb{C}})\right] \cdot \left[T(\Omega')\right] \begin{Bmatrix} x'_{\oplus,\mathbb{C}\to\Delta} \\ y'_{\oplus,\mathbb{C}\to\Delta} \\ z'_{\oplus,\mathbb{C}\to\Delta} \end{Bmatrix} \quad (21)$$

and in terms of geocentric equatorial coordinates by use of Eqs (15) through (18):

$$\begin{Bmatrix} x_{S\Delta} \\ y_{S\Delta} \\ z_{S\Delta} \end{Bmatrix} = \left[T(\Lambda_M)\right] \cdot \left[T(i_{\mathbb{C}})\right] \cdot \left[T(\Omega')\right] \begin{Bmatrix} x'_{\oplus\Delta} - x'_{\oplus\mathbb{C}} \\ y'_{\oplus\Delta} - y'_{\oplus\mathbb{C}} \\ z'_{\oplus\Delta} - z'_{\oplus\mathbb{C}} \end{Bmatrix} \quad (22)$$

The matrix multiplication indicated by Eq (22) can be performed to yield the position of the vehicle in selenographic coordinates when the position of the vehicle and of the moon in geocentric equatorial coordinates as well as the parameters $i_{\mathbb{C}}$, Ω', Λ_M ($\alpha, \delta, \pi_{\mathbb{C}}, \ell, b$) of the moon are known:

$$x_{S\Delta} = (x'_{\oplus\Delta} - x'_{\oplus\mathbb{C}})(\cos\Lambda_M \cos\Omega' - \sin\Lambda_M \sin\Omega' \cos i_{\mathbb{C}}) + (y'_{\oplus\Delta} - y'_{\oplus\mathbb{C}})(\cos\Lambda_M \sin\Omega' + \sin\Lambda_M \cos\Omega' \cos i_{\mathbb{C}}) + (z'_{\oplus\Delta} - z'_{\oplus\mathbb{C}})(\sin\Lambda_M \sin i_{\mathbb{C}}) \quad (23)$$

$$y_{S\Delta} = (x'_{\oplus\Delta} - x'_{\oplus\mathbb{C}})(-\sin\Lambda_M \cos\Omega' - \cos\Lambda_M \sin\Omega' \cos i_{\mathbb{C}}) + (y'_{\oplus\Delta} - y'_{\oplus\mathbb{C}})(-\sin\Lambda_M \sin\Omega' + \cos\Lambda_M \cos\Omega' \cos i_{\mathbb{C}}) + (z'_{\oplus\Delta} - z'_{\oplus\mathbb{C}})(\cos\Lambda_M \sin i_{\mathbb{C}}) \quad (24)$$

$$z_{S\Delta} = (x'_{\oplus\Delta} - x'_{\oplus\mathbb{C}})(\sin\Omega' \sin i_{\mathbb{C}}) + (y'_{\oplus\Delta} - y'_{\oplus\mathbb{C}})(-\cos\Omega' \sin i_{\mathbb{C}}) + (z'_{\oplus\Delta} - z'_{\oplus\mathbb{C}}) \cos i_{\mathbb{C}} \quad (25)$$

The selenographic longitude and latitude of a vehicle and the altitude of the vehicle above the moon's surface are illustrated in the following sketch and can be calculated from Eqs (21) and (22) as follows:

Selenographic latitude:

$$\phi_{\mathbb{C}} = \sin^{-1}\left(\frac{z_{S\Delta}}{r_{S\Delta}}\right), \quad -90° \le \phi_{\mathbb{C}} \le +90° \quad (26)$$

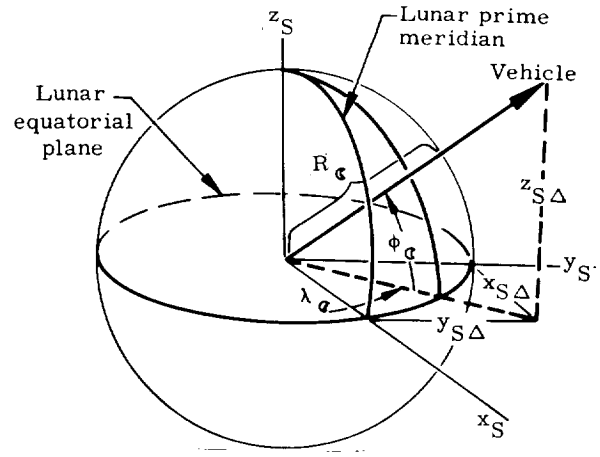

Selenographic longitude:

$$\lambda_{\mathbb{C}} = \sin^{-1}\left(\frac{y_{S\Delta}}{\left[x^2_{S\Delta} + y^2_{S\Delta}\right]^{1/2}}\right) = \cos^{-1}\left(\frac{x_{S\Delta}}{\left[x^2_{S\Delta} + y^2_{S\Delta}\right]^{1/2}}\right), \quad -180° \le \lambda_{\mathbb{C}} \le 180° \quad (27)$$

Altitude of the vehicle above surface of moon:

$$h_{\mathbb{C}} = r_{S\Delta} - R_{\mathbb{C}} \quad (28)$$

where $R_{\mathbb{C}}$ is the mean radius of the moon and $r_{S\Delta}$ is the magnitude of the vector $\vec{r}_{S\Delta}$.

e. Vehicle velocity in selenographic coordinates

Before we give an expression for the vehicle velocity, we have to introduce some notation and make some definitions.

Let a dot over a symbol denote differentiation with respect to time, i.e.,

$$\dot{x} = \frac{dx}{dt}, \quad \ddot{x} = \frac{d^2x}{dt^2}.$$

In addition, define the following velocities:

The vehicle velocity vector in the geocentric equatorial coordinate system,

$$\dot{\vec{r}}_{\oplus\Delta} = \dot{x}'_{\oplus\Delta}\hat{x}'_{\oplus} + \dot{y}'_{\oplus\Delta}\hat{y}'_{\oplus} + \dot{z}'_{\oplus\Delta}\hat{z}'_{\oplus} \quad (29)$$

The velocity vector of the moon in the geocentric equatorial system,

$$\dot{\vec{r}}_{\oplus\mathbb{C}} = \dot{x}'_{\oplus\mathbb{C}}\hat{x}'_{\oplus} + \dot{y}'_{\oplus\mathbb{C}}\hat{y}'_{\oplus} + \dot{z}'_{\oplus\mathbb{C}}\hat{z}'_{\oplus} \quad (30)$$

The velocity vector of the vehicle in the selenocentric equatorial system,

$$\dot{\vec{r}}_{\oplus,\mathbb{C}\to\Delta} = \dot{x}'_{\oplus,\mathbb{C}\to\Delta}\hat{x}'_{\oplus} + \dot{y}'_{\oplus,\mathbb{C}\to\Delta}\hat{y}'_{\oplus} + \dot{z}'_{\oplus,\mathbb{C}\to\Delta}\hat{z}'_{\oplus} \quad (31)$$

The velocity vector of the vehicle in the selenographic system is

$$\dot{\vec{r}}_{S\Delta} = \dot{x}_{S\Delta}\hat{x}_S + \dot{y}_{S\Delta}\hat{y}_S + \dot{z}_{S\Delta}\hat{z}_S \tag{32}$$

Differentiation of Eq (19) yields

$$\dot{\vec{r}}_{\oplus\Delta} = \dot{\vec{r}}_{\oplus\mathbb{C}} + \dot{\vec{r}}_{\oplus,\mathbb{C}\to\Delta} \tag{33}$$

However,

$$\dot{\vec{r}}_{\oplus,\mathbb{C}\to\Delta} = \dot{\vec{r}}_{S\Delta} + \vec{\omega}_{\mathbb{C}} \times \vec{r}_{S\Delta} \tag{34}$$

due to the rotation of the selenographic system with respect to the geocentric inertial coordinate system. Hence, the velocity in selenographic coordinates can be written,

$$\dot{\vec{r}}_{S\Delta} = \dot{\vec{r}}_{\oplus\mathbb{C}} - \dot{\vec{r}}_{\oplus\Delta} - \vec{\omega}_{\mathbb{C}} \times \vec{r}_{S\Delta} \tag{35}$$

where

$$\vec{\omega}_{\mathbb{C}} \times \vec{r}_{S\Delta} = \begin{vmatrix} \hat{x}_S & \hat{y}_S & \hat{z}_S \\ 0 & 0 & \omega_{\mathbb{C}} \\ x_{S\Delta} & y_{S\Delta} & z_{S\Delta} \end{vmatrix} = -\omega_{\mathbb{C}}\, y_{S\Delta}\hat{x}_S + \omega_{\mathbb{C}}\, x_{S\Delta}\hat{y}_S \tag{36}$$

The velocity components of the vehicle in selenographic coordinates ($\dot{x}_{S\Delta}$, $\dot{y}_{S\Delta}$, $\dot{z}_{S\Delta}$) in terms of geocentric equatorial velocity components of the moon and vehicle as well as selenographic vehicle position are:

$$\begin{Bmatrix} \dot{x}_{S\Delta} \\ \dot{y}_{S\Delta} \\ \dot{z}_{S\Delta} \end{Bmatrix} = \left[T(\Lambda_M)\right] \cdot \left[T(i_{\mathbb{C}})\right] \cdot \left[T(\Omega')\right] \begin{Bmatrix} \dot{x}'_{\oplus\Delta} - \dot{x}'_{\oplus\mathbb{C}} \\ \dot{y}'_{\oplus\Delta} - \dot{y}'_{\oplus\mathbb{C}} \\ \dot{z}'_{\oplus\Delta} - \dot{z}'_{\oplus\mathbb{C}} \end{Bmatrix} + \begin{Bmatrix} \omega_{\mathbb{C}}\, y_{S\Delta} \\ -\omega_{\mathbb{C}}\, x_{S\Delta} \\ 0 \end{Bmatrix} \tag{37}$$

which can be multiplied to yield:

$$\begin{aligned} \dot{x}_{S\Delta} = {} & (\dot{x}'_{\oplus\Delta} - \dot{x}'_{\oplus\mathbb{C}})(\cos\Lambda_M \cos\Omega' \\ & - \sin\Lambda_M \sin\Omega' \cos i_{\mathbb{C}}) \\ & + (\dot{y}'_{\oplus\Delta} - \dot{y}'_{\oplus\mathbb{C}})(\cos\Lambda_M \sin\Omega' \\ & + \sin\Lambda_M \cos\Omega' \cos i_{\mathbb{C}}) \\ & + (\dot{z}'_{\oplus\Delta} - \dot{z}'_{\oplus\mathbb{C}})(\sin\Lambda_M \sin i_{\mathbb{C}}) + \omega_{\mathbb{C}}\, y_{S\Delta} \end{aligned} \tag{38}$$

$$\begin{aligned} \dot{y}_{S\Delta} = {} & (\dot{x}'_{\oplus\Delta} - \dot{x}'_{\oplus\mathbb{C}})(-\sin\Lambda_M \cos\Omega' \\ & - \cos\Lambda_M \sin\Omega' \cos i_{\mathbb{C}}) \\ & + (\dot{y}'_{\oplus\Delta} - \dot{y}_{\oplus\mathbb{C}})(-\sin\Lambda_M \sin\Omega' \\ & + \cos\Lambda_M \cos\Omega' \cos i_{\mathbb{C}}) \\ & + (\dot{z}'_{\oplus\Delta} - \dot{z}'_{\oplus\mathbb{C}})(\cos\Lambda_M \sin i_{\mathbb{C}}) - \omega_{\mathbb{C}}\, x_{S\Delta} \end{aligned} \tag{39}$$

$$\begin{aligned} \dot{z}_{S\Delta} = {} & (\dot{x}'_{\oplus\Delta} - \dot{x}'_{\oplus\mathbb{C}})(\sin\Omega' \sin i_{\mathbb{C}}) \\ & + (\dot{y}'_{\oplus\Delta} - \dot{y}'_{\oplus\mathbb{C}})(-\cos\Omega' \sin i_{\mathbb{C}}) \\ & + (\dot{z}'_{\oplus\Delta} - \dot{z}'_{\oplus\mathbb{C}})(\cos i_{\mathbb{C}}) \end{aligned} \tag{40}$$

f. Vehicle acceleration in selenographic coordinates

The acceleration of the vehicle in selenocentric equatorial coordinates can be obtained by differentiation of both sides of Eq (33).

$$\ddot{\vec{r}}_{\oplus\Delta} = \ddot{\vec{r}}_{\oplus\mathbb{C}} + \ddot{\vec{r}}_{\oplus,\mathbb{C}\to\Delta} \tag{41}$$

where, by differentiation of Eq (34) with respect to time in the geocentric equatorial coordinate system, and if we assume tnat $\dot{\vec{\omega}}_{\mathbb{C}} = 0$

$$\ddot{\vec{r}}_{\oplus,\mathbb{C}\to\Delta} = \ddot{\vec{r}}_{S\Delta} + 2\,\vec{\omega}_{\mathbb{C}} \times \dot{\vec{r}}_{S\Delta} + \vec{\omega}_{\mathbb{C}} \times (\vec{\omega}_{\mathbb{C}} \times \vec{r}_{S\Delta}). \tag{42}$$

The vehicle acceleration in selenographic coordinates can be obtained by solving for $\ddot{\vec{r}}_{S\Delta}$ from Eqs (41) and (42):

$$\ddot{\vec{r}}_{S\Delta} = \ddot{\vec{r}}_{\oplus\Delta} - \ddot{\vec{r}}_{\oplus\mathbb{C}} - 2\,\vec{\omega}_{\mathbb{C}} \times \dot{\vec{r}}_{S\Delta} - \vec{\omega}_{\mathbb{C}} \times (\vec{\omega}_{\mathbb{C}} \times \vec{r}_{S\Delta}) \tag{43}$$

where

$$\vec{\omega}_{\mathbb{C}} \times \dot{\vec{r}}_{S\Delta} = -\omega_{\mathbb{C}}\, \dot{y}_{S\Delta}\hat{x}_S + \omega_{\mathbb{C}}\, \dot{x}_{S\Delta}\hat{y}_S \tag{44}$$

and

$$\vec{\omega}_{\mathbb{C}} \times (\vec{\omega}_{\mathbb{C}} \times \vec{r}_{S\Delta}) = -\omega_{\mathbb{C}}^2\, x_{S\Delta}\hat{x}_S - \omega_{\mathbb{C}}^2\, y_{S\Delta}\hat{y}_S . \tag{45}$$

The components of vehicle acceleration in selenographic coordinates ($\ddot{x}_{S\Delta}$, $\ddot{y}_{S\Delta}$, $\ddot{z}_{S\Delta}$) in terms of the moon's and vehicle's geocentric equatorial components of acceleration as well as selenographic vehicle position and velocity are:

$$\begin{Bmatrix} \ddot{x}_{S\Delta} \\ \ddot{y}_{S\Delta} \\ \ddot{z}_{S\Delta} \end{Bmatrix} = \left[T(\Lambda_M)\right] \cdot \left[T(i_{\mathbb{C}})\right] \cdot \left[T(\Omega')\right] \begin{Bmatrix} \ddot{x}'_{\oplus\Delta} - \ddot{x}'_{\oplus\mathbb{C}} \\ \ddot{y}'_{\oplus\Delta} - \ddot{y}'_{\oplus\mathbb{C}} \\ \ddot{z}'_{\oplus\Delta} - \ddot{z}'_{\oplus\mathbb{C}} \end{Bmatrix} + \begin{Bmatrix} 2\omega_{\mathbb{C}}\,\dot{y}_{S\Delta} \\ -2\omega_{\mathbb{C}}\,\dot{x}_{S\Delta} \\ 0 \end{Bmatrix} + \begin{Bmatrix} \omega_{\mathbb{C}}^2\, x_{S\Delta} \\ \omega_{\mathbb{C}}^2\, y_{S\Delta} \\ 0 \end{Bmatrix} . \qquad (46)$$

g. Lunar maps

Several lunar map series exist which represent the lunar surface to the best of our present knowledge:

USAF Lunar Atlas (edited by Dr. Gerard P. Kuiper). This atlas contains 280 photographs of the moon, sheet size 16 x 20 inches, scale 2.54 m to the lunar diameter or about 12.7 km to the cm and bound in a looseleaf ring binder. The photographs were from a collection of lunar plates taken at Mt. Wilson, Lick, Yerkes and McDonald Observatories in the United States and the Pic du Midi Observatory in France.

Orthographic Atlas of the Moon (edited by Dr. Gerard P. Kuiper), supplement No. 1 to the USAF Lunar Atlas. This volume contains 60 plates from the USAF Lunar Atlas which carry the orthographic grid established from a control net of 5000 points. Grid spacing is approximately 1.25 cm on the published copy. Meridians and parallels are printed in color at 2° intervals on each of the sheets which are bound in an 18 in. x 24 in. post-type hardback cover.

Rectified Lunar Atlas, supplement No. 2 to the USAF Lunar Atlas. This atlas consists of photographs of the entire visible hemisphere of the moon, rectified by projection on a globe 91.4 cm in diameter. Each of thirty fields on the globe were rephotographed at three different illuminations, corresponding to full moon, early morning and late afternoon.

USAF Lunar Mosaic. The lunar mosaic is a composite photograph of the moon made from the best imagery selected from photographs taken at Yerkes, McDonald and Mt. Wilson Observatories. The photography has been fitted to an orthographic projection which portrays the moon at mean libration as a sphere in true perspective. It is published in two sizes, LEM 1, scale 1:5,000,000 (lunar diameter 69 cm) and LEM 1A, scale 1:10,000,000 (lunar diameter 34 cm).

Lunar Aeronautical Charts (LAC Series). The Lunar Aeronautical Charts consist of a coordinated series requiring a total of 144 charts to cover the entire moon. Approximately 80 charts can be produced of the visible surface (59% of the total). Surface features are shown by a combination of shaded relief, contours and tones representing surface color variations. A spherical figure of the moon is assumed with a radius of $R_{\mathbb{C}}$ = 1738 km. Elevations are shown by 300-m approximate contours and referenced to the datum which was taken at 1735.4 km. The scale is 1:1,000,000 (10 km to the cm), and the sheet size is 22 in. x 29 in.

Atlas of the Moon's Far Side. This atlas, issued by the USSR Academy of Sciences and published in the United States by Interscience Publishers, gives the results of the Lunik III reconnaissance of the lunar far side. The volume gives a description of the interpretative technique used and 30 integrated photographs of the moon's far side obtained by the space vehicle camera. The results include a catalog of 498 formations classified according to the reliability of the observation and 4 maps drawn to scale 1:10,000,000.

Topographic Lunar Maps. This series of maps, prepared by the Army Map Service, is on a scale of 1:2,500,000. It shows surface features by a combination of shaded relief, contours and tones representing surface color variations. The moon is assumed to be a sphere with $R_{\mathbb{C}}$ = 1737.988 km and the vertical datum of the 500-m approximate contour lines is based on an elevation of 7000 m at the center of the crater Möshing A. A complete listing of lunar formations derived from "Named Lunar Formations" (1935) by M. Blagg and K. Müller is included on the back of the map. One sheet, Mare Nectaris--Mare Imbrium, 113 x 134 cm has been published.

3. Trajectory Coordinates

The position of a vehicle in earth-moon space can be given either in geocentric, geographic, or topocentric coordinates. Similarly, its position and velocity may be given in the selenocentric, selenographic or topocentric coordinate systems when the vehicle is near the moon. For tracking, for instance, it is convenient to use a topocentric system centered at the station since the tracking measurements and errors are given in that system. In the same manner several specialized coordinate systems have been evolved for various trajectory digital computer programs.

a. Typical rectangular coordinate systems.

The choice of coordinate systems for trajectory computations depends to a large degree on the force model and the dynamical system as well as on the method used for integrating the equations of motion. A great simplification of motion in earth-moon space is achieved when in the dynamical system the spherical earth and moon are assumed to move in circular orbits around the common center of mass (barycenter) which is taken as inertially fixed. The coordinate systems of the Martin Simplified Lunar Trajectory Digital Program, Ref. 7, which uses the force model described above, will be given here.

A basic coordinate system in the digital program has its origin at the barycenter and rotates at the constant rate $\omega_{\oplus\mathbb{C}}$ of the earth-moon system (see following sketch). The x_R-axis is directed toward the moon, the z_R-axis coincides with the angular momentum vector of the earth-moon system, and the y_R-axis completes the right-handed Cartesian coordinate system.

Consider another coordinate system with origin at the barycenter and axes x_0, y_0, z_0. At time t = 0 the x_R-axis is rotated by an angle Φ from the x_0-axis, and subsequently the angular

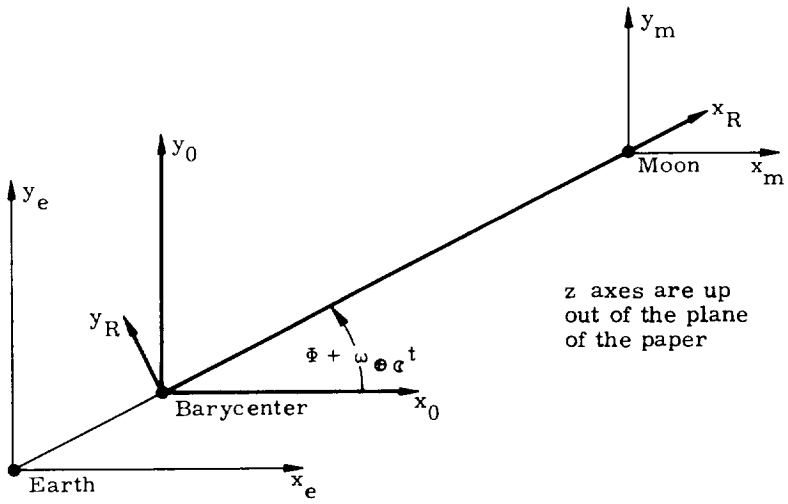

displacement of the rotating x_R -axis from the x_0 axis is $(\Phi + \omega_{\oplus\mathbb{C}} t)$. A third coordinate system, parallel to the nonrotating x_0, y_0, z_0 system but centered at the earth, will be denoted by x_e, y_e, z_e, and a fourth, moon-centered nonrotating coordinate system has axes x_m, y_m, z_m (see preceding sketch). Transformations from the nonrotating systems to the rotating coordinate system involve the same rotation through the angle $(\Phi + \omega_{\oplus\mathbb{C}} t)$ about the z-axis given by the matrix

$$\left[T\left(\Phi + \omega_{\oplus\mathbb{C}} t\right)\right] = \begin{bmatrix} \cos\left(\Phi + \omega_{\oplus\mathbb{C}} t\right) & -\sin\left(\Phi + \omega_{\oplus\mathbb{C}} t\right) & 0 \\ \sin\left(\Phi + \omega_{\oplus\mathbb{C}} t\right) & \cos\left(\Phi + \omega_{\oplus\mathbb{C}} t\right) & 0 \\ 0 & 0 & 1 \end{bmatrix} \tag{47}$$

and a translation which can be obtained by using the definition of the barycenter (see also Chapter IV). Position in the nonrotating systems is related to position in the rotating system by

$$\begin{Bmatrix} x_0 \\ y_0 \\ z_0 \end{Bmatrix} = \left[T\left(\Phi + \omega_{\oplus\mathbb{C}} t\right)\right] \begin{Bmatrix} x_R \\ y_R \\ z_R \end{Bmatrix}, \quad \begin{Bmatrix} x_e \\ y_e \\ z_e \end{Bmatrix} =$$

$$\left[T\left(\Phi + \omega_{\oplus\mathbb{C}} t\right)\right] \cdot \begin{Bmatrix} x_R + \nu\, \bar{r}_{\oplus\mathbb{C}} \\ y_R \\ z_R \end{Bmatrix}, \tag{48}$$

$$\begin{Bmatrix} x_m \\ y_m \\ z_m \end{Bmatrix} = \left[T\left(\Phi + \omega_{\oplus\mathbb{C}} t\right)\right] \begin{Bmatrix} x_R - \bar{r}_{\oplus\mathbb{C}}\,(1 - \nu) \\ y_R \\ z_R \end{Bmatrix},$$

where $\bar{r}_{\oplus\mathbb{C}}$ is the mean distance between the centers of the earth and moon, and $\nu = \dfrac{M_{\mathbb{C}}}{M_{\mathbb{C}} + M_{\oplus}}$ is the ratio of the mass of the moon to the total mass of the earth and moon.

It remains to relate the $x_e\, y_e\, z_e$ system to the geographic $x_G\, y_G\, z_G$ system which rotates about the z_G -axis at the constant angular velocity $\omega_{\oplus}$. The earth-moon orbital plane ($x_e\, y_e$ -plane) is inclined to the earth's equatorial plane ($x_G\, y_G$ -plane) at the constant angle i_{em} and their line of intersection does not rotate in inertial space. Since the initial value of Φ is arbitrary, we may assume that the intersection between the two planes is coincident with the y_e -axis. Thus Φ locates the moon in its orbit at time t = 0. Similarly we locate the Greenwich meridian (x_G -axis) relative to this intersection at time t = 0 by the angle Λ_G which is defined as the angle from the y_e - axis to the y_G -axis in the earth's equatorial plane (see following sketch).

The transformation from the $x_e\, y_e\, z_e$ coordinate systems to the $x_G\, y_G\, z_G$ system consists first of a rotation about the y_e -axis through the angle $(-i_{em})$ and then of a rotation about the z_G -axis through the angle $(\Lambda_G + \omega_{\oplus} t)$.

With $\left[T\left(-i_{em}\right)\right] = \left[T\left(i_{em}\right)\right]^{-1}$, the coordinate transformations between the various coordinate systems are given by,

$$\begin{Bmatrix} x_G \\ y_G \\ z_G \end{Bmatrix} = \left[T\left(\Lambda_G + \omega_{\oplus} t\right)\right] \left[T\left(i_{em}\right)\right]^{-1} \begin{Bmatrix} x_e \\ y_e \\ z_e \end{Bmatrix}$$

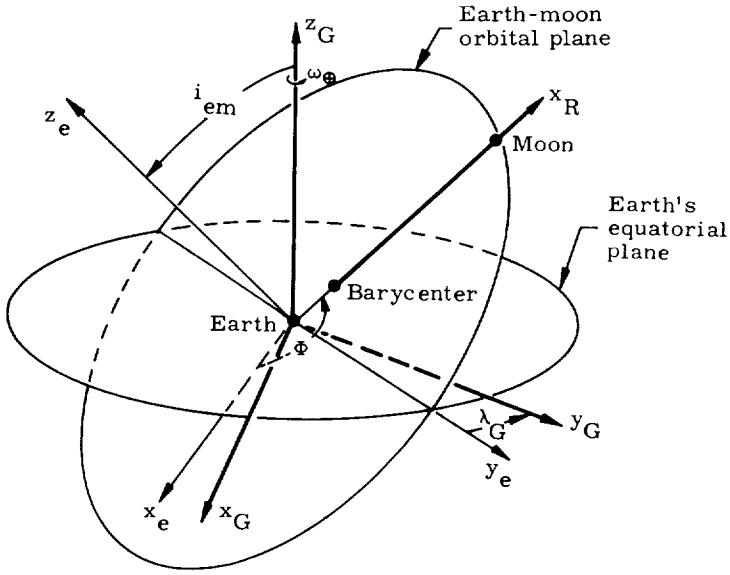

$$= \left[T\left(\Lambda_G + \omega_\oplus t\right)\right] \left[T\left(i_{em}\right)\right]^{-1} \left[T\left(\Phi + \omega_{\oplus\mathbb{C}}\, t\right)\right] \begin{Bmatrix} x_R \\ y_R \\ z_R \end{Bmatrix} \tag{49}$$

where

$$\left[T\left(\Lambda_G + \omega_\oplus t\right)\right] = \begin{bmatrix} \cos\left(\Lambda_G + \omega_\oplus t\right) & \sin\left(\Lambda_G + \omega_\oplus t\right) & 0 \\ -\sin\left(\Lambda_G + \omega_\oplus t\right) & \cos\left(\Lambda_G + \omega_\oplus t\right) & 0 \\ 0 & 0 & 1 \end{bmatrix}, \tag{50}$$

$$\left[T\left(i_{em}\right)\right]^{-1} = \begin{bmatrix} \cos i_{em} & 0 & -\sin i_{em} \\ 0 & 1 & 0 \\ \sin i_{em} & 0 & \cos i_{em} \end{bmatrix}, \tag{51}$$

and

$T\left[\Phi + \omega_{\oplus\mathbb{C}}\, t\right]$ is given by Eq (47).

The angles i_{em}, Φ and Λ_G are determined for any specific launch time t = 0 from the ephemerides of the earth and moon.

b. VOICE coordinate system

The coordinate system and force model used in the VOICE lunar trajectory program will be discussed in detail under that heading (Section IV C). Like the previous system, it is essentially based on the moon's orbital plane (MOP) as a fundamental plane and the lines of intersection of the trajectory planes with the MOP as reference directions. The earth-moon line as well as the earth and moon equatorial planes are defined with respect to this basic system.

c. Orbit plane system

Consider the dynamical system of a vehicle with negligible mass and one central spherical attracting body. It can be shown that in this case the vehicle moves in a fixed plane through the center of the attracting body which is known as the orbit plane.

The Cartesian coordinate systems given in Subsection 3a are essentially orbit plane systems with axes in and perpendicular to the orbit plane. Let us define an additional coordinate system with origin at the center of the attracting body and the z_P -axis normal to the orbit plane. The x_P -axis may be directed to perifocus, the closest approach to the central body, and denoted by x_ω, or to the ascending node and denoted by x_Ω. The y_P -axis is in the orbit plane, directed so as to complete the right-handed system. The unit vectors $\hat{x}_P$, $\hat{y}_P$ and $\hat{z}_P$ are in the x_P, y_P, z_P directions, respectively (see following sketch).

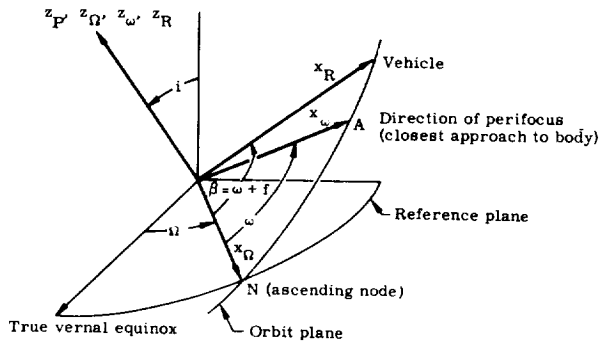

The orientation of the orbit plane may be given in terms of the orientation angles i, $0 \leq i \leq 180°$, inclination between the orbit plane and the reference plane measured from due east on the reference plane, Ω', longitude of the ascending node measured from the true vernal equinox, and ω, the argument of perifocus as measured from the ascending node. The angles i_{em}, Ω_G, and Φ given in Section 3a can similarly be regarded as orientation angles.

Since there are three second-order equations of motion for the vehicle, there are six constants of integration which enter into the solution of the equations of motion. These constants may be given in terms of initial position x_P, y_P, z_P and initial velocity $\dot{x}_P$, $\dot{y}_P$, $\dot{z}_P$ at time t_0 or in terms of six orbital elements, which do not involve the coordinates, velocity components, or time. In case of elliptic orbits customary sets of elements at epoch, t_0, are:

Ω' longitude of the ascending node

i inclination

ω argument of perifocus

a semi-major axis

e eccentricity

T_ω time of perifocal passage

The time of perifocal passage, T_ω may be replaced as an element by ℓ_0, the mean anomaly at an arbitrarily chosen epoch t_0, which is given by $\ell_0 = n(t_0 - T_\omega)$, where n is the mean motion of the vehicle in its orbit plane. Another set of elements is:

Ω' longitude of the ascending node

i inclination

$\tilde{\omega} = \Omega + \omega$, longitude of perifocus

n mean motion

e eccentricity

$\epsilon_0 = \tilde{\omega} + \ell_0$, mean longitude at epoch

Typical elements of a parabolic or hyperbolic orbit at epoch, t_0 are:

Ω' longitude of the ascending node

i inclination

ω argument of perifocus

q perifocus distance

e eccentricity

T_ω time of perifocal passage

while for a circular orbit only four elements are required at epoch t_0,

Ω' longitude of the ascending node

i inclination

r orbital radius

T_Ω time of ascending nodal crossing

since the eccentricity vanishes and the argument of perigee is undefined.

These elements remain constant for the dynamical system described at the beginning of the present section. In astronomy the concept of orbital elements is used even if other forces act on the vehicle, provided that they are small compared to the central force directed toward the attracting body. In this case the elements change slowly with time, and osculating elements at time t_0 are defined as the orbital elements of the vehicle if all forces except the central force due to the spherical attracting body were removed at t_0.

It has been found through experience that the orbital elements of a space vehicle are useful for descriptive purposes and to calculate approximate energy requirements only, but not suited to the analytical development of orbit determination and to precision work. In the latter case rectangular coordinates are more useful.

4. Vehicle--Centered Coordinates

In problems involving aerodynamic forces, stability, control and guidance of a space vehicle, it is sometimes convenient to introduce a body-axis system fixed in the vehicle with origin at its instantaneous center of gravity, the x_b-axis along the longitudinal axis of the vehicle in the forward direction, the y_b-axis directed laterally to the right and the z_b-axis completes the right-handed Cartesian system by being directed downward (see following sketch).

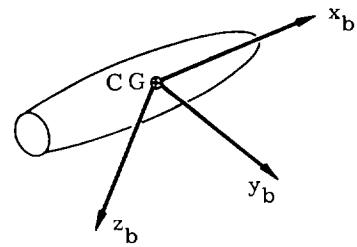

Additional specialized sets of axes which are required for particular equipment in the vehicle such as accelerometers, telescopes, rocket engines, etc. as well as transformations between the body axes and other coordinate systems will be discussed when they are used in the manual.

B. MOTION IN EARTH-MOON SPACE

The discussion in this section is based essentially on results of classical astronomy with Moulton's Celestial Mechanics (Ref. 8) used as the primary reference. Derivations that are important in the discussion of various force models used in the lunar trajectory digital programs, as well as special solutions of the equations of motion useful for space vehicle missions in earth-moon space are given. The material here is also introductory to a more complicated description of the motion of celestial bodies and vehicles in space which may be necessary for precision trajectories.

Assume a dynamical system of n bodies, which are homogeneous in spherical layers and move under the influence of their mutual gravitational attraction. The determination of the motion of these bodies reduces to finding 6n integrals of the 3n second-order simultaneous differential equations, and is known as the n-body problem. The gravitational attraction between celestial bodies is the most important force affecting their motion due to their enormous size and mass. The assumption of spherical celestial bodies is actually quite a good one. The equatorial semiaxes of the ellipsoidal earth model differ by only 21.4 km from the polar semiaxes with the radius of the equivalent sphere being 6371.02 km. The three dynamically determined semiaxes of the moon differ by at most 0.7 km from their arithmetic mean of 1738.5 km. The effect of asphericity of the earth on the motion of the moon at a mean distance of 384,402 km from the earth is thus very minor, even for comparatively long periods of time.

The effect of the asphericity of the earth and moon on the space vehicle will be important only when the space vehicle moves in the vicinity of these celestial bodies as will be shown later. Any irregularities in the shape of the sun and planets are completely negligible in earth-moon space over time periods of a week since these bodies are millions of kilometers away. Consider the two-body problem, n=2. Six integrals of the differential equations of motion can be found by considering the motion of the center of mass, and the other six constants of integration introduced by integrating the equations of motion of one body relative to the other.

The three initial coordinates and the initial velocity of one body with respect to the other, or 6 orbital elements, determine the motion of the two bodies completely. The motion of the smaller body takes place in a fixed plane through the center of the massive body which is known as the orbit plane.

For $n > 2$, however, only ten of the 6n integrals which are required in order to solve the problem completely have been found. If the dynamical system of n bodies which are homogeneous in spherical layers is subject to no forces except their mutual attractions, six of these integrals show that the center of mass (barycenter) exhibits rectilinear motion at constant speed, three more state that the angular momentum of the system is constant, and the tenth is simply an expression of the conservation of kinetic and potential energy. These 10 integrals are the only ones known since Bruns has proved that, when rectangular Cartesian coordinates are chosen as the dependent variables, there are no new algebraic integrals of existing functions. Also, Poincaré has demonstrated that use of orbital elements as the dependent variables yields no new uniform transcendental integrals even when the masses of all bodies except one are very small. However, the general system can be reduced still further by the mathematical trick of eliminating nodal position and time which reduces the requirement to 6 further integrals in the case n=3.

1. Three-body Problem

For lunar flight trajectories the problem of three bodies, n=3, which is concerned with the motion of a vehicle in the environment of the earth-moon system, is of primary interest. Although a general solution to the problem (which requires 18 arbitrary constants or integrals) has not as yet been found, there are a number of important results which have been established if the initial positions and velocities of the bodies satisfy certain conditions. While some of these special cases have not been found in nature, there are nevertheless some applications, for instance the libration point satellite buoys proposed by Buchheim and discussed further in Chapter IV. These special cases can be classified into: (1) study of the properties of motion of an infinitesimal body (i.e., one that is attracted by finite masses but in turn is assumed not to attract them) when it is attracted by two finite bodies which revolve in circles around their common center of mass; (2) construction of particular solutions for the motion of three finite bodies such that the ratios of their mutual distances are constants.

The former method will be discussed in the next section while, for the latter case, special methods will be described and references will be given here.

There are three special solutions for the case of 3 finite bodies: the three bodies at the vertices of an equilateral triangle, three bodies in a straight line, and the trivial case of the three bodies all at one point. The two nontrivial solutions are described among other places, in Moulton (Ref. 8) on pages 309-318 and in Finlay-Freundlich (Ref. 9).

a. Conditions for circular three-body orbits

Lagrange has shown that it is possible for three finite bodies to move in elliptical orbits around their common center of mass. The special case of circular orbits discussed in Ref. 8 will be presented in the following. Assume that the three bodies move in a common plane. Take the origin of coordinates at the common center of mass (barycenter) and the x_0y_0-plane as the plane of motion. Let the masses of the three bodies be M_1, M_2, M_3 and let G denote the universal gravitational constant. Then the differential equations of motion are:

$$\left.\begin{aligned} \ddot{x}_{0i} &= \frac{1}{M_i}\frac{\partial U}{\partial x_{0i}} \\ \ddot{y}_{0i} &= \frac{1}{M_i}\frac{\partial U}{\partial y_{0i}} \end{aligned}\right\} \quad , i = 1, 2, 3 \tag{56}$$

where

$$U = G\frac{M_1 M_2}{r_{1,2}} + G\frac{M_2 M_3}{r_{2,3}} + G\frac{M_3 M_1}{r_{3,1}} \tag{57}$$

is the gravitational potential, work function, or negative gravitational potential energy, of the dynamical system, and $r_{i,j}$ denotes the distance between the centers of M_i and M_j.

The motion of the system can be referred to axes $x_R\, y_R$ with origin at the barycenter and rotating with the uniform angular velocity ω_R with respect to the $x_0\, y_0$ axes by the transformation

$$\begin{Bmatrix} x_{0i} \\ y_{0i} \\ z_{0i} \end{Bmatrix} = \begin{bmatrix} \cos\omega_R t & -\sin\omega_R t & 0 \\ \sin\omega_R t & \cos\omega_R t & 0 \\ 0 & 0 & 1 \end{bmatrix} \begin{Bmatrix} x_{Ri} \\ y_{Ri} \\ z_{Ri} \end{Bmatrix} \tag{58}$$

Substitution of Eq (58) into Eq (56) yields, after simplification:

$$\left.\begin{aligned} \ddot{x}_{Ri} - 2\omega_R \dot{x}_{Ri} - \omega_R^2 x_{Ri} - \frac{1}{M_i}\frac{\partial U}{\partial x_{Ri}} &= 0 \\ \ddot{y}_{Ri} + 2\omega_R \dot{y}_{Ri} - \omega_R^2 y_{Ri} - \frac{1}{M_i}\frac{\partial U}{\partial y_{Ri}} &= 0 \end{aligned}\right\} \tag{59}$$

If the bodies are moving in circles around the origin with the angular velocity ω_R, their coordinates with respect to the rotating axes are constant and their time derivatives vanish. Equations (59) become, if we take the derivatives of the potential with respect to the coordinates as indicated and drop the time derivatives of x_{Ri} and y_{Ri},

$$\left.\begin{aligned} -\omega_R^2 x_{R1} + GM_2\frac{(x_{R1} - x_{R2})}{r_{1,2}^3} + GM_3\frac{(x_{R1} - x_{R3})}{r_{1,3}^3} &= 0 \\ -\omega_R^2 x_{R2} + GM_1\frac{(x_{R2} - x_{R1})}{r_{1,2}^3} + GM_3\frac{(x_{R2} - x_{R3})}{r_{2,3}^3} &= 0 \\ -\omega_R^2 x_{R3} + GM_1\frac{(x_{R3} - x_{R1})}{r_{1,3}^3} + GM_2\frac{(x_{R3} - x_{R2})}{r_{2,3}^3} &= 0 \end{aligned}\right\} \tag{60}$$

and three similar equations with x_R replaced by y_R.

The converse is also true, i.e., if the six equations (Eqs (60)) are satisfied, then the bodies move in circles around the origin with the uniform angular velocity ω_R. The system equations (Eqs (60)) can be reduced further by use of the condition that the origin is at the center of mass

$$\left.\begin{aligned} M_1 x_{R1} + M_2 x_{R2} + M_3 x_{R3} &= 0 \\ M_1 y_{R1} + M_2 y_{R2} + M_3 y_{R3} &= 0 \end{aligned}\right\} \tag{61}$$

to yield after simplification:

$$\left.\begin{aligned} -\omega_R^2 + GM_2\frac{(x_{R1} - x_{R2})}{r_{1,2}^3} + GM_3\frac{(x_{R1} - x_{R3})}{r_{1,3}^3} &= 0 \\ -\omega_R^2 x_{R2} + GM_1\frac{(x_{R2} - x_{R1})}{r_{1,3}^3} + GM_3\frac{(x_{R2} - x_{R3})}{r_{2,3}^3} &= 0 \\ -\omega_R^2 y_{R1} + GM_2\frac{(y_{R1} - y_{R2})}{r_{1,2}^3} + GM_2\frac{(y_{R1} - y_{R3})}{r_{1,3}^3} &= 0 \\ -\omega_R^2 y_{R2} + GM_1\frac{(y_{R2} - y_{R1})}{r_{1,2}^3} + GM_3\frac{(y_{R2} - y_{R3})}{r_{2,3}^3} &= 0 \end{aligned}\right\} \tag{62}$$

Equations (61) and (62) are the necessary and sufficient conditions for the existence of solutions in which the orbits of the three bodies are circles.

b. Equilateral triangle solutions

It remains to find solutions to the system of algebraic equations (Eqs (61) and Eqs (62)). It can be shown that the system is satisfied if the three bodies lie at the vertices of an equilateral triangle.

In that case $r = r_{1,2} = r_{2,3} = r_{1,3}$, and the system becomes:

$$\left.\begin{aligned}
&M_1 x_{R1} + M_2 x_{R2} + M_3 x_{R3} = 0\\
&\left(\frac{M_2}{r^3} + \frac{M_3}{r^3} - \frac{\omega_R^2}{G}\right) x_{R1} - \frac{M_2}{r^3} x_{R2} - \frac{M_3}{r^3} x_{R3} = 0\\
&\left(\frac{M_1}{r^3} + \frac{M_3}{r^3} - \frac{\omega_R^2}{G}\right) x_{R2} - \frac{M_1}{r^3} x_{R1} - \frac{M_3}{r^3} x_{R3} = 0\\
&M_1 y_{R1} + M_2 y_{R2} + M_3 y_{R3} = 0\\
&\left(\frac{M_2}{r^3} + \frac{M_3}{r^3} - \frac{\omega_R^2}{G}\right) y_{R1} - \frac{M_2}{r^3} y_{R2} - \frac{M_3}{r^3} y_{R3} = 0\\
&\left(\frac{M_1}{r^3} + \frac{M_3}{r^3} - \frac{\omega_R^2}{G}\right) y_{R2} - \frac{M_1}{r^3} y_{R1} - \frac{M_3}{r^3} y_{R3} = 0
\end{aligned}\right\} \quad (63)$$

The system of equations (Eqs (63)) is linear and homogeneous in $x_{R1}, x_{R2}, \ldots, y_{R3}$ and for a nontrivial solution to exist, the determinant of the coefficients must vanish. By defining $M = M_1 + M_2 + M_3$ this condition turns out to be

$M^2{}_3 \left(M - \frac{\omega_R^2 r^3}{G}\right)^4 = 0$ from which

$$\omega_R^2 = \frac{MG}{r^3} \quad (64)$$

Then two of the x_{Ri} and two of the y_{Ri} are arbitrary, and the equations have a solution compatible with $r_{i,j} = r$. Therefore, the equilateral triangular configuration with proper initial components of velocity is a particular solution of the three-body problem.

c. Straight line solutions

We can find a special solution to the system equations (Eqs (61) and (62)) by assuming $y_{R1} = y_{R2} = y_{R3} = 0$, i.e., all bodies are on the x_R-axis. Let them lie in the order M_1, M_2, M_3 from the negative end of the axis toward the positive. Then $x_{R3} > x_{R2} > x_{R1}$ and $r_{1,2} = x_{R2} - x_{R1} = r$, and the system of equations (Eqs (61) and (62)) become:

$$\left.\begin{aligned}
&M_1 x_{R1} + M_2 (x_{R1} + r) + M_3 x_{R3} = 0\\
&\frac{M_2}{r^2} + \frac{M_3}{(x_{R3} - x_{R1})^2} + \frac{\omega_R^2}{G} x_{R1} = 0\\
&-\frac{M_1}{r^2} + \frac{M_3}{(x_{R3} - x_{R1} - r)^2} + \frac{\omega_R^2}{G}(r + x_{R1}) = 0
\end{aligned}\right\} \quad (65)$$

Elimination of x_{R3} and ω_R^2 yields

$$\left.\begin{aligned}
&M_2 + (M_1 + M_2) x_{R1} + \frac{M_3^3 (r + x_{R1})}{(M x_{R1} + M_2 r)^2}\\
&- \frac{M_3^3 x_{R1}}{(M x_{R1} + M_2 r + M_3 r)^2} = 0
\end{aligned}\right\} \quad (66)$$

a quintic equation for x_{R1} whose coefficients are all positive. Therefore, there is no real positive root but there is at least one real negative root, and consequently at least one solution of the problem.

Instead of adopting x_{R1} as the unknown, $A = x_{R3} - x_{R2}$ may be used. The distance x_{R1} must be expressed in terms of this new variable. The relations among x_{R1}, x_{R2}, x_{R3} and A are

$$M_1 x_{R1} + M_2 x_{R2} + M_3 x_{R3} = 0$$

$$x_{R2} - x_{R1} = r$$

$$x_{R3} - x_{R2} = A$$

from which

$$x_{R1} = -\frac{\left[r (M_2 + M_3) + M_3 A\right]}{M} \quad (67)$$

Substitution of Eq (67) into Eq (66) letting $r = 1$, and subsequent simplification yields:

$$\left.\begin{aligned}
&(M_1 + M_2) A^5 + (3 M_1 + 2 M_2) A^4\\
&+ (3 M_1 + M_2) A^3\\
&-(M_2 + 3 M_3) A^2 - (2 M_2 + 3 M_3) A\\
&- (M_2 + M_3) = 0
\end{aligned}\right\} \quad (68)$$

which is Lagrange's quintic equation in A. Equation (68) has only one real positive root since the coefficients change sign only once. The only A valid in the problem for the chosen order of the masses is positive; hence, the solution of Eq (68) is unique and gives the location of the three bodies

in the straight line solution. Two more distinct straight line solutions can be obtained by cyclically permuting the order of the three bodies.

Moulton (Ref. 8) also discusses special solutions in which the orbits of the three bodies are conic sections with $e \neq 0$.

2. Restricted Three-Body Problem

If the mass of one of the three bodies is small compared to that of the other two, in fact so small that it does not influence the motion of the more massive bodies, then the determination of the motion of the small body is known as the restricted three-body problem. Since the mass of any space vehicle in earth-moon space ($M_\triangle$= order of 10^5 kg or less) is very small compared to that of the earth ($M_\oplus$= 5.9758 x 10^{24} kg) or that of the moon ($M_\mathbb{C}$= 7.3451 x 10^{22} kg), this approximation is permissible for the study of motion in earth-moon space. In addition,we assume that the earth and moon rotate in circular orbits around their common center of mass with the angular velocity $\omega_{\oplus\mathbb{C}}$. This is not quite true since the eccentricity of the moon's orbit around the earth is about 0.055 and,hence, the angular velocity varies with the moon's orbital position. Nongravitational forces such as atmospheric drag, electromagnetic forces, meteoritic drag, and solar radiation pressure may become important for unorthodox space vehicle shapes even though they can be utterly neglected in the motion of celestial bodies. Thrust forces will also be neglected in the following discussion. The equations of motion of the space vehicle and some results of the restricted three-body problem will be presented in this section with the discussion following that given by Moulton (Ref. 8, pages 278-307). General characteristics of lunar flight trajectories have been deduced from the restricted three-body problem, notably by Egorov (Ref. 10) and Buchheim (Ref. 11). We will discuss these applications to lunar flight missions in detail in the next chapter.

a. Equations of motion

Let the origin of coordinates be at the center of mass (barycenter) of the earth-moon system, and let the direction of the axes be so chosen that the $x_0\, y_0$-plane is the plane of their motion. (See Section A-3.) Denote the masses of the earth and moon by $M_\oplus$ and $M_\mathbb{C}$ and the universal gravitational constant by G. Let the coordinates of $M_\oplus$, $M_\mathbb{C}$ and the vehicle be $(x_{0\oplus}, y_{0\oplus}, 0)$; $(x_{0\mathbb{C}}, y_{0\mathbb{C}}, 0)$; and $(x_{0\triangle}, y_{0\triangle}, z_{0\triangle})$, respectively, so that the distance of the vehicle from the earth and moon is,respectively:

$$r_{\oplus\triangle} = \left[\left(x_{0\triangle} - x_{0\oplus}\right)^2 + \left(y_{0\triangle} - y_{0\oplus}\right)^2 + \left(z_{0\triangle}\right)^2\right]^{1/2}$$

$$r_{\mathbb{C}\triangle} = \left[\left(x_{0\triangle} - x_{0\mathbb{C}}\right)^2 + \left(y_{0\triangle} - y_{0\mathbb{C}}\right)^2 + z_{0\triangle}^2\right]^{1/2}$$

Note that the vehicle is not restricted to motion in the $x_0 y_0$-plane. (See following sketch.)

Then the equations of motion of the vehicle are:

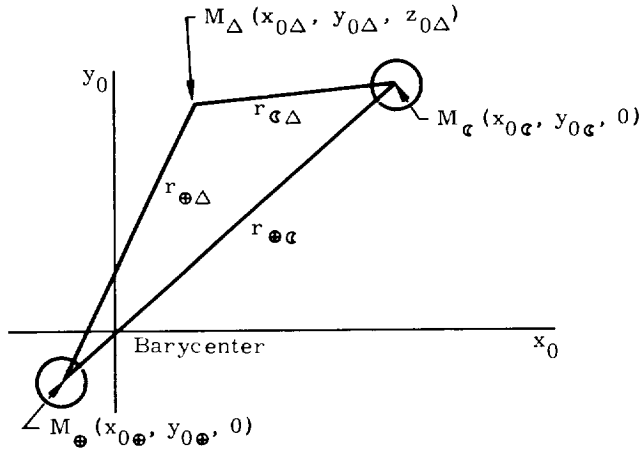

$$\ddot{x}_{0\triangle} = -GM_\oplus \frac{(x_{0\triangle} - x_{0\oplus})}{r^3_{\oplus\triangle}} - GM_\mathbb{C} \frac{(x_{0\triangle} - x_{0\mathbb{C}})}{r^3_{\mathbb{C}\triangle}}$$

$$\ddot{y}_{0\triangle} = -GM_\oplus \frac{(y_{0\triangle} - y_{0\oplus})}{r^3_{\oplus\triangle}} - GM_\mathbb{C} \frac{(y_{0\triangle} - y_{0\mathbb{C}})}{r^3_{\mathbb{C}\triangle}}$$

$$\ddot{z}_{0\triangle} = -GM_\oplus \frac{z_{0\triangle}}{r^3_{\oplus\triangle}} - GM_\mathbb{C} \frac{z_{0\triangle}}{r^3_{\mathbb{C}\triangle}} \qquad (69)$$

Let the motion of the bodies be referred to a new system of axes (x_R, y_R, z_R) having the same origin as the old, and rotating in the $x_0\, y_0$-plane in the same direction as the earth-moon system with the uniform angular velocity $\omega_{\oplus\mathbb{C}}$. The transformation from the inertial to the moving coordinate system is given by Eq (58). After computing the velocity and acceleration in the rotating coordinate system and substituting into Eqs (69), the equations of motion of the vehicle in the rotating coordinate system became:

$$\ddot{x}_{R\triangle} - 2\omega_{\oplus\mathbb{C}}\dot{y}_{R\triangle} = \omega^2_{\oplus\mathbb{C}} x_{R\triangle} - \frac{GM_\oplus\left(x_{R\triangle} - x_{R\oplus}\right)}{r^3_{\oplus\triangle}} - \frac{GM_\mathbb{C}\left(x_{R\triangle} - x_{R\mathbb{C}}\right)}{r^3_{\mathbb{C}\triangle}}$$

$$\ddot{y}_{R\triangle} + 2\omega_{\oplus\mathbb{C}}\dot{x}_{R\triangle} = \omega^2_{\oplus\mathbb{C}} y_{R\triangle}$$

$$- \frac{GM_{\oplus}(y_{R\Delta} - y_{R\oplus})}{r_{\oplus\Delta}^3} - \frac{GM_{\leftmoon}(y_{R\Delta} - y_{R\leftmoon})}{r_{\leftmoon\Delta}^2} \tag{70}$$

$$\ddot{z}_{R\Delta} = - \frac{GM_{\oplus} z_{R\Delta}}{r_{\oplus\Delta}^3} - \frac{GM_{\leftmoon} z_{R\Delta}}{r_{\leftmoon\Delta}^3}$$

The direction of the $x_R\, y_R$-axes can be chosen so that the x_R-axis is in the direction of the moon (see sketch on page 11); then $y_{R\oplus} = 0$, $y_{R\leftmoon} = 0$, and the equations of motion of the vehicle simplify to:

$$\ddot{x}_{R\Delta} - 2\omega_{\oplus\leftmoon}\dot{y}_{R\Delta} = \omega_{\oplus\leftmoon}^2 x_{R\Delta} - \frac{GM_{\oplus}(x_{R\Delta} - x_{R\oplus})}{r_{\oplus\Delta}^3} - \frac{GM_{\leftmoon}(x_{R\Delta} - x_{R\leftmoon})}{r_{\leftmoon\Delta}^3}$$

$$\ddot{y}_{R\Delta} + 2\omega_{\oplus\leftmoon}\dot{x}_{R\Delta} = \omega_{\oplus\leftmoon}^2 y_{R\Delta} - \frac{GM_{\oplus} y_{R\Delta}}{r_{\oplus\Delta}^3} - \frac{GM_{\leftmoon} y_{R\Delta}}{r_{\leftmoon\Delta}^3} \tag{71}$$

$$\ddot{z}_{R\Delta} = - \frac{GM_{\oplus} z_{R\Delta}}{r_{\oplus\Delta}^3} - \frac{GM_{\leftmoon} z_{R\Delta}}{r_{\leftmoon\Delta}^3}$$

where

$$r_{\oplus\Delta} = \left[(x_{R\Delta} - x_{R\oplus})^2 + y_{R\Delta}^2 + z_{R\Delta}^2\right]^{1/2} \tag{72}$$

and

$$r_{\leftmoon\Delta} = \left[(x_{R\Delta} - x_{R\leftmoon})^2 + y_{R\Delta}^2 + z_{R\Delta}^2\right]^{1/2} \tag{73}$$

For the particular force model (circular orbits of earth and moon about the barycenter) and the coordinate system (rotating system with the x_R-axis along the earth-moon line) chosen, $x_{R\oplus}$ and $x_{R\leftmoon}$ have become constants, and the equations of motion do not involve time explicitly.

The equations of motion (Eqs (71)) of the space vehicle are of sixth order and require six integrals for the determination of the three-dimensional motion of the vehicle; if it moves in the earth-moon plane, then the last equation of Eqs (71) vanishes, and only four integrals are required for the determination of the two-dimensional motion of the vehicle. In general, solutions of the equations of motion (Eqs (71)) are obtained by step-by-step integration with six vehicle initial conditions in the three-dimensional case as well as the initial positions of the earth and moon given.

b. Jacobi's integral and implications

Equations (71) admit an integral first given by Jacobi and which has been discussed by Hill in his Lunar Theory. Let

$$W = \frac{1}{2}\omega_{\oplus\leftmoon}^2\left(x_{R\Delta}^2 + y_{R\Delta}^2\right) + \frac{GM_{\oplus}}{r_{\oplus\Delta}} + \frac{GM_{\leftmoon}}{r_{\leftmoon\Delta}} \tag{74}$$

then Eqs (71) can be written in the form

$$\left.\begin{aligned} \ddot{x}_{R\Delta} - 2\omega_{\oplus\leftmoon}\dot{y}_{R\Delta} &= \frac{\partial W}{\partial x_{R\Delta}} \\ \ddot{y}_{R\Delta} + 2\omega_{\oplus\leftmoon}\dot{x}_{R\Delta} &= \frac{\partial W}{\partial y_{R\Delta}} \\ \ddot{z}_{R\Delta} &= \frac{\partial W}{\partial z_{R\Delta}} \end{aligned}\right\} \tag{75}$$

If these equations are multiplied by $2\dot{x}_{R\Delta}$, $2\dot{y}_{R\Delta}$ and $2\dot{z}_{R\Delta}$, respectively, and added, the resulting equation can be integrated, since W is a function of $x_{R\Delta}$, $y_{R\Delta}$, and $z_{R\Delta}$ alone, and this gives Jacobi's integral:

$$\left(\dot{x}_{R\Delta}\right)^2 + \left(\dot{y}_{R\Delta}\right)^2 + \left(\dot{z}_{R\Delta}\right)^2 = V_{R\Delta}^2 = 2W - C$$

$$V_{R\Delta}^2 = \omega_{\oplus\leftmoon}^2\left(x_{R\Delta}^2 + y_{R\Delta}^2\right) + \frac{2GM_{\oplus}}{r_{\oplus\Delta}} + \frac{2GM_{\leftmoon}}{r_{\leftmoon\Delta}} - C \tag{76}$$

where $V_{R\Delta}$ is the magnitude of the velocity of the vehicle in the rotating coordinate system and C is the Jacobian constant. We can obtain some qualitative and quantitative information from trajectories in the earth-moon system from Jacobi's integral.

When the constant of integration C has been determined numerically from the initial conditions, $x_{R\Delta}$, $y_{R\Delta}$, $z_{R\Delta}$, $\dot{x}_{R\Delta}$, $\dot{y}_{R\Delta}$, $\dot{z}_{R\Delta}$, Eq (76) determines the velocity $V_{R\Delta}$ of the vehicle at all points in the rotating coordinate system; and conversely, for a given $V_{R\Delta}$, Eq (76) gives the locus of points accessible to the space vehicle. In particular, $V_{R\Delta} = 0$ in Eq (76) defines surfaces of zero relative velocity. On one side of these surfaces the velocity $V_{R\Delta}$ will be real and on the other side imaginary; or, in other words, the space vehicle can move on the real side of this surface only. Thus the surfaces of zero relative velocity indicate the regions of space to which the space vehicle is constrained.

The equation of the surfaces of zero relative velocity for an arbitrary point $x_{R\Delta}$, $y_{R\Delta}$, $z_{R\Delta}$ denoting the space vehicle can be obtained by letting $V_{R\Delta} = 0$ in Eq (76):

$$\omega_{\oplus\mathbb{C}}(x_{R\Delta}^2 + y_{R\Delta}^2) + \frac{2GM_\oplus}{r_{\oplus\Delta}} + \frac{2GM_\mathbb{C}}{r_{\mathbb{C}\Delta}} = C \quad (77)$$

where $r_{\oplus\Delta}$ and $r_{\mathbb{C}\Delta}$ are given by Eqs (72) and (73). Since only the squares of $y_{R\Delta}$ and $z_{R\Delta}$ enter into Eq (77), the surfaces defined are symmetrical with respect to the $x_R y_R$ and $x_R z_R$-planes. We obtain the intersection of the surfaces (Eq (77)) with the $x_R y_R$-plane or the trace in the $x_R y_R$-plane by letting $z_{R\Delta} = 0$ in that equation:

$$\omega_{\oplus\mathbb{C}}^2(x_{R\Delta}^2 + y_{R\Delta}^2) + \frac{2GM_\oplus}{\left[(x_{R\Delta} - x_{R\oplus})^2 + y_{R\Delta}^2\right]^{1/2}} + \frac{2GM_\mathbb{C}}{\left[(x_{R\Delta} - x_{R\mathbb{C}})^2 + y_{R\Delta}^2\right]^{1/2}} = C \quad (78)$$

The curves (Eq (78)) are shown, not to scale, in Fig. 2, and from them the general characteristics of motion in the moon's orbital plane can be deduced.

The values of C in Fig. 2 are numerically in the order $C_1 > C_2 > C_3 > \ldots$. For initial conditions corresponding to $C = C_1$, the vehicle can move either in a closed region about the earth or in a closed region about the moon; it remains a satellite of the earth or the moon. If the initial conditions correspond to $C = C_3$, the vehicle can move within a closed contour around the earth-moon system such that motion from earth to moon is possible. The limiting case separating earth or moon orbits from earth-moon or moon-earth trajectories is represented by $C = C_2$. For the value $C = C_5$, the vehicle can escape entirely from the earth-moon system since the region of possible vehicle motion is open behind the moon. The value $C = C_4$ separates the earth-moon or moon-earth trajectories from possible escape trajectories from the earth-moon system. Besides these inner bounds of vehicle motion there are, for the same C values, closed outer boundaries around the earth-moon system beyond which motion is also possible. A vehicle coming from very far away with $C > C_4$ cannot approach the earth or moon any closer than the outer boundary of the $C = C_4$ contour of Fig. 2. When $C = C_4$ the inner and outer branches of the curve of zero relative velocity coalesce. For $C < C_4$ a vehicle starting near the earth or moon can escape from the system and one starting from a remote point can reach either body. As C decreases to C_5 and beyond, the opening in the contour behind the moon widens. When $C = C_6$ the contour also begins to open behind the earth and when $C = C_7$ the only portions of the plane excluded from motion of a vehicle are the interiors of 2 kidney-shaped regions above and below the x_R-axis. As C decreases further to a value of C_8, the regions of exclusion shrink to two points, each completing an equilateral triangle with the earth and moon. No region of the $x_R y_R$-plane is excluded if $C < C_8$.

The points at which the contours corresponding to $C = C_2$, C_4 and C_6 coalesce together with the 2 points for which $C = C_8$ are called double points. From the equation for the surfaces of zero relative velocity (Eq (77)) and from the traces of these surfaces in the $x_R y_R$, $x_R z_R$ and $y_R z_R$-planes such as Fig. 2, it can be seen that all the double points are in the $x_R y_R$-plane. Hence it it sufficient to consider the trace in the $x_R y_R$-plane, Eq (78), for the determination of the double points. These double points are of interest as critical points of the curves:

$$F(x, y) = \omega_{\oplus\mathbb{C}}^2(x_{R\Delta}^2 + y_{R\Delta}^2) + \frac{2GM_\oplus}{\left[(x_{R\Delta} - x_{R\oplus})^2 + y_{R\Delta}^2\right]^{1/2}} + \frac{2GM_\mathbb{C}}{\left[(x_{R\Delta} - x_{R\mathbb{C}})^2 + y_{R\Delta}^2\right]^{1/2}} - C = 0 \quad (79)$$

The condition for a critical point is that the first derivatives of Eq (78) with respect to $x_{R\Delta}$ and $y_{R\Delta}$ be zero, i.e.:

$$\omega_{\oplus\mathbb{C}}^2 x_{R\Delta} - \frac{GM_\oplus(x_{R\Delta} - x_{R\oplus})}{\left[(x_{R\Delta} - x_{R\oplus})^2 + y_{R\Delta}^2\right]^{3/2}} - \frac{GM_\mathbb{C}(x_{R\Delta} - x_{R\mathbb{C}})}{\left[(x_{R\Delta} - x_{R\mathbb{C}})^2 + y_{R\Delta}^2\right]^{3/2}} = 0$$

$$\omega_{\oplus\mathbb{C}}^2 y_{R\Delta} - \frac{GM_\oplus y_{R\Delta}}{\left[(x_{R\Delta} - x_{R\oplus})^2 + y_{R\Delta}^2\right]^{3/2}} - \frac{GM_\mathbb{C} y_{R\Delta}}{\left[(x_{R\Delta} - x_{R\mathbb{C}})^2 + y_{R\Delta}^2\right]^{3/2}} = 0 \quad (80)$$

It should be noted that Eqs (80) are identical to the equations of motion (Eqs (71)) with $z_{R\Delta} = 0$, and which can be written:

$$\left.\begin{aligned} \ddot{x}_{R\Delta} - 2\omega_{\oplus\mathbb{C}}\dot{y}_{R\Delta} &= \frac{1}{2}\frac{\partial F\left(x_{R\Delta}, y_{R\Delta}\right)}{\partial x_{R\Delta}} \\ \ddot{y}_{R\Delta} - 2\omega_{\oplus\mathbb{C}}\dot{x}_{R\Delta} &= \frac{1}{2}\frac{\partial F\left(x_{R\Delta}, y_{R\Delta}\right)}{\partial y_{R\Delta}} \end{aligned}\right\} \quad (81)$$

Since at the critical points

$$\frac{\partial F}{\partial x_{R\Delta}} = 0, \frac{\partial F}{\partial y_{R\Delta}} = 0$$

and since we are on a surface of zero relative velocity

$$V_{R\Delta} = \left[\dot{x}^2_{R\Delta} + \dot{y}^2_{R\Delta}\right]^{1/2} \equiv 0$$

we obtain from Eqs (81)

$$\ddot{x}_{R\Delta} = 0, \ddot{y}_{R\Delta} = 0.$$

Hence the coordinates of the vehicle at the critical points satisfy the differential equations and it will remain at the critical point unless it is disturbed by forces from outside of the dynamical system. We proceed to obtain the critical points. The second equation of Eq (80) is satisfied by $y_{R\Delta} = 0$ and the double points on the x_R-axis or the straight line solutions to the problem are given by:

$$\omega^2_{\oplus\mathbb{C}} x_{R\Delta} - \frac{GM_{\oplus}\left(x_{R\Delta} - x_{R\oplus}\right)}{\left[\left(x_{R\Delta} - x_{R\oplus}\right)^2\right]^{3/2}} - \frac{GM_{\mathbb{C}}\left(x_{R\Delta} - x_{R\mathbb{C}}\right)}{\left[\left(x_{R\Delta} - x_{R\mathbb{C}}\right)^2\right]^{3/2}} = 0 \quad (82)$$

If, as in Ref. 8, the units are normalized such that the sum $M = M_{\oplus} + M_{\mathbb{C}}$ is the unit of mass and the distance between the earth and moon or lunar unit (LU) is the unit of length, then the double points can be given in a convenient form. Let the double points on the x_R-axis be denoted by x_{Ri}, x_{RM} and x_{Re} which correspond to C_2, C_4 and C_6, respectively. Then from Moulton (Ref. 8, pages 292-293), for $M_{\mathbb{C}}$ small compared to $M_{\oplus}$ and hence small ν, the three straight line solutions can be obtained by expressing them as power series in $\nu^{1/3}$ and determining the coefficients. The result is:

$$\left.\begin{aligned} x_{Ri} - x_{R\mathbb{C}} &= \left(\frac{\nu}{3}\right)^{1/3} - \frac{1}{3}\left(\frac{\nu}{3}\right)^{2/3} - \frac{1}{9}\left(\frac{\nu}{3}\right) + \cdots \\ x_{RM} - x_{R\mathbb{C}} &= \left(\frac{\nu}{3}\right)^{1/3} + \frac{1}{3}\left(\frac{\nu}{3}\right)^{2/3} - \frac{1}{9}\left(\frac{\nu}{3}\right) + \cdots \\ x_{Re} - x_{R\mathbb{C}} &= 2 - \frac{7}{12}\nu - 23\frac{(7)^2}{12^4}\nu^3 + \cdots \end{aligned}\right\} \quad (83)$$

in LU, and where $\nu = \frac{M_{\mathbb{C}}}{M} = 0.01214226$.

Since $x_{R\mathbb{C}} = (1 - \nu)$ LU, the double points in terms of distances along the x_R-axis are:

$$x_{Ri} = 0.83741 \text{ LU}$$

$$x_{RM} = 1.15524 \text{ LU}$$

$$x_{Re} = 1.00506 \text{ LU}$$

For this force model of the earth-moon system (see Chapter IV, Section B), a consistent value is 1 LU = 384, 747.2 km. Hence, in MKS units

$$x_{Ri} = 322,190 \text{ km}$$

$$x_{RM} = 444,480 \text{ km}$$

$$x_{Re} = -386,690 \text{ km}$$

Substituting these values into Eq (78) with $y_{R\Delta} = 0$, C_2, C_4 and C_6 can be found. These values are:

$$C_2 = 3.34367 \left(\frac{\text{km}}{\text{sec}}\right)^2$$

$$C_4 = 3.322621 \left(\frac{\text{km}}{\text{sec}}\right)^2$$

$$C_6 = 3.15895 \left(\frac{\text{km}}{\text{sec}}\right)^2$$

From Eq (80), the double points corresponding to C_8 are found to be equidistant from the earth and moon, and form an equilateral triangle with these two and with coordinates

$$x_{RS} = 187,702 \text{ km}$$

$$y_{RS} = \pm 333,201 \text{ km}$$

The value of C_8 from this equilateral triangle solution is:

$$C_8 = 3.13365 \left(\frac{\text{km}}{\text{sec}}\right)^2.$$

These values of C_2, C_4, C_6 and C_8 can be made more meaningful if the velocity of a vehicle near the earth is calculated using these values. For the calculations, the positions of the vehicle will be chosen as 100 km and 1000 km from the surface of the earth on the x_R-axis both adjacent and opposite to the moon. If the equatorial radius of the earth (6, 378.2 km) is used, these coordinates are:

$x_{\Delta 1} = 1,006.5$ km Case I: 100 km above surface of earth adjacent to moon

$x_{\Delta 2}$ = 2,706.5 km Case II: 1000 km above surface of earth adjacent to moon

$x_{\Delta 3}$ = -11,149.9 km Case III: 100 km above surface of earth opposite to moon

$x_{\Delta 4}$ -12,049.9 km Case IV: 1000 km above surface of earth opposite to moon

The following sketch shows the position of the five double points.

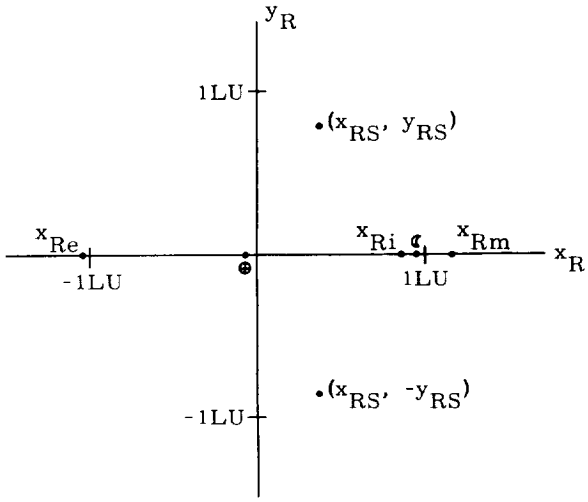

The velocities are then found from Jacobi's integral to be:

	I	II	III	IV
C_2 = 3.34367	10942.2	10233.3	10942.2	10233.2
C_4 = 3.32621	10943.4	10234.6	10943.4	10234.6
C_6 = 3.15895	10951.1	10242.8	10951.1	10242.8
C_8 = 3.13365	10952.3	10244.1	10952.3	10244.1

The magnitude of $V_{R\Delta}$ is the same regardless of direction although it is seen to vary from point to point (Cases I to IV correspond to different points). From Eq (76), Fig. 2 and the preceding sketch, it follows that on a circle with small radius about the earth, the velocity is relatively insensitive to position on the circle. This is also evident from the table by comparing Cases I and II (altitude 100 km, radius 6478.2 km with positions adjacent and opposite to the moon) where the difference is too small to detect. According to Egorov at an altitude of 200 km (radius 6578.2 km), the variations in $V_{R\Delta}$ are of order less than 0.01 m/sec and by comparing Cases II and IV (altitude 1000 km, radius 7378.2 km with positions adjacent and opposite to the moon), the variations are of order 0.1 m/sec. The radius of the circle around the earth has a very pronounced effect on the required $V_{R\Delta}$. A change in altitude from 100 to 1000 km lowers the values of the critical $V_{R\Delta}$'s by 709 m/sec, indicating that the minimum required injection velocity for lunar trajectories is quite sensitive to the injection altitude.

The table also reveals that the velocities corresponding to C_4 are lower than those corresponding to C_6; therefore, it is easier to escape from the vicinity of the earth by projecting toward the moon than it is by projecting away from the moon. The large qualitative difference between the $C = C_2$ and $C = C_4$, as well as the $C = C_6$ and $C = C_8$ contours of Fig. 2, should be compared with the small differences in projection velocities, indicating the sensitivity of lunar trajectories to initial velocities.

The velocities $V_{R\Delta}$ given in table are measured in the rotating $x_R y_R z_R$ coordinate system and are defined as

$$V_{R\Delta}^2 = \dot{x}_{R\Delta}^2 + \dot{y}_{R\Delta}^2 + \dot{z}_{R\Delta}^2 \qquad (84)$$

while velocities in lunar trajectories are usually given in the earth-centered $x_e y_e z_e$ coordinate system defined as

$$V_{e\Delta}^2 = \dot{x}_{e\Delta}^2 + \dot{y}_{e\Delta}^2 + \dot{z}_{e\Delta}^2 \qquad (85)$$

The transformation between the velocity components is

$$\begin{Bmatrix} \dot{x}_{e\Delta} \\ \dot{y}_{e\Delta} \\ \dot{z}_{e\Delta} \end{Bmatrix} = \left[T\left(\Phi + {}^{\omega}\oplus\mathbb{C}\ t\right)\right] \begin{Bmatrix} \dot{x}_{R\Delta} - {}^{\omega}\oplus\mathbb{C}\ y_{R\Delta} \\ \dot{y}_{R\Delta} + {}^{\omega}\oplus\mathbb{C}\left(x_{R\Delta} + {}^{\bar{r}}\oplus\mathbb{C}\ \nu\right) \\ \dot{z}_{R\Delta} \end{Bmatrix} \qquad (86)$$

where $\left[T\left(\Phi + {}^{\omega}\oplus\mathbb{C}\ t\right)\right]$ is given by Eq (47).

Equations (84) to (86) show that $V_{e\Delta}$ depends on $V_{R\Delta}$, the position of the vehicle, as well as the direction of $V_{R\Delta}$. Since the magnitude of each $V_{R\Delta}$ in the previous table is independent of direction to each such value of $V_{R\Delta}$, there would correspond a range of values of $V_{e\Delta}$.

c. Stability of the double points

The five double points given here are special solutions of the equations of motion and are analogous to the special solutions of the three-body problem (see Section B-1). The question of stability of these five points is of importance; i.e., will the vehicle stay near the point if given a small displacement and velocity (stable solution) or will it rapidly depart from that point (unstable solution)? These small displacements and velocities may be regarded as due to small forces neglected in the present model, which

means that the space vehicle will actually remain near the stable double points but depart rapidly from the unstable ones. It can be shown (Ref. 8, pp 299 to 305 and Ref. 11, pp 7-25 to 7-28) that the straight-line solutions are unstable, while the equilateral triangle solutions are stable.

Equilateral triangle solutions have been observed in the solar system. With the Sun and Jupiter considered as the massive bodies, asteroids have been discovered at approximately the equilateral point and with a mean angular velocity equal to that of Jupiter (Ref. 12; p 243). Buchheim (Ref. 11) has proposed to establish satellites at the equilateral triangle points of the earth-moon system which could serve as space buoys.

It has been suggested by Moulton (Ref. 8) that the phenomenon of gegenschein, a hazy patch of light opposite to the sun, is caused by meteors temporarily trapped in unstable periodic orbits around the straight-line point opposite to the sun in the sun-earth system.

C. MOTION OF THE MOON

The position of the moon and its orientation in space are of paramount importance in lunar flight: the position is important in determining the required injection conditions, as well as the exact value of the gravitational force of the moon on the vehicle during flight, and the position together with the particular orientation of the moon are important for landings at specified lunar sites. For these reasons, the orbit of the moon assumed in the discussion of the three-body and restricted three-body problems is not accurate enough for precision trajectories, and a consideration of neglected forces in that model and a comparison with astronomical observations of the moon is necessary. It has been observed that the mean period of the moon's rotation about its axis is equal to its sidereal period of revolution around the earth. Because of this fact and since lunar vehicles originate and are observed from earth, it is advantageous to define the orientation of the moon with respect to earth. The moon rotates at a very nearly constant rate about its axis while its orbital angular velocity varies slightly due to the eccentricity of the lunar orbit. Thus, during different orbital positions of the moon, some areas on either side of the moon become visible. Similarly, the rotational axis of the moon is inclined by about 6.7° to the normal of the moon's orbital plane and areas beyond the north and south poles of the moon become visible from earth at various times. These apparent side-to-side and tilting movements of the moon which occur periodically, are known as optical librations. In addition, the gravitational attractions of the sun and planets on the triaxially ellipsoidal figure of the moon cause a slight wobble of the rotational axis of the moon which is called physical libration. At any given time, lunar librations are determined by the moon's precise orbital motion, its rotational rate, and dynamical effects of its asymmetrical figure.

The first part of this section discusses very briefly the methods used for computing the position of the moon, the comparison between computed and observed positions, and the tabulated lunar ephemerides. The latter part is devoted to a brief discussion of lunar librations and to an approach for determining librations in a digital computer trajectory program which has stored positional data of the moon in geocentric equatorial coordinates.

1. Lunar Theory

Lunar theory in celestial mechanics is generally understood to be the analytical theory of the motion of the moon. The gravitational attraction of the earth and sun, and the earth's and lunar asphericity, as well as gravitational attractions of the planets as they affect the motion of the moon are considered. The methods employed in various lunar theories differ, but at present three methods, those of Delaunay, Hansen, and Hill-Brown, are referred to most frequently. A detailed discussion of these and other lunar theories can be found in Ref. 13. The brief discussion of lunar theories given here follows Refs. 13 and 14, as well as Ref. 2. The discussion is restricted to the "main problem" of lunar theory, which is the three-body problem of astronomy as applied to finding the motion of the spherical moon under the gravitational attraction of the spherical earth and sun.

a. Delaunay's lunar theory

Choose an inertial right-handed Cartesian coordinate system with origin at the center of mass of the dynamical system earth, moon, sun and axes $x'_0\ y'_0\ z'_0$. Let the mass of the earth be $M_\oplus$ with position $x'_{0\oplus}\ y'_{0\oplus}\ z'_{0\oplus}$. The position of the moon with mass $M_\leftmoon$ in this coordinate system is given by $x'_{0\leftmoon}$, $y'_{0\leftmoon}$, $z'_{0\leftmoon}$ and that of the sun with mass $M_\odot$ by $x'_{0\odot}$, $y'_{0\odot}$, $z'_{0\odot}$. The equations of motion of the moon are (compare with Eqs 56 and 57):

$$\left.\begin{aligned} \ddot{x}'_{0\leftmoon} &= \frac{1}{M_\leftmoon}\,\frac{\partial U}{\partial x'_{0\leftmoon}} \\ \ddot{y}'_{0\leftmoon} &= \frac{1}{M_\leftmoon}\,\frac{\partial U}{\partial y'_{0\leftmoon}} \\ \ddot{z}'_{0\leftmoon} &= \frac{1}{M_\leftmoon}\,\frac{\partial U}{\partial z'_{0\leftmoon}} \end{aligned}\right\} \qquad (87)$$

where

$$U = \frac{G M_\oplus M_\leftmoon}{r_{0,\oplus\to\leftmoon}} + \frac{G M_\oplus M_\odot}{r_{0,\oplus\to\odot}} + \frac{G M_\leftmoon M_\odot}{r_{0,\leftmoon\to\odot}} \qquad (88)$$

is the gravitational potential (work function) which is the negative of the gravitational potential energy of the dynamical system.

Since the three-body equations of motion (Eq (87)) cannot be solved in closed form, successive approximations must be used to obtain solutions in analytical form.

In the earth, moon, sun configuration $r_{0,\oplus\to\leftmoon}$ is small compared to $r_{0,\oplus\to\odot}$ or $r_{0,\leftmoon\to\odot}$ while $M_\odot$ is large compared to

$M_\oplus + M_\leftmoon$, and the earth-moon barycenter approximates unperturbed motion around the sun very well. It is, therefore, helpful to introduce coordinates of the moon relative to the earth,

$$\begin{aligned} x_{\oplus\leftmoon} &= x'_{0\leftmoon} - x'_{0\oplus} \\ y_{\oplus\leftmoon} &= y'_{0\leftmoon} - y'_{0\oplus} \\ z_{\oplus\leftmoon} &= z'_{0\leftmoon} - z'_{0\oplus}, \end{aligned} \tag{89}$$

and coordinates of the sun relative to the earth-moon barycenter,

$$\begin{aligned} x_{0\,\odot} &= x'_{0\odot} - \frac{M_\oplus x'_{0\oplus} + M_\leftmoon x'_{0\leftmoon}}{M_\oplus + M_\leftmoon} \\ y_{0\,\odot} &= y'_{0\odot} - \frac{M_\oplus y'_{0\oplus} + M_\leftmoon y'_{0\leftmoon}}{M_\oplus + M_\leftmoon} \\ z_{0\,\odot} &= z'_{0\odot} - \frac{M_\oplus z'_{0\oplus} + M_\leftmoon z'_{0\oplus}}{M_\oplus + M_\leftmoon} \end{aligned} \tag{90}$$

The precise orientation of the axes need not be specified for this discussion, but, for agreement with previous notation, $x_{\oplus\leftmoon}$, $y_{\oplus\leftmoon}$, $z_{\oplus\leftmoon}$ are equatorial coordinates of the moon referred to the mean equator and equinox. After making the necessary transformations, the equations of motion (Eq (87)) become

$$\begin{aligned} \ddot{x}_{\oplus\leftmoon} &= \frac{M_\oplus + M_\leftmoon}{M_\oplus M_\leftmoon} \frac{\partial U}{\partial x_{\oplus\leftmoon}} \\ \ddot{y}_{\oplus\leftmoon} &= \frac{M_\oplus + M_\leftmoon}{M_\oplus M_\leftmoon} \frac{\partial U}{\partial y_{\oplus\leftmoon}} \\ \ddot{z}_{\oplus\leftmoon} &= \frac{M_\oplus + M_\leftmoon}{M_\oplus M_\leftmoon} \frac{\partial U}{\partial z_{\oplus\leftmoon}} \end{aligned} \tag{91}$$

It remains to express U in terms of the new coordinates. Let $r^2_{\oplus\leftmoon} = x^2_{\oplus\leftmoon} + y^2_{\oplus\leftmoon} + z^2_{\oplus\leftmoon}$ be the square of the distance from the earth to the moon, $r^2_{\oplus\odot} = x^2_{0\odot} + y^2_{0\odot} + z^2_{0\odot}$ be the square of the distance from the earth to the sun with components in the respective coordinate systems (the earth-moon barycenter is very close to the earth), and S the angle at earth between the earth-moon and earth-sun lines (see following sketch). Then, as in Ref. 14, page 270, $r^{-1}_{0,\oplus\to\leftmoon}$, $r^{-1}_{0,\oplus\to\odot}$ and $r^{-1}_{0,\leftmoon\to\odot}$ can be expressed in terms of $r_{\oplus\leftmoon}$, $r_{\oplus\odot}$ and Legendre polynomials of cos S, P_n (cos S), to yield for the gravitational potential:

$$\begin{aligned} U = G\Bigg[& \frac{M_\oplus M_\leftmoon}{r_{\oplus\leftmoon}} + \frac{(M_\oplus + M_\leftmoon) M_\odot}{r_{\oplus\odot}} \\ & + \frac{M_\oplus M_\leftmoon M_\odot}{M_\oplus + M_\leftmoon} \frac{r^2_{\oplus\leftmoon}}{r^3_{\oplus\odot}} P_2(\cos S) \\ & + \frac{M_\oplus M_\leftmoon M_\odot (M_\oplus - M_\leftmoon)}{(M_\oplus + M_\leftmoon)^2} \frac{r^3_{\oplus\leftmoon}}{r^4_{\oplus\odot}} P_3(\cos S) \\ & + \frac{M_\oplus M_\leftmoon M_\odot (M^2_\oplus - M_\oplus M_\leftmoon + M^2_\leftmoon)}{(M_\oplus + M_\leftmoon)^3} \\ & \frac{r^4_{\oplus\leftmoon}}{r^5_{\oplus\odot}} P_4(\cos S) + \ldots \Bigg] \end{aligned} \tag{92}$$

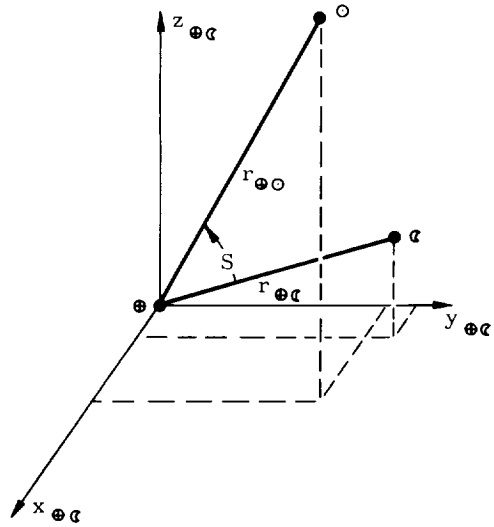

The equations of motion of the moon (Eq (91)) can now be written in the form

$$\begin{aligned} \ddot{x}_{\oplus\leftmoon} + \frac{G(M_\oplus + M_\leftmoon)}{r^3_{\oplus\leftmoon}} x_{\oplus\leftmoon} &= \frac{\partial R}{\partial x_{\oplus\leftmoon}} \\ \ddot{y}_{\oplus\leftmoon} + \frac{G(M_\oplus + M_\leftmoon)}{r^3_{\oplus\leftmoon}} y_{\oplus\leftmoon} &= \frac{\partial R}{\partial y_{\oplus\leftmoon}} \\ \ddot{z}_{\oplus\leftmoon} + \frac{G(M_\oplus + M_\leftmoon)}{r^3_{\oplus\leftmoon}} z_{\oplus\leftmoon} &= \frac{\partial R}{\partial z_{\oplus\leftmoon}} \end{aligned} \tag{93}$$

where, if we substitute the expressions for the Legendre polynomials,

$$\begin{aligned} R = \frac{G M_\odot}{r_{\oplus\odot}} \Bigg[& \left(\frac{r_{\oplus\leftmoon}}{r_{\oplus\odot}}\right)^2 \left(-\frac{1}{2} + \frac{3}{2}\cos^2 S\right) \\ & + \frac{M_\oplus - M_\leftmoon}{M_\oplus + M_\leftmoon} \left(\frac{r_{\oplus\leftmoon}}{r_{\oplus\odot}}\right)^3 \cdot \left(-\frac{3}{2}\cos S + \frac{5}{2}\cos^3 S\right) \end{aligned} \tag{94}$$

$$+\frac{M_\oplus^2 - M_\oplus M_\mathbb{C} + M_\mathbb{C}^2}{(M_\oplus + M_\mathbb{C})^2}\left(\frac{r_{\oplus\mathbb{C}}}{r_{\oplus\odot}}\right)^4\left(\frac{3}{8} - \frac{15}{4}\cos^2 S - \frac{35}{8}\cos^4 S\right) + \ldots\Bigg]. \tag{94}$$

In this expression for R the term $\frac{G(M_\oplus + M_\mathbb{C})M_\odot}{M_\oplus M_\mathbb{C} r_{\oplus\odot}}$ has been omitted since it is independent of $x_{\oplus\mathbb{C}}$, $y_{\oplus\mathbb{C}}$ and $z_{\oplus\mathbb{C}}$.

The second term on the left-hand side of the equations of motion (Eq (93)) is due to the gravitational attraction of the moon by the earth, and R is the disturbing function which in this case is due to the gravitational attraction of the sun by the earth. If $R \equiv 0$ the intermediate orbit, or first approximation to the path of the moon, is an ellipse.

The expression for R may be modified further by using Kepler's third law for the motion of the earth-moon barycenter,

$$G(M_\odot + M_\oplus + M_\mathbb{C}) = n_\odot^2 a_\odot^3, \tag{95}$$

where $n_\odot$ and $a_\odot$ are the sun's mean motion and semimajor axis, respectively. If we ignore the mass of the earth and moon compared to that of the sun, and that of the moon with respect to the earth, then we obtain after some manipulations:

$$R = n_\odot^2 a_\mathbb{C}^2\Bigg[\left(\frac{r_{\oplus\mathbb{C}}}{a_\mathbb{C}}\right)^2\left(\frac{a_\odot}{r_{\oplus\odot}}\right)^3\left(-\frac{1}{2} + \frac{3}{2}\cos^2 S\right) + \frac{a_\mathbb{C}}{a_\odot}\left(\frac{r_{\oplus\mathbb{C}}}{a_\mathbb{C}}\right)^3\left(\frac{a_\odot}{r_{\oplus\odot}}\right)^4\left(-\frac{3}{2}\cos S + \frac{5}{2}\cos^3 S\right) + \left(\frac{a_\mathbb{C}}{a_\odot}\right)^2\left(\frac{r_{\oplus\mathbb{C}}}{a_\mathbb{C}}\right)^4\left(\frac{a_\odot}{r_{\oplus\odot}}\right)^5\left(-\frac{3}{8} - \frac{15}{4}\cos^2 S - \frac{35}{8}\cos^4 S\right) + \ldots\Bigg] = R_1 + R_2 + R_3 + \ldots \tag{96}$$

In Delaunay's lunar theory the orbit of the earth around the sun is a fixed ellipse in a fixed plane. The expression (Eq (96)) for R can now be expanded in terms of elliptic elements of the moon's and sun's orbits. Delaunay's series for R consists of one constant and 320 periodic terms (Ref. 13).

The method of variation of parameters, also known as variation of elements and variation of arbitrary constants, is used in the solution of the lunar equations of motion. Consider the case $R = 0$. Then the instantaneous coordinates and velocity components of the moon allow the determination of a unique set of six orbital elements for the intermediate orbit of the moon which are constants of the motion. In actual motion $R \neq 0$ and the orbital elements vary with time for the true orbit. The requirement of the method is that the coordinates and velocity components expressed in terms of the elements and time have the same form for the intermediate ($R = 0$) and the true ($R \neq 0$) orbit. For the actual motion, one can obtain six first-order differential equations (called variation of parameter equations) which give the time-variation of the elements and are fully equivalent to the equations of motion (Eq (93)). The procedure calls for integration of the variation of parameter equations to obtain the orbital elements as functions of time and expressed as sums of trigonometric series. Finally the coordinates as well as velocity components may be obtained as functions of time by a coordinate transformation.

Delaunay chooses a set of elements so that the system of differential equations takes the canonical form:

$$\left.\begin{aligned}\frac{dL}{dt} &= \frac{\partial \tilde{F}}{\partial \ell}, \frac{d\ell}{dt} = -\frac{\partial \tilde{F}}{\partial L}\\ \frac{dG}{dt} &= \frac{\partial \tilde{F}}{\partial g}, \frac{dg}{dt} = -\frac{\partial \tilde{F}}{\partial G}\\ \frac{dH}{dt} &= \frac{\partial \tilde{F}}{\partial h}, \frac{dh}{dt} = -\frac{\partial \tilde{F}}{\partial H}\end{aligned}\right\} \tag{97}$$

These canonical elements or Delaunay variables are, in terms of μ and the elliptic elements given in section A-3.

$$\begin{aligned}L &= (\mu a)^{1/2}\\ G &= (\mu a)^{1/2}(1-e^2)^{1/2}\\ H &= (\mu a)^{1/2}(1-e^2)^{1/2}\cos i\\ h &= \Omega\\ g &= \omega\\ \ell_0 &= \int_{\text{time}} n\,dt + \ell, \text{ the mean anomaly at any}\end{aligned} \tag{98}$$

and

$$\tilde{F} = \frac{\mu^2}{2L^2} + R \tag{99}$$

is the Hamiltonian of the system.

The variation of parameter equations (Eq (97)) cannot be solved in closed form, just as one cannot solve in closed form the equations of motion of the three-body problem, and some approximation procedure has to be used. The coefficients of the disturbing function R are expanded in power series in $e_\mathbb{C}$, $\sin\frac{1}{2} i_{\epsilon m}$, $e_\odot$ and $\frac{a_\mathbb{C}}{a_\odot}$ (and not explicitly in canonical elements), while the general

argument is a function of the angles h, g, ℓ referring to the moon's orbit, and the mean anomaly of the sun $\ell_\odot$. During the integration, powers of $\frac{n_\odot}{n_\mathbb{C}}$ appear as part of the power series.

The principle of Delaunay's method consists of introducing a force function

$$\bar{F} = \frac{\mu^2}{2L^2} + P_1 + Q_1 \cos\theta, \qquad (100)$$

where P_1 denotes the nonperiodic terms in the expansion of R, and $Q_1 \cos\theta$ is one single periodic term selected from the expansion of R. Delaunay then integrated the canonical equations by using $\bar{F}$ instead of $\tilde{F}$ by applying a canonical transformation to new canonical variables L', G', H', ℓ', g' and h'. This transformation is applied to $\tilde{F}$ and the term $Q_1 \cos\theta$ has disappeared from R. Delaunay used a succession of canonical transformations (or contact transformations) until the coefficients of the periodic series became sufficiently small to be neglected.

By use of this method Delaunay has obtained a literal solution to the main problem of lunar theory which was presented in two volumes. His results may be readily extended to include other effects on the motion of the moon (Ref. 13).

The utilization of systems of differential equations in canonical form has the advantage that general rules can be established governing transformations from one set of variables to another, which is helpful if one considers the large number of transformations required. One drawback to Delaunay's method is the slow convergence of the coefficients in powers of $\frac{n_\odot}{n_\mathbb{C}}$ = 0.00748 in the case of the moon. Convergence in terms of the other parameters is generally satisfactory.

b. Hansen's lunar theory

Hansen considers the motion of the moon in its instantaneous orbit plane and starts with the variation of parameters differential equations. For the orbital elements Ω, i, ω, a, e and ℓ_0 these equations, which are equivalent to Delaunay's canonical equations (Eq (97)) (Refs. 3 and 14), become

$$\left.\begin{aligned}
\frac{d\Omega}{dt} &= \frac{1}{na^2(1-e^2)^{1/2}\sin i}\frac{\partial R}{\partial i} \\
\frac{di}{dt} &= \frac{\cot i}{na^2(1-e^2)^{1/2}}\frac{\partial R}{\partial \omega} - \frac{1}{na^2(1-e^2)^{1/2}\sin i}\frac{\partial R}{\partial \Omega} \\
\frac{d\omega}{dt} &= \frac{(1-e^2)^{1/2}}{na^2 e}\frac{\partial R}{\partial e} - \frac{\cot i}{na^2(1-e^2)^{1/2}}\frac{\partial R}{\partial i} \\
\frac{da}{dt} &= \frac{2}{na}\frac{\partial R}{\partial \ell_0} \\
\frac{de}{dt} &= \frac{1-e^2}{na^2 e}\frac{\partial R}{\partial \ell_0} - \frac{(1-e^2)^{1/2}}{na^2 e}\frac{\partial R}{\partial \omega} \\
\frac{d\ell_0}{dt} &= -\frac{2}{na}\frac{\partial R}{\partial a} - \frac{1-e^2}{na^2 e}\frac{\partial R}{\partial e}
\end{aligned}\right\} \qquad (101)$$

(continued)

These equations have been derived in Chapter IV of Ref. 3.

In Hansen's method, the plane of the sun need not be fixed, and the fixed plane of reference may be chosen as the ecliptic of a given date or any other plane inclined at a small angle to the ecliptic. However, the motion of the sun must be known.

Consider first the motion of the moon in its instantaneous orbit plane. Define an intermediate orbit in the plane of the moon's instantaneous orbit and one focus at the origin. Let it have constant elements n, a, e and mean anomaly nz where z is a variable with units of time. Let the elements of the intermediate orbit satisfy $n^2 a^3 = G(M_\oplus + M_\mathbb{C})$ and let its perigee have a forward motion ny in the plane of the orbit where y is an unknown constant depending on the attraction of the moon. Impose the additional condition that the point on the intermediate orbit with true anomaly f and radius r lies on the actual radius to the moon. If the true radius to the moon is r, then put

$$r = \tilde{r}(1 + k), \qquad (102)$$

where k is the fraction of the lunar radius between the intermediate and lunar orbits. The motion of the moon in the instantaneous plane of the orbit can be given as soon as z and k are determined in terms of time and the introduced constants. In the determination of k and z a single function W of the variable elements is used. Hence, in Hansen's method, the angular perturbations in the plane of the orbit are added to the mean anomaly of the intermediate orbit and the radial perturbations are expressed by the ratio of the true and intermediate radius vectors.

Next the differential equations for the latitude of the moon above the fixed reference plane are obtained by considering the motion of the instantaneous orbit plane.

The motion of the instantaneous orbit plane is independent of the motion of the moon in that plane. Finally, by a transformation of coordinates it can be shown that some very small corrections have to be added to the true orbital longitude in the instantaneous orbit in order to

obtain the true orbital longitude ($\Omega + \omega + f$) referred to a fixed direction in a fixed reference plane. The differential equations are solved by successive approximations, with the expansion of R in terms of elliptic elements and time being now somewhat different from the form used by Delaunay since the sun's orbit is not fixed.

The slow convergence of the coefficients in powers of $\frac{n_\odot}{n_\mathbb{C}}$ has been overcome by starting with assumed numerical values of all parameters entering into the theory as obtained from observation. If the observations improve, then small changes in these values have to be taken into account. Tables based on Hansen's lunar theory were introduced into the calculation of the lunar ephemeris in 1862 (Ref. 14).

c. Hill-Brown lunar theory

Both Delaunay's and Hansen's lunar theories consider the motion of the moon in the osculating plane, or the plane which at each instant contains the origin of coordinates, the radius, and velocity vectors of the moon. The method of variation of parameters is then used to obtain the motion of the moon. The Hill-Brown lunar theory, on the other hand, uses rectangular coordinates referred to axes moving with the constant angular velocity of the sun's mean motion, $n_\odot$. Advantages in using rectangular coordinates are: the development of R in terms of elliptic elements is unnecessary, and the perturbations are obtained in a form more immediately suitable for ephemeris calculations (Ref. 14).

The theory begins with the expansion of those perturbations that depend on $\frac{n_\odot}{n_\mathbb{C}}$ with the following simplifications in the original equations:

(1) The disturbing function R is given by R_1 only (see Eq (96)) which means that $\frac{a_\mathbb{C}}{a_\odot}$ is neglected in the series expansion.

(2) The moon is assumed to move in the plane of the ecliptic ($i_{\epsilon m} = 0$).

(3) The sun's orbit about the earth-moon barycenter is circular ($e_\odot = 0$, $a_\odot = r_{\oplus\odot}$).

The remaining differential equations thus give all terms depending on $\frac{n_\odot}{n_\mathbb{C}}$ and $e_\mathbb{C}$, and the terms depending on $e_\mathbb{C}$ may be eliminated by obtaining a particular solution of those equations.

Choose an ecliptic coordinate system with origin at the center of the earth as in Section A-1 and the $x_{\epsilon\mathbb{C}}$, $y_{\epsilon\mathbb{C}}$ axes in the fixed plane of the ecliptic. By assumption (2) above $z_{\epsilon\mathbb{C}} \equiv 0$.

The results of Section C-1a carry over directly since the orientation of the axes was not specified rigorously in this development. With the other assumptions the equations of motion (Eq (93)) become, by use of Eq (96) and a change in notation,

$$\left.\begin{aligned} \ddot{x}_{\epsilon\mathbb{C}} + \frac{G(M_\oplus + M_\mathbb{C})}{r^3_{\epsilon\mathbb{C}}} x_{\epsilon\mathbb{C}} &= \frac{\partial R_1}{\partial x_{\epsilon\mathbb{C}}} \\ \ddot{y}_{\epsilon\mathbb{C}} + \frac{G(M_\oplus + M_\mathbb{C})}{r^3_{\epsilon\mathbb{C}}} y_{\epsilon\mathbb{C}} &= \frac{\partial R_1}{\partial x_{\epsilon\mathbb{C}}} \end{aligned}\right\} \quad (103)$$

where

$$\left.\begin{aligned} R_1 &= n^2_\odot r^2_{\oplus\mathbb{C}} \left(-\tfrac{1}{2} + \tfrac{3}{2}\cos^2 S\right) \\ r^2_{\epsilon\mathbb{C}} &= x^2_{\epsilon\mathbb{C}} + y^2_{\epsilon\mathbb{C}} \end{aligned}\right\} \quad (104)$$

Introduce a coordinate system $x_R\, y_R\, z_R$ rotating with angular velocity $n_\odot$ so that the x_R-axis is always in the direction of the sun. The equations of motion of the moon become in this coordinate system (compare with Eqs (74) and (75)):

$$\left.\begin{aligned} \ddot{x}_{R\mathbb{C}} - 2n_\odot \dot{y}_{R\mathbb{C}} &= \frac{\partial W}{\partial x_{R\mathbb{C}}} \\ \ddot{y}_{R\mathbb{C}} + 2n_\odot \dot{x}_{R\mathbb{C}} &= \frac{\partial W}{\partial y_{R\mathbb{C}}} \end{aligned}\right\} \quad (105)$$

with

$$W = \frac{G(M_\oplus + M_\mathbb{C})}{r_{\epsilon\mathbb{C}}} + \tfrac{1}{2} n^2_\odot (x^2_{R\mathbb{C}} + y^2_{R\mathbb{C}}) + R_1 \quad (106)$$

Introduction of $r_{\epsilon\mathbb{C}} \cos S = x_{R\mathbb{C}}$ into the expression (Eq (104)) for R_1 permits us to write

$$W = \frac{G(M_\oplus + M_\mathbb{C})}{r_{\epsilon\mathbb{C}}} + \tfrac{3}{2} n^2_\odot x^2_{R\mathbb{C}}, \quad (107)$$

and yields for the equations of motion:

$$\left.\begin{aligned} \ddot{x}_{R\mathbb{C}} - 2n_\odot \dot{y}_{R\mathbb{C}} + \frac{G(M_\oplus + M_\mathbb{C})}{r^3_{\epsilon\mathbb{C}}} x_{R\mathbb{C}} \\ - 3n^2_\odot x^2_{R\mathbb{C}} = 0 \\ \ddot{y}_{R\mathbb{C}} + 2n_\odot \dot{x}_{R\mathbb{C}} + \frac{G(M_\oplus + M_\mathbb{C})}{r^3_{\epsilon\mathbb{C}}} y_{R\mathbb{C}} = 0 \end{aligned}\right\} \quad (108)$$

To obtain a solution to Eq (108) that depends on $\frac{n_\odot}{n_\mathbb{C}}$ only, consider the initial conditions

$$\left.\begin{aligned} x_{R\,\mathbb{C}}(t=t_0) &= c_1 \\ y_{R\,\mathbb{C}}(t=t_0) &= 0 \\ \dot{x}_{R\,\mathbb{C}}(t=t_0) &= 0 \\ \dot{y}_{R\,\mathbb{C}}(t=t_0) &= c_2 \end{aligned}\right\} \qquad (109)$$

that is, the moon is in conjunction with the sun at $t = t_0$.

Poincaré has shown that the initial conditions (Eq (109)) yield in the rotating coordinate system a periodic solution of the form

$$\left.\begin{aligned} x_{R\,\mathbb{C}} &= A_0 \cos (n_{\mathbb{C}} - n_{\odot})(t - t_0) + A_1 \cos 3 \\ &\quad (n_{\mathbb{C}} - n_{\odot})(t - t_0) + A_2 \cos 5\,(n_{\mathbb{C}} - n_{\odot}) \\ &\quad (t - t_0) + \ldots \\ y_{R\,\mathbb{C}} &= B_0 \sin (n_{\mathbb{C}} - n_{\odot})(t - t_0) + B_1 \sin 3 \\ &\quad (n_{\mathbb{C}} - n_{\odot})(t - t_0) + B_2 \sin 5\,(n_{\mathbb{C}} - n_{\odot}) \\ &\quad (t - t_0) + \ldots \end{aligned}\right\} \qquad (110)$$

where A_i and B_i, $i = 0, 1, 2, \ldots$ are constants. This periodic solution is taken as the intermediate orbit in the Hill-Brown lunar theory. The intermediate orbit allows one to determine the coefficients with any accuracy in $\frac{n_{\odot}}{n_{\mathbb{C}}}$, which circumvents the slow convergence of the coefficients in the expansion of R in powers of $\frac{n_{\odot}}{n_{\mathbb{C}}}$ encountered in Delaunay's lunar theory (Ref. 13).

The first step for solving the main problem of lunar theory consists of determining the intermediate orbit, i.e., the coefficients A_i, B_i in Eq (110) in terms of the parameter $m = \frac{n_{\odot}}{n_{\mathbb{C}} - n_{\odot}}$ for which Hill adopted a numerical value of $m = 0.080848933808312$. Next the general solution of the differential equations (Eq (108)) is obtained, i.e., terms in R whose coefficients depend on m and $e_{\mathbb{C}}$ are considered. Then the simplification $e_{\odot} = 0$, $a_{\odot} = r_{\epsilon\odot}$ is lifted and terms in R whose coefficients depend on m and $e_{\odot}$ are considered. This procedure is continued by considering terms in R whose coefficients depend on m, $a_{\odot}^{-1}$; m, $\sin \frac{1}{2} i_{\epsilon m}$; as well as m and combinations of $e_{\odot}$, $e_{\mathbb{C}}$, $\sin \frac{1}{2} i_{\epsilon m}$, $a_{\odot}^{-1}$ and higher powers thereof.

The Hill-Brown lunar theory consists first of the development of a solution to the equations of motion of the moon for the main problem of lunar theory as outlined above and secondly of the perturbations of this solution due to the direct and indirect gravitational attraction of the planets, the shape of the earth and triaxiality of the moon. The obtained coordinates of the moon are expressed as explicit functions of time. Thirdly, Brown (Ref. 15) computed tables deriving coefficients of all periodic terms to an accuracy of the order of $0''.001$ in true orbital longitude ($\Omega + \omega + f$), celestial latitude ϕ_{ϵ}, and $0''.0001$ in sine parallax (Ref. 16) by keeping terms of the order $\left(\frac{n_{\odot}}{n_{\mathbb{C}}}\right)^6$, $e_{\mathbb{C}}^6$, $e_{\odot}^4$, $\sin^6 \frac{1}{2} i_{\epsilon m}$, $\left(\frac{a_{\mathbb{C}}}{a_{\odot}}\right)^3$ in the disturbing function R for the main problem in the lunar theory.

Brown's tables have been used for the calculation of lunar ephemerides from 1923 to 1959. However, in order to obtain the position of the moon to the desired precision of $0^s.001$ in right ascension and $0''.01$ in declination, the lunar ephemeris since 1960 is based on values of true orbital longitude, celestial latitude and horizontal parallax calculated directly from the trigonometric series obtained from the Hill-Brown theory, not Brown's tables. It has been shown in Ref. 16, pages 364 through 417, that there exist discrepancies in the calculation of the moon's position from the theory and from the tables which amount to an amplitude of approximately $0''.1$ in lunar true orbital longitude, $0''.15$ in lunar celestial latitude and $0''.01$ in sine parallax.

At present the position of the moon for ephemeris calculations is expressed in the form of a trigonometric series as given in the explanation in Brown's tables (Ref. 15). Each argument is a linear function of time with small secular and periodic additions due to the planetary attractions. Each coefficient of the series is a constant for the main problem of lunar theory with small secular and periodic additions due to the attractions of the planets.

Consider only the main problem of lunar theory. Each argument in the series expression is in turn a function of four fundamental arguments*

$$\left.\begin{aligned} \ell &= \mathbb{C} - \Gamma', \text{ mean anomaly of the moon} \\ \ell', \ell_{\odot}, g_{\odot} &= L - \Gamma, \text{ mean anomaly of the sun} \\ F &= \mathbb{C} - \Omega, \text{ argument of lunar perigee plus mean anomaly of the moon} \\ D &= \mathbb{C} - L, \text{ mean elongation of the moon from the sun} \end{aligned}\right\} \qquad (111)$$

*The notation adopted in Ref. 1 has been used here, with the astronomical notation as well as the one used in Brown's tables indicated.

$\mathbb{C}$ (L) $= \Omega + \omega + \ell$ is the mean longitude of the moon, measured in the ecliptic from the mean equinox of date to the mean ascending node, then along the orbit

L (L') $= \tilde{\omega}_{\odot} + \ell_{\odot}$ ($g_{\odot}$) is the mean longitude of the sun, measured from the mean equinox of date

Γ' ($\tilde{\omega}$) = the mean longitude of lunar perigee, measured from the mean equinox of date along the ecliptic to the mean ascending node, then along the orbit

Γ ($\tilde{\omega}_{\odot}$) = the mean longitude of solar perigee measured from the mean equinox of date

Ω = the longitude of the mean ascending node of the lunar orbit on the ecliptic measured from the mean equinox of date

The arguments of each periodic term of the series can be expressed in the form

$$p_1 \ell + p_2 g_{\odot} + p_3 F + p_4 D \qquad (112)$$

where

$$p_i = 0, \pm 1, \pm 2, \pm 3, \ldots$$

If the attractions of the planets are taken into account, then secular and periodic terms are added to the solar arguments and for each planet a new argument appears which is a linear function of time. Effects of the shape of the earth and moon are included in the solar arguments.

The coefficients in the trigonometric series for the position of the moon are functions of four of the lunar and solar orbits:

e, $e_{\mathbb{C}}$ = 0.054900489, constant of the eccentricity of the moon's orbit

γ = $\sin \frac{1}{2} i_{\epsilon m}$ = 0.044886967, constant of the inclination of the moon's orbit

e', $e_{\odot}$ = eccentricity of the sun's orbit

α = 3422".5400, constant of sine parallax

(113)

The numerical value of $\frac{n_{\odot}}{n_{\mathbb{C}}}$, which can be obtained very accurately by observation, is introduced at the beginning of the theory. Each coefficient of the periodic terms consists of a numerical factor multiplied by the principal characteristic, which can be expressed in the form

$$e_{\mathbb{C}}^{q_1} e_{\odot}^{q_2} \gamma^{q_3} \alpha^{q_4} \qquad (114)$$

where $q_i = 0, 1, 2, 3, \ldots$ The gravitational attraction of the planets introduces secular and periodic terms in the parameters $e_{\odot}$, γ.

The independent variable is time counted from the epoch 1900, January 0.5 ET (Greenwich mean noon) which corresponds to the Julian Date 2415020.0. The position of the moon is usually given in spherical coordinates, i.e., true orbital longitude ($\Omega + \omega + f$), celestial latitude ϕ_{ϵ}, and horizontal parallax $\pi_{\mathbb{C}}$ (which is a measure of $r_{\epsilon\mathbb{C}}$). Its position in geocentric rectangular, or any other coordinate system can then be obtained by suitable transformations.

The trigonometric series as used for the calculation of the lunar position contains 1629 periodic terms which are tabulated in Ref. 16, together with 50 additive terms to the fundamental arguments.

Most of these periodic terms are very small but some of the principal ones, all due to the disturbing effects of the sun, have sizable coefficients. The better known terms are: The variation is a periodic perturbation in the moon's mean longitude $\mathbb{C}$ with a coefficient +39' 29".9 and a period of one-half mean synodic month (new moon to new moon), or approximately 14.8 days. Evection is the largest periodic perturbation in $\mathbb{C}$ due to periodic variations in the osculating eccentricity and longitude of perigee $\tilde{\omega}$ of the moon's orbit. Its coefficient is +1° 16' 26".4 and the period approximately 31.8 days. This term was known to Hipparchus from observations of the moon. The annual equation is another perturbation in $\mathbb{C}$ with coefficient -11'8".9 and period of an anomalistic year (the time between successive solar perigees in the orbit of the sun as seen from earth) of approximately 365.3 days. This perturbation is due primarily to the eccentricity of the earth's orbit around the sun. The parallactic inequality is a secondary perturbation in $\mathbb{C}$ (i.e., it comes from a term of R_2) with a coefficient -2'4".8 and period of mean synodic month (approximately 29.5 days). The principal perturbation in latitude has a coefficient of +10' 23".7 and a period of approximately 32.3 days.

d. Theory and observation

From lunar theory one can obtain the true coordinates of the moon as a function of time. This lunar position given by theory must be compared with observation and usually several corrections and coordinate transformations have to be applied before this comparison can be made accurately.

The geometric ephemeris is a table giving the actual or true position of the body at various times. However, actual positions cannot be observed directly since light emitted by the body takes a finite time to travel from the body to the observer (correction for light time), and during this time the body as well as the observer have been displaced from their original position (stellar aberration). These two corrections are known as planetary aberration, and if applied to the observed or apparent position of the body, they yield its true position. A table giving the apparent position of the body as a function of time

is known as an apparent ephemeris. Ephemerides of the sun, the principal planets, and the moon are usually apparent ephemerides. In the case of the moon the entire planetary aberration consists of the correction for light time which amounts to approximately 0".7 in geocentric mean orbital longitude ☾ with a variation of 0".05 due to the eccentricity of the moon's orbit (Ref. 14), and will be neglected in this manual. For observations of the moon from the surface of the earth, such as moonrise and moonset, three additional corrections, the diurnal aberration due to the earth's rotation which is a part of the stellar aberration, the atmospheric refraction, and a parallax correction, must be applied to reduce the observation to an apparent ephemeris. Formulas for these corrections are given in Ref. 2.

Furthermore, the fundamental reference planes in celestial mechanics, the ecliptic and the celestial or earth's equatorial plane, as well as one of their points of intersection on the celestial sphere, the vernal equinox, are in constant motion. Hence, the geocentric coordinates of the body vary due to this motion. The secular terms of this motion, which are independent of the positions of the earth and moon, are termed precessional terms. There are also periodic terms in this motion with arguments ℓ, $\ell_{\odot}$, F, D, Ω which are termed nutational terms. The principal term in nutation depends on Ω and has an amplitude of 9".210 and a period of 18.6 years.

The tabulated positions of the sun, moon, and planets in the ephemerides are usually apparent positions, that is, the coordinates of the body as an observer at the center of the earth would see them, and referred to a coordinate system defined by the instantaneous equator, ecliptic, and equinox. If the corrections for planetary aberration are applied to apparent positions, true positions are obtained. If the periodic effects of nutation are neglected, mean positions are obtained, which are the coordinates of the body referred to a coordinate system defined by the mean equator, ecliptic and equinox of date. Sometimes the effects of precession are removed for some time in order to provide a fixed reference for theoretical calculations. The selected epoch is usually chosen at the beginning of the year 1950.0 in order that data from various sources can most easily be combined. In Ref. 1 some positions are referred to the mean equator and equinox at the beginning of the year for which the ephemerides have been published. Transformations between the various reference systems are given in Ref. 6.

e. Available lunar ephemerides

The principal reference for lunar ephemerides is the American Ephemeris and Nautical Almanac (Ref. 1) which is published annually about two years in advance. On page 51 of Ref. 1 the following items are tabulated for every tenth day: the values of the fundamental arguments Γ', Ω, ☾, and D (see the following sketch); $i_{☾}$, the inclination of the mean equator of the moon to the true equator of the earth; Δ, the angle along the mean equator of the moon from its ascending node on the true equator of the earth to its ascending node on the ecliptic of date; $\Omega_{☾}$, the right ascension of the ascending node of the mean lunar equator measured from true equinox of date.

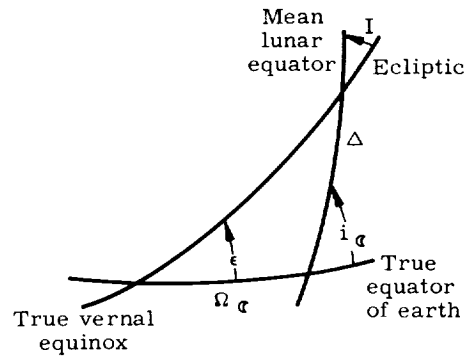

On pages 52 to 67, Ref 1 tabulates the following items for every half day: the apparent true orbital longitude referred to the mean equinox of date; the apparent celestial latitude referred to the ecliptic of date; the horizontal parallax, the semidiameter and ephemeris transit (time of crossing of the ephemerides meridian which is 1.002738 ΔT east of the Greenwich meridian). In Ref. 1, pages 68 to 159, the apparent right ascension, the apparent declination referred to true equator and equinox of date, together with differences for interpolation and fully corrected for planetary aberration, are tabulated to the nearest $0^s.001$ and 0".01, respectively for each hour of ephemeris time (pages 68 through 159). This accuracy has been recommended for national ephemerides by a resolution of the International Astronomical Union in 1952 and has been introduced into the lunar ephemeris from 1960 on. The phases of the moon and lunar perigee and apogee have also been tabulated on page 159.

The ephemerides for physical observations of the moon are based on the apparent coordinates given in the fundamental ephemerides described above and tabulated to a lesser degree of accuracy, usually to 0.01°.

The age, or number of days since the previous new moon, and the fraction of the illuminated disk, the earth's and sun's selenographic coordinates, the physical librations, and the position angles of the axis and bright limb, tabulated for 0^h Universal Time (UT) of each day, are given in Ref. 1, pages 310 through 317. The earth's selenographic coordinates are the sum of the optical and physical librations of the moon. They are the coordinates of the point on the lunar surface where the moon-earth line intersects it, and are given in the customary selenographic coordinate system described in Section A·2 of this Chapter. The sun's selenographic coordinates are the coordinates of the point of

intersection of the moon-sun line with the lunar surface and are given in terms of selenographic latitude (see Section A-2) and colongitude. The selenographic colongitude, $\lambda'_{\odot}$, $0° \leq \lambda'_{\odot} < 360°$, can be obtained by subtracting the selenographic longitude, $0° < \lambda < 360°$, from 90° or 450°. The sun's selenographic colongitude determines the illuminated regions of the lunar surface because the sun's selenographic latitude is small $|\phi_{\odot}| < 2°$: at new moon $\lambda'_{\odot} \approx 270°$, at first quarter $\lambda'_{\odot} \approx 0°$, at full moon $\lambda'_{\odot} \approx 90°$, and at last quarter $\lambda'_{\odot} \approx 180°$. The terminator is defined as the orthogonal projection of the great circle bounding the illuminated (by the sun) hemisphere of the moon on a plane perpendicular to the line of sight from the center of the earth or EML. The selenographic colongitude of the sun can thus be regarded as the selenographic longitude of the morning terminator. The selenographic longitude of the evening terminator differs by 180° from that of the morning terminator. The position angle of the axis is the angle between north on the lunar meridian which passes through the apparent central point of the lunar disk and the declination circle through this central point, measured positive eastward from the north point of the disk. The position angle of the bright limb is the angle between north on the same lunar meridian and the moon-sun line. Both position angles are analogous to the azimuth of topocentric coordinates. In addition to the selenographic coordinates of the earth, the physical librations in longitude, latitude, and position angle are tabulated separately.

For lunar mission planning purposes, positions of the moon are often needed in advance of the published ephemerides. In principle, it is possible to determine lunar ephemerides from the Hill-Brown Lunar Theory for all time. However, some parameters such as orbital elements and the masses of the planets must be supplied by observation, and due to observational inaccuracies, the position computed from theory by use of these observed parameters will differ more and more from the true position at the same time the farther ahead one tries to predict. However, the position of the moon can be determined with essentially ephemeris accuracy for decades and the Nautical Almanac Office of the United States Naval Observatory is prepared to supply ephemerides outside of the scope of Ref. 1 for special purposes. To aid the lunar mission planner, a future addendum will give the geocentric rectangular coordinates of the moon referred to mean equator and equinox of date for the years 1965 through 1969 in half-day intervals. The components of lunar position $x_{\oplus\odot}$, $y_{\oplus\odot}$, $z_{\oplus\odot}$ are given in units of earth radii.

Woolston (Ref. 17) gives additional lunar data for the years 1961 through 1971 useful for the mission planner: the phases of the moon are tabulated to within approximately one minute of time, and graphs giving the declination of the moon with phases indicated as well as its radial distance are presented for a rapid visualization of trajectory and solar illumination data. From the graphs the declination can be obtained to within approximately 0.5° and the radial distance to within 600 km for any given date. Some of these graphs are presented in Chapter XI.

2. Librations of the Moon

An important factor in planning lunar missions, whether they be circumlunar, reconnaissance, or landing flights, is the libration of the moon, or its orientation with respect to earth. Libration is defined as the "position of the moon-earth line with respect to the Moon's Mean Center point." This mean center point* is the fundamental base for the mapping of lunar features. The following sketch illustrates the orientation of the mean center point (MCP) and how latitude and longitude are measured in the selenographic coordinate

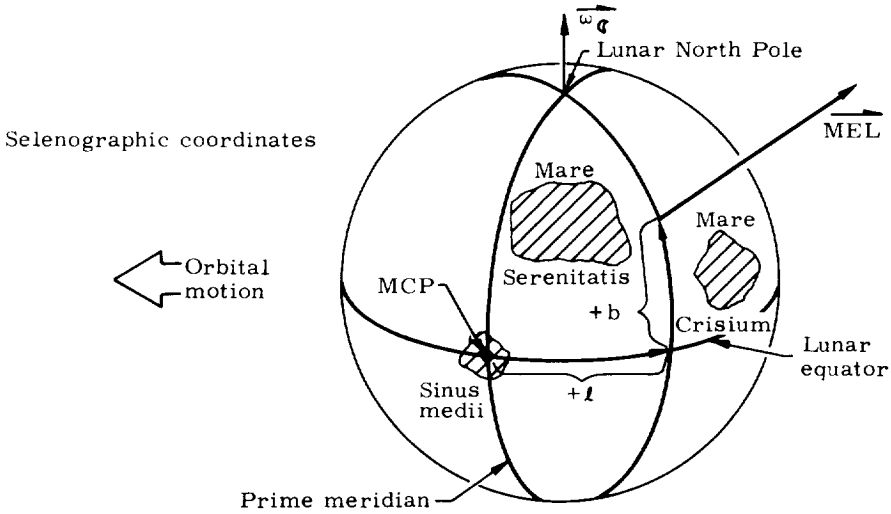

*Definition of MCP: The mean center point is the point on the lunar surface where the surface is intersected by the radius of the moon that would be directed toward the earth's center, were the moon to be at the mean ascending node when the node coincided with either the mean perigee or mean apogee.

system. The lunar equatorial plane is perpendicular to the moon's spin axis and the magnitude of the moon's angular velocity $\omega_{\mathbb{C}}$ is practically constant.

Selenographic longitudes are measured from the MCP (located in Sinus Medii-Central Bay) positive in the direction toward Mare Crisium (Sea of Crises). Selenographic latitudes are positive in the hemisphere containing Mare Serentatis (Sea of Serenity). Also in the sketch, the positive librations in longitude (+ℓ) and latitude (+b) are shown in the selenographic system. These coordinates are the sum of both the optical and physical librations in longitude and latitude, respectively. Therefore as the position of the moon-earth line (MEL) changes with respect to the MCP so does any specific lunar feature vary with respect to the MEL.

The causes of lunar librations are essentially twofold: First there are the optical librations which are the result of the dynamical properties of the moon's orbit about the earth, and secondly, the physical librations which are caused by the motion of $\vec{\omega}_{\mathbb{C}}$ in inertial space due to the small triaxiality in the moon's figure.

The following sketch is a view of the earth-moon system as seen from a point in the ecliptic plane. Effects of physical librations on I ($\rho < 0.045°$) are ignored for the purpose of this demonstration.

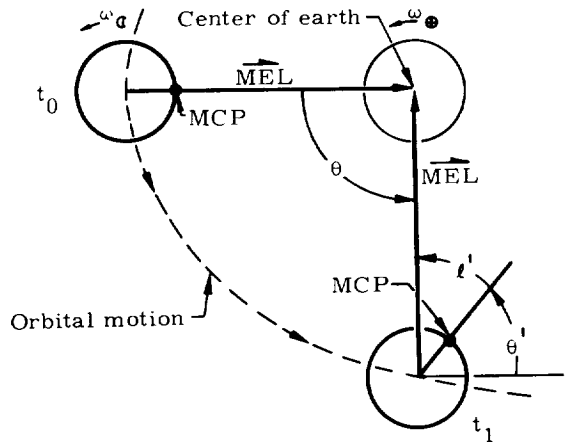

has a constant rotational rate $\omega_{\mathbb{C}}$ and rotates through an angle $\theta' = (t_1 - t_o)\,\omega_{\mathbb{C}}$. Because the orbital motion of the moon about the earth is elliptic, the central angle $\theta \neq \theta'$. The difference (ℓ') is called the "optical libration in longitude" with a variation from approximately + 8° to - 8° in a period of approximately 1 lunar month.

The much smaller physical librations (order of 0.04°) are the result of rigid body dynamics

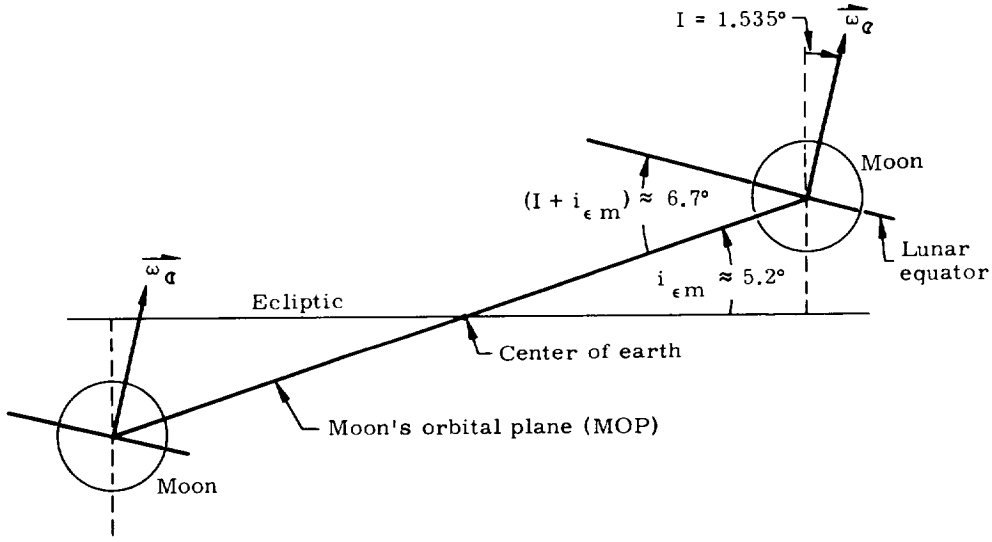

The inclination of the mean lunar equator to the ecliptic is denoted by I and is constant (1.535°). Now an observer at the earth's center would note a more exposed northern hemisphere at $(I + i_{em} \approx -6.7°)$ and one-half month later would view a more exposed southern hemisphere $(I + i_{em} = +6.7°)$. This apparent oscillation of the moon is termed the "optical libration in latitude" with a variation from approximately +7° to -7° in a period of approximately 1 lunar month.

The following sketch illustrates the earth-moon system when viewed from above the ecliptic. During the interval $(t_1 - t_o)$ the moon

and the moon's triaxial characteristics. These characteristics cause the direction of the moon's spin axis ($\vec{\omega}_{\mathbb{C}}$) to oscillate in inertial space about a "mean" position. The periods of the physical librations in longitude and latitude are approximately 1 year and 6 years, respectively. If these minor librations are ignored, an uncertainty of 1000 m can arise for any given surface coordinates. Thus it can be seen that for preliminary mission planning, the physical librations can be disregarded. However they cannot be eliminated from detailed planning, especially for "landing" type missions. This becomes more

evident when considering the fact that landing vehicles within this decade will be severely limited in hovering and translational capability. Furthermore, guidance inaccuracies may demand a large part of this capability. Physical librations can be compensated for prior to leaving earth or at a later time during flight depending on the guidance scheme. From the above discussion, it is seen that the librations are continually changing in magnitude. Also, the path traced by the $\overrightarrow{MEL}$ about the MCP is complex. This is evidenced in Fig. 3. In this figure the $\overrightarrow{MEL}$ loci are shown for the month of October in the years 1966 and 1967. Note the almost complete change in the trace characteristics and particularly the rapid movement across the moon's equatorial plane (up to 2°/day).

This movement has considerable influence on the planning of translunar and transearth trajectory orientations. Even during an earth launch time tolerance of 2 hr, a landing site can be displaced from a planned translunar trajectory to the site by 5000 m if librations are not accounted for during this time. Aborts occurring during a stay on the moon will markedly influence the earth return trajectories as compared to the original flight plan. Thus, the librations of the moon add both position and time constraints to the lunar mission.

Methods given in literature (Refs. 2 and 6) for determining librations can become cumbersome because interplanetary digital trajectory programs do and will most likely use stored positional data of the moon in geocentric rectangular coordinates. Thus, the following approach for simulating or determining librations on the computer is practical. The object is to obtain librations in longitude and latitude beyond published ephemeris data from geocentric equatorial coordinates of the moon using transformations of coordinates in terms of fundamental arguments.

First, the reference coordinate systems are shown in the following sketch. The numerical values in the following equations have been obtained from Ref. 1:

$\overrightarrow{EML}$ (earth moon line) has components $(x_{\mathbb{C}}, y_{\mathbb{C}}, z_{\mathbb{C}})$ in geocentric equatorial coordinates

ϵ (mean obliquity of the ecliptic)

$$\epsilon = 23.452294^{\circ} - 0.0130125^{\circ}\, T - 0.164^{\circ} \cdot 10^{-5}\, T^2 + 0.0503^{\circ} \cdot 10^{-5}\, T^3 \qquad (115)$$

T denotes the time measured in Julian centuries of 36525 ephemeris days from the epoch (1900 Jan 0.5 ET). See Table 1 for Julian day numbers for the years 1950 through 2000.

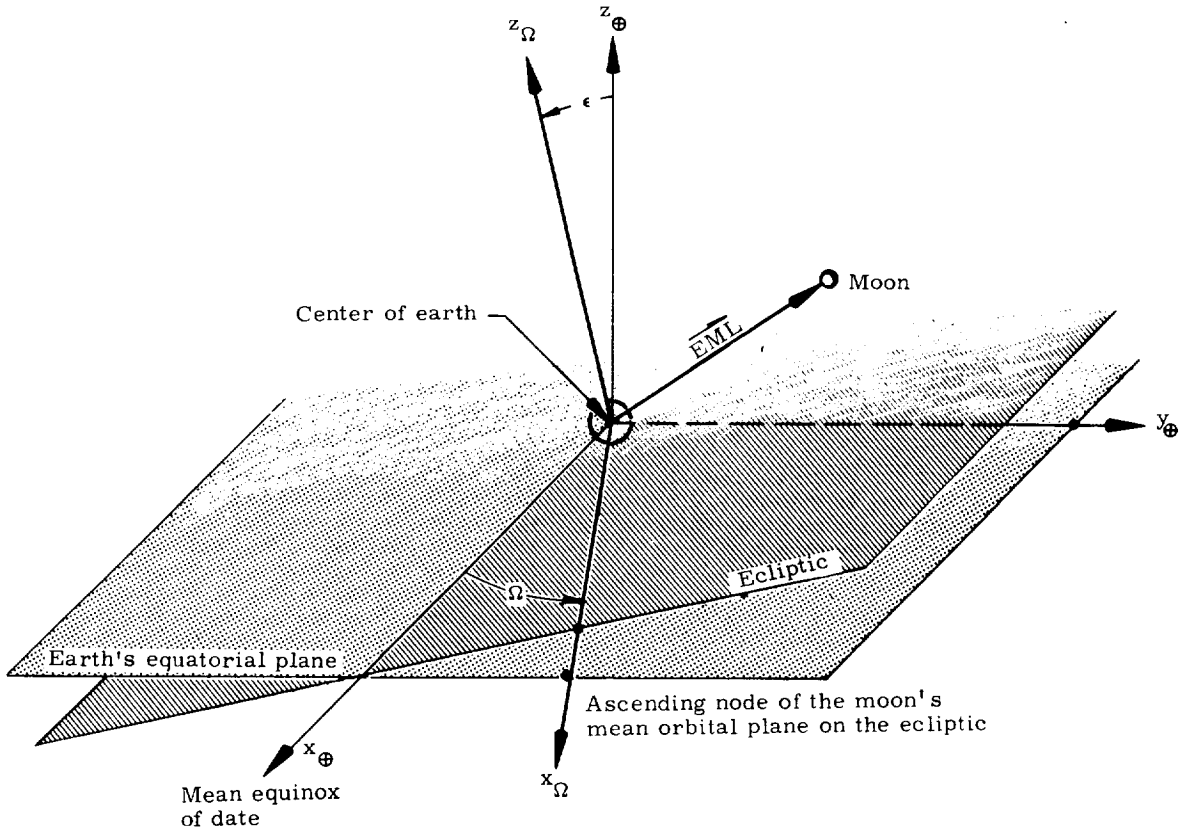

Ω (the longitude of the mean ascending node of the lunar orbit on the ecliptic, measured from the mean equinox of date)

$$\Omega = 259.183275° - 0.052953922° \, d + 0.002078° \, T^2 + 0.2° \cdot 10^{-5} T^3 \quad (116)$$

d denotes the number of ephemeris days from the epoch.

The transformation matrix giving $\overrightarrow{EML}$ in the ecliptic reference frame is:

$$(\overrightarrow{EML})_\Omega = \begin{pmatrix} x_\Omega \\ y_\Omega \\ z_\Omega \end{pmatrix} = \begin{bmatrix} \cos\Omega & \cos\epsilon \sin\Omega & \sin\epsilon \sin\Omega \\ -\sin\Omega & \cos\epsilon \cos\Omega & \sin\epsilon \cos\Omega \\ 0 & -\sin\epsilon & \cos\epsilon \end{bmatrix} \begin{pmatrix} x_{\oplus\mathbb{C}} \\ y_{\oplus\mathbb{C}} \\ z_{\oplus\mathbb{C}} \end{pmatrix} \quad (117)$$

In Ref. 2, optical librations are calculated using Hayn's value of 1.535° for the inclination (I) of the mean lunar equator to the ecliptic. The ascending node of the mean lunar equator on the ecliptic is at the descending node of the mean lunar orbit ($\Omega \pm 180°$). From the following sketch the $\overrightarrow{MEL}$ relative to the mean equatorial plane of the moon can be found.

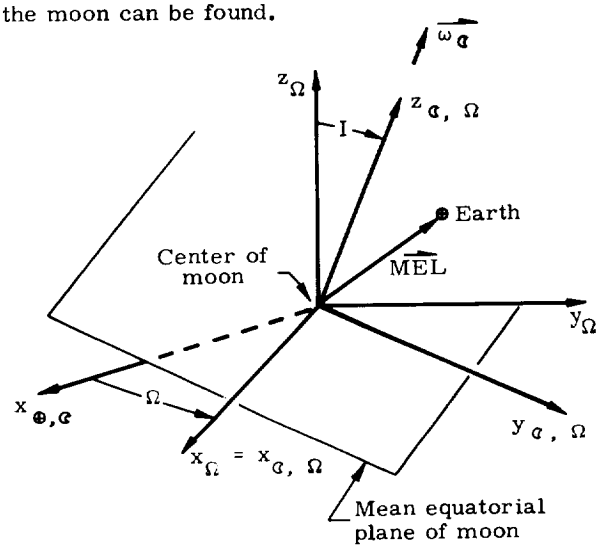

$\overrightarrow{MEL}$ (moon-earth line) = $-\overrightarrow{EML}$

The transformation is given by:

$$(\overrightarrow{MEL})_{\mathbb{C},\Omega} = \begin{pmatrix} x_{\mathbb{C},\Omega} \\ y_{\mathbb{C},\Omega} \\ z_{\mathbb{C},\Omega} \end{pmatrix} = \begin{bmatrix} 1 & 0 & 0 \\ 0 & \cos I & -\sin I \\ 0 & \sin I & \cos I \end{bmatrix} \begin{pmatrix} x_\Omega \\ y_\Omega \\ z_\Omega \end{pmatrix} \quad (118)$$

From the following sketch and the aforementioned definition of the MCP (the condition that the center of the apparent disk of the moon be at the mean center), the librations in longitude and latitude vanish simultaneously when $\mathbb{C} = \Omega$ and $\beta = 180°$.

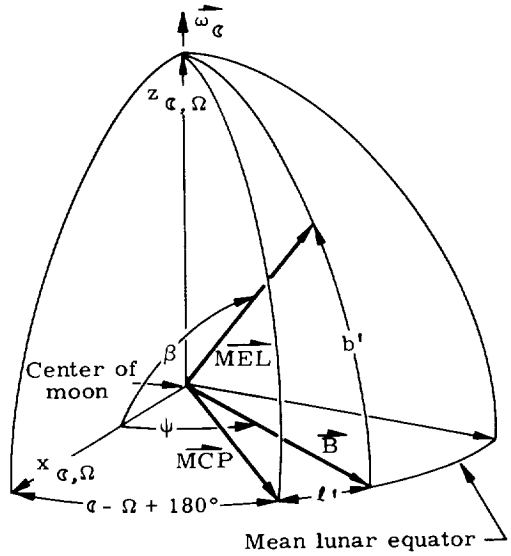

The symbols ℓ' and b' are the optical librations in longitude and latitude, respectively. The mean longitude of the moon $\mathbb{C}$, is given by the following series from Ref. 1.

$$\mathbb{C} = 270.434164° + 13.1763965286° \, d - 0.001133° \, T^2 + 0.19 \cdot 10^{-5°} T^3 \quad (119)$$

and is measured in the ecliptic from the mean equinox of date to the mean ascending node of the lunar orbit and then along the orbit. The prime meridian rotates at a rate ($\omega_{\mathbb{C}}$) which is equal to the mean orbital motion $n_{\mathbb{C}}$ of the moon. The optical libration in latitude is given by:

$$b' = 90° - \cos^{-1}\left(\frac{z_{\mathbb{C},\Omega}}{|\overrightarrow{MEL}|}\right) \quad (120)$$

Now the vector $\vec{B}$ is found by taking the vector triple product $\hat{z}_{\mathbb{C},\Omega} \times (\overrightarrow{MEL} \times \hat{z}_{\mathbb{C},\Omega})$. Therefore ψ, the angle measured from $x_{\mathbb{C},\Omega}$ to $\vec{B}$ is

$$\psi = \cos^{-1}\left(\frac{\vec{B} \cdot \hat{x}_{\mathbb{C},\Omega}}{|\vec{B}|}\right)$$

or

$$\psi = \cos^{-1}\left(\frac{x_{\mathbb{C},\Omega}}{|\vec{B}|}\right) \quad (121)$$

Thus, the optical libration in longitude equals:

$$\ell' = \psi - (\mathbb{C} - \Omega) - 180°. \quad (122)$$

These librations must be adjusted to account for the 'wobble' motion mentioned previously of the lunar north pole ($\vec{\omega}_{\mathbb{C}}$). Because of this

motion, the actual inclination and descending node of the lunar equator on the ecliptic are $I + \rho$ and $\Omega + \sigma$. It is well to note here that the physical librations are made up of forced and free librations. Free libration of the moon due to the gyroscopic motion has not been detected with certainty by observation and is neglected. The above equation represents the forced librations due to external torques (sun, earth, planets) on the moon.

From the Explanatory Supplement, Ref. 2, the physical librations ($\delta\ell$ and δb) can be found by the use of the following formulas:

$$\left.\begin{aligned} \delta\ell &= 0.003 \sin (\mathbb{C} - \Gamma') - 0.005 \sin 2 (\Gamma' - \Omega) \\ &\quad - 0.016 \sin g_{\odot} + 0.018\, \delta C b' \\ \delta b &= M + N \sin \ell' \end{aligned}\right\} \quad (123)$$

where

Γ' ~ the mean longitude of the lunar perigee, measured in the ecliptic from the mean equinox of date to the mean ascending node of the lunar orbit, and then along the orbit

$$\Gamma' = 334.329556^\circ + 0.1114040803^\circ d - 0.010325^\circ T^2 - 0.12^\circ \cdot 10^{-4} T^3 \quad (124)$$

$\ell_{\odot}$ ~ mean anomaly of the sun

$$\ell_{\odot} = 358.47583 + 0.98560267^\circ d - 0.00015^\circ T^2 - 0.3^\circ \cdot 10^{-5} T^3 \quad (125)$$

$$\delta C = M \sin \ell' - N$$

$$M = 0.04^\circ \sin (\Gamma' - \Omega) - 0.003^\circ \sin (\mathbb{C} - \Omega)$$

$$N = 0.02^\circ \cos (\Gamma' - \Omega) + 0.003^\circ \cos (\mathbb{C} - \Omega) \quad (126)$$

The values of the fundamental arguments given in Eqs (115), (119), (124) and (125) have been calculated from the Hill-Brown lunar theory. The actual librations are the sums of the optical and physical librations in longitude and latitude, respectively

$$\left.\begin{aligned} \ell \text{ (libration in longitude)} &= \ell' + \delta\ell \\ b \text{ (libration in latitude)} &= b' + \delta b \end{aligned}\right\} \quad (127)$$

For reference and mission planning purposes, a future addendum will contain the actual librations in one-day intervals.

As mentioned in Section C-1 above, a future addendum will present the geocentric rectangular coordinates of the moon referred to the mean equinox of date in one-half day intervals. The components $(x_{\oplus\mathbb{C}}, y_{\oplus\mathbb{C}}, z_{\oplus\mathbb{C}})$ are in earth radii for the years 1965 to 1969 and stored in the interplanetary trajectory program (Ref. 18). A continuous readout of librations can be obtained by curve fitting the positional data of the moon and utilizing the formulas presented in this section.

D. REFERENCES

1. "American Ephemeris and Nautical Almanac," published annually by the Nautical Almanac Office, United States Naval Observatory, Washington, D.C. (obtainable from the Supt. of Documents, U.S. Govt. Printing Office, Washington 25, D.C.)

2. "Explanatory Supplement to the Astronomical Ephemeris and the American Ephemeris and Nautical Almanac," Her Majesty's Stationery Office, London, 1961.

3. "Orbital Flight Handbook," Martin Company, Space Systems Division, Baltimore, Md., ER 12684, 1963.

4. Koskela, P., "Selenographic Coordinates for the Air Force Lunar Trajectory Program," Aeronutronic Systems Interim Technical Note 3 ASI Publication U-325, January 6, 1959.

5. Baker, R. M. L., and Makemson, M. W., "An Introduction to Astrodynamics," Academic Press, New York, 1960.

6. Kalensher, B. E., "Selenographic Coordinates," Jet Propulsion Laboratory, Pasadena, Calif., Technical Report 32-41, February 24, 1961.

7. Novak, D., "Simplified Lunar Trajectory Digital Program," Martin Marietta Corp., Space Systems Division, Baltimore, Md.

8. Moulton, F. R., "An Introduction to Celestial Mechanics," MacMillan, New York, 1914.

9. Finlay-Freundlich, E., "Celestial Mechanics," Pergamon Press, New York, 1958.

10. Egorov, V. A., "Certain Problems of Moon Flight Dynamics," Russian Literature of Satellites, Part 1, Intern. Phys. Index, New York, 1958.

11. Buchheim, R. W., "Lunar Flight Trajectories," The Rand Corp, Report P-1268, January 30, 1958.

    Also: Seifert, H. S., ed., "Space Technology," John Wiley and Sons, New York, Chapter 7, 1959.

12. Plummer, H. C., "An Introductory Treatise on Dynamical Astronomy," Dover Publications, New York, 1960.

13. Brown, E. W., "An Introductory Treatise on the Lunar Theory," Dover Publications, New York, 1960.

14. Brouwer, D., and Clemence, G. M., "Methods of Celestial Mechanics," Academic Press, New York, 1961.

15. Brown, E. W., "Tables of the Motion of the Moon," Yale University Press, New Haven, Conn., 1919.

16. Anon., "Improved Lunar Ephemeris 1952 to 1959," Nautical Almanac Office, United States Naval Observatory, Washington, 1954.

17. Woolston, D. S., "Declination, Radial Distance and Phases of the Moon for the Years 1961 to 1971 for Use in Trajectory Considerations," NASA Technical Note D-911, Washington, August 1961.

18. Pines, S., and Wolf, H., "Interplanetary Trajectory by Encke Method Programmed for the IBM 704," Republic Aviation Corp., Report RAC-656-450, December 15, 1959.

TABLE AND ILLUSTRATIONS

		Page
Table 1	Julian Day Numbers for the Years 1950 to 2000	III-39
Fig. 1	Selenographic Coordinate System Superimposed on a Lunar Photograph	III-40
Fig. 2	Curves of Zero Relative Velocity in the $x_R y_R$ Plane	III-41
Fig. 3	Lunar Librations During October 1966 and October 1967	III-42

TABLE 1

Julian Day Numbers for the Years 1950-2000
(based on Greenwich Noon)

Year	Jan. 0.5	Feb. 0.5	Mar. 0.5	Apr. 0.5	May 0.5	June 0.5	July 0.5	Aug. 0.5	Sept. 0.5	Oct. 0.5	Nov. 0.5	Dec. 0.5
1950	243 3282	3313	3341	3372	3402	3433	3463	3494	3525	3555	3586	3616
1951	3647	3678	3706	3737	3767	3798	3828	3859	3890	3920	3951	3981
1952	4012	4043	4072	4103	4133	4164	4194	4225	4256	4286	4317	4347
1953	4378	4409	4437	4468	4498	4529	4559	4590	4621	4651	4682	4712
1954	4743	4774	4802	4833	4863	4894	4924	4955	4986	5016	5047	5077
1955	243 5108	5139	5167	5198	5228	5259	5289	5320	5351	5381	5412	5442
1956	5473	5504	5533	5564	5594	5625	5655	5686	5717	5747	5778	5808
1957	5839	5870	5898	5929	5959	5990	6020	6051	6082	6112	6143	6173
1958	6204	6235	6263	6294	6324	6355	6385	6416	6447	6477	6508	6538
1959	6569	6600	6628	6659	6689	6720	6750	6781	6812	6842	6873	6903
1960	243 6934	6965	6994	7025	7055	7086	7116	7147	7178	7208	7239	7269
1961	7300	7331	7359	7390	7420	7451	7481	7512	7543	7573	7604	7634
1962	7665	7696	7724	7750	7785	7816	7846	7877	7908	7938	7969	7999
1963	8030	8061	8089	8120	8150	8181	8211	8242	8273	8303	8334	8364
1964	8395	8426	8455	8486	8516	8547	8577	8608	8639	8669	8700	8730
1965	243 8761	8792	8820	8851	8881	8912	8942	8973	9004	9034	9065	9095
1966	9126	9157	9185	9216	9246	9277	9307	9338	9369	9399	9430	9460
1967	9491	9522	9550	9581	9611	9642	9672	9703	9734	9764	9795	9825
1968	9856	9887	9916	9947	9977	*0008	*0038	*0069	*0100	*0130	*0161	*0191
1969	244 0222	0253	0281	0312	0342	0373	0403	0434	0465	0495	0526	0556
1970	244 0587	0618	0646	0677	0707	0738	0768	0799	0830	0860	0891	0921
1971	0952	0983	1011	1042	1072	1103	1133	1164	1195	1225	1256	1286
1972	1317	1348	1377	1408	1438	1469	1499	1530	1561	1591	1622	1652
1973	1683	1714	1742	1773	1803	1834	1864	1895	1926	1956	1987	2017
1974	2048	2079	2107	2138	2168	2199	2229	2260	2291	2321	2352	2382
1975	244 2413	2444	2472	2503	2533	2564	2594	2625	2656	2686	2717	2747
1976	2778	2809	2838	2869	2899	2930	2960	2991	3022	3052	3083	3113
1977	3144	3175	3203	3234	3264	3295	3325	3356	3387	3417	3448	3478
1978	3509	3540	3568	3599	3629	3660	3690	3721	3752	3782	3813	3843
1979	3874	3905	3933	3964	3994	4025	4055	4086	4117	4147	4178	4208
1980	244 4239	4270	4299	4330	4360	4391	4421	4452	4483	4513	4544	4574
1981	4605	4636	4664	4695	4725	4756	4786	4817	4848	4878	4909	4939
1982	4970	5001	5029	5060	5090	5121	5151	5182	5213	5243	5274	5304
1983	5335	5366	5394	5425	5455	5486	5516	5547	5578	5608	5639	5669
1984	5700	5731	5760	5791	5821	5852	5882	5913	5944	5974	6005	6035
1985	244 6066	6097	6125	6156	6186	6217	6247	6278	6309	6339	6370	6400
1986	6431	6462	6490	6521	6551	6582	6612	6643	6674	6704	6735	6765
1987	6796	6827	6855	6886	6916	6947	6977	7008	7039	7069	7100	7130
1988	7161	7192	7221	7252	7282	7313	7343	7374	7405	7435	7466	7496
1989	7527	7558	7586	7617	7647	7678	7708	7739	7770	7800	7831	7861
1990	244 7892	7923	7951	7982	8012	8043	8073	8104	8135	8165	8196	8226
1991	8257	8288	8316	8347	8377	8408	8438	8469	8500	8530	8561	8591
1992	8622	8653	8682	8713	8743	8774	8804	8835	8866	8896	8927	8957
1993	8988	9019	9047	9078	9108	9139	9169	9200	9231	9261	9292	9322
1994	9353	9384	9412	9443	9473	9504	9534	9565	9596	9626	9657	9687
1995	244 9718	9749	9777	9808	9838	9869	9899	9930	9961	9991	*0022	*0052
1996	245 0083	0114	0143	0174	0204	0235	0265	0296	0327	0357	0388	0418
1997	0449	0480	0508	0539	0569	0600	0630	0661	0692	0722	0753	0783
1998	0814	0845	0873	0904	0934	0965	0995	1026	1057	1087	1118	1148
1999	245 1179	1210	1238	1269	1299	1330	1360	1391	1422	1452	1483	1513
2000	245 1544	1575	1604	1635	1665	1696	1726	1757	1788	1818	1849	1879

1900 Jan 0.5 ET = Julian Day 2,415,020.0 = Greenwich Noon, January 1, 1900, a common epoch
1950 Jan 0.5 ET = Julian Day 2,433,282.0 = Greenwich Noon, January 1, 1950, another common epoch and first entry in this table

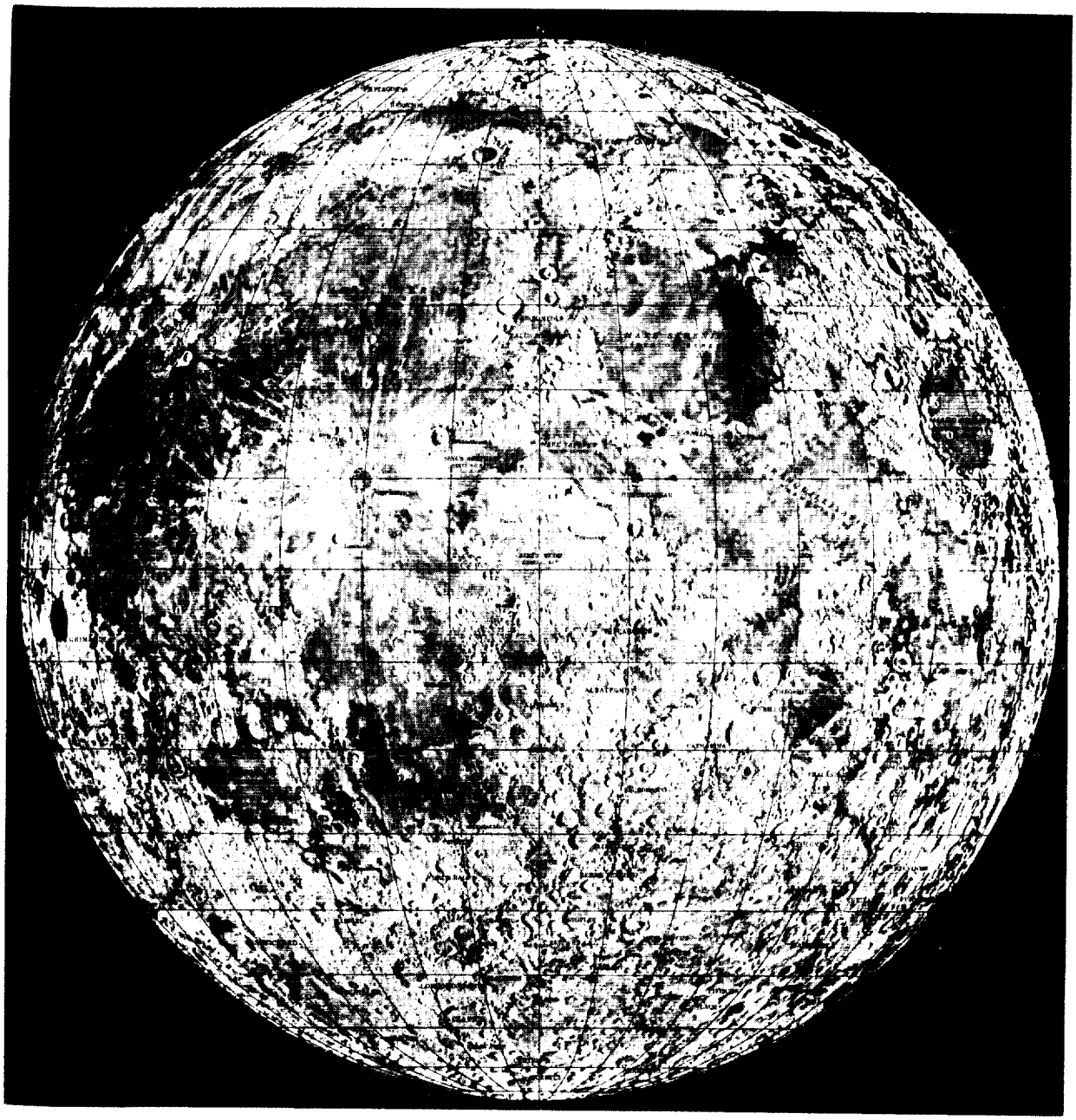

Fig. 1. Selenographic Coordinate System Superimposed on a Lunar Photograph

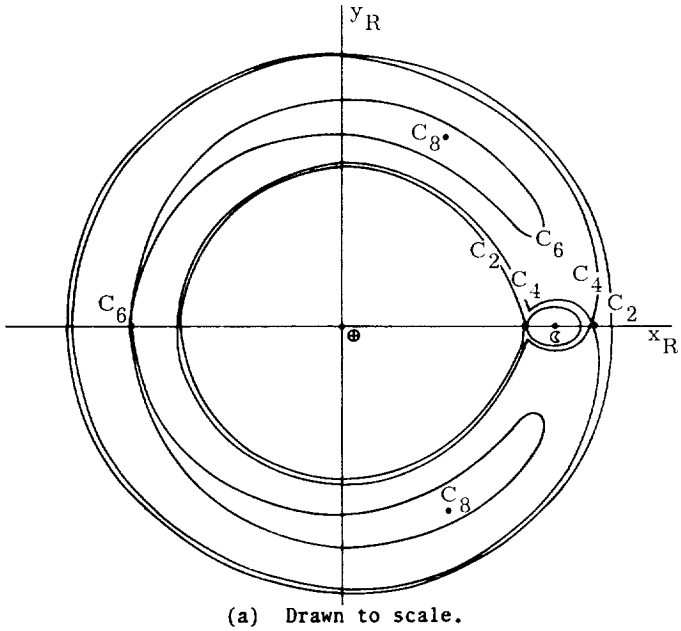

(a) Drawn to scale.

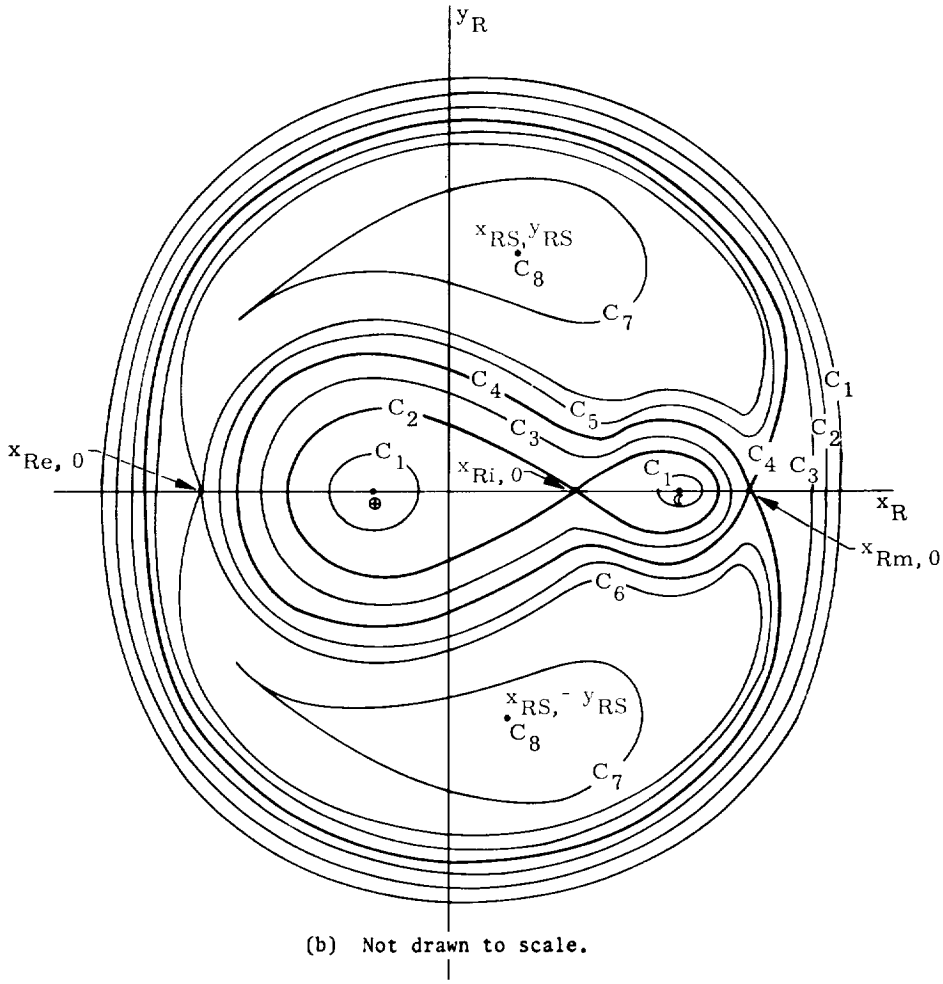

(b) Not drawn to scale.

Fig. 2. Curves of Zero Relative Velocity in the $x_R y_R$ Plane

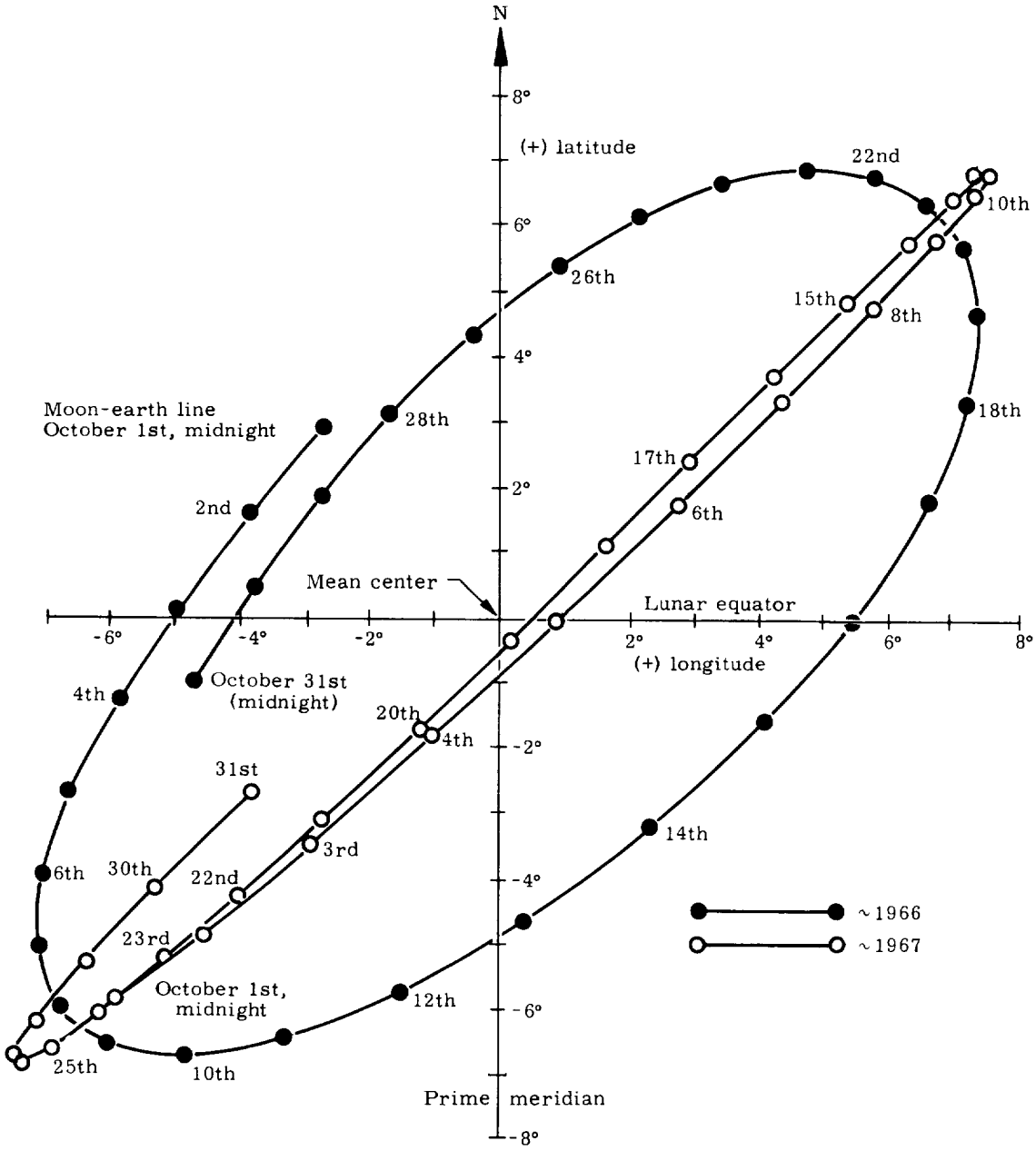

Fig. 3. Lunar Librations During October 1966 and October 1967

CHAPTER IV

TRAJECTORIES IN THE EARTH-MOON SYSTEM

Prepared by:

F. Martikan, L. Emery, F. Santora,
T. Garceau and A. Jazwinski
Martin Company (Baltimore)
Aerospace Mechanics Department
March 1963

Page

A. Classification and Nomenclature of Lunar Missions and Trajectories IV-1

B. Force Models for Lunar Trajectory Calculations IV-13

C. The Voice Technique IV-39

D. Additional Class of Circumlunar Orbits IV-42

E. References IV-43

Tables and Illustrations IV-45

IV. TRAJECTORIES IN THE EARTH-MOON SYSTEM

This chapter will apply the introductory material on kinematics and dynamics of the earth-moon system from Chapter III to space vehicle trajectories in earth-moon space. The force models and methods of solving the equations of motion will be discussed with emphasis on the approximations introduced and the usefulness of various trajectory programs. Some typical trajectories in earth-moon space will be sketched and described briefly in order to illustrate the types of lunar missions to be contemplated in succeeding chapters.

Section A gives a classification of lunar trajectories, and introduces the nomenclature of lunar trajectories to facilitate their visualization when results will be presented later in the manual. Section B describes the various force models that are used in lunar trajectory calculation, i.e.: (1) the restricted two-body trajectories for which analytical solutions are available, (2) their patching to form a complete earth-moon trajectory, (3) restricted three-body trajectories, (4) n-body trajectories with earth oblateness and triaxiality of the moon included, as well as a discussion of nongravitational forces and their simulation on the digital computer. Finally, Section C gives a description of the Voice trajectory computation technique which has been used extensively in obtaining lunar trajectories in this manual.

A. CLASSIFICATION AND NOMENCLATURE OF LUNAR MISSIONS AND TRAJECTORIES

1. General Considerations

Trajectory studies can be divided into two broad groups, feasibility and precision trajectories. Feasibility trajectories are used for preliminary vehicle performance studies such as injection requirements, maneuvering requirements, tolerances on flight parameters, guidance accuracies, observational constraints. Precision trajectories, on the other hand, are used for the detailed planning of an actual flight. In this latter approach the best values of parameters influencing the trajectory may be used to compute a nominal path, or to include correctional information, based on observations of the vehicle, in the trajectory calculation to obtain a path that is frequently updated during the flight. In this handbook most of the computed trajectories are of the feasibility type.

For the present qualitative discussion of lunar trajectories and missions it is not necessary to consider all the forces that act on the space vehicle, but only those which determine the characteristics of the lunar trajectories. The assumptions made in this section are:

(1) Gravitational effects of the sun and planets on lunar trajectories can be neglected because the region where the gravitational attraction of the earth and moon predominate extends in all directions about three times the earth-moon distance from earth.

(2) Atmospheric drag is neglected during the brief portion of the lunar trajectory in the earth's atmosphere, since the space vehicle reaches the required velocity for passage to the moon while it is more than 100 km above the surface of the earth.

(3) Lunar trajectories are assumed ballistic, i.e., no thrust forces act on the vehicle. Lunar missions, on the other hand, may include phases when large thrust forces alter the subsequent vehicle trajectory. Lunar missions with a continuous low thrust will not be considered here.

(4) The earth and moon are in circular orbits around the earth-moon barycenter (the small eccentricity of the lunar orbit can be neglected in qualitative trajectory discussions).

These facts suggest the use of the restricted three-body problem discussed in Chapter III as a force model for discussion of lunar trajectories. Sometimes an even simpler force model may describe the trajectory:

Two-body equations (earth-space vehicle) are used on most of the trajectory to the moon, and at some point near the moon a transformation to selenocentric coordinates is performed and two-body equations (moon-space vehicle) are used to describe the trajectory near the moon. This last simplification will be discussed further in Sections B-1 and C of the present chapter.

Any sketches of trajectories will be made either in nonrotating coordinates $x_e y_e z_e$ with origin at the center of the earth, nonrotating coordinates $x_m y_m z_m$ with origin at the center of the moon, or in rotating coordinates $x_R y_R z_R$ with origin at the barycenter and the x_R-axis along the earth-moon line in the direction of the moon (see sketch on page IV-20). A typical lunar trajectory is plotted to scale in geocentric nonrotating coordinates in Fig. 1 and in barycentric rotating coordinates in Fig. 2 with the time from injection indicated on each trajectory. The nonrotating trajectory shows the characteristic shape of a two-body conic section near the earth, and it is not until the moon is approached closely that the moon's gravitational attraction modifies the shape of this conic section. The path in the rotating coordinate system is approximately as it would appear to an observer at the center of the moon, since the moon's mean orbital motion is equal to the rotational rate about its axis. The qualification "approximately" is included because the difference between the true and mean orbital motion due to eccentricity $e_{\mathbb{C}}$ and the small inclination of the lunar spin axis to its orbital plane (both given by optical librations) cause the lunar observer to see a slightly different trajectory as the $x_R y_R$ coordinate trace.

As the title of this section indicates, lunar flights may be classified either into classes of trajectories, as was done notably by Egorov (Ref. 1) and Buchheim (Ref. 2), i.e., the trajectories are subdivided by their shape in an inertial or rotating coordinate system, or lunar flights may be classified into classes of missions according to the purpose of the flight. In general, the mission classification is broader since one mission, or one lunar flight, may consist of several trajectory classes. In this chapter, a lunar flight is defined as a space flight, on which the velocity at the initial point of the trajectory equals or exceeds the minimum velocity to leave the earth at the initial point and whose primary mission goal is in earth-moon space. Thus the boost or earth orbit phase of any trajectory will not be considered here, nor will any part of it outside of a region where the gravitational attraction of the earth and moon predominate. The table below classifies such lunar flights into the various mission and trajectory classes:

Mission Class	Trajectory Class
1. Lunar probes	Trajectories near minimum velocities
	Approach trajectories
	Impact trajectories (hard landing)
	Impact trajectories (soft landing)
2. Circumlunar and allunar missions	Circumlunar trajectories (nonperiodic and periodic)
	Allunar trajectories (nonperiodic and periodic)
3. Lunar orbit missions	Impact trajectories Approach trajectories Circumlunar trajectories Allunar trajectories Orbits around the moon
4. Landing missions	Approach trajectories Circumlunar trajectories Allunar trajectories Orbits around the moon Ascent and descent trajectories Impact trajectories
5. Space stations	Libration point buoys
6. Lunar passages to escape	Approach trajectories (accelerating or braking approaches)

The lunar missions in the classification above have been arranged chronologically, i.e., a planned exploration of the moon and solar system would at first involve lunar probes, then circumlunar (passing behind the moon) or allunar (passing in front of the moon) missions, lunar orbits, landings on the moon, establishment of long-term space stations in earth-moon space, and finally the use of the gravitational attraction of the moon to accelerate or decelerate space vehicles on their journey to the planets. Of course there may be a certain amount of overlapping so that for any given time the plan may call for lunar probes as well as circumlunar missions, or for circumlunar, lunar orbit, as well as landing missions. Most of the classes of lunar missions may be used for research and exploration, for military roles, as well as exploitation and colonization of the moon. Since the lunar flight manual is essentially mission-oriented, it is preferable to discuss qualitatively each class of mission and describe the various types of trajectories associated with the mission in the order of their first appearance.

Prior to this classification it is instructive to compare approximate propulsion requirements for typical lunar missions from earth launch. These requirements are given below in terms of the characteristic velocity increment ΔV, or the velocity the space vehicle would attain in gravity-free space if it were accelerated in a straight line by the equivalent amount of rocket burning:

Mission	ΔV (km/sec)
1. Lunar probe without rocket burning near the moon	12.5
2. Circumlunar mission	12.5
3. Circumlunar mission with deceleration by rockets to earth orbit velocity	16
4. Establishment of a lunar orbit	13.5
5. Establishment of a lunar orbit return to earth and deceleration by rockets to earth orbit velocity	18
6. Landing on the moon	14.5
7. Landing on the moon with return to earth orbit velocity	20.0

The higher velocities in missions 3 through 7 reflect additional rocket burning in the vicinity of the moon or during earth return. The return to earth orbit and eventually to an earth landing base may be accomplished largely by aerodynamic maneuvering and hence reduce the total propulsion requirements for a mission with earth return.

2. Lunar Probes

A lunar probe is defined as a one-way, unmanned space vehicle for the collection of scientific data passing the vicinity of the moon but which does not pass behind the moon. The trajectory classes associated with probes are ballistic except for possible braking prior to lunar impact. Probes are used to obtain scientific data in earth-moon space, near the moon, and on the lunar surface as the name implies. Typical measurements may include (Ref. 2):

(1) A determination of the mass of the moon.

(2) Measurement of magnetic fields, electromagnetic and corpuscular radiation, meteoritic densities and of other environmental data in earth-moon space.

(3) Determination of the physical properties of the very tenuous lunar atmosphere.

(4) Determination of the composition, properties, temperature variation, and radioactivity of the lunar surface.

(5) Determination of the seismic properties of the lunar interior.

In addition, lunar probes may serve as engineering test vehicles for the evaluation of space vehicle systems such as tracking, communication, environmental control and power systems.

The associated trajectory classes may be:

(1) Trajectories near minimum velocities, or those which have just sufficient energy to eventually leave the earth, and will, at least initially, return to the vicinity of the earth several times.

(2) Approach trajectories, which have a higher energy, and are defined as trajectories which reach the vicinity of the moon on the first orbit but miss it by some distance.

(3) Impact trajectories which directly strike the moon either without rocket braking or with rocket braking near the moon. Impact trajectories can be classified further. If the impact velocity on the lunar surface is of the order of tens of m/sec, the impact can be classified as a soft landing while impact speeds of about 100 m/sec and above are called hard landings.

a. Trajectories near minimum velocities; transit time

In this section the results of the previous restricted three-body discussion will be applied to this trajectory class, its characteristics will be discussed in detail, and the strong effect of injection velocity on transit time near minimum velocities will be illustrated.

The ballistic trajectory of a space vehicle is completely determined by its initial position and velocity. These injection conditions (or initial conditions for lunar trajectories near earth) are usually given either in earth-centered trajectory coordinates $x_e y_e z_e$ and velocity components $\dot{x}_e \dot{y}_e \dot{z}_e$, where $\dot{x}_e = \frac{dx_e}{dt}$, or in terms of $r_{e\Delta}$, $V_{e\Delta}$, γ_e and η_e (for trajectories in the moon's orbital plane) as illustrated in the following sketch:

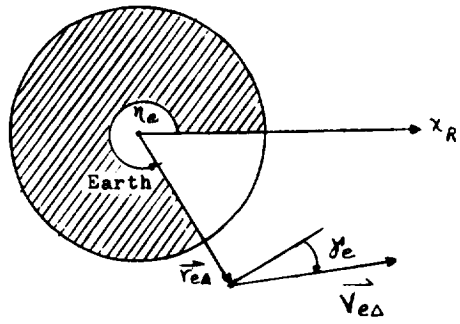

A subscript zero is used to specify injection conditions. Injection time must be held within close tolerances since the earth, moon, and space vehicle all move quite rapidly with respect to each other.

It was shown in Subsection B-2, Chapter III that the minimum velocity to reach the moon from earth corresponded to a value of $C_2 = 3.34367$ $(km/sec)^2$ for the Jacobi constant. This value was related to the injection velocity in the rotating $x_R y_R z_R$ coordinate system, $\vec{V}_{R\Delta}$, the magnitude of $V_{R\Delta}$ being independent of its direction and nearly independent of the angle between the initial radius vector $\vec{r}_{R\Delta} = \vec{r}_{e\Delta}$ and the x_R-axis. The maximum variation of $V_{R\Delta}$ with this angle was of the order of 0.1 m/sec for $r_{e\Delta} = 7378.2$ km and less for smaller values of $r_{e\Delta}$. However, a change in injection altitude from 100 km ($r_{e\Delta} = 6478.2$ km) to 1000 km ($r_{e\Delta} = 7378.2$ km) decreased the minimum $V_{R\Delta}$ from 10942.2 m/sec to 10233.2 m/sec.

It is now necessary to relate the injection velocity in rotating coordinates, $\vec{V}_{R\Delta 0}$ ($\dot{x}_{R\Delta 0}$, $\dot{y}_{R\Delta 0}$, $\dot{z}_{R\Delta 0}$) to the velocity in geocentric nonrotating coordinates $\vec{V}_{e\Delta 0}$ ($\dot{x}_{e\Delta 0}$, $\dot{y}_{e\Delta 0}$, $\dot{z}_{e\Delta 0}$). The general transformation between the velocity components of the two coordinate systems was given by Eq (86) of Chapter III,

$$\begin{Bmatrix} \dot{x}_{e\Delta} \\ \dot{y}_{e\Delta} \\ \dot{z}_{e\Delta} \end{Bmatrix} = \begin{bmatrix} \cos(\Phi + \omega_{\oplus\mathbb{C}} t) & -\sin(\Phi + \omega_{\oplus\mathbb{C}} t) & 0 \\ \sin(\Phi + \omega_{\oplus\mathbb{C}} t) & \cos(\Phi + \omega_{\oplus\mathbb{C}} t) & 0 \\ 0 & 0 & 1 \end{bmatrix} \cdot \begin{Bmatrix} \dot{x}_{R\Delta} - \omega_{\oplus\mathbb{C}} y_{R\Delta} \\ \dot{y}_{R\Delta} + \omega_{\oplus\mathbb{C}} (x_{R\Delta} + \bar{r}_{\oplus\mathbb{C}} \nu) \\ \dot{z}_{R\Delta} \end{Bmatrix} \quad (1)$$

where

$\nu = \frac{M_{\leftmoon}}{M_{\oplus} + M_{\leftmoon}} = 0.01214216$, $\bar{r}_{\oplus\leftmoon} = 384747.2$ km

is the lunar unit or earth-moon distance used for the circular restricted three-body problem, $\omega_{\oplus\leftmoon} = 2.661699484 \times 10^{-6}$ rad/sec is the rotational rate of the earth-moon line around the barycenter, and Φ is the initial angle between the nonrotating and rotating coordinate systems.

If the matrix multiplication is performed $V_{e\Delta}^2$ is obtained as:

$$V_{e\Delta}^2 = V_{R\Delta}^2 + \omega_{\oplus\leftmoon}^2 \left[y_{R\Delta}^2 + (x_{R\Delta} + \bar{r}_{\oplus\leftmoon}\ \nu)^2 \right] + 2\omega_{\oplus\leftmoon} \left[\dot{x}_{R\Delta}\ y_{R\Delta} + \dot{y}_{R\Delta}\ (x_{R\Delta} + \bar{r}_{\oplus\leftmoon}\ \nu) \right] \quad (2)$$

This expression can be transformed further by reference to the following sketch:

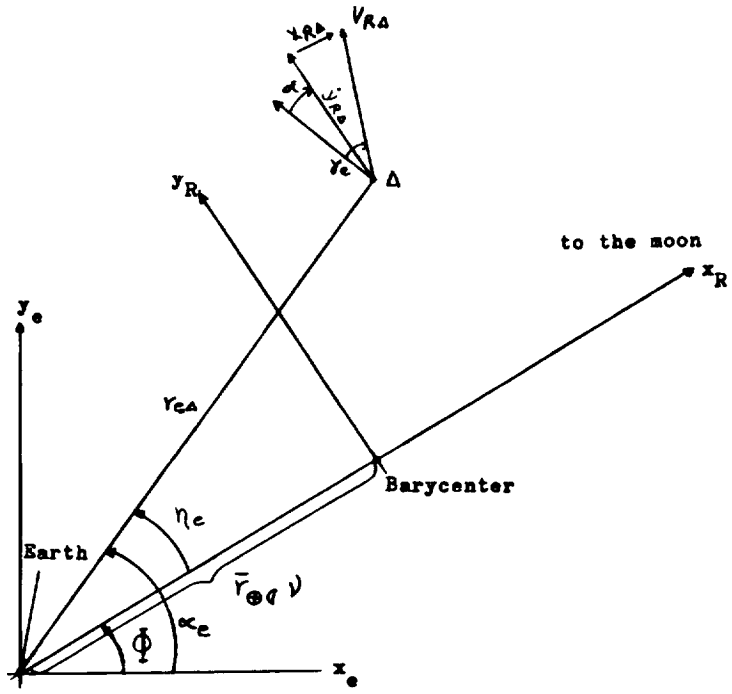

The following relations can be obtained from the previous sketch:

$$r_{e\Delta}^2 = x_{e\Delta}^2 + y_{e\Delta}^2 = (x_{R\Delta} + \bar{r}_{\oplus\leftmoon}\ \nu)^2 + y_{R\Delta}^2 \quad (3)$$

and

$$y_{R\Delta} = r_{e\Delta} \sin \eta_e,\quad x_{R\Delta} + \bar{r}_{\oplus\leftmoon}\ \nu = r_{e\Delta} \cos \eta_e \quad (4)$$

which yield, after substitution into Eq (2):

$$V_{e\Delta}^2 = V_{R\Delta}^2 + r_{e\Delta}^2\, \omega_{\oplus\leftmoon}^2 + 2\omega_{\oplus\leftmoon}\, r_{e\Delta} (\dot{x}_{R\Delta} \sin \eta_e + \dot{y}_{R\Delta} \cos \eta_e) \quad (5)$$

In terms of the flight path angle relative to earth γ_e

$$\dot{x}_{R\Delta} \sin \eta_e + \dot{y}_{R\Delta} \cos \eta_e = V_{R\Delta} \cos \gamma_e,$$

so that the square of the velocity relative to earth becomes:

$$V_{e\Delta}^2 = V_{R\Delta}^2 + r_{e\Delta}^2\, \omega_{\oplus\leftmoon}^2 + 2\omega_{\oplus\leftmoon}\, r_{e\Delta}\, V_{R\Delta} \cos \gamma_e. \quad (6)$$

For given values of $r_{e\Delta}$ and $V_{R\Delta}$ in the earth-moon system the velocity relative to earth $V_{e\Delta}$ is a maximum if $\cos \gamma_e = 1$ ($\gamma_e = 0°$) and it is a minimum if $\cos \gamma_e = -1$ ($\gamma_e = 180°$), or

$$\left[V_{R\Delta}^2 + r_{e\Delta}^2\, \omega_{\oplus\leftmoon}^2 - 2\omega_{\oplus\leftmoon}\, r_{e\Delta}\, V_{R\Delta} \right]^{1/2} \leq V_{e\Delta} \leq \left[V_{R\Delta} + r_{e\Delta}^2\, \omega_{\oplus\leftmoon}^2 + 2\omega_{\oplus\leftmoon}\, r_{e\Delta}\, V_{R\Delta} \right]^{1/2} \quad (7)$$

For injection at 100-km altitude:

$$r_{e\Delta 0} = 6478.2 \text{ km},\ V_{R\Delta 0} = 10942.2 \text{ m/sec},$$

$$10925.0 \text{ m/sec} \leq V_{e\Delta 0} \leq 10959.4 \text{ m/sec},$$

and the minimum velocity relative to earth for sending a vehicle to the moon is 10925.0 m/sec, while for injection at 1000-km altitude:

$$r_{e\Delta} = 7378.2 \text{ km},\ V_{R\Delta 0} = 10233.2 \text{ m/sec},$$

$$10213.6 \text{ m/sec} \leq V_{e\Delta 0} \leq 10252.8 \text{ m/sec}$$

and the minimum velocity relative to earth for lunar injection at that altitude is 10213.6 m/sec. In each case the maximum value of $V_{e\Delta 0}$, $(V_{e\Delta})_{max}$, occurs when $V_{e\Delta 0}$ is perpendicular to $r_{e\Delta}$ in the direction of the moon's rotation as illustrated in the following sketch:

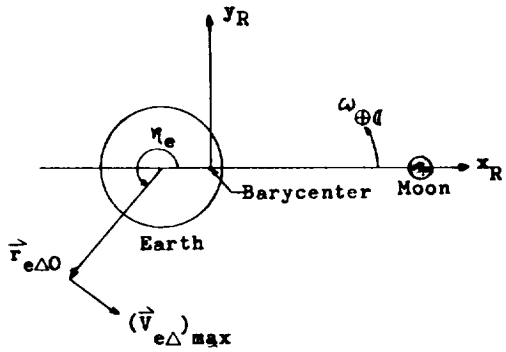

The injection flight path angle γ_{e0} may be used to classify lunar trajectories. Thus, a space vehicle trajectory in the direction of the earth-moon orbital motion($\gamma_{e0} < 90°$) illustrated in the previous sketch is known as a direct trajectory. Since the angular velocity vector of the earth $\vec{\omega}_{\oplus}$ has a component $\omega_{\oplus} \cos i_{em}$ perpendicular to the earth-moon orbital plane (MOP), a vehicle in a direct trajectory can capitalize on the rotation of the earth as well as the orbital motion of the earth in the MOP as illustrated above. Trajectories with injection in a sense opposite to $\omega_{\oplus}$ ($\gamma_{e0} > 90°$) are called retrograde trajectories. The ΔV penalty from launch for a retrograde trajectory as compared to a direct trajectory may be as high as 740 m/sec.

The gravitational attraction of the moon on the lunar trajectory near injection is very small, and it is possible to approximate the first stages of a lunar trajectory by a two-body earth-space vehicle problem. In a two-body approximation, the escape or parabolic velocity at 100 km is

$$V_{ep} = \sqrt{\frac{2\mu_{\oplus}}{r_{e\Delta}}} = 11093.2 \text{ m/sec}$$

which compares with a minimum restricted three-body velocity of

$$(V_{e\Delta})_{min} = 10925.0 \text{ m/sec.}$$

The corresponding minimum two and restricted three-body velocities for injection at 1000 km are:

$$V_{ep} = 10394.6 \text{ m/sec}, \quad (V_{e\Delta})_{min} =$$

$$10213.6 \text{ m/sec}$$

Thus, the minimum three-body velocity is only about 170 m/sec less than the two-body parabolic velocity. This indicates that lunar trajectories for near minimum velocities will approximate two-body ellipses with initial eccentricities near 1 (i.e., when the gravitational effect of the earth is predominant). As the injection velocity is increased, the trajectories will approximate two-body parabolas and hyperbolas in their initial stages. The extent along the trajectory to the moon to which this two-body approximation can be carried will be discussed in Subsection B-1c.

Egorov (Ref. 1) has made a systematic study of trajectories in the MOP near minimum velocities. These trajectories with a Jacobi constant of C_3 (refer to Fig. 2, Chapter III) have the characteristic of an extremely long transit time in the order of months. For example, consider trajectories with $\gamma_{e0} = 0°$. In geocentric $x_e y_e$ coordinates these trajectories closely approximate two-body ellipses with large eccentricities (near 1). The apogee of these trajectories increases slowly due to lunar perturbations as illustrated in the following sketch; only the first several orbits of a typical earth-moon trajectory near minimum velocity are shown.

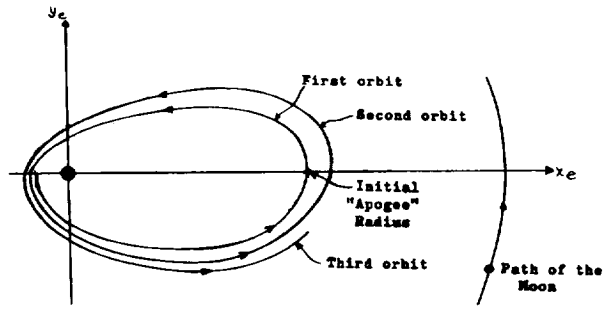

The space vehicle must traverse many such near-elliptical orbits before it can pass through the constriction in the C_3 contour near the double point between the earth and moon and approach the moon (Fig. 2, Chapter III). Increase of γ_{e0} will increase the required $V_{e\Delta 0}$ as well as the initial apogee radius of the trajectory.

The time required for a passage from the earth to the moon depends strongly on the injection velocity. It has been estimated (Ref. 1) that trajectories at the minimum velocity reach the boundary of their region C_2 in about three years. This type of trajectory thus is impractical for most lunar missions. A slight increase in injection velocity reduces the transit time significantly as can be noted from the following trajectories to the moon in the MOP with an injection altitude of $h_{\oplus 0} = r_{e\Delta 0} - R_e = 175.7$ km and with $\gamma_{e0} = 0°$:

Injection Velocity, $V_{e\Delta 0}$ (m/sec)		
γ_{e0} = 0°	γ_{e0} = 0°	
$r_{e\Delta 0}$ = 6478.2 km	$r_{e\Delta 0}$ = 6553.9 km	Transit Time to the Moon (hr)
$h_{\oplus 0}$ = 100 km	$h_{\oplus 0}$ = 175.7 km	
10,997	10,932	120
11,008	10,943	80
11,097	11,033	50
11,278	11,215	35
11,660	11,600	24
13,450	13,400	13

The injection velocity for an injection altitude of 100 km has been calculated from the energy integral of a two-body force model, Eq (9) below, to allow a direct comparison with the minimum restricted three-body velocity of 10959 m/sec.

An increase in injection velocity of 100 m/sec or about 1% near the minimum velocity decreases the transit time from five to about two days, but for any further significant decrease in transit time the injection velocity must be increased considerably. Hence, for each lunar mission there is a tradeoff between a higher injection velocity and the correspondingly higher fuel load and a longer transit time with larger power requirements and support systems.

b. Approach trajectories

Approach trajectories differ from trajectories near minimum velocities in that with the former class the vicinity of the moon may be reached much quicker than with the latter. The transit time for typical approach trajectories is approximately 120 hr at 40 m/sec above minimum restricted three-body escape velocity. This time is approximately 50 hr at parabolic velocity, which is 170 m/sec above the minimum restricted three-body escape velocity, and it decreases to approximately 24 hr at 500 m/sec above parabolic velocity. A further increase of injection velocity above the two-body escape or parabolic velocity will not reduce the transit time as markedly as was possible near the two-body escape velocity. Practical transit times for lunar approach and impact trajectories vary from about 30 to 80 hr, which seems to be a good compromise between rocket fuel requirements on one hand, and power and support system requirements on the other.

Approach trajectories may miss the moon by a small or large distance, the major differences between an approach trajectory from a trajectory near minimum velocity being that the "initial apogee" of the approach trajectory would be beyond the orbit of the moon and the transit time for passage to the orbit of the moon is less than five days. If the approach trajectory passes near the moon, the concept of "apogee" becomes illusory since the gravitational attraction of the moon modifies the trajectory shape considerably. Possible approach trajectories in the vicinity of the moon are given in the following sketch in selenocentric coordinates $x_m y_m$, where $\vec{V}_{\infty\Delta}$ is constant vehicle velocity in selenocentric coordinates at entry into the circular region around the moon, and $\vec{V}_{e\mathbb{C}}$ is the velocity of the moon in geocentric coordinates which is directed along the negative y_m-axis:

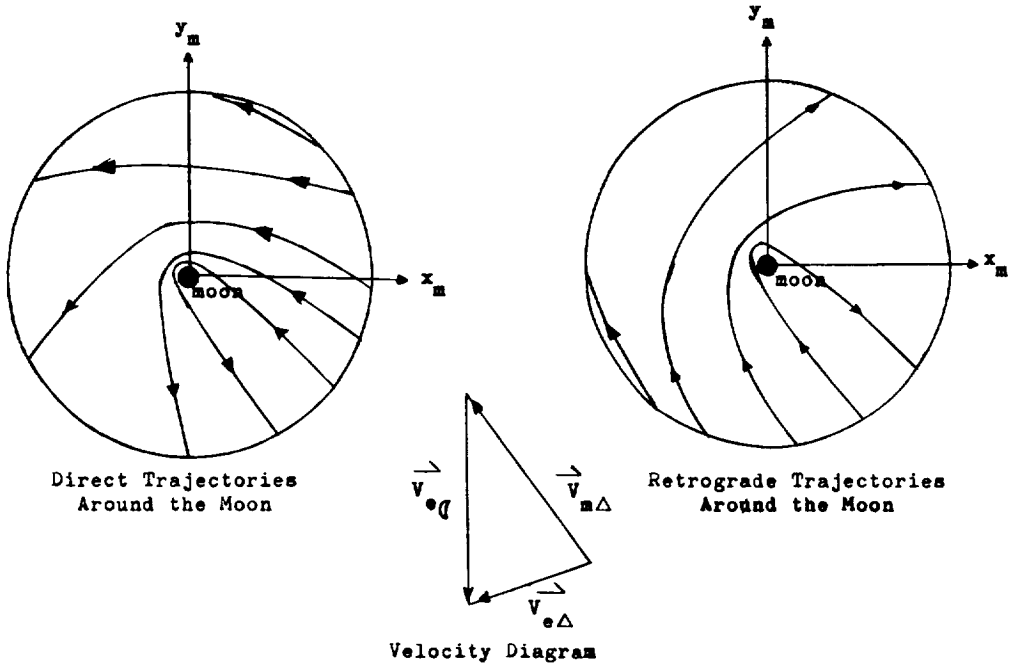

As can be seen from this sketch, the approach trajectory leaves the vicinity of the moon. It was shown by Egorov (Ref. 1) that the moon cannot capture a space vehicle on an approach trajectory since the vehicle energy corresponds to that of a hyperbolic selenocentric trajectory if the attraction of the earth is neglected. The preceding sketch also shows that the closer the approach to the moon, the greater is the "turning effect" of the moon on the trajectory. While in the vicinity of the moon, the approach trajectories may be either direct or retrograde, depending on whether they pass around the moon in the direction or against the direction of the lunar rotation, as illustrated in the preceding sketch. However, it is more common (Ref. 1, for example) to classify approach trajectories direct ($\gamma_{e0} < 90°$) or retrograde ($\gamma_{e0} > 90°$) at injection near earth.

c. Impact trajectories

In any study of lunar flight the first trajectory considered is usually an impact trajectory. Such a trajectory is simply an approach trajectory which intersects the surface of the moon. Since the impact may occur on the way out or on the return, there are now four types of impact trajectories as opposed to two types of approach trajectories:

The first type leaves the earth direct and intercepts the moon on an ascending arm. A second type leaves the earth direct but intercepts the moon on a descending arm. The following sketch depicts these two types of trajectories in the geocentric ($x_e y_e$) coordinate system with t_0 denoting the injection time and t_i the impact time:

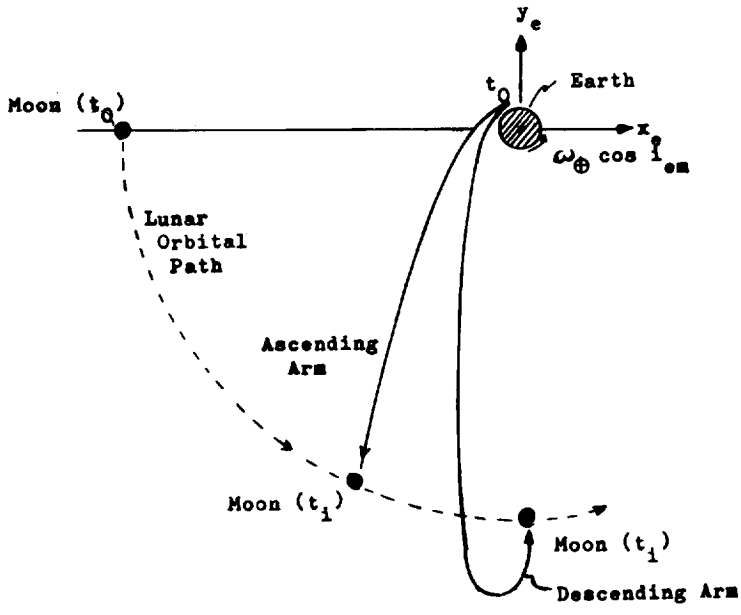

The third and fourth types are identical to the first two except that they leave the earth retrograde.

The retrograde trajectories are usually avoided due to the larger fuel requirements. Since interception of the moon on a descending arm has been shown to increase the required guidance accuracies by two to five times, the most practical impact probe trajectories are direct ones which strike the moon on the ascending arm.

Impact trajectories will hit the surface of the moon with a velocity of approximately 3000 m/sec unless they are retarded by rocket braking during the descent phase. Hard landings, with impact velocities approximately between 3000 and 100 m/sec, can be used for relatively simple experiments, while the impact velocity has to be braked to the order of tens of m/sec for soft landings of delicate equipment for experiments on the moon. Lunar impacts on the ascending arm are essentially limited to the visible disk while impacts on the descending arm occur essentially behind the moon. An impact trajectory with rocket burning before the landing will also require some control of the orientation of the vehicle before and during rocket burning.

3. Circumlunar and Allunar Missions

The next missions of interest are circumlunar and allunar missions, which may be manned or unmanned. Specific lunar and earth return conditions are somewhat more difficult to achieve than for lunar probes because of the tighter injection tolerances. A very desirable feature for these missions is that the vehicle returns to the vicinity of the earth ballistically after passing arbitrarily close to the lunar surface. The nomenclature of the associated trajectories is analogous to the mission nomenclature and the exact definition of each trajectory class will be given when it is discussed in detail.

Of primary interest are the nonperiodic circumlunar missions since they allow reconnaissance, surveillance and mapping of the back of the moon. The other trajectory classes are of less practical interest, but will nevertheless be mentioned briefly.

Trajectories that depart from earth, pass behind the moon while crossing the earth-moon line in the vicinity of the moon, and again return to earth ballistically are called nonperiodic circumlunar trajectories or circumlunar trajectories for short. Basically, these trajectories can leave the earth either direct as shown in the following sketch, or retrograde (not shown), where t_p is the time of pericynthion, or closest approach to the moon.

A circumlunar trajectory leaving the earth either direct or retrograde can return to earth by establishing either a direct or retrograde (and highly elliptic, parabolic or hyperbolic) orbit around it or impact the earth as indicated in the following sketch. This would account for six different types of circumlunar trajectories.

The general type of trajectory is one of the easiest to achieve, but specific conditions at the moon and on earth return are difficult to obtain due to the fact that error sensitivities are

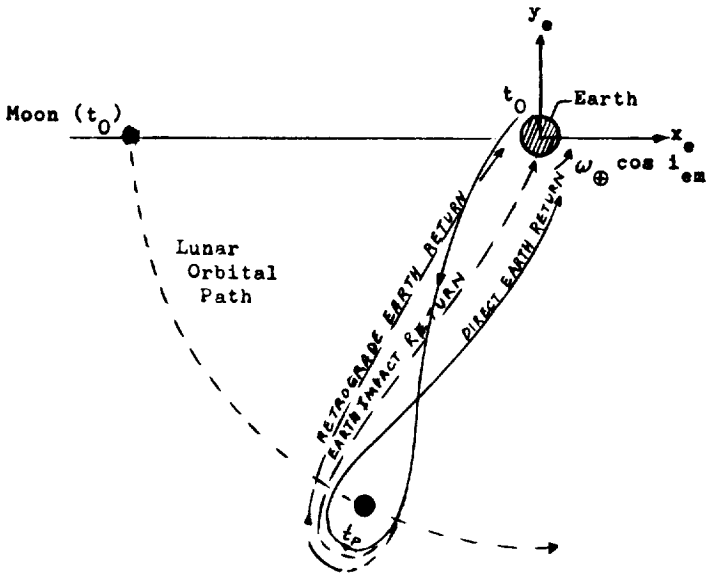

very high. For instance, an error of 1 m/sec in injection velocity (at t_0) can alter the miss distance by 870 km at the moon and 6650 km at earth. Although highly sensitive, these types of trajectories are especially suited for photographic missions on the back side of the moon. These missions may be manned or unmanned and may be highly desirable for future landing flights. In fact, actual landing missions may utilize such trajectories because of their inherent safety features (no lunar impact, ballistic departure and return). One drawback of circumlunar trajectories is the inaccessibility of higher lunar latitudes. This is due to the fact that their inclination to the lunar equatorial plane is limited to approximately 15° (see Chapter VI).

The total flight time for circumlunar missions is rather limited by the nature of the trajectory and depends strongly on the pericynthion altitude. The following figures are quoted for injection at an earth altitude of 200 km. For a pericynthion altitude of 200 km the total flight time to the moon and back can vary between 138 and 142 hr, for a pericynthion altitude of 1000 km it can vary between 147 and 152 hr, and for a pericynthion altitube of 2000 km it can vary between 155 and 165 hr. In each case the vacuum perigee of the return trajectory is at 50 km.

An interesting problem of lunar trajectories is the possibility of establishing periodic orbits around the earth and moon which pass behind the moon, or periodic circumlunar trajectories. The existence of such orbits was established and several orbits were calculated in Ref. 1. The closest approach to the earth, $(r_{e\Delta})_{min}$, and to the moon, $(r_{m\Delta})_{min}$, of several typical orbits is given below from Ref. 1*:

Orbit No.	$(r_{e\Delta})_{min}$ (km)	$(r_{m\Delta})_{min}$ (km)	Remarks
1	6,571	150	Lunar impact
2	42,203	825	Lunar impact
3	82,824	1500	Lunar impact
4	116,371	2000	A possible periodic orbit

As can be seen, the only case that does not impact the moon, $(r_{m\Delta})_{min} > 1738$ km, is Orbit No. 4. For this trajectory the closest approach to earth, $(r_{e\Delta})_{min}$, is almost 20 earth radii or about one-third of the distance to the moon. Such an orbit would seem to be of little practical interest, especially since this class of trajectories is also unstable, and small perturbations would cause the space vehicle to depart from this orbit.**

Opposed to the circumlunar classes of the corresponding nonperiodic and periodic trajectories described above are allunar trajectories, which pass only in front of the moon while they cross the earth-moon line in the vicinity of the moon. This feature is most clearly seen in rotating x_R y_R coordinates as shown in the following sketch of a direct nonperiodic allunar trajectory with an impact return to earth. Very frequently the descriptive term "nonperiodic" is dropped, and periodic allunar trajectories are referred to as allunar orbits to distinguish them from the allunar trajectories.

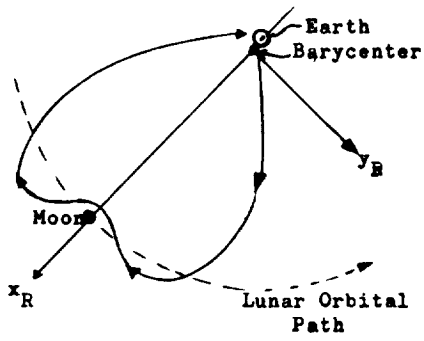

Analogous to the six types of circumlunar trajectories one may distinguish six types of allunar trajectories. A typical mission employing an allunar trajectory is photography of the front face of the moon without the aid of lunar satellite orbits.

Although there is but one class of periodic circumlunar trajectories there are an unlimited number of possible periodic allunar trajectories.

*These numerical values are based on Egorov's values of the earth-moon system constants and are to be regarded as illustrative rather than accurate.

**Note added in proof: A new class of circumlunar orbits has recently been described. A brief summary of this class of orbits is given as Section D.

Periods of these allunar orbits vary from 0.5 to 1.5 mo, and while they pass in front of the moon as they cross the earth-moon line, their farthest point from earth is well beyond the moon's orbit. Circumlunar and allunar periodic orbits are of interest, but it is doubtful that such orbits could be established for a very long time due to their unstable nature.

4. Lunar Orbit Missions

Lunar orbit missions are complex from a trajectory viewpoint since a single mission may consist of several phases, each utilizing a different class of trajectories. The characteristic feature of lunar orbit missions is that the primary purpose of the mission is accomplished during the lunar orbiting phase. In other respects the space vehicle may be manned or unmanned; it may make a one-way trip to the moon or eventually return to earth if this is a manned mission.

The primary advantage of lunar orbits lies in the almost unlimited time that the vehicle can spend in the vicinity of the moon, time which can be utilized for the gathering of scientific data, the reconnaissance, surveillance, and mapping of the moon. Also, no actual landing on the moon is necessary, and all the attendant structural and fuel problems do not appear.

The first question in a lunar orbit mission is whether the moon can capture a space vehicle launched with a velocity higher than the one corresponding to the Jacobi constant C_2 (see Chapter III, Subsection B-2). It was shown by Egorov (Ref. 1) that it is impossible for the moon to capture a vehicle on an approach trajectory, no matter what the initial conditions. The question of lunar capture without thrust remains open for trajectories near minimum velocities which make more than one orbit around earth before reaching the vicinity of the moon. When the injection velocity is between the one corresponding to the Jacobi constants C_2 and C_4, then the space vehicle can pass through the constriction near the critical point between the earth and moon (see Fig. 2, Chapter III) after more than one orbit around earth and become a temporary satellite of the moon before it returns to the vicinity of the earth.

This class of trajectories is not very practical since (1) the possible range of injection velocities is about 1 m/sec (see table on page 21 in Chapter III), and the trajectory is very sensitive to solar and other perturbations, and (2) the transit time is very long and the transit time is very sensitive to injection velocity in the possible range of about 1 m/sec. Thus in practice a lunar orbit can only be achieved by reducing the velocity of the space vehicle through thrust application near the moon.

A typical lunar orbit mission with return to earth, illustrated in the sketch at the top of the next page, will consist of:

(1) An earth-to-moon transfer phase which may be an approach, the first half of a circumlunar, or, less likely, an impact trajectory.

(2) An entry maneuver into the desired lunar orbit.

(3) A lunar orbit phase which may last for several revolutions.

(4) A departure maneuver from the lunar orbit.

(5) A moon-to-earth transfer phase which may be the second half of a circumlunar trajectory, or an approach or impact trajectory, and is illustrated in the following sketch in geocentric nonrotating coordinates x_e y_e.

The different types of approach, impact, or circumlunar trajectories have been discussed above. Lunar orbits may be classified either into direct or retrograde orbits; they may be either circular or elliptical with respect to the moon, but their actual shape is continually changing due to perturbations of the earth, the sun, and the moon's figure. A more quantitative characterization of orbits is by their elements (Chapter III, Subsection A-3).

Entry to and departure maneuvers from lunar orbits are generally characterized by the characteristic velocity ΔV of the maneuver.

5. Landing Missions

Closely related to lunar orbit missions are the lunar landing missions, in which the space vehicle is on the lunar surface during one phase of the mission where its primary purpose will be accomplished. Landing missions are the most complex missions from a trajectory point of view. They may be manned or unmanned, one-way or round trip. Most likely the lunar landing mission will use a circumlunar or approach trajectory in the earth-moon transfer phase, and a lunar "parking" orbit to reach the desired landing site, primarily because of the flexibility in the choice of landing site and because of the safety features of the circumlunar or approach trajectory. This type of mission is known as lunar orbital landing. As propulsion systems become more reliable, impact trajectories with a soft landing may be used for landing missions in areas of the moon which are easily accessible for impact trajectories. The latter type of mission is a lunar direct landing. Lunar landing missions are used for exploration, supply and logistics, and for establishment of lunar bases.

A typical lunar landing mission with round trip to earth consists of:

(1) An earth-to-moon transfer phase which may be an approach, the first half of a circumlunar, or, less likely, an impact trajectory.

(2) An entry maneuver into the desired lunar orbit (this phase is deleted for direct landings).

(3) A lunar orbit phase which may last from a fraction of one to several revolutions (this phase is deleted for direct landings.)

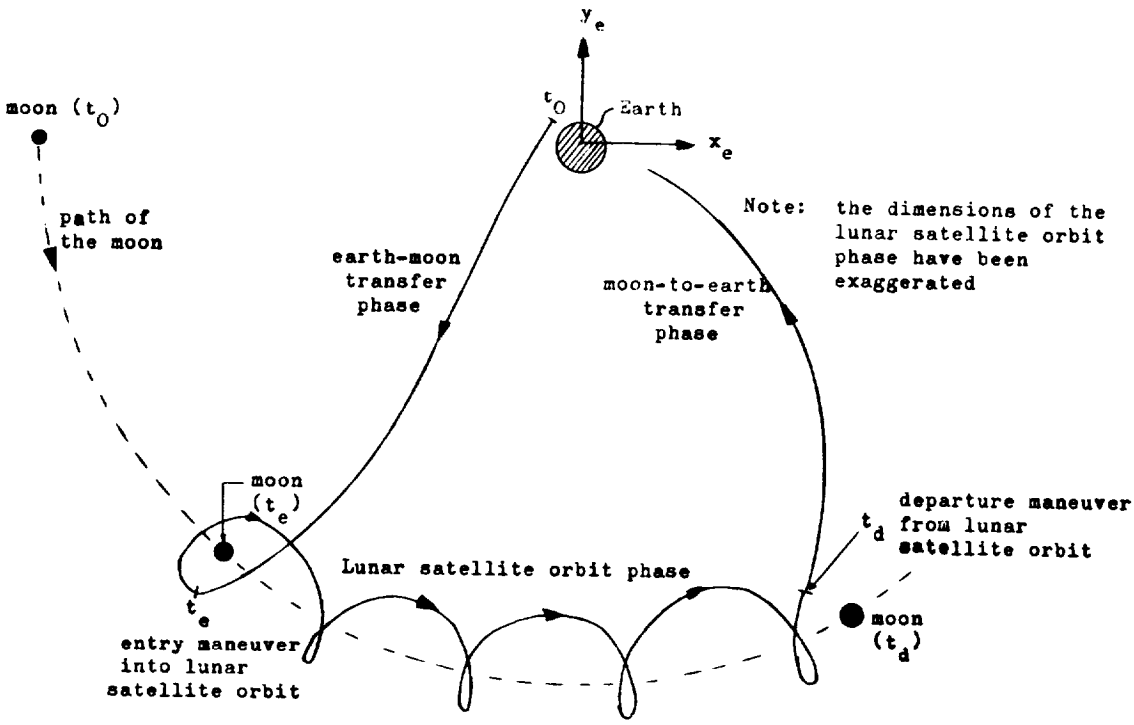

(4) A descent phase to the lunar surface and landing (possibly using lunar orbit rendezvous concept as described in the following paragraph).

(5) A lunar stay of arbitrary duration.

(6) An ascent phase from lunar surface.

(7) A lunar orbit phase which may last from a fraction of one to several revolutions (this phase is deleted for direct landings).

(8) A departure maneuver from lunar orbit (this phase is deleted for direct landings).

(9) A moon-to-earth transfer phase which may be the second half of a circumlunar trajectory, an approach or impact trajectory.

For one-way landing missions, phases (6) through (9) are deleted. The classes of trajectories utilized for each phase of the landing mission may be classified further as was discussed above.

A typical one-way lunar orbital landing mission has been illustrated in the following in geocentric nonrotating coordinates x_e y_e.

A mission which may be regarded as a hybrid between the lunar orbit and landing missions is the lunar orbit rendezvous mission (LOR). In this mission the space vehicle establishes a lunar orbit.

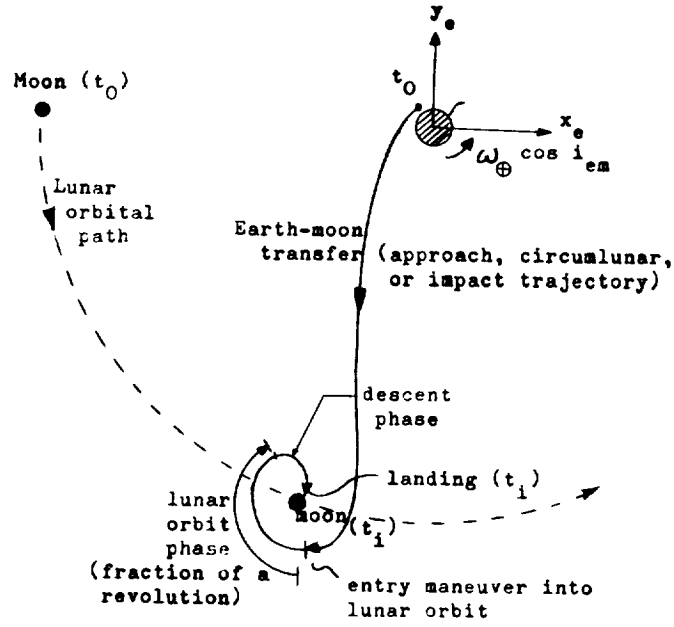

At the proper time a segment of the vehicle, called the shuttle vehicle, detaches itself, descends to and lands on the lunar surface. After the purpose of the mission on the lunar surface has been accomplished, the shuttle vehicle ascends to lunar orbit and makes a rendezvous with the orbiting space vehicle. The men and any equipment are

transferred to the space vehicle, which then returns to earth while the empty shuttle is abandoned in lunar orbit.

6. Space Stations

It has been proposed by Buchheim (Ref. 2) that space stations may be established at the five double points in earth-moon space. He calls such vehicles libration center buoys. These double points are in the MOP, they rotate around the barycenter with the same angular velocity as the earth and moon, and their fixed location in the rotating x_R y_R coordinate system is given in Subsection B-2 of Chapter III.

Three of the five double points are on the earth-moon line, two fairly near the moon and the third is on the opposite side of the moon about one lunar unit from earth. The double points on the earth-moon lines are unstable and the space vehicle would have to make corrective maneuvers to counteract perturbing forces in order to stay near the double points for a longer time. The other two double points form equilateral triangles with the earth and moon and they are stable. Thus, a space vehicle could stay at these points indefinitely. The sketch on page III-21 in the preceding chapter shows the location of the double points.

Space stations at the double points have also been called synodic or selenoid satellites. They could be used for beacons in space, as astronomical observatories, for conducting long-term experiments in earth-moon space and for space surveillance.

7. Lunar Passages to Escape

The moon can be used to accelerate or decelerate a space vehicle for interplanetary missions or solar probes since the moon and most planets are very close to the plane of the ecliptic. Acceleration of the space vehicle can be accomplished by planning the approach trajectory to pass very close to the moon and pass out of the vicinity of the moon in the general direction of the moon's orbital motion around earth. The following sketch in geocentric nonrotating coordinates illustrates this special case.

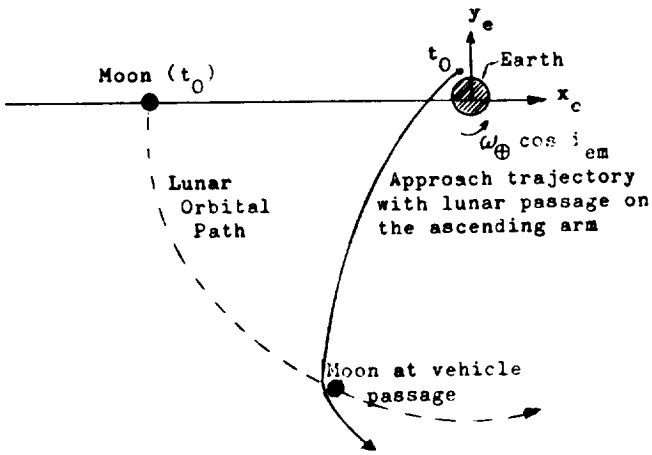

The maximum velocity increment that can be gained is approximately 1480 m/sec. The vehicle acceleration can be accomplished on a descending arm as well. Retrograde trajectories can also be used, but are not really practical because of the larger ΔV required for earth departure. In addition, the moon can be used to decelerate a space vehicle. Deceleration would be obtained by passing out of the moon's vicinity in a direction opposite to the moon's orbital motion around the earth.

The practicality of planning probes in this fashion is debatable at this time due to the increased guidance accuracy required. To take full advantage of the gravitational attraction of the moon, the following items are necessary:

(1) The approach to the moon should be as close as possible.

(2) The pericynthion, or point of closest approach to the moon, has to be controlled closely in order to turn the trajectory in the desired direction (see the preceding sketch.

(3) The launch time tolerance is very stringent since both the moon and planet or sun must be in a favorable position at time of pericynthion.

8. Nomenclature and Characteristics of a Circumlunar Trajectory

The ballistic lunar trajectories discussed above behave very similarly during transit to and from the moon. A fundamental plane of reference for such trajectories is the moon's orbital plane (MOP) used earlier in this section. For this discussion a circumlunar trajectory which is not restricted to the MOP is used as an example. The nomenclature used here is identical with that given in the Voice discussion of Section C and that describing all trajectory data throughout the remaining chapters.

The outgoing trajectory to the moon is termed a translunar trajectory. It is assumed that the injection of the space vehicle into the translunar trajectory occurs near earth, and a series of two-body force models is used in the approximation of the entire trajectory. The connection or patching between the different two-body trajectories occurs near the moon. The eccentricity of the translunar and transearth (a trajectory from the vicinity of the moon to the vicinity of the earth) trajectories is larger than 0.95.

The space vehicle can leave the earth in four directions, direct north, direct south, retrograde north, and retrograde south. These departure directions are illustrated in the following sketch. These departure directions are based on whether the trajectory at injection is direct or retrograde, above (north), or below (south) the MOP. The injection position is given by the angle ψ_0 which is measured from the intersection of the translunar trajectory plane with the MOP, which is the x_E-axis, to the injection point. The vectors $\vec{r}_{e\Delta 0}$ and $\vec{V}_{e\Delta 0}$ define the translunar trajectory

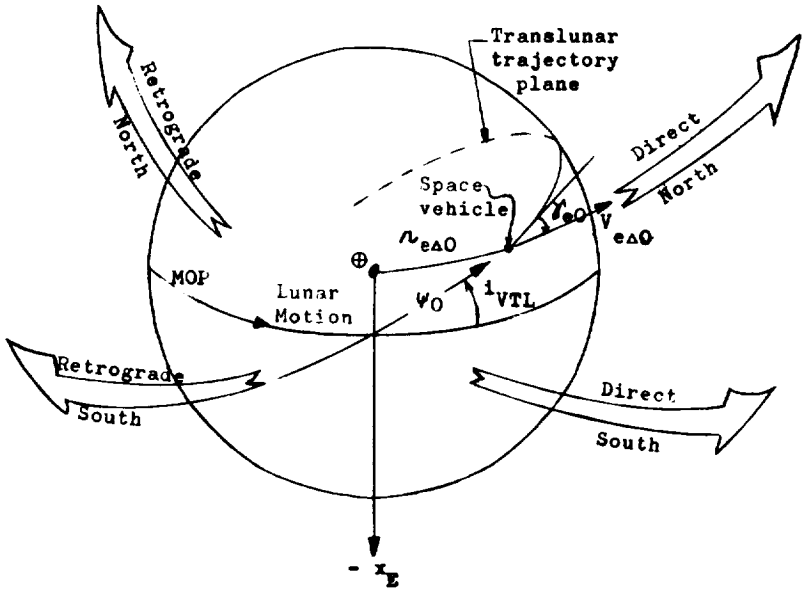

plane where $\vec{r}_{e\Delta 0}$ is the radius vector at injection. The injection flight path angle γ_{e0} is measured from the local horizontal (a plane perpendicular to $\vec{r}_{e\Delta 0}$) in the direction of the moon's motion to the velocity vector in the translunar plane (see preceding sketch). The positive x_E-axis is directed approximately toward the moon at the time of pericynthion while i_{VTL} is the inclination of the translunar plane to the MOP at the time of injection. In the vicinity of the earth ($r_{e\Delta} < 200{,}000$ km), i_{VTL} is essentially constant being affected primarily by the oblateness of the earth. As the vehicle nears the moon ($r_{e\Delta} > 200{,}000$ km), the trajectory is influenced to a greater degree by the gravitational attraction of the moon, thereby causing i_{VTL} to change. This is demonstrated in the following sketch.

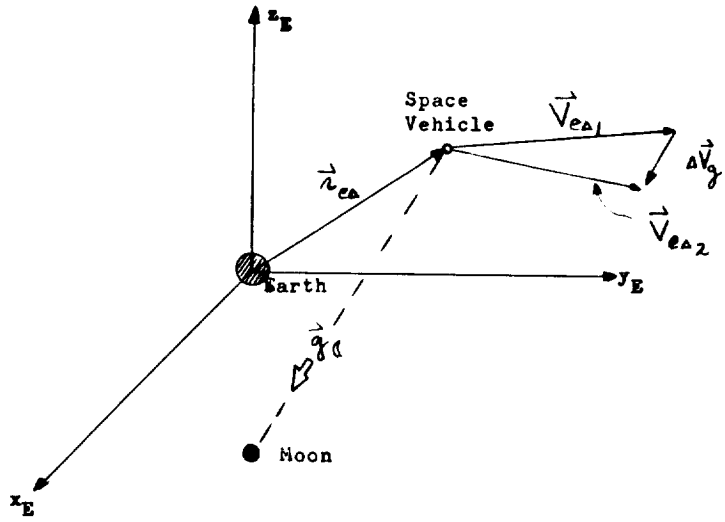

Consider a space vehicle with a position vector $\vec{r}_{e\Delta}$ and a velocity vector $\vec{V}_{e\Delta}$ relative to earth. The space vehicle will be accelerated toward the moon by the lunar gravity $\vec{g}_q$. During a short time interval Δt the velocity of the vehicle will be changed by an amount ΔV_g along the line of action of $\vec{g}_q$.

By assuming that $\vec{r}_{e\Delta}$ remains unchanged, the resultant velocity of the space vehicle is $\vec{V}_{e\Delta 2} = \vec{V}_{e\Delta 1} + \Delta\vec{V}_g$. The plane formed by $\vec{r}_{e\Delta 1}$ and $\vec{V}_{e\Delta 1}$ is different from that formed by $\vec{r}_{e\Delta 1}$ and $\vec{V}_{e\Delta 2}$, and its translunar inclination differs from the original translunar inclination by Δi_{VTL}. Hence, lunar gravity causes the space vehicle to drift from the original translunar plane, and the rate of drift, directed toward the moon, increases as the moon is approached since $\vec{g}_q$ increases. This drift has occasionally been referred to as the focusing effect of the moon. In addition, the speed of the space vehicle relative to earth increases as the moon is neared. The following sketch shows the drift characteristic of a lunar trajectory.

A similar drift is experienced on the trip back to earth (transearth trajectory) except that the vehicle drifts into the final return inclination i_{VTE}.

On return to earth, the transearth trajectory may approach it from various directions. As was the case for the translunar injection, the directions

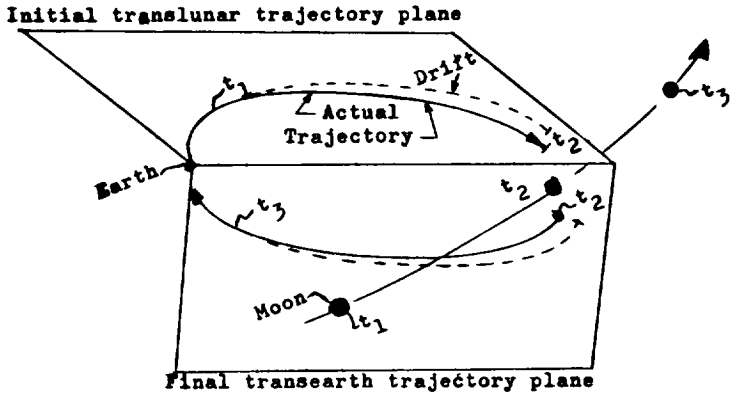

of return are classified as depicted in the following sketch, where i_{VTE} is the final inclination of the transearth trajectory:

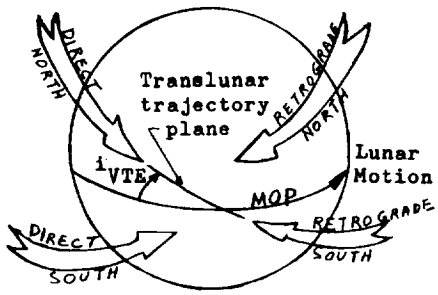

B. FORCE MODELS FOR LUNAR TRAJECTORY CALCULATIONS

In the preceding section the characteristics and nomenclature of lunar trajectories were introduced. These trajectory characteristics could be introduced with very little attention to the physical and mathematical background of how the position of the space vehicle as a function of time, or its trajectory, is obtained. However, in any quantitative work, be it precise or approximate, it is necessary to know what physical model underlies the calculations and by what mathematical method the trajectory was obtained. The emphasis in the present section will be on the assumed force model for deriving the equations of motion since the analytical and numerical methods of solving these equations have been discussed in Chapter IV of Ref. 3.

Various degrees of sophistication are possible in the description of the forces acting on a vehicle in the earth-moon environment. These force models vary in complexity as does the ease as well as cost of generating trajectories and obtaining values for trajectory parameters for a given lunar mission. Rough approximations should not be discarded simply because they are approximations. Different approximations in the force model vary in their sensitivity to different parameters, and a very crude approximation for one parameter may be an excellent or at least an adequate one for another, depending on the ultimate use of the generated trajectories.

In general, the relative error between two separate trajectories of a given force model is smaller than the absolute error between a trajectory using the given force model and one actually flown in the earth-moon environment. Hence, a very simple force model may be used to restrict the range of each trajectory parameter for the required lunar mission as well as to obtain the allowable errors in initial conditions for successful completion of the mission and to obtain guidance sensitivities. Any conclusions drawn from trajectories obtained from the simple model may then be verified by generating a small number of trajectories using a more sophisticated force model.

In the following text, various force models that have been employed in generating lunar trajectories are discussed in the order of increasing complexity, and quantitative differences between the models are given whenever possible.

1. Succession of Two-Body Trajectories

The simplest approach to lunar trajectory studies is to treat the transit of a vehicle from earth to moon as a succession of restricted two-body problems. In the initial phase of flight the vehicle is assumed to be in the earth's gravitational field alone and its mass M_Δ is negligible compared to the mass of the earth $M_\oplus$. At some point along the trajectory the vehicle will pass into a region where the moon's field is predominant. It will then be assumed to be in the moon's field alone and its mass M_Δ is negligible compared to the mass of the moon $M_\mathbb{q}$. This approach allows a splitting of the trajectory determination into various phases, namely the study of (1) planar dynamics of the earth's field, (2) transition from earth to moon influence where the criteria for passing from phase (1) to the next phase are discussed, (3) planar dynamics of the lunar field, and (4) three-dimensional effects when the vehicle is not in the moon's orbital plane. Many characteristics of lunar trajectories may be introduced logically and studied on the basis of this approach.

It is obvious that this force model, like any other model, will be more accurate for short lunar missions than for longer ones, since the neglected effects (discussed below) result from accelerations acting over the entire transit time. This approach is expected to be reasonably good for lunar impact trajectories, and for circumlunar flight. However, prolonged flights near the moon, such as lunar satellites, should be analyzed by use of more exact models.

a. Planar dynamics of the earth's field

For this two-body problem the vehicle moves in a plane passing through the earth's center. The moon revolves around the earth in the same plane

with an angular velocity $\omega_{\oplus\mathbb{C}}$ at a mean distance $\bar{r}_{\oplus\mathbb{C}}$ = 1 LU. The moon is treated here as a massless point without influence on the vehicle trajectory. Thus any nonrotating coordinate system at the earth's center of mass is inertial. In inertial plane polar coordinates $r_{e\Delta}$, $\theta_{e\Delta}$, as shown in the following sketch, the equations of motion of the space vehicle are:

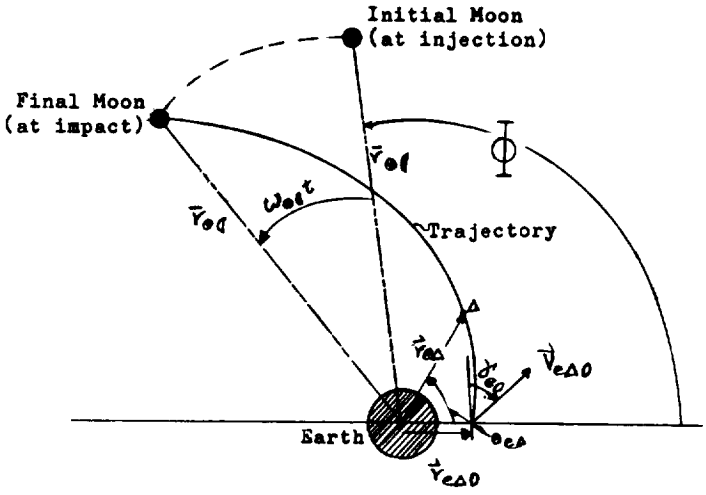

$$\ddot{r}_{e\Delta} - r_{e\Delta}\dot{\theta}_{e\Delta}^2 = -\frac{\mu_\oplus}{r_{e\Delta}^2}$$

$$r_{e\Delta}\ddot{\theta}_{e\Delta} + 2\dot{r}_{e\Delta}\dot{\theta}_{e\Delta} = 0 \qquad (8)$$

Equation (8) yields two first integrals,

$$E_e = \frac{1}{2}\left\{\dot{r}_{e\Delta}^2 + \left(r_{e\Delta}\dot{\theta}_{e\Delta}\right)^2\right\} - \frac{\mu_\oplus}{r_{e\Delta}} = \frac{1}{2}V_{e\Delta 0} - \frac{\mu_\oplus}{r_{e\Delta 0}} \qquad (9)$$

$$h_e = r_{e\Delta}^2\dot{\theta}_{e\Delta} = r_{e\Delta 0}\, V_{e\Delta 0} \cos\gamma_{e0}$$

where E_e and h_e are its energy and the magnitude of its angular momentum per unit mass, respectively. Equation (9) yields the final two integrals (see Ref. 4, for example)

$$t = \int_{r_{e\Delta 0}}^{\bar{r}_{\oplus\mathbb{C}}} \frac{dr}{\dot{r}} = \int_{r_{e\Delta 0}}^{\bar{r}_{\oplus\mathbb{C}}} \frac{dr}{\sqrt{2E_e + \frac{2\mu_\oplus}{r} - \frac{h_e^2}{r}}} \qquad (10)$$

$$\theta_{0\mathbb{C}} = \int_{r_{e\Delta 0}}^{\bar{r}_{\oplus\mathbb{C}}} \frac{h_e\, dr}{r^2\dot{r}} = \int_{r_{e\Delta 0}}^{\bar{r}_{\oplus\mathbb{C}}} \frac{h_e\, dr}{2E_e + \frac{2\mu_\oplus}{r} - \frac{h_e^2}{r^2}} \qquad (11)$$

where t is the total time of flight and $\theta_{0\mathbb{C}}$ the total in-plane angle from $r_{e\Delta 0}$ to $\bar{r}_{\oplus\mathbb{C}}$.

As is well known, the trajectory obtained from Eq (8) is a conic section in the plane of the trajectory with focus at the center of the earth. It remains to orient the injection point on this conic section with respect to the moon at injection by the angle

$$\Phi = \theta_{0\mathbb{C}} \pm \omega_{\oplus\mathbb{C}} t, \qquad (12)$$

where the negative sign applies for direct and the positive sign for retrograde trajectories.

A consistent set of constants required in Eqs (8) through (11) is:

$$\mu_\oplus \equiv GM_\oplus = 398{,}601.5 \text{ km}^3/\text{sec}^2$$

$$\omega_{\oplus\mathbb{C}} = 2.661{,}699{,}484 \times 10^{-6} \text{ rad/sec} \qquad (13)$$

$$\bar{r}_{\oplus\mathbb{C}} = 384{,}747.2 \text{ km}$$

Inspection of Eqs (10) and (11) in the light of Eq (9) reveals (Ref. 4) that the time of flight is insensitive to the burnout flight path angle γ_{e0}, but is a strong function of energy or burnout velocity $V_{e\Delta 0}$. The total in-plane angle $\theta_{0\mathbb{C}}$, on the other hand, is rather insensitive to $V_{e\Delta 0}$ and is a strong function of γ_{e0}. These relations are depicted in the following sketches for a representative injection radius of $r_{e\Delta 0}$ = 6740 km.

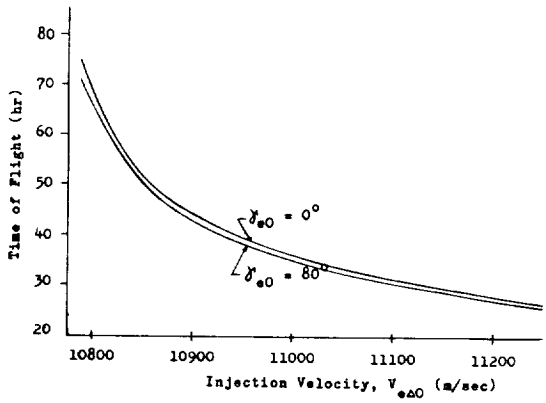

Since the effect of the moon has been ignored, the flight time and total in-plane angle for earth-moon transfer calculated from Eqs (10) and (11) are approximate. This approximation is relatively poor near minimum velocities $(V_{e\Delta})_{min}$ and becomes progressively better as the injection velocity $V_{e\Delta 0}$ is increased (for some comparison between these approximate and more exact results see Ref. 5). For the determination of visibility from earth, for instance, Eqs (10) and (11) are sufficiently accurate.

b. Transition from earth-to-moon influence

The transition from the earth to the lunar gravitational field may be made in various ways. Perhaps the simplest is to stop the translunar

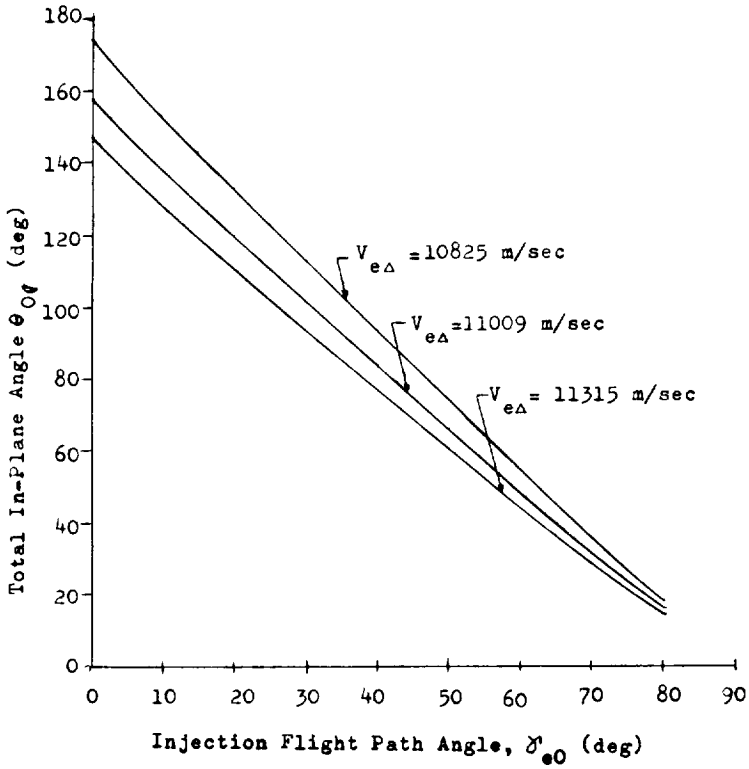

trajectory, as was done in the previous subsection, at a radius $\bar{r}_{\oplus\mathbb{C}}$, the mean distance to the moon, and regard these conditions at $r_{e\Delta} = \bar{r}_{\oplus\mathbb{C}}$ as occurring at infinity relative to the moon. This approach has been taken in Ref. 4, for example, and it may be referred to as the massless moon assumption.

However, a more natural transition from the earth's to the moon's gravitational field may be taken at the location in space when the ratio of the lunar disturbing force to the central force due to the earth's gravitational attraction becomes larger than the ratio of the earth's disturbing force to the central force of the lunar attraction. This region is called the sphere of influence of the moon, although it is slightly egg-shaped with the blunt end facing the earth, rather than spherical. The boundary of the sphere of influence of the moon can be found as follows.

Define distances by the following sketch: where the plane of the paper is the plane of the earth, moon, and space vehicle at its entry into the sphere of influence:

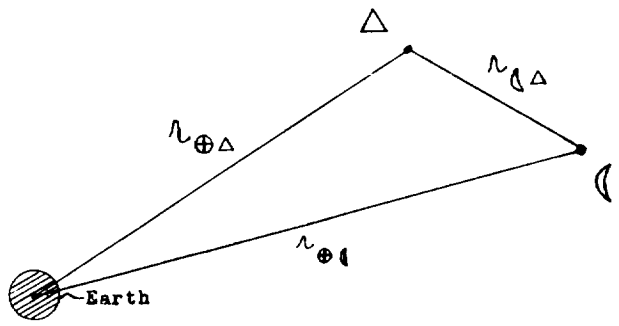

$r_{\oplus\mathbb{C}}$ = earth-moon distance

$r_{\oplus\Delta}$ = earth-space vehicle distance

$r_{\mathbb{C}\Delta}$ = moon-space vehicle distance

The gravitational acceleration or force per unit mass, on the space vehicle due to the moon, or the lunar gravitational field intensity at the space vehicle has the magnitude

$$f_{\mathbb{C}\Delta} = \frac{GM_{\mathbb{C}}}{r^2_{\mathbb{C}\Delta}}, \tag{14}$$

its acceleration due to the earth has the magnitude

$$f_{\oplus\Delta} = \frac{GM_{\oplus}}{r^2_{\oplus\Delta}}, \tag{15}$$

and the gravitational acceleration of the moon due to the earth

$$f_{\oplus\mathbb{C}} = \frac{GM_{\oplus}}{r^2_{\oplus\mathbb{C}}} \tag{16}$$

The ratio of the disturbing force of the earth to the attraction of the moon is given by

$$\frac{f_{\oplus\Delta} - f_{\oplus\mathbb{C}}}{f_{\mathbb{C}\Delta}} = \left(\frac{M_{\oplus}}{M_{\mathbb{C}}}\right) r^2_{\mathbb{C}\Delta} \cdot \frac{(r_{\oplus\mathbb{C}} + r_{\oplus\mathbb{C}})(r_{\oplus\mathbb{C}} - r_{\oplus\Delta})}{r^2_{\oplus\Delta}\, r^2_{\oplus\mathbb{C}}} \tag{17}$$

Similarly, the ratio of the disturbing force of the moon to the attraction of the earth is given by:

$$\frac{f_{\mathbb{C}\Delta} - f_{\mathbb{C}\oplus}}{f_{\oplus\Delta}} = \left(\frac{M_{\mathbb{C}}}{M_{\oplus}}\right) r^2_{\oplus\Delta} \cdot \frac{(r_{\oplus\mathbb{C}} + r_{\mathbb{C}\Delta})(r_{\oplus\mathbb{C}} - r_{\mathbb{C}\Delta})}{r^2_{\mathbb{C}\Delta}\, r^2_{\oplus\mathbb{C}}}, \tag{18}$$

where

$$f_{\mathbb{C}\oplus} = \frac{GM_{\mathbb{C}}}{r^2_{\oplus\mathbb{C}}} \tag{19}$$

is the gravitational acceleration of the earth due to the moon. The sphere of influence of the moon is the region

$$\frac{f_{\oplus\Delta} - f_{\oplus\mathbb{C}}}{f_{\mathbb{C}\Delta}} < \frac{f_{\mathbb{C}\Delta} - f_{\mathbb{C}\oplus}}{f_{\oplus\Delta}} \tag{20}$$

and its boundary is given by

$$\frac{f_{\oplus\Delta} - f_{\oplus\mathbb{C}}}{f_{\mathbb{C}\Delta}} = \frac{f_{\mathbb{C}\Delta} - f_{\mathbb{C}\oplus}}{f_{\oplus\Delta}} \tag{21}$$

or, if we substitute from the right-hand sides of Eqs (17) and (18), the boundary is defined as:

$$r^4_{\mathbb{C}\Delta} = \left(\frac{M_{\mathbb{C}}}{M_\oplus}\right)^2 \cdot r^4_{\oplus\Delta} \cdot \frac{(r_{\oplus\mathbb{C}} + r_{\mathbb{C}\Delta})(r_{\oplus\mathbb{C}} - r_{\mathbb{C}\Delta})}{(r_{\oplus\mathbb{C}} + r_{\oplus\Delta})(r_{\oplus\mathbb{C}} + r_{\oplus\Delta})}. \quad (22)$$

It can be deduced from the previous sketch that the disturbing effect is largest when the vehicle is on the earth-moon line between the earth and moon, and smallest when it is on the opposite side of the moon from the earth. Calling $r_{\mathbb{C}\Delta}$ positive in the former case, negative in the latter, the radii at these two points of conjunction are:

$$r_{\oplus\Delta} = r_{\oplus\mathbb{C}} - r_{\mathbb{C}\Delta}$$

$$r_{\mathbb{C}\Delta} = r_{\oplus\mathbb{C}} - r_{\oplus\Delta}$$

and Eq (22) can be written:

$$r_{\mathbb{C}\Delta} = \left(\frac{M_{\mathbb{C}}}{M_\oplus}\right)^{2/5} r_{\oplus\Delta}\left(\frac{r_{\oplus\mathbb{C}}}{2r_{\oplus\mathbb{C}}} + \frac{r_{\mathbb{C}\Delta}}{-r_{\mathbb{C}\Delta}}\right)^{1/5}. \quad (23)$$

Equation (23) can be solved by iteration, and the boundary of the "sphere of influence" of the moon on the earth-moon line is 51,870 km in front of the moon and 63,790 km behind the moon for a value of $\frac{M_\oplus}{M_{\mathbb{C}}} = 81.357$. As can be seen from Eq (23), the "sphere" of influence is not a true sphere but has a bulge behind the moon.

It is instructive to compute the sphere of influence of the earth in its assumed circular orbit around the sun. Equation (23) can be used directly if we replace the earth symbol by the sun symbol and the moon symbol by the earth symbol in that equation:

$$r_{\oplus\Delta} = \left(\frac{M_\oplus}{M_\odot}\right)^{2/5} r_{\odot\Delta}\left(\frac{r_{\odot\oplus} + r_{\oplus\Delta}}{2r_{\odot\oplus} - r_{\oplus\Delta}}\right)^{1/5} \quad (24)$$

In the sun-earth system $\frac{M_\odot}{M_\oplus} = 332{,}440$. Hence $r_{\odot\oplus} \gg r_{\oplus\Delta}$ and the spherical region approximating the earth's sphere of influence is given by

$$r_{\oplus\Delta} \simeq \left(\frac{1}{2}\right)^{1/5} r_{\odot\oplus}\left(\frac{M_\oplus}{M_\odot}\right)^{2/5}. \quad (25)$$

For a mean solar distance of $r_{\odot\oplus} = 149.53 \times 10^6$ km, the "radius" of the earth's sphere of influence is

$$r_{\oplus\Delta} = 805{,}000 \text{ km},$$

which is more than twice the mean distance of the moon from the earth. The moon, as well as lunar trajectories, is within the earth's sphere of influence, which justifies the omission of the gravitational attraction of the sun as a first approximation to the motion in earth-moon space.

When the space vehicle enters the lunar sphere of influence, its geocentric inertial position $(x_{e\Delta}, y_{e\Delta}, z_{e\Delta})$ and velocity $(\dot{x}_{e\Delta}, \dot{y}_{e\Delta}, \dot{z}_{e\Delta})$ will be transformed to a selenocentric inertial position $(x_{m\Delta}, y_{m\Delta}, z_{m\Delta})$ and velocity $(\dot{x}_{m\Delta}, \dot{y}_{m\Delta}, \dot{z}_{m\Delta})$ and its trajectory in the lunar gravitational field will be computed (see the sketch on page IV-40).

For typical lunar trajectory injection velocities, the velocity at the moon as given by the method of residual velocity at infinity is higher than that given by the method of sphere of influence by about 1%.

Another region around the moon that has been defined is the lunar gravisphere or sphere inside of which the gravitational attraction of the space vehicle by the moon exceeds the attraction by earth. On the boundary of the lunar gravisphere, from Eqs (14) and (15):

$$f_{\mathbb{C}\Delta} = f_{\oplus\Delta} \text{ or } r^2_{\mathbb{C}\Delta} = \frac{M_{\mathbb{C}}}{M_\oplus} r^2_{\oplus\Delta} \quad (26)$$

Numerically, this amounts in the earth-moon system to a ratio of the vehicle radii of

$$\frac{r_{\mathbb{C}\Delta}}{r_{\oplus\Delta}} = \left(\frac{M_{\mathbb{C}}}{M_\oplus}\right)^{1/2} = 0.1109 \quad (27)$$

It is more convenient to replace the vehicle distance from earth on the RHS of Eq (26) by application of the cosine law in the triangle shown in the following sketch (not drawn to scale).

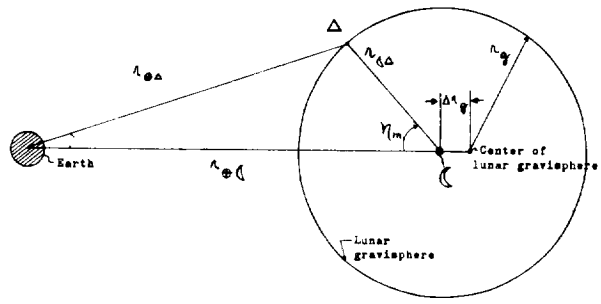

$$r^2_{\oplus\Delta} = r^2_{\oplus\mathbb{C}} + r^2_{\mathbb{C}\Delta} - 2r_{\oplus\mathbb{C}}\, r_{\mathbb{C}\Delta} \cos \eta_m$$

to obtain the boundary of the lunar gravisphere.

$$\frac{r_{\leftmoon\Delta}}{r_{\oplus\leftmoon}} = \frac{-\cos\eta_m + \left(\frac{M_\oplus}{M_\leftmoon} - \sin^2\eta_m\right)^{1/2}}{\frac{M_\oplus}{M_\leftmoon} - 1} \tag{28}$$

From the preceding sketch it can be seen that the lunar gravisphere has a radius r_g and center at $r_{\oplus\leftmoon} + \Delta r_g$, where

$$r_g = r_{\oplus\leftmoon} \frac{\left(\frac{M_\oplus}{M_\leftmoon}\right)^{2/5}}{\frac{M_\oplus}{M_\leftmoon} - 1} =$$

$$43186.6 \text{ km}, \frac{r_g}{r_{\oplus\leftmoon}} = 0.1122467 \text{ LU}$$

$$\Delta r_g = r_{\oplus\leftmoon} \frac{1}{\frac{M_\oplus}{M_\leftmoon} - 1} =$$

$$4788.0 \text{ km}, \frac{\Delta r_g}{r_{\oplus\leftmoon}} = 0.0124445 \text{ LU} \tag{29}$$

The volume of influence of the moon, which is used in the Voice computer program, is defined by the relation

$$\frac{r_{\leftmoon\Delta}}{r_{\oplus\Delta}} < 0.175, \tag{30}$$

a number which was determined empirically from lunar trajectories. The boundary of the volume of influence is given by

$$\frac{r_{\leftmoon\Delta}}{r_{\oplus\Delta}} = 0.175 = k_v \left(\frac{M_\leftmoon}{M_\oplus}\right)^{2/5}, \tag{31}$$

where $k_v = 1.578$ is a constant of proportionality. Hence, the volume of influence is a type of gravisphere with a scale factor k_v, larger than the lunar gravisphere, but one that gives the best location for transforming from earth to moon influence in typical lunar trajectories. Similar to the gravisphere, the volume of influence has a radius r_v and center at $r_{\oplus\leftmoon} + \Delta r_v$, where

$$r_v = r_{\oplus\leftmoon} \frac{k_v^{-1}\left(\frac{M_\oplus}{M_\leftmoon}\right)^{2/5}}{k_v^{-2}\frac{M_\oplus}{M_\leftmoon} - 1} = \tag{32}$$

$$69436.1 \text{ km}, \frac{r_v}{r_{\oplus\leftmoon}} = 0.1804719 \text{ LU}$$

$$\Delta r_v = r_{\oplus\leftmoon} \frac{1}{k_v^{-2}\frac{M_\oplus}{M_\leftmoon} - 1} =$$

$$12147.7 \text{ km}, \frac{\Delta r_v}{r_{\oplus\leftmoon}} = 0.0315732 \text{ LU}$$

At the boundary of the volume of influence the ratio of the lunar to the earth's gravitational attraction on the space vehicle is:

$$\frac{f_{\leftmoon\Delta}}{f_{\oplus\Delta}} = \frac{M_\leftmoon}{M_\oplus}\left(\frac{r_{\oplus\Delta}}{r_{\leftmoon\Delta}}\right)^2 \simeq 0.4014 \tag{33}$$

The lunar gravisphere has little significance from the standpoint of trajectories. The erroneous belief that it is sufficient to reach the point of equal gravitational attraction or the boundary of the lunar gravisphere in order to hit the moon was revealed in trajectory calculations made by Egorov (Ref. 1). A much more significant region for trajectory calculations is the lunar volume of influence since it allows the use of two-body force models for the best approximation of three-body or n-body trajectories.

At this point it would be helpful to illustrate the lunar sphere of influence, gravisphere, and volume of influence as well as the boundary of the closed region around the moon obtained from the Jacobi integral of the restricted three-body problem (see also Fig. 2 of Chapter III). These regions around the moon are drawn to scale in Fig. 3. However, since their maximum and minimum radii are on the earth-moon line, the table below gives the intersection of these regions with the EML and their characteristics:

Region of Lunar Influence	EML Intersection (in front of moon) (km)	EML Intersection (behind moon) (km)	Description of Region
Restricted three-body region from the Jacobi integral	57,890	48,350	Nearly elliptical region around the moon defined by the Jacobi constant C_2 (see Fig. 2 and Eq (77) of Chapter III). The boundary separates purely lunar orbits from moon escape trajectories.
Sphere of influence	51,870	63,790	Near-spherical region with the boundary given by Eq (23). The less the ratio of the mass of the smaller to that of the larger body, the more spherical this region.
Gravisphere	38,398.6	47,974.6	Region where the gravitational attraction of the moon exceeds that of the earth. It is spherical with center 4788.0 km behind the moon on the EML and with radius 43186.6 km.
Volume of influence	57,288.4	81,583.8	A type of gravisphere which gives the best successive two-body approximation for lunar trajectories. It is spherical with center 12147.7 km behind the moon on the EML and with radius 69436.1 km.

It should be remarked that the size of these various regions changes with the change of $\frac{M_\oplus}{M_\leftmoon}$ from the value 81.357 adopted in this manual and with any change in $\omega_{\oplus\leftmoon} = 2.661\,699484 \times 10^{-6}$ rad/sec.

(c) Planar dynamics of the lunar field

At the boundary of the lunar region of influence (sphere of influence, gravisphere or volume of influence) the geocentric (and so far inertial) position and velocity are transformed to the selenocentric system by the equations

$$\vec{r}_{m\Delta} = \vec{r}_{e\Delta} - \vec{r}_{e\leftmoon}$$
$$\vec{V}_{m\Delta} = \vec{V}_{e\Delta} - \vec{V}_{e\leftmoon} \qquad (34)$$

In selenocentric coordinates, which are assumed inertial inside the lunar region of influence, the energy of the vehicle relative to the moon is positive and its approach trajectory in this region is a hyperbola (see sketch on page IV-6). The equation of this trajectory in plane polar coordinates ($r_{m\Delta}$, $\theta_{m\Delta}$) centered at the moon is given by

$$r_{m\Delta} = \frac{\frac{h_m^2}{\mu_\leftmoon}}{1 + e_{m\Delta} \cos \theta_{m\Delta}} \qquad (35)$$

where h_m is the magnitude of the angular momentum per unit mass of the vehicle relative to the moon, the angle $\theta_{m\Delta}$ is measured from pericynthion, and the eccentricity is given by

$$e_{m\Delta} = \left(1 + \frac{2 E_m h_m^2}{\mu_\leftmoon^2}\right)^{1/2} \qquad (36)$$

where E_m is the energy per unit mass of the vehicle relative to the moon. The value for the lunar gravitational constant is

$$\mu_\leftmoon = GM_\leftmoon = 4899.4 \frac{km^3}{sec^2} \qquad (37)$$

All the results of Keplerian motion (restricted two-body problem, i.e., infinitesimal mass of the space vehicle compared to the mass of the moon) are now available for further study of the trajectory.

When the method of "residual" velocities at infinity is used (Ref. 4), two useful parameters of the orbit are illustrated in the following sketch:

$V_{m\Delta\infty}$ = the velocity relative to the moon at infinity

b_m = the impact parameter, which is the perpendicular distance between the asymptote of the hyperbolic orbit (direction of $V_{m\Delta\infty}$) and the center of the moon.

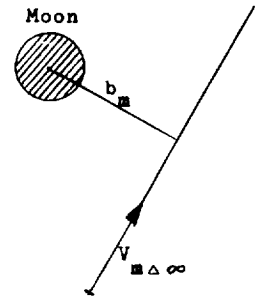

In the method of "residual" velocities at infinity the magnitude of the angular momentum and energy per unit mass of the vehicle are given by

$$h_m = b_m V_{m\Delta\infty}$$
$$E_m = \frac{1}{2} V_{m\Delta\infty}^2 \qquad (38)$$

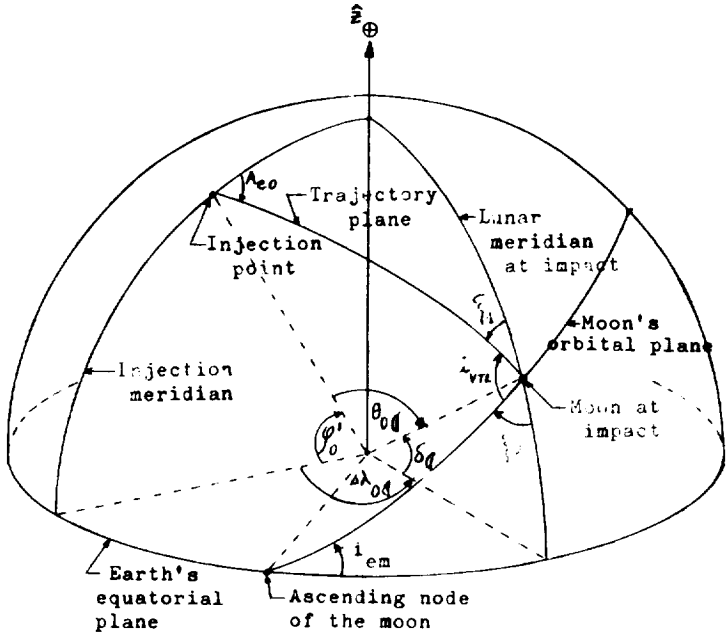

(d) Three-dimensional effects

It was seen in the previous sections that the planar trajectories were completely described by the injection conditions $r_{e\Delta 0}$, $V_{e\Delta 0}$, γ_{e0}. In addition, the orientation of the conic section with focus at the center of the earth (which is determined by the injection conditions) relative to the moon may be specified by the angle Φ (see sketch on page IV-14). Since the plane of the moon's motion is inclined to earth's equatorial plane, and the trajectory plane is, in general, inclined to both, three-dimensional effects must be considered (Refs. 4, 6, and 7). The geometry is portrayed in the following sketch.

A_{e0} = injection azimuth

ϕ_0' = injection latitude (geocentric)

$\Delta\lambda_{0\mathbb{C}}$ = longitude difference

$\delta_{\mathbb{C}}$ = instantaneous declination of the moon

i_{em} = inclination of the moon's orbital plane to the earth's equatorial plane or maximum declination of moon

$\theta_{0\mathbb{C}}$ = total in-plane angle

i_{VTL} = inclination of the translunar trajectory plane to the moon's orbital plane

Additional injection parameters required to describe three-dimensional trajectories are the geocentric injection latitude ϕ_0', the injection azimuth A_{e0}, the longitude difference between the injection point and the moon at impact $\Delta\lambda_{0\mathbb{C}}$, the instantaneous declination of the moon $\delta_{\mathbb{C}}$, and the inclination of the moon i_{em}.

From spherical trigonometry the total in-plane angle $\theta_{0\mathbb{C}}$ is given by

$$\cos\theta_{0\mathbb{C}} = \left[\sin\phi_0' \sin\delta_{\mathbb{C}} - \cos\phi_0' \cos A_{e0} \left(1 - \sin^2 A_{e0} \cos^2\phi_0' - \sin^2\delta_{\mathbb{C}}\right)^{1/2}\right] \left(1 - \sin^2 A_{e0} \cos^2\phi_0'\right)^{-1} \quad (39)$$

the longitude difference $\Delta\lambda_{0\mathbb{C}}$ is

$$\cos\Delta\lambda_{0\mathbb{C}} = \frac{\cos\theta_{0\mathbb{C}} - \sin\phi_0' \sin\delta_{\mathbb{C}}}{\cos\phi_0' \cos\delta_{\mathbb{C}}} \quad (40)$$

and the translunar inclination angle i_{VTL} in degrees is

$$i_{VTL} = 180° - (\xi_1 + \xi_2) \quad (41)$$

where

$$\xi_1 = \sin^{-1}\left(\frac{\cos\phi_0' \sin A_{e0}}{\cos\phi_0'}\right)$$

$$\xi_2 = \sin^{-1}\left(\frac{\cos i_{em}}{\cos\delta}\right)$$

In the following sketches, which have been taken from Ref. 6, the parameters $\theta_{0\mathbb{C}}$, $\Delta\lambda_{0\mathbb{C}}$, and i_{VTL} are plotted as functions of $\delta_{\mathbb{C}}$ and A_{e0}, respectively.

In each case injection is assumed to occur at $\phi_0' = +28.5°$, the latitude of Cape Canaveral, and lunar inclination i_{em} is assumed to be 20°. Of course, in the general case, the injection latitude may vary between +90° and -90°, and the lunar inclination between 18° and 28.5°.

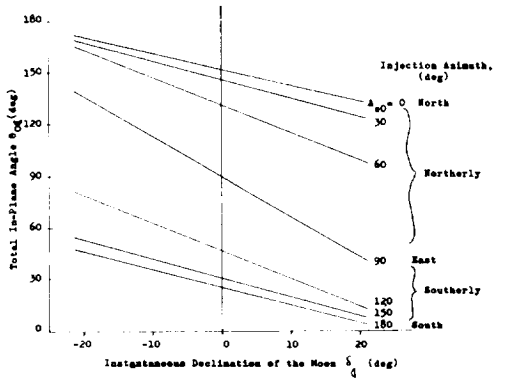

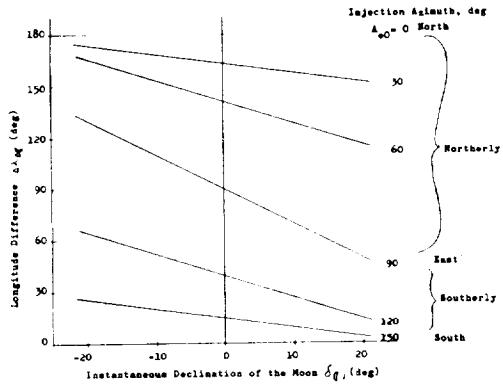

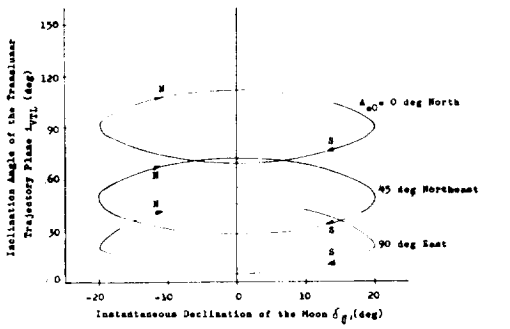

It is seen from the first of the previous three sketches, that $\theta_{0\mathbb{C}}$ decreases with increasing declination of the moon, for an injection in the northern hemisphere. The total in-plane angle also decreases as the injection azimuth is increased. Since it is also a function of $V_{e\Delta 0}$, $r_{e\Delta 0}$, γ_{e0}, the injection time depends also on the trajectory initial conditions.

The longitude difference $\Delta\lambda_{0\mathbb{C}}$ behaves similarly to the in-plane angle as can be noted from the middle sketch shown previously. In the first two sketches the abscissa coincides with the curve $A_{e0} = 180°$, or an injection toward the south. The last sketch shows that the minimum inclination angle i_{VTL} for lunar impact occurs when the moon is southbound in its orbit at zero declination. On the other hand, impact at the moon when it is at its maximum southern declination corresponds to a larger $\theta_{0\mathbb{C}}$ and consequently for a given injection velocity a smaller flight path angle at injection, which means lower gravity losses during powered flight from launch to injection. The inclination angle in this case is somewhat larger, however, resulting in lower tolerances on initial velocity due to three-dimensional effects. Initial azimuths of 90° (east) take greatest advantage of the earth's surface rotational velocity. Thus some compromise in these parameters is necessary.

This brief discussion shows that the geometry of the earth-moon and vehicle planes places constraints on injection conditions and defines preferred launch times throughout the lunar month. It must be remembered that the above discussion does not consider the use of parking orbits to ease the aforementioned injection constraints. Chapters V, VI, IX and XI present data reflecting more practical aspects of the injection into lunar trajectories.

2. Restricted Three-Body Trajectories

The simplified model discussed in Subsection B-1, where analytical solutions of the equations of motion were possible, may be complicated by adding the moon to the earth-vehicle, restricted two-body problem. The resultant restricted three-body problem was discussed in some detail in Chapter III, Section B in terms of Jacobi's integral. An analytical solution of the equations of motion is no longer possible and recourse must be taken to numerical methods.

In this subsection, vehicle motion, in terms of the restricted three-body problem, will be considered, i.e., the mass of the vehicle is negligible in comparison to the mass of the earth and moon, and with the earth and moon as spherical bodies so that they may be considered as point masses. The earth-moon system is considered isolated in space, the two bodies revolving in circles about their center of mass with an angular velocity $\omega_{\oplus\mathbb{C}}$.

The coordinate systems used in conjunction with this model have been defined in Section A of Chapter III and they are shown again in the following sketch.

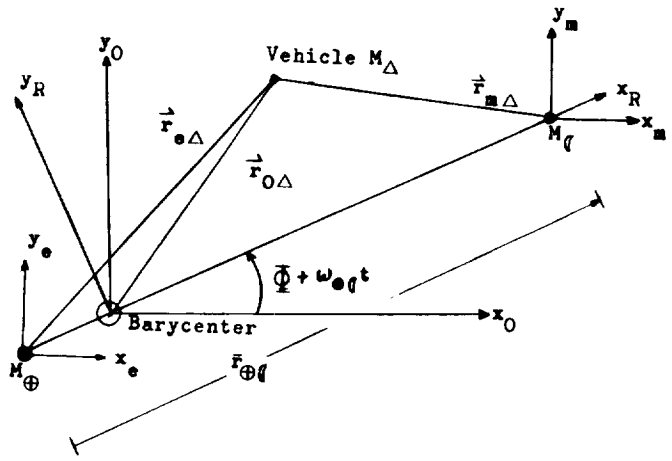

The transformations between the coordinates and velocity components of the various coordinate systems are summarized in Table 1. In the above sketch $\vec{r}_0$ (x_0, y_0, z_0) is an inertial reference system with origin at the barycenter (center of mass of the earth and moon system). The $\vec{r}_R$ (x_R, y_R, z_R) system rotates at the same rate as the earth and moon about the z_0-axis (up from the paper). The $\vec{r}_0$ and $\vec{r}_R$ systems have a common origin and coincident z_0, z_R axes. The $\vec{r}_e$ (x_e, y_e, z_e) system is a nonrotating system with origin at the center of mass of the earth, and the $\vec{r}_m$ (x_m, y_m, z_m) system is a nonrotating system with origin at the center of mass of the moon.

In the inertial reference system, where Newton's second law is valid, the equations of motion of a point mass representing the space vehicle are,

$$\ddot{\vec{r}}_{0\Delta} = -\frac{GM_\oplus}{r_{0,e\to\Delta}^3}\,\vec{r}_{0,e\to\Delta} - \frac{GM_\mathbb{C}}{r_{0,m\to\Delta}^3}\,\vec{r}_{0,m\to\Delta}, \tag{42}$$

where

$$\vec{r}_{0,e\to\Delta} = \vec{r}_{0\Delta} - \vec{r}_{0e}$$
$$\vec{r}_{0,m\to\Delta} = \vec{r}_{0\Delta} - \vec{r}_{0m} \tag{43}$$

It is convenient to transform the equations of motion (42) to the rotating coordinate system $(\vec{r}_R)$ for the purpose of numerical calculations,

because in the latter system several terms are constant. This may be done with the aid of the rotation matrix $T(\Phi + \omega_{\oplus \leftmoon} t)$ given by Eq (47) of Chapter III and the equations of motion become,

$$\ddot{x}_{R\Delta} - 2\omega_{\oplus \leftmoon} \dot{y}_{R\Delta} = \omega^2_{\oplus \leftmoon} x_{R\Delta} - \frac{GM_\oplus}{r^3_{R,e\to\Delta}} (x_{R\Delta} - x_{R\oplus}) - \frac{GM_{\leftmoon}}{r^3_{R,m\to\Delta}} (x_{R\Delta} - x_{R\leftmoon})$$

$$\ddot{y}_{R\Delta} + 2\omega_{\oplus \leftmoon} \dot{x}_{R\Delta} = \omega^2_{\oplus \leftmoon} y_{R\Delta} - \frac{GM_\oplus}{r^3_{R,e\to\Delta}} y_{R\Delta} - \frac{GM_{\leftmoon}}{r^3_{R,m\to\Delta}} y_{R\Delta} \qquad (44)$$

$$\ddot{z}_{R\Delta} = - \frac{GM_\oplus}{r^3_{R,e\to\Delta}} z_{R\Delta} - \frac{GM}{r^3_{R,m\to\Delta}} z_{R\Delta} ,$$

compare with Eq (70) of Chapter III, where

$$\vec{r}_{R,e\to\Delta} = \vec{r}_{R\Delta} - \vec{r}_{R\oplus} , \quad \vec{r}_{R,m\to\Delta} = \vec{r}_{R\Delta} - \vec{r}_{R\leftmoon} \qquad (45)$$

$y_{Re} = y_{Rm} = 0$, and (x_{Re}, x_{Rm}) are constants. The terms $2\omega_{\oplus \leftmoon} \dot{y}_{R\Delta}$ and $2\omega_{\oplus \leftmoon} \dot{x}_{R\Delta}$ are known as components of the Coriolis acceleration, and the terms $\omega^2_{\oplus \leftmoon} x_{R\Delta}$ and $\omega^2_{\oplus \leftmoon} y_{R\Delta}$ are components of the centrifugal acceleration. The equations of motion, Eq (44), can be integrated numerically subject to initial conditions on position and velocity $x_{R\Delta}, y_{R\Delta}, z_{R\Delta}, \dot{x}_{R\Delta}, \dot{y}_{R\Delta}, \dot{z}_{R\Delta}$.

These equations are for ballistic flight. Space vehicles, however, may be subject to thrust forces. These can be included in the trajectory calculations in two different ways: The thrust forces on the vehicle may be simulated by additional terms in the equations of motion, or a large thrust of short duration may also be simulated by an impulsive change $\Delta\vec{V}$ in inertial velocity $\vec{V}_{0\Delta}$ of the vehicle. This new vehicle velocity $\vec{V}_{0\Delta} + \Delta\vec{V}$ must be transformed to the rotating x_R, y_R, z_R coordinate system and the new vehicle velocity components together with the position at the time of the simulated thrust can be regarded as new initial conditions for a ballistic trajectory.

Before Eq (44) can be solved numerically, values of the constants G, $M_\oplus$, $M_{\leftmoon}$, $\omega_{\oplus \leftmoon}$, and $\bar{r}_{\oplus \leftmoon}$ are required for the restricted three-body model. In reality, only four constants are needed since G never occurs alone. The following consistent set of constants is given for this model:

$$\begin{aligned} \mu_\oplus &\equiv GM_\oplus = 398,\ 601.5\ \text{km}^3/\text{sec}^2 \\ \mu_{\leftmoon} &= GM_{\leftmoon} = 4899.4\ \text{km}^3/\text{sec}^2 \\ \omega_{\oplus \leftmoon} &= 2.661\,699\,484 \times 10^{-6}\ \text{rad/sec} \\ \bar{r}_{\oplus \leftmoon} &= 384,\ 747.2\ \text{km} \equiv 1\ \text{LU (lunar unit)} \end{aligned} \qquad (46)$$

The consistency of the above set of constants can be checked by Kepler's third law as applied to two-body (earth, moon) motion,

$$\tau^2_{\oplus \leftmoon} = \frac{(2\pi)^2 \bar{r}^3_{\oplus \leftmoon}}{\mu_\oplus + \mu_{\leftmoon}} ,$$

where $\tau_{\oplus \leftmoon}$ is the period of rotation of the earth-moon system. In terms of angular velocity

$$\omega_{\oplus \leftmoon} = \frac{2\pi}{\tau_{\oplus \leftmoon}} ,$$

the consistency relation becomes

$$\bar{r}^3_{\oplus \leftmoon} = \frac{\mu_\oplus + \mu_{\leftmoon}}{\omega^2_{\oplus \leftmoon}} \qquad (47)$$

Since the angular velocity can be observed very accurately, it is customary to assume the angular velocity as well as the gravitational constants of the earth and moon as known, and to determine a consistent value of lunar unit $\bar{r}_{\oplus \leftmoon}$. The lunar unit may be regarded, from Eq (47), as the distance to a fictitious moon in a circular orbit around the earth (of mass as determined by experiment) whose mass and Keplerian period coincide with those observed for the moon.

3. Many-Body Trajectories (oblate earth, triaxial moon)

In the discussion of the previous two force models, several forces have been neglected. These can be conveniently divided into gravitational and nongravitational forces. Examples of gravitational forces to be considered in the earth-moon trajectories are the attraction of the sun and planets, the oblateness of the earth, the triaxiality of the

moon, any inhomogeneities in the earth, and the dynamical effect of the eccentricity and inclination of the moon's orbit around the earth. Nongravitational forces include solar radiation pressure, atmospheric and meteoritic drag, electromagnetic forces, rocket thrust, and relativistic effects. Many of these forces such as earth oblateness and atmospheric drag are strongly related to position, and are significant only in the vicinity of the earth.

The influence of these factors on translunar trajectories has been investigated (Refs. 2, 8). The integrated effect of these factors over the whole trajectory depends on trajectory shape transit time, and the actual magnitude of the forces varies throughout the trajectory. The corrections $\Delta V_{e\Delta 0}$ to the initial velocity near earth $V_{e\Delta 0}$ because of these effects are listed below. They are intended to convey the magnitude of each factor compared to the restricted three-body initial velocity of 10.7 km/sec.

Factor	$\Delta V_{e\Delta 0}$ m/sec*	Percent $V_{e\Delta 0}$
1. Gravitational field of the sun	3.0 (Ref. 8)	0.03*
2. Gravitational fields of planets	0.006	--
3. Oblateness of the earth	6.0 (Ref. 8)	0.06*
4. Asphericity of the moon	--	--
5. Eccentricity of moon's orbit	13.5 (Ref. 8)	0.13*
6. Inclination of orbit of moon	6.0 (Ref. 8)	0.06*
7. Solar radiation pressure	0.012 (Ref. 8)	--
8. Meteoroid disturbances	--	--

*Transit time, 2.5 days. Nominal injection velocity, 10.7 km/sec. Vehicle with projected area of about 1 m^2 and weighing 1300 newtons.

It is seen that the $\Delta V_{e\Delta 0}$ corrections for the sun, oblateness of the earth, eccentricity of moon's orbit, and the inclination of the orbit of the moon are significant enough to necessitate the inclusion of these effects in the determination of initial velocity in actual trajectory calculations. The asphericity of the moon will be important in near-moon trajectory computations. These, as well as the other factors, will be discussed in some detail later in this chapter.

The equations of motion even in the restricted three-body problem could not be integrated in closed form, and with the present more complicated force model, numerical integration is necessary to obtain the position and velocity of the vehicle as a function of time. Since the integration technique can improve the speed and accuracy of obtaining a trajectory on the digital computer, a brief discussion of several techniques useful for lunar trajectory calculations will be included in this section.

a. Equations of motion

Consider the equatorial coordinate system described in Chapter III, Subsection A-1, with origin at the barycenter and unit vectors $\hat{x}_{\oplus\leftmoon}$, $\hat{y}_{\oplus\leftmoon}$, $\hat{z}_{\oplus\leftmoon}$, $\hat{x}_{\oplus\leftmoon}$ in the direction of the mean vernal equinox, and the $x_{\oplus\leftmoon}$ $y_{\oplus\leftmoon}$ -plane parallel to the mean equatorial plane of the earth. Let $M_\oplus$ represent the mass of the earth, $M_\leftmoon$ that of the moon, and M_Δ the mass of the vehicle, where $M_\Delta << M_\leftmoon$, $M_\Delta << M_\oplus$

Then, since $\hat{x}_\oplus$, $\hat{y}_\oplus$, $\hat{z}_\oplus$ constitute the unit vectors of an inertial coordinate system with origin chosen at the center of mass of the bodies considered in the physical model, the equations of motion of the space vehicle, or the equations of absolute motion, are

$$M_\Delta \ddot{\vec{r}}_{\oplus,0\to\Delta} = \sum_{i=\oplus}^{n} \left\{ (-G) \frac{\vec{r}_{\oplus,0\to\Delta} - \vec{r}_{\oplus,0\to i}}{r^3_{\oplus,i\to\Delta}} M_i M_\Delta + \vec{f}_i M_\Delta \right\} + \vec{n}_\Delta M_\Delta \qquad (48)$$

$$i = \oplus, \leftmoon, 1, 2, \ldots, n$$

The term $\vec{r}_{\oplus,0\to\Delta}$ is the radius vector of the vehicle from the barycenter (center of mass) equatorial coordinates with origin of the barycenter, $\vec{r}_{\oplus,i\to\Delta} = \vec{r}_{\oplus,0\to\Delta} - \vec{r}_{\oplus,0\to i}$, $\vec{f}_i$ represents the forces per unit mass due to the asphericity of the celestial bodies, and $\vec{n}_\Delta$ are the nongravitational forces per unit mass acting on M_Δ.

To obtain the equations of motion of the space vehicle, Eq (48), in a coordinate system with the origin at the center of the earth, Eq (49), the equations of motion of the earth (neglecting the gravitational attraction of the space vehicle since $M_\Delta << M_\oplus$),

$$\ddot{\vec{r}}_{\oplus,0\to\oplus} = \sum_{i=\text{(}}^{n} \left[-GM_i \frac{\vec{r}_{\oplus,0\to\oplus} \; \vec{r}_{\oplus,0\to i}}{r^3_{i\oplus}} \right] ,$$

$$i = \text{(}, 1, 2, \ldots n \qquad (49)$$

is multiplied by M_Δ and subtracted from Eq (48) to yield Eq (50), the equations of relative motion.

$$M_\Delta \ddot{\vec{r}}_{\oplus\Delta} = -G \frac{\vec{r}_{\oplus\Delta}}{r^3_{\oplus\Delta}} M_\oplus M_\Delta + \vec{f}_\oplus M_\Delta \sum_{i=\text{(}}^{n} \left[(-G) \left(\frac{\vec{r}_{\oplus\Delta}}{r^3_{\oplus\Delta}} - \frac{\vec{r}_{i\oplus}}{r^3_{i\oplus}} \right) M_i M_\Delta + \vec{f}_i M_\Delta \right] + \vec{n}_\Delta M_\Delta, \; i = \text{(}, 1, 2, \ldots n \qquad (50)$$

where

$$\vec{r}_{\oplus\Delta} = \vec{r}_{\oplus,0\to\Delta} - \vec{r}_{\oplus,0\to\oplus}$$

$$\vec{r}_{i\oplus} = \vec{r}_{\oplus,0\to\oplus} - \vec{r}_{\oplus,0\to i}$$

Actually any other body, such as the moon, could have been chosen as a reference with an appropriate change of symbols in Eq (50). The geometry is illustrated in the following sketch:

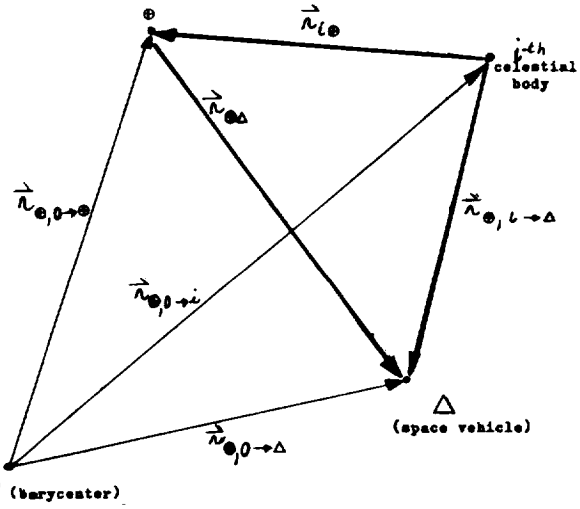

The unit vectors $\hat{x}_\oplus$, $\hat{y}_\oplus$, $\hat{z}_\oplus$ define the geocentric equatorial coordinate system in which the equations of motion, Eq (50), are given. The unit vector, $\hat{x}_\oplus$, is in the direction of the mean vernal equinox, and the $x_\oplus\, y_\oplus$ plane forms the mean equatorial plane of the earth. All vectors defined in the preceding sketch are assumed to be resolved into components in this coordinate system.

The vectors $\sum_{i=\oplus}^{n} \vec{f}_i$, representing the forces acting on M_Δ due to asphericity of the i celestial bodies, i = ⊕, (, 1, 2, . . . n can be written:

$$\vec{f}_i = \vec{f}_\oplus + \vec{f}_\text{(} + \vec{f}_1 + \vec{f}_2 + \ldots + \vec{f}_n \qquad (51)$$

Any asphericity of the sun and planets f_i, i = 1, 2, . . . n, is insignificant in its effect on lunar trajectories since even the effect of the central force is small, as can be seen in the preceding table.

Consider $\vec{f}_\oplus$ first. It arises from the expansion terms of the earth's gravitational potential in terms of spherical harmonics. In theory a large number of harmonic terms should be included; however, the coefficient of the oblateness term (second zonal harmonic) is larger by three orders of magnitude than the others (i.e., of order 10^{-3} as compared to the order 10^{-6} for the others). Thus all but the oblateness term can be neglected in lunar trajectory studies. The effect of local gravitational anomalies of the earth on the lunar trajectory is very small and will also be neglected.

If $U_\oplus$ represents the earth's gravitational potential, then the expansion of $U_\oplus$ in terms of zonal spherical harmonics (tesseral and sectoral harmonics have not yet been determined well enough for their inclusion) can be written

$$U_\oplus = \frac{GM_\oplus}{r_{\oplus\Delta}} \left[1 - \sum_{n=1}^{\infty} J_n \left(\frac{R_e}{r_{\oplus\Delta}} \right)^n P_n (\sin \phi') \right] \qquad (52)$$

where $r_{\oplus\Delta}$ is the distance of the vehicle from the earth, J_n, n = 1, 2, . . . are empirical constants (determined from geodetic and satellite measurements) and given in Chapter II, R_e is the mean equatorial radius of the earth (R_e = 6,378,163 m), ϕ' is the geocentric latitude, and $P_n (\sin \phi')$ is the associated Legendre polynomial of $\sin \phi'$. The above form of $U_\oplus$ has been adopted by the International Commission on Celestial Mechanics (Ref. 9). Let $U_\oplus = U_0 + U_2 + U_3$, where, by comparison with Eq (51)

$$U_0 = \frac{GM_\oplus}{r_{\oplus\Delta}}$$

$$U_2 = -\frac{GM_\oplus}{r_{\oplus\Delta}} J_2 \left(\frac{R_e}{r_{\oplus\Delta}} \right)^2 \frac{3 \sin^2 \phi' - 1}{2} \qquad (53)$$

$$U_3 = -\frac{GM_\oplus}{r_{\oplus\Delta}} \sum_{n=3}^{\infty} J_n \left(\frac{R_e}{r_{\oplus\Delta}} \right)^n P_n (\sin \phi')$$

U_0 represents the spherically symmetric earth, which has already been acounted for by the term $-G \frac{\vec{r}_{\oplus \Delta}}{r^3_{\oplus \Delta}} M_\oplus$ in Eq (50). U_1, the term corresponding to n = 1 in Eq (52), vanishes if the center of gravity of the earth coincides with the origin of coordinates (Ref. 10, p 43).

U_2 is the oblateness term (or second zonal harmonic) which is the largest term in the expansion, while U_3 represents the higher order zonal harmonics of the earth which may be neglected for lunar trajectory studies as mentioned above. The numerical value for

$$J_2 = 1082.28 \times 10^{-6}.$$

Let $f_{\oplus x}$, $f_{\oplus y}$ and $f_{\oplus z}$ be the $x_\oplus$, $y_\oplus$, $z_\oplus$ components of $\vec{f}_\oplus$ as defined by Eq (50), respectively. Then these components are given by

$$f_{\oplus x} = \frac{\partial U_2}{\partial x}, \quad f_{\oplus y} = \frac{\partial U_2}{\partial y}, \quad f_{\oplus z} = \frac{\partial U_2}{\partial z} \tag{54}$$

Next we turn to $\vec{f}_\mathbb{C}$. To obtain $\vec{f}_\mathbb{C}$, it is convenient to find an expression for the lunar gravitation potential $U_\mathbb{C}$ and define the gravitational force as the gradient of the potential. $U_\mathbb{C}$ is defined by

$$U_\mathbb{C} = G \int_\mathbb{C} \frac{dM_\mathbb{C}}{s} \tag{55}$$

where $dM_\mathbb{C}$ is an element of mass of the moon, s is the distance from $dM_\mathbb{C}$ to the space vehicle, and $\int_\mathbb{C}$ indicates integration over the total mass of the moon. The function $\frac{1}{s}$ can be expanded in terms of Legendre polynomials,

$$U_\mathbb{C} = U_{\mathbb{C}0} + U_{\mathbb{C}1} + U_{\mathbb{C}2} + \cdots \tag{56}$$

where Alexandrov (Ref. 11) and Baker, Makemson (Ref. 12) have given the following values for $U_{\mathbb{C}0}$, $U_{\mathbb{C}2}$ and $U_{\mathbb{C}3}$, after a slight change in notation*.

$$U_{\mathbb{C}0} = \frac{GM_\mathbb{C}}{r_{S\Delta}}$$

$$U_{\mathbb{C}1} = 0$$

$$U_{\mathbb{C}2} = \frac{GM_\mathbb{C}\, a^2}{2r^3_{S\Delta}} \left[\frac{I_b - I_a}{I_c} (1 - 3\cos^2 \beta_\mathbb{C}) + \frac{I_c - I_a}{I_c} (1 - 3\sin^2 \phi'_\mathbb{C}) \right] \tag{57}$$

The term a is the semiaxis of inertia of the moon, in the direction of the earth, $r_{S\Delta}$ is the distance from the center of the moon to the vehicle, $U_{\mathbb{C}0}$ is the central force term arising from the spherically symmetric moon, $U_{\mathbb{C}1}$ shows that the moment about the center of mass vanishes by symmetry, and $U_{\mathbb{C}2}$ comes about since the moon is a triaxial ellipsoid (i.e., an ellipsoid with different semimajor axes in three mutually orthogonal directions from the center). I_a, I_b and I_c are the moments of inertia about the three principal semiaxes of inertia, a, b and c of the moon, such that c is along the lunar polar axis, a is in the earth's direction (excluding small librations) and b completes the right-hand system in the lunar equatorial plane.

The selenographic coordinate axes x_S, y_S, z_S coincide with the principal axes of inertia a, b, c. The angles $\phi'_\mathbb{C}$ and $\beta_\mathbb{C}$ are then defined to be the angle between the radius vector to the vehicle and the lunar equatorial plane (or the selenographic latitude), and the angle between the y_S-axis and the radius vector, respectively. These relationships are illustrated in the following sketch:

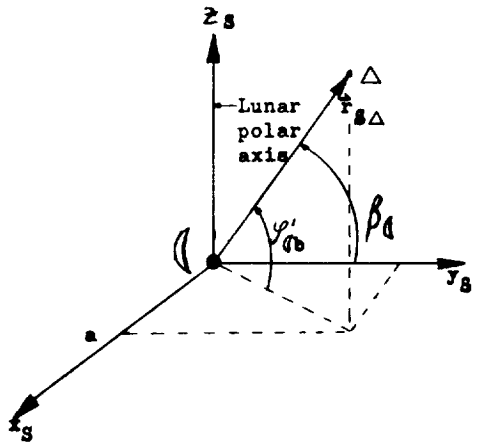

The expressions for $U_{\mathbb{C}2}$ given by Pines and Wolf (Ref. 13) agree with this expression if their symbol γ^3_{VM} is replaced by R^3_{VM} (which corresponds to $r^3_{S\Delta}$ in the notation of the present chapter).

---

*Actually, Baker and Makemson (Ref. 11) define a unit vector $\hat{r}_{S\Delta}$ in the direction of the vehicle radius vector $\vec{r}_{S\Delta}$ with components $x_{S\Delta}$, $y_{S\Delta}$, $z_{S\Delta}$ along the selenographic axes. Clearly,

$$\frac{y_{S\Delta}}{r_{S\Delta}} = \cos \beta_\mathbb{C}, \quad \frac{z_{S\Delta}}{r_{S\Delta}} = \cos (90 - \phi_\mathbb{C}) = \sin \phi_\mathbb{C}.$$

The form of $U_{\ell 2}$ in Eq (57) is given in the selenographic coordinate system which rotates with the moon (see preceding sketch). From this point one may proceed in two different ways. The first would be to transform $U_{\ell 2}$ to the geocentric equatorial coordinates used in the equations of motion, Eq (50). Since the influence of $U_{\ell 2}$ on the trajectory is strongest near the moon, it is more practical to write the equations of motion in a selenocentric equatorial or, preferably, lunar equatorial system and consequently transform $U_{\ell 2}$ to that coordinate system. If the second approach is taken, and the new perturbative expression is denoted by $U'_{\ell 2}$, then the components of the perturbative acceleration $\vec{f}_\ell$ in the lunar equatorial system are given formally by

$$f_{\ell x} = \frac{\partial U'_{\ell 2}}{\partial x_{\ell \Delta}}, \quad f_{\ell y} = \frac{\partial U'_{\ell 2}}{\partial y_{\ell \Delta}}, \quad f_{\ell z} = \frac{\partial U'_{\ell 2}}{\partial z_{\ell \Delta}} \tag{58}$$

Expressions for $\vec{f}_\ell$ and $U'_{\ell 2}$ will be given in Chapters VII and II.

At this time the knowledge of the lunar shape and the density distribution inside of the moon is slight and terms beyond $U_{\ell 2}$ in the expansion of U_ℓ given by Eq (56) are too uncertain for their inclusion. In the expressions for U_ℓ, Eqs (56 and (57), the numerical values of a, b, c, I_a, I_b, I_c given in Chapter II, are based on observations of the moon and the assumption that the lunar density is constant over concentric ellipsoidal shells. More accurate numerical values and expressions for U_ℓ together with local lunar gravity anomalies will become available as soon as a long-term lunar satellite can be observed from the lunar surface and when gravity measurements can be made on the moon.

b. Brief discussion of integration methods and techniques

Expressions for all gravitational terms in the equation of motion of the space vehicle, Eq (50), have been given previously. Before turning to the nongravitational force term $\vec{n}_\Delta M_\Delta$ in Eq (50), it is helpful to discuss the method of solution of this vector differential equation which corresponds to three second-order scalar differential equations, or an equivalent system of six first-order differential equations.

The problem is to find the position of the space vehicle as a function of time subject to its position and velocity at some initial time $t = t_0$, or its motion or trajectory. Mathematically speaking, this is an initial value problem in ordinary differential equations with time t as the independent variable and the coordinates $x_\oplus$, $y_\oplus$, $z_\oplus$ as the dependent variables. In order to proceed with the solution, the positions of the moon, sun and planets must be known in geocentric equatorial coordinates. These positions can be obtained from the yearly American Ephemeris (Ref. 14). If earth oblateness and the triaxiality of the moon are included in the physical model, then numerical values for certain other constants of the shape and density distribution of these celestial bodies are required as described in the previous subsection.

For lunar trajectories, the differential equation, Eq (50), is solved numerically on a digital computer. There are several methods of integration available (Cowell's method, Encke's method, for example), each with its own advantages and disadvantages for a specific physical problem. In addition one can use various numerical integration techniques (Runge-Kutta technique, for example), in which the integrand is represented by a polynomial of finite order at each computation step. Two types of errors arise from the integration technique, one due to the finite number of terms in the series, called the truncation error, and an error due to the finite number of digits carried on the computer, called the round-off error. In general it can be stated that the fewer the total number of computation steps in a given physical problem, the less the error. The term special perturbations is given to the determination of a trajectory by numerical integration; a more complete discussion of special perturbations can be found in Chapter IV of Ref. 3.

The numerical integration of space vehicle trajectories and the orbits of celestial bodies is based upon one of three methods, and variations thereof. The most direct in concept is Cowell's method. In this method the rectangular components of acceleration in the equations of motion are integrated directly, yielding the rectangular components of velocity and position. One disadvantage of the method is that the acceleration term in the integration changes rapidly with time, thereby necessitating the use of small computation steps (or time intervals). A second method, and the one most often used in ballistic trajectory computations, is Encke's method. Here, instead of obtaining the actual position and velocity coordinates, the difference between the actual position and velocity coordinates and that of a Keplerian orbit are computed. Some time, designated the epoch of osculation, is utilized to define the reference curve. This implies that for times near the epoch of osculation, the effects of the perturbations are small and can thus be summed over relatively large time intervals. A disadvantage lies in the fact that a new epoch of osculation must be introduced when the effects of the perturbations become large. This procedure is known as rectifying the Keplerian reference orbit. Another method is the Variation of Parameters which is discussed by Brouwer and Clemence (Ref. 15). There have been some recent studies (Baker et al., Ref. 16, Pines et al., Ref. 17, for example) of the advantages of the various integration methods in terms of simplicity, area of applicability and computing time, as well as accuracy and interpretation.

For long-term ephemerides, such as long-term artificial satellites of the earth and moon and periodic circumlunar and allunar trajectories, numerical methods are not well suited since a

very large number of computation steps are required and hence the accumulated error becomes excessive. In these cases one must resort to general perturbations, which is the analytical integration of series expansions of the perturbing forces, or a combination of special and general perturbations. Examples of general perturbations are the various lunar theories discussed in Chapter III. A discussion of general perturbations can be found in Chapter IV of Ref. 3.

For short transit trajectories as envisioned for approach, impact, lunar landing, the accuracy afforded by general perturbation theory is offset by its following inadequacies: (1) the theories have not yet included a complete analysis of all perturbing accelerations such as solar radiation pressure, and (2) the theories are very complicated to program (although short in machine time) and almost impossible to check. For these reasons general perturbation theories will not be discussed any further in this chapter.

In order to compare the various special perturbation methods, the following table taken primarily from page F-2 of Ref. 18 is useful:

Method	Advantages	Disadvantages
Cowell's	Simplicity in programming and analysis Universally applicable Coordinate conversion unnecessary	Increased number of integration steps Excessive error accumulation Increased computing time Detection of small perturbations difficult
Encke's	Smaller number of integration steps than Cowell's method Reduced computing time as compared with Cowell's method Improved accuracy Detection of small perturbations	Increased computing time for each step Complex program Special program for near-parabolic orbits
Variation of Parameters	Smaller number of integration steps than Cowell's Reduced computing time relative to Cowell's Improved accuracy as compared with Cowell's (about same as Encke's) Detection of small perturbations	Most complex to program Most computing time Most useful for earth-satellites of moderate eccentricity

Another consideration in numerical calculations is the integration technique to be used. The choice is between use of a single computation step technique such as the Runge-Kutta, a fourth-order multistep predictor-corrector technique such as Milne's and Adams-Moulton's or a higher order multistep technique such as Adams' Backward Difference, Obrechkoff, and Gauss-Jackson. There exist also special techniques for second-order differential equations such as the special Runge-Kutta and Milne-Stormer. For each multistep technique special formulas (for example, a Runge-Kutta technique or a Taylor series expansion) must be devised for starting the scheme at the given initial conditions. The most important factors in the choice of an integration technique for space vehicle trajectories are high speed and good accuracy. The latter involves low truncation or round-off error, ease of changing step size and little error growth. The round-off error can be reduced by using a double precision process, i.e., by carrying all dependent variables in double precision. The advantages and disadvantages of the various schemes are discussed more fully in Chapter IV of Ref. 3 (see also Refs. 15 and 18).

For ballistic lunar trajectories Encke's integration method or a variation thereof seems to be best suited due to the smallness of the perturbations throughout the trajectory (this can be seen by the way successive two-body problems can be used to describe the trajectory relatively accurately). The epoch of osculation should be changed whenever the sphere or volume of influence of the moon is entered or left. For an accurate simulation of large thrusts during the flight, Cowell's method is preferable during rocket burning. Of the various integration techniques Ref. 18 seems to favor slightly the Gauss-Jackson scheme over the others, while the Obrechkoff scheme has been found useful in the reduction of computing time. The interplanetary (and lunar) trajectory program described in Ref. 13 uses a modified Encke's method with an Adams' sixth-order backward difference integration technique which is initiated by a Runge-Kutta scheme.

Encke's method. Due to its widespread use in ballistic lunar trajectories, Encke's method will be described in this subsection. This method is used with some modifications in the trajectory program described in Ref. 13. This trajectory program, in turn, has been used with some minor modifications for the calculation of n-body lunar trajectories in this manual.

For the discussion of the basic Encke's method without modifications, consider Eq (50) repeated here:

$$M_\Delta \ddot{\vec{r}}_{\oplus\Delta} = -G \frac{\vec{r}_{\oplus\Delta}}{r^3_{\oplus\Delta}} M_\oplus M_\Delta + \vec{f}_\oplus M_\Delta + \sum_{i=\text{◀}}^{n} \left[(-G) \left(\frac{\vec{r}_{\oplus\Delta}}{r^3_{\oplus\Delta}} - \frac{\vec{r}_{i\oplus}}{r^3_{i\oplus}} \right) M_i M_\Delta + \vec{f}_i M_\Delta \right] + \vec{n}_\Delta M_\Delta, \quad i = \text{◀}, 1, 2, \ldots n$$

Dividing this equation by M_Δ and taking the dot product with $\hat{x}_\oplus$, $\hat{y}_\oplus$, $\hat{z}_\oplus$, respectively, yields the $x_\oplus$ $y_\oplus$ $z_\oplus$ components of vehicle acceleration. The $x_\oplus$-component of vehicle acceleration becomes

$$\ddot{x}_{\oplus\Delta} = -G\frac{x_{\oplus\Delta}}{r^3_{\oplus\Delta}} M_\oplus + f_{\oplus x} + \sum_{i=(}^{n} \left[(-G)\left(\frac{x_{\oplus\Delta}}{r^3_{\oplus\Delta}} - \frac{x_{i\oplus}}{r^3_{i\oplus}}\right) M_i + f_{ix}\right] + n_{\Delta x}$$

$$i = (\ ,1,2,\ldots n \qquad (59)$$

with similar expressions for $\ddot{y}_{\oplus\Delta}$ and $\ddot{z}_{\oplus\Delta}$.

Here f_{ix} represents the $x_\oplus$-component, in $x_\oplus$ $y_\oplus$ $z_\oplus$ coordinates, of the aspherical gravitational terms of the ith body affecting vehicle motion, and $n_{\Delta x}$ is the x-component of the resultant of all nongravitational accelerations acting on the vehicle in $x_\oplus$ $y_\oplus$ $z_\oplus$ coordinates.

For brevity neglect all but the spherical gravitational terms, i.e., n-body motion, since the other may be superimposed at the end. Then Eqs (59) become:

$$\ddot{x}_{\oplus\Delta} = -\frac{Gx_{\oplus\Delta}}{r^3_{\oplus\Delta}} M_\oplus + \sum_{i=(}^{n} (-G)\left(\frac{x_{\oplus\Delta}}{r^3_{\oplus\Delta}} - \frac{x_{i\oplus}}{r^3_{i\oplus}}\right) M_i,$$

$$i = (\ ,1,2,\ldots n \qquad (60)$$

with similar expressions for $\ddot{y}_{\oplus\Delta}$ and $\ddot{z}_{\oplus\Delta}$.

Consider the path that the vehicle would follow if acted on only by the gravitational attraction of the earth. Let the vehicle radius vector, its components of position and acceleration in this unperturbed restricted two-body motion be $\vec{r}_{\oplus u}$, $x_{\oplus u}$, $y_{\oplus u}$, $z_{\oplus u}$, and $\ddot{x}_{\oplus u}$, $\ddot{y}_{\oplus u}$, $\ddot{z}_{\oplus u}$, respectively. The unperturbed vehicle equations of motion for this case are:

$$\ddot{x}_{\oplus u} = -\frac{Gx_{\oplus u}}{r^3_{\oplus u}} M_\oplus \qquad (61)$$

and similar expressions for $\ddot{y}_{\oplus u}$ and $\ddot{z}_{\oplus u}$.

Subtract Eqs (61) from Eqs (60), and define new coordinates $\xi_{\oplus\Delta}$, $\eta_{\oplus\Delta}$, $\zeta_{\oplus\Delta}$ by the relations $x_{\oplus\Delta} - x_{\oplus u} = \xi_{\oplus\Delta}$, $y_{\oplus\Delta} - y_{\oplus u} = \eta_{\oplus\Delta}$, $z_{\oplus\Delta} - z_{\oplus u} = \zeta_{\oplus\Delta}$.

Then

$$\ddot{\xi}_{\oplus\Delta} = -GM_\oplus\left(\frac{x_{\oplus\Delta}}{r^3_{\oplus\Delta}} - \frac{x_{\oplus u}}{r^3_{\oplus u}}\right) + \sum_{i=(}^{n} (-G)\left(\frac{x_{\oplus\Delta}}{r^3_{\oplus\Delta}} - \frac{x_{i\oplus}}{r^3_{i\oplus}}\right) M_i,$$

$$i = (\ ,1,2,\ldots n \qquad (62)$$

and similar expressions hold for $\ddot{\eta}_{\oplus\Delta}$ and $\ddot{\zeta}_{\oplus\Delta}$.

Consider the first term in Eq (62). Taking only the term in parentheses and multiplying by (-1), it can be written

$$-\left(\frac{x_{\oplus u}}{r^3_{\oplus u}} - \frac{x_{\oplus\Delta}}{r^3_{\oplus\Delta}}\right) = -\frac{1}{r^3_{\oplus u}}\left(x_{\oplus u} - \frac{r^3_{\oplus u}}{r^3_{\oplus\Delta}} x_{\oplus u}\right)$$

$$= -\frac{1}{r^3_{\oplus u}}\left(x_{\oplus\Delta} - \xi_{\oplus\Delta} - \frac{r^3_{\oplus u}}{r^3_{\oplus\Delta}} x_{\oplus\Delta}\right)$$

$$= -\frac{1}{r^3_{\oplus u}}\left[\left(1 - \frac{r^3_{\oplus u}}{r^3_{\oplus\Delta}}\right) x_{\oplus\Delta} - \xi_{\oplus\Delta}\right] \qquad (63)$$

Now, expressing $r_{\oplus\Delta}$ in terms of $x_{\oplus 0}, y_{\oplus 0}, z_{\oplus 0}$, $\xi_{\oplus\Delta}, \eta_{\oplus\Delta}, \zeta_{\oplus\Delta}$

$$r^2_{\oplus\Delta} = x^2_{\oplus\Delta} + y^2_{\oplus\Delta} + z^2_{\oplus\Delta}$$

$$= (x_{\oplus u} + \xi_{\oplus\Delta})^2 + (y_{\oplus u} + \eta_{\oplus\Delta})^2 + (z_{\oplus u} + \zeta_{\oplus\Delta})^2$$

$$= r^2_{\oplus u} + 2x_{\oplus u}\xi_{\oplus\Delta} + 2y_{\oplus u}\eta_{\oplus\Delta} + 2z_{\oplus u}\zeta_{\oplus\Delta} + \xi^2_{\oplus\Delta} + \eta^2_{\oplus\Delta} + \zeta^2_{\oplus\Delta} \qquad (64)$$

Then

$$\frac{r^2_{\oplus\Delta}}{r^2_{\oplus u}} = 1 + 2\,\frac{(x_{\oplus u} + 1/2\,\xi_{\oplus\Delta})\xi_{\oplus\Delta} + (y_{\oplus u} + 1/2\,\eta_{\oplus\Delta})\eta_{\oplus\Delta} + (z_{\oplus u} + 1/2\,\zeta_{\oplus\Delta})\zeta_{\oplus\Delta}}{r^2_{\oplus u}} \qquad (65)$$

Put

$$q = \frac{(x_{\oplus u} + 1/2\,\xi_{\oplus\Delta})\xi_{\oplus\Delta} + (y_{\oplus u} + 1/2\,\eta_{\oplus\Delta})\eta_{\oplus\Delta} + (z_{\oplus u} + 1/2\,\zeta_{\oplus\Delta})\zeta_{\oplus\Delta}}{r^2_{\oplus u}} \qquad (66)$$

Then

$$\left(\frac{r_{\oplus\Delta}}{r_{\oplus u}}\right)^2 = 1 + 2q$$

and

$$\left(\frac{r_{\oplus u}}{r_{\oplus\Delta}}\right)^3 = (1 + 2q)^{-3/2}$$

Assume that the true orbit, Eq (60), does not differ much from the Keplerian orbit, Eq (61), so that $\xi_{\oplus\Delta}, \eta_{\oplus\Delta}, \zeta_{\oplus\Delta}$, are very small in comparison to $x_{\oplus u}, y_{\oplus u}, z_{\oplus u}$. In that case the squares of the increments can be neglected. Thus,

$$q \simeq \frac{x_{\oplus u}\,\xi_{\oplus\Delta} + y_{\oplus u}\,\eta_{\oplus\Delta} + z_{\oplus u}\,\zeta_{\oplus\Delta}}{r^2_{\oplus u}} \qquad (67)$$

Further, assume q is small compared to unity, thus enabling the first few terms of the binomial expansion to approximate the term $\left[1 - \left(\frac{r_{\oplus u}}{r_{\oplus\Delta}}\right)^3\right]$ in Eq (63).

Then,

$$\left[1 - \left(\frac{r_{\oplus u}}{r_{\oplus\Delta}}\right)^3\right] = 1 - (1+2q)^{-3/2} \simeq 3q - \frac{15}{2}q^2 \qquad (68)$$

The series used in the expansion of Eq (68) can be shown to converge for $-\frac{1}{2} < q < \frac{1}{2}$ which is well outside its practical limit of applicability in the n-body trajectory program.

Define

$$f = \frac{1 - (1+2q)^{-3/2}}{q} \qquad (69)$$

Note that f changes much less rapidly than q, staying very close to 3 when q is small. It is thus easy to interpolate giving q as a function of f.

Equation (63) then becomes by use of Eqs (64), (67) and (69):

$$-\frac{x_{\oplus u}}{r^3_{\oplus u}} - \frac{x_{\oplus\Delta}}{r^3_{\oplus\Delta}} = -\frac{1}{r^3_{\oplus u}}\left(fqx_{\oplus\Delta} - \xi_{\oplus\Delta}\right) \qquad (70)$$

Substitution of Eq (70) into Eq (62) and addition of the terms that have been neglected yields the following perturbation equations of motion:

$$\ddot{\xi}_{\oplus\Delta} = -\frac{GM_\oplus}{r^3_{\oplus u}}\left(fqx_{\oplus\Delta} - \xi_{\oplus\Delta}\right) + f_{\oplus x} + \sum_{i=1}^{n}\left[(-G)\left(\frac{x_{\oplus\Delta}}{r^3_{\oplus\Delta}} - \frac{x_{i\oplus}}{r^3_{i\oplus}}\right)M_i + f_{ix}\right] + n_{\Delta x}$$

$$\ddot{\eta}_{\oplus\Delta} = -\frac{GM_\oplus}{r^3_{\oplus u}}\left(fqy_{\oplus\Delta} - \eta_{\oplus\Delta}\right) + f_{\oplus y} + \sum_{i=1}^{n}\left[(-G)\left(\frac{y_{\oplus\Delta}}{r^3_{\oplus\Delta}} - \frac{y_{i\oplus}}{r^3_{i\oplus}}\right)M_i + f_{iy}\right] + n_{\Delta y} \qquad (71)$$

$$\ddot{\zeta}_{\oplus\Delta} = -\frac{GM_\oplus}{r^3_{\oplus u}}\left(fqz_{\oplus\Delta} - \zeta_{\oplus\Delta}\right) + f_{\oplus z} + \sum_{i=1}^{n}\left[(-G)\left(\frac{z_{\oplus\Delta}}{r^3_{\oplus\Delta}} - \frac{z_{i\oplus}}{r^3_{i\oplus}}\right)M_i + f_{iz}\right] + n_{\Delta z}$$

These are the fundamental equations of Encke's method. Sometimes they will be encountered having been multiplied by the constant factor, h^2, where h represents the width of the interpolation interval. An actual numerical example using this method is given by Brouwer (Ref. 15, p 179).

The reference orbit used in this description of Encke's method is the restricted two-body orbit, Eq (61). The method may be modified to use other types of reference orbits which would be more advantageous for the particular geometry and force model.

d. Description of the n-body trajectory program

The trajectory program used for obtaining n-body integrated lunar trajectories in this manual is described in detail in Ref. 13. Some additions have been made, so that the program at present is able to give the motion of a point mass with mass M_Δ (simulating the space vehicle) under the gravitational attraction of the oblate earth, the triaxially ellipsoidal moon, the sun, Venus, Mars and Jupiter. The positions of these celestial bodies as obtained from the U. S. Naval Observatory are stored in the program in geocentric equatorial rectangular coordinates ($x_\oplus, y_\oplus, z_\oplus$) for 12-hr intervals for the moon and for 24-hr intervals for the sun and planets. A special input variable allows the use of this position data for the specified time period. In addition a subroutine for computing lunar librations from the rectangular position coordinates of the moon exists, and is described in Section C of Chapter III. It will be incorporated in the program as soon as a satisfactory interpolation routine can be established.

The force model for this trajectory has also provisions for including drag due to a spherically symmetric atmosphere rotating with the earth. The atmospheric drag terms in the equations of motion are described in the next subsection. There are plans to include solar radiation pressure and other nongravitational forces.

The n-body trajectory program uses a modified Encke numerical integration method as described in Subsection 3d. The unperturbed restricted two-body orbit is rectified as soon as the ratios of the perturbative distance, speed, or numerical

value of acceleration exceeds 1% of the respective restricted two-body reference orbit. The procedure is essentially as follows:

(1) The most significant body in the system is selected (initially this is the earth, and if the trajectory approaches the moon, the moon); Eqs (61) are solved numerically on the computer. This numerical solution can always be checked by the known analytical solution.

(2) Equations (60) are then solved using a sixth-order Adams backward difference technique which is started by a Runge-Kutta scheme.

(3) The corrected coordinates of the body are then obtained by using the relations: $x_{\oplus\Delta} = x_{\oplus u} + \xi_{\oplus\Delta}$, $y_{\oplus\Delta} = y_{\oplus u} + \eta_{\oplus\Delta}$, $z_{\oplus\Delta} = z_{\oplus u} + \zeta_{\oplus\Delta}$ and similar ones for velocity and acceleration components. When the perturbations exceed the above limits, new solutions are obtained for Eq (61), and the orbit is rectified.

4. Nongravitational Forces

Having discussed all gravitational terms appearing in Eq (50), which are significant for lunar trajectories, let us turn our attention to the nongravitational forces acting on the vehicle, the resultant of which was termed $\vec{n}_\Delta M_\Delta$ in Eq (50). It should be noted that if the forces discussed subsequently are to be used in Eq (50) and the trajectory program, they must be expressed in component form in equatorial geocentric coordinates.

Let

$$\vec{n}_\Delta M_\Delta = \vec{D}_s + \vec{D} + \vec{D}_E + \vec{D}_M + \vec{T} + \vec{R}_{rel} \qquad (72)$$

where

$\vec{D}_s$ = force due to the solar radiation pressure

$\vec{D}$ = atmospheric drag force

$\vec{D}_E$ = electromagnetic forces

$\vec{D}_M$ = meteoritic drag force

$\vec{T}$ = rocket thrust force

$\vec{R}_{rel}$ = relativistic corrections to the equations of motion.

These forces will be discussed more fully in the above order in the following subsections.

a. Solar radiation pressure

Outside the confines of the earth's atmosphere, the most significant natural nongravitational force acting on a vehicle arises from solar radiation pressures can be seen from the table on page IV-22. It is due to the absorption and emission of photons by the space vehicle and is a consequence of the photon nature of light. Studies have been made previous to the launching of space vehicles concerning the effects of this solar radiation pressure on the orbits of micrometeorites around the sun. These studies by Poynting and Robertson indicated that the orbits of micrometeorites became more circular due to solar radiation, while simultaneously, slowly spiraling into the sun. More recently investigators have studied the effects of this force on satellites and, have found that for a vehicle mass to area ratio $\frac{M_\Delta}{A_\Delta} \leq 0.04$ gm/cm^2, a sizable perturbation occurs in the orbital elements (see Ref. 12). The essential qualitative effect of radiation pressure is a displacement of the center of the orbit, which is especially evident for circular and near-circular orbits (Ref. 19).

In these studies one of two possible approaches is taken. Either this force is obtained neglecting those times when the space vehicle is eclipsed by the earth or moon and hence the radiation pressure does not act (this is termed the shadow time), or the shadow time is included by expressing the force as a function of the orbital elements of the vehicle (i.e., as a perturbation in the variation of parameters method).

For the present analysis, the shadow time will be neglected and the rectangular components of the radiation pressure will be given in terms of vehicle-centered coordinates. This analysis essentially follows Kochi and Staley (Ref. 20).

Let P be the magnitude of the momentum of a photon, E_P its energy, m its equivalent mass, and c the speed of light; then

$$P = mc \qquad (73)$$

and

$$E_P = h\nu_P = mc^2 \qquad (74)$$

where $h = 6.625 \times 10^{-39}$ joule-sec is Planck's constant and ν is the frequency of the radiation. From Eqs (73) and (74)

$$P = \frac{h\nu_P}{c} \qquad (75)$$

The magnitude of the force per unit area due to radiation pressure, p_s, then is

$$p_s = \frac{h\nu_P}{c} N \qquad (76)$$

where N is the number of photon collisions with the vehicle per unit time on a unit area. If W_Δ is the radiated power arriving at the space vehicle per unit area of the vehicle, then $N = \frac{W_\Delta}{E_P} = \frac{W_\Delta}{h\nu_P}$

and

$$p_s = \frac{h\nu_P}{c} \cdot \frac{W_\Delta}{h\nu_P} = \frac{W_\Delta}{c} .$$

The type of photon collision with the vehicle must also be taken into consideration. To do this, a factor q_s will be introduced such that $0 \leq q_s \leq 1$ where $q_s = 0$ represents total momentum transfer, or perfect absorber, black body, i.e., an inelastic photon collision, and $q_s = 1$ represents a perfect

reflector, i.e., an elastic photon collision. Hence

$$p_s = \frac{W_\Delta}{c}(1 + q_s) \tag{77}$$

Let $W_\odot$ represent the total radiated power (in watts/cm^2 per hemisphere) of the sun at all frequencies. Then by the Stefen-Boltzmann Law:

$$W_\odot = \epsilon \sigma T^4 A_\odot \tag{78}$$

where ϵ is the total empirically determined emissivity of the sun ($\epsilon = 1.0$, i.e., the sun is a perfect radiator), $\sigma = 5.67 \times 10^{-8}$ watts/m^2 (°K)^4 is the Stefan-Boltzmann constant, a constant of proportionality determined experimentally and defined by Eq (78),

T is the absolute temperature in °K,

$A_\odot$ is the surface area of the sun.

Now the radiant energy per second, W_Δ, impinging upon a unit area of the vehicle perpendicular to the line-of-sight to the sun, which is regarded as a point source, at a distance $r_{\oplus,\odot\to\Delta}$ is given by

$$W_\Delta = \frac{W_\odot}{\pi r^2_{\oplus,\odot\to\Delta}} = \frac{\epsilon \sigma T^4 A_\odot}{\pi r^2_{\oplus,\odot\to\Delta}} \tag{79}$$

The point source approximation is reasonable since any trajectory in the vicinity of the earth is more than 100 solar diameters from the sun. Hence the solar radiation pressure per unit area is given by

$$p_s = \frac{\epsilon \sigma T^4 A_\odot}{\pi c r^2_{\oplus,\odot\to\Delta}}(1 + q_s) \times 10^7 \ \frac{\text{dynes}}{\text{cm}^2} \tag{80}$$

where p_s is in the opposite direction from the sun along the vehicle-sun line, and 10^7 is a conversion factor from watts to $\frac{\text{dyne-cm}}{\text{sec}}$. An approximate value for the solar radiation pressure at the distance of the earth is $p_s = 4.5 \times 10^{-5} \ \frac{\text{dynes}}{\text{cm}^2}$ for a black body space vehicle (Ref. 21).

The acceleration of the vehicle due to the solar radiation pressure, $\vec{D}_s$, is given by

$$\frac{\vec{D}_s}{M_\Delta} = \frac{p_{s0}(1 + q) A_s}{M_\Delta r^2_{\oplus,\odot\to\Delta}} \frac{\vec{r}_{\oplus,\odot\to\Delta}}{r_{\oplus,\odot\to\Delta}} \tag{81}$$

where

$$p_{s0} = \frac{\epsilon \sigma T^4 A_\odot \times 10^7}{\pi c} \simeq 10^{22} \text{ dynes}$$

is the total force due to solar radiation divided by π, q_s, $0 \le q_s \le 1$, is the space vehicle reflectivity, zero for a black body and 1 for a perfect reflector, A_s the area of the vehicle perpendicular to the vehicle-sun line, M_Δ its mass, and $\vec{r}_{\oplus,\odot\to\Delta}$ is the radius vector of the vehicle from the sun. Next write $\vec{r}_{\oplus,\odot\to\Delta} = \vec{r}_{\oplus\Delta} - \vec{r}_{\oplus\odot}$ so that Eq (81) becomes

$$\frac{\vec{D}}{M_\Delta} = \frac{p_{s0}(1 + q_s) A_s}{M_\Delta \left| \vec{r}_{\oplus\Delta} - \vec{r}_{\oplus\odot} \right|^3} (\vec{r}_{\oplus\Delta} - \vec{r}_{\oplus\odot}) \tag{82}$$

Since the position of the vehicle is continually computed during a trajectory run on the computer and since the positions of the sun are stored, Eq (82) may be solved as soon as A_s is specified. For all but spherical space vehicles the computation of A_s requires a knowledge of vehicle orientation with respect to the vehicle-sun line. This line can be given with respect to body axes x_b, y_b, z_b with origin at the vehicle center of gravity, and these axes can be transformed to the geocentric equatorial coordinates by the transformation given in Table 2. The following sketch illustrates the geometry in this case.

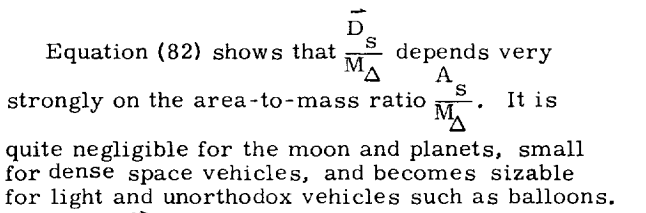

Equation (82) shows that $\frac{\vec{D}_s}{M_\Delta}$ depends very strongly on the area-to-mass ratio $\frac{A_s}{M_\Delta}$. It is quite negligible for the moon and planets, small for dense space vehicles, and becomes sizable for light and unorthodox vehicles such as balloons. The term $\frac{\vec{D}_s}{M_\Delta}$ also depends on the type of surface--thus q_s may approach 0.98 for highly polished metals. The shadow time may be neglected for lunar trajectory studies since the trajectory will be in sunlight during most approach, impact, and circumlunar trajectories. However, during earth or moon orbital phase the shadow time may approach half of the total time in orbit for low-altitude orbits. A discussion and graphical presentation of shadow time as a function of orbital elements is given in Chapter XIII of Ref. 3.

b. Atmospheric drag and lift

In connection with lunar trajectories, the contribution of atmospheric drag need only be considered in the short time period when the vehicle is in the immediate vicinity of the earth. Thus, its significance is much less important than in the case of earth satellite vehicles. However, during parking orbits around the earth, atmospheric drag becomes of decisive importance in the selection of orbital radius and eccentricity; a discussion of this force will be included here.

The acceleration of a space vehicle due to the drag force can be expressed as

$$\frac{\vec{D}}{M_\Delta} = -\frac{1}{2} C_D \frac{A_a}{M_\Delta} \rho V_a^2 \frac{\vec{V}_a}{V_a} \tag{83}$$

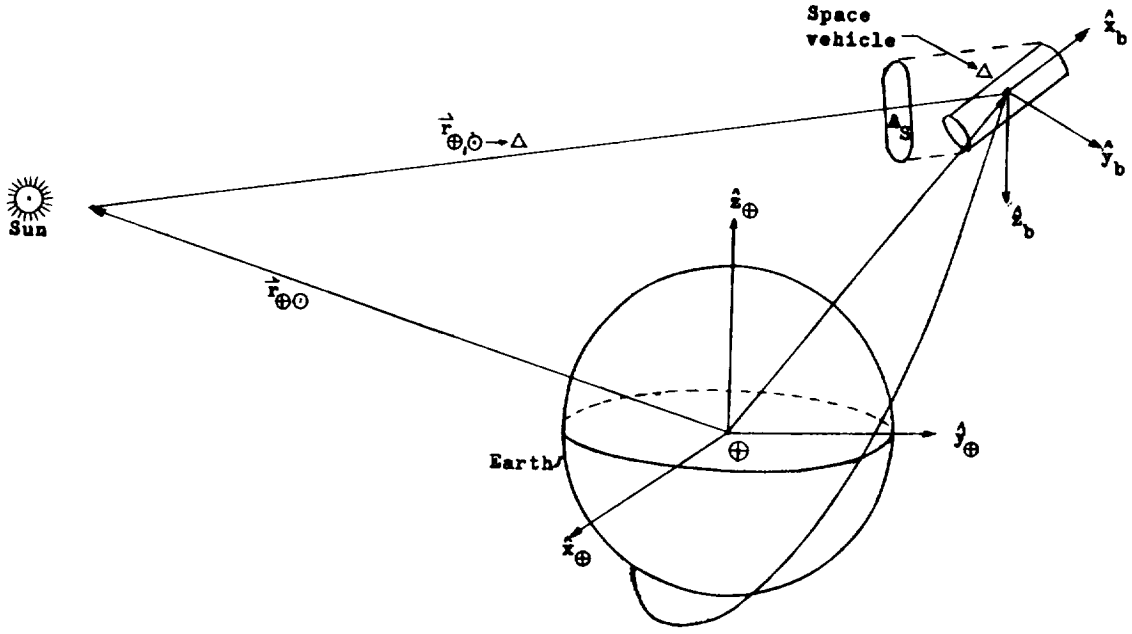

where

C_D is the drag coefficient (usually the one for free molecular flow in the case of earth satellites and space vehicles)

A_a is the area of the space vehicle perpendicular to $\vec{V}_a$

ρ_a is the density of the atmosphere

$\vec{V}_a$ is the velocity of the vehicle relative to the atmosphere.

For parametric studies it is useful to introduce a ballistic coefficient $B = \frac{C_D A_a}{2M_\Delta}$ which gives for the drag acceleration

$$\frac{\vec{D}}{M_\Delta} = -B\rho V_a \vec{V}_a \tag{84}$$

The drag coefficient C_D can be calculated from free molecular flow assumption in the kinetic theory of gases. It depends on the geometry and orientation of the vehicle as well as the interaction of the air molecules with its surface. The value of C_D is 2.0 for spherical vehicles, and slightly larger for other vehicle shapes. For all but spherical vehicles A_a as well as C_D will vary with the orientation of the vehicle relative to $\vec{V}_a$. In the case of a vehicle in a random tumble with a short period of tumble compared to the orbital period or compared to the time in the atmosphere for lunar trajectories, a good approximation is $A_a = \frac{A_\Delta}{4}$, where A_Δ is the surface area of the vehicle.

$\vec{V}_a$ can be written as the difference of the vehicle velocity with respect to the geocentric equatorial system frame $\vec{V}_{\oplus\Delta}$ and the velocity of the atmosphere $\vec{V}_{\oplus a}$. Thus,

$$\vec{V}_a = \vec{V}_{\oplus\Delta} - \vec{V}_{\oplus a} \tag{85}$$

At altitudes below 500 km, the atmosphere can be assumed to rotate with the earth so that under this assumption the velocity of the atmosphere with respect to the equatorial system is given by

$$\vec{V}_{\oplus a} = \vec{\omega}_\oplus \times \vec{r}_{\oplus\Delta} \tag{86}$$

Substituting (86) into (85)

$$\vec{V}_a = \vec{V}_{\oplus\Delta} - \vec{\omega}_\oplus \times \vec{r}_{\oplus\Delta} \tag{87}$$

In order to express V_a in rectangular geocentric coordinates, note that

$$\vec{V}_{\oplus\Delta} = \dot{x}_{\oplus\Delta}\hat{x}_\oplus + \dot{y}_{\oplus\Delta}\hat{y}_\oplus + \dot{z}_{\oplus\Delta}\hat{z}_\oplus \tag{88}$$

$$\vec{\omega}_\oplus \times \vec{r}_{\oplus\Delta} = \begin{vmatrix} \hat{x}_\oplus & \hat{y}_\oplus & \hat{z}_\oplus \\ 0 & 0 & \omega_\oplus \\ x_{\oplus\Delta} & y_{\oplus\Delta} & z_{\oplus\Delta} \end{vmatrix} = \omega_\oplus x_{\oplus\Delta}\hat{y}_\oplus - \omega_\oplus y_{\oplus\Delta}\hat{x}_\oplus$$

If Eqs (88) are substituted into Eq (87) and the result into Eq (84), the magnitude of the drag acceleration is given by:

$$\frac{D}{M_\Delta} = -B\rho\left(\dot{r}^2_{\oplus\Delta} - 2\omega_\oplus \dot{x}_{\oplus\Delta} y_{\oplus\Delta} + 2\omega_\oplus x_{\oplus\Delta}\dot{y}_{\oplus\Delta} + \omega^2_\oplus x^2_{\oplus\Delta}\right) \tag{89}$$

The number of molecules per unit volume, N_0, can be obtained from the kinetic theory of gases. In the case of an isothermal atmosphere (T = constant) and constant molecular weight and composition

$$N_0 = N_1 \exp\left[-\frac{mg_\oplus}{kT}(h_e - h_{e1})\right] \qquad (90)$$

where

- m = the constant mass of each molecule
- h_e = altitude above earth
- $g_\oplus$ = the constant value of the gravitational acceleration
- k = 1.380×10^{-23} joules/°K, Boltzmann's constant
- T = absolute temperature in °K
- h = altitude.

Subscript 1 designates some reference condition. The atmospheric density is then given by $\rho = N_0 m$. However, this is a very poor approximation of the atmosphere, and usually a variation of temperature T, $g_\oplus$, as well as molecular weight is assumed with altitude and the density, pressure, and any other quantities are computed from this assumption. The latest such "standard atmosphere" is the 1961 U. S. Standard Atmosphere, which is used in all work in this manual. The density in this atmosphere varies with altitude and is given to an altitude of 700 km. Actually the density varies additionally with latitude due to the latitude-dependence of the earth's gravitational potential $U_\oplus$ by about ±2% and with the solar activity (which at the higher altitudes may cause very large deviations from the standard density). These variations from the standard atmospheric density may be neglected, however, as long as only lunar trajectories or a few orbits near the earth are considered.

Just as in the case of solar radiation pressure the drag acceleration is small for small area-to-mass ratio or dense vehicles and becomes more significant for light vehicles such as balloons. The drag force decreases very substantially with altitude and may be neglected for all but long-time operations above 700 km.

For accurate drag computations and when the vehicle orientation is significant it is more convenient to express the drag force $\vec{D}$ in component form along the body axes x_b, y_b, z_b,

$$D_x = -\frac{1}{2} C_x A_{ref} \rho V_a^2$$
$$D_y = -\frac{1}{2} C_y A_{ref} \rho V_a^2 \qquad (91)$$
$$D_z = -\frac{1}{2} C_z A_{ref} \rho V_a^2$$

where all the variations in the force are absorbed in the coefficients C_x, C_y, C_z and A_{ref} is a constant reference area characterizing the space vehicle. Once the orientation of the vehicle is known, the transformation from body axes to geocentric equatorial coordinates as given in Table 2 can be performed.

Atmospheric lift will be neglected for parking orbits and lunar trajectories since it is several orders of magnitude less than the drag at orbital altitudes. However, during the intermediate stages of ascent to orbit or injection, and in the initial stages of a nonballistic re-entry, this force becomes important. The magnitude of the lift L is defined, analogously to the magnitude of the drag D, by the equation

$$L = \frac{1}{2} C_L A_a \rho V_a^2, \qquad (92)$$

where C_L is the lift coefficient which can be computed similarly to C_D from free molecular assumption in the kinetic theory of gases. The lift force $\vec{L}$ is in a plane perpendicular to $\vec{V}_a$ by definition, and its direction in this plane is specified by the bank angle ξ. Consider a unit vector in this plane perpendicular to $\vec{r}_{\oplus\Delta}$ and $\vec{V}_a$, namely $\hat{y}_w \equiv \frac{\vec{r}_{\oplus\Delta}}{r_{\oplus\Delta}} \times \frac{\vec{V}_a}{V_a}$. A unit vector orthogonal to $\hat{y}_w$ is given by $\hat{z}_w \equiv \frac{\vec{V}_a}{V_a} \times \frac{\vec{r}_{\oplus\Delta}}{r_{\oplus\Delta}} \times \frac{\vec{V}_a}{V_a}$

The unit vectors $\hat{x}_w \equiv \frac{\vec{V}_a}{V_a}$, $\hat{y}_w$ and $\hat{z}_w$ define wind axes, where a rotation about the x_w-axis is defined as the bank angle ξ, a rotation about the y_w-axis is the angle of attack α, and a rotation about the z_w-axis is the yaw angle β. Wind axes and the bank angle ξ between $\hat{z}_w$ and $\vec{L}$ are illustrated in the following sketch:

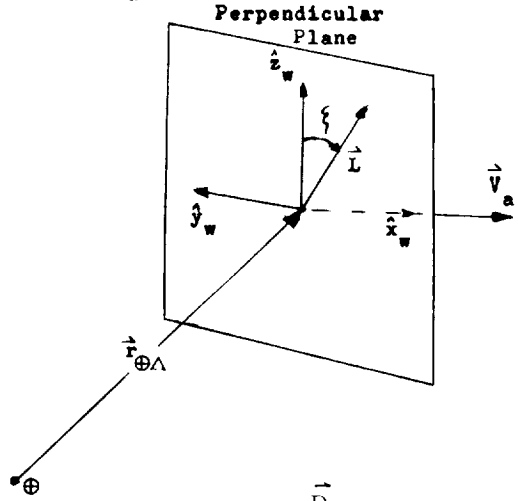

The drag acceleration $\frac{\vec{D}}{M_\Delta}$ as given by Eq (83) is in the negative $\hat{x}_w$-direction.

c. Electromagnetic forces

In most trajectory calculations the vehicle on a lunar trajectory is assumed to be electrically neutral, and beyond some altitude (700 km), which is regarded as the upper limit of the atmosphere, it is assumed to move in a vacuum. This ideal condition does not exist in space, and the effects of several electromagnetic phenomena will influence the vehicle trajectory very slightly. Even though these effects are small, upper limits to the deceleration of space vehicles should be determined and they should be considered in a detailed trajectory analysis.

The medium through which the space vehicle moves consists of charged particles. Baker (Ref. 12) states that even interplanetary space contains between 100 and 1000 charged particles per cubic centimeter which originate from solar eruptions (flares and solar winds), cosmic ray ionization (the ionization of neutral particles caused by cosmic rays and gamma radiation). Higher concentrations of charged particles occur near earth in the inner and outer Van Allen belts which consist of solar particles trapped in the earth's magnetic field. Recently a temporary radiation belt was created by a high-altitude hydrogen bomb explosion of July 9, 1962 which is expected to last for several years.

A space station in a stationary plasma (an electrically neutral medium containing charged particles) will collide with both slow moving positive ions and fast moving electrons and build up a small excess of net negative change on its surface.

Another factor affecting the potential of the vehicle, ϕ_Δ, stems from its motion with respect to the plasma.

As the vehicle travels at several km/sec, its collision rate with the positive ions, which move more slowly, increases as compared to the stationary plasma collision rate, whereas the collision rate with the electrons, which move much faster than the positive ions, remains essentially unaltered. Thus, vehicle motion tends to decrease the induced negative voltage from the source discussed above.

Beard and Johnson (Ref. 21) have derived an expression for the potential, ϕ_Δ, of a satellite moving through such a plasma with speed V_p. It is:

$$\phi_\Delta = - \frac{kT}{q_e} \ell n \left(\frac{1}{2} \frac{\bar{V}_{e\ell}}{V_p} \right) \qquad (93)$$

where

k = 1.380 x 10^{-23} joules/° K, Boltzmann's constant

T = absolute temperature of the plasma in ° K

q_e = 1.602 x 10^{-19} coulomb, the charge of an electron

V_p = speed of space vehicle relative to the plasma

$\bar{V}_{e\ell}$ = the average thermal speed of an electron in the medium, given by

$$\bar{V}_{e\ell} = 0.145 \quad T/m_e$$

where m_e is the atomic weight of an electron. This negative potential obtained from Eq (93) amounts to only a few volts in typical cases.

Singer and Walker (Ref. 22) have proposed that the ejection of electrons caused by high-energy solar radiation striking the vehicle need not be considered due to the buildup of a screen of ejected electrons surrounding the vehicle, thus reducing any further electron ejection.

An expression for the total force on a space vehicle which is electrically conductive and magnetically permeable has been given by M. Z. V. Krzywoblocki, et al., in Ref. 23. Starting from Maxwell's equation for moving media he derived the force on a body due to the electrostatic field, the magnetic field and a final expression for the force acting on a moving body in an electromagnetic field.

Due to our scant knowledge of the cislunar and interplanetary medium and the large and unpredictable fluctuation of its number-density with solar eruptions, the material given in this subsection has been primarily of an illustrative nature. The presence of these particles and the radiation will influence the trajectory of the lunar vehicle only slightly; their pressure, however, is of primary importance from the standpoint of shielding requirements for any human occupants in the space vehicle.

d. Meteoritic drag

In the attempts to analyze the force acting upon a space vehicle due to meteoritic drag, experimental evidence is taken primarily from past observation of meteoritic contact with the earth (Ref. 20) to which some space probe data has been added recently. Due to the rarity of large meteorites impinging even upon a body the size of the earth, it can be assumed that the probability of a small lunar vehicle being hit by such a meteorite would be extremely small; therefore, it will be neglected. Hence, it will be assumed that micrometeorites contribute the only significant meteoritic drag perturbation. Ideally one would like to know meteor density, mass flux, velocity and spatial distribution as a function of position and time for the sporadic background as well as for meteoritic showers. Only the sporadic background flux can be considered here. Estimates of the accretion of meteoritic material by the earth vary widely, but extensive geophysical evidence from both optical and radio experiments indicates that the maximum amount of meteoritic material hitting the earth per day is 2000 tons (Refs. 20, 24). This would correspond to a meteoritic density of $\rho_M = 5 \times 10^{-21}$ g/cm^3 outside of the atmosphere. Furthermore, it is believed that micrometeorites (i.e., meteorites

with magnitudes between the ranges 20 and 30 or radii less than about 100 microns) constitute 95% of the meteoritic material hitting the earth (Ref. 20). Also, meteorites can enter the earth's atmosphere only with velocities between 11 and 72 km/sec relative to the earth. The lower limit on velocities of entry is due to the gravitational acceleration of the particle by the earth, while the upper limit is the sum of the parabolic velocity for a solar orbit at the distance of the earth (42 km/sec) and the earth's orbital velocity (30 km/sec).

Assume that the direction of motion of the meteorites is random along the lunar trajectory (this hypothesis is invalid near the surface of the earth or the moon which shield the vehicle from below) and that the meteorites are so small as to evenly distributed in space. Then the mass, M_M of meteorites striking the vehicle in the time interval Δt from any one direction is:

$$M_M = \frac{1}{6} \rho_M A_M V_{\oplus M} \Delta t \qquad (94)$$

where

ρ_M = is the average density of meteoritic material in space

A_M = the cross-sectional area of the vehicle perpendicular to the particular direction

$V_{\oplus M}$ = the average speed of the meteorites

and it has been assumed that the velocity of the micrometeorites is much larger than the velocity of the vehicle. The net momentum imparted to the vehicle sides per second is zero since the momentum of the micrometeoritic hits from the left is cancelled by those from the right, and similarly for the top and bottom of the vehicle. However, the micrometeorites striking the space vehicle from behind have a relative velocity of $(V_{\oplus M} - V_{\oplus \Delta})$ with respect to the vehicle, and those from the front have a relative velocity of $-(V_{\oplus M} + V_{\oplus \Delta})$. The net rate of momentum transfer, or the magnitude of the force on the vehicle due to meteoritic impact is

$$D_{M1} = -\frac{1}{3} \rho_M A_M V_{\oplus M} V_{\oplus \Delta} \qquad (95)$$

where the negative sign indicates that this force is directed against the vehicle geocentric velocity vector $\vec{V}_{\oplus \Delta}$. As an illustrative example, for $\rho_M = 5 \times 10^{-21}$ g/cm^3, $A_M = 10 m^2 = 10^5$ cm^2, an average meteoritic speed of $V_{\oplus M} = 40$ km/sec $= 4 \times 10^6$ cm/sec and a representative vehicle speed of 3 km/sec $= 3 \times 10^5$ cm/sec, the magnitude of the force due to meteoritic impacts is $D_{M1} = -2 \times 10^{-4}$ dynes.

Also to be considered is the type of meteoritic impact. In a perfectly elastic collision the micrometeorite will leave the space vehicle with the same relative speed as that at which it hit and the magnitude of this total force on the space vehicle becomes

$$D_M = 2D_{M1} = -4 \times 10^{-4} \text{ dynes.}$$

In a perfectly inelastic collision, on the other hand, all the micrometeorites stay with the vehicle and must be accelerated to its speed. In this case the magnitude of the total force on the space vehicle becomes

$$D_M = D_{M1} - \rho_M A_M V_{\oplus M} V_{\oplus \Delta} = 4D_{M1}$$

$$= -8 \times 10^{-4} \text{ dynes.}$$

In the case where the micrometeorite blasts material from the skin of the space vehicle, and where it, together with some satellite material, is left behind, the meteoritic drag force should probably be decreased.

This discussion shows that regardless of the type of collision and even for the maximum meteoritic density assumed for these calculations the force on the satellite is extremely small. The major importance of meteoritic impacts lies in their effect on the material of the satellite skin, i.e., the probability of puncture with resulting fuel or gas losses, or damage to some subsystem, and the sandblasting or pitting of the skin or of optical surfaces such as lenses, windows, etc. The probabilities of a catastrophic encounter between a space vehicle and a large meteor are extremely small. A more complete discussion of meteoritic densities, representative values for fluxes, classifications, models, and the effect of micrometeorites on space vehicle materials is given in Chapter II and Chapter II of Ref. 3.

e. Rocket thrust

The thrust due to rocket burning is another force acting on the space vehicle which must be considered in the complete analysis of a lunar trajectory. As a first approximation it is possible to assume that the vehicle is accelerated by an initial large thrust during the boost stage to the predetermined injection velocity, and that the lunar trajectory approaches the moon ballistically on a path determined by the injection conditions. In this case thrust forces need not be considered. However, even the earliest lunar vehicles had provisions for applying corrective accelerations by both midcourse and terminal thrust to overcome any errors in initial conditions and due to our imperfect knowledge of the physical environment. More sophisticated missions such as lunar orbit and landing missions require one or several large decelerations and accelerations of the space vehicle during the mission. Thus at some time in the planning of any lunar mission the simulation of thrust becomes necessary.

In most cases the thrust force is large and the time for rocket burning is small compared to the transit time. Then Encke's integration method should be stopped at the onset of rocket burning (since the perturbing acceleration by the thrust force is too large), and Cowell's method of integration should be used to simulate vehicle motion

during rocket burning. The end conditions, i.e., the time when the thrust is terminated, can be used to define a new rectified orbit and the numerical calculations of the subsequent trajectory can be continued by use of Encke's integration method. Since the trajectory after injection is outside the denser parts of the atmosphere, low-thrust propulsion by ion engines or other devices is possible. The thrust perturbation will then act during the major part of the lunar trajectory, but it will be small enough so that Encke's method of integration may be used throughout for some small thrust accelerations, without large errors arising from rectification.

Let $\vec{T}$ be the thrust force acting on the space vehicle. It enters the equations of motion Eq (50) through the term n_Δ which is defined by Eq(72) where the mass M_Δ of the vehicle is its instantaneous mass, which decreases due to the exhaust of mass in a stream of particles during rocket burning. The magnitude, direction, and time-variation of $\vec{T}$ must be specified. A natural coordinate system in which the components of $\vec{T}$ might be given is the body-axis system defined in Chapter III since the rocket engine is mounted in the body of the space vehicle. With the orientation of the vehicle known, it is possible to obtain the $x_\oplus$, $y_\oplus$, $z_\oplus$ components of $\vec{T}$ by the transformation of Table 2.

In some cases such as in lunar landing optimization studies the thrust force will be resolved into components in and normal to the vehicle trajectory plane. The transformation from these thrust components to $x_\oplus$, $y_\oplus$, $z_\oplus$ components of $\vec{T}$ is given below.

Define a coordinate system $x_v\ y_v\ z_v$ with origin at the center of gravity of the vehicle, the z_v-axis in the direction of the radius vector (or up), the x_v-axis perpendicular to the z_v-axis in the general direction of vehicle motion in the trajectory plane, and the y_v-axis perpendicular to the instantaneous trajectory plane to complete the right-handed Cartesian coordinate system. Denote the thrust components in the $x_v y_v z_v$ directions by T_u, T_v, T_w respectively. The problem, then, is to transform the T_u, T_v, T_w components to T_x, T_y, T_z components in the $x_\oplus$, $y_\oplus$, $z_\oplus$ directions, respectively (see the following sketch):

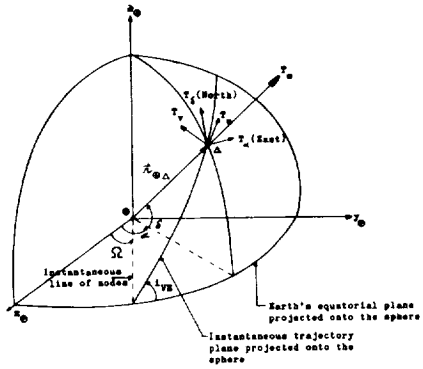

Define thrust components T_δ and T_α in the north and east directions, respectively. Then, as can be seen from the preceding sketch, the angle between T_v and T_δ as well as T_u and T_α is $(360°-A_e)$, where A_e is the azimuth of the T_v direction measured from geographic north. A rotation about T_w by the angle A_e will transform from T_u, T_v, T_w components to T_α, T_δ, T_ω components. Further rotations about T_α by the angle $-(90-\delta) = \delta-90$ and then about T_z by the angle $(270-\alpha)$ will yield the following transformation equations:

$$\begin{Bmatrix} T_x \\ T_y \\ T_z \end{Bmatrix} = \left[T\,(270-\alpha)\right] \cdot \left[T\,(\delta-90)\right] \cdot \left[T(A_e)\right] \begin{Bmatrix} T_u \\ T_v \\ T_w \end{Bmatrix}$$

$$= \begin{bmatrix} -\sin\alpha & -\cos\alpha & 0 \\ \cos\alpha & -\sin\alpha & 0 \\ 0 & 0 & 1 \end{bmatrix} \begin{bmatrix} 1 & 0 & 0 \\ 0 & \sin\delta & -\cos\delta \\ 0 & \cos\delta & \sin\delta \end{bmatrix}$$

$$\begin{bmatrix} \cos A_e & \sin A_e & 0 \\ -\sin A_e & \cos A_e & 0 \\ 0 & 0 & 1 \end{bmatrix} \begin{Bmatrix} T_u \\ T_v \\ T_w \end{Bmatrix} \qquad (96)$$

In the above equation

$$\sin\alpha = \frac{y_{\oplus\Delta}}{\left(x^2_{\oplus\Delta} + y^2_{\oplus\Delta}\right)^{1/2}} \qquad (97)$$

$$\cos\alpha = \frac{x_{\oplus\Delta}}{\left(x^2_{\oplus\Delta} + y^2_{\oplus\Delta}\right)^{1/2}}$$

$$\sin\delta = \frac{z_{\oplus\Delta}}{r_{\oplus\Delta}}$$

$$\cos\delta = \frac{\left(x^2_{\oplus\Delta} + y^2_{\oplus\Delta}\right)^{1/2}}{r_{\oplus\Delta}}$$

(compare with the preceding sketch). It remains to give $\cos A_e$ and $\sin A_e$ in terms of $x_{\oplus\Delta}$ $y_{\oplus\Delta}$ $z_{\oplus\Delta}$. We have

$$\cos A_e = \frac{\cos i_{VE}}{\cos \delta}$$

$$\sin A_e = -\left(1 - \frac{\cos^2 i_{VE}}{\cos^2 \delta}\right)^{1/2} \qquad (98)$$

where

$$\cos i_{VE} = \frac{\left(\vec{r}_{\oplus\Delta} \times \vec{V}_{\oplus\Delta}\right) \cdot \hat{z}_{\oplus}}{\vec{r}_{\oplus\Delta} \times \vec{V}_{\oplus\Delta}}$$

$$= \frac{x_{\oplus\Delta}\, \dot{y}_{\oplus\Delta}}{\left[\left(y_{\oplus\Delta}\, \dot{z}_{\oplus\Delta} - \dot{y}_{\oplus\Delta}\, z_{\oplus\Delta}\right)^2 + \left(z_{\oplus\Delta}\, \dot{x}_{\oplus\Delta} - \dot{z}_{\oplus\Delta}\, x_{\oplus\Delta}\right)^2 + \left(x_{\oplus\Delta}\, \dot{y}_{\oplus\Delta} - \dot{x}_{\oplus\Delta}\, y_{\oplus\Delta}\right)^2\right]^{1/2}} \qquad (99)$$

$$- \frac{\dot{x}_{\oplus\Delta}\, y_{\oplus\Delta}}{\left[\left(y_{\oplus\Delta}\, \dot{z}_{\oplus\Delta} - \dot{y}_{\oplus\Delta}\, z_{\oplus\Delta}\right)^2 + \left(z_{\oplus\Delta}\, \dot{x}_{\oplus\Delta} - \dot{z}_{\oplus\Delta}\, x_{\oplus\Delta}\right)^2 + \left(x_{\oplus\Delta}\, \dot{y}_{\oplus\Delta} - \dot{x}_{\oplus\Delta}\, y_{\oplus\Delta}\right)^2\right]^{1/2}}$$

The expressions (98) become, by use of (99):

$$\cos A_e = \left\{\left(x_{\oplus\Delta}\, \dot{y}_{\oplus\Delta} - \dot{x}_{\oplus\Delta}\, y_{\oplus\Delta}\right) r_{\oplus\Delta}\right\} \left\{\left(x^2_{\oplus\Delta} + y^2_{\oplus\Delta}\right) \left[\left(y_{\oplus\Delta}\, \dot{z}_{\oplus\Delta} - \dot{y}_{\oplus\Delta}\, z_{\oplus\Delta}\right)^2 + \left(z_{\oplus\Delta}\, \dot{x}_{\oplus\Delta} - \dot{z}_{\oplus\Delta}\, x_{\oplus\Delta}\right)^2 + \left(x_{\oplus\Delta}\, \dot{y}_{\oplus\Delta} - \dot{x}_{\oplus\Delta}\, y_{\oplus\Delta}\right)^2\right]\right\}^{-1/2} \qquad (100)$$

$$\sin A_e = -\left[1 - \left\{\left(x_{\oplus\Delta}\, \dot{y}_{\oplus\Delta} - \dot{x}_{\oplus\Delta}\, y_{\oplus\Delta}\right)^2 r^2_{\oplus\Delta}\right\} \left\{\left(x^2_{\oplus\Delta} + y^2_{\oplus\Delta}\right) \left[\left(y_{\oplus\Delta}\, \dot{z}_{\oplus\Delta} - \dot{y}_{\oplus\Delta}\, z_{\oplus\Delta}\right)^2 + \left(z_{\oplus\Delta}\, \dot{x}_{\oplus\Delta} - \dot{z}_{\oplus\Delta}\, x_{\oplus\Delta}\right)^2 + \left(x_{\oplus\Delta}\, \dot{y}_{\oplus\Delta} - \dot{x}_{\oplus\Delta}\, y_{\oplus\Delta}\right)^2\right]\right\}^{-1}\right]^{1/2} \qquad (101)$$

Equations (96), (97), (100) and (101) completely define T_x, T_y, T_z in terms of T_u, T_v, T_w and the instantaneous position and velocity coordinates $x_{\oplus\Delta}$, $y_{\oplus\Delta}$, $z_{\oplus\Delta}$, $\dot{x}_{\oplus\Delta}$, $\dot{y}_{\oplus\Delta}$, $\dot{z}_{\oplus\Delta}$. This latter method of determining the components of the thrust force is advantageous since the vehicle orientation does not enter the computations explicitly but rather implicitly as an input through the specification of the time variation of T_u, T_v, T_w. When one starts with the components of thrust in the body axis, the vehicle orientation must be specified explicitly.

f. Relativistic effects

Before relativistic effects are mentioned, a brief description of the various systems of mechanics which deal with the motion of bodies on the astronomical scale is required. The earliest formulation of mechanics in mathematical form is due to Newton. Two postulates underlie his formulation of the laws of motion: (1) there exists a universal absolute time t in terms of which all events can be described, (2) any particle can be placed in an absolute euclidean three-dimensional space. The metric, or distance ds between any two neighboring points, of this space is given by

$$ds^2 = dx^2 + dy^2 + dz^2 \qquad (102)$$

where x, y, z are the three cartesian coordinates of this space, and time t is regarded as a parameter. An inertial system in newtonian mechanics is defined as a coordinate system in which Newton's laws of motion preserve their mathematical form during a transformation of coordinates. Newton avoided complications by not specifying this absolute space and this absolute time (i.e., the inertial system). They have to be specified for each experiment that is performed.

Newtonian mechanics was very successful in interpreting experimental data, and it was not until two centuries later that this theory was modified by Einstein. Einstein's special theory of relativity is based on (1) the postulate of relativity, which states that it is impossible to detect unaccelerated motion through space and (2) the velocity of light in vacuo is the same for all observers, regardless of the relative velocity of the light source with respect to the observer. The most striking distinction between special relativity and newtonian mechanics is the introduction of a finite maximum velocity c in special relativity while the maximum velocity in newtonian mechanics does not have any limit. As a tribute to the success of newtonian mechanics the absolute euclidean three-dimensional space has been retained by special relativity. However, the notion of an absolute time which could be fixed in some way by two observers at two different places has been abandoned. Each event now needs four numbers to specify it: three space coordinates and time, and they can be plotted as points in the four-dimensional space-time with metric·

$$ds^2 = dt^2 - \frac{1}{c^2}\left(dx^2 + dy^2 + dz^2\right) \qquad (103)$$

(Eq 103 is called the Minkowski space-time.)

Similar to its definition in newtonian mechanics, an inertial system in special relativity is defined as a coordinate system in which the laws of mathematical physics retain their form during a transformation of coordinates. The most general transformation between two inertial system S (x, y, z, t) and S' (x', y', z', t') in newtonian mechanics is given by the Galileo transformation

$$t' = t,\ x' = x - Vt,\ y' = y,\ z' = z \qquad (104)$$

where V is the uniform speed with which S' moves parallel to the x-axis with respect to S. In special relativity the most general transformation between

S and S' is given by the Lorentz transformation

$$t' = \beta\left(t - \frac{V}{c^2}x\right), \quad x' = \beta(x - Vt),$$

$$y' = y, \quad z' = z, \tag{105}$$

where $\beta = \left(1 - \frac{V^2}{c^2}\right)^{-1/2}$, and c is the velocity of light in vacuo. Both of these transformations are invariants, i.e., we may exchange the primed and unprimed coordinate systems without altering the form of the equations.

The theory of general relativity attempts to extend the postulate of relativity to accelerated types of motion (not only to unaccelerated motion as in special relativity) such as to motion in a gravitational field. The euclidean geometry of the previous systems of mechanics has been abandoned, and all events can be plotted as points in some four-dimensional riemannian (curved) space-time with the metric

$$ds^2 = \sum_{i=1}^{4} \sum_{j=1}^{4} g_{ij}(x_i)\, dx_i\, dx_j, \tag{106}$$

where x_i are the coordinates and $g_{ij}(x_i)$ are the components of the fundamental metric tensor characterizing the particular space-time used in the problem. The coordinates x_i are not necessarily known a priori but will be assigned in some way later, the only restriction being that the same method of assigning coordinates be used throughout. The laws of physics are assumed to be unaffected by the choice of coordinates and can therefore be expressed in an invariant form. This means that as a guide one uses the principle of covariance: There must be no preferred coordinate system. This principle of covariance can be insured by use of tensors and tensor equations which have the same form in all coordinate systems.

The equations of mathematical physics in special relativity and general relativity should reduce to the corresponding equations in newtonian mechanics if the finite maximum velocity c in the relativistic equations is replaced by an infinite one. Thus, in the problem of space vehicle motion, special relativity may be regarded as a "correction" to newtonian mechanics at high space vehicle speeds and general relativity as a "correction" to Newton's law of gravitation.

Contributions to special relativistic rocket kinematics and dynamics have been made by many investigators and the fundamental equations have been presented by many authors, for example by Krause in Ref. 25. To illustrate special relativistic effects, the following summary of equations for the motion of a rocket in a straight line and without any external forces acting on it has been taken from Ref. 25.

The following table shows that special relativistic effects on a space vehicle become important when its velocity or the velocity of the exhaust gases are an appreciable fraction of the speed of light, c = 299792.5 km/sec. It should be noted that by letting $c \to \infty$, $\beta \to 1$ the above relativistic rocket equations reduce to the newtonian rocket equations. For lunar vehicles these relativistic corrections are very small and can be neglected in most practical cases.

Since the theories of special nor general relativity do not employ a universal absolute time as newtonian mechanics does, the readings of clocks moving relative to each other and/or being in a different gravitational field will not agree. It is therefore possible to employ the different gravitational environment and the relative velocity between an earth observer and a space vehicle to measure special and general relativistic "time dilation" effects.

The problem of rocket motion has not yet been attacked in the theory of general relativity. However, equations of motion analogous to the n-body and restricted n-body problems of newtonian mechanics have been obtained in general form by Einstein, Fock, and Papapetrou among others. The general relativistic equations of motion are so complicated that no method of solution has as yet been given. By using a simplified dynamical system of a massive body and a space vehicle analogous to the classical restricted two-body problem of newtonian mechanics, three general relativistic effects have been deduced:

(1) The advance of perihelion (closest approach to the sun) of the planets.

(2) The deflection of light by gravitational fields.

(3) The red-shift of spectral lines by the gravitational field near its source.

Krause derived in Ref. 25, by use of the above simplifying assumption, the secular and long-periodic perturbations in the osculating orbital elements of a near-earth satellite.

The theory of general relativity gives the effect of gravitational fields, and the stronger the field, the more pronounced its effect on the trajectory. But, just as in the case of special relativity, general relativistic effects are very small for lunar vehicles and can be neglected in practical trajectory calculations. For example, the advance of perigee of a near-earth satellite, as calculated by LaPaz (Ref. 26) amounts only to several hundreds of seconds of arc per century.

5. Accuracy of Computed Trajectories

Before closing the discussion on force models and trajectory calculations it is helpful to summarize the deviations of a computed from an actual trajectory. The main sources of error in a computed trajectory are:

Rocket in Rectilinear Motion

Quantity	Expression in Coordinate System $S_\oplus$ of Stationary Earth Observer	Expression in Body-Fixed Coordinate System S_Δ Centered in the Moving Rocket
Velocity	$\vec{V}$	0
Mass	$M = \dfrac{M_\Delta}{\left(1 - \dfrac{V^2}{C^2}\right)^{1/2}} \equiv \beta M_\Delta$	M_Δ
Time element	$dt = \beta\, dt_\Delta$	dt_Δ
Acceleration	$\vec{f}_c = \dfrac{1}{\beta^2}\left[\vec{f}_\Delta - \left(1 - \dfrac{1}{\beta}\right)\dfrac{\vec{f}_\Delta \cdot \vec{V}}{V}\dfrac{\vec{V}}{V}\right]$	$\vec{f}_\Delta$
Exhaust velocity	$\vec{V}_{ex} = \left\{\dfrac{\vec{V}_{ex\Delta}}{\beta} + \vec{V}\left[\left(1 - \dfrac{1}{\beta}\right)\dfrac{\vec{V}_{ex\Delta}\cdot\vec{V}}{V^2} - 1\right]\right\}\left\{1 - V_{ex}\right\}^{-1}$	$\vec{V}_{ex\Delta}$
Element of mass flow after ejection	$dM = \dfrac{dM_\Delta^*}{\left(1 - \dfrac{V_{ex}^2}{c^2}\right)^{1/2}}$	$dM_\Delta = \dfrac{dM_\Delta^*}{\left(1 - \dfrac{V_{ex\Delta}^2}{c^2}\right)^{1/2}}$
Mass flow rate	$-\dfrac{dM}{dt} = \dfrac{\frac{-1}{\beta}\frac{dM_\Delta^*}{dt_\Delta}}{\left(1 - \dfrac{V_{ex}^2}{c^2}\right)^{1/2}}$	$-\dfrac{dM_\Delta}{dt_\Delta} = \dfrac{-\frac{dM_\Delta^*}{dt_\Delta}}{\left(1 - \dfrac{V_{ex\Delta}^2}{c^2}\right)^{1/2}}$
Thrust force	$\vec{T} = -\dfrac{dM}{dt}V_{ex} = \dfrac{-\frac{1}{\beta}\frac{dM_\Delta^*}{dt_\Delta}}{\left(1 - \dfrac{V_{ex}^2}{c^2}\right)^{1/2}}\vec{V}_{ex}$	$\vec{T}_\Delta = \dfrac{dM_\Delta}{dt_\Delta}V_{ex\Delta} = \dfrac{\frac{dM_\Delta}{dt_\Delta}}{\left(1 - V_{ex}^2/c^2\right)^{1/2}}\vec{V}_{ex\Delta}$

where M_Δ or M_Δ^* is the rest mass (i.e., mass if $\vec{V} = 0$) of the rocket,

$\beta = \dfrac{1}{1 - \dfrac{V^2}{c^2}}$, c is the speed of light in vacuo, $\vec{V}_{ex}$ is the exhaust velocity, $\vec{V}$ is the velocity of the rocket and $\vec{f}$ its thrust acceleration.

a. Use of simplified force models

In the discussion of the various force models it is pointed out what approximations have been made in each. One would expect to use a simpler force model for preliminary trajectory selection and then use a more complicated model to verify some more desirable trajectories. It is to be expected that the many-body force model with the inclusion of nongravitational forces yields the most accurate trajectory. With each force model, many questions of computer simulation arise, such as the type of buildup and tail-off of thrust, the drag and lift coefficients, the reflectivity of the vehicle skin, the type of interaction between neutral and charged particles with the skin, etc. The computer simulation of some forces presents major problems and may be costly in programming and computation time.

b. Use of approximate physical constants

With each force there are in general some associated constants. Thus we need the gravitational constants of the moon $\mu_{\leftmoon} = GM_{\leftmoon}$, the earth $\mu_{\oplus} = GM_{\oplus}$, the mean angular velocity of the moon $\omega_{\oplus\leftmoon}$, constants associated with the expansion of the earth's and the moon's gravitational potentials, the variation of atmospheric temperature and molecular weight with altitude above the earth and many more constants depending on the force model. Each one of these constants is known imprecisely; this fact will cause errors in the computed trajectories. There should ideally be a balance between our knowledge of these constants and the type of force model to be used on the computer. The constants in any force model should be consistent among each other; and if they are not, a justification of each such departure should be given.

c. Errors in the lunar, solar, and planetary positions

The coordinates of celestial bodies have been obtained at the US Naval Observatory by use of general perturbation theories with certain values of physical constants which may differ from the values of the same constants used in the trajectory program.

d. Errors in initial conditions

The initial conditions of the vehicle, the celestial bodies and the launch site on earth as used in the computer simulation may be in error.

e. Computational errors

The programming of a trajectory computer program requires careful attention to the accumulation of error during the numerical integration of the equations of motion. Computational errors include those due to round-off, truncation, approximation, cancellation, and due to the presence of small divisors.

f. Human error

Last, but not least there is the possibility of human error in the handling of the data from assembling the machine input to the evaluation of the trajectory output.

C. THE VOICE TECHNIQUE

The discussion of the accuracy of computed trajectories in the preceding subsection pointed out the need of a simplified force model for parametric studies of lunar trajectories. The n-body force model is very complex because of the number of trajectory variables involved and the lack of exact solutions to the equations of motion. In fact, even the restricted three-body model (Subsection B-1) does not afford solutions for lunar trajectories efficiently. Although computer programs exist that determine trajectories by use of various integration schemes, the inputs to these programs are the unknown position and velocity of the spacecraft at some time. Since lunar trajectories are very sensitive to these initial conditions, these unknowns must be estimated very accurately. For example, a typical trajectory that passes behind the moon and returns to earth (circumlunar) requires an initial speed at the earth of approximately 11,000 m/sec. Perturbing this speed by 1 m/sec can change pericynthion (closest approach to moon) altitude by hundreds of kilometers, and the return perigee by thousands of kilometers. Thus, systematic studies using computer programs that integrate numerically can become long, tedious, and expensive, if the initial conditions are determined by a trial and error approach. The most desirable means around this problem is via a simplified technique that is relatively accurate and free of integration logic.

1. Description

To this end, a three-dimensional patched conic program using a succession of two-body trajectories, and with a transition region similar to the gravisphere transition to lunar influence was developed. However, instead of a gravisphere or sphere of influence, a lunar "volume of influence" is used which is defined by the locus of points that satisfy $r_M/r_E = 0.175$ (see Subsection B-1b). This volume, empirically determined to give the best results, is a sphere as was shown in the referenced subsection.

The following assumptions are made in any patched conic program: The earth and moon are spherical homogeneous bodies with the moon rotating about the earth's center. Motion within the lunar volume of influence is free of gravitational forces from the earth and sun. Likewise, motion toward or away from the volume is free of forces due to the moon and sun. Thus, a trajectory in this earth-moon model can be described by the classic two-body equations which are "patched" at the boundary of the lunar volume of influence.

Figure 4 presents a definition of the terms and the coordinate system used in the Voice (Volume of Influence-Calculated Envelopes) trajectory program. A geocentric coordinate system is employed with the positive x_E-axis defined by the vector lying along the intersection of the translunar trajectory plane and the moon's orbital plane in the direction of the moon. The z_E-axis is normal to the moon's orbital plane, i.e., in the direction of the angular momentum vector of the moon with the y_E-axis completing the right-handed system in the MOP. The lead angle of the moon, Φ *, is measured from the x_E-axis to the position of the moon at the time of injection.

The relative inclination of the translunar trajectory plane i_{VTL} and the transearth trajectory plane i_{VTE} to the MOP are determined at the time of injection and volume of influence exit, respectively.

The program first computes the translunar trajectory to the point of entry into the volume of influence, at which point the velocity and position vectors are determined relative to the geocentric coordinate system. At volume entry the velocity and position vectors are transformed to a selenocentric reference frame as illustrated in the following sketch for the simple case of a trajectory in the MOP ($i_{VTL} = 0$):

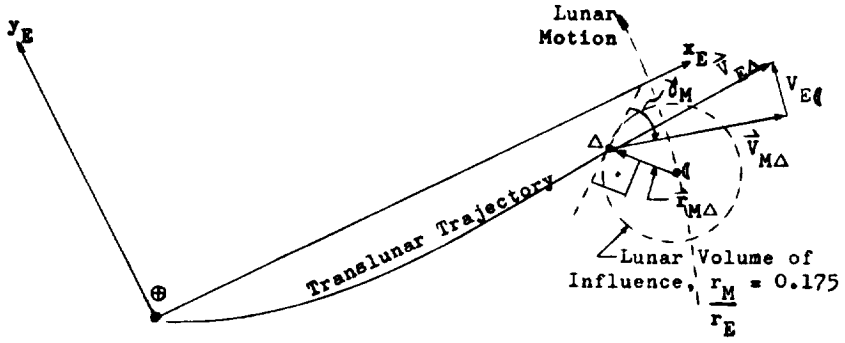

where $\vec{V}_{E\Delta}$ is the velocity of the space vehicle and $\vec{V}_{E\,(}$ is that of the moon relative to earth. From the preceding sketch it can be seen that the velocity of the space vehicle relative to the moon $\vec{V}_{M\Delta}$ is given by $\vec{V}_{M\Delta} = \vec{V}_{E\Delta} - \vec{V}_{E\,(}$.

The geocentric vehicle position and velocity at entry into the lunar volume of influence ($\vec{r}_{E\Delta}$, $\vec{V}_{E\Delta}$) are transformed to a selenocentric coordinate system $x_M\ y_M\ z_M$, i.e. to ($\vec{r}_{M\Delta}$, $\vec{V}_{M\Delta}$) for the trajectory computation around the moon. The $x_M\ y_M\ z_M$ coordinate system is illustrated in the following sketch:

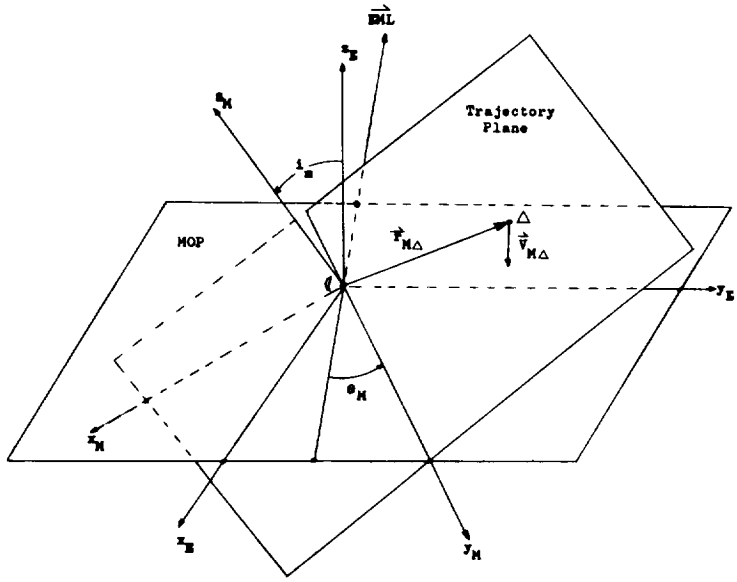

The z_M-axis is in the direction of $\vec{V}_{M\Delta} \times \vec{r}_{M\Delta}$ or perpendicular to the trajectory plane around the moon. The y_M axis defines the intersection between the trajectory or $x_M\ y_M$-plane and MOP (or the $x_E\ y_E$-plane), with the x_M axis completing the right-handed coordinate system. The inclination i_m of the trajectory to the moon's orbital plane inside the volume of influence is given by $i_m = \cos^{-1}\left(\frac{\vec{z}_M \cdot \vec{z}_E}{z_M z_E}\right)$. Knowing the direction of the earth-moon line $\overrightarrow{EML}$ at the time of entry into the volume, the time to reach pericynthion and the moon's rotational rate about the earth, $\omega_{\oplus \mathbb{C}}$, the orientation θ_M of the lunar trajectory with respect to the earth-moon line EML at pericynthion can be found.

Upon leaving the lunar volume of influence, the vehicle position and velocity are again transformed to the $x_E\ y_E\ z_E$ coordinate system and the transearth trajectory is then computed.

The above discussion acquaints the reader with the technique. In order to understand exactly what the Voice program can do, one must look at the inputs and outputs. The following trajectory variables are specified in the input for circumlunar mission trajectories:

(1) Earth launch base position (geocentric latitude and longitude).

(2) Injection altitude h_{e0} and flight path angle γ_{e0} for the translunar trajectory.

(3) Pericynthion altitude h_{PL}, closest approach to moon.

(4) Return vacuum perigee altitude h_{PE} or the closest approach to the earth if the earth's atmosphere is neglected.

(5) Translunar trajectory inclination i_{VTL} to the MOP.

(6) Transearth trajectory inclination i_{VTE} to the MOP.

(7) Declination of the moon when the spacecraft is at pericynthion.

(8) Return base geocentric latitude.

As can be seen, the major characteristics of the entire lunar trajectory are specified. The essence of the program is thus a matter of iteration within the program in order to satisfy these desired characteristics or trajectory variables, thus allowing one to explicitly state mission parameters as input.

The program output consists of other requirements to fulfill the mission and additional pertinent data as listed below:

(1) Injection position ψ_0 and geocentric latitude and longitude. The injection position ψ_0 is measured from the MOP along the translunar trajectory plane to the point of injection.

(2) Injection velocity $V_{E\Delta 0}$.

(3) Lunar lead angle Φ^* at injection.

(4) Position and velocity of the space vehicle at pericynthion.

(5) Inclination i_m of the vehicle trajectory to the MOP in the lunar volume of influence.

(6) Orientation θ_M of the trajectory with respect to the $\overrightarrow{EML}$ at pericynthion.

(7) Position and velocity at return vacuum perigee.

(8) Flight time to pericynthion and to return vacuum perigee.

(9) Longitude of first two intersections of the return trajectory.

(10) Range angle in parking orbit and range to return base latitude extended beyond perigee to the return base latitude.

Another program exists using the same principles as the Voice technique wherein one-way transearth trajectories from lunar orbit can be determined. Entitled, "Ejection from Lunar Orbit," this program has the following inputs and outputs which are illustrated in the following sketch:

Inputs:

(1) Inclination of the circular lunar orbit to the moon's orbital plane i_m. The program is restricted to circular lunar orbits.

(2) Orientation of the circular lunar orbit with respect to the earth-moon line θ_M.

(3) Altitude of the circular lunar orbit h_{PL}.

(4) Ejection point from lunar orbit β_{M0}.

(5) Flight path angle at ejection γ_{M0}.

(6) Desired vacuum perigee altitude h_{PE}.

Outputs:

(1) Ejection velocity $V_{M\Delta 0}$.

(2) Transearth inclination i_{VTE}.

(3) Time to return to vacuum perigee.

(4) Position and velocity at perigee.

With proper interpretation this program is also used for one-way translunar trajectories. Again note the ease by which specific mission requirements can be obtained.

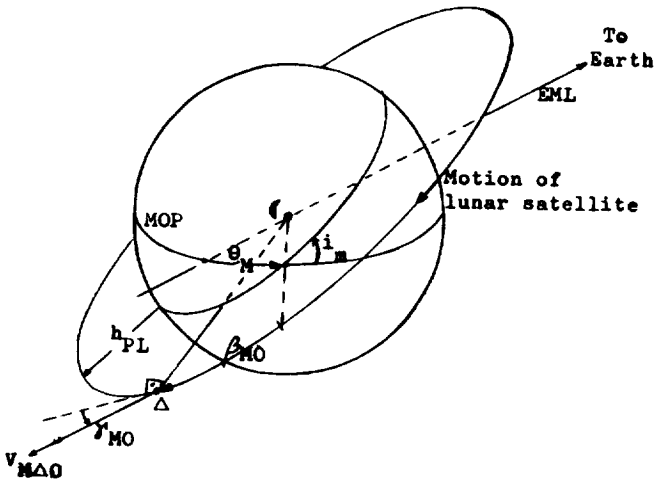

2. Comparison with Integrated Trajectories

The Voice technique, although an approximation to a complex physical model, compares very favorably with integrated restricted three-body and n-body trajectories. The following table illustrates this point by comparing two typical integrated trajectories (one restricted 3-body and one n-body) with their respective Voice trajectories. The integrated trajectories were obtained by an iterative scheme utilizing the Voice program. The table, which is self-explanatory, shows that there is good agreement between the initial conditions obtained with the Voice technique and the initial conditions for the actual integrated trajectory. All mission constraints are closely matched, thereby proving trends established by Voice.

Thus the Voice technique can be used with reasonable accuracy to perform parametric studies of lunar trajectory characteristics. In addition the technique can be used for obtaining actual n-body integrated trajectories.

Further comparisons between Voice trajectory characteristics and those using the restricted 3-body and n-body force models for various types of lunar trajectories are given in Chapters VI and IX.

Comparison of Voice Trajectories with Integrated Trajectories

Inject North--Direct			Restricted 3-Body Force Model Comparison		n-Body Force Model Comparison	
Item			Voice	Integrated	Voice	Integrated
Injection into translunar orbit	Altitude (h_{e0})	km	231.648	231.648	182.88	182.88
	Velocity ($V_{E\Delta 0}$)	m/sec	10905.545	10903.951	10962.32	10963.786
	Flight path angle (γ_{e0})	deg	3.0	3.0	2.6682	2.6682
	Inclination to MOP (i_{VTL})	deg	30.	30.	29.2495*	29.3822*
	Injection position (ψ_0)	deg	12.259	11.94	13.502125	13.198678
	Lunar lead angle (ϕ *)	deg	44.0596	45.0258	37.3314	38.02945
At moon	Pericynthion altitude (h_{PL})	km	1852.	1851.44	185.015	186.867
At earth	Vacuum perigee altitude (h_{PE})	km	45.72	46.086	36.81	37.5
	Total flight time (t)	hr	154.31	154.3	147.736	147.078
	Inclination to MOP (i_{VTE})	deg	7.92	6.96	35.206*	35.387*
	Direction and mode of return		Direct from south	Direct from south	Direct from south	Direct from south

*i_{VTL} and i_{VTE} are relative to earth equatorial plane, i.e., they are actually i_{VE} and i_{VTEQ}, respectively.

D. ADDITIONAL CLASS OF CIRCUMLUNAR ORBITS

A new class of circumlunar orbits, i.e., periodic circumlunar trajectories, has been described and an outline of the proof of existence for these orbits had been given by Arenstorf (Ref. 27) just as the Lunar Flight Manual went to press. These orbits were obtained for the restricted three-body problem, and they exist for small mass ratios of the two primary bodies. The circumlunar orbits exist near Keplerian, or restricted two-body, ellipses which represent a zero mass ratio between the two primary bodies or the existence of only one primary body. Two typical circumlunar orbits as calculated by Arenstorf have been plotted below for the earth-moon-space vehicle system in rotating $x_R y_R$ coordinates:

By a judicious choice of trajectory parameters these orbits can be made to pass arbitrarily close to the earth and moon, and small perturbations from forces arising outside of the framework of the restricted three-body problem can be counteracted by thrust. Reference 27 suggests the use of circumlunar orbits for shuttling passengers and materials from the vicinity of the earth to the vicinity of the moon.

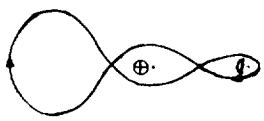

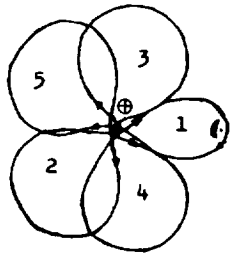

E. REFERENCES

1. Egorov, V. A., "Certain Problems of Moon Flight Dynamics," The Russian Literature of Satellites, Part I International Physics Index, Inc., New York, 1958.

2. Buchheim, R. W., "Lunar Flight Trajectories," Report P 1268, Rand Corporation, January 30, 1958. Also Chapter 7, "Lunar Flight Trajectories," in H. S. Seifert, ed. "Space Technology," John Wiley and Sons, Inc., New York, 1959.

3. Anonymous, "Orbital Flight Manual," ER 12684, Martin Marietta Corporation, Space Systems Division, Baltimore, 1963.

4. Mickelwait, A. B., "Lunar Trajectories," ARS Journal, Vol. 29, December 1959, pp 905 to 914.

5. Mickelwait, A. B., and Booton, R. C., Jr., "Analytical and Numerical Studies of Three-Dimensional Trajectories to the Moon," Journal of Aerospace Sciences, Vol. 27, August 1960, pp 561 to 573.

6. Koelle, H. H., Editor-in-Chief, "Handbook of Astronautical Engineering," McGraw-Hill, New York, 1961.

7. Weber, R. J., Pauson, W. M., and Burley, R. R., "Lunar Trajectories," NASA Technical Note TN D-866, August 1961.

8. Buchheim, R. W., "Motion of a Small Body in Earth-Moon Space," RM 1726, Rand Corporation, June 4, 1956.

9. Hagihara, Y., "Recommendations on Notation of the Earth Potential," Astronomical Journal, Vol. 67, February 1962, p 108.

10. Heiskanen, W. A., and Vening-Meinesz, F. A., "The Earth and Its Gravity Field," McGraw-Hill, New York, 1958.

11. Alexandrov, I., "The Lunar Gravitational Potential," in "Astronautical Science," Vol. 9, Plenum Press, New York, 1960, pp 320 to 324.

12. Baker, R. M. L., Jr., and Makemson, M. W., "An Introduction to Astrodynamics," Academic Press, New York, 1960.

13. Pines, S., and Wolf, H., "Interplanetary Trajectory by the Enckes Method Programmed for the IBM 704 and 7090," Republic Aviation Corporation, New York.

14. Anonymous, "American Ephemeris and Nautical Almanac," published annually by the Nautical Almanac Office, United States Observatory, Washington, D. C. (obtainable from Superintendent of Documents, U. S. Government Printing Office, Washington 25, D. C.).

15. Brouwer, D., and Clemence, G. M., "Methods of Celestial Mechanics," Academic Press, New York, 1961.

16. Baker, R. M. L., Jr., Westrom, G. B., et al., "Efficient Precision Orbit Computation Techniques," ARS Journal, August 1960, pp 740 to 747.

17. Pines, S., Payne, M., and Wolf, H., "Comparison of Special Perturbation Methods in Celestial Mechanics," Report No. 60-281, Aero Research Laboratory, Wright-Patterson AFB, Ohio, August 1960.

18. Anonoymous, "Flight Performance Handbook for Orbital Operations," Space Technology Laboratories, Inc., Redondo Beach, Calif., September 1961.

19. Parkinson, R. W., Jones, H. M., and Shapiro, I. J., "Effects of Solar Radiation Pressure on Earth Satellite Orbits," Science, Vol. 131, 1960. pp 920 and 921.

20. Kochi, K. C., and Staley, R. M., "Methods for Analysis of Satellite Trajectories," Aeronautical Research Laboratories, Wright-Patterson AFB, Ohio, September 1960.

21. Beard, D., and Johnson, F., "Charge and Magnetic Field Interaction with Satellites," Journal of Geophysical Research, Vol. 65, No. 1, 1960, pp 1 to 7.

    Singer, S. F., and Walker, E. H., "Electrostatic Screening of Bodies in Space," Report of the Physics Department, University of Maryland, College Park, September 1961.

23. Krzywoblocki, M. Z. v., et al., "A Study of Special Interplanetary Flight Problems," Report No. 2, PR-DW-58-43, IOD 2446-58, Engineering Experiment Station, Aeronautical Engineering Department, University of Illinois, Urbana, June 1959.

24. Lovell, A. C. B., "Meteor Astronomy," Clarendon Press, Oxford, 1954.

25. Krause, H. G. L., "Astrorelativity," Report MTP-P & VE-F-62-4, NASA, George C. Marshall Space Flight Center, Huntsville, Alabama, May 22, 1962. Also Chapter II, H. H. Koelle, Editor-in-Chief, "Handbook of Astronautical Engineering," McGraw-Hill, New York, 1961.

26. LaPaz, L., "Advances of the Perigees of Earth Satellites Predicted by General Relativity," Publications of the Astronautical Society of the Pacific, Vol. 66, 1954, pp 13 to 18.

27. Arenstorf, R. F., "Existence of Periodic Solutions Passing Near Both Masses of the Restricted Three-Body Problem," AIAA Journal, Vol. 1, No. 1 (January 1963), pp 238 to 240.

TABLES AND ILLUSTRATIONS

LIST OF TABLES

Table	Title	Page
1	Transformations Between Position and Velocity Components of the Restricted Three-Body Problem	IV-48
2	Transformation Between Body-Axes and Vehicle-Centered Equatorial Coordinates	IV-49

LIST OF ILLUSTRATIONS

Figure	Title	Page
1	Typical Earth-Moon Trajectory in Nonrotating $x_e y_e$ Coordinates	IV-51
2	The Earth-Moon Trajectory of Fig. 1 in Rotating $x_R y_R$ Coordinates	IV-52
3	Gravitational Regions Around the Moon	IV-53
4	Voice Geometry	IV-54

TABLE 1

Transformations Between Position and Velocity Components of the Restricted Three-Body Problem

Define the following rotation matrices:

$$\left[T_1\right] \equiv \left[T\left(\phi + \omega_{\oplus \mathbb{C}} t\right)\right] =$$

$$\begin{bmatrix} \cos\left(\phi + \omega_{\oplus \mathbb{C}} t\right) & -\sin\left(\phi + \omega_{\oplus \mathbb{C}} t\right) & 0 \\ \sin\left(\phi + \omega_{\oplus \mathbb{C}} t\right) & \cos\left(\phi + \omega_{\oplus \mathbb{C}} t\right) & 0 \\ 0 & 0 & 1 \end{bmatrix}$$

$$\left[T_2\right] \equiv \left[T^{-1}\left(\phi + \omega_{\oplus \mathbb{C}} t\right)\right] =$$

$$\begin{bmatrix} \cos\left(\phi + \omega_{\oplus \mathbb{C}} t\right) & \sin\left(\phi + \omega_{\oplus \mathbb{C}} t\right) & 0 \\ -\sin\left(\phi + \omega_{\oplus \mathbb{C}} t\right) & \cos\left(\phi + \omega_{\oplus \mathbb{C}} t\right) & 0 \\ 0 & 0 & 1 \end{bmatrix}$$

Position and velocity components in the three nonrotating coordinate systems are related to the rotating systems by the transformations:

$$\begin{Bmatrix} x_0 \\ y_0 \\ z_0 \end{Bmatrix} = \left[T_1\right] \begin{Bmatrix} x_R \\ y_R \\ x_R \end{Bmatrix} ,$$

$$\begin{Bmatrix} \dot{x}_0 \\ \dot{y}_0 \\ \dot{z}_0 \end{Bmatrix} = \left[T_1\right] \begin{Bmatrix} \dot{x}_R - \omega_{\oplus \mathbb{C}}\, y_R \\ \dot{y}_R + \omega_{\oplus \mathbb{C}}\, x_R \\ \dot{z}_R \end{Bmatrix}$$

$$\begin{Bmatrix} x_e \\ y_e \\ z_e \end{Bmatrix} = \left[T_1\right] \begin{Bmatrix} x_R + \bar{r}_{\oplus \mathbb{C}}\, \nu \\ y_R \\ z_R \end{Bmatrix},$$

$$\begin{Bmatrix} \dot{x}_e \\ \dot{y}_e \\ \dot{z}_e \end{Bmatrix} = \left[T_1\right] \begin{Bmatrix} \dot{x}_R - \omega_{\oplus \mathbb{C}}\, y_R \\ \dot{y}_R + \omega_{\oplus \mathbb{C}}\,(x_R + \bar{r}_{\oplus \mathbb{C}}\, \nu) \\ \dot{z}_R \end{Bmatrix}$$

$$\begin{Bmatrix} x_m \\ y_m \\ z_m \end{Bmatrix} = \left[T_1\right] \begin{Bmatrix} x_R - \bar{r}_{\oplus \mathbb{C}}\,(1-\nu) \\ y_R \\ z_R \end{Bmatrix}$$

$$\begin{Bmatrix} \dot{x}_m \\ \dot{y}_m \\ \dot{z}_m \end{Bmatrix} = \left[T_1\right] \begin{Bmatrix} \dot{x}_R - \omega_{\oplus \mathbb{C}}\, y_R \\ \dot{y}_R + \omega_{\oplus \mathbb{C}}\left[x_R - \bar{r}_{\oplus \mathbb{C}}\,(1-\nu)\right] \\ \dot{z}_R \end{Bmatrix}$$

and the inverse transformations must be given since the initial conditions are usually given in nonrotating coordinates, while the computation is performed in rotating coordinates:

$$\begin{Bmatrix} x_R \\ y_R \\ z_R \end{Bmatrix} = \left[T_2\right] \begin{Bmatrix} x_0 \\ y_0 \\ z_0 \end{Bmatrix} ,$$

$$\begin{Bmatrix} \dot{x}_R \\ \dot{y}_R \\ \dot{z}_R \end{Bmatrix} = \left[T_2\right] \begin{Bmatrix} \dot{x}_0 + \omega_{\oplus \mathbb{C}}\, y_0 \\ \dot{y}_0 - \omega_{\oplus \mathbb{C}}\, x_0 \\ \dot{z}_0 \end{Bmatrix}$$

$$\begin{Bmatrix} x_R + \bar{r}_{\oplus \mathbb{C}}\, \nu \\ y_R \\ z_R \end{Bmatrix} = \left[T_2\right] \begin{Bmatrix} x_e \\ y_e \\ z_e \end{Bmatrix},$$

$$\begin{Bmatrix} \dot{x}_R \\ \dot{y}_R \\ \dot{z}_R \end{Bmatrix} = \left[T_2\right] \begin{Bmatrix} \dot{x}_e + \omega_{\oplus \mathbb{C}}\, y_e \\ \dot{y}_e - \omega_{\oplus \mathbb{C}}\, x_e \\ \dot{z}_e \end{Bmatrix}$$

$$\begin{Bmatrix} x_R - \bar{r}_{\oplus \mathbb{C}}\,(1-\nu) \\ y_R \\ z_R \end{Bmatrix} = \left[T_2\right] \begin{Bmatrix} x_m \\ y_m \\ z_m \end{Bmatrix},$$

$$\begin{Bmatrix} \dot{x}_R \\ \dot{y}_R \\ \dot{z}_R \end{Bmatrix} = \left[T_2\right] \begin{Bmatrix} \dot{x}_m + \omega_{\oplus \mathbb{C}}\ y_m \\ \dot{y}_m - \omega_{\oplus \mathbb{C}}\ x_m \\ \dot{z}_m \end{Bmatrix}$$

*The coordinate systems are defined by the sketch on page IV-20.

TABLE 2

Transformation Between Body-Axes and Vehicle-Centered Equatorial Coordinates

The coordinates in the body-axis (x_b, y_b, z_b) coordinate system with origin at the instantaneous center of mass of the vehicle are related to nonrotating coordinates ($x_{\oplus,\Delta}$, $y_{\oplus,\Delta}$, $z_{\oplus,\Delta}$) fixed in the vehicle with origin at the instantaneous center of mass and axes parallel to the $x_\oplus$, $y_\oplus$, $z_\oplus$ directions by the relations (where the order of rotation is ψ, θ, ϕ around the z, y, and x axes, respectively)

$$\begin{Bmatrix} x_b \\ y_b \\ z_b \end{Bmatrix} = \left[T(\phi)\right]\left[T(\theta)\right]\left[T(\psi)\right] \begin{Bmatrix} x_{\oplus,\Delta} \\ y_{\oplus,\Delta} \\ z_{\oplus,\Delta} \end{Bmatrix}$$

or

$$\begin{Bmatrix} x_b \\ y_b \\ z_b \end{Bmatrix} = \begin{bmatrix} 1 & 0 & 0 \\ 0 & \cos\phi & \sin\phi \\ 0 & -\sin\phi & \cos\phi \end{bmatrix} \begin{bmatrix} \cos\theta & 0 & -\sin\theta \\ 0 & 1 & 0 \\ \sin\theta & 0 & \cos\theta \end{bmatrix} \begin{bmatrix} \cos\psi & \sin\psi & 0 \\ -\sin\psi & \cos\psi & 0 \\ 0 & 0 & 1 \end{bmatrix} \begin{Bmatrix} x_{\oplus,\Delta} \\ y_{\oplus,\Delta} \\ z_{\oplus,\Delta} \end{Bmatrix}$$

The inverse transformation is given by

$$\begin{Bmatrix} x_{\oplus,\Delta} \\ y_{\oplus,\Delta} \\ z_{\oplus,\Delta} \end{Bmatrix} = \left[T(\psi)\right]^{-1}\left[T(\theta)\right]^{-1}\left[T(\phi)\right]^{-1} \begin{Bmatrix} x_b \\ y_b \\ z_b \end{Bmatrix}$$

or

$$\begin{Bmatrix} x_{\oplus,\Delta} \\ y_{\oplus,\Delta} \\ z_{\oplus,\Delta} \end{Bmatrix} = \begin{bmatrix} \cos\psi & -\sin\psi & 0 \\ \sin\psi & \cos\psi & 0 \\ 0 & 0 & 1 \end{bmatrix} \begin{bmatrix} \cos\theta & 0 & \sin\theta \\ 0 & 1 & 0 \\ -\sin\theta & 0 & \cos\theta \end{bmatrix} \begin{bmatrix} 1 & 0 & 0 \\ 0 & \cos\phi & -\sin\phi \\ 0 & \sin\phi & \cos\phi \end{bmatrix} \begin{Bmatrix} x_b \\ y_b \\ z_b \end{Bmatrix}$$

or, when the matrix multiplication is performed,

$$\begin{Bmatrix} x_{\oplus,\Delta} \\ y_{\oplus,\Delta} \\ z_{\oplus,\Delta} \end{Bmatrix} = \begin{bmatrix} (\cos\psi\ \cos\theta) & (\cos\psi\ \sin\theta\ \sin\phi - \sin\psi\ \cos\phi) & (\cos\psi\ \sin\theta\ \cos\phi + \sin\psi\ \sin\phi) \\ (\sin\psi\ \cos\theta) & (\sin\psi\ \sin\theta\ \sin\phi + \cos\psi\ \cos\phi) & (\sin\psi\ \sin\theta\ \cos\phi - \cos\psi\ \sin\phi) \\ (-\sin\theta) & (\cos\theta\ \sin\phi) & (\cos\theta\ \cos\phi) \end{bmatrix} \begin{Bmatrix} x_b \\ y_b \\ z_b \end{Bmatrix}$$

This can also be written formally in the form of direction cosines

$$\begin{Bmatrix} x_{\oplus,\Delta} \\ y_{\oplus,\Delta} \\ z_{\oplus,\Delta} \end{Bmatrix} = \begin{bmatrix} \ell_{11} & m_{11} & n_{11} \\ \ell_{12} & m_{12} & n_{12} \\ \ell_{13} & m_{13} & n_{13} \end{bmatrix} \begin{Bmatrix} x_b \\ y_b \\ z_b \end{Bmatrix}$$

which are given by direct comparison of the preceding two equations

$$\ell_{11} = \cos\psi \cos\theta$$

$$\ell_{12} = \sin\psi \cos\theta$$

$$\ell_{13} = -\sin\theta$$

$$m_{11} = \cos\psi \sin\theta \sin\phi - \sin\psi \cos\phi$$

$$m_{12} = \sin\psi \sin\theta \sin\phi + \cos\psi \cos\phi$$

$$m_{13} = \cos\theta \sin\phi$$

$$n_{11} = \cos\psi \sin\theta \cos\phi + \sin\psi \sin\phi$$

$$n_{12} = \sin\psi \sin\theta \cos\phi - \cos\psi \sin\phi$$

$$n_{13} = \cos\theta \cos\phi$$

and must satisfy

$$\ell_{11}^2 + m_{11}^2 + n_{11}^2 = 1$$

$$\ell_{12}^2 + m_{12}^2 + n_{12}^2 = 1$$

$$\ell_{13}^2 + m_{13}^2 + n_{13}^2 = 1$$

and

$$\ell_{11} m_{11} + \ell_{12} m_{12} + \ell_{13} m_{13} = 0$$

$$m_{11} n_{11} + m_{12} n_{12} + m_{13} n_{13} = 0$$

$$n_{11} \ell_{11} + n_{12} \ell_{12} + n_{13} \ell_{13} = 0$$

$$\ell_{11} \ell_{12} + m_{11} m_{12} + n_{11} n_{12} = 0$$

$$\ell_{12} \ell_{13} + m_{12} m_{13} + n_{12} n_{13} = 0$$

$$\ell_{13} \ell_{11} + m_{13} m_{11} + n_{13} n_{11} = 0$$

$$\begin{vmatrix} \ell_{11} & \ell_{12} & \ell_{13} \\ m_{11} & m_{12} & m_{13} \\ n_{11} & n_{12} & n_{13} \end{vmatrix} = 1$$

$$\ell_{11}^2 + \ell_{12}^2 + \ell_{13}^2 = 1$$

$$m_{11}^2 + m_{12}^2 + m_{13}^2 = 1$$

$$n_{11}^2 + n_{12}^2 + n_{13}^2 = 1$$

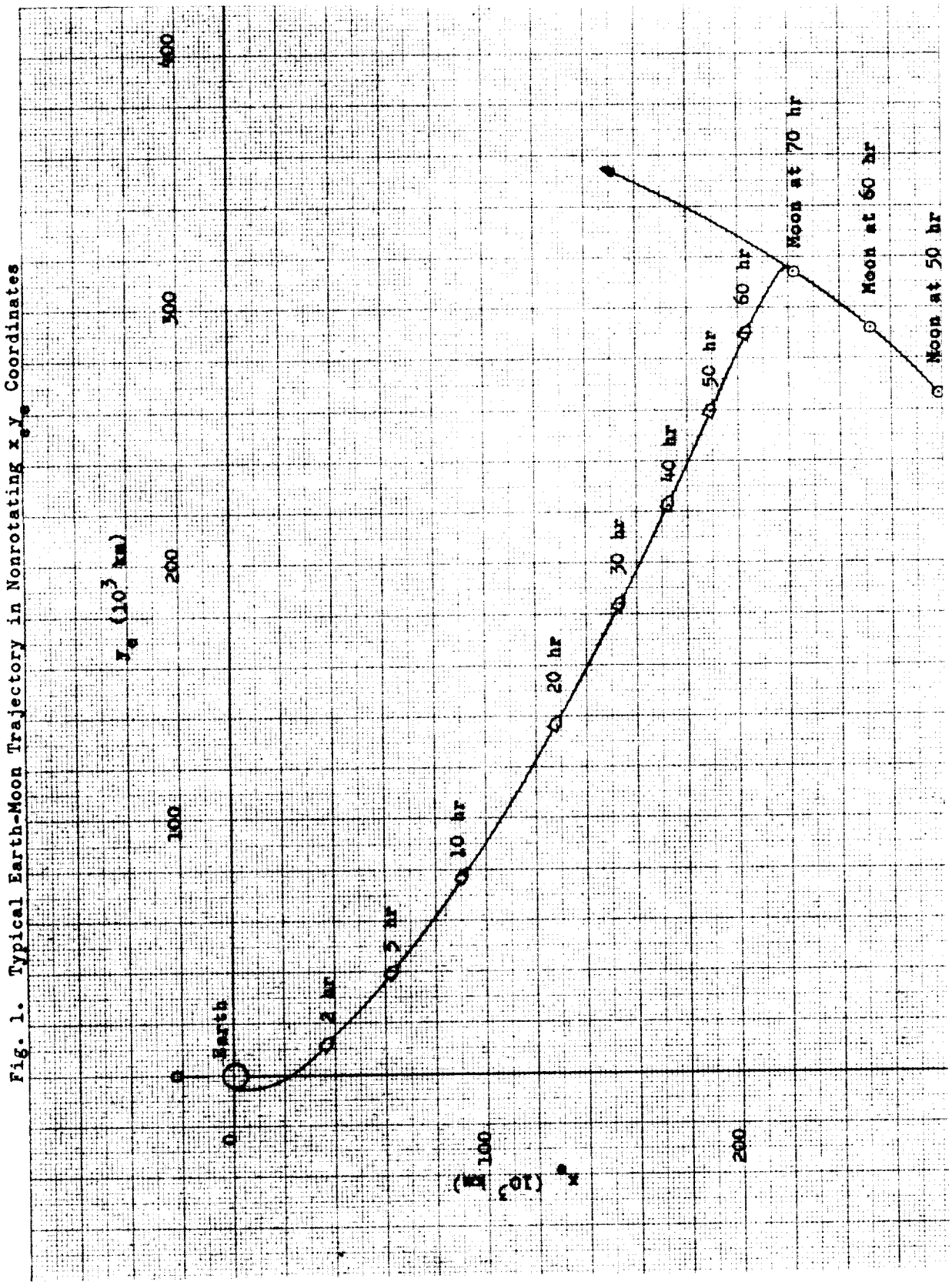

Fig. 1. Typical Earth-Moon Trajectory in Nonrotating $x_e y_e$ Coordinates

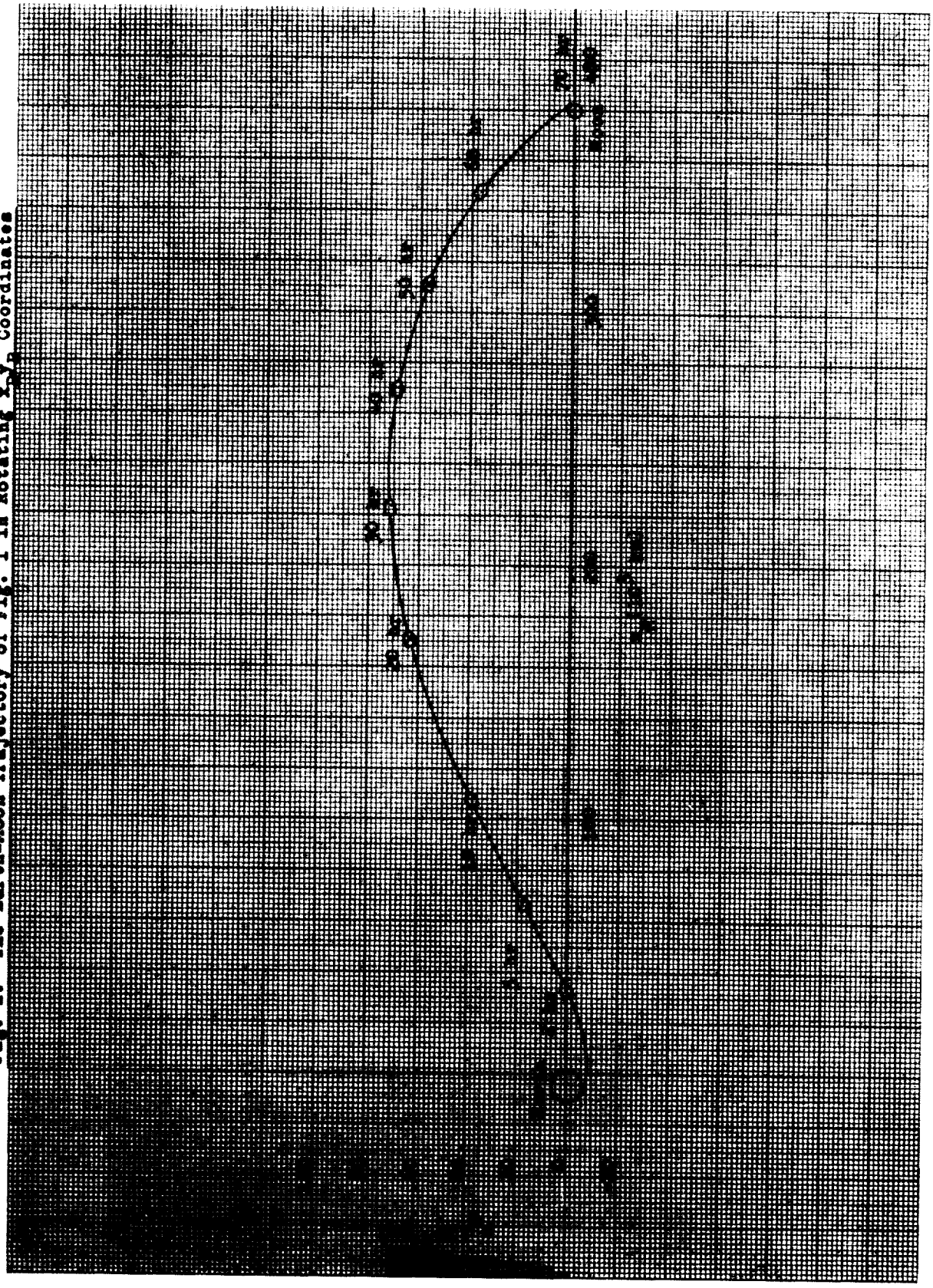

Fig. 2. The Earth-Moon Trajectory of Fig. 1 in Rotating x_1y_1 Coordinates

Fig. 3. Gravitational Regions Around the Moon

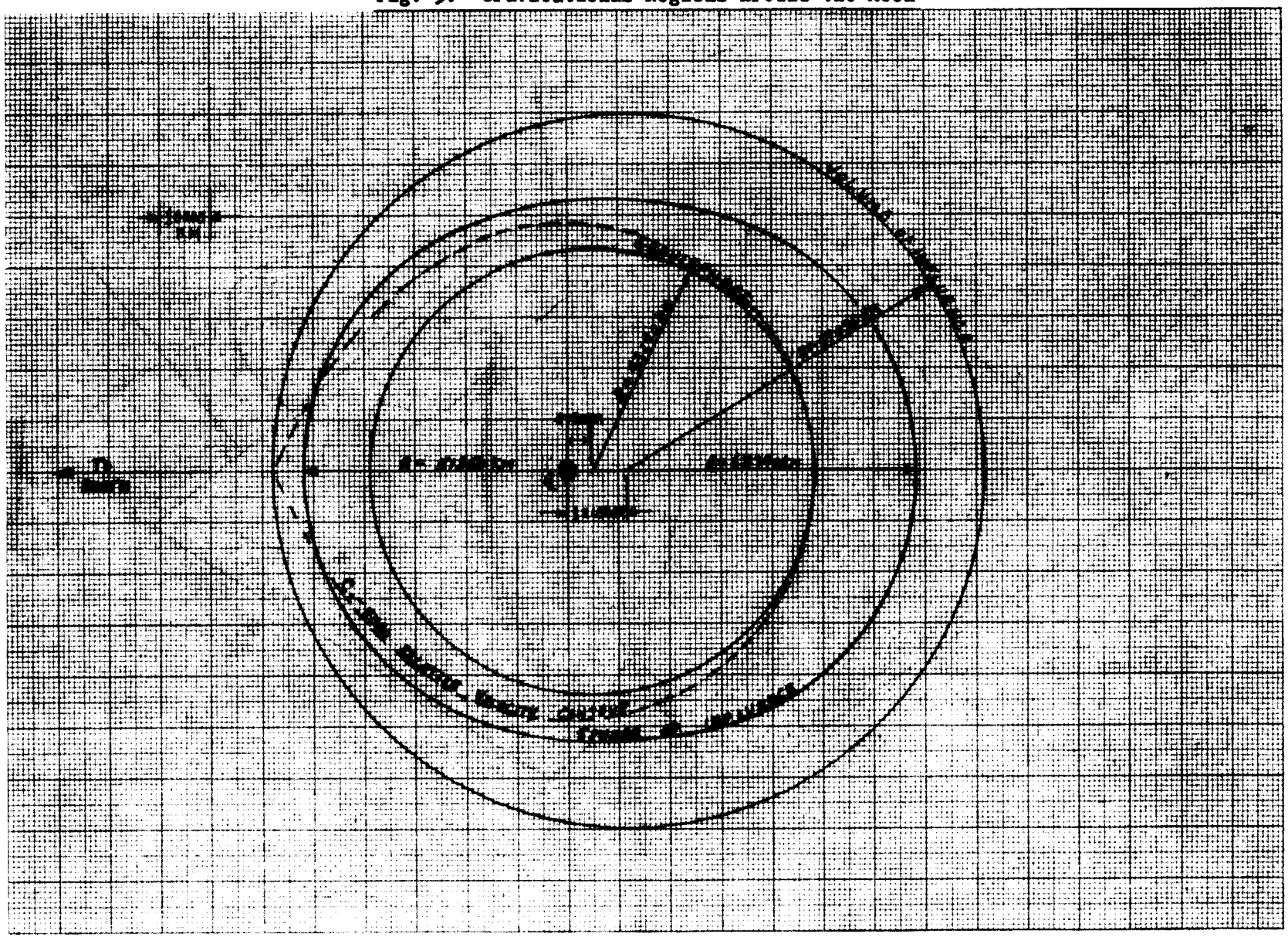

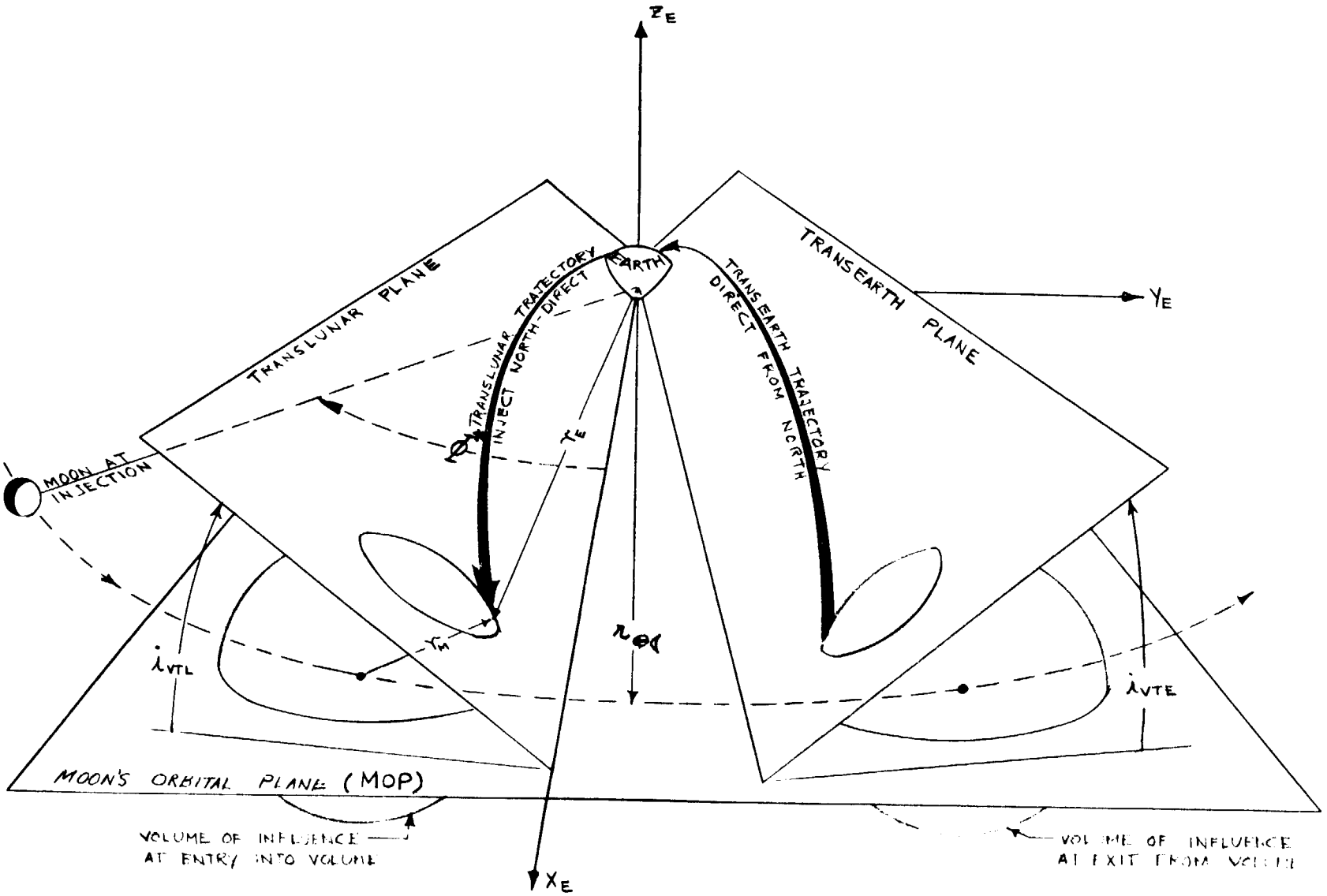

FIG 4 VOICE GEOMETRY

CHAPTER V

EARTH DEPARTURE

Prepared by:

F. Santora
Martin Company (Baltimore)
Aerospace Mechanics Department
March 1963

A. Fixed Translunar Trajectory Technique V-2

B. Variable Translunar Trajectory Technique V-12

C. Translunar Injection V-14

D. References V-21

Illustrations V-23

List of Illustrations V-25

V. EARTH DEPARTURE

INTRODUCTION

Chapters II, III and IV presented material introductory to the problem of lunar flight such as analysis of the environment in which the space vehicle moves (including some numerical values of constants describing this environment), the geometry and dynamics of motion in earth-moon space and finally, a general classification of missions and trajectories and trajectory simulation in earth-moon space. The material in Chapters II, III and IV has been qualitative, or--if quantitative--designed to provide background for a discussion of lunar trajectories. The present chapter is the first of six which present detailed trajectory data for the various phases of a lunar mission, giving detailed analyses and approaches to the problems, illustrating them with numerical examples, or giving parametric variations of trajectory variables whenever necessary. Chapter V discusses earth departure--that part of the total trajectory of any lunar mission between launch at a given time and site and injection into the desired translunar trajectory at the correct time and position. However, no discussion will be given of ascent trajectories from launch to booster burnout.

To accomplish its mission, a lunar spacecraft must be placed at a precise position at a precise time with a very accurate velocity. In order to attain these injection conditions, the spacecraft must first be launched from the earth's surface with the proper ascent trajectory. It is thus of utmost importance that this earth departure phase be as flexible as possible to ease the complexity of mission planning and to minimize the introduction of additional launch constraints. This consideration precludes discussion of direct ascent from launch to lunar trajectory injection (i.e., direct earth departure) by continuous rocket burning during this phase of the trajectory.

Generally the most practical, efficient, and likely technique of earth departure utilizes parking orbits about the earth prior to injection. Additionally, these parking orbits allow greater mission flexibility by providing:

(1) Time for final onboard and ground checkouts before injection is initiated.

(2) Injection capability any time of the month, twice a day.

(3) The same nominal ascent and injection trajectory profile for any mission.

The major disadvantages of this technique are the increased requirements for tracking, communication and computational facilities. Even so, these disadvantages will become less severe as more ground support equipment becomes operational and available for lunar mission support. Hence, parking orbits have been assumed for the earth departure phase throughout this chapter.

Flexibility from a flight mechanics point of view, as used here, is assessed in terms of launch frequency and launch tolerance. Launch frequency is defined as the number of time periods for a possible launch during the month (lunar position in orbit) or during the day (earth rotation), while launch tolerance is the interval of time by which the launch can be expedited or delayed from the nominal launch time, still yielding the desired injection conditions.

There are two basic launch techniques that can be used to obtain launch frequency and launch tolerance. In the first technique, the earth parking orbit and translunar trajectory are fixed for a given injection time. Direct or indirect ascents are performed to attain the required parking orbit. The direct ascent solves the timing problem of arriving at the proper injection point at the correct time on the ground before launch. In the indirect ascent method, the spacecraft is launched at any time, and the timing problem is solved while in the parking orbit. The former method results in launch tolerances measured in terms of a few minutes and a launch frequency varying from one to four times a day. The indirect method is characterized by launch tolerances measured in hours, a frequency of one or two times a day, and a requirement of two additional rocket engine ignitions. Furthermore, waiting times in parking orbit prior to injection can easily be 24 hr for the indirect as compared to 2 hr for the direct ascent.

The second technique assumes a variation of the translunar trajectory with delay time resulting in a launch frequency of twice a day, with a corresponding launch tolerance of approximately 5 hr. Since no excess propellant is required to obtain this launch tolerance, there is no payload penalty. However, this is not the case for the first technique, where launch tolerances are governed by the amount of excess propellant available. This latter technique appears to be most favorable if an earth rendezvous is not required.

Additional propellant may also be required to salvage a mission in the event the vehicle cannot be injected at the preplanned time. Essentially, this propellant provides an injection frequency and injection time tolerance once the spacecraft is in its parking orbit. Excess propellant is also desirable for manned missions if an abort is required during the injection phase, when the spacecraft is being accelerated from earth-orbital to translunar injection speed.

The numerical data presented in this chapter represent launches from Cape Canaveral alone. Magnitudes of launch tolerances are obtained by assuming a hypothetical launch vehicle and are included solely for the purpose of giving insight into and comparison of the various aspects of the problem.

All data presented in this chapter is based on Keplerian orbits during ballistic flight, i.e., the earth is assumed spherically symmetric in concentric layers, and atmospheric drag and other nongravitational forces on the vehicle are neglected. (On occasion, effects of atmospheric drag and earth oblateness on the ascent trajectory will be mentioned.) In most cases, rocket thrust is simulated by an impulsive change in the veloc-

ity--ΔV; more details concerning the effects of finite burning times and a discussion of general orbital maneuvers are presented in Chapter VI of Ref. 1.

A. FIXED TRANSLUNAR TRAJECTORY TECHNIQUE

The timing and planning of a lunar mission reduces to the selection of a moon arrival date and time which depends on such mission considerations as solar illumination of the moon, the ability to establish prescribed orbits around the moon with circumlunar trajectories, and the ability to land at designated landing sites which are librating relative to earth. This selection of arrival time then fixes the translunar injection position ψ_0, the injection time and the inclination of the translunar plane i_{VTL} (Chapter IV, Section B). These fixed values, together with the injection radius and velocity, are then specific requirements for the lunar mission which must be met if the mission objectives are to be attained with the particular vehicle. This is illustrated by considering a one-minute delay in the arrival at the predetermined injection point. A late injection of this magnitude into a ballistic translunar trajectory can change the miss distance (pericynthion) at the moon by - 26 km, the vacuum perigee altitude (for a circumlunar trajectory) by + 305 km, and the return inclination i_{VTE} by 2 deg. Another, and more severe example is an error in injection position. If the spacecraft is injected at the correct time but with an along-track position error of + 11 km, the pericynthion of the ballistic circumlunar trajectory can change by + 135 km, the return vacuum perigee by - 14, 250 km and the return trajectory inclination by 7.5 deg. Therefore, regardless of how the spacecraft leaves the earth's surface, it must satisfy the translunar injection requirements quite closely. Understandably, midcourse guidance can correct small errors at injection; but they must be small if the correction fuel requirements are not to become excessive and if the midcourse guidance scheme is to be easily mechanized. Major trajectory changes after injection require too much energy to be practical at this time and they should be avoided.

1. Launch Tolerance with Direct Ascent

a. Direct ascent without earth rendezvous

With the ballistic translunar trajectory fixed, the injection conditions of the spacecraft (radius and velocity vector) are also fixed. To achieve these injection conditions, a coast period and parking orbits are likely to be used during the ascent phase.

The inclination of the parking orbit to the equatorial plane is quite important. If this inclination is not the same as the inclination of the translunar trajectory to the equatorial plane, a lateral maneuver will be required at velocities between earth orbital and escape speed. This is expensive in fuel since a large velocity vector must be changed in direction or "turned." Therefore, throughout the handbook, the parking orbit prior to injection is assumed to lie in the same plane as the initial translunar trajectory, and any lateral maneuvers, if required, will be performed during ascent into the parking orbit.

In order to satisfy the injection conditions, one can first visualize a "phantom" satellite in the parking orbit having the correct position for achieving the injection conditions at some predetermined time.

The problem now reverts to one that requires the spacecraft to ascend from the earth's surface and rendezvous with the phantom satellite. For mission planning, information is required as to the fuel penalty if the launch of the spacecraft is delayed on the ground.

In the direct ascent method, the spacecraft is boosted directly to the altitude of the parking orbit. The time of arrival at this altitude is planned such that the spacecraft and phantom satellite are coincident. The spacecraft is then injected into orbit, and it executes any turns that may be required to establish itself in the parking orbit plane during the orbit injection. In other words, a fictitious rendezvous is made with the phantom satellite. The direct ascent method is illustrated in the following sketch.

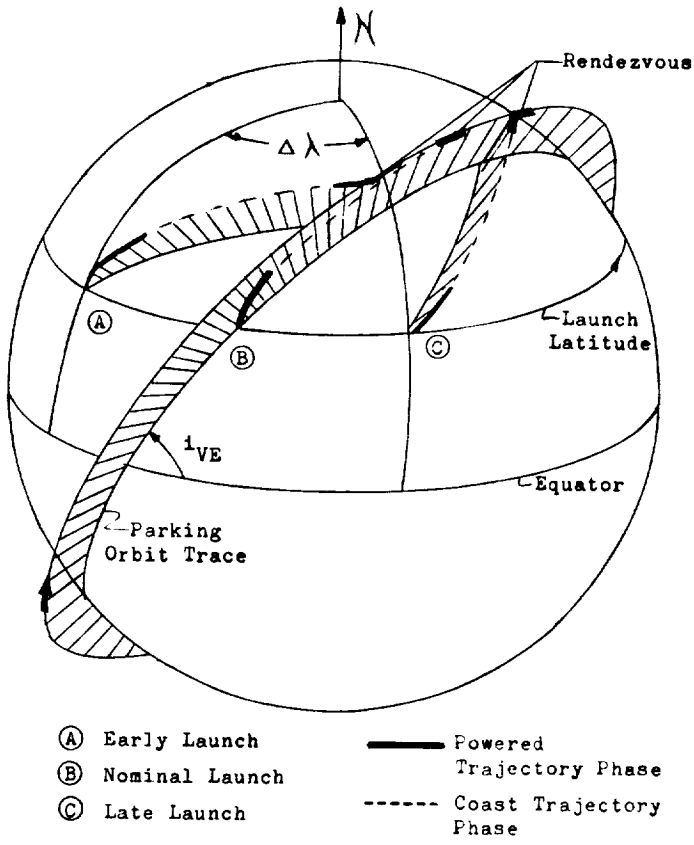

As can be seen, the spacecraft is accelerated from launch to some cutoff altitude. It then coasts to the parking orbit altitude, where ren-

dezvous is made with the phantom satellite. If a turn (i.e., orbit inclination change) is required, it is made during the second powered phase, as shown.

First, consider Case B in the sketch, where the launch site lies in the parking orbit plane and the phantom satellite is in the correct position, such that rendezvous occurs at the end of the ascent phase. For this case, no turn is required at the rendezvous point, and Case B will be considered as the nominal ascent trajectory in this discussion.

The next sketch shows three ascent trajectories (1, 2, 3) and the times of arrival at apogee (t_1, t_N, t_3). Trajectory number two is the nominal ascent, and t_N is the nominal apogee arrival time, with the nominal launch time being t_L.

Now consider that for Case B, the phantom satellite was not at the correct position at launch (t_L), but instead was at ($t_L - \Delta t_1$) as shown

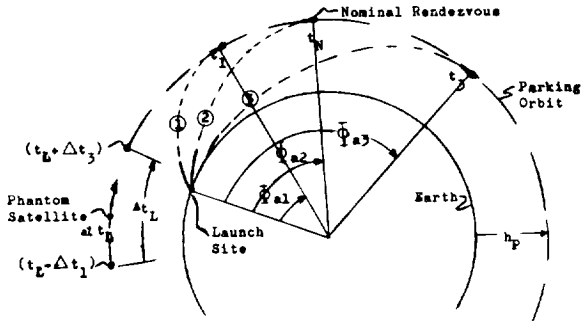

If Δt_1 is equal to the difference between the nominal apogee arrival time and t_1 ($t_N > t_1$), the spacecraft can still perform the rendezvous by flying the number 1 trajectory. This is called an early launch. The same reasoning applies if the phantom satellite occupies the position ($t_L + \Delta t_3$) at launch (late launch). If Δt_3 is equal to ($t_3 - t_N$) the spacecraft can rendezvous by flying the number 3 trajectory. In other words, by extending the ascent range Φ_a the spacecraft can be launched at any time in the interval $\Delta t_L = (t_3 - t_1)$, where Δt_L is the launch tolerance obtained by extending Φ_a from Φ_{a1} to Φ_{a3}.

Another method of obtaining launch tolerance consists of shaping the ascent trajectory. Consider the nominal ascent which arrives at the parking orbit altitude h_P with zero flight path angle ($\gamma = 0$). Now, for a given range angle Φ_a, allow the spacecraft to intersect the parking orbit with $\gamma \neq 0$, as shown in the following sketch:

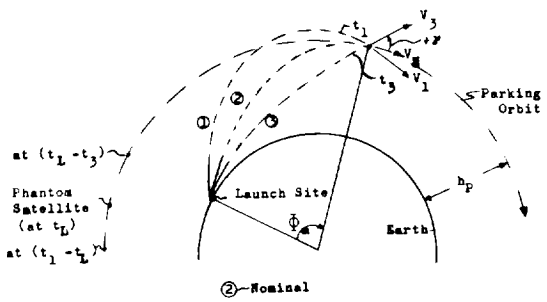

Assume further that upon arrival at the parking orbit altitude h_P a rendezvous is performed, and the flight path angle is reduced to zero. Trajectory number 1 (early launch) arrives at t_1, where $t_1 > t_N$, and trajectory number 3 (late launch) arrives at $t_3 < t_N$. By utilizing the same approach presented for the range extension method, it is similarly found that the launch tolerance from trajectory shaping is $\Delta t_L = (t_1 - t_3)$.

Thus far, the discussion has been restricted to Case B where the launch site lies in the parking orbit plane. However, this is not true in general because as the phantom satellite progresses in its orbit, the launch site, on the rotating earth, rotates out of the parking orbit plane. The real situation, greatly exaggerated, is depicted in the sketch on page V-2 by the ascent trajectories A and C. Because of the earth's rotation, Case A occurs prior to the nominal launch time t_L and Case C after t_L, and it is evident that some turn is required if launch took place at those times. The following sketch gives the pertinent geometry for determining the required turn angle ΔA which can be obtained from spherical trigonometry:

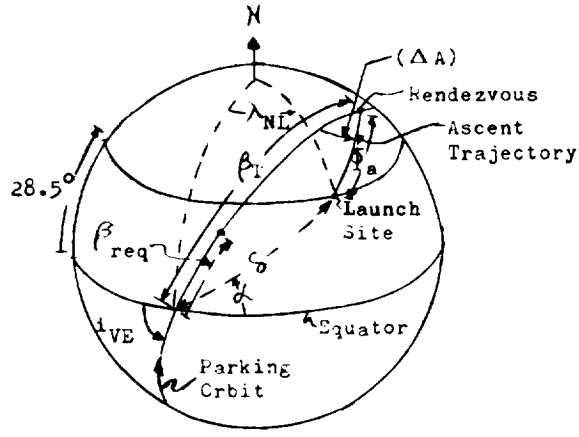

Ascent Turn Angle Geometry

$$\Delta A = \sin^{-1}\left[\pm \frac{\sin 28.5^\circ \cos i_{VE}}{\sin \Phi_a} - \frac{\cos 28.5^\circ \sin i_{VE} \sin \lambda_{NL}}{\sin \Phi_a} \right] \quad (1)$$

where the launch site is assumed in the northern hemisphere for this formula to hold, and

(+) = launch site on the polar side of the orbital ground trace (not shown)

(-) = launch site on the equatorial side of the ground trace

+28.5° = latitude of Cape Canaveral, the launch site

Equation (1) shows that the longitude of the launch site λ_L, the ascent range Φ_a, and the parking orbit inclination to the earth's equator i_{VE}, determine the magnitude of the required turn angle ΔA. Furthermore, the minimum turn angle occurs when $\Phi_a = 90$ deg. Assuming that the launch site is Cape Canaveral, which is at a latitude of +28.5 deg and i_{VE} is limited to between 28.5 and 35 deg, typical values of ΔA are shown in Fig. 1 for the nominal case Φ_a = 90 deg. Since the phantom satellite moves along the parking orbit at approximately 4 deg/min, and the launch site rotates with the earth at approximately 0.25 deg/min, the value of $\Delta\lambda$ will always be small for a given nominal phantom satellite pass (see sketch on page V-2). Consequently, because of the short interval of time the phantom satellite is in a favorable rendezvous position in a given revolution, the required ΔA is small. This particular point will become quite clear when the actual magnitudes of the launch tolerances are discussed below.

If ΔA and Φ_a are known, the required position of the phantom satellite β_{req} can be determined by use of spherical trigonometry (see the above sketch):

$$\beta_T = \cos^{-1}\left[\left\{ \cos \Phi_a \cos \delta - \sin \Phi_a \sin \delta \cos \Delta A \cdot \cos \left[\pm (\alpha - i_{VE}) \right] \right\} \left\{ 1 - \sin \Phi_a \sin \Delta A \cdot \sin \delta \sin \left[\pm (\alpha - i_{VE}) \right] \right\}^{-1} \right] \quad (2)$$

where

(+) = launch site on the polar side of the orbital ground trace

(-) = launch site on the equatorial side of the orbital ground trace

$$\alpha = \tan^{-1}\left[\frac{\tan 28.5^\circ}{\sin \lambda_L} \right]$$

$$\delta = \sin^{-1}\left[\frac{\sin 28.5^\circ}{\sin \alpha} \right]$$

then $\beta_{req} = \beta_T$ - ascent time $\left(\frac{\partial \beta_T}{\partial t} \right)$.

β_T is the orbital central angle of the rendezvous point (measured northward from the ascending node of the parking orbit--see previous sketch).

But first, the required ascent range as a function of launch delay time must be determined. If a nominal launch (Φ_a = 90 deg) is possible at a given time (t_L), there are only two parameters which can be changed to effect a rendezvous at a later instant. These variables are the actual launch time t and the ascent range Φ_a. The motion of the phantom satellite as a function of these variables is given by:

$$d\beta_{req} = \frac{\partial \beta_T}{\partial t} dt + \left(\frac{\partial t}{\partial \Phi_a} \right) \left(\frac{\partial \beta_T}{\partial t} \right) d\Phi_a. \quad (3)$$

Likewise, the motion of the intersection point of the parking orbit and ascent trajectory is given by

$$d\beta_T = \left(\frac{\partial \beta_T}{\partial t} \right)_{\Phi_a = \text{constant}} dt + \left(\frac{\partial \beta_T}{\partial \Phi_a} \right)_{t = \text{const}} d\Phi_a \quad (4)$$

In order to effect a rendezvous, the phantom satellite and the intersection point must be coincident. Therefore, by equating Eqs (3) and (4), the range extension as a function of launch time can be found as

$$\frac{d\Phi_a}{dt} = \frac{\frac{\partial \beta_T}{\partial t} - \left(\frac{\partial \beta_T}{\partial t} \right)_{\Phi_a = \text{constant}}}{\left(\frac{\partial \beta_T}{\partial \Phi_a} \right)_{t = \text{const}} - \frac{\partial t}{\partial \Phi_a} \frac{\partial \beta_T}{\partial t}} \quad (5)$$

A typical magnitude of $d\Phi_a/dt$ for near-earth parking orbits is 55 deg/min. Thus if a nominal launch calls for Φ_a = 90 deg, a launch can be made one minute before nominal by decreasing Φ_a to 35 deg or one minute after nominal by increasing Φ_a to 145 deg. In other words, for this practical range variation, launch tolerances obtained by range extension for the direct ascent technique are measured in minutes rather than hours. Note that Eqs (3), (4) and (5) apply to the range extension method only. Besides being used individually, the methods of range extension and trajectory shaping also can be used together to

obtain a launch tolerance as shown in the numerical example of Subsection A-1c below.

b. Direct ascent with earth rendezvous

It becomes immediately evident that if the phantom satellite were replaced by an orbiting vehicle, the launch tolerances given by the previous discussion are directly applicable. Therefore, if a mission entails a physical rendezvous with a fueling vehicle in earth orbit, for example, the methods for launching the spacecraft are not altered.

For the fixed translunar trajectory technique, the methods for launching and the launch tolerances for the fueling vehicle are identical to those of the spacecraft, since for an earth rendezvous mission with a subsequent translunar injection requirement, the fueling vehicle must first rendezvous with a phantom satellite and then the spacecraft must rendezvous with the fueling vehicle. Part of the mission planning must include the time required in parking orbit to perform the rendezvous maneuver, mate the vehicles and make final preparation for injection into the translunar trajectory.

c. Numerical example for direct ascent

The various concepts for direct ascents to the parking orbit and their relative merits can best be illustrated by a numerical example. Figure 2 presents launch tolerances obtained by range extension for a hypothetical launch vehicle with a burnout altitude of 185.2 km. The data shows that launch tolerance increases with increasing parking orbit altitude, and for the same range extension, it decreases with increasing initial ascent range. Both of these effects are evident from Eq (5), the first being due to the decrease of $\partial \beta_T / \partial t$ with increasing altitude, and the second due to increasing $(\partial t / \partial \Phi)_{\text{const launch time}}$ with increasing initial range.

Another aspect of the direct launch involves a set of orbit injection conditions (discussed in Section C) as well as launch tolerances for each orbital pass of the phantom satellite, since launch and rendezvous can take place on orbital revolutions prior to and after the nominal. This is also illustrated in the sketch showing direct ascent, whereby in Case A (early launch) the rendezvous with the phantom satellite may occur one revolution before the nominal, and in Case C (late launch) the rendezvous may occur one revolution after the nominal. Since the parking orbit period is approximately 90 min for the orbital altitudes considered, the launch site will have approximately a 22.5-deg longitude difference from the parking orbit plane for a pass before or after the nominal revolution. It becomes quite clear, for these cases, that much larger turns are required when the spacecraft intersects the parking orbit (Fig. 1). The additional ΔV of launching one revolution before nominal (due to turn) is approximately 1311 m/sec for the parking orbit inclination i_{VE} = 35 deg. This ΔV decreases with decreasing i_{VE}, but it still is 549 m/sec above nominal for i_{VE} = 29 deg. For launches after nominal, the additional fuel requirement rises, but not nearly as sharply as for launches before nominal. A launch one revolution after nominal requires an additional ΔV = 762 m/sec for i_{VE} = 35 deg and only 91.5 m/sec for i_{VE} = 29 deg. For some cases, three or four launches per day are possible.

The velocity capability required V_{req} for the nominal ascent (Case B) is given for the hypothetical booster in Table 1.

TABLE 1

Total Velocity Required for Nominal, No Turn, Rendezvous, V_{req} (m/sec)

h_{BO} = 185.2 km

Parking Orbit Altitude h_P (km)	Ascent Range Angle, Φ_a (deg)			
	60	90	120	180
277.8	7848.3	7848.0	7847.4	7847.1
466.7	7964.7	7958.0	7955.9	7955.9
740.8	8136.9	8114.4	8107.1	8104.3

By extending the ascent range, the total velocity requirements are affected, the total velocity required being defined as

V_{req} = velocity at burnout + ΔV (injection and turns)

Table 1 shows that the required velocity decreases slightly with increasing ascent range. Thus, for the nominal case, launch tolerance is obtained with an attendant reduction in V_{req} and hence in fuel expenditure. Of course, V_{req} increases with parking orbit altitude, as can be seen from Table 1.

For the off-nominal case and the parking orbit inclinations of interest, practical turn angles from a standpoint of fuel requirements will vary from 0 to 4°.

Figure 3 shows that for a constant turn angle at h_P = 466.7 km the required velocity drops with decreasing range angle (see solid curves). However, the turn angle required will not remain constant as Φ_a changes and the "dashed" curves in Fig. 3 show how the total velocity requirement varies. For range extensions from 60° to 90°, no additional velocity is required; but by extending the range beyond 90° and below 60°, the velocity required increases rapidly.

Launch tolerances as obtained from trajectory shaping have not been considered thus far. Essentially, the tolerances derived from the "shaping" method are limited only by the velocity capability of the booster and are dependent on the booster characteristics. Figure 1 presents the velocity requirement above nominal for obtaining launch tolerances by this method with the assumed booster and for h_P = 466.7 km. For a fixed h_P

and a fixed launch time tolerance, the velocity requirement increases with decreasing ascent range angle.

It should be noted that the slopes of the ΔV versus Δt_L curves are quite steep and increase (not shown), with decreasing parking orbit altitude. In addition, more velocity is required to obtain a (+) launch tolerance (launch late) than a (-) tolerance. Practical tolerances ($\Delta V \simeq 300$ m/sec) again are measured in minutes.

A third method for generating tolerances is by combining the first two methods. This is possible by shaping the ascent trajectory for an early launch at the minimum ascent range angle and a late launch at the maximum range angle. Consider as an example a parking orbit (h_P = 466.7 km, i_{VE} = 30.25°) and a booster (V_{req} = 8186 m/sec, h_{BO} = 185.2 km). At this inclination ($i_{VE} > 28.5°$, the launch latitude) three launches daily are possible--two for Case B, since the parking orbit ground trace intersects the launch parallel at two points, and one for Case C, since the maximum turn angle required at Φ_a = 90° is approximately 2°, which is within the velocity capability of the booster, as illustrated in Fig. 3. Case B and Case C are illustrated in the sketch on page V-2.

Tables 2, 3 and 4 show the launch tolerances for this velocity capability using range extension only, trajectory shaping only, and a combination of the two methods for parking orbit altitudes of 277.8 km, 466.7 km, and 740.8 km. The nominal ascent range angle is 60° and, for the range extension method only, was varied to 180° for launch tolerance. For the maximum turn case, the maximum ascent range angle is reduced to 125° because of the increased cost for turning (see Fig. 3). The nominal ascent range for trajectory shaping is 90° for the no-turn cases and approximately 65° for the turn cases.

Note that for the lower parking orbit altitudes ($h_P < 703.8$ km) and for the no-turn case ($\Delta A = 0$), it is best to use the combination method. Above 703.8 km, the range extension method becomes the most efficient. Also note that if it is not practical to extend the ascent range from 60° to 180°, for example, limit $\Phi_{a_{max}}$ to 120°, then the combination method is the most efficient. For the example, presented (V_{req} = 8186.6 m/sec and i_{VE} = 30.25), a launch time tolerance of 3 min is available for the no-turn case at the parking orbit altitudes of interest. At h_P = 888.9 km, the entire velocity capability V_{req} is required to establish a circular orbit, and therefore there is no excess velocity available for range extension or trajectory shaping. Consequently, there is zero launch tolerance at this altitude.

Tables 2, 3 and 4 also point out how the launch tolerances are reduced considerably for the maximum turn case because part of the excess velocity must be used to perform the turn.

One way of increasing the launch tolerances is to increase the velocity capability. For instance, by increasing the velocity capability of the previous example from 8186.6 to 8338.7 m/sec, the launch tolerance can be increased by one minute for a parking orbit altitude of 466.7 km.

TABLE 2

Launch Tolerance (min)

h_{BO} = 185.2 km, h_P = 277.8 km, V_{req} = 8186.6 m/sec

Method	No Turn (Case B)			Maximum Turn (Case C)		
	-Tolerance	+Tolerance	Total Tolerance	-Tolerance	+Tolerance	Total Tolerance
Range extension	0	0.54	0.54	0	0.28	0.28
Trajectory shaping	1.76	0.85	2.61	0.68	0.42	1.10
Combination	1.76	1.24	3.00	0.67	0.56	1.23

TABLE 3

Launch Tolerance (min)

h_{BO} = 185.2 km, h_P = 466.7 km, V_{req} = 8186.6 m/sec

Method	No Turn (Case B)			Maximum Turn (Case C)		
	-Tolerance	+Tolerance	Total Tolerance	-Tolerance	+Tolerance	Total Tolerance
Range extension	0	1.68	1.68	0	0.86	0.86
Trajectory shaping	1.48	0.82	2.30	0.70	0.46	1.16
Combination	1.45	1.85	3.30	0.70	0.85	1.55

TABLE 4

Launch Tolerance (min)

h_{BO} = 185.2 km, h_P = 740.8 km, V_{req} = 8186.6 m/sec

Method	No Turn (Case B)			Maximum Turn (Case C)		
	-Tolerance	+Tolerance	Total Tolerance	-Tolerance	+Tolerance	Total Tolerance
Range extension	0	3.28	3.28	0	0	0
Trajectory shaping	0.81	0.66	1.47	0	0	0
Combination	0.62	2.37	2.99	0	0	0

2. Launch Tolerance with Indirect Ascent

a. Indirect ascent without earth rendezvous

The indirect ascent method can be regarded as a generalization of the direct ascent method. The former method is illustrated in the following sketch.

In an indirect ascent, the spacecraft is launched at an arbitrary time into an ascent trajectory which intersects the parking orbit plane 90° downrange from burnout. This ascent range angle minimizes the turn angle as given by Eq (1). At the intersection of the ascent plane with the parking orbit plane, the spacecraft has reached the apogee of its ascent coast trajectory and is turned into and accelerated to the velocity of the predetermined intermediate or waiting orbit. The circular waiting orbit may be below or above the parking orbit, its most important characteristic being that it has a period different from the parking orbital period. This allows the spacecraft to wait in the intermediate orbit until the desired phase relationship with the phantom satellite is established. At this time the spacecraft transfers to the parking orbit by a Hohmann transfer and effects a rendezvous with the phantom satellite.

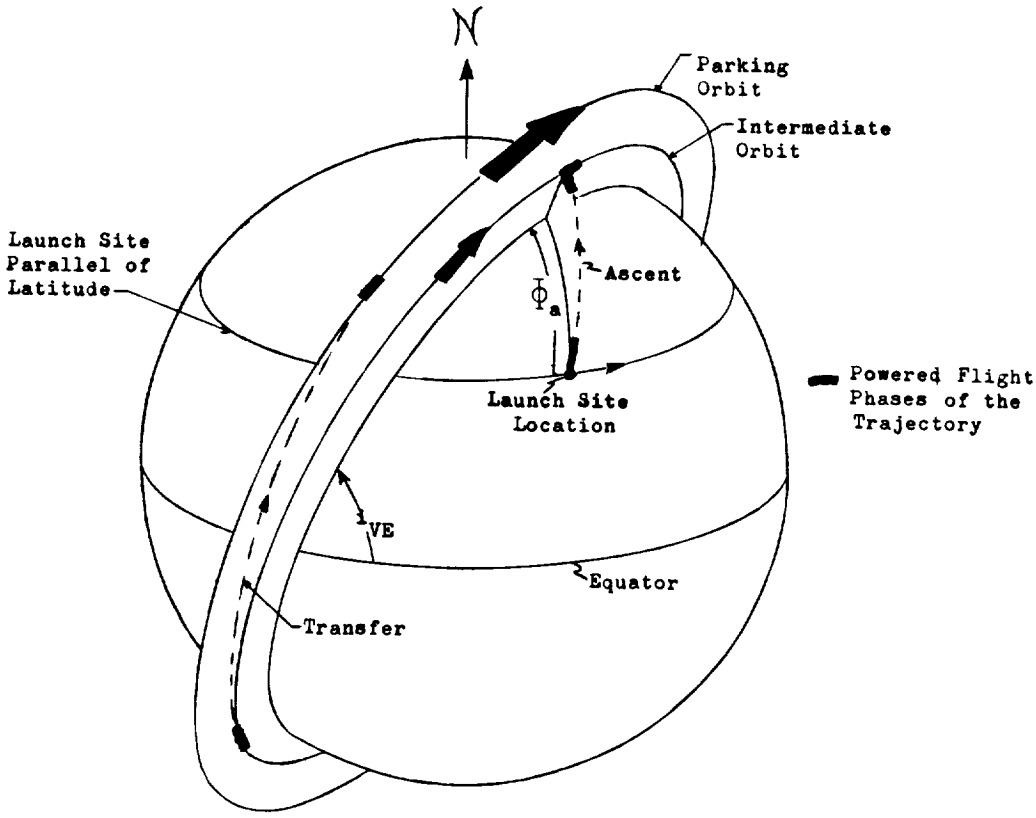

The indirect ascent method has the following characteristics: (1) Since the phantom satellite's position is ignored at launch, the launch tolerance is significantly larger than in the case of the direct ascent method. (2) Since there is generally a waiting period in the intermediate orbit and the transfer range angle is 180°, the time from launch to rendezvous can be many hours as compared to less than an hour for the direct ascent method. (3) Two additional powered phases are required. (4) The actual position of the rendezvous point cannot generally be controlled without excessive fuel penalties or longer wait times in the intermediate orbit. (5) The launch vehicle or booster must possess sufficient capability to deliver the spacecraft to higher altitudes than the nominal parking orbit because otherwise this method may become impractical due to the very long waiting times in the intermediate orbit.

In the numerical example which will be given later, it is assumed that the booster can deliver the spacecraft to any waiting orbit altitude between 185.2 and 740.8 km. The lower altitude limit is the result of unacceptably high drag decay rates for space vehicles with "normal" area-to-mass ratios, while the upper limit is the result of increasing radiation from the inner Van Allen belt, which may require heavier shielding of the spacecraft, and to a lesser degree it is the result of increased energy requirements for the mission if the parking orbit is at a lower altitude.

In this range of waiting orbital altitudes, the time required to change the phase relationship between the spacecraft and the phantom satellite can be determined as soon as the parking orbit altitude is fixed. The following sketch shows the phantom satellite near the middle of the altitude band at 466.7 km. Assume that at a time t_0, the spacecraft and phantom satellite are in phase, $\Delta\beta' = 0$, as shown. After one complete revolution of the phantom satellite t_1 the relative position of the spacecraft to the phantom satellite has changed ($\Delta\beta' \neq 0$). In other words, the spacecraft has "gained" on the satellite for altitudes less than 466.7 km and has "lost" for altitudes greater than 466.7 km. The gain in central angle per revolution (i.e., angular displacement of spacecraft ahead of phantom satellite) is given by:

$$\Delta\beta' = t_1 (\omega_i - \omega_P) \tag{6}$$

where ω_i is the angular velocity of the satellite in the waiting or intermediate orbit

or in terms of time the gain per revolution is

$$\Delta t = \Delta\beta'/\omega_i \tag{7}$$

The maximum gain per revolution obtained from above is 5.7 min for a waiting orbit at 185.2 km, and the maximum loss is 5.7 min for one at 740.8 km if the parking orbit altitude is 466.7 km. Utilizing the same nomenclature but referring to t_1 as the position of the spacecraft at any time, and $\Delta\beta'_{req}$ as the required phase relationship to

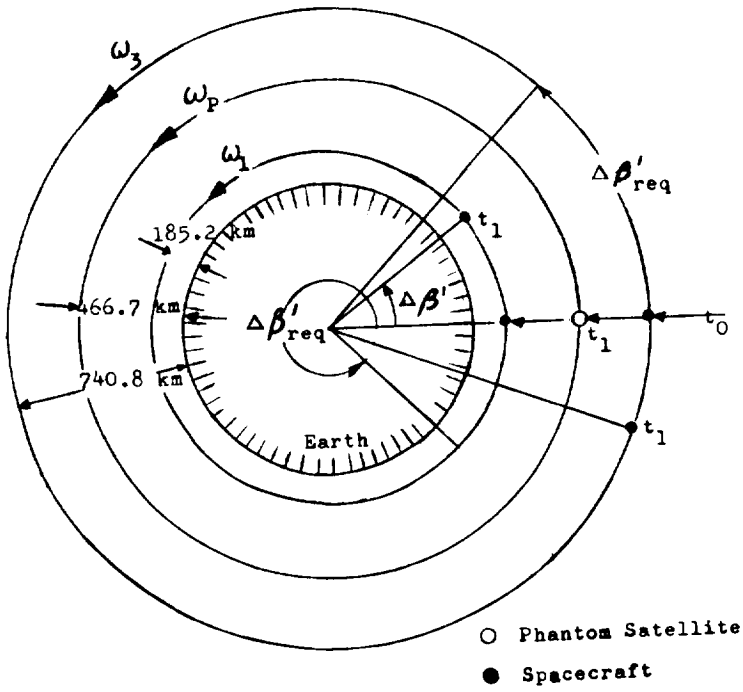

effect a Hohmann transfer to the parking orbit for rendezvous, the angle β to be gained or lost is:

$$\beta = \left| \Delta\beta'_{req} - \Delta\beta' \right| \text{ , gain for } \omega_1 \text{ , loss for } \omega_3 \qquad (8)$$

$$\beta = 360 - \left| \Delta\beta'_{req} - \Delta\beta' \right| \text{ , loss for } \omega_1 \text{ , gain for } \omega_3 \qquad (9)$$

with the number of spacecraft revolutions n required to achieve the proper phase relationship for rendezvous given by

$$n = \beta / \Delta\beta' \qquad (10)$$

where $\Delta\beta'$ is obtained from Eq (6) and n is not necessarily an integer.

Now assume that the nominal ascent trajectory corresponds to Case B (in the parking orbit plane, direct with $\Phi_a = 90°$). After a few minutes of possible direct launches (direct launch tolerance) the phantom satellite is no longer in the proper phase relationship for rendezvous. The spacecraft must now ascend to a different altitude to correct for this phase differential, but in doing so, generates another differential because of the difference in ascent time from the nominal. Furthermore, the interception of the parking orbit plane occurs at a different location from the nominal, thereby introducing an additional phase differential. Finally, the transfer from the intermediate orbit requires a phase differential. Therefore, the total phase angle β to be made up in the intermediate orbit can be obtained from:

$$\beta = \Delta t_L \, \omega_P + (t_a - t_{aN}) \, \omega_P + (\beta_T - \beta_{TN}) + (180 - t_{tr} \, \omega_P) \qquad (11)$$

where

Δt_L = launch tolerance

t_a = ascent time

t_{aN} = nominal ascent time

β_T = central angle from parking orbit node to interception of the parking orbit plane with the ascent trajectory

β_{TN} = same as β_T except the ascent trajectory is nominal

t_{tr} = transfer time from the intermediate orbit to the parking orbit.

Any booster burnout dispersions can be included in the second term on the right-hand side, waiting orbit dispersions into the third term; however transfer orbit and parking orbit injection dispersions will alter β.

Thus with knowledge of $\Delta\beta'$ for the intermediate orbit and of β for a particular launch tolerance, the number of revolutions required in the intermediate orbit can be found from Eq (10). But in order to obtain t_a, β_T and t_{tr} for Eq (11), the intermediate orbit altitude relative to the parking orbit must be known. This altitude can be established through use of the previous sketch and Fig. 5. The constraints for ascent to a higher or lower intermediate orbit altitude are as follows--either set may be used; both reflect the phase conditions at injection into the intermediate orbit.

Set (1)

$$\Delta\beta'_{req} - 180° \leq \Delta\beta' \leq \Delta\beta'_{req} \text{ (lower alt)}$$

$$\Delta\beta'_{req} - 180° > \Delta\beta' > \Delta\beta'_{req} \text{ (higher alt)} \qquad (12)$$

Set (2)

$$\Delta\beta'_{req} + 180° \geq \Delta\beta' \geq \Delta\beta'_{req} \text{ (higher alt)}$$

$$\Delta\beta'_{req} + 180° < \Delta\beta' < \Delta\beta'_{req} \text{ (lower alt)} \qquad (13)$$

For a parking orbit altitude h_P = 740.8 km, the waiting or intermediate orbit lies below it and there is no choice but to have an intermediate orbit lower than the parking orbit. In this case it is possible to have a phase difference β of 360°, which means that a maximum waiting time of 12.8 hr is possible at an altitude h_i = 185.2 km of the intermediate orbit. If the intermediate altitude is higher, for example, h_i = 466.7 km, the waiting time is doubled. The same waiting time applies if h_P = 185.2 km and the intermediate orbit is necessarily higher. Consider the case h_P = 466.7 km, h_i = 185.2 km where the maximum phase differential is 360°, the maximum waiting time is 25.6 hr. Of course, the maximum waiting time increases for 185.2 km < h_i < 466.7 km. If 185.2 km < h_i < 740.8 km, both constraints given by Eq (12) or Eq (13) can be utilized and the maximum waiting time is again reduced to 12.8 hr.

In the determination of parking and waiting orbit parameters, some neglected forces should be considered. Thus, at the lower orbital altitudes, i.e., near 200 km, atmospheric drag has a considerable effect on the trajectory of the spacecraft. The lifetime for a dense spacecraft, or low area-to-mass ratio, is of the order of days, while for a spacecraft with a high area-to-mass ratio it may be as low as a few hours. (For more details on lifetime, see Chapter V of Ref. 1.) Considering also orbit injection errors, a practical lower altitude limit for intermediate or parking orbits is 250 km.

Other corrections to Keplerian orbits are due to earth oblateness. For a circular orbit, the major secular effects are a correction to the orbital period and a correction to the location of the ascending node (regression of the nodes). During the earth departure phase, the motion of the phantom satellite in the parking orbit must be simulated from the translunar trajectory injection point back in time to the launch time t_L. In other words, the phantom satellite position in orbit should reflect oblateness effects of the earth.

If the intermediate orbit altitude is different from that of the parking orbit, there will be a difference in regression rates between the two. Therefore, at the time of injection into the intermediate orbit, the plane of the intermediate orbit is established with the same inclination i_{VE} as the parking orbit, but with an orbital plane that has a slightly different ascending node, or an offset. This offset gradually decreases due to nodal regression until, at the time of rendezvous, both the intermediate and parking orbit planes are coincident.

Oblateness effects can also be counteracted by applying small thrust impulses at the intersection of the intermediate and parking orbit planes or by one pulse at rendezvous, or one at the intersection just prior to the rendezvous transfer maneuver. The additional ΔV requirement to counteract earth oblateness effects can be as high as 67 m/sec for a parking orbit altitude of 466.7 km and for a maximum of 24 hr in orbit.

b. Indirect ascent with earth rendezvous

Just as in Subsection A-1b, if the phantom satellite is replaced by a physical vehicle, the discussion given in the previous subsection, A-2-a, is directly applicable for indirect ascents of lunar spacecraft employing an earth rendezvous. The same launch tolerances and velocity requirements apply to the launch of the physical vehicle.

c. Numerical example for indirect ascent

Again, the various concepts for an indirect ascent will be illustrated by a numerical example. In order to allow a comparison with the direct ascent method, the parking orbit and hypothetical booster characteristics are assumed to be the same.

It has been established that the inclination of the parking orbit, the launch site latitude, and the launch delay time all have a bearing on the magnitude of the turn angle ΔA. It is assumed that the launch site is Cape Canaveral at a latitude of 28.5° N and that orbit inclinations, i_{VE}, are limited from 28.5 to 34.5°. Figure 5 presents the required ΔA for ϕ_a = 90° from Cape Canaveral to various values of i_{VE} within the allowable band. The data are presented versus a time scale in increments of 1-hr launch delay time. The origin in time, t = 0, is arbitrarily chosen in Fig. 5; it by no means represents the nominal launch time for the nominal, no-turn, direct ascent. This choice of time origin also applies to Figs. 6 through 12.

Again a hypothetical launch vehicle is assumed whose burnout altitude is 185.2 km. Typical velocity requirements for this booster are given in Table 5 below for parking orbit altitudes h_P of 185.2, 466.7 and 740.8 km.

TABLE 5

Velocity Required for Indirect Ascents for Translunar Missions (m/sec)

Parking Orbit Altitude h_P	185.2 km	466.7 km		740.8 km
Intermediate Orbit Altitude h_i	740.8 km	185.2 km	740.8 km	185.2 km
V (burnout)	7816.9	7793.1	7816.9	7793.1
ΔV (injection)	297.8	0	297.8	0
ΔV (transfer)	311.2	162.8	164.6	311.2
ΣV (required to rendezvous)	8425.9	7955.9	8279.3	8104.3
ΔV (escape)	3226.0	3159.3	3159.3	3098.0
ΣV (required for mission)	11651.9	11115.2	11438.6	11202.3

However, the remainder of the discussion will assume that h_P = 466.7 km, which is very close to a "rendezvous compatible orbit" of $\simeq$ 485.2 km. A rendezvous compatible, or synchronous satellite orbit has an integral number of revolutions per sidereal day, and hence passes over the same areas each day. For circular orbits, the altitude alone determines rendezvous compatibility, but with earth oblatness effects taken into account, the altitude-inclination combination determines compatibility of orbits for rendezvous.

Figures 6 through 9 show the excess velocity requirements ΔV, i.e., the velocity required over a nominal, no-turn, direct ascent, for h_i = 185.2, 370.4, 555.6, 740.8 km, respectively. This velocity excess includes the excess increments for the launch, injection and turn, transfer and rendezvous phases. Note that in Figs. 6 through 9 the minimum excess velocity increases for $h_i > h_P$, since the spacecraft must lose altitude and hence potential energy to return to the parking orbit for rendezvous. The minimum excess is ΔV = 99.1 m/sec for h_i = 555.6 km and ΔV = 304.8 m/sec for h_i = 740.8 km.

The sketches below serve as an aid for interpreting Figs. 6 through 9.

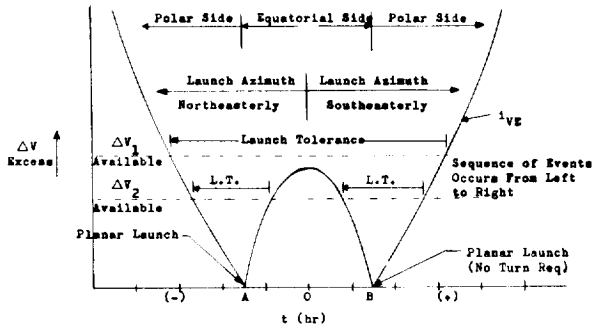

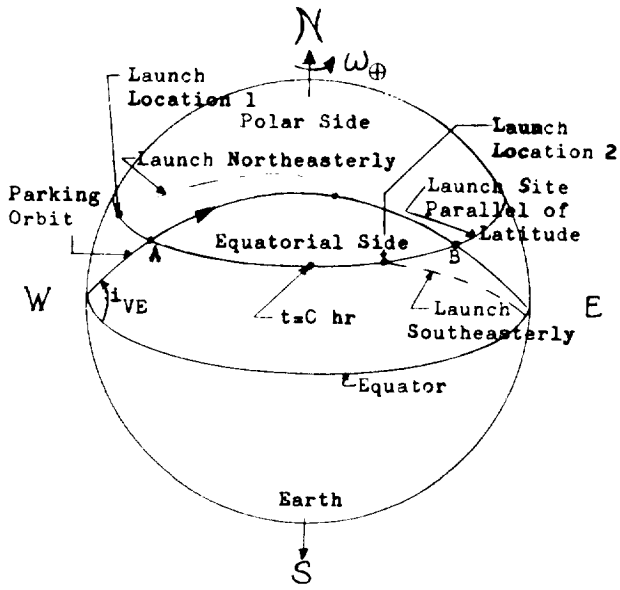

At t = 0, the launch site is halfway between the intersections of the parking orbit plane with the launch latitude on the equatorial side. Prior to this time, ascents are made northeasterly, A < 90° and southeasterly, A > 90°, afterward. The inertial launch azimuth A (great circle course on a nonrotating earth) is measured clockwise from geographic north through 360°. If the launch vehicle has an excess ΔV_1 available, it will have a continuous launch period (see sketch on page V-2). However, if only an excess ΔV_2 is available, the possible launch period LT will be discontinuous as shown in the first sketch.

Referring again to Figs. 5 to 9, it is possible to have a continuous launch tolerance for all parking orbit inclinations and the maximum ΔV excess required is on the order of 900 m/sec. The resulting launch tolerance can vary from 6 to 8 hr, depending on i_{VE}. For excess ΔV's less than about 900 m/sec, discontinuous and shorter launch tolerances will be experienced for the higher values of i_{VE}. However, continuous launch tolerances may still be realized for lower values of i_{VE}.

If the phantom satellite has the proper phase relation at the time the launch site is in the parking orbit plane, the nominal, no-turn, direct ascent to rendezvous is conducted. In this case no waiting time is required. If the launch vehicle and spacecraft are ready prior to the nominal time, and an ascent is performed, the proper phase relationship will not exist and the spacecraft must wait in an intermediate orbit. The spacecraft also must wait if a late launch is performed.

The waiting time in the intermediate orbit depends on the launch time. Figures 10 through 12 give the waiting time, in hours, for h_i = 185.2, 370.4, 555.6 and 740.8 km. Each figure represents a different i_{VE} in the possible band that can be established from Cape Canaveral launches. Data is shown emanating from a northeasterly nominal launch direction. Below is another auxiliary sketch illustrating the interpretation and use of the figures.

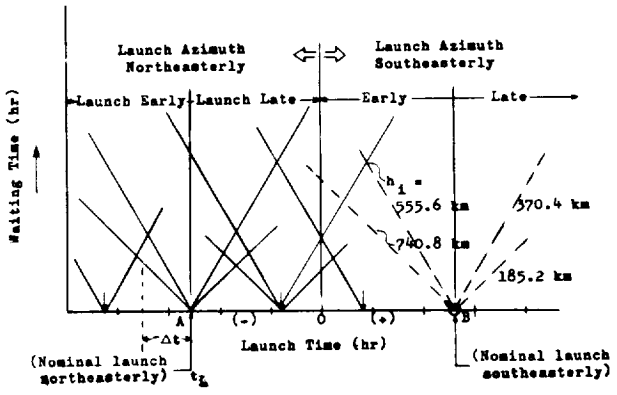

The sketch shows the regions of northeasterly and southeasterly launch azimuths. Since in general $i_{VE} > 28.5°$, the launch latitude, the launch

site will be in the parking orbit plane twice a day (points A and B in the previous sketches). If the launch took place at the nominal north-of-east launch time there would be zero waiting time. However, if the spacecraft is launched early, say at $t_L - \Delta t$, then, depending on h_i, the waiting time will vary accordingly as illustrated in the above sketch. Note the cyclic nature of the curves that originate at the "arrowheads." This is due to the phantom satellite achieving the proper phase relationship on succeeding revolutions. The interval of time between "phasings" is attained after one revolution plus an increment to account for the launch site rotation, i.e., the interval is slightly greater than the orbital period of the parking orbit. These "phasings" are denoted by arrows on the abscissas in Figs. 10 to 12 and the construction of the curves is accomplished by utilizing the same slopes for the straight lines as for the nominal launch. The phasing points do not necessarily occur on the southeasterly planar launch. However, if the nominal ascent is planned to occur at the southeast orbital plane intersection (point B and dashed curves in sketches), the phasing points are constructed in the same manner and with the same time intervals as they were for the northeasterly nominal launch. It becomes evident from the above discussion that the nominal ascent is not necessarily planned for either orbital plane intersection (points A and B). In fact, direct ascent (nominal launch) frequency may be higher for a given excess velocity if the phasing points are offset from the planar crossings.

Figures 10 to 12 essentially present minimum waiting times and the corresponding intermediate orbital altitudes as reflected by the constraints, Eqs 12 and 13.

B. VARIABLE TRANSLUNAR TRAJECTORY TECHNIQUE

This technique is based on the fact that for any given translunar trajectory inclination i_{VTL} a specific trajectory can be found to satisfy constraints in flight time, pericynthion altitude, and transearth inclination i_{VTE}. For the class of circumlunar trajectories discussed in Chapter IV, this suggests that translunar trajectories with variable i_{VTL} be used to obtain a launch time tolerance (see Ref. 2, and also Chapter VI). This is opposed to the technique discussed in Section A, which assumes that the translunar trajectory inclination, i_{VTL}, is fixed by the mission during the launch tolerance.

1. Launch Tolerance

a. Without earth rendezvous

Three assumptions will be made to simplify this discussion. (1) It can be shown for lunar trajectories that when the spacecraft is at pericynthion, t_p, the lunar position is nearly along the intersection x_E of the MOP and the translunar trajectory plane established at injection, t_0 (see sketch below). This will be assumed exactly true

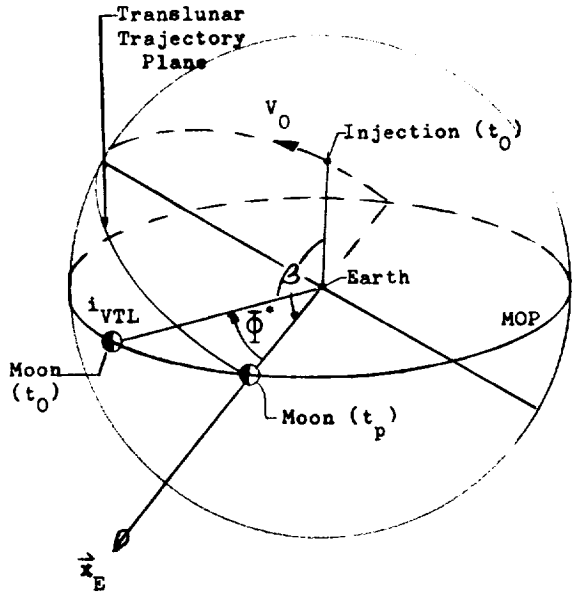

throughout this section. (2) Parking orbits around the earth are permissible; in fact, they are desirable because they allow the use of one efficient nominal ascent and orbit injection trajectory profile, provide final on-board and ground checkouts, and open the launch window considerably. (3) The moon's position at pericynthion (t_p) is assumed fixed on $\vec{x}_E$ throughout the period of the launch time tolerance, and consequently the orientation of the earth's equatorial plane and MOP are assumed similarly fixed. The relatively slow motion of the moon around earth (about 1° of Φ^* in 2 hr) makes this assumption valid over a period of a few hours.

The next sketch illustrates how a launch time tolerance is obtained by varying i_{VTL}. Theoretically, there is an infinite launch tolerance for this technique if there are no launch azimuth restrictions and if the launch vehicle possesses the additional energy requirements for retrograde launches (against the earth's rotation). Practically, however, this is not the case, since Cape Canaveral, for instance, has range safety constraints that restrict launch azimuths to $45° \leq A \leq 110°$. In the illustrative example the launch azimuth is restricted to $70° \leq A \leq 110°$.

The following sketch shows the moon ($\vec{x}_E$) near its ascending node $\vec{B}$ at the time of pericynthion. The launch site is at 28.5° north latitude and is rotating with the earth, as indicated by the sequence of points, A, B, C on the sketch. At point A the launch site longitude is less than 180° west of the moon's longitude and A = 70°. This heading allows a parking orbit plane to be established (denoted by ① on the sketch) that passes through $\vec{x}_E$ and remains within the launch azimuth restriction. The resulting inclinations to the equator and

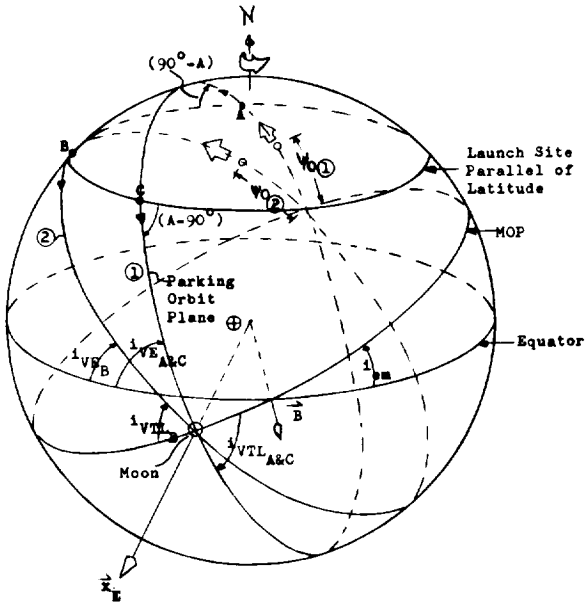

MOP are i_{VE_A} and i_{VTL_A}, respectively. The spacecraft remains in the parking orbit until it reaches the proper injection point $\psi_{0\,①}$ and then is injected into a northerly direction relative to the MOP. North, relative to the MOP, is defined by the angular momentum vector of the lunar orbital motion.

If the spacecraft is launched due east (A = 90°), there is a launch point B that also allows the parking orbit (denoted by ② on the sketch) to pass through $\vec{x}_E$. Again the spacecraft remains in the parking orbit until position $\psi_{0\,②}$ at which time a northerly injection takes place. This launch results in the minimum i_{VE} and i_{VTL}, as is evident from the sketch.

As the launch site rotates with the earth, point C is reached, requiring the maximum allowable launch azimuth (A = 110°) in order to pass through $\vec{x}_E$. Here, the parking orbit plane is the same as established when the launch was made at point A. Consequently i_{VE} and i_{VTL} are the same as for launch location A.

A launch is possible at any time that the launch site is between A and C. The translunar trajectories for this example are necessarily northerly and direct relative to the MOP, since a central angle $\beta > 150°$ is required (see previous sketch) to intercept the moon if injection occurs close to perigee of the translunar trajectory.

When the launch site is east, but less than 180° east of the lunar longitude, another possible launch period exists. However, in this period translunar trajectories that depart from the earth southerly relative to the MOP are required as illustrated by the sketch below:

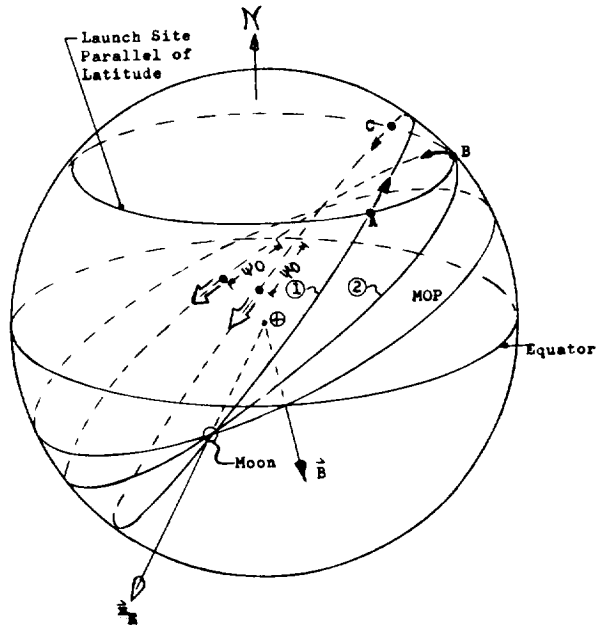

As before, in the time the launch site rotates from point A to B to C, the launch azimuths are 70°, 90° and 110° respectively, and within the azimuth restriction. The spacecraft waits in parking orbit ① or ② until the proper injection point ψ_0 is reached. At this time the spacecraft is injected in a southerly direction relative to the MOP. The shorter time required in the parking orbit for this case as compared to the inject north case can be noted by comparing the two sketches on this page. When the moon is near its descending node the opposite is true.

The two sketches above imply that dA/dt, the change in launch azimuth with launch time, is constant. This is true when the moon is at its descending or ascending node, but not when the moon is at some other orbital position, as shown below.

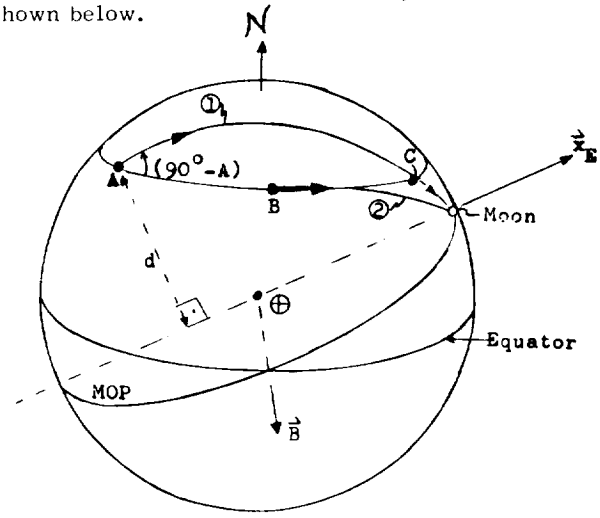

Here the moon is at its maximum northerly declination, and again the longitudes between A and B represent northeasterly launches and the longitudes from B to C represent southeasterly launches. Note that the perpendicular distances d between A and $\vec{x}_E$ and C and $\vec{x}_E$ are different. This causes a rapid variation in dA/dt when the site nears C, as can be visualized when the moon is considered as a pivot point. This is illustrated in Fig. 13, where the northeasterly and southeasterly launch tolerances are plotted separately for different lunar positions. Independently, the launch tolerance varies from 10 min to 4.74 hr. For the full range of launch azimuths the total available launch tolerance is 4.91 hr.

As pointed out previously, there are two launch periods available in one day. One period results in translunar trajectories that are northerly relative to the MOP, and the other period results in southerly translunar trajectories. Figure 13, although shown for northerly departures, also is applicable for southerly departures if the curve of northeasterly launches in Fig. 13 is used to represent southeasterly launches and vice versa.

Below is a table presenting typical delay times between injection during period I and injection during period II:

TABLE 6

Lunar Position	Max North	Max South	Desc/Asc Node
Injection (Period I)	Northerly	Northerly	Northerly
Launch time tolerance	4.91 hr	4.91 hr	4.91 hr
Delay time	38 sec	38 sec	7.19 hr
Injection (Period II)	Southerly	Southerly	Southerly
Launch time tolerance	4.91 hr	4.91 hr	4.91 hr

These data show a very short delay time between available launch periods for the moon at its maximum northerly or southerly declinations. For all practical purposes, a launch period of 9.82 hr is available at these times if both inject north and south trajectories are permitted.

The data presented in Fig. 13 and the above table are calculated for the year 1968, when the inclination of the MOP to the equatorial plane $i_{em} = 28.5°$. Approximately nine years later, $i_{em} = 18.5°$. The effect of this change on launch tolerance presented in Fig. 13 is to increase the minimum tolerance and decrease the maximum tolerance of the individual northeasterly or southeasterly launches. The total launch time tolerance will not be affected.

It is important to note that the technique outlined above does not require any turning of the velocity vector in flight at any time, although such maneuvers could be used to further increase the launch time tolerance. The only ΔV penalty of the launch vehicle is approximately 25 m/sec due to the varying component of the earth's rotational velocity in the flight direction for the range $70° \leq A \leq 110°$.

b. Launch tolerance with earth rendezvous

If a fueling vehicle is injected first into a parking orbit utilizing the variable trajectory technique, its launch tolerance can be obtained from the previous subsection. However, the spacecraft must now be launched to perform a rendezvous with the fueling vehicle. Since the parking orbit inclination of the fueling vehicle is fixed, the launch tolerance for the spacecraft is the same as for direct or indirect ascent of the fixed translunar trajectory technique.

The techniques for earth departure discussed in Sections A and B illustrate how the launch tolerance can be increased from minutes to many hours by the use of parking or parking and intermediate (waiting) orbits with only moderate fuel expenditure (ΔV's of the order of 300 m/sec). The increased launch tolerance is obtained at the expense of some increase in complexity and the number of rocket burning phases from launch to lunar injection. On the other hand, each burning phase can be used to correct for dispersions from previous phases, dispersions due to variable densities, earth oblateness, etc., and the additional time near earth can be used for tracking, checkout of equipment, and refueling by shuttle vehicles. Thus the small allowable delay time at the launch site for the one burning phase of a direct departure from earth has been traded for a large delay time at the launch site and small tolerances for each of several burning phases for an indirect departure from earth (i.e., one using parking or waiting orbits) which are simpler to achieve and give more control and reaction time during the earth departure phase of a lunar mission.

C. TRANSLUNAR INJECTION

Sections A and B have discussed launch techniques that result in the spacecraft arriving at the correct position at the correct time for injection into the translunar trajectory. Prior to injection, the spacecraft is in a parking orbit. But the question arises as to what can be done to salvage the mission if the spacecraft cannot be injected from this orbit at the proper time. This may be the result of a system malfunction that requires repair, a hold for injection because of the need of further verification of system status, or an off-design parking orbit.

Furthermore, some missions require long waiting periods in a parking orbit prior to injection. Such a mission may be a lunar logistics mission wherein the freighter waits in a parking orbit while supplies are shuttled to it from the earth's surface. The following discussion is applicable to both the cases of a missed injection point and the logistics mission.

1. Injection Tolerance

A nominally ballistic translunar trajectory used for fulfilling a preplanned lunar mission is determined by the injection conditions: at a given time during the lunar month and during the launch tolerance at a given day there will be a resultant translunar trajectory plane inclined at an angle i_{VTL} to the MOP (see sketch below).

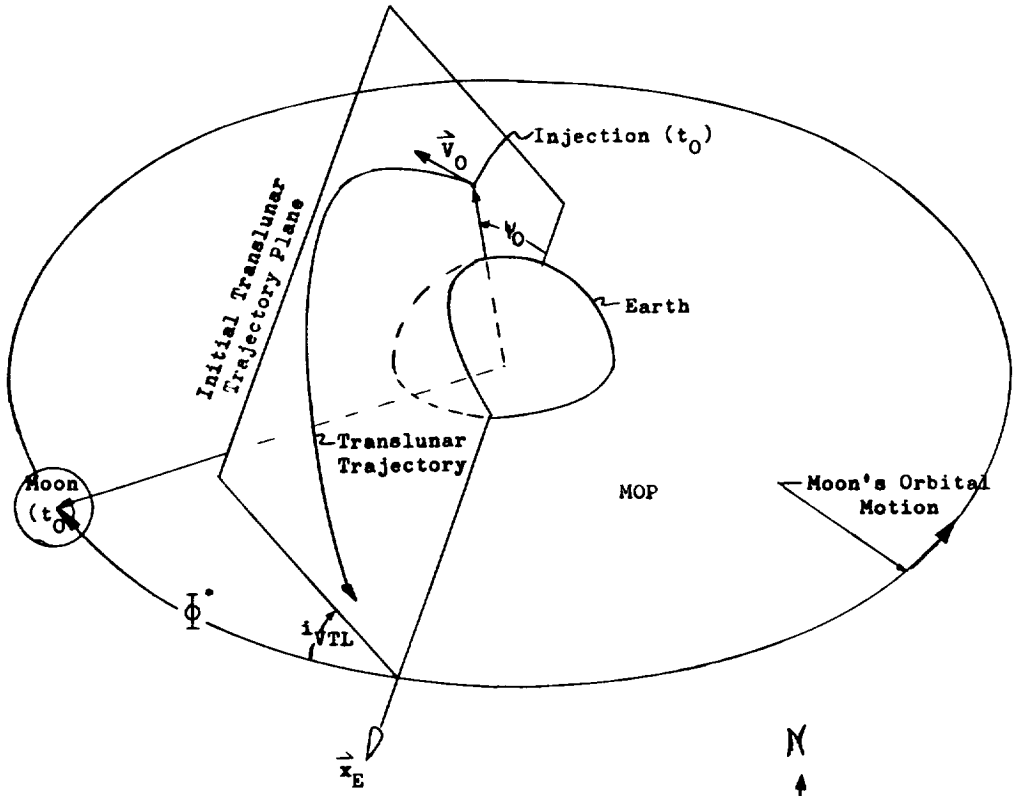

For this i_{VTL}, there corresponds a particular injection velocity vector $\vec{V}_0$, injection position ψ_0, and moon lead angle Φ^*, to satisfy certain mission constraints such as miss distance at the moon, flight time to the moon, resultant orbital orientation about the moon, etc.

If the injection is not performed at time t_0, then the spacecraft will continue in its parking orbit until the next opportune time for injection arises. This time may occur after approximately one or several revolutions in the parking orbit provided the vehicle has a certain maneuvering capability. If the delay is such that the maneuvering capability becomes insufficient to cope with the off-design conditions, then a return to earth must be made, or the spacecraft continues in its parking orbit until its maneuvering capability allows an injection into the desired translunar trajectory. These cases will be discussed below.

Consider a delayed injection, where the spacecraft continues its flight in the parking orbit. Assume that the inclination of the MOP relative to the equatorial plane i_{em} remains constant and that its nodal regression rate due to earth oblateness is negligible. The inclination of the parking orbit, i_{VE}, is also constant, but its nodal regression rate cannot be ignored. The following sketch shows the physical situation and the nomenclature on the celestial sphere.

After the injection point has been missed, the moon continues in its orbit as indicated. The parking orbit regresses in a westerly direction for direct parking orbits and easterly for retrograde orbits; however, the launch restrictions

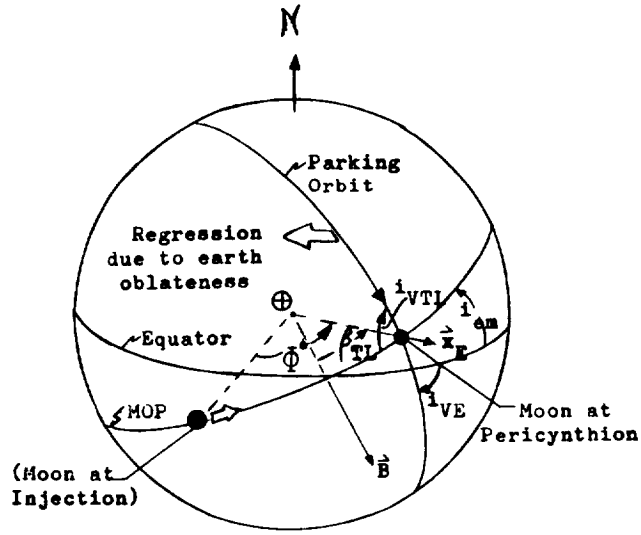

at Cape Canaveral permit only easterly launches. The angle β_{TL} is measured from the ascending node of the MOP to the intersection of the parking orbit or translunar plane with the MOP ($\vec{x}_E$ axis) and is a function of i_{VE} and i_{em}. As can be seen the angle β_{TL} also varies with time as plotted under the title "Parking Orbit Regression Time Traces" in Figs. 14 to 16. The first two figures present

data for $i_{em} = 26.5°$ and $i_{em} = 28.5°$, respectively. This represents the period from early 1966 when $i_{em} = 26.5°$ through late 1968 when $i_{em} = 28.5°$ to early 1972 when i_{em} is once again 26.5°. The parking orbit altitude assumed in these figures is that of a rendezvous compatible orbit (approximately 480 km) as explained previously in Subsection A-2b. The actual altitude varies slightly with i_{VE} and the figures reflect data for $28.57° \leq i_{VE} \leq 33.7°$. Figure 16 shows the variation of β_{TL} for $h_P = 185.2$ km and $i_{em} = 26.5°$ for comparison purposes.

Once the injection is missed, it will take approximately one revolution in the parking orbit (approximately 1.5 hr for a near-earth satellite) before another attempt is made. During this time the lunar position changes by $\Delta\Phi^*$ in its orbit (see sketch below), and the parking orbit shifts an amount $\Delta\beta_{TL}$ to $\vec{x}'_E$.

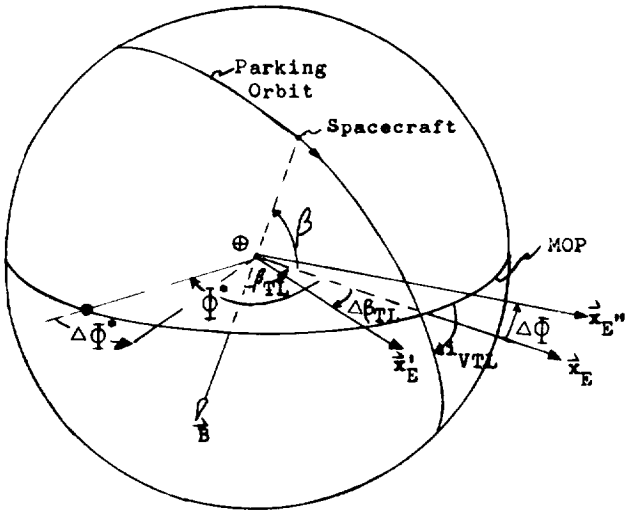

The inclination i_{VTL} also changes slightly (Fig. 17), and now the resulting lead angle after one revolution is equal to $(\Phi^* - \Delta\Phi^* - \Delta\beta_{TL})$. However, if the change in i_{VTL} is small the required lead angle remains essentially constant (see Chapter VI); therefore, if $\vec{x}_E$ is shifted by an amount $\Delta\Phi$ to $\vec{x}''_E$ prior to one revolution, another injection becomes possible.

where $\Delta\Phi \simeq \Delta\Phi^* + \Delta\beta_{TL}$

This technique can be extended for more than one revolution in the parking orbit and is only limited by the maneuvering capability ΔV to perform the shift.

This shift, or parking orbit adjustment, can be accomplished by two methods. First, the orbital maneuver or adjustment takes place at $\beta = \pm 90°$ so that the ΔV requirements are minimized. Second, the adjustment takes place at a point in the parking orbit that allows the nominal or design i_{VTL} and Φ^* to be kept constant.

Only the former adjustment technique is discussed; the steps necessary to determine the amount of correction ΔV are listed below.

(1) Determine the i_{VTL}, Φ^* required curve that satisfies the lunar mission from Chapters VI and XI.

(2) Starting from the design or nominal injection time t_0, determine β_{TL} as a function of time.

(3) From (2), also determine actual i_{VTL} as a function of time.

(4) From (3) and (1), ascertain Φ^* required as a function of time.

(5) From (2), knowing the moon's orbital position at any time, determine the actual lead angle Φ^* as a function of time.

(6) From (5) and (4), find $\Delta\Phi$ by subtraction.

(7) The orbital maneuver turn angle ΔA is given by

$$\Delta A = \sin^{-1}\left(\sin \Delta\Phi \sin i_{VTL_{(actual)}}\right). \quad (14)$$

(8) Find the required ΔV through the following geometry, where V_P is the spacecraft speed in the parking orbit:

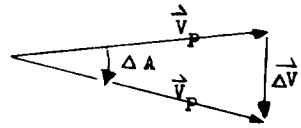

$$\Delta V = 2V_P \sin(\Delta A/2) \approx V_P \Delta A \quad \text{for small angles } \Delta A \quad (15)$$

The above steps are then repeated in an iteration procedure, since $i_{VTL_{(actual)}}$ varies slightly with ΔV. This variation, shown in Fig. 17 as a function of β_{TL}, is very insensitive to modest values of ΔV. Also shown in Fig. 17 is the capability of shifting the parking orbit by $\Delta\Phi$, which is strongly dependent on the approximate time of pericynthion or β_{TL}.

Below is a rough replica of a parking orbit regression time trace (see Figs. 14 to 16) to illustrate the above-described method for obtaining injection tolerances. The sketch shows one trace reflecting one value of i_{em}.

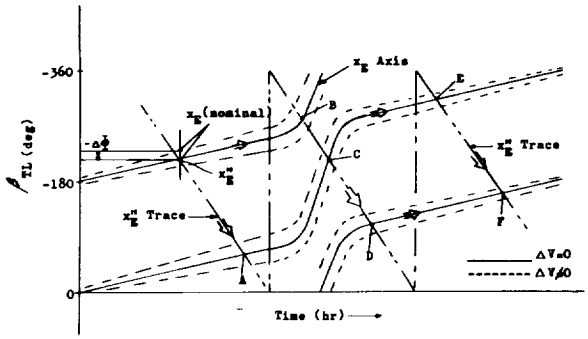

Assume that for a particular lunar mission the x_E axis is located at the designated point in the sketch for a nominal or design injection. Assume further that the nominal translunar trajectory injection is south relative to the MOP and that there is a ΔV capability for adjusting the parking orbit. As was noted in the previous discussion, this ΔV capability can be used to shift the x_E axis by an amount equal to $\pm \Delta\Phi$. Therefore, the solid curves can be altered during any parking orbit revolution to another starting point on the dashed curves. It must be remembered that the nominal x_E axis on the solid curve also satisfies the required moon lead angle relationship Φ^*; and the relationship, given by x''_E, moves at the same rate as the moon in its orbit and thereby establishes a second trace. The traces are coincident for the nominal injection but are separated until they are coincident again at points A, B, C, D, E and F. These coincident points represent other possible injection times.

Before discussing these points it is helpful to examine in more detail what is occurring at the nominal injection point as shown by the following sketch.

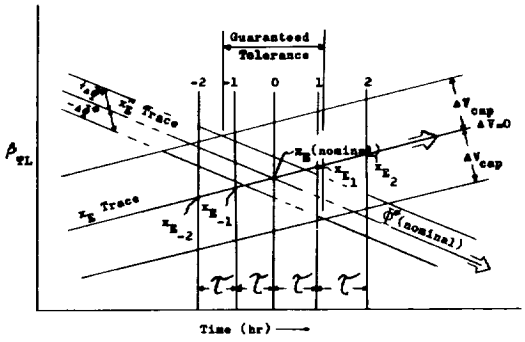

The nominal point, x_E, is shown with its initial parking orbit at the injection point ψ_0. One revolution later, or after a time interval equal to the period τ of the parking orbit, the x_E axis lies at x_{E_1}. After two revolutions, the axis lies at x_{E_2}, etc. Considering the point x_{E_1}, it is noticed that the x''_E trace is no longer coincident and a parking orbit adjustment must be made to shift x_{E_1} to the x''_E trace. As can be seen, the amount of shift is within the ΔV capability of the spacecraft even for the off-nominal x''_E traces. These off-nominal x''_E traces ($\pm \Delta\Phi^*$) are to be expected, since a change in i_{VTL} will necessitate a change in the lead angle, Φ^*, as pointed out previously. However, from Chapter VI, lead angle data indicates that $\Delta\Phi^*$ will generally be no greater than $\pm 1°$ for an entire month and for the same mission. Therefore another chance for injection is possible at x_{E_1}. If injection does not occur at x_{E_1}, another time interval τ must elapse before injection can take place at x_{E_2}. But at this point, one can see that x_{E_2} cannot under all conditions be shifted to x''_E because of insufficient maneuvering capability. Thus the injection tolerance in terms of injection frequency is 1 and in terms of time is a little longer than τ, or $\tau+$. The maneuvering capability ΔV_{cap} again becomes sufficient at point A in the previous sketch, where another injection frequency can be established. For purposes of illustration, let the above sketch also apply to point A, although the zero parking orbit revolution generally will not be coincident with the x_E and x''_E traces. Here, it is seen that an injection can be made at $x_{E_{-1}}$, $x_{E_{nominal}}$ and x_{E_1} because both traces are starting from the far left before becoming coincident, whereas in the initial nominal case, both traces started at the coincident point. The injection frequency now is 3 and the guaranteed injection tolerance is $2\tau+$. The same reasoning applies to points B, C, D, E and F.

It was assumed that the nominal case resulted in an "inject south" case. At points A, C and E the resulting injection will be toward the north relative to the MOP and again toward the south at points B, D and F. If the nominal injection was toward the north, then the injections would be cycled correspondingly for the points.

Figures 18 and 19 present actual data for two nominal cases occurring at $\beta_{TL} = -220°$ and $-65°$ The first value represents conditions that result in a minimum injection frequency, and the second value gives a maximum frequency. A parking orbit altitude of 525.8 km is assumed together with $i_{em} = 27.5°$ and $i_{VE} = 30°$.

Table 7 gives the guaranteed launch frequency and tolerance for the case where the injection is planned during the first parking orbit revolution after ascent from earth.

TABLE 7

ΔV_{cap} (m/sec)	β_{TL}=-220°		β_{TL}= -65°	
	Frequency	Tolerance (hr)	Frequency	Tolerance (hr)
76.2	0	0	2	3.5
152.4	0	0	4	6
304.8	1	2.7	8	13

Table 8 gives launch frequency and tolerance for an injection planned many orbital revolutions in advance, such as a logistics mission or injection under circumstances similar to point A on the sketch on page V-17, is mentioned above.

TABLE 8

ΔV_{cap} (m/sec)	β_{TL} = -220°		β_{TL} = -65°	
	Frequency	Tolerance (hr)	Frequency	Tolerance (hr)
76.2	0	0	5	7
152.4	1	1.5	10	15.6
304.8	4	5.8	20	31.5

As can be seen ΔV_{cap} = 304.8 m/sec will provide a launch frequency of at least 1 for the most unfavorable situation.

If an injection must be delayed until the next opportune time or a few succeeding opportune times (points A, B, C, D, E, F on the sketch on page V-17), necessary fuel and life support requirements must reflect this possible waiting time.

As a matter of interest, in Figs. 14 and 15, the minimum and maximum waiting times between possible translunar injections are noted. In Fig. 14, for example, the minimum waiting time between opportune injection times is 10 hr for i_{VE} = 28.57° and 12.4 hr for i_{VE} = 33.7°. The maximum waiting time is 253 hr for an i_{VE} = 28.57° and 250 hr for i_{VE} = 33.7°.

2. Propulsion System Requirements and Limitations During Injection

In the introductory paragraphs of the present chapter three advantages of earth departure by parking orbits were mentioned. The first, feasibility of final onboard and ground checkouts, should properly be discussed by the systems designer of a particular vehicle, so this point will not be elaborated in this Handbook. The increase in launch and injection capability has been discussed in detail in Sections A and B and Subsection C-1 of the present chapter. It remains to show why a parking orbit prior to injection leads to a single and most efficient injection trajectory profile. Additional use of the variable translunar trajectory technique (Section B), as opposed to the direct ascent, ensures a single and most efficient ascent trajectory.

The first sketch below illustrates on the celestial sphere the possible launch periods, points A to C, A' to C' on the launch parallel of latitude, for arrival at the moon when the moon is at its ascending node (see also Subsection C-1 for a more detailed discussion), while the second sketch illustrates the translunar trajectory injection parameters in the trajectory plane for the same conditions.

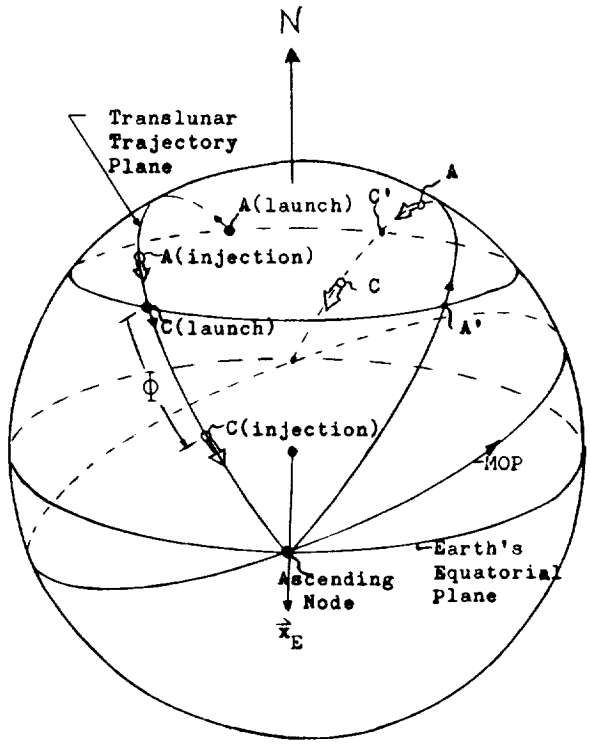

If a direct injection is performed (no parking orbit), the ascent range Φ from launch to injection is essentially constant or small for a given launch vehicle and it can only be launched during the period when the launch site is between points A, C, A', or C'. When Cape Canaveral is near position A, ψ_0 is typically 67°, with an ascent range angle Φ = 15°, and an injection flight path angle $\gamma_0 \simeq 30°$. Similarly, when Cape Canaveral is near position C, ψ_0 = 143°, Φ = 15°, $\gamma_0 \simeq 70°$. If Cape Canaveral is located near point A' or point C', the required γ_0 is negative and the spacecraft would lose altitude and atmospheric drag would cause a reentry. Another, completely impracticable, alternative would be to reverse the direction of vehicle motion. In fact, with a launch site in the northern hemisphere it becomes very difficult to perform direct departure lunar missions at all. For instance, with direct launches during the period when the moon is near its maximum northerly declination, zero launch frequency for many days of the lunar month can be expected.

In order to demonstrate the sensitivity of the flight path angle to energy expenditure, two representative plots of injection energy requirements to parabolic speed from a circular parking orbit are presented in Figs. 20 and 21. The characteristic

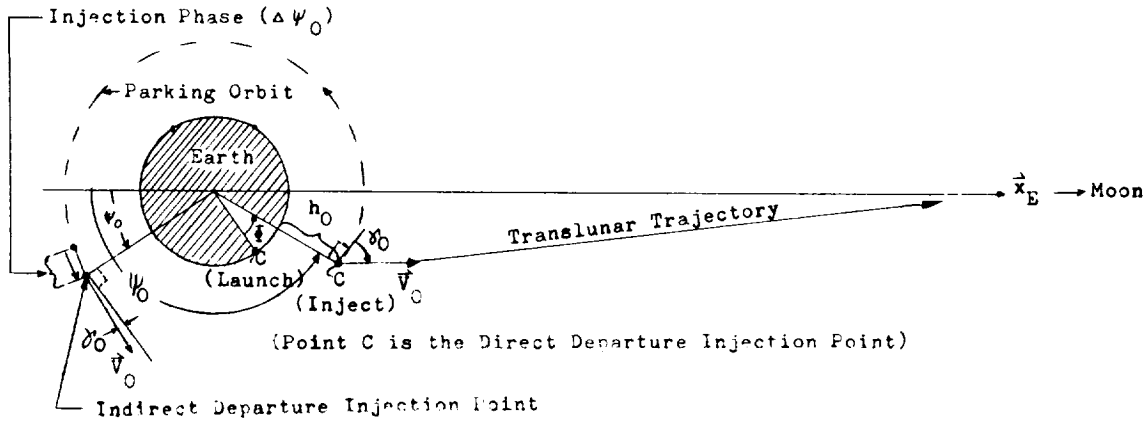

velocity of the maneuver is presented as a function of h_0 (injection altitude) and γ_0 (injection flight path angle) for representative solid or liquid launch vehicles.

Figure 20 is for an initial thrust-to-weight ratio $T/W_0 = 0.5$ and Fig. 21 for $T/W_0 = 1.5$. A specific impulse $I_{sp} = 420$ sec is used, and the initial parking orbit altitude at which the maneuver is started is $h_P = 183$ km.

Note that the best flight path angle to minimize the energy requirements for this departure from the parking orbit is greater than 2° but less than 7° for values of T/W_0 considered. The data presented in these figures are also indicative of the trends that can be expected for direct launches. An increase of γ_0 beyond 7° drastically increases the ΔV requirements. Therefore flight path angles of 30° or 70° would require very large quantities of fuel to counteract gravity losses during ascent, an inefficiency which is entirely unnecessary if parking orbits are employed prior to injection. It is obvious that if a given set of values (V_0, h_0, γ_0, $\Delta\psi_0$) represent the most efficient injection, the ψ_0 required to fulfill a lunar mission with these injection conditions can be achieved by a parking orbit, as indicated in the previous sketch.

3. Abort During Injection

When the proper position of the spacecraft relative to the moon has been achieved in the parking orbit phase, the vehicle is accelerated to the translunar trajectory injection velocity. This maneuver is the injection phase, ($\Delta\psi_0$) and it establishes a ballistic trajectory with sufficient energy and the proper characteristics for the lunar mission. For a manned mission, it is highly desirable to provide for the safety of the crew in the event of a system malfunction, which means guaranteeing the safe return of the spacecraft to earth. Two methods can be used for a safe return during the injection phase. The first immediate return employs an abort maneuver that results in a re-entry of the spacecraft within a few minutes, while the second method, normal return, requires one revolution prior to re-entry.

a. Immediate return

The abort maneuver technique used for an immediate return calls for a maximum deflection of the spacecraft's velocity vector toward the earth as shown in the following sketch.

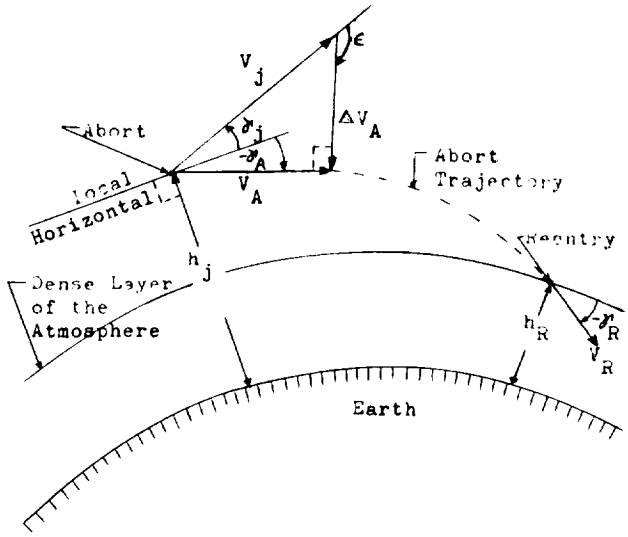

The spacecraft initially has a speed V_j and flight path angle γ_j at the time of abort. Thrust is then applied at a firing angle ϵ resulting in a characteristic velocity ΔV_A of the abort maneuver. The thrust orientation angle ϵ is such that the total deflection angle ($\gamma_j - \gamma_A$) is a maximum for a given ΔV_A and is determined by:

$$\epsilon = \cos^{-1}\left(\frac{-\Delta V}{V_j}\right) \qquad (16)$$

Although the velocity of the spacecraft after the abort maneuver, V_A, is somewhat less than V_j, the flight path angle $-\gamma_A$ is the prime criterion for establishing the abort trajectory. γ_A must be negative (V_A below the local horizontal) if re-entry is to be accomplished immediately.

However, at the re-entry point, the abort trajectory results in a re-entry velocity V_R and a re-entry flight path angle γ_R. If γ_R is not sufficiently negative for V_R at the re-entry altitude h_R, then the spacecraft will skip back out of the atmosphere. Conversely, if γ_R is too steep, the spacecraft will undergo re-entry decelerations and heating rates beyond design limitations. Thus, there is an acceptable range of V_R and γ_R at altitude h_R that permits a safe re-entry. By neglecting the atmosphere for the moment, the range of re-entry conditions (h_R, V_R, γ_R) results in minimum and maximum vacuum perigee altitudes. This difference in altitudes is referred to as the "safe re-entry corridor" and is further discussed in Chapter X. Of course, this corridor depends on the configuration of the re-entering spacecraft.

In executing the abort maneuver, a minimum ΔV_A is needed if the abort trajectory is planned so as to acquire the upper limit or "skip boundary" of the re-entry corridor, since by doing this, $(\gamma_j - \gamma_A)$ is minimum. This upper limit is more commonly referred to as the "single pass overshoot boundary."

Such a boundary is shown in the lower left corner of Fig. 22 for a re-entering spacecraft with a lift-to-drag ratio of $\frac{L}{D} = -0.5$, which is representative of a blunt-body spacecraft configuration. The propellant requirement W_f for an L/D = 0 increases the mass ratio by about $\zeta = \frac{W_f}{W_0} \simeq 0.03$, which corresponds to an additional ΔV_A of approximately 150 m/sec over the value obtained from Fig. 22, as was pointed out in Ref. 3.

The boundary is presented as a function of the speed V_j and flight angle γ_j for various altitudes during the injection phase, and it assumes $h_P \leq 198.1$ km. It should be noted that the higher h_P, the more difficult it is to perform an immediate return. Figure 22 also allows the determination of the required ΔV_A for an immediate return abort during the injection phase for various values of T/W_0 and $I_{sp} = 420$ sec.

A source of ΔV_A losses arises from the implementation of the abort maneuver itself. Usually, the sequence of events consists of separating the spacecraft from the injection stage and orienting the spacecraft to the desired thrust attitude ϵ. This takes time, and it has been shown (Ref. 3) that a delay of only 30 sec requires an additional amount of propellant equivalent to a mass ratio of $\zeta = \frac{W_f}{W_0} \simeq 0.07$ to 0.10, which corresponds to $\Delta V_A \simeq 350$ to 500 m/sec. The reason for this is that the spacecraft velocity is near the parabolic speed, resulting in a centrifugal acceleration almost twice as large as the acceleration due to gravity and hence a rapid increase in γ_j ($\frac{d\gamma_j}{dt} = 0.05°/\text{sec}$).

b. Normal return

From the previous subsection, it was found that an immediate return abort may require large amounts of propellant, especially if $T/W_0 < 4.0$ and $h_P > 200$ km. This implies the use of high-thrust rocket engines, and possibly more than 40% of the spacecraft weight must be in the form of fuel and propellant system dead weight. If design consideration or operational concepts prohibit the immediate return method, then the abort must be conducted differently.

The normal return method is pictured in the sketch below.

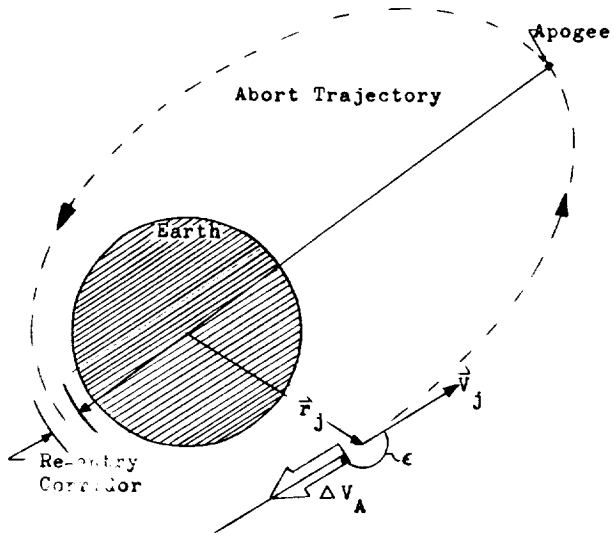

If at a certain point in the injection phase $(\vec{V}_j, \vec{r}_j)$ an abort becomes necessary, thrust is applied parallel to the velocity vector $\vec{V}_j$ but in the opposite direction (retrograde, $\epsilon = 180°$). This technique can be used since it minimizes the return time to earth and consequently provides a form of time control. After the abort burning phase, the spacecraft continues along its abort

trajectory until apogee. At this time, small midcourse corrections are made in order to ensure that the vacuum perigee of the abort trajectory lies in the re-entry corridor. There are two reasons for making the midcourse correction near or at apogee: (1) Perigee conditions can be changed most efficiently; (2) There is sufficient time for tracking and calculation of the actual abort trajectory prior to and after the midcourse correction.

Although the spacecraft may have a certain ΔV_A potential, it does not mean that the entire potential should be used for the abort maneuver. Generally only a portion of this capability will be used, as can be seen from Fig. 23. It presents the time to return to earth from abort to re-entry as a function of speed V_j at the time of abort for various ΔV_A's. Data are shown for an initial T/W_0 of approximately 1.1 and I_{sp} = 420 sec. In this figure, for a typical injection trajectory profile as given in Table 9 below, it is noticed that if there is a limited control on ΔV_A application there is a corresponding limited control on the return time. This in turn allows some control of the geographical re-entry point. In the lower speed range, time of re-entry can be controlled within 2 hr for the ΔV_A's quoted. This results in being able to vary the re-entry point by 30° in longitude. In the higher speed range, re-entry longitude control can vary from 150° to 360°. Thus, suitable and specific landing sites can be reached, thereby reducing the size of recovery forces and the number of required landing areas.

Also given in Fig. 23 are the apogee altitudes that result from an abort maneuver. These altitudes may be as high as 50,000 km, in which case two or more midcourse corrections are required to ensure safe re-entry. Depending on the inclination of the trajectory, there may be restrictions on apogee altitude because of the Van-Allen radiation belt.

In addition, the immediate return capability is shown to exist only in the very low-speed regime for the conditions presented.

TABLE 9

Typical Injection Trajectory Profile

V_j (m/sec)	h_j (km)	γ_j (deg)	Notes
7,924.8	198.1	0	Parking orbit conditions
8,534.4	199.6	0.7	↑
9,144	203.6	1.8	↑
9,753.6	210.3	3	Injection phase
10,363.2	220.1	5	↓
10,972.8	233.2	7.6	Injection conditions

This concludes the discussion of abort during the injection phase. Abort and re-entry, prior to the parking orbit phase and while in the parking orbit, are considered earth-orbital type aborts. Re-entry and recovery data for earth satellites are presented in Chapters VIII and IX of Ref. 1, and abort data for the parking and intermediate orbit phases can be obtained from this reference.

D. REFERENCES

1. "Orbital Flight Handbook," Martin Marietta Corporation, Space Systems Division, Baltimore, Md., ER 12684, 1963.

2. Pragluski, W., "Launch Time Tolerance for Manned Lunar Missions," given at the "Proceedings of the Aerospace Support and Operations Meeting" of the Institute of the Aerospace Sciences in Orlando, Fla., 4 January 1961.

3. Slye, R., "Velocity Requirements for Abort from the Boost Trajectory of a Manned Lunar Mission," NASA TN D-1038, 1961.

ILLUSTRATIONS

LIST OF ILLUSTRATIONS

Figure	Title	Page
1	Minimum Ascent Turn Angle	V-27
2	Earth Launch Time Tolerance from Range Extension	V-28
3	Required Velocity Capability Versus Ascent Range	V-29
4	ΔV Versus Launch Time	V-30
5	Rendezvous Turn Angle Versus Launch Time	V-31
6	ΔV Required for Launch Tolerance	V-32
7	ΔV Required for Launch Tolerance	V-33
8	ΔV Required for Launch Tolerance	V-34
9	ΔV Required for Launch Tolerance	V-35
10	Waiting Time in Intermediate Orbit for Indirect Launches	V-36
11	Waiting Time in Intermediate Orbit for Indirect Launches	V-37
12	Waiting Time in Intermediate Orbit for Indirect Launches	V-38
13	Launch Tolerance	V-39
14	Parking Orbit Regression Time Trace	V-40
15	Parking Orbit Regression Time Trace	V-41
16	Parking Orbit Regression Time Trace	V-42
17	Moon Lead Angle and i_{VTL} Change Curves	V-43
18	Injection Tolerance and Frequency for "Missed" Scheduled Injections (Case 1, $\beta_{TL} = -220°$)	V-44

LIST OF ILLUSTRATIONS (continued)

Figure	Title	Page
19	Injection Tolerance and Frequency for "Missed" Scheduled Injections (Case 2, $\beta_{TL} = -65°$)	V-44
20	Injection Energy Requirements to Parabolic Speed from a Circular Parking Orbit	V-45
21	Injection Energy Requirements to Parabolic Speed from a Circular Parking Orbit	V-46
22	Abort Velocity Impulse Required to Arrive at a Single-Pass Overshoot Boundary	V-47
23	Time to Return Versus Initial Abort Speed for a Typical Injection Phase	V-48

Fig. 1. Minimum Ascent Turn Angle

———— Polar Side
– – – – Equator Side
Ascent Range $\Phi_a = 90^\circ$
Launch Site -- Cape Canaveral

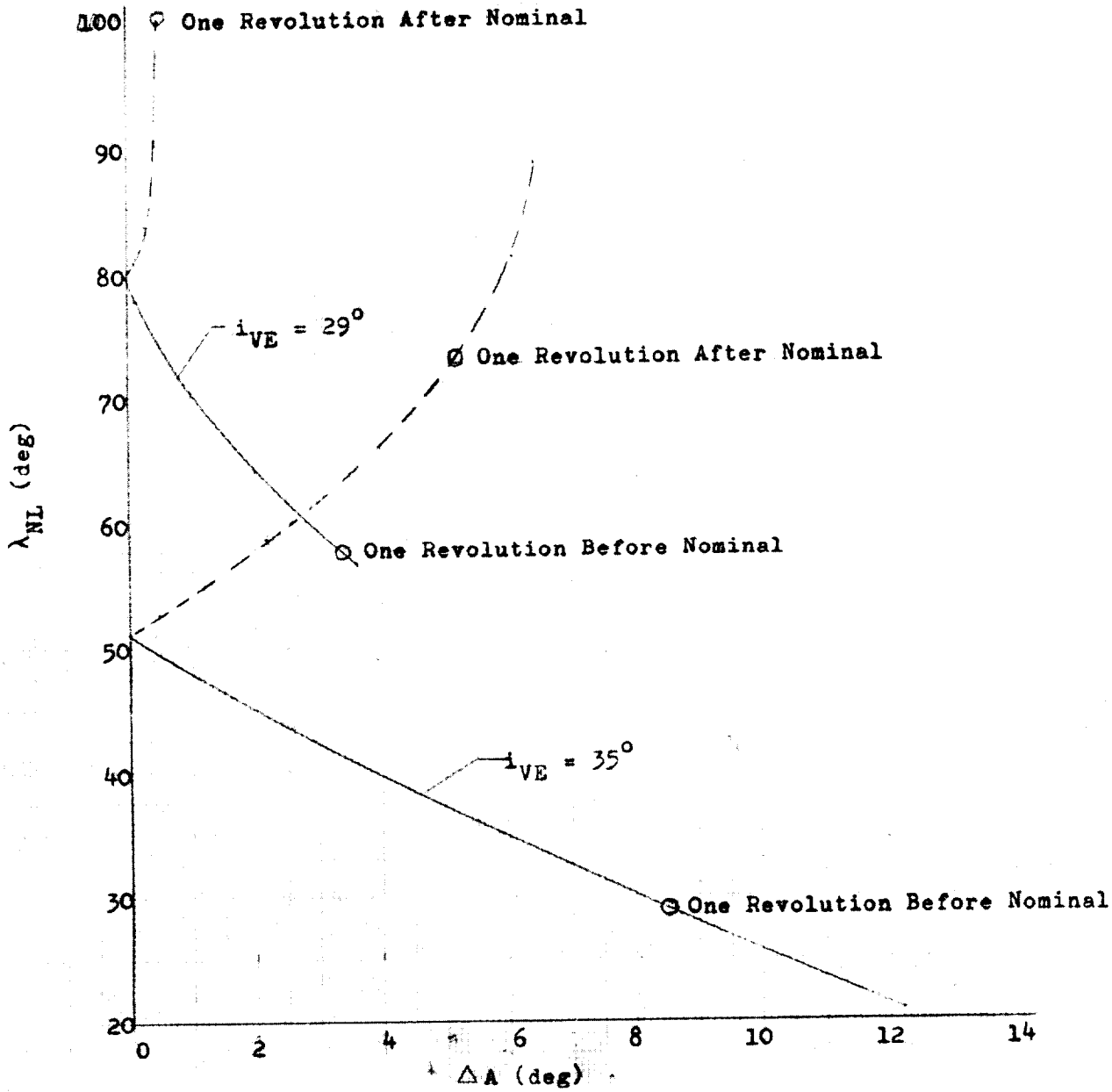

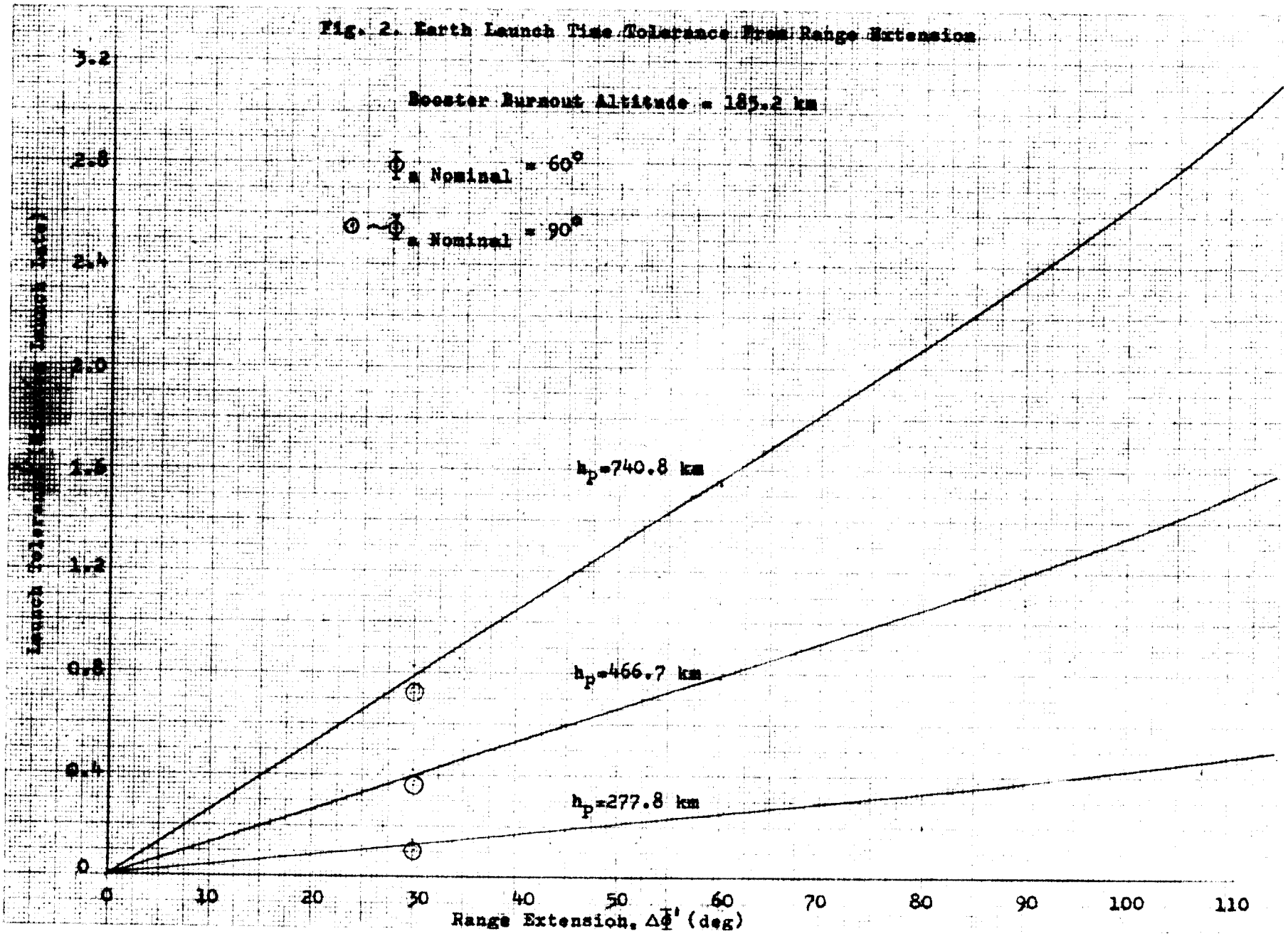
Fig. 2. Earth Launch Time Tolerance From Range Extension
Booster Burnout Altitude = 185.2 km
$\Phi_{a\ Nominal} = 60°$
$\Phi_{a\ Nominal} = 90°$
h_p=740.8 km
h_p=466.7 km
h_p=277.8 km
Launch Tolerance, Hours
3.2
2.8
2.4
2.0
1.6
1.2
0.8
0.4
0
0
10
20
30
40
50
60
70
80
90
100
110
Range Extension, $\Delta\Phi'$ (deg)

Fig. 3. Required Velocity Capability Versus Ascent Range

h_p = 466.7 km

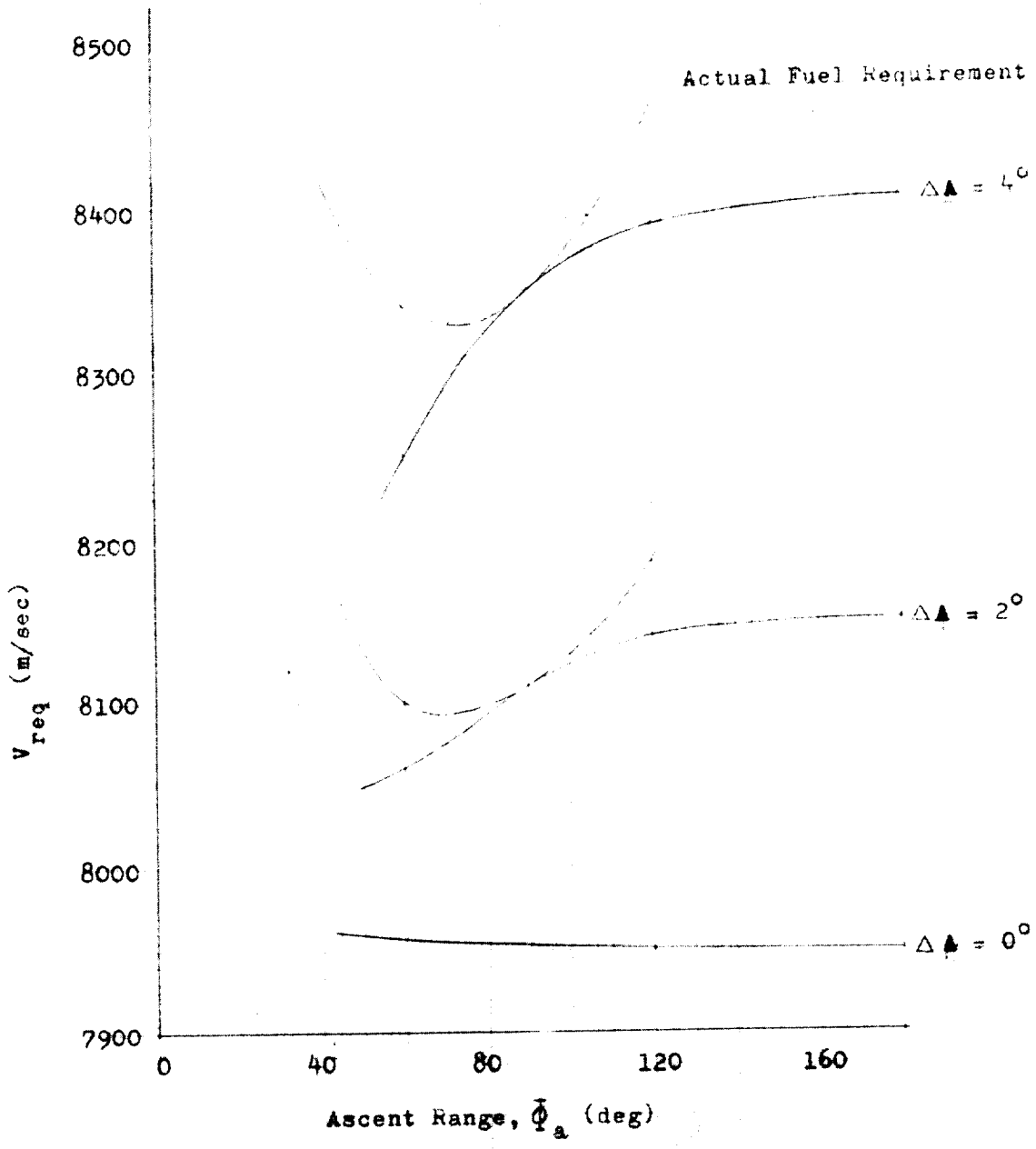

Fig. 4. ΔV Versus Launch Time

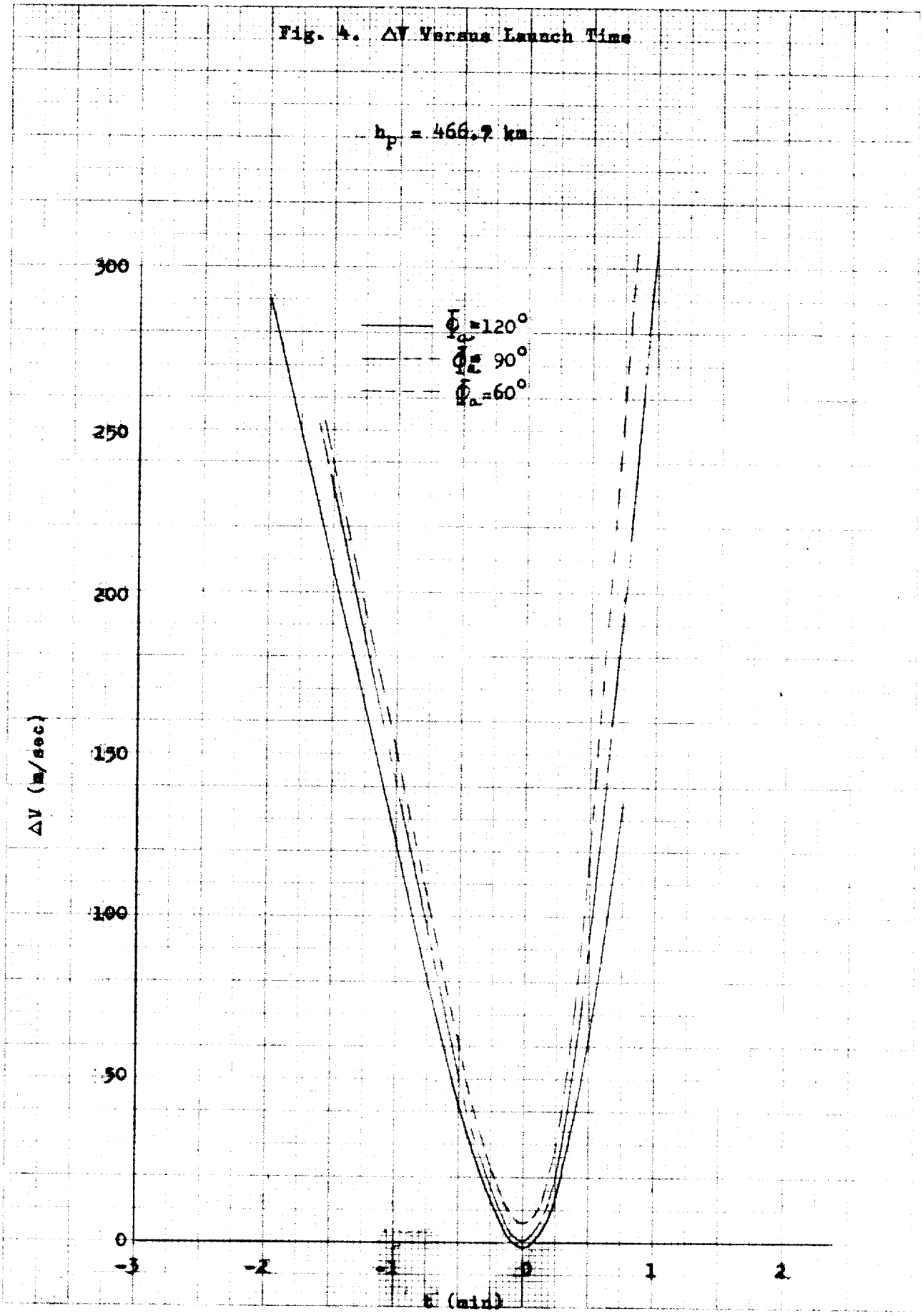

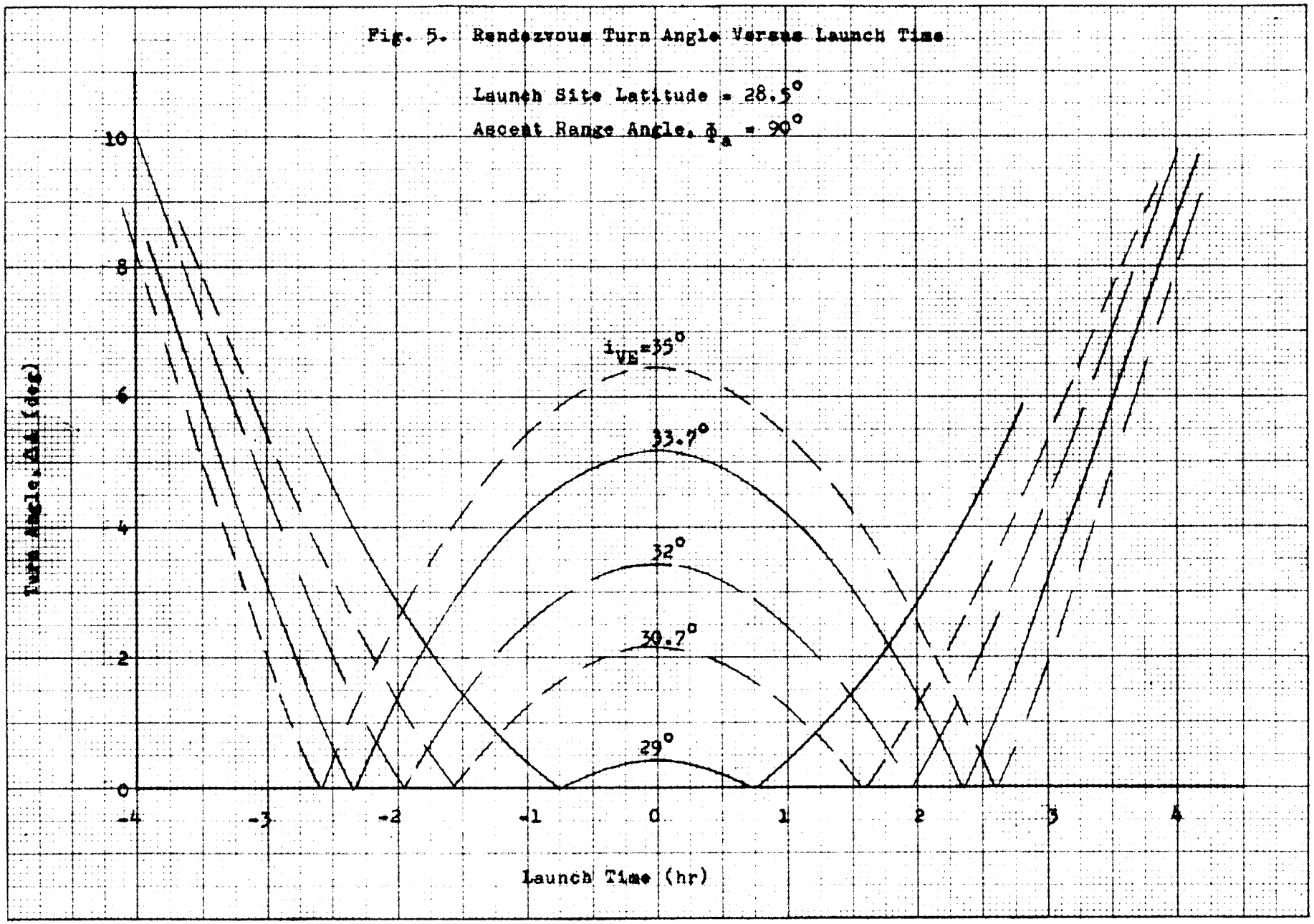

Fig. 5. Rendezvous Turn Angle Versus Launch Time

Fig. 6. ΔV Required For Launch Tolerance

h_p = 466.7 km

h_i = 185.2 km

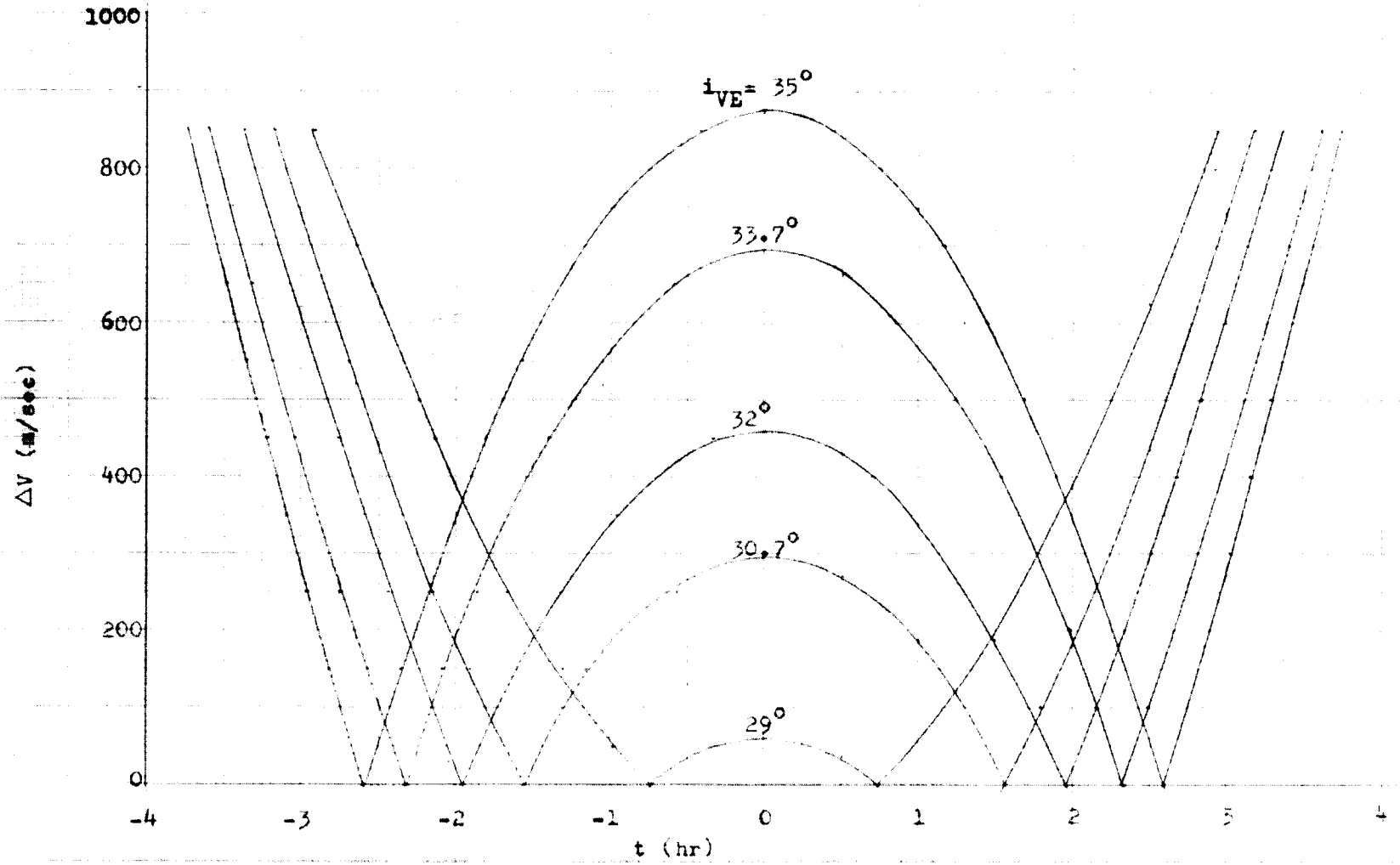

Fig. 7. ΔV Required For Launch Tolerance

h_p = 466.7 km

h_i = 370.4 km

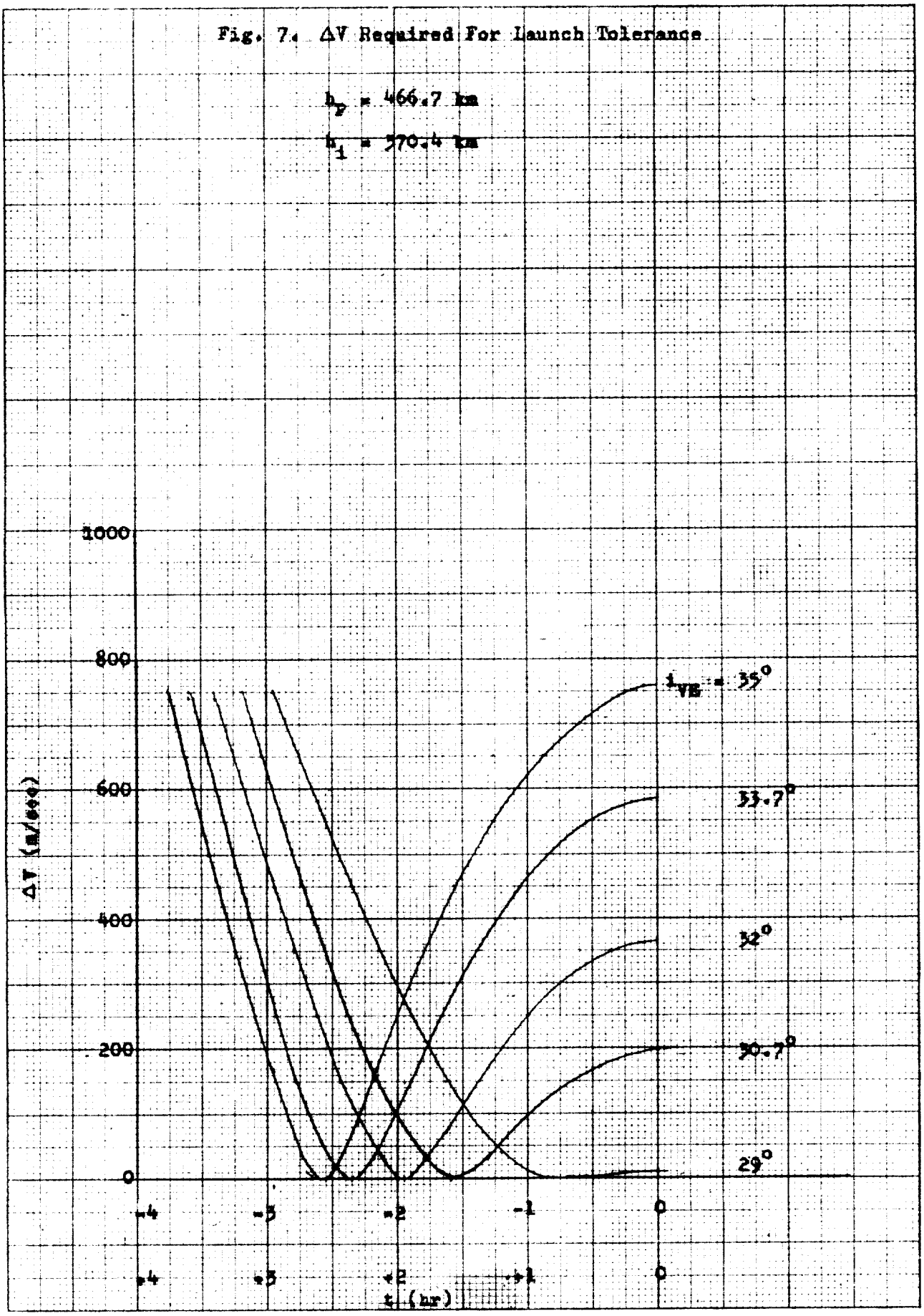

Fig. 8. ΔV Required For Launch Tolerance

h_p = 466.7 km

h_i = 555.6 km

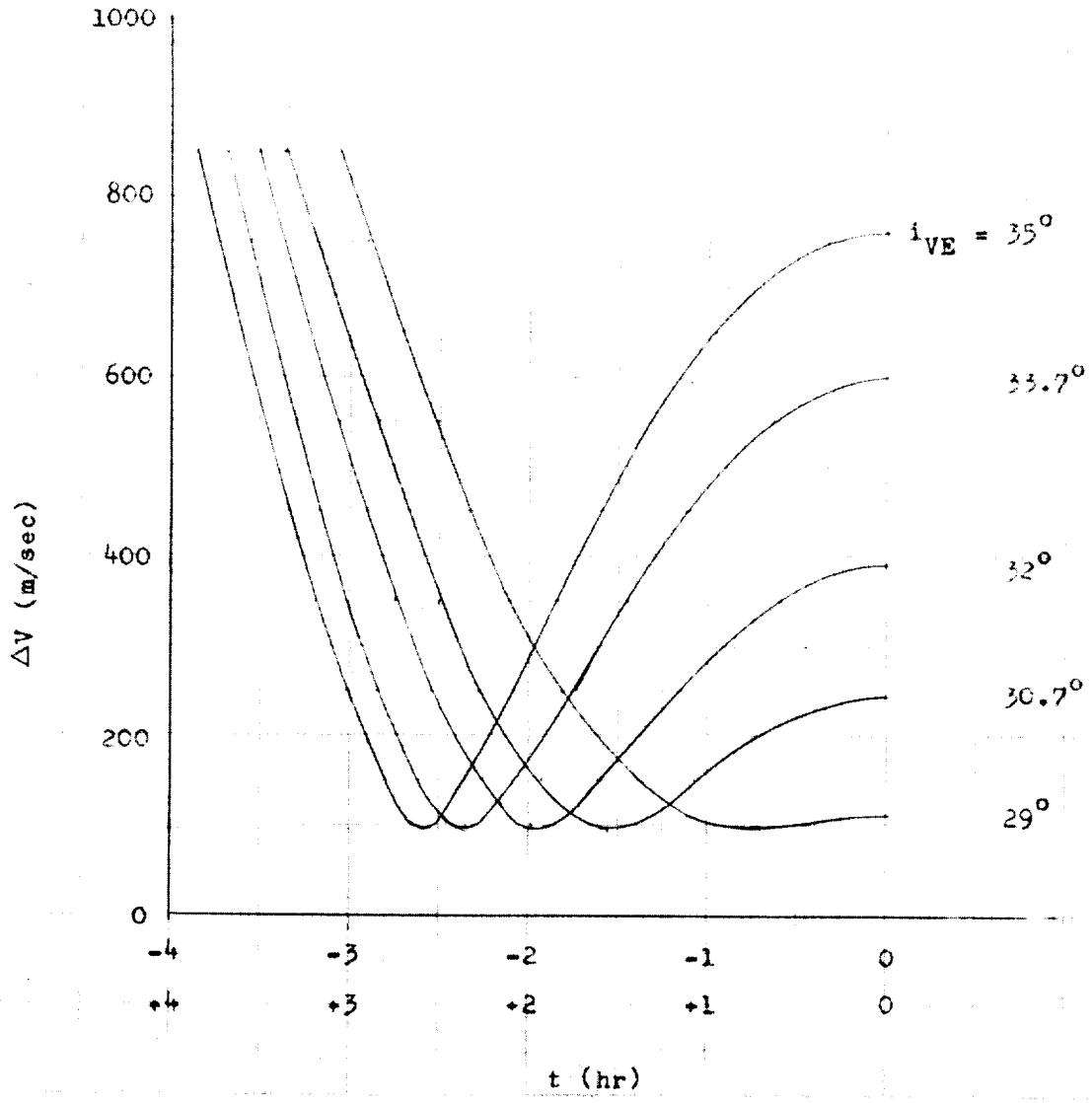

Fig. 9. ΔV Required For Launch Tolerance

h_p = 466.7 km

h_i = 740.8 km

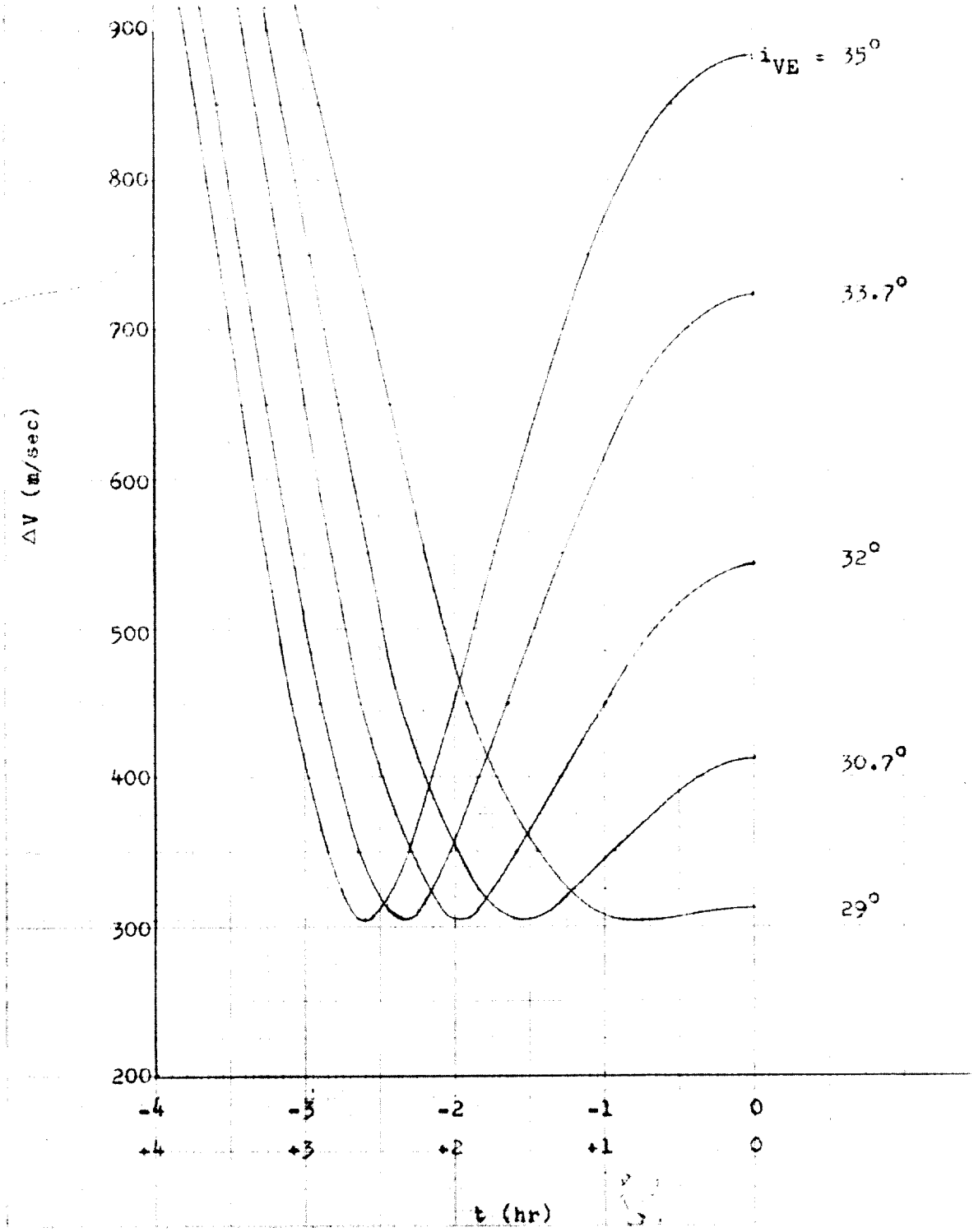

Fig. 10. Waiting Time In Intermediate Orbit For Indirect Launches

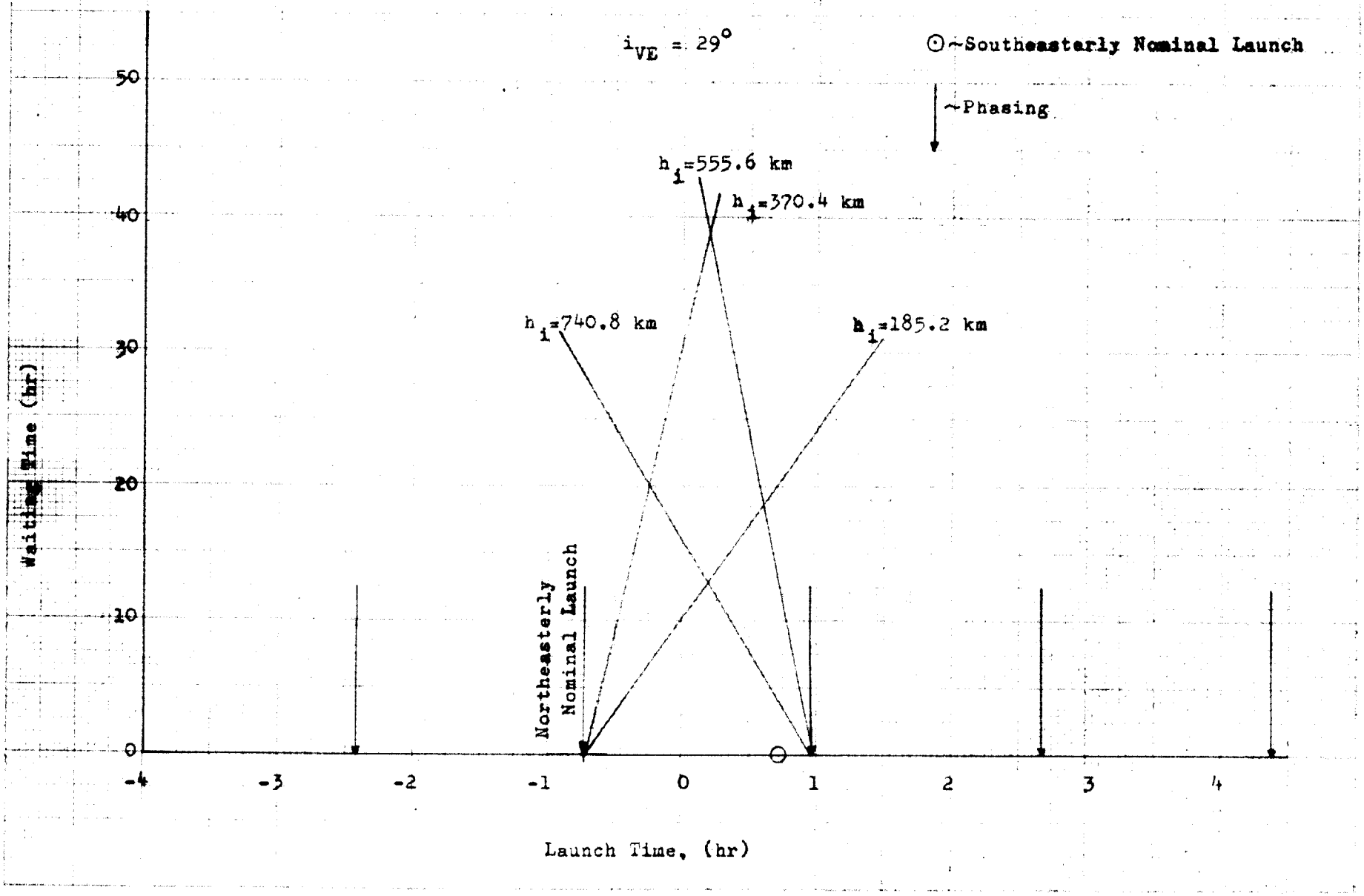

Fig. 11. Waiting Time In Intermediate Orbit For Indirect Launches

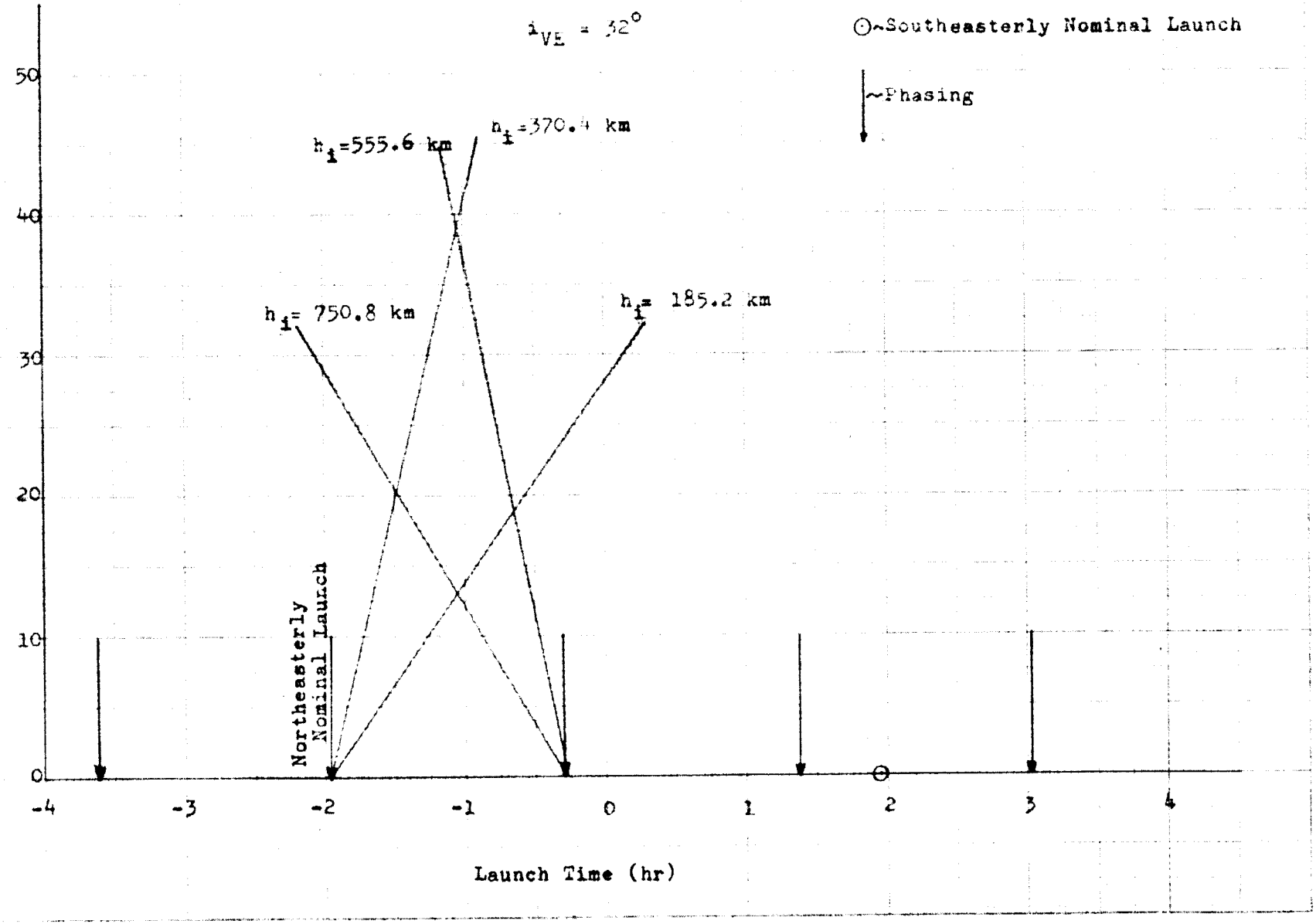

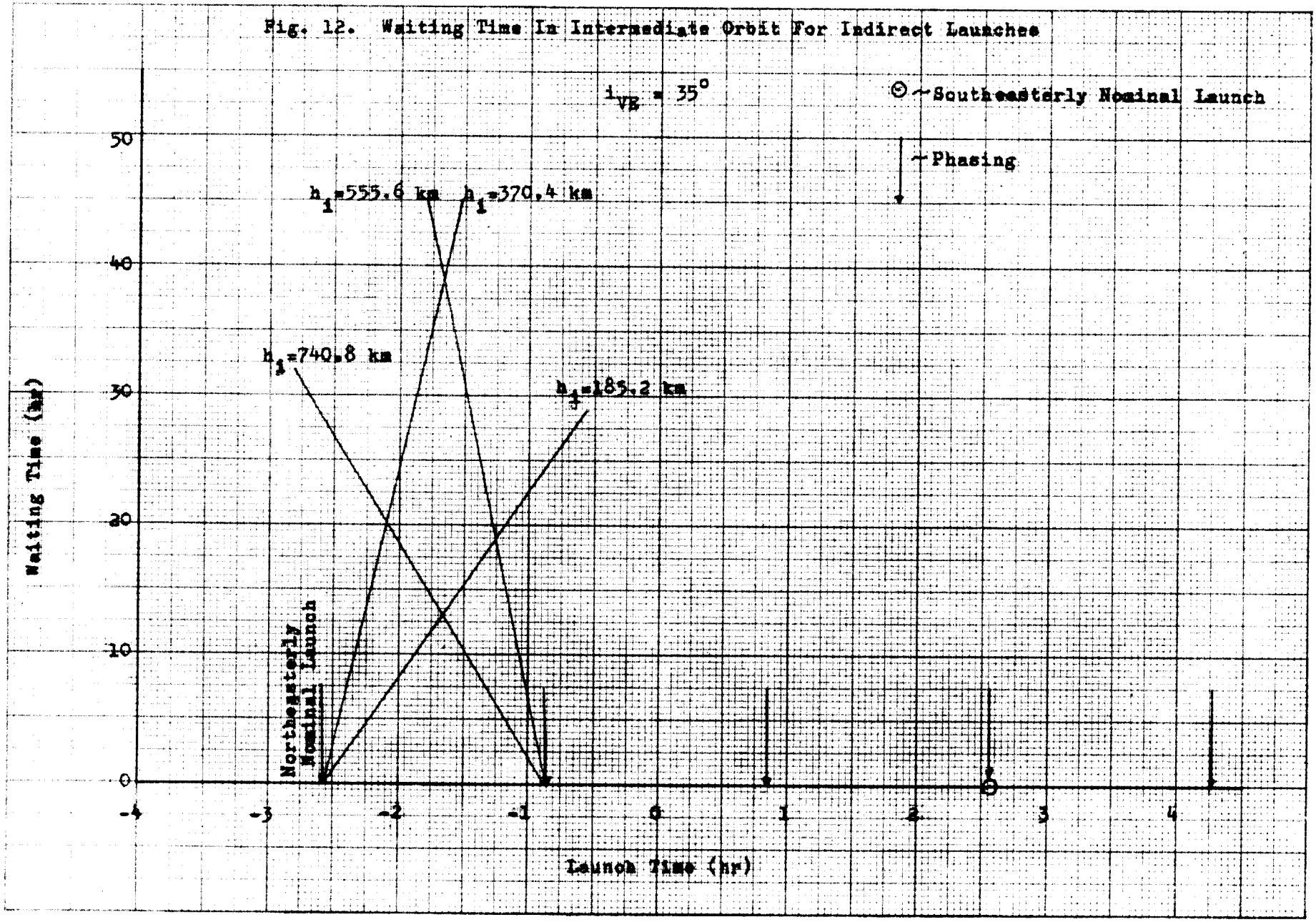
Fig. 12. Waiting Time In Intermediate Orbit For Indirect Launches
i_{VE} = 35°
⊙ ~ Southeasterly Nominal Launch
~ Phasing
h_1=555.6 km
h_1=370.4 km
h_1=740.8 km
h_1=185.2 km
Northeasterly Nominal Launch
Waiting Time (hr)
Launch Time (hr)
50
40
30
20
10
0
-4
-3
-2
-1
0
1
2
3
4

Fig. 13. Launch Tolerance

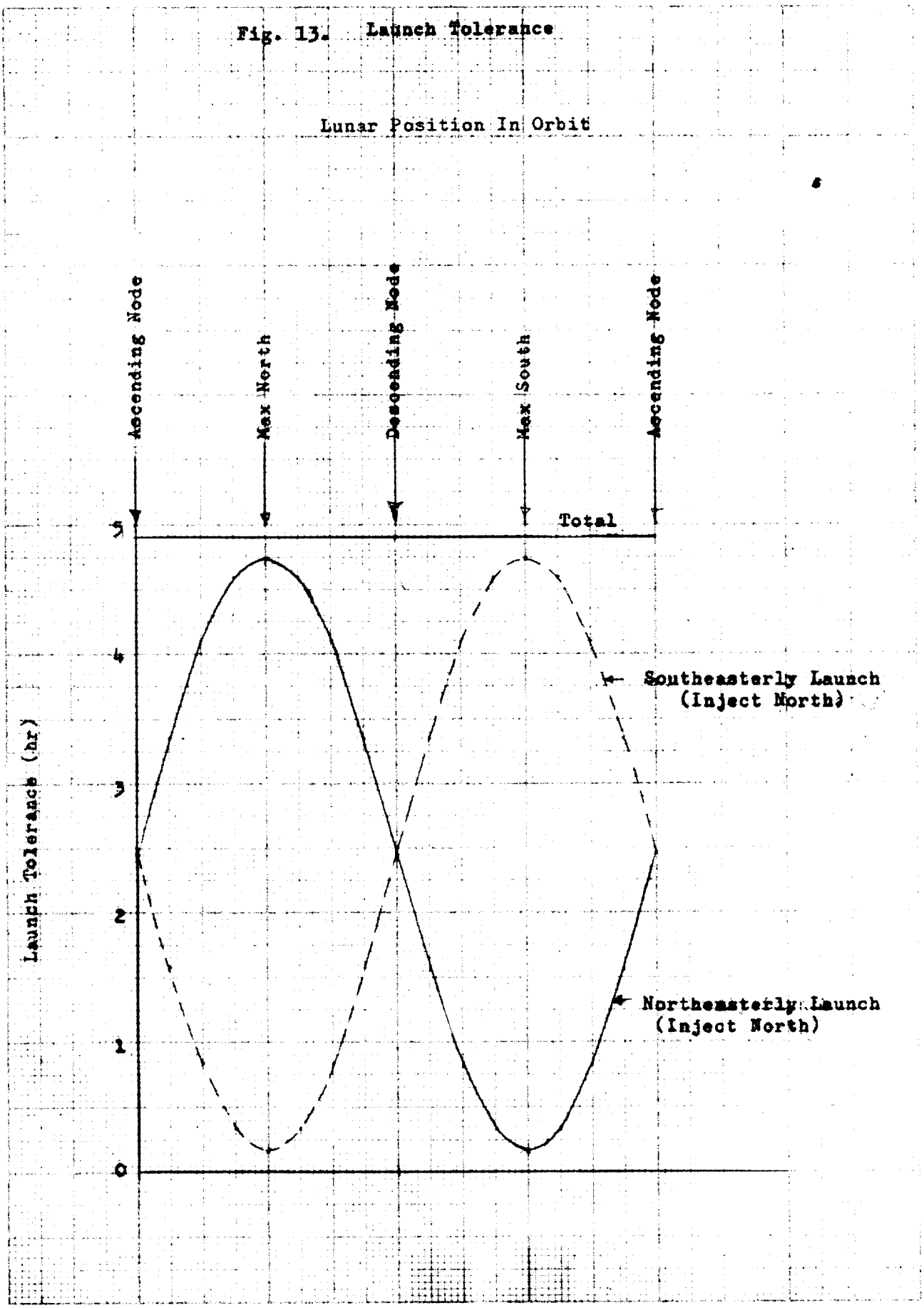

FIG. 19. PARKING ORBIT REGRESSION TIME TRACE

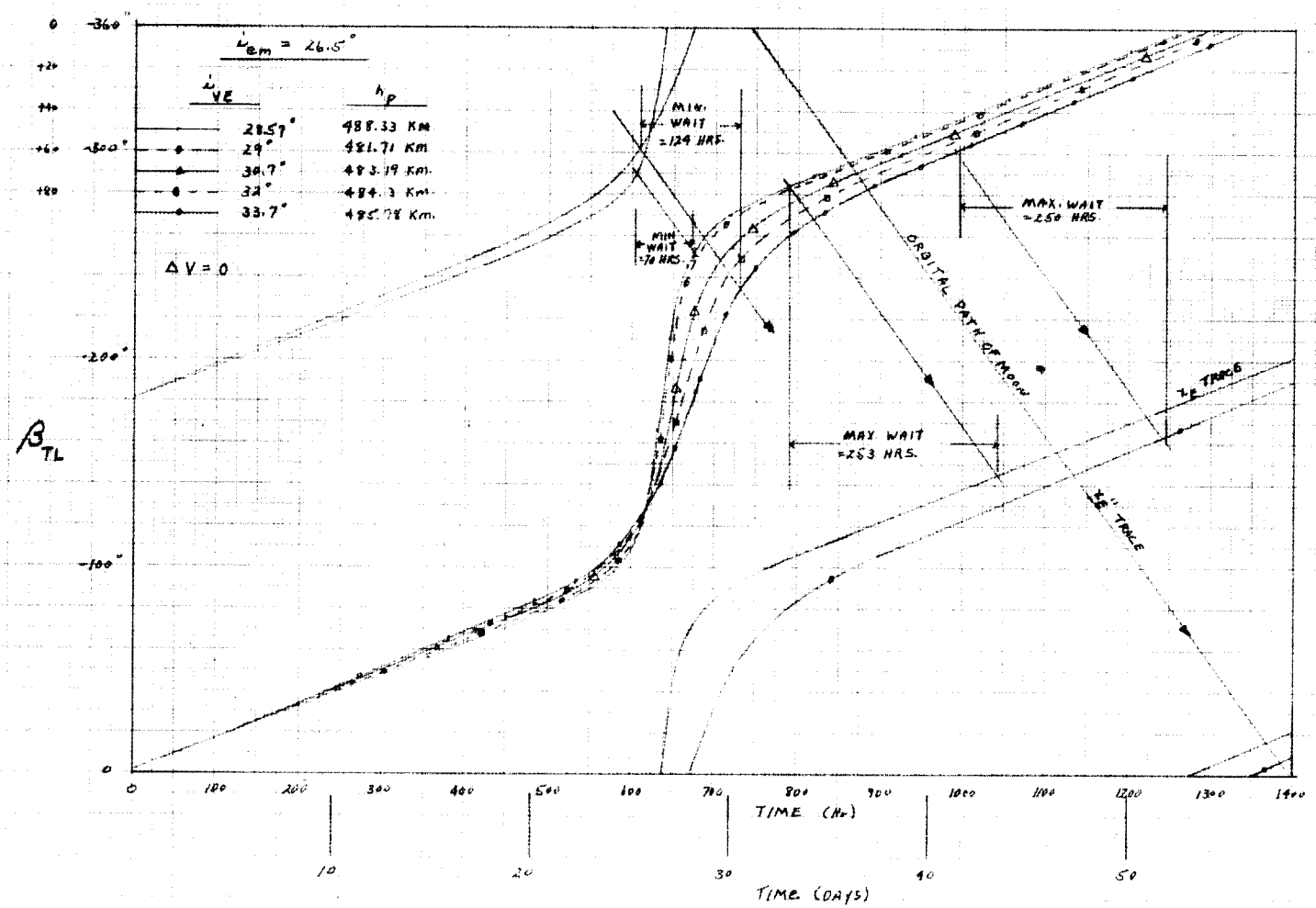

FIG. 15 PARKING ORBIT REGRESSION TIME TRACE

FIG. 1b. PARKING ORBIT REGRESSION TIME TRACE

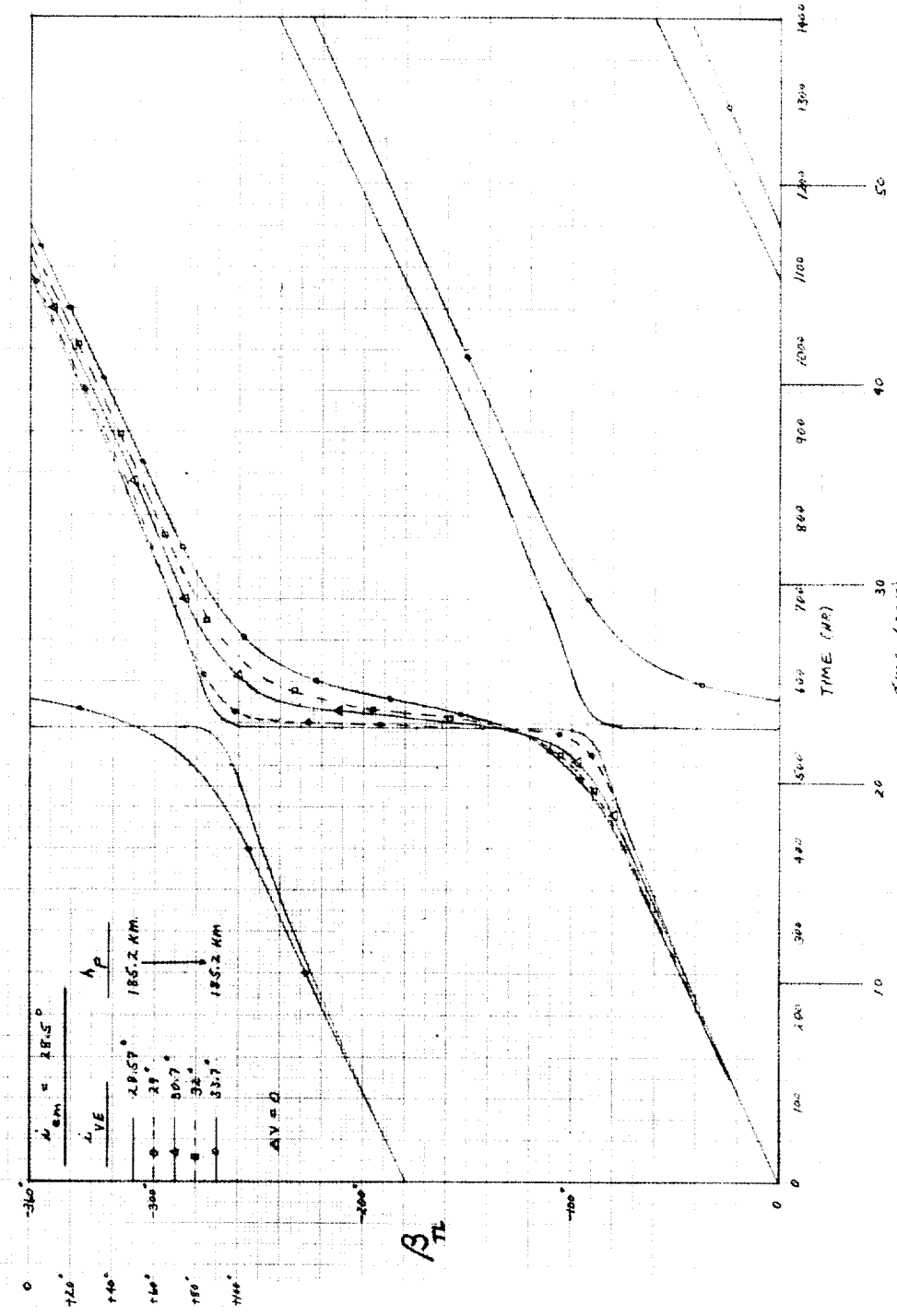

FIG. 17. MOON LEAD ANGLE AND i_{VTL} CHANGE CURVES

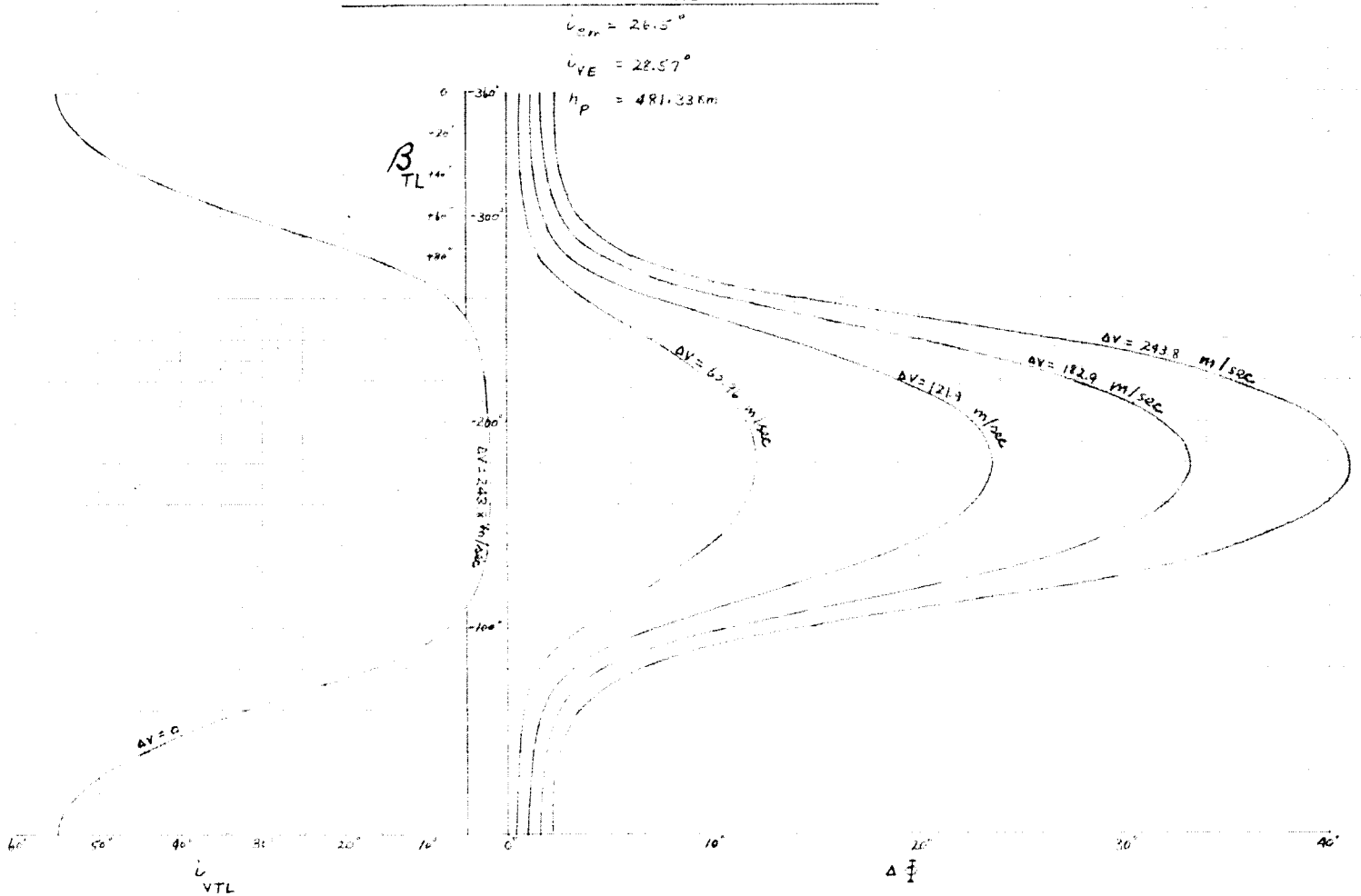

Fig. 18. Injection Tolerance And Frequency For 'Missed' Scheduled Injections (Case 1, $\beta_{TL} = -220^\circ$)

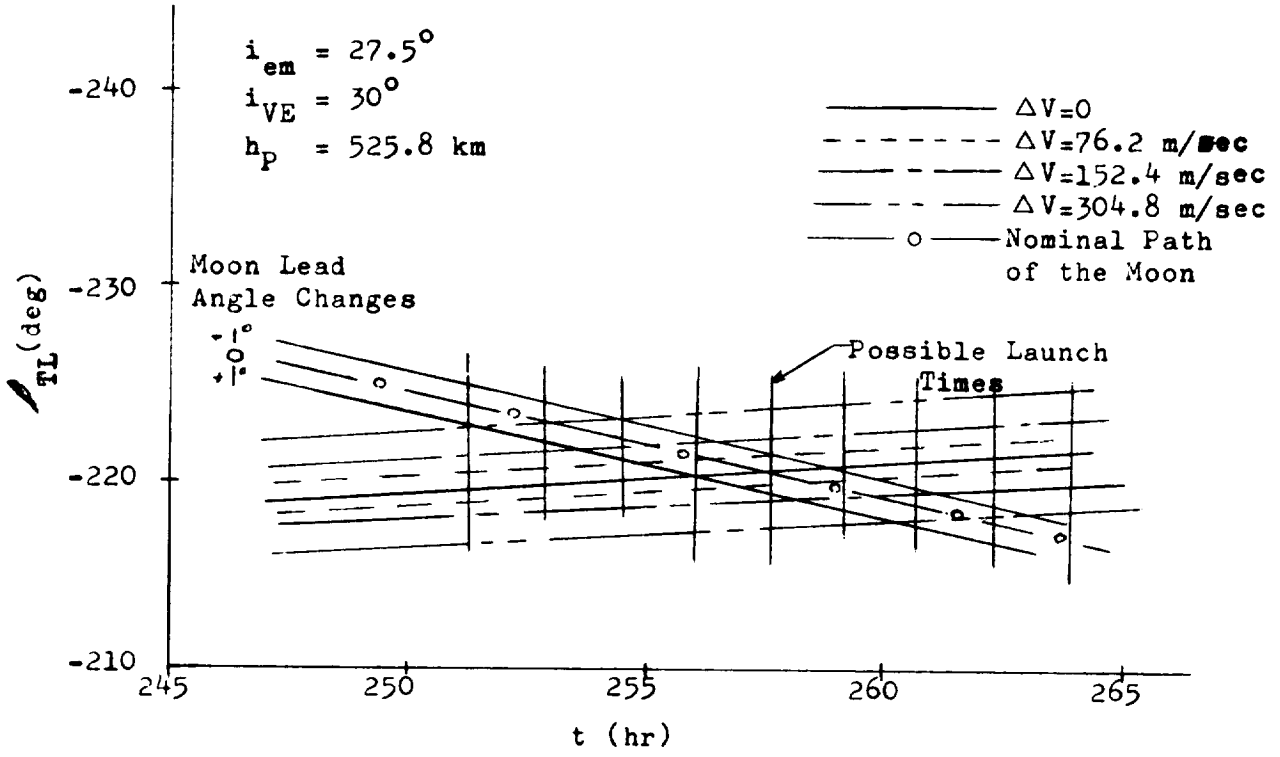

Fig. 19. Injection Tolerance And Frequency For 'Missed' Scheduled Injections (Case 2, $\beta_{TL} = -65^\circ$)

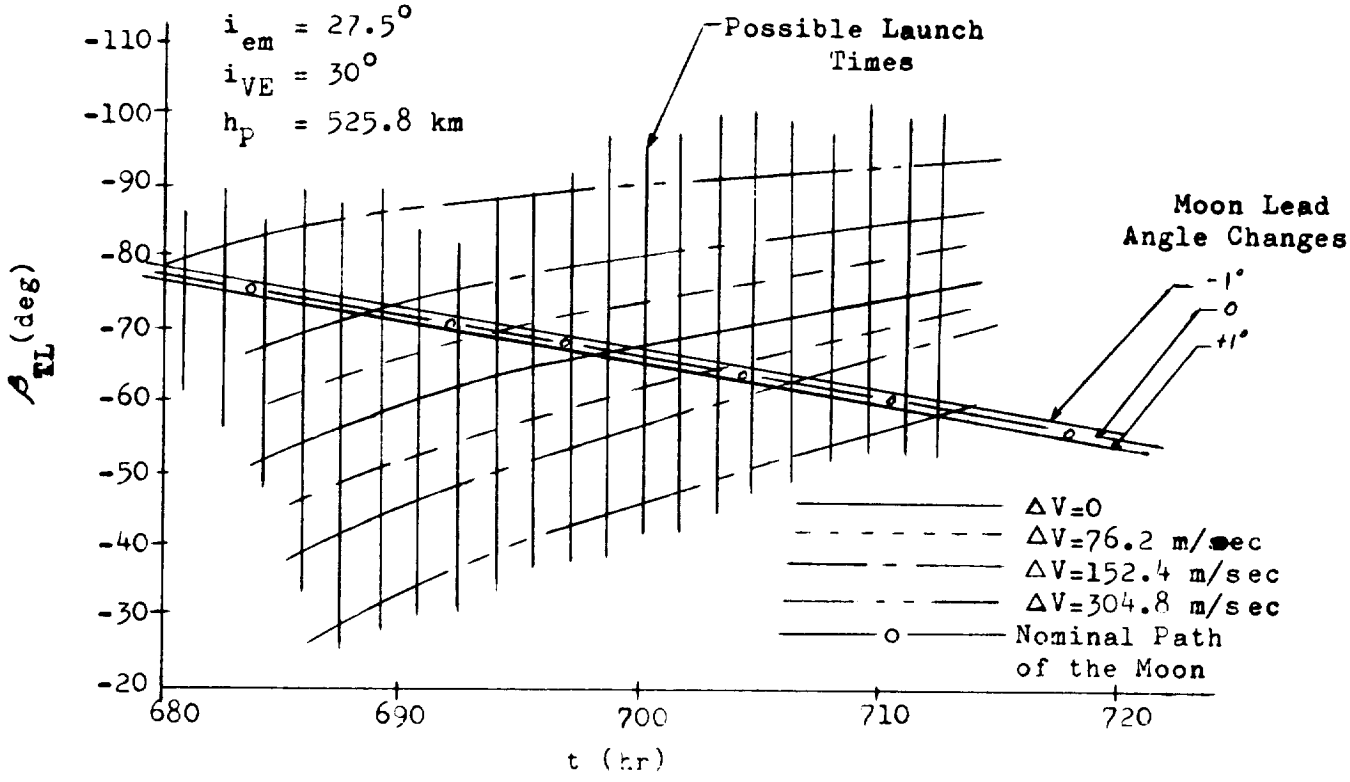

Fig. 20. Injection Energy Requirements To Parabolic Speed From A Circular Parking Orbit

$T/W_0 = 0.5$

$h_p = 183$ km

$I_{sp} = 420$ sec

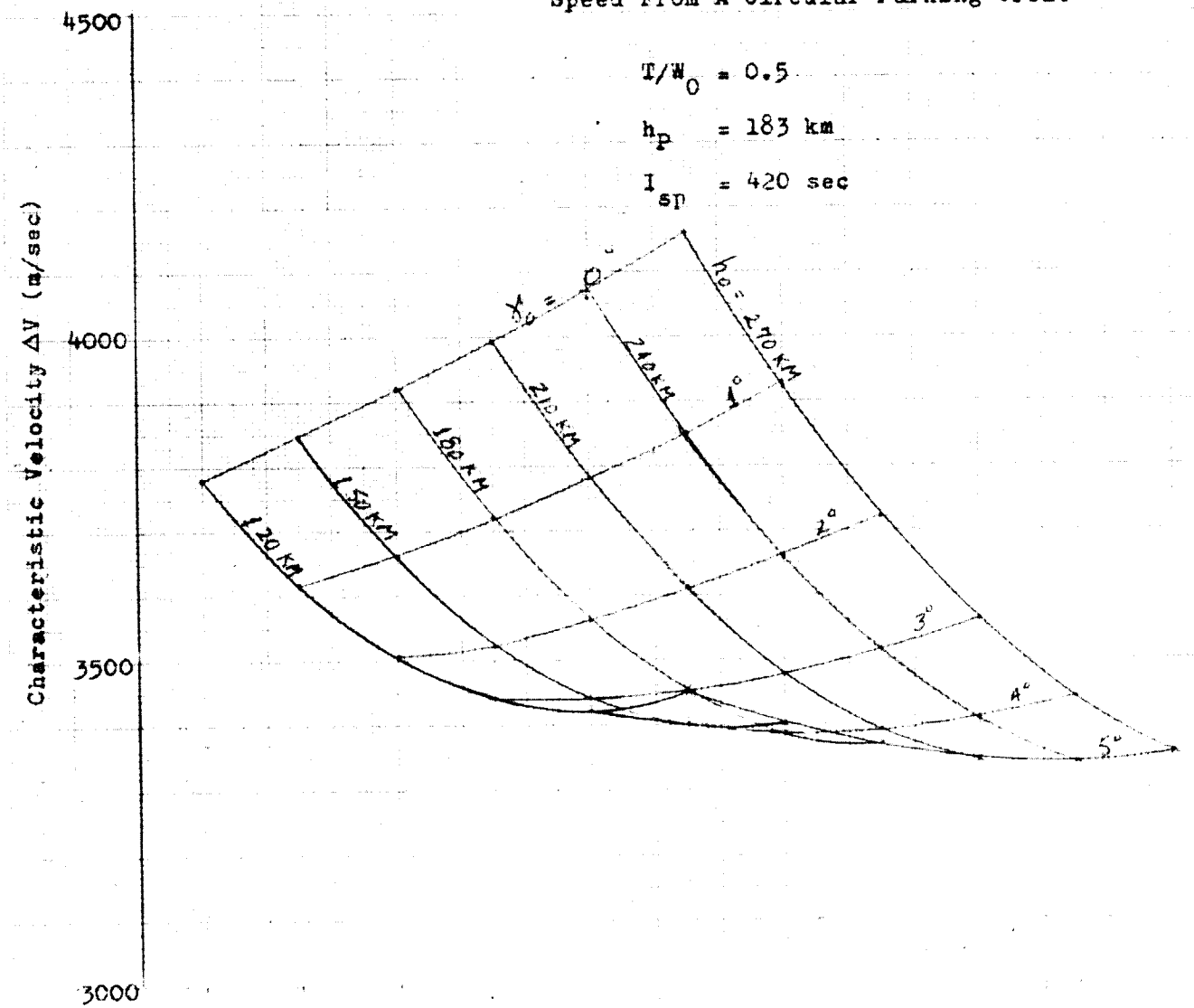

Fig. 21. Injection Energy Requirements To Parabolic Speed From A Circular Parking Orbit

$T/W_0 = 1.5$

$h_p = 183$ km

$I_{sp} = 420$ sec

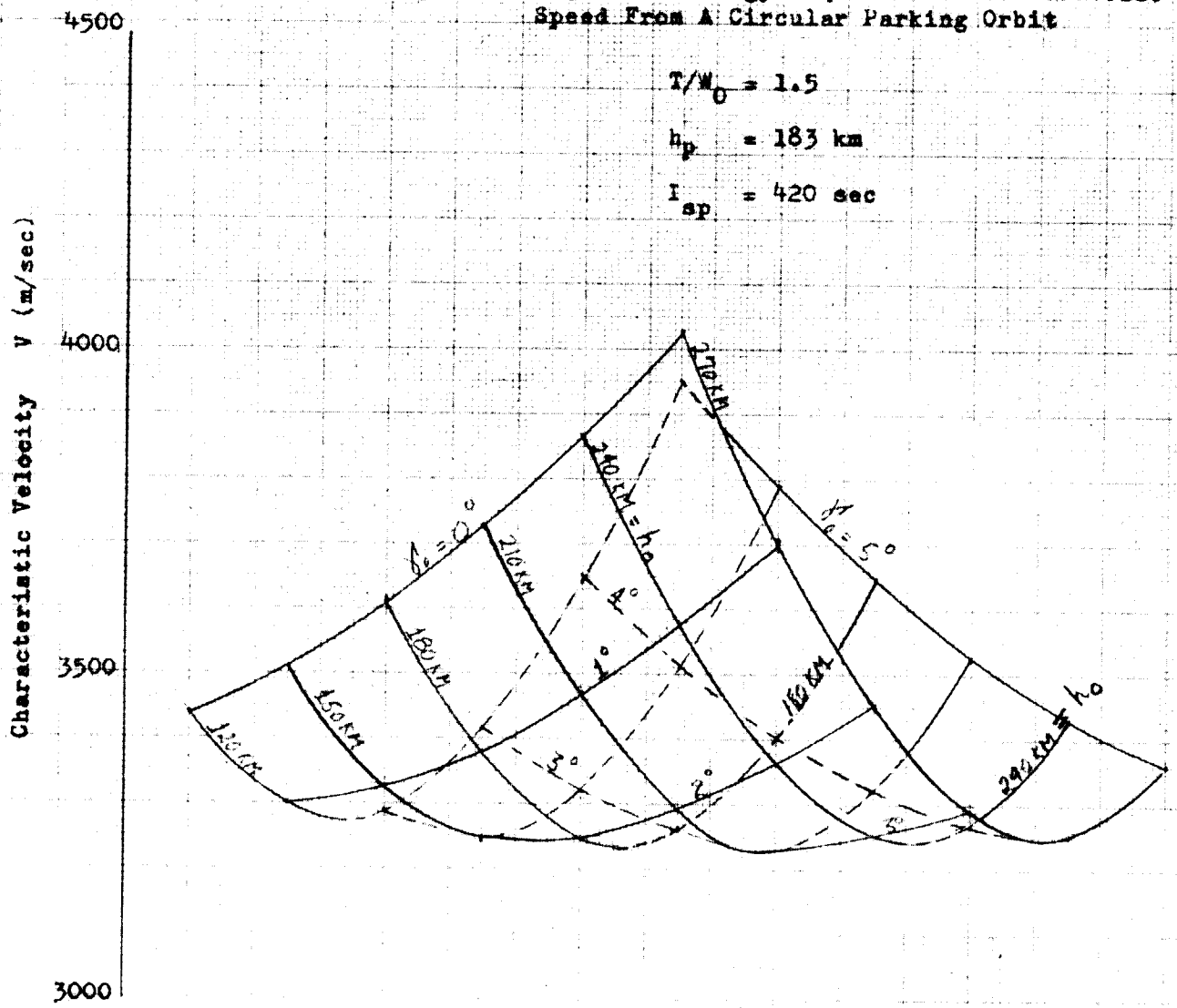

FIG. 22. ABORT VELOCITY IMPULSE REQUIRED TO ARRIVE AT A SINGLE-PASS OVERSHOOT BOUNDARY

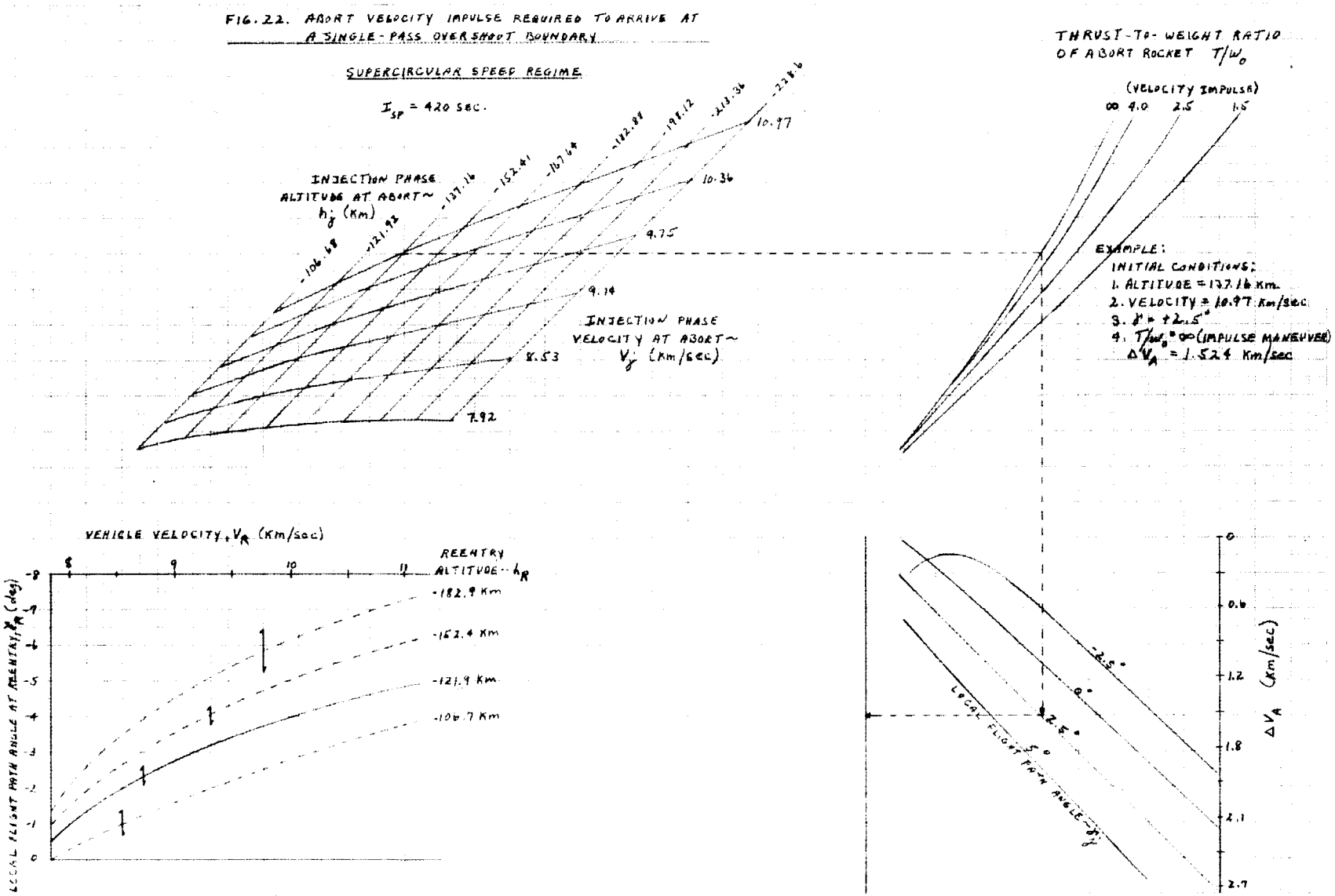

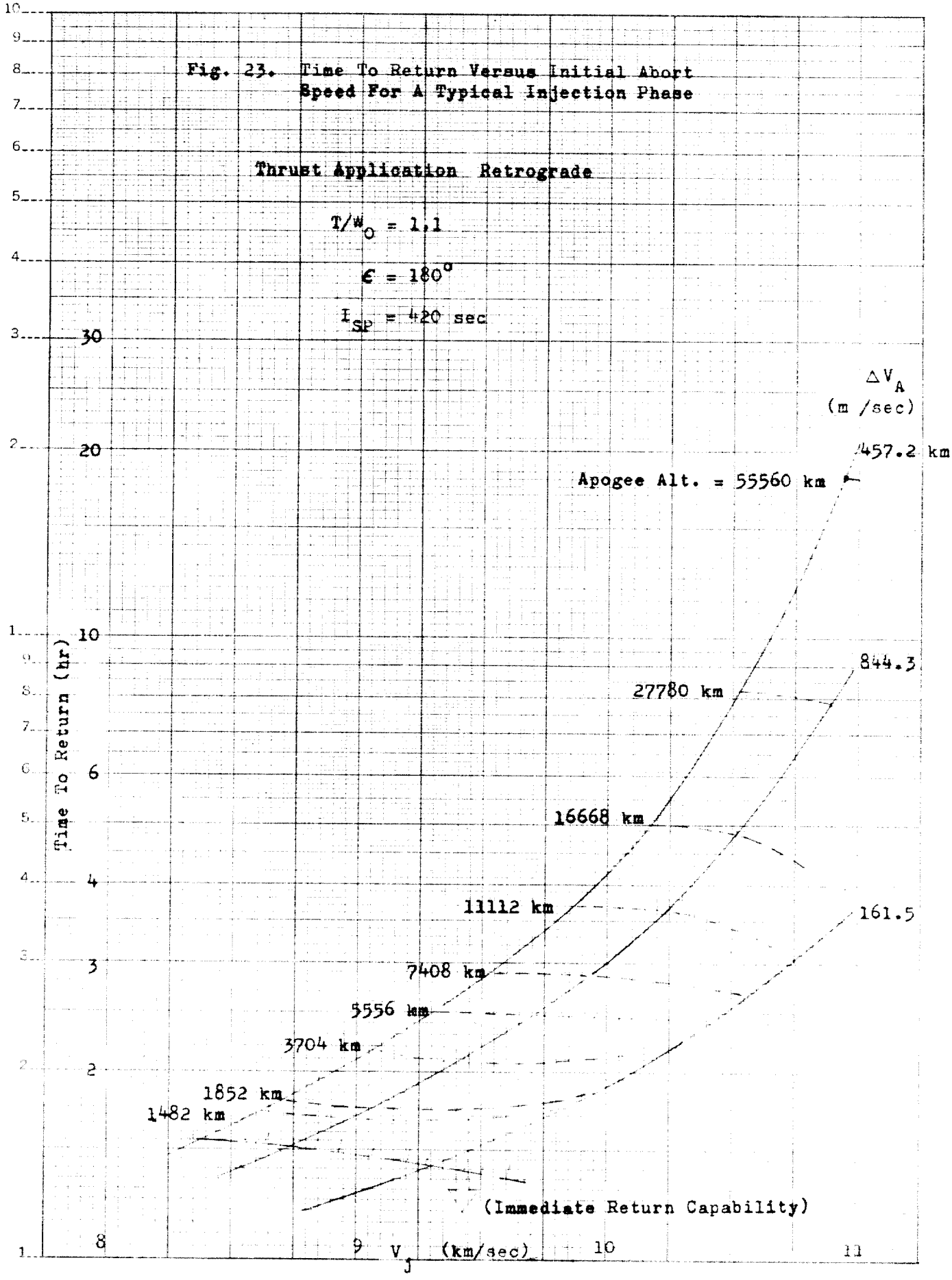
Fig. 23. Time To Return Versus Initial Abort Speed For A Typical Injection Phase
Thrust Application Retrograde
T/W_o = 1.1
ϵ = 180°
I_{SP} = 420 sec
ΔV_A (m /sec)
457.2 km
Apogee Alt. = 55560 km
844.3
27780 km
16668 km
11112 km
161.5
7408 km
5556 km
3704 km
1852 km
1482 km
(Immediate Return Capability)
Time To Return (hr)
V_j (km/sec)
10
9
8
7
6
5
4
3
2
1
30
20
11

CHAPTER VI

EARTH-TO-MOON TRANSFER

Prepared by:

F. Santora, R. Salinger, F. Martikan, T. Garceau,
L. Emery, and D. Kuhn
Martin Company (Baltimore)
Aerospace Mechanics Department
March 1963

A. Injection Requirements for Lunar Trajectories VI-1

B. Navigational and Tracking Requirements VI-7

C. Midcourse Guidance and Energy Requirements VI-15

D. Translunar Abort VI-22

E. References VI-27

Illustrations VI-31

Circumlunar Trajectory Catalogue VI-43

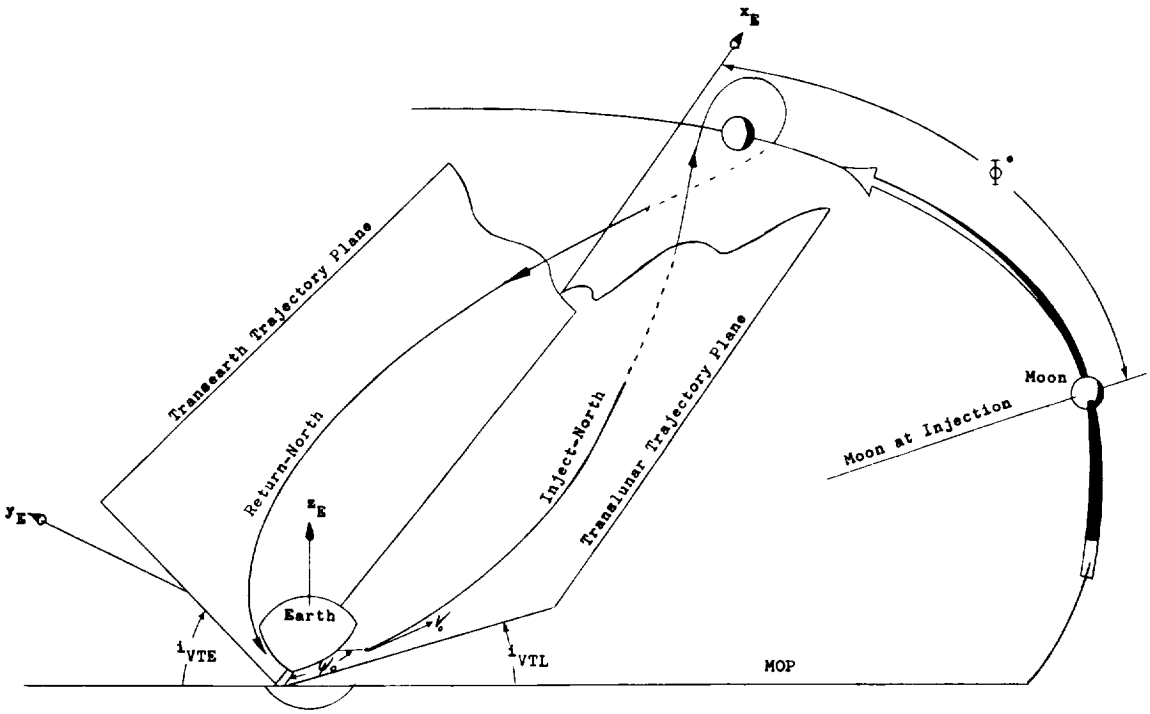
x_E
Φ°
Transearth Trajectory Plane
Return-North
Inject-North
Translunar Trajectory Plane
Moon
Moon at Injection
y_E
z_E
Earth
i_{VTE}
i_{VTL}
MOP

VI. EARTH TO MOON TRANSFER

Chapter V presented various techniques for leaving the launch site on the earth's surface and arriving at the proper injection conditions to establish a translunar trajectory satisfying certain mission constraints. These injection conditions consist of a specific time, velocity vector and radius vector. One purpose of Chapter VI is to graphically catalogue all possible injection conditions that reflect certain mission constraints in sufficient detail to serve as a primary source for design and mission planning work. Heavy emphasis is placed on circumlunar trajectories which return ballistically to earth; these were defined in Chapter IV and are described qualitatively and quantitatively in Section A, below. Although no data is presented in Chapter VI for the class of lunar trajectories that do not return ballistically to the immediate vicinity of the earth or approach trajectories, such data is included in Chapter IX. No injection data for lunar impact trajectories is included in the handbook except in discussion form in Chapters IV and VIII.

Chapter IV gives a description of the Voice technique which is used here to generate lunar trajectories by means of the patched two-body conics around the earth and moon. It is this technique that was used to generate the trajectory data found in this chapter and Chapters IX and XI. By referring trajectory data to the moon's orbital plane (MOP), which is a plane of symmetry, trends and tradeoffs between the various trajectory parameters are easily obtained and understood, and the number of graphs can be reduced. For the same reason, all data is general and thus applicable for any lunar position in orbit. If the lunar position in orbit at a certain date is needed, Chapter XI gives auxiliary graphs that allow interpretation of the general data of this chapter for specific dates. Comparisons with numerically integrated trajectories are also presented to prove the validity of the Voice data and to illustrate its accuracy.

Sections B and C of this chapter present the better-known concepts of navigation and guidance used for lunar missions, mostly in qualitative form. Some numerical data is given to compare and illustrate the various concepts. Of special interest are the ground traces of several circumlunar trajectories shown in Figs. 4 and 5, and discussed in Subsection B-2 on tracking.

Finally, implications of performing an abort from a translunar trajectory are included in Section D, in which will be discussed and illustrated the timing of aborts for return to a particular earth base, nonplanar abort maneuvers and their consequences, and the possibility of establishing "abort way-stations" along the translunar trajectory.

A. INJECTION REQUIREMENTS FOR LUNAR TRAJECTORIES

The data of this chapter concerns only circumlunar trajectories, as they are most likely to be used for manned lunar missions. A spacecraft in a circumlunar trajectory departs from the earth, transfers ballistically to the vicinity of the moon, and achieves its closest approach, or pericynthion, as it passes behind the moon. The gravitational attraction of the moon turns the trajectory in the general direction of the earth, and the vehicle continues in a trajectory which brings it to the vicinity of the earth. The passage from the earth to the moon is referred to as the "translunar trajectory," while the return passage is termed the "transearth trajectory." This class of trajectory and possible related missions has been discussed and illustrated in Chapter IV.

1. The Circumlunar Trajectory Catalogue

The nomenclature of the Voice technique, which has been introduced in Sections B-8 and C of Chapter IV, is repeated here for convenience and discussed more fully because the graphical data of this chapter has been derived from this technique. The leading sketch, opposite, is a schematic showing the Voice Cartesian coordinate axes and some of the trajectory nomenclature and parameters. The x_E-axis is defined by the intersection of the translunar trajectory plane with the moon's orbital plane (MOP) and is directed toward the moon. The z_E-axis is defined by the angular momentum vector of the moon about the earth's center, while the y_E-axis completes the right-hand coordinate system. The inclination of the translunar plane to the MOP is given by i_{VTL}, $0° \leq i_{VTL} \leq 180°$, and is measured as shown in the leading sketch. The velocity and radius vectors at injection, or the initial conditions of the lunar trajectory, define the translunar plane.

The injection conditions are specified as described below and illustrated on the following sketch:

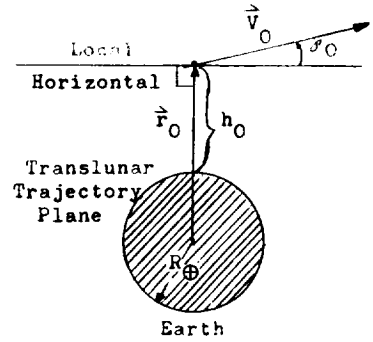

$\vec{V}_0$ is the injection velocity measured relative to the nonrotating $x_E y_E z_E$ system centered at the earth; γ_0 is the local flight path angle measured from the local horizontal to the velocity vector. The injection altitude, h_0, is defined by $h_0 = r_0 - R_\oplus$, where $\vec{r}_0$ is the radius vector at injection and $R_\oplus = 6371.02$ km is the radius of an equivalent spherical model of the earth. The specification of the injection is completed by the angle ψ_0, which orients the injection point with respect

to the Voice coordinate system and is measured from the negative x_E-axis to $\vec{r}_0$, as shown in the leading sketch, facing page VI-1.

A very important concept is that of the cardinal directions when the MOP is used as a reference plane for the trajectories in this handbook. By definition, the z_E-axis is designated as the "North" direction and "East" is in the same direction as the moon's orbital motion about the earth. Thus, when $0 < i_{VTL} < 90°$, injection is in the northern hemisphere (relative to the MOP) and is direct, or in the direction of the lunar motion in orbit, or "East" (see Subsection A-8 of Chapter IV). When $90° < i_{VTL} < 180°$ the injection is again north of the MOP, but in this case the direction is a retrograde or, westward injection. The same reasoning applies for injections taking place in the southern hemisphere relative to the MOP. Since all data is presented with positive values of i_{VTL}, the type of injection must be specified together with the value of i_{VTL}; e.g., $i_{VTL} = 60°$ (inject north), or $i_{VTL} = 60°$ (inject south). In Chapters V and XI, Cape Canaveral is the launch site, and launch azimuths A_e are arbitrarily restricted to $70° < A_e < 110°$. These values of A_e result in values of i_{VTL} equal to or greater than 0° but always less than 75°, as can be noted from Figs. 11 and 12 in Chapter XI. For this reason, data is given for $2° \leq i_{VTL} \leq 75°$. The material is presented for the "inject north" case and must be reinterpreted for the "inject south" case, as will be discussed later in the chapter. A similar situation exists for the transearth trajectory, as was noted in Chapter IV. The transearth inclination to the MOP is denoted by i_{VTE} and is measured positively, as shown. For convenience, the sketch is repeated here with an explanatory table relating return direction to quadrant.

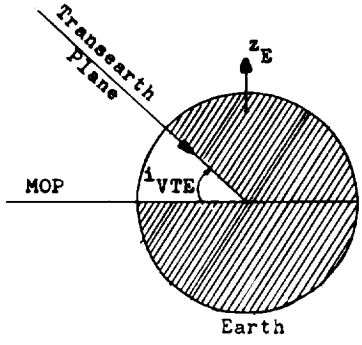

Transearth Trajectory Inclination	Return Direction
$0° < i_{VTE} < 90°$	Direct from the north
$90° < i_{VTE} < 180°$	Retrograde from the north
$-90° < i_{VTE} < 0°$	Direct from the south
$-180° < i_{VTE} < -90°$	Retrograde from the south

The circumlunar trajectories have been graphically catalogued for specific mission constraints--namely, the pericynthion altitude h_{PL}, the earth-moon distance $R_{\oplus\mathbb{C}}$, and vacuum perigee altitude of the transearth trajectory h_{PE}. The circumlunar trajectory catalogue includes data for h_{PL} from 185.2 km to 5000 km where $h_{PL} = r_{PL} - R_{\mathbb{C}}$ with r_{PL} the radius from the vehicle to the center of the moon at pericynthion and $R_{\mathbb{C}} = 1738.16$ km is the radius of the spherical moon model. $R_{\oplus\mathbb{C}}$ is varied from 56 ER (earth radii) to 64 ER, which represent the minimum lunar perigee radius and maximum lunar apogee radius, respectively, that can be encountered because of the eccentricity of the lunar orbit. The Voice data for these $R_{\oplus\mathbb{C}}$ was generated by keeping the angular momentum of the moon constant and assuming the moon to be in a circular orbit around the earth. All transearth trajectories have a vacuum perigee altitude of $h_{PE} = 46$ km.

In addition to the injection conditions of i_{VTL}, V_0, γ_0, h_0 and ψ_0, the flight time to pericynthion t_p and the total flight time from injection to perigee (T) also are recorded.

It is well to note at this time exactly what the catalogue contains and then to discuss each item separately in detail sufficient to provide a working knowledge of the material. The catalogue itself consists of Figs. C-1 to C-83 and contains the following trajectory constraints:

TABLE 1

Circumlunar Trajectory Catalogue

Case	$R_{\oplus\mathbb{C}}$ (earth radii)	h_{PL} (km)	Figure Numbers	Pages
1	56	185.2	C-1 to 8	IV-48 to 56
2	56	1000	C-9 to 16	IV-57 to 64
3	56	5000	C-17 to 24	IV-65 to 72
4	60	185.2	C-25 to 32	IV-73 to 80
5	60	1000	C-33 to 41	IV-81 to 89
6	60	3000	C-42 to 50	IV-90 to 98
7	60	5000	C-51 to 59	IV-99 to 107
8	64	185.2	C-60 to 67	IV-108 to 115
9	64	1000	C-68 to 75	IV-116 to 123
10	64	5000	C-76 to 83	IV-124 to 131

Trajectory data is given by the following variables as a function of i_{VTE} for each of the above constraints:

(1) V_0
(2) ψ_0
(3) Φ^*
(4) ΔV
(5) t_p
(6) T
(7) i_m
(8) θ_M

The variables Φ^*, ΔV, i_m and θ_M have not been mentioned previously in this chapter but will be discussed in sequence along with the others.

(1) V_0 --the required injection velocity for the circumlunar mission. Figure C-1 shows V_0 as a function of i_{VTE} for $R_{\oplus\mathbb{C}}$ = 56 ER and h_{PL} = 185.2 km. The independent parameter is i_{VTL}, and its particular values are 2°, 30°, 60° and 75°. The first trend noticed is the fact that V_0 increases as i_{VTL} decreases. By referring to Figs. C-9 and C-17, it is observed that this trend remains the same and that the variation in V_0 due to i_{VTL} is 6 to 20 m/sec, depending on h_{PL}. For $R_{\oplus\mathbb{C}}$ of 60 and 64 ER (Figs. C-25, C-34, C-35, C-42, C-43, C-51, C-52, C-60, C-68 and C-76), this variation does not substantially change. Another trend indicates that V_0 is lower if the trans-earth trajectory is direct rather than retrograde. The difference between returning direct in the MOP and retrograde in the MOP is approximately 25 m/sec for all cases. It is also noticed that V_0 decreases as h_P increases but increases as $R_{\oplus\mathbb{C}}$ increases. The maximum V_0 encountered for the above cases is 10922.8 m/sec and occurs for $R_{\oplus\mathbb{C}}$ = 64 ER, i_{VTE} = 180°, h_{PL} = 185.2 km and i_{VTL} = 2°.

(2) ψ_0--the injection position as given in Figs. C-2, C-10, C-18, C-26, C-35, C-44, C-53, C-61, C-69 and C-77. There is no appreciable change in the value of ψ_0 as $R_{\oplus\mathbb{C}}$ is varied if h_{PL} is maintained constant. However, if h_{PL} is varied a significant change does occur.

(3) Φ^*--moon lead angle. This variable is discussed in Chapter IV, Section C, but for convenience is depicted in the sketch on page (ii) of this chapter. It is measured from the lunar position at injection to the x_E-axis, and its magnitude varies from 30° to 60°. This is a very important angle when obtaining numerically integrated trajectories.

(4) ΔV--required velocity impulse to enter a circular lunar orbit from the circumlunar trajectory. If the spacecraft were to enter a circular orbit about the moon at the time of pericynthion, a characteristic velocity impulse would be required to reduce the speed of the space vehicle to circular orbit velocity (see Chapter IV, Subsection A-4). Figures C-4, C-12, C-20, C-28, C-37, C-46, C-55, C-63, C-71 and C-79 present ΔV as a function of i_{VTE}, and it is immediately noticed that ΔV increases as i_{VTL} increases. By varying i_{VTL} from 2° to 75°, a ΔV change of 30 to 60 m/sec may be realized, depending on h_{PL}. $R_{\oplus\mathbb{C}}$ has little effect on this change but does influence the magnitude of the impulse by as much as 50 m/sec (ΔV decreases as $R_{\oplus\mathbb{C}}$ increases). Again, as is the case for V_0, smaller values of ΔV are required for direct return trajectories. The maximum ΔV encountered for the cases in the above table is 1045 m/sec, which occurs for the following conditions: $R_{\oplus\mathbb{C}}$ = 56 ER, i_{VTL} = 75°, i_{VTE} = 180°, h_{PL} = 185.2 km.

(5) t_p--time from injection to pericynthion. As expected, t_p increases with i_{VTL}, since V_0 decreases with i_{VTL}; t_p also increases as h_{PL} and $R_{\oplus\mathbb{C}}$ increase, and the longest times are realized with "direct" returns. This data is presented in Figs C-5, C-13, C-21, C-29, C-38, C-47, C-56, C-64, C-72 and C-80.

(6) T--total flight time measured from injection to perigee. This particular variable is markedly influenced by h_{PL}. In fact, one may expect an increase of 35 to 65 hr (depending on i_{VTE}) by increasing h_{PL} from 185.2 km to 5000 km. T is also increased by approximately 25 hr if $R_{\oplus\mathbb{C}}$ varies from 56 to 64 ER (with h_{PL} held constant). The data giving T versus i_{VTE} is found in Figs. C-6, C-14, C-22, C-30, C-39, C-48, C-57, C-65, C-73 and C-81.

(7) i_m--inclination of the lunar orbit to the MOP, $0° \leq i_m \leq 90°$. If the spacecraft enters a lunar orbit at the pericynthion point (item 4), the resulting lunar orbit will be inclined to the MOP by an angle i_m. Because of the importance of this angle, a sketch showing i_m is repeated at this time from Chapter IV. Figures C-7, C-15, C-23, C-31, C-40, C-49, C-58, C-66, C-74 and C-82 present i_m, and a very interesting and significant result is that i_m is limited to 25° for h_{PL} = 5000 km and to less than 15° for h_{PL} = 185.2 km. This clearly implies that high selenographic latitudes (25°) are inaccessible for landing or reconnaissance missions unless the velocity vector is turned at pericynthion. This maneuver requires relatively much fuel, and hence, circum-

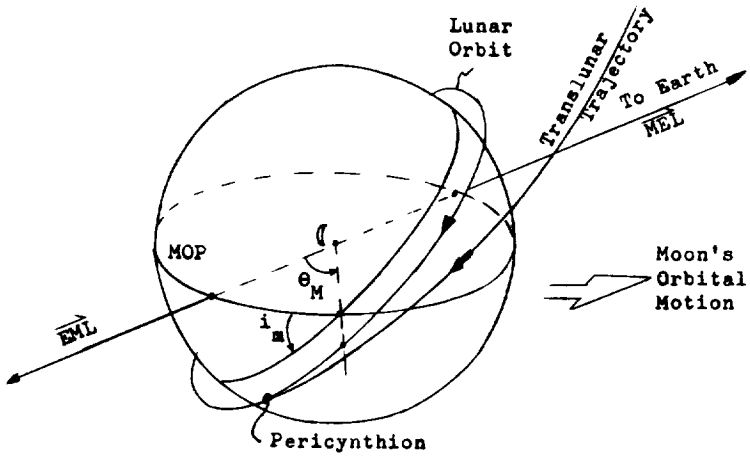

lunar trajectories will result in fly-bys and lunar orbits that lie in a narrow band above and below the MOP. Furthermore, lunar librations will not improve this coverage to any great extent.

(8) θ_M--angle between the earth-moon line and the descending node of the lunar orbit, $-180° \leq \theta_M \leq 180°$. At the time of pericynthion (t_p), the descending node of the trajectory plane is displaced θ_M degrees from the earth-moon line ($\overrightarrow{EML}$). This angle is also shown in the above sketch, and it, together with i_m, completely describes the orientation of the trajectory plane at t_p as well as the orientation of the circular lunar orbit that may be established at this point. Data relating θ_M with i_{VTE} for various i_{VTL} are given in Figs. C-8, C-16, C-24, C-32, C-41, C-50, C-59, C 67, C-75 and C-83. Another important fact, not mentioned above, is that for a constant value of i_{VTL}, an earth return is possible from any direction. This can be extremely useful in establishing operational concepts for lunar missions.

2. Generalization of the Catalogued Data

The catalogued data, extensive as it is, does not cover all parameters of the translunar trajectory. The material presented is applicable only for an injection flight path angle $\gamma_0 = 5°$ and an injection altitude $h_0 = 250$ km. The following discussion presents methods whereby γ_0 and h_0 may be extended to other values.

First, consider that h_0 remains 250 km and it is desired to change γ_0 to a value γ_0' other than 5°. It has been found that all data in the catalogue, except for ψ_0, remains essentially the same and any changes that do occur are altogether insignificant on the scale of the graphs. A new ψ_0, denoted by ψ_0' can be estimated to within ±0.2° for $\Delta\gamma_0$ as high as ±20° by means of the following empirical relation:

$$\psi_0' = \psi_0 + 2\,\Delta\gamma_0 \qquad (1)$$

where ψ = catalogue value
ψ_0' = revised value of ψ_0
$\Delta\gamma_0 = \gamma_0' - \gamma_0 = \gamma_0' - 5°$
γ_0 = catalogue value
γ_0' = desired value of γ_0

Values of $\gamma_0' > 25°$ are improbable for earth departure by present boosters because of the higher fuel requirements, while values of $\gamma_0' < -15°$ cause the spacecraft to re-enter the earth's atmosphere.

Next, consider that γ_0 remains unchanged, i.e., $\gamma_0' = \gamma_0$, and that it is desired to alter h_0 by an amount Δh_0. For Δh_0 less than ±250 km, the data in the catalogue again does not change, with the exception of the injection velocity V_0. A new value of V_0, denoted by V_0', can be determined for the desired h_0, which is denoted by h_0' through use of this equation derived from the conservation of energy in a restricted 2-body system:

$$V_0' = \left[V_0^2 - V_p^2 \left(\frac{\Delta h_0}{r_0} \right) \right]^{1/2} \qquad (2)$$

where V_0 = catalogue value of injection velocity
V_p = parabolic speed at the desired h_0
$\Delta h_0 = h_0' - h_0$
h_0 = catalogue value of injection altitude
r_0 = radius from the center of earth to h_0.

Observing that Eqs (1) and (2) are independent of each other, both γ_0 and h_0 may be varied together. An example of the use of these equations

is included in the second sample mission in Chapter XI.

If h_0' is extended to 2000 km by means of Eq (2), small errors appear in the other parameters. These errors may be acceptable for feasibility trajectory calculations. The brief table below gives the maximum magnitude of these errors for the various parameters if the catalogued data is extended to $h_0' = 2000$ km:

	Maximum Error
V_0	±1.5 m/sec
ψ_0	+1.3°
Φ^*	±0.2°
ΔV	-5 m/sec
t_p	±0.3 hr
T	±0.6 hr
i_m	-0.7°
θ_M	-3°

where:

parameter error = actual parameter value - estimated parameter value (from Eq (2)).

Therefore, the catalogued data in Figs. C-1 through C-83 can be applied to most circumlunar trajectories of interest. The catalogued trajectories are for the "inject north" case only as was mentioned previously. Since the reference plane is a plane of symmetry, the material can easily be reinterpreted for the "inject south" case by redefining the return inclination (i_{VTE}) scale on the figures by:

$$i_{VTE}\,(\text{inject south}) = -\,i_{VTE}\,(\text{inject north}) \quad (3)$$

A simple example illustrates this readily. Suppose that for the "inject north" case, $i_{VTL} = 60°$ and $i_{VTE} = +40°$, which is a return direct from the north. Therefore, for the "inject south" case, i_{VTL} remains the same, but $i_{VTE} = -40°$, which is a return direct from the south.

The lunar orbit orientation θ_M for the inject south case is interpreted in the following manner.

$$\theta_M\,(\text{inject south}) = \theta_M\,(\text{inject north}) + 180°$$

3. Accuracy of Injection Conditions and Trajectory Data

Since the data presented in Figs. C-1 to C-83 was derived from an approximate force model of the earth-moon system, it is necessary to ascertain the accuracy of such data. To this end, the catalogued Voice trajectory data (patched conic force model) was spotchecked with numerically integrated trajectories which were generated by using the more accurate restricted 3-body force model with the moon in a circular orbit about the earth (angular momentum is constant). The selected trajectories are considered extreme in the sense that they represent the maximum inaccuracy to be expected between the Voice and integrated trajectory results. For instance, high values of i_{VTL} (>60°) and small values of $R_{\oplus\mathbb{C}}$ (≃ 56 ER) produce larger errors in V_0, t_p and T.

Table 2 presents four circumlunar trajectories, giving the comparison of the previously discussed parameters. Trajectories 1 and 2 are presented to demonstrate the differences between the Voice and integrated results for the extreme conditions just mentioned. Below is a brief account of the likely errors that can be encountered in such extreme cases.

$\Delta V_0 \approx 2.3$ m/sec (error = Voice data - integrated trajectory data)
$\Delta \psi_0 \approx 0.4°$
$\Delta \Phi^* \approx -1°$
$\Delta h_{PL} \approx 0$
$\Delta(\Delta V) \approx -20$ m/sec
$\Delta i_m \approx -0.5°$
$\Delta \theta_M < -2°\ (i_{VTL} > 15°)$
$\Delta \theta_M \approx -0.6°$
$\Delta i_{VTE} \approx 0$
$\Delta t_p \approx 0.7$ hr

where the error is defined as the difference between the Voice and the restricted 3-body force model.

But more important than determining the acceptability of the Voice model is the substantiation of the trends indicated by Voice. Trajectory 1, for instance, shows the feasibility of leaving the earth with highly inclined trajectories and also returning with very high inclinations relative to the MOP. Trajectory 2 depicts in part the opposite case, i.e., injecting into a highly inclined translunar plane but returning with extremely low inclinations, in fact almost in the MOP. In trajectory 3, a complete reversal of trajectory 2 is shown. This trajectory has a very low inclined translunar plane ($i_{VTL} = 2°$) but returns to earth with a transearth inclination of approximately 75°. The last trajectory, number 4, has a remote pericynthion altitude ($h_{PL} = 5000$ km) and the moon is near apogee or at $R_{\oplus\mathbb{C}} = 64$ ER. In addition, the entire circumlunar trajectory is essentially in one plane. Thus, some important trends indicated by Voice are easily verified by the numerically integrated trajectories given in Table 2, and it is possible to conclude that the inaccuracies inherent in utilizing a patched conic method are acceptable for initial feasibility trajectory studies.

As a final point, the resulting lunar orbit orientation about the moon (i_m, θ_M) is in remarkable agreement with that obtained by integrated trajectories. This fact is a major reason that the use of Voice data for mission planning, further discussed in Chapter XI, is practical. If desired, a more accurate value of θ_M can be obtained by applying an empirical correction, given by

TABLE 2

Comparison of Voice Trajectories with Numerically Integrated Restricted 3-Body Trajectories
h_0 = 250 km, γ_0 = 5°, Inject North

Quantity	1		2		3		4	
	Voice	Integrated	Voice	Integrated	Voice	Integrated	Voice	Integrated
$R_{\oplus \mathbb{C}}$ (ER)	56.0	56.0	56.0	56.0	56.0	56.0	64.0	64.0
V_0 (m/sec)	10896.661	10894.788	10889.214	10887.064	10903.696	10902.030	10890.007	10889.463
i_{VTL} (deg)	75.0	75.0	75.0	75.0	2.0	2.0	60.0	60.0
ψ_0 (deg)	18.7534873	18.456858	17.497310	17.090264	22.30213	22.209816	14.787743	14.562976
Φ^* (deg)	40.488397	41.201542	43.093934	44.149837	35.934781	36.316359	46.632338	47.461369
h_{PL} (km)	185.0305	185.4452	185.0630	185.2193	185.0750	185.4256	4998.8867	4999.7675
ΔV (m/sec)	3237.672	3296.0677	3131.953	3189.2988	3129.7472	3187.0975	2161.8967	2261.009
t_p (hr)	62.220	62.554	66.204	66.942	59.078	59.044	93.202	93.160
T (hr)	125.584	126.376	125.294	126.009	125.346	126.067	188.215	188.447
i_{VTE} (deg)	98.145	98.128	-178.9526	-178.9658	105.1679	105.1248	-115.5457	-115.5227
h_{PE} (km)	45.7893	44.2087	45.2795	43.3567	45.6254	43.7711	45.8436	54.7968
i_m (deg)	13.792493	14.308571	8.86063	9.0893964	8.8545358	9.09866	9.7478268	9.810085
θ_M (deg)	90.310615	91.203772	42.873267	44.390196	134.93123	132.6791	-1.9753935	-0.859943
θ^*_M (deg)	91.162143	91.203772	43.7924	44.390196	133.2306	132.6791	-0.8012156	-0.859943

$$\Delta\theta_M = \pm \left[\frac{0.22 + 0.000156\, h_{PL}}{C_0 \sin i_{VTE} + 1} \right] . \quad (4)$$

where

+ holds for the "inject south" case

- holds for the "inject north" case

C_0 is obtained from Chapter XI, Section E; a constant derived from empirical data.

The corrected value of θ_M, $\theta_M{}^*$, is given by

$$\theta_M{}^* = \theta_M + \Delta\theta_M$$

and is also noted in Table 2.

B. NAVIGATIONAL AND TRACKING REQUIREMENTS

Navigation is defined as the process of determining the position and velocity of a space vehicle; this process is usually accomplished by making observations such as star occultations by the moon, bearing lines to certain stars, angular diameters of the moon, earth and sun and from these observations computing the vehicle position and velocity vector. The problems of navigation in cislunar space, discussed in this section, are greater than those encountered in earth orbit since vehicle trajectories far from earth are significantly influenced by the lunar gravitational attraction, since trajectory sensitivities (the partial derivatives of trajectory parameters with respect to initial conditions) increase drastically, and because of uncertainties in the force model and in the astronautical constants. Thus, some means must be developed to determine the vehicle trajectory in flight, or the deviation of the actual trajectory from the nominal trajectory. The procedure used to determine the new trajectory is referred to as the navigation technique. The observations fundamental to a particular technique may be made from the spacecraft itself, from tracking stations on the earth, or from the lunar surface. A number of feasible navigation techniques for cislunar space can be devised if the methods for making the necessary navigational observations are available. The techniques discussed in this section include navigation by means of nominal or precomputed trajectories and trajectories computed in flight. A third technique, described as a "homing" technique (Ref. 1) utilizes line-of-sight orientation to ensure interception with the target. However, this technique has not yet been adequately proven for lunar missions, so it will not be discussed further.

The question remains of what to do when the deviation of the actual from the nominal trajectory has been determined, that is, how to return to the original trajectory or correct the actual trajectory in order to fulfill the mission. These midcourse guidance and energy requirements will be discussed in Section C.

1. Navigational Techniques

a. Observational considerations

Before discussing the details of various navigational techniques, it is necessary to decide what observations are to be made and how they are to be used in order to provide an improved estimate of position and velocity. Battin, in Ref. 2, has developed a procedure for statistically optimizing navigation for space flight. The detailed analysis will not be presented here, but a short account is given to emphasize the necessity of such a procedure.

In a typical self-contained space navigation system, observational data is gathered and processed to produce estimated velocity corrections by rocket burning (i.e., guidance corrections). Observational data may be gathered either by optical means or by radio. Fundamental to the navigation system is a procedure for processing observations which permits incorporation of each individual observation as it is made to provide an improved estimate of position and velocity. In order to optimize a navigation technique a number of alternate courses of action must be evaluated. The various alternatives, which form the basis of a decision process, concern the following:

(1) Which navigational observation gives the most accurate position?

(2) Does the best observation give a sufficient reduction in the predicted target error to warrant making the observation?

(3) Is the uncertainty in the indicated guidance correction a small enough percentage of the correction itself to justify an engine restart and propellant expenditure?

The time interval from injection to arrival time at the aim point (near or on the moon) can be considered to be subdivided into a number of smaller intervals t_1, t_2, ... called "decision points." At each decision point one of three possible courses of action is followed: (1) a single observation is made; (2) a velocity correction is implemented; or (3) no action is taken. As a necessary step in the application of navigation schemes, certain rules must be adopted for the course of action to be taken at each "decision point." The number and frequency of observations must be controlled in some manner--ideally by a decision rule which is realistically compatible with both the mission objectives and the capabilities of the observing device. If an observation is to be made, a decision is required regarding the type and the celestial objects to be used. Periodic guidance corrections must be applied and the number of impulses and times of occurrence must be decided.

Once the decision rules have been specified, it is necessary to test their effectiveness with some measure of performance. One typical objective is to minimize the miss distance at the moon. However, a reduction in miss distance

usually implies an increase in either the required number of observations or a greater expenditure of corrective propulsion--or both. This fact is demonstrated in Section C. In the face of conflicting objectives, present in any technique, compromises are clearly necessary, and a statistical simulation helps in arriving at an acceptable balance.

A common assumption is that secondary effects arising from the finite speed of light, the finite distance of stars, etc., are ignored in the observations. For the calculations, these effects at a particular reference point on the trajectory may be lumped together as a modification to the stored data which represents nominal reference values for the quantities to be observed at that point. Also, the question of simultaneous observations does not arise if the vehicle dynamics are governed by known laws and if deviations from a predetermined reference trajectory are kept sufficiently small to permit a linearization by expanding around the nominal trajectory point in a Taylor series and neglecting second and higher-order terms.

The essential problem is to select those observations which are, in some sense, most effective. For example, the requirement might be to make the selected observation at a certain time in order to get the maximum reduction in mean-squared positional or velocity uncertainty at that time. Of perhaps greater significance would be the requirement to select the observation which minimizes the uncertainty in any linear combination of position and velocity deviations. Specifically, one might select the observation which minimizes the uncertainty in the required velocity correction. As a further example, one might wish to select that observation which, if followed immediately by a velocity correction, would result in the smallest position error at the target or aim point.

The common methods for making navigational observations may be subdivided into three principal areas:

(1) Optical observation of the angles between several celestial bodies as seen from the vehicle.

(2) Radio or optical tracking from the earth by determining the azimuth and elevation of the space vehicle.

(3) Radio range (interferometer) and doppler measurements on the vehicle, the earth, or the moon.

Methods (2) and (3) will not be discussed since they are treated in Chapter XI of Ref. 1. However, a brief remark on the interferometer method of tracking and navigation will be made. For lunar flights it is possible to use the earth-moon separation as an interferometric baseline (Ref. 3). If a receiver could be established on the moon or at the libration points, it could easily be synchronized with a series of such stations on the rotating earth by means of line-of-sight communications. In this case the interferometer scheme illustrated in Chapter X of Ref. 1, where two transmitters are used at the ends of the baseline, operates in reverse. The phases of the transmitted waves are compared in the vehicle and the radio range from the vehicle to the stations can be determined. If each vehicle can carry sufficient computing equipment to transform and act on the received phase difference data, any number of vehicles can track themselves simultaneously from the same ground system. This system is similar to the hyperbolic LORAN navigation scheme now widely used by aircraft and ships.

The emphasis in this subsection will be on method (1)--angular observations of celestial bodies from the vehicle by optical methods. This technique will be most useful in early lunar flights since it has been proposed that navigation on manned lunar missions be handled by the crew and self-contained optical units be used for unmanned missions. Two types of measurements, one for small angles and one for large angles, will be described.

Small angles, i.e., those less than a few degrees, may be measured within the field of view of an astronomical telescope. This type of measurement is particularly desirable for measuring the apparent diameter of the sun, earth or moon and the position of these bodies against their neighboring stellar background. The observations may be made directly, or the telescope may be used to photograph the sun, and/or moon and/or planets against the star background (Ref. 4). In the latter case the photographic plates could be read with an optical micrometer after developing. The photographic method has the advantage of "freezing" time, thus permitting a leisurely measurement of what was visible at a single instant. The technique requires local filtering to reduce the exposure of the image of the sun, moon or planet relative to the stellar background. It is presently used for determining the lunar ephemeris from the earth, yielding accuracies on the order of 0.''01. These accuracies, of course, can not be expected from space vehicle observations. The photographic method requires a plate-reading micrometer; however, on a manned voyage it is very likely that an astronomical telescope and plate-handling equipment are on board for other than navigational purposes.

Large angles as well as small ones can be measured by a type of sextant which may be either hand-held or mounted in the vehicle. The sextant has several advantages over the telescope, notably:

(1) Having separate light paths, a sextant requires no troublesome local filter; one light path or the other may be filtered as desired.

(2) It measures large angles as well as small ones.

(3) The optical requirements of a sextant's telescope are minimal, since the two objects whose separation is measured are brought into coincidence at a single point rather than being measured over an extended optical field.

Since a vehicle-borne sextant doesn't require manual support, it can be larger than a marine-

type sextant and can be equipped with a high-magnification telescope and a reading microscope for the vernier.

In a space vehicle, the optical system of such angular measuring instruments as sextants and star trackers have accuracies of the order of 0.''1 to 1.''0. However, the observational technique, reading errors, etc., permit practical accuracies of the order of only 10'' for a single observation. This accuracy is quoted for a single observation of point sources such as stars; the tracking of extended images such as the earth and moon degrade, while the combination of a number of individual observations and their smoothing to determine a small vehicle trajectory arc enhance the practically achievable accuracy.

All optical observations are subject to planetary aberration due to the finite velocity of light and the relative motion of the observer and the celestial body. If a stationary telescope is pointed at a celestial body, it is pointing at the position where the celestial body was when the observed light left it rather than where it is when the light arrives at the space vehicle. These errors could be of the order of 10''. The relative motion of the vehicle with respect to the observed object or stellar aberration causes celestial bodies to be displaced in the direction of the vehicle's velocity. This angular deviation, Δ, is given by the expression:

$$\Delta = \sin\phi \tan^{-1}\left(\frac{V_\Delta}{c}\right) \qquad (5)$$

where

ϕ = angle between the velocity vector and the line of sight to the observed object

V_Δ = velocity of the space vehicle relative to the celestial body

c = velocity of light, 299,792.5 ± 0.1 km/sec.

These errors are small and easy to correct because V_Δ/c is very small. For the worst case, $\phi = 90°$, the deviation is about 20'' for $V_\Delta = 29.8$ km/sec.

Several types of navigational observations can be made from a space vehicle simultaneously in order to arrive at the best determination of position and velocity. For example: gyroscopic techniques can be used for angular measurements; accelerometers for measuring acceleration, primarily during rocket burning or near the moon and earth; radar techniques for velocity measurements; distance measurements from the apparent diameters of celestial bodies in the solar system; and time measurements from clocks and from the motion of celestial bodies in the solar system. These are all discussed extensively in Ref. 5.

b. Analysis of two navigational techniques

Two navigational techniques, referred to as technique 1 and technique 2, for determining spacecraft position by means of optical observations of celestial bodies will now be analyzed in detail. In technique 1 it is assumed that the nominal spacecraft position and velocity vectors are known so that perturbation methods may be employed in determining the actual position and velocity from the nominal. All measurements are assumed to be made at exact instants of time. Technique 2 on the other hand does not require a nominal trajectory, but the actual trajectory is determined directly from the observations. The same type of observation may be used in either navigational technique.

In technique 1, one type of observation to be considered is that of the angle A subtended at the space vehicle by the moon-earth line. By passing to the limit of infinite distance from either the earth or moon, corresponding angular measurements of the earth-star or moon-star line can be made. Referring to the sketch below, Δ and $\mathcal{C}$ denote the nominal positions of the spacecraft and moon at the time of the measurement. Let $\vec{r}_{\oplus\Delta}$ be the vector from the earth $\oplus$ to Δ and $\vec{r}_{\Delta\mathcal{C}}$ the vector from Δ to $\mathcal{C}$. With A denoting the angle at the space vehicle from the radius to the earth to the radius to the moon, we have

$$\cos A = -(\vec{r}_{\oplus\Delta} \cdot \vec{r}_{\Delta\mathcal{C}})/r_{\oplus\Delta}\, r_{\Delta\mathcal{C}} \qquad (6)$$

where $r_{\oplus\Delta}$ and $r_{\Delta\mathcal{C}}$ denote magnitudes of the respective vectors $\vec{r}_{\oplus\Delta}$ and $\vec{r}_{\Delta\mathcal{C}}$. Treating all changes as first order differentials, it can be shown that

$$\delta A = \left(\frac{\hat{m} - (\hat{n}\cdot\hat{m})\hat{n}}{r_{\oplus\Delta}\sin A} + \frac{\hat{n} - (\hat{n}\cdot\hat{m})\hat{m}}{r_{\Delta\mathcal{C}}\sin A}\right)\delta\vec{r}_{\oplus\Delta} \qquad (7)$$

where $\delta\vec{r}_{\mathcal{C}\Delta}$ is the radius vector from the observed position to the nominal position of Δ with respect to earth, $\hat{n}$ and $\hat{m}$ are, respectively, the unit vectors from Δ toward $\oplus$ and toward $\mathcal{C}$. Hence $\vec{r}_{\oplus\Delta} = -r_{\oplus\Delta}\,\hat{n}$ and $\vec{r}_{\Delta\mathcal{C}} = r_{\Delta\mathcal{C}}\,\hat{m}$. The vector $\delta\vec{r}_{\oplus\Delta}$ is small compared to $\vec{r}_{\oplus\Delta}$. The two individual vector coefficients of $\delta\vec{r}_{\oplus\Delta}$ in Eq (7) are vectors in the same plane in which the observation takes place and normal to the lines of sight to the earth and to the moon.

A second observation determines position by taking a stadiametric reading, or measuring the diameter of a celestial body. If D is the apparent diameter of the moon, the apparent angular diameter 2γ is found from

$$\sin(\gamma) = D/2\, r_{\Delta\mathcal{C}} \qquad (8)$$

with the differential given by

$$\delta(2\gamma) = \frac{D\,\hat{m}\cdot\delta\vec{r}_{\oplus\Delta}}{(r_{\Delta\mathcal{C}})^2\cos(\gamma)} \qquad (9)$$

In technique 2, where the actual trajectory is computed without a nominal trajectory, this distance

measurement is usually used in conjunction with other measurements.

A third observation records the time of a stellar occultation by the moon. Let Δ and $\mathbb{C}$ be, respectively, the nominal positions of the spacecraft and the moon at the time of observation, and let $\hat{n}$ be a unit vector at the vehicle in the direction of the star occulted by the moon. With γ denoting the angle from the star radius to the moon radius as shown in the second sketch, we have, at the nominal instant of occultation,

$$\hat{n} \cdot \vec{r}_{\Delta\mathbb{C}} = r_{\Delta\mathbb{C}} \cos\gamma \qquad (10)$$

Treating changes as first order differentials we obtain

$$\hat{n} \cdot \delta\vec{r}_{\Delta\mathbb{C}} = (\cos\gamma)\delta r_{\Delta\mathbb{C}} - r_{\Delta\mathbb{C}} \sin\gamma\delta\gamma$$

$$= (\cos\gamma)\hat{m} \cdot \delta\vec{r}_{\Delta\mathbb{C}} - r_{\Delta\mathbb{C}} \sin\gamma\delta\gamma \qquad (11)$$

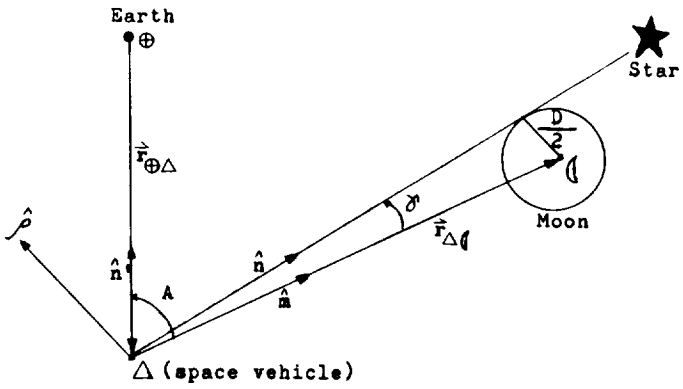

The angular deviation $\delta\gamma$ is computed from a first order differential of $2\, r_{\Delta\mathbb{C}} \sin\gamma = D$:

$$\delta\gamma = -D\,\hat{m} \cdot \delta\vec{r}_{\Delta\mathbb{C}} / 2\,(r_{\Delta\mathbb{C}})^2 \cos\gamma \qquad (12)$$

Furthermore, if $\vec{V}_{\mathbb{C}}$ and $\vec{V}_{\Delta}$ are the respective inertial velocities of the moon and the spacecraft, and if δt is the difference between the observed and the nominal time of occultation, we have:

$$\delta\vec{r}_{\Delta\mathbb{C}} = \vec{V}_{\mathbb{C}}\,\delta t - (\delta\vec{r}_{\oplus\Delta} + \vec{V}_{\Delta}\,\delta t)$$

$$= -\delta\vec{r}_{\oplus\Delta} - \vec{V}_{\mathbb{C}\Delta}\,\delta t \qquad (13)$$

where $\vec{V}_{\mathbb{C}\Delta}$ is the velocity of the spacecraft relative to the moon. Then by combining Eqs (11), (12) and (13) we have finally:

$$\delta t = -\frac{\hat{\rho} \cdot \delta\vec{r}_{\oplus\Delta}}{\hat{\rho} \cdot \vec{V}_{\mathbb{C}\Delta}} \qquad (14)$$

where $\hat{\rho}$ is a unit vector perpendicular to $\hat{n}$ in the plane determined by the lines of sight to the moon and the star. The procedure could be reversed by considering star occultations by the earth.

Consider next the technique wherein the angle between the lines of sight to a star and the edge of the lunar disc is measured. From the sketch below,

$$\hat{n} \cdot \vec{r}_{\Delta\mathbb{C}} = r_{\Delta\mathbb{C}} \cos(A^* + \gamma) \qquad (15)$$

where A^* is the angle to be measured. Taking total differentials and noting that $\delta\vec{r}_{\oplus\Delta} = -\delta\vec{r}_{\Delta\mathbb{C}}$, we obtain:

$$\frac{\rho \cdot \delta\vec{r}_{\oplus\Delta}}{r_{\Delta\mathbb{C}}} = \delta A^* + \delta\gamma$$

$$= \delta A^* + D\,\hat{m} \cdot \delta\vec{r}_{\oplus\Delta} / 2\,(r_{\Delta\mathbb{C}})^2 \cos\gamma$$

$$= \delta A^* + \tan\gamma\,\hat{m} \cdot \delta\vec{r}_{\oplus\Delta} / r_{\Delta\mathbb{C}} \qquad (16)$$

or finally:

$$\delta A^* = \frac{\rho \cdot \delta\vec{r}_{\oplus\Delta}}{r_{\Delta\mathbb{C}} \cos\gamma} \qquad (17)$$

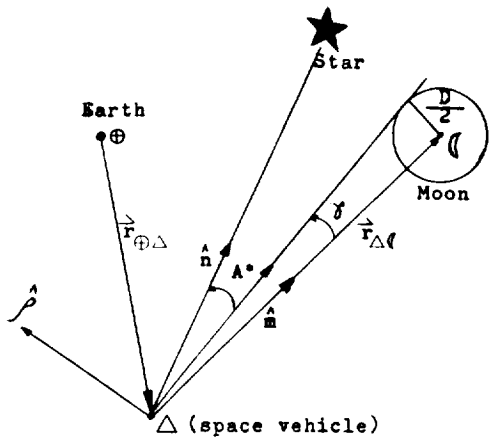

For the measurement of the angle between a landmark on a planet or lunar surface and a star, let $\hat{\rho}$ be a unit vector perpendicular to the line of sight to the landmark and in the plane of measurement. Then if $\vec{\rho}$ is the vector position of the landmark relative to the center of the object, we have

$$\delta A^* = \frac{\hat{\rho} \cdot \delta\vec{r}_{\oplus\Delta}}{|\vec{r}_{\Delta\mathbb{C}} + \vec{\rho}|}$$

Technique 2 does not use perturbations about a nominal trajectory, but angular measurements are converted directly to positional data. Optical instruments in the vehicle are used to establish bearing lines to point sources in the sky and the angles between the lines of sight are measured by a sextant. The conversion to positional information is illustrated in the following sketch, where the plane of the paper represents the plane of one set of two sextant readings. One bearing is assumed to be taken on the earth and the other sources, 1 and 2, are either stars, planets, or the moon. Define a nonrotating plane polar coordinate system $(r_{\oplus}, \theta_{\oplus})$ with origin at the earth, in which the stars are assumed fixed. The unknown polar coordinates of the vehicle, $(r_{\oplus\Delta}$,

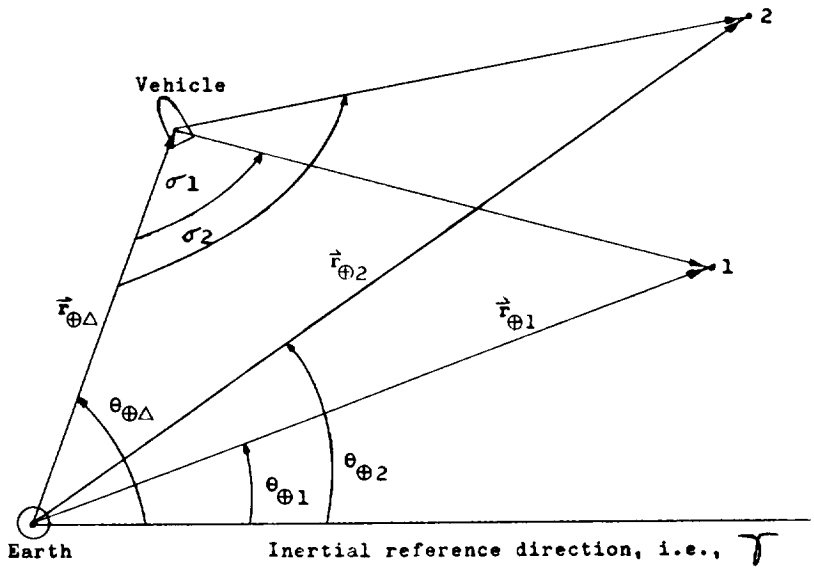

$\theta_{\oplus\Delta}$), can be expressed in terms of the measured angles σ_1, σ_2, $0° \leq \sigma_1, \sigma_2 \leq 180°$ and the known polar coordinates $(r_{\oplus 1}, \theta_{\oplus 1})$ and $(r_{\oplus 2}, \theta_{\oplus 2})$ of the sources 1 and 2, respectively, by use of trigonometry:

$$r_{\oplus\Delta} = \left[r_{\oplus 1} r_{\oplus 2} \sin(\sigma_1 - \theta_{\oplus 1} - \sigma_2 + \theta_{\oplus 2}) \right] \cdot \left[(r_{\oplus 1})^2 \sin^2 \sigma_2 + (r_{\oplus 2})^2 \sin^2 \sigma_1 - 2 r_{\oplus 2} r_{\oplus 1} \sin\sigma_1 \sin\sigma_2 \cos(\sigma_1 - \theta_{\oplus 1} - \sigma_2 + \theta_{\oplus 2}) \right]^{-1/2} \quad (18)$$

$$\tan\theta_{\oplus\Delta} = \frac{r_{\oplus 1} \sin\sigma_2 \sin(\sigma_1 - \theta_{\oplus 1}) - r_{\oplus 2} \sin\sigma_1 \sin(\sigma_2 - \theta_{\oplus 2})}{r_{\oplus 2} \sin\sigma_1 \cos(\sigma_2 - \theta_{\oplus 2}) - \sigma_1 \sin\sigma_2 \cos(\sigma_1 - \theta_{\oplus 1})} \quad (19)$$

If source 1 is a distant star and source 2 represents the moon, these formulas simplify considerably, since $r_{\oplus 2}/r_{\oplus 1} \to 0$. Then

$$r_{\oplus\Delta} = r_{\oplus 2} \frac{\sin(\sigma_1 - \theta_{\oplus 1} - \sigma_2 + \theta_{\oplus 2})}{\sin\sigma_2} \quad (20)$$

and

$$\theta_{\oplus\Delta} = \pi - \sigma_1 + \theta_{\oplus 1} \quad (21)$$

Differentials of Eqs (20) and (21) give an estimate of the errors induced in $r_{\oplus\Delta}$ and $\theta_{\oplus\Delta}$ by the measurement errors $\delta\sigma_1$ and $\delta\sigma_2$ and source position errors.

$$\delta r_{\oplus\Delta} = (\delta\sigma_1 + \delta\theta_{\oplus 2}) r_{\oplus 2} \frac{\cos(\sigma_1 - \theta_{\oplus 1} - \sigma_2 + \theta_{\oplus 2})}{\sin\sigma_2} - \delta\sigma_2 r_{\oplus 2} \frac{\sin(\sigma_1 - \theta_{\oplus 1} + \theta_{\oplus 2})}{\sin^2\sigma^2} + \delta r_{\oplus 2} \frac{\sin(\sigma_1 - \theta_{\oplus 1} - \sigma_2 + \theta_{\oplus 2})}{\sin\sigma_2} \quad (22)$$

$$\delta\theta_{\oplus\Delta} = -\delta\sigma_1 + \delta\theta_{\oplus 1} \quad (23)$$

The total effect of instrument and/or data errors in Eq (22) can be minimized by proper choice of sources 1 and 2. It is quite clear, for instance, that the cases $\sigma_2 = 0, \pi$, i.e., cases in which the moon, vehicle and earth are colinear, should be avoided. The simultaneous values $\sigma_1 - \theta_{\oplus 1} + \theta_{\oplus 2} = 0$, $\sigma_2 = 90°$ reduce all errors but those for $\delta r_{\oplus 2}$. Errors in the radial distance $r_{\oplus\Delta}$, $\delta r_{\oplus\Delta}$, therefore determined primarily by the uncertainty in $r_{\oplus 2}$, the distance of the moon from the earth.

If Eqs (22) and (23) are divided by dt, one obtains the time rates-of-change of $r_{\oplus\Delta}$ and $\theta_{\oplus\Delta}$:

$$\dot{r}_{\oplus\Delta} = \dot{\sigma}_2 \frac{\sin(\sigma_1 - \theta_{\oplus 1} - \sigma_2 + \theta_{\oplus 2})}{\sin\sigma_2} + \sigma_2 \left[(\dot{\sigma}_1 + \dot{\theta}_{\oplus 2}) \frac{\cos(\sigma_1 - \theta_{\oplus 1} - \sigma_2 + \theta_{\oplus 2})}{\sin\sigma_2} - \dot{\sigma}_2 \frac{\sin(\sigma_1 - \theta_{\oplus 1} + \theta_{\oplus 2})}{\sin^2\sigma_2} \right] \quad (24)$$

$$\dot{\theta}_{\oplus\Delta} = -\dot{\sigma}_1 \qquad (25)$$

The problem of obtaining these derivatives is discussed on p 21 of Ref. 3.

By combining the available observations and measurements, other approaches may be found through this technique. For instance, as an outgrowth of the above method, the position of a spacecraft in cislunar space may be determined by two stellar directions and a planetary source.

c. Application of navigational technique 2 to lunar flight

The choice of stars and celestial bodies is of some importance if technique 2 is used for navigation in cislunar space. This aspect is discussed to some extent and illustrated by one example in the present subsection.

If the position of three bodies in space is known at a given time from calculated ephemerides, triangulation can be used to determine the position of the spacecraft at that time. In cislunar space one of the bodies will either be the earth or the moon, due to their proximity. The sun, any of the planets, and any of their moons suggest themselves for the other two celestial bodies. Unfortunately, these bodies cannot be used for lunar missions because of the inaccuracy developing from the large interplanetary distances as compared to the relatively small earth-moon distance. Therefore, the stars must be used.

It can be assumed with excellent accuracy that the stars are at an infinite distance from the earth-moon-spacecraft region. Hence the position of the stars is defined by their direction only and two stars and the earth or moon are not sufficient to determine the exact location of the spacecraft, but only a line of positions. The observation of the angle between one star and the prime body (earth or moon) from the spacecraft specifies its position as being on a cone with apex at the prime body (earth or moon), whose center line is directed toward the star, and whose half-angle is given by the angle between the star and prime body. The additional observation of the angle between another star and the prime body specifies a second cone. The intersection between two cones with a common apex is specified by either one or two straight lines or no intersection occurs. However, since the spacecraft must be on the surface of both cones simultaneously, the last case is ruled out. If there is one line of intersection, which will be denoted "line of position," then the spacecraft is known to be located somewhere on it. If there are two lines of intersection, then a proper choice of stars or a third angular measurement to get another star may settle on which line of position the vehicle is on. Approximate knowledge of the vehicle trajectory, of course, also determines the line of position. The location of the space vehicle on this line can be determined by stadiametric readings, a star occultation by a second prime body which may be another planet or the moon, by using another line of position determined from two stars and the second prime body, or by tracking from the earth or moon and subsequent data transmission to the spacecraft. The choice between these methods is dependent upon where the vehicle is relative to the earth or moon at the time.

In this navigation technique, it is important to know an optimum orientation of the two stars and the prime body chosen for observation in order to give the minimum error in the line of position due to errors in the two angular measurements. Another important question is whether the more prominent navigation stars can be used for position determination within an acceptable error, or if some of the less well-known stars have to be employed as well.

The geometry is illustrated in the following sketch. The origin of coordinates is at the center of the prime body, with Cartesian axes $x_P y_P z_P$ as shown. Vectors $\hat{s}_1$ and $\hat{s}_2$ are unit vectors in the direction of stars 1 and 2, σ_s is the angle between $\hat{s}_1$ and $\hat{s}_2$ which is known quite accurately

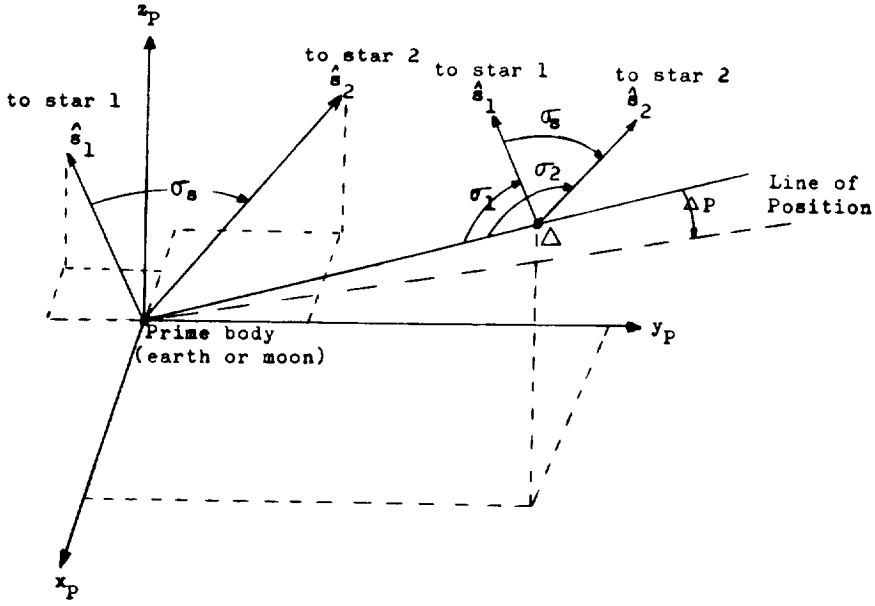

from the ephemeris, and the angles σ_1 and σ_2 are between the direction to the prime body and stars 1 and 2, respectively, $0° \leq \sigma_1, \sigma_2 \leq 180°$. The last two readings, made by the crew, establish the line of position.

The use of this navigation technique is illustrated below. The observational accuracy in the measurement of σ_1 and σ_2 is assumed at 6", and the worst possible combination of these two errors was used to define ΔP, the angular error in the line of position. Figure 1 shows the possible relationships between σ_1 and σ_2 which will result in $\Delta P = 0.006°$ or less for a star separation of $\sigma_s = 60°$ in the case of the worst possible combination of errors in σ_1 and σ_2. The line of position error (maximum) will be 0.006° on the boundary for the σ_1 and σ_2 combinations shown and will decrease as the σ_1 and σ_2 combinations move from the boundaries into the shaded area.

A natural goal is to choose stars which will keep the effect of reading errors to a minimum, but still make use of the more prominent navigation stars which have proved themselves to be easily identifiable over several centuries of naval navigation. With this in mind, the data presented in Fig. 2 is used in making the choice. The shaded areas shown represent the σ_1 and σ_2 combinations which will result in $\Delta P \leq 0.004°$ for any σ_s between 60° and 90°. For illustration, it can be seen that the range encompassed by σ_1 between 30° and 50° and σ_2 between 70° and 80° lies within the shaded area.

This data can be illustrated with an example using a circumlunar trajectory launched from Cape Canaveral on 14 June 1968 at 14:14 hr GMT. A view of the earth, as seen from the spacecraft three hours after injection into the translunar trajectory (a good time for first midcourse guidance corrections), is shown in Fig. 3 with the actual stellar background. The right side of the earth is illuminated by the sun, with Alaska and California appearing on the extreme right. The principal stellar constellations visible behind the earth are indicated on the figure. Using the earth's center as the celestial body, the σ_1 range (30° to 50°) and σ_2 range (70° to 80°) are shown traced on the celestial sphere. The required angular displacement between the two stars is 60° to 90° (shown on the bottom of the figure). Thus, star 1 must lie in the band labeled σ_1 range and star 2 in the band labeled σ_2 range. The distance between star 1 and star 2 must be 60° to 90°. Inspection of Fig. 3 shows many such separations between the prominent navigation stars. The spacecraft 3 hr after injection is typically 50,000 km from the earth, and an angular error of $\Delta P = 0.006°$ corresponds to a position error of 5 km in the line of position.

Figures similar to Fig. 3 can be prepared for various times throughout the lunar mission. In the case of the illustrated circumlunar trajectory, figures for a later time will differ from Fig. 3 by a decreasing size of the earth and the earth's displacement due to its motion toward the upper left. When the vehicle approaches the moon, the moon with its star background can be used for navigation.

The main advantages of this navigational technique are:

(1) Observations can be planned well ahead of the mission on the ground.

(2) In many cases the same pair of stars can be used for observations over long periods of time.

(3) Observational errors can be minimized by proper choice of stars for navigation.

(4) The time for navigational observations can be minimized.

The last point is important, as two observations must be made from the spacecraft for determining the line of position, and in the very early stages of lunar flight, the trajectory curves strongly (see Fig. 1 in Chapter IV), and the direction of the line of position changes relatively rapidly. This suggests that this navigational technique will yield better results farther from the prime body than in its immediate vicinity, and that it is not suitable for space vehicles in near-earth or near-moon orbits.

d. Concluding remarks

The problems of navigation are not completely solved even when position and velocity data are obtained and decision rules are applied. There still remains the problem of reducing this data to useful applications in corrections. For the case of smoothing and data reduction, reference can be made to Chapter XI of Ref. 1, while the differential correction technique is treated in Chapter VI of the same reference.

All navigational techniques mentioned have stringent data-processing requirements. Equations must be solved rapidly and accurately in order to support each technique.

The data processing could in principle be performed by analog computers, digital computers, or digital differential analyzers. Considerations of weight, volume, accuracy, and programming flexibility, however, preclude the use of the analog computer alone. For this reason, a navigational system must rely on digital data processors. The best compromise would appear to be a general-purpose digital computer capable of incremental computation for certain portions of the navigational problem. The mission duration anticipated for lunar flights requires a reliability sufficient for at least intermittent operation over long periods of time with a minimum of maintenance. Thus, the volume, weight, and secondary power available for the computer will necessarily be limited.

2. Tracking and Communications for Lunar Missions

The above discussion of navigation techniques illustrated the possibility of a vehicle in cislunar space performing the required navigational tasks independently of earth-based sensors. However, it remains extremely unlikely that ground monitoring, control, or coordination of a lunar mission for navigational or communication purposes will be dispensed with. This being the case, tracking of the spacecraft becomes a requirement for both manned and unmanned lunar missions. This subsection provides a qualitative description of tracking requirements for a typical lunar mission.

Since these requirements vary widely with the operational concept, a set of practical ground rules is needed. The following rules, illustrative of a typical lunar mission, have been established for the qualitative discussion of tracking:

(1) Launch is planned from Cape Canaveral, in anticipation that the majority of lunar missions will originate there.

(2) The launch azimuth A_e is restricted to between 70° and 110°, which is considered practical for the existing tracking facilities, range safety and launch tolerance requirements (see Chapter V).

(3) Parking orbits are permissible.

(4) The launch frequency must be twice a day.

(5) The return or re-entry (if applicable) is adequately tracked.

Detailed quantitative tracking data for a given set of ground rules is usually obtained as a by-product of the trajectory calculation.

The first three ground rules are effectively illustrated by Figs. 4 and 5, which show typical ground traces of circumlunar missions launched from Cape Canaveral for a southerly and northerly lunar declination. With regard to the fourth ground rule, a launch frequency of twice a day can only be realized if injection into the translunar trajectory is allowed to take place in either a southerly direction along the Atlantic Missile Range (AMR) area or in a northerly direction along the Pacific Missile Range (PMR) area. Figures 4 and 5 show how the ground trace corresponding to a particular lunar trajectory with a specified launch azimuth is replaced by a ground swath corresponding to the band of possible launch azimuths. These ground swaths cover a large part of AMR and PMR. Since launch tracking facilities must be provided in these areas, it can be assumed that re-entry (for circumlunar missions) also occurs there. In fact, for the ground swaths in Figs. 4 and 5, re-entry occurs along PMR and the landings in the western part of the U. S.

Lunar missions are similar to earth orbital missions in many respects, and therefore, present Project Mercury techniques developed for tracking and communications can readily be used. As mentioned previously, a logical assumption is that the overall coordination of the lunar mission will still be exercised by a ground control center. This control center will receive selected information concerning mission progress from the remote WTCN (Worldwide Tracking and Communications Network) stations during all phases of the mission and it uses this information to coordinate decisions and to advise and assist the vehicle if manned. Computational support for this control center is assumed to be provided by a computations and communications switching center (CCSC) such as exists at the Goddard Space Flight Center in Greenbelt, Maryland.

The CCSC computer determines trajectory parameters and steering corrections for normal or aborted missions and predicts the earth or lunar landing areas if applicable. WTCN stations exist at AMR and PMR in the Mercury Network, and as part of the DSIF (Deep Space Instrumentation Facilities). In addition, facilities are currently being planned for a primary landing site in southern Texas. An up-to-date list of the WTCN tracking facilities, their locations and a brief description is given in Chapter XI of Ref. 1.

In order to obtain an idea of tracking and communication requirements, a lunar mission is divided into several phases, as depicted in Figs. 4 and 5, and the requirements of each flight phase are briefly discussed.

During the launch phase and under direction of the ground control center, the CCSC computer predicts the boost phase trajectory, computes the look angles for the downrange radars, and transmits this data to the corresponding WTCN stations for use in vehicle acquisition. The vehicle boost phase is for the most part along the Project Mercury orbital mission range. These facilities are presently adequate to provide continuous tracking as well as voice and telemetry communications with the vehicle during the powered flight periods. Telemetry information is continuously collected at the ground stations with sufficient redundancy to minimize loss of data and obtain a smoothed trajectory from the many individual and overdetermining tracking observations. The ground control center also affirms the necessity for aborting the mission and in the case of an abort alerts the recovery forces for a manned mission. Injection into the parking orbit always takes place over an instrumented portion of the AMR, as the ascent range of "boosters" is small compared with the length of the AMR.

After parking orbit injection, the spacecraft waits for the proper moment to be injected into the translunar trajectory. For a northerly injection along PMR, this injection area varies from the vicinity of Australia to Hawaii. The actual injection point varies with the time of month and the launch time. To provide continuous tracking and monitoring during injection, it is very likely that additional tracking ships will be required to supplement the fixed site coverage along the PMR. The exact number will depend on launch azimuth variation, on injection requirements during the lunar month, on the operational concept and on the mobility of the tracking ships. If southerly injection along AMR is specified,

the same Project Mercury tracking range can be utilized. However, additional recovery forces may be required for manned missions in the event of an abort. It is also possible that additional tracking ships may be needed in this area, especially if the variable launch azimuth technique is used (see Chapter V).

Once the vehicle is injected into the translunar trajectory, its ground trace has the same general characteristics as indicated in Figs. 4 and 5. A very interesting feature of translunar and transearth trajectories is that for most of the mission, the ground trace will lie in a narrow band of almost constant latitude. This band will shift in latitude according to the time of month. In the above-mentioned figures, the maximum shift is from +35° latitude (northerly declination) to -35° latitude (southerly declination) under the present ground rules. This permits an easy plotting of the ground trace on maps using the Mercator projection. Another important and interesting characteristic of translunar and transearth trajectories is the "doubling back" or reversal of their ground traces. This characteristic is clearly shown in Figs. 4 and 5 and occurs within a few hours after injection and before re-entry. The reversal of the ground trace is due to the decrease of the angular velocity of the space vehicle with respect to the earth as it recedes from the earth (see Fig. 1 of Chapter IV), while the rotational rate of the earth about its axis remains constant. This becomes an advantage because the spacecraft will be overhead for a few hours when its angular velocity and the rotational rate of the earth are nearly the same, enabling continuous tracking at that time, which results in the determination of precise trajectory parameters.

During the translunar and transearth trajectory phases, the spacecraft is under continuous coverage by DSIF stations. They acquire and retain coverage from shortly after injection into a lunar trajectory until it returns to the vicinity of the earth (for a circumlunar trajectory) except for times when the vehicle is in the shadow of the moon. DSIF station coverage consists of two-way voice communications, telemetry and tracking, resulting in a steady updating of data and practically uninterrupted monitoring of mission progress. The ground control center, in turn, can refine the vehicle trajectory information and so inform a manned vehicle. Along the translunar and transearth trajectories, the CCSC computers systematically calculate and extrapolate the trajectory, and derive midcourse corrections. For a manned mission, these corrections are transmitted to the vehicle over a voice link for comparison with onboard navigational data. The onboard observations may provide the primary means of navigation, with ground-derived data providing redundancy, or vice-versa.

Since circumlunar and other lunar missions may involve passing behind the moon, and since the altitude and the predicted pericynthion point may be more accurately determined onboard than on the ground, data can be telemetered to earth just prior to occultation of the vehicle by the moon to permit ground computation of the trajectory so that the DSIF stations can reacquire the spacecraft when line of sight is re-established. Likewise, during lunar orbits, vehicle sensors gather lunar data continuously, store the data while behind the moon, and transmit when visible to DSIF stations. On the transearth trajectory, DSIF stations again continuously cover the vehicle, receive any backlog of telemetry data, and provide the CCSC computers with trajectory data and voice reports in case of an unmanned mission for comparison. Final course corrections will be made after tracking data from earth tracking facilities refine the computer predictions, and ground-derived data and corrections are transmitted to the vehicle.

For the case of a manned lunar landing, continuous telemetry information from the lunar investigations and, very likely, television pictures will be transmitted to earth. Positional data collected during the lunar stay will allow the CCSC computer to provide information via DSIF voice link for comparison with the onboard navigation system. Earth computation may be either a primary or a supplementary source of data during the lunar takeoff and transearth trajectory injections.

Since there is an obvious operational advantage in having all manned lunar missions re-entering over the same ground facilities, it is desirable that the re-entry phase of the transearth flight occur either in a northerly direction along PMR or in a southerly direction along AMR. In this case, AMR and PMR tracking stations, the southern USA tracking stations, and backup and alternate landing sites along the AMR and the PMR can be used. There should also be provisions for emergency takeoffs or aborts from the lunar surface with safe returns to earth, which could be made at any time. As in the case of lunar injection, ships may be required along the PMR to provide continuous tracking during re-entry. The ship locations for any given day are again determined by variations of the ground swath over the lunar month and the mobility of the tracking ships.

C. MIDCOURSE GUIDANCE AND ENERGY REQUIREMENTS

Sections A of this chapter and of Chapter IX give the required injection conditions near earth for lunar missions. A translunar trajectory injection is specified by particular values of time, V_0, γ_0, h_0, ψ_0 and i_{VTL} as defined in Section A above. But these nominal conditions cannot be achieved exactly because of injection guidance, navigation errors, and off-nominal booster performance. Therefore the actual translunar trajectory, as determined by the various navigation techniques, in all probability deviates from the desired or nominal trajectory, and thus may not satisfy the specific mission requirements. Hence, it becomes necessary that once or even several times during the flight to the moon, corrections be made to re-establish a trajectory that satisfies mission objectives. These corrections, more commonly called "midcourse guidance corrections," take the form of thrust impulses that adjust the actual or "errant" trajectory. Navigational observations and techniques as well as tracking and command from earth then serve as inputs which,

together with trajectory calculations, determine the magnitude and direction of the midcourse guidance correction.

In a general sense, there are two guidance concepts which can be used to correct the translunar trajectory:

(1) Correct the errant trajectory to the aim point, which may be the nominal pericynthion point at the nominal pericynthion time, or correct the errant trajectory to some other pericynthion point and time in the case of approach and circumlunar trajectories. For lunar impact trajectories, the aim point is at a specified distance in front of the moon, such as entry into the lunar volume of influence. This may be regarded as an explicit guidance scheme.

(2) Correct the errant trajectory back to the nominal trajectory (in position, velocity and time) some time prior to reaching the moon. This may be regarded as an implicit scheme.

The relative merits of these concepts are discussed below, together with some numerical data which was generated using a restricted three-body force model with the moon in a circular orbit at a radius of 60.32 earth radii except where noted otherwise.

1. Methods for Determining Midcourse Corrections

The problem of midcourse guidance is to compute the exact space vehicle velocity in an n-body force model (which for most cases of ballistic flight is sufficiently close to the actual trajectory as discussed in Section B, Chapter IV) for specified guidance objectives. Several approaches can be used, of which the following four are discussed below:

(1) A linear differential correction scheme utilizing a nominal trajectory and precomputed trajectory sensitivities which are assumed to be constant.

(2) A linear differential correction scheme utilizing trajectory sensitivities computed after launch (either on-board or on the ground).

(3) A corrective trajectory technique which designs a new trajectory that satisfies mission specifications by means of the same method used to design the nominal trajectory.

(4) A virtual mass technique utilizing two-body equations.

The first two methods involve the use of trajectory sensitivities. They are obtained by linearizing the nonlinear equations of motion by expanding in a Taylor series about a point of the trajectory and neglecting all but the zeroth and first order term. The coefficients of the first order term, which are the partial derivatives of trajectory parameters with respect to some such independent parameters as initial conditions, astronautical constants or time, are called trajectory sensitivities.

The first and best-known method used for determining the magnitude and direction of the midcourse correction is a linear differential correction scheme. In this scheme, a nominal translunar trajectory is assumed to satisfy all mission requirements, which in the case of a circumlunar trajectory consist of translunar inclination i_{VTL}, pericynthion altitude h_{PL}, inclination and orientation (i_m, θ_M) of the orbit about the moon, and the transearth inclination i_{VTE}. Due to injection errors, however, the actual trajectory will be displaced from the nominal, as shown below.

It is also assumed that the errant trajectory has been adequately determined by navigation or tracking before the point A_1 is reached. The point A_1 corresponds to a time t_1, after injection, when the midcourse correction is applied. Point A is the corresponding point on the nominal trajectory at time t_1 with B and B_1 being the points on the nominal and errant trajectory, respectively, at a time t_2, when it is desired to again "match" or intersect the nominal trajectory by a corrective trajectory. Since the errant trajectory is known prior to t_1 through tracking and celestial navigation, the generalized position and velocity coordinates of the errant trajectory q_B $\dot{q}_B$ can be predicted at time t_2. These coordinates are then

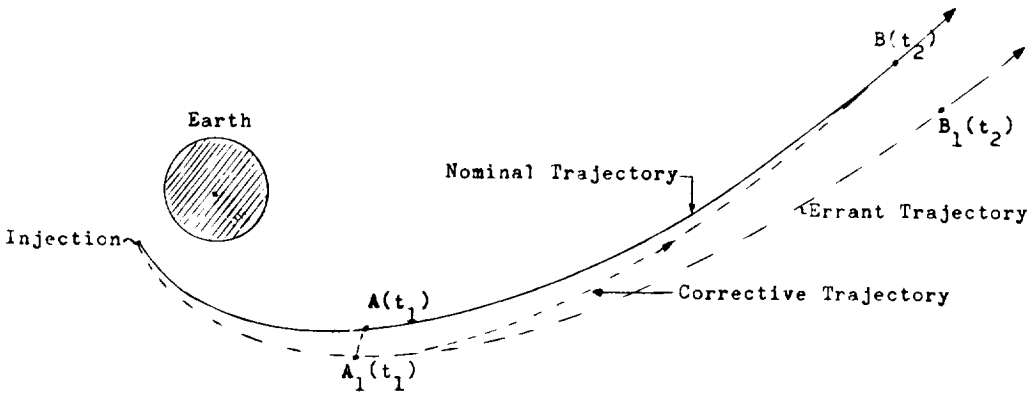

compared to those of the nominal trajectory at point B and the differences Δq_B, $\Delta \dot{q}_B$ are obtained.

A first approach to defining the magnitude and direction of the midcourse direction involves the determination of the change in position and velocity components of the nominal trajectory as a result of characteristic velocity perturbations $\Delta \dot{q}_A$ at point A by means of integrated trajectories using a three-body force model. These partial derivatives $\left(\frac{\partial q_B}{\partial \dot{q}_A}, \frac{\partial \dot{q}_B}{\partial \dot{q}_A}\right)$ are the trajectory sensitivites and are used in the following fashion to define the midcourse correction $\Delta \dot{q}_{iA}$:

$$\Delta q_{jB} = \sum_{i=1}^{n} \frac{\partial q_{jB}}{\partial \dot{q}_{iA}} \Delta \dot{q}_{iA} \quad j = 1, 2, \ldots, m$$

$$\Delta \dot{q}_{jB} = \sum_{i=1}^{n} \frac{\partial \dot{q}_{jB}}{\partial \dot{q}_{iA}} \Delta \dot{q}_{iA} \quad j = 1, 2, \ldots, m \qquad (26)$$

where j and i are integers denoting the coordinate directions. For the rotating rectangular coordinate system $x_R\ y_R\ z_R$ of the restricted 3-body problem discussed in Subsection B-2 of Chapter III, Eq (26) take the form:

$$\Delta x_{RB} = \frac{\partial x_{RB}}{\partial \dot{x}_{RA}} \Delta \dot{x}_{RA} + \frac{\partial x_{RB}}{\partial \dot{y}_{RA}} \Delta \dot{y}_{RA} + \frac{\partial x_{RB}}{\partial \dot{z}_{RA}} \Delta \dot{z}_{RA}$$

$$\Delta y_{RB} = \frac{\partial y_{RB}}{\partial \dot{x}_{RA}} \Delta \dot{x}_{RA} + \frac{\partial y_{RB}}{\partial \dot{y}_{RA}} \Delta \dot{y}_{RA} + \frac{\partial y_{RB}}{\partial \dot{z}_{RA}} \Delta \dot{z}_{RA}$$

$$\Delta z_{RB} = \frac{\partial z_{RB}}{\partial \dot{x}_{RA}} \Delta \dot{x}_{RA} + \frac{\partial z_{RB}}{\partial \dot{y}_{RA}} \Delta \dot{y}_{RA} + \frac{\partial z_{RB}}{\partial \dot{z}_{RA}} \Delta \dot{z}_{RA} \qquad (27)$$

In these three equations: the sensitivities $\frac{\partial x_{RB}}{\partial \dot{x}_{RA}}$, etc., are known from the ground-computed trajectories; the errors in position at the aim point, Δx_{RB}, etc., are known from the trajectory prediction; and the required midcourse correction at A ($\Delta \dot{x}_{RA}$, $\Delta \dot{y}_{RA}$, $\Delta \dot{z}_{RA}$) can be obtained. Application of the midcourse correction at A_1 results in a corrective trajectory which arrives at the aim point B with a velocity $\dot{q}_{jB} + \Delta \dot{q}_{jB}$ with components ($\dot{x}_{RB} + \Delta \dot{x}_{RB}$, $\dot{y}_{RB} + \Delta \dot{y}_{RB}$, $\dot{z}_{RB} + \Delta \dot{z}_{RB}$). This velocity is not necessarily equal to the nominal trajectory velocity $(\dot{q}_j)_{nominal}$ If it is desired to match the trajectory in velocity as well as position at B, the midcourse correction at B is given by $\left[\dot{q}_{j\ nominal} - (\dot{q}_{jB} + \Delta \dot{q}_{jB})\right]$.

The above approach tacitly assumes that the position errors at injection (not shown on the preceding sketch) are so small that they do not influence trajectory sensitivities and that the trajectory sensitivities at A are very nearly the same as those at A_1 and therefore can be computed on the ground before the mission. This assumption has been validated by numerical integration for expected small errors at injection. Numerical data embodying the linear differential correction scheme is presented in the next subsection.

The second approach does not make this assumption, and, therefore, sensitivities are computed while in flight for the midcourse correction point A_1 after the parameters of the errant trajectory have been determined by navigation and tracking. In both approaches trajectory sensitivities are obtained through the generation of integrated trajectories whose initial conditions are the slightly perturbed nominal conditions at t_1. This fact has led to the almost universal acceptance of the idea that a capability for numerically integrating the n-body equations, or at least the 3-body equations for lunar trajectories (Chapter IV), is required from a guidance computer in the space vehicle if the second approach is used.

A third method which may also be employed, consists of designing an entirely new corrective trajectory in the same manner as the nominal trajectory was designed to satisfy the mission constraints. This new corrective trajectory intersects the errant trajectory at point A_1, and it can be computed between injection and time t_2 by use of a perturbative scheme or an iterative scheme using a combination of n-body trajectories and the Voice technique. The midcourse correction is found very easily by determining the magnitude of ΔV_p and its direction necessary to reorient the errant velocity vector at A_1 to the corrective trajectory velocity vector at the same point.

A midcourse guidance scheme for cislunar space has been developed which would alleviate the demands for computers in the space vehicle (Ref. 6). The scheme uses modified 2-body trajectories to simulate n-body velocities by introduction of a

virtual mass into the earth-moon system which changes the earth's mass and relocates the barycenter. The use of the simple and inaccurate 2-body equations paradoxically permits an operational flexibility which cannot be attained so easily by numerically integrated 3-body and n-body trajectories due to the extreme sensitivity of trajectories to initial conditions.

The virtual mass technique essentially depends upon computing 2-body trajectories relative to a force center defined by the combined earth and virtual mass. The location of this force center is selected so that the plane, defined by the force center and points A and B, coincides with the initial n-body trajectory plane at A (as defined by the radius and velocity vectors relative to the force center). This force center is on the earth-moon line and lies between the center of the earth and the earth-moon barycenter. It represents an origin which defines the location for a Keplerian central mass that properly accounts for the out-of-plane distortion (drift) of the true trajectory (Chapter IV, Subsection A-8). The magnitude of the mass, or the strength of the central force field, must be adjusted so that the position and velocity at t_1, corresponding to measurement from the force, define a trajectory which in fact passes through the aim point B. This technique of "biasing" the gravitational constant to account for the in-plane and out-of-plane distortion of course means that the flight time will differ from the actual time and must itself also be biased.

Thus, by knowing the position and velocity components of point B at t_2 in this biased reference frame, the velocity vector required at A_1 to intercept B can be found by 2-body equations. This velocity vector is then compared to the actual velocity vector at A_1 and the direction and magnitude of the midcourse ΔV_p can be readily obtained. Preliminary analyses indicate that this biasing is independent of i_{VTL}. A compact catalogue of virtual masses (location and magnitude) and time biases as a function of the time of the month can be prepared in advance for use during the mission. The virtual mass approach is a welcome step toward simplicity in determining guidance corrections and can be used as the primary method or as a manual backup for lunar missions.

2. Guidance Concepts

a. Guidance concept 1

Guidance concept 1 consists of correcting the errant trajectory to the nominal pericynthion point at the nominal pericynthion time--or correcting the errant trajectory to some other pericynthion point and time.

This concept suggests the use of the pericynthion position at t_2 as an aim point, which appears desirable since full advantage is taken of the focusing effect of the moon (Chapter IV, Subsection A-8). However, consideration must be given to the direction of flight at the pericynthion point as well. Discussion of this facet of the problem is simplified if reference is made to the geometry of the lunar approach trajectory and the resulting lunar orbit as shown by the sketch in Section A page 4 of this chapter. The sketch shows the moon, the direction to earth (MEL) when the spacecraft reaches pericynthion, and the resultant lunar orbit if the spacecraft were injected into orbit at pericynthion with a retarding velocity impulse ΔV. The orientation of the resultant lunar orbit is specified by the inclination i_m to the moon's orbital plane and the angle θ_M between the earth-moon line and the descending node. The pericynthion point is specified by β_M, which is the orbital central angle measured positively toward the north from the descending node of the lunar orbit.

The nominal translunar trajectory will have a specific i_m, θ_M, and β_M associated with it. A single midcourse correction to an errant trajectory (a t_1 = 3 hr after injection, for instance) cannot result in arrival at the moon with the same i_m, θ_M, and β_M. Any single impulse technique can be expected to fix one of the quantities, but not all three. The guidance concept under consideration fixes the pericynthion point. The resultant i_m and θ_M cannot be matched without the addition of another velocity impulse at pericynthion. Yet, the correct i_m and θ_M is necessary. If the mission is circumlunar, an error in any of the required characteristics will result in an error in both vacuum perigee altitude and transearth trajectory inclination i_{VTE} at vacuum perigee. The total mission flight time will also be affected. If it is a lunar orbit mission, the desired lunar orbit would not be attained. This has more serious implications than the immediate situation mentioned. If it were a lunar landing mission, the resultant orbit would not go over the desired landing site. For illustrative purposes a completely ballistic circumlunar trajectory with i_{VTL} = 63.3°, h_{PL} = 463 km and h_{PE} = 45.720 km is used.

The injection velocity errors are based on typical standard deviations (1σ values) as given here in x_v, y_v and z_v coordinates, respectively, where z_v is in the direction of the local vertical, x_v along the local horizontal in the flight direction, and y_v completes the right-handed Cartesian coordinate system by defining a lateral direction normal to the trajectory plane.

σ_x = 0.46 m/sec

σ_y = 0.34 m/sec

σ_z = 2.4 m/sec

These errors are used for the remainder of the discussion and are combined in various ways to yield a total velocity error, at injection, with a 99% probability.

In this example the total injection velocity errors in the rotating trajectory coordinate system $x_R y_R z_R$ become

$$\Delta\dot{x}_R = 1.18 \text{ m/sec}$$

$$\Delta\dot{y}_R = 0 \text{ m/sec}$$

$$\Delta\dot{z}_R = 5.23 \text{ m/sec}$$

which are the same as those used in the third sketch below.

Trajectory sensitivities are determined for $t_1 = 3$ hr and the first adjustment method is used to calculate that a midcourse correction $\Delta V_p = 7.3$ m/sec is required to correct to the nominal pericynthion point and time. The second correction, to reorient the velocity vector along the nominal trajectory, was $\Delta V_v = 13.7$ m/sec at pericynthion, and the total required $\Delta V_{TOT} = 21.0$ m/sec.

A feature of this concept which is somewhat expensive in fuel is the reorientation of the velocity vector to the desired direction at the aim point. This disadvantage can be eliminated, or almost eliminated, by changing the aim point to a new pericynthion position.

A large amount of data has been assembled in the present chapter and Chapter IX showing the relationships between the lunar orbit orientation (θ_M and i_m) and pericynthion point position β_M. The data are presented as a function of i_{VTL} for approach trajectories (Chapter IX) and as a function of i_{VTE} and i_{VTL} for circumlunar trajectories which return to a specific vacuum perigee (Section A). A curve of required θ_M versus i_m can be determined as demonstrated in the sample mission I of Chapter XI (also Section A of Chapter XI). This data then fixes the i_{VTE} for circumlunar flights and consequently β_M (see Section D Chapter XI). The required θ_M and i_m curve can be obtained directly if a constant i_{VTE} is desired. Trajectories that do not return to a specific and safe vacuum perigee (Chapter IX) have a pericynthion position that varies with translunar flight time for a given $i_m - \theta_M$ relationship. Thus, the corrected trajectory can be aimed at a new pericynthion point that satisfies the $i_m - \theta_M$ conditions. It must be remembered that, in general, a velocity correction is still required at this point.

This technique was used to correct the errant trajectory above. Again, midcourse corrections at 3 hr after injection were made along the velocity vector $\vec{V}_{\oplus\Delta}$, normal to the velocity vector in the plane of $\vec{r}_{\oplus\Delta}$ and $\vec{V}_{\oplus\Delta}$ (relative to earth) and a correction normal to this trajectory plane. These corrections will be referred to as $\Delta V_{\oplus\Delta}$, $\Delta\gamma$, and Δi, respectively.

It was found that $\Delta V_{\oplus\Delta}$ changed h_{PL} efficiently, but not i_m or θ_M. On the other hand, $\Delta\gamma$ changed i_m and θ_M, but did not change h_{PL} effectively. The Δi correction changed all of the pericynthion conditions, but not always in the correct directions or proportions. Therefore, a combination of $\Delta V_{\oplus\Delta}$ and $\Delta\gamma$ corrections was used in the midcourse maneuver, plus another correction at the new pericynthion point. The total velocity impulse required ΔV_{TOT} was approximately 10.7 m/sec, compared to the 21.0 m/sec correction of the first approach above. Percentage-wise the differences in the two techniques may be large at times but in magnitude the differences may be wholly acceptable.

However, some difficulty may be encountered in determining the required midcourse maneuver. It has been shown analytically (Ref. 7) that the lunar miss distance or pericynthion is a linear function of the injection errors for an infinitesimal lunar mass (massless moon assumption). However, if the finite lunar mass is considered (patched conic or restricted 3-body technique), then the miss distance is related quadratically to the injection errors. It follows that for the linear trajectory sensitivities generated for conditions near the moon, a certain amount of cross-coupling in the sensitivities can be expected. This can be handled either by taking second-order terms in the Taylor series expansion or by repeated (and hopefully convergent) iteration by improved guesses at sensitivities. This cross coupling has indeed been noted in the above numerical example. The injection errors are large enough that the required midcourse correction was not readily obtained, in fact, a minimum of three iterations were required to obtain a satisfactory midcourse correction at the 3-hr point.

The following table shows a comparison between the linear differential correction scheme (methods one and two in Subsection C-1) and the third method for determining midcourse corrections in Subsection C-1, wherein a corrective trajectory is designed by use of the Voice technique (Chapter IV, Section C) and n-body force model trajectory calculations in conjunction determining the midcourse corrections. The trajectory under consideration is a circumlunar trajectory with the desired mission requirements noted in Table 3. The errant trajectory fulfills all the requirements satisfactorily except for the return vacuum perigee altitude. A hypothetical case is taken for which it is assumed that the mid course correction takes place at the injection point. When the linear differential correction method without iterations was used, the obtained return perigee altitude was completely unacceptable and the pericynthion altitude was less satisfactory. However, use of the Voice technique and n-body trajectory calculations for obtaining the necessary correction, the resultant return perigee altitude becomes acceptable and all other mission parameters remain essentially the same. One trajectory can of course not be used as the basis of a final conclusion. However, together with the results of Egorov for impact trajectories (Ref. 7), the third method seems superior to the first two for the case of circumlunar trajectories,

TABLE 3

Comparison of Various Midcourse Guidance Schemes
for a Typical Circumlunar Trajectory

Trajectory Variable	Mission Requirements	Errant Trajectory (n-body)	Corrected Trajectory (linear diff. correct.) (n-body)	Corrected Trajectory (iteration with Voice) (n-body)
V_0 (injection velocity) (m/sec)		10,963.736	10,963.756	10,963.786
γ_0 (injection flight angle) (°)	2.668174	2.668174	2.668174	2.668174
h_0 (injection altitude) (km)	182.88	182.88	182.88	182.88
ψ_0 (injection position) (°)		13.9936314	13.1875706	13.1986777
i_{VE} (translunar inclination) (°)	29.24953	29.384214	29.383332	29.382176
i_{VTEQ} (transearth inclination) (°)	35.206	35.098407	35.566	35.386665
t_p (time to pericynthion) (hr)		73.734375	73.734	73.64034
T (total mission time) (hr)		147.101562	150	147.07816
h_{PL} (pericynthion altitude) (km)	185.0148	185.2000	173.1620	186.8668
h_{PE} ($^{\text{return vacuum}}_{\text{perigee altitude}}$) (km)	36.8061	215.4936	-1402.080	37.5
Φ^* (moon lead angle) (°)		37.4512316	38.038309	38.0294507

when the trajectory passes from a earth-dominated gravitational field to a moon-dominated gravitational field and back again. It should be noted that the return vacuum perigee, i.e., when the vehicle passes through all three gravitational regions, is hardest to obtain by a linear differential correction scheme.

b. Guidance concept 2

Guidance concept 2 consists of correcting the errant trajectory back to the nominal trajjectory (in position, velocity and time) sometime prior to reaching the moon (Ref. 8).

Two approaches may also be used in implementing this concept with the linear differential correction scheme. Either the midcourse correction can be made to return to the nominal trajectory as soon as possible (a truly explicit scheme) or to return to the nominal trajectory at some prearranged point and time. Ideally, either of these midcourse corrections is made in two parts. The first, at t_1, is a velocity impulse which will return the spacecraft to the nominal trajectory at a specific point and time t_2. The second correction is made at t_2, to reorient the spacecraft's velocity vector along the nominal velocity vector. The velocity impulses required are referred to as ΔV_p, the first impulse to correct position, and ΔV_v, the second impulse to realign the spacecraft trajectory along the nominal trajectory.

The graphical data shown below is presented in a manner that allows a quick understanding of the orders of magnitude involved and of the efficiency of this concept.

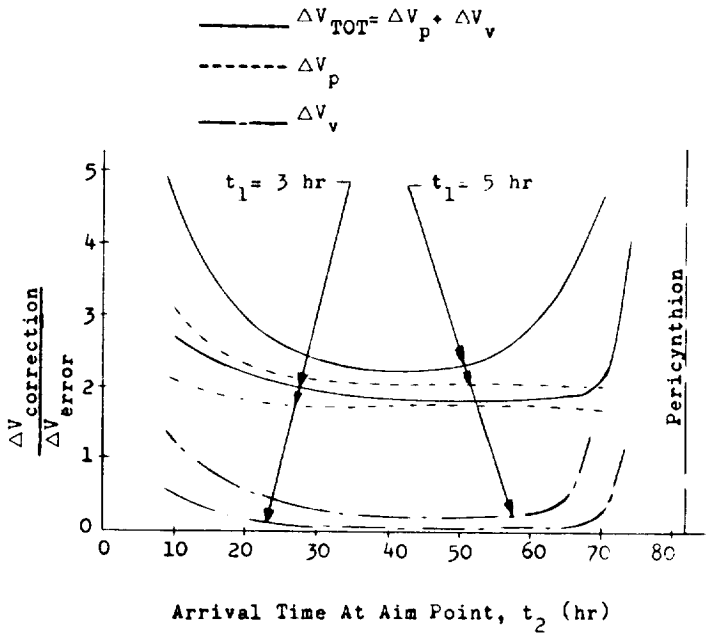

For this example, the nominal circumlunar trajectory has h_{PL} = 1852 km and an i_{VTL} = 9.1° at injection. The injection error is only in velocity. This error was applied in arbitrary directions, but only one set of typical data is presented. ΔV_p, ΔV_v and their sum ΔV_{TOT} per velocity error are shown as a function of arrival time t_2 on the nominal trajectory. The curves are shown for the midcourse correction being made at t_1 = 3 hr and at t_1 = 5 hr after injection.

For the effect of i_{VTL} at injection on the midcourse requirements, several trajectories have been investigated. All nominal trajectories are circumlunar, returning ballistically to a vacuum perigee of h_{PL} = 45.7 km, with h_{PL} = 463 km. The i_{VTL} of the trajectories is varied from 30° to 63.3°. The effect of i_{VTL} on midcourse requirements is shown below. The error conditions noted are for the most extreme cases encountered, and the coordinate system is that previously presented for the 1σ errors. Only ΔV_{TOT} is shown, and the initial midcourse correction ΔV_p has been assumed at t_1 = 3 hr.

This example typifies the differences between the first and second concepts. The first correction, ΔV_p, decreases as the aim point gets closer to pericynthion. The second correction, ΔV_v, increases as the moon is approached, a trend which becomes more severe with increasing values of i_{VTL}. In comparison, this concept requires a ΔV_{TOT} = 7.9 m/sec which is 25 to 60% less than required in the first concept.

The obvious points of the above figures are that:

(1) Delay in the midcourse correction results in increased propulsion requirements.

(2) The required correction is greater when the inclination of the translunar trajectory plane (at injection) is increased.

(3) For this concept, the best aim point on the nominal trajectory is approximately 75,000 km before reaching the moon.

Finally, most midcourse adjustment methods are readily adaptable to this guidance concept.

c. Midcourse guidance accuracy requirements

Several questions arise regarding midcourse guidance:

(1) How accurate must be the navigational position and velocity determinations or the tracking of the vehicle from the earth and moon?

(2) How accurately can the errant and corrective trajectories be predicted to the aim point?

(3) How accurately must the magnitude and orientation of the corrective velocity impulse be controlled in order to achieve the desired corrective trajectory?

$\Delta \dot{x}_R$ = .70 m/sec

$\Delta \dot{y}_R$ = .51 m/sec

$\Delta \dot{z}_R$ = 6.20 m/sec

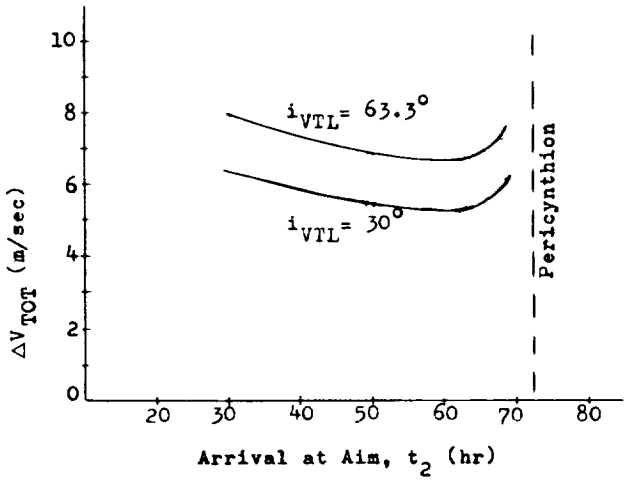

$\Delta \dot{x}_R$ = 1.18 m/sec

$\Delta \dot{y}_R$ = 0

$\Delta \dot{z}_R$ = 5.23 m/sec

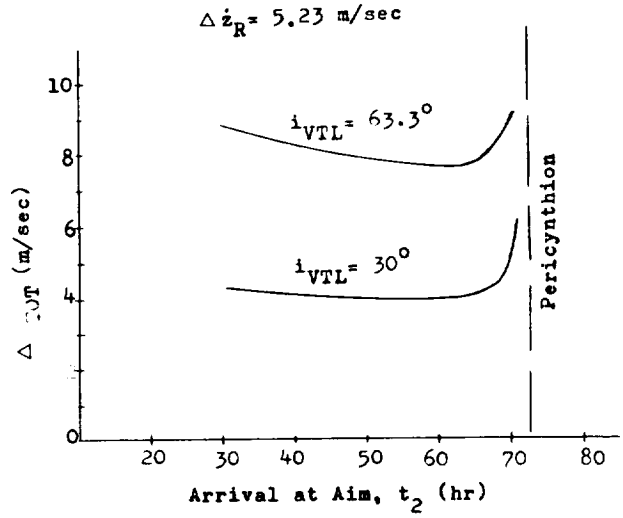

Again, since numerical values of position determination differ widely with the particular tracking and navigational equipment used, since the prediction depends on the force model and constants used in the trajectory simulation, and since the corrective velocity impulse depends on rocket engine characteristics, no quantitative results will be given.

A brief account of observational accuracies and some results of one navigational technique have been presented in Subsection B-1. Tracking by electronic means depends on the type of

measurement made by the equipment, i.e., range, azimuth, elevation, photography against the star background, range measurements from several stations, etc., and on the accuracy of each individual tracking measurement. Usually, many measurements are taken, thus overdetermining the trajectory of the vehicle. The random errors can then be minimized by some smoothing technique which results in a trajectory which is better than one derived from the minimum number of tracking observations. Equipment bias errors, station location errors and atmospheric refraction errors (if the tracking is from earth) cannot be removed in this fashion but may be isolated by many observations with the tracking equipment in question. A more quantitative discussion of tracking equipment and smoothing techniques can be found in Chapter XI of Ref. 1.

The problems in trajectory simulation have been discussed in Section B of Chapter IV, and numerical comparisons between results obtained by use of several simple force models are scattered throughout the Handbook, most recently in Section A-2 of the present chapter.

The control of the corrective velocity impulses ΔV_p or ΔV_v depends on the thrust level of the rocket motor used for midcourse guidance, the burning time required to achieve the desired ΔV_p or ΔV_v, the accuracy of the accelerometers which control the thrust as well as the roundoff and truncation errors of the computer integrating the thrust acceleration to obtain ΔV_p or ΔV_v. These aspects have been discussed quantitatively in Chapters VI and XII of Ref. 1, and only a very brief description will be given here. The magnitude of the velocity impulse can be controlled by two different methods, with representative errors in each technique.

(1) Monitor propulsive inputs, a technique which attempts to control each of the propulsive parameters contributing to the velocity increment. The errors depend on the rocket engine control system and engine and fuel characteristics. Typical errors are:

Burning time	$\Delta t_b = 0.030$ sec
Mass flow rate	$\Delta M_f = 0.005\ M_f$
Specific impulse	$\Delta I_{sp} = 0.004\ I_{sp}$
Initial mass	$\Delta M_0 = 0$

(2) Monitor the velocity increment directly, a technique requiring accelerometers and integrating computers. This system is more appropriate for the small midcourse corrections to be made; it has a typical error of $\Delta(\Delta V) = 10^{-4}\ \Delta V$ in the increment itself and $\Delta t_b = 0.030$ sec in shutdown time.

The individual midcourse velocity impulse can be controlled to within 0.01 to 0.1 m/sec by a conventional midcourse propulsion system. More accurate control is not necessary, but could be achieved by unconventional propulsion systems.

The directional control of ΔV_p and ΔV_v is not as critical since these velocity impulses are very small compared to the vehicle velocity vector V_Δ. Directional control of the thrust vector to within 1 to 5° from the nominal is considered sufficient in most cases, which can be achieved by a rudimentary attitude control system based on navigational observations.

If the navigational observations for position determination are in error, and the trajectory has not been determined or predicted accurately enough, or the midcourse velocity correction is in error, multiple midcourse corrections are required. These are not discussed here. However, additional data on nominal transearth midcourse guidance requirements will be given in Section B of Chapter IX.

D. TRANSLUNAR ABORT

In the translunar trajectory phase of a lunar mission, the vehicle is assumed to be in a ballistic two-body trajectory in the general direction of the moon. If a malfunction occurs on an unmanned mission which jeopardizes it or causes a mission failure, usually little action will be taken. However, if an emergency such as a solar flare or a meteoritic penetration occurs on a manned mission, it is abandoned and a turnaround or abort maneuver is performed to return the crew safely back to earth. This abort maneuver uses rocket burning to establish an abort trajectory with a prescribed vacuum perigee altitude and re-entry angle, within the safe re-entry corridor of the spacecraft. The essential parameters in such a maneuver are the propulsion requirements, the point along the translunar trajectory at which the abort is executed, and the eccentricity of the translunar trajectory. These parameters affect very strongly the time to return to earth and the possibility of landing at a preselected site.

In this section, requirements for abort maneuvers which result in the safe recovery of the vehicle will be presented. A simple method of obtaining acceptable return trajectories will be given in the first part. The problem of reaching preselected landing sites will then be discussed together with a consideration of aborts that occur both in and out of the plane of the initial trajectory. Finally, the requirements for establishing abort way-stations along the nominal trajectory will be discussed.

Only abort maneuvers initiated after injection and before the vehicle reaches a distance of approximately 200,000 km from earth will be considered. Beyond this distance, the effect of the moon begins to play a major role in determining the translunar trajectory, and the two-body trajectory assumption will no longer be accurate enough.

1. Abort to the Vicinity of Earth

In order to obtain a general idea of the requirements of the turnaround problem, several assumptions are made which simplify the calcu-

lations but allow the various parameters of interest to be found with sufficient accuracy. These assumptions are:

(1) The model used for translunar and abort trajectories is a restricted two-body model, i.e., a vehicle of negligible mass moving in the central force field of a spherical earth. This allows the use of constant orbital elements for the description of these trajectories.

(2) The abort maneuver consists of a single velocity impulse, ΔV_A.

(3) The translunar and abort trajectories are confocal and have a perigee radius of 1 ER (earth radius).

(4) Radiation belts are ignored.

The first concern is to determine ΔV_A requirements for abort together with the time to return to earth when performing abort maneuvers. Before this can be done, the velocity V_T and flight path angle γ_T must be known for any point along any translunar trajectory. In a system of units which measures the distance from the earth R in earth radii, and $\mu_\oplus = 1$ is the gravitational constant of the earth, the resulting normalized velocity is expressible as:

$$V = \left[\frac{2}{R} - (1 - e_T)\right]^{1/2} \qquad (28)$$

where e_T is the orbital eccentricity of the translunar trajectory.

The flight path angle γ, which is measured from the local horizontal to the velocity vector, may be found by use of the following equation:

$$\gamma = \cos^{-1}\left[\frac{(1+e_T)/R}{2 - R(1-e_T)}\right]^{1/2} \qquad (29)$$

Next, the limit of allowable eccentricities for the abort trajectories is required. For one constant and continuous band, an abort eccentricity $e_A = 1$ is arbitrarily selected. Actually, this may be interpreted as a design limit and will be referred to as such. For a given distance from earth and a required perigee altitude, the minimum e_A obtainable is realized when the semi-major axis a_A is as small as possible. This requires that the radius at abort, R_A, is the apogee, and, by assumption 3, above,

$$a_A = \frac{R_A + 1}{2}. \qquad (30)$$

The resulting equation for the minimum allowable eccentricity is:

$$(e_A)_{min} = \frac{(R_A - 1)}{(R_A + 1)}. \qquad (31)$$

Figure 6 shows an envelope of allowable return eccentricities as a function of distance from the earth. There is actually no real upper limit above $e_A = 1$ provided that a proper negative abort flight path angle γ_A is achieved.

Knowing the orbital elements of the translunar trajectory and the required abort eccentricity, both the translunar trajectory conditions prior to abort (V_T, γ_T) and immediately after the maneuver (V_A, γ_A) are easily found.

The time to return to earth along any of the allowable orbits is computed with the classic two-body time equations of Ref. 1 and the results are shown in Fig. 7. This plot is true regardless of the eccentricity, e_T, of the translunar trajectory and shows the return time as a function of the allowable e_A for any R_A.

The time to return may be altered for a given ΔV_A if the abort maneuver is such that the abort trajectory plane is different from the translunar plane. This is referred to as a "change in azimuth" and the consequences of such a maneuver are described here.

The change in azimuth ΔA is the angle between the original translunar trajectory plane defined by $\vec{R}_T$ and $\vec{V}_T$ or the $x_v y_v$ plane and the trajectory plane defined by $\vec{R}_A$ and $\vec{V}_A$.

Taking the dot product of the initial and final velocities, $\vec{V}_T \cdot \vec{V}_A$, the angle ϵ between $\vec{V}_T$ and $\vec{V}_A$ is obtained as

$$\epsilon = \cos^{-1}\left[\sin\gamma_T \sin\gamma_A + \cos\gamma_T \cos\gamma_A \cos\Delta A\right].$$

Thus, for a given γ_T and γ_A, ϵ increases with ΔA.

From the law of cosines,

$$(\Delta V_A)^2 = V_T^2 + V_A^2 - 2V_T V_A \cos\epsilon$$

it is seen that as ϵ increases, the required velocity impulse also increases for a given V_T and V_A. Therefore, for given initial conditions of V_T and V_A and a specific time to return, any change in heading will result in an increase in the required maneuvering impulse ΔV_A.

Figure 8 shows the ΔV_A needed to perform the abort maneuver at various distances from the earth without changes in heading. $A(+\gamma_A)$ in Figs. 7 and 8 indicates the region where, after the abort maneuver, the flight path angle is positive, and $(-\gamma_A)$ is the region where the final flight path angle after abort is negative. For positive values of γ_A, the spacecraft must pass

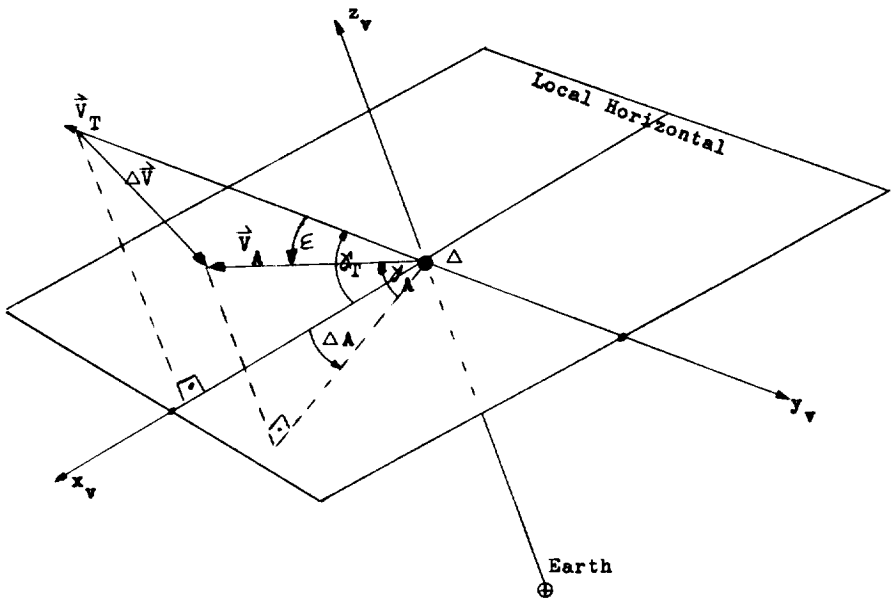

through the apogee of the abort trajectory prior to returning to earth and perigee, while for the latter case, the spacecraft returns directly to the perigee of the abort trajectory. However, for obtaining a specific perigee latitude and longitude it may be more efficient, timewise, to maneuver out of the initial trajectory plane. This is demonstrated later in the section. The data given in Fig. 8 applies for $e_T = 1.0$. For $e_T < 1.0$ the ΔV_A required to return to earth in a given time also decreases. In fact, the ΔV_A is reduced by 10 to 15% if e_T is lowered from 1.0 to 0.98.

2. Abort to Preselected Landing Sites

Even during emergency situations, the problems of recovery might be reduced by the use of preselected landing sites. The results of performing in-plane abort maneuvers that return to a given perigee longitude will be presented in this section. They were obtained by using classical two-body results and by assuming that the abort maneuver is characterized by an impulsive change of velocity ΔV_A at a distance R_A (in earth radii) from earth.

The nominal translunar trajectory prior to the abort maneuver used as an example is elliptical with injection at perigee $h_0 = 45.720$ km, $V_0 = 11,055.1$ m/sec, corresponding to an eccentricity $e_T = 0.9668$. This ellipse has an apogee radius approximately equal to the moon's average orbital radius of about 60 ER and an inclination $i_{VE} = 36.5°$ to the equator.

Figure 9 presents the necessary information to estimate return perigee longitudes for various values of ΔV_A and R_A. The right-hand side of Fig. 9 shows the return time (time from the abort maneuver to return perigee which is also at $h_{PE} = 45.720$ km) as a function of R_A and ΔV_A. The left-hand side of the graph converts the return time into the longitude of abort trajectory perigee relative to the translunar trajectory (injection) perigee with the assumption that the latitude of the translunar trajectory perigee is equal to the latitude of the abort trajectory perigee. This assumption results in the removal of orbital inclination from the problem. However, the inclination and injection perigee latitude enter indirectly when the return perigee longitude is chosen. For example, assume that the injection latitude is 16.5° S and it is desired to land in Australia after an abort from a southeasterly launch from Cape Canaveral. This launch azimuth results in an approach to Australia from the northwest. Therefore, return perigee longitudes somewhat to the west of Australia are desirable.

Figures 10 and 11 have been obtained from Fig. 5 for three typical situations. Figure 10 shows ΔV_A and return time for abort maneuvers at various values of R_A with the requirement of landing in Australia. The injection perigee longitude and latitude are taken as 8.8° W and 16.5° S, which is representative for lunar launches from Cape Canaveral. The longitudes used for landings in Australia reflect an approach from the northwest. Figure 10 denotes the number of revolutions the earth has made (i.e., the number of sidereal days) before re-entry takes place, and the shaded band represents the width of the Australian continent.

Figure 11 presents the same information for landing in the United States and off the west coast. The injection perigee is assumed to be directly over Edwards Air Force Base which is representative of a lunar launch from Cape Canaveral on a trajectory inclination to the earth's equator of $i_{VE} = 35°$ with a parking orbit prior to injection. The selection of return perigee longitude depends on the aerodynamic maneuvering capability of the lifting body re-entry vehicle, which is nearly tangent to the landing site latitude.

Therefore, four possible return perigee longitudes have been shown in Fig. 11. Perigee at 170° E longitude is representative of a return to Edwards Air Force Base with 7200 km of re-entry glide range. The other extreme would be a return perigee longitude at the east coast of the United States. This would represent the minimum re-entry that could still remain within the boundaries of the United States. The much wider selection of return times compared to the Australian landings is apparent. This is due primarily to the fact that re-entry longitudinal maneuverability can be used to extend the choice of return perigee longitudes.

Subsection D-1 mentioned abort maneuvers that result in an abort trajectory out of the translunar trajectory plane. The discussion below demonstrates the feasibility of performing an abort maneuver with a change in azimuth ΔA resulting in reduced return flight times to reach a specific landing site.

In order to obtain representative data, a typical translunar trajectory was selected from which abort maneuvers were conducted in and out of the translunar plane at various distances from earth. The landing site is Edwards Air Force Base and the translunar trajectory is characterized by the following injection conditions:

Velocity	V_0	10,907 m/sec
Altitude	h_0	231.953 km
Flight Path Angle	γ_0	3°
Longitude	λ_0	165° west
Latitude	ϕ_0	26.35° north
Orbital Inclination	i_{VE}	35°
Orbital Eccentricity	e_T	0.9728

Results are presented in Fig. 12 which give the time-to-return from an abort as a function of R_A and ΔA for abort and translunar trajectories. The translunar (nominal) trajectory represents a no-maneuver condition and just gives the time to complete a circumlunar mission as a function of R on the translunar portion of the trajectory. The time-to-return from an abort maneuver depends on whether one particular landing site is desired, or a number of sites are available or simple earth return is sufficient. In the last case, it has been shown that the least ΔV_A is realized when the abort maneuver occurs in the nominal translunar trajectory plane. Figure 12 also gives the absolute minimum return time to earth for the values $(\Delta V_A)_{max} = 549$ m/sec and $(\Delta V_A)_{max} = 1829$ m/sec illustrating that simple earth return requires less time than return to a specific site.

If return to a particular landing site such as Edwards Air Force Base is desired, then the arrival must be timed correctly because of the earth's rotation. The step functions on Fig. 9 represent the minimum time to return to Edwards Air Force Base for variable values of $\Delta V_A \leq (\Delta V_A)_{max}$ and show the timing problem for two values of $(\Delta V_A)_{max}$ for abort trajectories with $\Delta A = 0°$, $\Delta A = 10°$ and $\Delta A = 20°$. The return times for out-of-plane abort to Edwards Air Force Base are in certain cases less than for in-plane aborts. The intersections of the out-of-plane step functions with the absolute minimum time curves in Fig. 12 denote these cases, and near these intersections the planar change ΔA should be decreased for increasing R_A to maintain minimum return times. As these intersections on the "return-to-Edwards" curves are approached, an increasingly larger ΔV_A is required and at the point of intersection the total available ΔV_A or $(\Delta V_A)_{max}$ is used for abort.

The data in Fig. 12 indicates that definite benefits may be gained in performing abort maneuvers out of the translunar trajectory plane when landing at a specific site is required. Reductions in time-to-return of up to 5 hr over the in-plane returns can be realized for Edwards Air Force Base landings. If several landing sites are available the time to return could be reduced further. The restriction imposed by available tracking facilities has so far been ignored (see Subsection B-2). Since abort maneuvers out of the nominal trajectory plane change the abort trajectory inclination, the capability to track the vehicle during re-entry from existing facilities must be re-examined.

A point not illustrated in Fig. 12 is that the total time from the translunar abort decision to re-entry, t_R, for landing at a particular site is the same for a large range of ΔV_A up to $(\Delta V_A)_{max}$, since for a successful abort the landing site which rotates with the earth must be near the abort trajectory plane. It does not matter whether the entire t_R is spent in an abort trajectory with a lower ΔV_A or whether part of it is used in reaching a point on the translunar trajectory where $(\Delta V_A)_{max}$ is used for the abort maneuver and the rest on the abort trajectory. This characteristic of translunar aborts to a given landing site suggests the selection of specific points or "abort way-stations" along the translunar trajectory for abort maneuvers, from which the vehicle can acquire the landing site with a fixed value of ΔV_A. "Abort way-stations" allow the use of abort trajectories which can be precomputed on the ground prior to the lunar mission. However, they represent the least efficient abort maneuver from a standpoint of fuel requirements (i.e., the maximum value of ΔV_A is used for a given time to return). More material on way-stations is presented in the next subsection.

3. Abort Way-Stations

A method for obtaining abort way-stations, or points on the nominal translunar trajectory from which precomputed abort trajectories characterized with a fixed value of ΔV_A can be used, has been presented by Kelly and Adornato (Ref. 9). The method as described briefly in the present subsection is a modification of the one used in Ref. 9.

The following sketch illustrates the geometry of translunar abort with return to a specific landing site.

Assume a restricted two-body force model for the translunar and abort trajectories, and assume that they are in a common plane ($\Delta A = 0°$). If we include the re-entry trajectory into the calculation, then an abort way-station as defined above must satisfy the following four constraints:

(1) Abort trajectories from the way-station must have acceptable flight path angles γ_R at re-entry:

$$\gamma_{min} \leq \gamma_R \leq \gamma_{max} \qquad (32)$$

(2) Referring to the previous sketch, let 0 denote the vehicle and C the position of the landing site at translunar injection, let A denote the abort maneuver, B the location of the vehicle and landing site at re-entry and L, f the coinciding positions of the landing site and space vehicle, respectively, at vehicle touchdown. In addition, a double subscript notation is introduced for time, i.e., Δt_{0-A} is the time for the space vehicle to travel from translunar injection to abort and Δt_{B-L} the time for the landing site to rotate with the earth from B to L. With this notation, the first abort way-station imposes the following time constraint.

$$\Delta t_{0-A} + \Delta t_{A-B} + \Delta t_{B-f} = \Delta t_{C-B} + \Delta t_{B-L} \qquad (33)$$

However, since the landing site rotates with the earth, it will be in the trajectory plane at the same location L once in each sidereal day (1 sidereal day = 86164.1 sec = $23^h\ 56^m\ 4^s.1$) as long as the latitude of the landing site is less than the trajectory inclination. Thus, further abort way-stations are characterized by

$$\Delta t_{0-A} + \Delta t_{A-B} + \Delta t_{B-f} = \Delta t_{C-B} + \Delta t_{B-L} + (n-1)\ 86164.1 \text{ sec} \qquad (34)$$

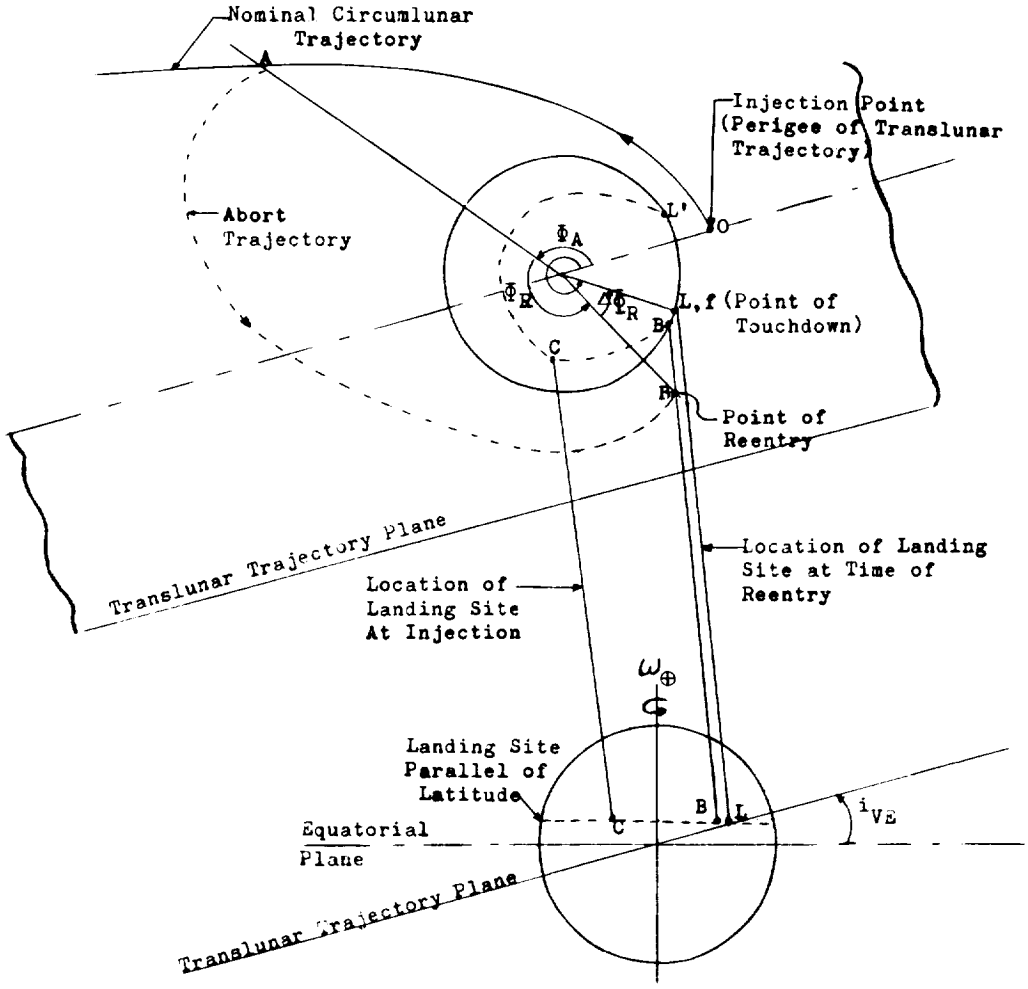

where n = 1, 2, . . . is the number of the abort way-stations or sidereal days or complete rotations of the earth from injection. As long as the latitude of the landing site is less than the trajectory inclination, the site will intersect the translunar trajectory plane also at L' and a second set of abort way-stations can be computed for this site.

(3) Let Φ_A be the range angle from injection to abort (or true anomaly since injection occurs at perigee), Φ_R the range angle from abort to re-entry, and $\Delta\Phi_R$ the required longitudinal maneuverability of the vehicle from re-entry. The total range angle Φ_0 from injection to the point L of intersection of the landing site with the trajectory plane must satisfy

$$\Phi_0 = \Phi_A + \Phi_R + \Delta\Phi_R \qquad (35)$$

(4) The range angle $\Delta\Phi_R$ is constrained by the longitudinal maneuvering capability of the vehicle, i.e.,

$$\left(\Delta\Phi_R\right)_{min} \leq \Delta\Phi_R \leq \left(\Delta\Phi_R\right)_{max} \qquad (36)$$

For preliminary calculations the re-entry portion of the flight can be neglected in comparison with the translunar and abort trajectories. Then $\Delta t_{B-f} = \Delta t_{B-L} = 0$, $\Delta\Phi_R = 0$, and the restricted two-body force model results compiled in Chapter III of Ref. 1 can be used to determine abort way-stations for certain translunar abort trajectory characteristics and landing sites. If available, the re-entry trajectory parameters Δt_{B-f} and $\Delta\Phi_R$ can be obtained for certain space vehicle characteristics and added to the restricted two-body results to obtain more realistic abort way-stations.

A typical graph for determining abort way-stations has been given in Fig. 13. The dashed lines represent the required time from injection to when the landing site intersects the trajectory plane at L or $(\Delta t_{0-A} + \Delta t_{A-B} + \Delta t_{B-f})$ = constant for the first, second and third day. The curve of minimum time to re-enter corresponds to a change in flight path angle only by the abort maneuver, while the maximum time to re-enter corresponds to a change in velocity only with no change in flight path angle at abort. Both curves are for the same $\Delta V_A = 1529$ m/sec. The intersections of the minimum time to re-enter curve with the dashed line represent abort way-stations and are denoted by dots on Fig. 13.

The abort way-stations on Fig. 13 correspond to the intersection of the $\Delta A = 0°$ step function with the curve labeled "absolute minimum time to return to earth $(\Delta V_A)_{max}$" in Fig. 12. It is obvious that Fig. 12 presents much more information than Fig. 13--it gives abort way-stations for $\Delta A = 0°$, $\Delta A = 10°$, and $\Delta A = 20°$ which are the intersections of the step functions with the $(\Delta V_A)_{max}$ curves. In addition, lower values of ΔV_A can be obtained at a glance from Fig. 12. The near-horizontal part of the two-step function on Fig. 12 can be connected to yield a four-parameter set of curves where ΔV_A and ΔA are presented in the field of the graph together with the nominal trajectory ($\Delta V_A = 0$), and R_A and time-to-return are the abscissa and ordinate, respectively. In this fashion, the maximum abort maneuver information can be presented on a single graph.

In practical design of abort trajectories (and way-stations), a set of graphs similar to Fig. 12 should be prepared for each prospective landing site and each location L and L' as soon as the nominal translunar portion of the trajectory has been determined. Results of re-entry trajectory calculations can be used to bias the curves obtained from the restricted two-body force model and thereby represent the actual situation more realistically.

E. REFERENCES

1. "Orbital Flight Handbook," ER 12684, The Martin Company, Baltimore, March 1963.
2. Battin, R. H., "A Statistical Optimizing Navigation Procedure for Space Flight," Instrumentation Laboratory, MIT, Cambridge, Massachusetts, May 1962.
3. Wheelon, A. D., "Midcourse and Terminal Guidance," Report No. 145, Space Technology Laboratories, Applied Physics Department, Los Angeles, California, June 1958.
4. Porter, J. G., "Navigation Without Gravity," Journal of the British Interplanetary Society, Vol. 13, No. 2, March 1954, p 68.
5. "Navigational Techniques for Interplanetary Space Flight," Report No. 2752-15-F, University of Michigan, Willow Run Laboratories, Ann Arbor, Michigan, 1958.
6. Novak, D. H., "Two-Body Navigation and Guidance in Cislunar Space," ER 12447, Martin Company, Aerospace Systems Division, Baltimore, Maryland, May 1962.
7. Egorov, V. A., "Certain Problems of Moon Flight Dynamics," The Russian Literature of Satellites, Part I, International Physical Index, Inc., New York, 1958.
8. Pragluski, W. J., "Lunar Mission Midcourse Guidance Concept Trajectory Analysis, Lunar Landing Module," Technical Report No. 11, Martin Company, Baltimore, February 1962. (Unpublished)
9. Kelly, T. J. and Adornato, R. J., "Determination of Abort Way-Stations on a Nominal Circumlunar Trajectory," ARS Journal, Vol. 32, June 1962, pp 887 to 893.

ILLUSTRATIONS

LIST OF ILLUSTRATIONS

Figure	Title	Page
1	Star Choice Angles	VI-32
2	Star Choice Angles	VI-32
3	View from Spacecraft Towards Earth	VI-33
4	Typical Lunar Flight Ground Swath (southerly declination of the moon)	VI-34
5	Typical Lunar Flight Ground Swath (northerly declination of the moon)	VI-34
6	Minimum Eccentricity Allowable for Safe Earth Return	VI-35
7	Time to Return to Earth from any Point in a Translunar Trajectory	VI-36
8	Characteristic Velocity Impulse ΔV_A of the Abort Maneuver (no changes in azimuth)	VI-37
9	Time to Return for an Abort Maneuver from a Typical Translunar Trajectory	VI-38
10	Abort Velocity Impulse Required to Land in Australia for a Typical Translunar Trajectory	VI-39
11	Abort Velocity Impulse Required to Land in or Near the United States for a Typical Translunar Trajectory	VI-40
12	Complete Abort Data for a Typical Circumlunar Trajectory	VI-41
13	Abort Way-Stations for a Typical Circumlunar Trajectory	VI-42

FIG. 1. STAR CHOICE ANGLES

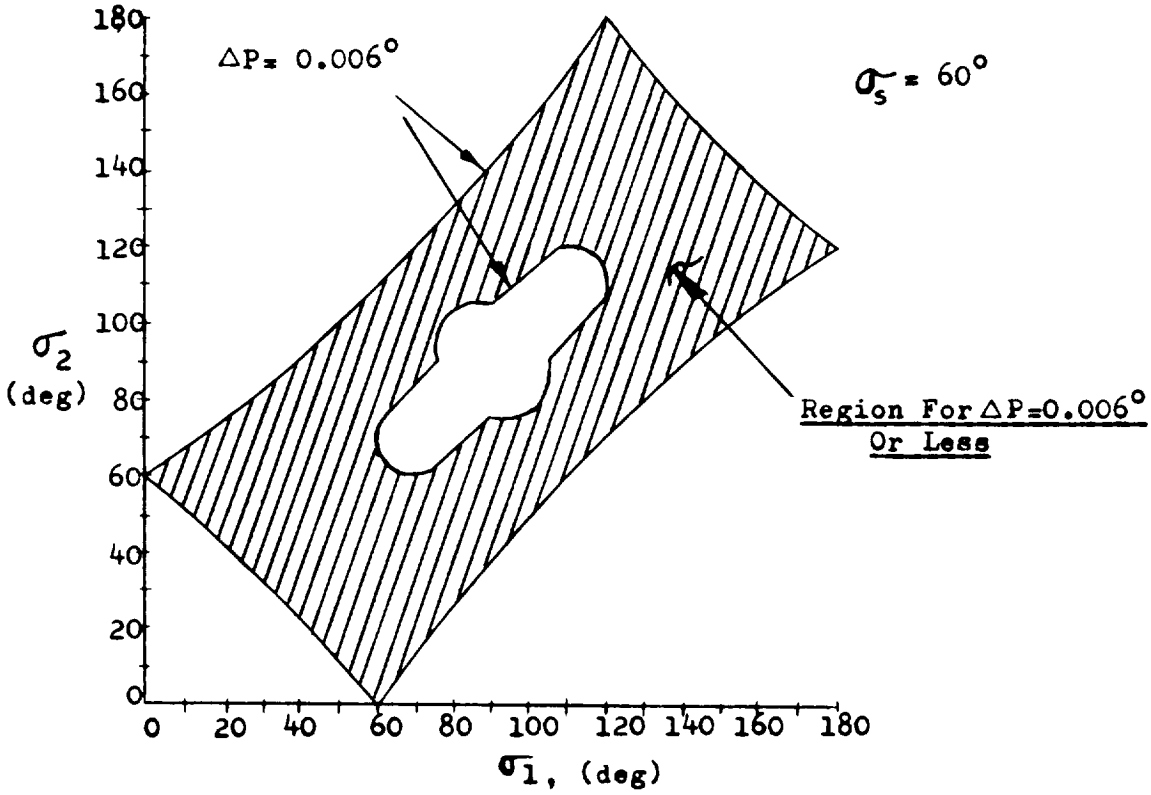

FIG. 2 STAR CHOICE ANGLES

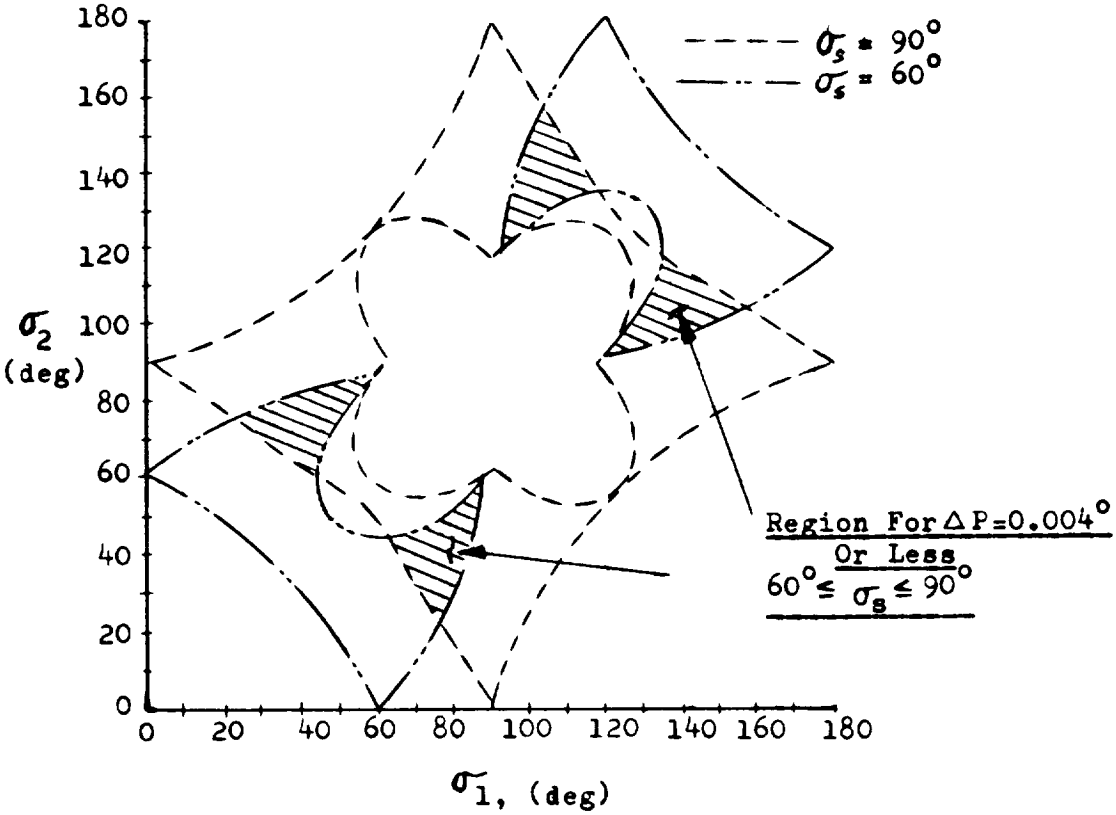

FIG. 3. VIEW FROM SPACECRAFT TOWARDS EARTH

Launch: 14 June, 1968, 14:14 Hr GMT
View 3 Hours After Injection

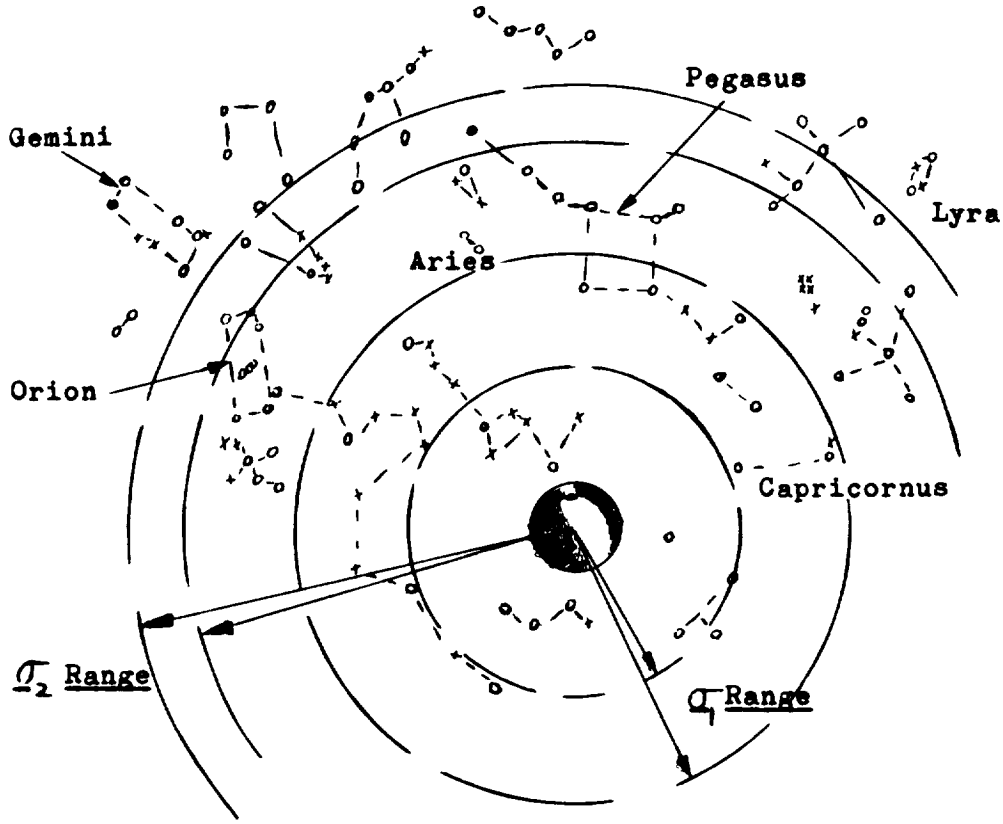

Star Code:

o 3rd. Magnitude or Brighter

× 5th. Magnitude or Brighter

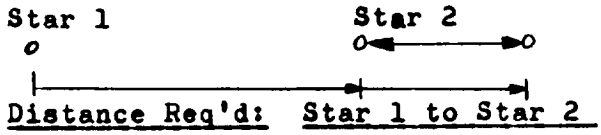

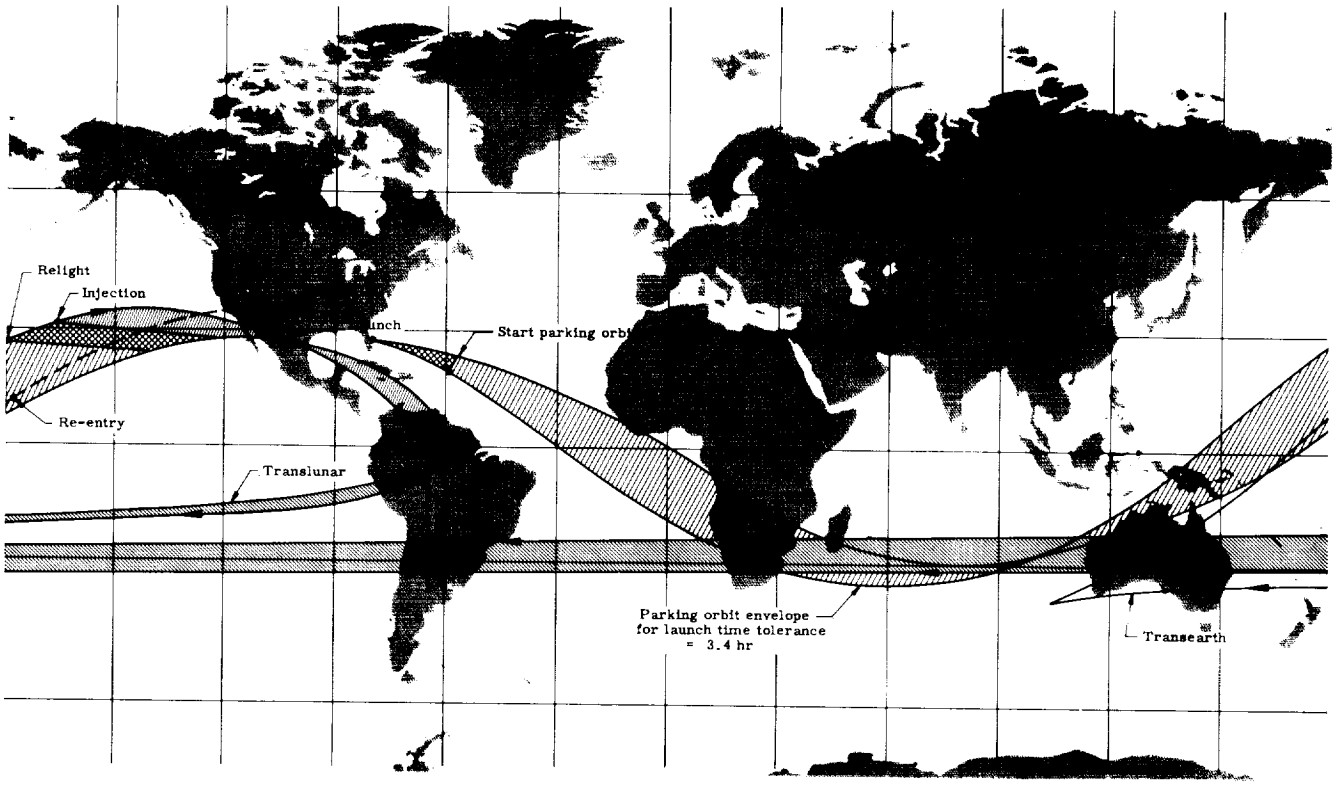

Fig. 4. Typical Lunar Flight Ground Swath (Southerly Declination of the Moon)

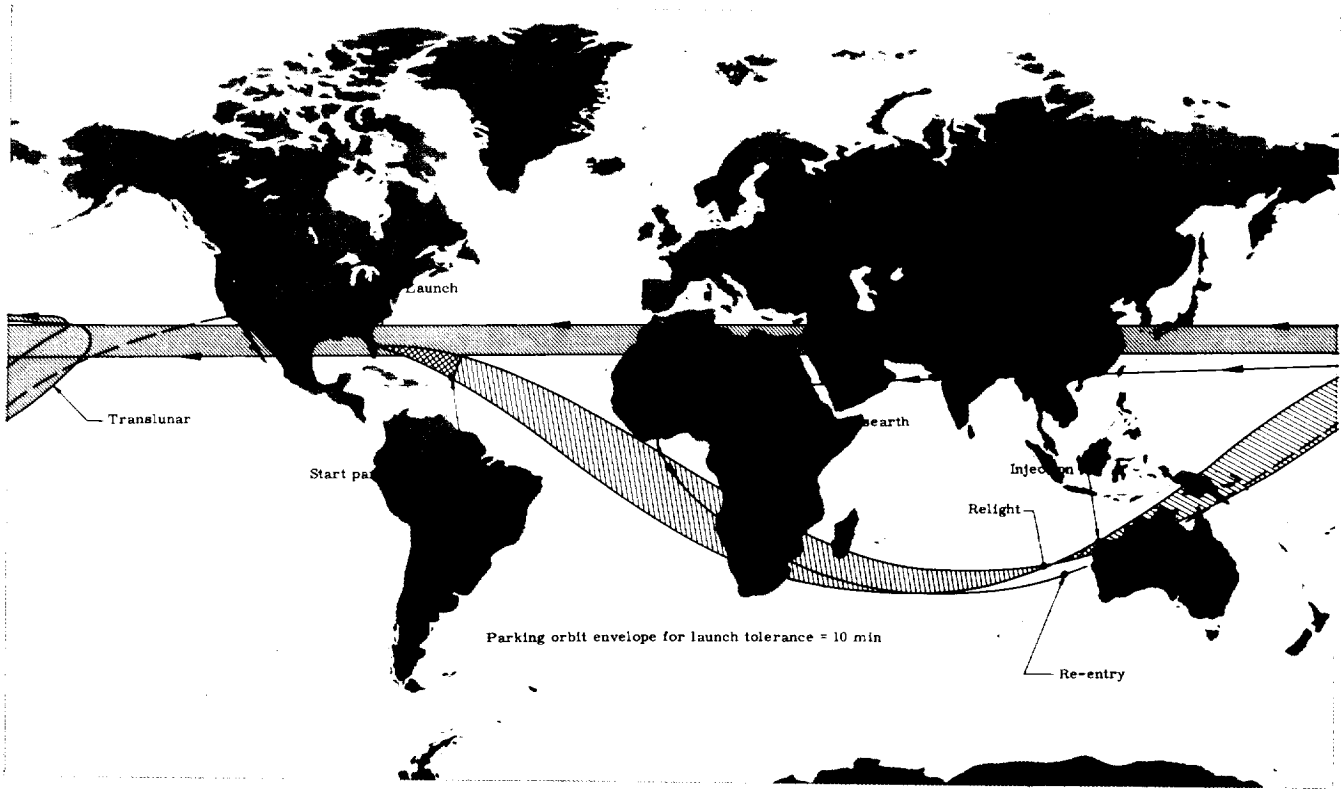

Fig. 5. Typical Lunar Flight Ground Swath (Northerly Declination of the Moon)

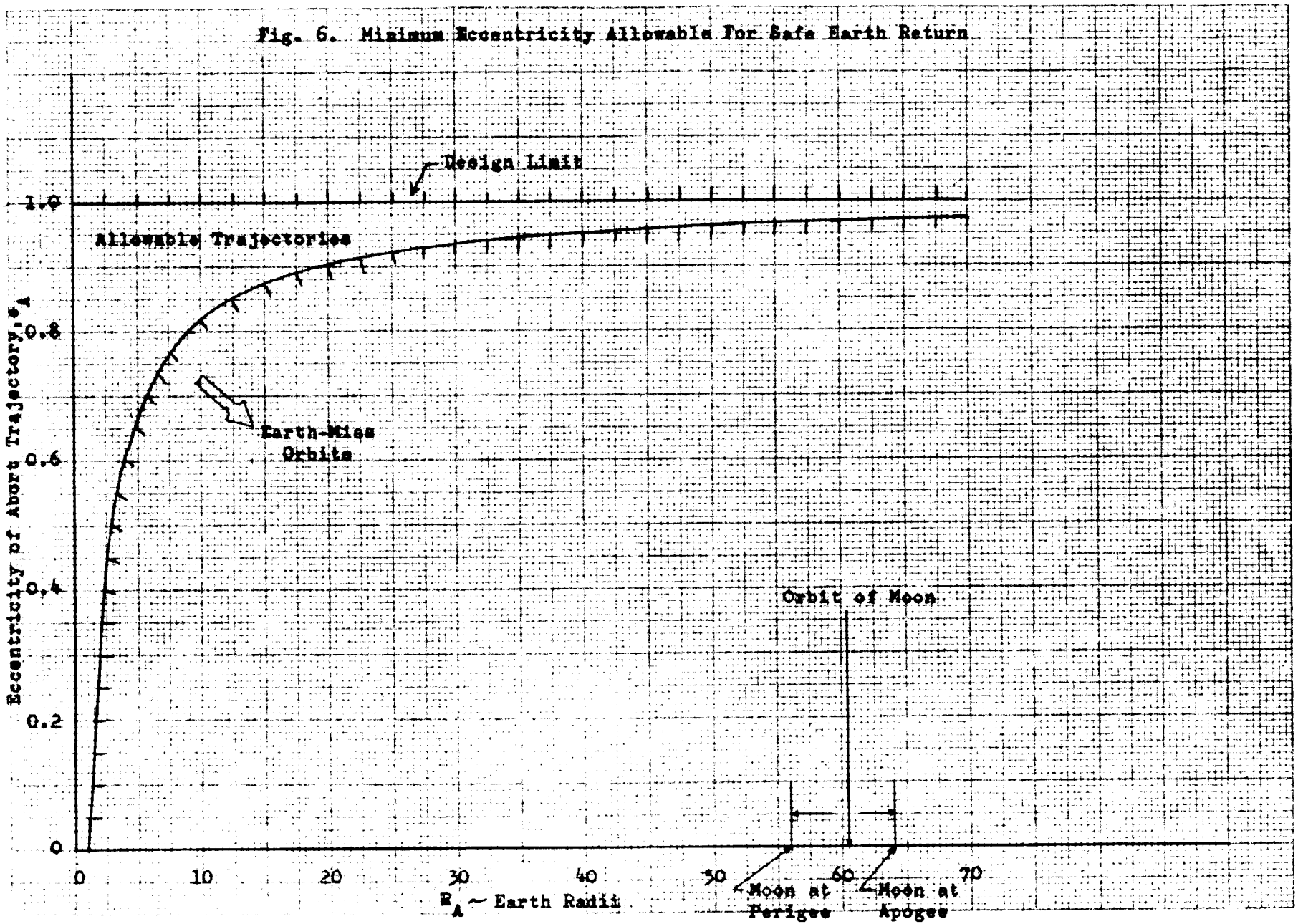

Fig. 6. Minimum Eccentricity Allowable For Safe Earth Return

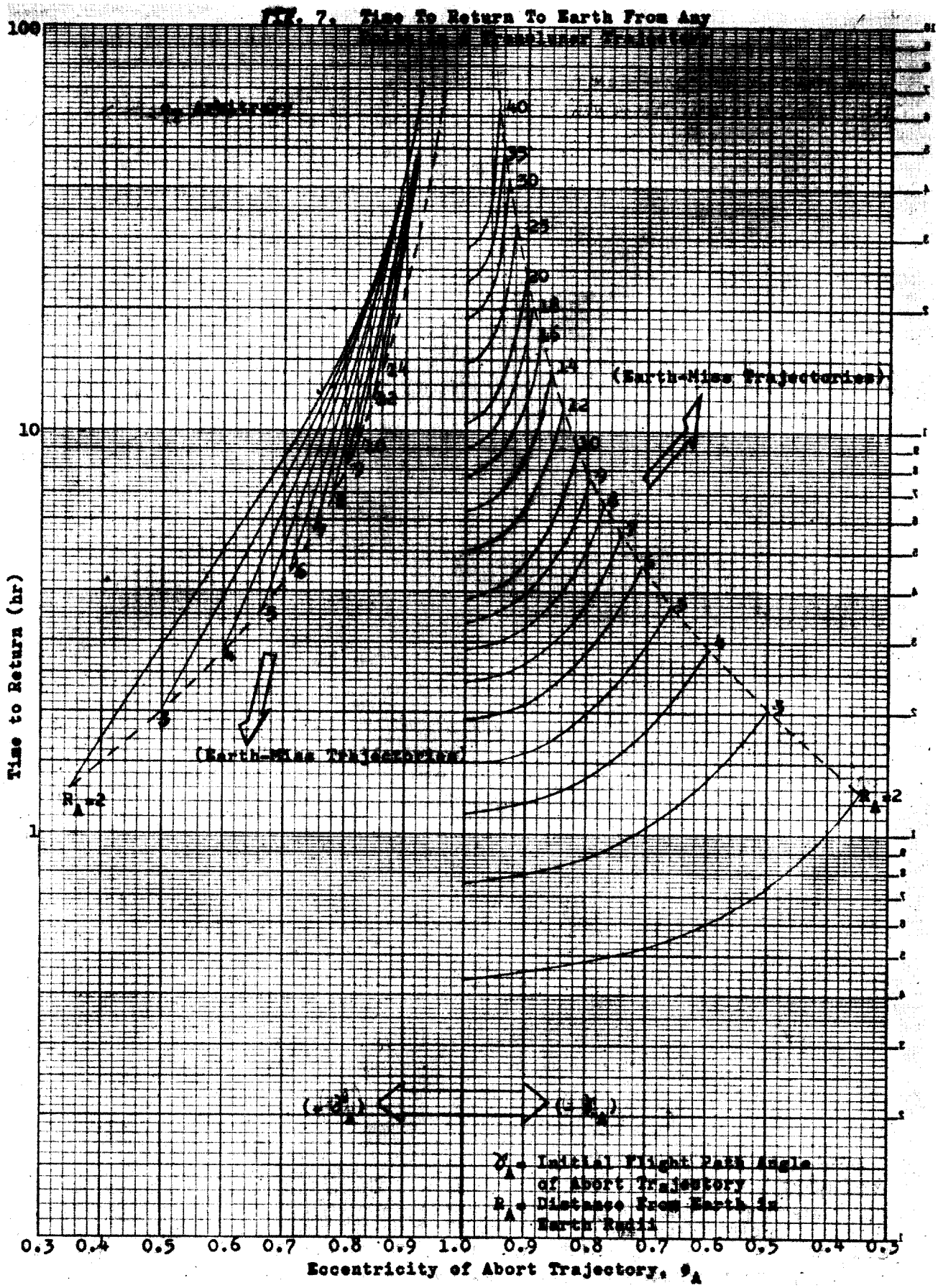

FIG. 7. Time To Return To Earth From Any Point On A Translunar Trajectory

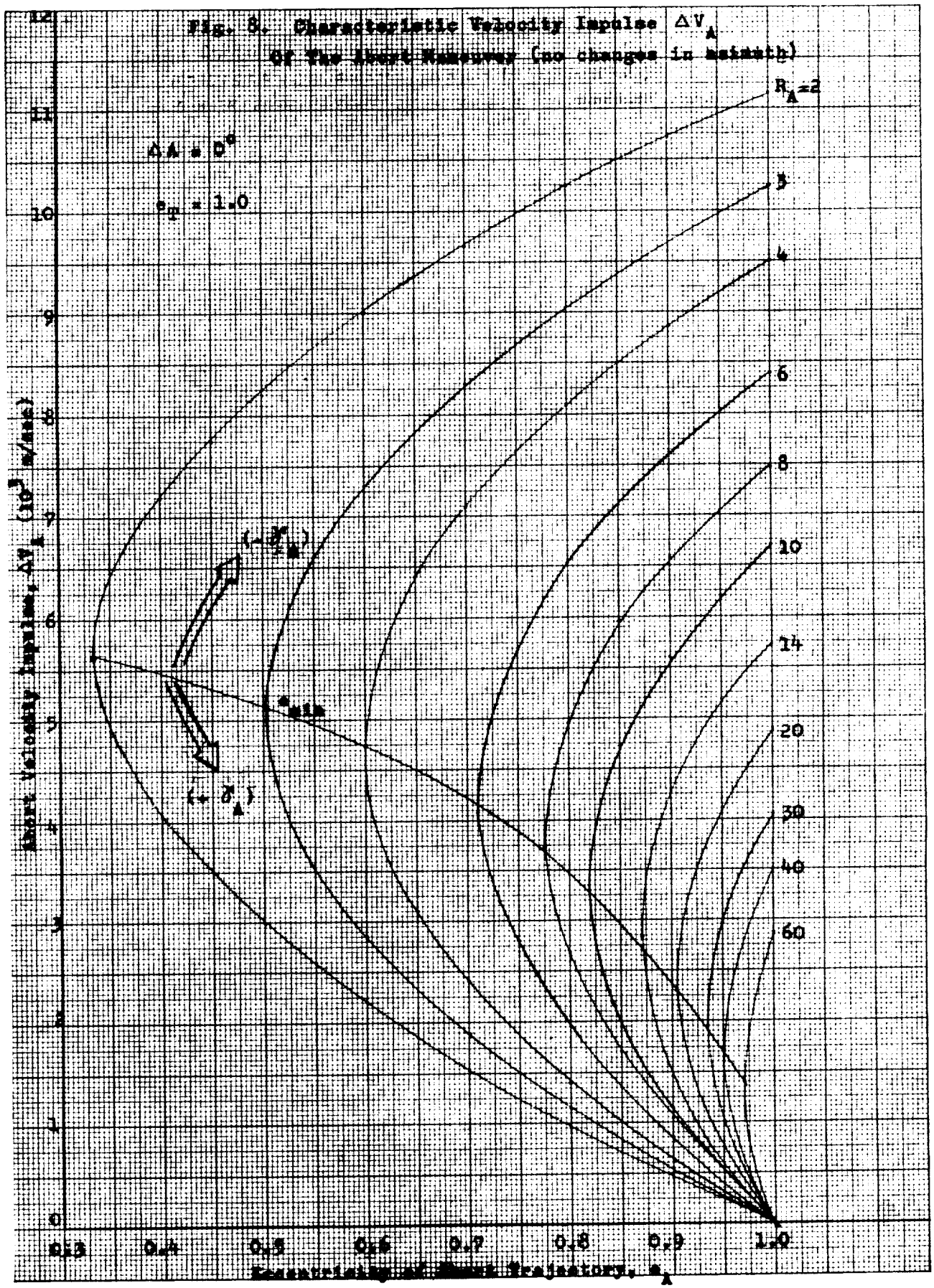
Fig. 8. Characteristic Velocity Impulse ΔV_A Of The Abort Maneuver (no changes in azimuth)
R_A=2
3
4
6
8
10
14
20
30
40
60
$\Delta A = 0^\circ$
$e_T = 1.0$
$(-\gamma_{EA})$
$(+\gamma_A)$
e_{min}
Abort velocity impulse, ΔV_A (10^3 ft/sec)
Eccentricity of abort trajectory, e_A
0.3
0.4
0.5
0.6
0.7
0.8
0.9
1.0

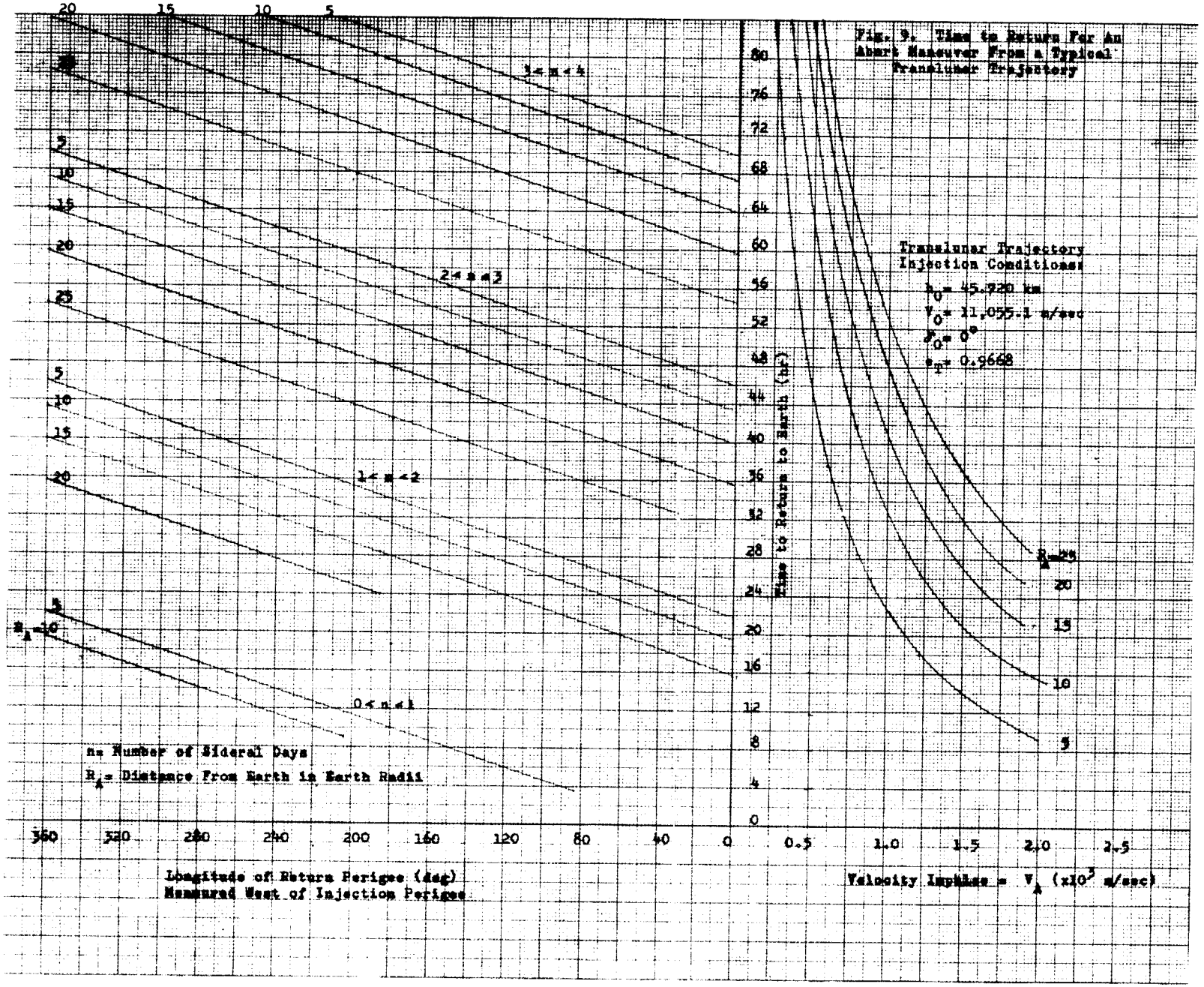
Fig. 9. Time to Return For An Abort Maneuver From a Typical Translunar Trajectory
Translunar Trajectory Injection Conditions:
h_0 = 45,720 km
V_0 = 11,055.1 m/sec
γ_0 = 0°
e_T = 0.9668
Time to Return to Earth (hr.)
R_A=25
20
15
10
5
1 ≤ n < 4
2 ≤ n < 3
1 ≤ n < 2
0 ≤ n < 1
R_A=10
5
n = Number of Sideral Days
R_A = Distance From Earth in Earth Radii
Longitude of Return Perigee (deg)
Measured West of Injection Perigee
Velocity Impulse = V_A (x10^3 m/sec)

Fig. 10. Abort Velocity Impulse Required To Land In Australia For a Typical Translunar Trajectory

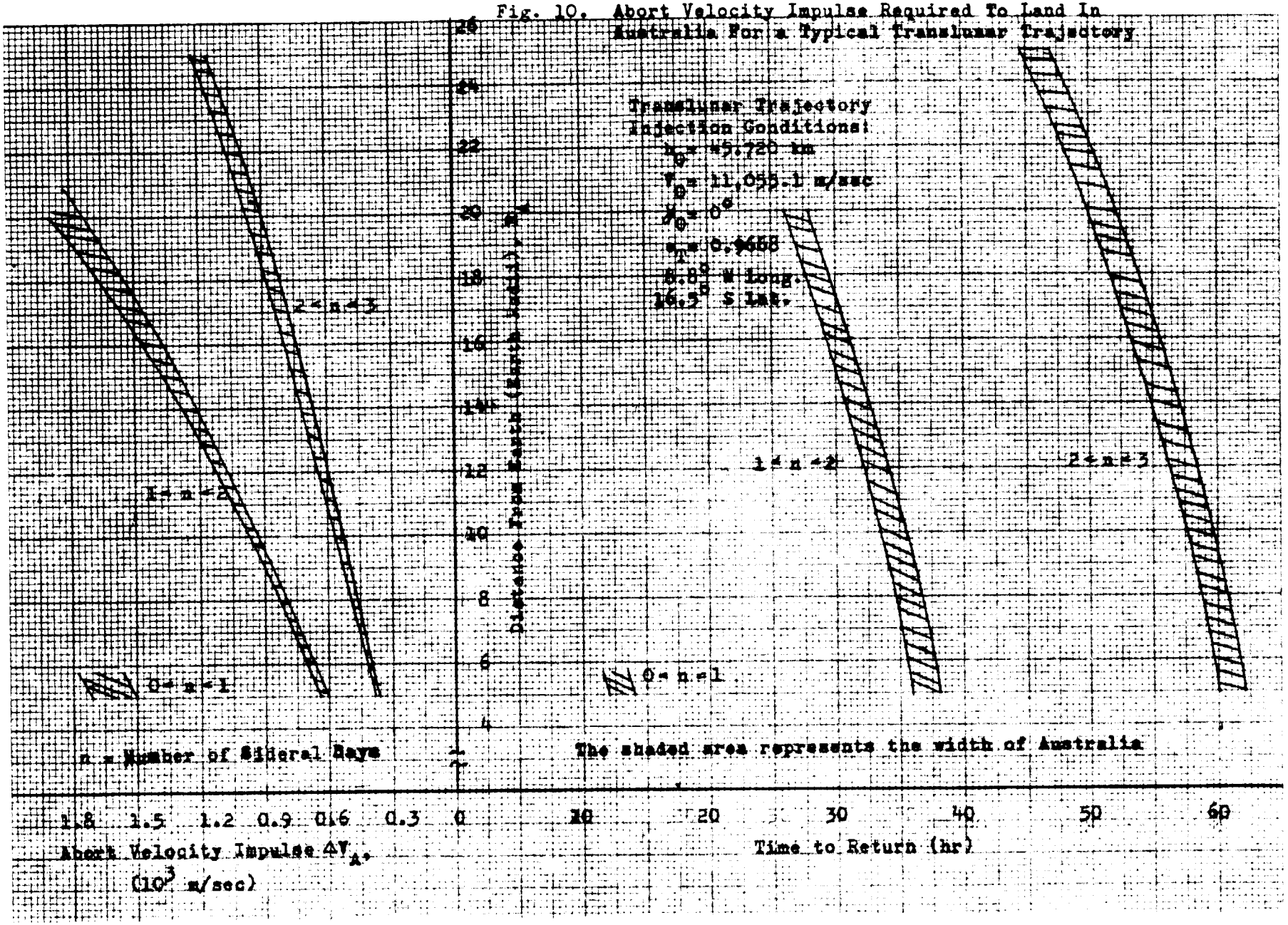

Fig. 11. Abort Velocity Impulse Required To Land In Or Near The United States For A Typical Translunar Trajectory

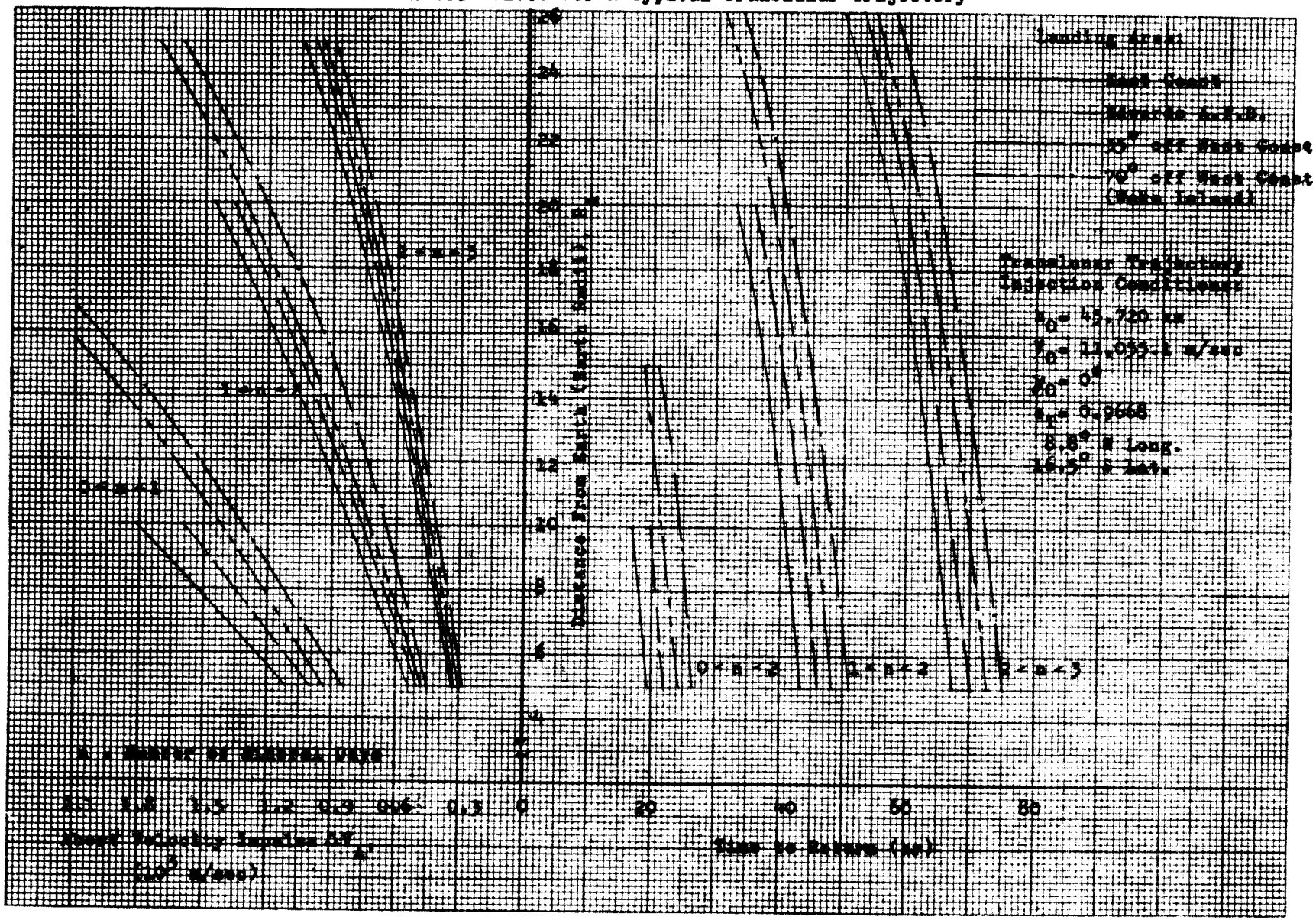

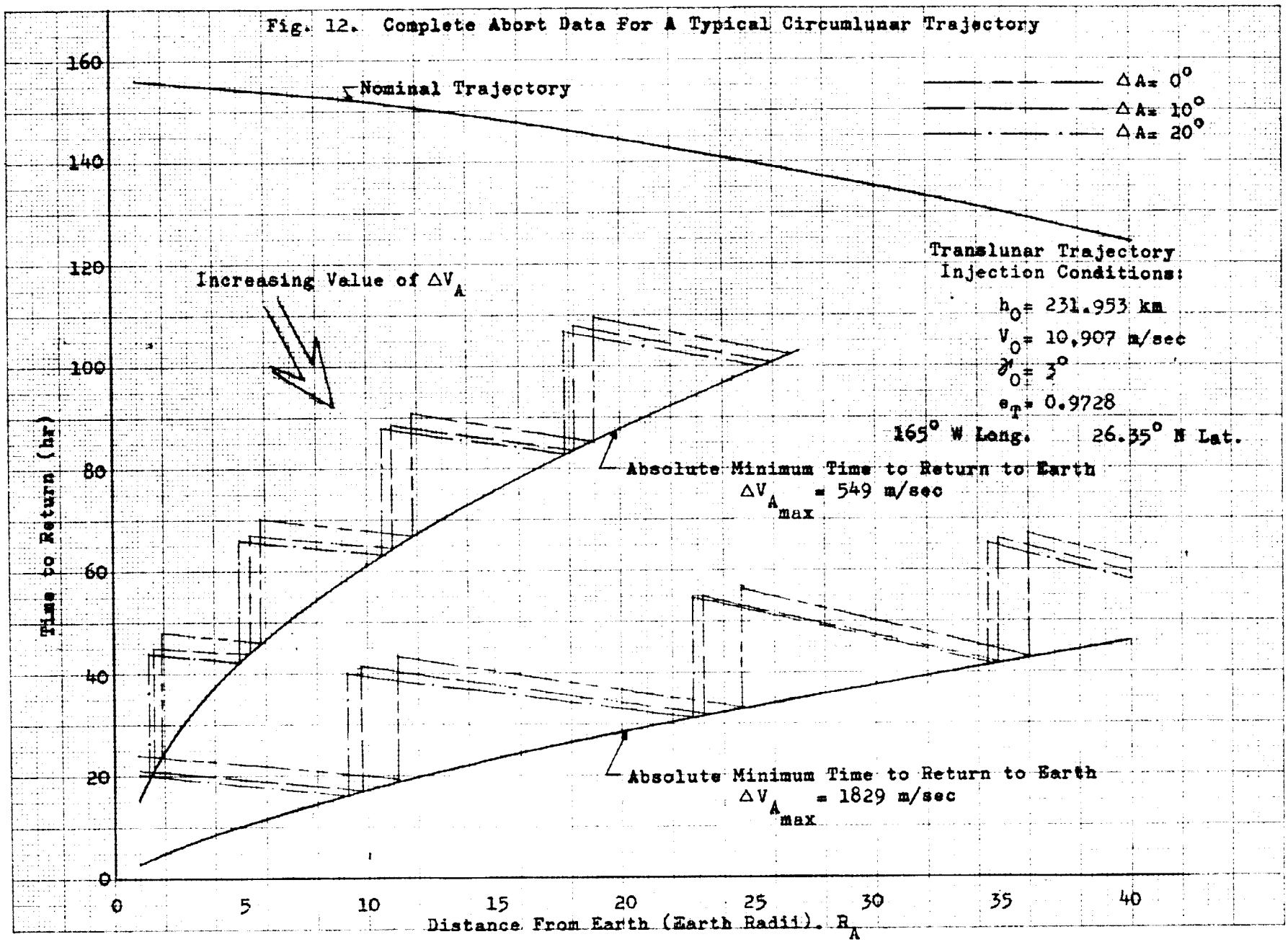

Fig. 12. Complete Abort Data For A Typical Circumlunar Trajectory

Fig. 13. Abort Way-Stations For A Typical Circumlunar Trajectory

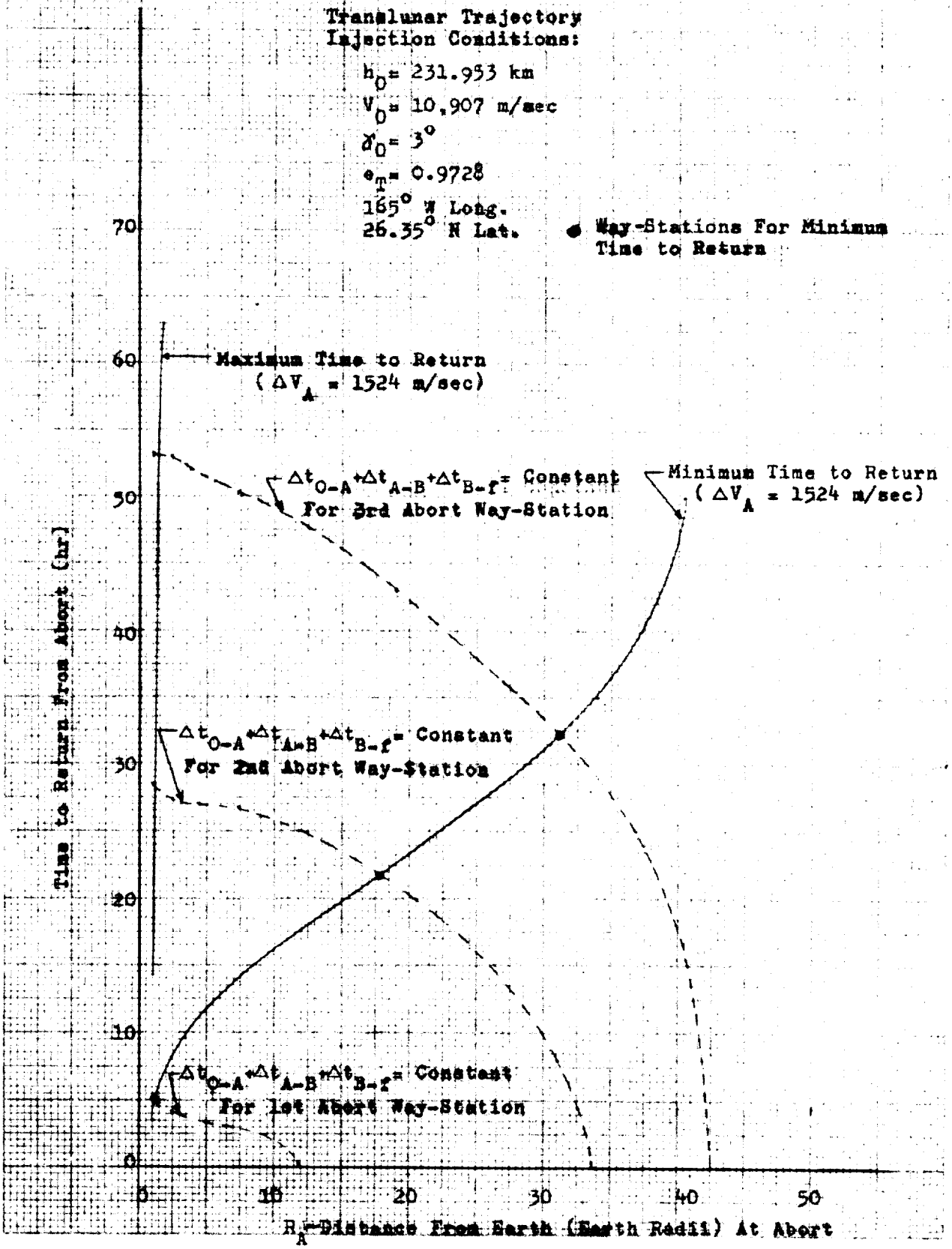

CIRCUMLUNAR TRAJECTORY CATALOGUE

Figures C-1 through C-83

Figure	Title	Page
C-1	Injection Velocity Versus Return Inclination	VI-49
C-2	Injection Point Position Versus Return Inclination	VI-50
C-3	Moon Lead Angle Versus Return Inclination	VI-51
C-4	ΔV Required to Enter Circular Lunar Orbit Versus Return Inclination	VI-52
C-5	Time of Pericynthion Versus Return Inclination	VI-53
C-6	Total Time Versus Return Inclination	VI-54
C-7	Lunar Orbit Inclination Versus Return Inclination	VI-55
C-8	Lunar Orbit Orientation Versus Return Inclination	VI-56
C-9	Injection Velocity Versus Return Inclination	VI-57
C-10	Injection Point Position Versus Return Inclination	VI-58
C-11	Moon Lead Angle Versus Return Inclination	VI-59
C-12	ΔV Required to Enter Circular Lunar Orbit Versus Return Inclination	VI-60
C-13	Time of Pericynthion Versus Return Inclination	VI-61
C-14	Total Time Versus Return Inclination	VI-62
C-15	Lunar Orbit Inclination Versus Return Inclination	VI-63
C-16	Lunar Orbit Orientation Versus Return Inclination	VI-64
C-17	Injection Velocity Versus Return Inclination	VI-65
C-18	Injection Point Position Versus Return Inclination	VI-66
C-19	Moon Lead Angle Versus Return Inclination	VI-67
C-20	Δ V Required to Enter Circular Lunar Orbit Versus Return Inclination	VI-68
C-21	Time of Pericynthion Versus Return Inclination	VI-69
C-22	Total Time Versus Return Inclination	VI-70
C-23	Lunar Orbit Inclination Versus Return Inclination	VI-71

Figure	Title	Page
C-24	Lunar Orbit Orientation Versus Return Inclination	VI-72
C-25	Injection Velocity Versus Return Inclination	VI-73
C-26	Injection Point Position Versus Return Inclination	VI-74
C-27	Moon Lead Angle Versus Return Inclination	VI-75
C-28	ΔV Required to Enter Circular Lunar Orbit Versus Return Inclination	VI-76
C-29	Time of Pericynthion Versus Return Inclination	VI-77
C-30	Total Time Versus Return Inclination	VI-78
C-31	Lunar Orbit Inclination Versus Return Inclination	VI-79
C-32	Lunar Orbit Orientation Versus Return Inclination	VI-80
C-33	Injection Velocity Versus Return Inclination	VI-81
C-34	Injection Velocity Versus Return Inclination	VI-82
C-35	Injection Point Position Versus Return Inclination	VI-83
C-36	Moon Lead Angle Versus Return Inclination	VI-84
C-37	ΔV Required to Enter Circular Lunar Orbit Versus Return Inclination	VI-85
C-38	Time of Pericynthion Versus Return Inclination	VI-86
C-39	Total Time Versus Return Inclination	VI-87
C-40	Lunar Orbit Inclination Versus Return Inclination	VI-88
C-41	Lunar Orbit Orientation Versus Return Inclination	VI-89
C-42	Injection Velocity Versus Return Inclination	VI-90
C-43	Injection Velocity Versus Return Inclination	VI-91
C-44	Injection Point Position Versus Return Inclination	VI-92
C-45	Moon Lead Angle Versus Return Inclination	VI-93
C-46	ΔV Required to Enter Circular Lunar Orbit Versus Return Inclination	VI-94
C-47	Time of Pericynthion Versus Return Inclination	VI-95
C-48	Total Time Versus Return Inclination	VI-96

Figure	Title	Page
C-49	Lunar Orbit Inclination Versus Return Inclination	VI-97
C-50	Lunar Orbit Orientation Versus Return Inclination	VI-98
C-51	Injection Velocity Versus Return Inclination	VI-99
C-52	Injection Velocity Versus Return Inclination	VI-100
C-53	Injection Point Position Versus Return Inclination	VI-101
C-54	Moon Lead Angle Versus Return Inclination	VI-102
C-55	ΔV Required to Enter Circular Lunar Orbit Versus Return Inclination	VI-103
C-56	Time of Pericynthion Versus Return Inclination	VI-104
C-57	Total Time Versus Return Inclination	VI-105
C-58	Lunar Orbit Inclination Versus Return Inclination	VI-106
C-59	Lunar Orbit Orientation Versus Return Inclination	VI-107
C-60	Injection Velocity Versus Return Inclination	VI-108
C-61	Injection Point Position Versus Return Inclination	VI-109
C-62	Moon Lead Angle Versus Return Inclination	VI-110
C-63	Δ V Required to Enter Circular Lunar Orbit Versus Return Inclination	VI-111
C-64	Time of Pericynthion Versus Return Inclination	VI-112
C-65	Total Time Versus Return Inclination	VI-113
C-66	Lunar Orbit Inclination Versus Return Inclination	VI-114
C-67	Lunar Orbit Orientation Versus Return Inclination	VI-115
C-68	Injection Velocity Versus Return Inclination	VI-116
C-69	Injection Point Position Versus Return Inclination	VI-117
C-70	Moon Lead Angle Versus Return Inclination	VI-118
C-71	ΔV Required to Enter Circular Lunar Orbit Versus Return Inclination	VI-119
C-72	Time of Pericynthion Versus Return Inclination	VI-120
C-73	Total Time Versus Return Inclination	VI-121

Figure	Title	Page
C-74	Lunar Orbit Inclination Versus Return Inclination	VI-122
C-75	Lunar Orbit Orientation Versus Return Inclination	VI-123
C-76	Injection Velocity Versus Return Inclination	VI-124
C-77	Injection Point Position Versus Return Inclination	VI-125
C-78	Moon Lead Angle Versus Return Inclination	VI-126
C-79	ΔV Required to Enter Circular Lunar Orbit Versus Return Inclination	VI-127
C-80	Time of Pericynthion Versus Return Inclination	VI-128
C-81	Time of Pericynthion Versus Return Inclination	VI-129
C-82	Lunar Orbit Inclination Versus Return Inclination	VI-130
C-83	Lunar Orbit Orientation Versus Return Inclination	VI-131

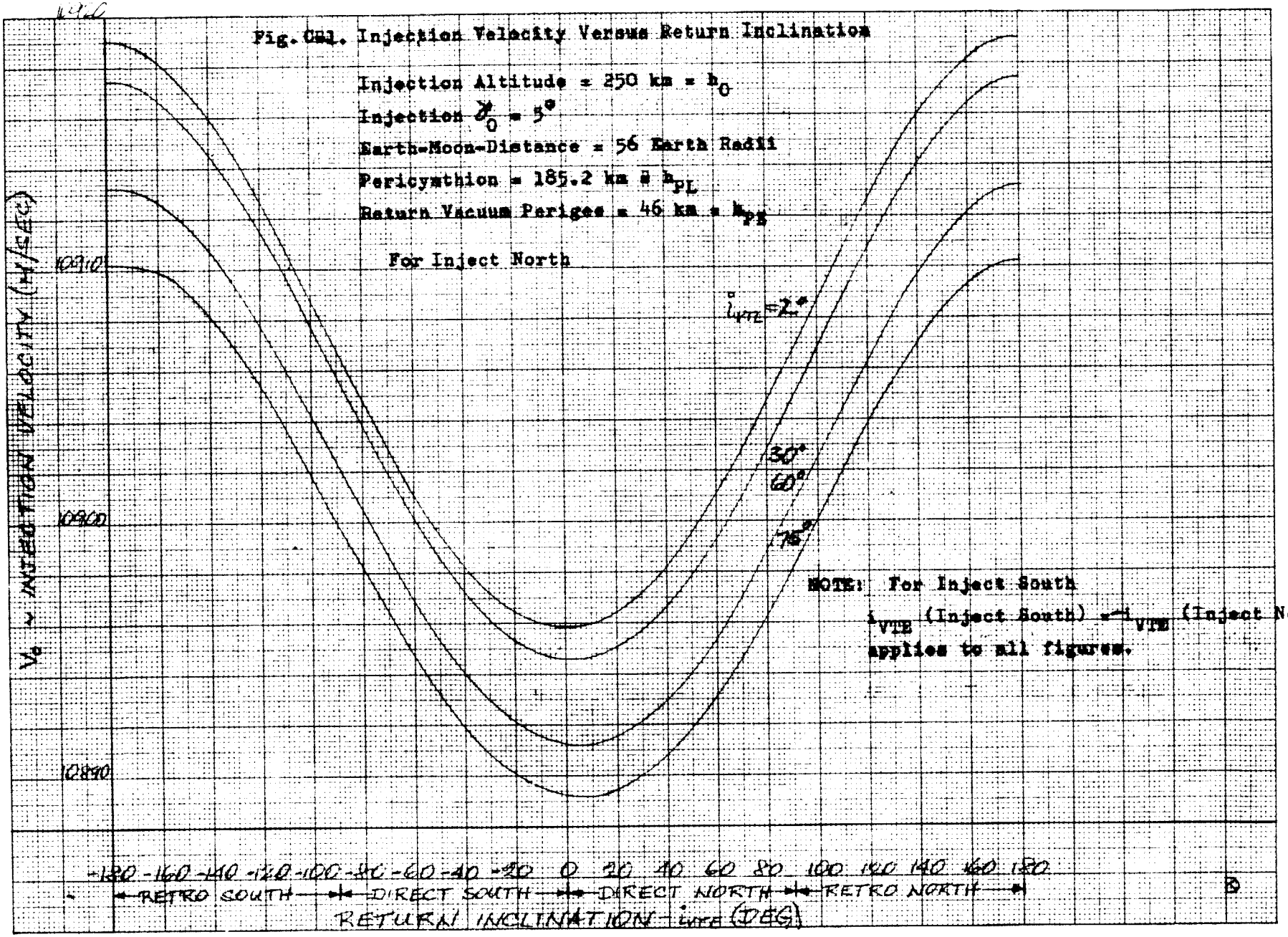
Fig. CM1. Injection Velocity Versus Return Inclination
Injection Altitude = 250 km = h_0
Injection γ_0 = 5°
Earth-Moon-Distance = 56 Earth Radii
Pericynthion = 185.2 km = h_{PL}
Return Vacuum Perigee = 46 km = h_{PE}
For Inject North
i_{VTE}=2°
30°
60°
75°
NOTE: For Inject South
i_{VTE} (Inject South) = $-i_{VTE}$ (Inject No.)
applies to all figures.
V_0 - INJECTION VELOCITY (FT/SEC)
10910
10900
10890
-180 -160 -140 -120 -100 -80 -60 -40 -20 0 20 40 60 80 100 120 140 160 180
RETRO SOUTH
DIRECT SOUTH
DIRECT NORTH
RETRO NORTH
RETURN INCLINATION - i_{VTE} (DEG)

Fig. 6.2. Injection Point Position Versus Return Inclination

Injection Altitude = 250 km = h_0

Injection γ_0 = 5°

Earth-Moon-Distance = 56 Earth Radii

Perisynthion = 185.2 km = h_{PS}

Return Vacuum Perigee = 46 km = h_{PR}

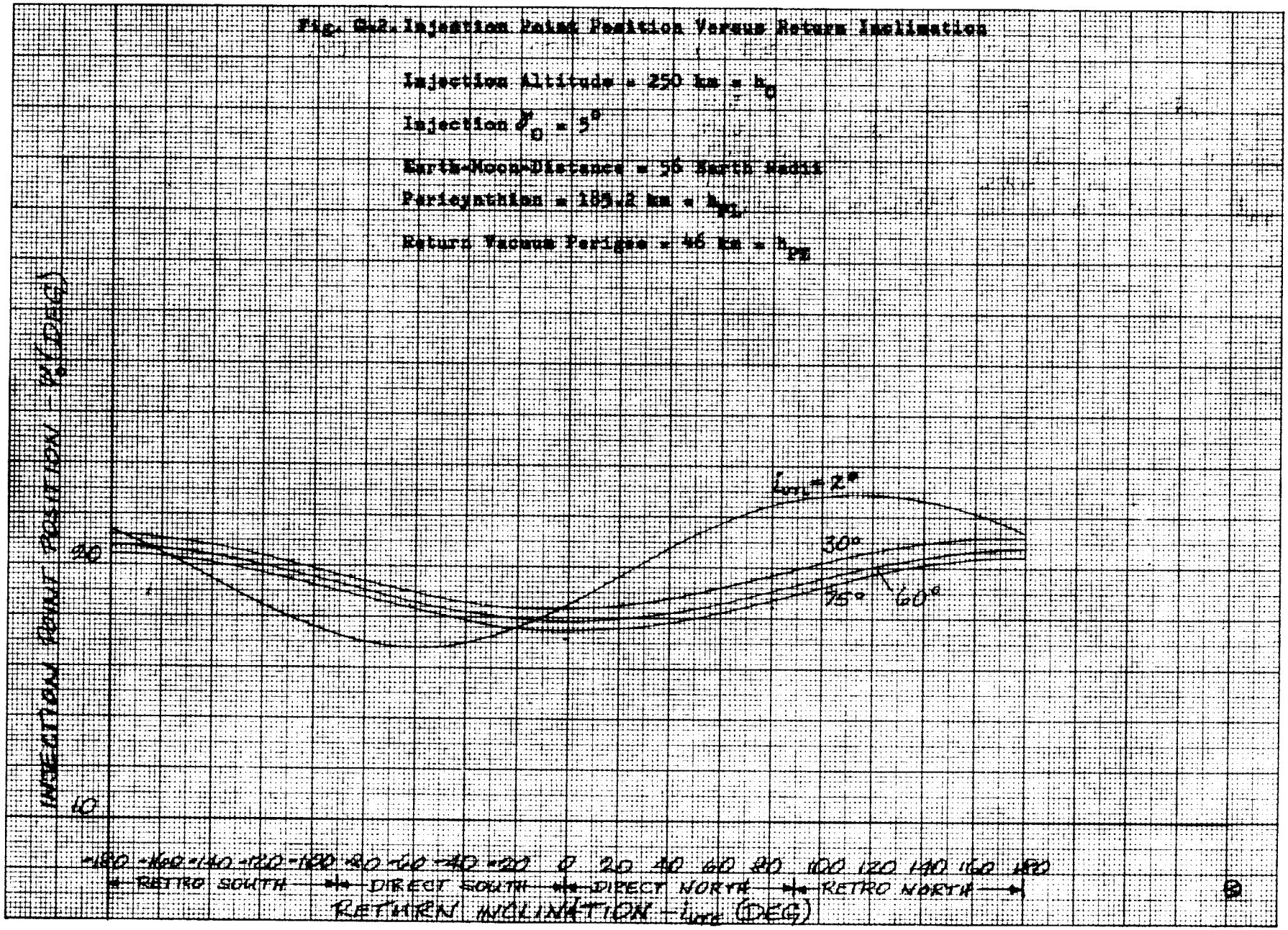

Fig. 6b; Moon Lead Angle Versus Return Inclination
Injection Altitude = 250 km = h_a
Injection γ_a = 5°
Earth-Moon Distance = 56 Earth Radii
Perigee Altitude = 185.2 km = h_p
Return Vacuum Perigee = 46 km = h_pR
MOON LEAD ANGLE - ψ (DEG)
i_ret = 45°
i_ret = 90°
i_ret = 135°
RETURN INCLINATION (i_ret) (DEG)
0 20 40 60 80 100 120 140 160 180
* RETRO SHIP — DIRECT NORTH — RETRO NORTH
** RETRO SHIP — DIRECT SOUTH — RETRO SOUTH
50
40
30
B

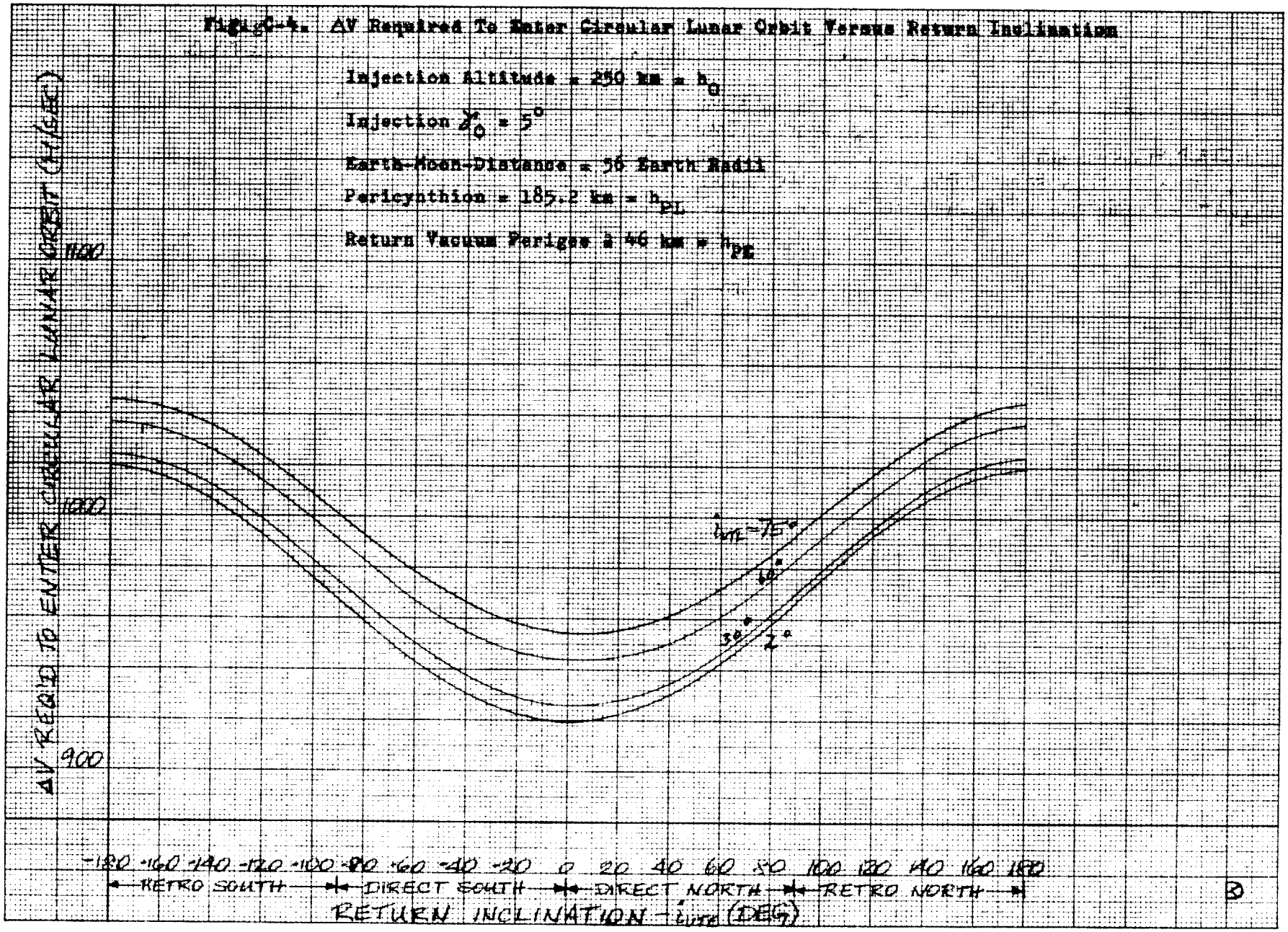
Fig. C-4. ΔV Required To Enter Circular Lunar Orbit Versus Return Inclination
Injection Altitude = 250 km = h_0
Injection γ_0 = 5°
Earth-Moon-Distance = 56 Earth Radii
Pericynthion = 185.2 km = h_{PL}
Return Vacuum Perigee = 46 km = h_{PE}
ΔV REQD TO ENTER CIRCULAR LUNAR ORBIT (M/SEC)
1100
1000
900
i_{VTL} = 75°
60°
30°
2°
-180 -160 -140 -120 -100 -80 -60 -40 -20 0 20 40 60 80 100 120 140 160 180
RETRO SOUTH
DIRECT SOUTH
DIRECT NORTH
RETRO NORTH
RETURN INCLINATION - i_{VTE} (DEG)
B

Fig. C-5, Time of Perigee Passage Versus Return Inclination
Injection Altitude = 250 km = h_0
Injection γ_0 = 5°
Earth-Moon-Distance = 56 Earth Radii
Perigee Radius = 185.2 km = h_{p1}
Return Versus Perigee = 46 km = h_{p2}
TIME OF RECROSSING THIGH - t_R (HR)
i_R
δ_R
i_R = RETRO SHOT INCLINATION (DEG)
δ_R = DIRECT SHOT DECLINATION (DEG)
i_R = RETRO SHOT INCLINATION (DEG)

Fig. G-6. Round-Trip Venus Return Inclination
Injection Altitude = 250 km = h_0
Injection γ_0 = 5°
Earth-to-Venus Distance = 76 Earth Radii
Periapsis = 1812 km = r_{pc}
Return Vacuum Periapse = 46 km = r_{pr}
i_{pr}
i_{pc}
i_{pr} = 45°
i_{pc} = 45°
RETURN INCLINATION (DEG)
DIRECT SOLUTION
RETRO SOLUTION
i_{pc} (DEG)
TOTAL TIME - T (DAYS)

Fig. C-7. Lunar Orbit Inclination Versus Return Inclination
Injection Altitude = 250 km = h_0
Injection γ_0 = 5°
Earth-Moon-Distance = 56 Earth Radii
Perigynthion = 185.2 km = h_{pt}
Return Vacuum Perigee = 46 km = h_{PE}
LUNAR DESCENT INCLINATION - i_{LD} (DEG)
i_{LR} = 45°
60°
30°
7°
0
-180 -160 -140 -120 -100 -80 -60 -40 -20 0 20 40 60 80 100 120 140 160 180
RETRO SOUTH
DIRECT SOUTH
DIRECT NORTH
RETRO NORTH
RETURN INCLINATION - i_{RE} (DEG)
B

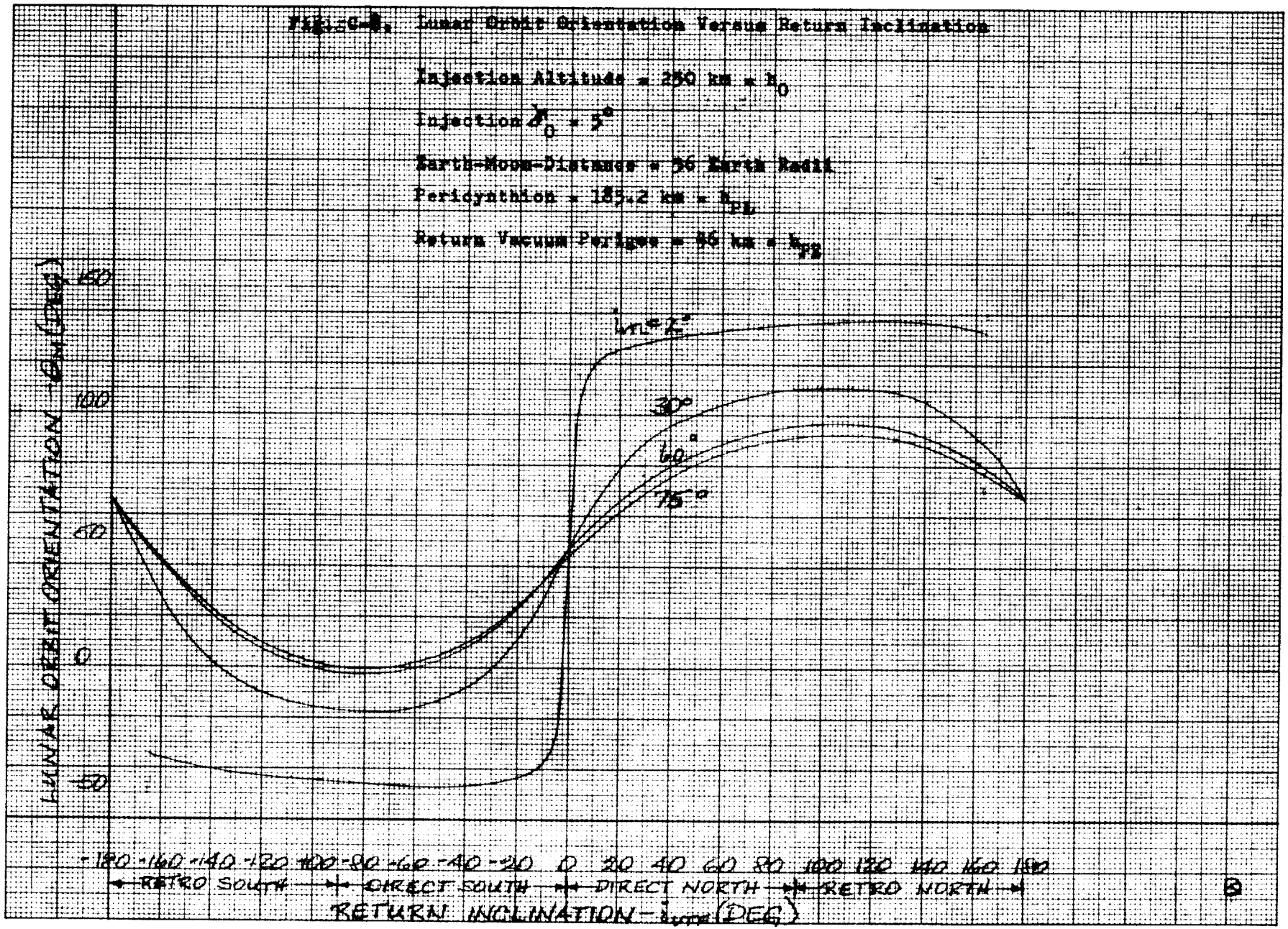
Fig. C-8x Lunar Orbit Orientation Versus Return Inclination
Injection Altitude = 250 km = h_0
Injection γ_0 = 5°
Earth-Moon-Distance = 56 Earth Radii
Perigynthion = 185.2 km = h_{Pl}
Return Vacuum Perigee = 96 km = h_{P2}
i_{WL} = 2°
30°
60°
75°
LUNAR ORBIT ORIENTATION - i_{LOR} (DEG)
150
100
50
0
-50
-180 -160 -140 -120 -100 -80 -60 -40 -20 0 20 40 60 80 100 120 140 160 180
RETRO SOUTH
DIRECT SOUTH
DIRECT NORTH
RETRO NORTH
RETURN INCLINATION - i_{RTN} (DEG)
B

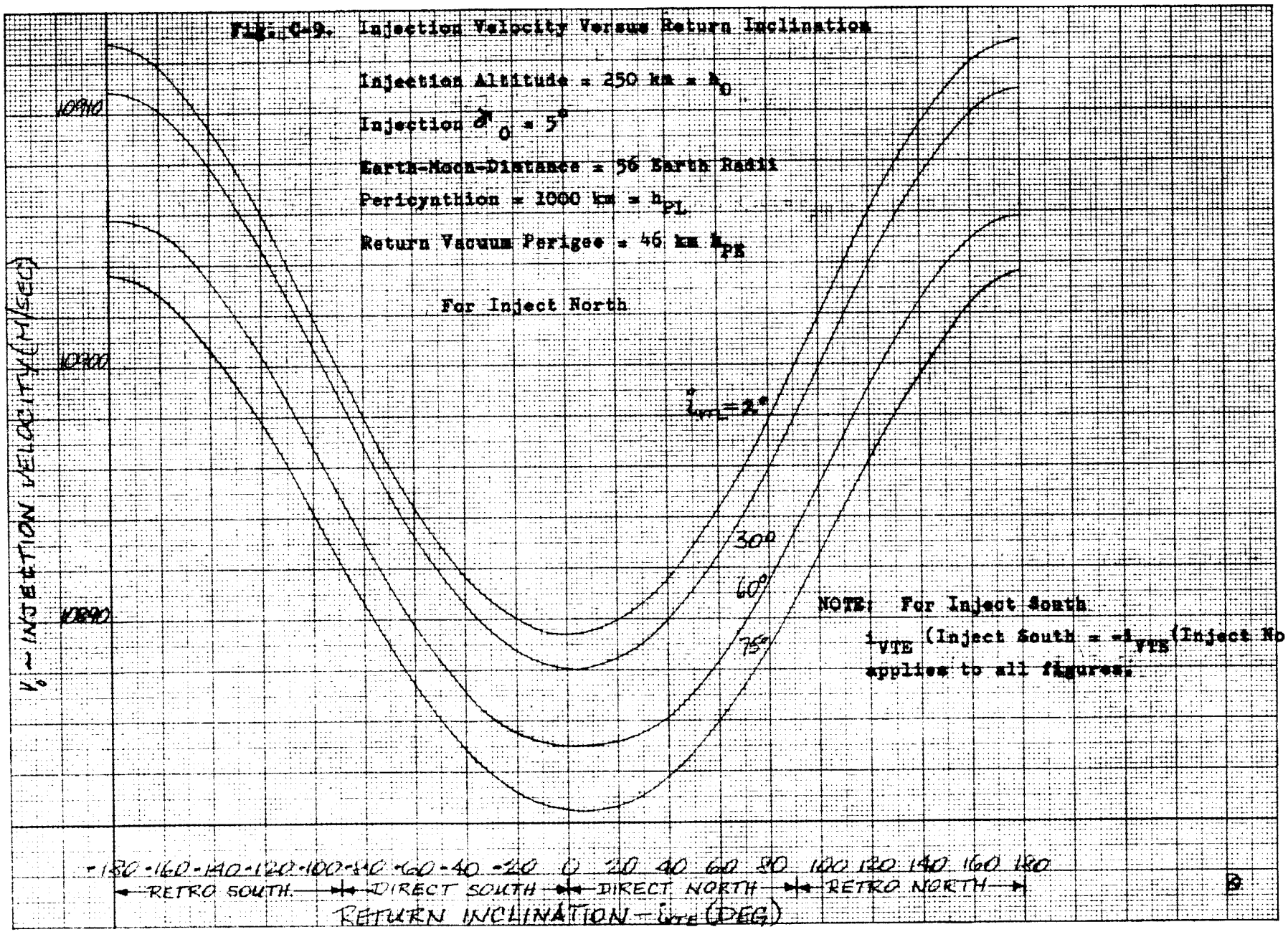
Fig. C-9. Injection Velocity Versus Return Inclination
Injection Altitude = 250 km = h_0
Injection γ_0 = 5°
Earth-Moon-Distance = 56 Earth Radii
Pericynthion = 1000 km = h_{PL}
Return Vacuum Perigee = 46 km h_{PE}
For Inject North
i_{VTL}=2°
30°
60°
75°
NOTE: For Inject South
i_{VTE} (Inject South) = $-i_{VTE}$ (Inject No.)
applies to all figures.
INJECTION VELOCITY (FT/SEC)
10990
10900
10890
-180 -160 -140 -120 -100 -80 -60 -40 -20 0 20 40 60 80 100 120 140 160 180
RETRO SOUTH
DIRECT SOUTH
DIRECT NORTH
RETRO NORTH
RETURN INCLINATION - i_{VTE} (DEG)

Fig. 6-10. Injection Point Position Versus Return Inclination

Injection Altitude = 250 km = h_0

Injection $\gamma_0 = 5^0$

Earth-Moon-Distance = 56 Earth Radii

Perigynthion = 1000 km = h_{PL}

Return Vacuum Perigee = 56 km = h_{PE}

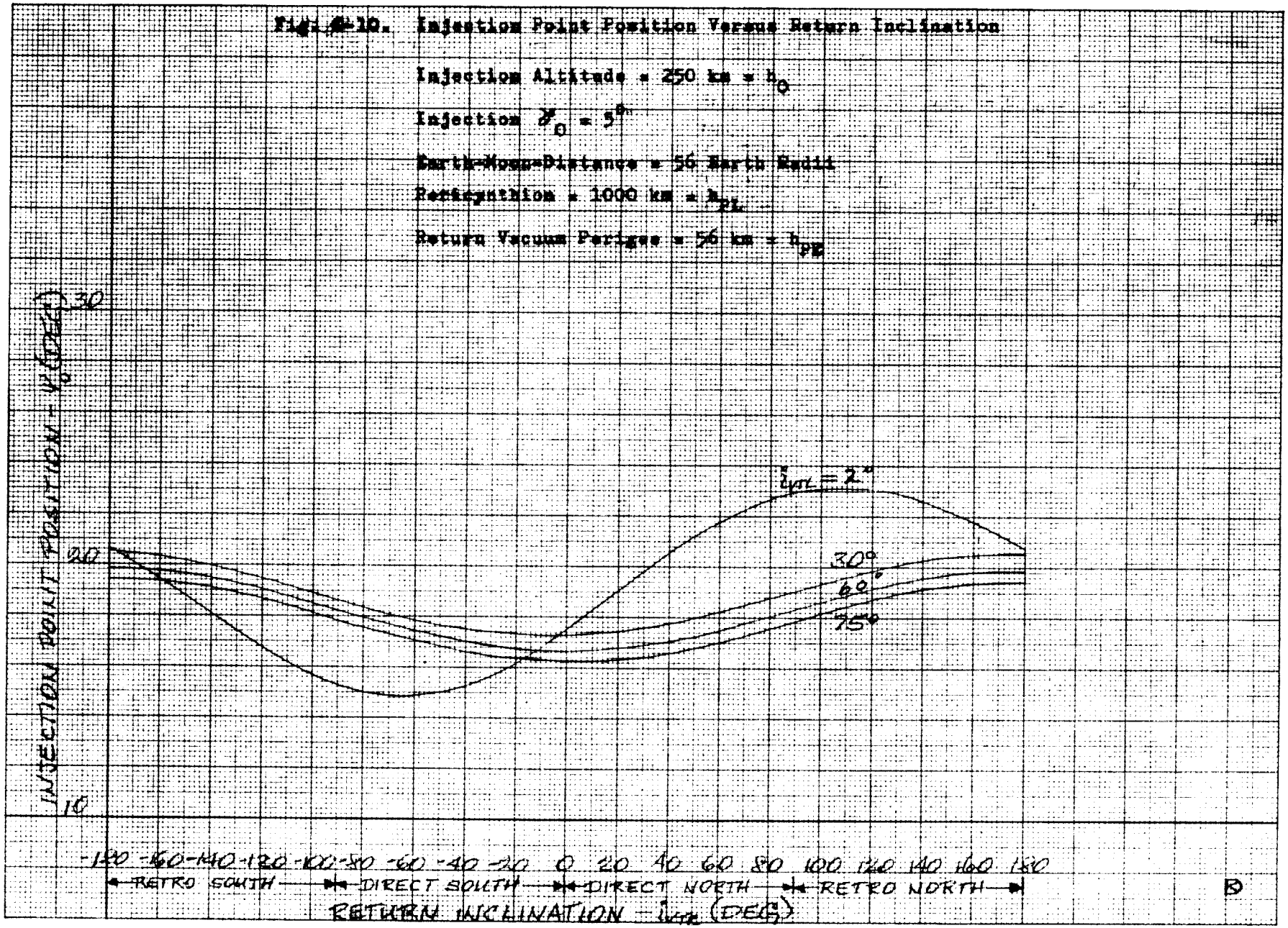

Fig. C.11: Moon Lead Angle Versus Return Inclination
Injection Altitude = 250 km = h_0
Injection $\gamma_0 = 5°$
Earth-Moon distance = 56 Earth Radii
Perisynthion = 1000 km = h_{PS}
Return Vacuum Perigee = 46 km = h_{PE}
MOON LEAD ANGLE - ψ_M (DEG)
50
30
B
RETURN INCLINATION - i (DEG)
RETRO SOUTH
DIRECT SOUTH
DIRECT NORTH
RETRO NORTH

Fig. C-12. ΔV Required To Enter Circular Lunar Orbit Versus Return Inclination

Injection Altitude = 250 km = h_0

Injection γ_0 = 5°

Earth-Moon-Distance = 56 Earth Radii

Pericynthion = 1000 km = h_{PL}

Return Vacuum Perigee = 46 km = h_{PE}

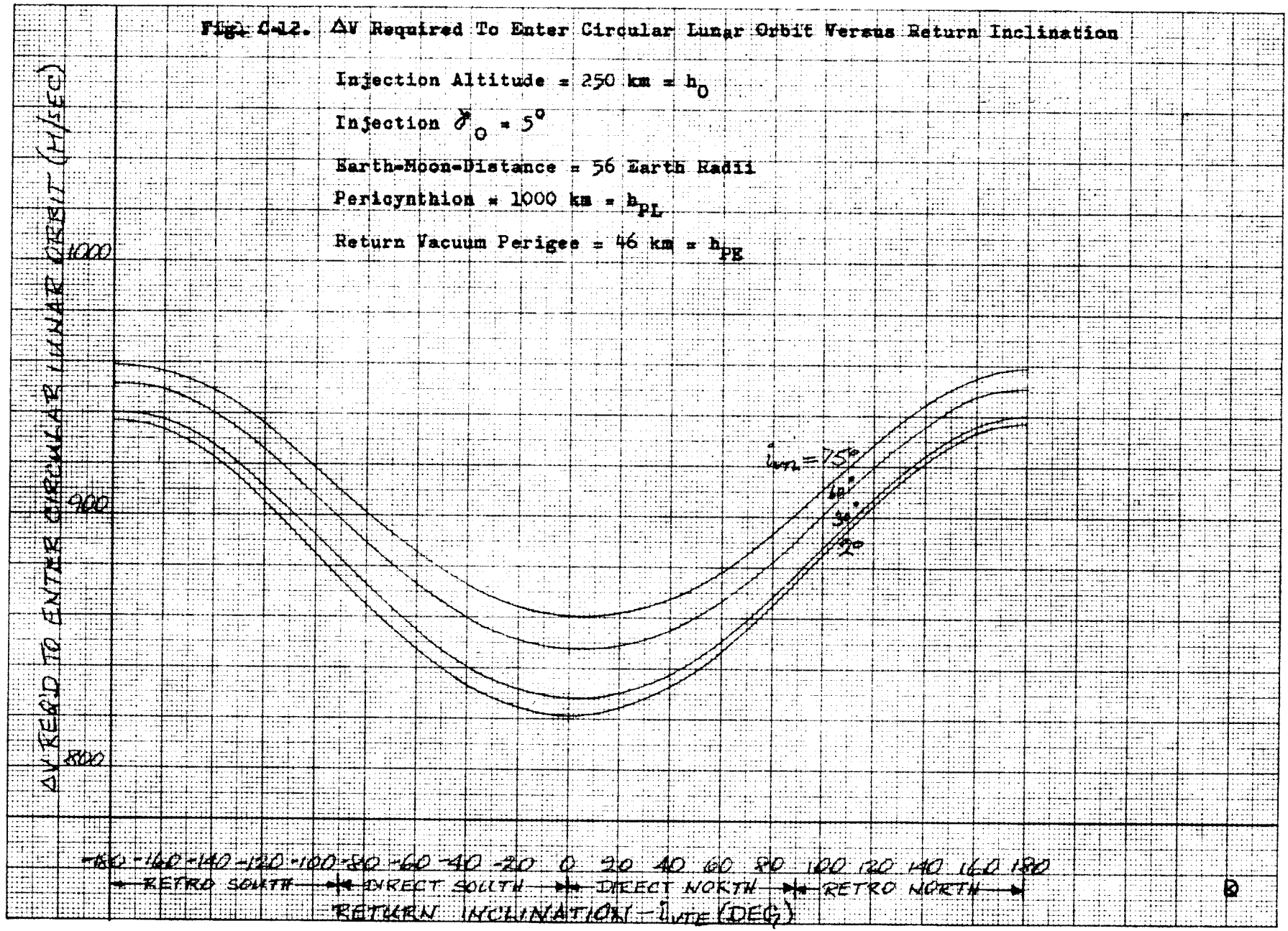

Fig. C13. Time of Perigeation Versus Return Inclination
Injection Altitude = 250 km = h_0
Injection γ_0 = 5°
Earth-Moon-Distance = 56 Earth Radii
Perigeebtion = 1060 km = h_p
Return Vacuum Perigee = 46 km = h_{pR}
TIME OF PERIGEE OCCULTATION — t_p (HR)
RETURN INCLINATION + LYDE (DEG)
i_R = 0°
i_R = 30°
i_R = 60°
i_R = 90°
-90 -60 -30 0 30 60 90 120 150 180
-120 -90 -60 -30 0 30 60 90 120 150
* RETRO SOUTH ** DIRECT SOUTH ** DIRECT NORTH ** RETRO NORTH *

Fig. G-14. Total Time Versus Return Inclination

Injection Altitude = 250 km = h_0

Injection $\gamma_0 = 5°$

Earth-Moon-Distance = 56 Earth Radii

Pericynthion = 1000 km = h_{PL}

Return Vacuum Perigee = 46 km = h_{PE}

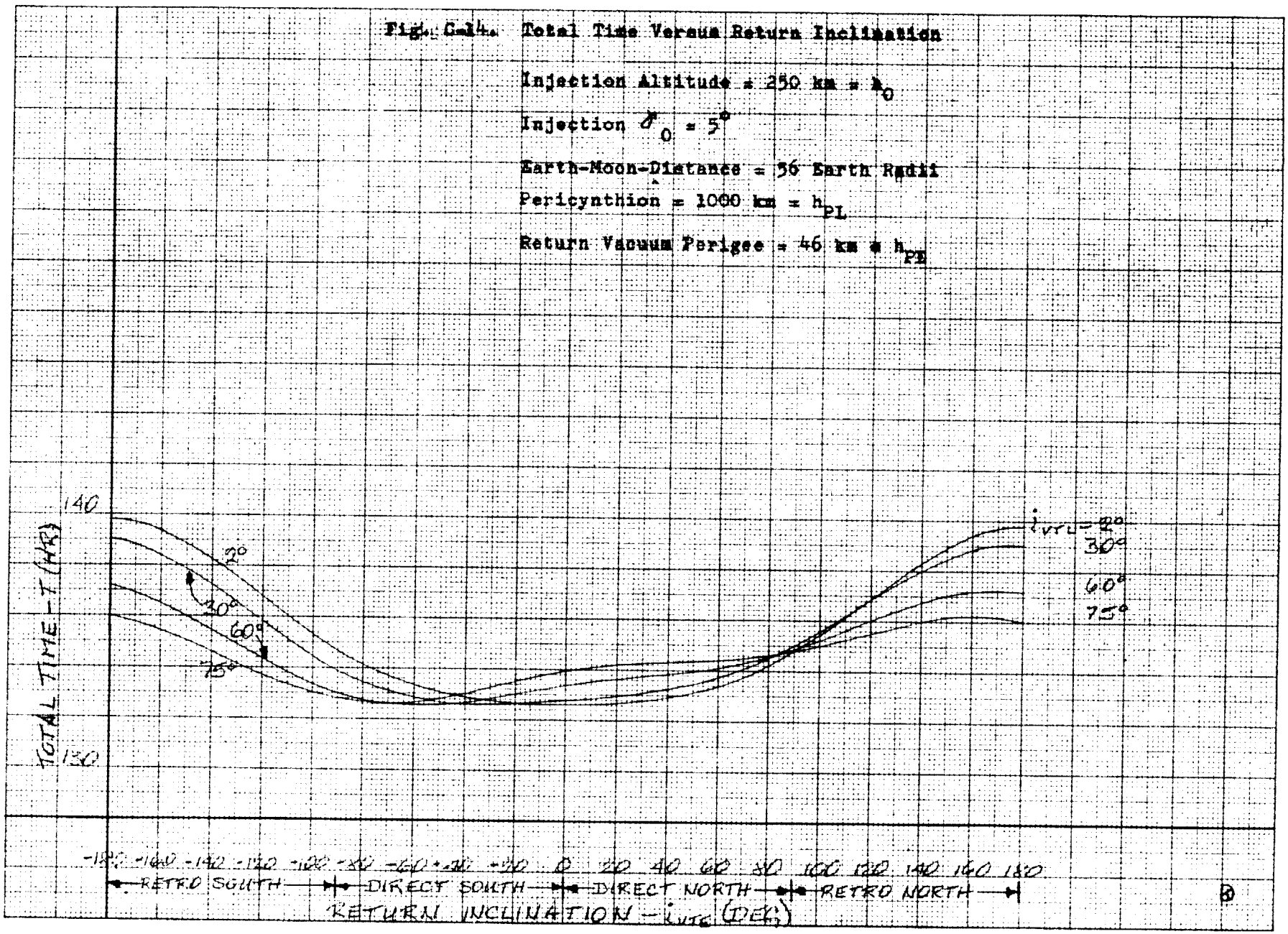

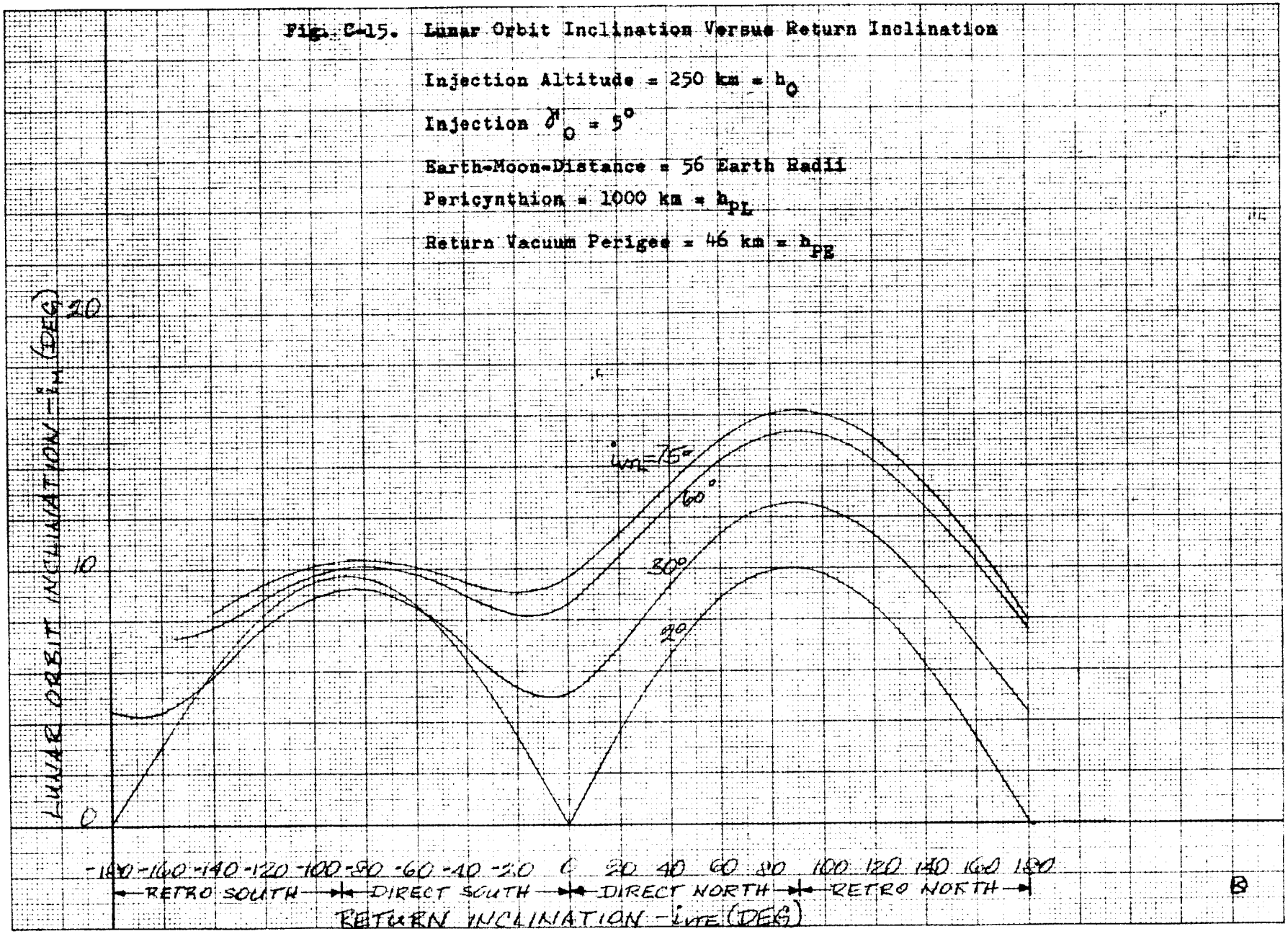
Fig. C-15. Lunar Orbit Inclination Versus Return Inclination
Injection Altitude = 250 km = h_0
Injection γ_0 = 5°
Earth-Moon-Distance = 56 Earth Radii
Pericynthion = 1000 km = h_{PL}
Return Vacuum Perigee = 46 km = h_{PE}
LUNAR ORBIT INCLINATION - i_{LM} (DEG)
20
10
0
i_{LM}=75°
60°
30°
90°
-180 -160 -140 -120 -100 -80 -60 -40 -20 0 20 40 60 80 100 120 140 160 180
RETRO SOUTH
DIRECT SOUTH
DIRECT NORTH
RETRO NORTH
RETURN INCLINATION - i_{RE} (DEG)

Fig. C-16. Lunar Orbit Orientation Versus Return Inclination

Injection Altitude = 250 km = h_0

Injection $\gamma_0 = 5°$

Earth-Moon-Distance = 56 Earth Radii

Pericynthion = 1000 km = h_{PL}

Return Vacuum Perigee = 46 km = h_{PE}

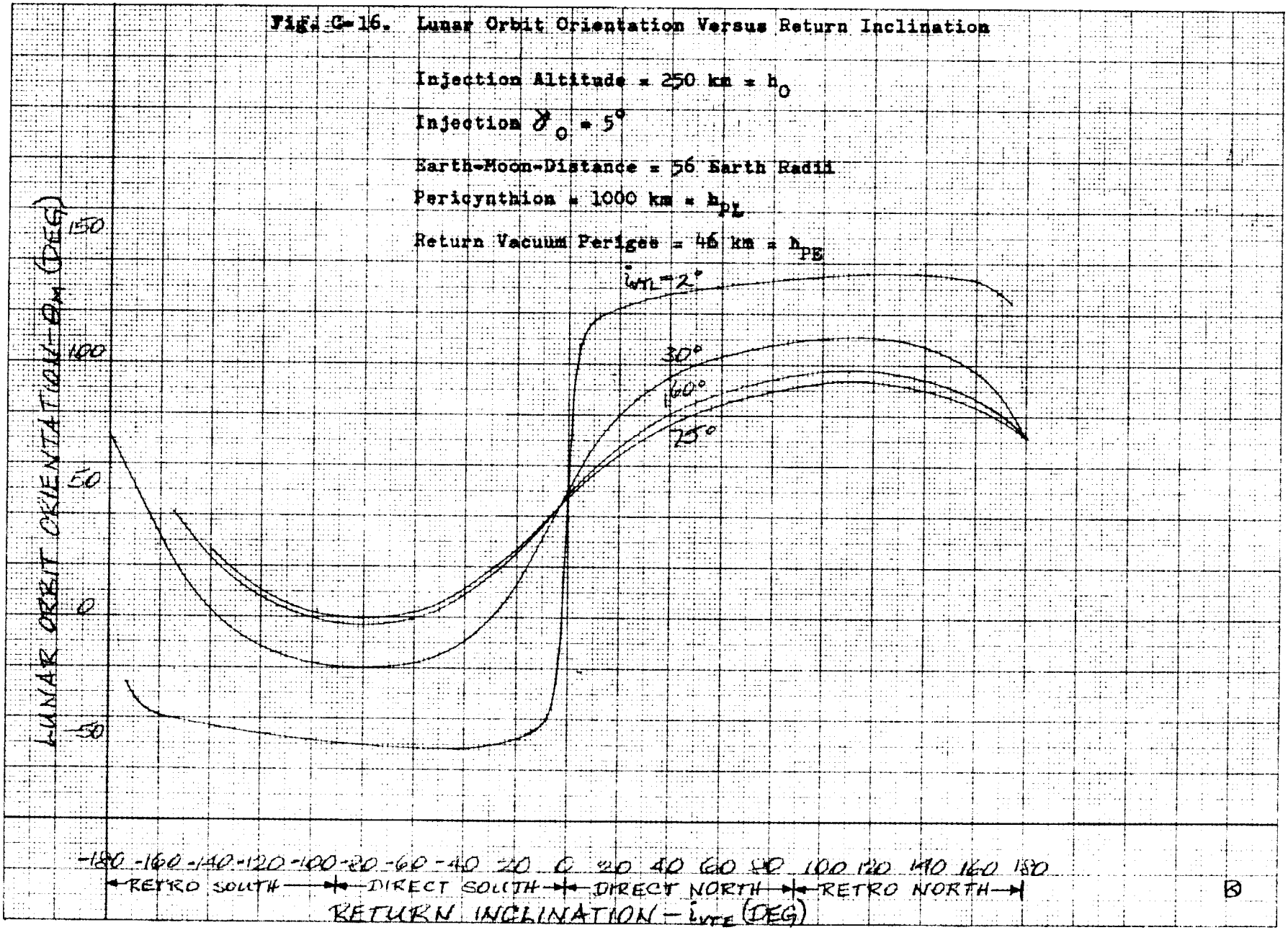

Fig. C-17. Injection Velocity Versus Return Inclination

Injection Altitude = 250 km = h_0

Injection $\gamma_0 = 5°$

Earth-Moon-Distance = 56 Earth Radii

Pericynthion = 5000 km = h_{PL}

Return Vacuum Perigee = 46 km = h_{PE}

For Inject North

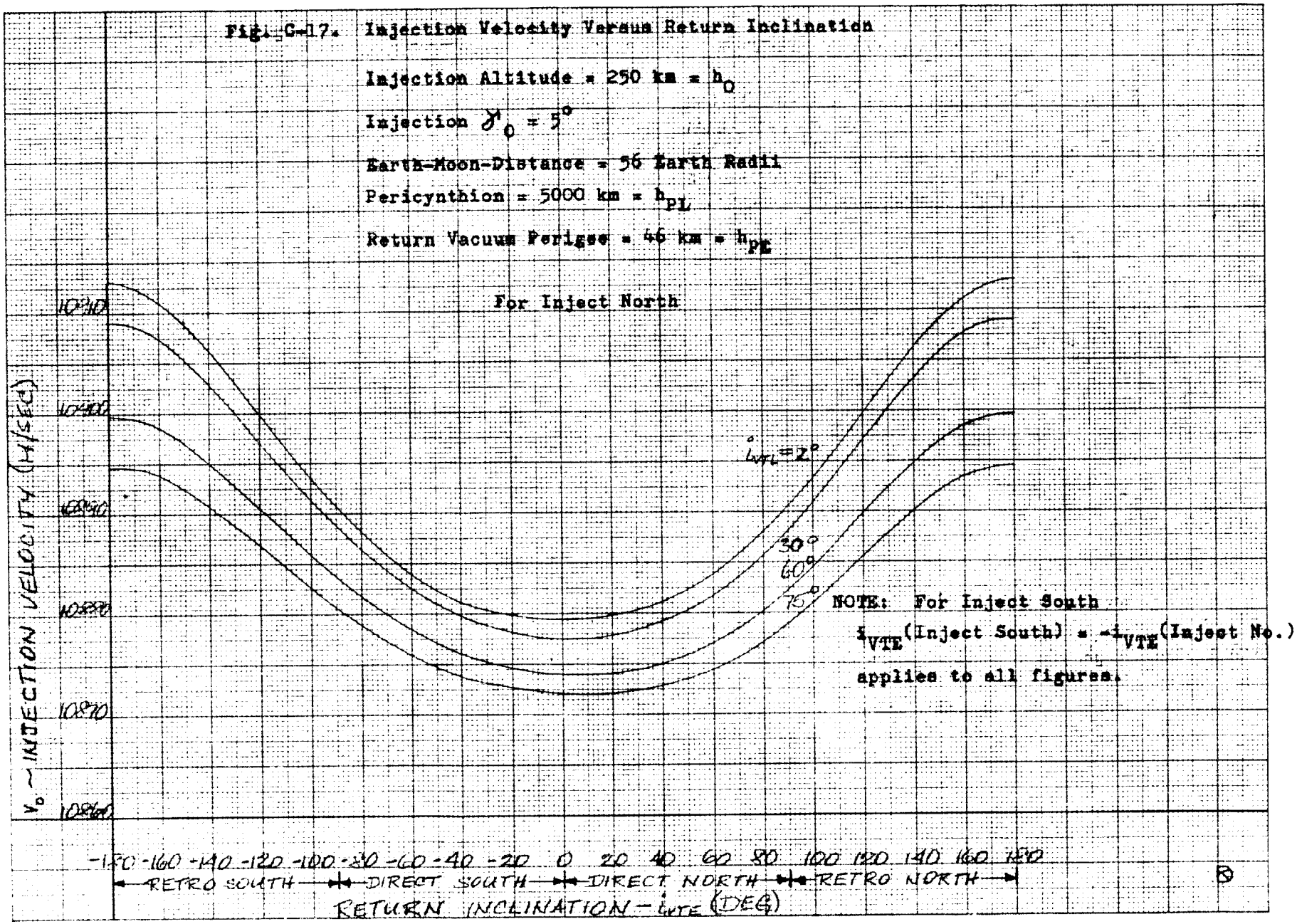

NOTE: For Inject South

i_{VTE}(Inject South) = $-i_{VTE}$(Inject No.)

applies to all figures.

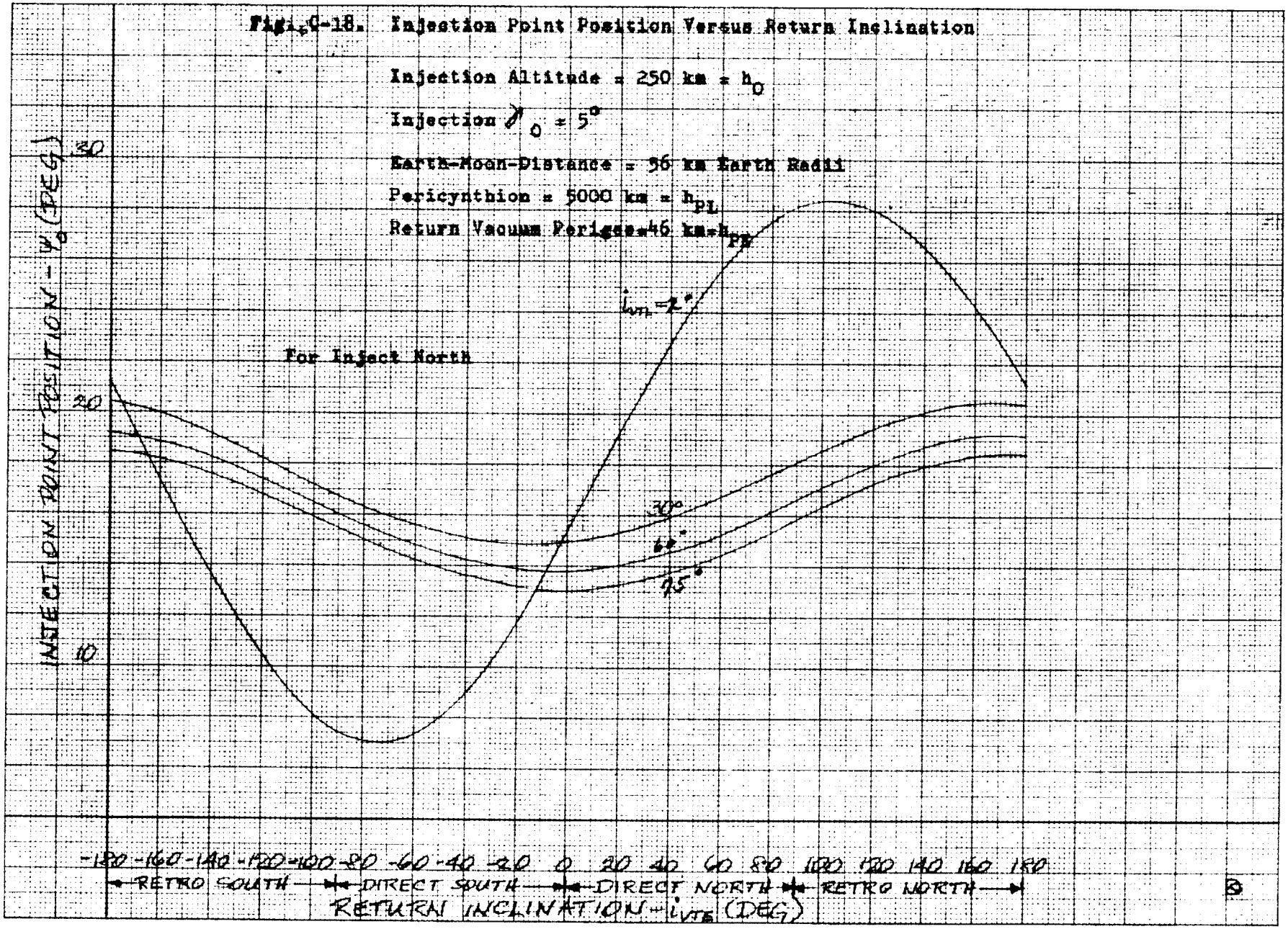
Fig. C-18. Injection Point Position Versus Return Inclination
Injection Altitude = 250 km = h_0
Injection γ_0 = 5°
Earth-Moon-Distance = 56 Earth Radii
Pericynthion = 5000 km = h_{PL}
Return Vacuum Perigee = 46 km = h_{PE}
i_{VTL} = 2°
For Inject North
30°
60°
75°
INJECTION POINT POSITION - ψ_0 (DEG)
30
20
10
-180 -160 -140 -120 -100 -80 -60 -40 -20 0 20 40 60 80 100 120 140 160 180
RETRO SOUTH
DIRECT SOUTH
DIRECT NORTH
RETRO NORTH
RETURN INCLINATION - i_{VTE} (DEG)

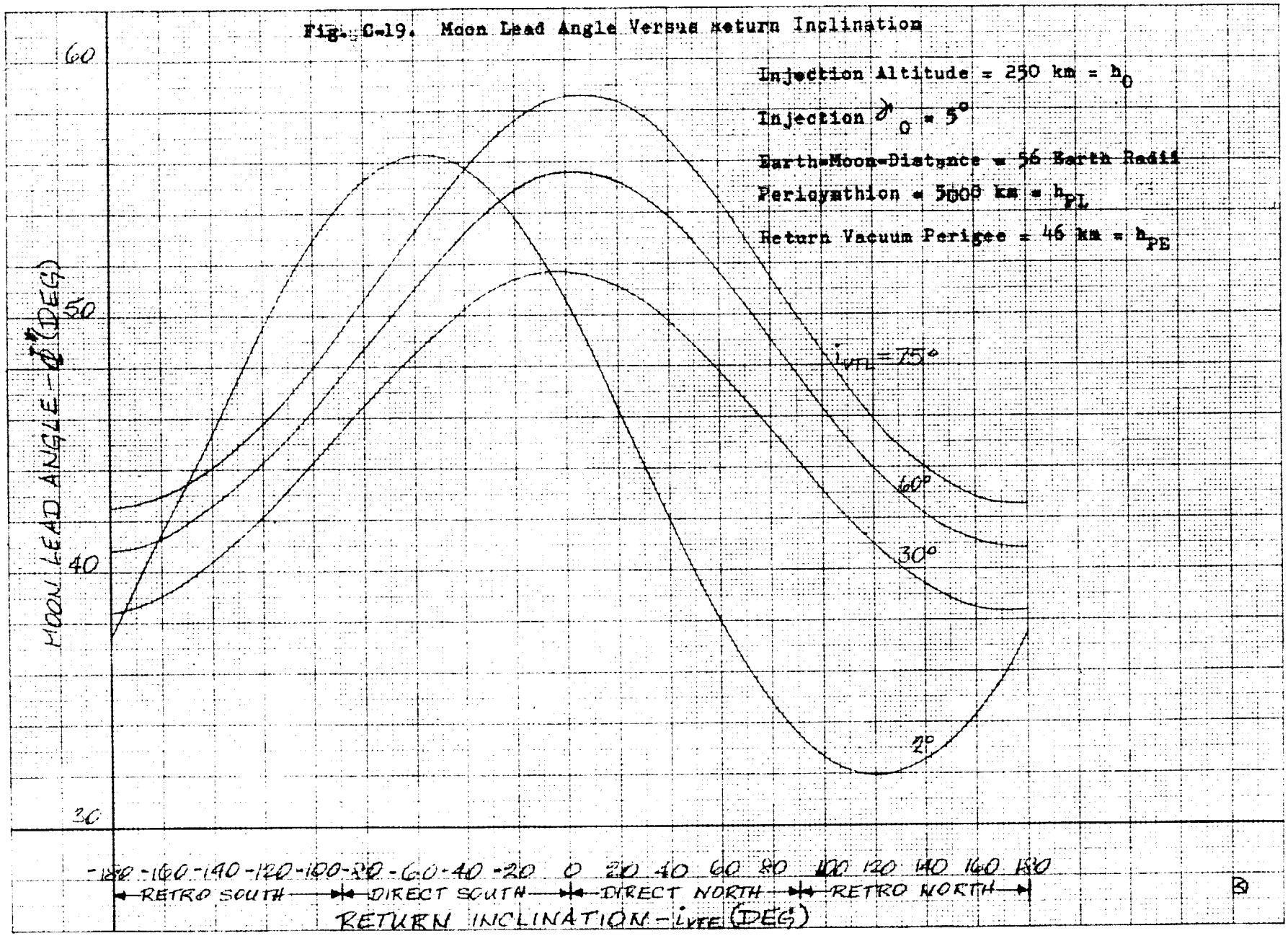

Fig. C-19. Moon Lead Angle Versus Return Inclination

Fig. C-20. ΔV Required To Enter Circular Lunar Orbit Versus Return Inclination

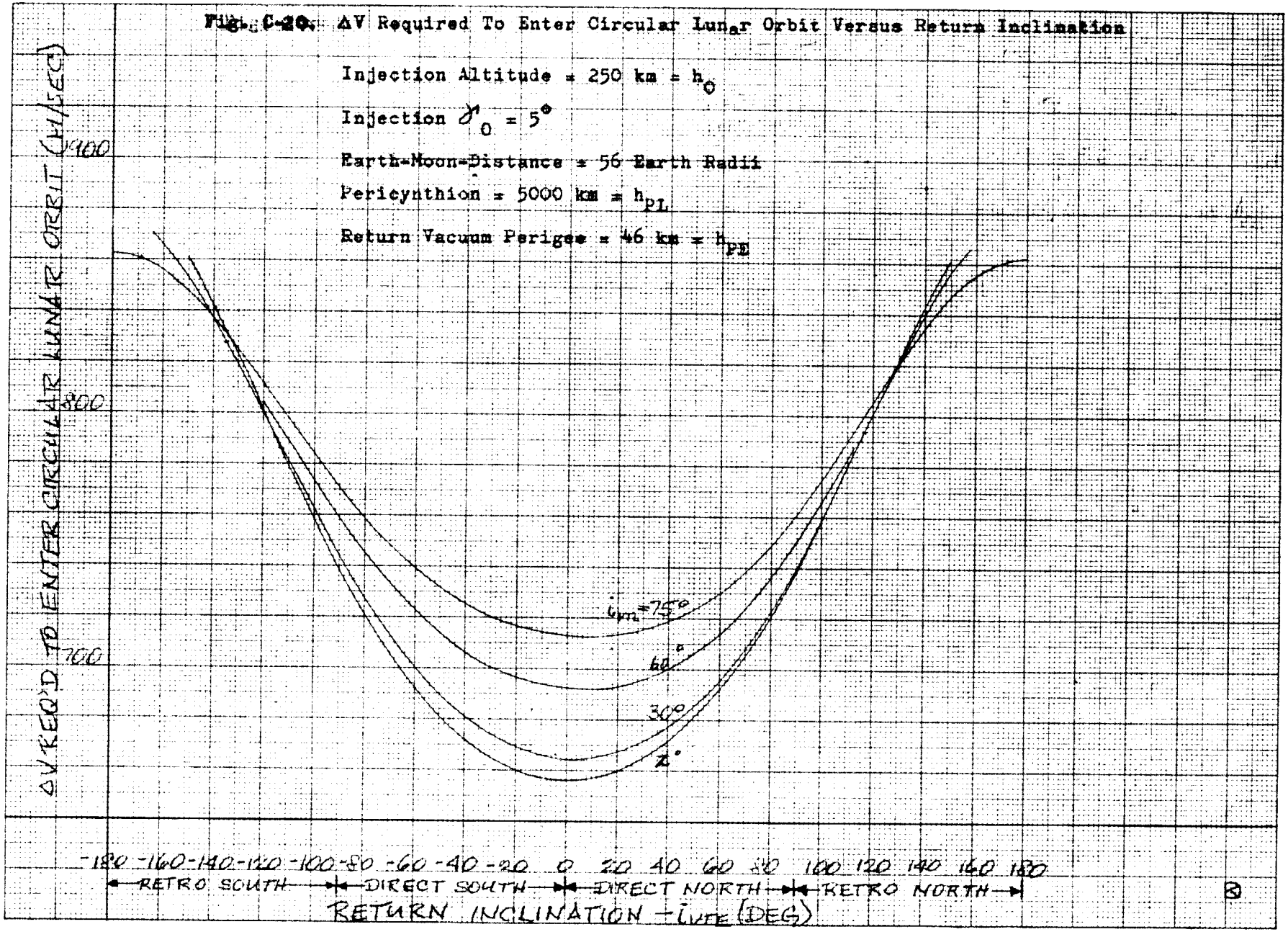

-180 -160 -140 -120 -100 -80 -60 -40 -20 0 20 40 60 80 100 120 140 160 180
RETURN INCLINATION ~ INTS (DEG)

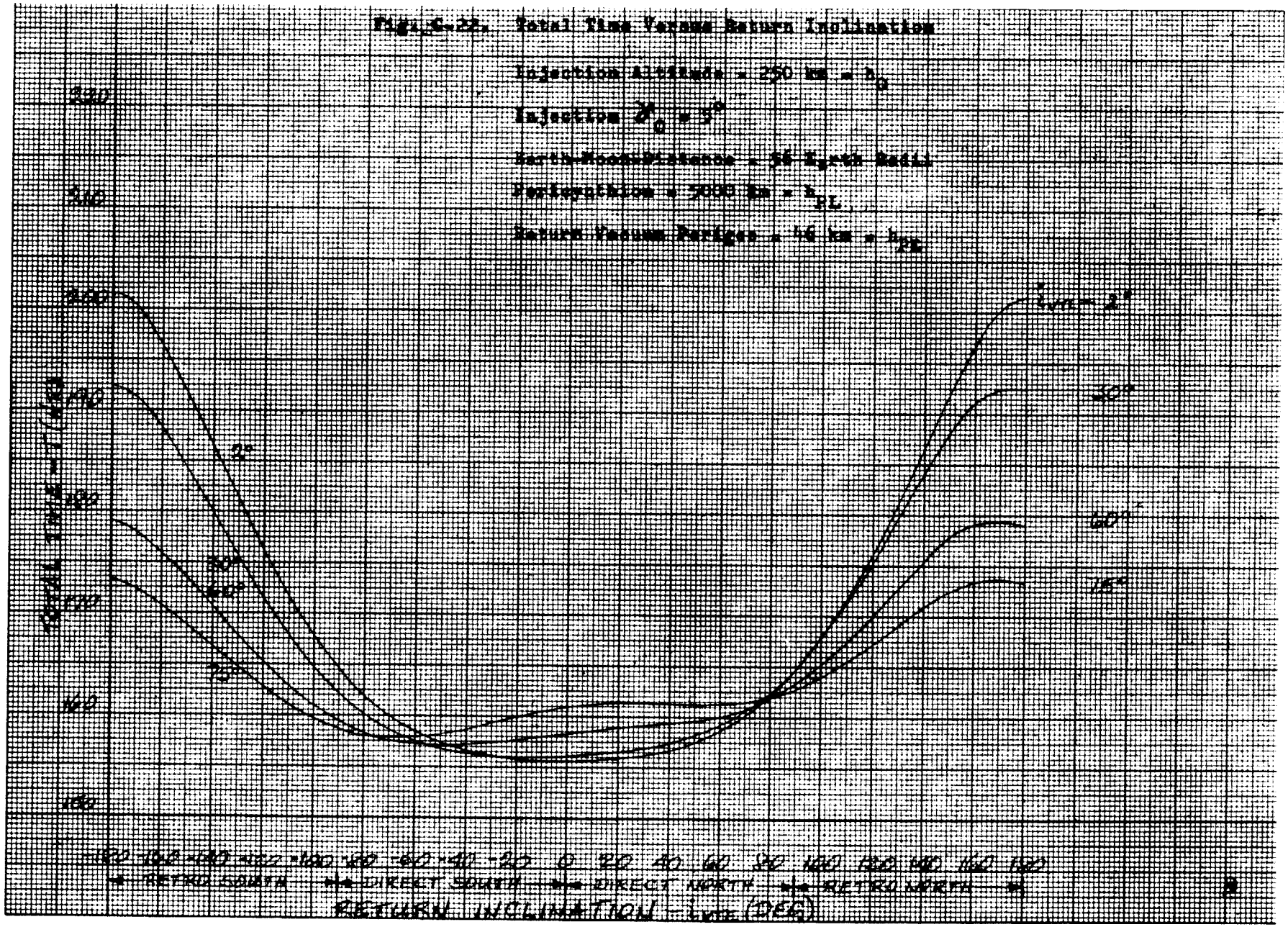
Fig. C-22. Total Time Versus Return Inclination
Injection Altitude = 250 km = h_0
Injection γ_0 = 3°
Earth-Moon Distance = 56 R_E each Radii
Perigee Altitude = 3000 km = h_{PL}
Return Vacuum Perigee = 46 km = h_{PR}
i_{ret} = 2°
30°
60°
75°
2°
30°
60°
75°
RETURN INCLINATION = i_{RET} (DEG)
RETRO SOUTH
DIRECT SOUTH
DIRECT NORTH
RETRO NORTH

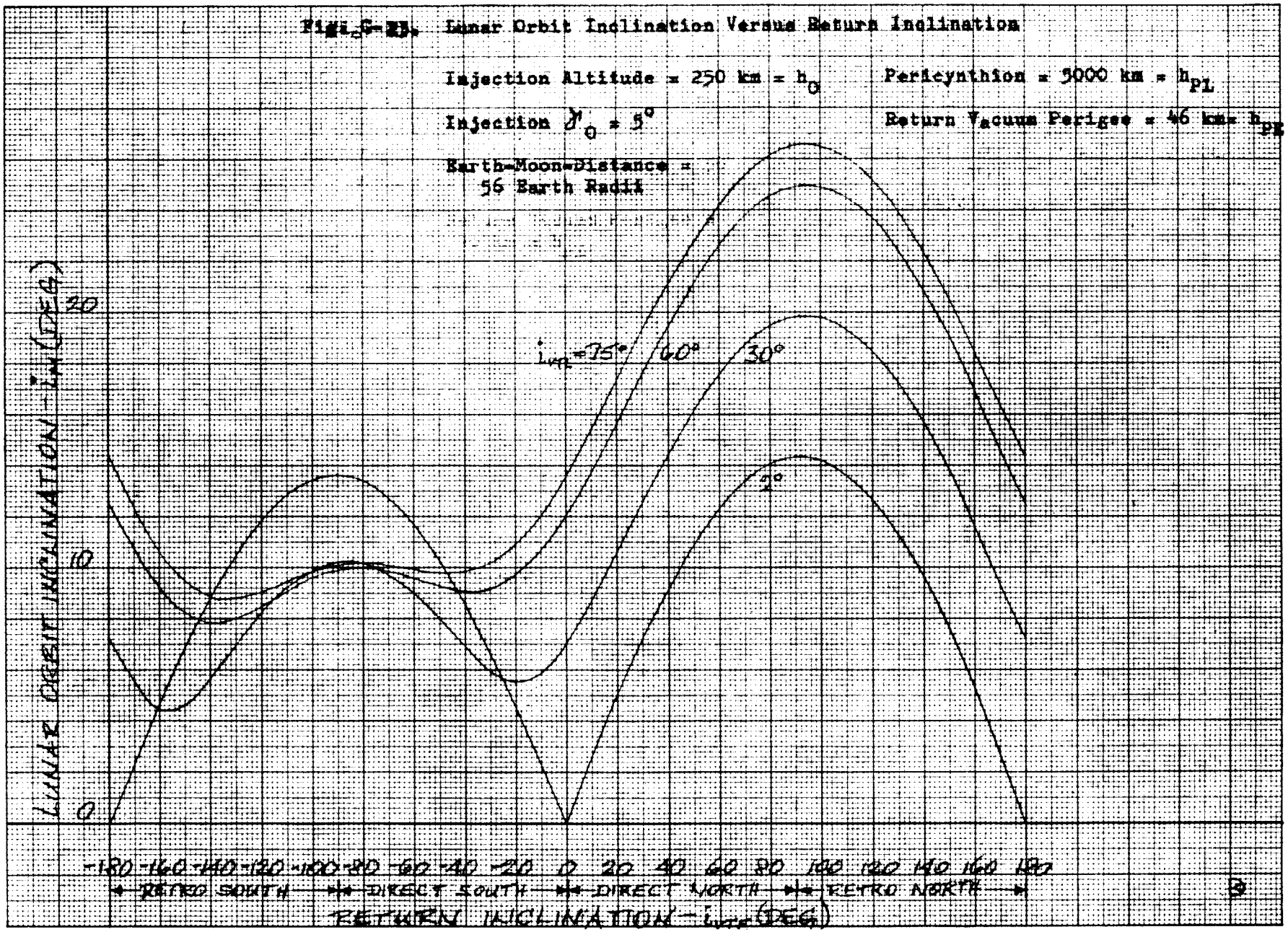
Fig. G-23. Lunar Orbit Inclination Versus Return Inclination
Injection Altitude = 250 km = h_0
Injection γ_0 = 5°
Earth-Moon-Distance = 56 Earth Radii
Pericynthion = 3000 km = h_{PL}
Return Vacuum Perigee = 46 km = h_{pr}
i_{vn}=75°
60°
30°
7°
LUNAR ORBIT INCLINATION - i_{vn} (DEG)
0
60
120
-180 -160 -140 -120 -100 -80 -60 -40 -20 0 20 40 60 80 100 120 140 160 180
RETRO SOUTH
DIRECT SOUTH
DIRECT NORTH
RETRO NORTH
RETURN INCLINATION - i_{vr} (DEG)

Fig. C-24. Lunar Orbit Orientation Versus Return Inclination

Injection Altitude = 250 km = h_0

Injection γ_0 = 5°

Earth-Moon-Distance = 56 Earth Radii

Pericynthion = 5000 km = h_{PL}

Return Vacuum Perigee = 46 km = $h_{PE_{VAC}}$

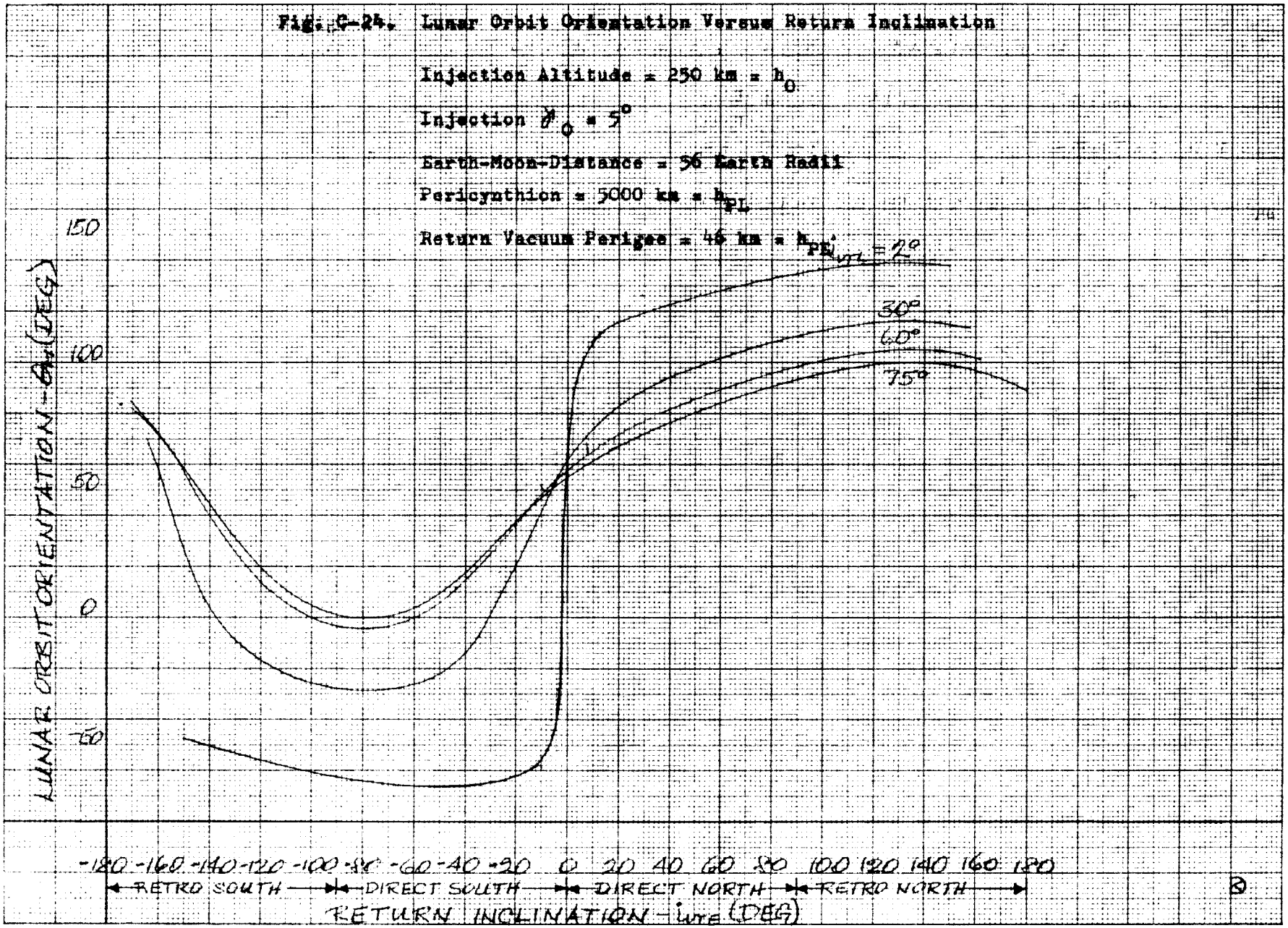

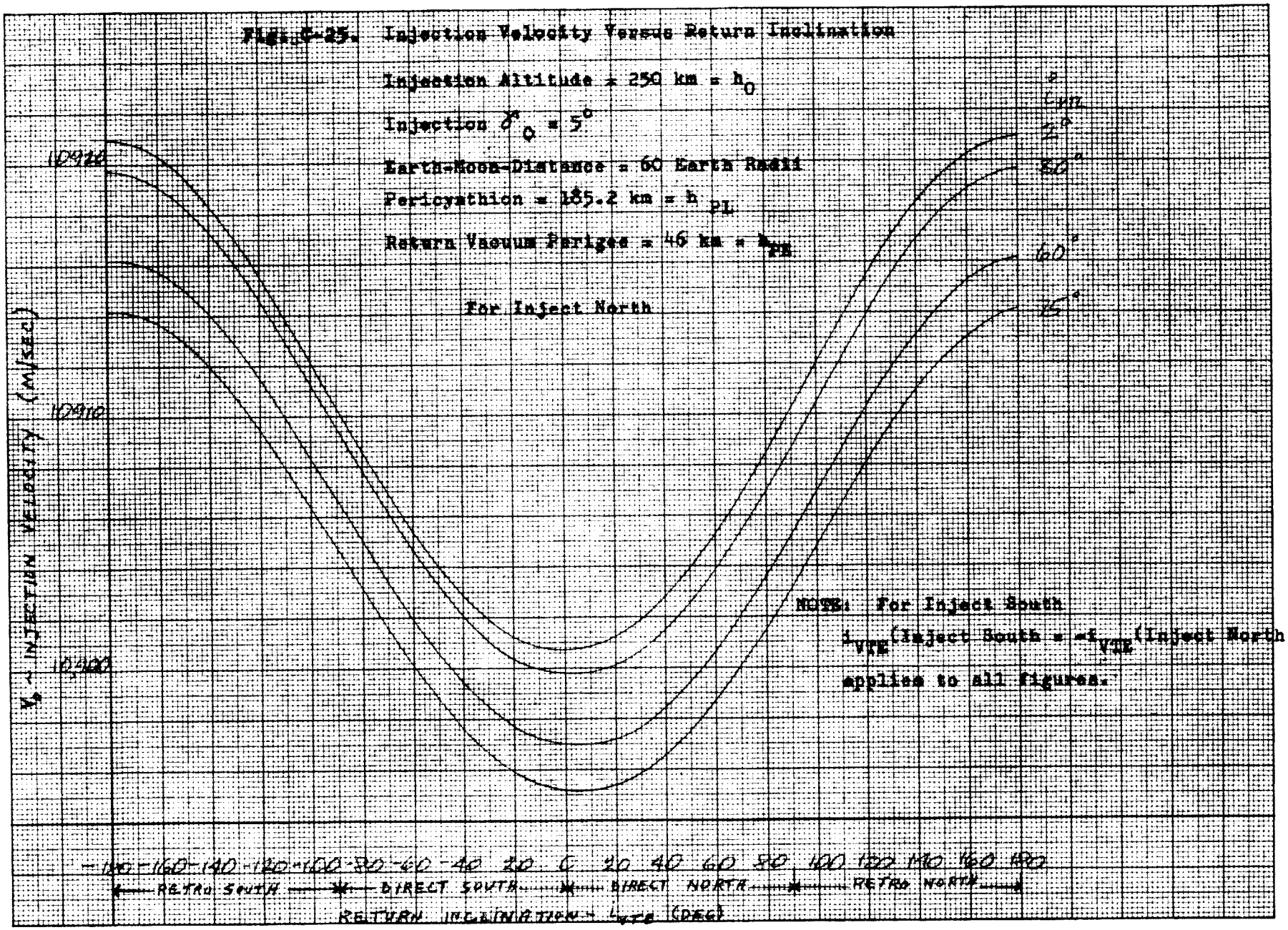
Fig. C-25. Injection Velocity Versus Return Inclination
Injection Altitude = 250 km = h_0
Injection $\delta^\circ_0 = 5^\circ$
Earth-Moon-Distance = 60 Earth Radii
Pericynthion = 185.2 km = h_{PL}
Return Vacuum Perigee = 46 km = h_{PE}
For Inject North
NOTE: For Inject South
i_{VRE}(Inject South) = $-i_{VRE}$(Inject North)
applies to all figures.
i_{VRE}
2°
30°
60°
45°
INJECTION VELOCITY (M/SEC)
V_0
10,900
10,800
10,400
-180 -160 -140 -120 -100 -80 -60 -40 -20 0 20 40 60 80 100 120 140 160 180
RETRO SOUTH
DIRECT SOUTH
DIRECT NORTH
RETRO NORTH
RETURN INCLINATION = i_{VRE} (DEG)

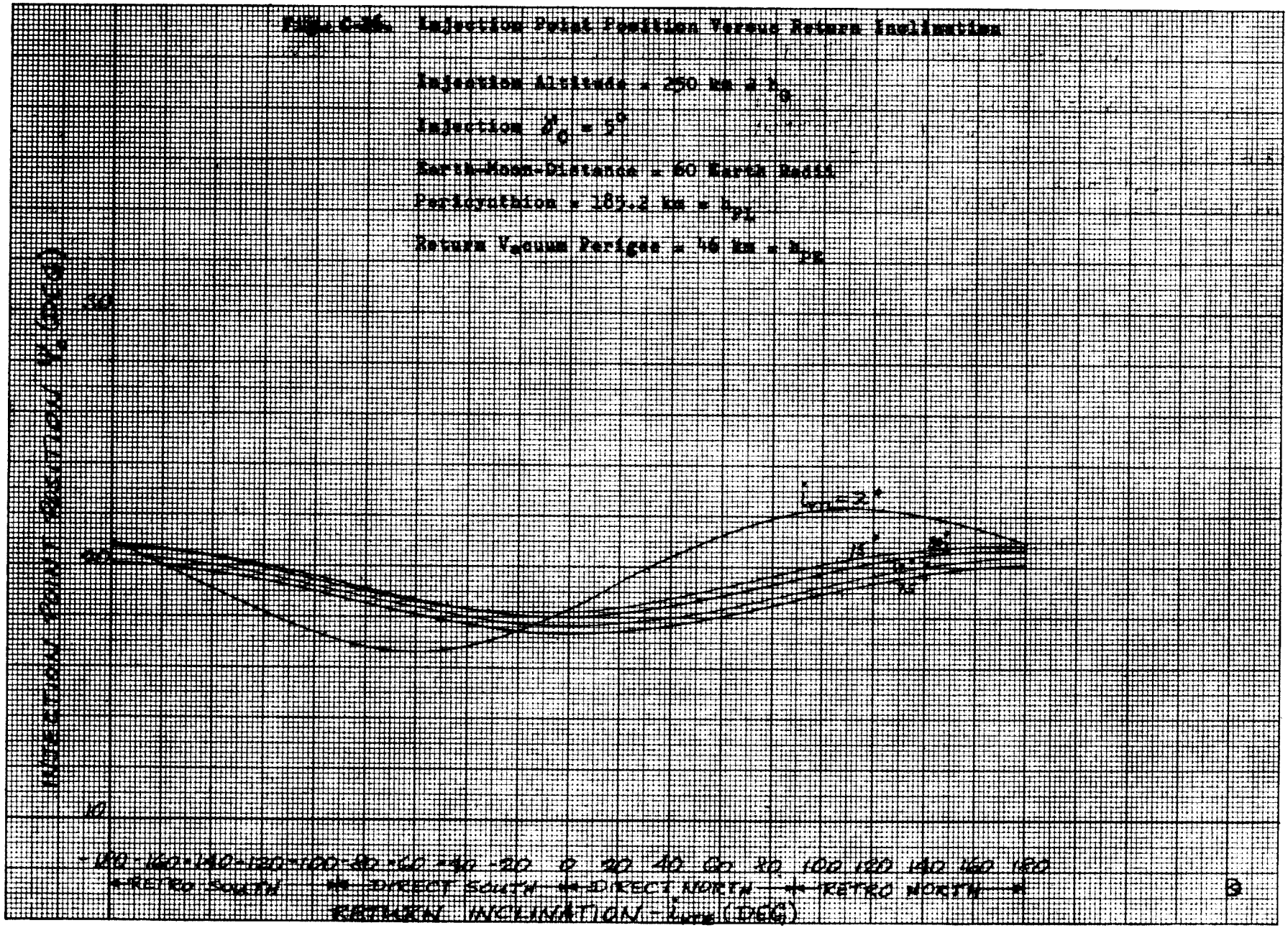
Fig. C-46. Injection Point Position Versus Return Inclination
Injection Altitude = 250 km = h_0
Injection δ_0^M = 5°
Earth-Moon-Distance = 60 Earth Radii
Perigee = 185.2 km = h_{p_1}
Return Vacuum Perigee = 46 km = h_{p_2}
INJECTION POINT POSITION δ_0^M (DEG)
$i_{ret} = 2°$
15°
RETURN INCLINATION - i_{ret} (DEG)
-160 -140 -120 -100 -80 -60 -40 -20 0 20 40 60 80 100 120 140 160 180
RETRO SOUTH
DIRECT SOUTH
DIRECT NORTH
RETRO NORTH

Fig. C-27. Moon Lead Angle Versus Return Inclination

Injection Altitude = 250 km = h_0

Injection $\gamma_0 = 5°$

Earth-Moon-Distance = 60 Earth Radii

Pericynthion = 185.2 km = h_{PL}

Return Vacuum Perigee = 46 km = h_{PE}

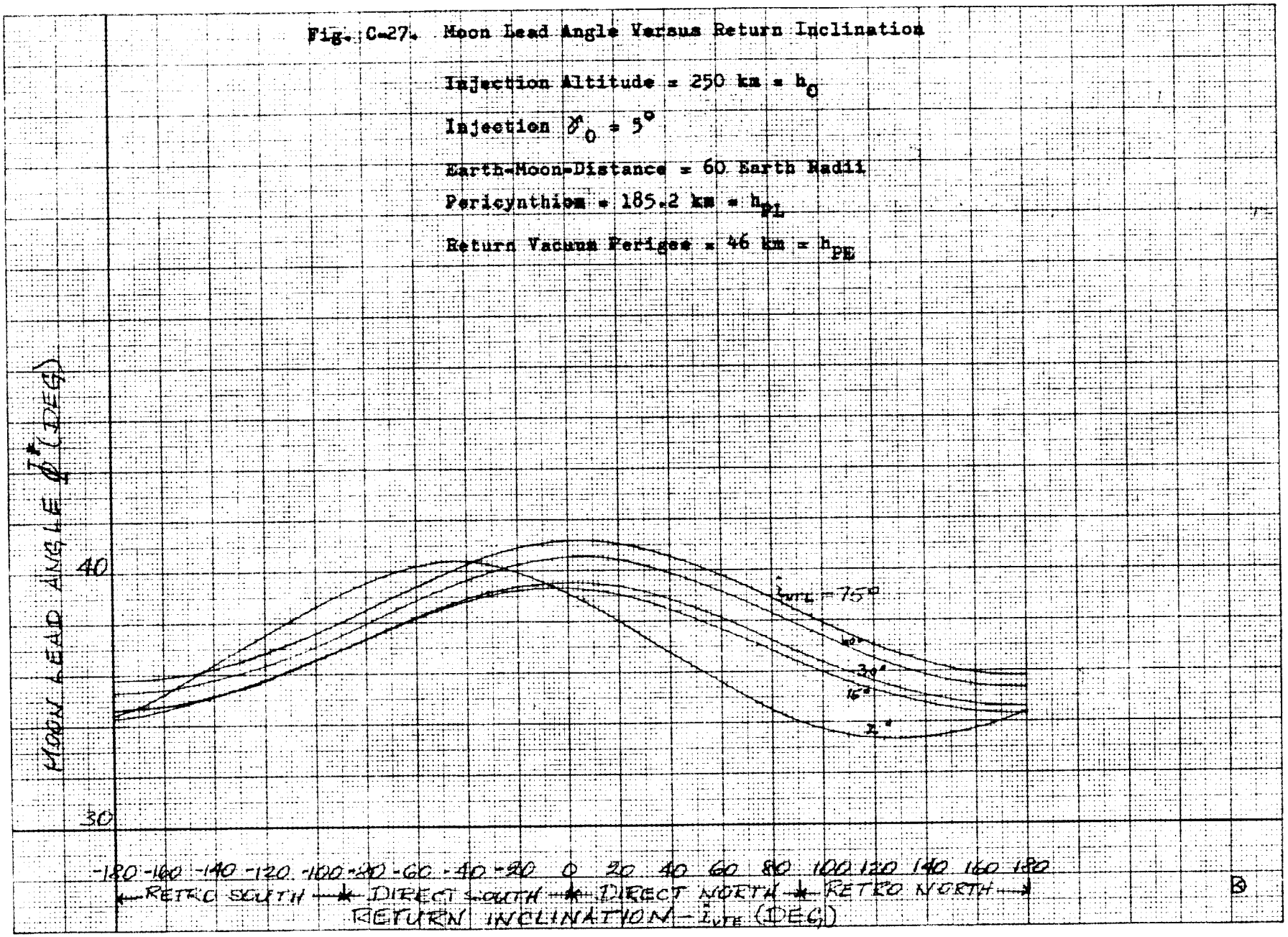

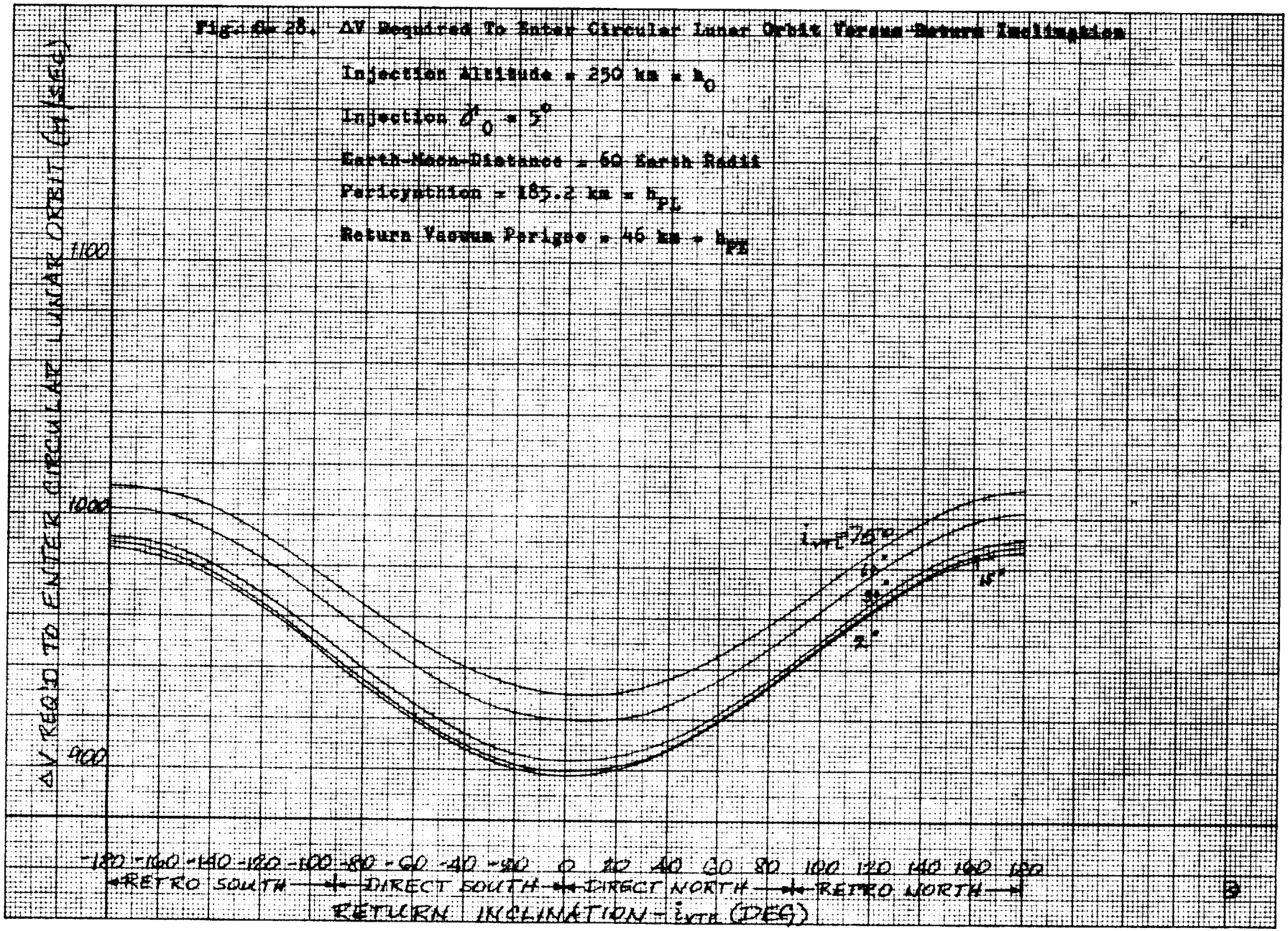
Fig. 6a-28. ΔV Required To Enter Circular Lunar Orbit Versus Return Inclination
Injection Altitude = 250 km = h_0
Injection δ°_0 = 5°
Earth-Moon-Distance = 60 Earth Radii
Pericynthion = 185.2 km = h_{PL}
Return Vacuum Perigee = 46 km = h_{PE}
ΔV REQ'D TO ENTER CIRCULAR LUNAR ORBIT (M/SEC)
1100
1000
900
i_{VTL} = 76°
64°
52°
40°
28°
16°
4°
-180 -160 -140 -120 -100 -80 -60 -40 -20 0 20 40 60 80 100 120 140 160 180
RETRO SOUTH
DIRECT SOUTH
DIRECT NORTH
RETRO NORTH
RETURN INCLINATION - i_{VTL} (DEG)

Fig. 6.29 Time of Perigynthion Versus Return Inclination
Injection Altitude = 250 km = h_0
Injection $\gamma_\oplus$ = 5°
Earth-Moon-Distance = 60 Earth Radii
Perigynthion = 185.2 km = h_{PL}
Return Vacuum Perigee = 46 km = h_{PE}
TIME OF DECAY/VARIATION - t_p (hrs)
i_{VTL} = 25°
60°
30°
2°
-180 -160 -140 -120 -100 -80 -60 -40 -20 0 20 40 60 80 100 120 140 160 180
RETRO SOUTH
DIRECT SOUTH
DIRECT NORTH
RETRO NORTH
RETURN INCLINATION - i_{VTE} (DEG)

Fig. C-30. Total Time Versus Return Inclination

Injection Altitude = 250 km = h_0

Injection γ_0 = 5°

Earth-Moon-Distance = 60 Earth Radii

Pericynthion = 185.2 km = h_{PL}

Return Vacuum Perigee = 46 km = h_{PE}

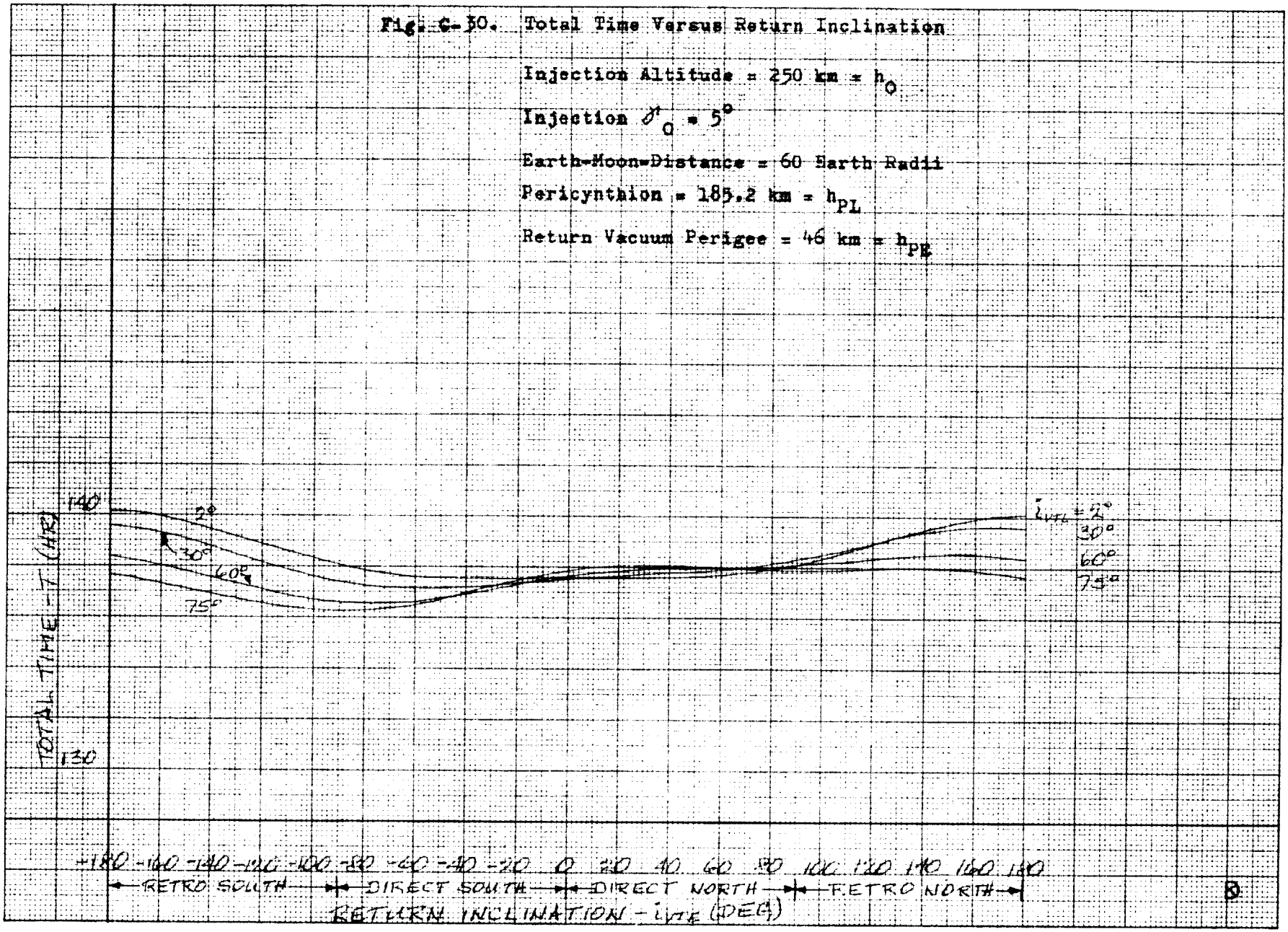

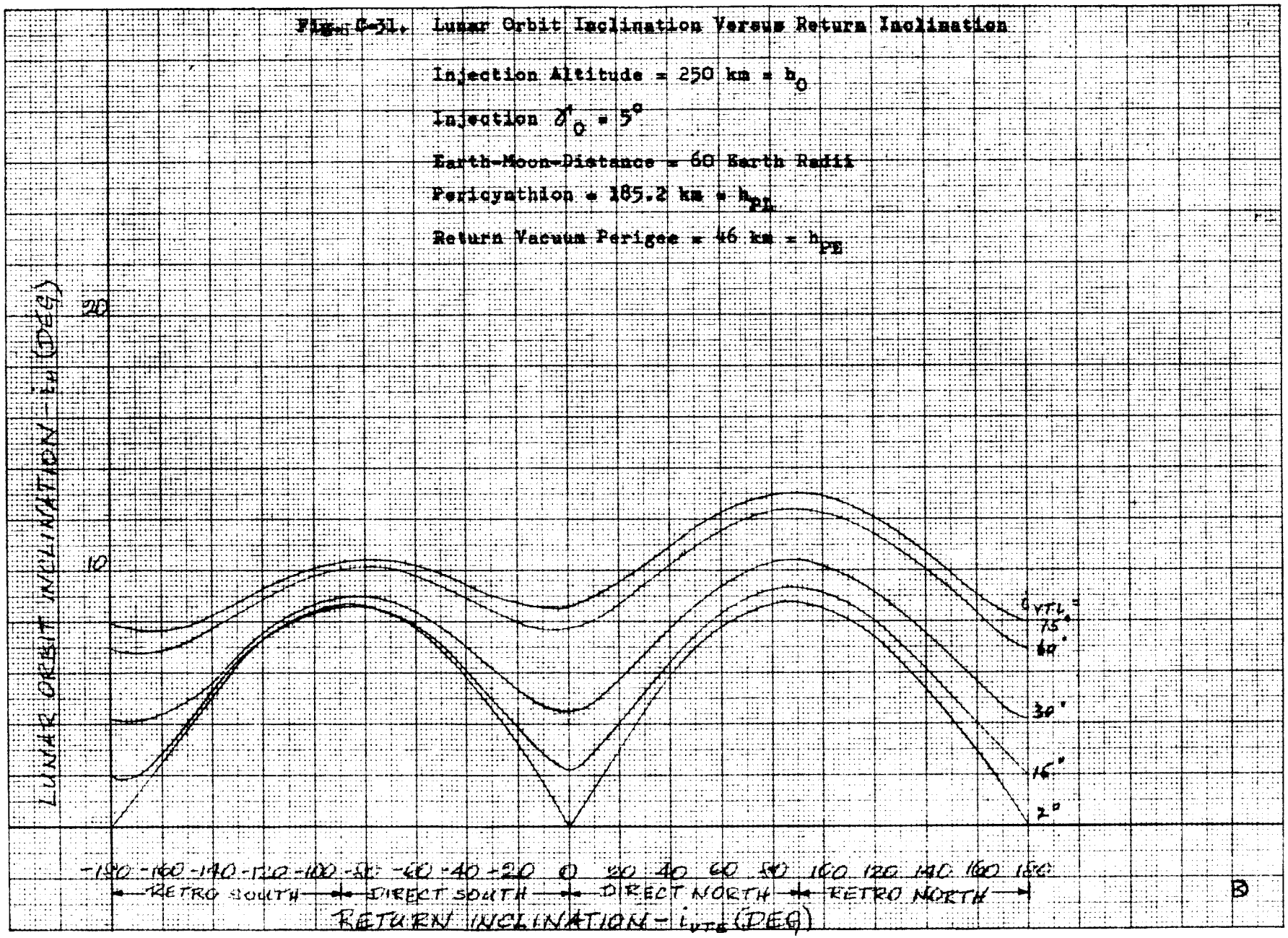
Fig. C-31. Lunar Orbit Inclination Versus Return Inclination
Injection Altitude = 250 km = h_0
Injection γ_0 = 5°
Earth-Moon-Distance = 60 Earth Radii
Pericynthion = 185.2 km = h_{PL}
Return Vacuum Perigee = 46 km = h_{PE}
LUNAR ORBIT INCLINATION - i_{LO} (DEG)
20
10
$\dot{G}_{VTL}$ = 75°
60°
30°
15°
2°
-180 -160 -140 -120 -100 -80 -60 -40 -20 0 20 40 60 80 100 120 140 160 180
RETRO SOUTH
DIRECT SOUTH
DIRECT NORTH
RETRO NORTH
RETURN INCLINATION - i_{VTE} (DEG)
B

Fig. C-32. Lunar Orbit Orientation Versus Return Inclination

Injection Altitude = 250 km = h_0

Injection $\gamma_0 = 5°$

Earth-Moon-Distance = 60 Earth Radii

Pericynthion = 185.2 km = h_{pL}

Return Vacuum Perigee = 46 km = h_{pE}

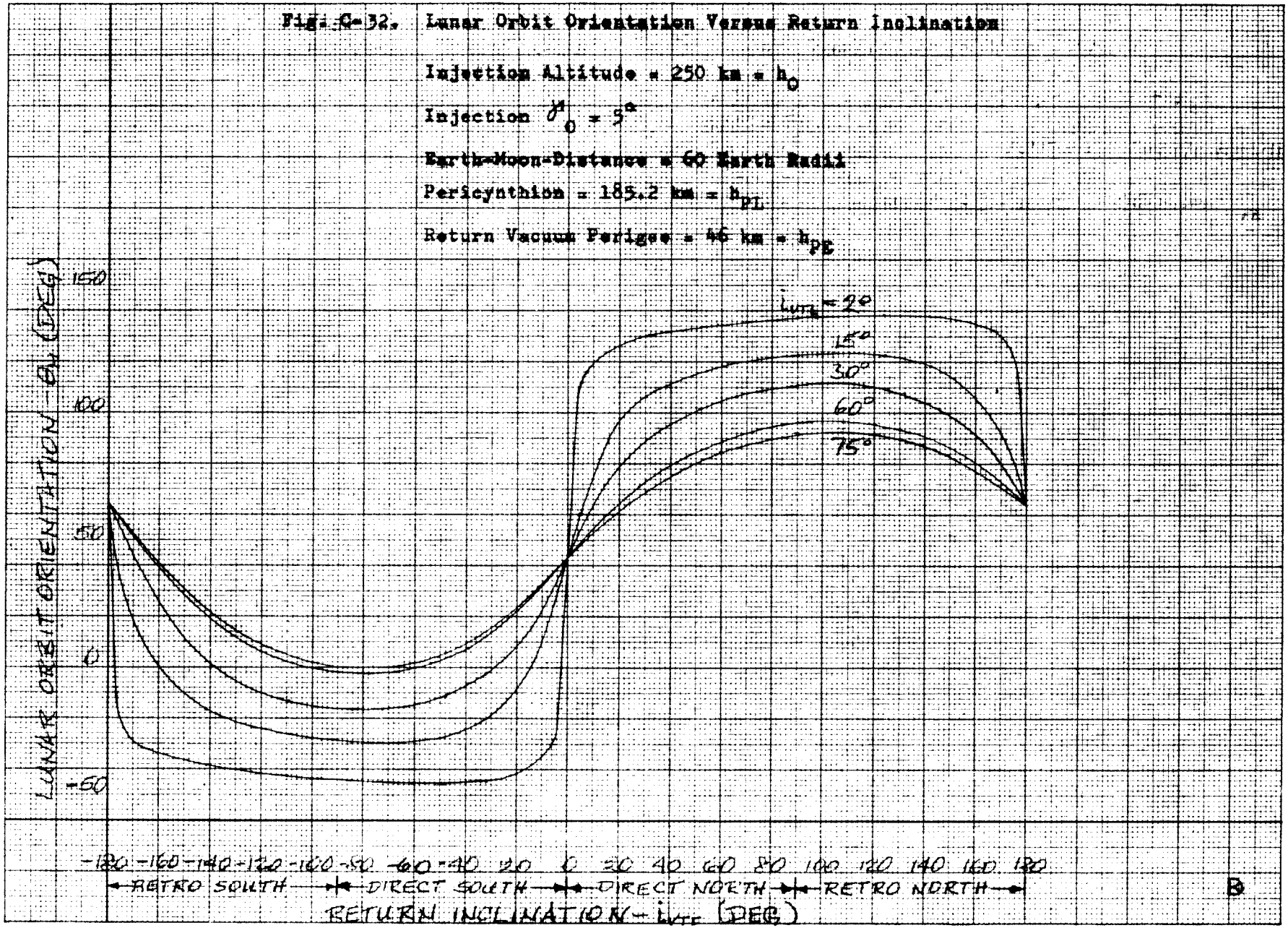

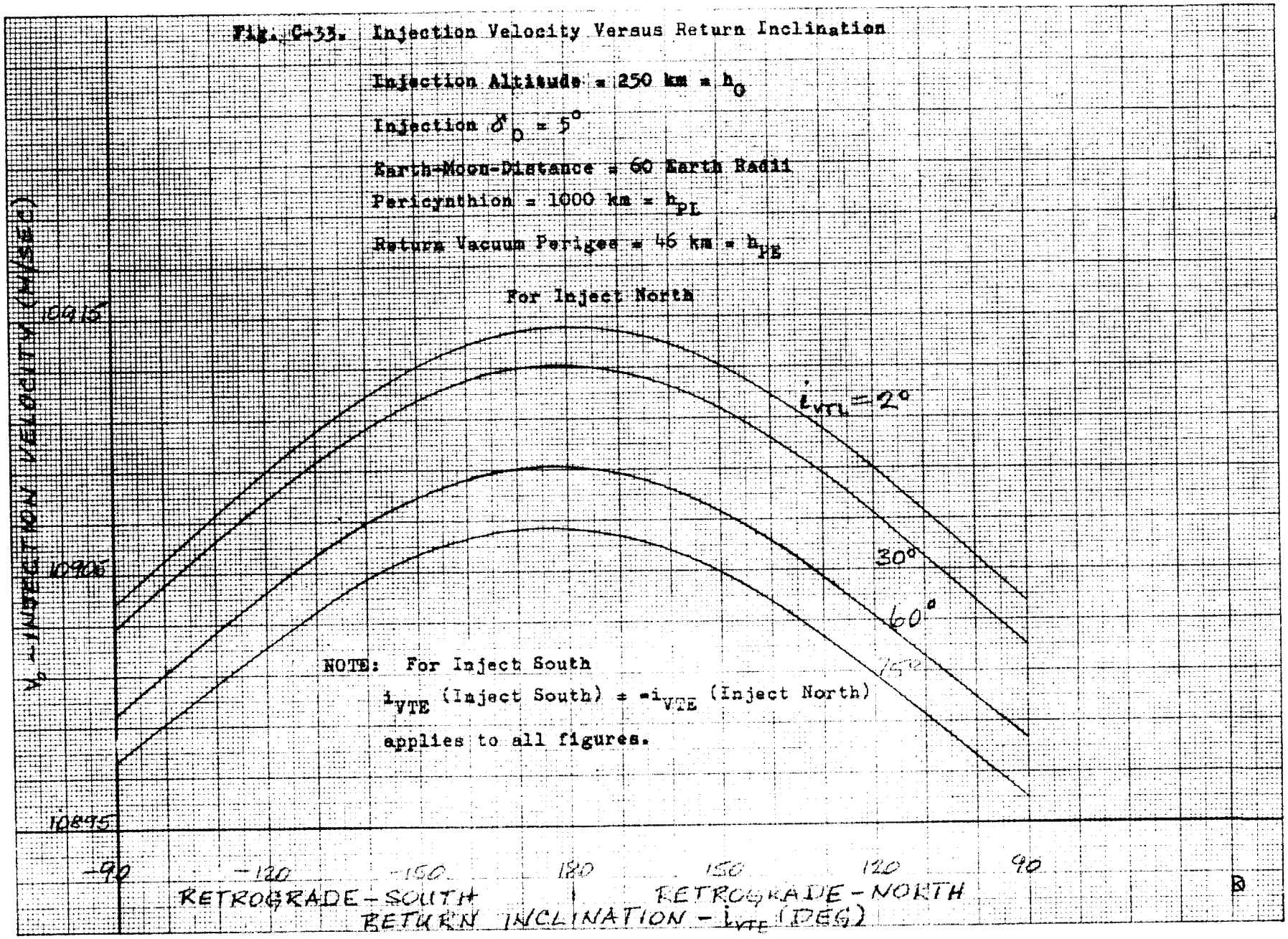
Fig. C-33. Injection Velocity Versus Return Inclination
Injection Altitude = 250 km = h_0
Injection $\delta_0 = 5°$
Earth-Moon-Distance = 60 Earth Radii
Pericynthion = 1000 km = h_{PL}
Return Vacuum Perigee = 46 km = h_{PE}
For Inject North
$i_{VTL} = 2°$
30°
60°
NOTE: For Inject South
i_{VTE} (Inject South) = $-i_{VTE}$ (Inject North)
applies to all figures.
10915
10910
10895
-90
-120
-150
180
150
120
90
RETROGRADE - SOUTH
RETROGRADE - NORTH
RETURN INCLINATION - i_{VTE} (DEG)

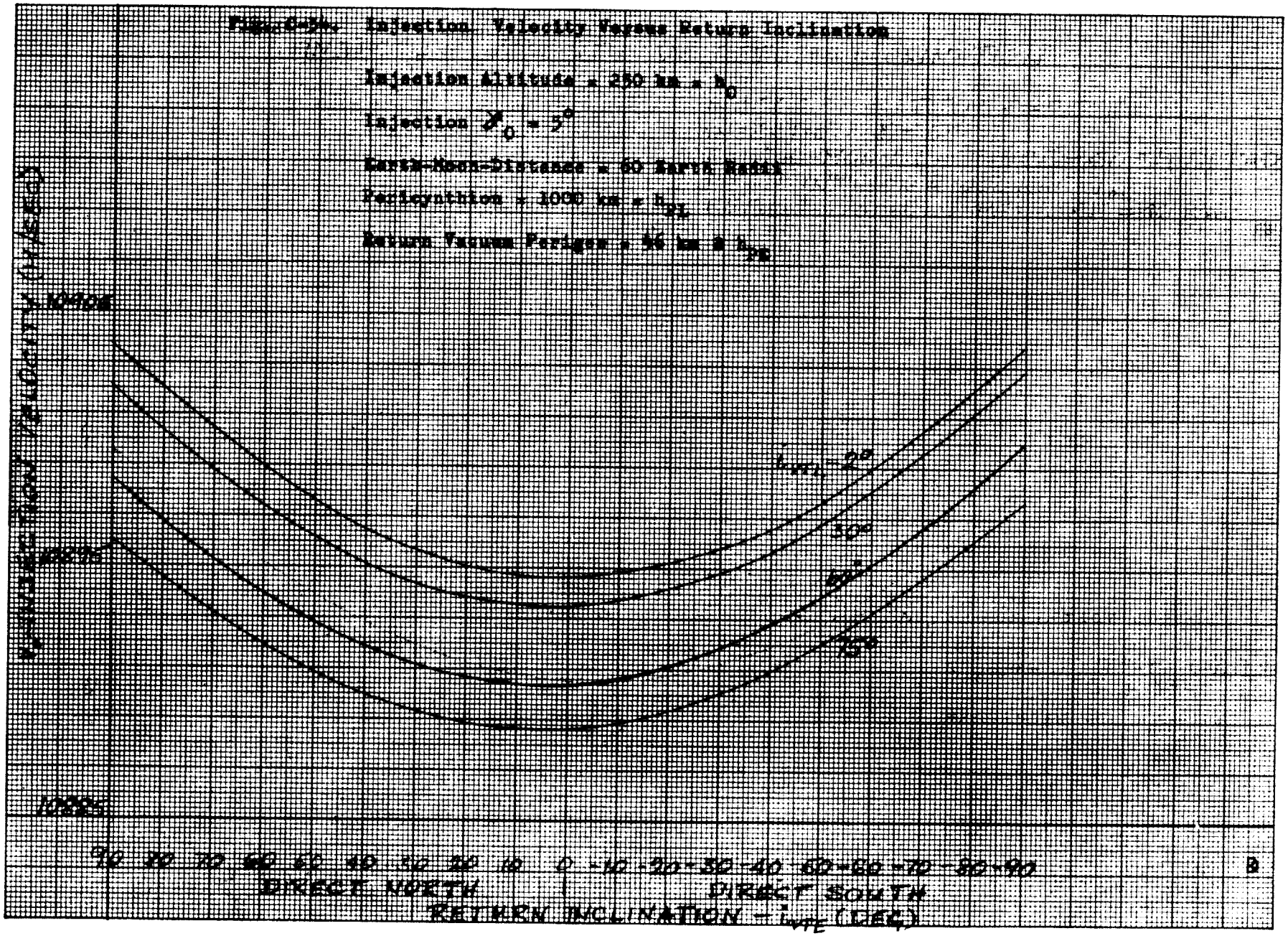
Injection Velocity Versus Return Inclination
Injection Altitude = 250 km = h_0
Injection $\gamma_0 = 5^\circ$
Earth-Moon-Distance = 60 Earth Radii
Perisynthion = 1000 km = h_{p_L}
Return Vacuum Perigee = 56 km = h_{p_E}
$i_{MIL} = 2^\circ$
30°
60°
75°
DIRECT NORTH
RETURN INCLINATION — i_{MIE} (DEG)
DIRECT SOUTH

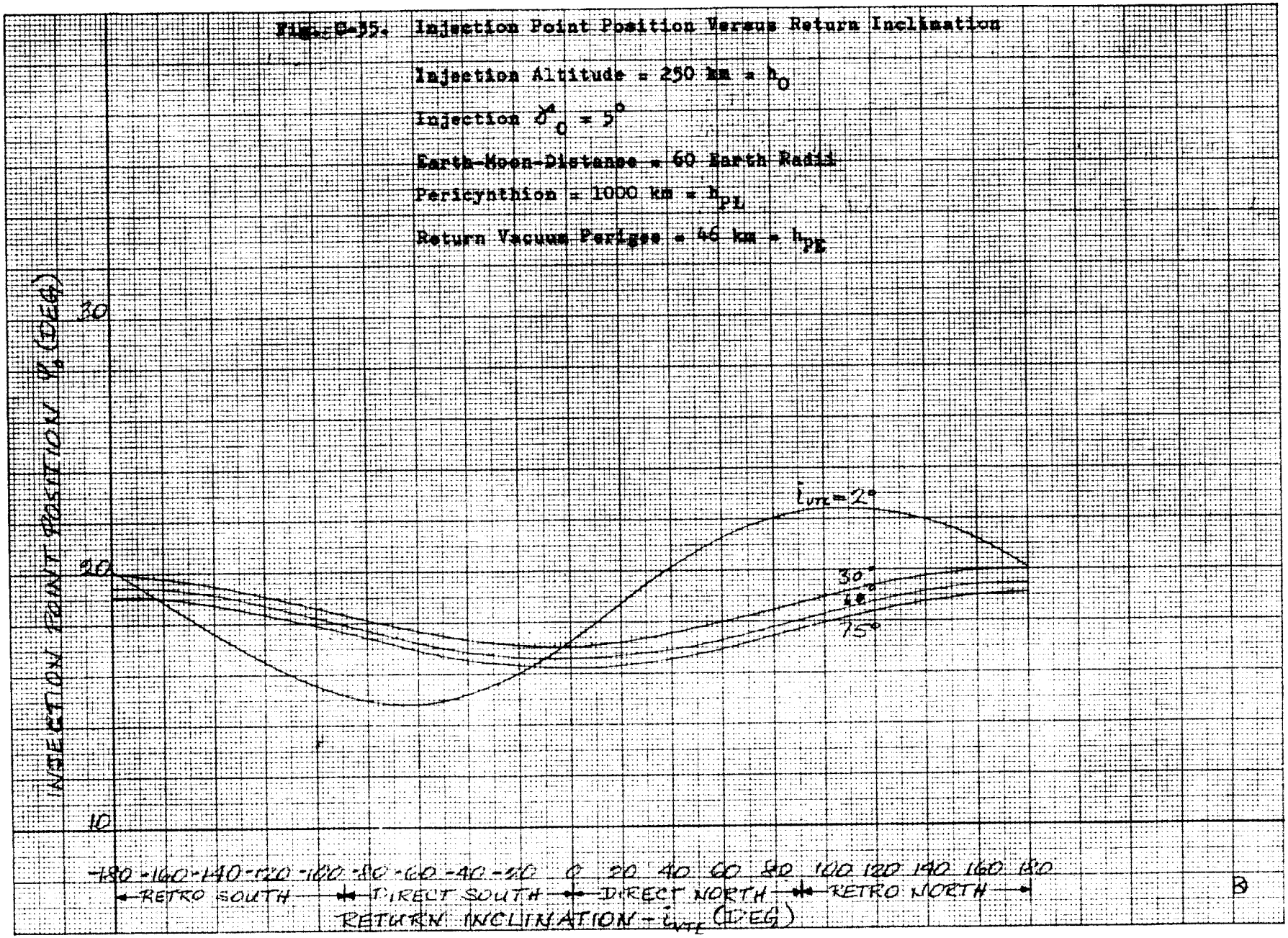
Fig. C-35. Injection Point Position Versus Return Inclination
Injection Altitude = 250 km = h_0
Injection $\gamma_0 = 5°$
Earth-Moon-Distance = 60 Earth Radii
Pericynthion = 1000 km = h_{PL}
Return Vacuum Perigee = 46 km = h_{PE}
INJECTION POINT POSITION ψ_0 (DEG)
30
20
10
i_{VTL}=2°
30°
15°
75°
-180 -160 -140 -120 -100 -80 -60 -40 -20 0 20 40 60 80 100 120 140 160 180
RETRO SOUTH
DIRECT SOUTH
DIRECT NORTH
RETRO NORTH
RETURN INCLINATION - i_{VTL} (DEG)
B

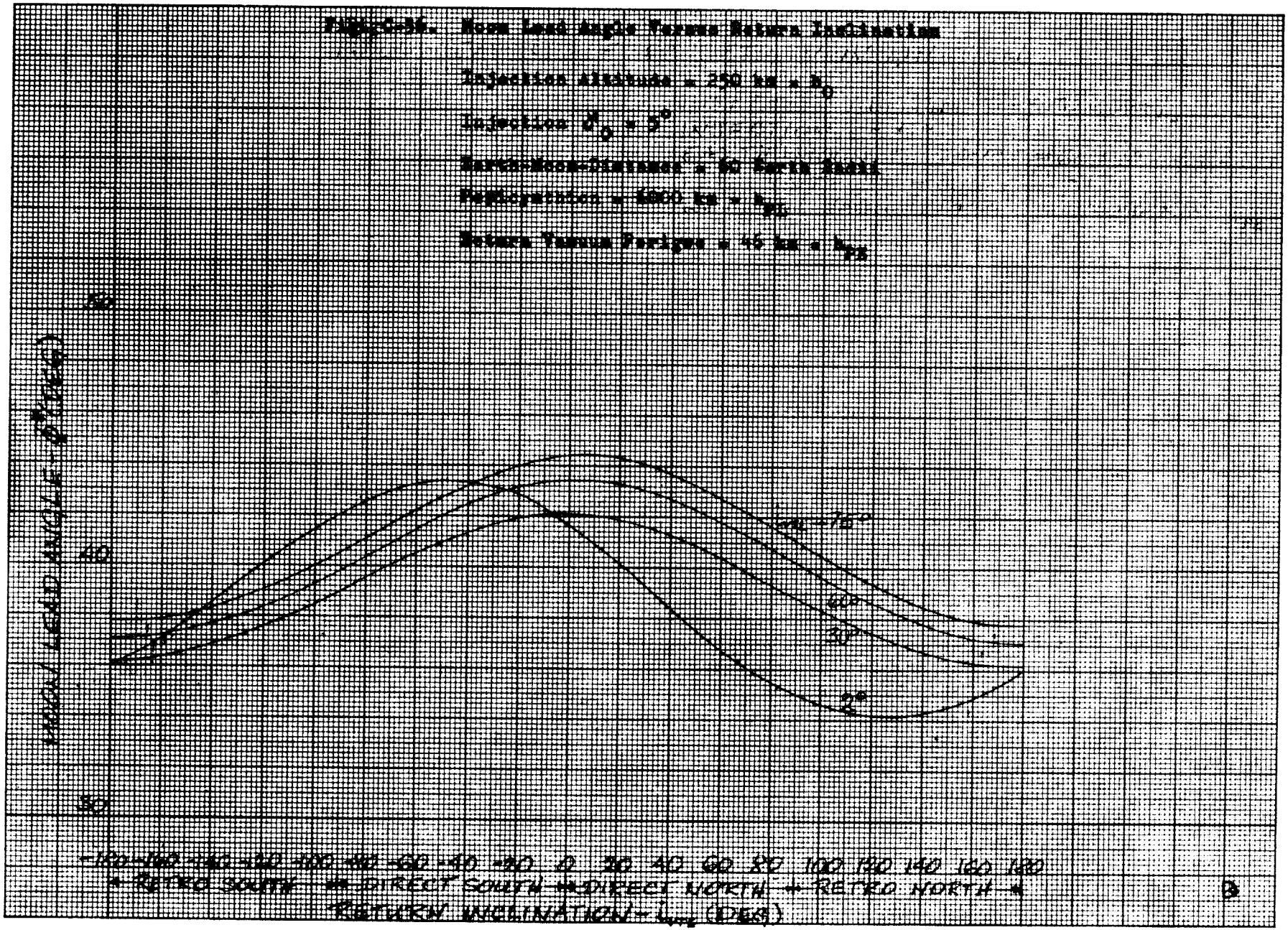
Figure 6-36. Nom Lead Angle Versus Return Inclination
Injection Altitude = 250 km = h_0
Injection γ_0 = 5°
Earth-Moon-Distance = 60 Earth Radii
Perigeeattitude = 6600 km = h_{p_E}
Return Fusion Perigee = 46 km = h_{p_R}
60
40
30
20
$i_{ret} = 75°$
60°
30°
2°
-160 -140 -120 -100 -80 -60 -40 -20 0 20 40 60 80 100 120 140 160 180
RETRO SOUTH
DIRECT SOUTH
DIRECT NORTH
RETRO NORTH
RETURN INCLINATION - i_{ret} (DEG)

Figure 37. Δv Required to Enter Circular Lunar Orbit Versus Return Inclination
Injection Altitude = 250 km = h_0
Injection β_0 = 5°
Earth-Moon Distance = 60 Earth Radii
Periapsis = 1000 km = A_{PL}
Sphere Vacuum Perigee = 46 km = A_{PE}
Δv REQUIRED TO ENTER CIRCULAR LUNAR ORBIT (km/sec)
RETURN INCLINATION (DEG)
180 160 140 120 100 80 60 40 20 0 20 40 60 80 100 120 140 160 180
RETRO SOUTH ← DIRECT SOUTH — DIRECT NORTH → RETRO NORTH
β_0 = 5°
h_0 = 250 km
A_{PL} = 1000 km
A_{PE} = 46 km
60 ER

Figure 6-38. Time of Reentry Versus Return Inclination

Injection Altitude = 250 km = h_0

Injection γ_0 = 5°

Earth-Moon Distance = 60 Earth Radii

Reentry Path = 1000 km = h_{EI}

Return Vacuum Perigee = 46 km = h_{PR}

Fig. 6-19. Total Time Versus Return Inclination
Injection Altitude = 250 km = h_0
Injection γ_0 = 5°
Earth-Moon-Distance = 60 Earth Radii
Perijunction = 1000 km = h_{pn}
Return Versus Perigee = 46 km = h_{PE}
TOTAL TIME — T (HRS)
RETURN INCLINATION — i_{RE} (DEG)
DIRECT SOUTH
DIRECT NORTH
RETRO SOUTH
RETRO NORTH
i_{MCC} = 0°
30°
60°
75°
2°
5°
10°
15°
20°
160
150
140
130
120
110
100
90
80
70
60
50
40
30
20
10
0
-10
-20
-30
-40
-50
-60
-70
-80
-90
-100
-110
-120
-130
-140
-150
-160
-170
-180

Lunar Orbit Inclination Versus Return Inclination
Injection Altitude = 250 km = h_0
Injection $\gamma_0 = 5°$
Earth-Moon-Distance = 60 Earth Radii
Perigynthion = 1000 km = h_{PL}
Return Vacuum Perigee = 46 km = h_{PE}
LUNAR ORBIT INCLINATION = i_M (DEG)
RETURN INCLINATION (DEG)
RETRO SOUTH
DIRECT SOUTH
DIRECT NORTH
RETRO NORTH
i_{MIN}
$i_M = 75°$
60°
30°
15°
0°

Fig. 6-40. Lunar Orbit Orientation Versus Return Inclination

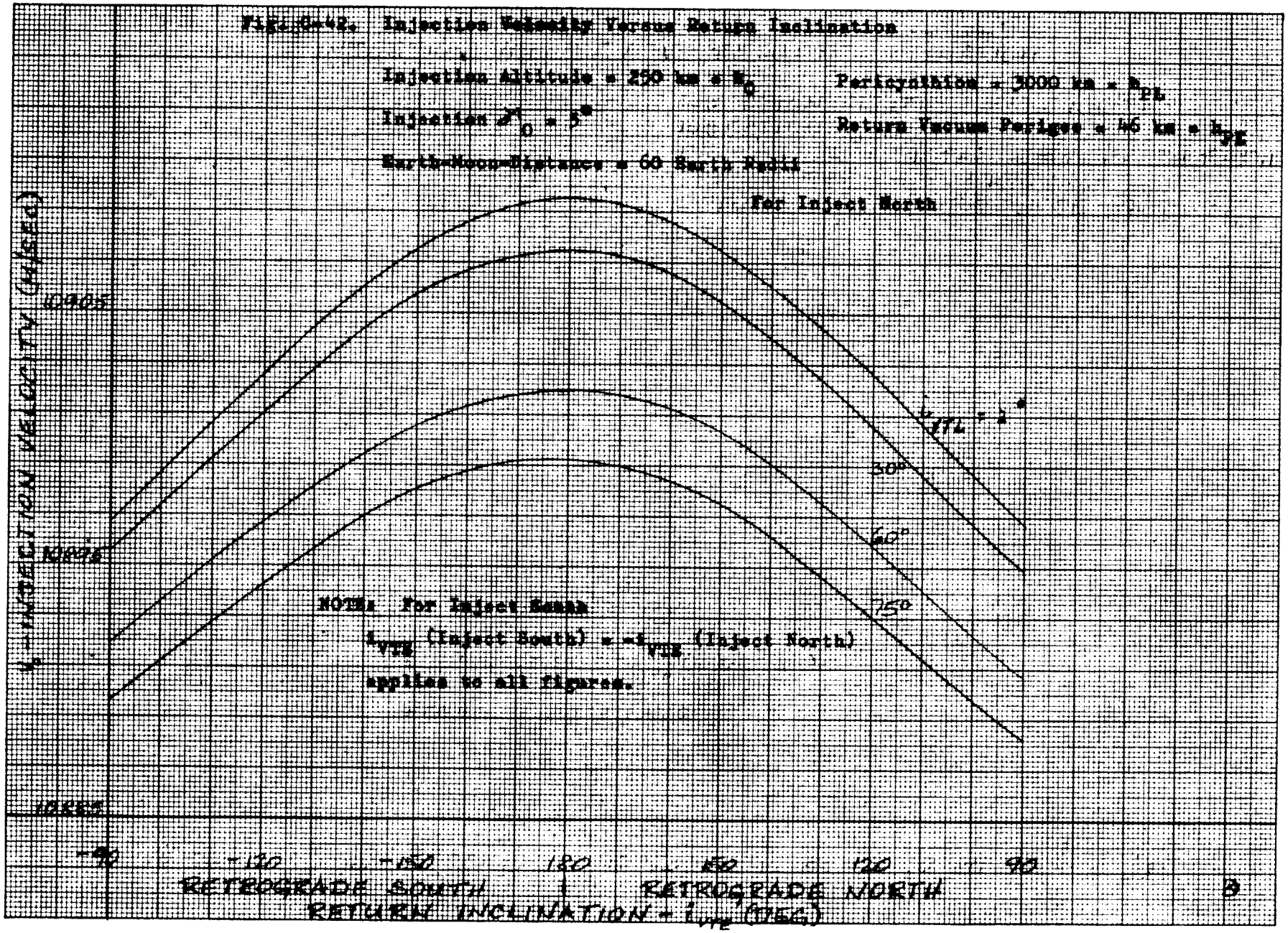
Fig. 6-42. Injection Velocity Versus Return Inclination
Injection Altitude = 250 km = H_0
Perigeeration = 3000 km = h_{Pk}
Injection γ_0 = 5°
Return Vacuum Perigee = 46 km = h_{PR}
Earth-Moon-Distance = 60 Earth Radii
For Inject North
i_{VTA} = 2°
30°
60°
75°
NOTE: For Inject South
i_{VTS} (Inject South) = $-i_{VTN}$ (Inject North)
applies to all figures.
INJECTION VELOCITY (Ft/Sec)
10905
10875
10845
-90
-120
-150
180
150
120
90
RETROGRADE SOUTH
RETROGRADE NORTH
RETURN INCLINATION = i_{VTE} (DEG)

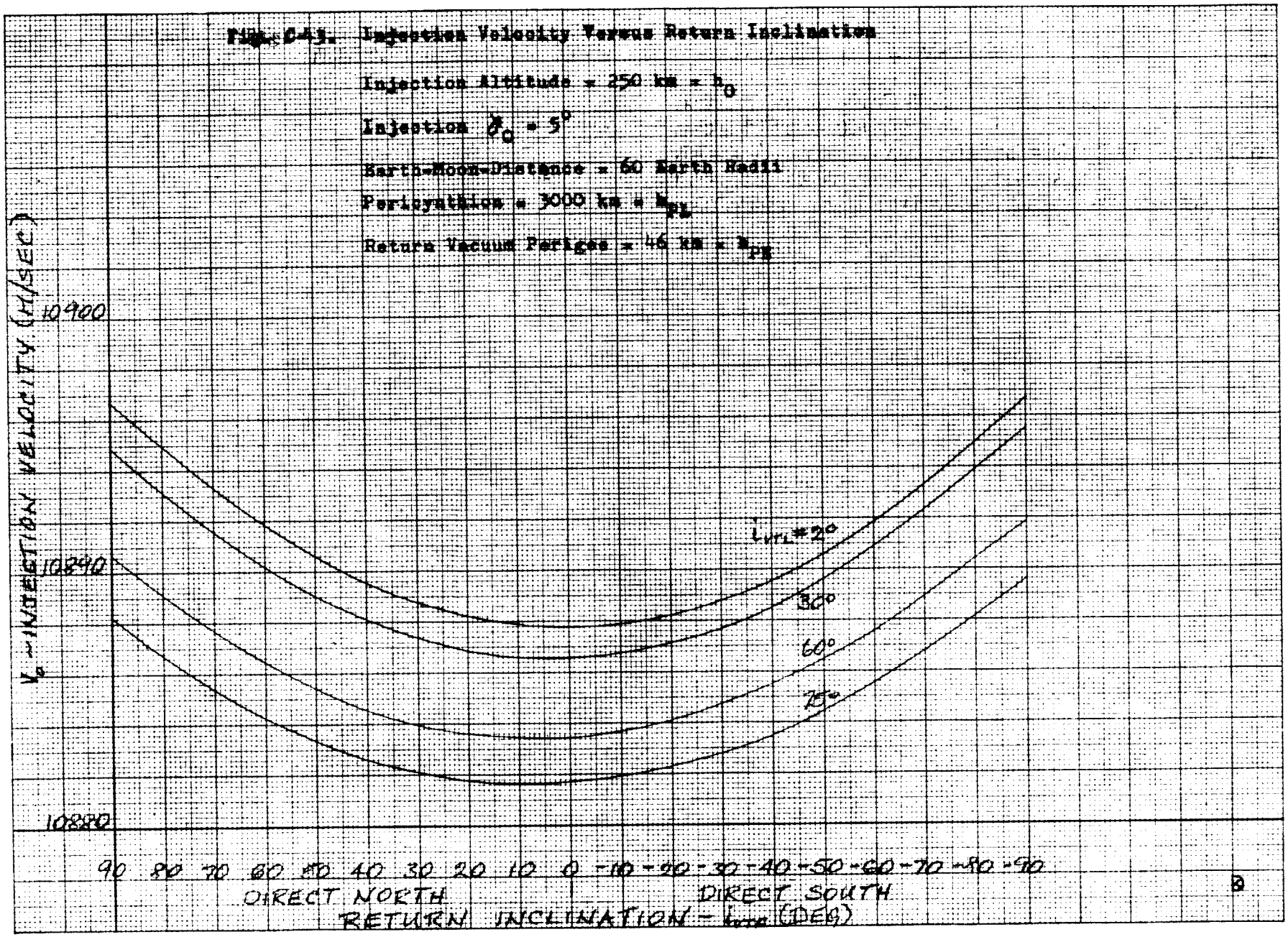
Fig. C-43. Injection Velocity Versus Return Inclination
Injection Altitude = 250 km = h_0
Injection γ_0 = 5°
Earth-Moon-Distance = 60 Earth Radii
Perigynthion = 3000 km = h_{pl}
Return Vacuum Perigee = 46 km = h_{pE}
V_0 - INJECTION VELOCITY (FT/SEC)
10900
10890
10880
i_{ret} = 2°
30°
60°
75°
90 80 70 60 50 40 30 20 10 0 -10 -20 -30 -40 -50 -60 -70 -80 -90
DIRECT NORTH
DIRECT SOUTH
RETURN INCLINATION - i_{ret} (DEG)

Fig. C-44. Injection Point Position Versus Return Inclination

Injection Altitude = 250 km = h_0

Injection γ_0 = 5°

Earth-Moon-Distance = 60 Earth Radii

Perisynthion = 5000 km = h_{PL}

Return Vacuum Perigee = 66 km = h_{PE}

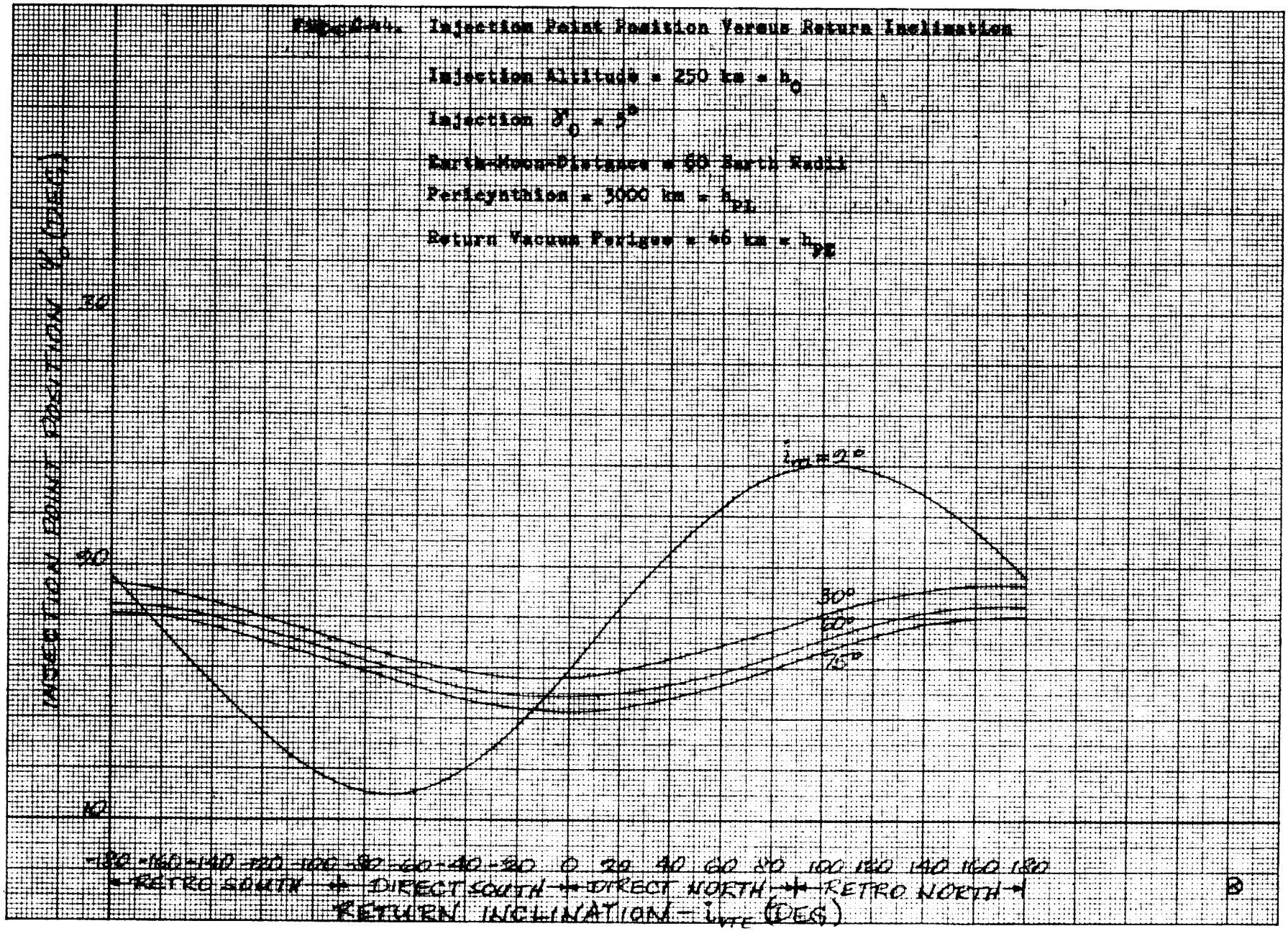

Fig. 6.45, Moon Head Angle Versus Return Inclination
Injection Altitude = 250 km = h_0
Injection γ_0 = 0°
Earth-Moon Distance = 60 Earth Radii
Perigynthion = 3000 km = h_{PE}
Return Vacuum Perigee = 46 km = h_{PR}
i_{CR} = 75°
60°
30°
0°
40
ϕ_0
MOON HEAD ANGLE ϕ_0 (DEG)
RETRO SOUTH → DIRECT NORTH → RETRO NORTH
RETURN INCLINATION (DEG)

Fig. 6-46. ΔV Required To Enter Circular Lunar Orbit Versus Return Inclination

Injection Altitude = 250 km = h_0

Injection $\gamma_0 = 5^\circ$

Earth-Moon-Distance = 60 Earth Radii

Pericynthion = 3000 km = h_{PL}

Return Vacuum Perigee = 46 km = h_{PE}

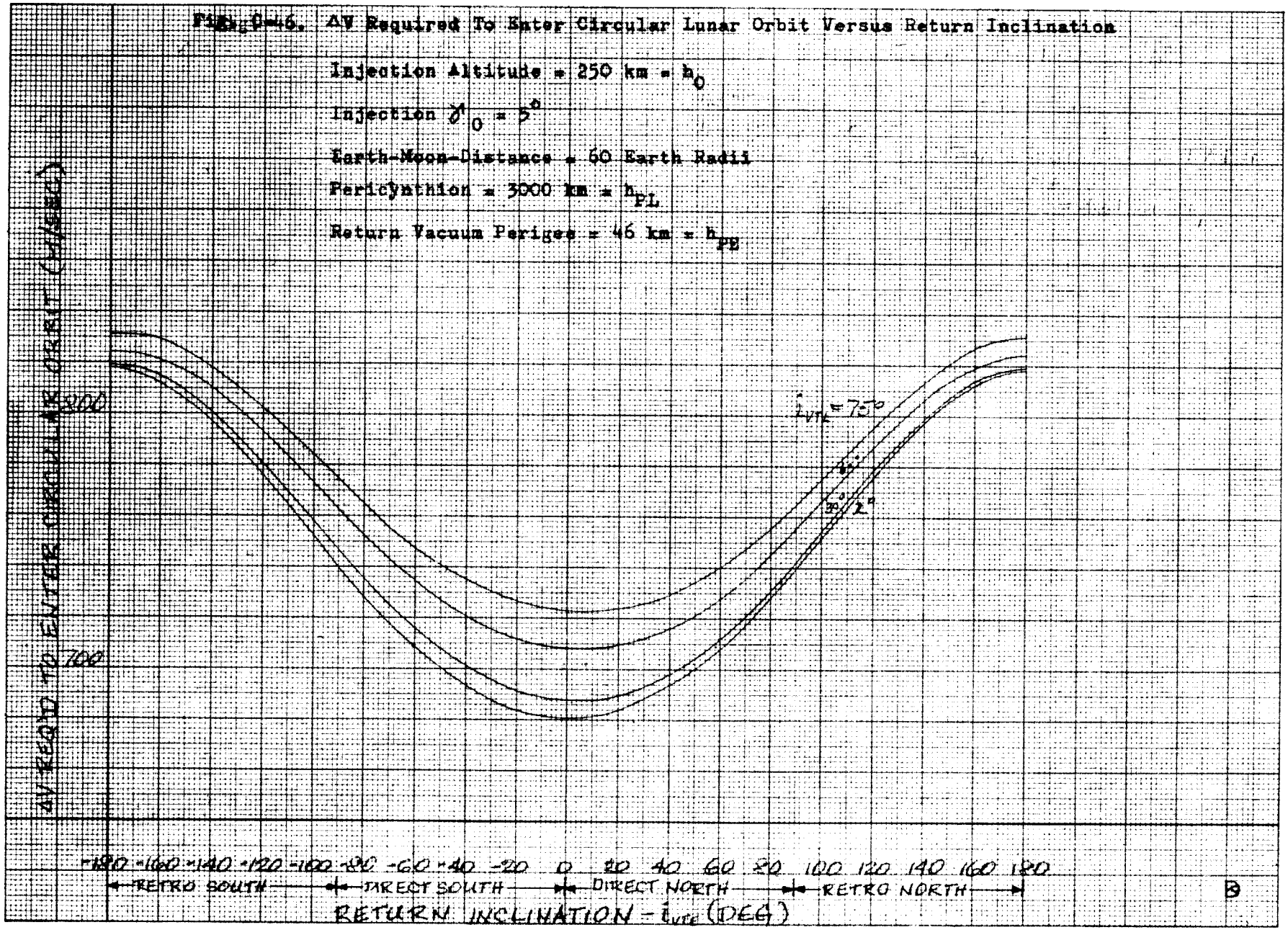

Flight Path Angle at Termination Versus Return Inclination
Earth-Moon-Distance = 60 Earth Radii
Perigee Altitude = 2000 km = h_p
Return Vacuum Perigee = 46 km = h_{pR}
Inclination = 250 NM = h_o
Inclination γ_o = 5°
TIME OF FLIGHT FROM INJECTION - t_F (HR)
FLIGHT PATH ANGLE AT TERMINATION - γ_F (DEG)
γ_o = -4.0°
γ_o = -4.5°
γ_o = -5.0°
γ_o = -5.5°
γ_o = -6.0°
γ_o = -6.5°
γ_o = -7.0°
γ_o = -7.5°
γ_o = -8.0°
γ_o = -8.5°
γ_o = -9.0°
γ_o = -9.5°
γ_o = -10.0°
γ_o =

Fig. C-48. Total Time Versus Return Inclination

Injection Altitude = 250 km = h_0

Injection γ_0 = 5°

Earth-Moon-Distance = 60 Earth Radii

Pericynthion = 3000 km = h_{PL}

Return Vacuum Perigee = 46 km = h_{PE}

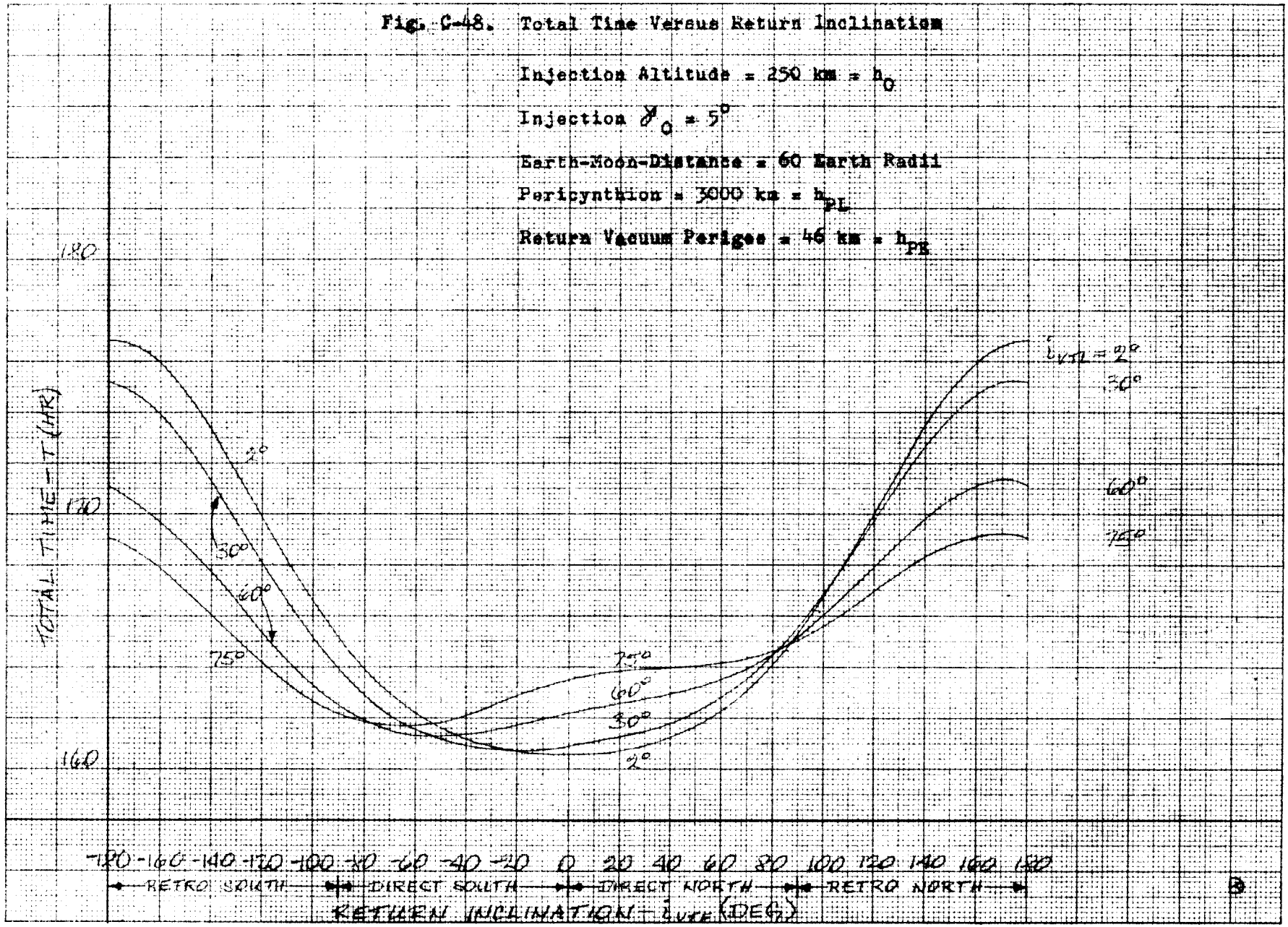

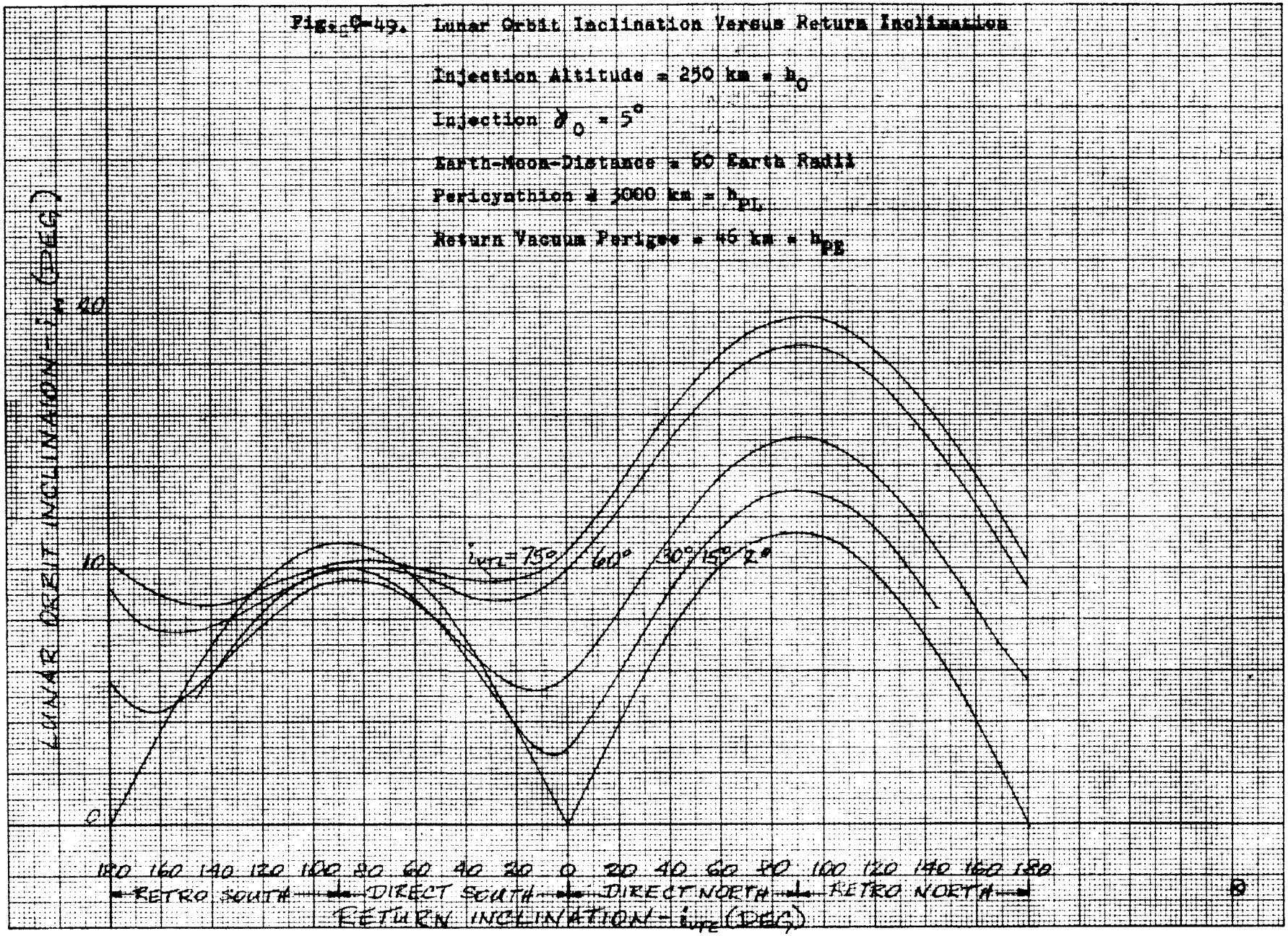
Fig. 6-49. Lunar Orbit Inclination Versus Return Inclination
Injection Altitude = 250 km = h_0
Injection γ_0 = 5°
Earth-Moon-Distance = 60 Earth Radii
Pericynthion = 3000 km = h_{PL}
Return Vacuum Perigee = 46 km = h_{PE}
LUNAR ORBIT INCLINATION - i_L (DEG)
i_{LTE} = 75°
60°
30°
15°
2°
180 160 140 120 100 80 60 40 20 0 20 40 60 80 100 120 140 160 180
RETRO SOUTH
DIRECT SOUTH
DIRECT NORTH
RETRO NORTH
RETURN INCLINATION - i_{RTE} (DEG)

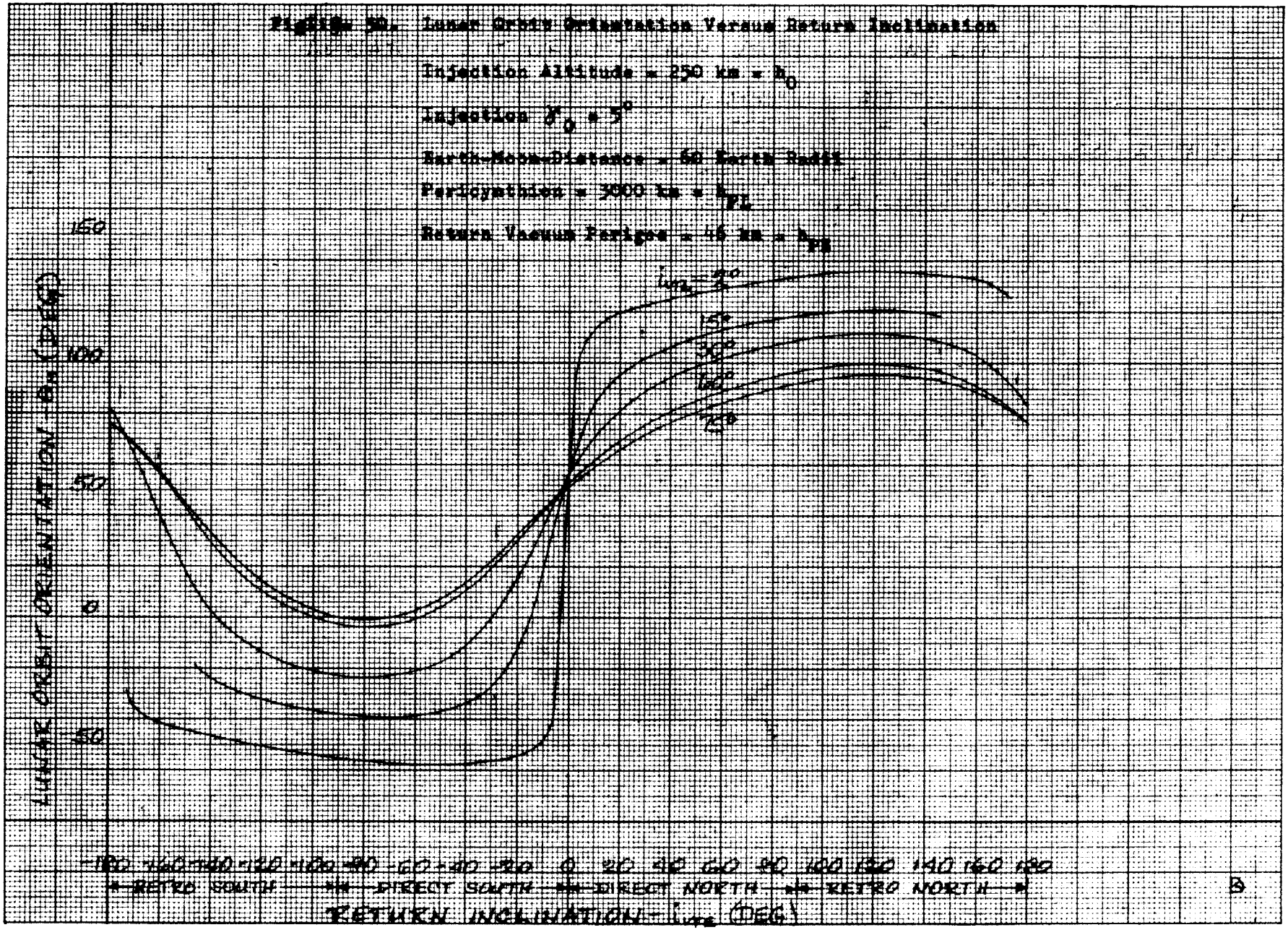
Figure 30. Lunar Orbit Orientation Versus Return Inclination
Injection Altitude = 250 km = h_0
Injection γ_0 = 5°
Earth-Moon-Distance = 60 Earth Radii
Pericynthion = 3000 km = h_{PL}
Return Vacuum Perigee = 46 km = h_{PE}
i_{ma} = 2°
15°
30°
60°
90°
150
100
50
0
-50
LUNAR ORBIT ORIENTATION - θ_m (DEG)
-180 -160 -140 -120 -100 -80 -60 -40 -20 0 20 40 60 80 100 120 140 160 180
RETRO SOUTH
DIRECT SOUTH
DIRECT NORTH
RETRO NORTH
RETURN INCLINATION - i_{re} (DEG)

Fig. C-51. Injection Velocity Versus Return Inclination
Injection Altitude = 250 km = h_0
Injection $\gamma_a = 5°$
Earth-Moon Distance = 60 Earth Radii
Perigee Vacuum Altitude = 5000 km = h_{PL}
Return Vacuum Perigee = 46 km = h_{PR}
For Inject North
$\gamma_a = 2°$
$\gamma_a = 3°$
$\gamma_a = 4°$
$\gamma_a = 5°$
NOTE: For Inject South, γ_a = Plus (Inject North) minus (Inject South)
applies to all figures.
V_∞ - INJECTION VELOCITY (M/SEC)
RETROGRADE SOUTH INCLINATION - Line (DEG)
RETROGRADE NORTH
RETURN INCLINATION (DEG)
-90
-120
-150
180
150
120
90
60
30
0

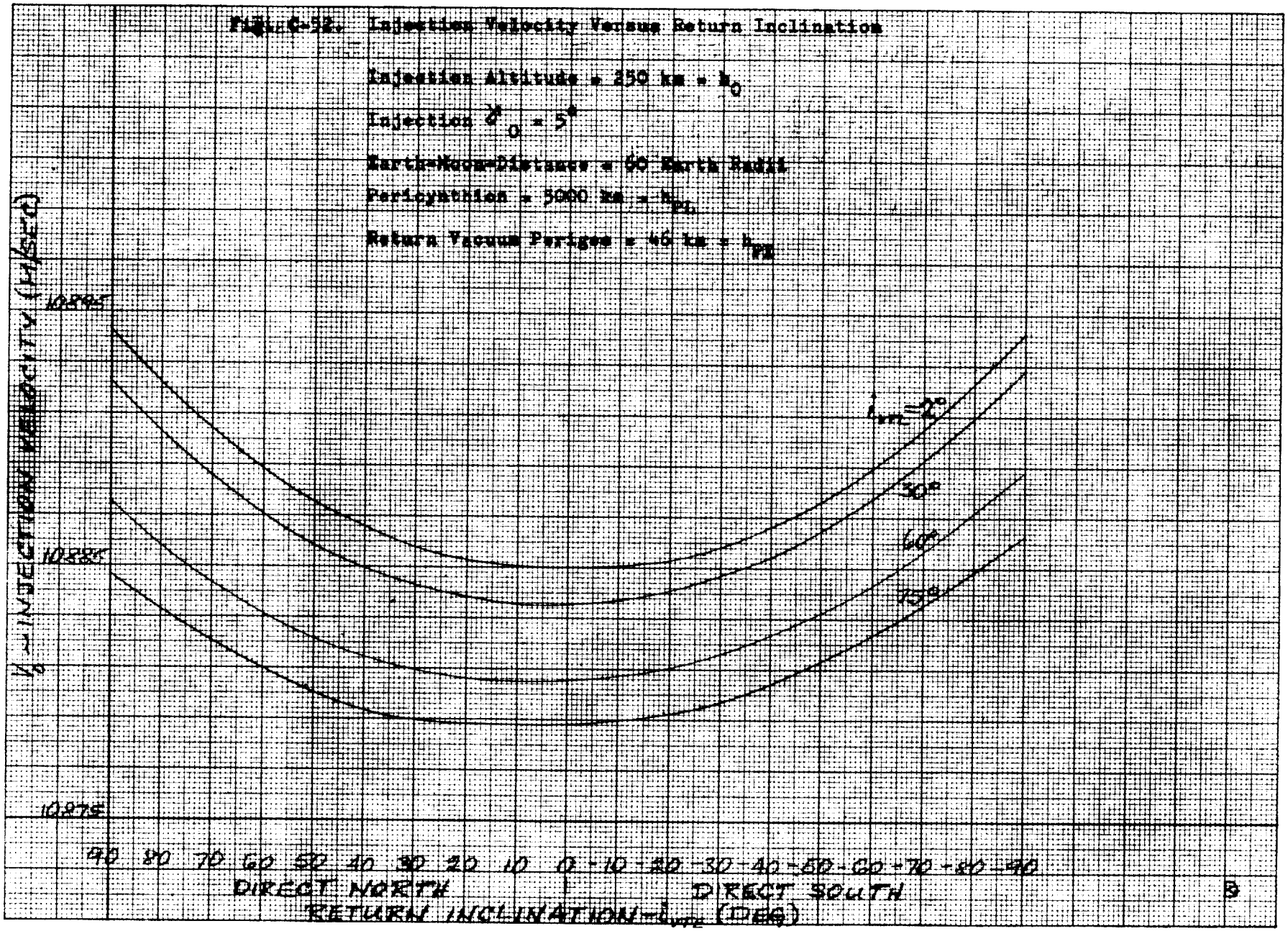
Fig. C-52. Injection Velocity Versus Return Inclination
Injection Altitude = 250 km = h_0
Injection $\gamma_0 = 5°$
Earth-Moon-Distance = 60 Earth Radii
Perisynthion = 5000 km = h_{P_1}
Return Vacuum Perigee = 46 km = h_{P_2}
i_{sm}=2°
30°
60°
90°
10895
10885
10875
INJECTION VELOCITY (FPS)
90 80 70 60 50 40 30 20 10 0 -10 -20 -30 -40 -50 -60 -70 -80 -90
DIRECT NORTH
DIRECT SOUTH
RETURN INCLINATION - i_{sm_2} (DEG)

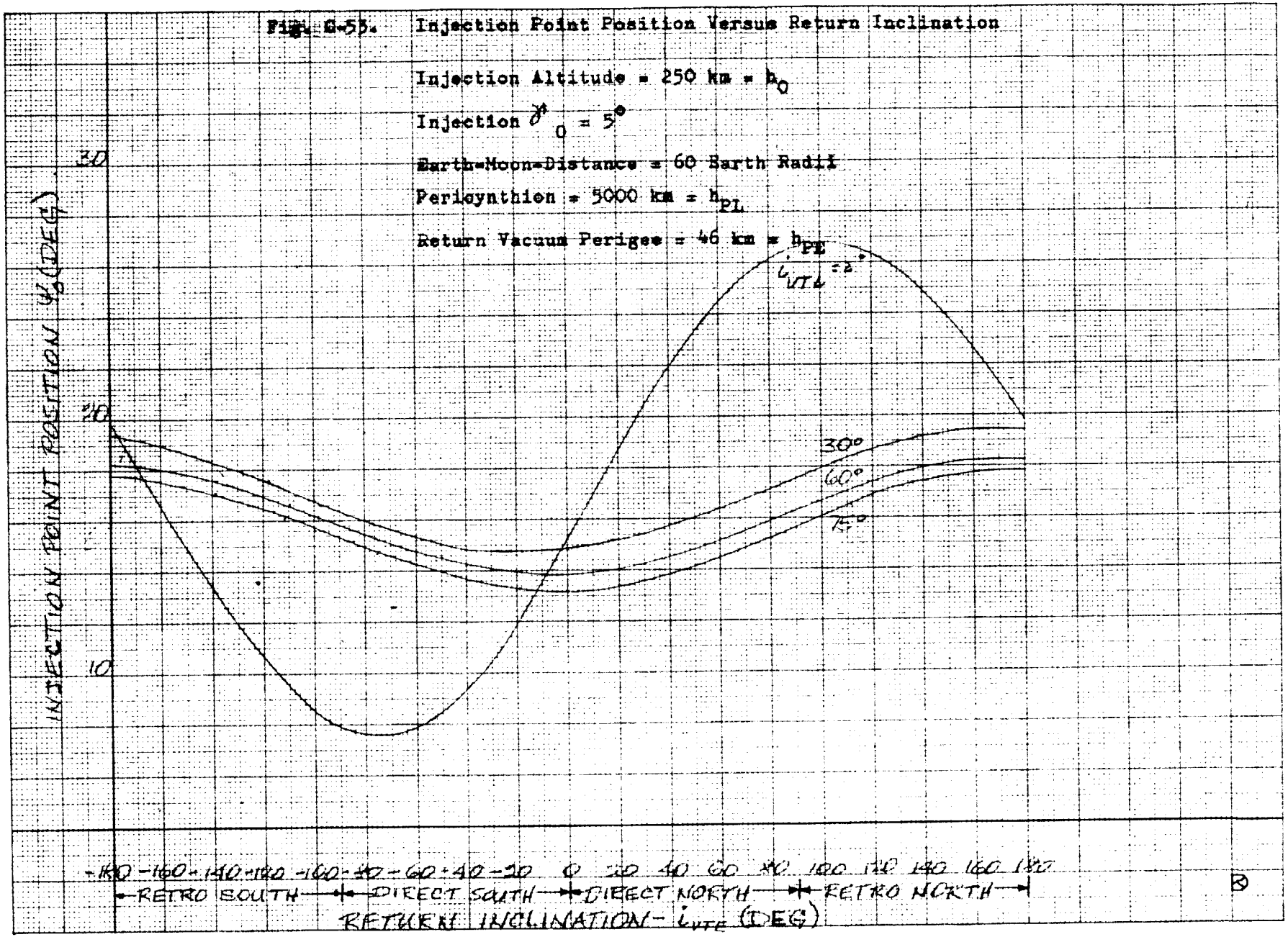
Fig. C-55. Injection Point Position Versus Return Inclination
Injection Altitude = 250 km = h_0
Injection γ_0 = 5°
Earth-Moon-Distance = 60 Earth Radii
Perisynthion = 5000 km = h_{PI}
Return Vacuum Perigee = 46 km = h_{PE}
i_{VTE} = 2°
30°
60°
75°
INJECTION POINT POSITION ψ_0 (DEG)
30
20
10
-180 -160 -140 -120 -100 -80 -60 -40 -20 0 20 40 60 80 100 120 140 160 180
RETRO SOUTH
DIRECT SOUTH
DIRECT NORTH
RETRO NORTH
RETURN INCLINATION - i_{VTE} (DEG)

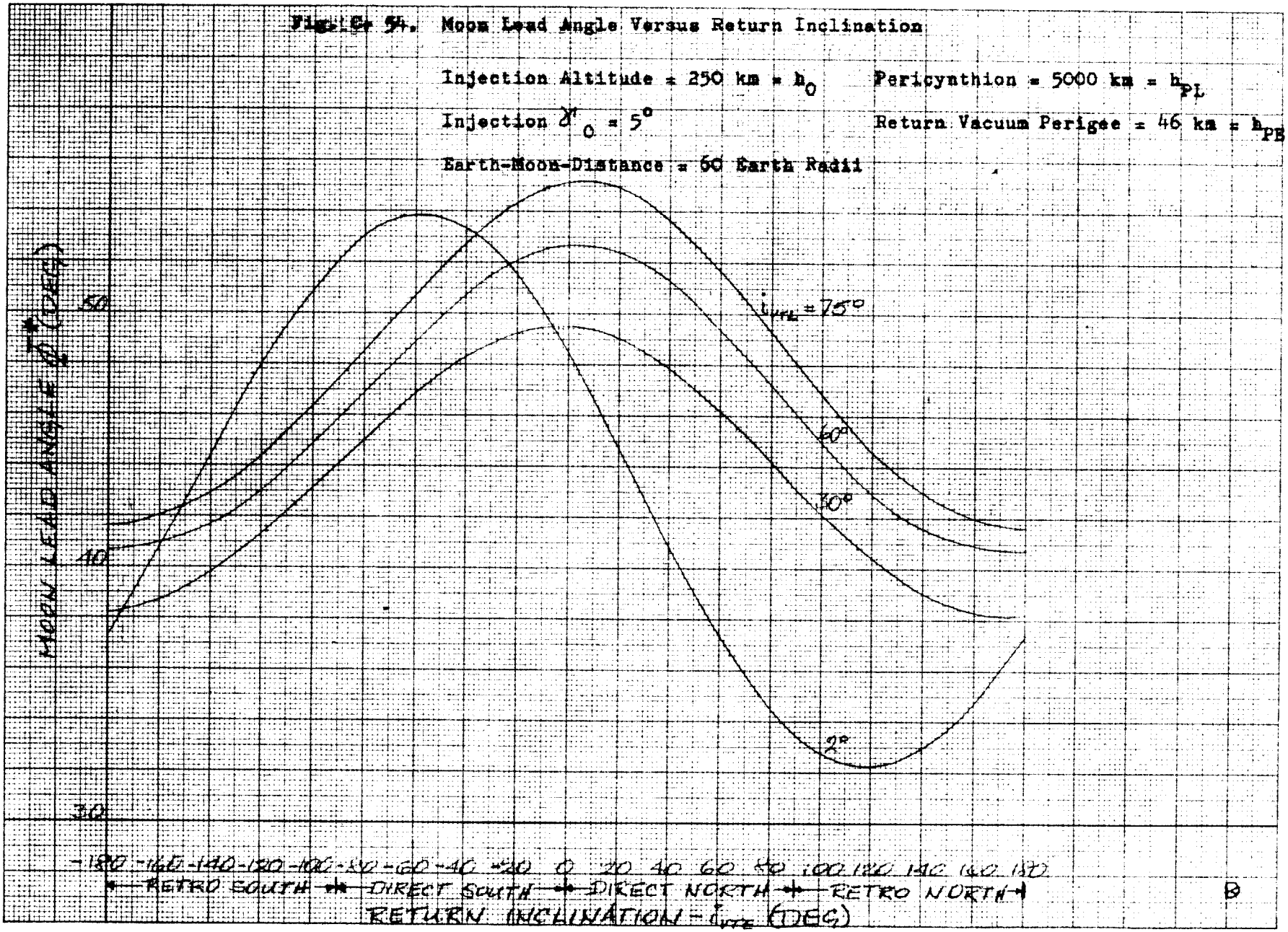
Fig. C-54. Moon Lead Angle Versus Return Inclination
Injection Altitude = 250 km = h_0
Pericynthion = 5000 km = h_{PL}
Injection γ_0 = 5°
Return Vacuum Perigee = 46 km = h_{PE}
Earth-Moon-Distance = 60 Earth Radii
MOON LEAD ANGLE = ϕ (DEG)
50
40
30
i_{MPL} = 75°
60°
30°
2°
-180 -160 -140 -120 -100 -80 -60 -40 -20 0 20 40 60 80 100 120 140 160 180
RETRO SOUTH
DIRECT SOUTH
DIRECT NORTH
RETRO NORTH
RETURN INCLINATION = i_{MPE} (DEG)
B

Figure 6.3
Air Assisted 90 Meter Circular Lunar Orbit Versus Return Inclination
Inclination of 0
Injection Altitude = 250 km = h_0
Injection γ_0 = 5
Aerodynamic Coefficients = 50 Earth Result
Reservoir Pressure = 500 atm = P_{01}
Return Vacuum Perigee = 40 km = h_p
Lunar Orbit
Earth
Return Inclination (DEG)
RETURN INCLINATION - DEG
RETURN SOUTH — DIRECT SOUTH — DIRECT NORTH — RETRO NORTH
AV REQ'D TO ENTER CIRCULAR LUNAR ORBIT (km/sec)

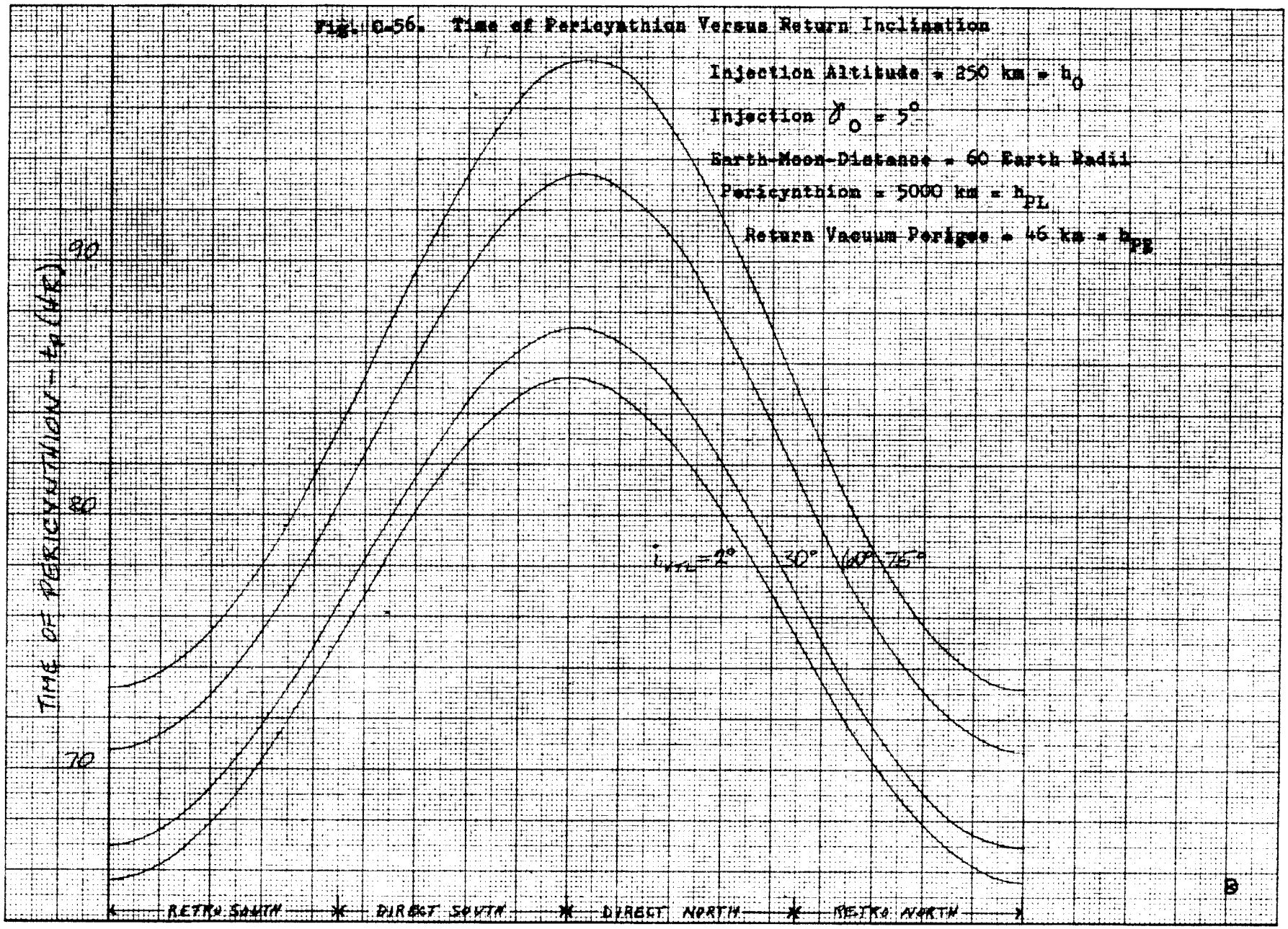
Fig. C-56. Time of Pericynthion Versus Return Inclination
Injection Altitude = 250 km = h_0
Injection $\gamma_0 = 5°$
Earth-Moon-Distance = 60 Earth Radii
Pericynthion = 5000 km = h_{PL}
Return Vacuum Perigee = 46 km = h_{PE}
TIME OF PERICYNTHION - t_0 (HR)
90
80
70
i_{RTE}=2° 30° 60° 75°
RETRO SOUTH
DIRECT SOUTH
DIRECT NORTH
RETRO NORTH
RETURN INCLINATION - i_{RTE} (DEG.

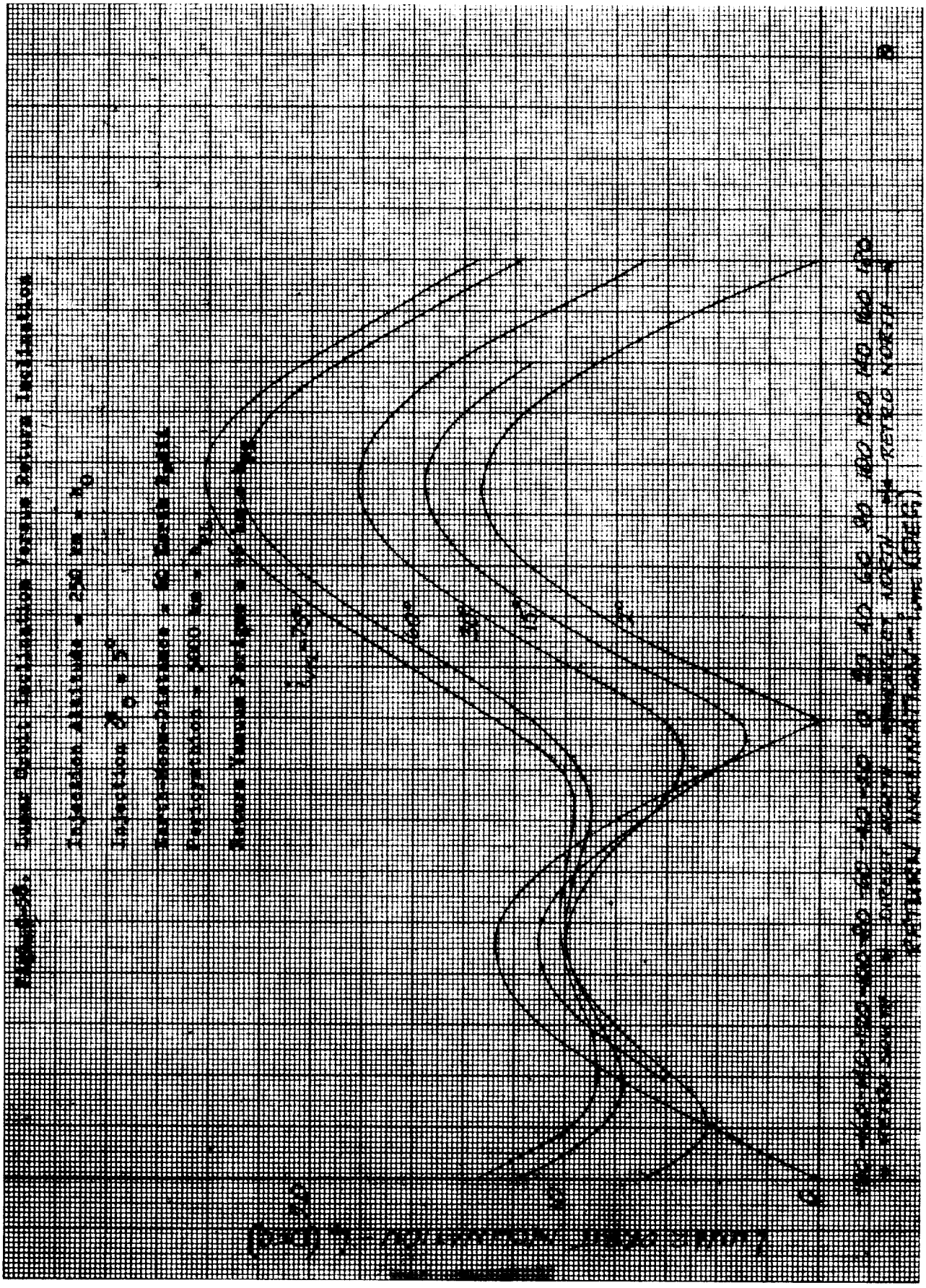

Figure 29. Lunar Orbital Orientation Versus Return Inclination
Inclination Altitude = 250 km = h_p
Inclination = i
Earth-Moon Distance = 60 Earth Radii
Earth-Moon Radius = 900 km = R_M
Return Velocity = 4.0 km/sec
Return Velocity = 4.5 km/sec
Return Velocity = 5.0 km/sec
-180 -160 -140 -120 -100 -80 -60 -40 -20 0 20 40 60 80 100 120 140 160 180
* RETRO SOUTH ** DIRECT NORTH *** RETRO NORTH
RETURN INCLINATION (DEG)
(DEG) to Translunar Injection Asymptote

Reflection Point Position Versus Return Inclination
Elevation altitude = 250 km = h
Reflection β_0 = 5°
Earth-Observer distance = 24 degree Radii
Periapsis = 185.2 km = Alt
Return Vacuum Perigee = 46 km = Rp
β_0
β
β_0 = 2°
30°
75°
RETURN INCLINATION (DEG)
RETURN SOUTH
DIRECT NORTH
DIRECT SOUTH
RETRO NORTH
RETURN INCLINATION (DEG)

Moon Lead Angle Versus Return Inclination
Injection Altitude = 250 km = h_0
Injection γ_0 = 5°
Earth-Moon-Distance = 60 Earth Radii
Perisynthion = 185.2 km = h_{p_1}
Return Perigee = 46 km = h_{p_2}
i_{ret} = 75°
30°
0°
Moon Lead Angle (DEG)
Return Inclination (DEG)
* RETRO SOUTH ** DIRECT SOUTH ** DIRECT NORTH ** RETRO NORTH
B

Figure 6-53. ΔV Required to Enter Circular Lunar Orbit Versus Return Inclination
Injection Altitude = 250 km = h_0
Injection γ_0 = 5°
Earth-Moon Distance = 64 Earth Radii
Periapsis = 185.2 km = h_{PL}
Return Vacuum Perigee = 46 km = h_{PE}
ΔV REQ'D TO ENTER CIRCULAR LUNAR ORBIT (ft/sec)
RETURN INCLINATION - i_RE (DEG)
RETRO SOUTH → DIRECT SOUTH → DIRECT NORTH → RETRO NORTH

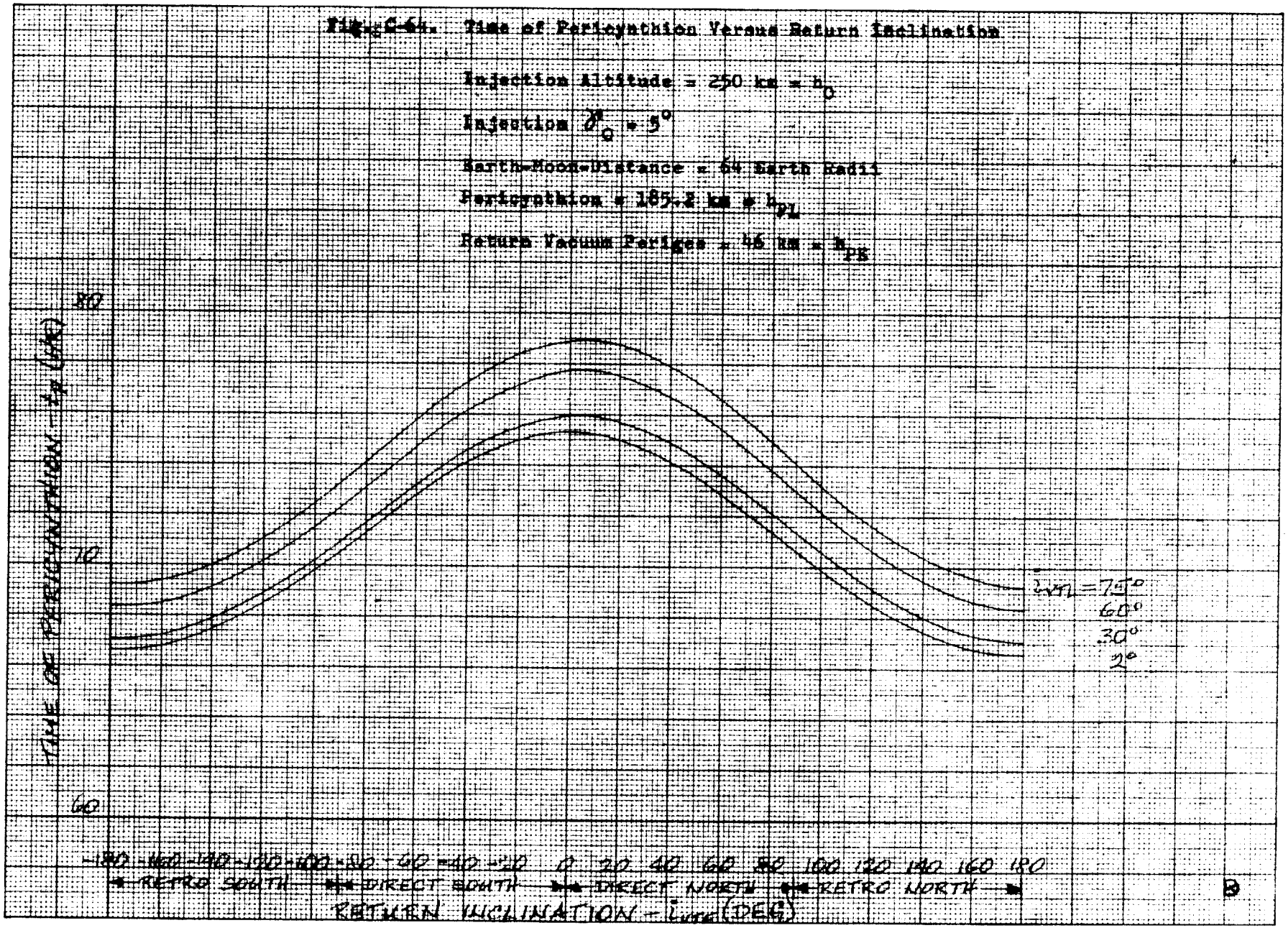
Fig. C-64. Time of Pericynthion Versus Return Inclination
Injection Altitude = 250 km = h_0
Injection γ_0 = 5°
Earth-Moon-Distance = 64 Earth Radii
Pericynthion = 185.2 km = h_{PL}
Return Vacuum Perigee = 46 km = h_{PE}
80
40
0
-40
-80
i_{RM} = 75°
60°
30°
0°
-180 -160 -140 -120 -100 -80 -60 -40 -20 0 20 40 60 80 100 120 140 160 180
RETURN INCLINATION - i_{RM} (DEG)

Total Time Return Inclination
Reflection Altitude = 250 km = h_0
Radiation λ_0 = 5°
Earth-moon distance = 24 earth radii
Perigee radius = 185.2 km = R_{pr}
Earth radius = 6,378 km = R_E
ϕ_{pr}
ϕ_{pr} = 20°
30°
40°
50°
60°
70°
75°
DIRECT NORTH
RETRO NORTH
DIRECT SOUTH
RETRO SOUTH
RETRO SOUTH
DIRECT SOUTH
RETRO NORTH
DIRECT NORTH
ϕ_{pr} (DEG)
ϕ_{pr} (DEG)
ϕ_{pr} (DEG)

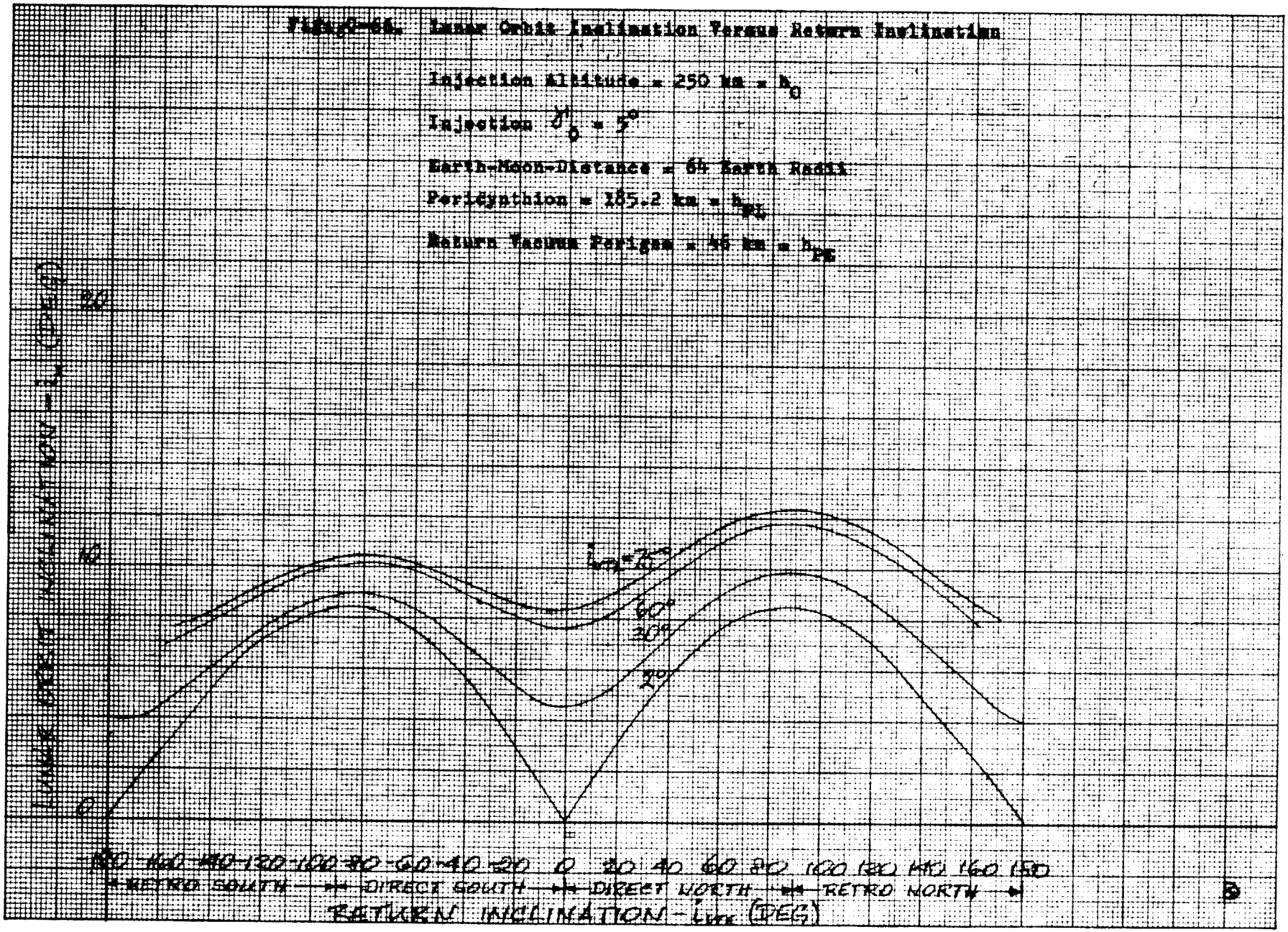

Fig. 6-64. Lunar Orbit Inclination Versus Return Inclination

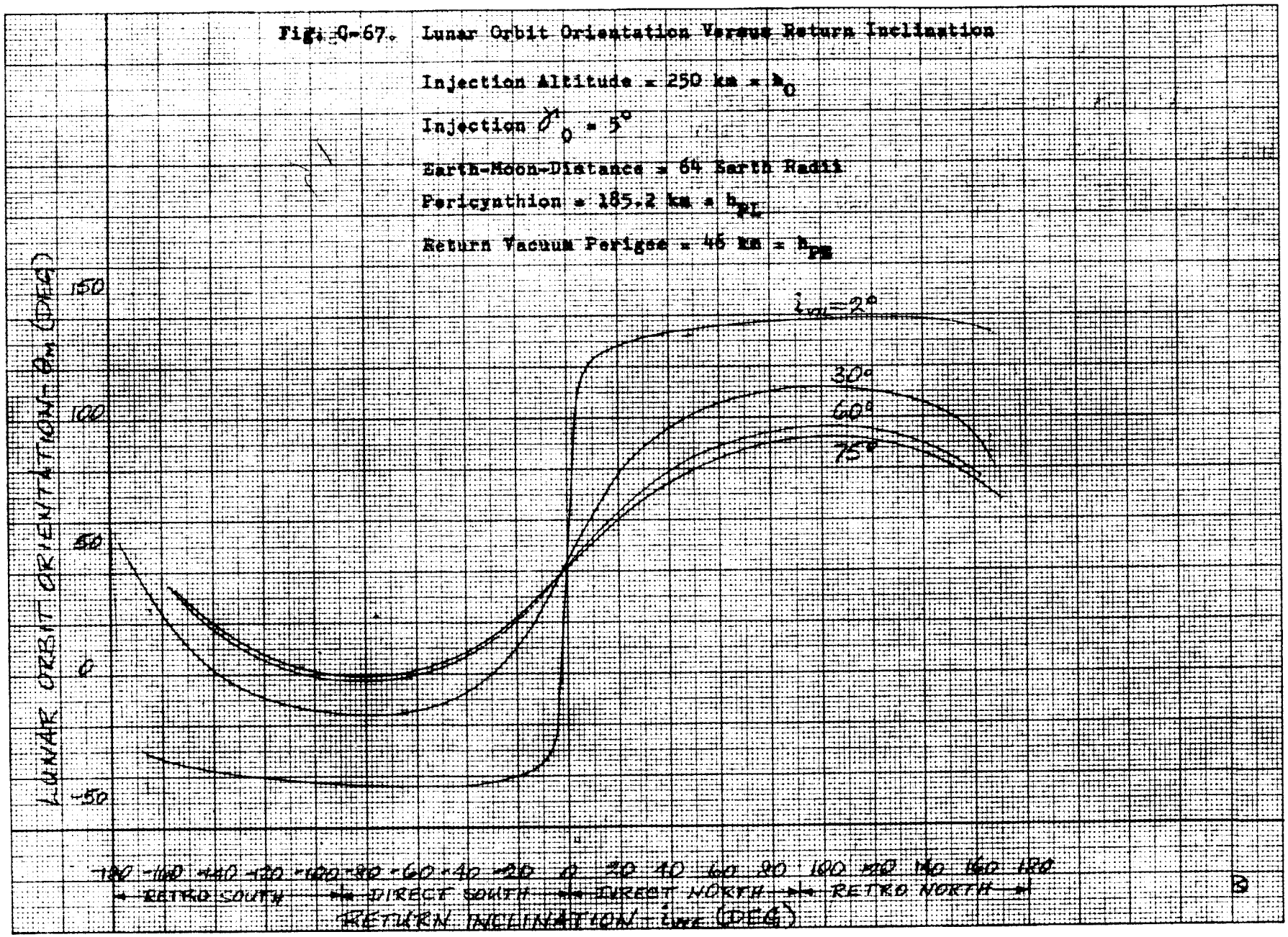
Fig. C-67. Lunar Orbit Orientation Versus Return Inclination
Injection Altitude = 250 km = h_0
Injection $\gamma_0 = 5°$
Earth-Moon-Distance = 64 Earth Radii
Pericynthion = 185.2 km = h_{PL}
Return Vacuum Perigee = 46 km = h_{PE}
$i_{VR} = 2°$
30°
60°
75°
LUNAR ORBIT ORIENTATION θ_M (DEG)
150
100
50
0
-50
-180 -160 -140 -120 -100 -80 -60 -40 -20 0 20 40 60 80 100 120 140 160 180
RETRO SOUTH
DIRECT SOUTH
DIRECT NORTH
RETRO NORTH
RETURN INCLINATION - i_{VR} (DEG)

Figure C-68. Injection Velocity Versus Return Inclination

Injection Altitude = 250 km = h_0

Injection $\gamma_0 = 5°$

Earth-Moon-Distance = 64 Earth Radii

Pericynthion = 1000 km = h_{PL}

Return Vacuum Perigee = 46 km = h_{PE}

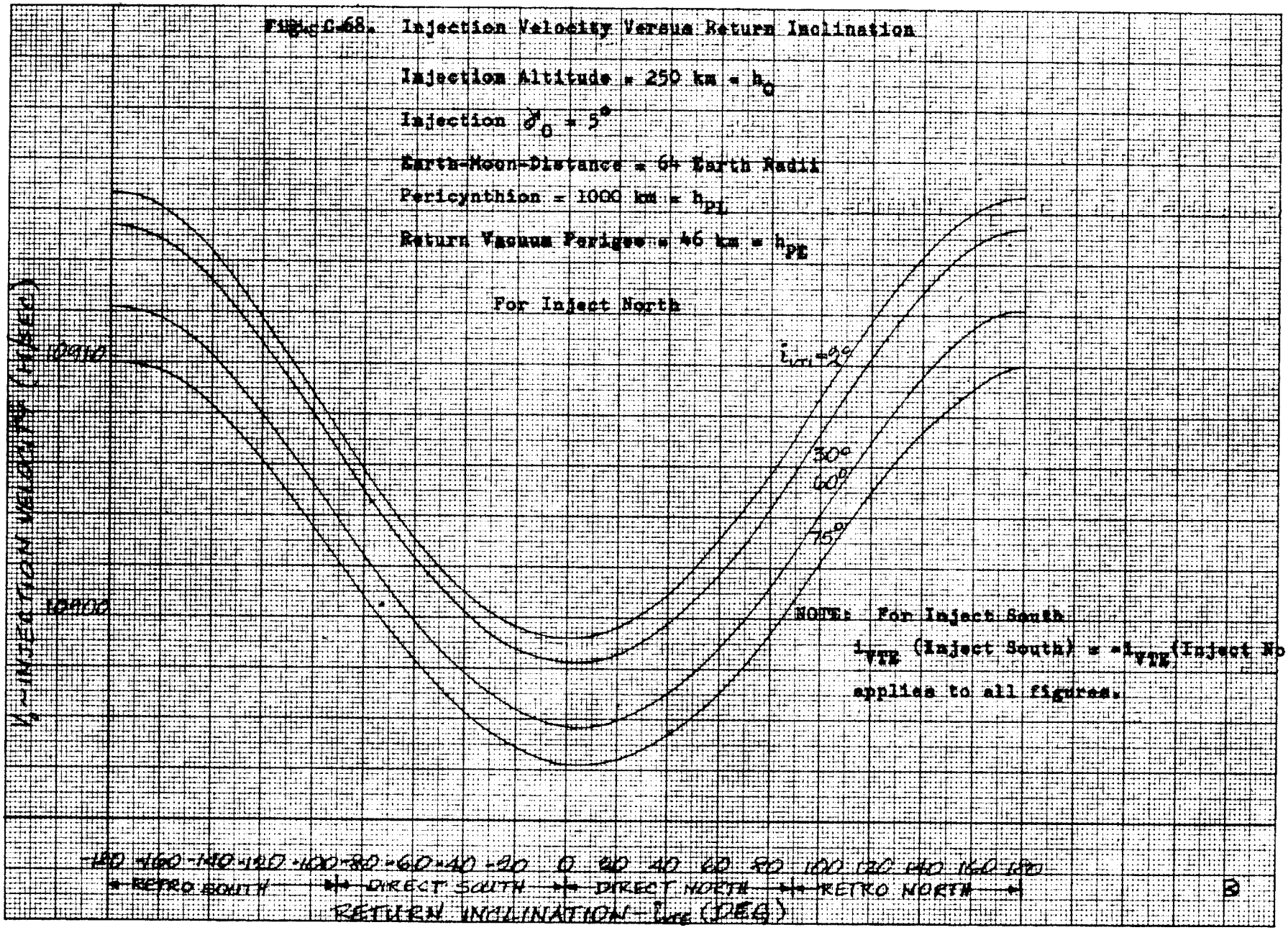

Injection Point Position Versus Return Inclination
Injection Altitude = 250 km = h_0
Injection $\gamma_0 = 5°$
Earth-Moon-Distance = 64 Earth Radii
Pericynthion = 1000 km = h_{pi}
Return Vacuum Perigee = 46 km = h_{pr}
Ω_E
Ω_M
i_{re}
$i_{re} = 90°$
30°
20°
10°
0°
B
-RETRO SOUTH
-DIRECT SOUTH
-DIRECT NORTH
-RETRO NORTH
RETURN INCLINATION - i_{re} (DEGS)

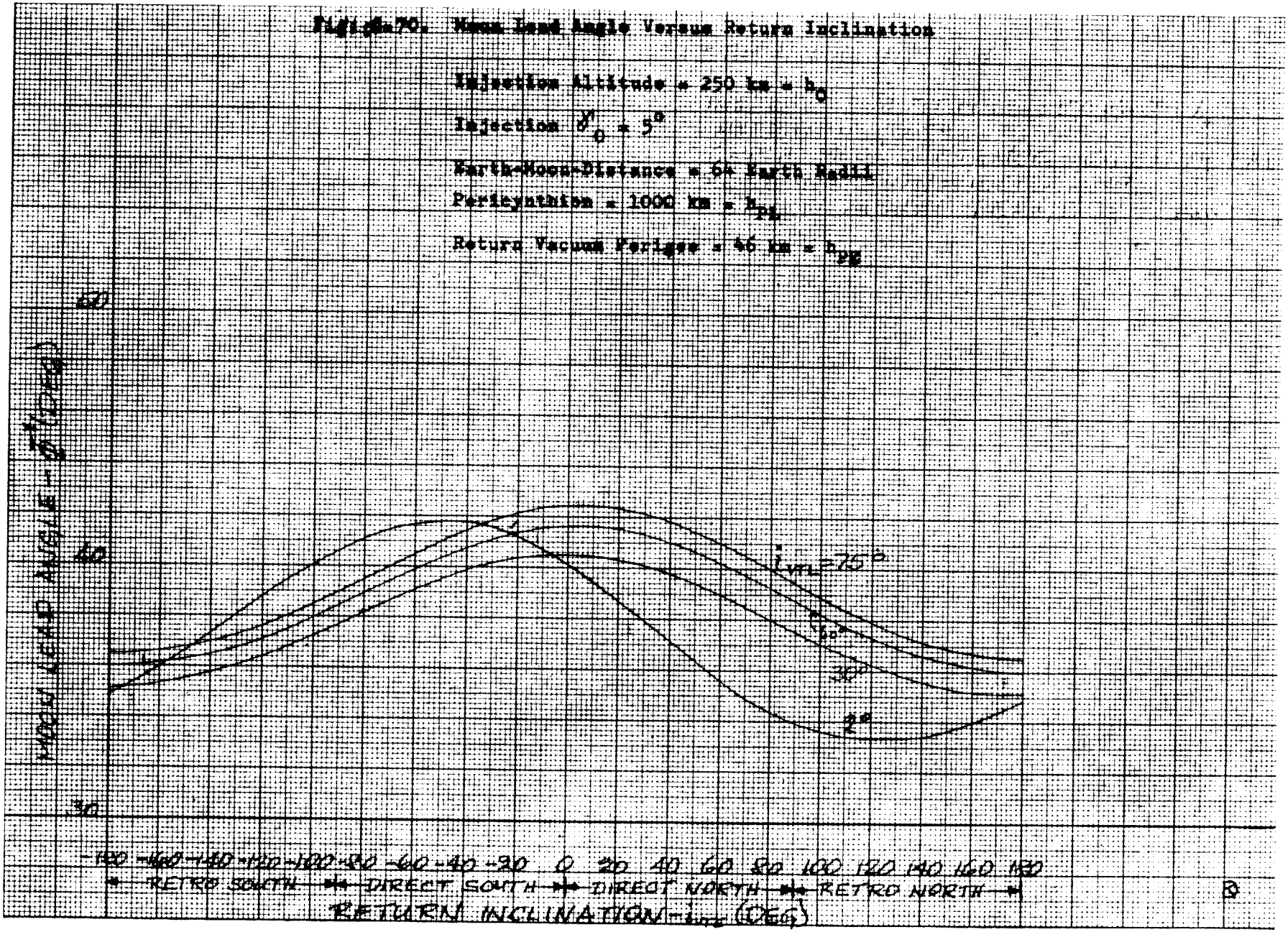
Figure 70. Vacuum Load Angle Versus Return Inclination
Injection Altitude = 250 km = h_0
Injection $\gamma'_0 = 5^\circ$
Earth-Moon-Distance = 64 Earth Radii
Perisynthion = 1000 km = h_{PA}
Return Vacuum Perigee = 46 km = h_{PR}
LOAD ANGLE (DEG)
60
40
30
$i_{VPL} = 75^\circ$
60°
30°
2°
-180 -160 -140 -120 -100 -80 -60 -40 -20 0 20 40 60 80 100 120 140 160 180
RETRO SOUTH
DIRECT SOUTH
DIRECT NORTH
RETRO NORTH
RETURN INCLINATION - i_{VPR} (DEG)

Apollo Earth Return Circular Lunar Orbit Versus Return Inclination
Injection Altitude = 250 km = h_0
Injection γ_0 = 0°
Earth-Moon Distance = Mean Mean
Perigee Radius = 1000 km = h_{pE}
Return Radius Perigee = 46 km = h_{pE}
ΔV (ECO to Lunar Circular Orbit Insertion) (km/sec)
ΔV_{ECO}
ΔV_{LOI}
ΔV_{TOT}
-90 -80 -70 -60 -50 0 40 50 60 70 80 90
DIRECT SOUTH
DIRECT NORTH
RETROGRADE
RETROGRADE
DIRECT
DIRECT
RETROGRADE
RETROGRADE
RETROGRADE
DIRECT

Flight Time of Particles Versus Return Inclination
Injection Altitude = 250 km = h_0
Injection β_0 = 5°
Antipodal Distance = 40 Earth Radii
Perigee Altitude = 1000 km = h_p
Return Vacuum Radius = 46 r_e = R_p
TIME OF PERIGEE PENETRATION = t_p (hrs)
α_0
α_R
i_{max} = 90°
75°
60°
30°
0°
RETRO SOUTH
DIRECT SOUTH
DIRECT NORTH
RETRO NORTH
RETURN INCLINATION (i_R)

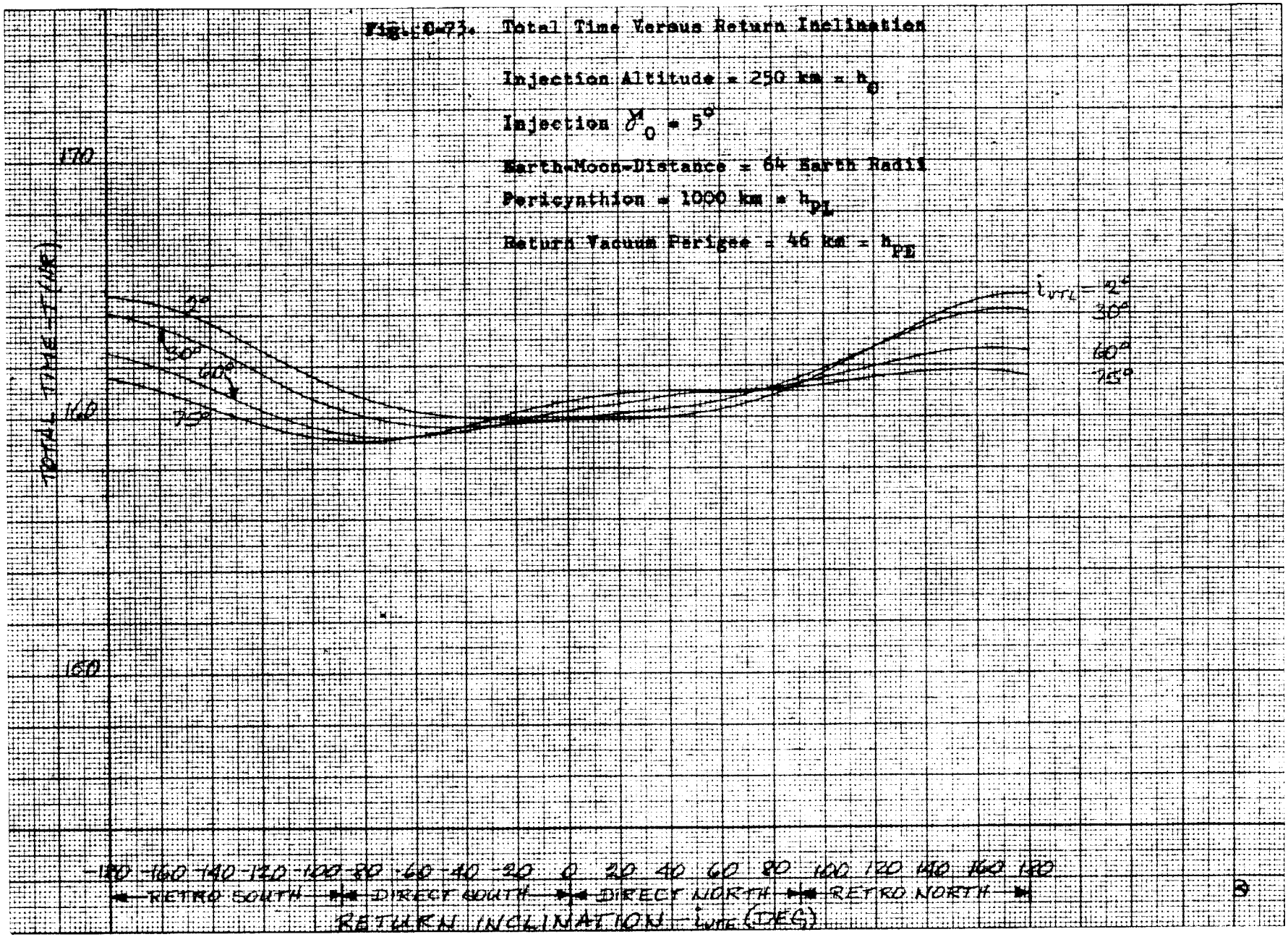
Fig. C-73. Total Time Versus Return Inclination
Injection Altitude = 250 km = h_0
Injection γ_0 = 5°
Earth-Moon-Distance = 64 Earth Radii
Pericynthion = 1000 km = h_{PL}
Return Vacuum Perigee = 46 km = h_{PE}
i_{VTL} = 2°
30°
60°
75°
180
160
140
2°
30°
60°
75°
-180 -160 -140 -120 -100 -80 -60 -40 -20 0 20 40 60 80 100 120 140 160 180
RETRO SOUTH
DIRECT SOUTH
DIRECT NORTH
RETRO NORTH
RETURN INCLINATION - i_{VTL} (DEG)

Fig. C-7b. Lunar Orbit Inclination Versus Return Inclination
Injection Altitude = 250 km = h0
Injection γ0 = 5°
Earth-Moon-Distance = 64 Earth Radii
Periapsis = 1000 km = h2
Return Vacuum Perigee = 45 km = h3
Return Inclination (Deg)
Lunar Orbit Inclination (Deg)
Direct Return
Retro Return
Direct Return
Retro Return

Fig. 6-29. Lunar Orbit Orientation Versus Return Inclination
Injection Altitude = 250 km = h_0
Injection γ_0 = 5°
Earth-Moon-Distance = 64 Earth Radii
Periapsis = 1000 km = h_{PL}
Return Vacuum Perigee = 46 km = h_R
i_{RE} = 0°
i_{RE} = 20°
i_{RE} = 30°
i_{RE} = 40°
i_{RE} = 50°
LUNAR ORBIT ORIENTATION - Ω_M (DEG)
RETURN INCLINATION - i_{RE} (DEG)
-180 -160 -140 -120 -100 -80 -60 -40 -20 0 20 40 60 80 100 120 140 160 180
RETRO SOUTH ← DIRECT SOUTH → DIRECT NORTH ← RETRO NORTH →

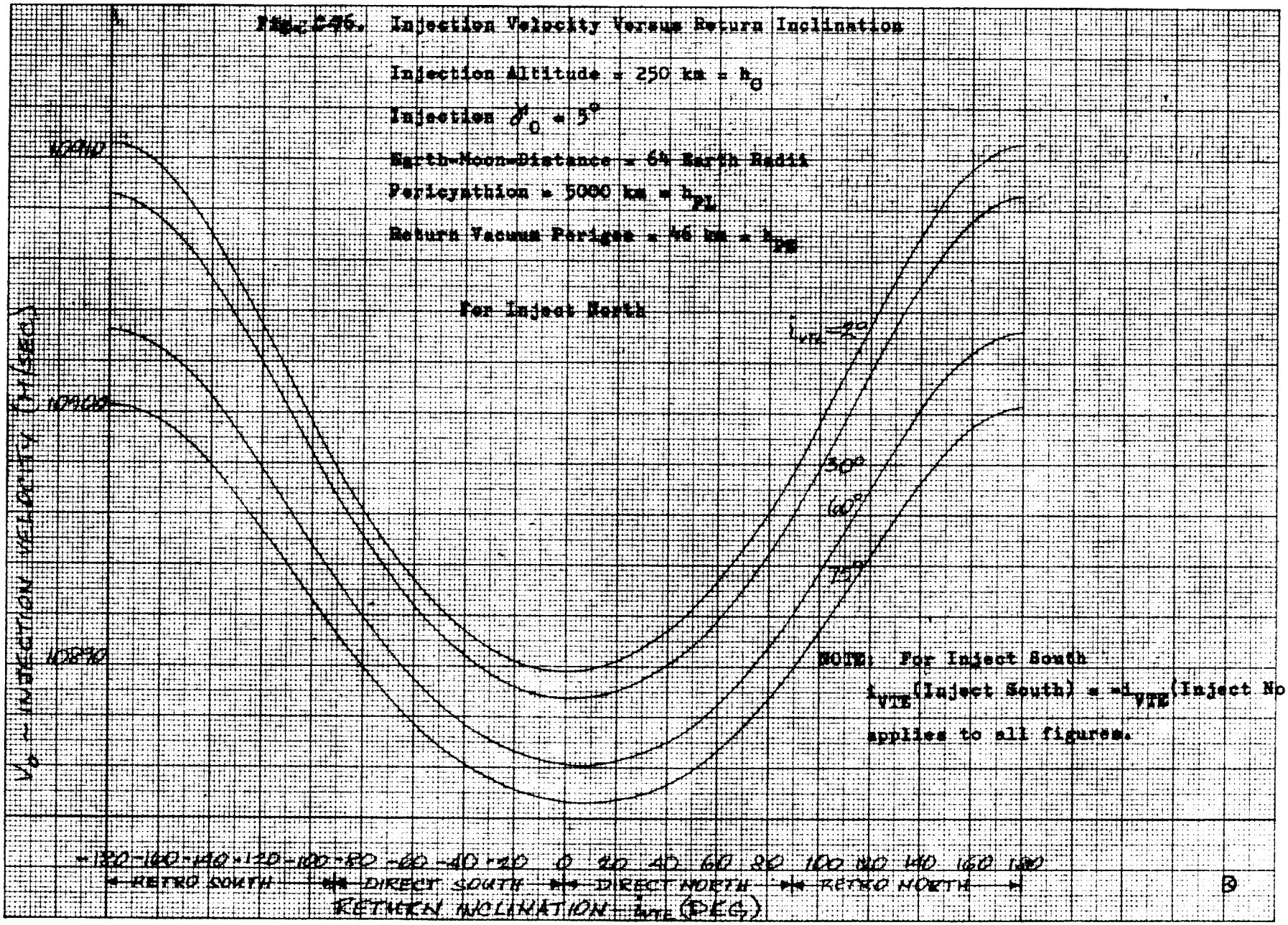
Fig. C-26. Injection Velocity Versus Return Inclination
Injection Altitude = 250 km = h_0
Injection γ_0 = 5°
Earth-Moon-Distance = 64 Earth Radii
Pericynthion = 5000 km = h_{PL}
Return Vacuum Perigee = 46 km = h_{PE}
For Inject North
i_{VTE}=-20°
-30°
-60°
-75°
NOTE: For Inject South
i_{VTE}(Inject South) = -i_{VTE}(Inject No.)
applies to all figures.
INJECTION VELOCITY - V_0 (FEET/SEC)
RETURN INCLINATION - i_{VTE} (DEG)
-120 -100 -80 -60 -40 -20 0 20 40 60 80 100 120 140 160 180
RETRO SOUTH
DIRECT SOUTH
DIRECT NORTH
RETRO NORTH

Figure 6-28. Moon Earth Lunar Return Inclination
Injection Altitude = 250 km = h_0
Injection γ_0 = 0°
Earth-Moon Distance = 64 Earth Radii
Perkyzelian = 5000 km = h_{pz}
Return Perilune = 40 km = h_{pl}
i_{max}=175°
150°
120°
90°
60°
30°
0°
RETURN INCLINATION (DEG)
RETROGRADE
DIRECT
DIRECT SOUTH
RETRO SOUTH
RETRO NORTH
DIRECT NORTH
MOON AT APOGEE
MOON AT PERIGEE

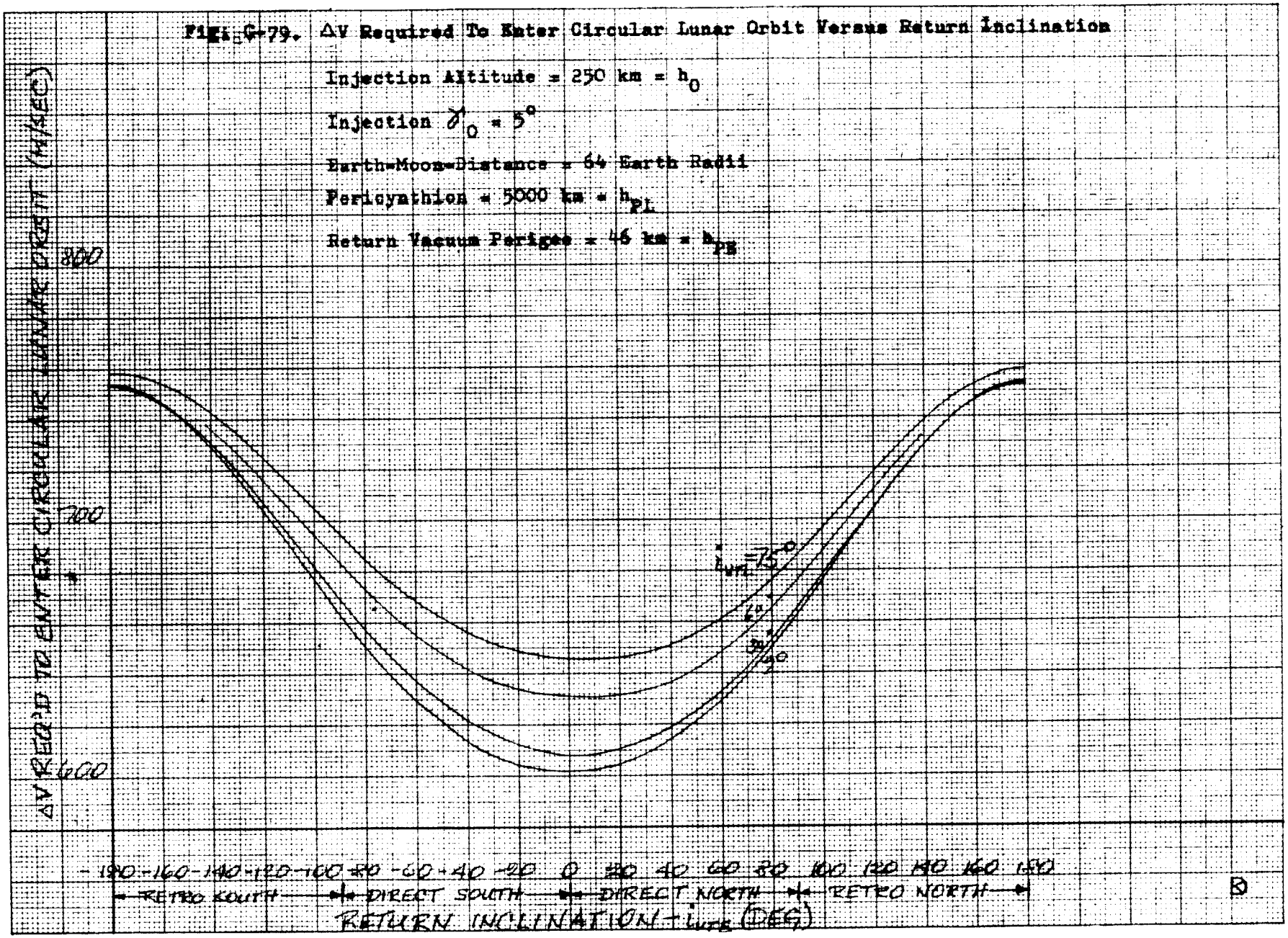
Fig. C-79. ΔV Required To Enter Circular Lunar Orbit Versus Return Inclination
Injection Altitude = 250 km = h_0
Injection γ_0 = 5°
Earth-Moon-Distance = 64 Earth Radii
Pericynthion = 5000 km = h_{PL}
Return Vacuum Perigee = 46 km = h_{PE}
ΔV REQ'D TO ENTER CIRCULAR LUNAR ORBIT (M/SEC)
800
700
600
i_{INC}=75°
70°
30°
0°
-180 -160 -140 -120 -100 -80 -60 -40 -20 0 20 40 60 80 100 120 140 160 180
RETRO SOUTH
DIRECT SOUTH
DIRECT NORTH
RETRO NORTH
RETURN INCLINATION - i_{INC} (DEG)

Time of Perigulation Versus Return Inclination
Injection Altitude = 250 km = h_0
Injection $\gamma_0 = 5°$
Earth-Moon-Distance = 60 Earth Radii
Perigyaction = 5000 km = h_{p_2}
Return Vacuum Perigee = 46 km = h_{p_1}
$i_{eff} = 5°$
30°
60°
75°
DIRECT SOUTH
DIRECT NORTH
RETRO NORTH
RETROGRADE INCLINATION (DEG)
B

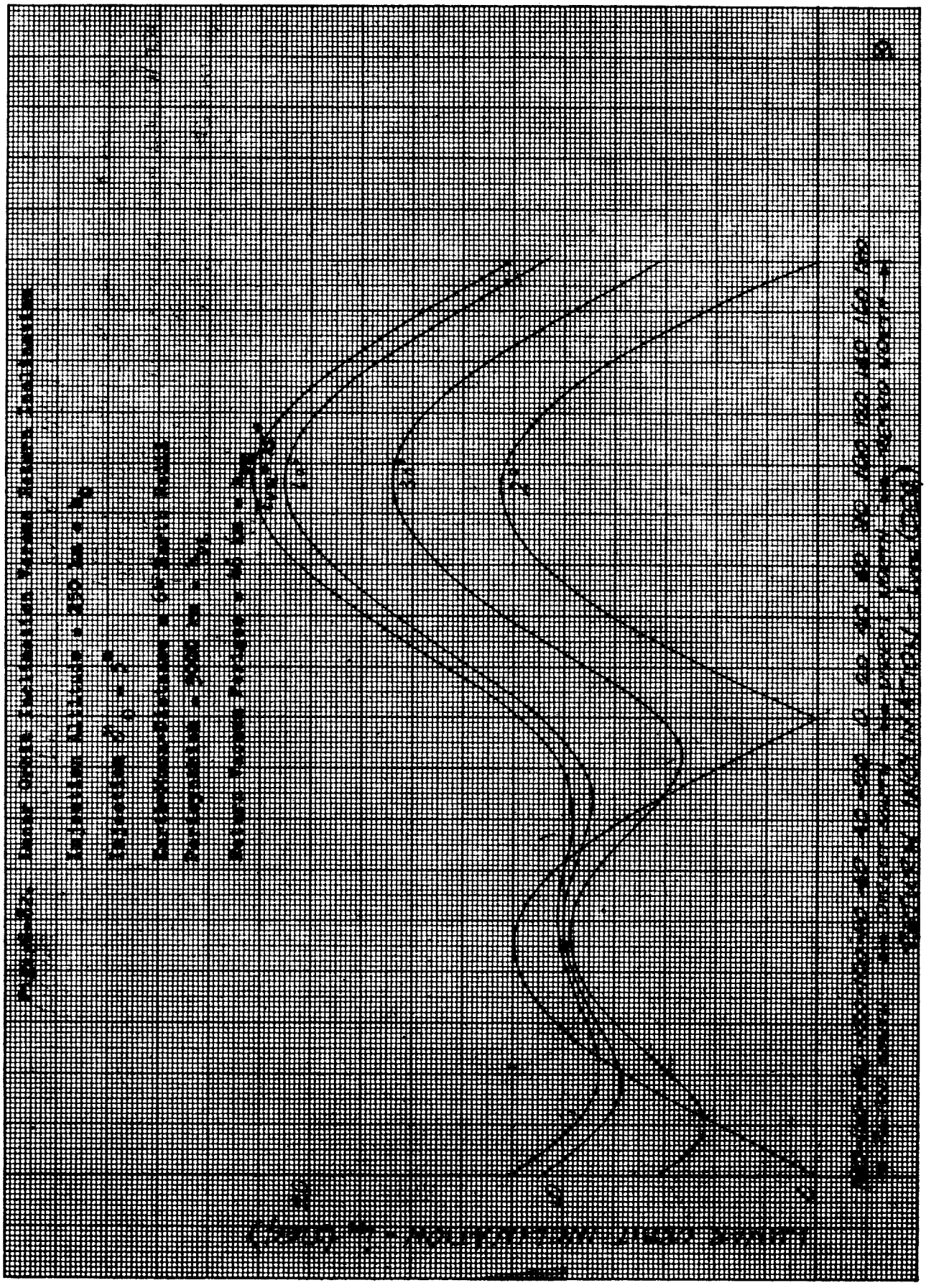

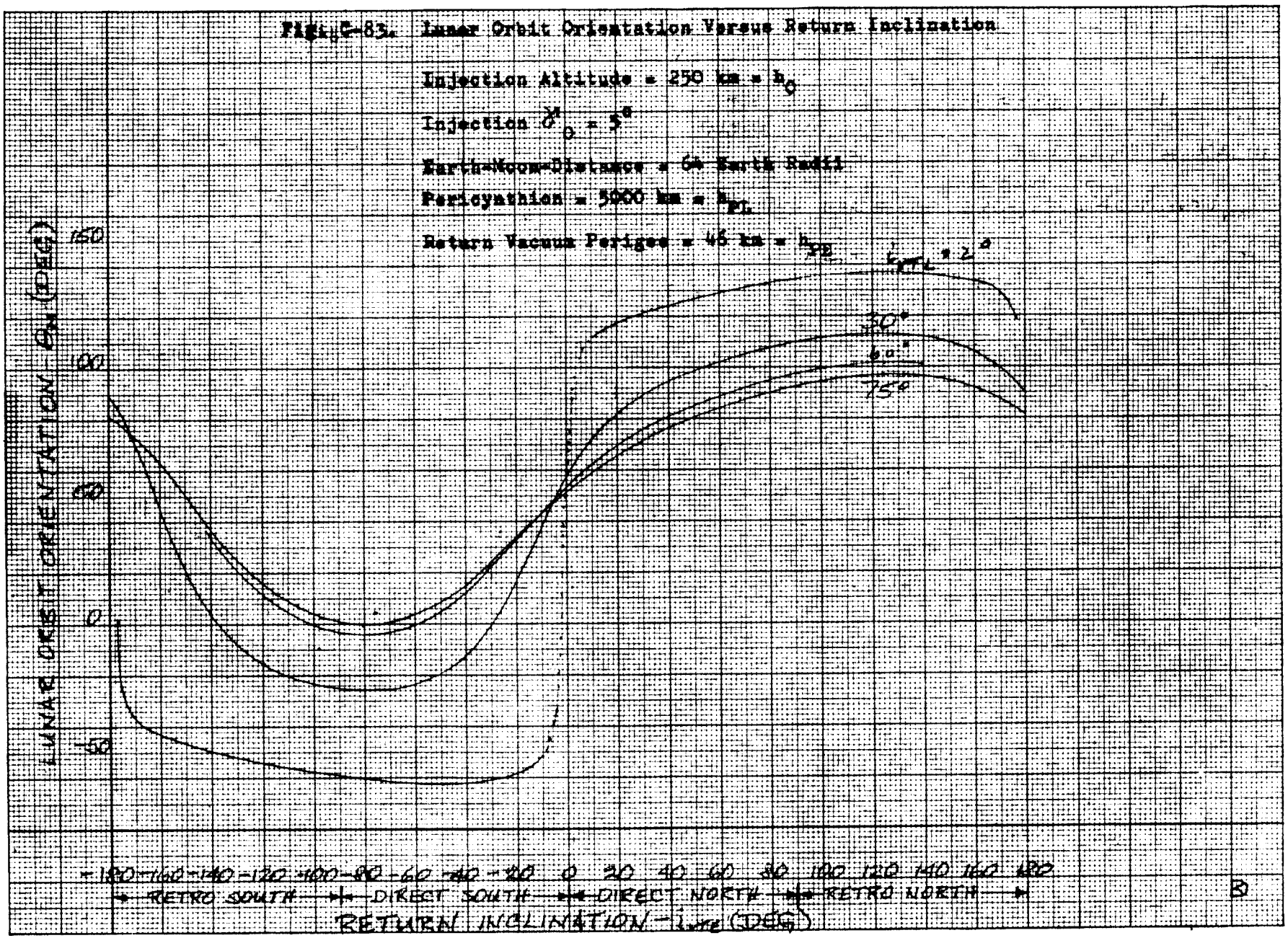
Fig. 6-83. Lunar Orbit Orientation Versus Return Inclination
Injection Altitude = 250 km = h_0
Injection $\gamma_0 = 5°$
Earth-Moon-Distance = 60 Earth Radii
Pericynthion = 5000 km = h_{PL}
Return Vacuum Perigee = 46 km = h_{PE}
$t_{FL} = 2^d$
30°
60°
75°
LUNAR ORBIT ORIENTATION ON (DEG)
80
60
0
-60
-180 -160 -140 -120 -100 -80 -60 -40 -20 0 20 40 60 80 100 120 140 160 180
RETRO SOUTH
DIRECT SOUTH
DIRECT NORTH
RETRO NORTH
RETURN INCLINATION - i_{VE} (DEG)

CHAPTER VII

LUNAR ORBIT

Prepared by:

F. Martikan and R. Salinger

Aerospace Mechanics Department
Martin Company (Balto.)
March, 1963

A.	Lunar Orbit Missions	VII-1
B.	Characteristics of Lunar Orbits	VII-1
C.	Entry and Departure Maneuvers Between Lunar Orbits and Transfer Trajectories	VII-9
D.	Lunar Orbit Determination Schemes	VII-11
E.	References	VII-12
	Illustrations	VII-15

VII. LUNAR ORBIT

A. LUNAR ORBIT MISSIONS

Lunar orbits are here defined as space vehicle trajectories which lie wholly within the Jacobi C_2 region around the moon (Chapter III). They are very well suited for reconnaissance and surveillance missions where the objective is to obtain mapping and close-range scientific data. Orbits are useful in that a properly placed lunar satellite can stay in lunar orbit almost indefinitely, with its usefulness only limited by the life of the equipment. At the present time, it is planned that manned lunar missions will include a lunar orbit. In this case, the lunar orbit provides the safety feature of ballistic earth return prior to orbit entry, longer reaction time prior to landing at a preselected lunar site, smaller total fuel requirements, and smaller abort fuel requirements when compared to soft-landing lunar impacts (see Chapter VIII). In the lunar orbit phase, the space vehicle crew can determine repeatedly its position in orbit and the position of the landing site before the initiation of the deorbit maneuver. A logistics mission can employ a lunar "freighter" shuttling between an earth orbit and a lunar orbit, leaving material in lunar orbit for later use by the lunar expedition, to be called down at the time and place desired. When lunar exploration has advanced beyond the initial stage, rescue, communication, navigation, and possibly even travel between distant lunar bases may be accomplished by use of lunar orbits.

The lunar orbit phase is thus vital for almost all future missions, as soon as lunar exploration progresses beyond the stage of probes on approach or impact trajectories and beyond approach trajectories near minimum velocities. A brief description and classification of lunar orbit missions and missions using a lunar orbit phase has been given in Section A of Chapter IV. Lunar orbit parameters have also been discussed qualitatively and quantitatively in connection with the circumlunar trajectory catalogue (Section A of Chapter VI) and the transearth trajectory catalogue (Section A of Chapter IX). Both sample missions discussed in Chapter XI, Section G, one a landing and the other a reconnaissance mission, use a lunar orbit phase. In the mission discussion, the lunar orbital parameters, as they are limited by mission constraints, and methods for obtaining a first estimate of orbital parameters have been given.

In the present chapter, near-lunar satellite orbits are discussed in relative detail. In Section B, the characteristics of an orbit around the moon as affected by the triaxiality of the moon, the sun and the earth are discussed. These effects are compared, and it is shown that for a close lunar satellite, the sun's effects can be neglected. The equations of motion in a selenocentric coordinate system are derived from a potential function based on a triaxial moon. First-order secular changes in the orbital elements due to the moon's oblateness are presented in graphical form as a function of orbital inclination. Stability of a lunar orbit is briefly discussed. Finally, relationships for determining ground traces and longitude increments between successive ground traces are given. This data is important for orbital parameter choice in lunar mapping, reconnaissance and surveillance missions.

Velocity requirements for entry into a lunar orbit in the form of summary plots are presented in Section C. The bulk of the material is based on the assumption that the effects of finite burning times are negligible. Results for two different types of trajectories (circumlunar and approach), based on a simplified earth-moon model, are presented and compared. It is seen that there are certain restrictions on the trajectory paramters that must be taken into account when planning a lunar mission.

In Section D, a qualitative discussion of lunar orbit determination schemes for both manned and unmanned vehicles in a lunar orbit is presented.

B. CHARACTERISTICS OF LUNAR ORBITS

In the design of lunar orbits the first and foremost concern is the determination of orbital parameters which best fulfill the mission objective. In most cases this requires eventually a rather accurate determination of space vehicle position with time, which involves either the use of general perturbation theories or a numerical integration on the digital computer if only short-time ephemerides of a lunar satellite are required. However, since very little graphical data on orbits around the moon has been published in the literature, and hardly any numerical evaluation of general perturbation theories as applied to lunar orbits has appeared, the discussion of this section will be directed toward a summary of important analytical results and the presentation of graphical material.

1. Keplerian Orbit Parameters

To obtain gross orbital characteristics, the moon may be considered a spherically symmetric body as a first approximation, with the influence of the earth and the sun neglected. Theoretically, this model is equivalent to one in which the lunar mass is concentrated at the center of the moon. The gravitational potential for this lunar model is

$$U_{\mathbb{C}} = \frac{\mu_{\mathbb{C}}}{r_0} \tag{1}$$

and the well-known restricted two-body Keplerian equations apply, as given in Chapter III, Section K (Ref. 1), for elliptic and circular orbits.

From a flight mechanics point of view, the period of revolution τ_0 for an elliptic orbit with semimajor axis a_0 as a function of a_0,

$$\tau_0 = 2\pi \sqrt{\frac{a_0^3}{\mu_{\mathbb{C}}}} \tag{2}$$

and the velocity of a satellite $V_{\mathbb{C}c}$ in a circular orbit with radius r_0 as a function of r_0,

$$V_{\mathbb{C}\,c} = \sqrt{\frac{\mu}{r_0}} \qquad (3)$$

are of special interest. These parameters have been presented as a function of mean altitude $h_0 = a_0 - R_{\mathbb{C}}$, where $R_{\mathbb{C}} = 1738.16$ km is the radius of the equivalent spherical moon, and of circular orbit altitude $h_0 = r_0 - R_{\mathbb{C}}$ in Figs. 1 and 2 for lunar orbits and close lunar orbits, respectively. For preliminary design calculations and for orbits of short duration, these numbers are a good approximation to the actual orbit.

However, these gross orbital characteristics are not good enough for a long-time satellite of the moon and for more accurate calculations. In this case, perturbing forces, which are small effects compared to the principal force of lunar attraction, have to be taken into account. The perturbing forces that will be discussed here are due to the gravity fields of the earth and of the sun and to the asphericity of the lunar gravity field.

2. Orbit Perturbations

a. Solar perturbation

Consider the gravitational attraction of the sun on a lunar satellite first. It can be shown that for a lunar satellite orbit, the effects of the sun can be neglected when compared to those of the earth. Let the masses of the lunar satellite, sun, moon, and earth be denoted by M_Δ, $M_\odot$, $M_{\mathbb{C}}$, and $M_\oplus$, respectively. Assume an inertial frame of reference centered at the sun (which is a good assumption, since $M_\odot \gg M_\oplus, M_{\mathbb{C}}, M_\Delta$) as shown in the sketch below:

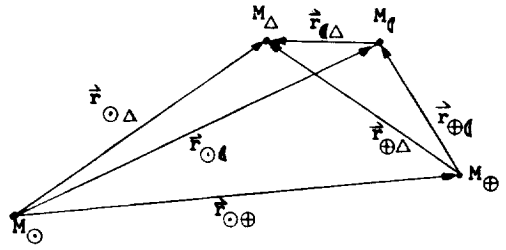

The equation of motion of the lunar satellite is in vector form

$$M_\Delta \left(\frac{d^2 \vec{r}_{\odot\Delta}}{dt^2}\right) = \vec{F}_{M_\Delta}(M_\odot) + \vec{F}_{M_\Delta}(M_{\mathbb{C}}) + \vec{F}_{M_\Delta}(M_\oplus) \qquad (4)$$

or:

$$M_\Delta \left(\frac{d^2 \vec{r}_{\odot\Delta}}{dt^2}\right) = \vec{F}\left(\vec{r}_{\odot\Delta}\right) + \vec{F}\left(\vec{r}_{\mathbb{C}\Delta}\right) + \vec{F}\left(\vec{r}_{\oplus\Delta}\right) \qquad (5)$$

where $F_{M_\Delta} \equiv F_{M_\Delta}(M_\odot) \equiv F(r_{\odot\Delta}) = \dfrac{GM_\odot M_\Delta}{r_{\odot\Delta}^2} = \dfrac{\mu_\odot M_\Delta}{r_{\odot\Delta}^2}$ is the magnitude of the gravitational attraction of the sun on the lunar satellite, etc.

The motion of the moon is given by:

$$M_{\mathbb{C}} \left(\frac{d^2 \vec{r}_{\odot\mathbb{C}}}{dt^2}\right) = \vec{F}\left(\vec{r}_{\odot\mathbb{C}}\right) + \vec{F}\left(\vec{r}_{\oplus\mathbb{C}}\right) \qquad (6)$$

where the force of the satellite on the moon is neglected (i.e., these equations are for a restricted 4-body problem). Using Eqs (4) and (5) and the relation $\vec{r}_{\mathbb{C}\Delta} = \vec{r}_{\odot\Delta} - \vec{r}_{\odot\mathbb{C}}$, it follows that:

$$M_\Delta \left(\frac{d^2 \vec{r}_{\mathbb{C}\Delta}}{dt^2}\right) = \vec{F}\left(\vec{r}_{\mathbb{C}\Delta}\right) + \left[\vec{F}\left(\vec{r}_{\mathbb{C}\Delta}\right) + \frac{M_\Delta}{M_{\mathbb{C}}}\vec{F}\left(\vec{r}_{\odot\mathbb{C}}\right)\right] + \left[\vec{F}\left(\vec{r}_{\oplus\Delta}\right) - \frac{M_\Delta}{M_{\mathbb{C}}}\vec{F}\left(\vec{r}_{\oplus\mathbb{C}}\right)\right] \qquad (7)$$

or

$$M_\Delta \left(\frac{d^2 \vec{r}_{\mathbb{C}\Delta}}{dt^2}\right) = \vec{F}\left(\vec{r}_{\mathbb{C}\Delta}\right) + \mu_\odot M_\Delta \left[\frac{\vec{r}_{\odot\mathbb{C}}}{r_{\odot\mathbb{C}}^3} - \frac{\vec{r}_{\odot\Delta}}{r_{\odot\Delta}^3}\right] + \mu_\oplus M_\Delta \left[\frac{\vec{r}_{\oplus\mathbb{C}}}{r_{\oplus\mathbb{C}}^3} - \frac{\vec{r}_{\oplus\Delta}}{r_{\oplus\Delta}^3}\right] \qquad (8)$$

The magnitude of the second term on the RHS of Eq (8), which is due to the sun, can be approximated by $\mu_\odot M_\Delta \left(\dfrac{r_{\mathbb{C}\Delta}}{r_{\odot\mathbb{C}}^3}\right)$ since $r_{\mathbb{C}\Delta} << r_{\odot\mathbb{C}}$; the magnitude of the last term of Eq (8), which is due to the earth, can be approximated by $\mu_\oplus M_\Delta \left(\dfrac{r_{\mathbb{C}\Delta}}{r_{\oplus\mathbb{C}}^3}\right)$ since $r_{\mathbb{C}\Delta} << r_{\oplus\mathbb{C}}$. The ratio of these terms is given by:

$$\frac{M_\odot}{M_\oplus}\left(\frac{r_{\oplus\mathbb{C}}}{r_{\odot\mathbb{C}}}\right)^3 \simeq \frac{M_\odot}{M_\oplus}\left(\frac{r_{\oplus\mathbb{C}}}{r_{\odot\oplus}}\right)^3 \simeq 0.00565, \qquad (9)$$

which justifies the omission of the effects due to the sun when compared to those of the earth. Schechter (Ref. 2) uses Pontecoulant's lunar theory to obtain an idea of the sun's perturbative effect. Schechter considers a coplanar restricted four-body problem in the ecliptic plane; he expands the sun's gravitational field in a Taylor series around the instantaneous lunar position, and retains only the leading term of the series. The magnitude of the solar effect on a lunar satellite obtained there is roughly 0.3% as large as the effect exerted by the earth, or less than half of the approximate value obtained in Eq (9). Solar effects on lunar satellites can thus be considered higher-order effects and neglected.

b. Lunar asphericity perturbations

Before considering the actual magnitude of the earth's gravitational attraction, effects of lunar asphericity on lunar satellite orbits will be dis-

cussed; the earth perturbations will be compared later to those of lunar asphericity. Thus, we consider next the effects of the triaxially ellipsoidal shape of the moon on the satellite orbit. Assume that the moon and space vehicle are the only bodies in the dynamical system, and that the lunar potential is expanded in terms of spherical harmonics. By the use of MacCullagh's theorem (Ref. 3), the lunar potential U can also be written in terms of the lunar moments of inertia. Several forms of $U_{\mathbb{C}}$ which are widely used have been presented in Chapter II.

Another form of $U_{\mathbb{C}}$ which is given in terms of the selenographic coordinate system x_S, y_S, z_S is

$$U_{\mathbb{C}} = \frac{\mu_{\mathbb{C}}}{r_S}\left\{1 + \left(\frac{R}{r_S}\right)^2\left[\frac{3}{2}J_2\left(\frac{1}{3} - \left(\frac{z_S}{r_S}\right)^2\right) + 3\,C_{2,2}\left(\frac{x_S^2 - y_S^2}{r_S^2}\right)\right]\right\} \tag{10}$$

where R is the radius of the moon in the direction of the earth (denoted by a in Chapters II and IV) and J_2, $C_{2,2}$ are the constant expansion coefficients, which can be defined in terms of the lunar moments of inertia as given in Chapter II. An advantage of Eq (10) is that it shows explicitly the two perturbative terms which are due to the asphericity of the moon. The J_2 term represents the oblateness of the moon (i.e., the latitude dependence of the lunar radius), and the $C_{2,2}$ term represents the ellipticity of the equator (longitude dependence of the lunar radius).

The selenographic coordinate system rotates with the moon, and before an explicit form for the gravitational force of the moon on the vehicle can be given, a transformation to the inertial (for this dynamical system) lunar equatorial coordinate system $x_{\mathbb{C}}$, $y_{\mathbb{C}}$, $z_{\mathbb{C}}$ must be made.

This transformation is given by Eq (2) of Chapter III, and $U_{\mathbb{C}}$ in the inertial coordinate system becomes:

$$U_{\mathbb{C}} = \frac{\mu_{\mathbb{C}}}{r_{\mathbb{C}}}\left\{1 + \left(\frac{R}{r_{\mathbb{C}}}\right)^2\left[\frac{3}{2}J_2\left(\frac{1}{3} - \left(\frac{z_{\mathbb{C}}}{r_{\mathbb{C}}}\right)^2\right) + \frac{3\,C_{2,2}}{r_{\mathbb{C}}^2}\left[\left(x_{\mathbb{C}}^2 - y_{\mathbb{C}}^2\right)\cos 2\left(\Lambda_S + \omega_{\mathbb{C}}\,t\right) + 2\sin^2\left(\Lambda_S + \omega\,t\right)x_{\mathbb{C}}\,y_{\mathbb{C}}\right]\right]\right\} \tag{11}$$

The equations of motion in the $x_{\mathbb{C}}$, $y_{\mathbb{C}}$, $z_{\mathbb{C}}$ coordinate system can be obtained by partial differentiation:

$$\ddot{x}_{\mathbb{C}} = \frac{\partial U_{\mathbb{C}}}{\partial x_{\mathbb{C}}}\,;\quad \ddot{y}_{\mathbb{C}} = \frac{\partial U_{\mathbb{C}}}{\partial y_{\mathbb{C}}}\,;\quad \ddot{z}_{\mathbb{C}} = \frac{\partial U_{\mathbb{C}}}{\partial z_{\mathbb{C}}} \tag{12}$$

Carrying out the indicated operations, one obtains:

$$\ddot{x}_{\mathbb{C}} = \frac{\mu_{\mathbb{C}}\,x_{\mathbb{C}}}{r_{\mathbb{C}}^3}\left\{1 + \frac{3\,J_2\,R^2}{2\,r_{\mathbb{C}}^2}\left[1 - 5\left(\frac{z_{\mathbb{C}}}{r_{\mathbb{C}}}\right)^2\right] - \frac{3\,C_{2,2}\,R^2}{r_{\mathbb{C}}^4}\left(x_{\mathbb{C}}^2 + 3\,y_{\mathbb{C}}^2 + 2\,z_{\mathbb{C}}^2\right)\cos 2\left(\Lambda_S + \omega_{\mathbb{C}}\,t\right) - \frac{6\,C_{2,2}\,R^2}{r_{\mathbb{C}}^2}\left(\frac{y_{\mathbb{C}}}{x_{\mathbb{C}}}\right)\left[1 - 5\left(\frac{x_{\mathbb{C}}}{r_{\mathbb{C}}}\right)^2\right]\sin 2\left(\Lambda_S + \omega_{\mathbb{C}}\,t\right)\right\} \tag{13}$$

$$\ddot{y}_{\mathbb{C}} = -\frac{\mu_{\mathbb{C}}\,y_{\mathbb{C}}}{r_{\mathbb{C}}^3}\left\{1 + \frac{3\,J_2\,R^2}{2\,r_{\mathbb{C}}^2}\left[1 - 5\left(\frac{z_{\mathbb{C}}}{r_{\mathbb{C}}}\right)^2\right] - \frac{3\,C_{2,2}\,R^2}{r_{\mathbb{C}}^4}\left(x_{\mathbb{C}}^2 + 3y_{\mathbb{C}}^2 + 2\,z_{\mathbb{C}}^2\right)\cos 2\left(\Lambda_S + \omega_{\mathbb{C}}\,t\right) - \frac{6\,C_{2,2}\,R^2}{r_{\mathbb{C}}^2}\left(\frac{x_{\mathbb{C}}}{y_{\mathbb{C}}}\right)^2\left[1 - 5\left(\frac{y_{\mathbb{C}}}{r_{\mathbb{C}}}\right)^2\right]\sin 2\left(\Lambda_S + \omega_{\mathbb{C}}\,t\right)\right\} \tag{14}$$

$$\ddot{z}_{\mathbb{C}} = -\frac{\mu_{\mathbb{C}}\,z_{\mathbb{C}}}{r_{\mathbb{C}}^3}\left\{1 + \frac{3\,J_2\,R^2}{2\,r_{\mathbb{C}}^2}\left[3 - 5\left(\frac{z_{\mathbb{C}}}{r_{\mathbb{C}}}\right)^2\right] + \frac{15\,C_{2,2}\,R^2\left(x_{\mathbb{C}}^2 - y_{\mathbb{C}}^2\right)}{r_{\mathbb{C}}^4}\cos 2\left(\Lambda_S + \omega_{\mathbb{C}}\,t\right) + \frac{30\,R^2\,C_{2,2}\,x_{\mathbb{C}}\,y_{\mathbb{C}}}{r_{\mathbb{C}}^4}\sin 2\left(\Lambda_S + \omega_{\mathbb{C}}\,t\right)\right\} \tag{15}$$

These rather complicated equations of motion can be solved by numerical integration to yield the satellite position.

Another approach to the problem is to express U_ℓ in terms of the orbital elements a, e, i, ω, Ω', and f, which were defined in Subsection A-3c of Chapter III:

$$U_\ell = \frac{\mu_\ell}{r_\ell}\left\{1 + \left(\frac{R}{r_\ell}\right)^2\left[\frac{3}{2}J_2\left(\frac{1}{3} - \sin^2 i \sin^2(f+\omega)\right)\right.\right.$$
$$+ 3\,C_{2,2}\left((\cos 2(\Omega' - \omega_\ell t)\left[\cos^2(f+\omega)\right.\right.\right. \quad (16)$$
$$\left.\left.\left. - \sin^2(f+\omega)\cos^2 i\right]\right.\right.$$
$$\left.\left.\left. - \sin 2(f+\omega)\sin 2(\Omega' - \omega_\ell t)\cos i\right)\right]\right\}$$

where r_ℓ can be expressed in terms of the elliptical elements of the satellite by:

$$r_\ell = \frac{a(1 - e^2)}{1 + e\cos f} \quad (17)$$

and where f, the true anomaly, is related to ℓ the mean anomaly, by the differential equation:

$$\frac{df}{d\ell} = \frac{a^2}{r_\ell^2}\sqrt{1 - e^2} \quad (18)$$

It is now possible to form the perturbing function:

$$\Phi_\ell = U_\ell - \frac{\mu_\ell}{r_\ell} \quad (19)$$

and to use general perturbation methods to determine the time-variation of the orbital elements. The perturbing function Φ_ℓ can be divided into terms that arise due to J_2 and terms that arise due to $C_{2,2}$. The function Φ_ℓ can additionally be divided into secular terms, or terms that keep increasing with time, into long-period terms, or terms that are periodic with an approximate period of the rotation of pericynthion, and into short-period terms, which are periodic with approximately the same period as the satellite period τ_0. The desired term of Φ_ℓ can be substituted into the variation-of-parameter equations, one form of which is given by Eq (101) of Chapter III and other forms in Chapter III of Ref. 1, which form a set of six first-order ordinary differential equations completely equivalent to the equations of motion (13) through (15). These equations can then be solved for the secular, long-periodic and short-periodic variations in satellite orbital elements due to the lunar potential.

Consider the oblateness coefficient J_2. From Chapter II, it is seen that this expansion coefficient is the largest one in the lunar potential, and, hence, oblateness effects can be expected to be the most notable asphericity effects on the lunar satellite orbit. Of particular interest to the mission designer are the secular effects, since these increase with time and since it is often desired to obtain the average satellite behavior over a long period of time for lunar orbital missions. Since the earth is also oblate, analytic work on near-earth satellites is also applicable for lunar satellites. In the following discussion of lunar oblateness effects, the secular effects will be discussed qualitatively, quantitatively, and finally, graphically. Periodic effects on the radius will be described only.

Due to the small oblateness of the moon ($J_2 < 1$), the lunar satellite orbit is very nearly a circle or an ellipse. To first order in oblateness (using terms to J_2 in the expansion of the gravitational potential), the orbital plane precesses around the lunar polar axis at a variable rate (nodal regression). In addition, the line of apsides defining the orientation of the satellite trajectory in the orbital plane rotates in this plane at a variable rate (apsidal rotation). The dependence of the mean motion, or the average rate of rotation of the satellite in the orbital plane, on the orbital inclination results in an oblateness correction to the period of the unperturbed (or restricted 2-body) motion. Restricted 2-body motion is referred to as zero-order or unperturbed motion; if J_2 is used, in addition, the motion is defined as second-order; the inclusion of $C_{2,2}$ defines third-order motion; and all other, yet-to-be-defined spherical harmonic expansion coefficients of U_ℓ define fourth-order motion and are negligible.

The mean rate of nodal regression to first-order has been found by many authors (Refs. 4 through 11 and others). In units of degrees per nodal period (time between successive ascending nodes), it is:

$$\frac{d\Omega}{dt} = -360 \cdot \frac{3}{2}J_2\frac{R^2}{\bar{a}^2(1 - e^2)^2}\cos i_0 \quad (20)$$

Since $\frac{d\Omega}{dt} = 0\left(J_2\frac{d\beta}{dt}\right)$, any one of the following expressions can be used to second-order in the denominator:

$$a^2(1 - e^2)^2,\ a_0^2(1 - e^2)^2,\ \bar{a}^2(1 - e^2)^2,\ p^2,\ \bar{p}^2$$

where a_0 is the Keplerian value of the semimajor axis, $p^2 = a^2(1 - e^2)^2$ is the semilatus rectum of the orbit, r_0 is the average orbital radius ($r_0 \equiv p$ for Keplerian orbits), and a bar denotes an average value of the quantity about which it varies periodically for oblate moon orbits. The value of $\frac{d\Omega}{dt}$ is negative for a direct orbit ($i_0 < 90°$), i.e., it is a shift toward the west; while $\frac{d\Omega}{dt}$ is positive for a retrograde orbit ($i_0 > 90°$). For an equatorial orbit ($i_0 = 0°$, $180°$), the ascending node Ω is undefined, but $\frac{d\Omega}{dt}$ can be defined in the limit as $i_0 \to 0°$ or $i_0 \to 180°$. In Fig. 3, $\left(-\frac{d\Omega}{dt}\right)$ is plotted as a function of i_0 for three values of p.

It is seen from this figure that the nodal regression is largest for an equatorial orbit and zero for a polar orbit; it is larger for a circular orbit (e = 0) than for an elliptic orbit $0 < e < 1$, and since it is a gravitational force, it decreases with the inverse square of the distance from the center of the moon.

The mean rate of apsidal rotation has been found by many authors (Refs. 4 through 11 and others); in units of degrees per nodal period, it is

$$\frac{d\omega}{dt} = 360 \frac{3J_2}{2} \frac{R^2}{\bar{a}^2 (1 - e^2)^2} \cdot (2 - \frac{5}{2} \sin^2 i_0) \qquad (21)$$

For near-polar orbits, the perigee regresses, i.e., it moves against the direction of satellite motion, and $\frac{d\omega}{dt}$ is negative in value, while for near-equatorial orbits the perigee advances--i.e., it moves in the direction of satellite motion, and $\frac{d\omega}{dt}$ is positive in value. The inclination angles at which $2 - \frac{5}{2} \sin^2 i_0 = 0$, or $i_0 \simeq 63.45°$ and $i_0 \simeq 116.55°$ are known as critical inclination angles. Near the critical inclination, when $2 - \frac{5}{2} \sin 2 i_0 = O(J_2)$, or approximately for inclinations between 62.45 and 64.45°, as well as between 115.55 and 117.55°, a second-order theory is insufficient to describe the apsidal motion, and Eq (21) does not hold. This case has been discussed by Struble (Ref. 12). Figure 4 presents the rate of apsidal rotation as a function of orbital inclination for three values of p. The perifocus location ω is undefined for circular orbits, but it is possible to define $\frac{d\omega}{dt}$ in the limit as $e \to 0$. The same general comments on the dependence of $\frac{d\omega}{dt}$ on e, p apply as in the case of $\frac{d\Omega}{dt}$.

The orbital period in unperturbed satellite motion is given by Eq (2) which has been plotted in Figs. 1 and 2.

In perturbed satellite motion, or when second-order perturbing forces due to lunar oblateness act on the satellite, one can define three, in general distinct, periods of motion:

(1) The anomalistic period, the time from one pericynthion to the next. In that time the elliptic angles (true, mean, and eccentric anomaly) increase by 360°, while the orbital central angle $\beta = \omega + f$ increases by more or less than 360°, depending on whether the apsidal rotation is against or in the direction of satellite motion.

(2) The nodal period, also called draconic period, the time from one ascending node to the next. In that time the orbital central angle $\beta = \omega + f$ increases by 360°, since β is measured from the instantaneous position of the ascending node. The satellite does not, except at an orbit inclination of 90°, return to the same relative position in inertial space after one nodal period due to the regression of the nodes.

(3) The sidereal period, the time for the satellite to return to the same relative position in inertial space. In that time the satellite central angle as measured from a fixed reference, which is not to be confused with the central angle as measured from the ascending node, increases by 360°. In artificial satellite theory, the sidereal period is less important than the other two periods; it is rarely used, and it will not be discussed any further.

In many satellite calculations, especially in approximate ephemeris prediction, it is more convenient to use the nodal period τ_β than the anomalistic period, τ_r, since (especially for circular and near-circular orbits) the ascending node is a more easily identifiable point than pericynthion, except in the case of equatorial lunar orbits. Unfortunately, however, differing expressions have been obtained for it in the literature (compare the nodal periods derivable from mean motions given in Refs. 6, 7, 8, 10, 13, 14, 15, 16, 17, 18 among others).

An expression for the nodal period was derived from Struble's (Ref. 12) first-order theory by Martikan and Kalil (Ref. 13) for small eccentricities, $e = O(J_2)$, and shown to be compatible with expressions for the anomalistic period for large values of eccentricity by some numerical examples in Ref. 13:

$$\tau_\beta = \frac{2\pi}{\sqrt{\mu_\oplus}} (\bar{a})^{\frac{3}{2}} \left\{ 1 - \frac{3}{8} J_2 \frac{R^2}{\bar{a}^2 (1 - e^2)^2} (7 \cos^2 i_0 - 1) \right\}, \qquad (22)$$

where $\bar{a}$ is the mean semimajor axis of the perturbed orbit defined in terms of a reference Keplerian semimajor axis (which should not be used, since it is but a first estimate for a):

$$\bar{a} = a_0 \left\{ 1 - \frac{3}{4} J_2 \frac{R^2}{a_0^2 (1 - e^2)^2} \cdot (3 \cos^2 i_0 - 1) \sqrt{1 - e^2} \right\} \qquad (23)$$

The oblateness correction to the period as described by

$$\Delta\tau_\beta = \tau_\beta - \tau_0 \qquad (24)$$

has been presented in Fig. 5 as a function of inclination for three values of $\bar{p} = \bar{a}(1 - e^2)$.

Again the corrections are larger for a circular orbit (e = 0) than for an elliptic orbit $0 < e < 1$, and it decreases with the inverse square of the distance from the center of the moon since it is a gravitational force.

Another important quantity of a lunar orbit is the variation of the orbital radius $r_\mathbb{C}$ with time. The radius in terms of orbital elements is given by Eq (17), and since the semimajor axis a and eccentricity e exhibit no first-order secular changes, $r_\mathbb{C}$ undergoes short-periodic changes since the term cos f in the expression for $r_\mathbb{C}$ undergoes short-periodic changes. If one uses Kork's form (Ref. 19) for the radius, which is equivalent to expressions derivable from Struble (Ref. 12), Kozai (Refs. 4, 20) and Izsak (Ref. 21) for eccentricities of order J_2, then the expression for the instantaneous radius in one satellite revolution can be written.

$$r_\mathbb{C} = \bar{a}\left[1 - e\cos(\beta - \omega) + \frac{1}{4}J_2\left(\frac{R}{\bar{a}}\right)^2 \sin^2 i_0 \cos 2\beta\right], \quad e = O(J_2) \tag{25}$$

The maximum variation in radius about the Keplerian orbit radius $r_{\mathbb{C}\,0} = \bar{a}\left[1 - e\cos(\beta - \omega)\right]$, if Eq (25) is compared with Eq (17), occurs for a polar close lunar satellite orbit ($i_0 = 90°$, $\bar{a} \to R$). In this extreme case the radius variation due to lunar oblateness is given by

$$\Delta r_\mathbb{C} = r_\mathbb{C} - r_{\mathbb{C}\,0} \simeq \pm\frac{1}{4}J_2\,\bar{a} = \pm 0.09 \text{ km} \tag{26}$$

This radius variation decreases as the inclination decreases, $i_0 \gtrless 90°$, and it decreases with semimajor axis $\frac{R}{\bar{a}} < 1$, but altogether it is a very small variation. Similarly the short-periodic variations in e, i are rather small and result in position variations of about the same magnitude.

No explicit expressions exist for the effects of the terms of $\Phi_\mathbb{C}$ containing the equatorial ellipticity coefficient $C_{2,2}$ on lunar satellite orbit parameters. The numerical value of $C_{2,2}$ is one order of magnitude less than the value of J_2, and one can expect the effects of equatorial ellipticity to be less than those of oblateness. Direct effects of $C_{2,2}$ on orbital elements can again be obtained by solving the variation-of-parameter equations using only the terms in $\Phi_\mathbb{C}$ which contain $C_{2,2}$ as a coefficient.

c. Earth perturbations

The next step in determining the motion of a lunar satellite is to compare the perturbing effect of the earth with that of the lunar asphericity, where both effects vary with the altitude above the lunar surface. Lass and Solloway (Ref. 22) obtain an approximation for the earth's potential in the selenographic coordinate system. The acceleration of the lunar satellite due to gravitational attraction of the earth, which is the third term on the RHS of Eq (7), can be written as:

$$\frac{\vec{F}(\vec{r}_{\oplus\Delta}) - \frac{M_\Delta}{M_\mathbb{C}}\vec{F}(\vec{r}_{\oplus\mathbb{C}})}{M_\Delta} = \mu_\oplus\left\{\frac{(x_S - \bar{r}_{\oplus\mathbb{C}})\hat{x}_S + y_S\hat{y}_S + z_S\hat{z}_S}{\left[(x_S - \bar{r}_{\oplus\mathbb{C}})^2 + y_S^2 + z_S^2\right]^{3/2}} + \frac{\hat{x}_S}{\bar{r}_{\oplus\mathbb{C}}^2}\right\} \tag{27}$$

Equation (27) becomes for $\bar{r}_S^2 << \bar{r}_{\oplus\mathbb{C}}^2$, with $\bar{r}_{\oplus\mathbb{C}}$ the fixed distance between the earth and the moon,

$$\frac{\vec{F}(\vec{r}_{\oplus\Delta}) - \frac{M_\Delta}{M_\mathbb{C}}\vec{F}(\vec{r}_{\oplus\mathbb{C}})}{M_\Delta} \simeq \frac{\mu_\oplus}{\bar{r}_{\oplus\mathbb{C}}^3}(2x_S\hat{x}_S - y_S\hat{y}_S - z_S\hat{z}_S) = -\overrightarrow{\text{grad}}\left[\frac{\mu_\oplus}{2\bar{r}^3}(r_S^2 - 3x_S^2)\right] \tag{28}$$

where $\overrightarrow{\text{grad}}$ is the gradient operator $\overrightarrow{\text{grad}} \equiv \frac{\partial}{\partial x_S}\hat{x}_S + \frac{\partial}{\partial y_S}\hat{y}_S + \frac{\partial}{\partial z_S}\hat{z}_S$. The earth's potential for a lunar satellite can thus be approximated by

$$U_\oplus \simeq \frac{\mu_\oplus}{2\bar{r}_{\oplus\mathbb{C}}^3} r_S^2\left[1 - 3\left(\frac{x_S}{r_S}\right)^2\right] \tag{29}$$

The earth's potential $U_\oplus$ can now be compared with the terms in the lunar potential $U_\mathbb{C}$, or more properly, the gradients of the potential, which are the gravitational forces, should be compared.

Numerical values for the ratio of the earth's potential as given by Eq (29), to the J_2 and $C_{2,2}$ terms of the lunar potential, as given by Eq (10), have been obtained. The approximations are only valid for close lunar satellites and crude enough so that no differentiation can be made if the satellite is between the earth and moon or on the opposite side of the moon. The results are presented in the following table where the ratios

$$\frac{J_2}{\text{earth}} = \frac{3\mu_\mathbb{C} R^2 J_2}{r_S^3}\Big/\frac{\mu_\oplus r_S^2}{2\bar{r}_{\oplus\mathbb{C}}^3} = 3\left(\frac{\mu_\mathbb{C}}{\mu_\oplus}\right)\left(\frac{\bar{r}_{\oplus\mathbb{C}}}{R}\right)^3 J_2 \tag{30}$$

and

$$\frac{C_{2,2}}{\text{earth}} = \frac{3\mu_{\mathbb{C}} R^2 C_{2,2}}{r_S^3} \Big/ \frac{\mu_{\oplus} r_S^2}{2\bar{r}_{\oplus\mathbb{C}}^3} = 6\left(\frac{\mu_{\mathbb{C}}}{\mu_{\oplus}}\right)\left(\frac{\bar{r}_{\oplus\mathbb{C}}}{R}\right)^3 C_{2,2} \tag{31}$$

are given as a function of lunar satellite altitude in lunar radii (LR):

h (LR)	$J_{2/\text{earth}}$	$C_{2,2/\text{earth}}$
0	84.7	15.0
1	10.6	1.87
2	3.14	0.55
3	1.32	0.23
4	0.68	0.12

The earth's perturbation equals the lunar $C_{2,2}$ term at an altitude of approximately 2700 km, and it equals the lunar J_2 term at an altitude of approximately 6100 km. For a close lunar satellite, the lunar asphericity terms predominate; these terms can be considered a first approximation to the motion of the lunar satellite.

d. Lunar atmospheric perturbations

The moon has an atmosphere which, at the surface, is estimated to be less than 10^{-12} times the density of the earth's atmosphere at sea level. Since the atmospheric drag forces are proportional to the density times velocity squared (for more data on aerodynamic forces see Subsection B-4b of Chapter IV), a hypothetical ratio of drag forces of a satellite of the earth orbiting at sea level and one of the moon at distance $R_{\mathbb{C}}$ can be found. This ratio is given by

$$\frac{D_{\mathbb{C}\,SL}}{D_{\oplus\,SL}} \simeq \frac{\rho_{\mathbb{C}\,SL} V_{\mathbb{C}\,c}^2}{\rho_{\oplus\,SL} V_{\oplus\,c}^2} \simeq 10^{-12} \frac{(1.7)^2}{(7.9)^2} \simeq 5 \times 10^{-14} \tag{32}$$

where $\rho_{\mathbb{C}\,SL}$ and $\rho_{\oplus\,SL}$ are the sea-level atmospheric densities of the moon and earth, respectively, and $V_{\mathbb{C}\,c}$, $V_{\oplus\,c}$ are the circular satellite velocities at zero altitude. This ratio might change by several orders of magnitude with lunar and earth orbital altitude, but by all accounts atmospheric drag is an utterly negligible force in lunar satellite orbits. Atmospheric drag acting on a circular lunar satellite orbit at an altitude of 10 km is less than the atmospheric drag of an earth satellite in a 1000-km circular orbit. Of course, data on the lunar atmosphere is still subject to conjecture.

e. Solar radiation pressure perturbations

The effect of solar radiation pressure has been discussed in Subsection B-4a of Chapter IV. The magnitude of the force is of the same order as in the case of earth satellites, since the moon and earth are about the same distance from the sun and, for close lunar satellites, shadow time must be considered, since for certain orbital parameters it may be as much as 40% of the total time in orbit.

3. Stability of Lunar Orbits

The final question in establishing orbital parameters for lunar satellites concerns stability of the orbit. The moon exerts a much smaller force on a lunar satellite than does the earth on an earth satellite at a comparable distance. Also, the perturbations on a near-lunar satellite due to the earth are much larger than the perturbations of the moon on near-earth satellites at a comparable distance. Only the effects of asphericity are more pronounced in the case of the earth than the moon, while solar perturbing effects are about the same for near-earth and near-moon satellites. Hence, stability of a lunar satellite is much more of a problem than the stability of an earth satellite. In particular, it is important to determine whether the combined gravitational attractions of the earth and sun (or other forces) can distort a lunar orbit sufficiently to cause the satellite to impact on the lunar surface.

The time period from the initially established orbit until impact has been given the name "lifetime" by some investigators. This term should not be confused with the term "lifetime" as it is applied to earth satellites, where it is the time period from the initially established orbit until atmospheric drag causes the satellite to re-enter the denser portions of the earth's atmosphere.

No investigations into stability have been performed for this chapter, but one note on the stability of lunar satellites has been reviewed. Schechter (Ref. 2) applies a modified version of Pontecoulant's lunar theory (see Ref. 23 for more details on this lunar theory) to the problem of motion of a lunar satellite. Schechter finds the maximum decrease of pericynthion radius Δr_{PL} as a function of $r_{PL} = a(1 - e)$ is given approximately by

$$\frac{\Delta r_{PL}}{r_{PL}} \equiv \frac{(r_{PL})_{min} - r_{PL}}{r_{PL}} \simeq -\frac{15}{8} \text{ em } (1 + e) \tag{33}$$

where $m = \dfrac{2\pi/\tau_0}{\omega_{\mathbb{C}}}$ is the ratio of angular velocity of the satellite in its orbit to the rotational rate of the moon. Schechter takes a conservative lunar orbit (from a perturbation standpoint) of $e = 0.2$, $m = 1/15$ (or a $\simeq$ 14,500 km), and the maximum decrease in pericynthion radius $r_{PL} = a(1 - e) = 11{,}600$ km is $\Delta r_{PL} = -\frac{15}{8}$ em $r_{PL} \cdot (1 + e) = -350$ km, or about 3%. The particular lunar satellite will have an infinite lifetime. However, these perturbations may in time increase the apocynthion radius sufficiently so that the mission requirements are not met.

4. Ground Traces and Longitude Increments

For reconnaissance, surveillance and mapping missions of the lunar surface from a near-moon orbit, the ground trace, or succession of subsatellite points on the lunar surface, and the longitude increments between successive ground traces are important. Both depend on the choice

of orbital parameters, and an orbit may be designed to cover certain regions of the moon and to provide a specific value for the longitude increment. The longitude increment that can be achieved for certain lunar orbits in turn is constrained by mission requirements, sensor limitations such as the field of view, the resolution, the image motion compensation required, and the maintainability of the system in the near-lunar environment.

In the following, only oblateness effects of the moon are considered, with lunar ellipticity and earth effects neglected. Also, since uniform picture quality and a simple image motion compensation system require circular or near-circular orbits for reconnaissance, surveillance and mapping missions, the case of a circular orbit around the moon will be treated separately.

During each revolution, the satellite ground track experiences a longitude increment of $\Delta\lambda_{\mathbb{C}}$ degrees per nodal period to the west, where, under the preceding assumptions:

$$\Delta\lambda_{\mathbb{C}} = -\omega_{\mathbb{C}}\,(\tau_0 + \Delta\tau_\beta) - \frac{d\Omega}{dt}\ \frac{\text{degrees}}{\text{nodal period}}$$

$$= -\omega_{\mathbb{C}}\ 2\pi\left(\frac{r_S^3}{\mu_{\mathbb{C}}}\right)^{1/2}\left[1 - \frac{3}{8}J_2\left(\frac{R}{r_S}\right)^2(7\cos^2 i_0 - 1)\right]$$

$$- 360\cdot\frac{3}{2}J_2\left(\frac{R}{r_S}\right)^2\cos i_0\ \frac{\text{deg}}{\text{nodal period}} \qquad (34)$$

where $R \equiv a$, the longest semiaxis of the moon, r_S is the radius of the circular lunar orbit, the minus signs indicate a shift to the west or negative selenographic longitude, $\lambda_{\mathbb{C}}$, and the nodal period is chosen because it gives the longitude increment at the same point in orbit. The first term on the right-hand side of Eq (34) above is due to the moon's rotation in one nodal period, while the second term is the average regression rate of the ascending node (or any other point on the ground track in this first approximation) due to lunar oblateness, as given by Eq (20), applied to a circular orbit. Since τ_0 is at least 6500 sec (see Fig. 2) and $\Delta\tau_\beta$ is at most 3 sec (see Fig. 5), the oblateness effect on the period is less than 1/2000 of the central force effect, and in view of the other approximations it can be neglected. Hence,

$$\Delta\lambda_{\mathbb{C}} \tilde{=} -\omega_{\mathbb{C}}\ 2\pi\left(\frac{r_S^3}{\mu}\right)^{1/2} - 540\ J_2\left(\frac{R}{r_S}\right)^2\cos i_0\ \frac{\text{deg}}{\text{rev}} \qquad (35)$$

In order to obtain a qualitative idea of the magnitude of these effects for a 100-km circular equatorial orbit around the moon, one can obtain from Figs. 2 and 3 and from Eq (35), with $\omega_{\mathbb{C}} \tilde{=} 1.52504 \times 10^{-4}$ deg/sec:

$$\Delta\lambda_{\mathbb{C}} \tilde{=} -1.079 - 0.102 \text{ deg/rev} = -1.181 \text{ deg/rev} \qquad (36)$$

In this extreme case the second term in Eq (35) (due to nodal regression, -0.102 deg/rev) is about one-tenth of the first term (due to the lunar rotation during one period, -1.079 deg/rev). Lunar oblateness effects on $\Delta\lambda_{\mathbb{C}}$ are very significant, and cannot be ignored. They are as significant as in the case of a satellite orbit around the earth, primarily due to the much slower rotational rate $\omega_{\mathbb{C}}$ of the moon about its axis. This smaller $\omega_{\mathbb{C}}$ counteracts the effects of a smaller oblateness coefficient J_2 for the moon, as well as the weaker central force, as given by the gravitational constant $\mu_{\mathbb{C}}$ of the moon as compared with $\mu_\oplus$.

Consider next a 1000-km circular equatorial orbit around the moon, for which

$$\Delta\lambda_{\mathbb{C}} \tilde{=} -2.059 - 0.047 \text{ deg/rev} = 2.106 \text{ deg/rev}. \qquad (37)$$

For this higher orbit, lunar oblateness accounts for only about one fortieth of the total $\Delta\lambda_{\mathbb{C}}$, showing that the weaker central force, as given by the gravitational constant $\mu_{\mathbb{C}}$ of the moon, increases the period and decreases the oblateness effects, or $\frac{d\Omega}{dt}$, considerably with altitude. Of course, there is a dependence of $\frac{d\Omega}{dt}$ on inclination--i.e., it decreases with increasing inclination and is zero for a polar orbit--while the period, and hence the first term of $\Delta\lambda_{\mathbb{C}}$, remains the same in this approximation.

For elliptic orbits, the term $\left(\frac{r_S^3}{\mu_{\mathbb{C}}}\right)^{1/2}$ in Eqs 34 and 35 should be replaced by $\left(\frac{\bar{a}^3}{\mu_{\mathbb{C}}}\right)^{1/2}$ and the term $\left(\frac{R}{r_S}\right)^2$ by $\left(\frac{R}{p}\right)^2$ in the same equations, where $\bar{a}$ and $p = \bar{a}\,(1 - e^2)$ have been defined in Subsection B-2b.

However, besides the longitudinal increment between revolutions, the location of the subsatellite point at any time during one revolution is of interest. To this end, consider a circular orbit around the moon and secular lunar oblateness effects with the exception of the oblateness effect on the period. The orbit ground trace, or the selenographic latitudes and longitudes of the subsatellite points as a function of time, can be computed in several steps. The satellite ground trace in a selenocentric nonrotating lunar equatorial coordinate system $x_S\ y_S\ z_S$ can be found by spherical trigonometry. The declination δ_S of the subsatellite point is

$$\delta_S = \sin^{-1}(\sin i_0 \sin\beta),\ -90° \le \delta_S \le 90° \qquad (38)$$

where

$\beta = \beta_0 + \frac{d\beta}{dt} dt$, $0° \leq \beta \leq 360°$ is the orbital central angle measured from the ascending node

$\beta_0 = 0$ is the orbital central angle at the time of ascending nodal crossing of the satellite

$\frac{d\beta}{dt} = \frac{360}{\tau_0} \left(\frac{deg}{sec}\right)$ is the constant angular velocity of the satellite in its circular orbit,

dt, $0 \leq dt \leq \tau_0$ is an increment of time, measured from the ascending node to Δ.

The longitude of the subsatellite point relative to the ascending node, $\Delta\lambda_{N\Delta}$ is

$$\Delta\lambda_{N\Delta} = \pm\cos^{-1}\left(\frac{\cos\beta}{\cos\delta_S}\right), \quad 0° \leq |\Delta\lambda_{N\Delta}| \leq 360° \tag{39}$$

where the positive sign applies for direct orbits ($i_0 < 90°$), the negative sign applies for retrograde orbits ($i_0 > 90°$), and $\Delta\lambda_{N\Delta} = 0$ for polar orbits ($i = 90°$). The geometry of the satellite ground trace is illustrated in the following sketch:

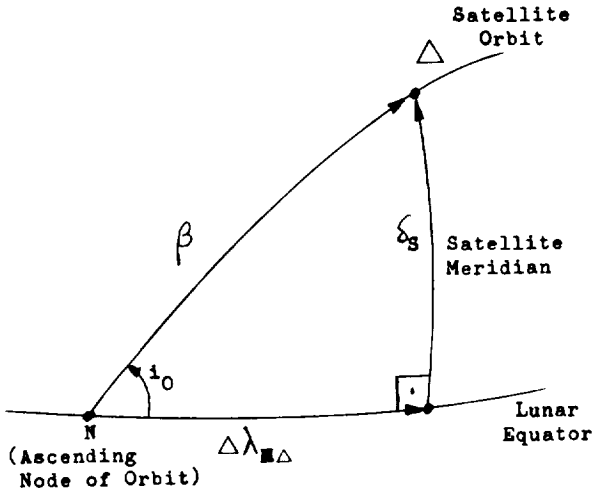

By use of the vector relation,

$$\sin\Delta\lambda_{N\Delta} = \frac{\tan\delta_S}{\tan i_0}$$

and by use of Eq (38), Eq (39) can be written

$$\Delta\lambda_{N\Delta} = \pm\tan^{-1}(\cos i_0 \tan\beta) \tag{40}$$

where + is for direct, - for retrograde and $\Delta\lambda_{N\Delta} = 0$ for polar orbits. In applying Eqs (38) and (40), great care must be taken to use the correct quadrants of the angles β and $\Delta\lambda_{N\Delta}$.

On a rotating moon, the declination of the subsatellite point δ_S becomes the selenographic latitude $\phi_{\mathbb{C}}$ directly, while an increment $\omega_{\mathbb{C}}\, dt$ must be added to $\Delta\lambda_{N\Delta}$ in order to obtain the selenographic longitude $\Delta\lambda_{\mathbb{C}\Delta}$ relative to the ascending node. The major effect of the lunar oblateness (the regression of the nodes) contributes the term

$$+\frac{d\Omega}{dt} dt = -540\, J_2 \left(\frac{R}{r_S}\right)^2 \cos i_0\, dt \tag{41}$$

to the longitude of the subsatellite point.

To summarize, the ground trace equations for circular orbits on a rotating moon, including the nodal regression, become

$$\begin{aligned} \phi_{\mathbb{C}} &= \sin^{-1}(\sin i_0 \sin\beta) \\ \lambda_{\mathbb{C}} &= \lambda_{AN} \pm \tan^{-1}(\cos i_0 \tan\beta) + \omega_{\mathbb{C}}\, dt \\ &\quad - 540\, J_2 \left(\frac{R}{r_S}\right)^2 \cos i_0\, dt \end{aligned} \tag{42}$$

where the positive sign applies for $i_0 < 90°$, the negative sign for $i_0 > 90°$, and $\tan^{-1}(\cos i_0 \tan\beta) = 0$ for $i_0 = 90°$,

$\beta = \beta_0 + \frac{d\beta}{dt} dt$

λ_{AN} is the selenographic longitude of the ascending node.

Equations (42) can be used for elliptic lunar orbits if

(1) β is replaced by

$$\omega + f = \omega_0 + \frac{d\omega}{dt} dt + f_0 + \frac{df}{dt} dt, \tag{43}$$

where $\frac{d\omega}{dt}$ is the apsidal advance given by Eq (21) and the subscript zero denotes conditions at the time of the ascending nodal crossing of the satellite.

(2) $\frac{df}{dt}$ is not constant, but the true anomaly f must be expressed as a function of time through Kepler's equation.

(3) The angle $\omega_{\mathbb{C}}\, dt$ is a function of f, as well as the angle $\frac{d\Omega}{dt} dt$.

(4) The factor $\left(\frac{R}{r_S}\right)^2$ in $\frac{d\Omega}{dt}$ must be replaced by $\left(\frac{R}{p}\right)^2$, where $p = \bar{a}(1 - e^2)$.

C. ENTRY AND DEPARTURE MANEUVERS BETWEEN LUNAR ORBITS AND TRANSFER TRAJECTORIES

The material in Section B described the effects of various forces on lunar orbits once they are

established. In this section, the ΔV requirements to establish lunar orbits from translunar trajectories and to inject into transearth trajectories from lunar orbits will be discussed. These maneuvers may be divided into three categories:

(1) Velocity requirements assuming finite burning times and variable thrust-to-weight ratios of the rocket engine.

(2) Velocity requirements for circumlunar trajectories assuming an impulsive maneuver.

(3) Velocity requirements for one-way trajectories (injection into lunar orbit from a translunar trajectory or injection from a lunar orbit into a transearth trajectory) assuming an impulsive maneuver.

Figure 6 presents the ΔV requirements for entry into a circular lunar orbit at an altitude of 185.2 km from a typical approach trajectory when finite burning times and variable thrust-to-weight ratios are employed. These results were obtained by assuming that the entire maneuver was conducted in the trajectory plane, and that during rocket burning the thrust vector was parallel to the velocity vector at all times. The effect of off-nominal conditions as the entry maneuver was initiated is not included.

Under these assumptions, the required change in velocity can be obtained from the rocket equation:

$$\Delta V = g_{\oplus 0}\, I_{sp} \ln\left(\frac{M_0}{M_e}\right) + \int_0^{t_b} g_\ell \sin\gamma \, dt. \qquad (44)$$

where M_0 is the initial mass and M_e the final mass of the space vehicle, t_b is the burning time, γ the flight path angle, $g_{\oplus 0}$ the earth sea-level value and g_ℓ the local value of the acceleration due to gravity. The first term on the right is an expression of the conservation of linear momentum and depends on the propellant consumed. This term takes into account the thrust-to-weight ratio, $\frac{T}{W_0}$, since the specific impulse I_{sp} is defined as:

$$I_{sp} = \frac{T}{\dot{W}_f} \qquad (45)$$

where $\dot{W}_f$ is the propellant weight flow rate of the rocket engine. The second term takes into account the gravitational effects during rocket burning (change in flight path angle and change in altitude). The increase in vehicle velocity due to the local lunar gravity (the second term in Eq (44)) must be counterbalanced by an increase in total impulse of the vehicle's rocket engines. From Fig. 6 it can be seen that as T/W_0 increases, the velocity requirement reaches a lower limit. It has been found that for practical lunar vehicles, the T/W_0-ratios are large enough so that the differences between finite burning time and a velocity impulse maneuver (infinite thrust-to-weight ratio and infinitesimal burning time) are very small.

A general idea of the impulsive velocity maneuver requirements can be gained from Fig. 7 which presents a summary plot of these ΔV requirements for circumlunar trajectories. The manuever is performed at the pericynthion point of a circumlunar trajectory, and the lunar vehicle enters a circular orbit at the pericynthion altitude. The ΔV required to enter the circular orbit is the difference between the velocity of the vehicle on the trajectory at pericynthion and the circular lunar satellite velocity at the pericynthion altitude. The plot shows ΔV as a function of h_{PL} for a maximum, average, and minimum earth-moon distance $R_{\oplus\ell}$. Requirements for ΔV depend on the translunar trajectory inclination, and a value of $i_{VTL} = 75°$ with respect to the MOP was selected as this represents a limit for lunar missions launched from Cape Canaveral. For a translunar trajectory close to the MOP, e.g., 2°, the values of ΔV of Fig. 7 are reduced by an average of 33 m/sec. A transearth inclination of $i_{VTE} = 60°$ with a direct north earth return was chosen to ensure that the return would always be direct. Since the maximum inclination of the MOP to the earth's equatorial plane is approximately 28.5°, this condition is satisfied.

For a retrograde return, there is an increase in the required ΔV. Data in Fig. 7 is based on circumlunar trajectories which were obtained by use of the Voice technique (see Chapter IV). To obtain a more realistic model of the earth-moon system, computer runs were made utilizing a restricted three-body trajectory program, and the results for a circularizing velocity impulse were compared with those obtained from the Voice program. The following table presents a comparison of the two programs for various trajectory parameters.

ΔV Requirements for Lunar Orbit Entry
(m/sec)

	Voice	Restricted 3-body	$(\Delta V)_{\text{restricted 3-body}} - \Delta V_{\text{(Voice)}}$
$R_{\oplus\ell}$ = 56 ER h_{PL} = 185.2 km i_{VTL} = 75° i_{VTE} = 34.6°	1034.924	1052.876	18.852
$R_{\oplus\ell}$ = 56 ER h_{PL} = 185.2 km i_{VTL} = 75° i_{VTE} = 98.1°	986.842	1004.642	17.800
$R_{\oplus\ell}$ = 56 ER h_{PL} = 185.2 km i_{VTL} = 75° i_{VTE} = -178.9°	954.619	972.098	17.479
$R_{\oplus\ell}$ = 56 ER h_{PL} = 185.2 km i_{VTL} = 2° i_{VTE} = 105.2°	953.947	971.427	17.480
$R_{\oplus\ell}$ = 64 ER h_{PL} = 5000 km i_{VTL} = 60° i_{VTE} = -115.5°	658.946	689.156	30.210

As the table indicates, the velocity impulses for the restricted three-body force model are higher because in the restricted three-body force model, the vehicle is always under the gravitational influence of the moon, while in the Voice model, the vehicle is attracted by the moon only when it is within the lunar volume of influence. Thus, the vehicle velocity relative to the moon at pericynthion will be higher for the former case. A better approximation for ΔV can be obtained if the Jacobi integral calculation (Eq (76), Chapter III) is incorporated in the Voice program. The values of ΔV obtained by this method are higher than those from the integrated program but closer in magnitude than those obtained from the Voice program alone. Also, this method requires only a single additional computation whereas several trajectories must be calculated by numerical integration if the restricted three-body force model is used.

One result of considering finite burning time effects rather than impulsive values of ΔV is that h_{PL} of the translunar trajectory will normally be 2 to 4 km higher than the lunar orbital altitude, h_0. For $\frac{T}{W_0} > 0.2$, the gravity losses for this maneuver are negligibly small.

For the case of one-way trajectories, i.e., translunar-to-lunar orbit or lunar orbit-to-transearth (Chapter IX), the values of the required ΔV vary over a larger range, since one set of constraints (either at the earth or at the moon) is removed. Figures 8 and 9 present the requirements for injection into a circular lunar orbit at an altitude of 185.2 km from a translunar trajectory using an impulsive maneuver. These figures differ from Fig. 7 in that lunar orbits with particular inclinations i_m and descending nodes θ_{MTL} are shown, while in the latter figure, these mission constraints were not indicated. As will be discussed in Chapter IX, this data can be used equally well for injection from a lunar orbit into a transearth trajectory by a slight change of notation.

Figure 8 is for $i_m = 2°$. This low inclination of the orbit results in almost equatorial lunar orbits with a maximum $i_0 = 8.7°$ due to the lunar librations in latitude which amount to 6.7°. In addition, the translunar trajectory inclination i_{VTL} is limited to a range of 30°, and θ_{MTL} varies from 60° to 180°. However, these values shown in Fig. 8 can be extended due to symmetry about the MOP as discussed further in Section A of Chapter IX. The minimum ΔV for orbit entry is $\Delta V = 770$ in./sec, for a transfer time about twice the usual transfer time of 60 hr.

In Fig. 9, $i_m = 15°$, and a wider range in all trajectory parameters is available. The maximum i_0 is 21.7° and i_{VTL} as well as θ_{MTL} is only restricted by the desired flight time and the available ΔV.

Additional plots for higher values of i_m can also be obtained with corresponding increases in the ranges of the lunar orbit and trajectory parameters.

The lunar orbit parameters referred to above (i_m and θ_{MTL}) are not defined directly with respect to selenographic coordinates, but rather with respect to coordinates referred to the MOP and the earth-moon line. Thus, to tie these orbits to ground traces on the lunar surface for a specific lunar mission date, a coordinate transformation must be made to obtain the selenographic latitude and longitude.

Figures 8 and 9 do not take into account the variation in the earth-moon distance or the variation in velocity requirements for lunar orbits higher than 185.2 km. A correction of $\Delta V = \pm 30$ m/sec must be made for distances other than the average earth-moon distance (60 ER). The higher the lunar orbit, the less ΔV is required to enter it. For $h_0 = 5500$ km the saving may be as high as 275 m/sec.

D. LUNAR ORBIT DETERMINATION SCHEMES

After a lunar vehicle (either manned or unmanned) has been placed in a lunar orbit, some means must be provided to determine the accuracy of the actual orbit achieved. This determination is important both for a reconnaissance mission and a lunar landing mission, since in both cases the location of certain lunar landmarks relative to the orbit plane is of the utmost importance. If the actual orbit differs much from the planned one, some corrections must be initiated in order to fulfill the mission objectives.

Lunar orbit determination schemes are similar for the manned and unmanned missions in that they both employ a combination of earth-based tracking facilities, instruments located in the vehicle, and possibly beacons on the lunar surface. However, for manned lunar missions, the primary responsibility for orbit determination will lie with the men in the space vehicle.

For a manned lunar mission, the essential instruments that will be required are the following:

(1) Horizon scanner (utilizing Doppler radar).

(2) Radar altimeter.

(3) Sextant.

(4) Clock.

A local vertical can be established with the horizon scanner, and thus measurements of the vehicle's orientation with respect to it can be made. By the use of the radar altimeter, an altitude-time history of the orbit is obtained. When the vehicle is over the lighted side of the moon, the horizon scanner and the sextant can be used in conjunction for angular readings between a star and a landmark on the moon. A similar measurement can be made between a star and the

local vertical when the vehicle is over the unlighted side of the moon. The period of the lunar orbit can be calculated by measuring the occultation of a star by the moon with the aid of the clock.

Since the orbital elements are not constants but will be continuously changing due to the triaxiality of the moon and the gravitational attractions of the earth and the sun, these readings by themselves will be useless. Therefore, some scheme for combining the individual instrument readings for determining the present and for predicting the future orbit of the space vehicle must be devised. One such method which will be described here is based upon a scheme used for midcourse guidance corrections.

At an arbitrary epoch (e.g., time of injection into lunar orbit), the position and rotational orientation of the earth and moon relative to the stars will be determined precisely. The position and velocity of the vehicle relative to the selenocentric nonrotating coordinate system (x_ζ, y_ζ, z_ζ; $\dot{x}_\zeta$, $\dot{y}_\zeta$, $\dot{z}_\zeta$) are assumed known at this time. Later several instrument readings $\sigma_R(t)$ are taken. Using the assumed initial conditions and the equations of motion for a lunar orbit, the vehicle's position and velocity at the times of the readings are calculated. From these coordinates, it is possible to determine what the readings would have been ($\sigma_c(t)$) under these assumptions. The differences between the actual and calculated readings are then found:

$$\Delta\sigma = \sigma_c(t) - \sigma_R(t) \tag{46}$$

There will be a set of these equations for each of the times that the readings are taken.

This process is then repeated for each set of assumed initial conditions except for a change in each one of them, e.g., $x_\zeta + \Delta x_\zeta$, y_ζ, z_ζ; $\dot{x}_\zeta$, $\dot{y}_\zeta$, $\dot{z}_\zeta$, etc. The differences in the actual and calculated readings are then expressible in terms of changes in coordinates by:

$$\Delta\sigma_i = \frac{\partial\sigma_i}{\partial x_\zeta}\Delta x_\zeta + \frac{\partial\sigma_i}{\partial y_\zeta}\Delta y_\zeta + \frac{\partial\sigma_i}{\partial z_\zeta}\Delta z_\zeta + \frac{\partial\sigma_i}{\partial \dot{x}_\zeta}\Delta\dot{x}_\zeta + \frac{\partial\sigma_i}{\partial \dot{y}_\zeta}\Delta\dot{y}_\zeta + \frac{\partial\sigma_i}{\partial \dot{z}_\zeta}\Delta\dot{z}_\zeta \tag{47}$$

where i denotes the i-th instrument reading. Utilizing a least squares technique which minimizes the differences $\Sigma\,(\Delta\sigma_i)^2$, Eq (47) is solved for Δx_ζ, Δy_ζ, Δz_ζ; $\Delta\dot{x}_\zeta$, $\Delta\dot{y}_\zeta$, and $\Delta\dot{z}_\zeta$. Thus, a set of initial conditions which when used with the equations of motion yield the best results consistent with the actual readings is obtained. These results might be improved by several refinements--using a more detailed set of equations of motion, including statistical and instrument errors in the calculations, and using a more refined smoothing technique which weighs each of the readings differently.

For an unmanned lunar mission, orbit determination will be primarily based on data obtained by DSIF (Chapter VI). This system will be able to obtain the orbital altitude by knowing the precise location and dimensions of the moon. The orbital period will be calculated by adding the time the vehicle spends behind the moon to the time it is observed by the tracking facilities. Automatic equipment which might be included in an unmanned vehicle are a star tracker and a radar altimeter. These will give additional values of the orbital period and altitude.

E. REFERENCES

1. "Orbital Flight Handbook," ER 12684, Martin Company, Space Systems Division (Baltimore), 1963.

2. Schechter, H. B., "Multibody Influence on the Least Altitude of a Lunar Satellite," ARS Journal, Vol. 32, December 1962, p 1921.

3. Jeffreys, H., "The Earth, Its Origin, History, and Physical Constitution," University Press (Cambridge, England), 1952.

4. Kozai, Y., "The Motion of a Close Earth Satellite," The Astronomical Journal, Vol. 64, No. 9, November 1959, p 367.

5. Brouwer, D., "Solution of the Problem of Artificial Satellite Theory Without Drag," The Astronomical Journal, Vol. 64, No. 9, November 1959, p 378.

6. King-Hele, D. G., "The Effect of the Earth's Oblateness on the Orbit of a Near Satellite," Proceedings of the Royal Society, Vol. 247A, No. 4, August 1958, p 49.

7. Vinti, J. P., "New Method of Solution for Unretarded Satellite Orbits," Journal of Research, N.B.S., Vol. 62B, No. 2, October-December, p 105.

8. Blitzer, L., "Effect of Earth's Oblateness on the Period of a Satellite," Jet Propulsion, Vol. 27, No. 4, April 1957, pp 405-406.

9. Jaramillo, T. J., "The Combined Non-Linear Effects of Earth Oblateness and Atmospheric Drag on a Near-Earth Satellite," Wright Air Development Center WADC TR 59-513, AD No. 233184, October 1959.

10. Groves, G. V., "Motion of a Satellite in the Earth's Gravitational Field," Proceedings of the Royal Society, Vol. 254A, No. 1276, January 19, 1960, pp 48-69.

11. Anthony, M. L., and Fosdick, G. E., "Satellite Motions About an Oblate Planet," IAS Paper No. 60-57, IAS, National Summer Meeting, June, 1960, also published in Journal of Aerospace Sciences, Vol. 28, No. 10, October 1961, p 789.

12. Struble, R. A., "The Geometry of the Orbits of Artificial Satellites," Archive for Rational Mechanics and Analysis, Vol. 7, No. 2, 1961, pp 87-104.

13. Martikan, F. and Kalil, F., "A Derivation of Nodal Period of an Earth Satellite and Comparisons of Several First-Order Secular Oblateness Results," unpublished note, also ER 12202, Martin Company (Baltimore), February 28, 1962.

14. Sterne, T. E., "The Gravitational Orbit of a Satellite of an Oblate Planet," The Astronomical Journal, Vol. 63, No. 1255, January 1958, p 28.

15. Sterne, T. E., "Development of Some General Theories of the Orbits of Artificial Earth Satellites," The Astronomical Journal, Vol. 63, No. 1264, November 1958, p 424.

16. Vinti, J. P., "Theory of an Accurate Intermediary Orbit for Satellite Astronomy," Journal of Research, N.B.S., Vol. 65B, No. 3, July-September 1961, p 169.

17. King-Hele, D. G., Walker, D. M. C., "Methods for Predicting the Orbits of Near-Earth Satellites," Journal of the British Interplanetary Society, Vol. 17, No. 1, January-February 1959, pp 2-14.

18. Blitzer, L., Weisfeld, M., Wheelon, A. D., "Perturbations of a Satellite's Orbit Due to the Earth's Oblateness," Journal Applied Physics, Vol. 27, No. 10, October 1956, pp 1141-1149.

19. Kork, J., "First Order Satellite Motion in Near-Circular Orbits About an Oblate Earth: Comparison of Several Results and Optimization for Minimum Altitude Variation," ER 12202, Martin Company (Baltimore), January 1962.

20. Kozai, Y., "Note on the Motion of a Close Earth Satellite with Small Eccentricity," The Astronomical Journal, Vol. 66, No. 3, April 1961, p 132.

21. Izsak, I. G., "On Satellite Orbits with Very Small Eccentricities," The Astronomical Journal, Vol. 66, No. 3, April 1961, p 129.

22. Lass, H. and Solloway, C. B., "Motion of a Satellite of the Moon," ARS Journal, Vol. 31, February 1961, p 220.

23. Brown, E. W., "An Introductory Treatise on the Lunar Theory," Dover Publications (New York), 1960.

ILLUSTRATIONS

LIST OF ILLUSTRATIONS

Figure		Page
1	Keplerian Period and Circular Velocity for Lunar Orbits	VII-19
2	Keplerian Period and Circular Velocity for Near-Lunar Orbits	VII-20
3	Rate of Nodal Regression	VII-21
4	Rate of Apsidal Rotation	VII-22
5	First order Change in Nodal Period	VII-23
6	Entry into Lunar Orbit	VII-24
7	ΔV Required for Injection into Circular Orbit for Circumlunar Trajectories	VII-25
8	Lunar Mission Parameters--$i_m = 2°$	VII-26
9	Lunar Mission Parameters--$i_m = 15°$	VII-27

Fig. 1. Keplerian Period And Circular Velocity For Lunar Orbits

$$V_{\ell c} = \sqrt{\frac{\mu_\ell}{a_0}}$$

$$\tau_0 = 2\pi\sqrt{\frac{a_0^3}{\mu_\ell}}$$

$$a_0 = h_0 + R_\ell$$

$$r_0 = h_0 + R_\ell$$

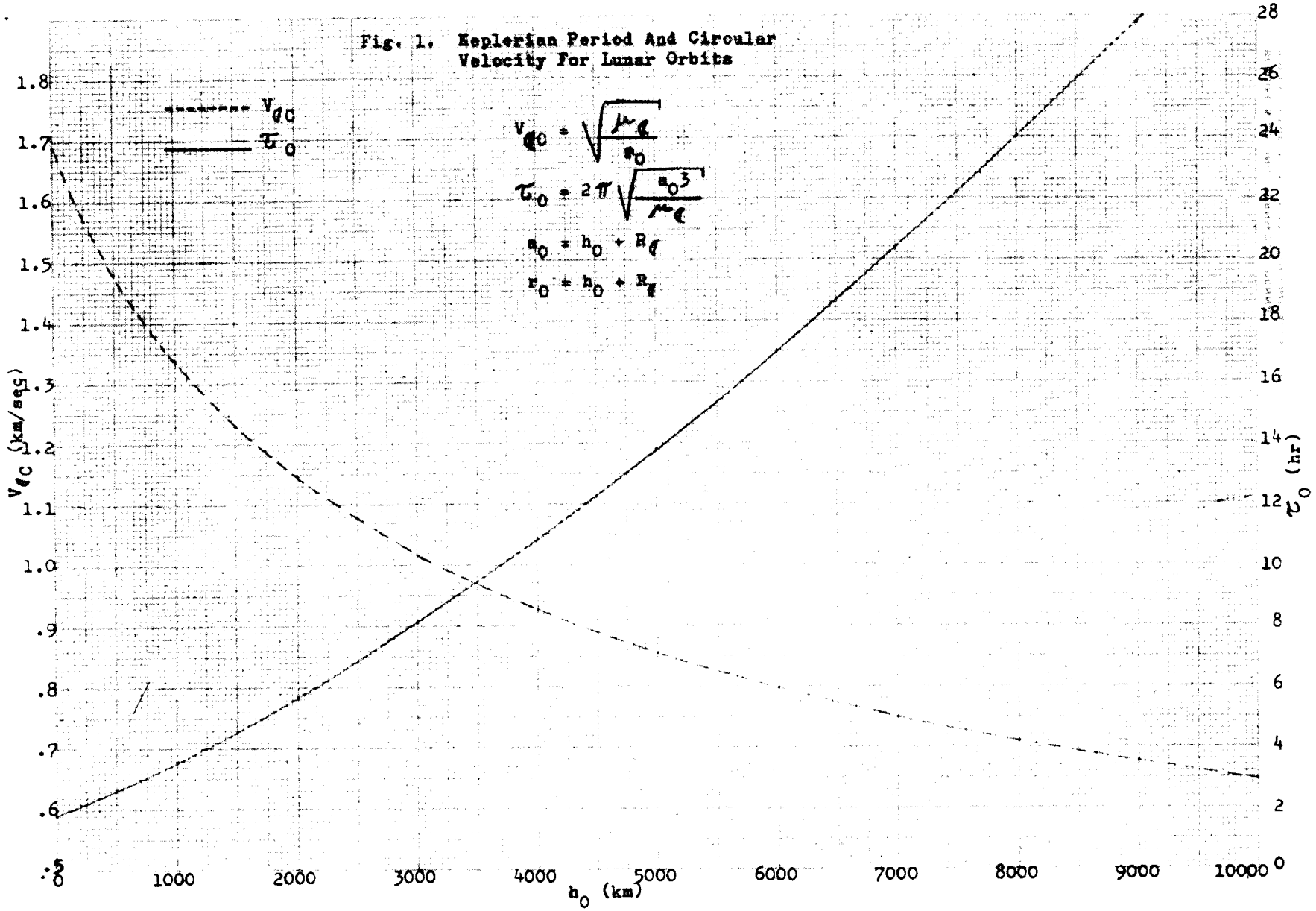

Fig. 2. Keplerian Period And Circular Velocity For Near-Lunar Orbits

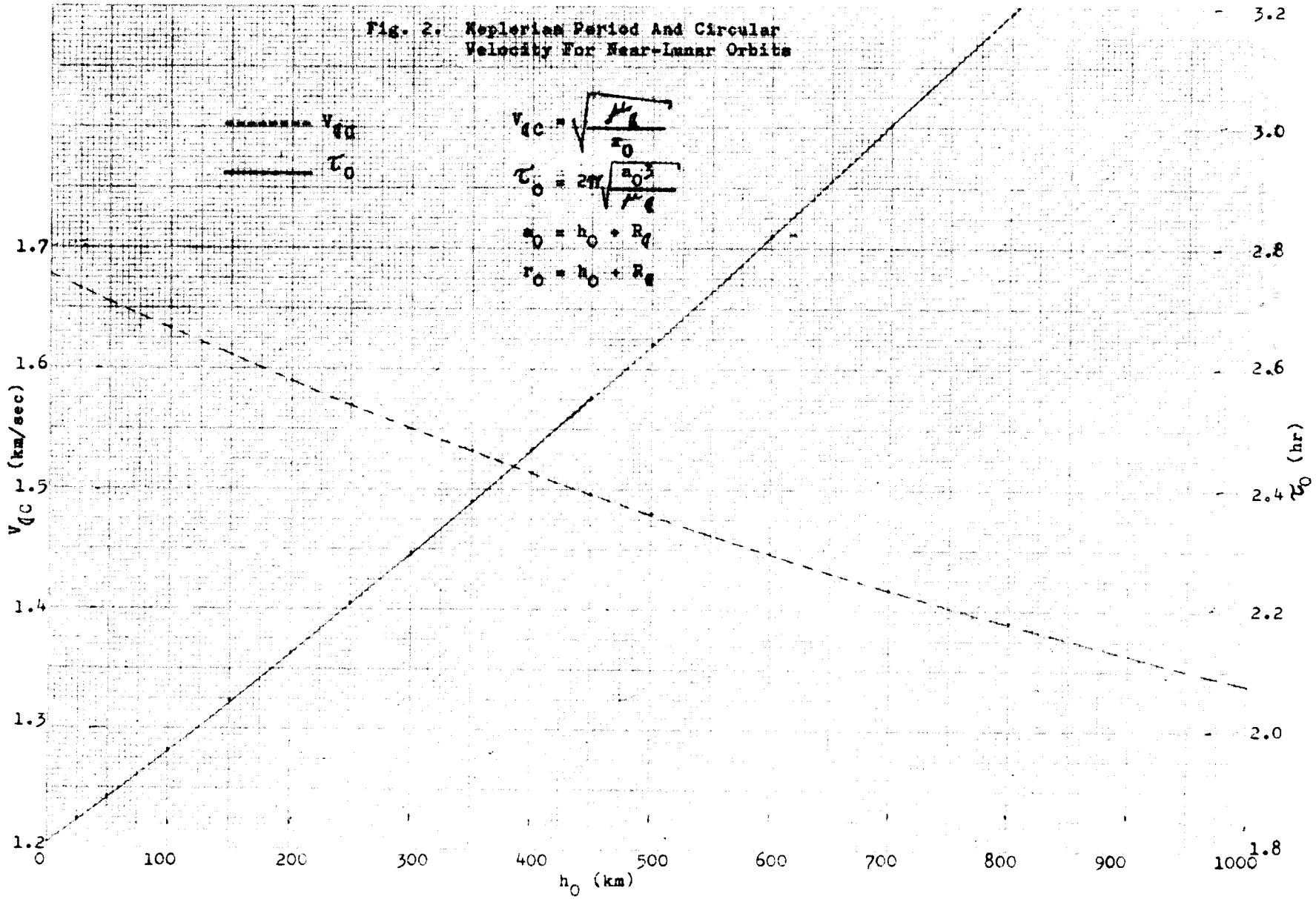

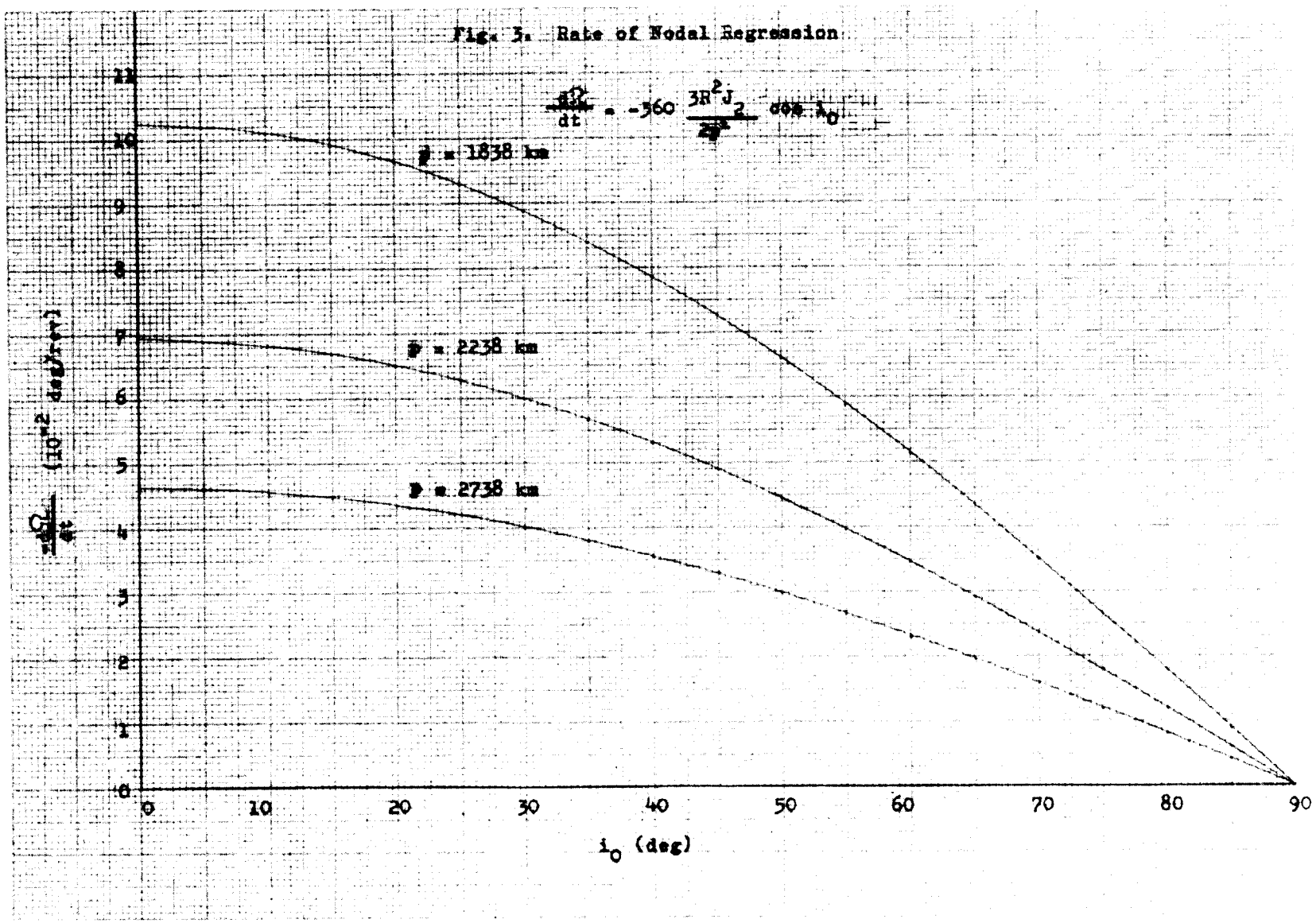
Fig. 3. Rate of Nodal Regression
$\frac{d\Omega}{dt} = -360 \frac{3R^2 J_2}{2p^2} \cos i_o$
p = 1838 km
p = 2238 km
p = 2738 km
$\frac{d\Omega}{dt}$ (10^{-2} deg/rev)
i_o (deg)
0
1
2
3
4
5
6
7
8
9
10
11
0
10
20
30
40
50
60
70
80
90

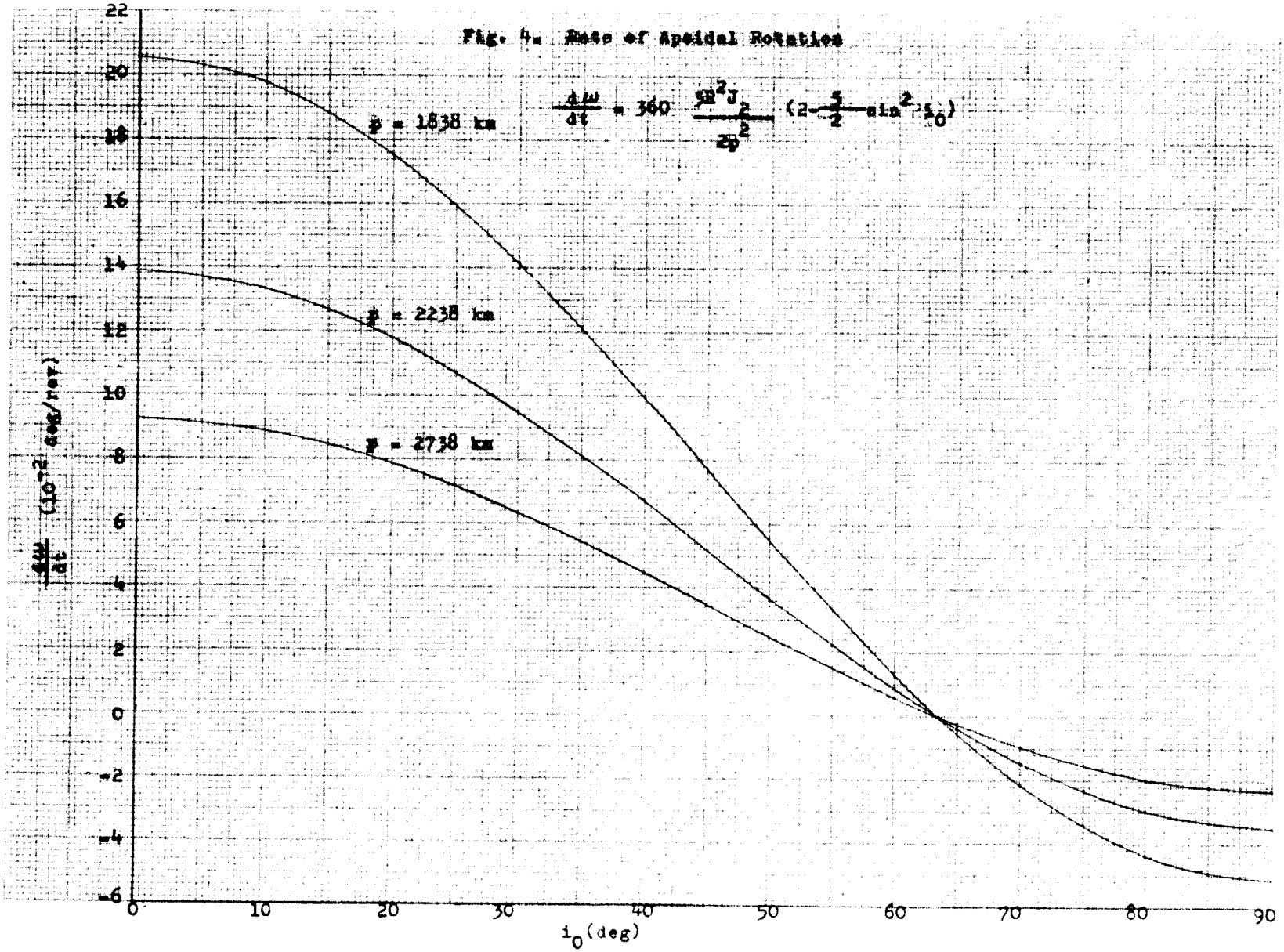
Fig. 4. Rate of Apsidal Rotation
$\frac{d\omega}{dt} = 360\ \frac{3R^2 J_2}{2p^2}\left(2-\frac{5}{2}\sin^2 i_0\right)$
p = 1838 km
p = 2238 km
p = 2738 km
$\frac{d\omega}{dt}$ (10^{-2} deg/day)
i_0 (deg)
22
20
18
16
14
12
10
8
6
4
2
0
-2
-4
-6
0
10
20
30
40
50
60
70
80
90

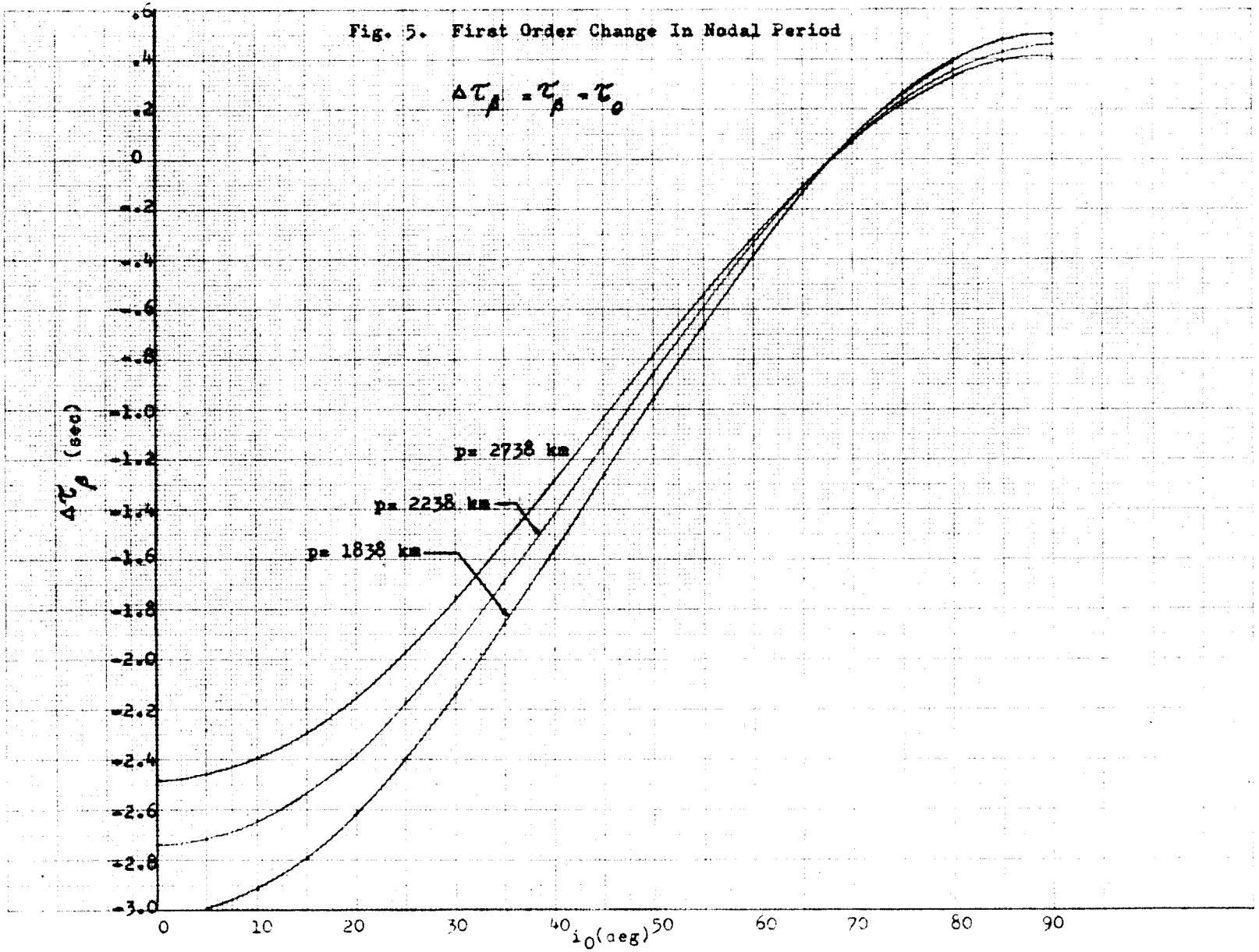
Fig. 5. First Order Change In Nodal Period
$\Delta\tau_p = \tau_p - \tau_o$
p= 2938 km
p= 2238 km
p= 1838 km
$\Delta\tau_p$ (sec)
.6
.4
.2
0
-.2
-.4
-.6
-.8
-1.0
-1.2
-1.4
-1.6
-1.8
-2.0
-2.2
-2.4
-2.6
-2.8
-3.0
0
10
20
30
40
50
60
70
80
90
i_o(deg)

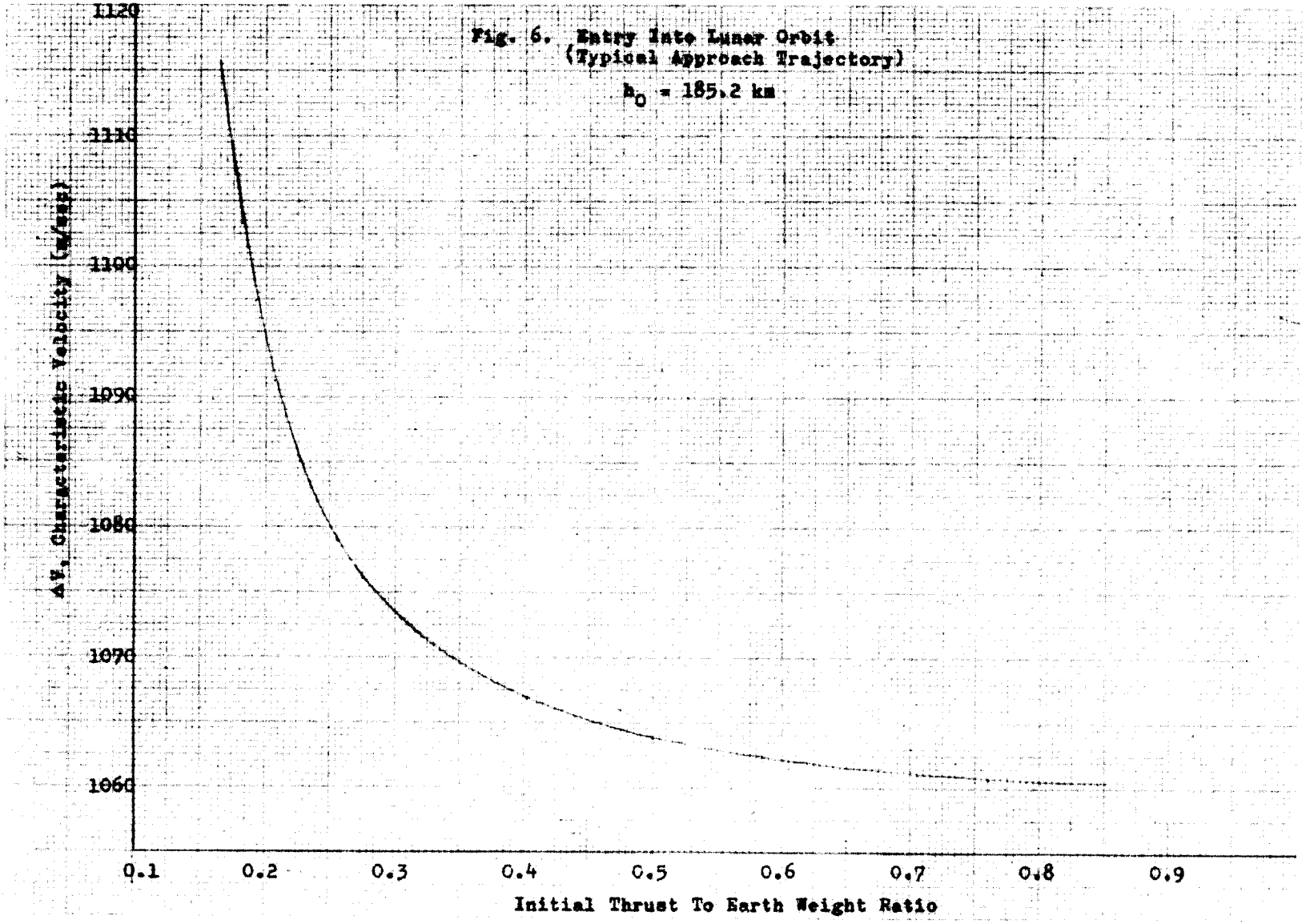
Fig. 6. Entry Into Lunar Orbit
(Typical Approach Trajectory)
h_0 = 185.2 km
Characteristic Velocity, V, (fps)
1120
1110
1100
1090
1080
1070
1060
0.1
0.2
0.3
0.4
0.5
0.6
0.7
0.8
0.9
Initial Thrust To Earth Weight Ratio

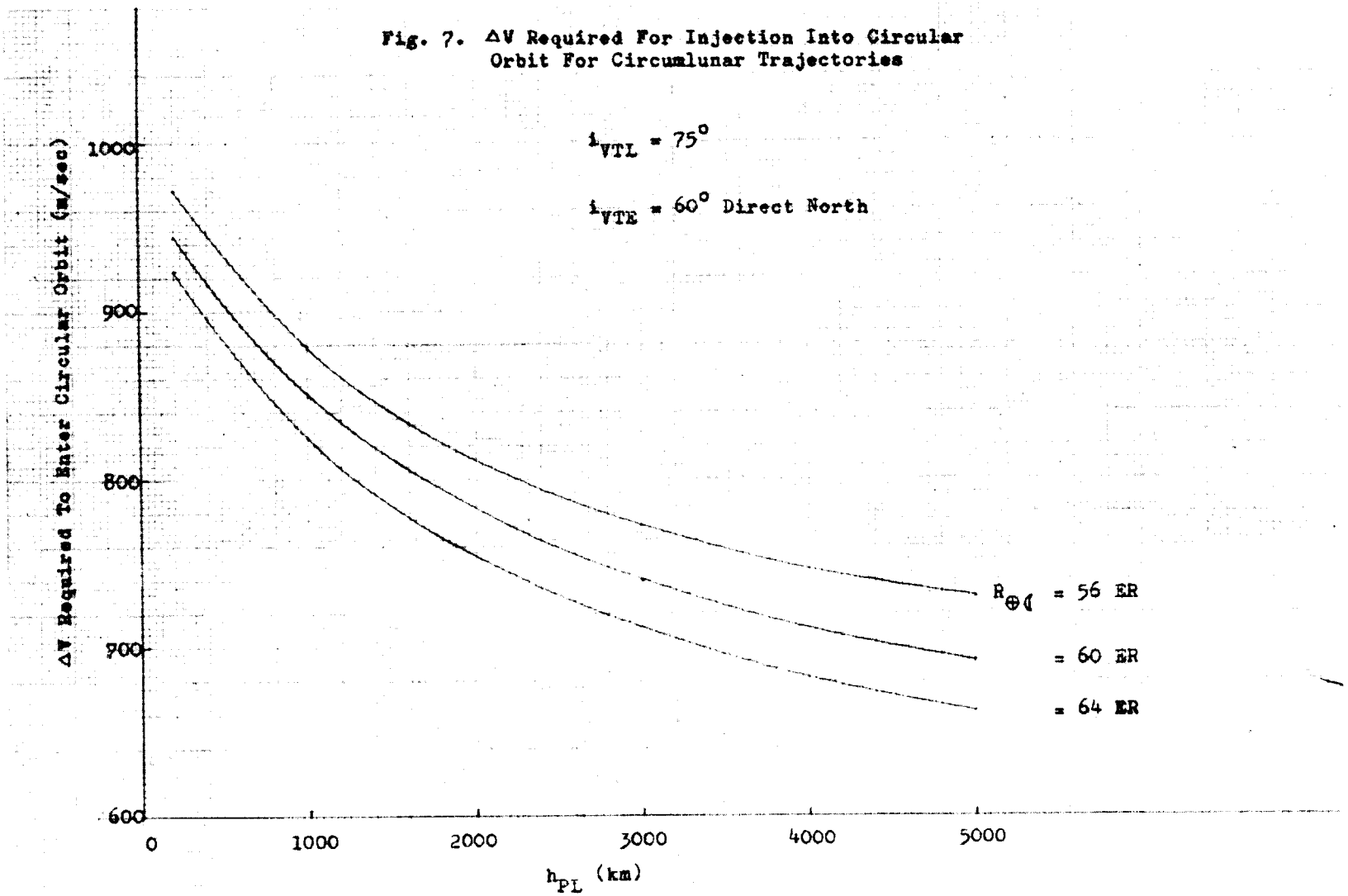
Fig. 7. ΔV Required For Injection Into Circular Orbit For Circumlunar Trajectories
i_{VTL} = 75°
i_{VTE} = 60° Direct North
ΔV Required To Enter Circular Orbit (m/sec)
1000
900
800
700
600
0
1000
2000
3000
4000
5000
h_{PL} (km)
$R_{\oplus C}$ = 56 ER
= 60 ER
= 64 ER

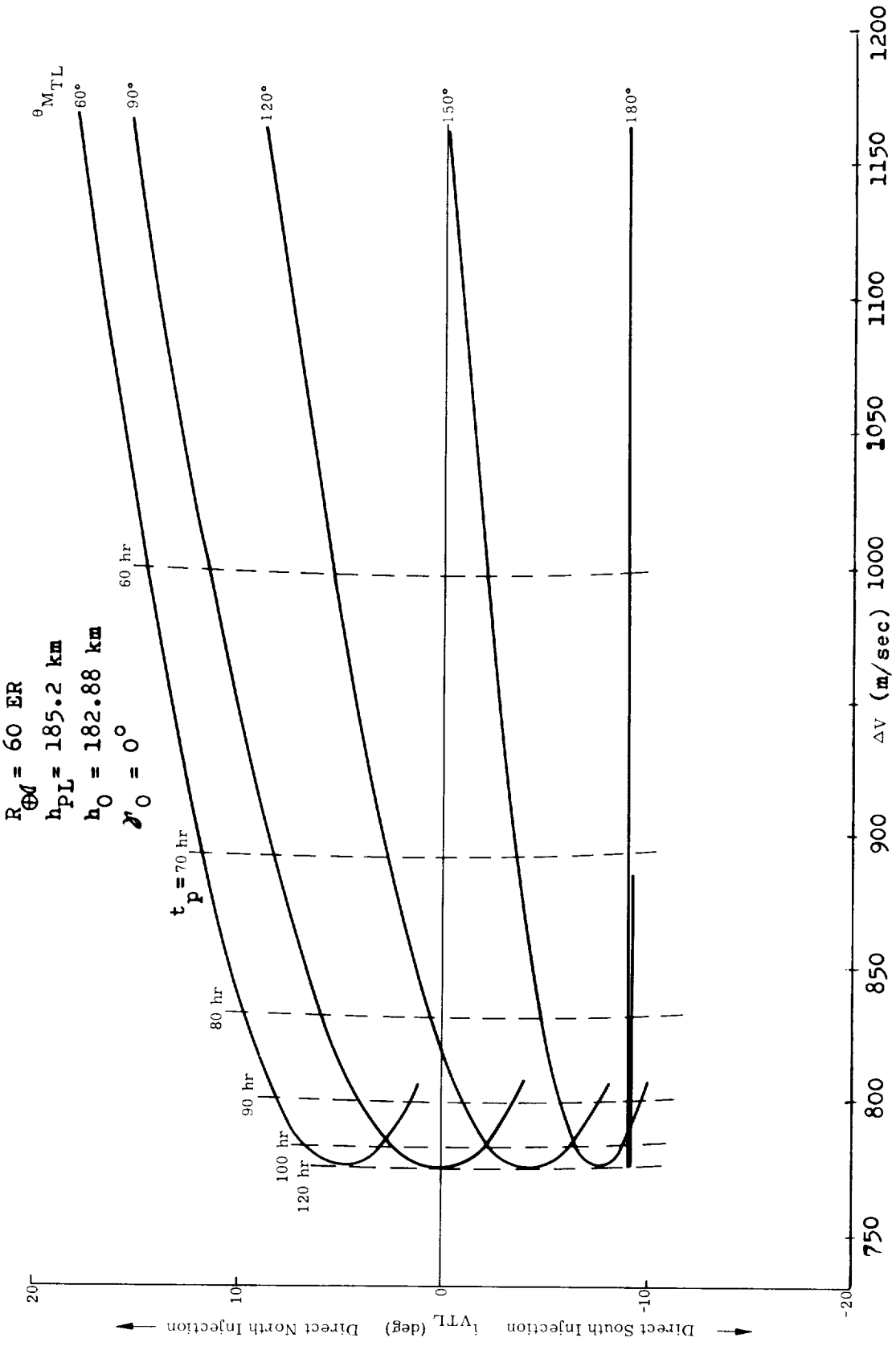

Fig. 8. Lunar Mission Parameters--i_m = 2°
(Approach Trajectories)

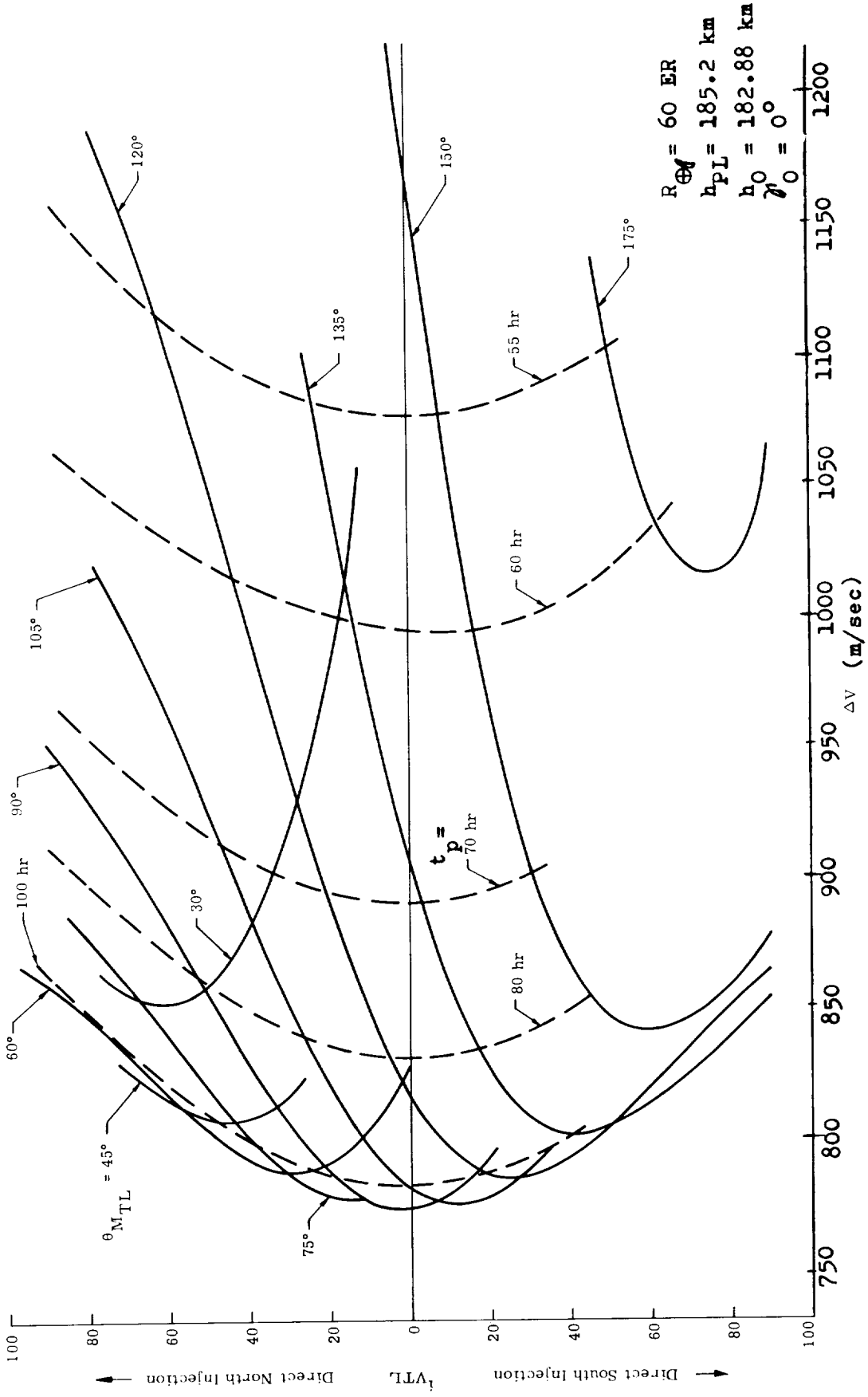

Fig. 9. Lunar Mission Parameters--i_m = 15° (Approach Trajectories)

CHAPTER VIII

DESCENT TO AND ASCENT FROM THE LUNAR SURFACE

Prepared by:

J. D. Kraft, F. Santora, A. Jazwinski, F. Martikan, and R. Salinger
Martin Company (Baltimore)
Aerospace Mechanics Department
March 1963

Page

A. Introduction VIII-1

B. Descent to Lunar Surface VIII-1

C. Ascent from Lunar Surface VIII-18

D. Hovering and Translation Requirements VIII-21

E. Lunar Landing Abort VIII-25

F. References VIII-32

Illustrations VIII-33

List of Illustrations VIII-35

VIII. DESCENT TO AND ASCENT FROM THE LUNAR SURFACE

A. INTRODUCTION

The landing of a space vehicle on the surface of the moon in general involves retro-rocket deceleration to significantly reduce a relative vehicle approach speed which is on the order of 3 km/sec. The degree of reduction required and the techniques for achieving this velocity reduction are different for high-speed hard landings than for soft-landing instrument carriers and manned vehicles. Two main classes of ascent and descent trajectories may be distinguished:

(1) Direct ascent from the lunar surface into a transearth trajectory or direct descent from a translunar trajectory to the lunar surface.

(2) Ascent to a lunar satellite orbit prior to entering a transearth trajectory, which will be referred to as indirect ascent, and descent from a lunar satellite orbit after entering the lunar orbit from a translunar trajectory, which will be referred to as indirect descent.

Although the direct case is straightforward and requires little explanation, various approaches are possible for achieving indirect ascent or descent, and these approaches are worthy of note. In the direct case, of course, the entire space vehicle, which is called landing module (LM), together with any related modules, descends from the translunar trajectory by use of one or more rocket deceleration phases to the lunar surface. On the other hand, in the indirect case, the space vehicle, on nearing the moon, is injected into a lunar satellite orbit. After this orbit is adequately determined, the indirect descent may proceed in either of two ways:

(1) The vehicle separates into two modules, one containing the propulsion system and return spacecraft for the return trip to earth and the other comprising a shuttle. The shuttle vehicle is a minimal vehicle which is capable of being landed on the lunar surface; it can be used as a base for explorations, and it can be launched for a rendezvous with the return space vehicle, which has in the meantime remained in lunar orbit.

(2) The entire orbiting space vehicle, including propulsion systems and fuel supply for the return to earth descends to the preselected point on the lunar surface. The portion of the vehicle which descends to the surface of the moon is known as the landing module (LM).

Both indirect approaches offer the advantages of greater flexibility in landing site selection and a longer period for final orbit determination. The shuttle approach offers the further advantage of smaller fuel requirements, since parts of the LM may be abandoned in lunar orbit, but it requires more complex space vehicle systems due to the rendezvous requirement after ascent.

All data presented in this chapter is based on the assumption of a moon which is the only celestial body affecting the trajectory, which is symmetric in spherical layers and without an atmosphere. Thus all ballistic trajectories are Keplerian orbits. These assumptions are justified, since the short time spent during ascent and descent keeps the secular perturbations, which are neglected by making these assumptions, quite small.

Specific areas considered in each class of lunar ascent and descent trajectory include propulsion system requirements, types of trajectories, abort capabilities, guidance laws and control system requirements. The lunar ascent and descent phase of an impact probe or lunar landing mission can be further classified into such subphases as descent braking, hovering and translation prior to landing, launch from the lunar surface, and rendezvous (if required) with a lunar satellite vehicle. Each phase will be discussed separately. Material related to lunar ascent and descent is given as follows: Injection requirements for moon-to-earth transfer are noted in Chapter IX, trajectory computation for the principal moon-to-earth or earth-to-moon transfers is considered in Chapters IV and VI, and some aspects of deorbit requirements are covered in Chapter VII. Keplerian orbit data is given in Chapter III of Ref. 1 in analytical and graphical form.

B. DESCENT TO LUNAR SURFACE

1. Direct Descent

Impact velocities with which an unretarded landing module (LM) strikes the moon vary from about 2.5 km/sec to 3.2 km/sec for typical earth-to-moon transfers. This terminal velocity (or unretarded impact velocity) is plotted as a function of transfer time in Fig. 1. Since the terminal velocity is equivalent to the velocity impulse required to stop the vehicle just before impact, it represents a lower bound on the velocity decrement required to decelerate and soft-land a vehicle with rocket burning. The actual deceleration or braking of the vehicle requires finite burning time and more fuel. Soft landings are characterized by impact velocities on the order of tens of meters per second. The degree by which the terminal velocity must be reduced by rocket braking depends on the nature of the mission.

a. Terminal velocity requirements

The greatest reduction in terminal velocity is required for manned vehicles. In this case impact should occur at less than about 5 m/sec (without shock absorption) so that the maximum impact deceleration be less than 15 $g_{\oplus o}$. For many instrument carriers, the soft landing requirement may be relaxed to several hundred $g_{\oplus o}$, resulting in a simplification of the landing guidance and control system. These missions may

employ mechanical or fluid shock absorbers or gas-filled balloons to reduce decelerations, but retro-rockets will still be required. Reference 2 estimates that a 200 newton payload, if slowed by retro-rocket to an impact speed of about 100 m/sec, could be landed by a collapsing balloon system with deceleration of 200 $g_{\oplus 0}$. References (3) and (4) consider stresses and penetrations with hard landings. Instrument packages may be mounted on top of high strength penetration spikes to avoid toppling and damage. Figure 2 shows the penetration of a rock surface material by a cylindrical body with a conical nose. The empirical Petry formula has been used to obtain the penetration depths plotted in Fig. 2:

$$P = K \frac{W}{D^2} f(V_i) \qquad (1)$$

where

P = maximum penetration depth

K = a constant varying with material and projectile shape

W = weight of projectile

D = diameter of projectile

$f(V_i)$ = a function of impact velocity

The maximum resistive pressure associated with this penetration is plotted in Fig. 3. This pressure is independent of projectile weight. Both figures employ the compressive strength of the rock as a parameter, thus avoiding a specification of the type of lunar surface. Although opinions still differ as to the nature of the lunar surface, the primary surface material is rather thought to consist of porous rock than a thick dust layer (Ref. 5). At any rate, even for lunar probes, impact speeds should be reduced by retro-rockets to at least 100 m/sec for most payloads.

b. Braking technique

Direct descent braking is, then, a matter of reducing impact velocity from about 3 km/sec to less than 100 m/sec. The braking could be done most economically by applying maximum thrust over a minimum burning time in order to reach zero velocity just at the lunar surface. In the limiting case, the most efficient braking technique would apply, just before impact, an impulse equal in magnitude to the impact velocity. Of course, optimization based on the sole criterion of fuel economy results in a system requiring tolerance to high decelerations and stringent guidance and control system performance. Design of the lunar landing system must be based on a compromise between fuel economy on one hand and low decelerations and a simple guidance system on the other hand.

A braking technique for direct descent which achieves such a compromise might have the following qualitative characteristics: In the initial phase of the approach, which comprises the principal part of the landing trajectory, a high constant-thrust stage is employed to reduce approach velocity significantly. During this phase only very crude guidance will be required. (The midcourse translunar guidance must achieve accuracies of the order of a few m/sec to assure impact, and errors of this order in the early braking phase can be tolerated.) A second phase, in which a variable thrust engine relying on accurate local velocity, altitude, and attitude sensors cancels the remaining velocity, must be initiated at a sufficiently high altitude to provide time to eliminate trajectory errors before touchdown. In manned missions this phase will probably terminate in a period of hovering and translation. Fuel economy of the vernier rocket is improved with increased throttleability, or range of thrust at which the engine can operate. The initial phase of constant-thrust burning could be accomplished in several periods of burning separated by a ballistic trajectory, although some means of attitude control is required at all times. The use of several periods of burning appears to relax certain guidance system requirements, but involves a more complicated propulsion system.

c. Direct descent trajectory analysis

All braking techniques considered for the descent phase must be evaluated in terms of fuel requirements, decelerations, complexity of the guidance scheme and similar parameters which can be obtained from the trajectory of the vehicle. The following sketch shows some typical ballistic lunar impact trajectories (i.e., those with no rocket braking in the vicinity of the moon) in the MOP which were obtained by use of the restricted three-body force model:

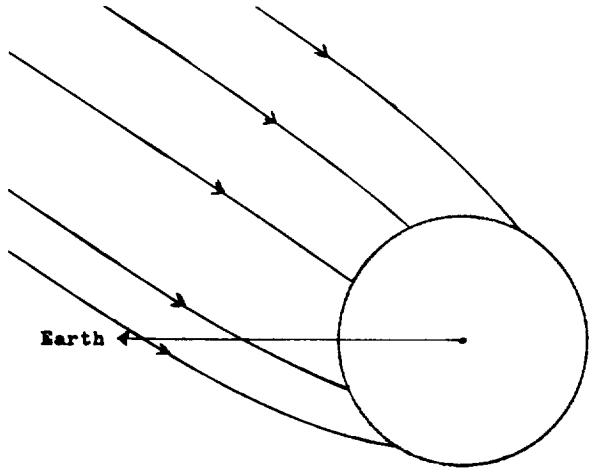

All strike the moon on the ascending arm; they leave earth direct, and the difference in injection velocity near earth between the outer trajectories on the sketch is approximately 25 m/sec.

In analyzing descent trajectories with rocket braking, or trajectories in general, analytic solutions are useful and desirable in that they show trends and provide a check on subsequent, more accurate, numerical solutions. On the other hand, these analytic trajectories may be unrealistic due to the restrictive assumptions that had to be made. The following assumptions underlie the simplest physical model which can

be used for analytical direct descent trajectories:

(1) The descent is vertical to the surface of the moon.

(2) The moon is homogeneous in spherical layers.

(3) The lunar gravitational acceleration is constant during the braking phase.

(4) Drag forces are neglected.

(5) The mass flow rate and exhaust velocity of the braking rocket are constant.

(6) The vehicle is a point mass and its attitude does not influence the trajectory; the attitude is only important in the correct aiming of the rocket engine.

The first assumption is justified for preliminary analysis since some typical direct descent trajectories approach the moon vertically, or nearly vertically, as can be seen from the preceding sketch. In addition, data generated from the vertical trajectory analysis is useful in describing off-vertical trajectories as long as thrust and vehicle velocity are colinear. The second assumption is quite reasonable, as can be seen from the lunar data in Section A of Chapter II, and it allows the treatment of all vertical trajectories as similar, regardless of the landing site location. Actually the first assumption implies the second. Concerning the third assumption, no serious inaccuracies result in the data if average values of gravitational acceleration are taken in each braking phase, especially when the altitude range during one braking phase is small compared to the lunar radius. Assumption (4) is certainly valid since the lunar atmospheric density at the surface is probably less than 10^{-12} of the sea level density of the earth's atmosphere. Assumptions (5) and (6) are the usual ones for a preliminary trajectory analysis. Furthermore, descent trajectories are usually so close to the primary body (in this case the moon) and of such a short duration that the gravitational attraction of other celestial bodies may be neglected.

With the foregoing assumptions, the equation of motion for vertical descent to the lunar surface with rocket burning becomes:

$$M \frac{d^2h}{dt^2} = - V_{ex} \frac{dM}{dt} - M\bar{g}_{\mathbb{C}} \qquad (2)$$

where

M = mass of the vehicle, $M = M_0 - \dot{M}t$, M is a positive constant, M_0 the initial mass.

h = altitude of the vehicle above the lunar surface

t = time

V_{ex} = effective exhaust velocity of retro-rocket (assumed constant)

$\bar{g}_{\mathbb{C}}$ = average gravitational acceleration during braking

Successive integration of Eq (1) and evaluation of the boundary conditions,

$$t = 0: h = h_0, V = V_0$$

$$t = t_b: h = h_1, V = V_1$$

gives equations for the velocity and altitude after any given braking phase, which can be expressed in the form:

$$V_1 = V_0 + V_{ex} \left[\ln (1 - \zeta) + \frac{\bar{g}_{\mathbb{C}}}{g_{\oplus 0}} \frac{\zeta}{\left(\frac{T}{W_0}\right)} \right] \qquad (3)$$

$$h_1 = h_0 + \frac{V_{ex}^2}{g_{\oplus 0}} \frac{1}{\left(\frac{T}{W_0}\right)} \left\{ (1 - \zeta) \ln (1 - \zeta) + \zeta \left[1 - \frac{V_0}{V_{ex}} - \frac{\zeta \frac{\bar{g}_{\mathbb{C}}}{g_{\oplus 0}}}{2 \left(\frac{T}{W_0}\right)} \right] \right\} \qquad (4)$$

where

V_0 = vehicle speed (positive downward) at retro-rocket ignition

h_0 = altitude above the lunar surface at retro-rocket ignition

V_{ex} = effective exhaust velocity of the retro-rocket (assumed constant)

ζ = mass ratio of retro-rocket

$$\left(\zeta = \frac{W_f}{W_0} = \frac{\dot{M}}{M_0} t_1 \right)$$

$\frac{T}{W_0}$ = initial thrust-to-weight ratio using sea level weight at earth

W_0 = earth sea level weight

$g_{\oplus 0}$ = acceleration of gravity at the surface of the earth

$\bar{g}_{\mathbb{C}}$ = average acceleration of lunar gravity over the altitude range during braking

Less accurately, the value of gravity at the lunar surface, $g_{\mathbb{C}0}$ will be used instead of $\bar{g}_{\mathbb{C}}$ in subsequent calculations and figures on vertical descent. For the case of one burning phase leading to a soft landing with zero relative velocity to the surface the end conditions are

$$t = t_b: h = h_1 = 0, V = V_1 = 0$$

and, for this special case, Eqs (3) and (4) reduce respectively to:

$$\frac{V_0}{V_{ex}} = -\left[\ln (1 - \zeta) + \frac{g_{\oplus 0}}{g_{\oplus 0}} \frac{\zeta}{\frac{T}{W_0}} \right] \quad (5)$$

$$\frac{h_0 g_{\oplus 0}}{V_{ex}^2} = - \frac{1}{\left(\frac{T}{W_0}\right)} \left[\zeta + \ln (1 - \zeta) + \frac{1}{2} \frac{g_{\oplus 0}}{g_{\oplus 0}} \frac{\zeta^2}{\left(\frac{T}{W_0}\right)} \right] \quad (6)$$

The nondimensional velocity parameter $\frac{V_0}{V_{ex}}$, and the nondimensional altitude parameter, $\frac{h_0 g_{\oplus 0}}{V_{ex}^2}$, are plotted in Figs. 4 and 5 as functions of mass ratio ζ and initial thrust-to-weight ratio $\frac{T}{W_0}$. If Eq (5) is solved for thrust-to-weight ratio, and the result substituted in Eq (6), the nondimensional altitude parameter is related to mass ratio and nondimensional velocity parameter as follows:

$$\frac{g_{\oplus 0} h_0}{V_{ex}^2} = \left[\frac{V_0}{V_{ex}} + \ln (1 - \zeta) \right] \left[1 - \frac{1}{2} \frac{V_0}{V_{ex}} + \left(\frac{1}{\zeta} - \frac{1}{2} \right) \ln (1 - \zeta) \right] \quad (7)$$

Since

$$t_b = \frac{\zeta V_{ex}}{g_{\oplus 0} \frac{T}{W_0}}$$

Equation (5) can be used to relate burning time to mass ratio and velocity at retro-rocket ignition and define a nondimensional burning time parameter $\frac{g_{\oplus 0} t_b}{V_{ex}}$ by the equation:

$$\frac{g_{\oplus 0} t_b}{V_{ex}} = - \left[\frac{V_0}{V_{ex}} + \ln (1 - \zeta) \right] \quad (8)$$

Equation (7) is plotted in Fig. 6, and Eq (8) is plotted in Fig. 7.

Error relationships for vertical descent may be evolved by taking differentials of Eq (3) and (4), where $\bar{g}_{\oplus}$ has been replaced by $g_{\oplus 0}$. The results are as follows:

$$dV_1 = dV_0 + \left[\ln (1 - \zeta) + \frac{g_{\oplus 0}}{g_{\oplus 0}} \frac{\zeta}{\left(\frac{T}{W_0}\right)} \right] dV_{ex} + V_{ex} \left[- \frac{1}{1 - \zeta} + \frac{g_{\oplus 0}}{g_{\oplus 0}} \frac{1}{\left(\frac{T}{W_0}\right)} \right] d\zeta$$

continued

$$- V_{ex} \frac{g_{\oplus 0}}{g_{\oplus 0}} \frac{\zeta}{\left(\frac{T}{W_0}\right)^2} d \left(\frac{T}{W_0}\right) \quad (9)$$

$$dh_1 = dh_0 + \left[\frac{2 (h_1 - h_0)}{V_{ex}} + \frac{V_0}{V_{ex}} t_b \right] dV_{ex} + \frac{1}{\left(\frac{T}{W_0}\right)} (h_0 - h_1 + t_b^2 \frac{g_{\oplus 0}}{2}) d \left(\frac{T}{W_0}\right) + \frac{V_1 V_{ex}}{g_{\oplus 0} \left(\frac{T}{W_0}\right)} d\zeta - t_b \, dV_0 \quad (10)$$

where $t_b = \frac{V_{ex} \zeta}{g_{\oplus 0} \left(\frac{T}{W_0}\right)}$

For the case of a single rocket braking period to a soft landing with zero velocity, nominal values are $V_1 = 0$ and $h_1 = 0$. Then

$$dV_1 = dV_0 - \frac{V_0}{V_{ex}} dV_{ex} + V_{ex} \left[- \frac{1}{1 - \zeta} + \frac{g_{\oplus 0}}{g_{\oplus 0}} \frac{1}{\left(\frac{T}{W_0}\right)} \right] d\zeta - V_{ex} \frac{g_{\oplus 0}}{g_{\oplus 0}} \frac{\zeta}{\left(\frac{T}{W_0}\right)^2} d \left(\frac{T}{W_0}\right) \quad (11)$$

$$dh_1 = dh_0 + \left(- \frac{2 h_0}{V_{ex}} + \frac{V_0}{V_{ex}} t_b \right) dV_{ex} + \frac{1}{\left(\frac{T}{W_0}\right)} (h_0 + t_b^2 \frac{g_{\oplus 0}}{2}) d \left(\frac{T}{W_0}\right) - t_b \, dV_0, \quad \left[V_1 = 0, \; h_1 = 0 \right] \quad (12)$$

De Fries (Ref. 6) derives results corresponding to Eq (11) for the case of n thrust on-off periods, i.e., n periods of constant thrust followed by periods of ballistic flight. The assumptions are the same as in the single-stage case. The value of the acceleration due to lunar gravity for the j-th powered phase is the constant value $g_{\oplus j}$ at the time of rocket cutoff, while it is assumed variable during the ballistic flight phases. The error due to this assumption can be accounted for by including lunar gravity as an independent error source in the analysis. The results are reproduced here for convenience, and the notation is illustrated in the following sketch.

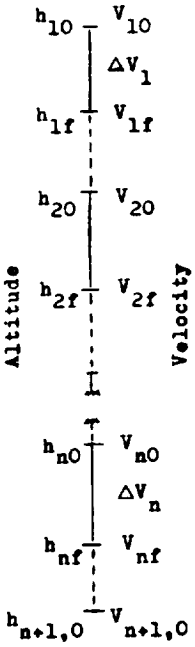

h_{j0} = initial altitude of the j-th powered phase

h_{jf} = final altitude of the j-th powered phase

$V_{j+1,0}$ = initial velocity of the $(j+1)^{th}$ powered phase

V_{jf} = final velocity of the j-th powered phase

$\Delta V_j = -V_{ex} \ln\left(1 - \frac{\zeta}{t_b} t\right)$ equivalent velocity increment of the j-th powered phase

The error analysis is made by using a Taylor series expansion of the touchdown velocity (the velocity at the end of the n-th coasting period. which may be regarded as the initial velocity of a fictitious $(n+1)^{th}$ powered phase and is denoted by $V_{n+1,0}$) involving only first-order terms.

$$V_{n+1,0}(h_{j0} + \Delta h_{j0},\ \Delta V_j + \Delta(\Delta V_j),\ T_j + \Delta T_j,\ g_{(j} + \Delta g_{(j},\ V_{10} + \Delta V_{10})$$

$$= V_{n+1,0}(h_{j0},\ V_j,\ T_j,\ g_{(j},\ V_{10}) + \sum_{j=1}^{n} \frac{\partial V_{n+1,0}}{\partial h_{j0}} \Delta h_{j0} + \sum_{j=1}^{n} \frac{\partial V_{n+1,0}}{\partial(\Delta V_j)} \Delta(\Delta V_j) + \sum_{j=1}^{n} \frac{\partial V_{n+1,0}}{\partial T_j} \Delta T_j + \sum_{j=1}^{n} \frac{\partial V_{n+1,0}}{\partial g_{(j}} \Delta g_{(j} + \frac{\partial V_{n+1}}{\partial V_{10}} \Delta V_{10} \qquad (13)$$

where the partial derivatives are given as follows:

$$\frac{\partial V_{n+1,0}}{\partial h_{j0}} = \frac{\partial V_{j+1,0}}{\partial h_{j0}} \frac{1}{V_{n+1,0}} \left(1 - \frac{\Delta V_n}{V_{n0}}\right) \psi \qquad (j \neq n)$$

$$\frac{\partial V_{n+1,0}}{\partial \Delta V_j} = \frac{\partial V_{j+1,0}}{\partial \Delta V_j} \frac{1}{V_{n+1,0}} \left(1 - \frac{\Delta V_n}{V_{n0}}\right) \psi \qquad (j \neq n)$$

$$\frac{\partial V_{n+1,0}}{\partial T_j} = \frac{\partial V_{j+1,0}}{\partial T_j} \frac{1}{V_{n+1,0}} \left(1 - \frac{\Delta V_n}{V_{n0}}\right) \psi \qquad (j \neq n)$$

$$\frac{\partial V_{n+1,0}}{\partial g_{(j}} = \frac{\partial V_{j+1,0}}{\partial g_{(j}} \frac{1}{V_{n+1,0}} \left(1 - \frac{\Delta V_n}{V_{n0}}\right) \psi \qquad (j \neq n)$$

$$\frac{\partial V_{n+1,0}}{\partial V_{10}} = \frac{\partial V_{20}}{\partial V_{10}} \frac{1}{V_{n+1,0}} \left(1 - \frac{\Delta V_n}{V_{n0}}\right) \psi \qquad (j \neq n) \quad (14)$$

$$\frac{\partial V_{n+1,0}}{\partial h_{n0}} = \frac{g_{(n}}{V_{n+1,0}} \qquad (j = n)$$

$$\frac{\partial V_{n+1,0}}{\partial \Delta V_n} = \frac{-V_{nf}}{V_{n+1,0}} \qquad (j = n)$$

$$\frac{\partial V_{n+1,0}}{\partial T_n} = \frac{1}{T_n} \frac{g_{(n} M_{on} V_{ex}^2}{T_n V_{n+1}} \left[\frac{\Delta V_n}{V_{ex}} - 1 + e^{-\frac{\Delta V_n}{V_{ex}}}\right] \qquad (j = n)$$

$$\frac{\partial V_{n+1,0}}{\partial g_{(n}} = -\frac{1}{2 g_{(n} V_{n+1,0}} \left[(V_n - \Delta V_n)^2 - V_{nf}^2\right] \qquad (j = n)$$

$$\frac{\partial V_{20}}{\partial V_{10}} = \frac{V_{10} - \Delta V_1}{V_{20}} \qquad (j = n)$$

where

$$\psi = \begin{cases} V_{j+1,0} & (n - j - 1 = 0) \\ V_{j+1,0} \prod \left(1 - \frac{\Delta V_{j+m}}{V_{j+m}}\right) & m = 1, 2, \ldots, (n - j - 1) \end{cases}$$

+ continued

$\prod$ denotes the product over m

M_{on} is the initial mass of the space vehicle at the n-th powered phase

The derivatives can be evaluated from Eqs (3) and (4), which are the solutions to the vertical descent equation of motion, with the subscript j denoting the j-th phase of rocket burning.

$$V_{jf} = V_{j,0} + g_{\ell j} \frac{M_{0j} V_{ex}}{T_j} \left(1 - e^{-\frac{\Delta V_j}{V_{ex}}}\right) - \Delta V_j$$

$$h_{jf} = h_{j0} - V_{j,0} \frac{M_{0j} V_{ex}}{T_j} \left(1 - e^{-\frac{\Delta V_j}{V_{ex}}}\right) - \frac{g_{\ell j}}{2} \frac{M_{0j}^2 V_{ex}^2}{T_j^2} \left(1 - e^{-\frac{\Delta V_j}{V_{ex}}}\right)^2 + \frac{M_{0j} V_{ex}^2}{T_j} \left[\left(1 - e^{-\frac{\Delta V_j}{V_{ex}}}\right) - \frac{\Delta V_j}{V_{ex}} e^{-\frac{\Delta V_j}{V_{ex}}}\right]$$

$$V_{j+1,0} = 2\mu_{\ell} \left[\frac{1}{h_{j0}} - \frac{1}{h_{jf}}\right] + V_{jf}^2 \qquad (15)$$

where M_{0j} is the initial mass of the vehicle at the j-th burning phase.

A complication is introduced when the assumption of vertical descent is dropped since the analytic solutions for descent trajectories comprised by Eqs (3) and (4), or (5) and (6), apply only for vertical descent. The accurate solution for nonvertical trajectories involves a numerical approach, since the equations of motion are not integrable in closed form. However, the vertical descent solutions are useful, rather than good, approximations for description of nonvertical trajectories when altitude and velocity in the vertical case are interpreted as range and range rate. Accuracy of the approximation is increased if the thrust and vehicle velocity vectors are colinear during the braking phases of descent, so that the trajectory is almost a straight line until the very final, low-velocity phase, when the trajectory curves over to the local vertical on the moon. The sketch on page VIII-2 shows that ballistic trajectories approach the moon almost on a straight line, since the maximum curvature of the hyperbolic selenocentric approach trajectory is near pericynthion, which is below the lunar surface for impact trajectories.

The next step in the calculation of descent trajectories would be the numerical solution of a general two-dimensional descent trajectory. The physical model implies that any phases of rocket burning take place in a trajectory plane which at the same time contains the center of the moon; its trace on the lunar surface is a great circle, and this model is compatible with the spherical moon assumption. The standard inverse-square variation of g_{ℓ} with vehicle distance from the center of the moon is assumed in two-dimensional trajectories, thus retaining only assumptions (2), (4), (5) and (6) of the ones listed on pages VIII-2 and -3 for the physical model underlying two-dimensional descent trajectory calculations.

Consider two coordinate systems in the trajectory plane. One is a selenocentric system which is regarded as inertial and has its origin at the center of the moon, the y_t axis directed toward the northernmost point of the trajectory plane and the x_t axis toward the ascending node in the lunar equatorial plane. The second coordinate system is a local one similar to the topocentric system, but with origin at the instantaneous subvehicle point and the y_{ℓ}-axis directed toward the vehicle. Both coordinate systems, the unit vectors $\hat{\sigma}$, $\hat{\tau}$, and the forces acting on the vehicle are illustrated in the following sketch (positive values for all quantities are shown):

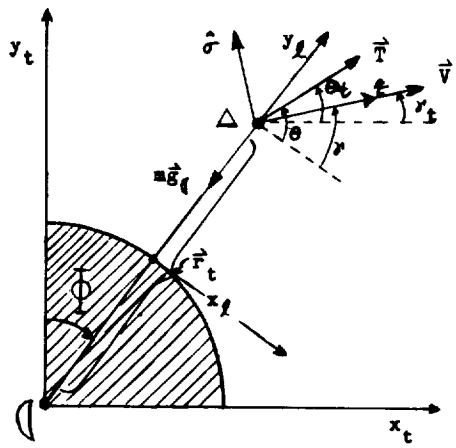

In inertial coordinates, the vector equation of motion is

$$M\ddot{\vec{r}}_t = \vec{T} + M\vec{g}_{\ell} , \qquad (16)$$

where

$M = M_0 - \frac{T}{V_{ex}} t_b$ = instantaneous vehicle mass

M_0 = constant vehicle initial mass (prior to rocket burning)

$\vec{T}$ = rocket thrust

V_{ex} = effective exhaust velocity

t_b = time of rocket burning

$\vec{r}_t$ = vehicle radius vector

The digital computer usually integrates the scalar equations of motion, which will be obtained next. The components of the forces tangential and normal to the flight path (which is along the unit vector $\hat{\tau} \equiv \frac{\vec{V}}{V}$), can be obtained from the preceding sketch.

$$F_\tau = T \cos(\theta - \gamma) - Mg_\ell \sin\gamma$$
$$F_\sigma = T \sin(\theta - \gamma) - Mg_\ell \cos\gamma \qquad (17)$$

where

θ = thrust attitude angle (the angle between local horizontal or x_ℓ-axis and the thrust direction)

γ = flight path angle (the angle between the local horizontal or x_ℓ-axis and the velocity vector).

If these force components are further resolved into the x_t and y_t directions, one can write the scalar equations of motion

$$\ddot{x}_t = \cos\gamma_t \left[\frac{T}{M}\cos(\theta - \gamma) - g_\ell \sin\gamma\right] - \sin\gamma_t \left[\frac{T}{M}\sin(\theta - \gamma) - g_\ell \cos\gamma\right] \qquad (18)$$

$$\ddot{y}_t = \sin\gamma_t \left[\frac{T}{M}\cos(\theta - \gamma) - g_\ell \sin\gamma\right] + \cos\gamma_t \left[\frac{T}{M}\sin(\theta - \gamma) - g_\ell \cos\gamma\right] \qquad (19)$$

where

γ_t = inertial flight path angle (for angle between the x_t - axis and the velocity vector)

$= \gamma - \Phi$

These differential equations are integrated to solve for $\dot{x}_t$ and $\dot{y}_t$, which in turn are integrated to solve for x_t and y_t. The following auxiliary definitions are of interest and they are usually computed for each trajectory printout interval.

$V = \sqrt{\dot{x}_t^2 + \dot{y}_t^2}$, the selenocentric (inertial) velocity of the vehicle

$r = \sqrt{x_t^2 + y_t^2}$, the distance of the vehicle from the center of the moon

$y_\ell \equiv h = r - R_\ell$, where R_ℓ is the radius of the spherical moon

$$\Phi = \tan^{-1}\left(\frac{x_t}{y_t}\right)$$

$$\gamma_t = \tan^{-1}\left(\frac{y_t}{x_t}\right)$$

$$\gamma = \sin^{-1}\left(\frac{y_t\dot{y}_t + x_t\dot{x}_t}{rV}\right)$$

In some cases it is convenient to write the component equations of motion tangential and normal to the instantaneous flight path. If we define a unit vector $\hat{\tau} = \frac{\vec{V}}{V}$ tangential to the flight path and define a unit vector $\hat{\sigma}$ normal to the flight path, the velocity is by definition $\dot{\vec{r}}_t \equiv \vec{V} = V\hat{\tau}$, and the acceleration is given by

$$\ddot{\vec{r}}_t = \dot{V}\hat{\tau} + V\dot{\hat{\tau}} = \dot{V}\hat{\tau} - V\dot{\gamma}_t\hat{\sigma}.$$

Thus the tangential and normal scalar equations of motion become

$$\dot{V} = F_\tau, \quad V\dot{\gamma}_t = -F_\sigma, \qquad (20)$$

where F_τ and F_σ are given by Eqs (17).

Once the range of possible trajectory parameters for the direct descent trajectory has been narrowed down, and the landing area has been selected, some typical precision trajectories should be calculated. The vehicle can now move in three dimensions, and the most accurate values are used for the physical constants. This would result in lifting the assumption of a moon homogeneous in spherical layers, but using a moon homogeneous in ellipsoidal shells. The buildup and tailoff of rocket thrust in a given burning period can also be simulated, and any lateral maneuvering which can reduce the hovering and translational requirements on the LM can be introduced into the computer simulation.

The equations of motion in selenocentric lunar equatorial coordinates x_ℓ y_ℓ z_ℓ (assumed inertial for this case), including the triaxially ellipsoidal shape of the moon, are given in Chapter VII. Thrust accelerations add terms $\frac{T_x}{M}$, $\frac{T_y}{M}$, $\frac{T_z}{M}$ to the equation of motion in the x_ℓ, y_ℓ, and z_ℓ directions, respectively. The transformations of T_x, T_y, T_z to components T_u, T_v, T_w, which are in a coordinate system x_v, y_v, z_v, are given in Chapter IV-B-4 e (the only change in the transformation equations is a formal change of the $\oplus$-symbol to the ℓ-symbol). This coordinate system has its origin at the center of gravity of the vehicle, the z_v-axis in the direction of the radius vector, the x_v-axis in the general direction of motion in the trajectory plane but perpendicular

to z_v, and the y_v-axis perpendicular to the trajectory plane to complete the right-hand Cartesian coordinate system.

d. Trajectory optimization

The previous subsection described the physical models and the corresponding equations of motion--the tools of the trajectory analyst. In order to obtain a particular solution to the equations of motion, or a trajectory, further information is needed, for example: the initial conditions for descent (position, velocity, vehicle mass) must be obtained from translunar trajectories, the characteristics of the rocket engine and the fuel must be specified, and the important question, "How should the space vehicle be steered, or, what is the variation of thrust attitude angle θ with time during rocket burning?" must be answered. Since there are an infinite number of possible trajectories between the initial position and velocity for a direct descent and the final lunar landing site position and touchdown velocity, the number of trajectories analyzed must be reduced drastically. This leads naturally to a problem of trajectory optimization: what trajectory maximizes or minimizes some criterion of performance Q, where Q might be the fuel expended during descent, payload on the lunar surface, cost, etc.? Of course, the lunar descent phase must be integrated with the other trajectory phases of the particular lunar mission.

Optimization problems may be classified into two categories:

(1) Pure trajectory problems, where all vehicle and rocket engine characteristics, such as initial weight, thrust, etc., are specified and the trajectory that optimizes some aspect of performance is sought.

(2) Space vehicle design problems, where the mission is specified, and payload weight, landing site location, rocket engine and fuel characteristics or similar parameters are sought.

Various trajectory optimization schemes, primarily based on the calculus of variations, the method of steepest descent, Pontryagin's maximum principle or dynamic programming have appeared in the literature. A general approach will be outlined in Subsection B-2e and applied to the case of descent from lunar orbit. Although this approach could also be used in analysis of direct descent, the discussion of this optimization scheme will be deferred until later, and only results of two simpler approaches, one a space vehicle design problem and the other a trajectory problem, will be given here for nominally vertical trajectories.

Reference 7 treats a space vehicle design problem. In it are treated the optimum thrust-to-mass ratios $f_0 = \frac{T}{M_0}$ for the simple, vertical descent with one burning phase to a soft landing at zero touchdown velocity under the assumption of constant thrust and constant gravity (the trajectory of Eqs (5) and (6)). A further assumption is that the total mass of the propulsion system M_p (mass of tanks, thrust chamber, propellant reserves, plumbing, etc.), can be expressed by the linear form

$$M_p = A + B M_f + CT \qquad (21)$$

where

M_f = total propellant mass

A = fixed propulsion system mass, i.e., the mass that does not vary with engine size

B, C are constants of proportionality, where

B = ratio of the propulsion system mass that depends on M_f (or the propellant scalable system mass) to M_p

C = ratio of the propulsion system mass that depends on T (or the thrust scalable system mass) to M_p

T = thrust.

The constants A, B and C are rocket engine design parameters. Figure 8 gives the optimum in terms of a nondimensional impact velocity parameter $\frac{V_i}{V_{ex}}$, where V_i is the ballistic lunar impact velocity given in Fig. 1 as a function of transit time, and in terms of the nondimensional propulsion system parameter $[(g_{\ell 0}C)/(1 + B)]$.

The region of the parameter $g_{\ell 0}C/(1 + B)$ for liquid propulsion systems is shaded in Fig. 8. The parameter C is smaller for solid rockets than for liquid systems because the solid rocket system mass is largely dependent upon the propellant mass and not too dependent upon thrust level. Therefore, payload acceleration tolerances would generally be exceeded if the optimum thrust for solid rockets were chosen. Figure 9, also from Ref. 7, shows the penalty in payload weight resulting from braking at other than optimum thrust level. For typical impact velocities, the payload is not too sensitive to changes in thrust-to-weight ratio.

Reference 8 outlines an optimization procedure for a trajectory problem based on a two-engine braking system. The basic braking technique to be optimized is chosen for simplicity and reliability as follows. A high constant-thrust, solid-propellant engine provides the major portion of the braking. After main retro-rocket burnout a variable-thrust, liquid-propellant engine reduces the remaining velocity before impact and corrects for dispersions in altitude and velocity at burnout of the solid engine. The nominal program of this vernier engine involves a descent at minimum thrust until sensors reveal a velocity-altitude combination which permits soft landing by maximum vernier thrust operation for the remainder

of flight. Based on this preliminarily defined braking technique, the optimization is then concerned with apportionment of velocity reduction between the two engines such that total braking system weight is minimized. The technique is indicated first in the case of vertical descent and then extended to off-vertical approaches. The numerical optimization procedure is illustrated in the following sketch and may be outlined as follows:

(1) From given main engine terminal conditions and engine characteristics, a dispersion ellipsoid in the h, V, γ space is established.

(2) The computer then iterates to find the point of tangency of this ellipsoid and a surface of constant vernier fuel. This point represents the maximum vernier fuel required for the chosen nominal burnout point.

(3) From the vernier fuel mass corresponding to the tangent surface, the total engine weight (vernier weight plus main engine weight) is computed.

(4) Curves of main engine weight and vernier weight as functions of nominal main engine terminal velocity are generated by repeated computer runs. The optimum terminal velocity is then the one corresponding to the minimum sum of vernier and main engine weight.

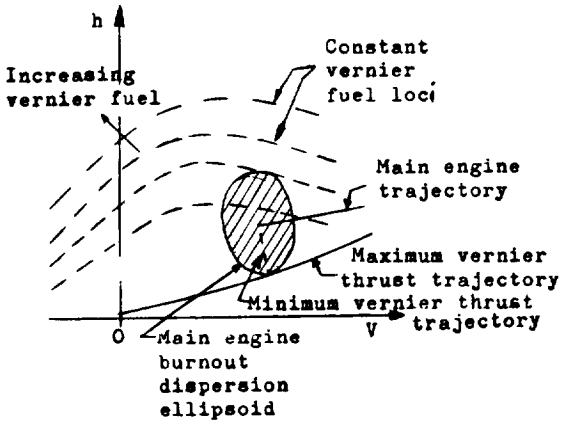

e. Guidance laws for direct descent soft landings

From the trajectory analysis and optimization phase of the design, one or several trajectories will have been selected for the proposed direct descent to the lunar surface. But how will the vehicle stay on the desired trajectory? The guidance, which is concerned with obtaining the input information required for the desired trajectory, such as altitude and velocity, and the guidance laws, which are used to control the vehicle so that it stays near the desired trajectory, for direct descent trajectories form the subject of the present subsection.

A multitude of guidance laws have been studied in connection with the lunar landing mission. However, only a few laws can be considered here in any detail. It is instructive to consider first a few simple guidance laws which can be used in connection with nominally vertical descent, the case for which analytic approximate solutions have been derived. These guidance laws for vertical descent will be considered in this section; a guidance law applicable to nonvertical trajectories will be analyzed in detail in Section B-2d (discussing indirect descent) since typical trajectories for ascent to or descent from a lunar satellite orbit deviate further from the vertical than do typical direct ascent and descent trajectories.

In the case of direct descent, guidance in the early phases of descent may be relatively simple. The system may consist of altimeter and horizon sensor, and a constant-thrust rocket engine.

Velocity need not be measured during initial braking, first because the velocity would have to be controlled by midcourse guidance to a few m/sec to avoid missing the moon completely and, secondly, because accurate velocity determination might be difficult at high altitude. In the final braking phase more refined guidance will be required to eliminate trajectory errors before touchdown. The altimeter must be supplemented by a Doppler system in the vehicle so that both altitude and velocity may be monitored. For this final phase a variable thrust engine will be required to implement the guidance commands.

Reference 9 considers several guidance laws for use in nominally vertical descent:

(1) Vertical channel

$$a_c = \frac{1}{2}\,\frac{\dot{h}^2 - \dot{h}_f^2}{h - h_f} + g_{\mathbb{C}} \qquad (22)$$

or

$$a_c = a_{nom} + K(t)\left\{\dot{h} - \left[2\,(a_{nom} - g_{\mathbb{C}})\,(h - h_f) + \dot{h}_f^2\right]^{1/2}\right\} \qquad (23)$$

where

a_c = command acceleration

$\dot{h}$ = instantaneous downward velocity

$\dot{h}_f$ = desired final downward velocity

h = instantaneous altitude

h_f = desired final altitude

a_{nom} = nominal acceleration

K(t) = programmed gain factor

(2) Horizontal channel

$$\omega_{vc} = -f(t)\frac{V_w}{V_u} = -k\frac{V_w}{r_t} \qquad (24)$$

$$\omega_{wc} = f(t)\frac{V_v}{V_u} = k\frac{V_v}{r_t} \qquad (25)$$

where

ω_{vc} = command pitch rate

ω_{wc} = command yaw rate

V_u = velocity component along roll (thrust) axis

V_v = velocity component along pitch axis

V_w = velocity component along yaw axis

k = gain constant

r_t = slant range along thrust axis to lunar surface

Next, these guidance laws will be discussed. By means of Eq (22), when a deviation from the nominal trajectory is sensed, the thrust is controlled to produce a new constant acceleration trajectory which terminates with the required final velocity and altitude. That is, this guidance law is explicit; it does not depend upon storage of the complete nominal trajectory. The law does not force the vehicle to fly the nominal trajectory but simply steers for the desired final values. It may be obtained by integration of the equation of motion during vertical descent, under the assumption that $\frac{T}{M}$ and g_ℓ are constant:

$$F \equiv M(f - g_\ell) = M\ddot{h} \qquad (26)$$

where

$f = \frac{T}{M}$ is the constant acceleration due to thrust.

From the conservation of energy

$$\int F\,dh = \text{change in kinetic energy}$$

or

$$\int_{h_0}^{h_f} M(f - g_\ell)\,dh = \frac{1}{2}M(\dot{h}_0^2 - \dot{h}_f^2) \qquad (27)$$

which becomes

$$f - g_\ell = \frac{1}{2}\frac{\dot{h}_0^2 - \dot{h}_f^2}{h_0 - h_f} \qquad (28)$$

after integration over the indicated interval.

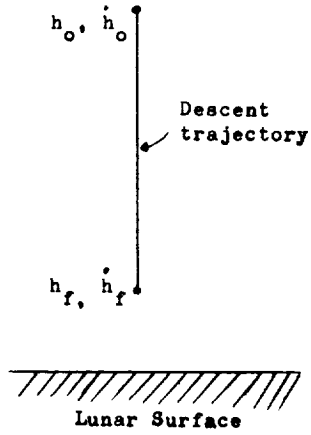

The guidance law of Eq (23) is an example of an implicit guidance law; that is, the vehicle follows a nominal trajectory in the guidance phase. A deviation of the actual velocity h from the desired instantaneous velocity,

$$\sqrt{2(a_{nom} - g_\ell)(h - h_f) + \dot{h}_f^2}\ , \qquad (29)$$

generates a command correction to the nominal acceleration. This law forces the vehicle to follow the nominal trajectory.

In the absence of errors, both laws would produce identical trajectories. However, Cheng and Pfeffer (Ref. 9) find that the closer adherence to the nominal trajectory resulting from use of Eq (23) results in less variation in acceleration. When the LM attitude is nearly vertical, the altitude h and altitude rate $\dot{h}$ may be replaced by slant range r_t and velocity along the thrust axis V_u, respectively, in Eqs (22) and (23), so that the raw data need not be transformed.

Equations (24) and (25) form a proportional rate guidance law for horizontal maneuvers. The angle between the velocity vector and the thrust vector is used to generate angular command rates ω_{vc} and ω_{wc}. The thrust and velocity are not forced to be colinear throughout flight as in the case of a gravity turn trajectory (Subsection C-2b), but this situation is gradually achieved by touchdown time.

2. Indirect Descent (descent from lunar orbit)

The direct descent method for achieving a hard or soft landing will probably only be used for instrument carriers, since any failure in the rocket braking system would result in a lunar impact speed of about 3 km/sec for the space vehicle. In contrast, the most commonly used descent technique for manned and even some unmanned vehicles will probably use an approach or circumlunar trajectory for the translunar portion of the flight. Of these two trajectories the latter would be preferable, since any failure in the rocket braking system would allow a ballistic return of the vehicle to the vicinity of the earth. Lunar descent from the approach and circumlunar trajectory is performed in two stages--a braking from the translunar trajectory,

which is a hyperbolic trajectory around the moon, to circular or elliptic lunar orbits and subsequently a descent from this orbit to the lunar surface by the entire landing module (LM). This approach allows maximum flexibility in choice of landing site, since with a lateral maneuver during or subsequent to the braking into lunar orbit, any orbital inclination can be obtained. Furthermore, with additional fuel consumption, the indirect descent technique allows more time for observations and corrections before landing. However, the technique is more complex than direct descent from a translunar trajectory.

a. Descent technique

Descent from a lunar satellite orbit to a soft landing on the lunar surface will probably involve the following routine, although other techniques are possible:

(1) In the shuttle concept, after separation from the orbiting vehicle, the shuttle vehicle experiences a retrothrust during what will be termed the deorbit phase of descent. Of course, this technique is not restricted to the shuttle case but can be applied to an indirect descent of the entire vehicle. The deorbit maneuver requires a velocity impulse of $\Delta V \approx 100$ m/sec.

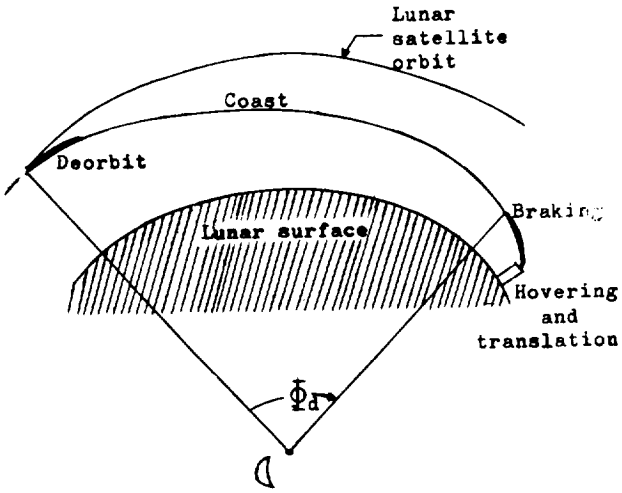

(2) Following deorbit the (LM) coasts in a ballistic elliptical trajectory to an altitude of perhaps 20 or 30 km.

(3) A final braking phase reduces the LM velocity to less than 50 m/sec by the time the vehicle has descended to an altitude of a few hundred meters.

(4) During the terminal braking phase, lateral velocity is reduced to zero and the thrust vector is pitched over into a vertical or hovering attitude.

(5) During the final phase of descent, the vehicle is capable of hovering and translation. This capability is discussed in Section D below.

Since descent from orbit, or indirect descent, necessarily involves curved, nonvertical trajectories, the analytic trajectory solutions possible for vertical direct descent (Section B-1c) are useful as approximations no longer. All indirect descent trajectories must be computed by numerical integration of the equations of motion. (Section B-1c includes various simple forms of the equations to be integrated.) Also, guidance law for indirect descent must be more general, and therefore more complicated, since these laws cannot rely on approximations which assume small angles between the thrust vector and the local vertical. On the other hand, many approaches which will be applied to analysis of indirect descent are obviously applicable in the cases of direct descent which deviate considerably from vertical.

b. Indirect descent trajectories

Various factors prevent a general analysis of descent trajectories. The number of parameters involved is very large (orbit altitude, descent range, individual propulsion system specifications, vehicle weight, to mention a few). Even after a descent technique such as the one discussed in the previous subsection has been chosen for a given mission, trajectories will differ somewhat, depending on the choice of guidance law or pitch program. Therefore, generality must be sacrificed, and trajectories will be presented for a particular hypothetical mission, a particular vehicle, and for limited ranges of trajectory variables.

The particular case investigated is descent from a circular orbit of 185.2-km altitude. Various trajectories were computed with a two-dimensional point-mass trajectory program and plotted in Figs. 10 through 14 for parameters given in the following table. Nominally constant pitch rates (θ_t = const) were used in generating these trajectories.

Sample Braking Trajectories

Figure No.	$\frac{T}{W_0}$	Descent Range, Φ_d (deg)	Initial Altitude, h_0 (km)	Terminal Altitude, h_f (km)	Specific Impulse I_{sp} (sec)
10	0.45	90	18.29	0.304	309
11	0.45	180	18.29	0.304	309
12	0.45	Synchronous* 95	18.29	0.304	309
13	0.45	Synchronous 95	12.19	0.304	309
14	0.45	Synchronous 95	27.43	0.304	309

*Synchronous, or equal period, descent is discussed in Section D

The ordinates for these figures give altitude in km (left-hand ordinate) and the corresponding time from braking ignition (right-hand ordinate). Time increments are also indicated along each curve by data points. For a given altitude or time the four curves on each figure determine the vehicle velocity magnitude, V; the local flight path angle, γ; the range from braking rocket ignition, and the pitch angle with respect to inertial coordinates, θ_t, on the appropriate abscissa scales.

c. Braking requirements

Figures 15, 16 and 17 summarize a parametric computer analysis of propulsion system requirements for descent from orbit and, in particular, for the braking phase. All of these figures relate to descent from a 185.2-km circular orbit, for which the braking phase trajectories of Figs. 10 through 14 are typical.

Figure 15 shows a typical complete descent trajectory. Figure 16 shows the characteristic velocity, $\Delta V \equiv -V_{ex} \ln (1 - \zeta)$, required during the braking phase as a function of initial thrust-to-weight ratio for several descent range angles.

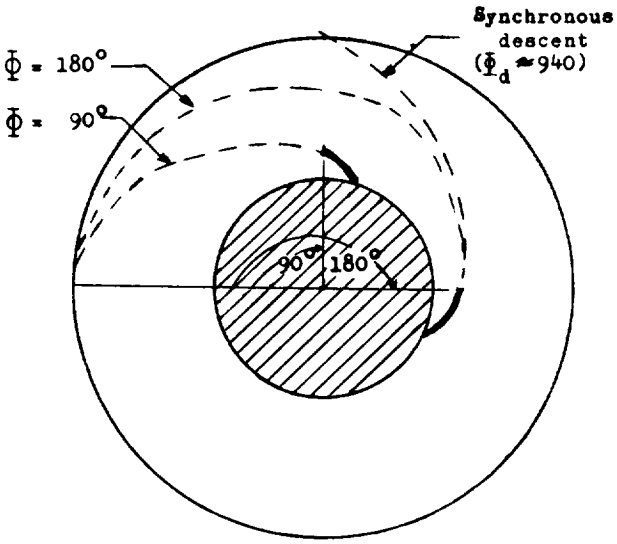

Whereas the $\Phi_d = 90°$ and $\Phi_d = 180°$ descents are initially tangent to the lunar satellite orbit, the synchronous descent (involving a coast phase of the same orbital period as the lunar satellite orbit) begins with a nontangential deorbit. This factor explains the greater economy of the $\Phi_d = 90°$ and $\Phi_d = 180°$ cases as shown in Fig. 16.

Figure 17 shows the same functional relationship, velocity decrement required versus initial thrust-to-weight ratio, for various initial braking altitudes for a synchronous descent. One curve for a higher value of specific impulse is also included for comparison. Figure 18 is a plot of the same variables as Figs. 16 and 17, except that Fig. 18 includes the deorbit phase requirements in addition to those for the braking phase. The forms of these curves indicate the existence of an optimum thrust level for each set of nominal system and orbit parameters from the flight mechanics point of view.

d. Guidance law for indirect descent braking

Just as there is an optimum thrust magnitude, there is also an optimum direction, and the guidance and control system must keep the vehicle reasonably close to this optimum for descent. The control law (or guidance law) for descent from lunar orbit should be as flexible, efficient, as simple as possible, and should permit man-in-the-loop operation for system reliability. A predictive guidance technique, which has been demonstrated in a simulation program (Ref. 10), appears to fulfill these requirements very well and will therefore be discussed in this subsection.

The guidance operational phase of the descent from orbit described in Subsection B-2a begins during the ballistic phase 30 sec before the braking thrust is initiated. During braking, the thrust vector must be controlled in such a manner that the range and range rate go to specific values simultaneously. The thrust magnitude should experience as small a variation as is practical to minimize the requirements for engine throttling. Fuel consumption must not be penalized by the thrust vector control.

These requirements are not compatible. For example, minimum fuel consumption dictates constant thrust (Ref. 11), but range control dictates variable thrust. Again, minimum fuel consumption with a range restraint dictates a complicated thrust vectoring system, whereas the guidance information must be displayed simply to reduce human reaction time. There are other conflicting requirements. The predictive law selected represents a reasonable compromise. Lawden (Ref. 12) has noted that an extremum of a payload function is obtainable for a point particle in a constant gravitational field with mass a function of time, if the thrust vector direction in the two-dimensional case is represented by the time-dependent bilinear function of the form

$$\tan \theta_t = \frac{a - bt}{c - dt} \qquad (30)$$

where θ_t is the thrust vector angle in an inertial two-dimensional coordinate system. Fried (Ref. 13) has shown that d = 0 if range is unrestrained, and Perkins (Ref. 14) has indicated that the law (30) is applicable to a braking type of maneuver. It can also be shown that another form similar to Eq (24) is obtained when a three-dimensional trajectory is considered, and the thrust vector is resolved in two directions. The thrust in this discussion is assumed to act along the longitudinal or roll axis of the vehicle.

Consider any set of orthogonal Cartesian axes $x_t\ y_t\ z_t$ and a rotation about one of these axes to form a new Cartesian set $x_t'\ y_t'\ z_t'$. Define a

rotation about the z_t-axis as yaw angle ψ_t, a rotation about the z_t-axis as pitch angle θ_t and a rotation about the x_t-axis as roll angle ϕ_t. Next consider a three-dimensional lunar landing trajectory.

A notable characteristic of solutions for a and b in Eq (30) is that the product (bt) is generally small for braking trajectories in selenocentric space and with initial decelerations greater than 5 m/sec^2. With this observation, it is possible in a first approximation to linearize the pitch angle θ_t and the yaw angle ψ_t:

$$\theta_t = \theta_{t0} + \dot{\theta}_t t$$
$$\psi_t = \psi_{t0} + \dot{\psi}_t t \qquad (30a)$$

Therefore, in a first approximation, an Euler angle program having constant first derivatives represents an efficient thrust vector control. Furthermore, the requirement that range and range rate be driven to specified values simultaneously is satisfied in two of the three dimensions. The third (longitudinal range) is satisfied if the thrust magnitude and ignition point are allowed to vary within specific bounds to accommodate errors in ignition time and system performance. Finally, an Euler angle program of this form is quickly assimilated and understood by a human pilot.

Solution of the differential equations of motion for guidance purposes needs to be only approximate, provided that the solution is convergent. That is, as the vehicle approaches the target, it becomes more accurate. It is necessary that the initial inaccuracies do not jeopardize the later stages of the trajectory. In addition, the predictive system exhibits a closed-loop response, so that inaccuracies due to constant errors or computational roundoffs are driven to zero.

The differential equation of motion in vector notation is

$$\frac{d^2\vec{r}}{dt^2} = -\frac{\mu_\oplus}{r^3}\vec{r} + \frac{\vec{T}}{M} \qquad (31)$$

In development of the prediction equations, the following approximations can be made:

(1) Thrust and mass flow are constant.

(2) The vehicle behaves like a point mass.

(3) The change in $\frac{\mu_\oplus}{r^3}$ is small when compared to $\frac{T}{M}$.

For these assumptions, Eq (25) becomes

$$\left(\frac{d^2}{dt^2} + \omega^2\right)\vec{r} = \frac{\vec{T}}{M_0 - \dot{M}t} \qquad (31a)$$

where

$$\omega = \sqrt{\frac{\mu_\oplus}{R_\oplus^3}} = \text{constant.} \qquad (31b)$$

This form of differential equation is amenable to solution by the method of variation of parameters. A complementary solution is:

$$\vec{r}_c = \vec{C}_1 \sin\omega t + \vec{C}_2 \cos\omega t \qquad (32)$$

where $\vec{C}_1$ and $\vec{C}_2$ are constant vectors

The particular solution has the form

$$\vec{r}_p = \vec{A}(t)\sin\omega t + \vec{B}(t)\cos\omega t \qquad (33)$$

The three dependent variables, $\vec{r}$, $\vec{A}$ and $\vec{B}$ must satisfy Eqs (31) and (33) and one additional, arbitrary condition which will be imposed. Differentiation of Eq (33) gives

$$\frac{d\vec{r}}{dt} = \vec{A}\omega\cos\omega t - \vec{B}\omega\sin\omega t + \dot{\vec{A}}\sin\omega t + \dot{\vec{B}}\cos\omega t$$

The third arbitrary condition may be specified as

$$\dot{\vec{A}}\sin\omega t + \dot{\vec{B}}\cos\omega t \triangleq 0 \qquad (34)$$

so that

$$\frac{d\vec{r}}{dt} = \vec{A}\omega\cos\omega t - \vec{B}\omega\sin\omega t \qquad (35)$$

Differentiation of Eq (35) and substitution of Eq (33) gives

$$\frac{d^2\vec{r}}{dt^2} = -\omega^2\vec{r} + \dot{\vec{A}}\omega\cos\omega t - \dot{\vec{B}}\omega\sin\omega t \qquad (36)$$

which, with Eq (31), reduces to

$$\dot{\vec{A}}\omega\cos\omega t - \dot{\vec{B}}\omega\sin\omega t = \frac{\vec{T}}{M} \qquad (37)$$

Simultaneous solution of Eqs (34) and (37) gives

$$\dot{\vec{A}} = \frac{\vec{T}}{\omega M}\cos\omega t \qquad (38)$$
$$\dot{\vec{B}} = \frac{\vec{T}}{\omega M}\sin\omega t$$

Then the solution becomes

$$\vec{r} = \left(\vec{r}_0 - \frac{1}{\omega}\int_0^\tau \frac{\vec{T}}{M}\sin\omega t\,dt\right)\cos\omega\tau + \frac{1}{\omega}\left(\dot{\vec{r}}_0 + \int_0^\tau \frac{\vec{T}}{M}\cos\omega t\,dt\right)\sin\omega\tau \qquad (39)$$

$$\dot{\vec{r}} = \left(\dot{\vec{r}}_0 + \int_0^\tau \frac{\vec{T}}{M}\cos\omega t\,dt\right)\cos\omega\tau - \left(\omega\vec{r}_0 - \int_0^\tau \frac{\vec{T}}{M}\sin\omega t\,dt\right)\sin\omega\tau$$

where τ denotes the final time.

For the case of short burning times,

$$\sin \omega\tau \cong \omega\tau$$

$$\cos \omega\tau \cong 1$$

and Eq (39) reduces to

$$\vec{r} \simeq \vec{r}_0 \cos \omega\tau - \int_0^\tau \frac{\vec{T}}{M} t\,dt + \left(\dot{\vec{r}}_0 + \int_0^\tau \frac{\vec{T}}{M}\,dt\right)\tau$$

$$\dot{\vec{r}} \simeq \dot{\vec{r}}_0 + \int_0^\tau \frac{\vec{T}}{M}\,dt - \left(\dot{\vec{r}}_0 - \int_0^\tau \frac{\vec{T}}{M} t\,dt\right)\omega^2\tau \qquad (40)$$

Equations (40) are the approximate prediction equations in this explicit guidance law. The components of the thrust vector $\vec{T}$ in the $x_t\ y_t\ z_t$ coordinate system at any time t are:

$$T_x(t) = T(t)\cos(\theta_t + \dot{\theta}_t t)\cos(\psi_t + \dot{\psi}_t t)$$

$$T_y(t) = T(t)\cos(\theta_t + \dot{\theta}_t t)\sin(\psi_t + \dot{\psi}_t t) \qquad (40a)$$

$$T_z(t) = T(t)\sin(\theta_t + \dot{\theta}_t t)$$

If the thrust is assumed constant, and $\dot{\theta}_t$ and $\dot{\psi}_t$ are assumed to be of the same order as ω, approximate analytic solutions for $\vec{A}$ and $\vec{B}$ may be derived. To the first order in ωt, the components of $\vec{A}$ and $\vec{B}$ in the $x_t\ y_t\ z_t$ coordinate system are:

$$A_x \approx \frac{1}{\omega}\left[J_1 \cos\theta_t \cos\psi_t - J_2(\dot{\theta}_t \sin\theta_t \cos\psi_t + \dot{\psi}_t \sin\psi_t \cos\theta_t)\right]$$

$$A_y \approx \frac{1}{\omega}\left[J_1 \cos\theta_t \sin\psi_t - J_2(\dot{\theta}_t \sin\theta_t \sin\psi_t - \dot{\psi}_t \cos\psi_t \cos\theta_t)\right]$$

$$A_z \approx \frac{1}{\omega}\left[J_1 \sin\theta_t + J_2 \dot{\theta}_t \cos\theta_t\right] \qquad (40b)$$

$$B_x \approx J_2 \cos\theta_t \cos\psi_t - J_3(\dot{\theta}_t \sin\theta_t \cos\psi_t + \dot{\psi}_t \sin\psi_t \cos\theta_t)$$

$$B_y \approx J_2 \cos\theta_t \sin\psi_t - J_3(\dot{\theta}_t \sin\theta_t \sin\psi_t - \dot{\psi}_t \cos\psi_t \cos\theta_t)$$

$$B_z \approx J_2 \sin\theta_t + J_3 \dot{\theta}_t \cos\theta_t$$

where

$$J_1 = -V_{ex} \ln(1 - \zeta)$$

$$J_2 = \frac{t}{\zeta}(J_1 - V_{ex}\zeta)$$

$$J_3 = \frac{t}{\zeta}\left(J_2 - \frac{V_{ex}}{2} t\zeta\right)$$

$V_{ex} = \frac{T}{\dot{M}}$ is the effective exhaust velocity

$\zeta = \frac{\dot{M}t}{M}$ is the mass ratio

The commanded pitch, pitch rate, yaw and yaw rate for the bilinear guidance law, θ_{tc}, $\dot{\theta}_{tc}$, ψ_{tc} and $\dot{\psi}_{tc}$, can be determined explicitly:

$$\sin\theta_{tc} = \frac{\omega A_z \frac{J_3}{J_2} - B_z}{J_1 \frac{J_3}{J_2} - J_2}$$

$$\dot{\theta}_{tc} = \frac{B_z - J_2 \sin\theta_{tc}}{J_3 \cos\theta_{tc}} \qquad (40c)$$

$$\sin\psi_{tc} = \frac{1}{\cos\theta_{tc}} \frac{\omega A_y \frac{J_3}{J_2} - B_y}{J_1 \frac{J_3}{J_2} - J_2}$$

$$\dot{\psi}_{tc} = \frac{\omega A_y + (\dot{\theta}_{tc} J_2 \sin\theta_{tc} - J_1 \cos\theta_{tc})\sin\psi_{tc}}{J_2 \cos\theta_{tc} \cos\psi_{tc}}$$

where ζ and t can be computed from the following empirical approximations, with the subscript k denoting the value at a given time t:

$$\zeta = 1 - \exp\left[\frac{1}{V_{ex}}\left(\dot{S} + 2g_0 \frac{h - h_k}{V + V_k}\right)\right] \quad ; \quad (V + V_k) > 0 \qquad (40d)$$

$$t = \left|\frac{S^2}{\vec{S}\cdot\vec{S}\left[\frac{1}{\ln(1-\zeta)} + \frac{1}{\zeta}\right] + \dot{\vec{r}}_k \cdot \vec{S}}\right| \frac{1}{K_k} \qquad (40e)$$

with

$$\vec{S} = \vec{r} - \vec{r}_k .$$

The function K_k depends on its value at the preceding step, K_{k-1}, and can be computed from the following relation:

$$K_k = \left(\frac{\vec{S}_{plp}\cdot\vec{S}_{plp}}{\vec{S}\cdot\vec{S}}\right)^{1/2} K_{k-1} \qquad (41)$$

where the predicted slant range vector is

$$\vec{S}_{plp} = \vec{r} - \vec{r}_{plp}$$

With a pilot in the loop, the equations for t and K_k are not required. The pilot performs the same function as these equations by manipulating the throttle.

During the manual mode, the predictions are acted upon directly by the pilot. He does not use

the angles θ_{tc} and $\dot{\theta}_{tc}$, or ψ_{tc} and $\dot{\psi}_{tc}$, but he sees the effects which the instantaneous values of θ_t, $\dot{\theta}_t$, ψ_t, $\dot{\psi}_t$ will have on the terminal (or landing) conditions. Then, using the appropriate control, he adjusts his attitude until the prediction is favorable. Thus, in a sense, the pilot is solving for the correct attitudes and attitude rates by trial and error by use of the predictive displays.

In the terminal phase, as in the braking phase, provision may be made for both automatic and manual control. A guidance law for the terminal phase (Ref. 15) is

$$\frac{\vec{T}}{M} = g_{\mathbb{C}} \frac{\vec{R}_{\mathbb{C}}}{R_{\mathbb{C}}} - \frac{(\dot{\vec{S}} - \dot{\vec{S}}_t)}{\left(1 + \frac{h}{h_0}\right)^2} K_1 - K_2 \vec{S} \quad (42)$$

where

$\vec{R}_{\mathbb{C}}$ = central body radius vector to landing site

$\vec{S}$ = slant range vector from target to vehicle

K_1, K_2 = thrust sensitivity coefficients

The capability of the guidance law has been tested in a lunar landing simulator which required a total of 294 operational amplifiers, utilizing four Reac C-400. Two Reac C-100 and an expanded EA 231R analog computers. Fuel consumption during the manual braking runs was generally within two percent of that required for an identical automatic run. Pilot displays are so simple for the predictive law that, in most cases, a "safe" flight was flown on the second or third attempt. The pilot's performance was best when augmenting the automatic system, and his inclusion, in general, improved the total system performance. In some cases, with marginal initial conditions, the pilot was able to recover control and save the vehicle in a situation in which use of the automatic system would have resulted in an impact.

e. Trajectory optimization

Up to this point optimum maneuvers have only been mentioned in passing. The purpose of this subsection is thus to include a more detailed discussion of trajectory optimization.

The trajectory optimization field, and for that matter the solution of variational problems in general, has acquired considerable impetus during the last few years. To the classical calculus-of-variations approach have been added methods based on steepest descent, the Pontryagin maximum principle, and dynamic programming. These latter are very closely related to the calculus of variations and are reducible to it, at least in the limit.

Most recently, steepest descent has dominated the scene. Considerable success has been realized in obtaining approximate optima by this method. The abandonment of the classical indirect approach (calculus of variations), which yields exact optima, in favor of this approximate method, was stimulated by the difficulty encountered in solving the two-point boundary value problem (in general with one unknown boundary) which results from the classical approach.

A new systematic scheme for solving the two-point boundary value problem with one unknown boundary has recently been developed (Ref. 16). Its feasibility and advantages have been demonstrated (Ref. 17) on a simple trajectory optimization problem which possesses an analytical solution (Ref. 18). The method of solving the variational boundary value problem is here applied to solve for the steering program resulting in maximum payload in the braking phase of a lunar landing maneuver. The method will now be briefly outlined, and some representative results will be presented.

It is assumed that the moon is spherical and does not rotate. Trajectories in a plane are considered so that the equations of motion may be written (see sketch below)

$$\begin{aligned}
\dot{V} &= -\frac{T}{M}\cos(-\gamma - \theta) - \frac{\mu_{\mathbb{C}}}{r^2}\sin\gamma \\
\dot{\gamma} &= \frac{T}{MV}\sin(-\gamma - \theta) + \frac{V}{r}\cos\gamma - \frac{\mu_{\mathbb{C}}\cos\gamma}{r^2 V} \\
\dot{r} &= V\sin\gamma \qquad (43) \\
\dot{\Phi} &= \frac{V\cos\gamma}{r}
\end{aligned}$$

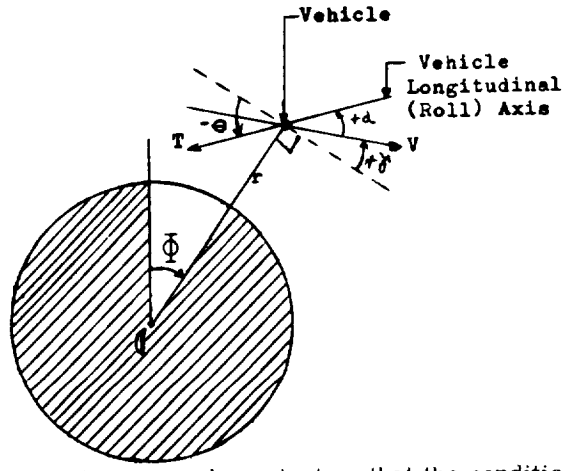

Thrust is assumed constant so that the condition of maximum payload is equivalent to that of minimum rocket burning time.

The first necessary condition of the calculus of variations (Euler-Lagrange equations) results in a boundary value problem. The constraint equations (43) have to be solved together with the Euler-Lagrange equations, where conditions are imposed at both boundaries, and where the terminal boundary--terminal (minimum) time--is unknown.

Linear perturbations around some nominal (nonoptimal) solution of this boundary value problem are considered. This new set of linear, ordinary differential equations defines an adjoint set. Solutions of the adjoint equations are Green's functions, which relate perturbations in initial conditions to terminal conditions. Appropriate linear combinations of the Green's functions yield the

desired perturbations in the unknown (estimated) initial conditions, and the terminal time, which will result in desired changes in the terminal conditions which have to be met. The process is iterative in nature, since the equations (43) are nonlinear, and converges rapidly to the solution of the Eulerian boundary value problem.

This method was applied to the problem at hand. The pertinent constants are:

$$\mu_{\oplus} \equiv GM_{\oplus} = 4905.927 \text{ km}^3/\text{sec}^2$$

$$R_{\oplus} = 1738.236 \text{ km}$$

$$T/W_0 = 0.45$$

$$I_{sp} = 309 \text{ sec}$$

$$g_{\oplus 0} = 9.80665 \text{ m/sec}^2$$

$$M_0 = 9979 \text{ kg.}$$

The Eulerian boundary value problem was solved for the initial conditions:

$$V_0 = 1.74 \text{ km/sec}$$

$$\gamma_0 = 0°$$

$$h_0 = 18{,}288 \text{ m,}$$

which represent the conditions during synchronous ballistic descent, at pericynthion, or at the start of braking. Two sets of terminal conditions were solved for:

(1) $V_1 = 0.001$ km/sec

$\gamma_1 = -90°$

$h_1 = 304.34$ m

(2) $V_1 = 0.001$ km/sec

$\gamma_1 = -10°$

$h_1 = 304.34$ m

The solutions appear in Fig. 19. Terminal flight path angle constraints were not accurately met because the simplicity of the integration scheme limited the accuracy. (This was a pilot program.) The other terminal conditions were satisfactorily met. It should be pointed out that the accuracy with which terminal constraints are met is strictly a function of accuracy in the integration (Ref. 18).

A few comments are in order. It may be observed that all the maneuvering necessary to change the terminal flight path angle occurs optimally at the end of the trajectory. This is a rather apparent result since it is easiest to change the flight path angle when velocity is lowest. It is observed that fuel expenditure for this maneuvering is rather low, so that the same optimum trajectory may be flown almost to the end no matter what the desired terminal orientation. The near-linearity of the θ-curve implies that a bilinear tangent steering program is an excellent approximation. (This is an exact optimum in a constant gravitational field; see previous subsection.)

It is pointed out that the trajectories shown in Fig. 19 yield maximum payload for the exact terminal conditions attained.

A second approach to the control optimization problem is presented in Ref. 19 and applied to the braking phase of lunar landing, i.e., that phase of descent from about 15 km to a few hundred meters above the lunar surface. Briefly, the method involves piecewise linear approximations to a nominal trajectory in a two-dimensional inertial coordinate system. The required control, as obtained from solving the matrix Riccati equation, is optimum in the sense that a performance index is minimized for a specified set of performance matrices.

The notation of Ref. 19, as defined in the following sketch, has been retained.

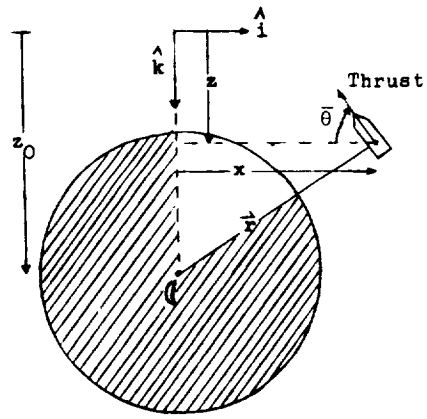

The equations which provide the mathematical model of the system to be controlled are the equations of motion in the two-dimensional inertial coordinate system, which become:

$$\ddot{x} = -\mu_{\oplus} \frac{x}{r^3} - g_{\oplus 0} I_{sp} \frac{\dot{M} \cos \bar{\theta}}{M_0 - M_f}$$

$$\ddot{z} = \mu_{\oplus} \frac{z - z_0}{r^3} - g_{\oplus 0} I_{sp} \frac{\dot{M} \sin \bar{\theta}}{M_0 - M_f} \qquad (44)$$

where

I_{sp} = specific impulse of the propellant

$g_{\oplus 0}$ = sea-level acceleration due to earth gravity

$\dot{M}$ = mass flow rate

M_0 = initial mass of the vehicle

M_f = mass of fuel expended

$\bar{\theta}$ = $180 - \theta_t$, pitch angle relative to the negative x-axis

Control of the vehicle is to involve a variation of $\bar{\theta}$ and $\dot{M}$. Linear approximations to these equations may be written in terms of perturbations about the nominal trajectory, $x_0 = x - x_{nom}$, $\dot{x}_0 = \dot{x} - \dot{x}_{nom}$, etc., by means of Taylor series. For example,

$$\ddot{x}_0 = \frac{\partial \ddot{x}_0}{\partial x} x_0 + \frac{\partial \ddot{x}_0}{\partial z} z_0 + \frac{\partial \ddot{x}_0}{\partial M_f} M_{f0} + \frac{\partial \ddot{x}_0}{\partial M} M_0 + \frac{\partial \ddot{x}_0}{\partial \bar{\theta}} \bar{\theta}_0 \qquad (45)$$

where all partial derivatives are evaluated for nominal values. The linearized equations can be written in matrix form as

$$\dot{\vec{X}} = [F(t)]\,\vec{X} + [G(t)]\,\vec{u} \qquad (46)$$

where $\vec{X}$ is the state vector which in this case has as components the variables which describe the behavior of the system, i.e.,

$$\vec{X} = \{ x_0, \dot{x}_0, z_0, \dot{z}_0, M_{f0} \}$$

and $\vec{u}$ is the control vector with the control variables as components, i.e.,

$$\vec{u} = \{ \dot{M}_0, \bar{\theta}_0 \}.$$

The time-varying coefficient matrices $[F(t)]$ and $[G(t)]$ are approximated by constant values for a given increment of time:

$$[F] = \begin{bmatrix} 0 & 1 & 0 & 0 & 0 \\ f_{21}(t) & 0 & f_{23}(t) & 0 & f_{25}(t) \\ 0 & 0 & 0 & 1 & 0 \\ f_{41}(t) & 0 & f_{43}(t) & 0 & f_{45}(t) \\ 0 & 0 & 0 & 0 & 0 \end{bmatrix}$$

$$[G] = \begin{bmatrix} 0 & 0 \\ g_{21}(t) & g_{22}(t) \\ 0 & 0 \\ g_{41}(t) & g_{42}(t) \\ 1 & 0 \end{bmatrix}$$

$$f_{21}(t) = \left.\frac{\partial \ddot{x}_0}{\partial x}\right|_{nom} = \mu \frac{2x_{nom}^2 - (z_{nom} - z_0)^2}{\left[x_{nom}^2 + (z_{nom} - z_0)^2\right]^{5/2}}$$

$$f_{23}(t) = \left.\frac{\partial \ddot{x}_0}{\partial z}\right|_{nom} = f_{41}(t) = \left.\frac{\partial \ddot{z}_0}{\partial x}\right|_{nom} = 3\mu x_{nom} \frac{z_{nom} - z_0}{\left[x_{nom}^2 + (z_{nom} - z_0)^2\right]^{5/2}}$$

$$f_{25}(t) = \left.\frac{\partial \ddot{x}_0}{\partial M_f}\right|_{nom} = -g_{\oplus 0} I_{sp} \dot{M}_{nom} \frac{\cos \bar{\theta}_{nom}}{(M_0 - M_{f_{nom}})^2}$$

$$f_{43}(t) = \left.\frac{\partial \ddot{z}_0}{\partial z}\right|_{nom} = \mu \frac{2(z_{nom} - z_0)^2 - x_{nom}^2}{\left[x_{nom}^2 + (z_{nom} - z_0)^2\right]^{5/2}}$$

$$f_{45}(t) = \left.\frac{\partial \ddot{z}_0}{\partial M_f}\right|_{nom} = -g_{\oplus 0} I_{sp} \dot{M}_{nom} \frac{\sin \bar{\theta}_{nom}}{(M_0 - M_{f_{nom}})^2}$$

$$g_{21}(t) = \left.\frac{\partial \ddot{x}_0}{\partial \dot{M}}\right|_{nom} = -g_{\oplus 0} I_{sp} \frac{\cos \bar{\theta}_{nom}}{M_0 - M_{f_{nom}}}$$

$$g_{22}(t) = \left.\frac{\partial \ddot{x}_0}{\partial \bar{\theta}}\right|_{nom} = -g_{\oplus 0} I_{sp} \dot{M}_{nom} \frac{\sin \bar{\theta}_{nom}}{M_0 - M_{f_{nom}}}$$

$$g_{41}(t) = \left.\frac{\partial \ddot{z}_0}{\partial \dot{M}}\right|_{nom} = -g_{\oplus 0} I_{sp} \frac{\sin \bar{\theta}_{nom}}{M_0 - M_{f_{nom}}}$$

$$g_{42}(t) = \left.\frac{\partial \ddot{z}_0}{\partial \bar{\theta}}\right|_{nom} = -g_{\oplus 0} I_{sp} \dot{M}_{nom} \frac{\cos \bar{\theta}_{nom}}{M_0 - M_{f_{nom}}}$$

These equations comprise the linear model.

The optimum control $\vec{u}$ will be that which minimizes the specified performance index, which is, in general, a function of the form

$$\mathcal{J}(\vec{u}) = \lambda \left[\vec{X}(t_f), t_f \right] + \int_0^{t_f} L(\vec{X}, \vec{u}, t)\, dt.$$

For the lunar landing problem the performance index selected is

$$\mathcal{J}(\vec{u}) = \frac{1}{2} \vec{X}^T(t_f) [S] \vec{X}(t_f) + \frac{1}{2} \int_0^{t_f} \left\{ \vec{X}^T [Q(t)] \vec{X} + \vec{u}^T [R(t)] \vec{u} \right\} dt$$

The matrices $[S]$, $[Q(t)]$ and $[R(t)]$ may be selected to meet such requirements as accuracy and the amount of control available. The significance of these matrices will be indicated by the solution.

Minimization of a given performance index may be based upon Pontryagin's maximum principle, which states that a necessary condition for an optimum $\vec{u}$ is that there must exist

a continuous vector $\vec{\psi}$ such that the Hamiltonian function

$$H = L + \vec{\psi}^T \dot{\vec{X}}$$

is minimized by $\vec{u}$. The conditions that $\vec{\psi}$ must satisfy are

$$\dot{\vec{\psi}}_i = - \frac{\partial H}{\partial X_i}$$

and

$$\vec{\psi}_i (t_f) = - \left. \frac{\partial \lambda}{\partial X_i} \right|_{t = t_f}$$

The Hamiltonian then becomes

$$H = \frac{1}{2} \vec{X}^T [Q] \vec{X} + \frac{1}{2} \vec{u}^T [R] \vec{u} + \vec{\psi}^T [F] \vec{X} + \vec{\psi}^T [G] \vec{u},$$

which is minimized with respect to $\vec{u}$ by setting

$$\frac{\partial H}{\partial u_i} = 0$$

which gives the optimum $\vec{u}$,

$$\vec{u} = - [R]^{-1} [G]^T \vec{\psi}.$$

The solution for $\vec{\psi}$ is assumed to have the form

$$\vec{\psi} = [P(t)] \vec{X}.$$

Then P(t) is found to satisfy the nonlinear matrix Riccati equation,

$$[\dot{P}(t)] - [P(t)] [G] [R]^{-1} [G]^T [P(t)] + [F]^T [P(t)] + [P(t)] [F] + [Q] = 0$$

An additional constraint is the final value of the Riccati equation,

$$[P(t_f)] = [S].$$

The $[S]$ matrix affects only the final values of control, whereas the $[Q]$ matrix influences the error of the state vector $\vec{X}$. The $[R]$ matrix penalizes the system for using too much control.

Detailed results from application of the optimum theory to the lunar landing problem are presented in Ref. (19). Final trajectory errors are on the order of one meter per 300 meters initial error in position and one m/sec per five m/sec initial error in velocity. Controls that would use small amounts of additional fuel for off-nominal trajectory conditions are obtained. For 3000-meter initial error in position, about 18.2 kg of additional fuel are required. For initial errors in velocity of 9 m/sec, 146 kg of additional fuel are required.

C. ASCENT FROM LUNAR SURFACE

1. Direct Ascent

The goal of the direct lunar ascent phase is accurate injection of the vehicle into a certain transearth trajectory. Since no intermediate or parking orbit is involved, the required injection conditions are the final values to be achieved by the direct ascent trajectory. Figures 20a and 20b give some indication of typical final value requirements for lunar ascent trajectories. The magnitude and direction of the final velocity vector required at an altitude of 93 km (50 naut mi) for injection into 70- and 80-hr return-time transearth trajectory are given as functions of lunar longitude for launch sites lying in or close to the MOP. The magnitude of the required velocity vector exhibits little variation with burnout point longitude. For example, variation for the 80-hr orbit injection is from 2497 to 2490 m/sec. Direct ascent from a lunar landing base is possible for bases over a wide range of the lunar surface if sufficient propellant is available.

Define an angle η measured from the moon-earth direction on the far side of the moon, positive in the direction of the moon's angular rotation, $\vec{\omega}_{\ell}$. From Fig. 20a it can be seen that, in the region of most probable landing sites in the MOP given by $-180° < \eta < -100°$, the required flight path angle is close to 90°, i.e., the ascent trajectory must be nearly vertical. For this reason, the vertical trajectory analysis of Subsection B-1c is again useful as a closed-form approximate solution. Under the assumptions of constant gravity $g_{\ell 0}$, constant mass flow rate $\dot{M}$, and constant exhaust velocity V_{ex}, Eqs (3) and (4) apply in the case of vertical ascent, except that the signs of all velocities (V_0 and V_1) should be reversed if vehicle speed is to be measured positive upward. These equations, evaluated for the initial conditions,

$$t = 0: \; h_0 = 0, \; V_0 = 0$$

give the following burnout conditions:

$$\frac{V_{B0}}{V_{ex}} = - \left[\ln (1 - \zeta) + \frac{g_{\ell 0}}{g_{\oplus 0}} \frac{\zeta}{T/W_0} \right] \quad (47)$$

$$\frac{h_{B0} \, g_{\oplus 0}}{V_{ex}^2} = \frac{1}{T/W_0} \left[(1 - \zeta) \ln (1 - \zeta) + \zeta - \frac{1}{2} \frac{g_{\ell 0}}{g_{\oplus 0}} \frac{\zeta^2}{T/W_0} \right] \quad (48)$$

Equation (47) has the same form as Eq (5), so that Fig. (4) gives $\frac{V_{B0}}{V_{ex}}$ for vertical ascent as well as $\frac{V_0}{V_{ex}}$ for vertical descent.

2. Indirect Ascent

a. Ascent technique

The ascent technique which will be investigated as being most typical is analogous to the descent technique discussed in Subsection B-2a.

(1) The term "ascent phase" will be ascribed to the initial powered liftoff portion of ascent.

(2) Following the initial powered phase, the space vehicle coasts in an elliptical orbit to a desired parking orbit altitude.

(3) The vehicle is injected into the parking orbit.

(4) For the shuttle concept, the shuttle vehicle (LM) executes a rendezvous with the orbiting module (MOM).

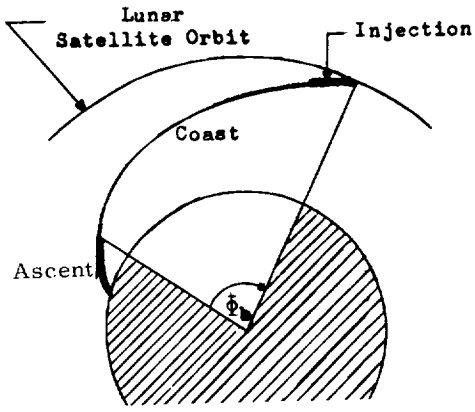

These phases are considered below.

b. Indirect ascent trajectories and requirements

Several sample trajectories for ascent to a 185.2-km circular orbit are shown in Figs. 21 through 25. These figures show range; velocity, V; flight path angle with respect to local horizontal, γ; and pitch angle with respect to inertial coordinates, θ_t, on the abscissa scales corresponding to altitude or flight time on the ordinates. The pitch program for these runs was based on a nominally constant pitch rate, $\dot{\theta}$ = const. Propulsion system and trajectory parameters for these sample ascents are given in the following table. Ascent range, as indicated in the previous sketch, is the lunar central angle between initial liftoff and orbit injection burnout.

Sample Ascent Trajectories
(initial phase only)

Figure No.	$\frac{T}{W_0}$	Ascent Burnout Range Altitude Φ_b (deg)	h_{BO} (km)	I_{sp}, (sec)
21	0.2	180	15.24	315
22	0.39741	60	36.58	315
23	0.39741	180	21.34	315
24	0.7	60	18.29	315
25	0.99138	180	15.24	315

Figure 26 shows a typical complete ascent trajectory.

The total velocity increment required for ascent and injection into a 185.2-km circular orbit is shown as a function of initial thrust-to-weight ratio for several range angles in Fig. 27. These curves are based on a parametric computer study utilizing approximately constant pitch rates. The improvement in fuel economy of this type of program over a gravity turn trajectory is indicated by a gravity turn data point on Fig. 27. For the particular conditions of the run (I_{sp} = 315 sec, Φ_b = 75°, $\frac{T}{W_0}$ = 0.4) the gravity turn trajectory was less efficient by about 30 m/sec.

Although, as indicated by Fig. 27, the gravity turn is not a particularly efficient pitch program, it is one of the basic types of ascent trajectories and deserves some mention. Reference 20 presents an analysis of this type of trajectory. A gravity turn is one in which the thrust is always maintained parallel to the vehicle velocity vector. (The special case of vertical descent, i.e., both thrust and vehicle velocity in the vertical direction during flight, was solved analytically in Subsection B-1c.) This type of trajectory is particularly useful for planetary ascents since it keeps the aerodynamic moments low during ascent in the denser parts of planetary atmospheres. The equation of motion for a gravity turn is the same as Eq (2) for one-dimensional descent, except that vector notation must be used to allow for two-dimensional motion:

$$M \frac{d\vec{V}}{dt} = \vec{T} - M g_\ell \hat{k} \tag{49}$$

where

M = instantaneous vehicle mass

$\vec{V}$ = vehicle velocity vector

$\vec{T}$ = thrust vector

$\hat{k}$ = unit vector normal to lunar surface

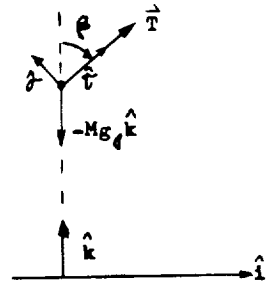

From the definition of the gravity turn,

$$\vec{T} = T \hat{\tau}$$

where the unit vector $\hat{\tau} = \frac{\vec{V}}{V}$.

With resolution of the equation of motion along $\hat{\tau}$ and $\hat{\sigma}$, a unit vector normal to $\hat{\tau}$ in the plane of motion, Eq (49) becomes, in component form

$$\frac{dV}{dt} = g_\ell \left(\frac{T}{W} - \cos \beta\right)$$
$$V\dot{\beta} = g_\ell \sin \beta \tag{50}$$

where β = thrust orientation angle with respect to vertical.

For constant g_ℓ, say $g_{\ell 0}$, and constant $\frac{T}{W}$ these equations can be integrated in closed form.

$$V = V_0 \frac{\left(\tan\frac{\beta}{2}\right)^{\left(\frac{T}{W}-1\right)}\left(1+\tan^2\frac{\beta}{2}\right)}{\left(\tan\frac{\beta_0}{2}\right)^{\left(\frac{T}{W}-1\right)}\left(1+\tan^2\frac{\beta_0}{2}\right)} \qquad (51)$$

$$\frac{\dot{M}}{M_0}t = \frac{V_0}{V_{ex}}\left(\frac{T}{W}\right) \frac{\left(\tan\frac{\beta}{2}\right)^{\left(\frac{T}{W}-1\right)}\left[\frac{1}{\frac{T}{W}-1}+\frac{\tan^2\frac{\beta}{2}}{\frac{T}{W}+1}\right]}{\left(\tan\frac{\beta_0}{2}\right)^{\left(\frac{T}{W}-1\right)}\left(1+\tan^2\frac{\beta_0}{2}\right)} \qquad (52)$$

However, this analytic solution is not as useful as that obtained for vertical descent (Subsection B-1c.). Reference 15 outlines a numerical solution to Eq (50) for the following conditions:

(1) Constant g_ℓ and T

(2) Constant mass flow rate $\dot{M}$

(3) The initial velocity is zero, and the trajectory is initially vertical.

The solution proceeds as follows:

$$u(\tau) = -\frac{T}{W_0}\ln(1-\tau)\dot{} + \int_0^\tau \psi(s)\,ds \qquad (53)$$

$$\tan\frac{\beta}{2} = \left(\frac{1+\psi}{1-\psi}\right)^{\frac{1}{2}} \qquad (54)$$

where

$$\psi(\tau) = \tanh\left[\int_\tau^1 \frac{ds}{\frac{T}{W_0}\ln(1-s) - \int_0^s \psi(s')\,ds'} - k\right]$$

(Solved by iteration)

$$u = \frac{V\frac{T}{W_0}}{V_{ex}}$$

$$\tau = \frac{\dot{M}}{M_0}t$$

c. Lunar rendezvous

A mission employing the shuttle concept requires that the shuttle be able to rendezvous with an orbiting module (MOM) in lunar orbit. In many ways, this rendezvous is easier to perform than an earth orbit rendezvous. Lunar orbit speed is much lower than earth orbit speed, and the ratio of lunar orbit period to lunar rotation rate is very favorable with regard to launch frequency. The more difficult aspects of the lunar orbit rendezvous are associated with the unfamiliar topography, the lack of ground facilities for tracking the orbiting vehicle, and the planning of the ascent guidance commands.

The rendezvous maneuver can be conveniently considered as consisting of three phases, the ascent phase, closing phase and docking phase. During the ascent phase the target vehicle (MOM) is acquired electronically or optically by the intercepting shuttle vehicle. The second phase includes the closing trajectory from acquisition to the vicinity of the target vehicle, where the third phase, docking, takes place.

The ascent phase must be considered in the problem of orbital rendezvous because it is in this phase that the timing problem of hitting the target is solved. A shuttle vehicle on the lunar surface (rotating with a period of about 28 days) must be launched with the objective of intercepting the target vehicle, which is orbiting with a period of about two hours. The ascent phase can accomplish the interception objective by either of two basic approaches, direct rendezvous or indirect rendezvous. The indirect rendezvous is illustrated and fully discussed in Chapter V. The shuttle vehicle is launched into an intermediate parking orbit without considering the position of the target vehicle in its orbit at launch time. The intermediate parking orbit and target orbit are coplanar but have different altitudes and, therefore, different orbital periods. Because of the period difference, the relative angular position of the two vehicles changes with time. When the proper relative position is achieved, the shuttle vehicle is accelerated into a transfer orbit which terminates in the vicinity of the target vehicle, where final acquisition can be made. Thus, the timing problem is solved with the shuttle in orbit.

The direct rendezvous technique is also fully discussed in Chapter V. Here, the shuttle vehicle is not launched until the relative position of the launch site and the orbiting vehicle is that required for direct ascent and acquisition. The timing problem is solved on the ground before launch in the case of direct rendezvous.

At only two times in every 28 days can the shuttle be launched into an intercept trajectory which is optimum from the standpoint of propellant consumption. Therefore, the shuttle must have more than the optimum amount of propellant in order to widen the launch time tolerance. Important considerations in allocating this fuel surplus are the desired launch-time tolerance, target orbital altitude and inclination, and the time available for rendezvous.

Two means of increasing the launch-time tolerance are available. These means, range extension and trajectory shaping, are discussed in detail in Chapter V. With range extension, the ascent trajectory reaches its apogee at the target orbit altitude, as in the optimum ascent case, but the ascent range is varied as a function of time to provide launch time tolerance. Direct ascent rendezvous timing involves matching the interception point of the ascent trajectory and the target orbit with the target vehicle (MOM) itself. The amount of launch time tolerance to be gained by range extension can be determined by comparing the motion of the interception point and the target and making them coincide.

The second means of increasing the launch time tolerance is by trajectory shaping (see Chapter V). If a nominal ascent is taken to be one in which the shuttle arrives at the parking orbit altitude with zero flight path angle, then launch-time tolerance can be obtained by flying an ascent trajectory that would pass through the target point with a nonzero positive or negative flight path angle. Such a flight path, of course, would require correction to zero flight path angle at orbit altitude. Ascents resulting in a positive flight path angle at intercept permit "launch late" launch time tolerance. When the ascent trajectory includes an apocynthion, time is lost in transfer, and "launch early" time tolerance is provided. Figure 28 shows the lunar launch time tolerance available from trajectory shaping. Figure 29 shows the total excess velocity requirement for increasing launch time tolerance by range extension and trajectory shaping for sample out-of-plane launches.

Launch tolerances for missions that do not entail the shuttle concept are essentially unlimited. From Chapter IX it is seen that a return to earth can be made in any transearth trajectory plane and the return is completely independent of the launch time. This and the fact that there are no launch azimuth restrictions result in the ability of launch at any time.

The second phase, the closing phase, may be accomplished in various ways, including tail chase, inverse tail chase, and lateral rendezvous techniques. In the tail chase, the shuttle overtakes the MOM from behind. The shuttle must travel at a speed greater than the circular orbit speed of the target and so will gain altitude during closing. Therefore, the closing phase for the tail chase method must begin behind and below the targets. In the inverse tail chase, the target (MOM) overtakes the intercepting shuttle, which must be placed ahead of and above the target. The tail chase and inverse tail chase are shown in Fig. 30. Lateral rendezvous, shown in Fig. 31, involves placing the shuttle in an orbit at the same altitude as the target orbit. The two orbits cross after a certain time to permit rendezvous.

Each of the techniques has its advantages and disadvantages. The tail chase permits radar sensing from the shuttle vehicle without lunar surface background, but requires excess fuel to catch up to the target. The inverse tail chase is relatively economical, but the lunar surface may provide an undesirable radar background to the target during acquisition. Both direct and inverse tail chases involve curved flight paths which make line-of-sight steering difficult. The lateral rendezvous approach does not entail any problems of surface background, and cross-coupling between velocity and altitude does complicate steering so much as in the other techniques. The lateral approach ranks between the two tail-chase techniques in economy.

After the closing phase, with the shuttle in the same orbit as the MOM with approximately 10 meters separation, the docking phase will complete the rendezvous. If the only reason for rendezvous is to permit refueling, docking may involve either structural mating of the two vehicles or simply use of a probe and drogue. On the other hand, if crew or supplies must be interchanged, then structural mating, seals and air locks are necessary. Precise attitude and translation control will be required on the "seeker" vehicle, and, at the minimum, the target vehicle (MOM) must be attitude-stabilized. Attitude control of the MOM may be necessary if there is a possibility of a large discrepancy in attitude between the two vehicles. In order that damaging impacts be precluded, closure rate should be reduced to zero when the vehicles are some distance apart. A docking mast could then be extended from one vehicle to engage a receptacle on the other vehicle and thus serve to pull the two vehicles together at a closely controlled rate.

Rendezvous has not been discussed in great detail, since there is essentially little difference in philosophy between lunar orbit rendezvous and earth orbit rendezvous, which has been considered extensively in the literature, e.g., Ref. 21 and Chapter VII of Ref. 1. There are only quantitative differences due to the weaker gravitational field and smaller radius of the moon. These differences will tend to make lunar orbit rendezvous easier than earth orbit rendezvous at the same altitude. Circular orbit speeds involved in lunar rendezvous closures are on the order of 2 km/sec as against 8.5 km/sec for low altitude earth orbit rendezvous. A typical lunar orbit rendezvous is shown in Fig. 32.

d. Guidance laws

While a wide variety of guidance laws are applicable to the problem of ascent from the lunar surface, only one will be singled out as an example. The law selected is that described in Subsection B-2d in connection with the descent braking trajectories. This law is equally applicable to the case of indirect ascent and, in fact, has been used to generate the thrust orientation program for the trajectories plotted in Figs. 21 through 26.

D. HOVERING AND TRANSLATION REQUIREMENTS

Most manned lunar landings will require the capability to hover above the landing site while final observations of the site are made. These observations will primarily concern the suitability of landing site terrain. Because the area immediately beneath the hovering vehicle (LM) might prove unfavorable (due to uneven rocks, large crevices or deep dust deposits, for example), the landing

module (LM) should be capable of translating, i.e., maneuvering laterally, during the final descent phase. This subsection considers propellant requirements and optimum conditions for hovering and translation.

Since hovering altitude and translation range are very small compared to the lunar radius R_{ℓ}, and since propellant weight required in this phase is small compared to vehicle weight, very good analytic approximate solutions of the equations of motion may be obtained. The case of constant vehicle acceleration and the case of constant thrust with constant propellant flow rate will be investigated. For convenience the analyses consider vertical and horizontal motion separately. Therefore, the results can be used directly if hovering and translation are accomplished by separate orthogonal rocket engines. However, if the required thrust orientation is obtained by gimbaling a single engine or by pitching the entire vehicle, the thrust, position, and velocity as computed should be interpreted as components of the resultant vector quantity.

1. Constant Acceleration

Although motion under constant thrust with constant flow rate is generally a more realistic basis for propulsion analysis, the small mass ratios required for hovering and the extreme simplicity ot analysis make the case of constant acceleration useful for preliminary investigations. Let the landing vehicle (LM) be required to translate with uniform acceleration and deceleration while hovering at constant altitude. The local $x_{\ell}\, y_{\ell}$ coordinate system can then be assumed an inertial system, and the total horizontal translation denoted by $x_{\ell t}$ can be obtained from the familiar expression for rectilinear motion,

$$x_{\ell t} = \left[\frac{1}{2} \frac{T_x}{M} \left(\frac{t_b}{2} \right)^2 \right] 2 = \frac{T_x}{M} \frac{t_b^2}{4} \tag{55}$$

where

$\frac{T_x}{M}$ = constant horizontal thrust acceleration

t_b = total hovering time (i.e., horizontal rocket burning time)

The constant thrust required is

$$T_x = \frac{4 x_{\ell t} W}{g_{\oplus 0} t_b^2}, \tag{56}$$

where $W = g_{\oplus 0} M$ is the constant vehicle weight.

Since $T_x = I_{sp} \dot{W}_{fx}$ and $W_{fx} = \dot{W}_{fx} t_b$, Eq 56 becomes

$$W_{fx} = \frac{4 x_{\ell t} W}{g_{\oplus 0} I_{sp} t_b}. \tag{57}$$

W_{fx} is the total fuel weight lost due to burning of the horizontal translation engine and $\dot{W}_{fx}$ is the fuel weight flow rate $\dot{W}_{fx} = \dot{M}_{fx} g_{\oplus 0}$.

The weight of the propellant required to hold the vehicle at constant altitude during translation, W_{fy}, is seen from

$$T_y \equiv I_{sp} \dot{W}_{fy} = M g_{\ell 0} \tag{58}$$

to be

$$W_y = \dot{W}_{fy} t_b = \frac{W g_{\ell 0} t_b}{g_{\oplus 0} I_{sp}} \tag{59}$$

The total propellant used for hovering and translation is

$$W_f = W_{fx} + W_{fy} = \frac{W}{g_{\oplus 0} I_{sp}} \cdot \left[\frac{4 x_{\ell t}}{t_b} + g_{\ell 0} t_b \right] \tag{60}$$

For minimum total fuel, to translate a given distance $x_{\ell t}$,

$$\frac{dW_f}{dt_b} = \frac{W}{g_{\oplus 0} I_{sp}} \left[- \frac{4 x_{\ell t}}{t^2} + g_{\ell 0} \right] = 0, \tag{61}$$

or

$$\left.\begin{aligned} t_b &= 2 \sqrt{\frac{x_{\ell t}}{g_{\ell 0}}} \\ T_x &= T_y = W \frac{g_{\ell 0}}{g_{\oplus 0}} \\ \frac{W_f}{W} &= \frac{4 \sqrt{x_{\ell t} g_{\ell 0}}}{g_{\oplus 0} I_{sp}}. \end{aligned}\right\} \text{ for minimum } W_f \tag{62}$$

2. Constant Thrust

a. Translation

It is possible to derive simple analytic solutions to the equation of translatory motion under the assumptions of constant thrust and constant mass flow rate. This case is much more realistic than that of constant acceleration previously considered. The equation of motion is

$$M \frac{d^2 x_{\ell}}{dt^2} = T_x \tag{63}$$

where

M = instantaneous total vehicle mass

x_{ℓ} = horizontal translation

T_x = constant thrust component in the horizontal (x_{ℓ}) direction

The thrust program selected is the simplest possible. A constant thrust T_x is applied for approximately half the burning time, at which point the thrust is reversed to decelerate the LM to zero horizontal velocity when the desired translation distance has been traversed. Velocity at the beginning of the translation will be assumed zero. Thus, this constant thrust routine is analogous to the constant acceleration scheme previously outlined. The time of thrust reversal, t_1, obviously will not be half the burning time, t_b, because the vehicle will be lighter during the deceleration phase than in the acceleration phase due to the weight of propellant expended during translation.

The equation of motion may be rewritten:

$$\ddot{x}_\ell = \frac{\frac{T_x}{M_0}}{1 - \frac{\dot{M}}{M_0} t} \tag{64}$$

where

M_0 = initial total vehicle mass

$\dot{M}$ = total constant mass flow rate (including any flow from vertical hovering rockets during the translation)

The first integration of this equation gives the expression for the horizontal velocity of the LM at any time during the acceleration phase:

$$\dot{x}_\ell = -\frac{T_x}{\dot{M}} \ln \left(1 - \frac{\dot{M}}{M_0} t\right) + \dot{x}_{\ell 0}; \quad \dot{x}_{\ell 0} = 0 \tag{65}$$

The second integration and evaluation of the constant of integration for the initial condition $x_\ell = 0$ at $t = 0$ gives the relation for horizontal position. In particular, at an arbitrary time t_1, the horizontal position and velocity components are as follows:

$$x_{\ell 1} = \frac{T_x M_0}{\dot{M}^2} \left[(1 - \zeta_1) \ln (1 - \zeta_1) + \zeta_1\right]$$

$$\dot{x}_{\ell 1} = -\frac{T_x}{\dot{M}} \ln (1 - \zeta_1) \tag{66}$$

where $\zeta_1 = \frac{\dot{M}}{M_0} t_1$ is the mass ratio for rocket burning from t_0 to t_1.

At this time the thrust is reversed, i.e., the vehicle obeys the equation of motion

$$\ddot{x}_\ell = -\frac{\frac{T_x}{M_0'}}{1 - \frac{\dot{M}}{M_0'} t} \tag{67}$$

where $M_0' = M_0 - \dot{M} t_1$ is the total vehicle mass at beginning of the deceleration phase.

Successive integration of this equation and evaluation of the constants of integration for the initial conditions of the deceleration phase, $x_\ell = x_{\ell 1}$ and $\dot{x}_\ell = \dot{x}_{\ell 1}$ at $t = t_1$, determine the position from the start of the translation and the velocity at any time during this phase.

$$\dot{x}_\ell = \frac{T_x}{\dot{M}} \ln \left(1 - \frac{\dot{M}}{M_0'} t\right) - \frac{T_x}{\dot{M}} \ln \left(1 - \frac{\dot{M}}{M_0'} t_1\right) + \dot{x}_{\ell 1}$$

$$x_\ell = \frac{T_x}{\dot{M}} \left[-\frac{M_0'}{\dot{M}} \left(1 - \frac{\dot{M}}{M_0'} t\right)\left\{\ln \left(1 - \frac{\dot{M}}{M_0'} t\right) - 1\right\}\right.$$

$$+ (t_1 - t) \ln \left\{\left(1 - \frac{\dot{M}}{M_0'} t_1\right) \cdot \left(1 - \frac{\dot{M}}{M_0} t_1\right)\right\}$$

$$+ \frac{M_0}{\dot{M}} \left(1 - \frac{\dot{M}}{M_0} t_1\right) \ln \left(1 - \frac{\dot{M}}{M_0} t_1\right) + t_1$$

$$\left. + \frac{M_0'}{\dot{M}} \left(1 - \frac{\dot{M}}{M_0'} t_1\right)\left\{\ln \left(1 - \frac{\dot{M}}{M_0'} t_1\right) - 1\right\}\right] \tag{68}$$

The rather formidable position equation simplifies considerably on evaluation at the end point $t = t_b$; $x_\ell = x_{\ell t}$, $\dot{x}_\ell = 0$. The velocity equation gives, for $\dot{x}_\ell = 0$ at $t = t_b$,

$$0 = \frac{T_x}{\dot{M}} \ln \left[\frac{1 - \frac{\dot{M}}{M_0'} t_b}{\left(1 - \frac{\dot{M}}{M_0'} t_1\right)\left(1 - \frac{\dot{M}}{M_0} t_1\right)}\right] \tag{69}$$

which provides a simple relation between total burning time and the thrust reversal time.

$$t_b = 2t_1 \left(1 - \frac{\dot{M}}{M_0} t_1\right) = 2 \frac{M_0'}{M_0} t_1 \tag{70}$$

Substitution of this relation in the position equation gives, in terms of mass ratio

$$x_{\ell t} = \frac{T_x M_0}{\dot{M}^2} \left[-(1 - \zeta_1)(1 - 2\zeta_1)\right.$$

$$\left\{ \ln (1 - 2\,\zeta_1) - 1 \right\}$$

$$- \zeta_1 (1 - 2\,\zeta_1) \ln (1 - 2\,\zeta_1)$$

$$+ (1 - \zeta_1) \ln (1 - \zeta_1) + \zeta_1$$

$$+ (1 - 2\,\zeta_1) \left\{ \ln (1 - 2\,\zeta_1) - \ln (1 - \zeta_1) - 1 \right\} \Bigg] \qquad (71)$$

which reduces to

$$x_{\ell t} = \frac{T_x}{\dot{M}}\, t_1 \left[\ln (1 - \zeta_1) + 2\,\zeta_1 \right]$$

$$\text{where } t_1 = \frac{1 - \sqrt{1 - 2\,\frac{\dot{M}}{M_0}\, t_b}}{2\,\frac{\dot{M}}{M_0}}$$

Mass ratios for hovering and translation generally should be less than $\zeta = 0.01$. For such small mass ratios the previous expression for translational distance can be approximated by:

$$x_{\ell t} \approx \frac{T_x}{M_0}\,\frac{t_b^2}{4} \left(1 + \frac{1}{4}\,\frac{\dot{M}}{M_0}\, t_b\right), \quad 1 >> \left(\frac{\dot{M}}{M_0}\, t_b\right)^2 \qquad (72)$$

This solution obviously approaches that for constant acceleration (or constant mass with constant thrust since acceleration $= \frac{T_x}{M}$) as $\dot{M}$ approaches zero. Translational distance is plotted as a function of initial thrust-to-weight ratio and burning time in Fig. 33.

b. Vertical descent from hover

If the LM is to descend and reach zero altitude at the end of the translation time, t_b, the vertical component of motion is described by the following equation.

$$M\,\frac{d^2 y_\ell}{dt^2} = T_y - M\, g_{\ell 0} \qquad (73)$$

or

$$\frac{d^2 y_\ell}{dt^2} = \frac{\frac{T_y}{M_0}}{1 - \frac{\dot{M}}{M_0}\, t} - g_{\ell 0} \qquad (74)$$

where

y_ℓ = altitude above the lunar surface

T_y = vertical component of thrust

$\dot{M}$ = total mass flow rate (including any flow from horizontal rockets).

With the assumptions of constant thrust T_y, constant mass flow rate, $\dot{M}$, and constant lunar gravity $g_{\ell 0}$, this equation can be integrated as in Subsection B-1c. However, in the case of final descent from hover, the initial conditions are $\dot{y}_\ell = 0$ and $y_\ell = y_{\ell 0}$ at $t = 0$. For this case, integration of the above equation of motion gives:

$$\dot{y}_\ell = -\frac{T_y}{\dot{M}} \ln \left(1 - \frac{\dot{M}}{M_0}\, t\right) - g_{\ell 0} t$$

$$y_\ell = \frac{T_y}{\dot{M}^2}\,\frac{M_0}{\dot{M}} \left[\left(1 - \frac{\dot{M}}{M_0}\, t\right) \ln \left(1 - \frac{\dot{M}}{M_0}\, t\right) + \frac{\dot{M}}{M_0}\, t \right] - \frac{g_{\ell 0}\, t^2}{2} + y_{\ell 0} \qquad (75)$$

For $\dot{y}_\ell = 0$, $y_e = 0$ at $t = t_b$, these equations give

$$t_b = -\frac{T_y}{g_{\ell 0} \dot{M}} \ln (1 - \zeta) \qquad (76)$$

$$y_{\ell 0} = -\frac{T_y}{\dot{M}}\, t_b \left[\left(\frac{1}{\zeta} - 1\right) \ln (1 - \zeta) + 1 \right] + \frac{g_{\ell 0} t_b^2}{2} \qquad (77)$$

where $\zeta = \frac{\dot{M}\, t_b}{M_0}$ is the total mass ratio. Substitution of the first equation for T_y in the second equation provides the relation

$$y_{\ell 0} = g_{\ell 0} t_b^2 \left[\frac{1}{\zeta} - \frac{1}{2} + \frac{1}{\ln (1 - \zeta)} \right] \qquad (78)$$

For small mass ratios, as will generally be the case for the final phase of descent, the following approximation is convenient.

$$y_{\ell 0} \approx \frac{g_{\ell 0} t_b^2}{12}\, \zeta \left(1 + \frac{\zeta}{2}\right), \quad 1 >> \zeta^2 \qquad (78a)$$

c. Hovering

Hovering precisely at a chosen altitude obviously requires variable vertical thrust,

$$T_y = M\, g_{\ell 0} = M_0\, g_{\ell 0} \left(1 - \frac{\dot{M}}{M_0}\, t\right).$$

If a constant thrust $T_y = M_a\, g_{\ell 0}$ were applied, the solution of the equation of motion with initial conditions $y_\ell = y_{\ell\,0}$, $\dot{y}_\ell = 0$ at $t = 0$ does not permit the constraints $\dot{y}_\ell\ (t_b) = 0$ or $y_\ell\ (t_b) - y_\ell\ (0) = 0$ except for the theoretical limit $t_b = \zeta = 0$. However, with choice of a slightly lower constant thrust level, the condition $\dot{y}_\ell\ (t_b) = 0$ can be achieved. From Eq (75) for the given initial conditions,

$$\dot{y}_{\ell t} = -\frac{T_y}{\dot{M}} \ln \left(1 - \frac{\dot{M}}{M_0}\, t_b\right) - g_{\ell 0} t_b$$

$$y_{\ell t} - y_{\ell 0} = \frac{T_y M_0}{\dot{M}^2}\left[\left(1 - \frac{\dot{M}}{M_0} t_b\right) \ln\left(1 - \frac{\dot{M}}{M_0} t_b\right) + \frac{\dot{M}}{M_0} t_b\right] - \frac{g_{\ell 0} t_b^2}{2} \quad (79)$$

where the subscript t signifies a value at time t_b. For small mass ratios the first equation gives

$$\dot{y}_{\ell t} \approx t_b\left[\frac{T_y}{M_0}\left(1 + \frac{1}{2}\zeta\right) - g_{\ell 0}\right], \quad 1 >> \zeta^2 \quad (80)$$

so that the end constraint $\dot{y}_{\ell t} = 0$ is possible if the constant thrust is selected such that

$$T_y \approx M_0 g_{\ell 0}\left(1 - \frac{\zeta}{2}\right) \quad (81)$$

Substitution of this value in the second equation of (46) determines the change in altitude during the "hover,"

$$y_{\ell 0} - y_{\ell t} \approx \frac{1}{12} g_{\ell 0} t_b^2 \zeta, \quad 1 >> \zeta^2 \quad (82)$$

d. Simultaneous translation and hovering or descent

If the vertical and horizontal components of thrust are provided by separate engines, the solutions of Subsections D-2a through D-2c apply directly for simultaneous translation and hovering or descent. For touchdown at the same instant as the required translation is completed, the simultaneous equations are, from Eqs (43) and (45) and $\dot{M} = \dot{M}_x + \dot{M}_y$

$$x_{\ell t} \simeq \frac{\zeta V_{ex} t_b}{4} - \frac{g_{\ell 0} t_b^2}{4} + \frac{1}{16} g_{\ell 0} \zeta t_b^2 + \frac{1}{16} \zeta^2 V_{ex} t_b \quad (83)$$

$$y_{\ell 0} \simeq \frac{g_{\ell 0} t_b^2}{12} \zeta \left(1 + \frac{\zeta}{2}\right) \quad (84)$$

where V_{ex} = exhaust velocity of each engine. For given mission requirements $x_{\ell t}$ and $y_{\ell 0}$, the required values of ζ and t_b are determined by these equations. No optimization is possible since the problem is completely determined. In the case of simultaneous translation and hovering with constant thrust components, only the first of the two previous equations is a condition. Therefore, a value of t_b can be selected which optimizes the mass ratio $\zeta = \frac{W_f}{W_0}$. Values of ζ and t_b selected in this way then determine the change in altitude which must be accepted,

$$y_{\ell 0} - y_{\ell t} \approx \frac{1}{12} g_{\ell 0} t_b^2 \zeta. \quad (85)$$

Conditions for minimum ζ, ζ_m, are obtained by setting

$$\frac{d\zeta}{dt_b} = 0 \quad (86)$$

in the equation resulting from differentiating Eq (83) with respect to ζ. The results are:

$x_{\ell t} \approx x_{\ell t}(\zeta, t_b)$, are

$$t_b \simeq \frac{\zeta_m V_{ex}}{2g}\left(1 + \frac{\zeta_m}{2}\right)$$

$$x_{\ell t} \simeq \frac{\zeta_m V_{ex} t_b}{4}\left(1 + \frac{1}{4}\zeta_m\right) - \frac{g_{\ell 0} t_b^2}{4}\left(1 - \frac{1}{4}\zeta_m\right)$$

$$y_{\ell 0} - y_{\ell t} \simeq \frac{1}{12} g_{\ell 0} t_b^2 \zeta_m \quad (87)$$

where ζ_m is the minimum ζ.

It can be seen that these expressions approach those derived in the constant acceleration case in the limit as $\zeta \to 0$,

$$\zeta = \frac{2 g_{\ell 0} t_b}{V_{ex}}$$

$$x_{\ell t} = \frac{g_{\ell 0} t_b^2}{4}.$$

These equations demonstrate the utility of Fig. 34 as an accurate approximation for the minimum fuel required to hover and translate simultaneously.

E. LUNAR LANDING ABORT

It is anticipated that the majority of landing missions in the near future will not employ direct (impact) trajectories to the landing site. In the case of manned landings, crew safety is jeopardized by use of direct trajectories, while for reconnaissance flights (manned or unmanned), the lunar areas that can be covered are severely limited. Since most impacting lunar probes have no abort requirements, this section is based on a flight wherein the spacecraft is maneuvered into a circular orbit about the moon from which the landing phase begins. This phase is initiated by a deorbit maneuver, after which the vehicle descends on a landing coast trajectory to a lunar altitude of approximately 18 km, at which point a braking maneuver is initiated. The braking maneuver decelerates the vehicle to hover condition at a low altitude of approximately 600 meters from which translation and final letdown are accomplished.

During the landing phase, it may become imperative to cut short the intended mission and to alter the course of the spacecraft. Typical reasons for such action could be propulsion failures, "unsafe" trajectories, guidance malfunctions, solar flare activity, etc.

In this section various techniques of abort during the landing phase will be discussed, with emphasis on the manned mission; these techniques are similar in most respects to those presented in Refs. 22 and 23. In Technique I the apocynthion altitude of the abort trajectory equals the initial circular orbit; in Technique II the apocynthion altitude of the abort trajectory exceeds the altitude of the initial

circular orbit; and in Technique III the abort trajectory is circular and has an altitude equal to the abort altitude. Each one of the abort techniques above can be performed with or without rendezvous. In addition, abort maneuvers occurring during the final braking and hovering phases will be discussed.

1. Abort with Return to Orbit (Technique I)

a. Abort Technique I without rendezvous

The pertinent orbital relations are illustrated in the following sketch:

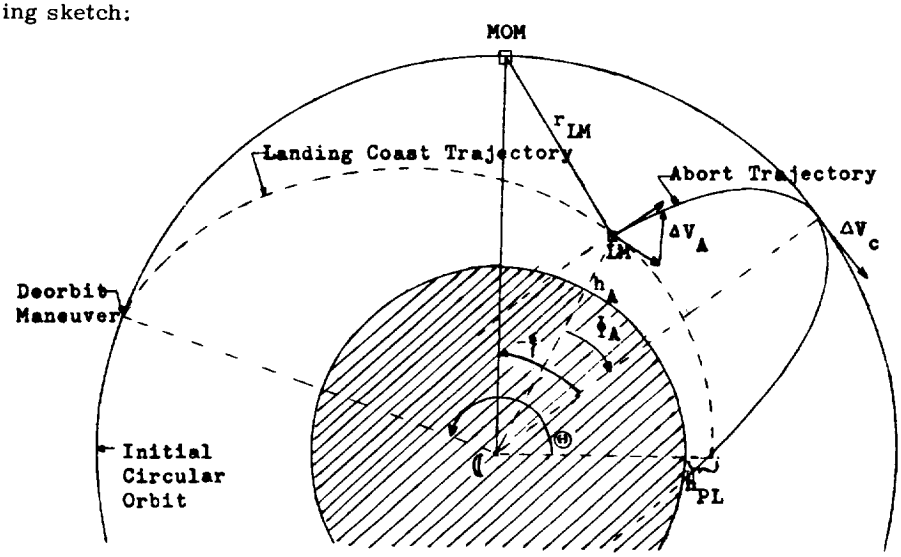

The vehicle is initially in a circular orbit of altitude h_0, and the orbit departure angle Θ is measured from the pericynthion point of the landing coast trajectory to the deorbit point along the circular orbit with origin taken at the center of the moon. A spherical moon is assumed and altitudes are measured with respect to the lunar surface. The abort trajectory has an apocynthion altitude of h_0, and a downrange aim angle (Φ_A) is defined as the central angle between the abort point and the apocynthion of the abort trajectory. All rocket burning is simulated by a velocity impulse ΔV, where ΔV_A is the characteristic velocity impulse required to establish the abort trajectory. Upon arrival at the apocynthion of the abort trajectory, the vehicle is injected back into the circular orbit by a circularizing velocity impulse ΔV_c. Hence, the total velocity impulse required to execute an abort and to inject into a circular orbit is $\Delta V_T = \Delta V_A + \Delta V_c$.

Figure 35 presents ΔV_T versus downrange angle (Φ_A) for three abort altitudes, namely, h_A = 152.4 km, 91.4 km, and 18.3 km, with an initial circular orbit altitude of h_0 = 185.2 km. For this case, the orbit departure angle is Θ = 178° and the pericynthion altitude of the landing coast trajectory is h_{PL} = 18.3 km. Decreasing the orbit departure angle Θ from 178° to 150° (not shown) increases the ΔV_T requirements from 3 to 10 m/sec. This figure shows that there is an optimum downrange angle to "aim" which minimizes the ΔV_T requirements. However, in some cases, where h_{PL} is negative, this aim point must be adjusted to avoid impact with the lunar surface. This physical limitation is indicated on the figure and refers to two types of abort trajectories as shown in the following sketch.

For the case of a type A abort trajectory, the vehicle ascends to the apocynthion after the abort maneuver. If at this time the vehicle fails to inject into the circular orbit, it will descend toward pericynthion, and if this pericynthion is less than some minimum altitude, there will be an impact.

A type B abort trajectory descends through its pericynthion first before attaining the circular orbit altitude. The limitation with this type of trajectory is again that the pericynthion altitude be above the lunar surface.

In the present discussion, an abort trajectory was designated as safe if it attained a pericynthion altitude of no less than 11 km. This choice was based on the moon's topographical characteristics and was taken to avoid lunar mountains with an ample margin of safety.

The restriction of a pericynthion above the lunar surface may be eliminated if the reliability is deemed high enough to assure that an injection into the circular orbit will always take place. It may also be eliminated if design features account for such a contingency. However, for the present, this restriction is not waived. As can be seen from Fig. 35, this restriction on the pericynthion altitude of the types A and B abort trajectories essentially describes a safe abort window which is defined by the angle α as shown in the following sketch. Figure 36 presents α as a function of circular orbit altitudes h_0 for several values of h_A. It

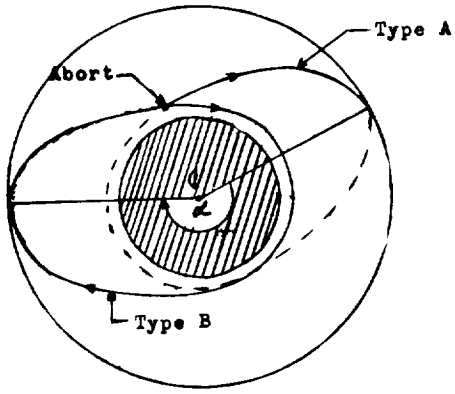

can be seen that α decreases rapidly with abort altitude. But even at low abort altitudes, the window is sufficiently wide ($\alpha \simeq 40°$) to affirm the success of manual or emergency backup control modes. The safe abort window is independent of the other orbital elements of the landing coast trajectory and is a function of the abort altitude and initial circular altitude alone. Active abort procedures as described above may become necessary because of unacceptable coast trajectories, probability of stage explosions, ease of planning the return flight to earth, etc. This abort procedure requires two rocket engine ignitions.

Passive abort procedures require one ignition, and they utilize a landing coast trajectory that returns to or intersects the initial circular orbit altitude where the circularizing maneuver is performed. If the braking phase has begun, an active abort becomes mandatory.

b. Abort Technique I with rendezvous

For the problem of rendezvous (shuttle concept) the vehicle consists of two modules, the landing module (LM) and the lunar orbital module (MOM). At the deorbit point the LM leaves the MOM and establishes a landing coast trajectory while the MOM continues in the original circular orbit (see next sketch). In the event of an abort during descent, the objective of the LM is to establish an abort trajectory whose apocynthion is at the circular orbit. The slant range (r_{LM}) is the distance between the LM (actually the shuttle) and the MOM at the time of abort.

The case for which the abort trajectory allows the LM to arrive coincident with the MOM is defined as a "perfect rendezvous." This, however, may not always be desirable because of velocity impulse requirements and lunar impact restrictions. Thus, the LM can either lead or lag the MOM after reestablishing the original circular orbit

If the LM lags the MOM, a "catch-up" maneuver (gain) is required. For separation angles ξ greater than a certain amount, such maneuvers result in trajectories that impact the moon if performed in one revolution.

Should the LM lead the MOM (a more likely case), a "drop-back" maneuver (loss) is required. The limiting factor for the loss maneuver can arbitrarily be chosen to be the loss of line of sight between the two vehicles. The limiting separation angles are given in Table 1 with the corresponding circular orbit altitude (h_0).

TABLE 1

Permissible Separation Angles (ξ)

h_0 (km)	$+\xi$	$-\xi$	
92.6	14n°	37°	where n is the number of revolutions of the MOM and LM
185.2	26n°	51°	
370.4	47n°	69°	

Performing an indirect rendezvous of this nature requires three rocket engine ignitions. By restricting the number of revolutions of the gain or loss orbits to one, the elapsed time from the maneuver to the closing phase is approximately two hours.

The total velocity impulse required to abort and rendezvous with these maneuvers is shown in Figs. 37, 38, and 39 for initial orbital altitudes of 92.6, 185.2, and 370.4 km, respectively. Each figure presents several abort altitudes for an orbit departure angle of 178°. The pericynthion altitude of the landing coast trajectory is chosen in all cases to be 18.3 km. The figures show that for a 1.0-km increase in h_0, the minimum ΔV increases $\simeq$0.5 m/sec and occurs at downrange aim angles ($\Phi_A > 160°$) greater than those required for perfect rendezvous.

Table 2 presents a comparison of the minimum total ΔV requirements with and without rendezvous considerations. The quantities shown do not include a perfect rendezvous with data for an orbit departure angle $\Theta = 178°$ and a circular orbit altitude $h_0 = 185.2$ km.

TABLE 2

h_{PL} (km)	h_A (km)	ΔV (indirect rendezvous) i.e., with gain or loss maneuvers (m/sec)	ΔV (no rendezvous) (m/sec)
18.3	18.3	105	37
	91.4	100	40
	152.4	70	38

Conditions for a perfect rendezvous are also indicated in Figs. 37, 38 and 39, and it is seen that compared with the minimum ΔV's listed above the ΔV requirements increase significantly by hundreds of meters per second. The required downrange aim angle for perfect rendezvous is less than 95°. Figure 40 presents the velocity requirements for direct rendezvous (i.e., without gain or loss maneuver) as a function of abort altitude and various initial orbital altitudes. Also shown in the figure are the requirements for an orbit departure angle $\Theta = 95°$ for $h_0 = 185.2$ km. This particular departure angle bears significant interest because it provides a passive abort capability (i.e., the LM is allowed to coast to the lunar orbit altitude and an adjustment of the velocity to

circular orbit velocity (ΔV_c) is included) that allows rendezvous to take place in approximately two hours, as explained below.

Consider an initial circular orbit altitude h_0 with the associated period τ_0:

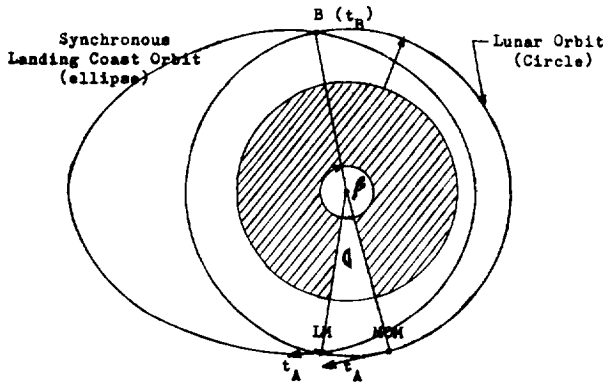

If the landing coast trajectory also has the period τ_0, then the LM will lead the MOM at t_A, but the modules will be coincident at t_B, or when the orbital central angle $\beta = 360°$ at which time the rendezvous maneuver is executed. The impulse requirement for this maneuver at the initial orbital altitude stated above (h_0 = 185.2 km) is 138.5 m/sec. For each initial orbit altitude, there is a departure angle that results in such a synchronous coast trajectory. Other departure angles may require several revolutions, or even days, before coincidence is attained.

The ΔV requirements versus downrange aim angle for an active abort (i.e., when the LM is put on the abort trajectory as soon as possible) from a synchronous orbit are given in Fig. 41. Data is presented for the case mentioned above (h_0 = 185.2 km), and the downrange aim angle required for a perfect rendezvous is indicated. The minimum velocity impulse is approximately 45 m/sec over the impulse required for the 178° orbit departure.

The downrange aim angle necessary for perfect rendezvous is shown in Figs. 42, 43, and 44 as a function of abort altitude for h_0 = 92.6, 185.2, and 370.4 km, respectively. Also included in these figures are the downrange angles that result in a plus and minus 1° separation angle between the LM and MOM when the LM arrives at apocynthion. These figures may be interpreted in several ways. First, assuming that the separation distance ($\approx$ 35 km) is the reasonable limit of the guidance and propulsion capability of the LM for the closing phase, the curves represent an acceptable rendezvous window. This window decreases rapidly as the abort altitude decreases. Secondly, if the position-time history of the MOM is not exactly as planned (for example, if there exists a separation angle of -1°), but the LM abort guidance is accurate, the increase in ΔV requirements may be found. This is accomplished by noting that a decrease in downrange angle (Figs. 42 through 44) is accompanied by an increase in abort velocity impulse (Figs. 37 through 41).

Figures 42 through 44 are presented for orbit departure angles of 178°. Included in Fig. 43, is the departure angle of 95° (synchronous orbit). A decrease of the departure angle results in a rotation of the Φ_A versus h_A curves in Figs. 42 through 44, which lowers the rendezvous window at higher abort altitudes and slightly decreases the window size. A reduction of pericynthion altitude h_{PL} of the coast trajectory (not shown) raises the rendezvous window and increases its size.

Superimposed on Figs. 42, 43 and 44 is the impact restriction for type A abort trajectories. As is noticed, if "safe" abort trajectories are specified, perfect rendezvous at all times is not possible and gain or loss maneuvers have to be performed. These maneuvers increase the rendezvous time by 2 hr. It was found that type B abort trajectories do not affect the rendezvous problem because the downrange angles at which they occur are far removed from those required for perfect rendezvous.

Another important aspect of rendezvous missions is the slant range between the LM and MOM during the landing phase. The maximum slant range occurs at the initiation of the braking phase (to hovering and landing) as shown in Fig. 45. This figure presents the slant range as a function of altitude during the landing coast trajectory for initial circular orbit altitudes of 92.6, 185.2 and 370.4 km. The maximum slant ranges for an orbit departure angle of 178° are 185, 410 and 820 km, respectively. After braking begins, the slant range decreases to values equivalent to the initial circular orbit altitudes, i.e., at some point during the braking or hovering phase MOM is directly overhead.

2. Abort with Return to Orbit and Perfect Lunar Rendezvous (Technique II)

The following sketch illustrates this technique. In this method the abort trajectory is such that its apocynthion altitude exceeds the circular orbit altitude. This allows the MOM to "catch up" while the LM is still in its abort trajectory above the circular orbit altitude, so that both arrive at the same time at the rendezvous point at altitude h_0. Figure 46 presents the total ΔV required to abort and rendezvous from a descent use of a synchronous orbit as a function of time from the deorbit maneuver. The solid curve corresponds to Technique I and the dashed curves to the present method (Technique II) for three values of time from abort to rendezvous. An auxiliary scale in Fig. 13 indicates the abort altitude h_A.

Depending on the time requirements, the savings in ΔV (i.e., fuel savings) by use of Technique II instead of Technique I can be quite large. Table 3 presents the velocity requirements for the two techniques when a perfect rendezvous is considered. The circular orbit altitude h_0 is

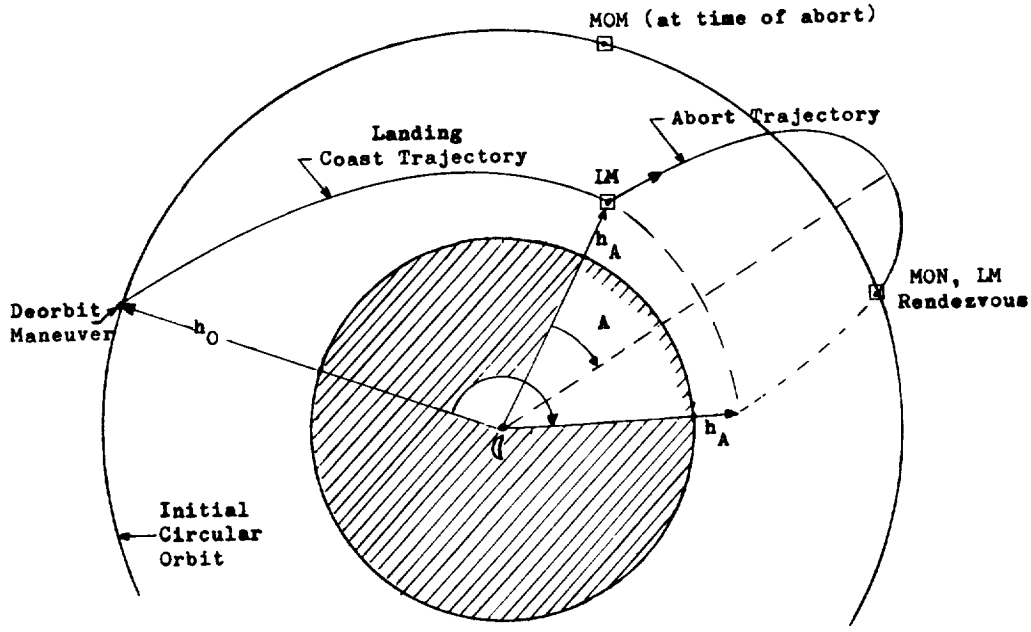

185.2 km, and the orbit departure angle is 95°.

TABLE 3

h_A (km)	Technique I ΔV (m/sec)	Technique II ΔV (m/sec) Time from Abort to Rendezvous 1000 sec	3000 sec	5000 sec
20	1290	960	425	205
30	940	765	390	220
60	595	560	330	210
100	360	390	260	190
160	195	195	170	150

It is seen from Table 3 that for low abort altitudes the velocity requirements using Technique II are significantly smaller. This is due to the fact that larger downrange angles are possible with this method. However, for high abort altitudes, the advantage is not as great and the differences reduce to zero as h_A approaches h_0. In addition, the ΔV requirements for a typical braking phase are included in Fig. 46. It is seen that during the braking phase, the fuel savings of Technique II diminish. The maximum propulsion requirement (≃ 1750 m/sec) for abort occurs, as is expected, at the end of braking.

3. Circular Abort Trajectory (Technique III)

This type of abort is pictured in the sketch at the right. If an abort becomes necessary during the landing coast trajectory, another alternative to the two previously discussed techniques is to establish a circular orbit at the abort altitude and leave the LM in this orbit for an indefinite time.

This abort technique is attractive for non-rendezvous missions and for missions that require establishment of very low circular orbits about the moon. Table 4 gives the ΔV requirements for orbit departure angles of 178° and 95° as well as the ΔV required for passive aborts. Passive aborts return to the initial circular altitude of 185.2 km and include the adjustment of the velocity to the circular orbit velocity. Impulse requirements may be either larger or smaller than the passive maneuver, depending on the orbit departure angle (Θ).

TABLE 4

h_0 = 185.2 km, h_{PL} = 18.3 km

h_A (km)	ΔV, Θ = 178° (m/sec) Passive	Active	ΔV, Θ = 95° (m/sec) Passive	Active
152.4	36.6	61.9	138.5	138.4
121.92	36.6	72.1	138.5	133.7
91.44	36.6	74.1	138.5	125.4
60.96	36.6	67	138.5	108.8
30.48	36.6	50	138.5	85.2

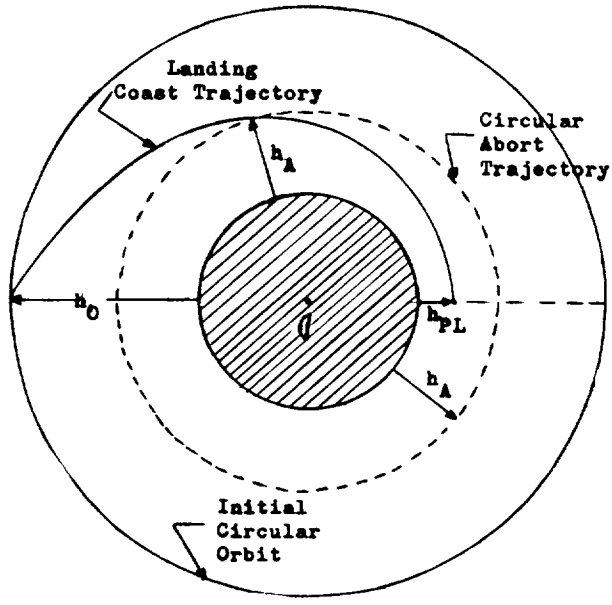

4. Abort During the Hovering Phase

Final letdown to the lunar surface requires that the landing module possess a rate of descent appropriate to the type of landing, whether for soft or hard landings. For soft landings, which are considered in this section, the most crucial stage of the letdown maneuver occurs within 30 meters of the lunar surface. If an abort becomes necessary during this time, important considerations are the abort thrust-to-weight ratio, the reaction time and the design structural limit of the LM.

The objective of the abort during this phase is to establish a positive rate of climb before impact with the lunar surface, or to ensure that a touchdown on the surface will be within mission design limits.

The landing safety boundaries are illustrated for a typical abort thrust-to-weight ratio of $\frac{T}{W_0} = 0.422$. It is assumed that the delay time to ignite the abort engines or increase engine thrust to the desired emergency value is one second. During this reaction interval, the LM is assumed to descend ballistically ($\frac{T}{W_0} = 0$) from an initial altitude and an initial rate of descent. Figure 47 gives a safety boundary for the case that impacts without use of emergency thrust and for the conditions stated above. If the initial conditions of the LM are to the left of the boundary, the module can recover before impact and initiate an ascent back to orbit. To the right, impact cannot be avoided. Included in the figure is an arbitrary impact structural limit of $6\, g_{\oplus,0}$ (with shock absorbers) based on free fall ($\frac{T}{W_0} = 0$). Initial conditions to the right of this limit are structurally unsafe for free fall to the surface.

Also included in the figure is a typical descent as executed by an automatic landing system. As long as the descent is to the left of the boundaries, the letdown is continued in a normal fashion. However, if the altitude is greater than 11 meters and the descent reaches the safety limit, abort propulsion is initiated followed by an ascent to orbit. When the altitude is less than 11 meters, the main landing propulsion is terminated at the limit and the module drops in. It is further assumed that the horizontal component of velocity is within the stability margin of the LM while it is below 11 meters of altitude.

5. Lunar Surface Abort

After completion of a lunar landing, the module will remain on the surface for a selected interval of time. If during this stay time an abort becomes necessary, the module will initiate an ascent phase. For missions that do not entail lunar rendezvous, the launch is accomplished in a normal manner. That is, the module is rolled to the desired azimuth, and the ascent is carried on without changes from the nominal ascent trajectory. However, for the case where lunar rendezvous is a consideration, the launch azimuth is somewhat restricted.

The sketch below illustrates how plane changes become necessary when aborting with the requirement to rendezvous for a launch-compatible orbit.

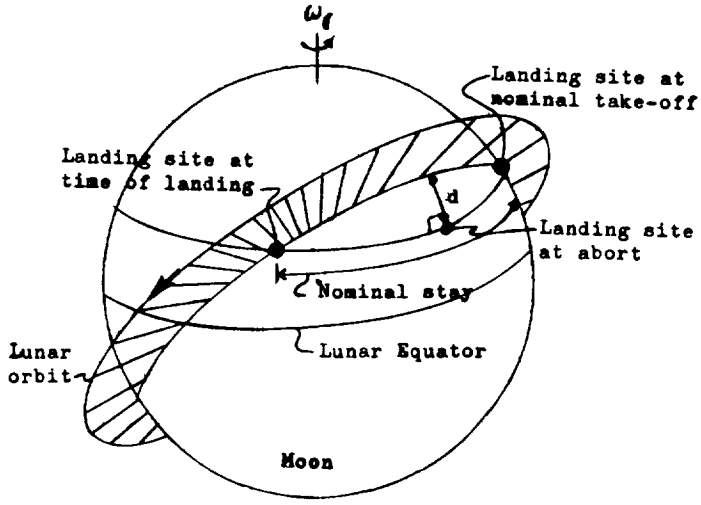

This type of orbit passes over the landing site once the landing phase, and again after a nominal stay time, so that both ascent and descent occur essentially in the orbit plane. Since the moon is rotating, the landing site will not lie in the plane of the orbiting MOM at all times. Therefore, a launch at any time during the nominal stay time and after the stay time will result in the site being displaced from the orbital plane.

The maximum displacement is given in Fig. 48 for aborts made after one-half the nominal stay time, for aborts one day past the nominal stay time, and for various landing-site latitudes. This range is zero for sites on the lunar equator and increases with site latitude.

Aborts from the lunar surface should be successful. Although any vehicle will be designed for high reliability, the question still arises as to what can be done in the event of a primary guidance failure. The possibility of such an emergency requires some type of backup guidance system.

For illustrative purposes, a backup system utilizing strapped down gyros and three orthogonally mounted accelerometers is assumed. Such a system would require a man to complete the guidance loop. Module attitude is related to him from the gyros and velocity from the accelerometers.

The above manual ascent technique is considered the simplest. It consists of lifting off and rising vertically for an interval of time. The module is then pitched to a desired inertial thrust attitude θ_t, which is measured from the x_t-axis to the thrust axis, and this attitude is maintained constant in inertial space until engine cutoff. It is assumed that the nominal mission specifies the establishment of a lunar orbit at 185.2 km. Therefore, after thrust cutoff, the module coasts

TABLE 5

T/W_0	t_t (sec)	θ_t (deg)	$\frac{\partial h_{AL}}{\partial t_t}$ (m/sec)	$\frac{\partial \Phi_0}{\partial t_t}$ (deg/sec)	$\frac{\partial h_{AL}}{\partial \theta_t}$ (m/deg)	$\frac{\partial \Phi_0}{\partial \theta_t}$ (deg/deg)	$\frac{\partial h_{AL}}{\partial t_b}$ (m/sec)	$\frac{\partial \Phi_0}{\partial t_b}$ (deg/sec)	t_b (sec)
0.4	60	20.7	0	-0.3	19507	0.5	8336	1.5	340
0.4	100	17.5	-204.2	-0.32	20970	0	10741	2	350
0.4	100	13	-1143.	0.4	25146	2.5	8918	3.2	360
0.6	60	17	0	-0.2	22068	0.75	14246	2.35	220
0.6	100	11.8	-323.1	-0.4	23590	0	7699	2.55	230

to an apocynthion altitude of 185.2 km, at which time injection into a circular orbit is made. Two thrust-to-weight ratios have been investigated for a fuel specific impulse of I_{sp} = 315 sec, and the results are presented in Fig. 49. The ascent range angle Φ_0, range angle measured from liftoff to orbit injection is shown as a function of tilt time with burning time as a parameter. Also noted in the figure are the acceptable limits of tilt time as determined from trajectory sensitivities. Sensitivities are determined by assuming errors of 1 second in tilt time (t_t) and burning time t_b plus 1° in θ_t (inertial thrust or pitch attitude), and with out-of-plane maneuvers not being considered. These errors are considered representative. The areas of decreasing, minimum, and rapidly increasing sensitivities for the thrust-to-weight ratios are shown in Fig. 49.

Typical sensitivities are listed in Table 5, where h_{AL} = apocynthion altitude.

Conditions in the area of decreasing sensitivity result in a maximum rectangular dispersion area from the nominal point of 66.6 km in altitude and 222 km in range on arrival at apocynthion for the above-mentioned errors. This maximum dispersion rectangle is shown by the curve marked "limit" in Fig. 49. Note also the limited amount of range control as shown in Fig. 49. For both values of T/W_0, the range angle Φ_0 can be varied from 40 to 70 degrees. As the tilt time is prolonged, the ΔV requirements increase, as can be seen in Table 6. Compared to guided ascents (Section C), the ΔV requirements increase by 60 to 90 m/sec. Also included in Table 6 is the required pitch attitude θ_t.

As can be seen from the above discussion, lunar ascent utilizing this backup technique is feasible. However, for missions involving a lunar rendezvous, launch time tolerances are drastically reduced because of the restricted range control.

This implies that additional stored pitch programs, preferably with constant rates, be used to increase range control. These pitch programs can be generated with clocked potentiometers, and the backup technique is again found to be quite feasible.

The initial pitch angle (θ_{t0}), pitch rate ($\dot{\theta}_t$), and burning time t_b required to extend (Φ_0) to 180° are shown in Fig. 50. The pitch rate ($\dot{\theta}_t$) is held constant throughout the burning phase, with data presented for T/W_0 = 0.4, T/W_0 = 0.7 and I_{sp} = 315 sec.

Much of the data on lunar abort presented in this section is illustrative of the various techniques and representative of some present plans for lunar landing abort, rather than being of a parametric nature. The number of parameters is too large to be presented over all values of each trajectory variable. Practical limits on the variables are often prescribed by the available hardware at the time of the mission, and they

TABLE 6

T/W_0	t_t (sec)	t_b (sec)	ΔV (m/sec)	θ_t (deg)
0.4	20	340	194.8	20.4
0.4	60	340	1962.9	20.7
0.4	100	340	200.2	20.4
0.4	20	350	1877.6	16.5
0.4	60	350	1941.6	17.0
0.4	100	350	2004.1	17.5
0.4	100	360	2276.3	13.0
0.6	20	220	1872.7	16.9
0.6	60	220	1910.2	17.0
0.6	100	220	1923.6	16.3
0.6	20	230	1851.4	8.3
0.6	60	230	1881.8	11.3
0.6	100	230	1929.1	11.8

can be further restricted by the choice of abort technique as was illustrated in this section.

F. REFERENCES

1. Orbital Flight Handbook, ER 12684, Martin Company, Space Systems Division (Baltimore), 1963.
2. Schrader, C. D., "Lunar and Planetary Soft Landings by Means of Gas-Filled Balloons," Technical Paper 2480-62, ARS Lunar Missions Meeting, 17 to 19 July 1962.
3. Lang, H. A., "Lunar Instrument Carrier--Landing Factors," Rand Corporation Report RM-1725, 4 June 1956.
4. Rinehart, J. S., "Stresses Associated with Lunar Landings," J. British Interplanetary Society, Vol. 17, 1960, pp 431 to 436.
5. "Proceedings of the Lunar and Planetary Exploration Colloquium," Vol. III, No. 1, 15 May 1962, p 75.
6. deFries, P. J., "Analysis of Error Progression in Terminal Guidance for Lunar Landing," NASA TN D-605, July 1961.
7. Wrobel, J. R., and Breshears, R. R., "Lunar Landing Vehicle Propulsion Requirements," Paper No. 1121-60, ARS Semi-Annual Meeting, 9 to 12 May 1960.
8. Mason, M., and Brainin, S. M., "Descent Trajectory Optimization for Soft Lunar Landings," IAS Paper No. 62-11, presented at the IAS 30th Annual Meeting, New York, 22 to 24 January 1962.
9. Cheng, R. K., and Pfeffer, I., "A Terminal Guidance System for Soft Lunar Landing," Technical Paper 1912-61, ARS Guidance Control and Navigation Conference, 7 to 9 August 1961.
10. Markson, E., Bryant, J., and Bergsten, F., "Simulation of Manned Lunar Landing," Paper No. 2482-62, ARS Lunar Missions Meeting, 17 to 19 July 1962.
11. Berman, L. J., "Optimum Soft Landing Trajectories, Part 1, Analysis," MIT, AFOSR 519, March 1961.
12. Lawden, D. F., "Dynamic Problems of Interplanetary Flight," Aeronautical Quarterly, Vol. 6, 1955, pp 165 to 180.
13. Fried, B. D., "Trajectory Optimization for Powered Flight in Two or Three Dimensions," Space Technology, J. Wiley and Sons, Inc., 1959.
14. Perkins, C. W., "Optimum Retro-Thrust Trajectories," M. S. Thesis, MIT, June 1960.
15. Markson, E. E., "Thrust Programming for Terminal Maneuvers in Space," Proceedings of IAS Meeting on Aerospace Support and Operations, Orlando, Florida, 4 to 6 December 1961.
16. Jazwinski, A. H., "Integration of Two-Point Boundary Value Problems with One Unknown Boundary," A-PD-113, General Dynamics/Astronautics, 17 May 1962.
17. Jurovics, S. A., and McIntyre, J. E., "The Adjoint Method and Its Applications to Trajectory Optimization," ARS Journal, 32 (9), September 1962, pp 1354 to 1358.
18. Jazwinski, A. H., "New Approach to Variational Problems in Trajectory Optimization," ER 12700, Martin Company Space Systems Division (Baltimore), November 1962.
19. Tyler, J., and Foy, W., "Application of Optimal Control Theory to a Lunar Landing Vehicle," RM-230, Martin Company (Baltimore), August 1962.
20. Culler, G. J., and Fried, B. D., "Universal Gravity Turn Trajectories," J. of Applied Physics, Vol. 28, No. 6, June 1957, pp 672 to 676.
21. Jensen, J., Townsend, G., Kork, J., and Kraft, D., "Design Guide to Orbital Flight," McGraw-Hill, 1962.
22. Bartos, G., and Greenberg, A., "Abort Problems of the Lunar Landing Mission," ARS Preprint 2490-62.
23. Kelly, T. J., "Abort Considerations for Manned Lunar Missions," ARS Preprint 2478-62.

ILLUSTRATIONS

LIST OF ILLUSTRATIONS

Figure	Title	Page
1	Lunar Impact Velocity Without Rocket Braking . . .	VIII-39
2	Target Penetration for Sectional Density, $W/D^2 = 1$ . . .	VIII-40
3	Maximum Resistive Pressure Between Payload and Rock Target. . . .	VIII-41
4	Vertical Descent . . .	VIII-42
5	Vertical Descent . . .	VIII-43
6	Vertical Descent . . .	VIII-44
7	Vertical Descent . . .	VIII-45
8	Variation of Optimum Thrust/Mass Ratio with Propulsion-System Mass Parameter . . .	VIII-46
9	Effect of Off-Optimum Thrust Level on Payload Soft-Landed with Zero Touchdown Velocity . . .	VIII-46
10	Braking Trajectory 1 . . .	VIII-47
11	Braking Trajectory 2 . . .	VIII-48
12	Braking Trajectory 3 . . .	VIII-49
13	Braking Trajectory 4 . . .	VIII-50
14	Braking Trajectory 5 . . .	VIII-51
15	Typical Lunar Landing Trajectory. . . .	VIII-52
16	Characteristic Velocity Requirement for Braking Phase. . . .	VIII-53
17	Characteristic Velocity Requirement for Braking Phase of Synchronous Orbit Descent . . .	VIII-54
18	Characteristic Velocity Requirement for Descent . . .	VIII-55

LIST OF ILLUSTRATIONS (continued)

Figure	Title	Page
19	Optimum Braking Phase of Lunar Landing	VIII-56
20a	Requirements for Injection into an 80-Hour Return-Time Transearth Trajectory	VIII-57
20b	Transearth Trajectory Injection Requirements. . . .	VIII-58
21	Ascent Trajectory 1	VIII-59
22	Ascent Trajectory 2	VIII-60
23	Ascent Trajectory 3	VIII-61
24	Ascent Trajectory 4	VIII-62
25	Ascent Trajectory 5	VIII-63
26	Typical Lunar Ascent Trajectory	VIII-64
27	Characteristic Velocity ΔV Required for Ascent to an 185.2-km Circular Orbit	VIII-65
28	Excess ΔV Required Versus Launch Time Tolerance for Lunar Rendezvous	VIII-66
29	Excess ΔV Required for Out-of-Plane Ascent	VIII-67
30	In-Plane Rendezvous Techniques.	VIII-68
31	Lateral Rendezvous	VIII-69
32	Typical Lunar Orbit Rendezvous Profile.	VIII-70
33	Horizontal Translation	VIII-71
34	Minimum Propellant for Translation While Hovering at Constant Altitude	VIII-72
35	Total ΔV Required to Abort from a Lunar Landing Coast Trajectory	VIII-73
36	Safe Abort Window (Non-Impact Trajectories)	VIII-74

LIST OF ILLUSTRATIONS (continued)

Figure	Title	Page
37	ΔV Required to Abort and Rendezvous at 92.6 km (50 N Mi) from a Landing Coast Trajectory	VIII-75
38	ΔV Required to Abort and Rendezvous at 185.2 km (100 N Mi) from a Landing Coast Trajectory	VIII-76
39	ΔV Required to Abort and Rendezvous at 370.4 km (200 N Mi) from a Landing Coast Trajectory	VIII-77
40	Total ΔV Required for Perfect Rendezvous Versus Abort Altitude	VIII-78
41	ΔV Required to Abort and Rendezvous at 185.2 km (100 N Mi) from a Landing Coast Trajectory	VIII-79
42	Down Range Angle Required for a Lunar Rendezvous from an Abort Along a Landing Coast Trajectory	VIII-80
43	Down Range Angle Required for a Lunar Rendezvous from an Abort Along a Lunar Landing Coast Trajectory	VIII-81
44	Down Range Angle Required for a Lunar Rendezvous from an Abort Along a Lunar Landing Coast Trajectory	VIII-82
45	Slant Range Versus Altitude of Landing Coast Trajectory	VIII-83
46	Velocity ΔV Required to Abort and Rendezvous from Synchronous Orbit Descent	VIII-84
47	Landing Safety Boundaries	VIII-85
48	Maximum Landing Site Out-of-Plane Range for Aborted Missions	VIII-86
49	Emergency Backup Guidance Capability	VIII-87
50	Pitch Rate and Initial Pitch Angle Required for Range Extension	VIII-88

Fig. 1. Lunar Impact Velocity Without Rocket Braking

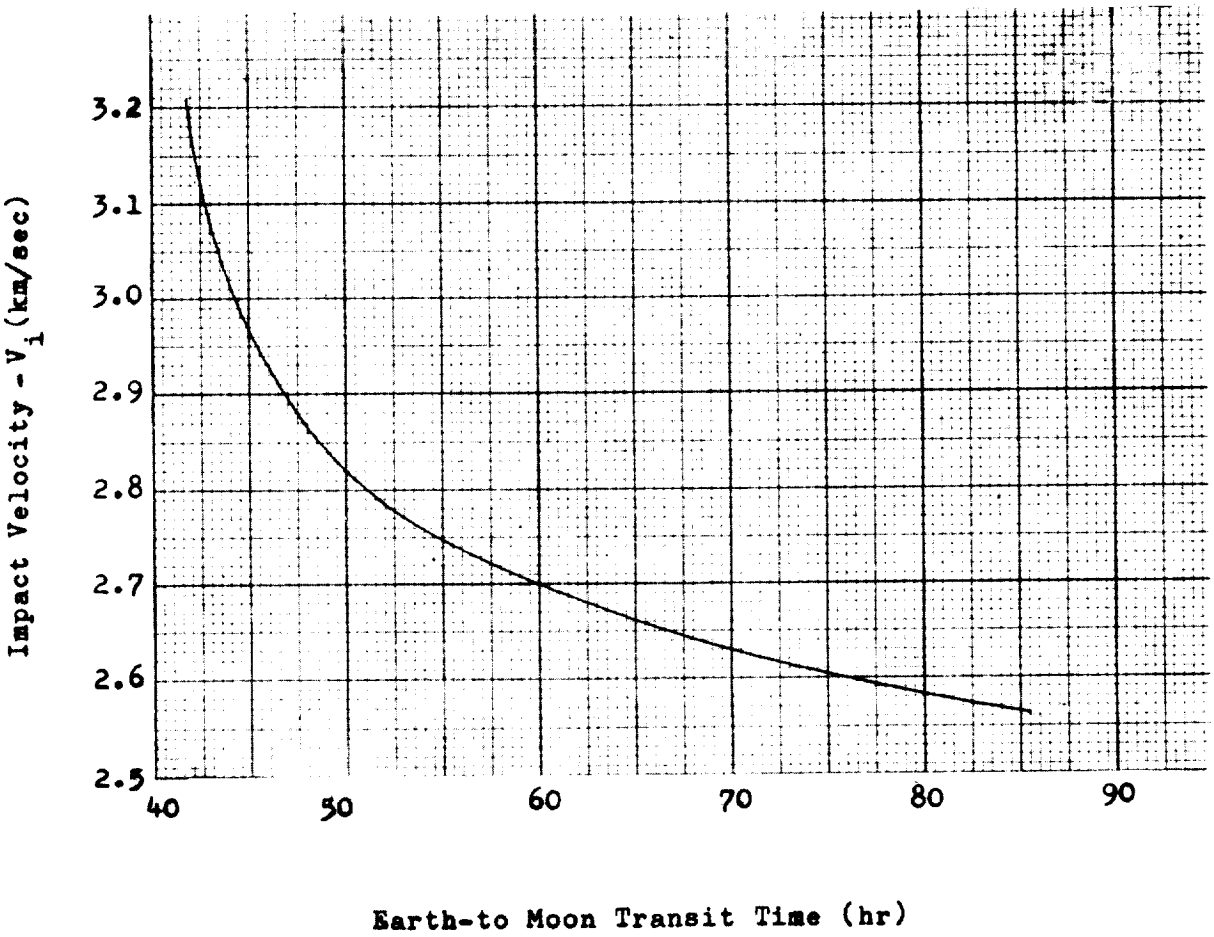

Fig. 2. Target Penetration for Sectional Density, $W/D^2=1$

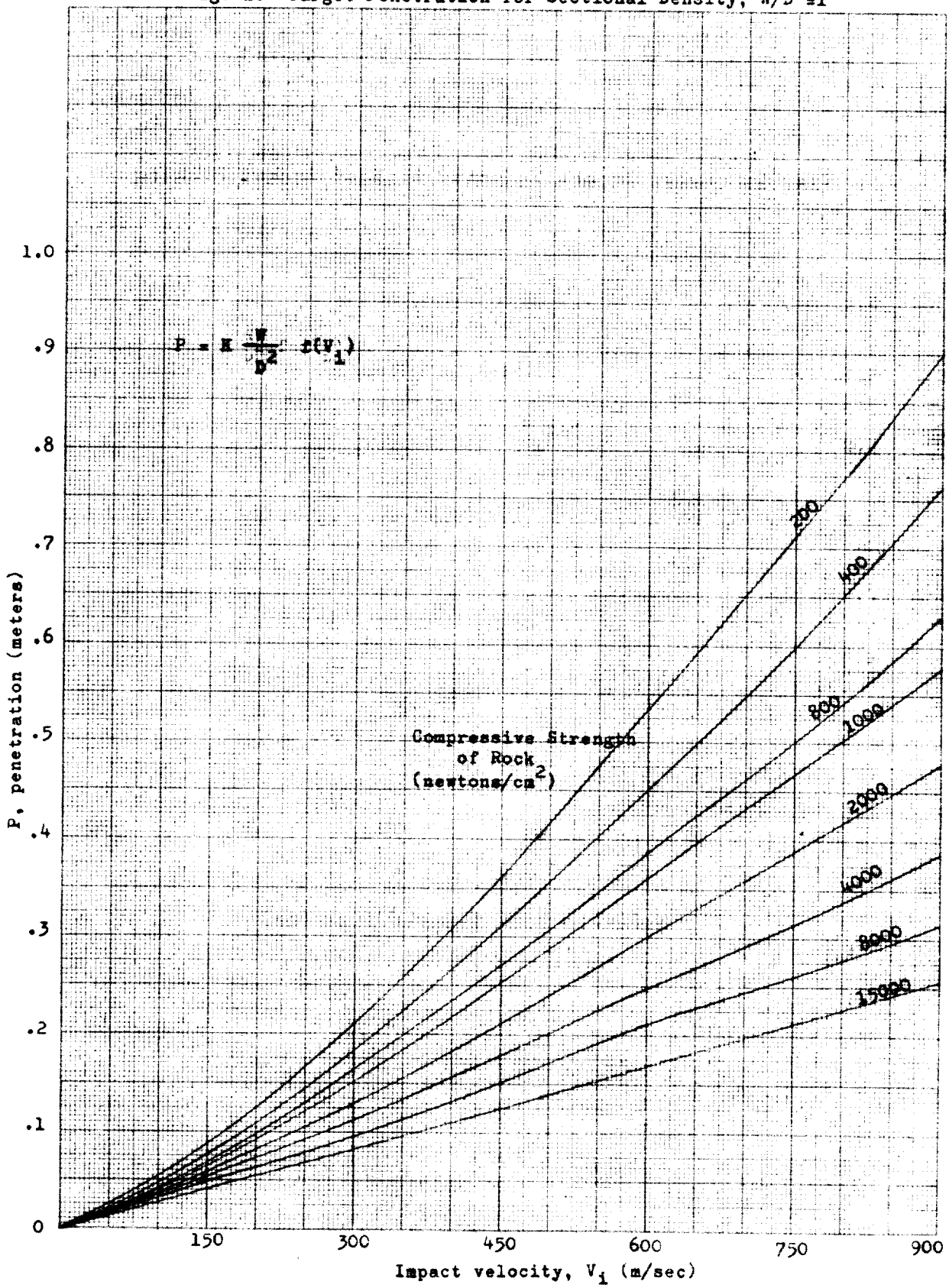

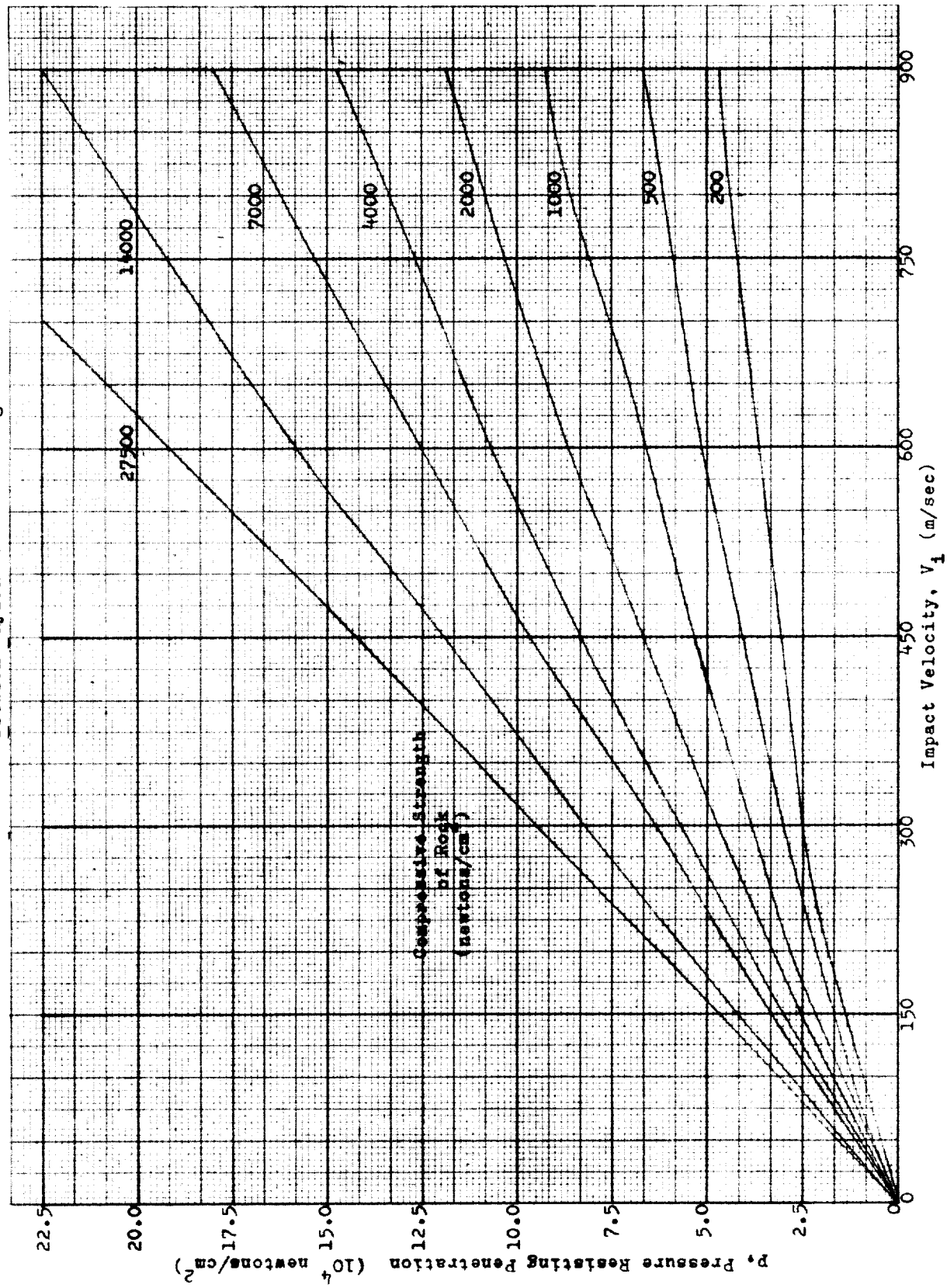

Fig. 3. Maximum Resistive Pressure Between Payload and Rock Target

Fig. 4. Vertical Descent

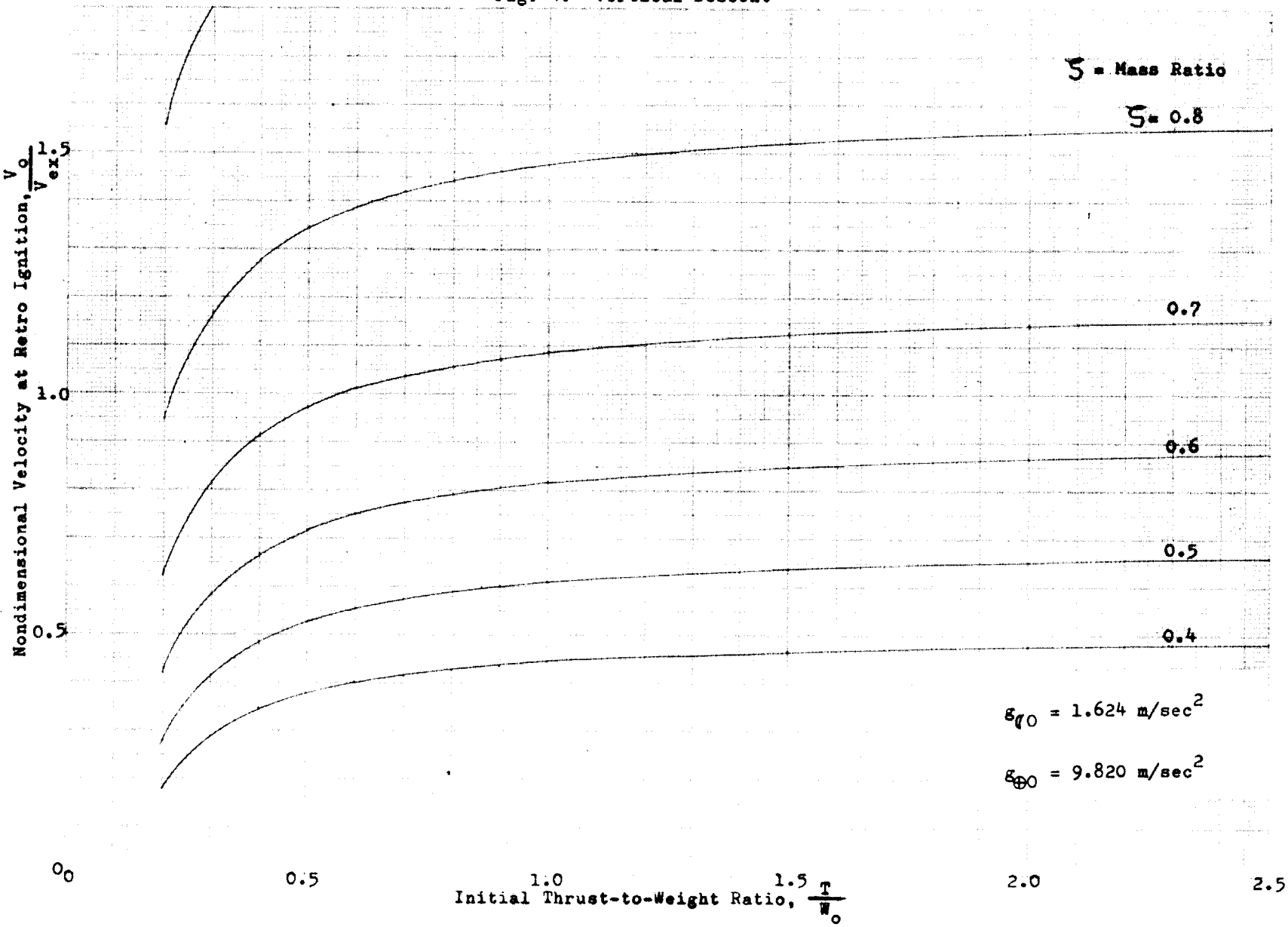

Fig. 5. Vertical Descent

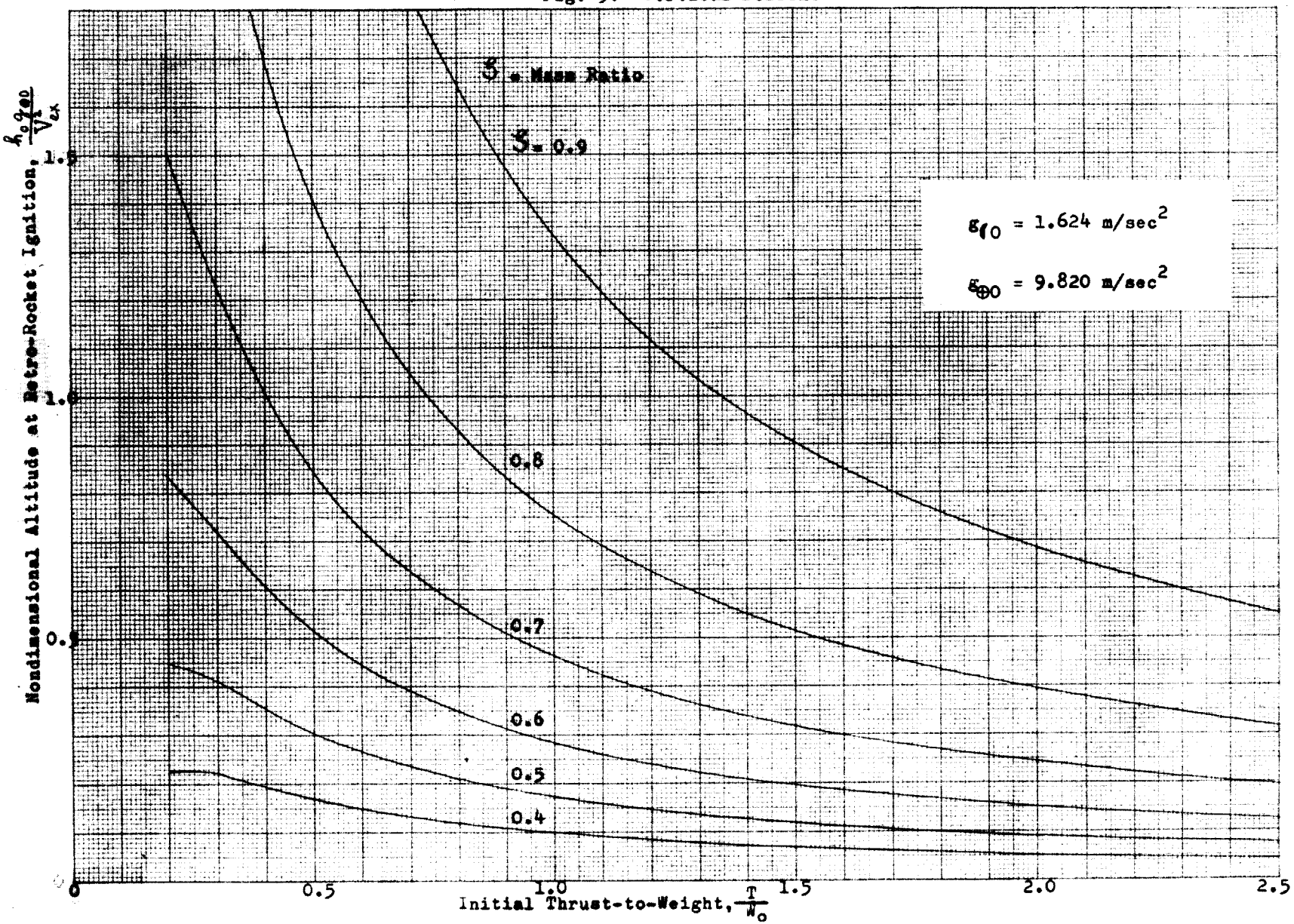

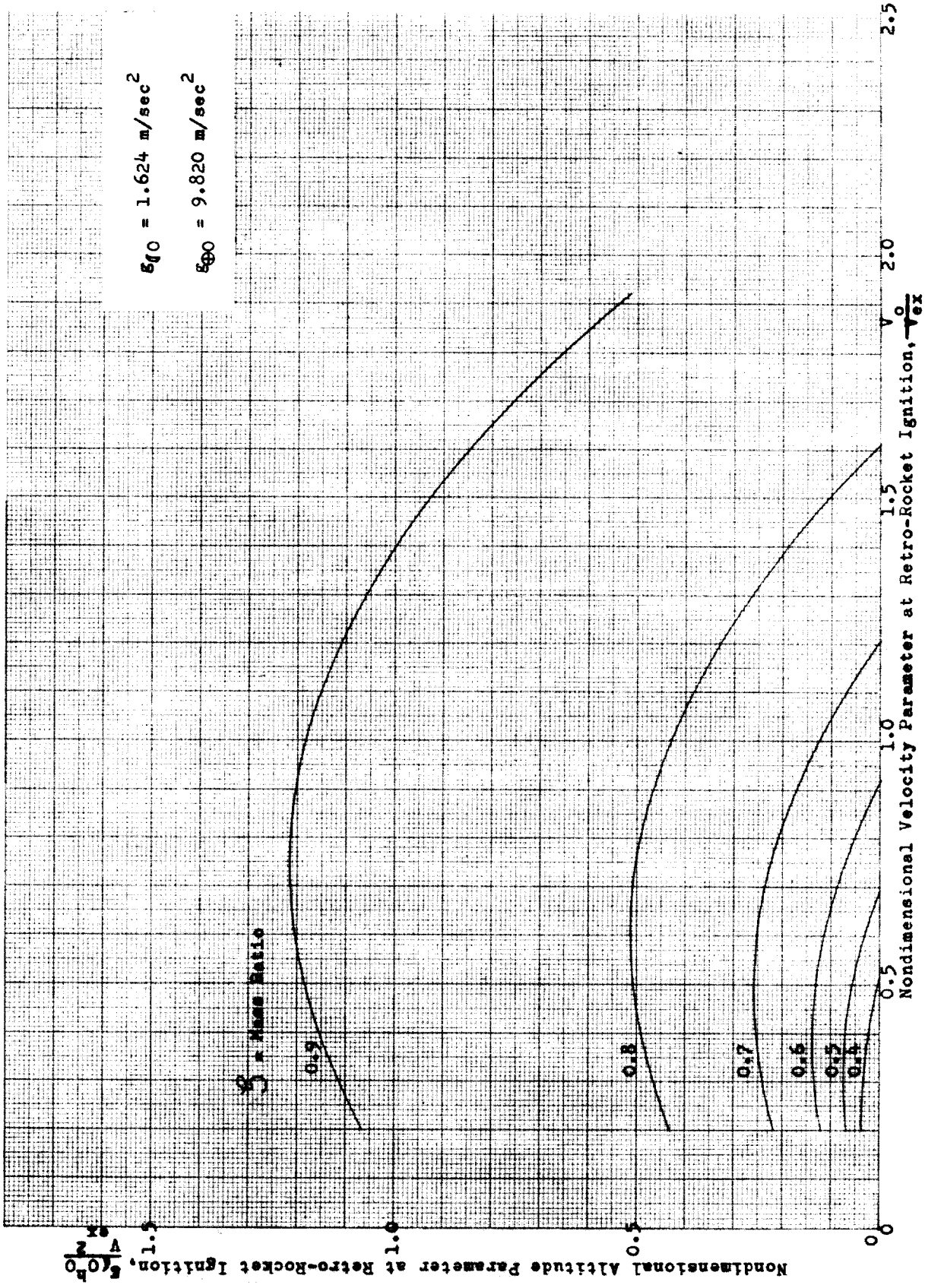

Fig. 6. Vertical Descent

Fig. 7. Vertical Descent

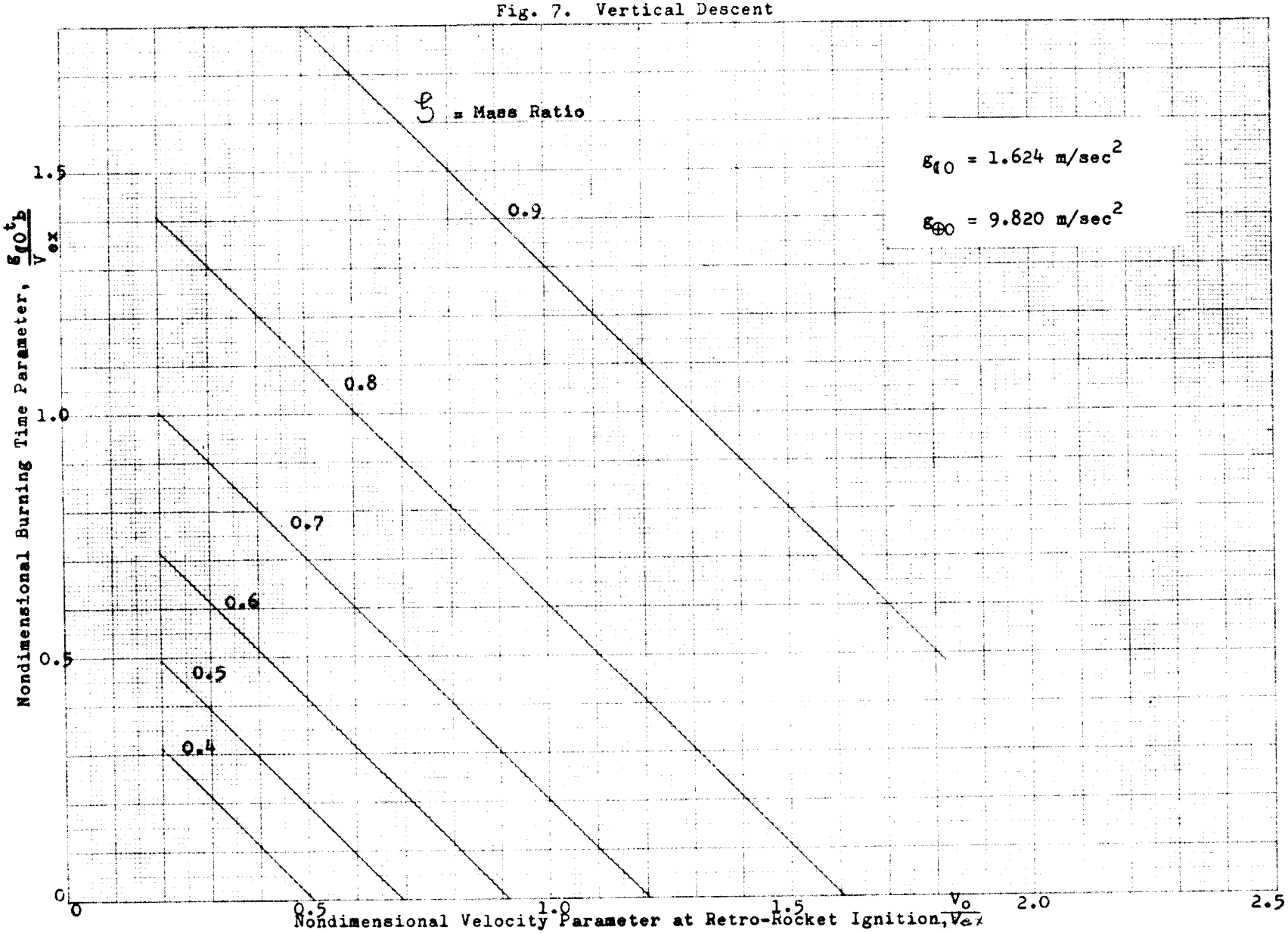

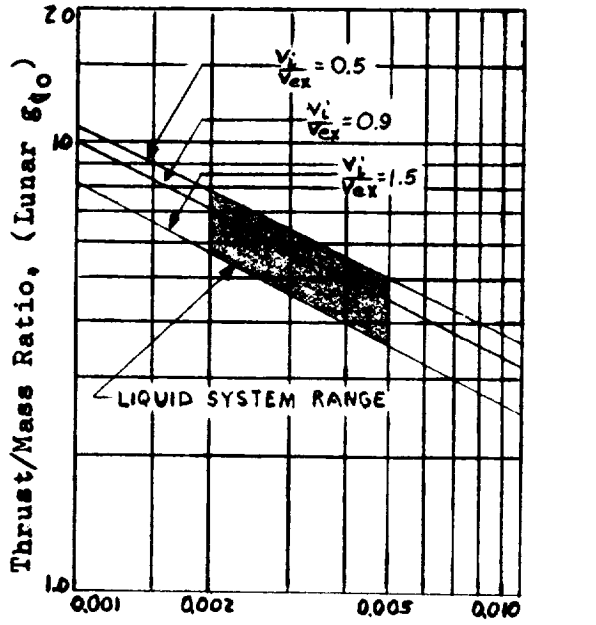

Fig. 8. Variation of optimum thrust/mass ratio with propulsion-system mass parameter

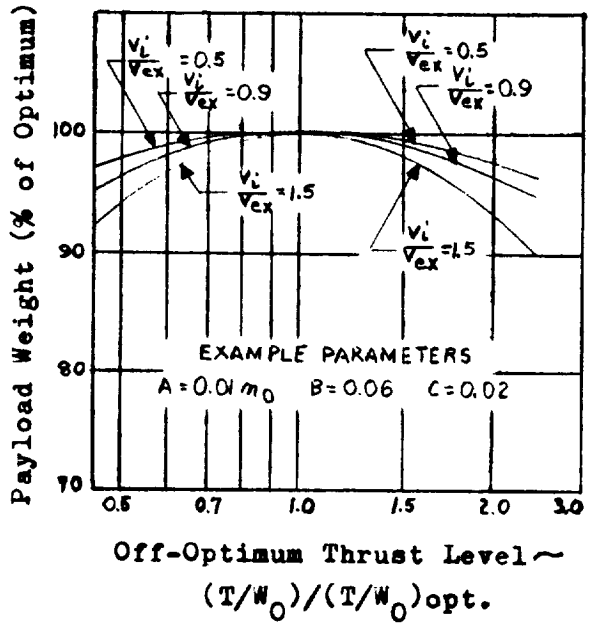

Fig. 9. Effect of off-optimum thrust level on payload soft-landed with zero touchdown velocity

Data For Vertical Descent With a Single Burning Phase.

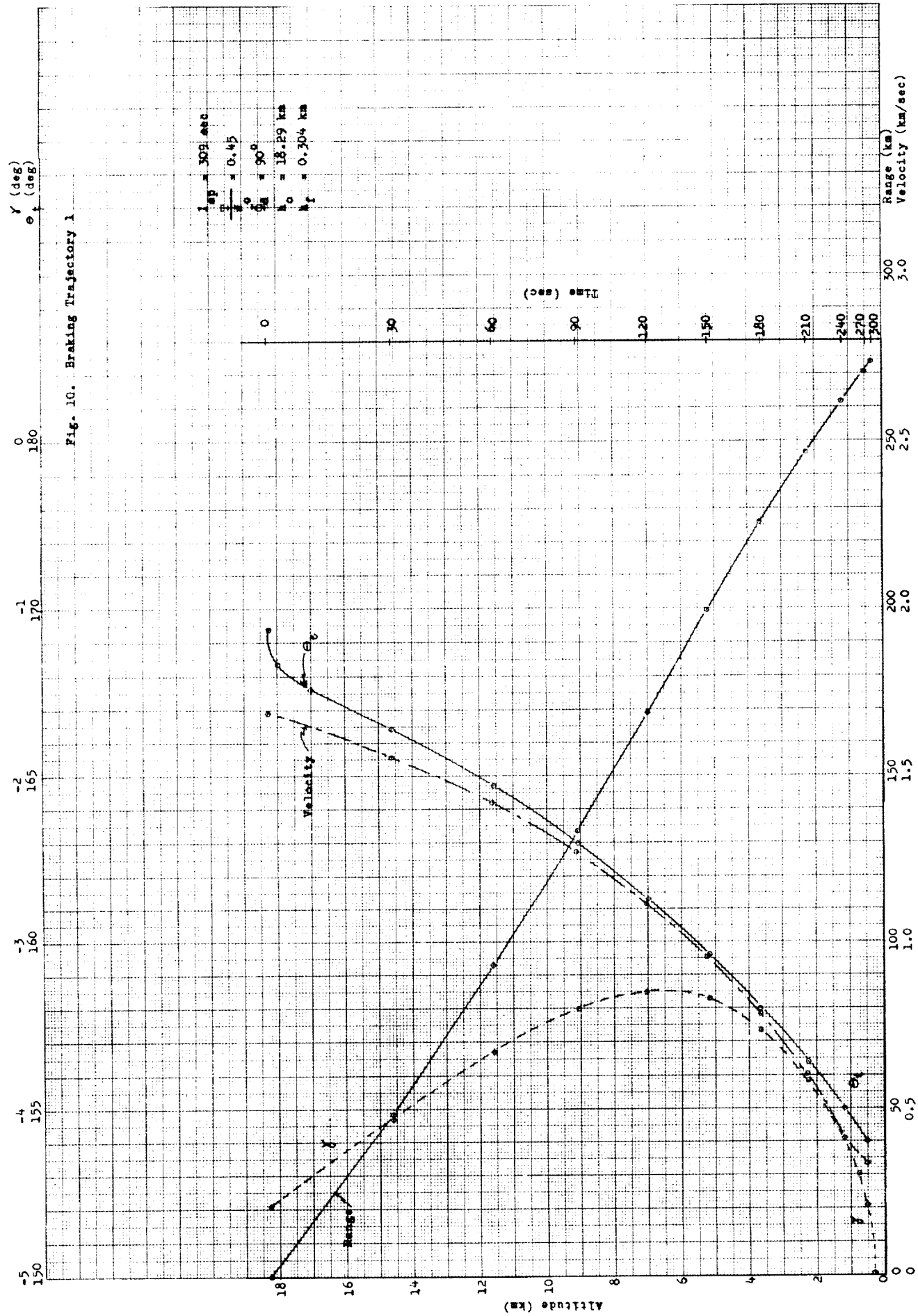
Fig. 10. Braking Trajectory 1
t_{ap} = 309 sec
$\frac{m}{S_a C_D}$ = 0.45
θ_a = 90°
h_o = 18.29 km
h_f = 0.304 km
Time (sec)
Altitude (km)
Range (km)
Velocity (km/sec)
γ (deg)
θ_t (deg)
Velocity
Range

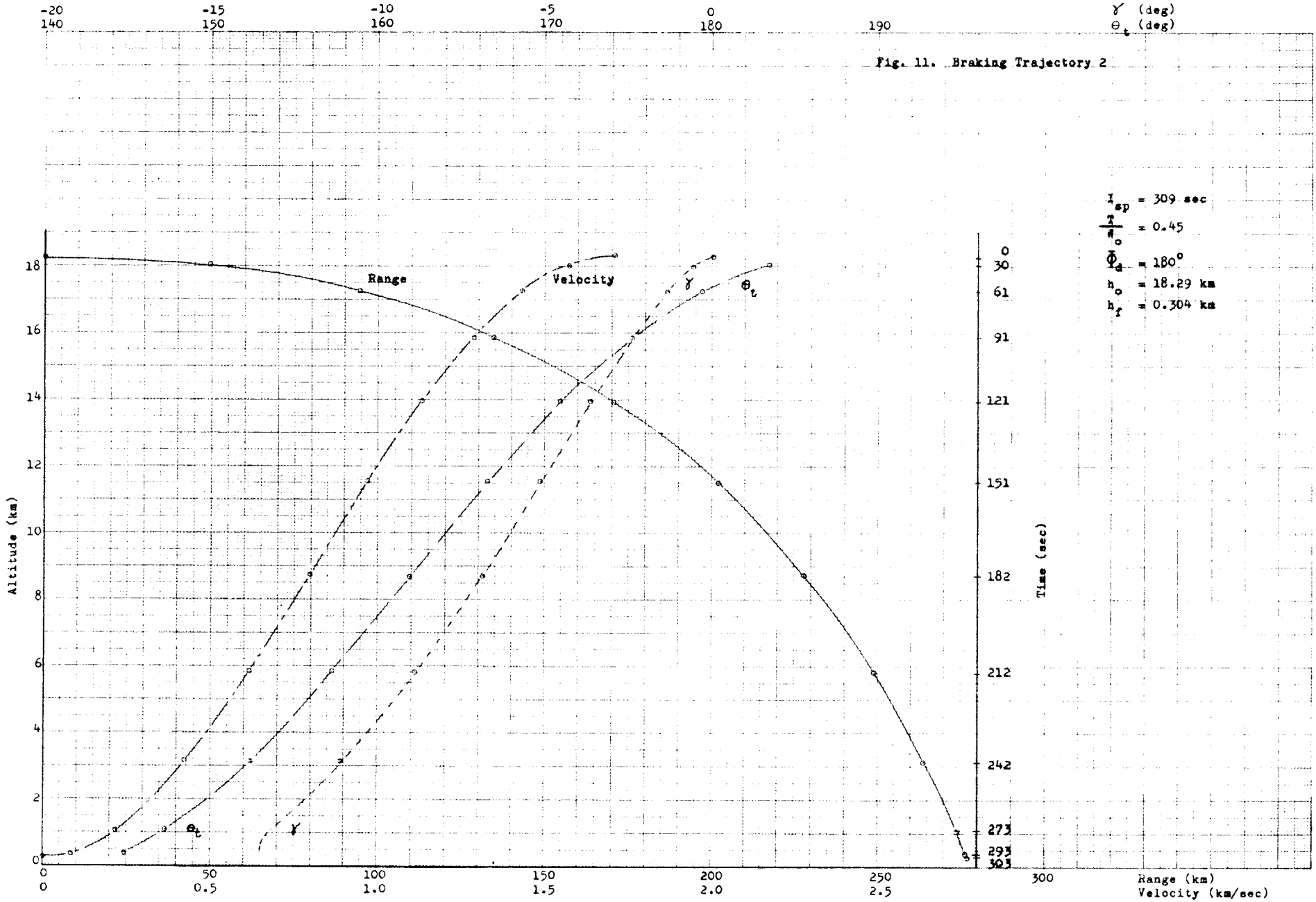

Fig. 11. Braking Trajectory 2

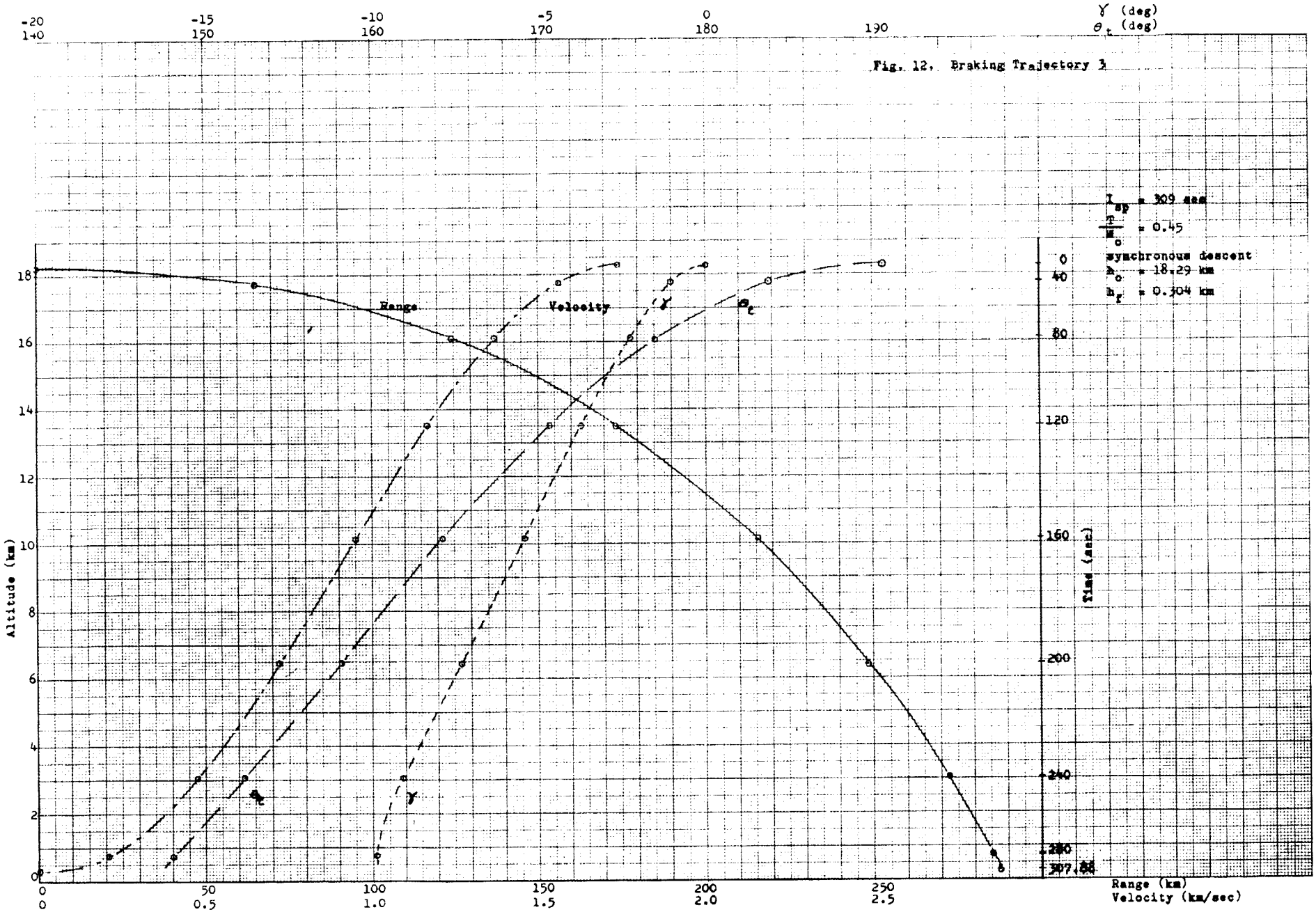
γ (deg)
θ_t (deg)
-20
140
-15
150
-10
160
-5
170
0
180
190
Fig. 12. Braking Trajectory 1
I_sp = 309 sec
T/m_o = 0.45
synchronous descent
h_o = 18.29 km
h_f = 0.304 km
Range
Velocity
Altitude (km)
Time (sec)
Range (km)
Velocity (km/sec)
0
2
4
6
8
10
12
14
16
18
0
40
80
120
160
200
240
280
307.88
0
50
100
150
200
250
0
0.5
1.0
1.5
2.0
2.5

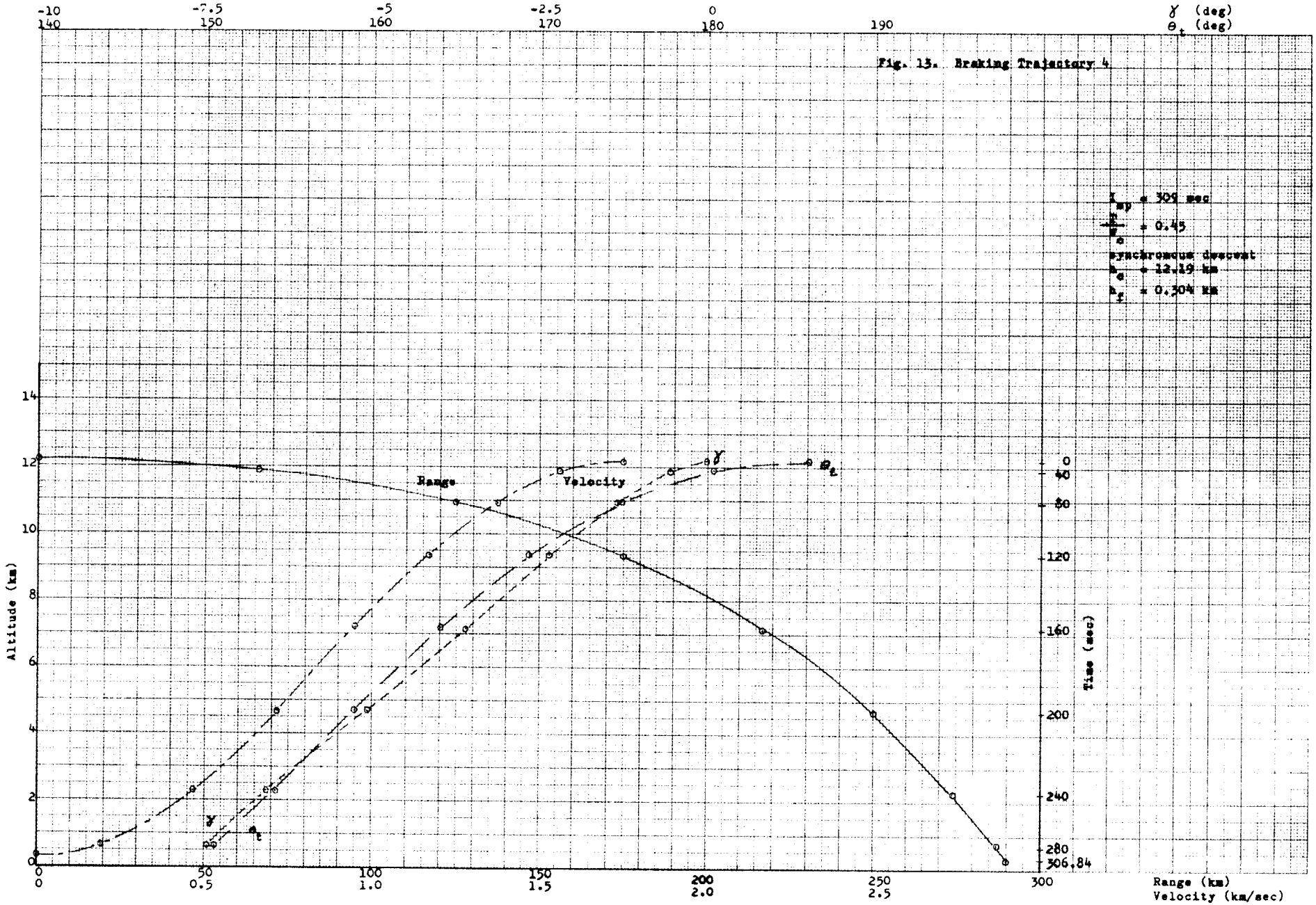

Fig. 13. Braking Trajectory 4

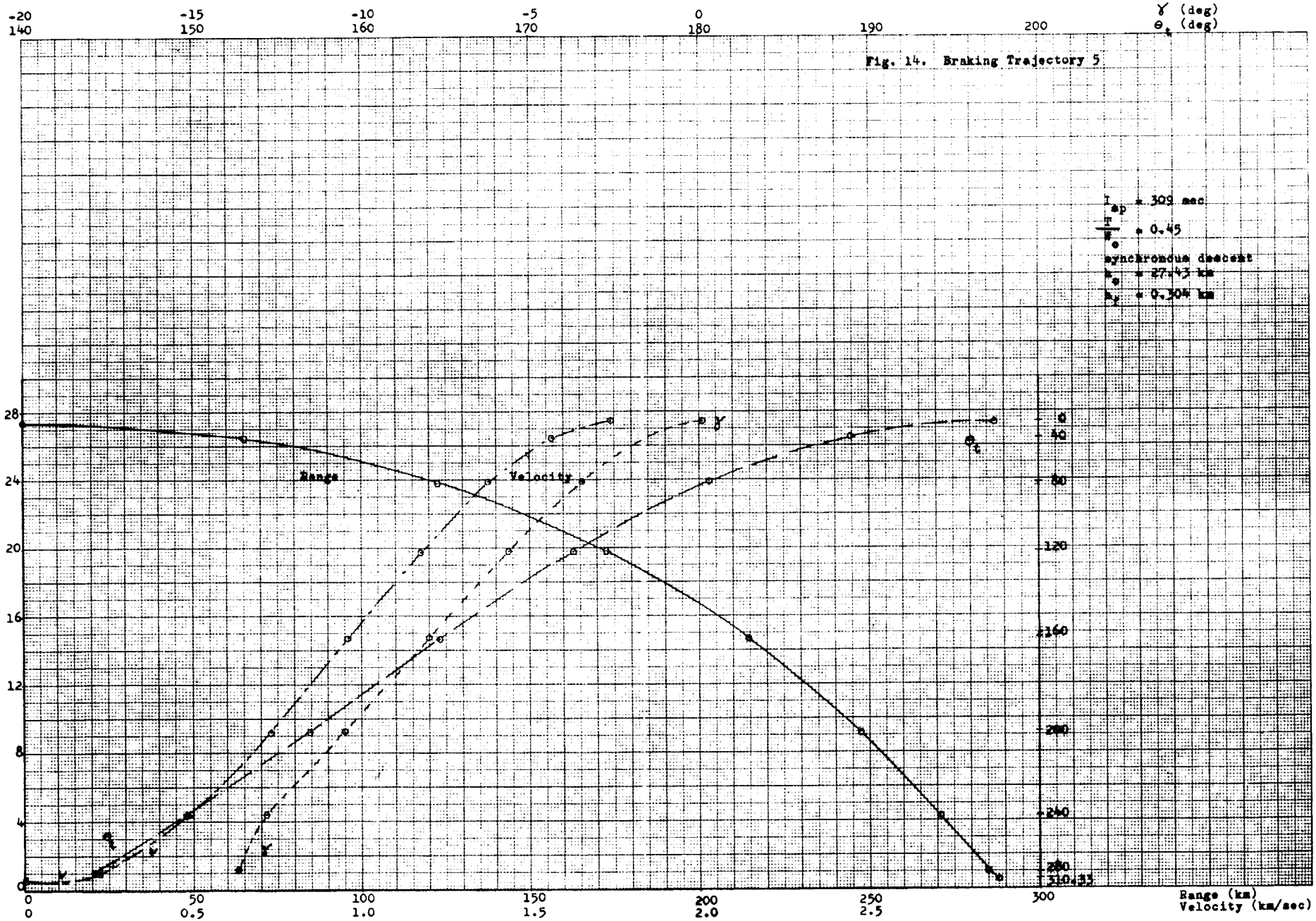

Fig. 14. Braking Trajectory 5

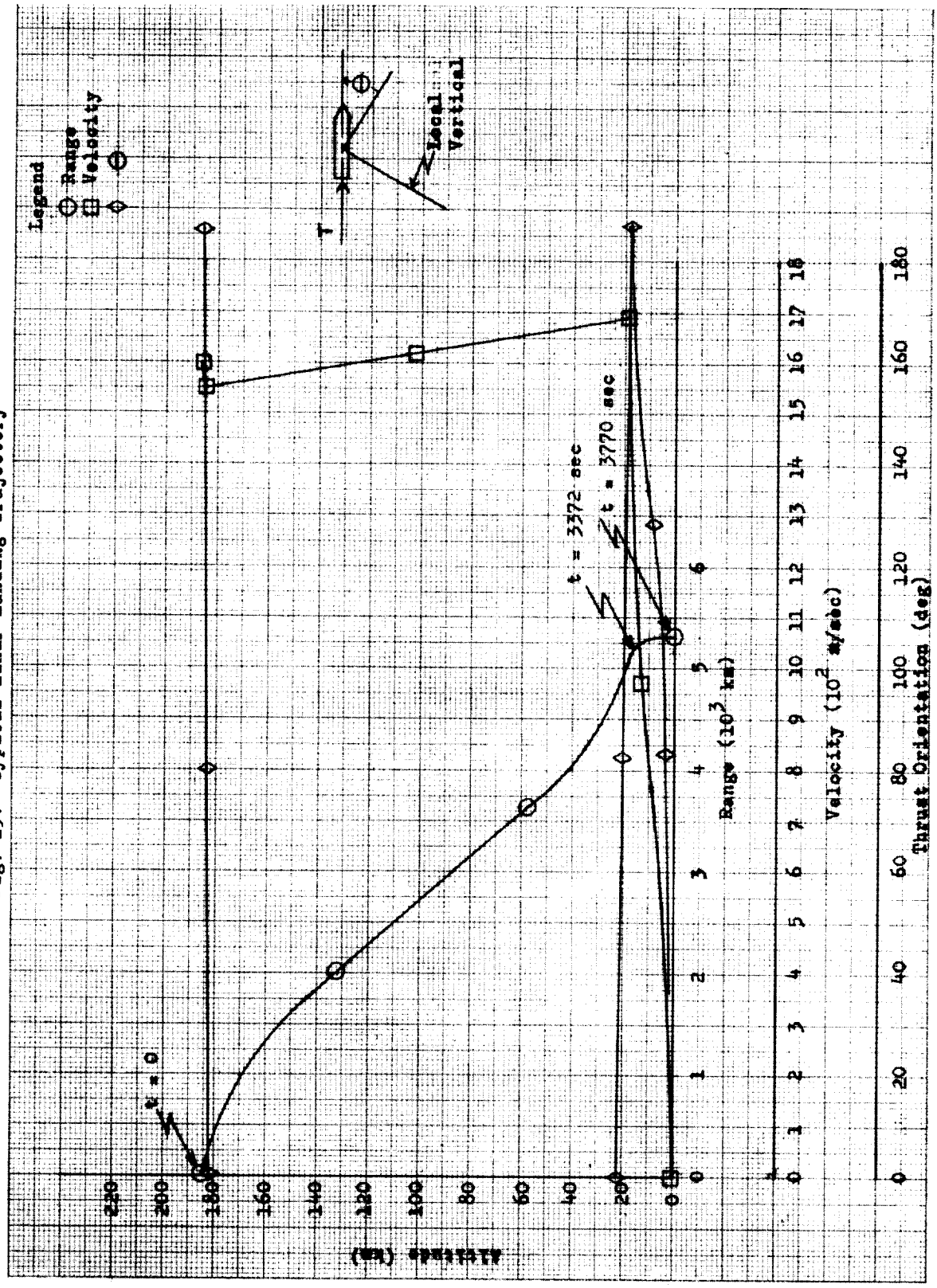

Fig. 15. Typical Lunar Landing Trajectory

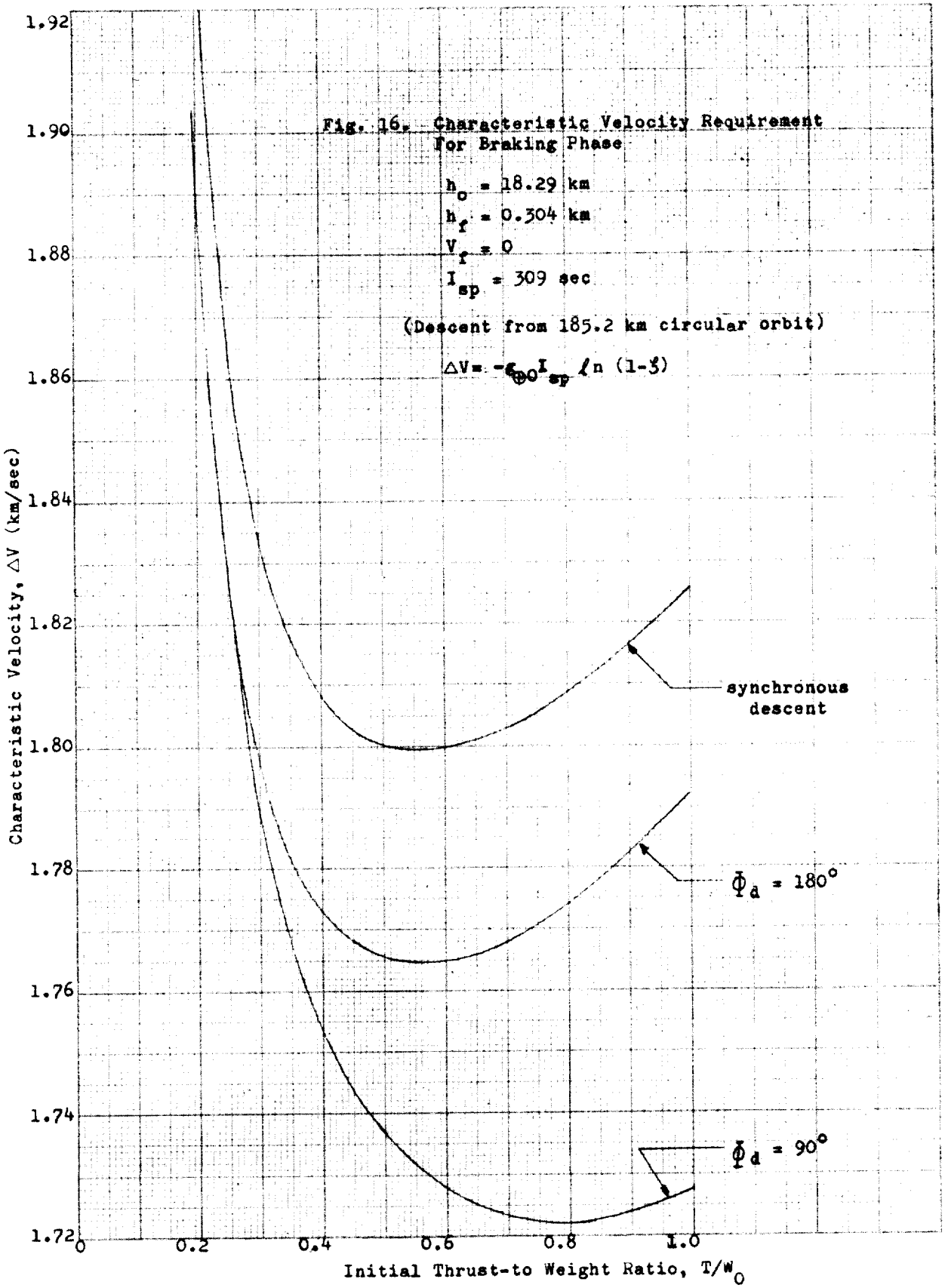

Fig. 16. Characteristic Velocity Requirement for Braking Phase

h_o = 18.29 km

h_f = 0.304 km

V_f = 0

I_{sp} = 309 sec

(Descent from 185.2 km circular orbit)

$\Delta V = -g_{\oplus 0} I_{sp} \ell n (1-\zeta)$

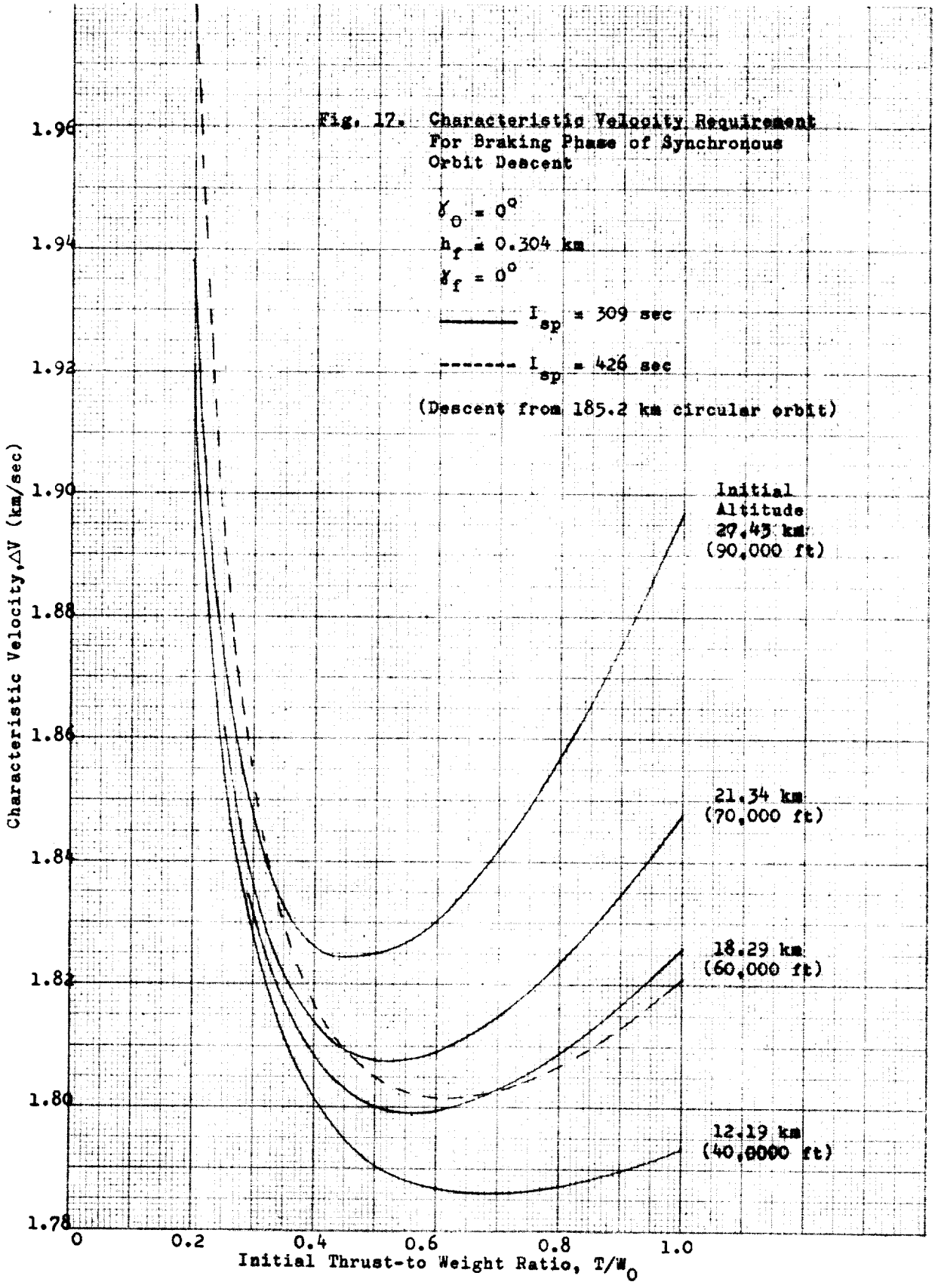

Fig. 17. Characteristic Velocity Requirement For Braking Phase of Synchronous Orbit Descent

$\gamma_0 = 0^\circ$

$h_f = 0.304$ km

$\gamma_f = 0^\circ$

——— $I_{sp} = 309$ sec

------- $I_{sp} = 426$ sec

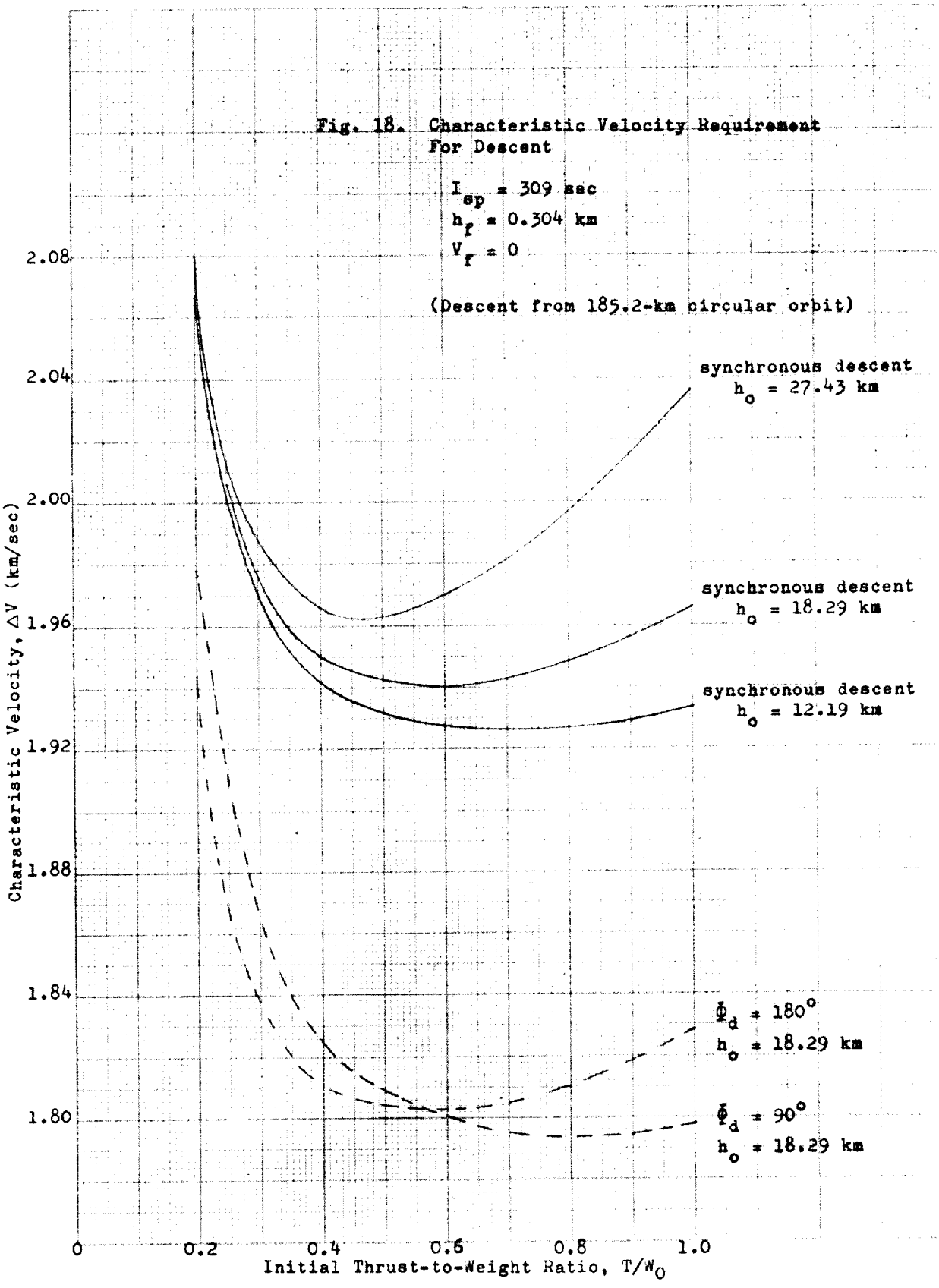
Fig. 18. Characteristic Velocity Requirement For Descent
I_{sp} = 309 sec
h_f = 0.304 km
V_f = 0
(Descent from 185.2-km circular orbit)
synchronous descent
h_o = 27.43 km
synchronous descent
h_o = 18.29 km
synchronous descent
h_o = 12.19 km
Φ_d = 180°
h_o = 18.29 km
Φ_d = 90°
h_o = 18.29 km
Characteristic Velocity, ΔV (km/sec)
2.08
2.04
2.00
1.96
1.92
1.88
1.84
1.80
0
0.2
0.4
0.6
0.8
1.0
Initial Thrust-to-Weight Ratio, T/W_0

Fig. 19. Optimum Braking Phase of Lunar Landing

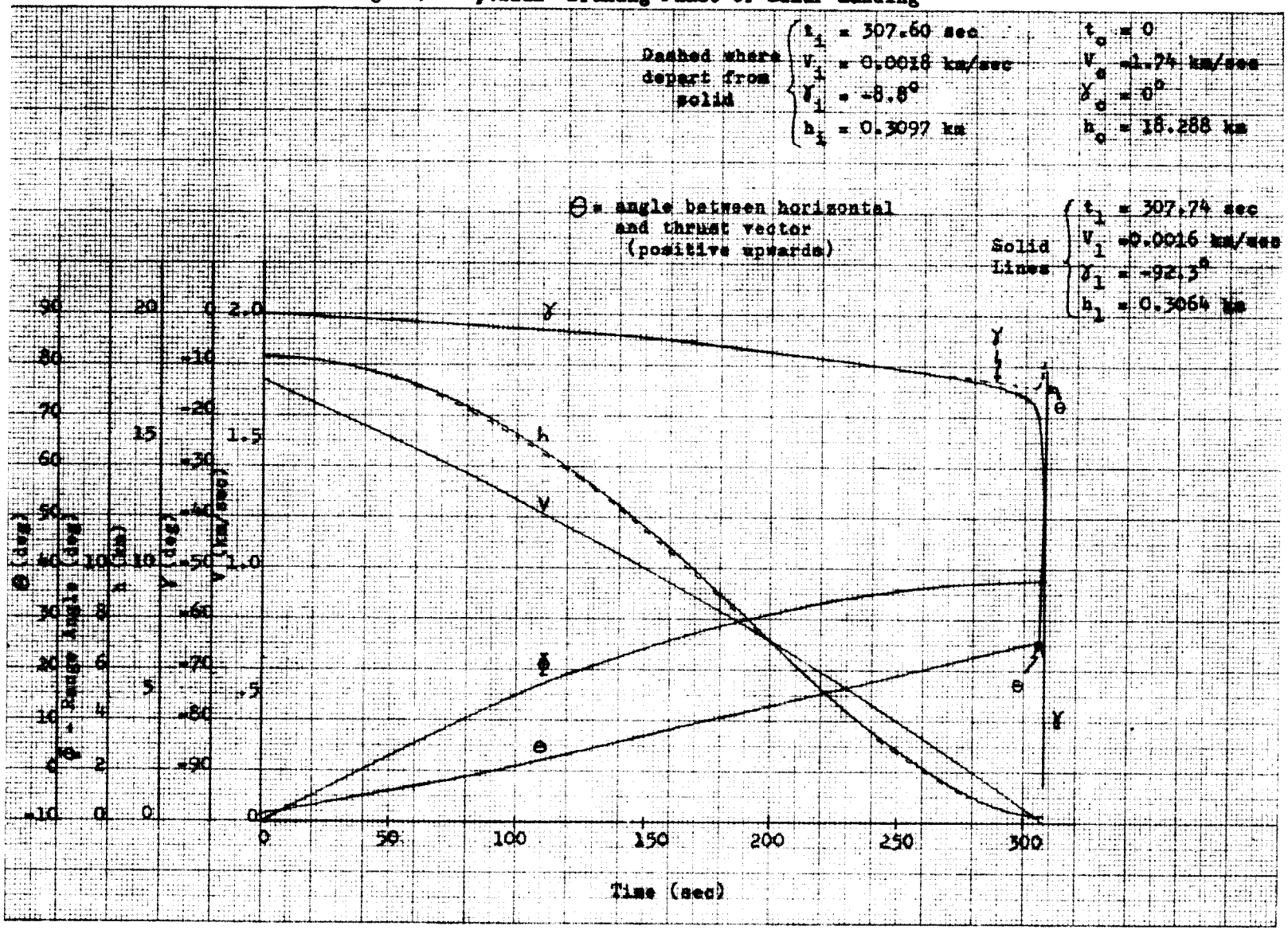

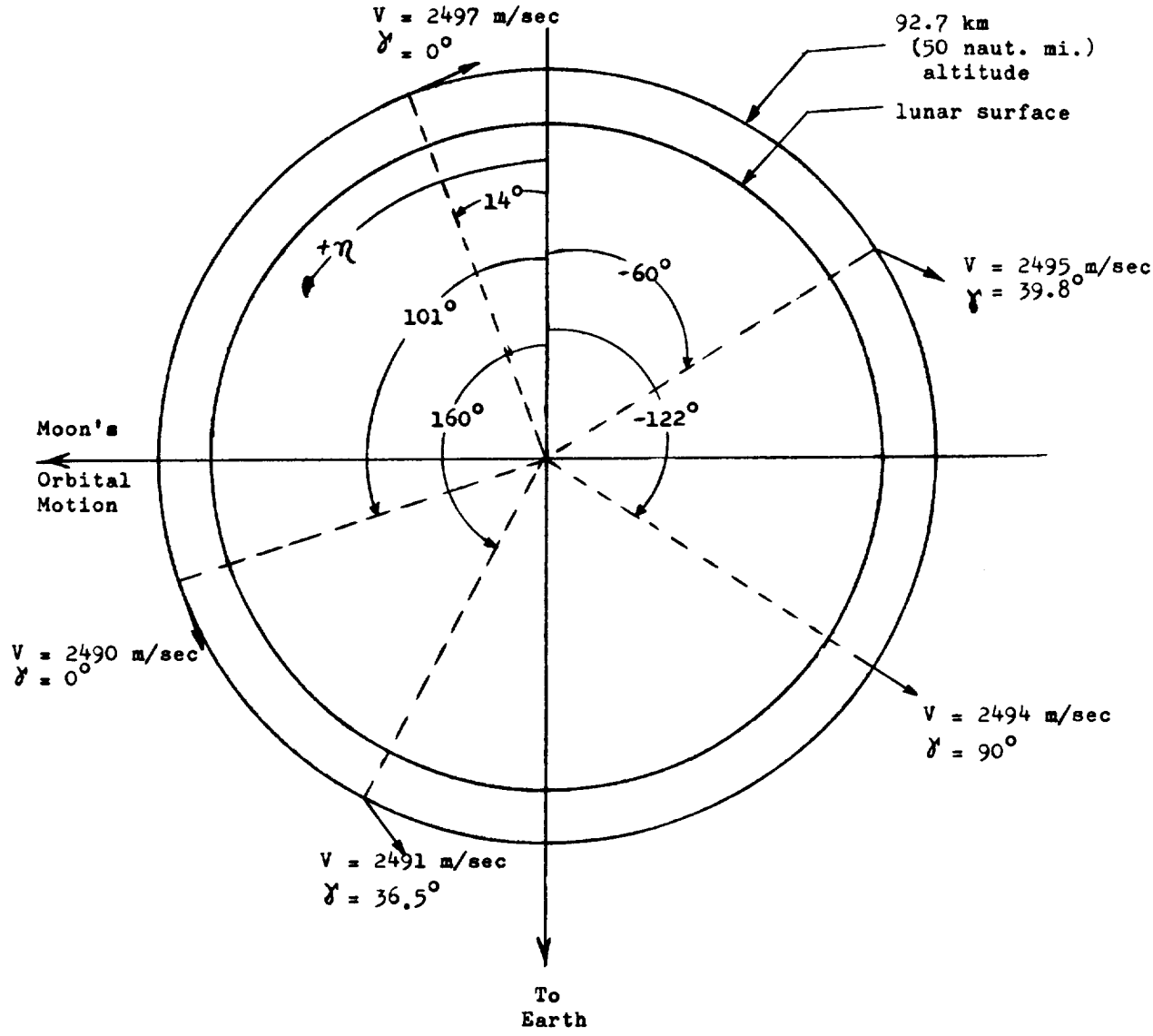

Fig. 20a. Requirements for Injection Into An 80-Hour Return-Time Trans-Earth Trajectory

Fig. 20b. Transearth Trajectory Injection Requirements

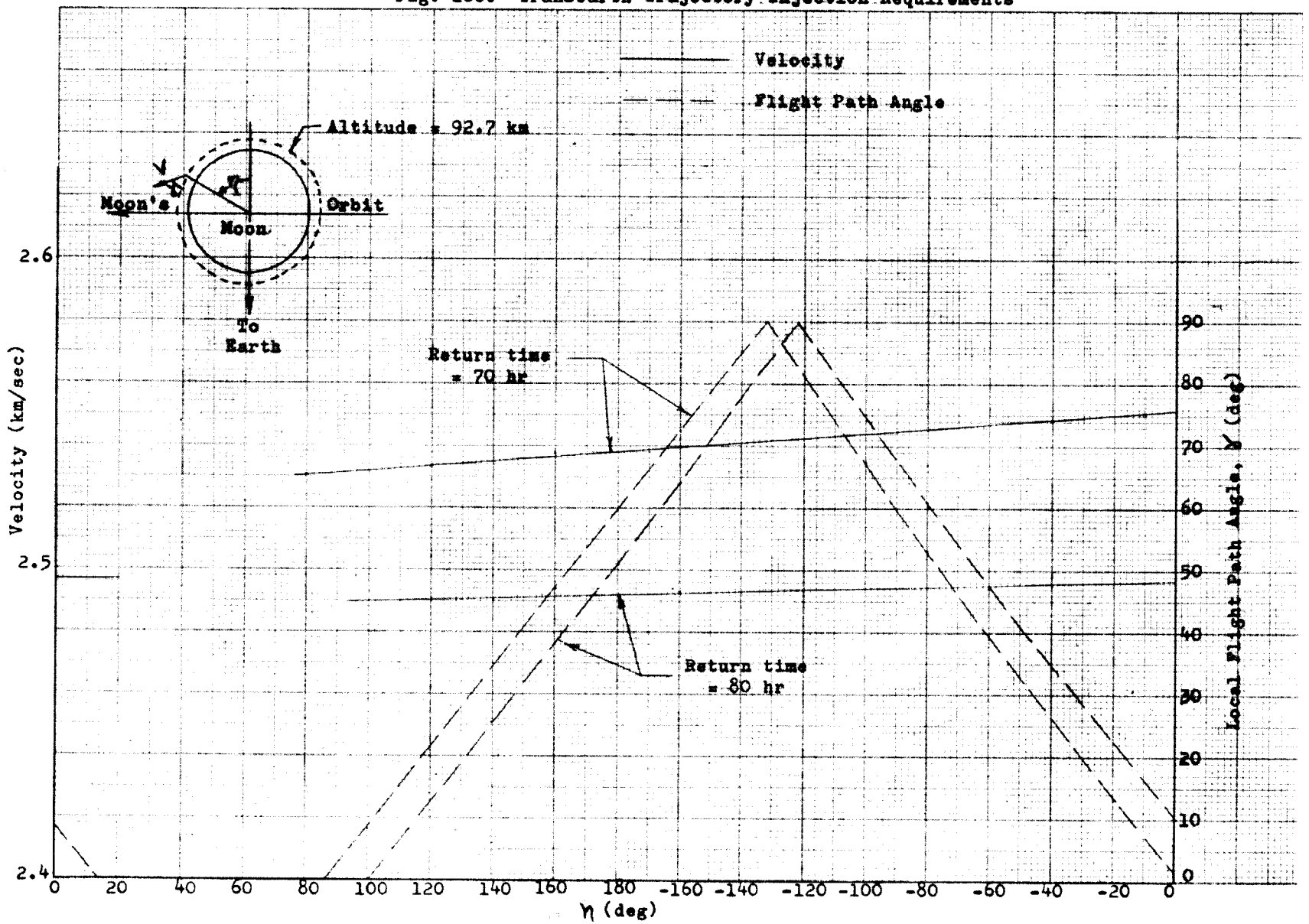

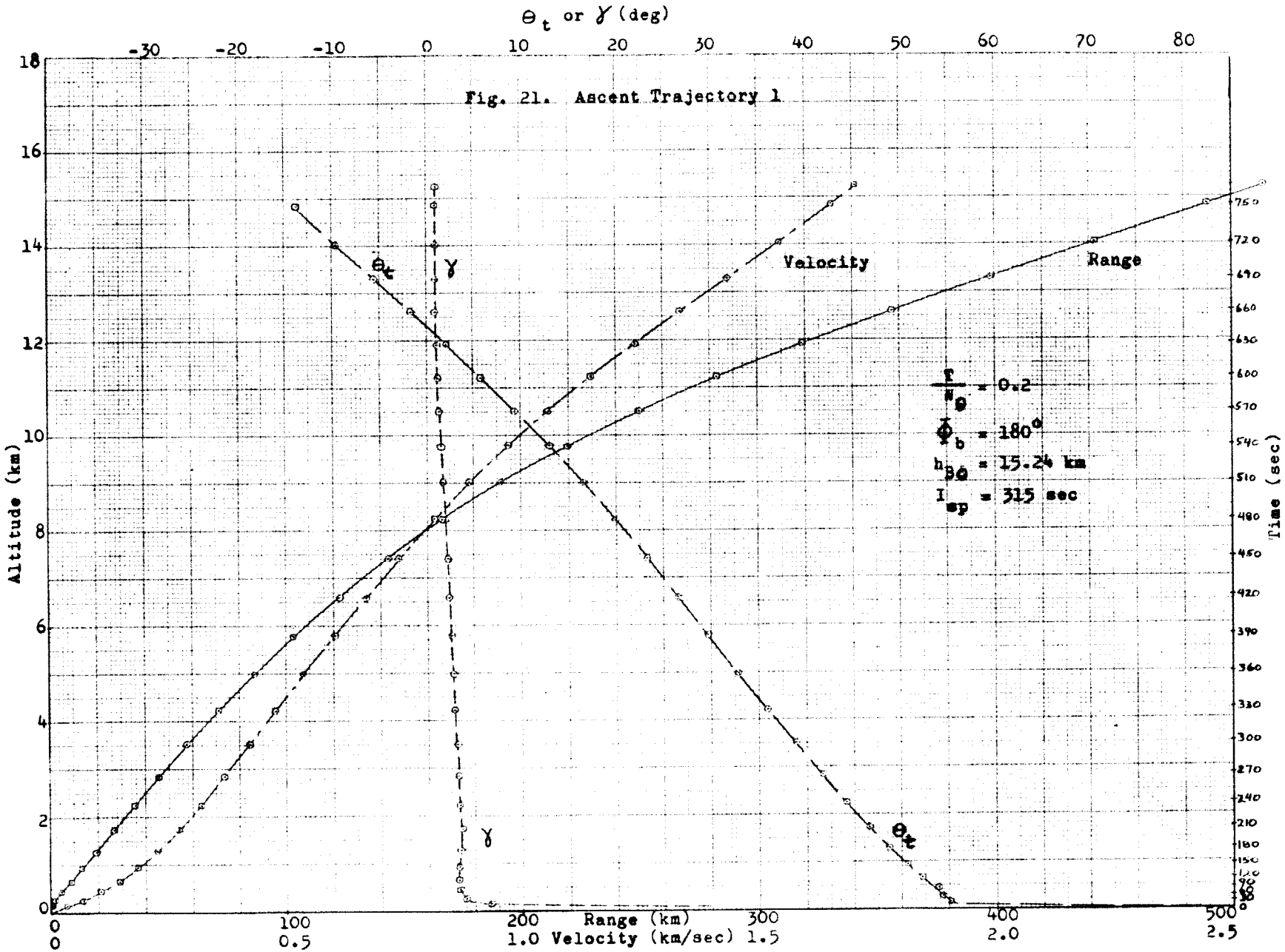

Fig. 21. Ascent Trajectory 1

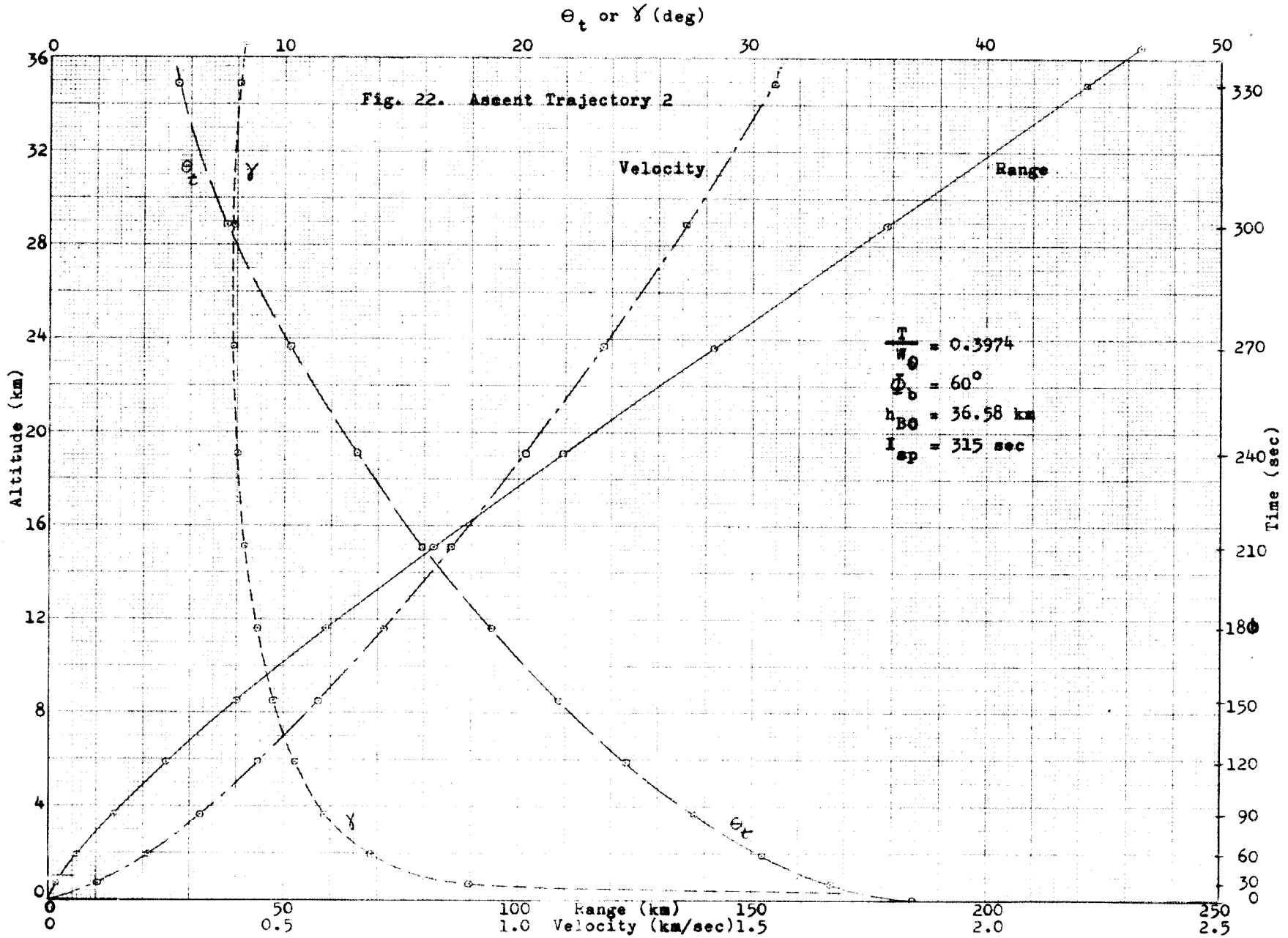
θ_t or γ (deg)
0
10
20
30
40
50
Fig. 22. Ascent Trajectory 2
θ_t
γ
Velocity
Range
$\frac{T}{W_0}$ = 0.3974
Φ_b = 60°
h_{BO} = 36.58 km
I_{sp} = 315 sec
Altitude (km)
0
4
8
12
16
20
24
28
32
36
Time (sec)
0
30
60
90
120
150
180
210
240
270
300
330
Range (km)
0
50
100
150
200
250
Velocity (km/sec)
0
0.5
1.0
1.5
2.0
2.5

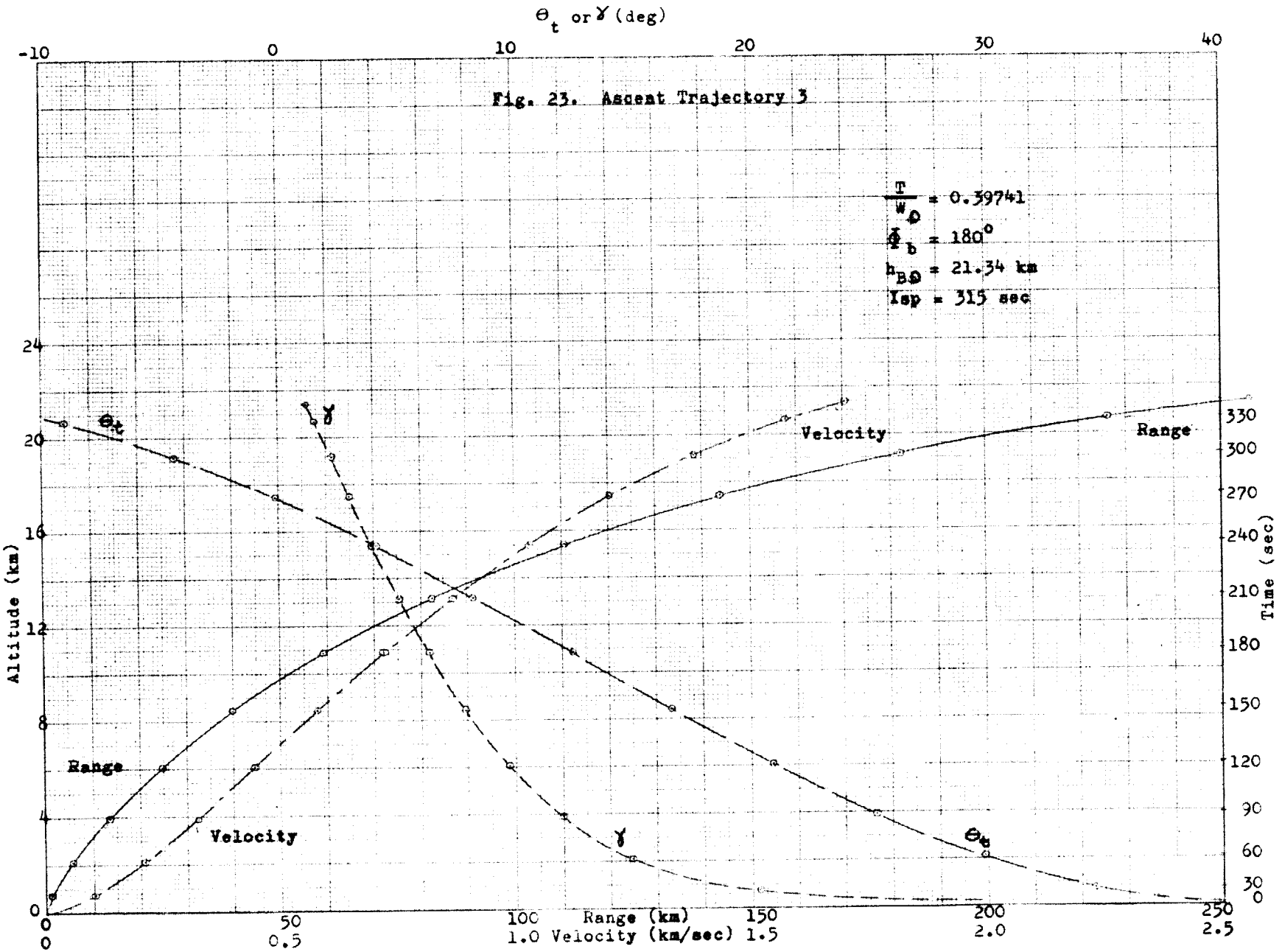
θt or γ (deg)
-10
0
10
20
30
40
Fig. 23. Ascent Trajectory 3
T/W0 = 0.39741
Φb = 180°
hBO = 21.34 km
Isp = 315 sec
θt
γ
Velocity
Range
Range
Velocity
γ
θt
Altitude (km)
0
4
8
12
16
20
24
Time (sec)
0
30
60
90
120
150
180
210
240
270
300
330
0
50
100
150
200
250
Range (km)
0
0.5
1.0
1.5
2.0
2.5
Velocity (km/sec)

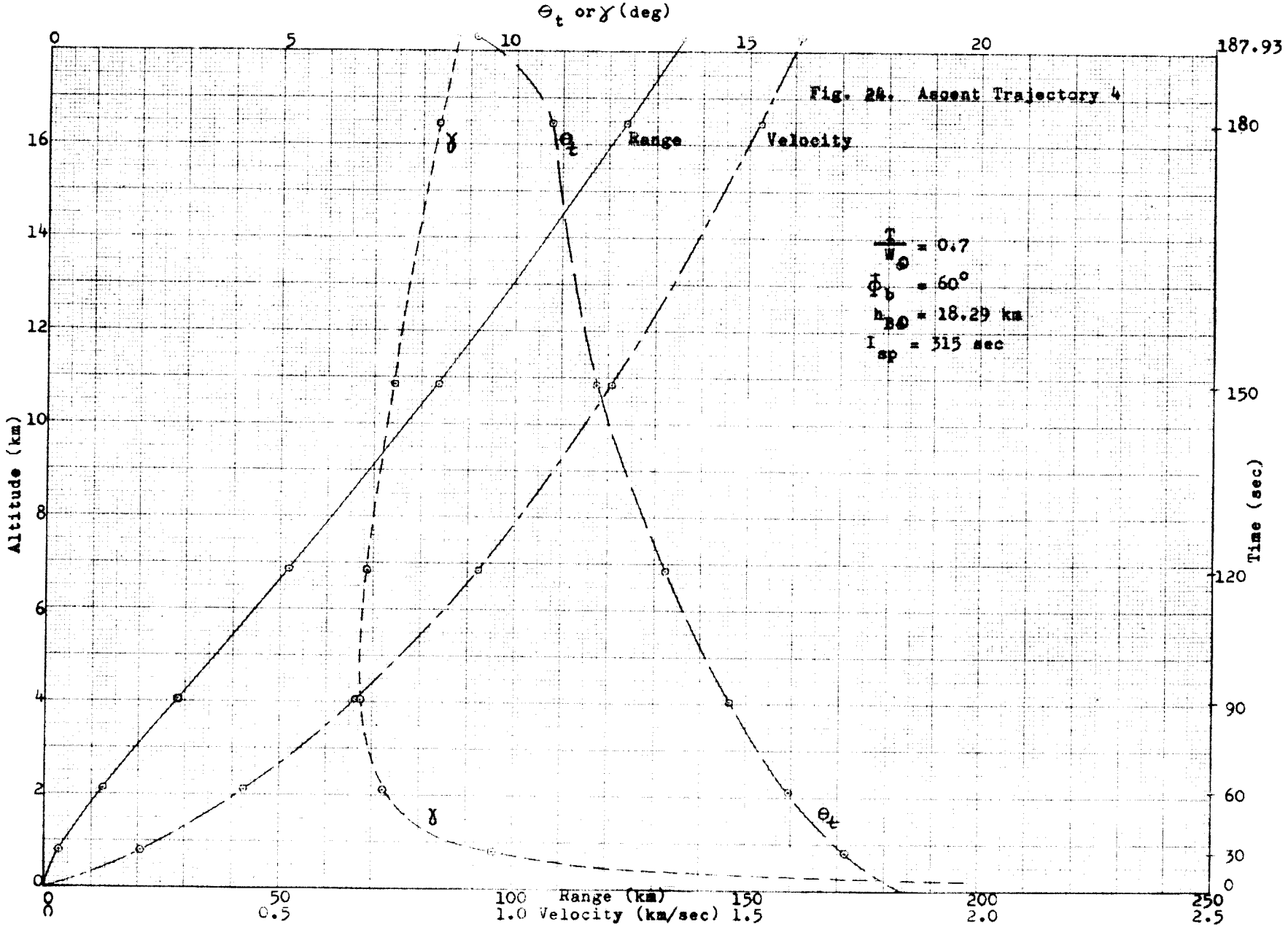

Fig. 28. Ascent Trajectory 4

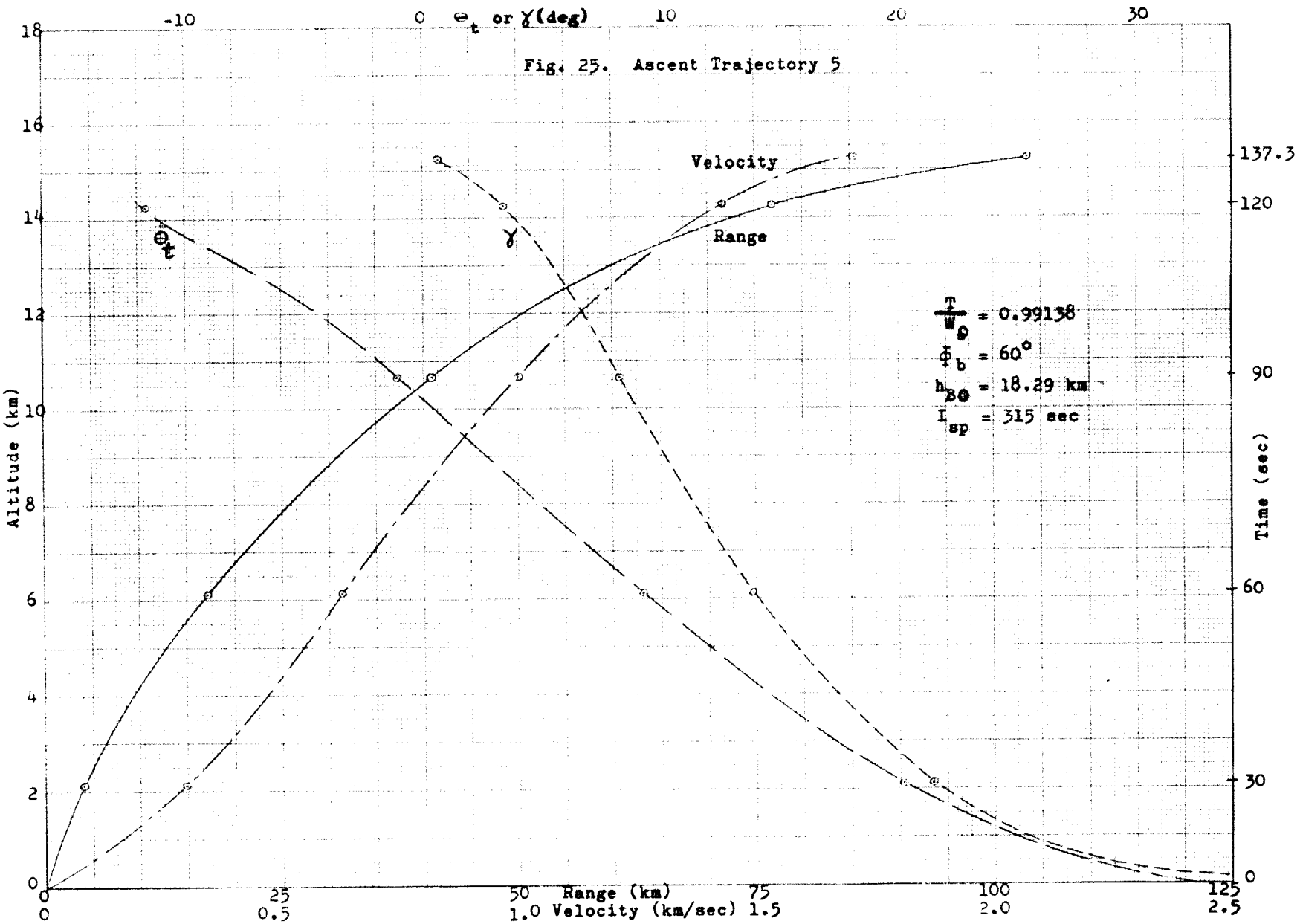

Fig. 25. Ascent Trajectory 5

Fig. 26. Typical Lunar Ascent Trajectory

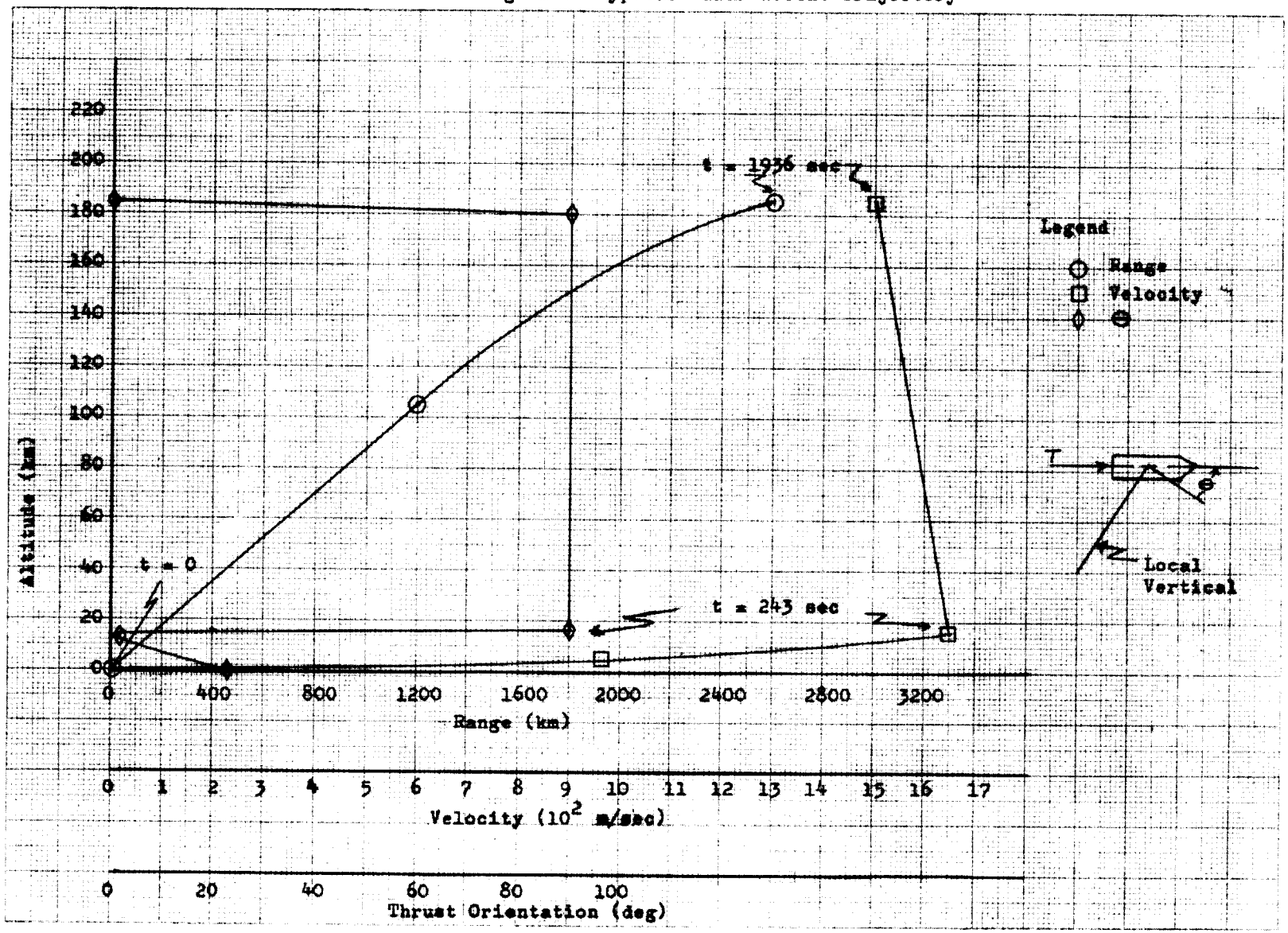

Fig. 27. Characteristic Velocity ΔV Required For Ascent to an 185.2-km Circular Orbit

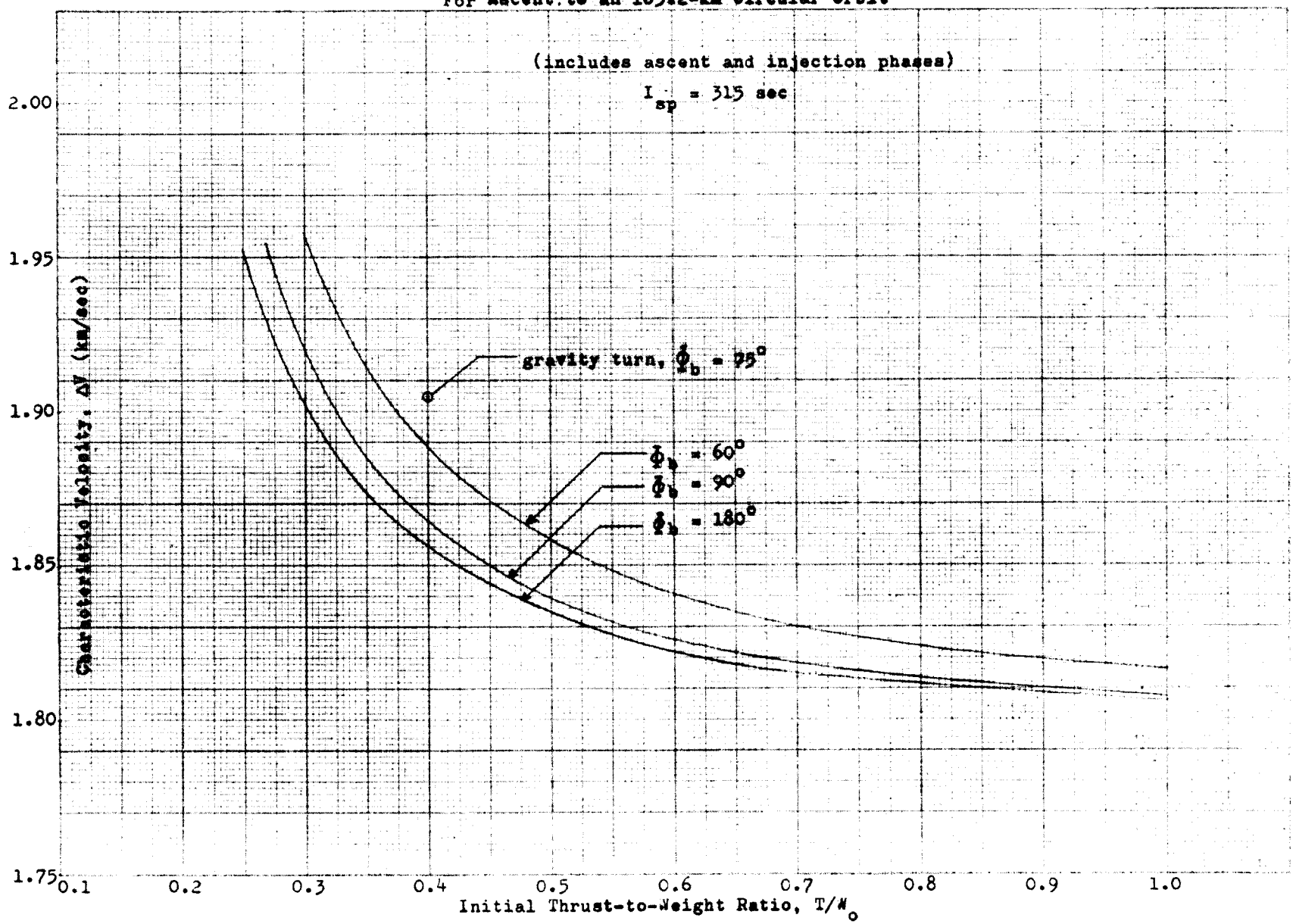

Fig. 28. Excess ΔV Required Versus Launch Time Tolerance for Lunar Rendezvous

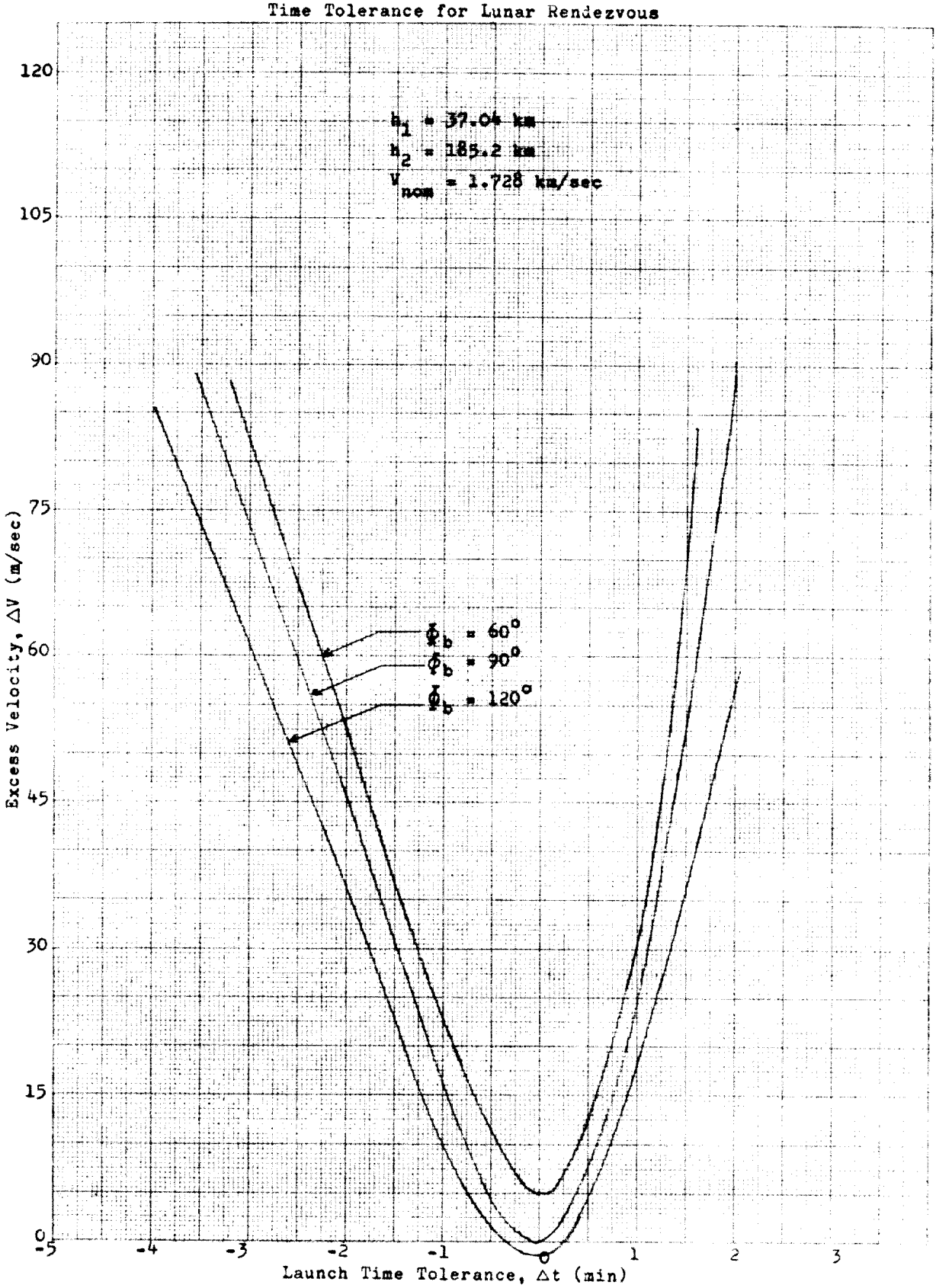

Fig. 29. Excess ΔV Required for Out-of-Plane Ascent

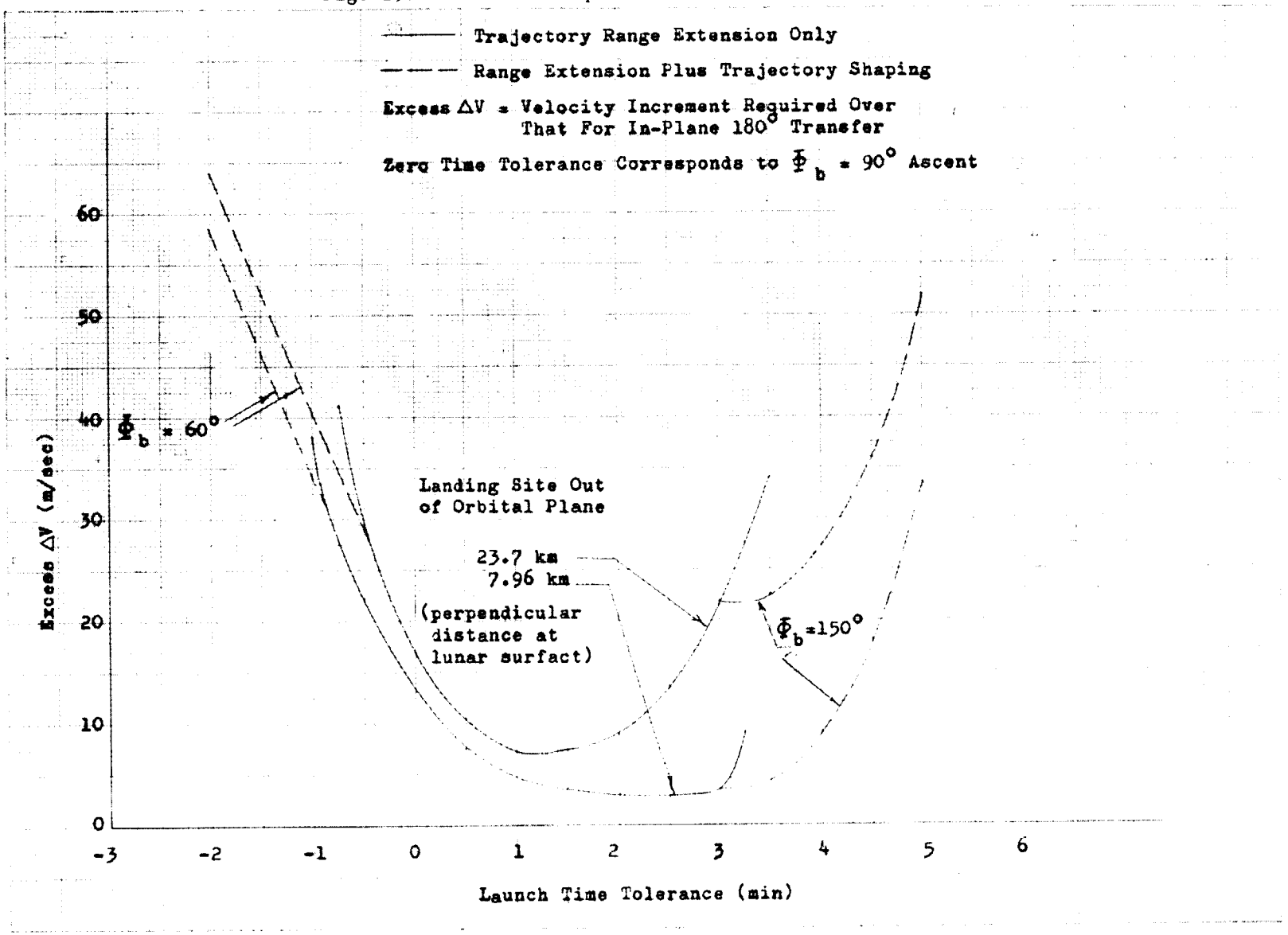

Fig. 30. In-Plane Rendezvous Techniques

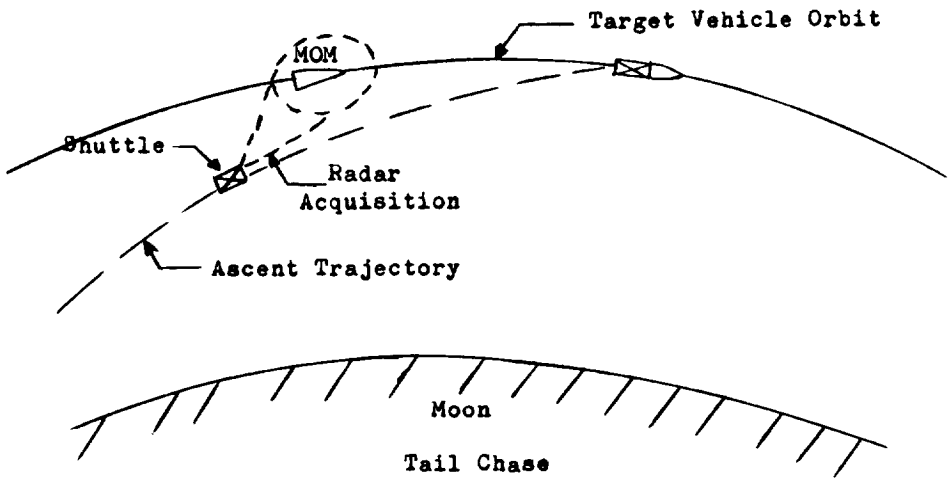

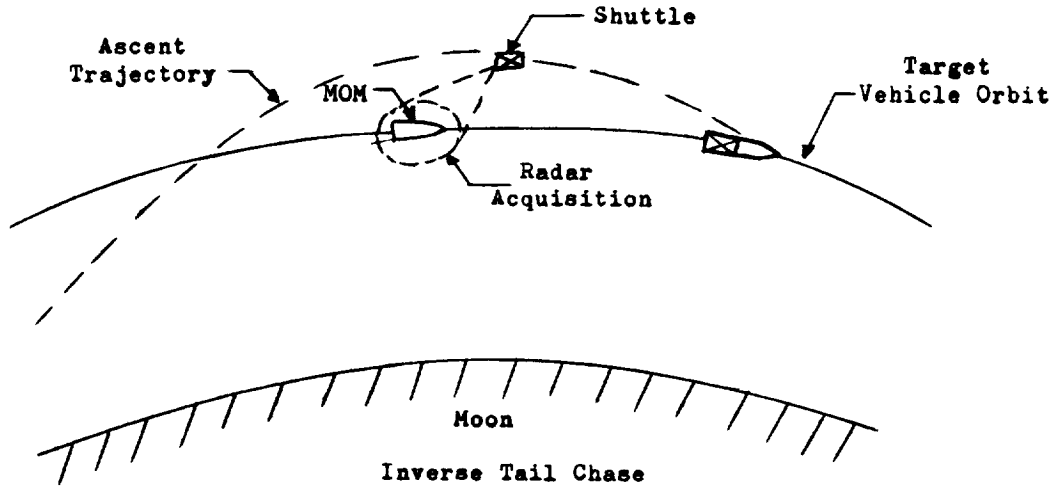

Fig. 31. Lateral Rendezvous

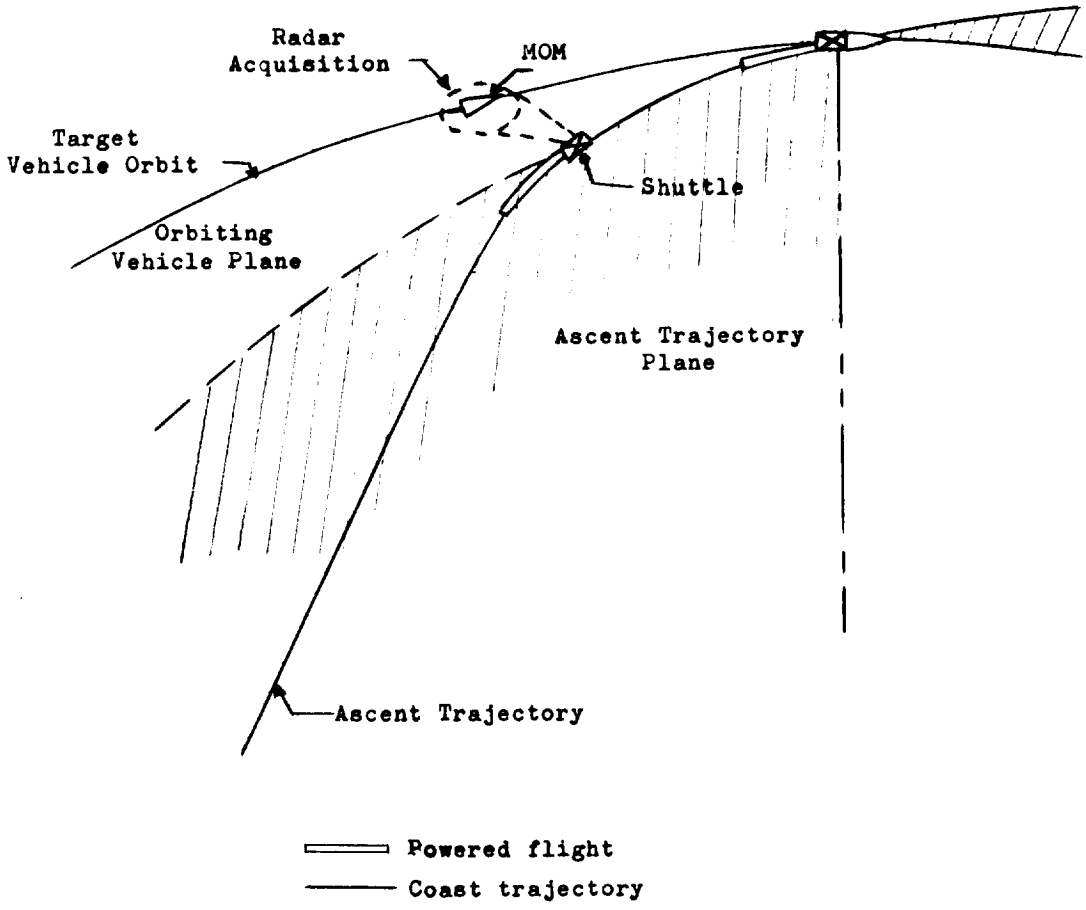

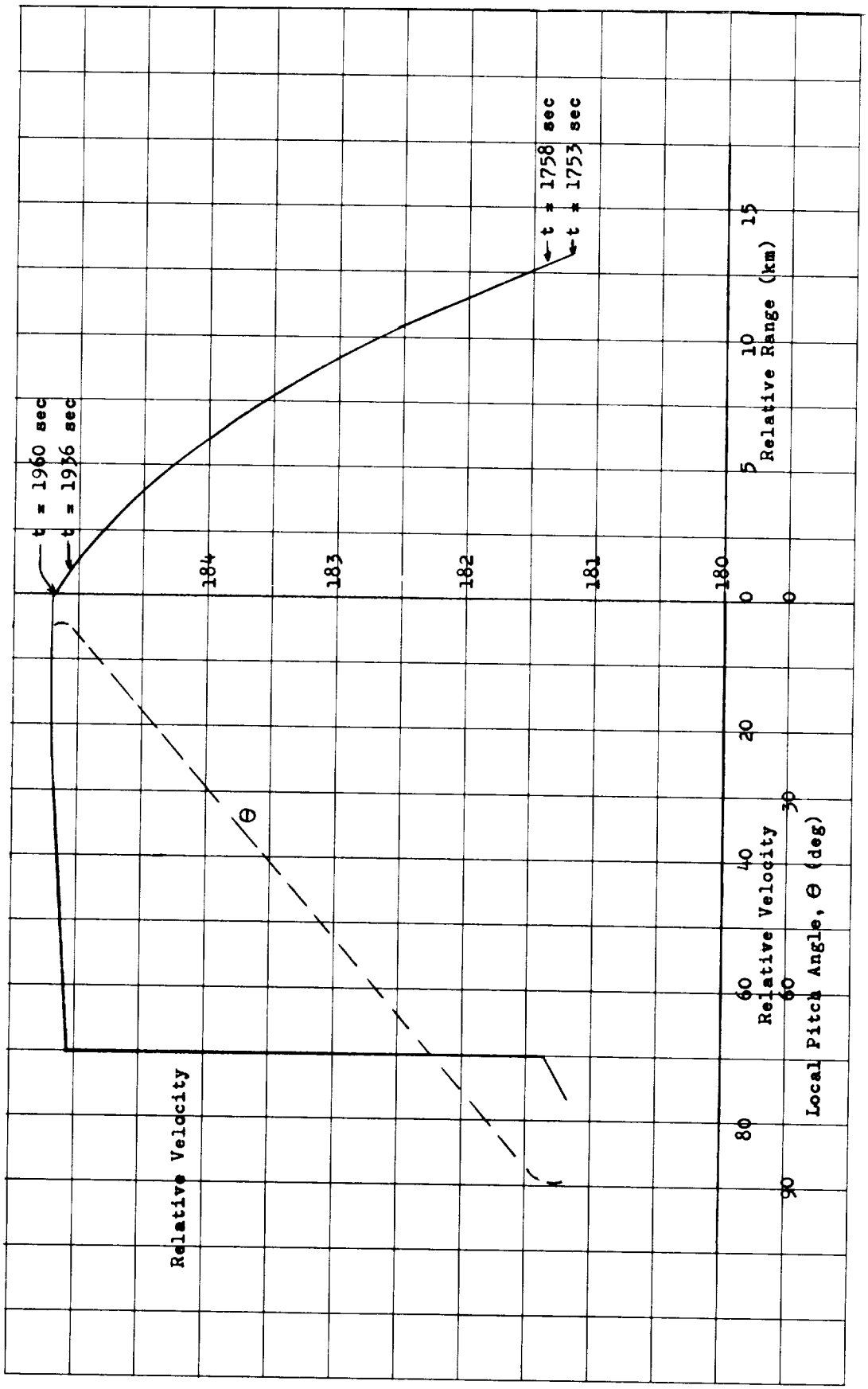

Fig. 32. Typical Lunar Orbit Rendezvous Profile

Fig. 33. Horizontal Translation

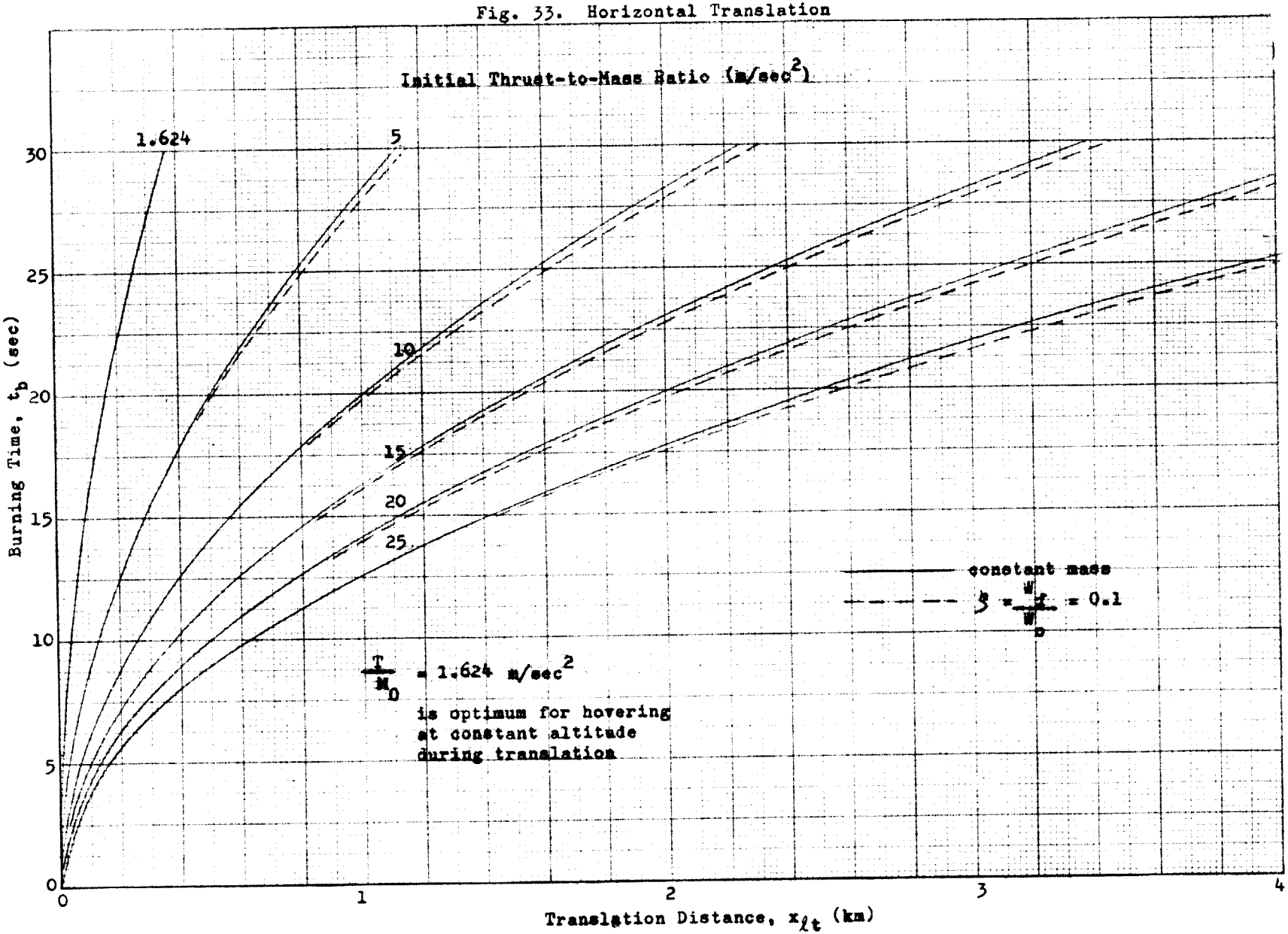

Fig. 34. Minimum Propellant for Translation While Hovering at Constant Altitude

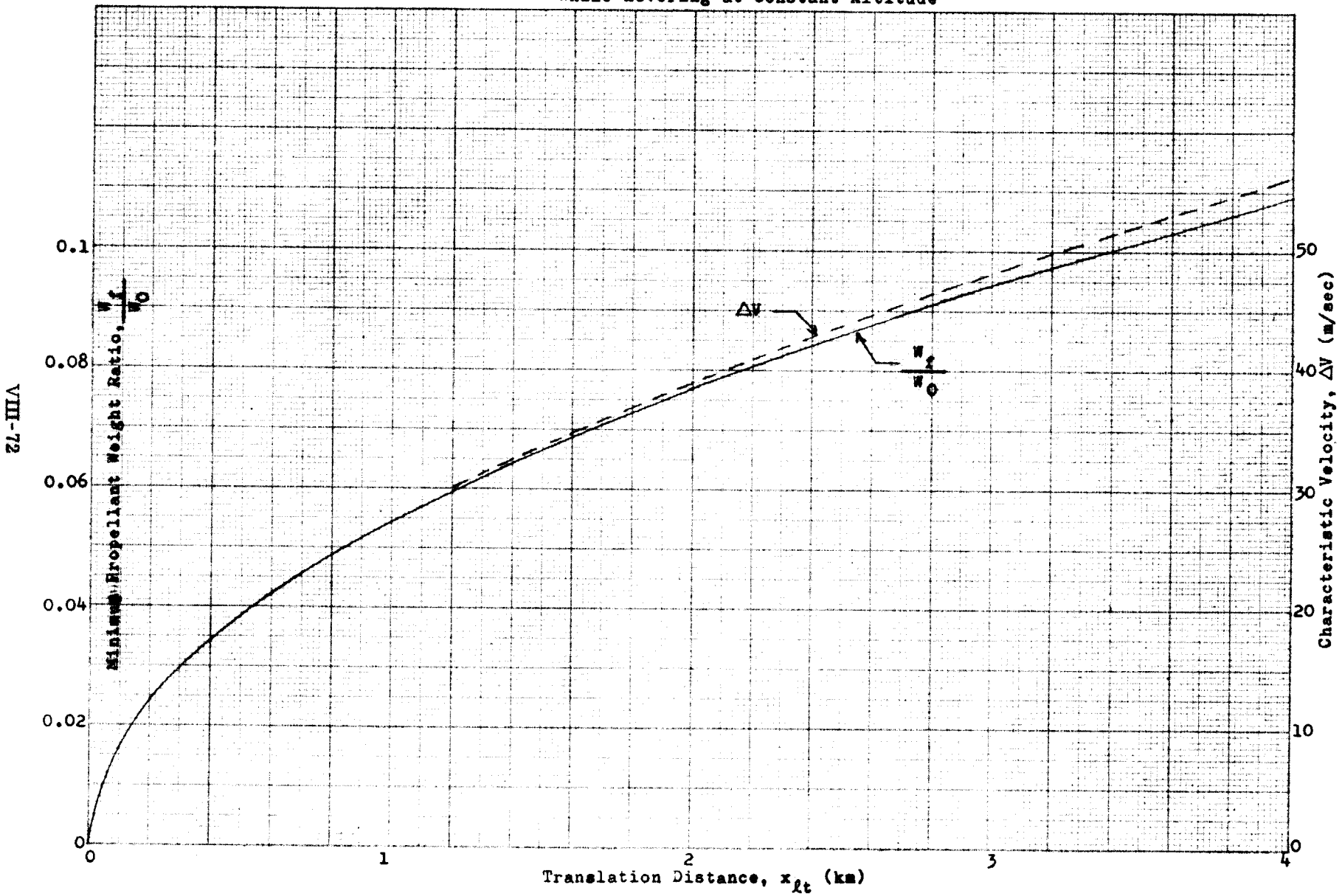

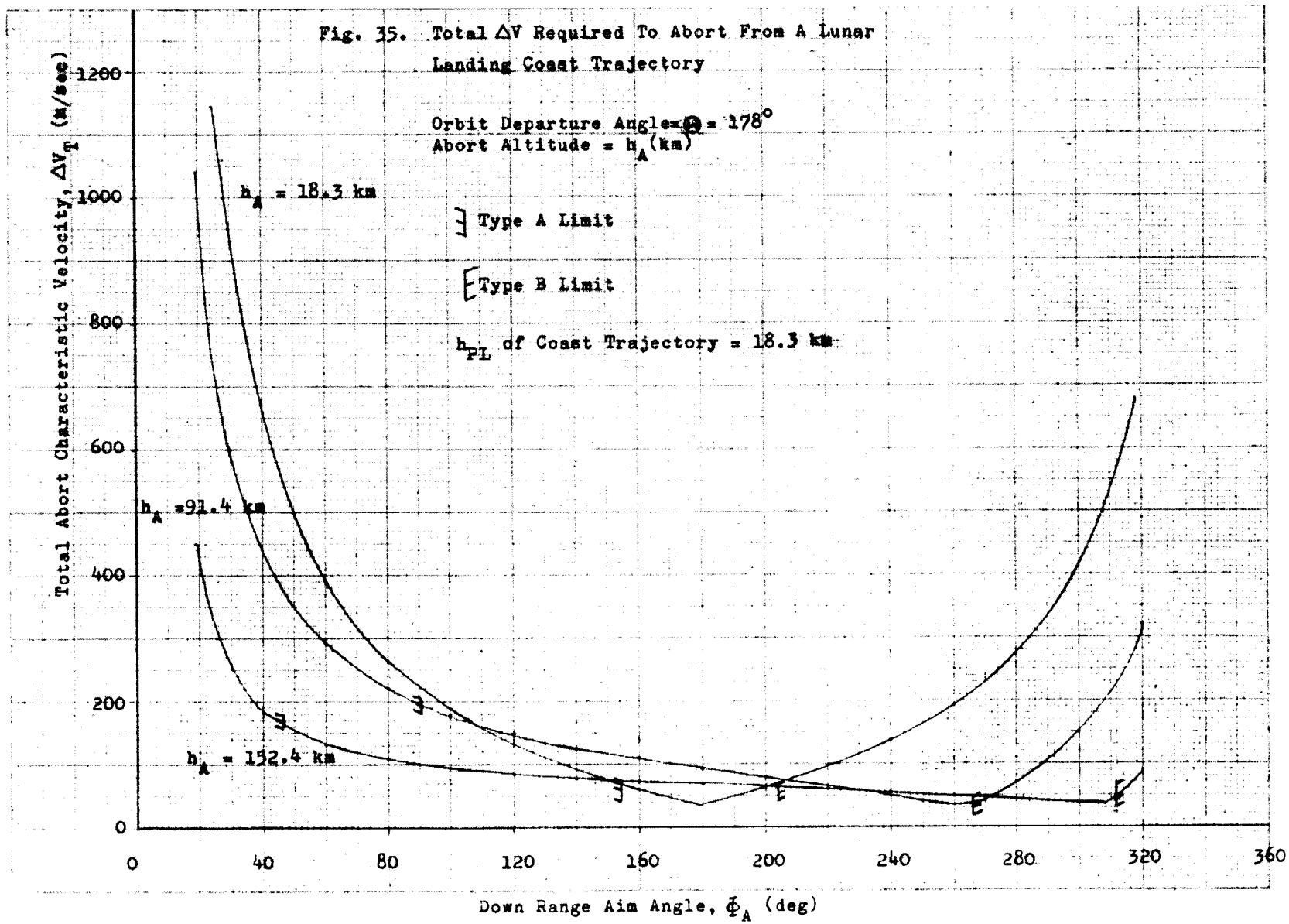

Fig. 35. Total ΔV Required To Abort From A Lunar Landing Coast Trajectory

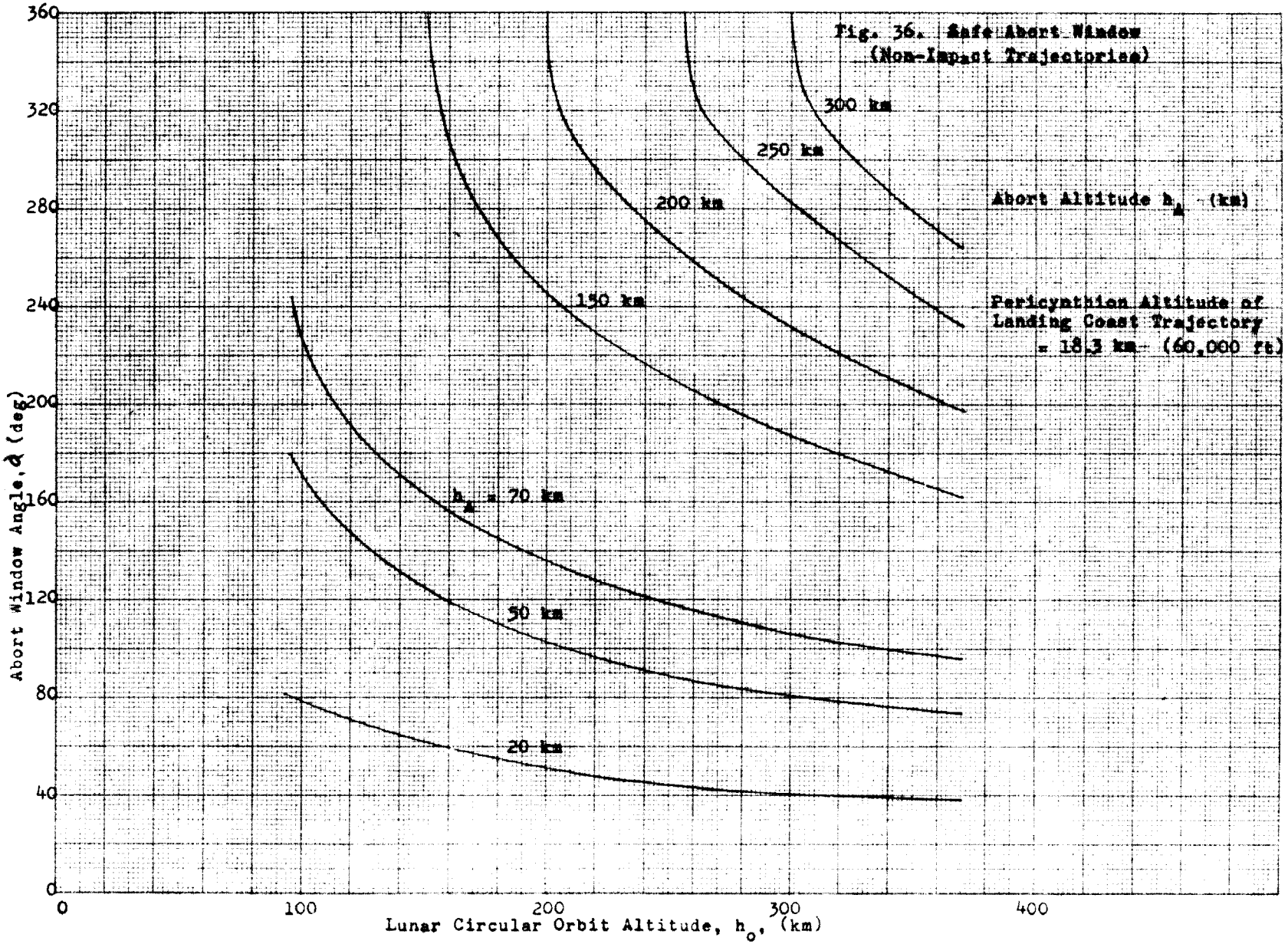

Fig. 36. Safe Abort Window (Non-Impact Trajectories)

Fig. 37. ΔV Required To Abort And Rendezvous At 92.6 km (50 N Mi) From a Landing Coast Trajectory

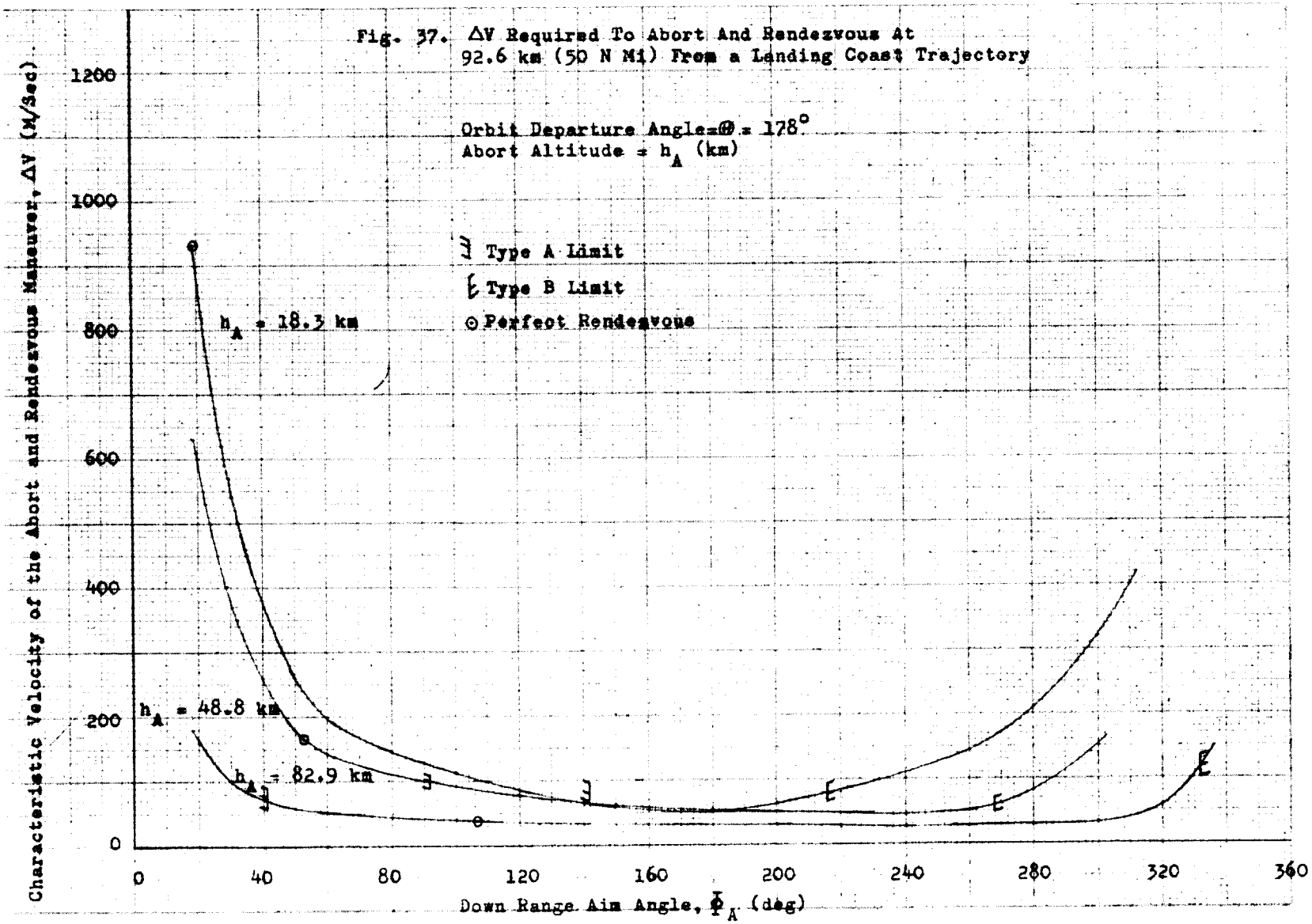

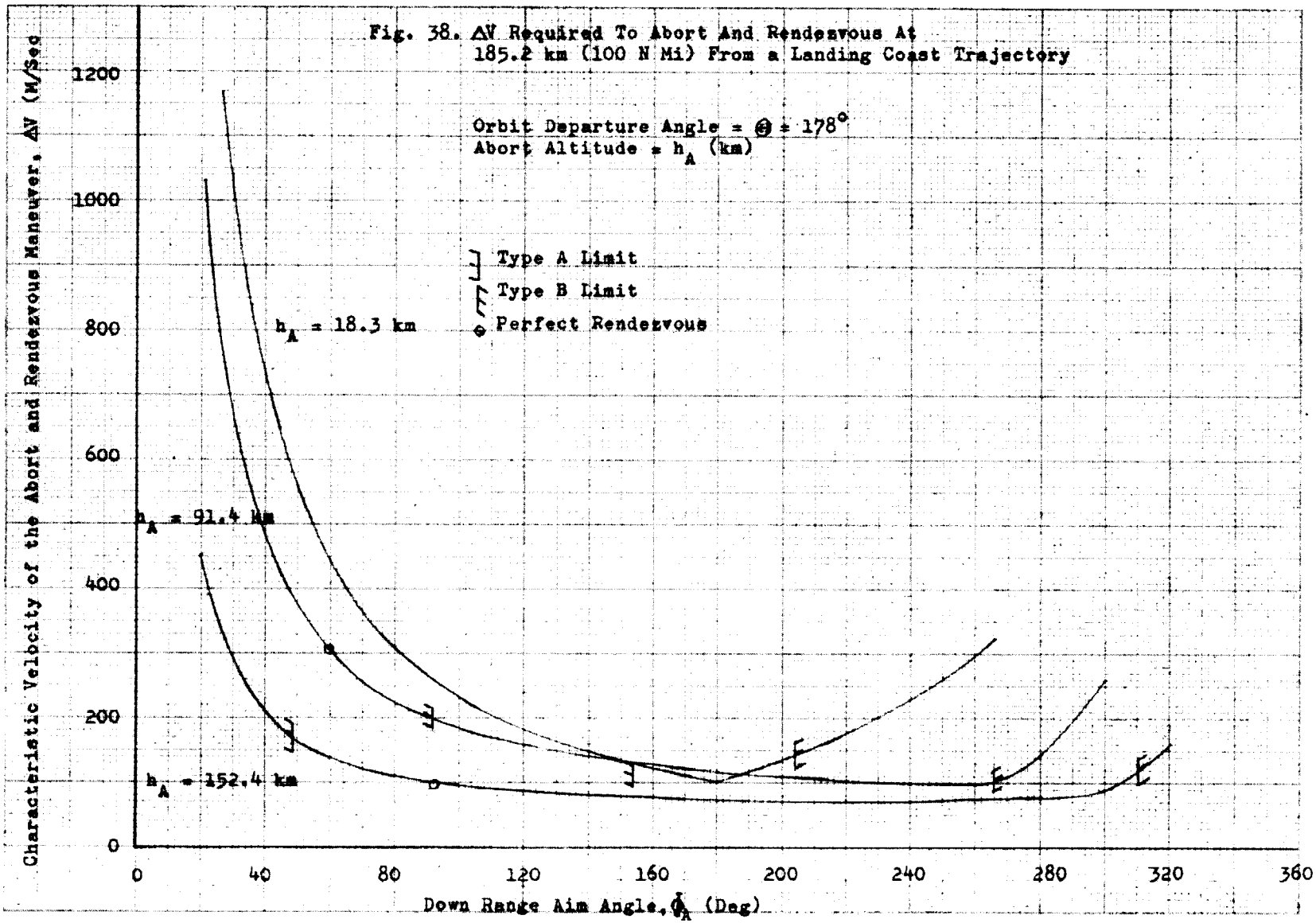

Fig. 38. ΔV Required To Abort And Rendezvous At 185.2 km (100 N Mi) From a Landing Coast Trajectory

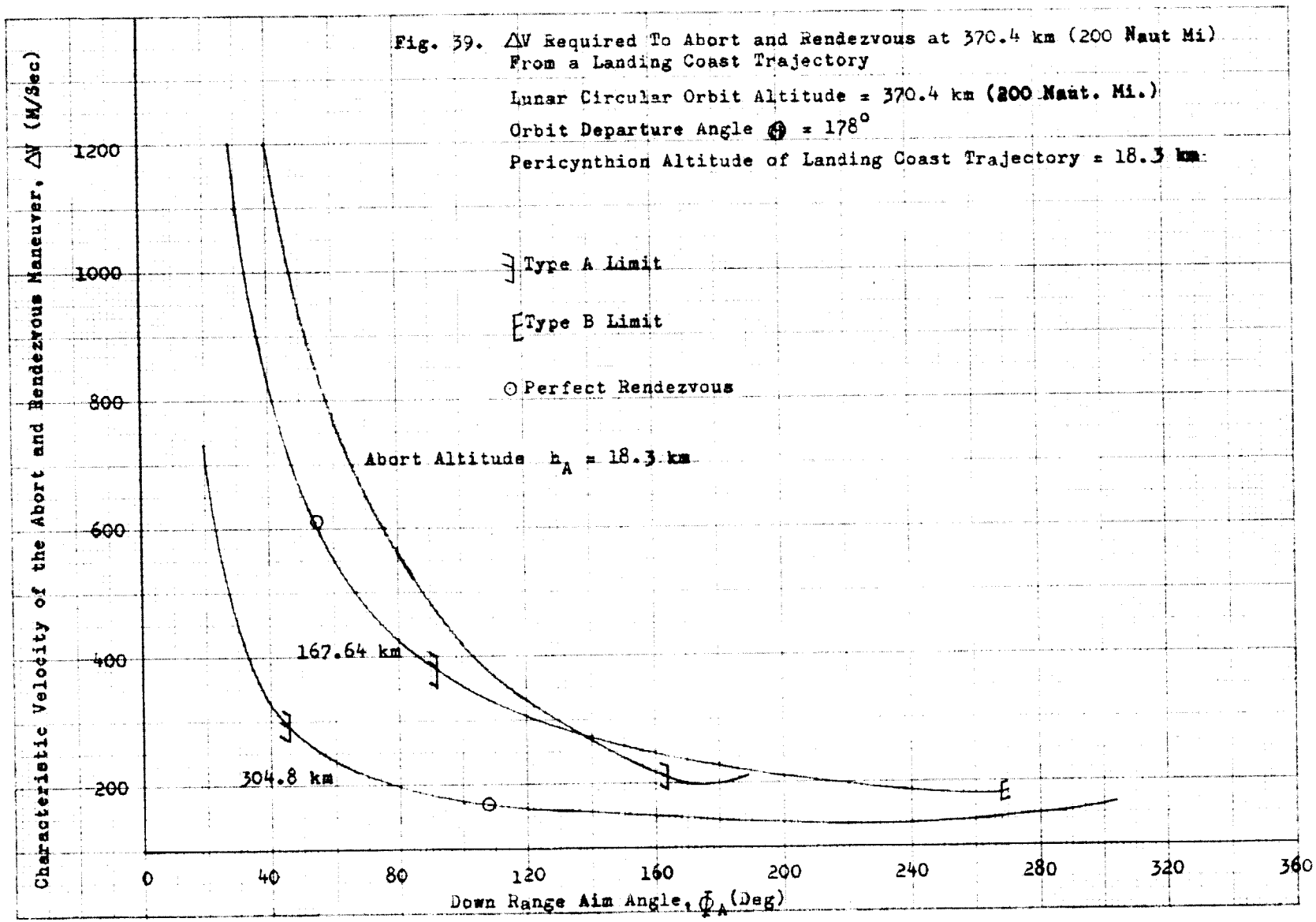

Fig. 39. ΔV Required To Abort and Rendezvous at 370.4 km (200 Naut Mi) From a Landing Coast Trajectory

Lunar Circular Orbit Altitude = 370.4 km (200 Naut. Mi.)

Orbit Departure Angle Θ = 178°

Pericynthion Altitude of Landing Coast Trajectory = 18.3 km

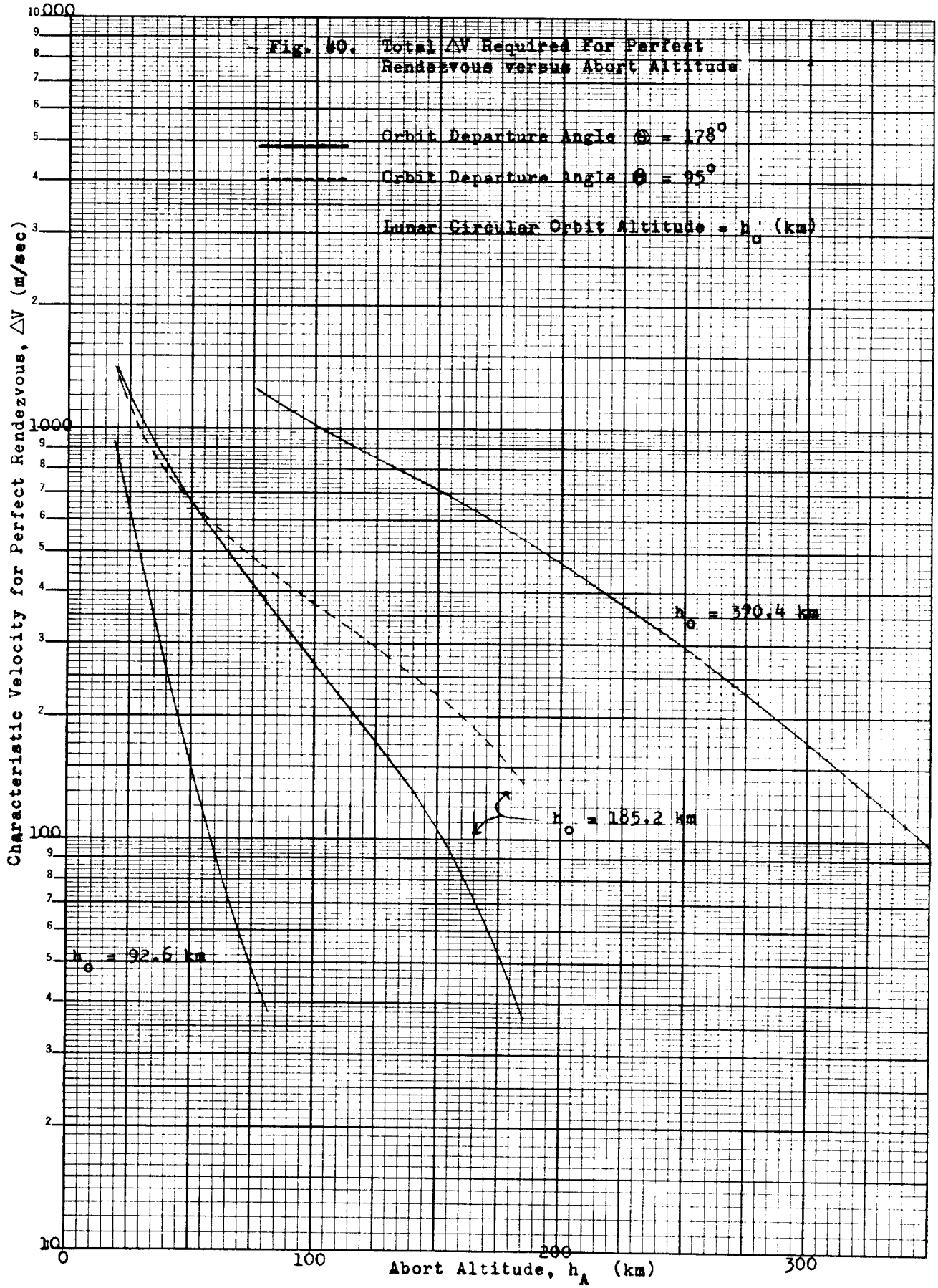
Fig. 40. Total ΔV Required For Perfect Rendezvous versus Abort Altitude
Orbit Departure Angle Θ = 178°
Orbit Departure Angle Θ = 95°
Lunar Circular Orbit Altitude = h_o' (km)
h_o = 370.4 km
h_o = 185.2 km
h_o = 92.6 km
Characteristic Velocity for Perfect Rendezvous, ΔV (m/sec)
Abort Altitude, h_A (km)
10,000
1000
100
10
0
100
200
300

Fig. 41. ΔV Required To Abort and Rendezvous At 185.2 km (100 Naut Mi) From a Landing Coast Trajectory
Orbit Departure Angle = Θ = 95°
Abort Altitude = h_A (km)
h_A = 18.3 km
Type A Limit
Type B Limit
Perfect Rendezvous
h_A = 91.4 km
h_A = 152.4 km
Characteristic Velocity of the Abort and Rendezvous Maneuver, ΔV (M/Sec)
Down Range Air Angle, ϕ_A (Deg)
1300
1100
900
700
500
300
100
0
40
80
120
160
200
240
280
320
360
A
B
C
D
E

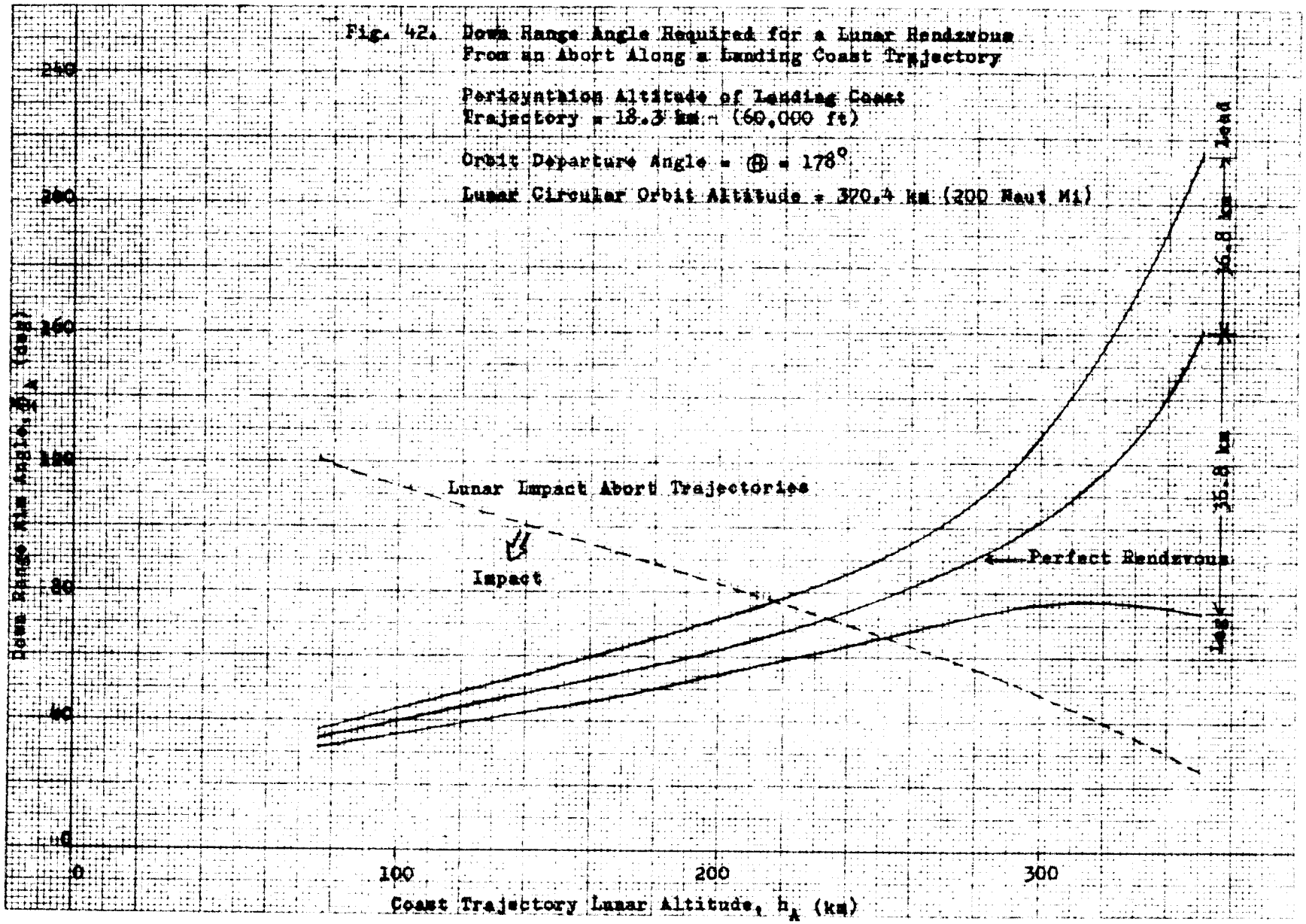
Fig. 42. Down Range Angle Required for a Lunar Rendezvous From an Abort Along a Landing Coast Trajectory
Perigynthion Altitude of Landing Coast Trajectory = 18.3 km (60,000 ft)
Orbit Departure Angle = ⊕ = 178°
Lunar Circular Orbit Altitude = 370.4 km (200 Naut Mi)
Down Range Arm Angle, Ψ_A (Deg)
Lunar Impact Abort Trajectories
Impact
Perfect Rendezvous
Lead
Lag
36.8 km
36.8 km
0
100
200
300
Coast Trajectory Lunar Altitude, h_A (km)

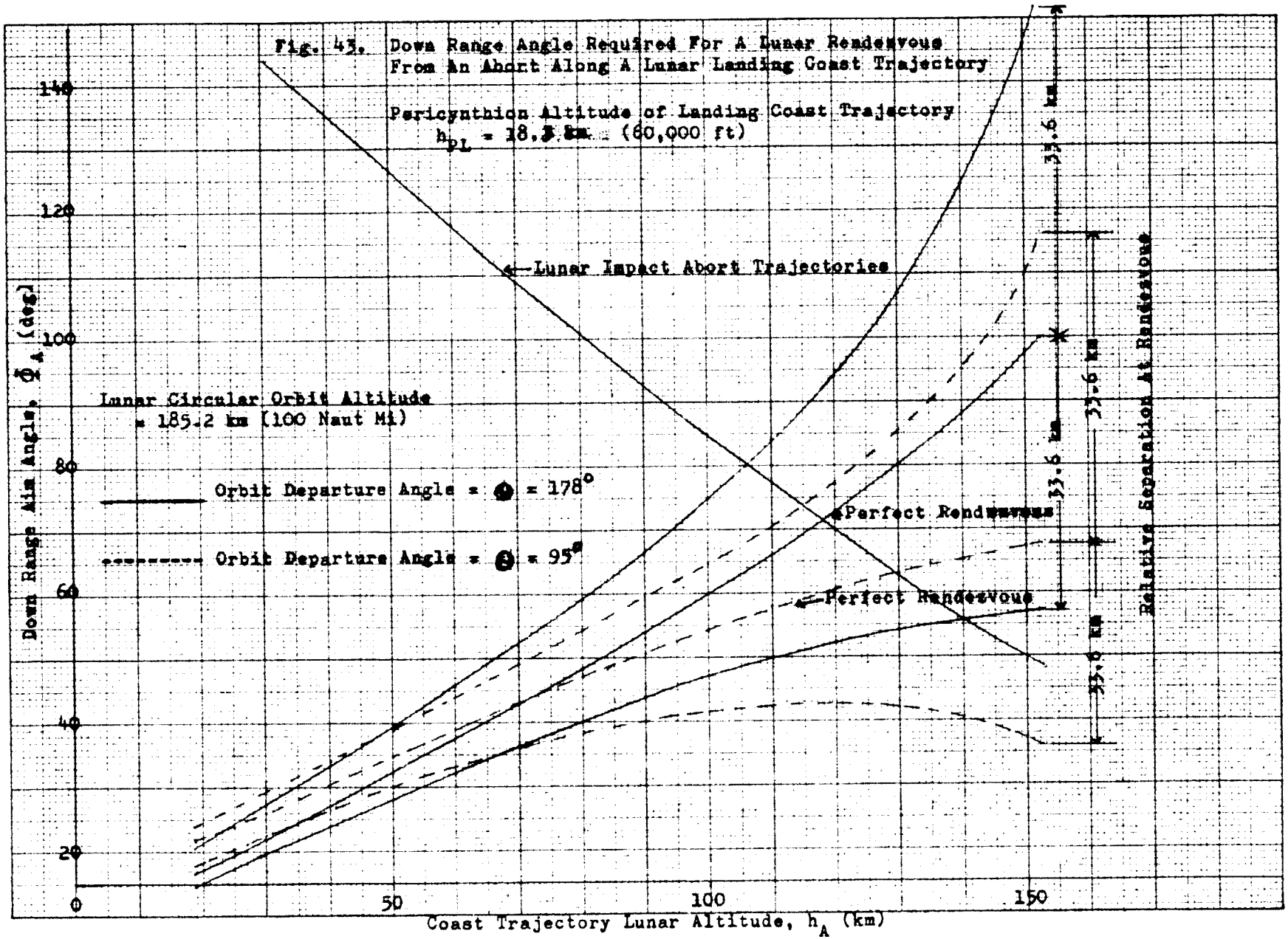

Fig. 43. Down Range Angle Required For A Lunar Rendezvous From An Abort Along A Lunar Landing Coast Trajectory

Pericynthion Altitude of Landing Coast Trajectory
h_{PL} = 18.3 km (60,000 ft)

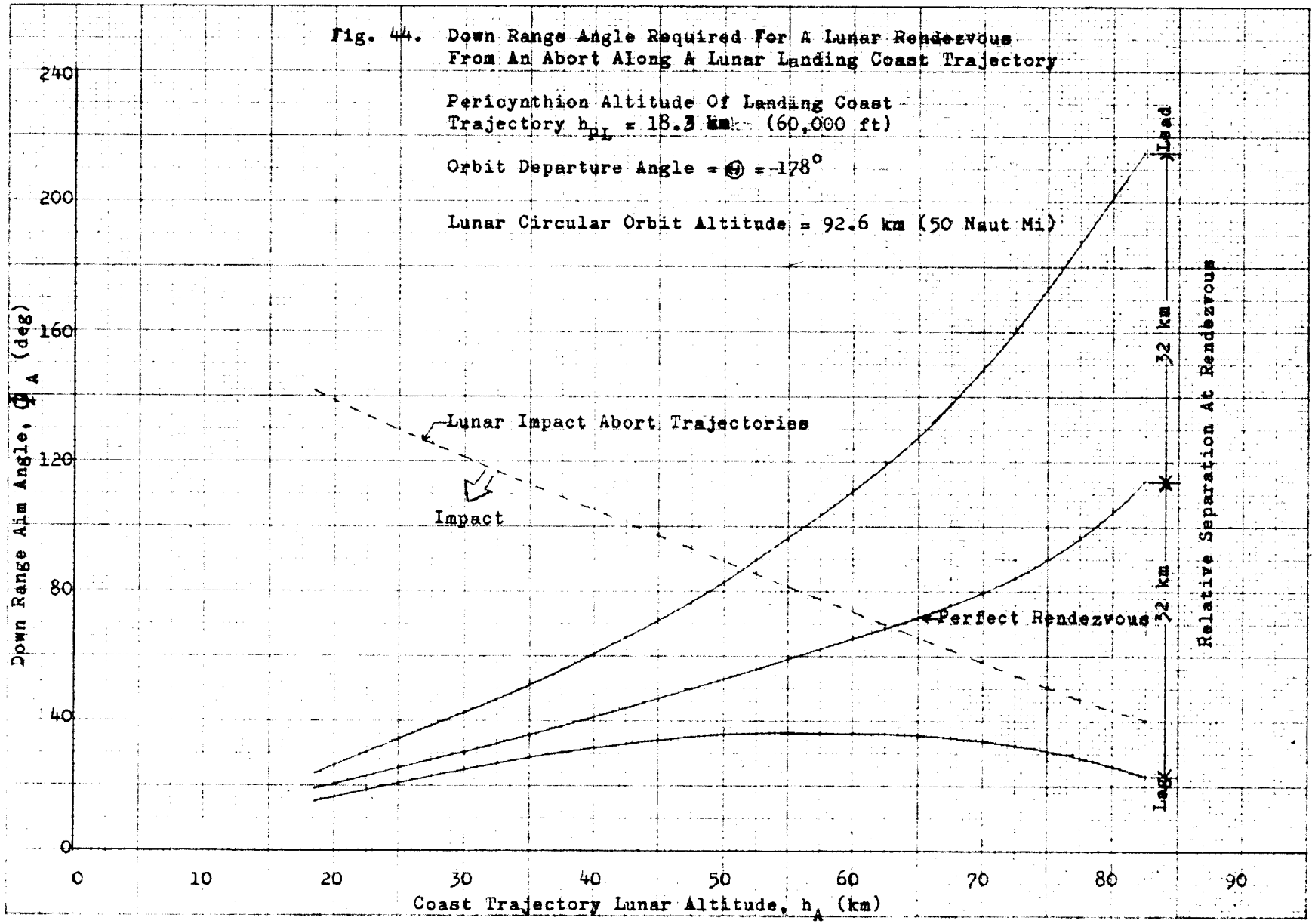

Fig. 44. Down Range Angle Required For A Lunar Rendezvous From An Abort Along A Lunar Landing Coast Trajectory

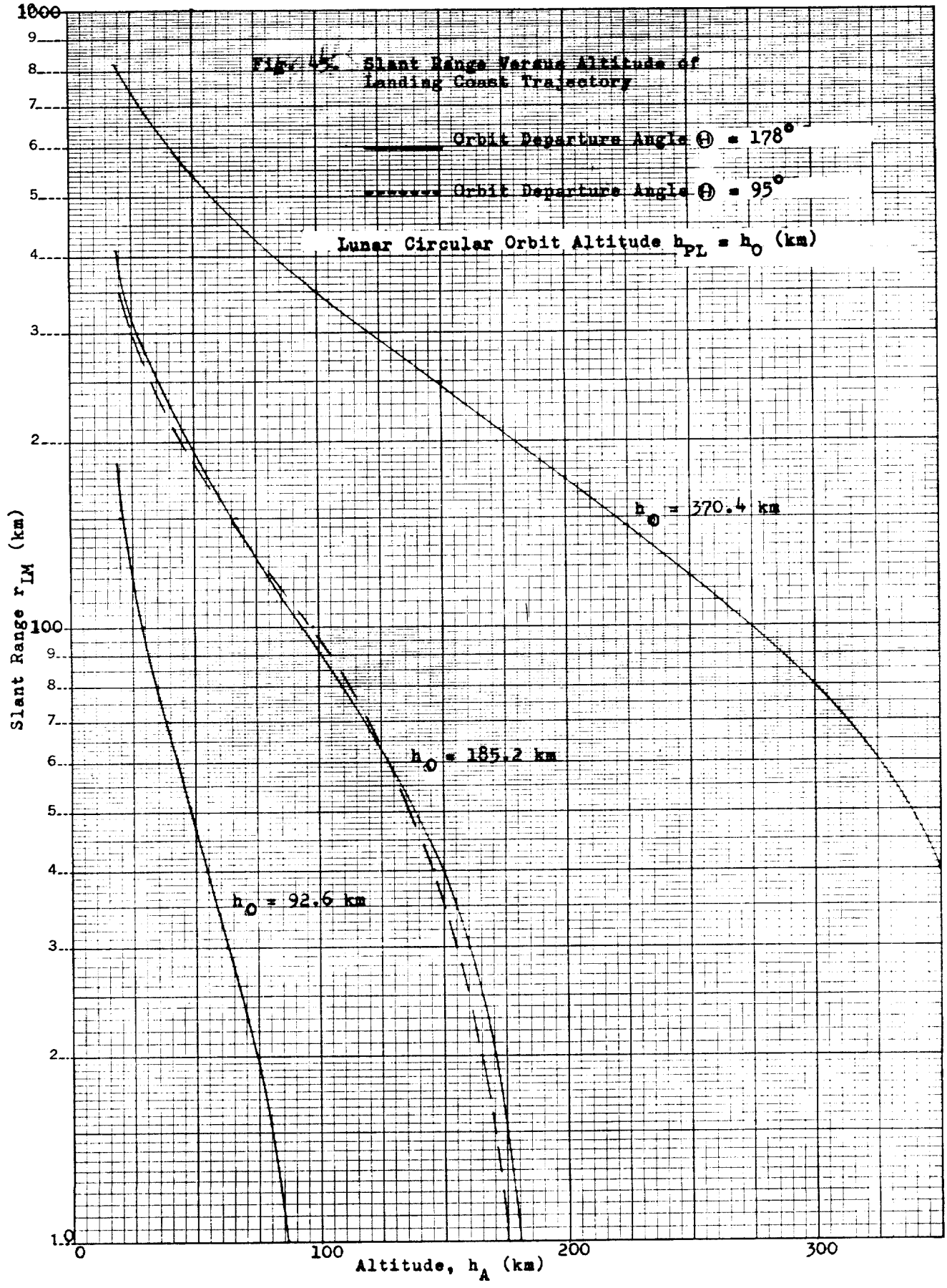
Fig. 45. Slant Range Versus Altitude of Landing Coast Trajectory
Orbit Departure Angle Θ = 178°
Orbit Departure Angle Θ = 95°
Lunar Circular Orbit Altitude $h_{PL} = h_O$ (km)
h_O = 370.4 km
h_O = 185.2 km
h_O = 92.6 km
Slant Range r_{LM} (km)
Altitude, h_A (km)
1000
100
1.0
0
100
200
300

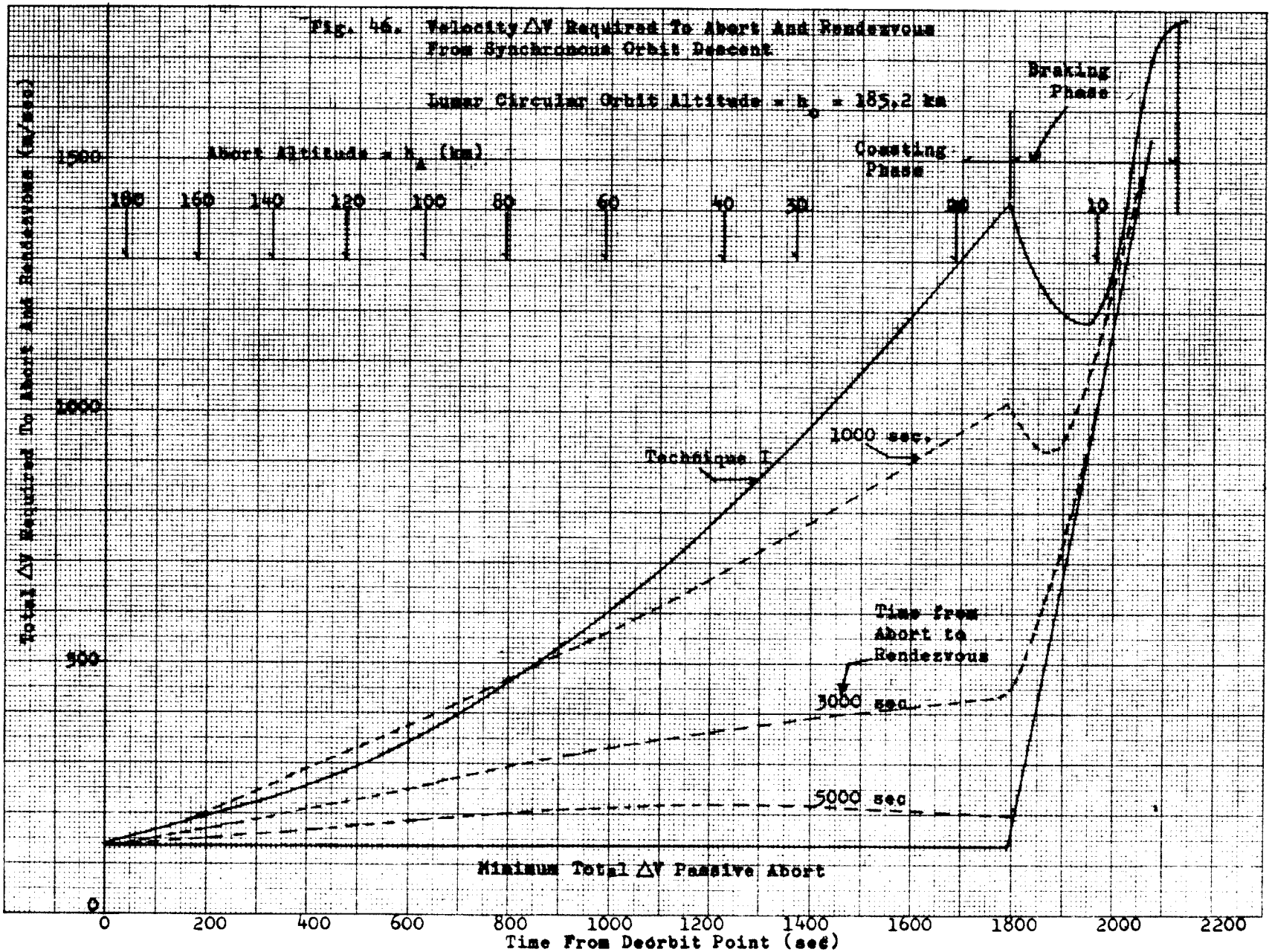
Fig. 46. Velocity ΔV Required To Abort And Rendezvous From Synchronous Orbit Descent
Lunar Circular Orbit Altitude = h_o = 185.2 km
Abort Altitude = h_A (km)
180
160
140
120
100
80
60
40
30
20
10
Braking Phase
Coasting Phase
Total ΔV Required To Abort And Rendezvous (m/sec)
1500
1000
500
0
Technique I
1000 sec.
Time from Abort to Rendezvous
3000 sec.
5000 sec
Minimum Total ΔV Passive Abort
0
200
400
600
800
1000
1200
1400
1600
1800
2000
2200
Time From Deorbit Point (sec)

Fig. 47. Landing Safety Boundaries

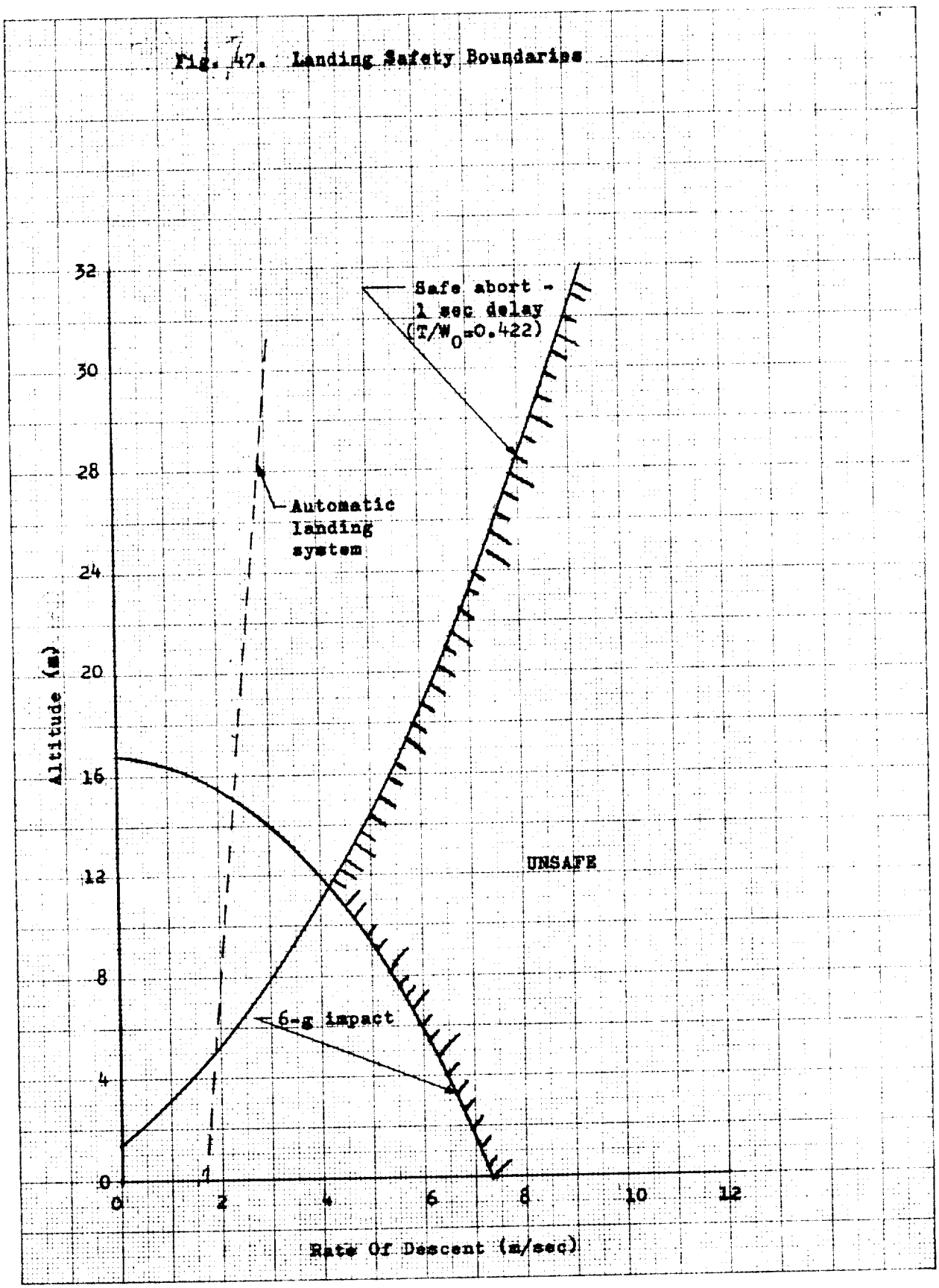

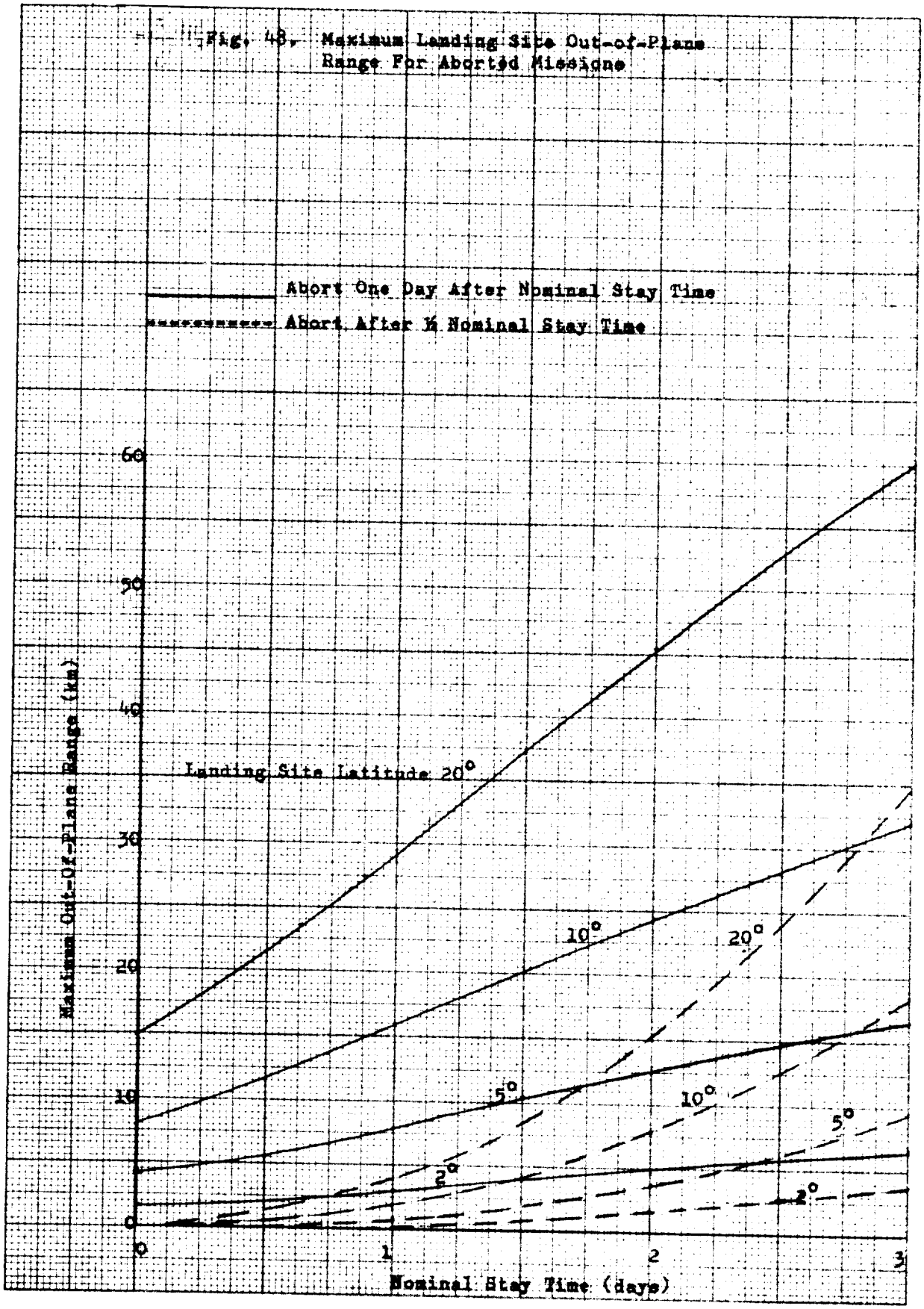

Fig. 48. Maximum Landing Site Out-of-Plane Range For Aborted Missions

Fig. 49. Emergency Backup Guidance Capability

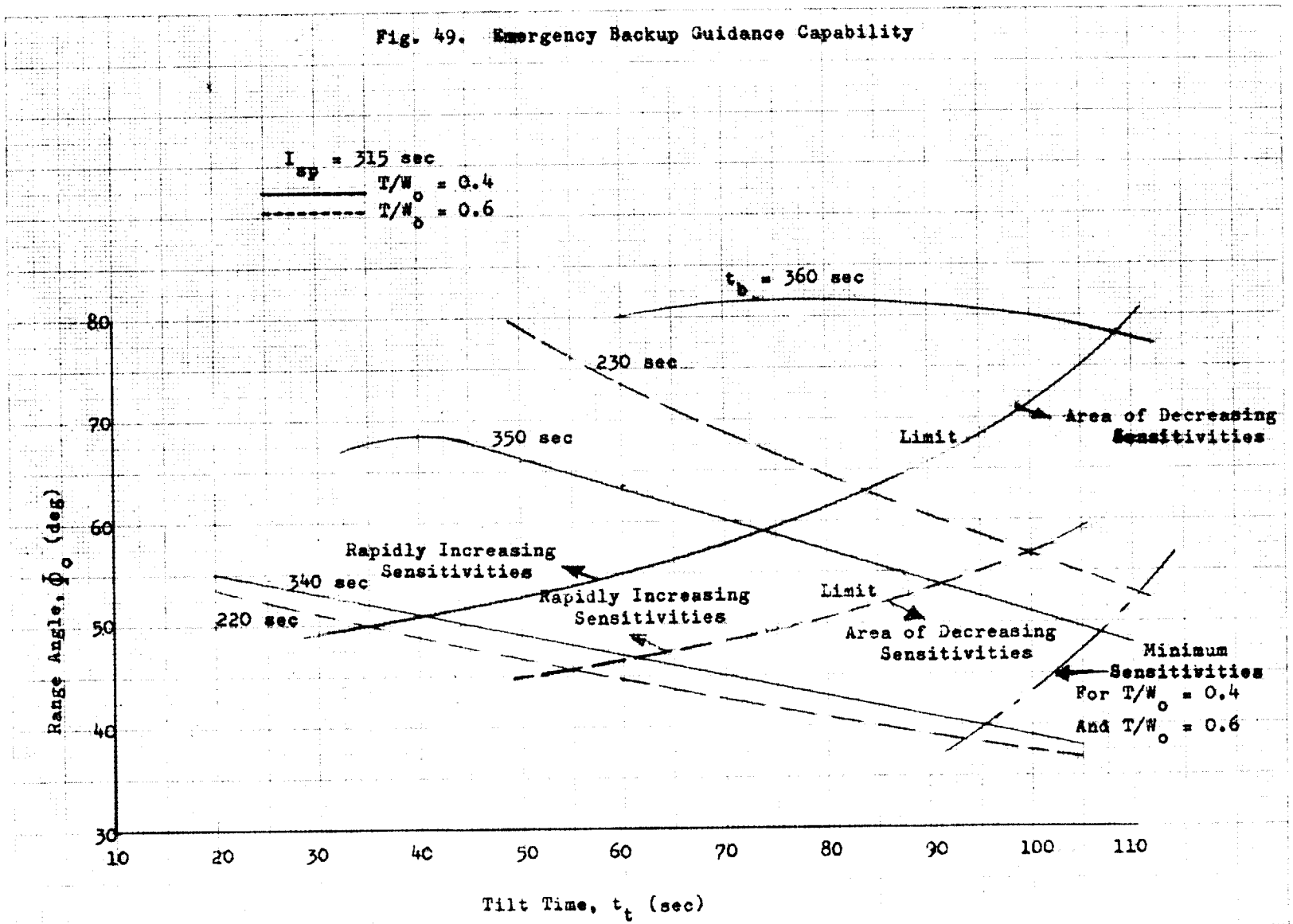

Fig. 50. Pitch Rate And Initial Pitch Angle Required For Range Extension

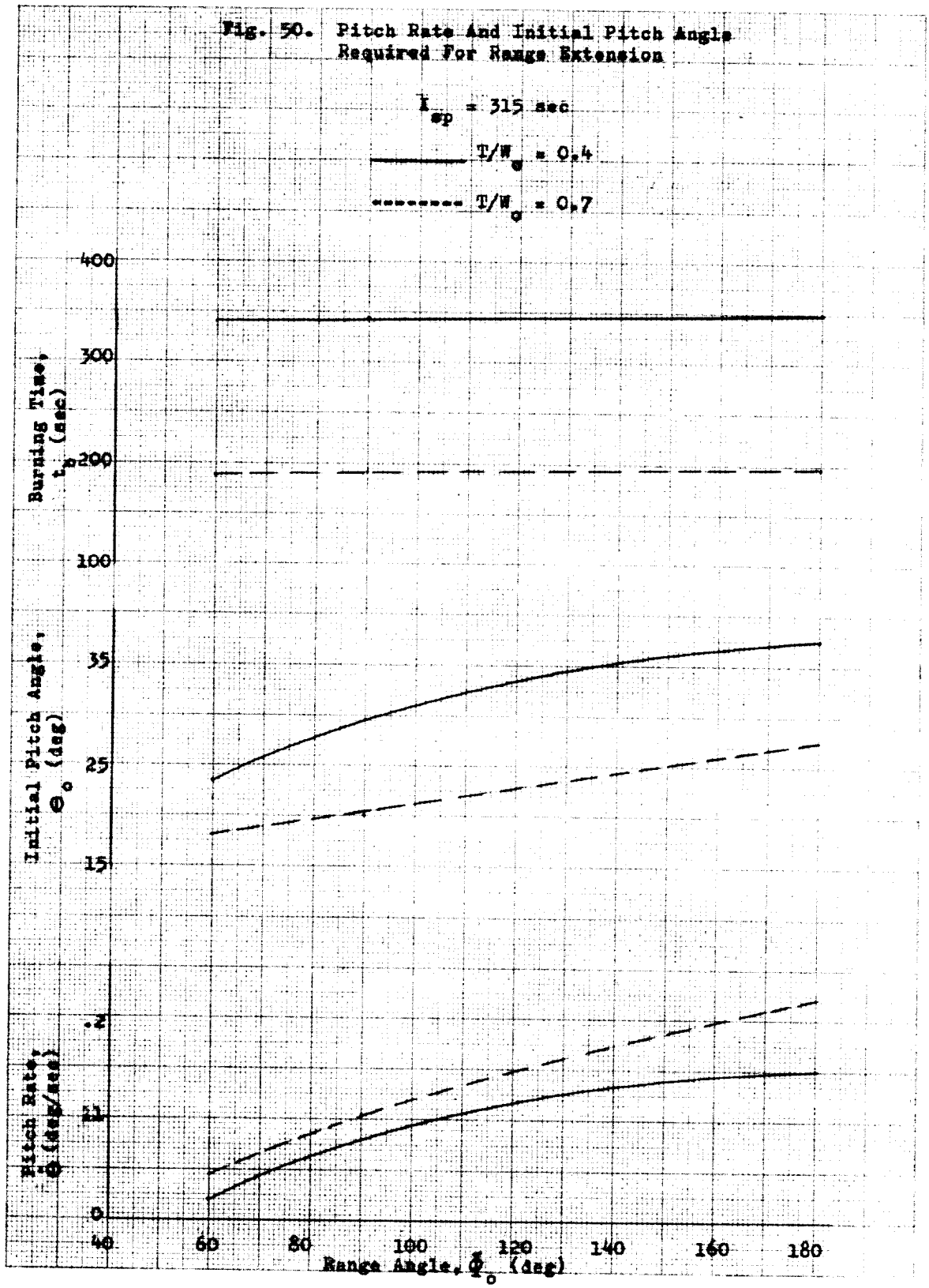

CHAPTER IX

MOON-TO-EARTH TRANSFER

Prepared by:

F. Santora, R. Salinger and D. Kuhn
Martin Company (Baltimore)
Aerospace Mechanics Department
March 1963

Page

A. Injection Requirements for Moon-to-Earth Trajectories IX-1

B. Midcourse Guidance and Energy Requirements. IX-7

Illustrations. IX-9

List of Illustrations. IX-11

IX. MOON-TO-EARTH TRANSFER

Chapter V focused attention on the techniques for ascending from the earth's surface to the translunar injection point where a ballistic trajectory that satisfies various mission constraints is established. Chapter VI then presented a catalogue of circumlunar trajectory data that specified the injection condition for the ballistic trajectory around the moon with a return to the vicinity of the earth. Another class of translunar trajectories which do not return ballistically to the vicinity of the earth, namely approach trajectories (Chapter IV, Section A), is catalogued in Subsection A-2 of this chapter.

When the objective of the mission is accomplished, whether it be exploration, surveillance, or logistics, etc., it may be desirable to return the vehicle to earth. (This requirement is mandatory if the mission is manned.) Therefore, there are also injection requirements at the moon that must be satisfied if the spacecraft is to return to the vicinity of earth. Two techniques exist whereby these lunar injection conditions can be achieved. The first is a "direct departure technique" in which the spacecraft is boosted directly from the lunar surface to the transearth injection point, inferring lunar landing missions only. In the second technique, the vehicle is in a lunar parking orbit or establishes one prior to injection into a transearth trajectory--hence it is called the "orbital departure technique." Because of the limited data available for the first technique, and since orbital departure is more general, in that the direct departure technique can be regarded as a special case of the orbital departure technique, only the second technique is discussed in this chapter.

Transearth trajectory data is catalogued in Section A in the same manner as was the circumlunar data. It will be seen that the flight times back to earth are for the most part unrestricted, thereby easing the timing problem for returning to specific earth sites. This same transearth catalogue can also be interpreted as a translunar catalogue. The interpreted trajectory data represents the approach class of translunar trajectories. For this class of lunar trajectories, two major improvements over the circumlunar class are realized, namely:

(1) A wider choice of translunar flight time is now available.

(2) Any lunar site or feature is accessible for landing, surveillance or rendezvous purposes.

The use of the catalogue material for mission planning is demonstrated for transearth trajectories by the first sample mission in Chapter XI and for the interpreted translunar trajectories by the second sample mission in that chapter.

Transearth trajectory energy requirements for guidance are briefly discussed in Section B and they exhibit essentially the same trends as presented in Chapter VI, Section C. Since navigation, tracking, and guidance techniques for transearth and translunar trajectories are identical, the discussion in Chapter VI applies. However, abort during the transearth phase is somewhat of a misnomer since the only action that can be taken is to maneuver to "speed up" the return or to change the transearth trajectory inclination to ensure arrival at a given earth landing site. The velocity impulse requirement to accomplish these two maneuvers separately is given in Chapter XI.

A. INJECTION REQUIREMENTS FOR MOON-TO-EARTH TRAJECTORIES

The data given in this chapter presents the injection requirements for returning from the moon to earth by use of a specific lunar departure technique, namely, the "orbital departure technique." In it, the spacecraft is assumed to be in a circular orbit around the moon. At the proper position in the orbit, the vehicle is accelerated by rocket burning to the desired injection conditions for a transearth trajectory which is ballistic and returns the spacecraft safely to the immediate vicinity of the earth. Again, as in Chapter VI, the data has been generated by the Voice technique except that the translunar portion of the Voice program was eliminated. Thus, the nomenclature and parameters referring to lunar trajectories that have been presented in previous chapters remain unchanged, the moon is assumed spherically symmetric and satellite motion around the moon occurs in a restricted two-body orbit. The effect of perturbations on the orbit, such as lunar triaxiality, and the attractions of the earth and sun have been discussed briefly in Section B of Chapter VII. Departure from elliptic orbits around the moon has not been considered since these orbits seem to offer few advantages over circular lunar orbits. Some disadvantages of elliptic lunar orbits include: (1) the more complicated navigation and guidance that is required for establishing elliptic orbits of arbitrary orientation around the moon, and (2) the possibility of vehicle impact with the moon for elliptic orbits with low pericynthion altitudes if perturbing forces act for a long time. Also, the addition of two new trajectory parameters by elliptic orbits would make the cataloguing of transearth trajectories almost impossible.

1. The Transearth Trajectory Catalogue

As was mentioned above, the spacecraft is assumed to be in circular orbit around the moon. The vehicle may have been placed into this orbit either at the terminal phase of a translunar trajectory, or by ascending from the lunar surface. Since in the general case there are no launch azimuth restrictions on the moon, and since an infinite number of lunar orbit orientations can be established by means of translunar trajectories, the parameters of the initial circular orbit around the moon are completely arbitrary from an operational viewpoint. Only optimization with respect to some aspect of the entire trajectory and mission constraints governs the selection of nominal orbital parameters. Therefore, it is desirable to obtain transearth injection requirements for an arbitrary injection point near the moon.

The catalogue again uses the MOP (moon's orbital plane), which is a plane of symmetry, as a reference plane and employs the trajectory parameters defined in Chapters IV and VI. As an aid to understanding the material in this chapter, the following sketch illustrates the geometry of a transearth injection near the moon:

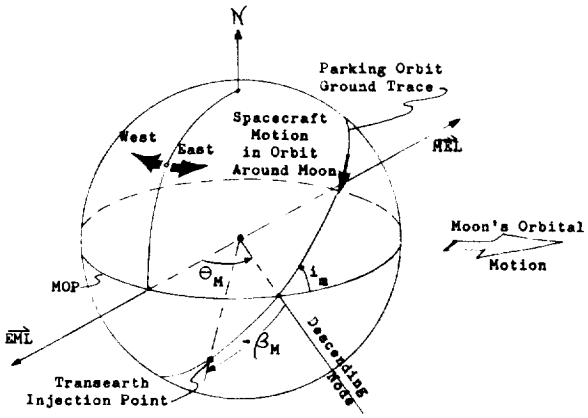

Here is shown the lunar ground trace of the circular lunar orbit which is called the parking orbit as in the case of earth departure. The orbit is inclined to the MOP by the angle i_m, $0° \leq i_m \leq 90°$, and the spacecraft's motion in this orbit is as indicated. The lunar satellite, as shown, may be regarded as being in a retrograde orbit relative to the MOP (i.e., its motion is "westward" or against the component of lunar rotation in the MOP). Since i_m varies only between 0° and 90°, the "eastward" or "westward" satellite motion around the moon must be specified together with the value of i_m. "North" is defined as in the direction of the angular momentum vector of the moon's orbital motion around the earth, and the "East" and "West" directions are defined with respect to the MOP by the same convention used for earth departure. These directions are not to be confused with the selenographic cardinal direction given in Chapter III. The intersection of the parking orbit plane with the MOP is designated by the angle θ_M ($-180° \leq \theta_M \leq 180°$) which is measured positively eastward from the earth-moon line ($\overrightarrow{EML}$) to the descending node of the parking orbit relative to the MOP. The values of i_m, θ_M specify the orientation of the circular lunar orbit, while its orbital radius $r_{\mathbb{C}\Delta}$ the orbital central angle β_M, and "eastward" or "westward" spacecraft motion specify the location of the spacecraft in the orbit at any time.

The injection into the transearth trajectory takes place at a central angle $-180° \leq \beta_{M0} \leq 180°$, where β_{M0} is measured positively toward north from the descending node. Transearth injection is also assumed to be in the direction of the spacecraft's motion. At the transearth injection point, and after the spacecraft has been accelerated, in addition to i_m, θ_M and β_{M0}, the parameters shown in the following sketch are needed for complete specification of the injection.

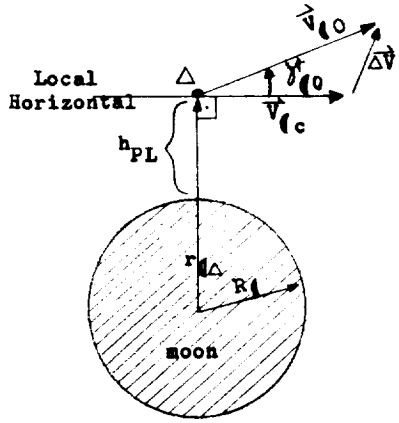

where

$V_{\mathbb{C}0}$ is the transearth injection velocity in the selenocentric lunar equatorial coordinate system

h_{PL} is the transearth injection altitude $h_{PL} = r_{\mathbb{C}\Delta} - R_{\mathbb{C}}$

$\gamma_{\mathbb{C}0}$ is the transearth injection flight path angle with respect to the lunar local horizontal.

It is also assumed that during transearth injection the spacecraft is accelerated instantaneously, or a velocity impulse ΔV is applied, as shown above.

$$\vec{V}_{\mathbb{C}0} = \vec{V}_{\mathbb{C}c} + \Delta\vec{V}$$

where $\vec{V}_{\mathbb{C}c}$ is the circular orbital velocity corresponding to the radius $r_{\mathbb{C}\Delta}$ in the selenocentric coordinate system $x_{\mathbb{C}}\ y_{\mathbb{C}}\ z_{\mathbb{C}}$. The effect of finite burning time and finite thrust-to-weight ratio on the fuel requirements of transearth injection is discussed in Chapter VII. The material presented in this catalogue is for $\gamma_{\mathbb{C}0} = 0°$, and hence the transearth injection altitude h_{PL} is also the pericynthion altitude, $|\Delta\vec{V}|$ is colinear with $|\vec{V}_{\mathbb{C}c}|$ and can be added algebraically to $|\vec{V}_{\mathbb{C}c}|$ to obtain $|\vec{V}_{\mathbb{C}0}|$; ΔV is considered an injection condition.

When the space vehicle approaches earth on the transearth trajectory, its inclination to the MOP, i_{VTE}, is defined in the same way as in Section A, Chapter VI. The value of i_{VTE}, $-180° \leq i_{VTE} \leq 180°$ is considered a trajectory parameter.

The transearth trajectories have been similarly catalogued as the circumlunar trajectories in Chapter VI. They have been graphically recorded in Figs. 1 to 90 for specific mission constraints

of i_m, lunar parking orbit inclination, $R_{\oplus \ell}$, earth-moon distance in terms of earth radii, h_{PL}, transearth injection and parking orbit altitude, and h_{PE}, the vacuum perigee altitude of the transearth trajectory. The transearth catalogue includes data for only one value of h_{PL}, namely h_{PL} = 185.2 km. The parking orbit inclination, i_m, is varied from 5° to 90° and the transearth perigee altitude h_{PE} = 183 km. Although this altitude is not in any safe re-entry corridor, it can be considered so since the small change required in h_{PE} for a safe re-entry corridor will have insignificant effects on the trajectory parameters. Again, as was the case in Chapter VI, $R_{\oplus \ell}$ is varied from 56 ER (earth radii) to 64 ER, which are the minimum lunar perigee radius and maximum lunar apogee radius, respectively, that can be encountered because of the eccentricity of the moon's orbit around the earth.

In addition to the transearth injection conditions of i_m, θ_M, β_{M0}, ΔV and h_{PL}, the flight time t_p from transearth injection to perigee is recorded. Although the symbol t_p denoted the flight time from the translunar injection to pericynthion in Chapter VI, it will become obvious in the next subsection why the same symbol was chosen here. The data contained in the catalogue is also given as a function of i_{VTE} but for the independent parameter of θ_M.

Table 1 gives the contents of the catalogue apportioned between the three trajectory constraints of i_m, $R_{\oplus \ell}$ and transearth injection direction.

TABLE 1

Case	$R_{\oplus \ell}$ (ER)	i_m (deg)	Injection Direction	Figures
1	56	5	Westward	1 to 3
2	56	15	Westward	6 to 8
3	56	30	Westward	11 to 13
4	56	60	Westward	16 to 18
5	56	90	Westward	21 to 23
6	60	5	Westward	26 to 28
7	60	15	Westward	31 to 33
8	60	30	Westward	36 to 38
9	60	60	Westward	41 to 43
10	60	90	Westward	46 to 48
11	64	5	Westward	51 to 53
12	64	15	Westward	56 to 58
13	64	30	Westward	61 to 63
14	64	60	Westward	66 to 68
15	64	90	Westward	71 to 73
16	60	5	Eastward	76 to 78
17	60	15	Eastward	79 to 81
18	60	30	Eastward	82 to 84
19	60	60	Eastward	85 to 87
20	60	90	Eastward	88 to 90

Trajectory data is given by the following variables as a function of i_{VTE} for each of the above constraints:

(1) t_p

(2) ΔV

(3) β_{M0}

The angle θ_M is not given as such in the figures, but rather with an additional subscript TE to ease the interpretation of the data when considering translunar trajectories as discussed in the next subsection. Therefore, when considering moon-to-earth transfers, the appropriate symbol is θ_{MTE} with the same definition as θ_M. The parameter θ_{MTE} is always given in the field of the graph.

The majority of catalogued data is for a westward transearth injection or retrograde relative to the MOP. This selection is based on the assumption that most approaches to the moon from a translunar trajectory will be in a westward direction and, thus, the presented data is more useful for the mission planner. However, some eastward transearth injection data is presented for $R_{\oplus \ell}$ = 60 ER, mainly for comparison purposes with westward injections $R_{\oplus \ell}$ = 60 ER and rough approximations for other values of $R_{\oplus \ell}$.

The trends in each of the three major trajectory variables as shown in the catalogue are discussed below:

(1) t_p--Flight time from transearth injection near the moon to vacuum perigee. Flight time is given in Figs. 1, 6, 11, 16, 21, 26, 31, 36, 41, 46, 51, 56, 61, 66, 71, 76, 79, 82, 85 and 88. It is immediately observed that for values of $i_m < 30°$ a discontinuous region exists on the graphs for certain values of θ_{MTE}, and as the region is approached, flight times increase very rapidly. This region has been denoted "Impractical Region" in the catalogued figures. Actually this "impractical region" also exists for larger i_m's but is not as pronounced since only a smaller range of θ_{MTE}'s are affected.

The discontinuity represents the situation where return times to earth become impractical or where the spacecraft escapes from the sphere of influence of the earth and moon into a heliocentric orbit. The sketch below illustrates this latter phenomenon for a trajectory in the MOP ($i_m = 0°$) and both a westward and eastward transearth injection. When the vehicle exits the lunar volume of influence, its velocity relative to the moon is $\vec{V}_{\ell \Delta}$. However, when its velocity relative to earth $\vec{V}_{\oplus \Delta}$ is found by adding the moon's velocity, $\vec{V}_{\oplus \ell}$, about the earth, the spacecraft is moving away from

the earth with sufficient energy to leave the sphere of influence of the earth and moon and be captured by the sun.

The figures show that the spacecraft can be made to return to earth in 50 hr or, if desired, 150 hr for any value of i_m and $R_{\oplus\mathbb{C}}$, and for one fixed value of h_{PL}, return time is not restricted to the degree as was the case for circumlunar trajectories of Chapter VI.

(2) ΔV--Velocity impulse required to inject the spacecraft into a transearth trajectory. The value for this variable is found in the figures immediately following the flight time figures. As expected, the higher the ΔV requirement, the lower the flight time. Another point worth mentioning is the fact that the minimum ΔV required is approximately 800 m/sec regardless of the values of $R_{\oplus\mathbb{C}}$, i_m, or θ_{MTE}

(3) β_{M0}--Orbital central angle of the transearth injection point, measured postively toward the north from the descending node, $-180° \leq \beta_{M0} \leq 180°$. Assuming for the moment that a return time to earth has been selected for given values θ_{MTE} and i_m along with the return inclination i_{VTE}, the required ΔV can be found. The final variable that completely describes the injection is the injection position β_{M0}, as defined above. It is determined by entering the catalogue with the additional mission constraints of i_{VTE}, θ_M, and i_m.

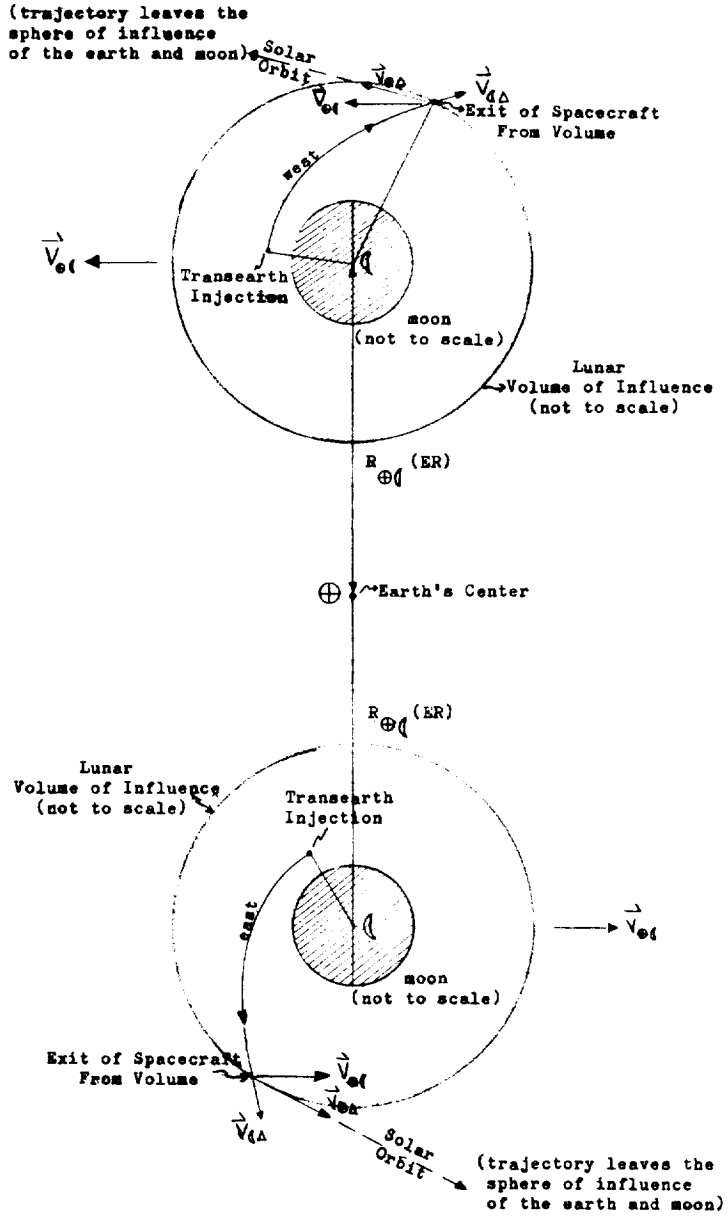

The material given in the catalogue can be extended significantly by use of symmetry about the MOP, and it is important that an understanding of this extension procedure be achieved. It is illustrated by means of an example. Assume that $i_m = 60°$, $\theta_{MTE} = 80°$, $i_{VTE} = 40°$, $t_p = 80$ hr, $\Delta V = 1700$ m/sec, $\beta_{M0} = -20°$ and the transearth injection is westward. This situation is shown in the following sketch (parking orbit ①).

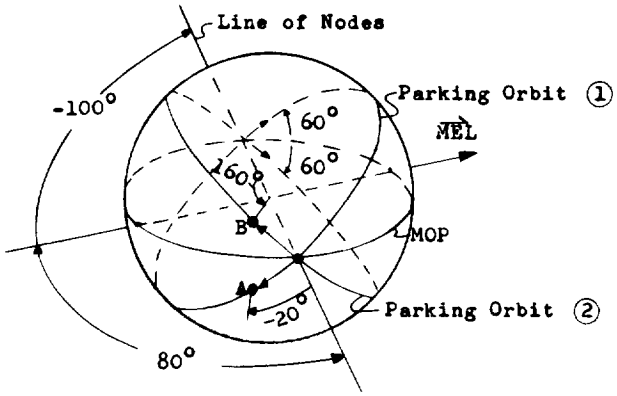

Since the MOP is a plane of symmetry, another parking orbit ② can be established that has the same value of i_m, 60°, but having an ascending node that is now coincident with the descending node of parking orbit ① . If the injection point B has the same orbital central angle as A from the line of nodes, the transearth trajectory established from parking orbit ② is a mirror image of the transearth trajectory established from parking orbit ① . Therefore the transearth trajectory data of parking orbit ① can be used for parking orbit ② by means of a few simple rules, for interpreting the catalogued data, namely:

$$\theta_{MTE}\ ② = \theta_{MTE}\ ① - 180° = -100° \quad (1a)$$

or

$$\theta_{MTE}\ ① + 180° = 260°$$

$$\beta_{M0}\ ② = 180° + \beta_{M0}\ ① = 160° \quad (1b)$$

$$i_{VTE}\ ② = -i_{VTE}\ ① = -40° \quad (1c)$$

$$\Delta V\ ② = \Delta V\ ① = 1700 \text{ m/sec} \quad (1d)$$

$$i_m\ ② = i_m\ ① = 60° \quad (1e)$$

$$t_p\ ② = t_p\ ① = 80 \text{ hr} \quad (1f)$$

both transearth injections are westward.

The next sketch illustrates the above procedure for a typical t_p versus i_{VTE} curve similar to Fig. 1 in the catalogue.

The "impractical region" has been shifted to the right and the curves are a mirror image about $i_{VTE} = 0°$.

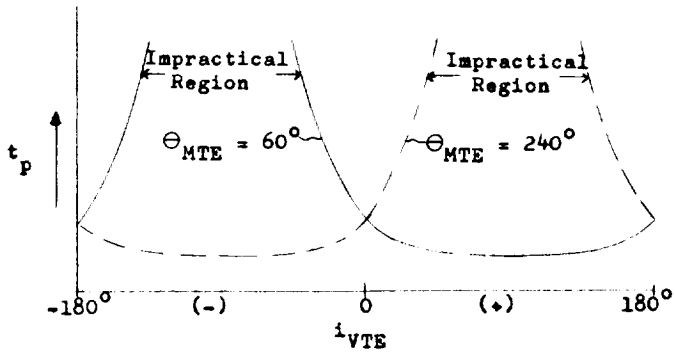

The extension of the catalogued transearth data by means of conservation of energy to other values of h_{PE} and $V_{\infty 0}$ can probably be performed for small changes in h_{PL}. However, due to the low velocity of the spacecraft relative to the moon, trajectory parameters other than $V_{\infty 0}$ would be affected, notably the flight time t_p. Thus the formula given by Eq (2) of Section A, Chapter VI for change in near-earth injection altitude of circumlunar trajectories is applicable for a smaller range of lunar injection altitudes. Before definite recommendations can be made on the useful range of injection altitudes, a comparison of empirically determined parameters with Voice and integrated trajectories is required.

2. Interpretation of Transearth Trajectory Data as Translunar Trajectory Data

The symmetry discussed above can also be employed in interpreting moon-to-earth trajectories as earth-to-moon trajectories, as can be visualized by means of the following sketch which shows the moon at the time of transearth injection t*. At this time, the orientation of the parking orbit about the moon is specified by i_m and θ_{MTE}. During the moon-to-earth transfer, the moon changes position from t* to the point P; and on arrival at earth the transearth trajectory has an inclination i_{VTE}.

If a mirror were placed along the $\overrightarrow{EML}$ perpendicular to the MOP, an image trajectory would be seen. When the moon is at P, its image is at Q and the spacecraft in the image trajectory is also at earth. Now if the motion of the moon were to be reversed, i.e., if it were to move from P to its initial location at t*, the motion of the spacecraft in the transearth trajectory would also be reversed. However, when viewing the image of this lunar reverse motion it is evident that as P moves towards t*, its image Q is also moving toward t*, and the spacecraft moves from the earth toward the moon along the image trajectory.

This image situation is identical to the actual translunar situation since Q moves in the same direction as does the moon in its orbital motion. Thus the transearth trajectory may be interpreted as a translunar trajectory.† The following rules

†For instance, if the transearth trajectory is direct north the translunar trajectory is also direct north.

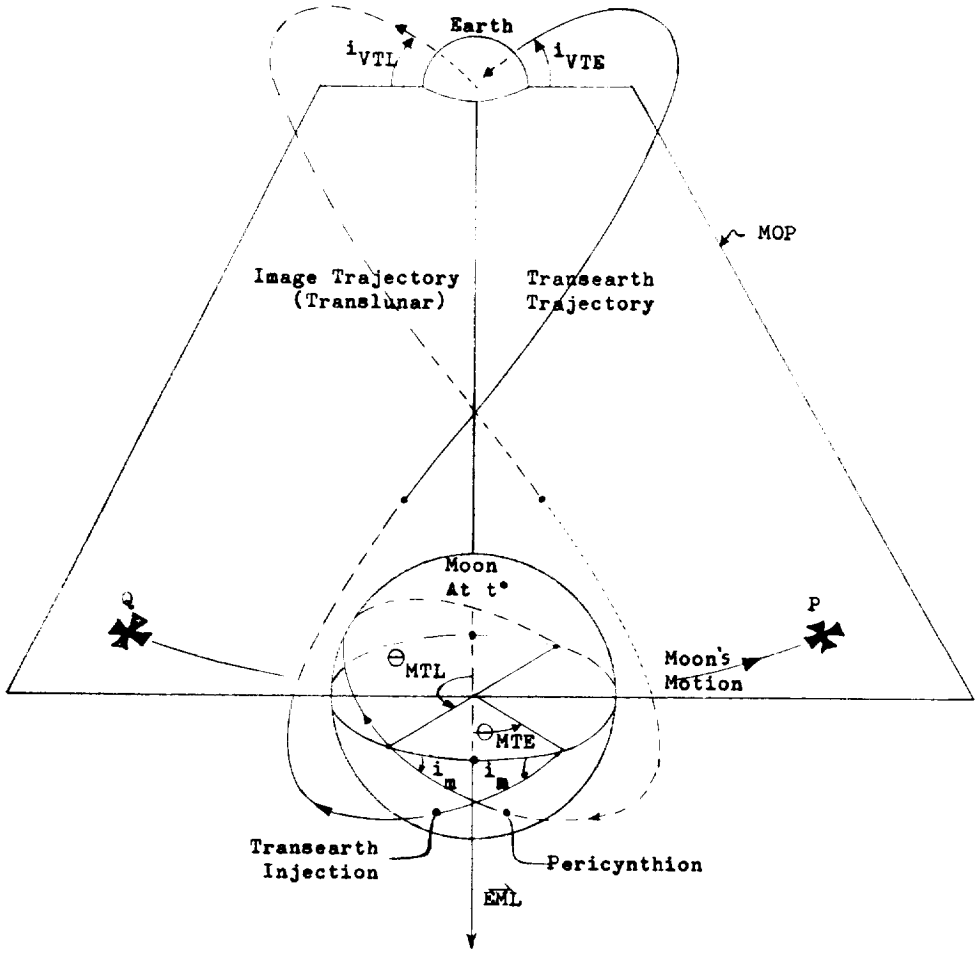

regarding this interpretation can now be made:

for i_{VTE} use i_{VTL} (2a)

for θ_{MTE} use $180° - \theta_{MTL}$ (2b)

where

θ_{MTL} locates the descending node of the parking orbit of the translunar trajectory

for i_m (transearth) use i_m (translunar) (2c)

for β_{M0} (transearth) use $180° - \beta_{M0}$ (translunar) (2d)

for ΔV (transearth injection) use ΔV (see definition in Chapter VI) (2e)

for t_p (transearth) use t_p (translunar) (2f)

Furthermore, a fixed value of i_{VTL} may represent either an inject north or inject south case, i.e., the image trajectory can be reflected below or above the MOP as well. For instance, in the above sketch the translunar injection is direct north. Since the MOP is a plane of symmetry, the image or translunar trajectory can also be reflected below the MOP to obtain a direct inject-south case for which the trajectory parameters at the moon must be interpreted properly. The rules governing the interpretation for the opposite case † are:

for i_{VTE} use i_{VTL} (3a)

for θ_{MTE} use $-\theta_{MTL}$ (3b)

for i_m (transearth) use i_m (translunar) (3c)

for β_{M0} (transearth) use $-\beta_{M0}$ (translunar) (3d)

† For instance, if the transearth trajectory is direct north, the translunar trajectory is opposite, i.e., direct south (see example in Fig. 4 of catalogue).

for ΔV (transearth injection) use ΔV (see definition in Chapter VI) (3e)

for t_p (transearth) use t_p (translunar) (3f)

for V_0 use V_0 (3g)

If the transearth trajectories in the catalogue are interpreted as translunar data, the injection conditions at earth need further discussion. The transearth data is for an injection altitude h_0 of 183 km, and the injection flight path angle γ_0 is 0°. The injection velocity V_0 is included in the catalogue along with the injection position ψ_0 (see Chapter VI for definition). The function ψ_0 is discontinuous when i_{VTL} is 0° or 180° due to a singularity in the equations of the Voice program when $i_{VTL} = 0°$ or 180°. However, this feature does not detract from the usefulness of the data for mission planning purposes since the value $i_{VTL} = 180°$ represents unlikely retrograde injections, and the singularity $i_{VTL} = 0°$ invalidates Voice data for mission planning if $i_{VTL} \leq 10$ for the inject-south or the inject-north cases.

The translunar injection conditions of h_0, V_0, ψ_0 and γ_0 can be extended to include other injection conditions by the use of the empirical relationships, Eqs (1) and (2), given in Chapter VI, Section A.

As pointed out previously, the translunar trajectories in this Chapter are not of the circumlunar class but of the approach class (Chapter IV). Two major advantages are to be gained by the use of the approach class of translunar trajectories.

(1) The freedom in selecting landing sites or surveillance areas

(2) The relative freedom in choosing a flight time to the moon. Although accessibility of lunar areas is vastly improved by the use of these trajectories, the problems associated with mission abort near the moon before entering lunar orbit make this approach more risky.

B. MIDCOURSE GUIDANCE AND ENERGY REQUIREMENTS

The navigation and guidance techniques presented in Chapter VI are also applicable to the transearth phase of a lunar mission and therefore will not be discussed further. However, there are some brief comments to be made regarding the energy requirements of this phase.

For circumlunar trajectories it is very difficult to determine the velocity impulses ΔV_{TOT} for the transearth portion of the trajectory because midcourse corrections are applied during the translunar phase. These corrections may be designed to return the errant trajectory back to a nominal trajectory or to ensure arrival at a specific aim point near the moon (not necessarily matching a nominal). Therefore the transearth trajectory depends on the accuracy of these translunar midcourse corrections and the off-nominal conditions of i_m, θ_M, h_{PL} and t_p at the moon. It was emphasized in Chapter VI that very stringent requirements exist on the trajectory at given instants of time if mission specifications are to be fulfilled.

The sensitivity of transearth vacuum perigee to variations in pericynthion altitude, h_{PL}, varies over a wide range, and a factor of 10 is not unreasonable. Not only does the return vacuum perigee altitude vary, but the transearth inclination, i_{VTE}, and the time of re-entry also vary, making the task of returning to a prescribed point on earth even more difficult. Unless midcourse corrections are made to reach the correct pericynthion altitude at the right time and orientation, the distortion in the transearth trajectory may require large transearth midcourse guidance corrections. A circumlunar trajectory will thus require multiple midcourse guidance corrections, one or more during the translunar phase, one at or near pericynthion, and one or more during the transearth phase.

1. Energy Requirements for Transearth Portion of Circumlunar Trajectories

If the first guidance concept given in Chapter VI with the aim point at pericynthion is used, then difficulties arise in simultaneous control of the four prime variables i_m, θ_M, h_{PL} and t_p at pericynthion which, in turn, control the transearth trajectory. Most likely a statistical approach will be used to determine the transearth guidance requirements for this concept. For the second concept, which is designed to return the spacecraft to the nominal trajectory prior to reaching the moon, the difficulty may arise from the small differences between the required velocity corrections and the accuracy to which the spacecraft's velocity vector is known at the time of correction.

In order to gain at least some insight to the transearth energy requirements, it is assumed that the final translunar midcourse guidance correction (for a typical circumlunar trajectory of Chapter VI) by use of guidance concept 2 is not made. In this case the spacecraft continues its trajectory around the moon with no further corrections until it is on the transearth portion some distance from the moon. The transearth midcourse correction is assumed at $t_1 = 105$ hr after translunar injection, 106,000 km from the moon. This correction is designed to return the spacecraft to the nominal transearth trajectory at various times t_2 which vary from 120 hr after injection to perigee. The total mission time (from injection to perigee) is approximately 151 hr

and the magnitude of the final translunar correction which is not made is ΔV_v of 0.7 m/sec. The following sketch shows the total corrective velocity requirements for the above conditions.

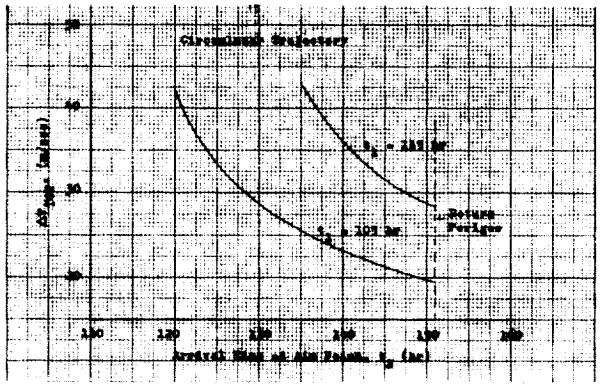

The magnitude of the required corrections, although felt to be quite conservative, indicates the need of controlling the translunar trajectory as closely as possible. The omission of a ΔV_v of 0.7 m/sec correction during the translunar trajectory at t = 50 hr results in a required 20 m/sec correction (at t_1 = 105 hr) on the transearth trajectory. Also included in the sketch is data for an initial transearth midcourse correction at t_1 = 115 hr. The data shows the expected trends of reduced ΔV_{TOT} for corrections made as early as possible and reduction of the total ΔV_{TOT} as the aim point approaches transearth vacuum perigee.

The initial correction times (t_1) assumed ensure that the vehicle position at t_1 is sufficiently beyond the effect of the moon's gravitational field to allow reasonable prediction of position and velocity at perigee. The previous sketch illustrates the necessity of obtaining ample position and velocity data as soon as possible after entering a region where reasonably accurate return midcourse guidance corrections can be computed.

2. Requirements for Transearth Trajectories Originating at the Moon

For transearth trajectories established from a lunar orbit, errors arise mainly from the ability of the guidance system to control the injection velocity vector. Although the correct position at transearth injection is also important, the intrinsic nature of the guidance concept to be used tends to keep position errors small. This is especially true if the guidance technique uses a phantom satellite as the aim point as discussed in Chapter V. The standard deviation in velocity, i.e., the 1σ error in the velocity, is assumed to be 0.3 m/sec in each coordinate direction, x_v, y_v, z_v,

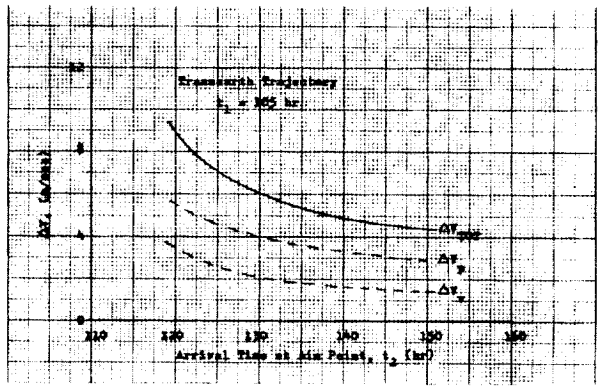

where x_v is along the local horizontal in the flight direction, z_v is in the direction of the local vertical and y_v completes the right-handed Cartesian coordinate system by defining a lateral direction normal to the trajectory plane. Injection velocity errors reflect a three-dimensional 99% probability (3.368 σ). The velocity error at transearth injection is propagated to a position corresponding to the point at t_1 = 105 hr used in the circumlunar case above. The previous sketch presents the initial (position) velocity correction (ΔV_p), the final (velocity) correction (ΔV_v) and ΔV_{TOT}, the total impulse required. As in the translunar case, the initial correction, made at the 105-hr point, corrects the position of the spacecraft so that it intercepts the nominal transearth trajectory at a predetermined aim position and time. This aim point has been varied from the 120-hr point to perigee on the sketch and the final correction at the aim point reorients the spacecraft's velocity vector along the nominal trajectory with the correct magnitude. The data presented in the sketch represents the highest midcourse energy requirements and as noted, it exhibits the same trends as the circumlunar trajectory of the previous subsection.

Guidance accuracy requirements have been discussed qualitatively in Subsection C-2c of Chapter VI with some reference to quantitative data given in that subsection. Again the discussion applies to midcourse guidance and energy requirements of translunar as well as transearth trajectories.

ILLUSTRATIONS

LIST OF ILLUSTRATIONS

Figure	Title	Page
1	Flight Time Versus Return Inclination (Inject West - Retrograde)	IX-17
2	ΔV Required For Transearth Injection Versus Return Inclination	IX-18
3	Transearth Injection Point Versus Return Inclination	IX-19
4	Injection Velocity Versus Translunar Inclination	IX-20
5	Translunar Injection Position Versus Translunar Inclination	IX-21
6	Flight Time Versus Return Inclination (Inject West - Retrograde)	IX-22
7	ΔV Required For Transearth Injection Versus Return Inclination	IX-23
8	Transearth Injection Point Versus Return Inclination	IX-24
9	Injection Velocity Versus Translunar Inclination	IX-25
10	Translunar Injection Position Versus Translunar Inclination	IX-26
11	Flight Time Versus Return Inclination (Inject West - Retrograde)	IX-27
12	ΔV Required For Transearth Injection Versus Return Inclination	IX-28
13	Transearth Injection Point Versus Return Inclination	IX-29
14	Injection Velocity Versus Translunar Inclination	IX-30
15	Translunar Injection Position Versus Translunar Inclination	IX-31
16	Flight Time Versus Return Inclination (Inject West - Retrograde)	IX-32

ILLUSTRATIONS (continued)

Figure	Title	Page
17	ΔV Required For Transearth Injection Versus Return Inclination	IX-33
18	Transearth Injection Point Versus Return Inclination	IX-34
19	Injection Velocity Versus Translunar Inclination	IX-35
20	Translunar Injection Position Versus Translunar Inclination	IX-36
21	Flight Time Versus Return Inclination (Inject West - Retrograde)	IX-37
22	ΔV Required For Transearth Injection Versus Return Inclination	IX-38
23	Transearth Injection Point Versus Return Inclination	IX-39
24	Injection Velocity Versus Translunar Inclination	IX-40
25	Translunar Injection Position Versus Translunar Inclination	IX-41
26	Flight Time Versus Return Inclination (Inject West - Retrograde)	IX-42
27	ΔV Required for Transearth Injection Versus Return Inclination	IX-43
28	Transearth Injection Point Versus Return Inclination	IX-44
29	Injection Velocity Versus Translunar Inclination	IX-45
30	Translunar Injection Position Versus Translunar Inclination	IX-46
31	Flight Time Versus Return Inclination (Inject West - Retrograde)	IX-47
32	ΔV Required For Transearth Injection Versus Return Inclination	IX-48

ILLUSTRATIONS (continued)

Figure	Title	Page
33	Transearth Injection Point Versus Return Inclination	IX-49
34	Injection Velocity Versus Translunar Inclination	IX-50
35	Translunar Injection Position Versus Translunar Inclination	IX-51
36	Flight Time Versus Return Inclination (Inject West - Retrograde)	IX-52
37	ΔV Required For Transearth Injection Versus Return Inclination	IX-53
38	Transearth Injection Point Versus Return Inclination	IX-54
39	Injection Velocity Versus Translunar Inclination	IX-55
40	Translunar Injection Position Versus Translunar Inclination	IX-56
41	Flight Time Versus Return Inclination (Inject West - Retrograde)	IX-57
42	ΔV Required For Transearth Injection Versus Return Inclination	IX-58
43	Transearth Injection Point Versus Return Inclination	IX-59
44	Injection Velocity Versus Translunar Inclination	IX-60
45	Translunar Injection Position Versus Translunar Inclination	IX-61
46	Flight Time Versus Return Inclination (Inject West - Retrograde)	IX-62
47	ΔV Required For Transearth Injection Versus Return Inclination	IX-63
48	Transearth Injection Point Versus Return Inclination	IX-64

ILLUSTRATIONS (continued)

Figure	Title	Page
49	Injection Velocity Versus Translunar Inclination	IX-65
50	Translunar Injection Position Versus Translunar Inclination	IX-66
51	Flight Time Versus Return Inclination (Inject West - Retrograde)	IX-67
52	ΔV Required For Transearth Injection Versus Return Inclination	IX-68
53	Transearth Injection Point Versus Return Inclination	IX-69
54	Injection Velocity Versus Translunar Inclination	IX-70
55	Translunar Injection Position Versus Translunar Inclination	IX-71
56	Flight Time Versus Return Inclination (Inject West - Retrograde)	IX-72
57	ΔV Required For Transearth Injection Versus Return Inclination	IX-73
58	Transearth Injection Point Versus Return Inclination	IX-74
59	Injection Velocity Versus Translunar Inclination	IX-75
60	Translunar Injection Position Versus Translunar Inclination	IX-76
61	Flight Time Versus Return Inclination (Inject West - Retrograde)	IX-77
62	ΔV Required For Transearth Injection Versus Return Inclination	IX-78
63	Transearth Injection Point Versus Return Inclination	IX-79

ILLUSTRATIONS (continued)

Figure	Title	Page
64	Injection Velocity Versus Translunar Inclination . . .	IX-80
65	Translunar Injection Position Versus Translunar Inclination	IX-81
66	Flight Time Versus Return Inclination (Inject West - Retrograde)	IX-82
67	ΔV Required For Transearth Injection Versus Return Inclination	IX-83
68	Transearth Injection Point Versus Return Inclination	IX-84
69	Injection Velocity Versus Translunar Inclination . .	IX-85
70	Translunar Injection Position Versus Translunar Inclination	IX-86
71	Flight Time Versus Return Inclination (Inject West - Retrograde)	IX-87
72	ΔV Required For Transearth Injection Versus Return Inclination	IX-88
73	Transearth Injection Point Versus Return Inclination	IX-89
74	Injection Velocity Versus Translunar Inclination	IX-90
75	Translunar Injection Position Versus Translunar Inclination	IX-91
76	Flight Time Versus Return Inclination (Inject East - Direct)	IX-92
77	ΔV Required For Transearth Injection Versus Return Inclination	IX-93
78	Transearth Injection Point Versus Return Inclination	IX-94
79	Flight Time Versus Return Inclination (Inject East - Direct)	IX-95

ILLUSTRATIONS (continued)

Figure	Title	Page
80	ΔV Required For Transearth Injection Versus Return Inclination	IX-96
81	Transearth Injection Point Versus Return Inclination	IX-97
82	Flight Time Versus Return Inclination (Inject East - Direct)	IX-98
83	ΔV Required For Transearth Injection Versus Return Inclination	IX-99
84	Transearth Injection Point Versus Return Inclination	IX-100
85	Flight Time Versus Return Inclination (Inject East - Direct)	IX-101
86	ΔV Required For Transearth Injection Versus Return Inclination	IX-102
87	Transearth Injection Point Versus Return Inclination	IX-103
88	Flight Time Versus Return Inclination (Inject East - Direct)	IX-104
89	ΔV Required For Transearth Injection Versus Return Inclination	IX-105
90	Transearth Injection Point Versus Return Inclination	IX-106

TRANSEARTH TRAJECTORIES

Fig. 1. Flight Time Versus Return Inclination
(Inject West - Retrograde)

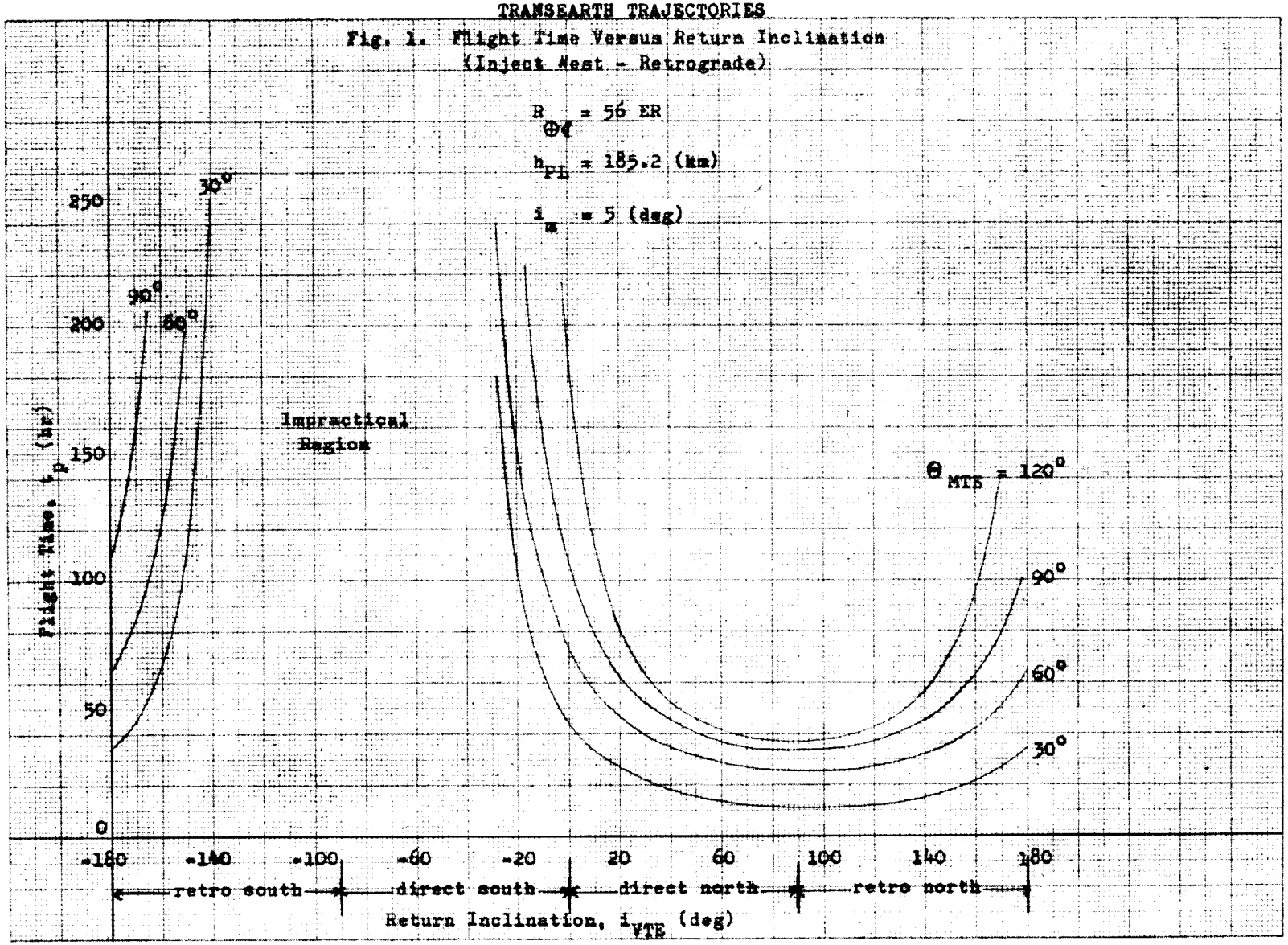

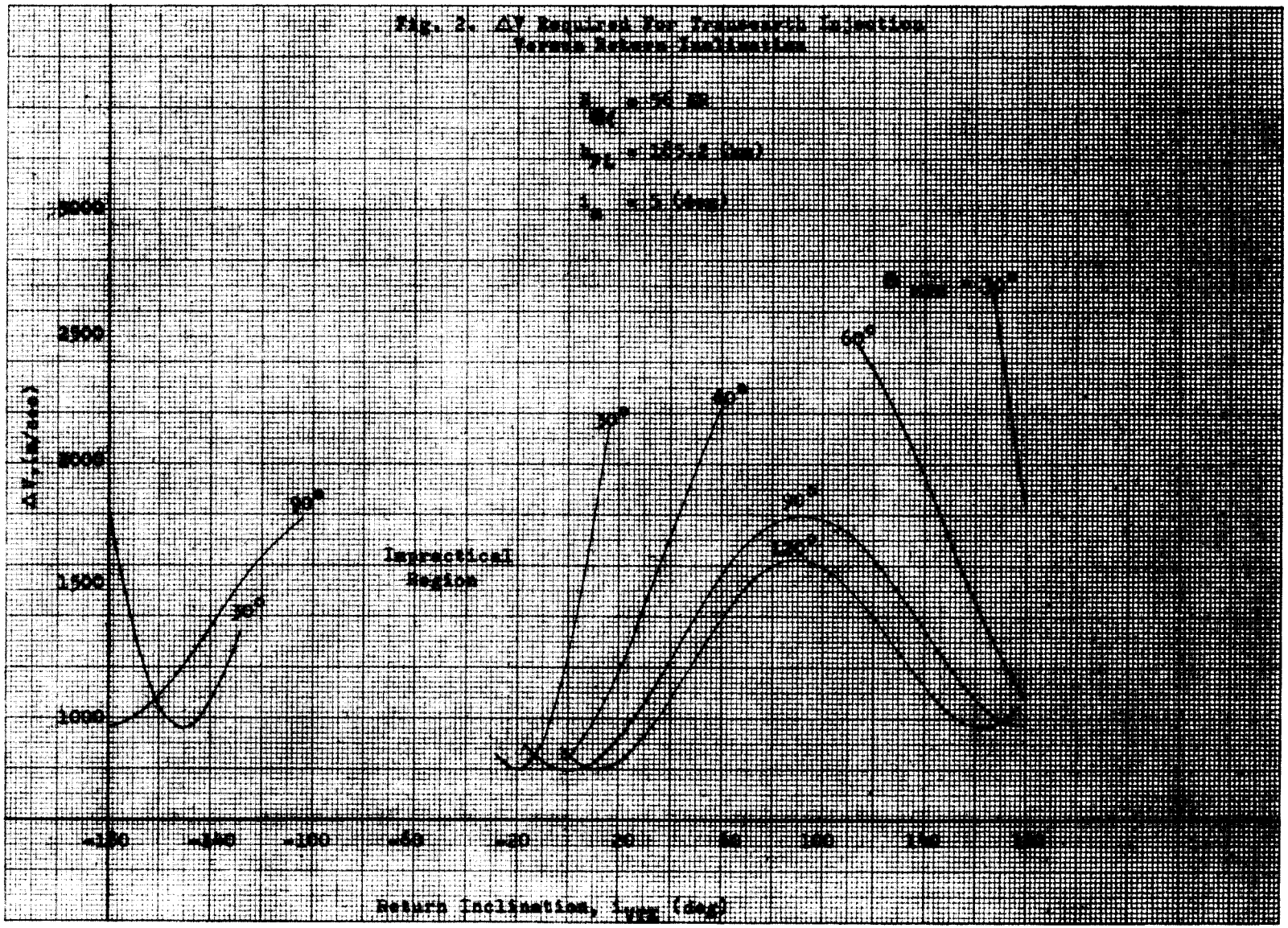
Fig. 2. ΔV Required For Transearth Injection Versus Return Inclination
h_{pk} = 50 nm
h_{pk} = 185.2 (km)
i_m = 5 (deg)
2500
2000
1500
1000
ΔV, (fps)
90°
30°
Impractical Region
30°
40°
60°
120°
-180
-140
-100
-60
-20
20
60
100
140
180
Return Inclination, i_{ret} (deg)

Fig. 3. Transearth Injection Point Versus Return Inclination

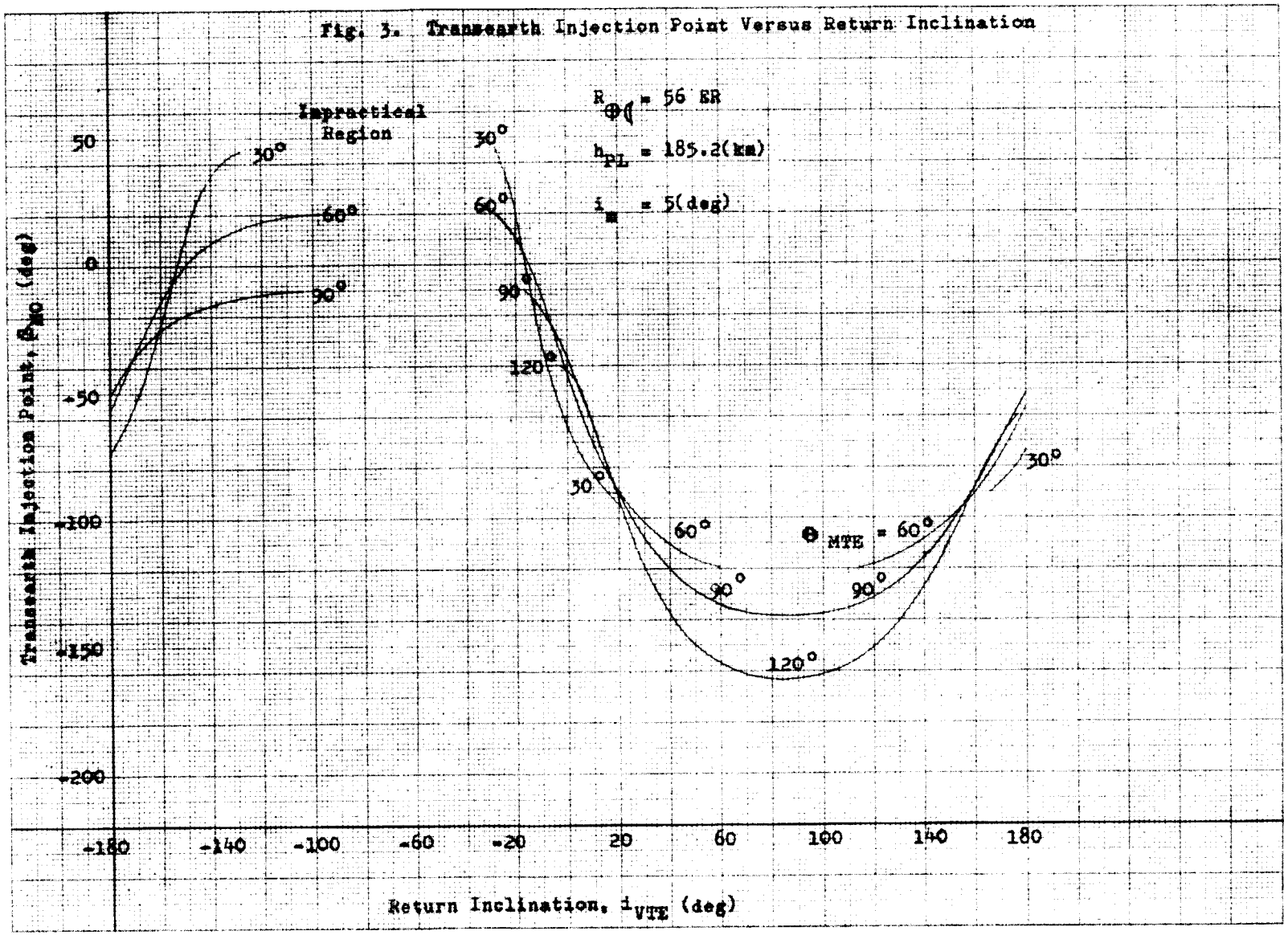

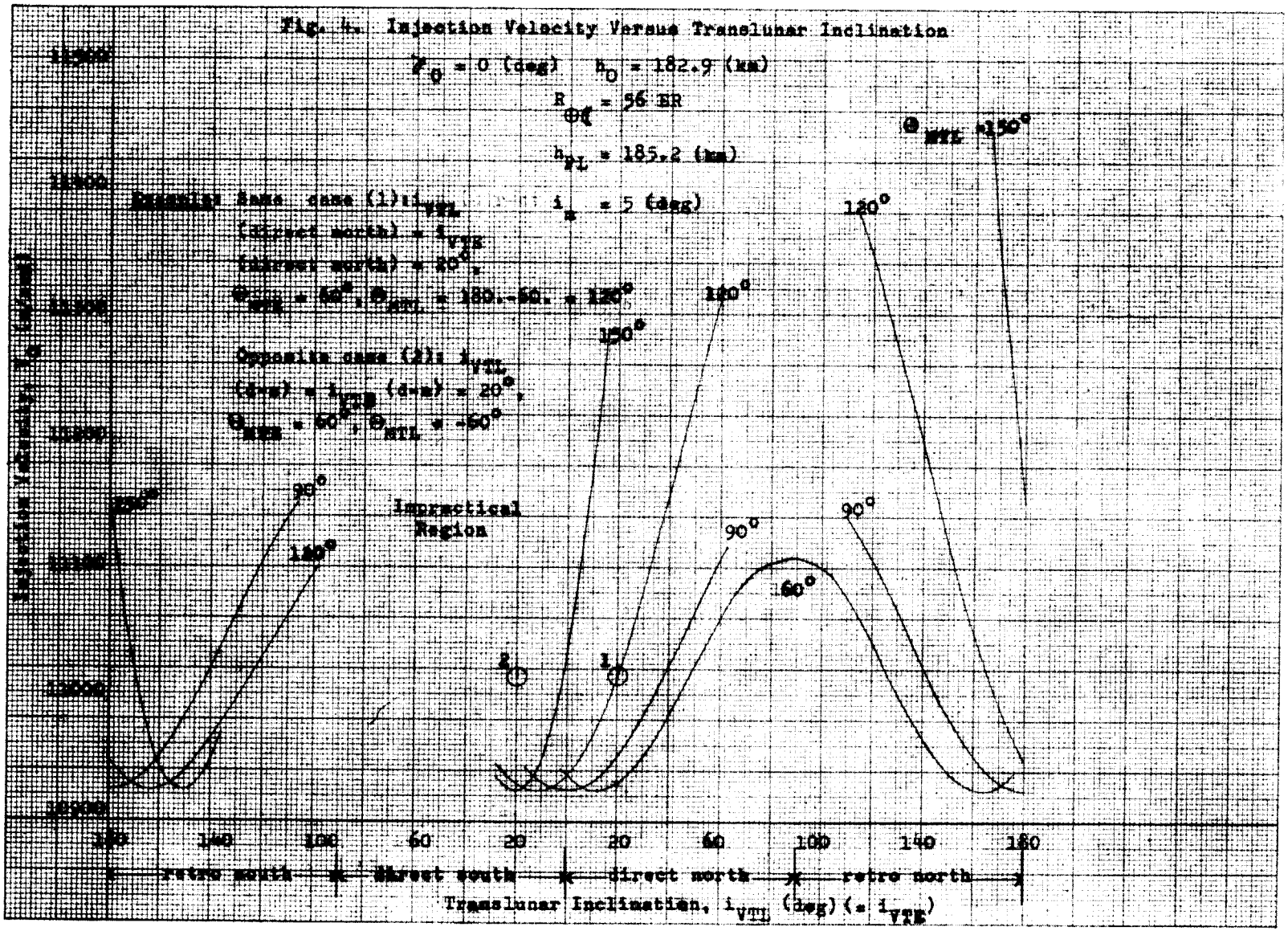
Fig. 4. Injection Velocity Versus Translunar Inclination
γ_0 = 0 (deg) h_0 = 182.9 (km)
$R_{\oplus}$ = 56 ER
h_{PL} = 185.2 (km)
i_x = 5 (deg)
Opposite case (1): i_{VTL} (direct north) = i_{VTE} (direct north) = 20°, Θ_{MTE} = 60°, Θ_{MTL} = 180.-60. = 120°
Opposite case (2): i_{VTL} (d-n) = i_{VTE} (d-n) = 20°, Θ_{MTE} = 60°, Θ_{MTL} = -60°
Impractical Region
Θ_{MTE} =150°
120°
180°
150°
90°
90°
90°
60°
i_0
γ_0
retro south
direct south
direct north
retro north
Translunar Inclination, i_{VTL} (deg) (= i_{VTE})

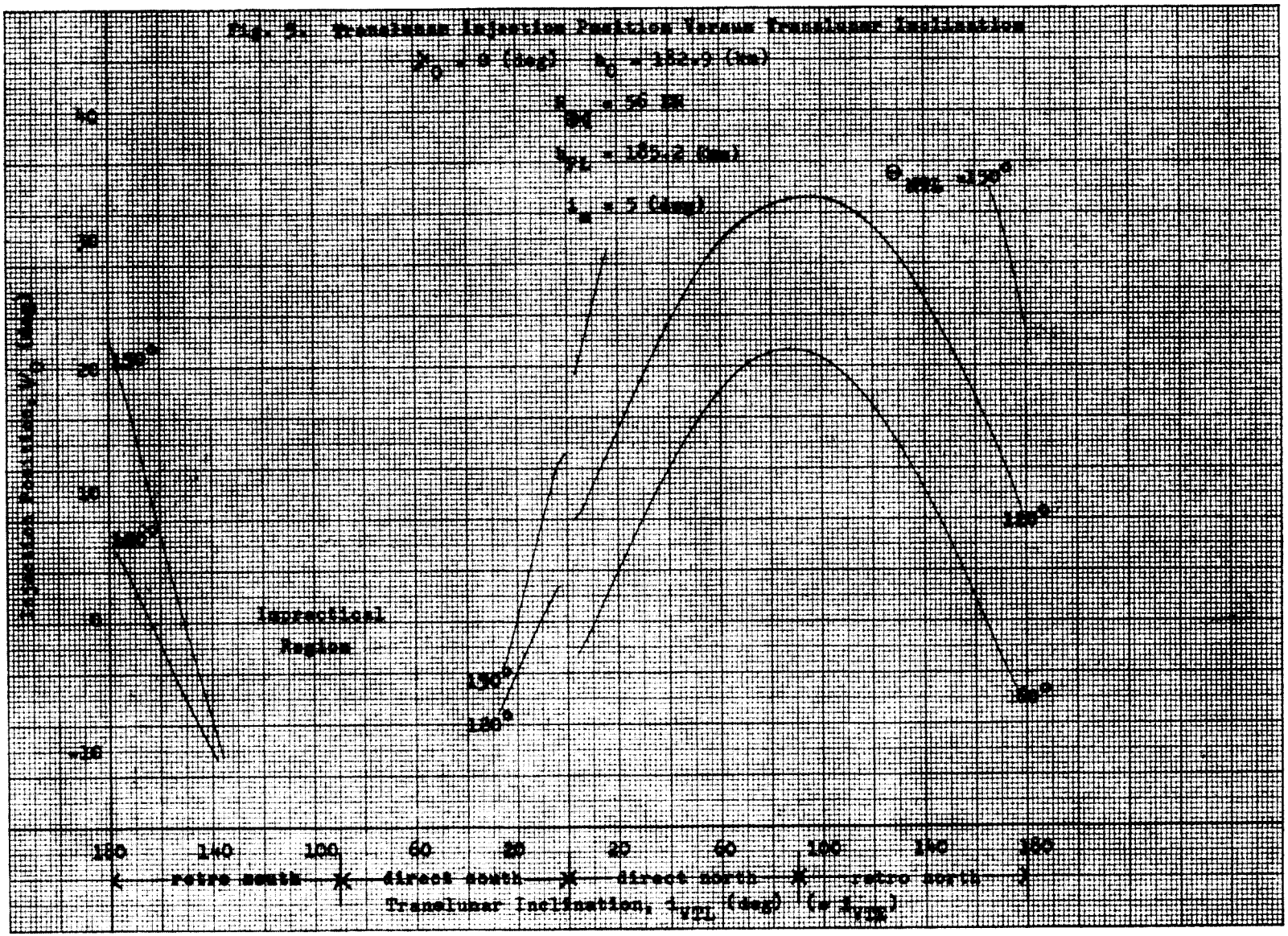
Fig. 9. Translunar Injection Position Versus Translunar Inclination
γ_0 = 0 (deg)
h_0 = 182.9 (km)
h_{pL} = 185.2 (km)
i_M = 5 (deg)
θ_{pos} = 120°
Translunar Injection Position, θ_{TLI} (deg)
Impractical Region
130°
120°
direct south
direct north
retro north
Translunar Inclination, i_{TPL} (deg) (or λ_{TPL})

Fig. 6. Flight Time Versus Return Inclination
(Inject West + Retrograde)

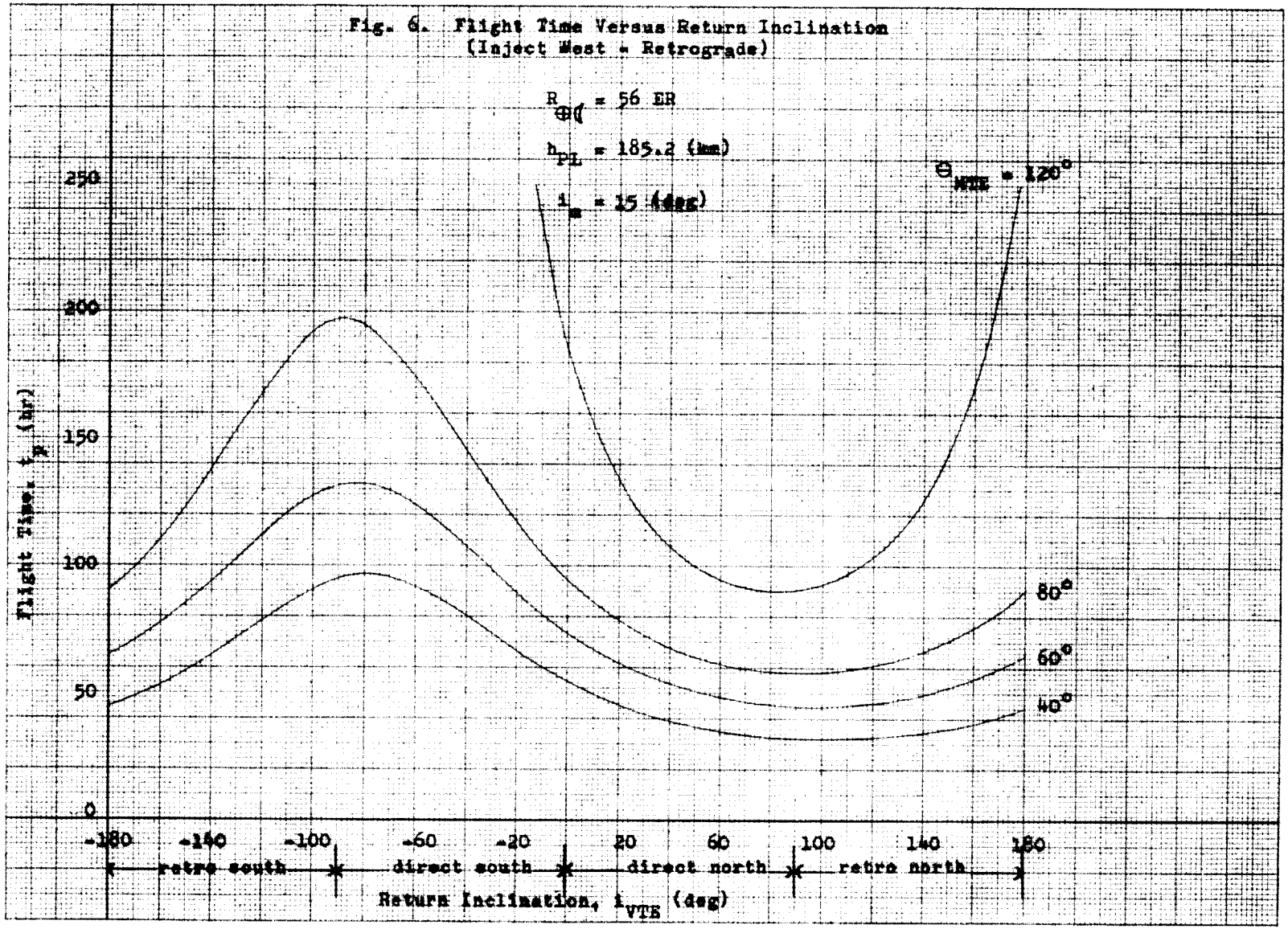

Fig. 7. ΔV Required For Transearth Injection Versus Return Inclination

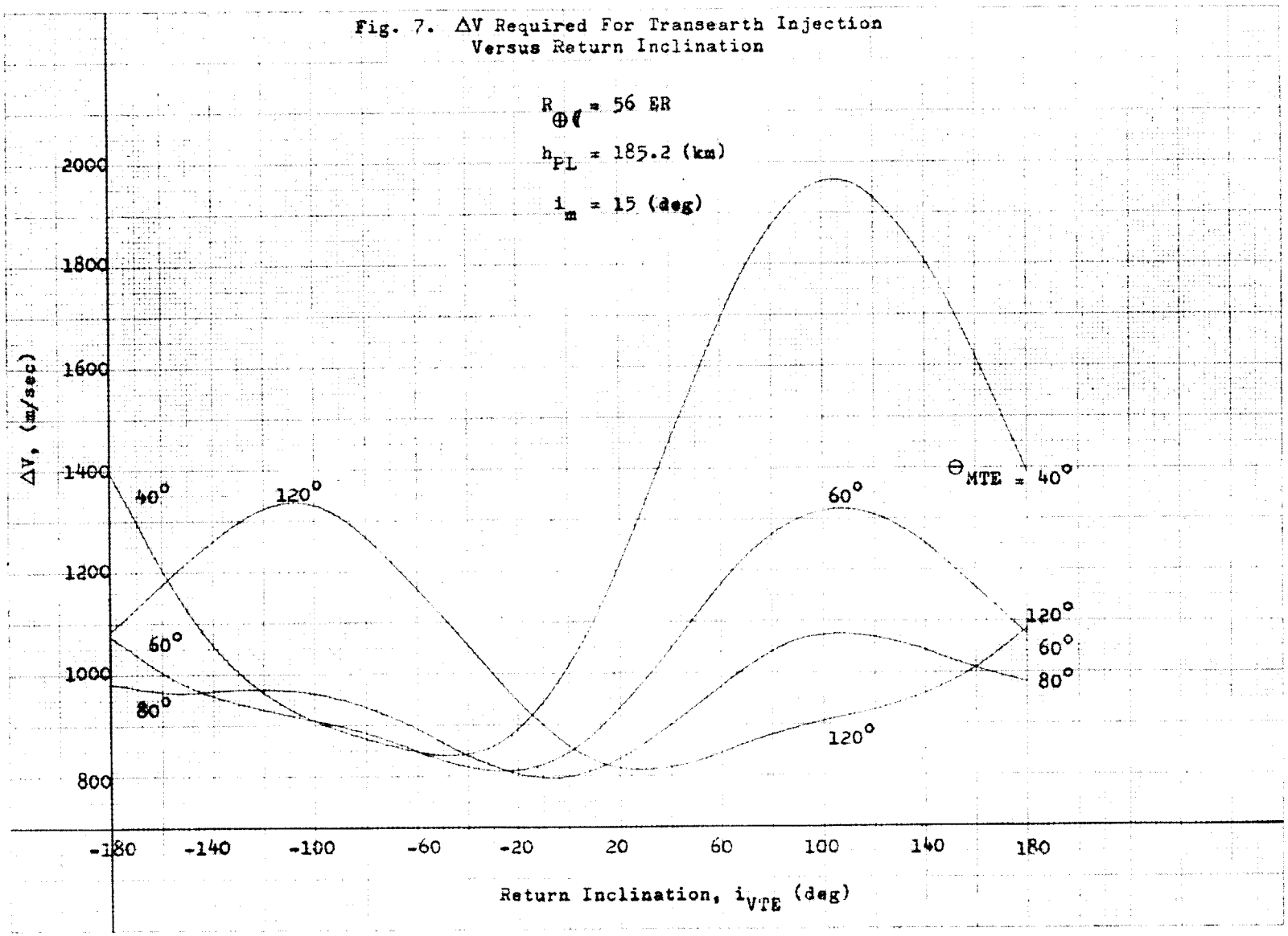

Fig. 8. Transearth Injection Point Versus Return Inclination

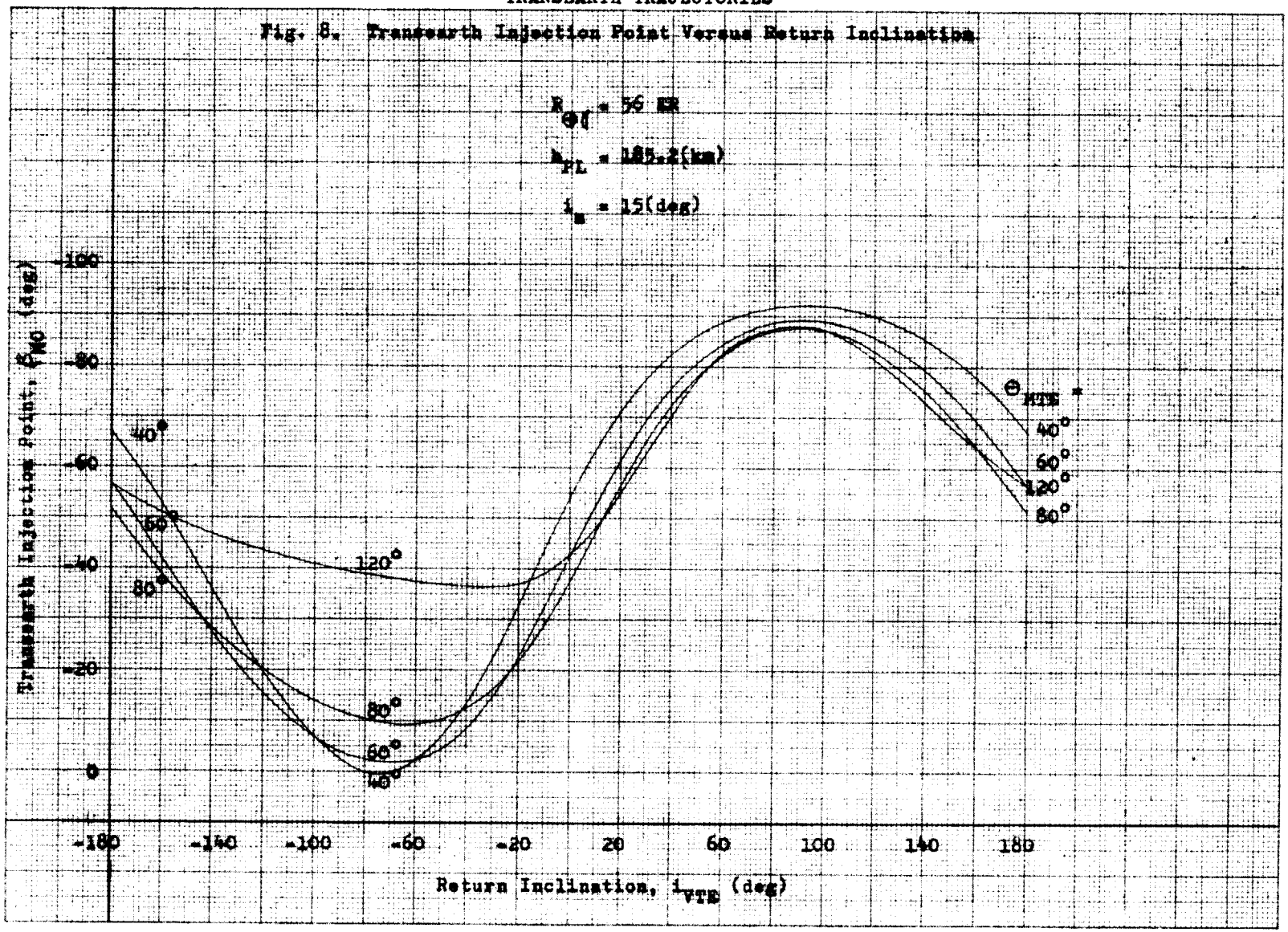

Fig. 9. Injection Velocity Versus Translunar Inclination

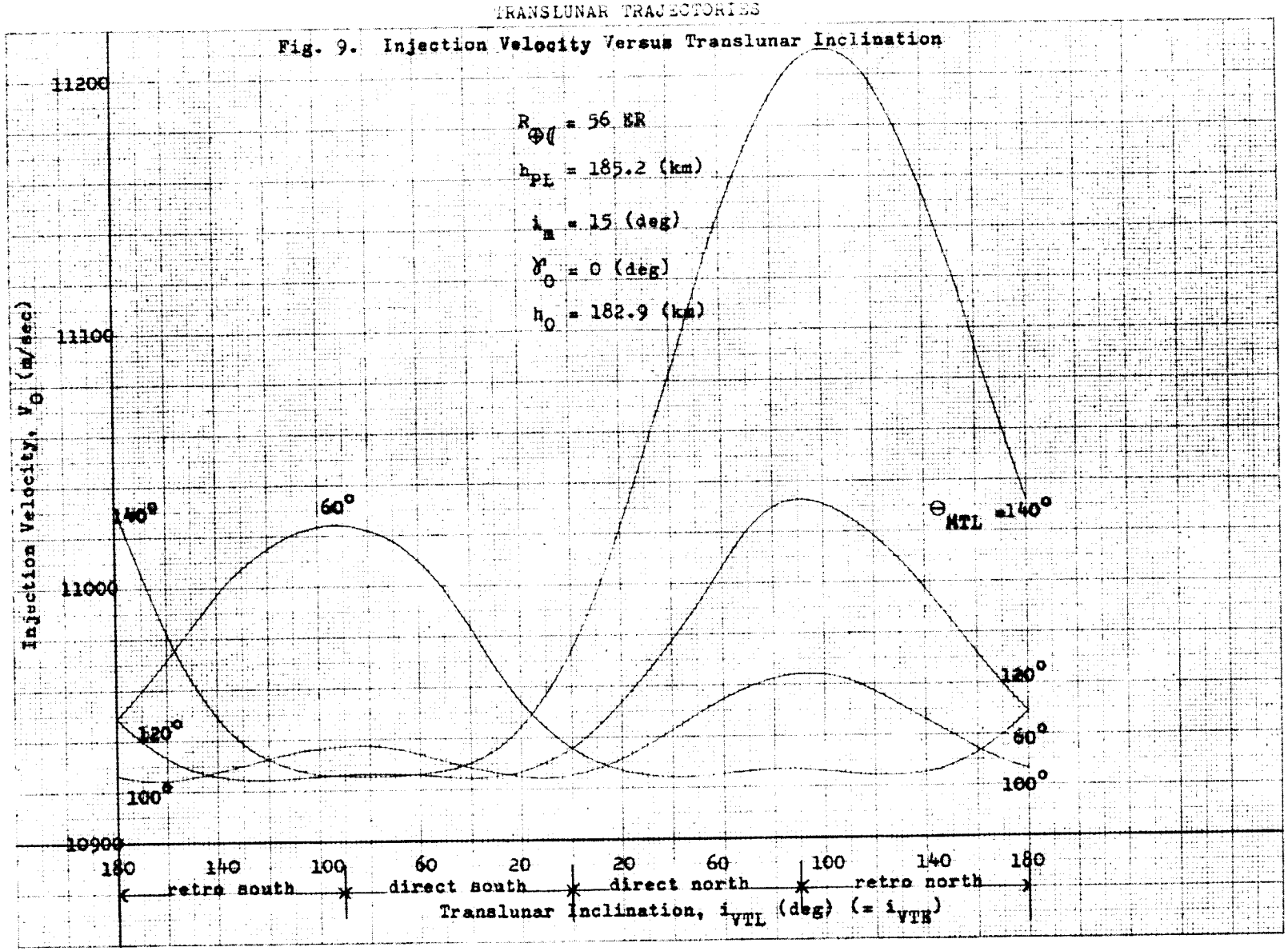

Fig. 10. Translunar Injection Position Versus Translunar Inclination

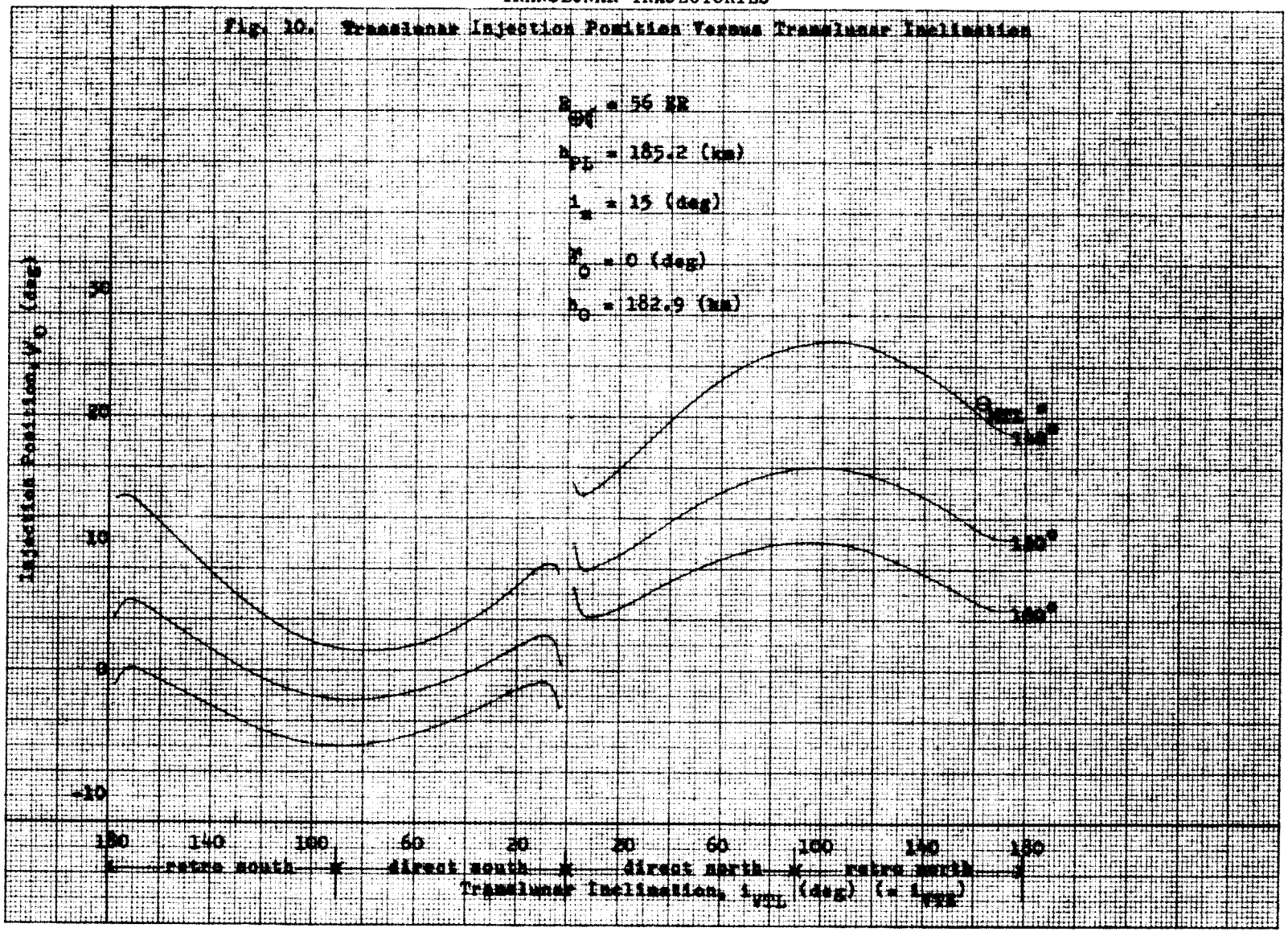

Fig. 11. Flight Time Versus Return Inclination
(Inject West - Retrograde)

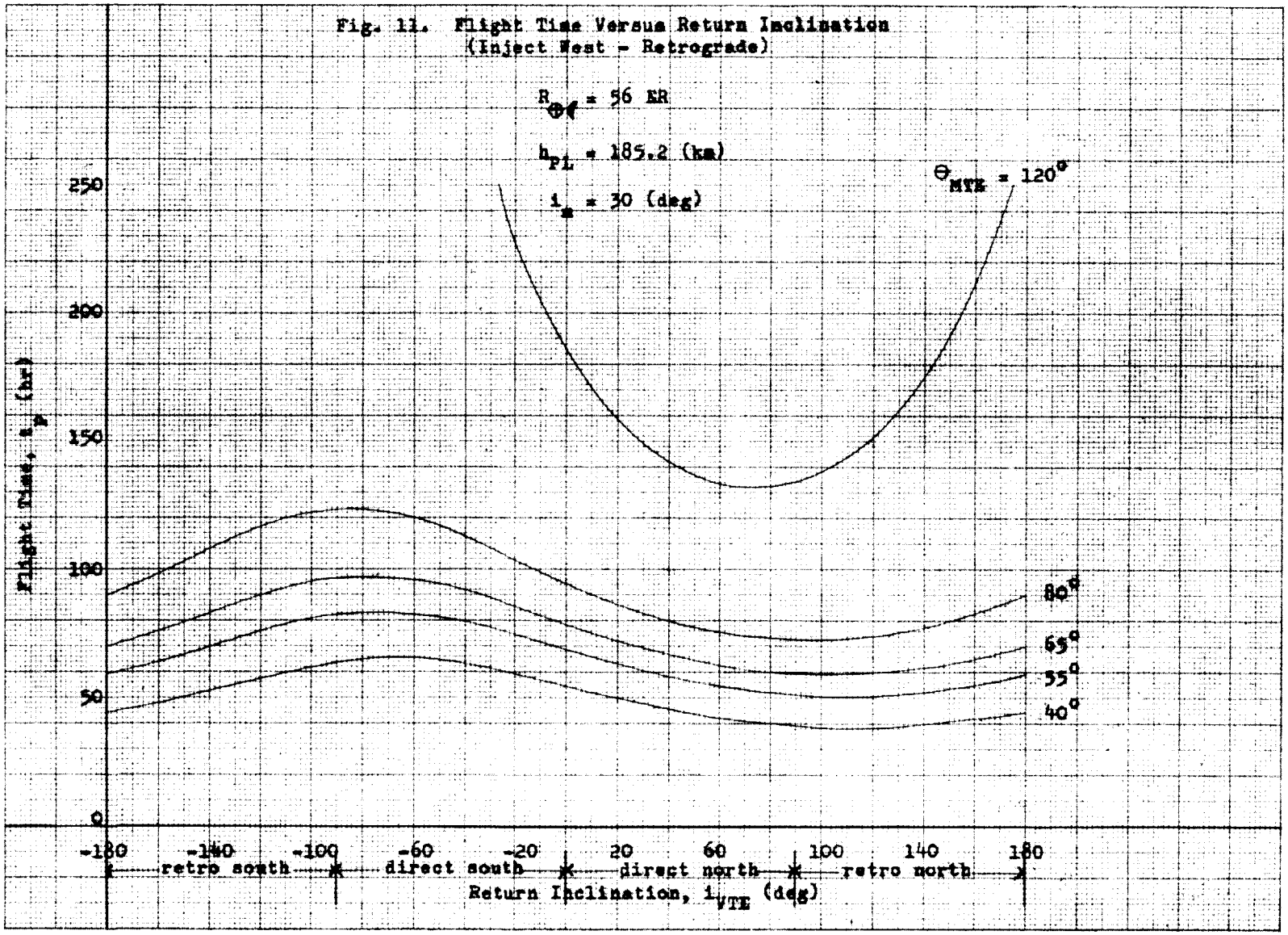

Fig. 12. ΔV Required For Transearth Injection Versus Return Inclination

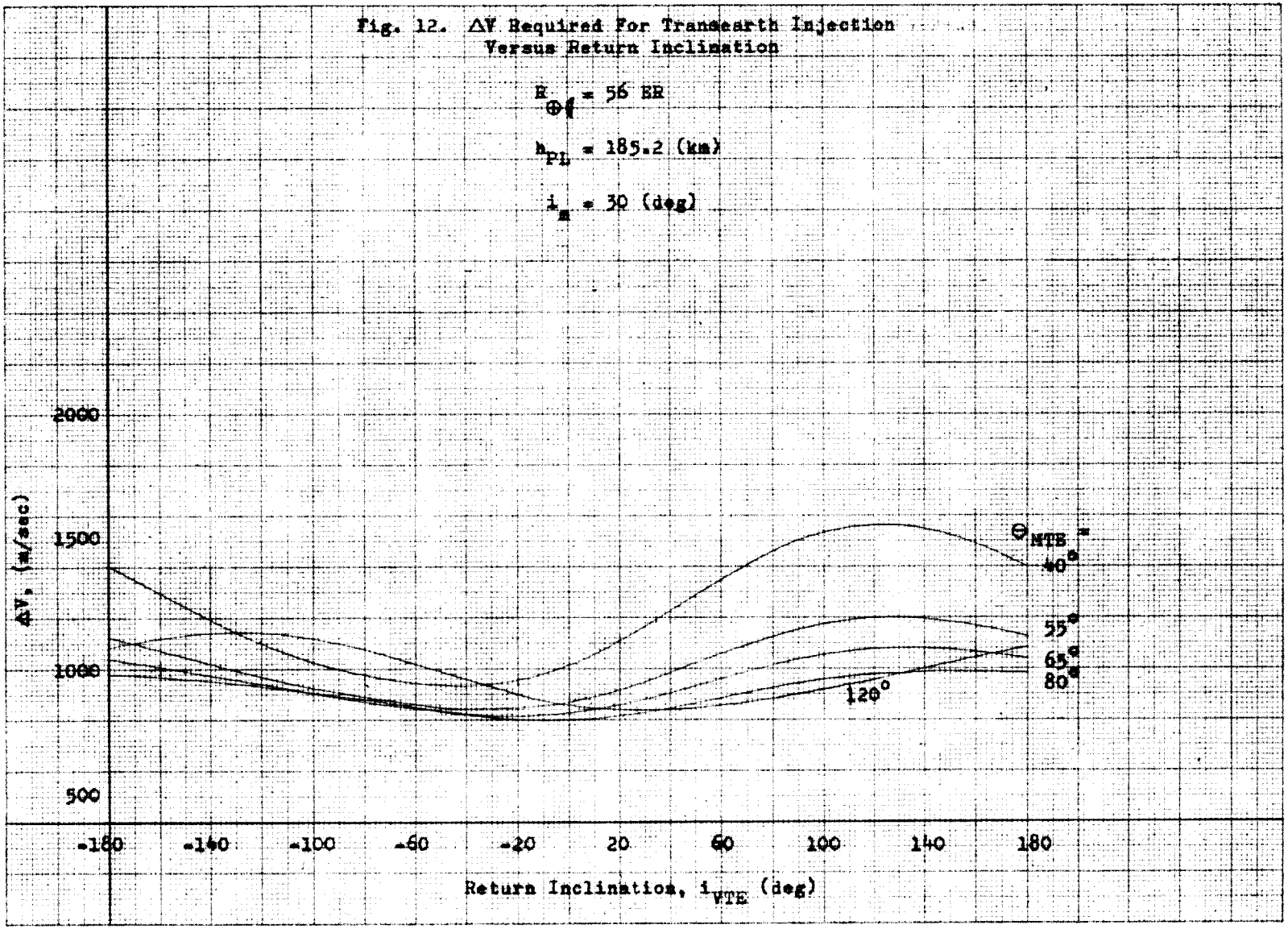

Fig. 13. Transearth Injection Point Versus Return Inclination

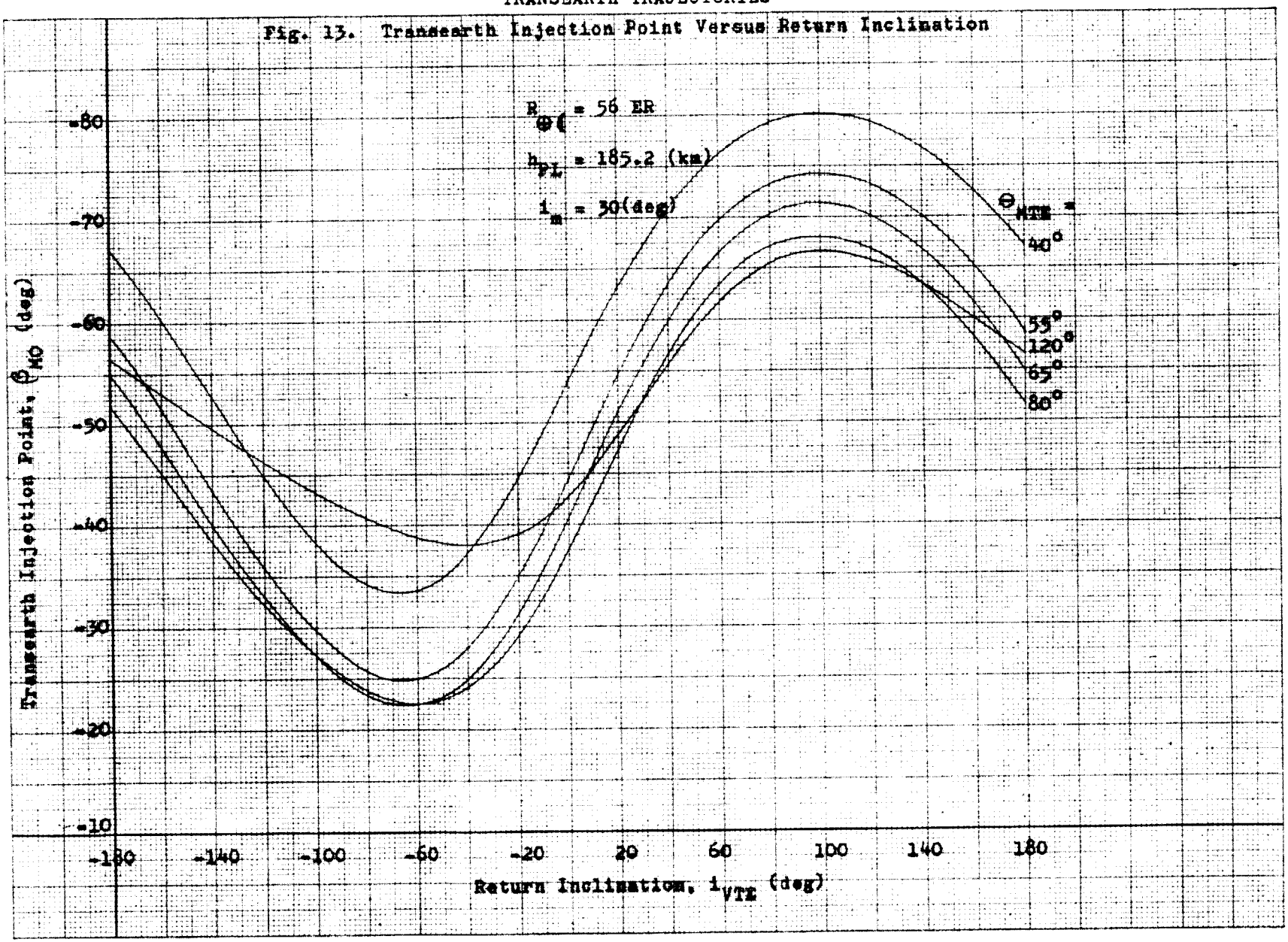

Fig. 14. Injection Velocity Versus Translunar Inclination

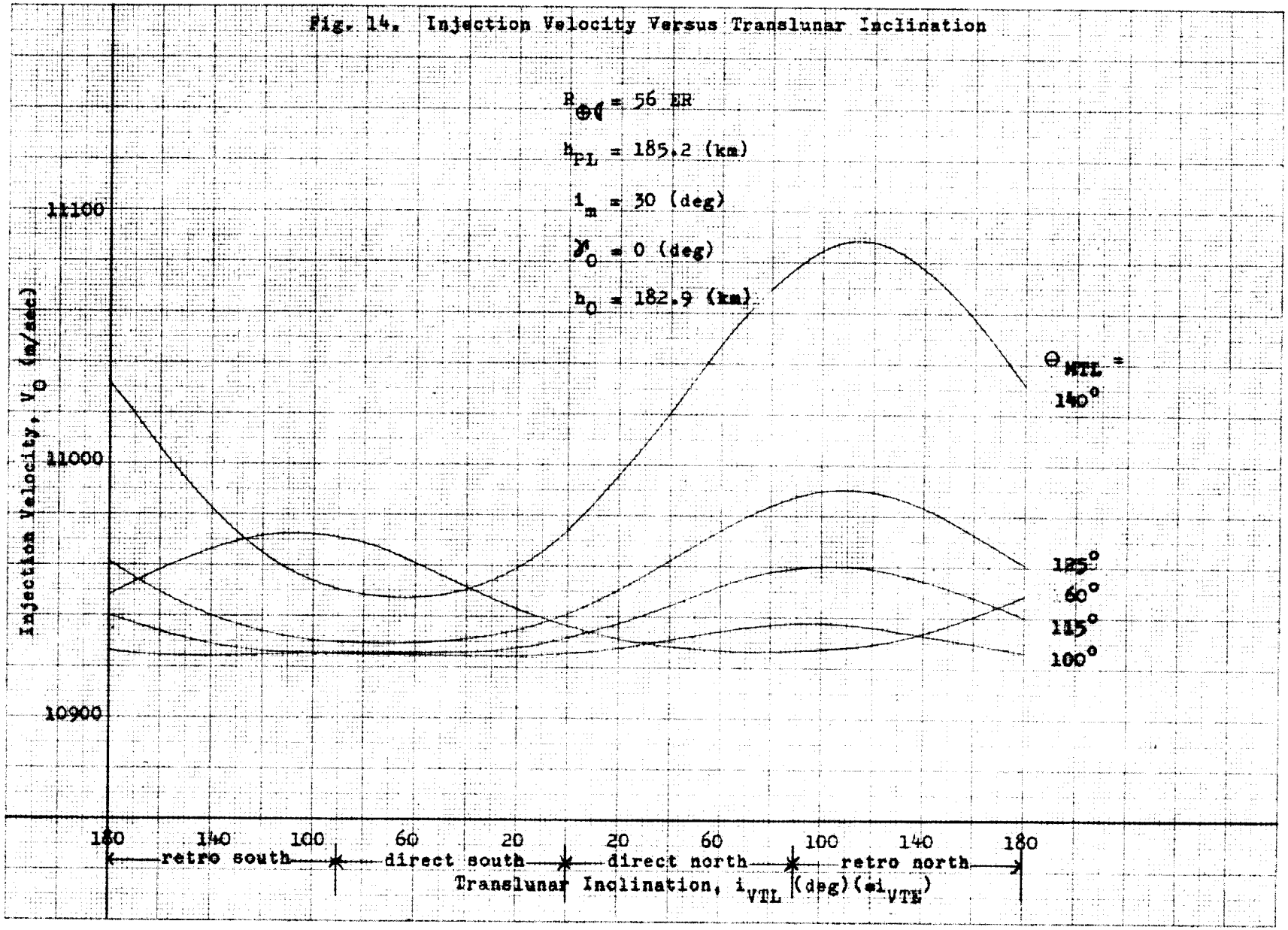

Fig. 15. Translunar Injection Position Versus Translunar Inclination

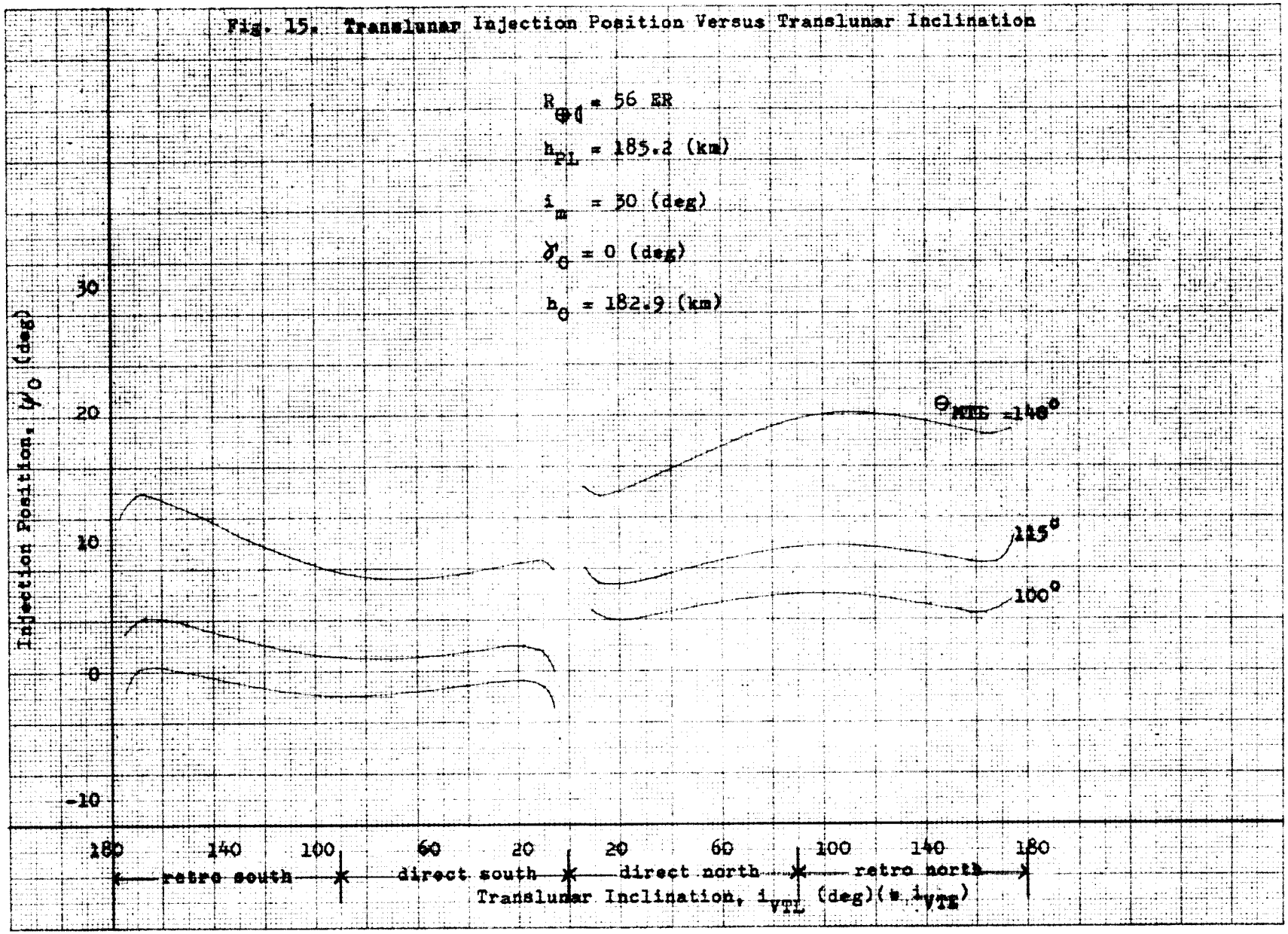

Fig. 16. Flight Time Versus Return Inclination
(Inject West - Retrograde)

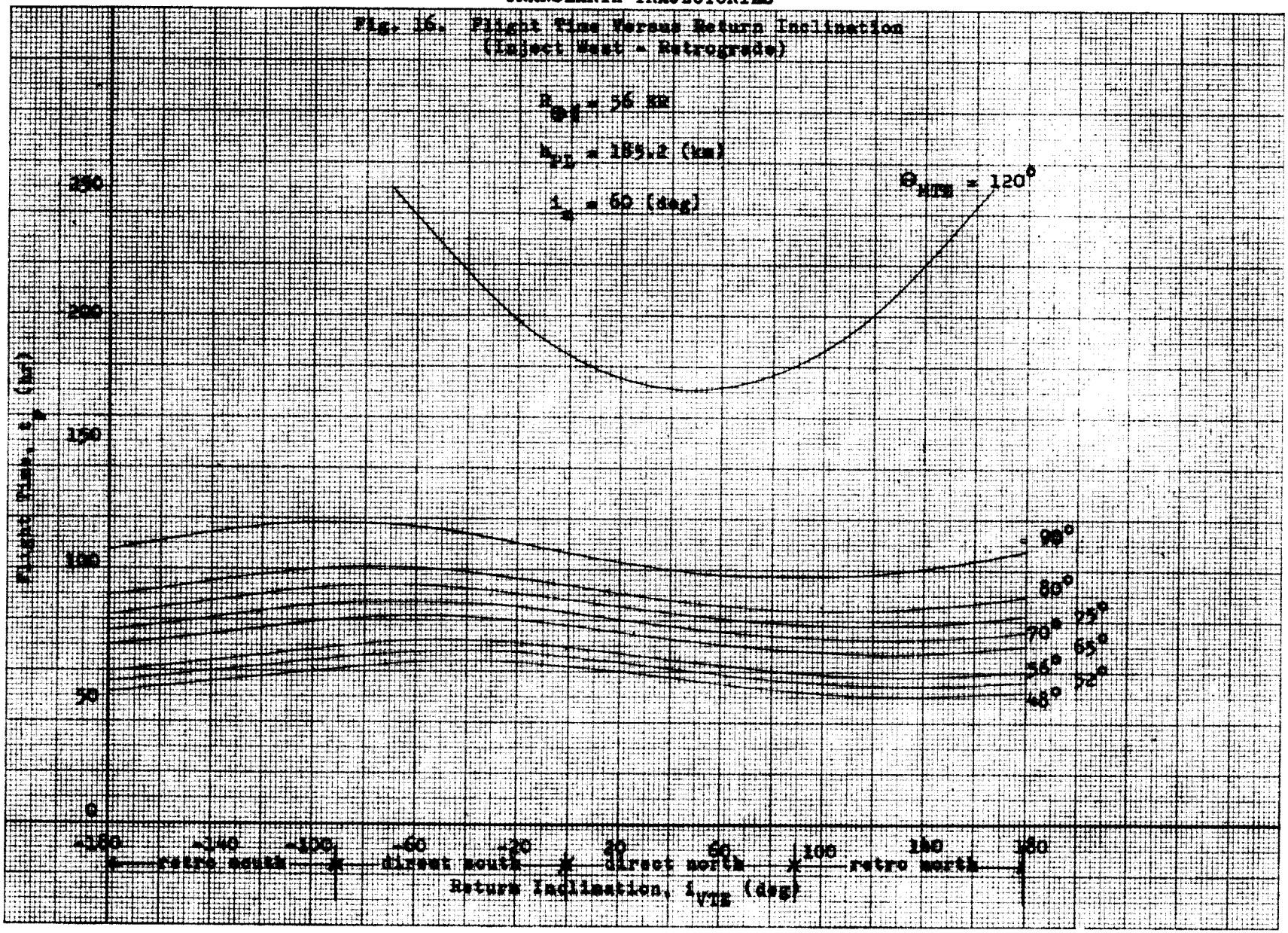

Fig. 17. ΔV Required For Transearth Injection Versus Return Inclination

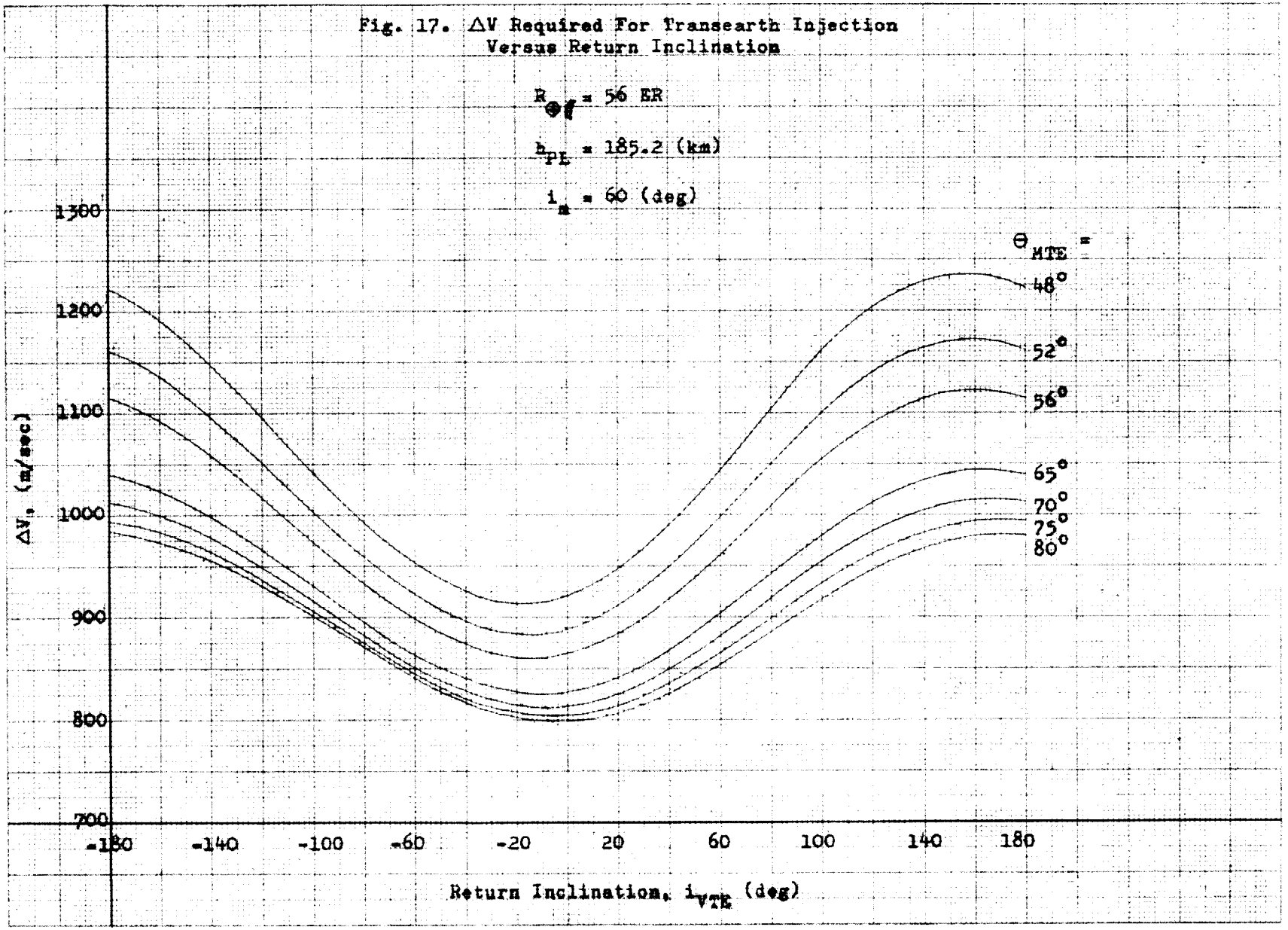

Fig. 18. Transearth Injection Point Versus Return Inclination

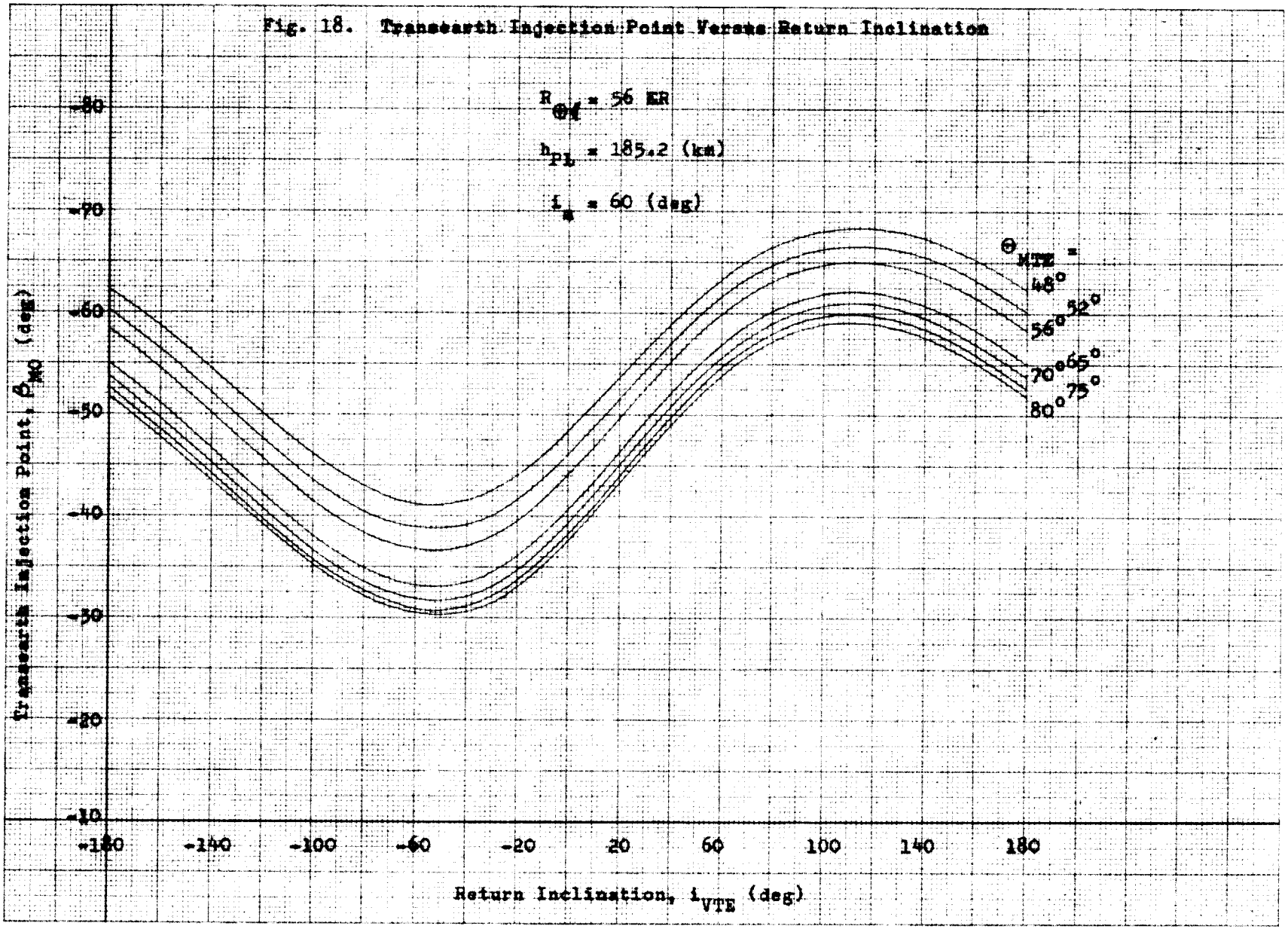

Fig. 19. Injection Velocity Versus Translunar Inclination

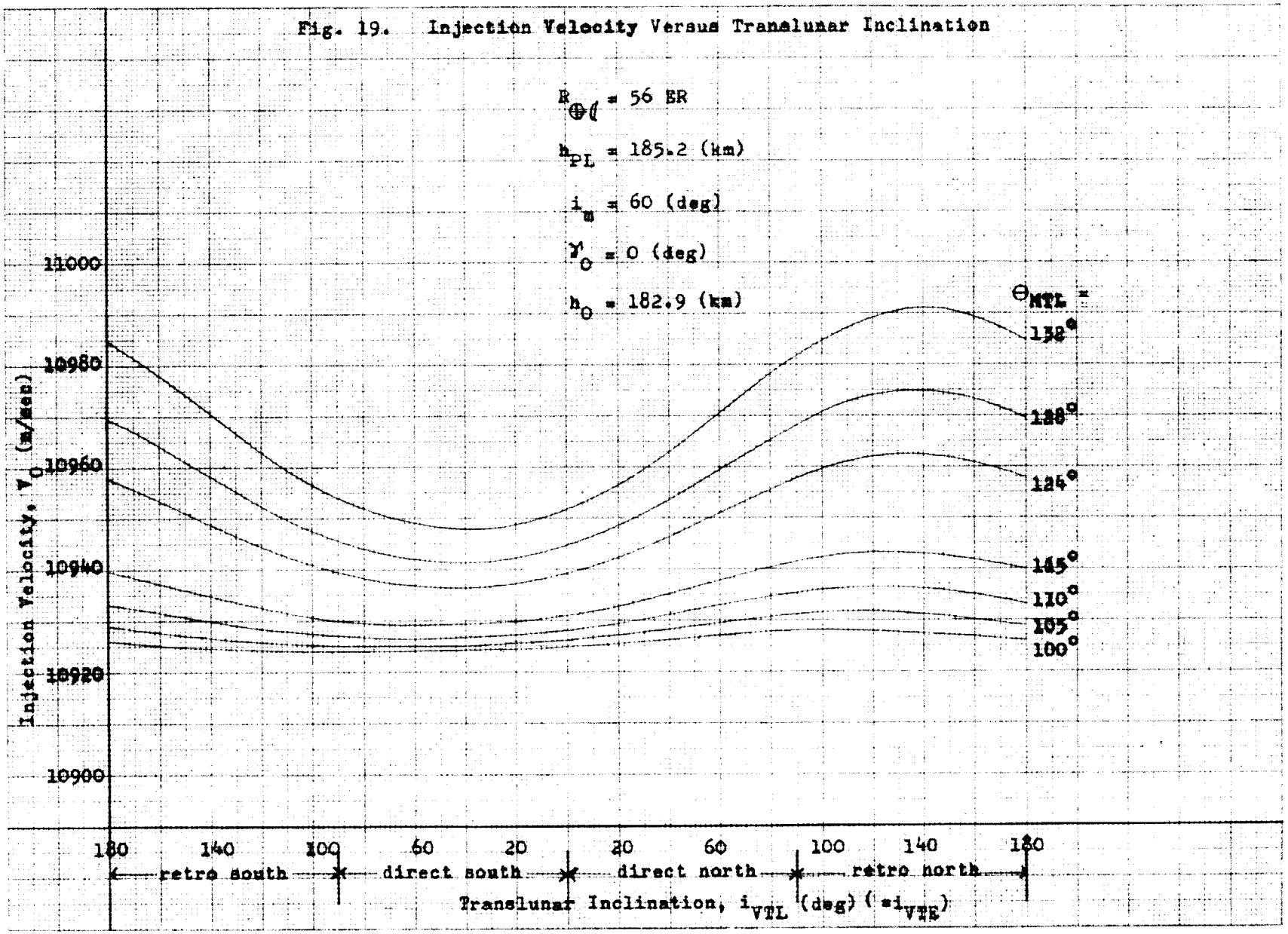

Fig. 20. Translunar Injection Position Versus Translunar Inclination

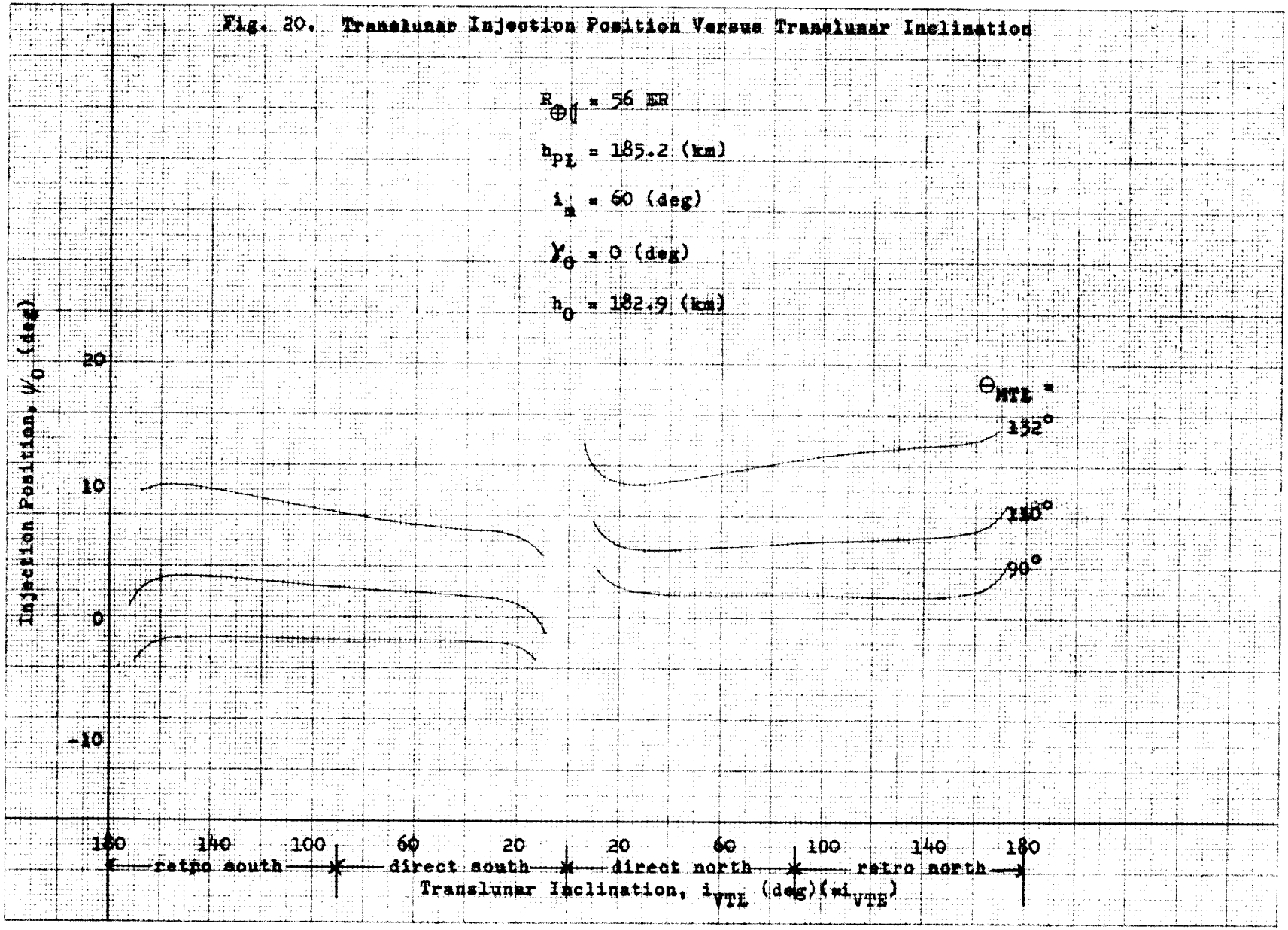

Fig. 21. Flight Time Versus Return Inclination
(Inject West - Retrograde)

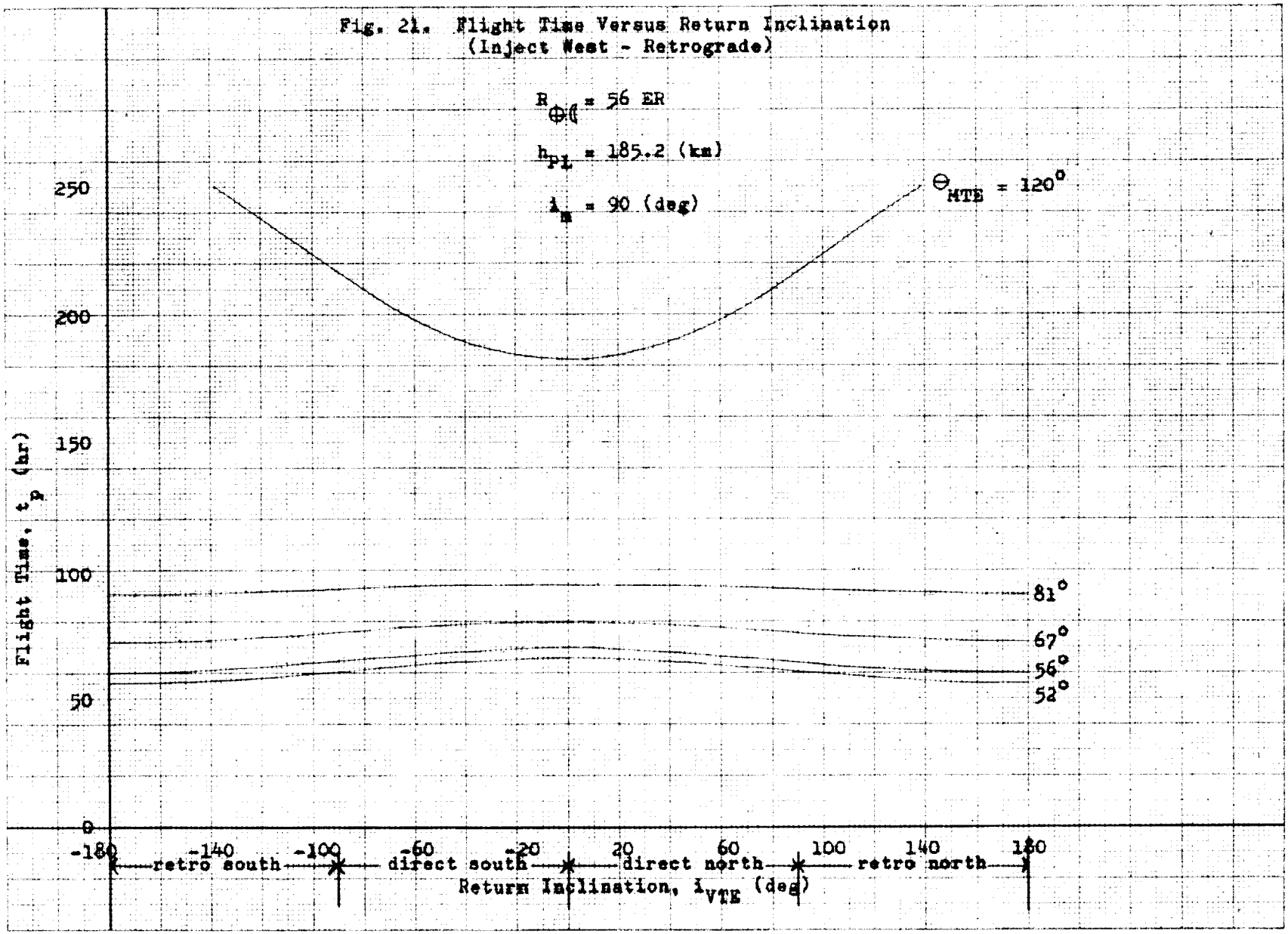

Fig. 22. ΔV Required For Transearth Injection Versus Return Inclination

$R_{\oplus C} = 56$ ER

$h_{PL} = 185.2$ (km)

$i_m = 90$ (deg)

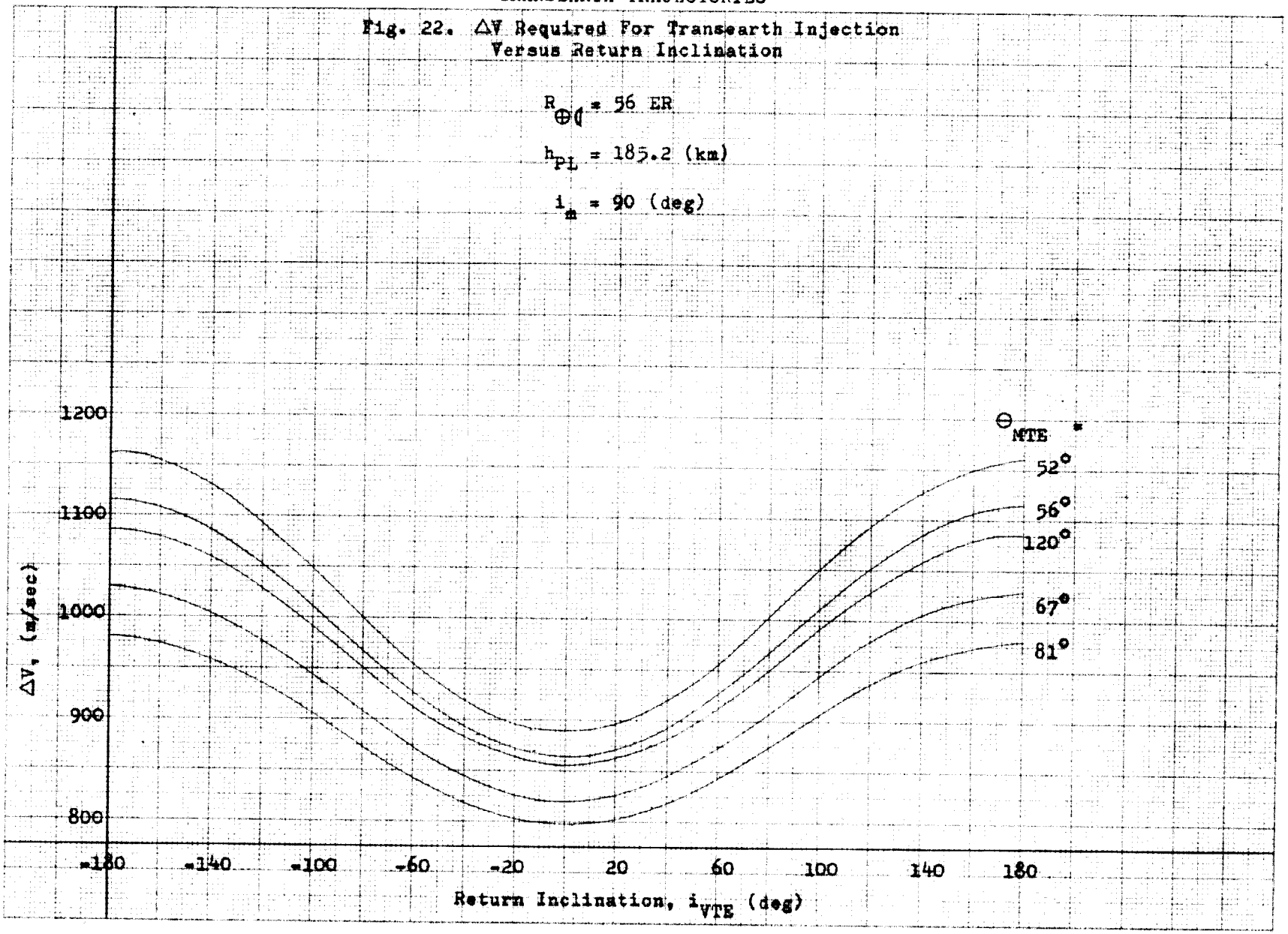

Fig. 23. Transearth Injection Point Versus Return Inclination

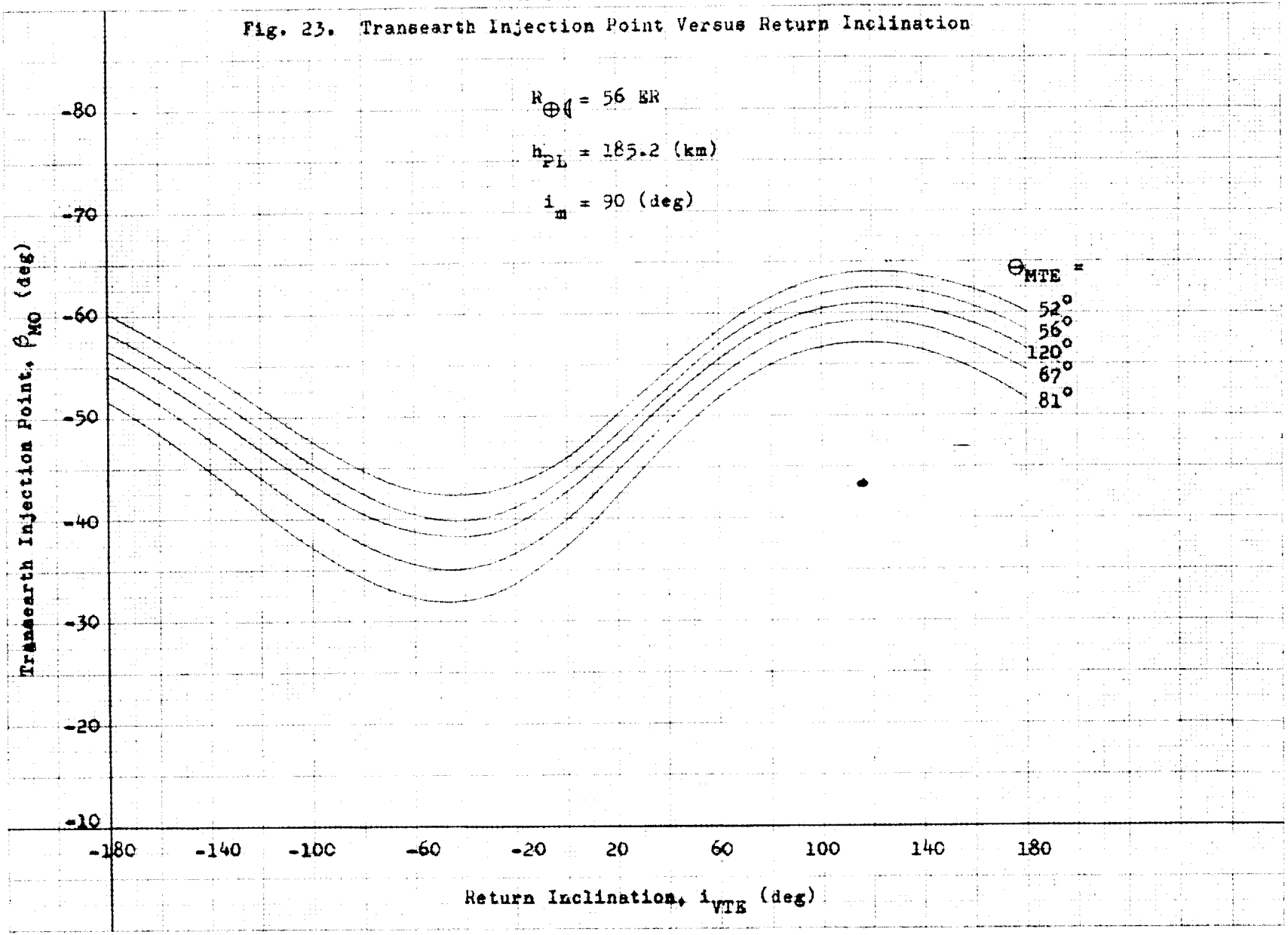

Fig. 24. Injection Velocity Versus Translunar Inclination

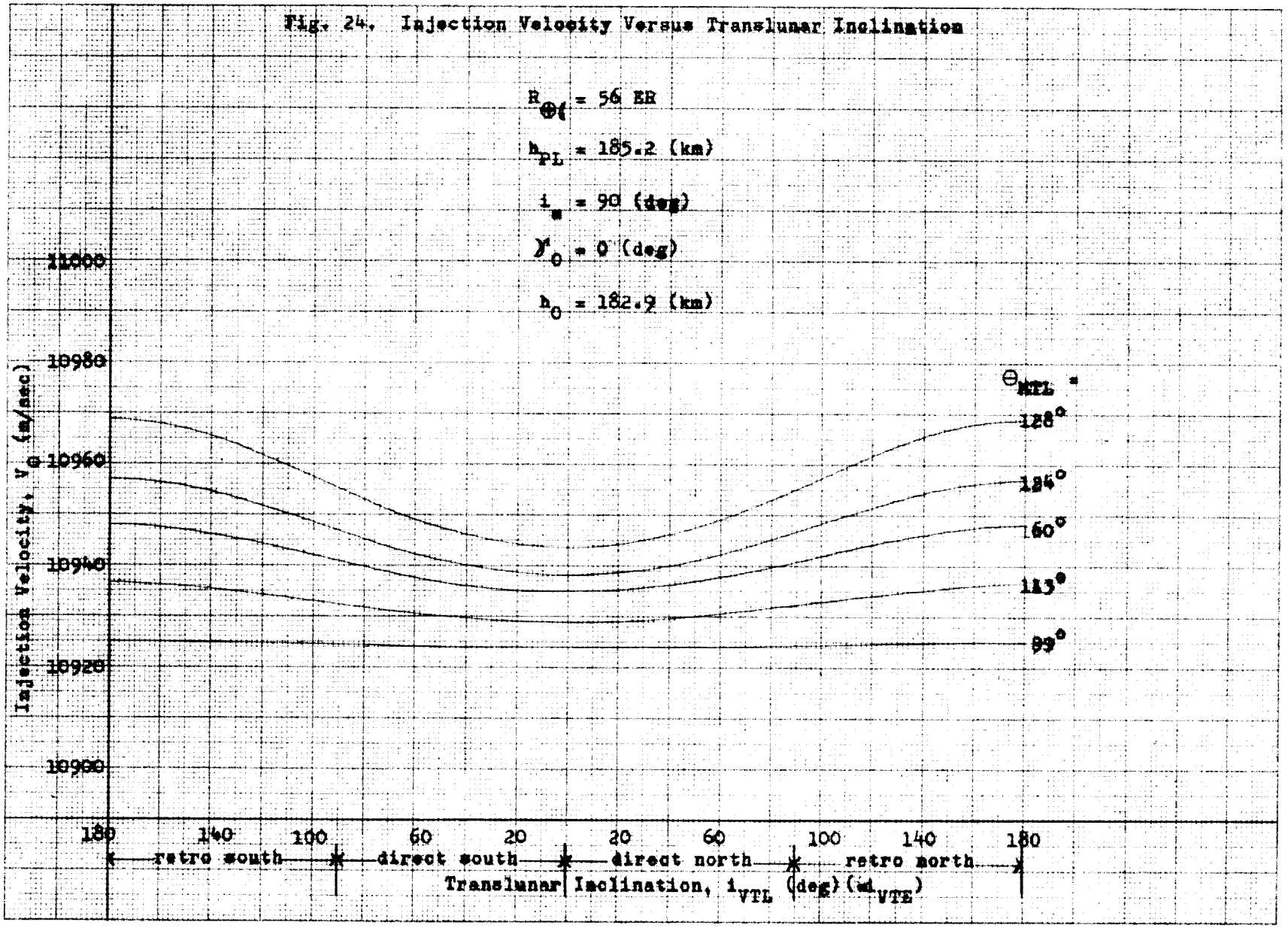

Fig. 25. Translunar Injection Position Versus Translunar Inclination

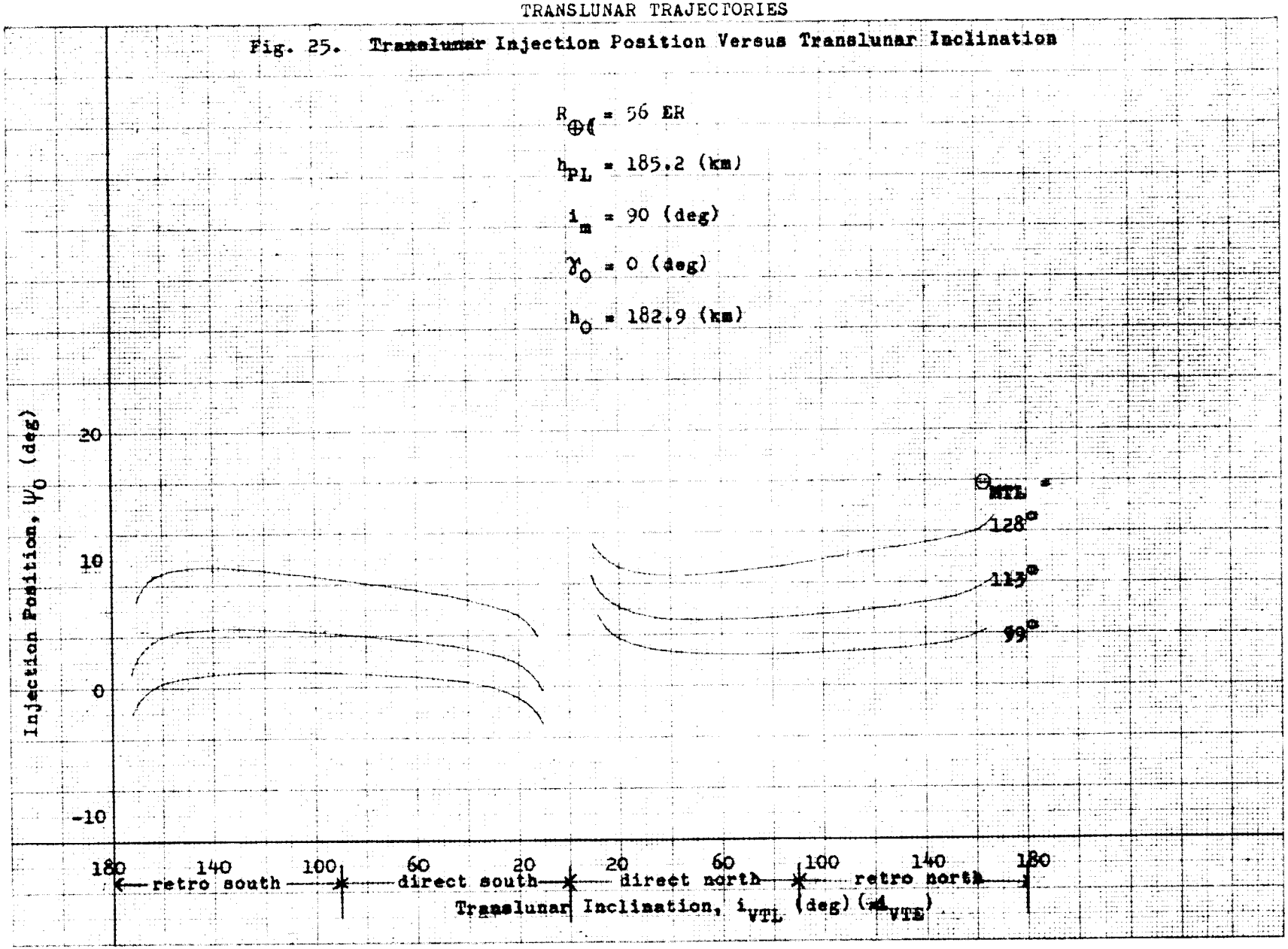

Fig. 26. Flight Time Versus Return Inclination
(Inject West - Retrograde)

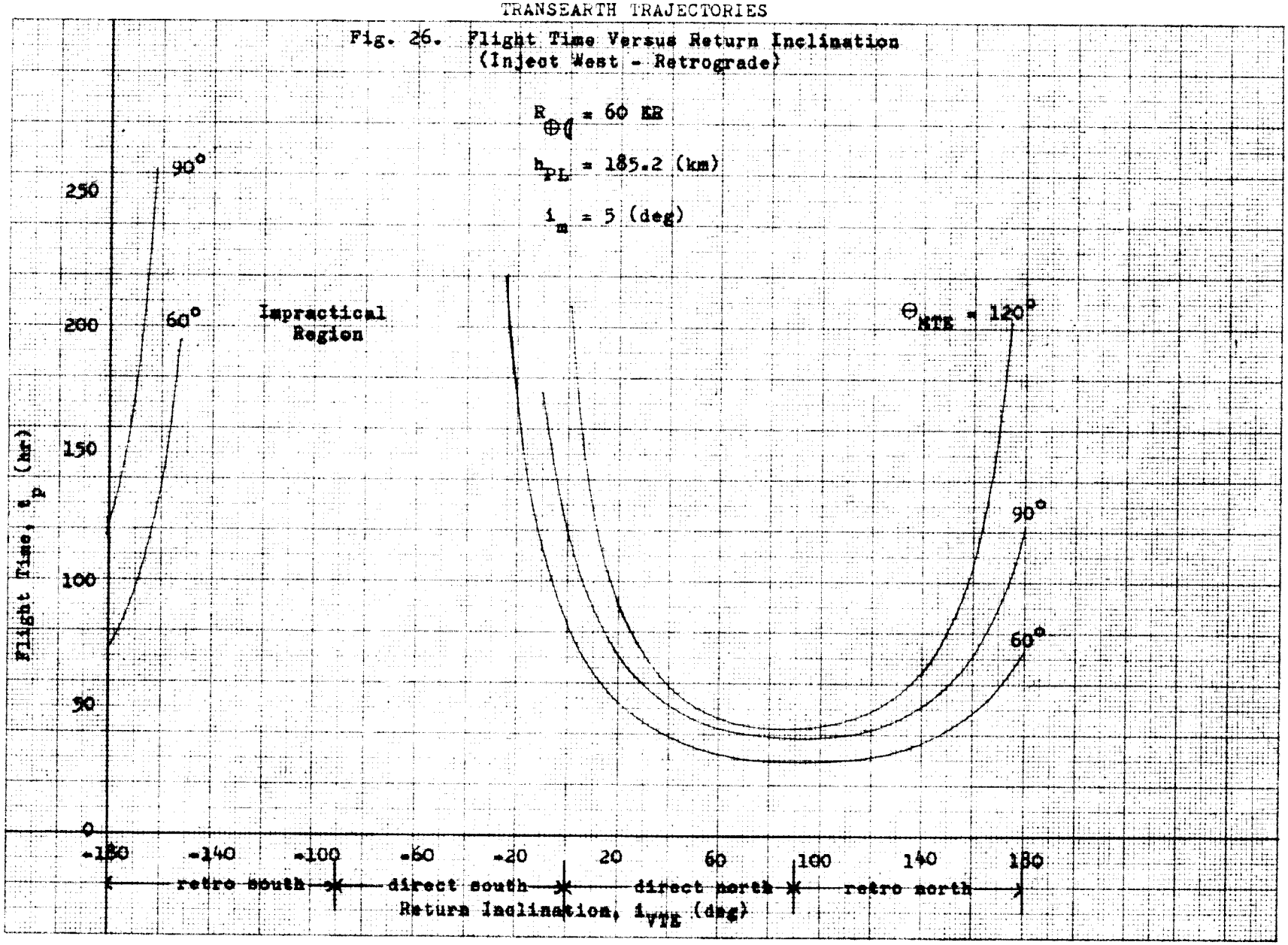

Fig. 27. ΔV Required For Transearth Injection Versus Return Inclination

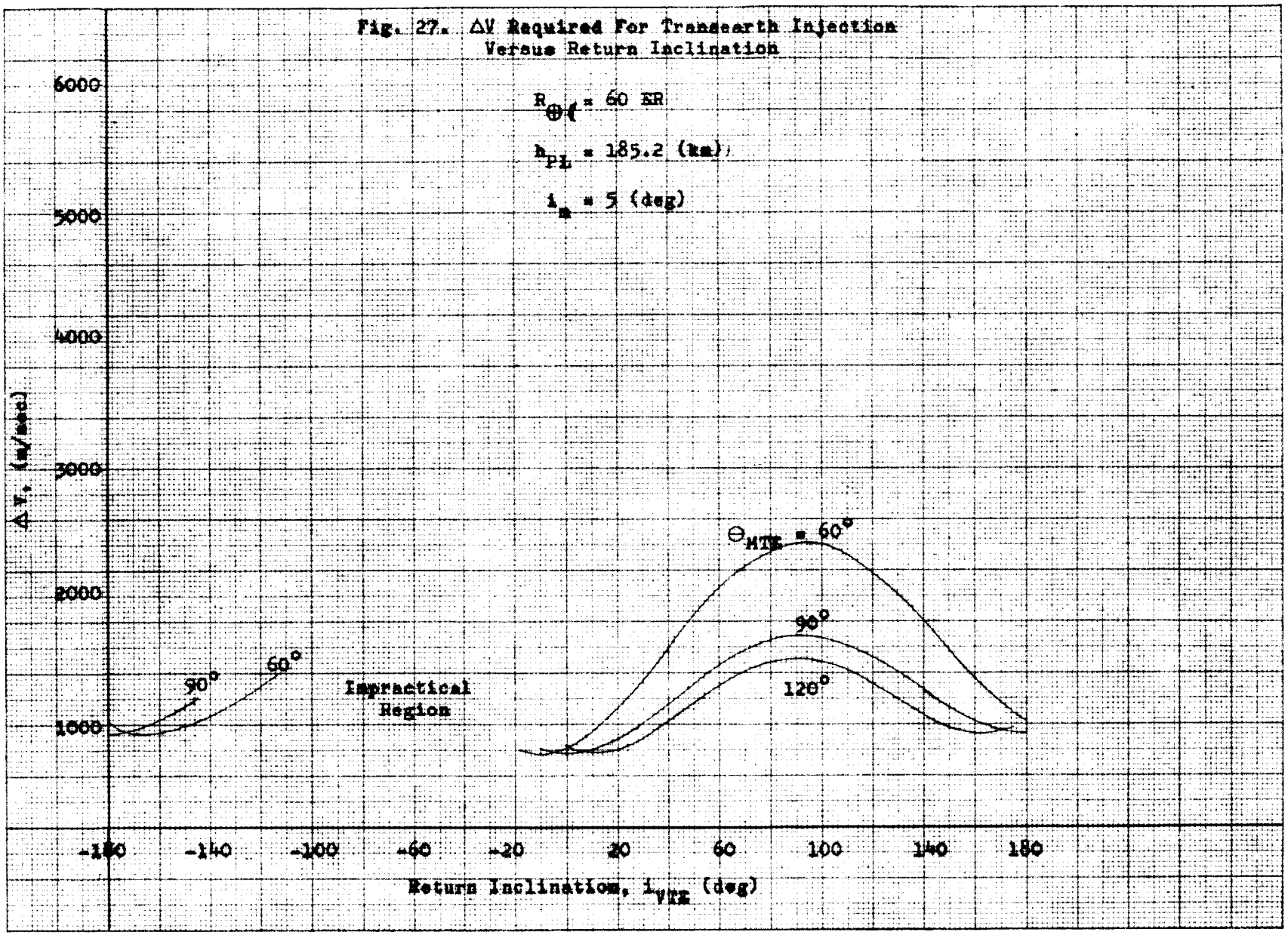

Fig. 28.- Transearth Injection Point Versus Return Inclination

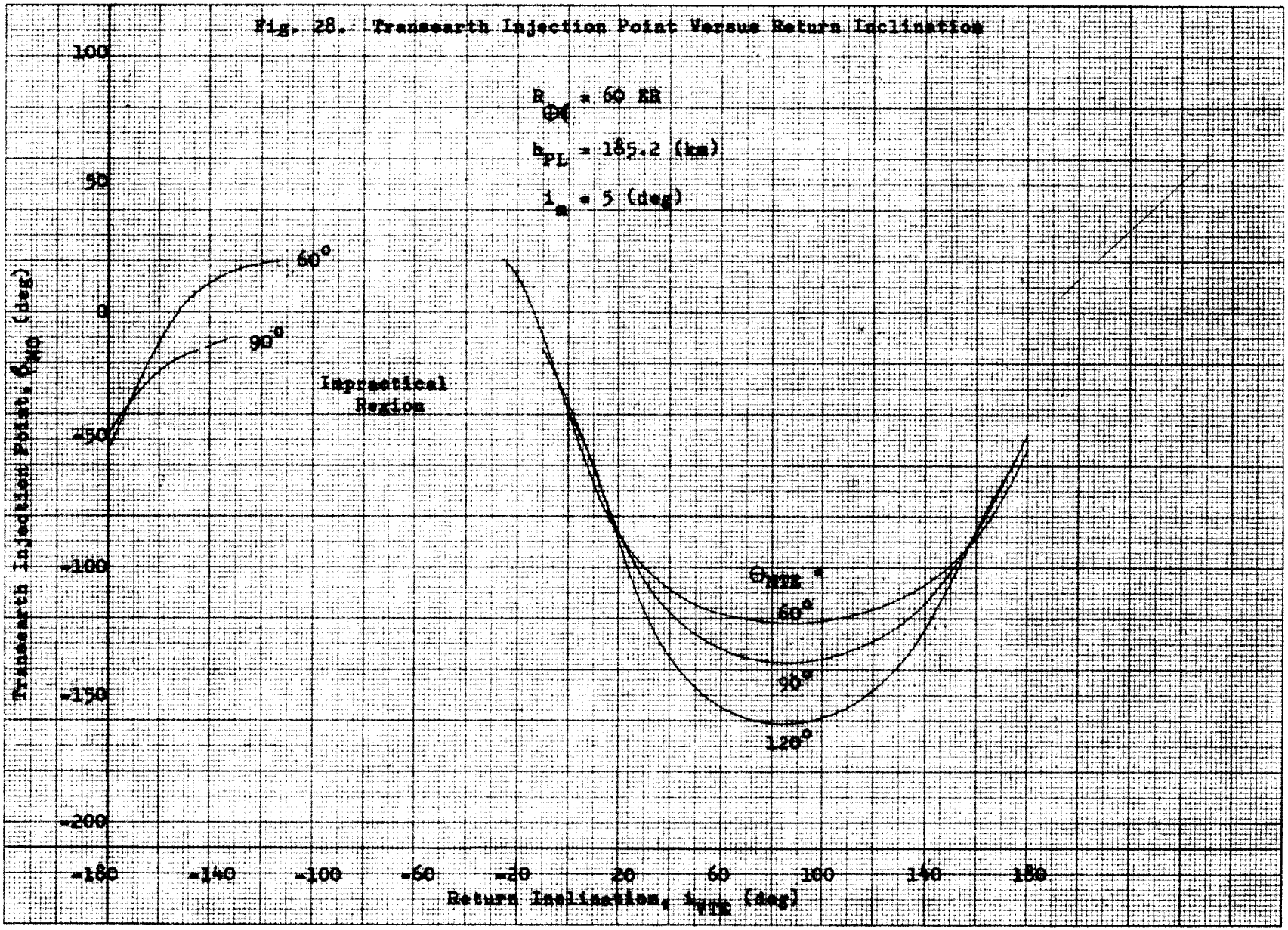

Fig. 29. Injection Velocity Versus Translunar Inclination

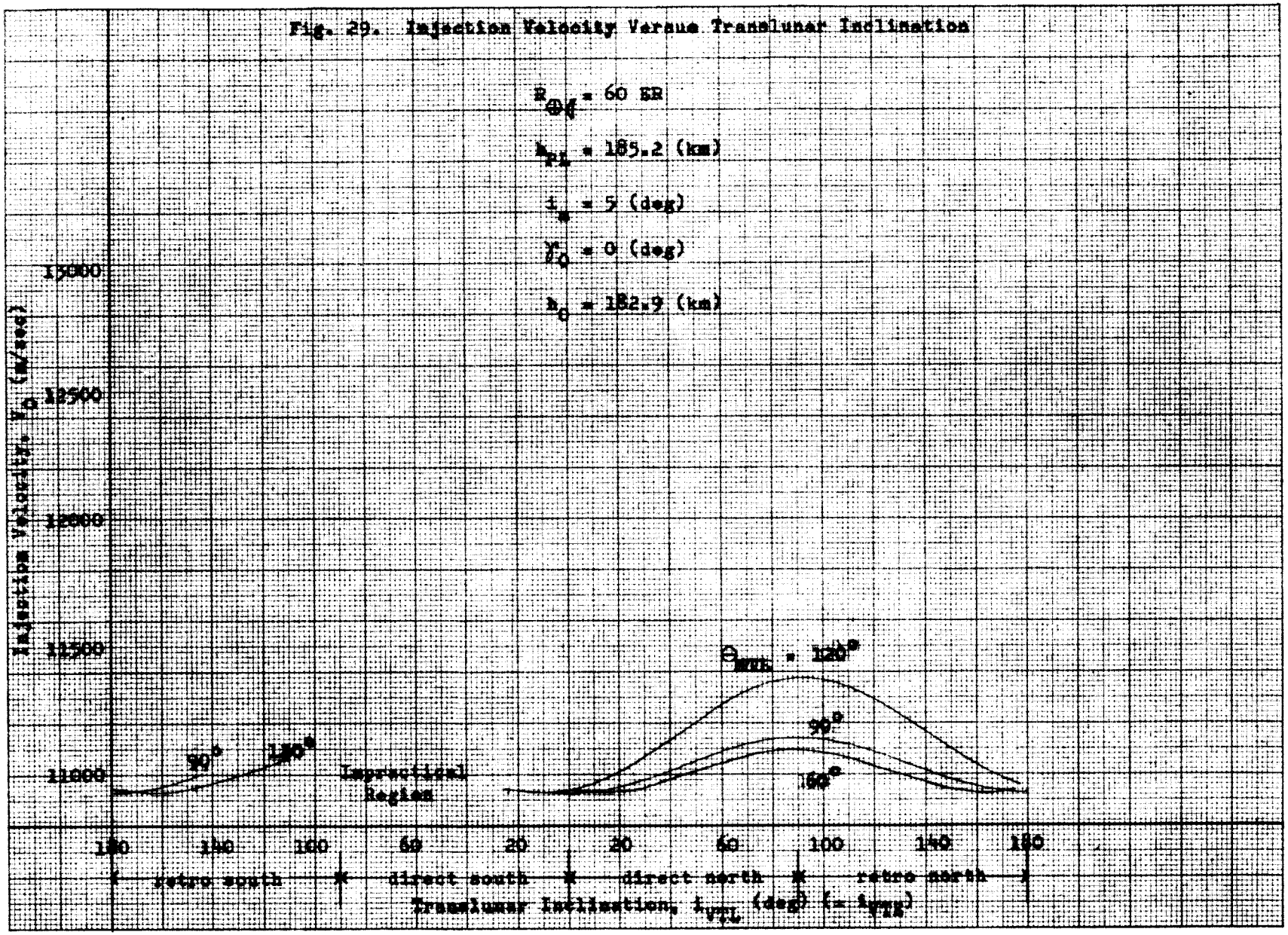

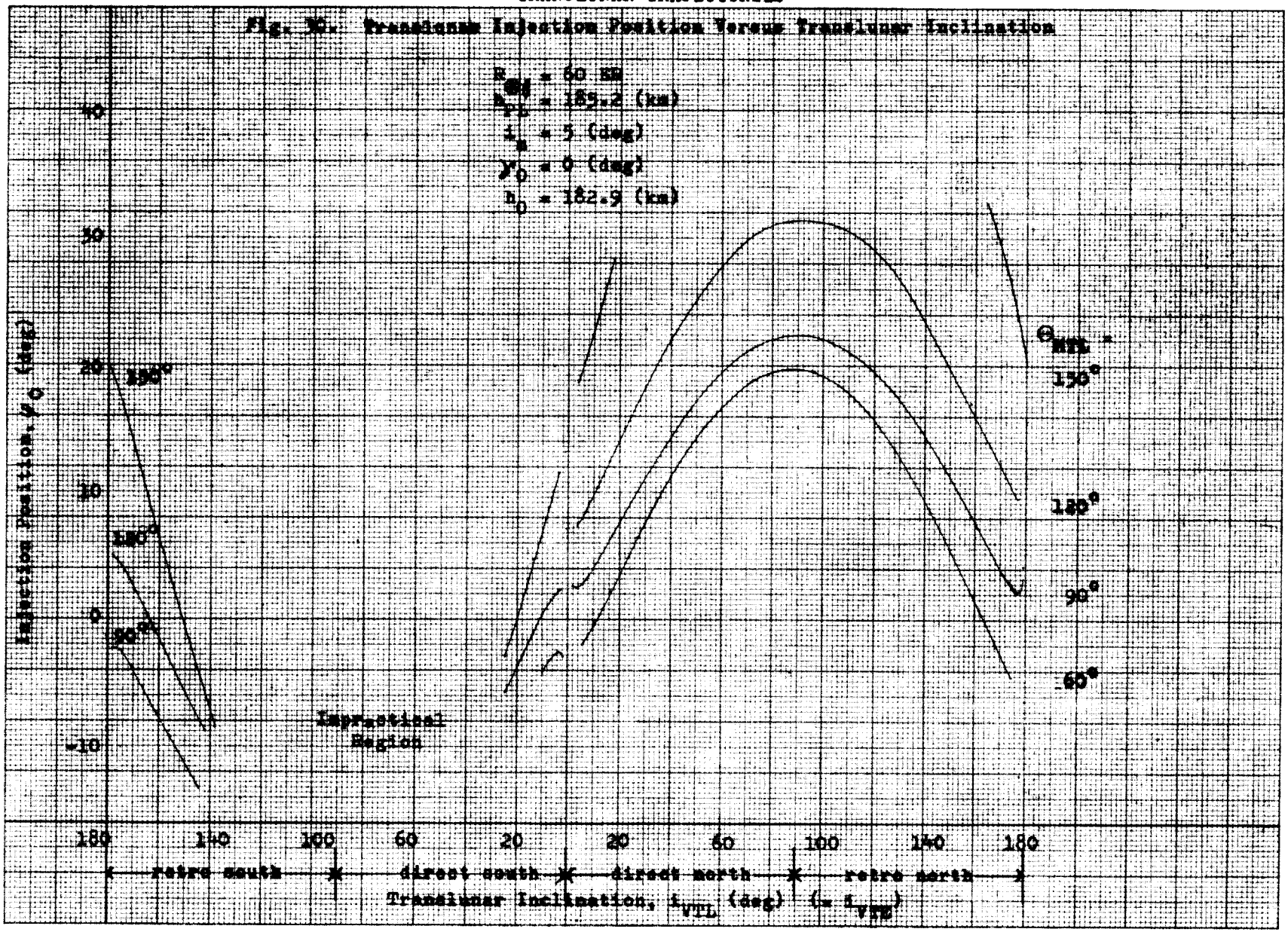
Fig. IX-x. Translunar Injection Position Versus Translunar Inclination
R_{EM} = 60 ER
h_{Pb} = 185.2 (km)
i_m = 5 (deg)
γ_0 = 0 (deg)
h_0 = 182.9 (km)
θ_{MTL} =
150°
180°
90°
-65°
Injection Position, γ_0 (deg)
40
30
20
10
0
-10
150°
120°
90°
Impractical Region
180
140
100
60
20
20
60
100
140
180
retro south
direct south
direct north
retro north
Translunar Inclination, i_{VTL} (deg) (= i_{VTE})

Fig. 31. Flight Time Versus Return Inclination
(Inject West - Retrograde)

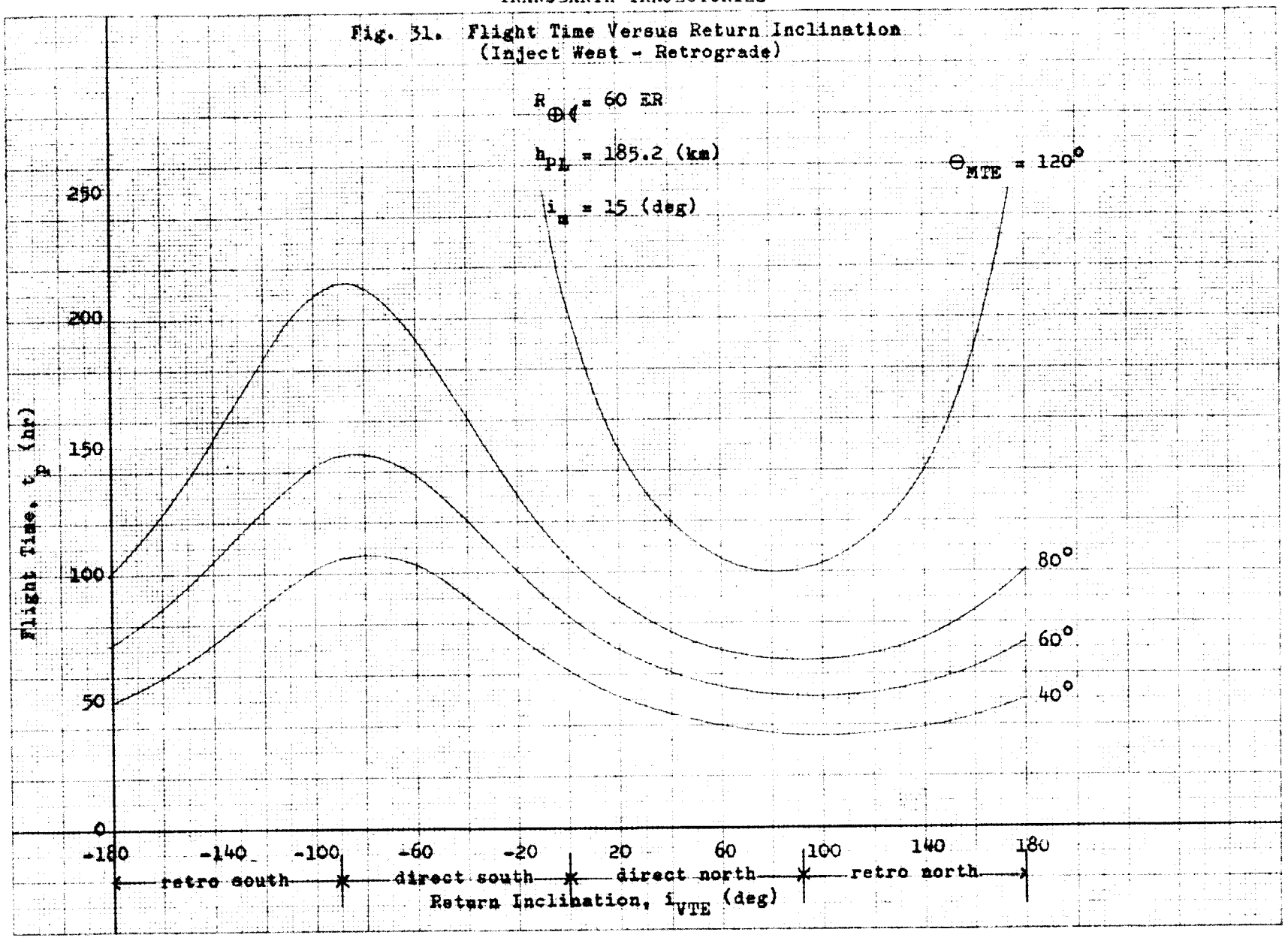

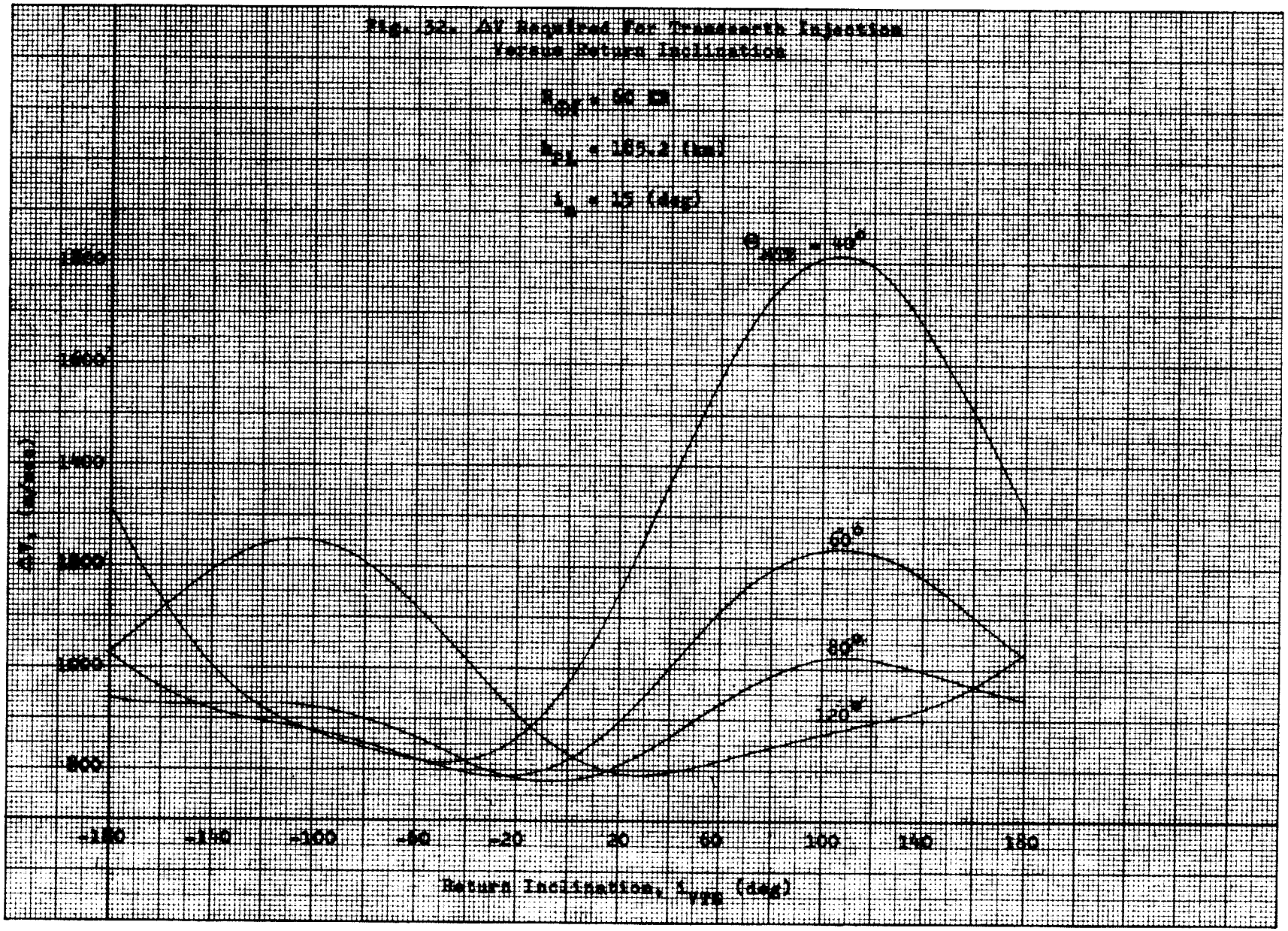

Fig. 32. ΔV Required For Transearth Injection Versus Return Inclination

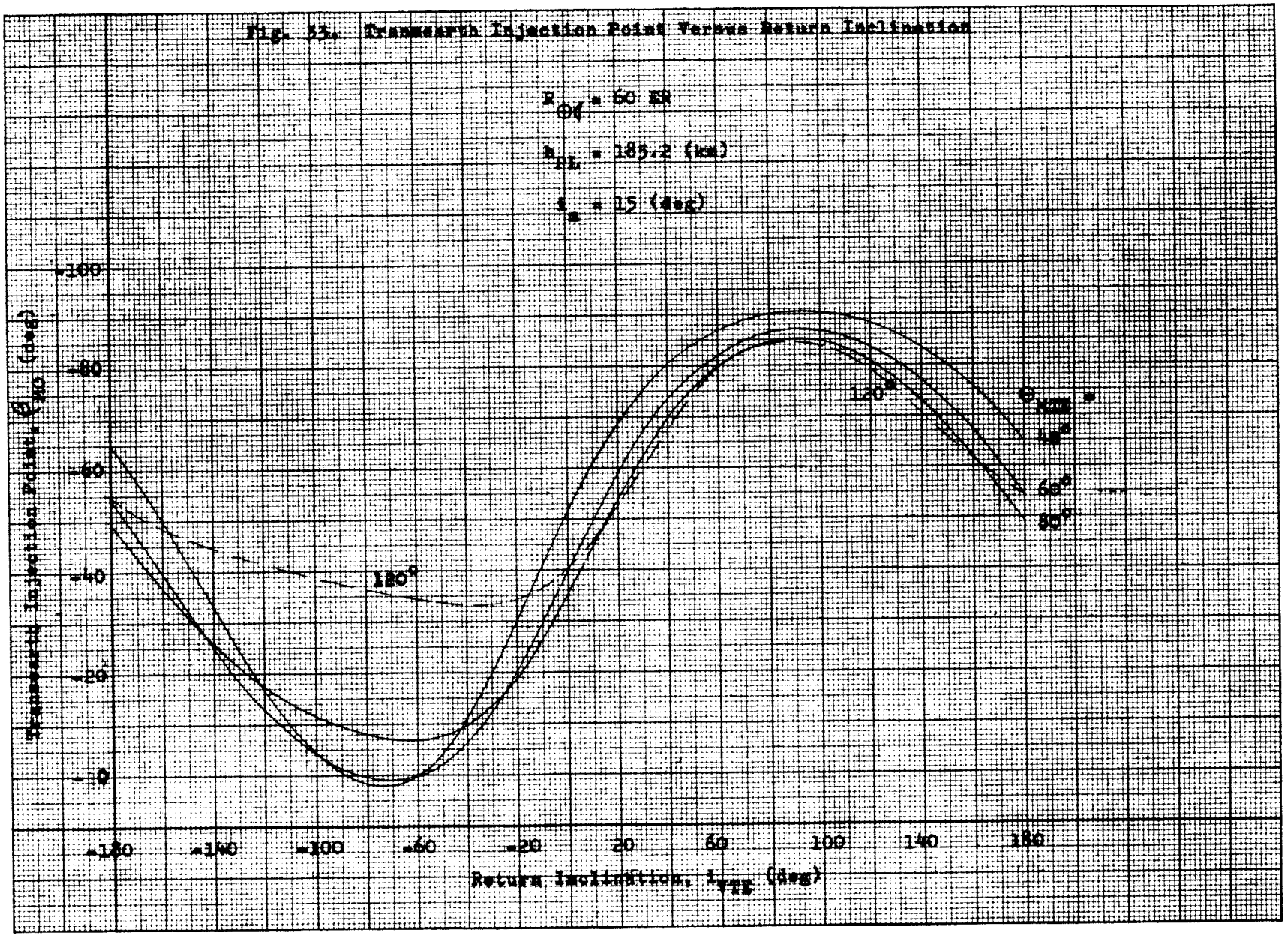

Fig. 33. Transearth Injection Point Versus Return Inclination

Fig. 34. Injection Velocity Versus Translunar Inclination

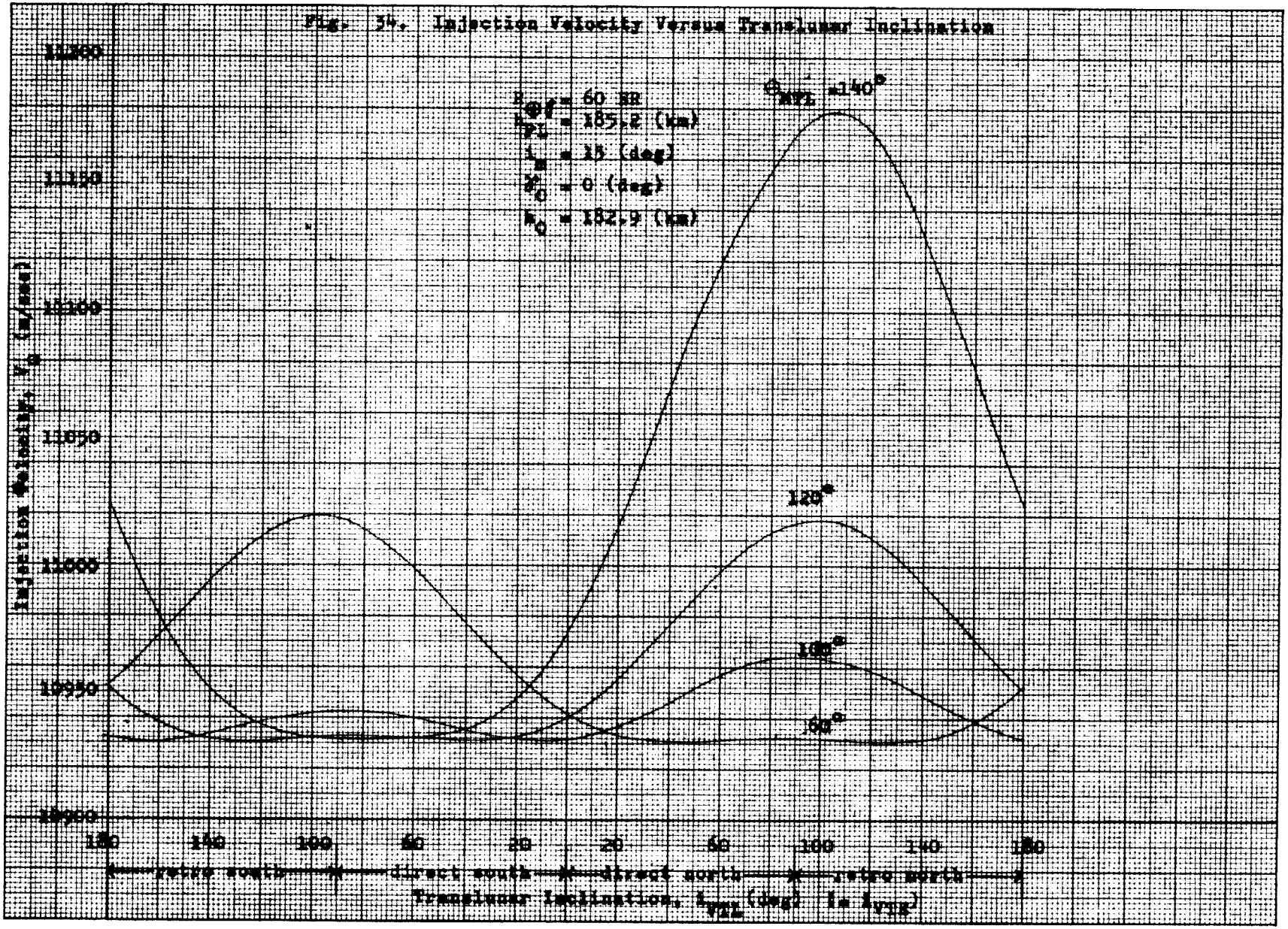

Fig. 33. Translunar Injection Position Versus Translunar Inclination

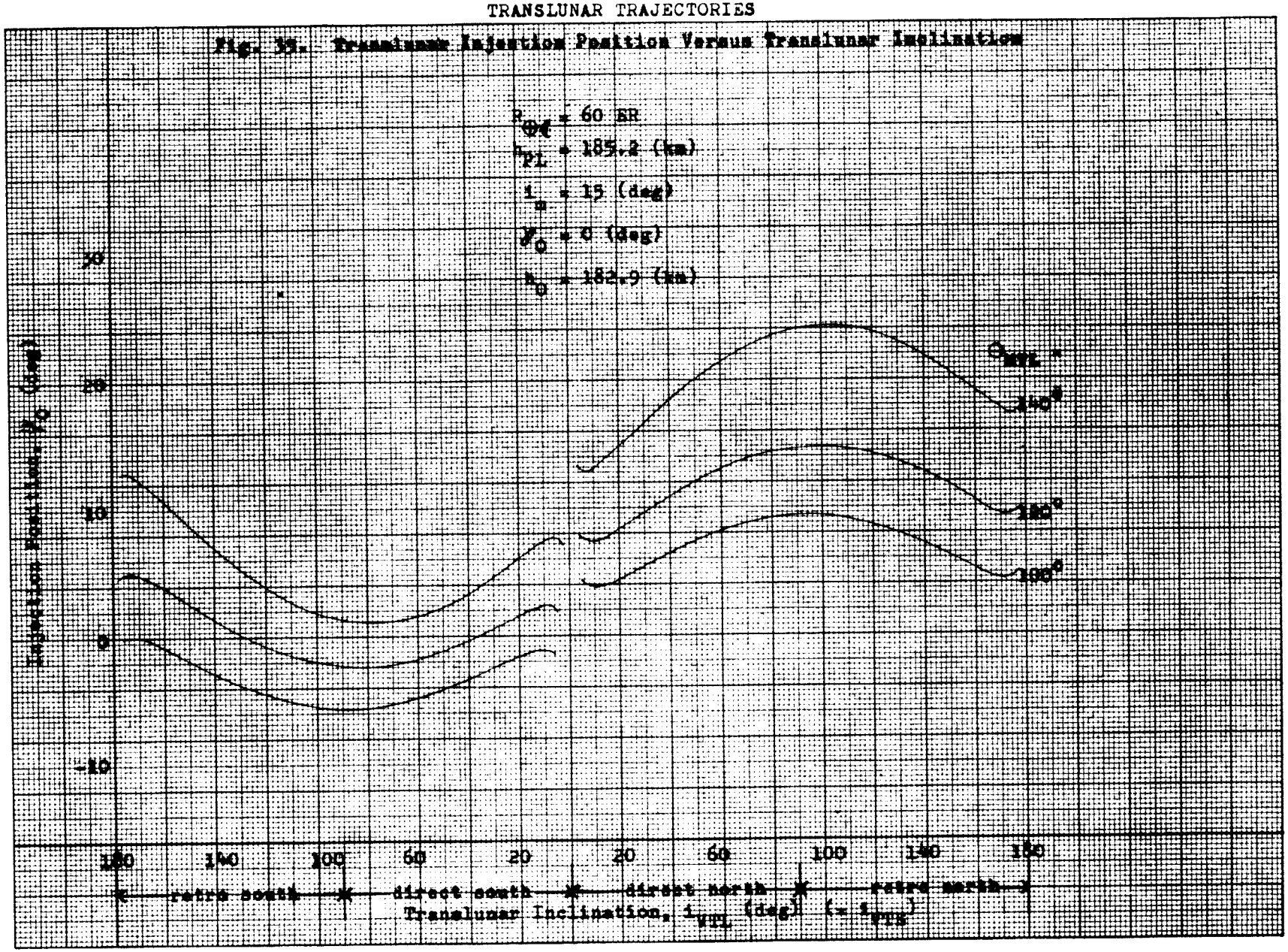

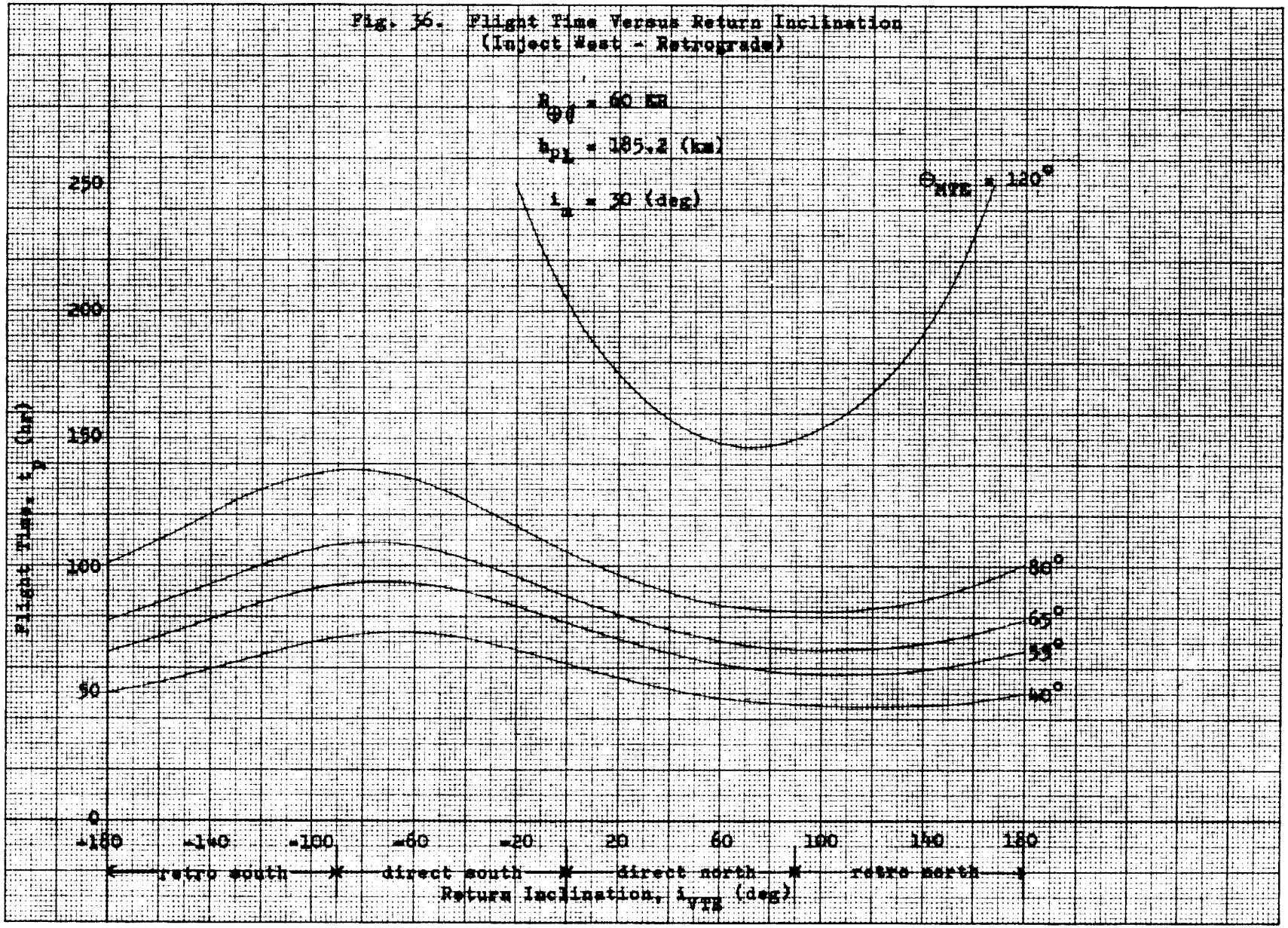

Fig. 16. Flight Time Versus Return Inclination (Inject West - Retrograde)

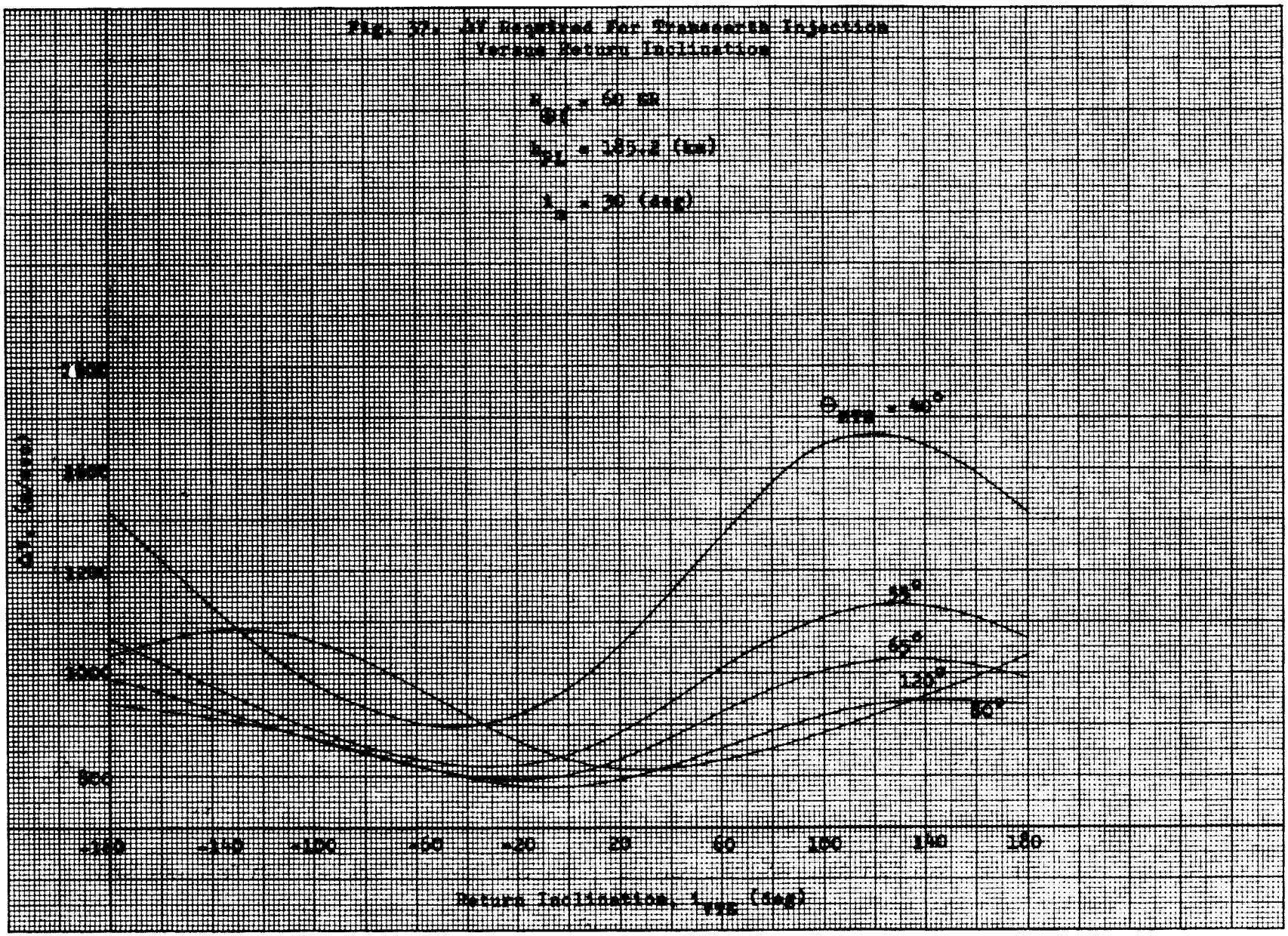

Fig. 32. ΔV Required for Transearth Injection versus Return Inclination

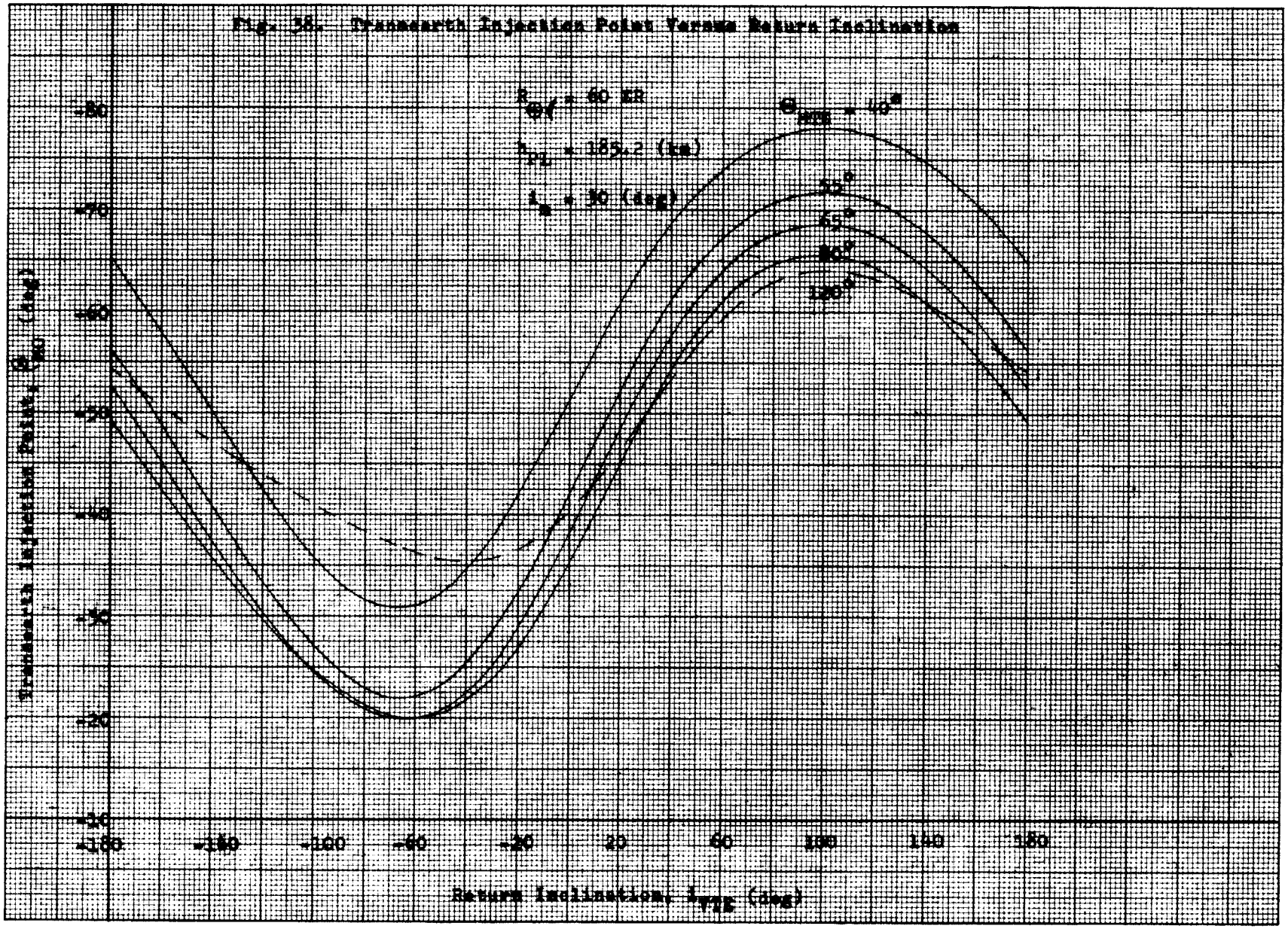

Fig. 38. Transearth Injection Point Versus Return Inclination

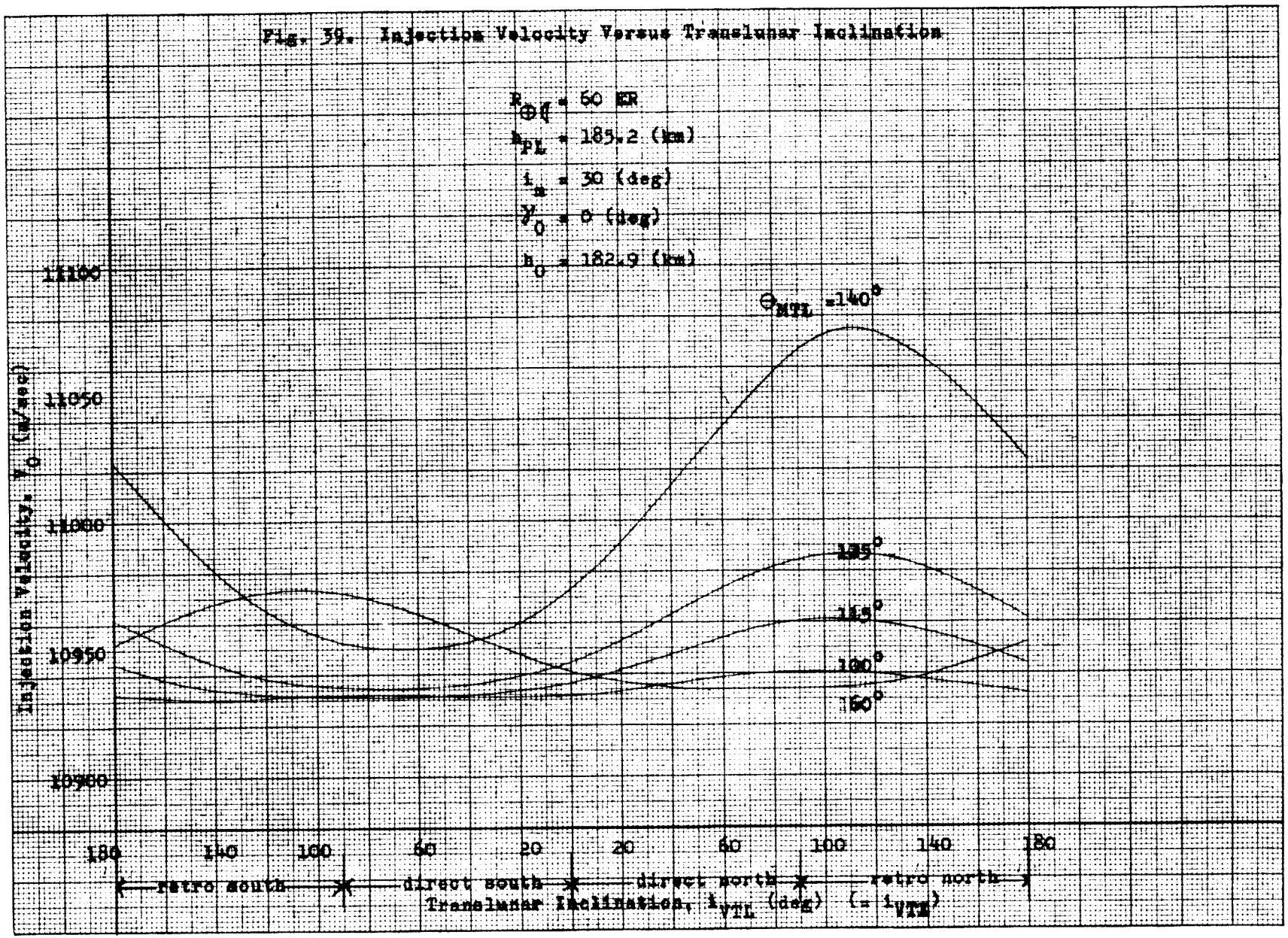

Fig. 39. Injection Velocity Versus Translunar Inclination

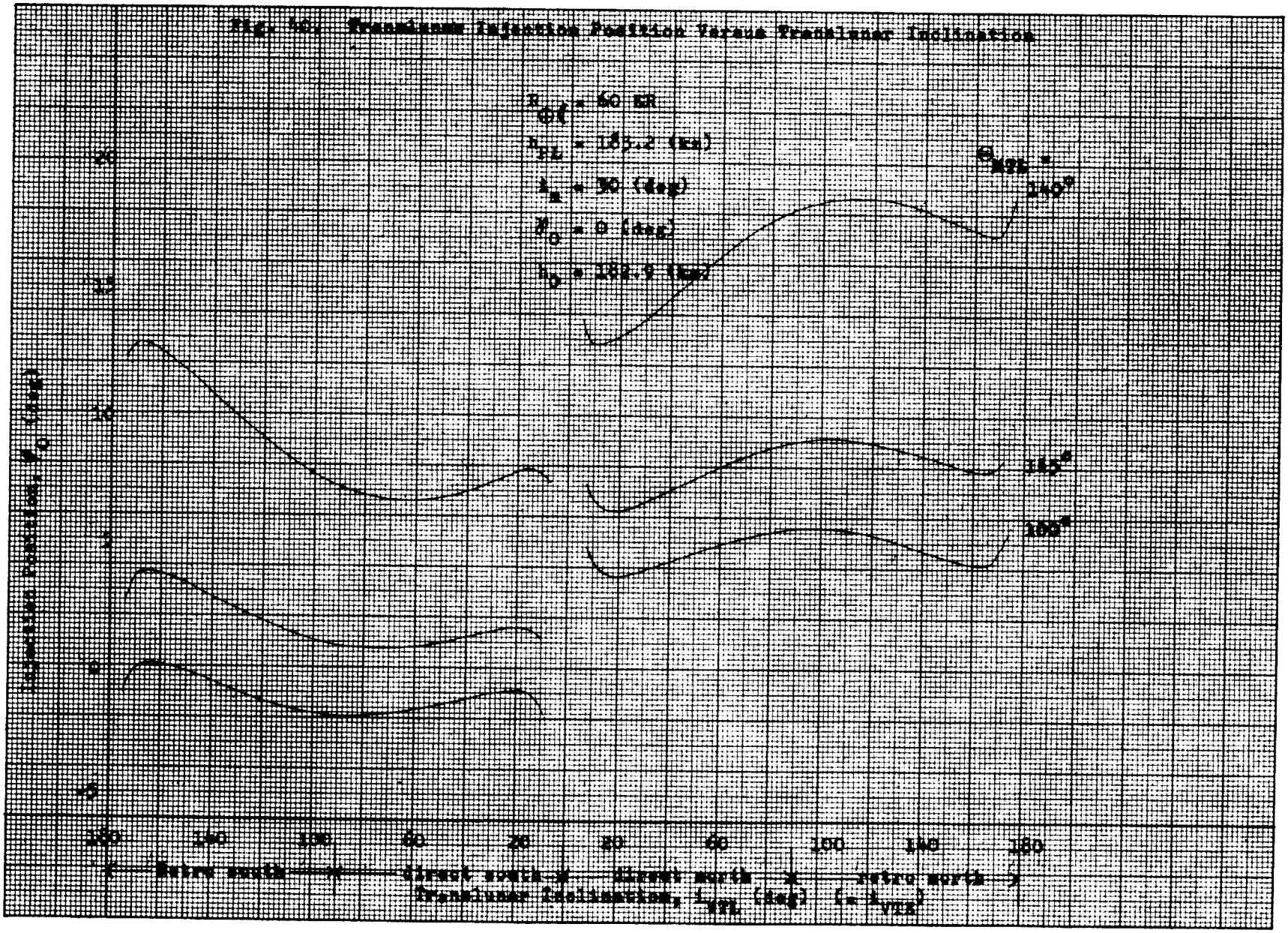
Translunar Injection Position Versus Translunar Inclination
$r_{\oplus f}$ = 60 ER
t_{FL} = 85.2 (hrs)
i_s = 30 (deg)
θ_0 = 0 (deg)
h_p = 282.9 (nm)
Ω_{MJD} = 240°
245°
100°
Declination of Injection Asymptote, δ_{VTL} (deg)
35
30
25
20
15
10
5
0
-5
180
140
100
60
20
20
60
100
140
180
Retro south
Direct south
Direct north
Retro north
Translunar Inclination, i_{VTL} (deg) (= i_{VTR})

Fig. 41. Fuller Time Versus Return Inclination
(Direct Heat + Retrograde)
R_{pl} = 60 MR
h_{pl} = 185.2 (km)
i_m = 60 (deg)
Φ_{arr} = 120°
90°
80°
75°
70°
65°
52°
30°
Direct north
Direct south
Return inclination, i_{arr} (deg)
Return south
Return north
t_{arr} (hr) Transit time

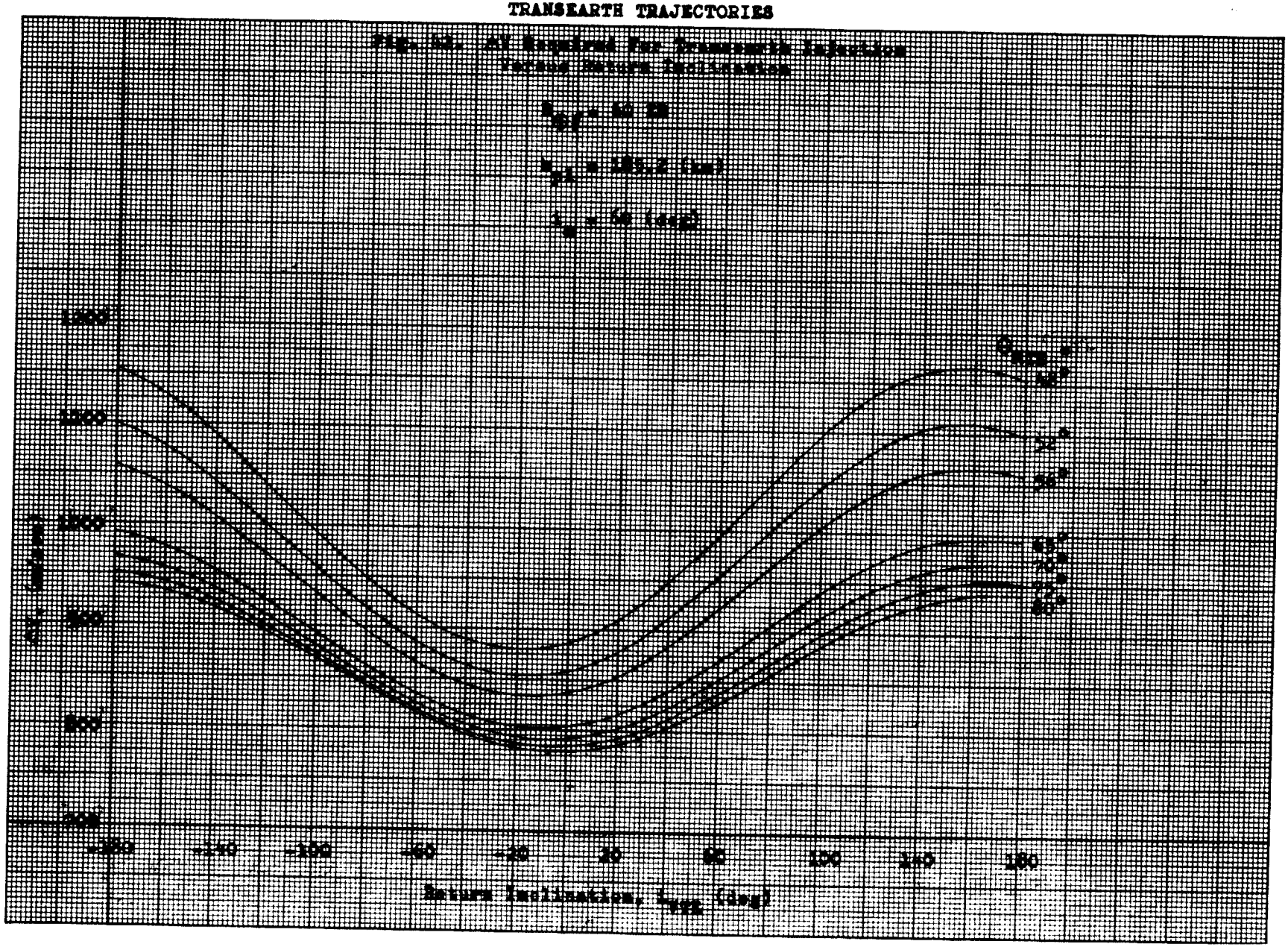

Fig. 5d. ΔV Required For Transearth Injection Versus Return Inclination

h_{pf} = 60 nm

h_{pA} = 185.2 (km)

i_M = 50 (deg)

Fig. 4.3. Transearth Injection Point Versus Return Inclination
r_{pf} = 60 n mi
h_{pf} = 185.2 (km)
γ_f = 0° (deg)
Return Inclination, i$_{RE}$ (deg)
Transearth Injection Velocity, V$_{TEI}$ (fps)

Fig. 44. Injection Velocity Versus Translunar Inclination

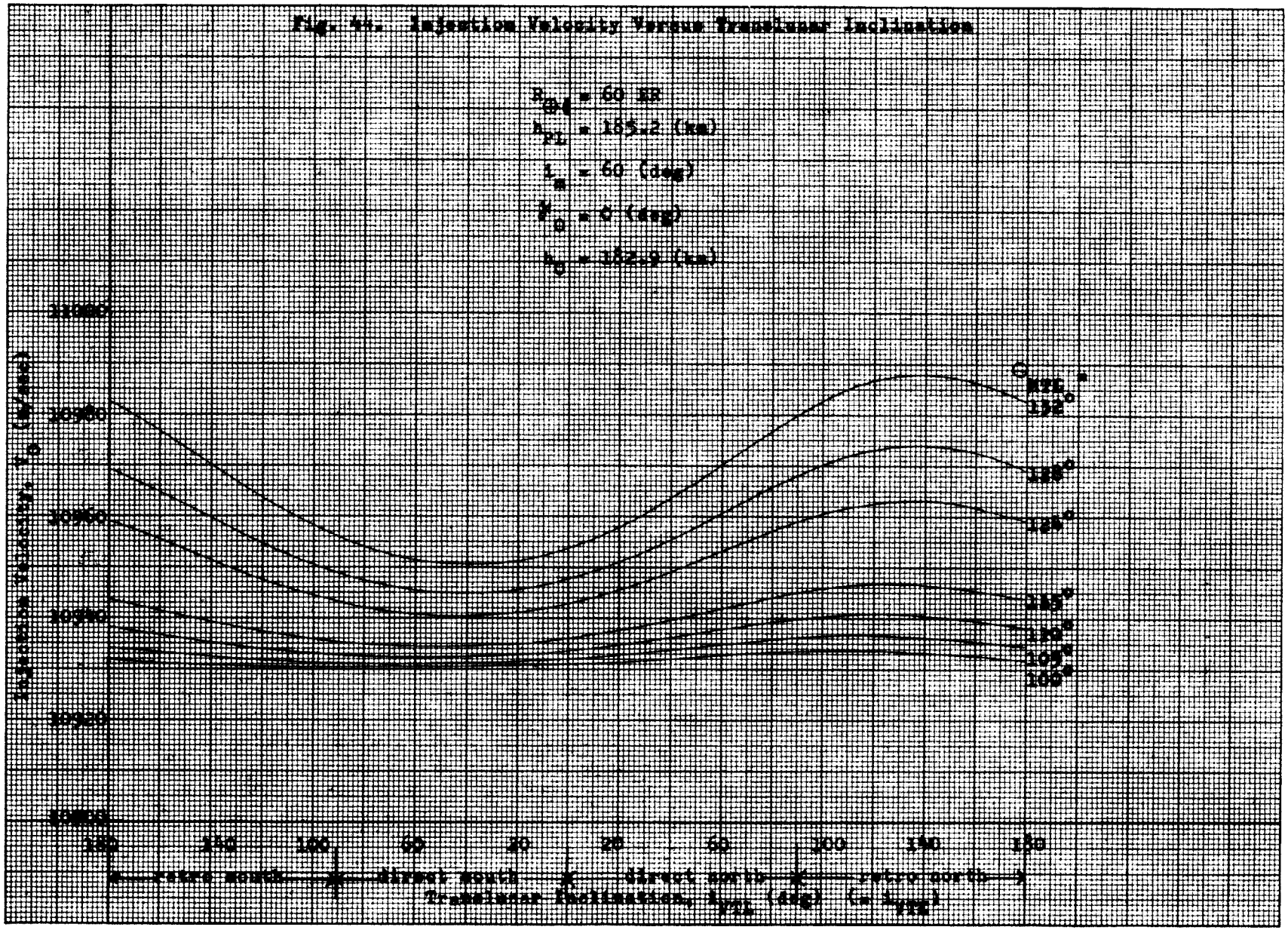

TRANSLUNAR TRAJECTORIES

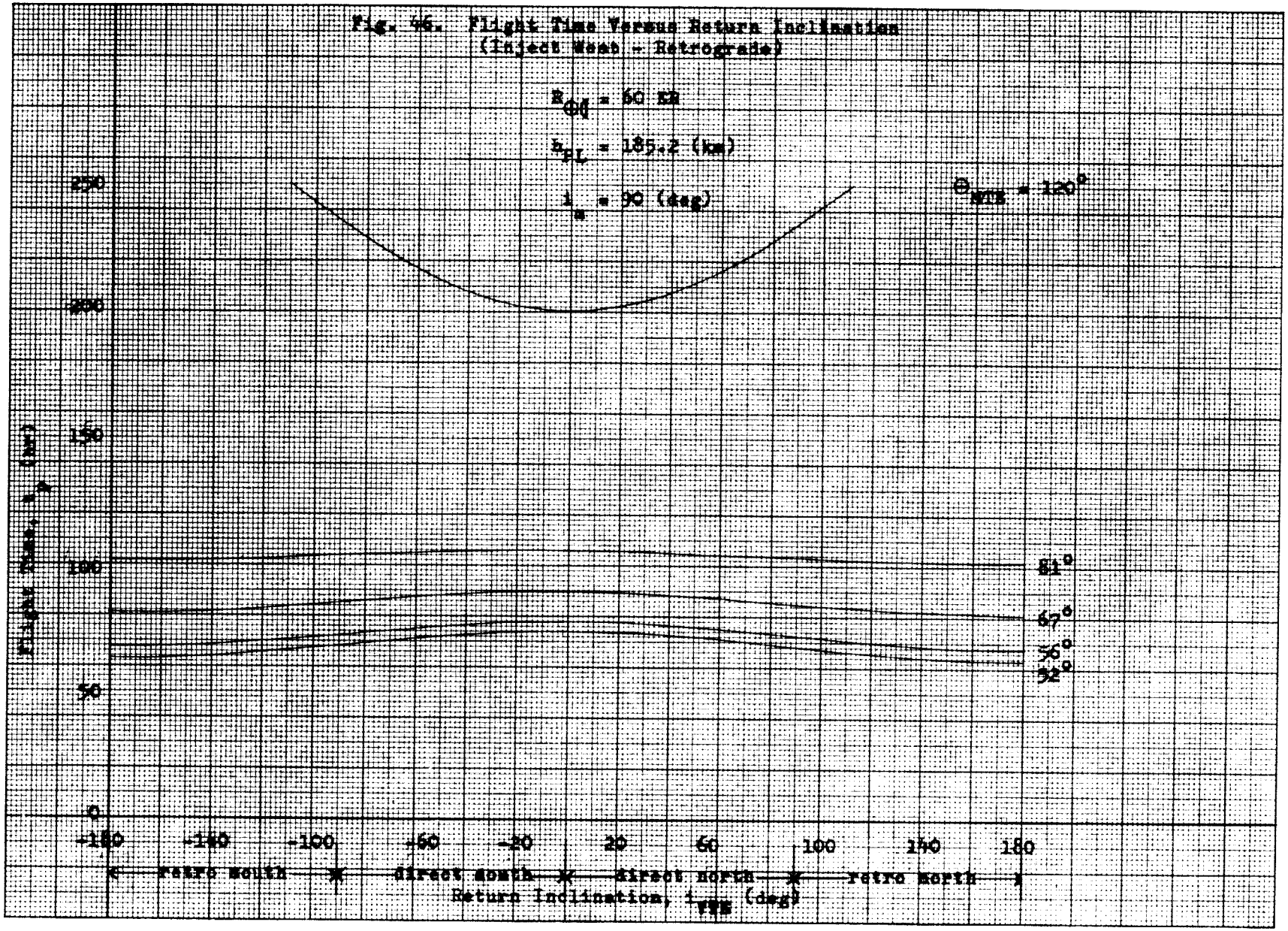

Fig. 46. Flight Time Versus Return Inclination (Inject West - Retrograde)

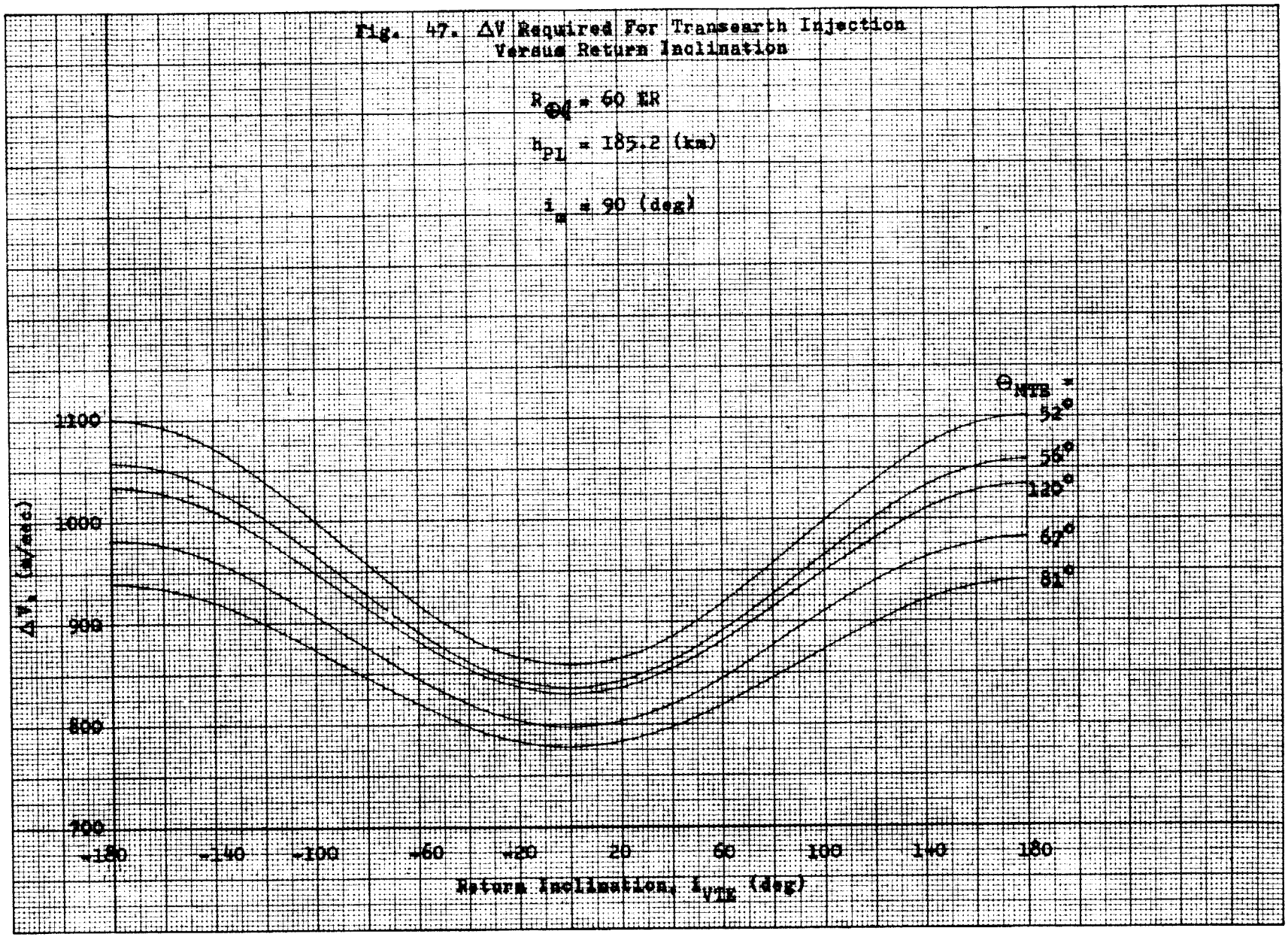

Fig. 47. ΔV Required For Transearth Injection Versus Return Inclination

Fig. 48. Transearth injection point versus return inclination

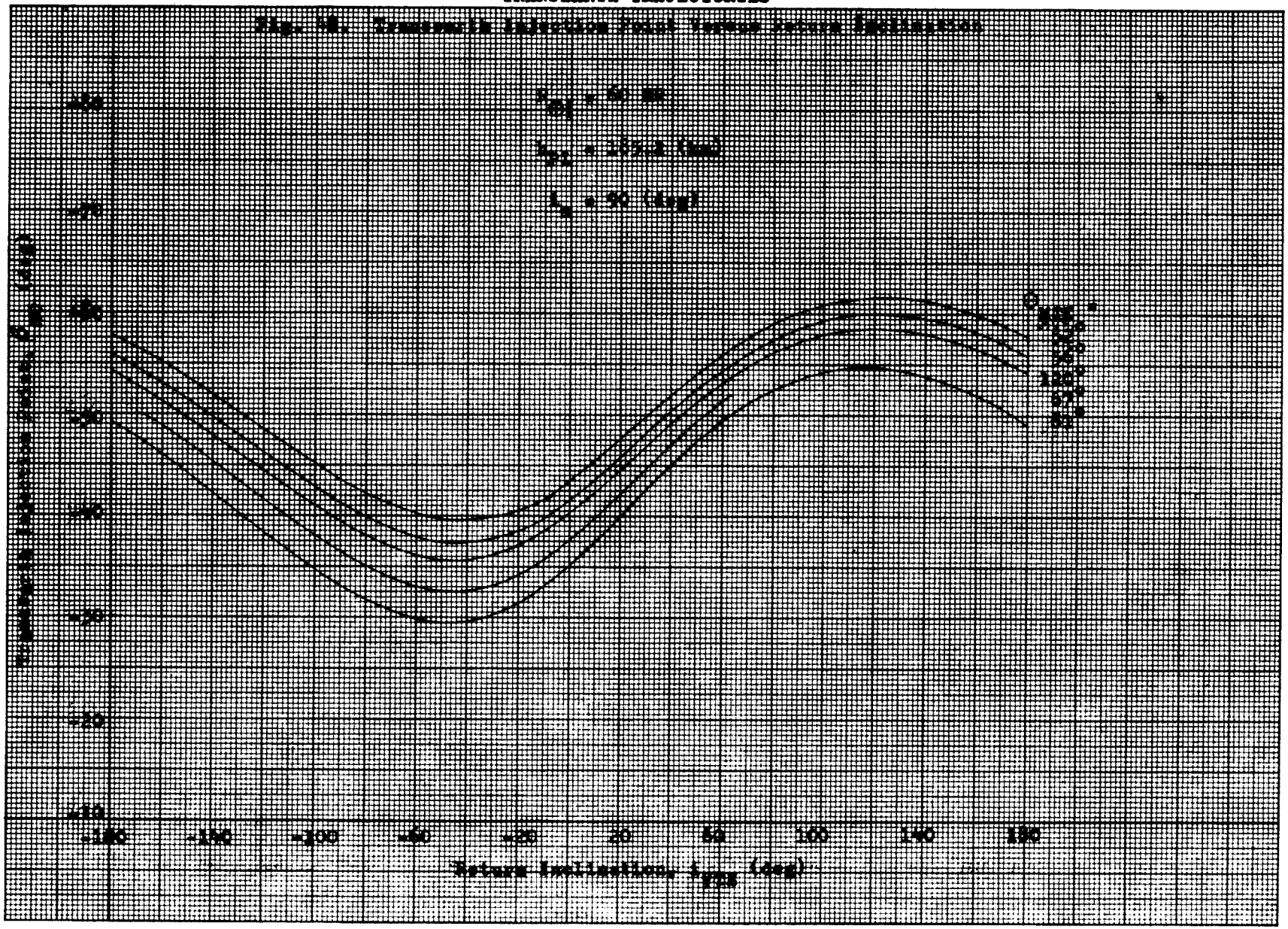

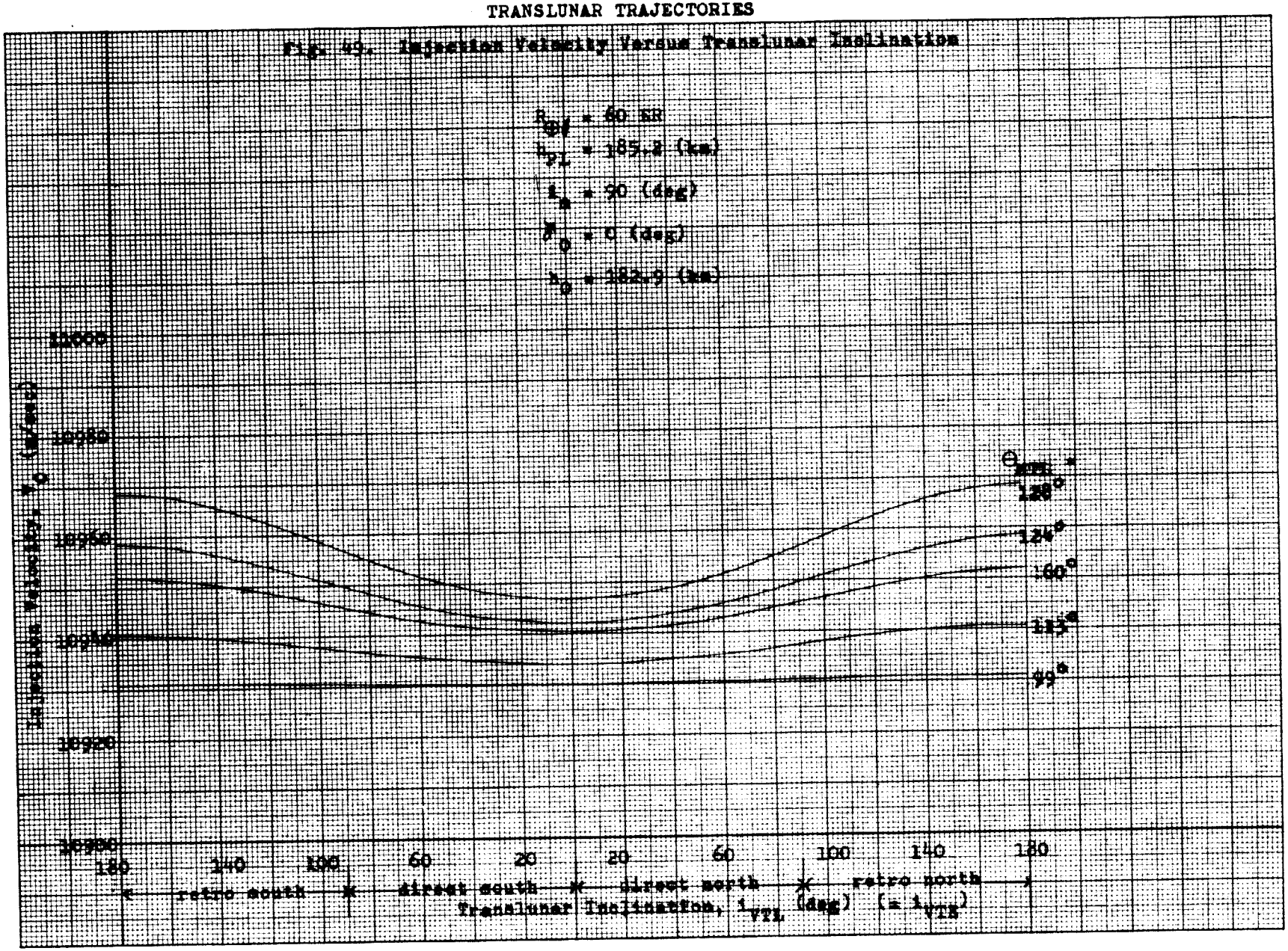

Fig. 49. Injection Velocity Versus Translunar Inclination

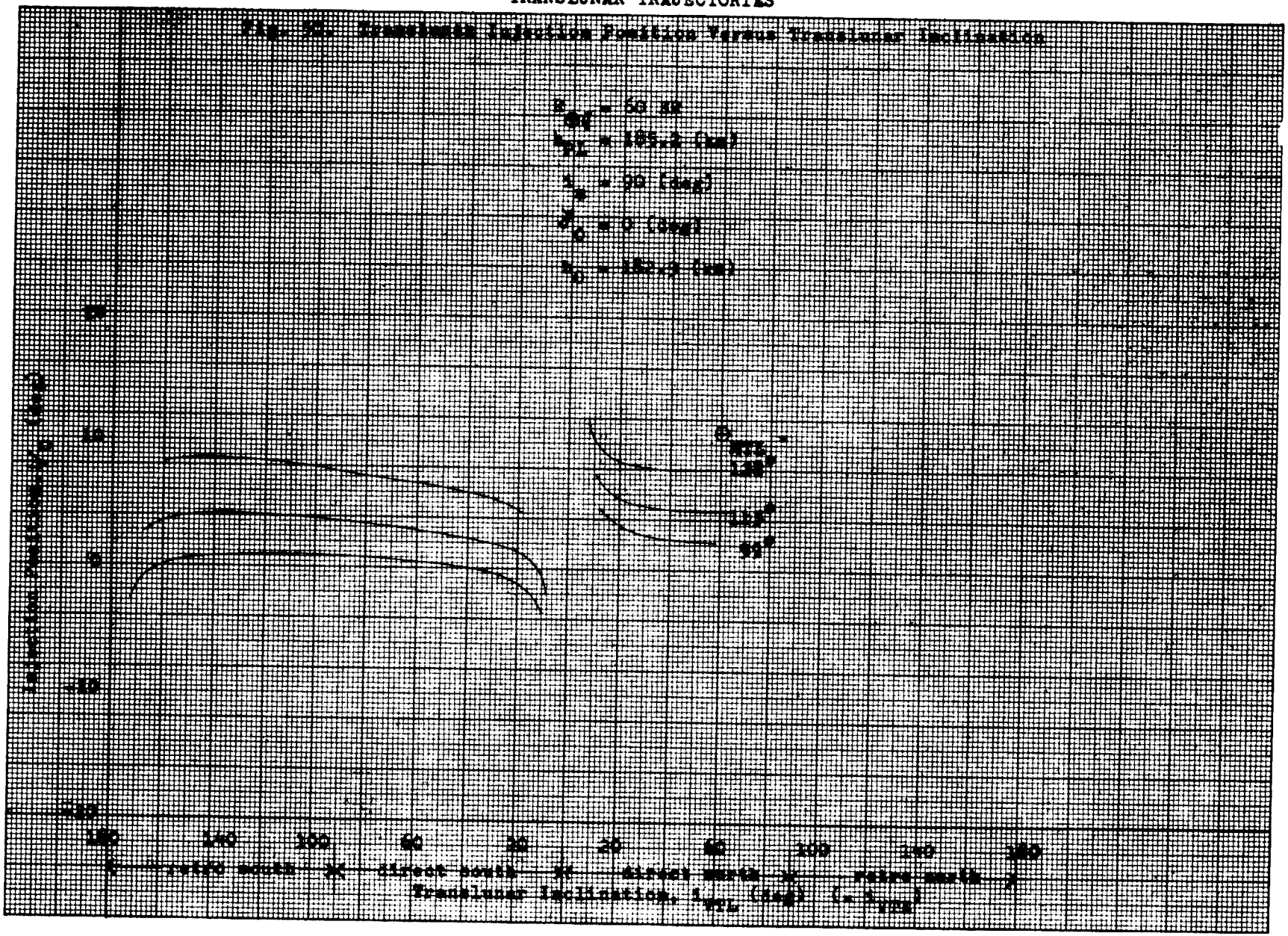
Fig. 20. Translunar Injection Position Versus Translunar Inclination
E_{GK} = 50 ER
h_{PL} = 185.2 (km)
λ_0 = 90 (deg)
γ_0 = 0 (deg)
s_0 = 152.9 (sec)
Translunar Inclination, i_{TL} (deg)
retro south
direct south
direct north
retro north

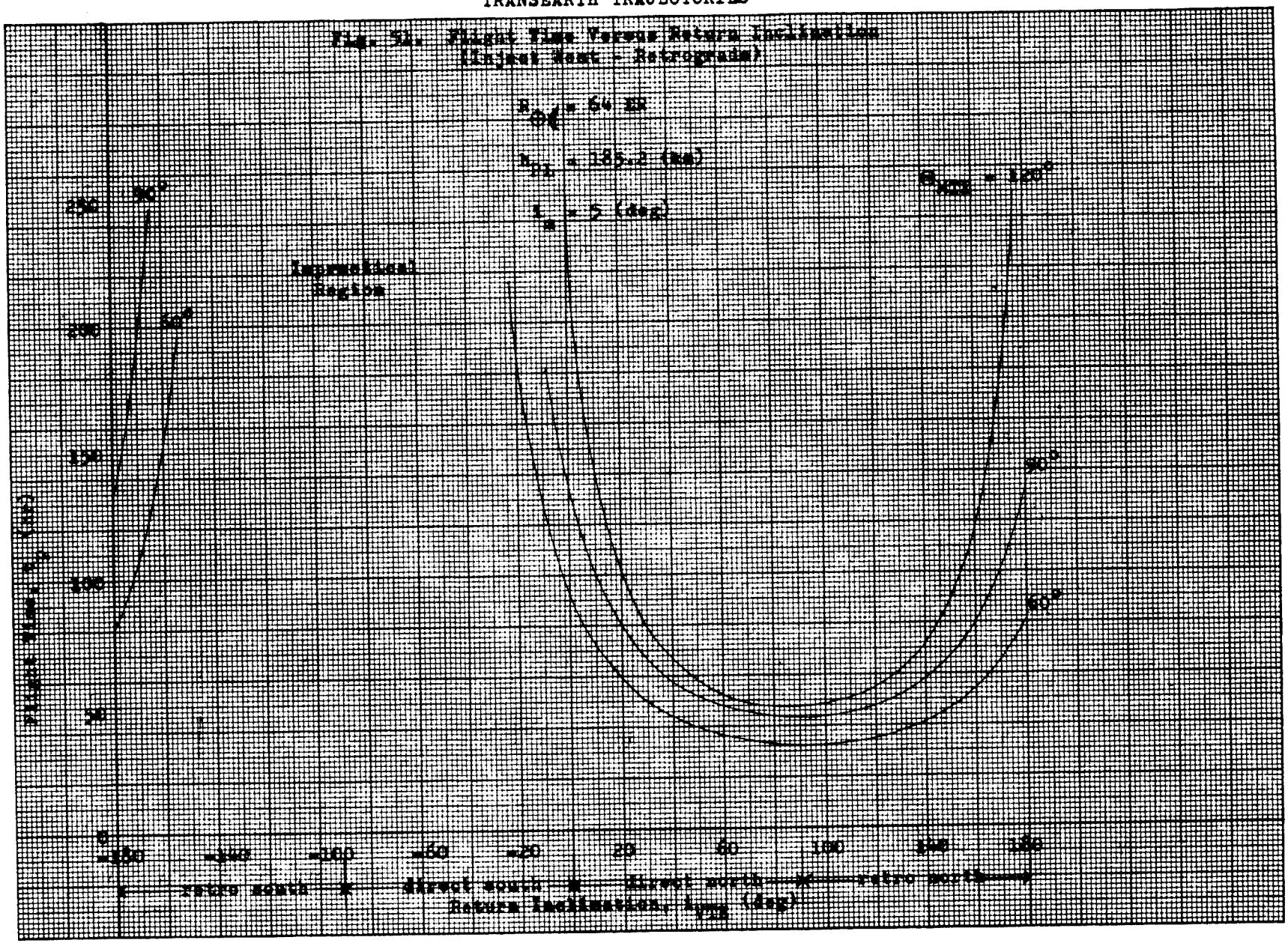
Fig. 51. Flight Time Versus Return Inclination
(Injection Node - Retrograde)
$R_{\oplus C}$ = 64 ER
h_{pc} = 185.2 (km)
i_s = 5 (deg)
θ_{max} = 120°
Impractical Region
90°
60°
Flight Time, T_{FT} (hr)
Return Inclination, i_{RE} (deg)
retro south
direct south
direct north
retro north

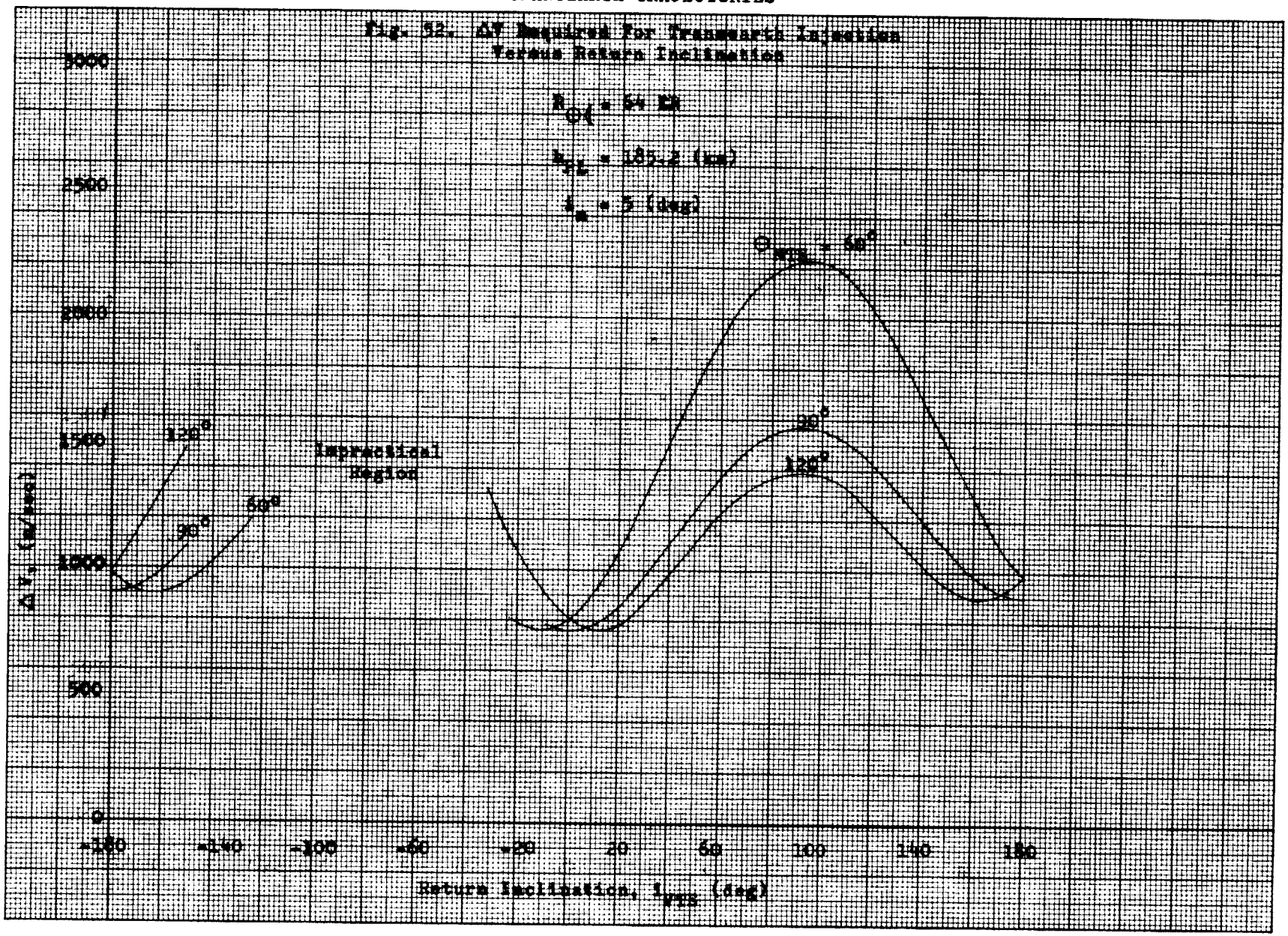
Fig. 32. ΔV Required For Transearth Injection
Versus Return Inclination
$R_{0(} = 54$ ER
$R_{PL} = 185.2$ (km)
$\lambda_m = 5$ (deg)
$\Theta_{arr} = 60°$
120°
90°
60°
30°
Impractical Region
3000
2500
2000
1500
1000
500
0
-180
-140
-100
-60
-20
20
60
100
140
180
ΔV, (fps)
Return Inclination, i_{rtn} (deg)

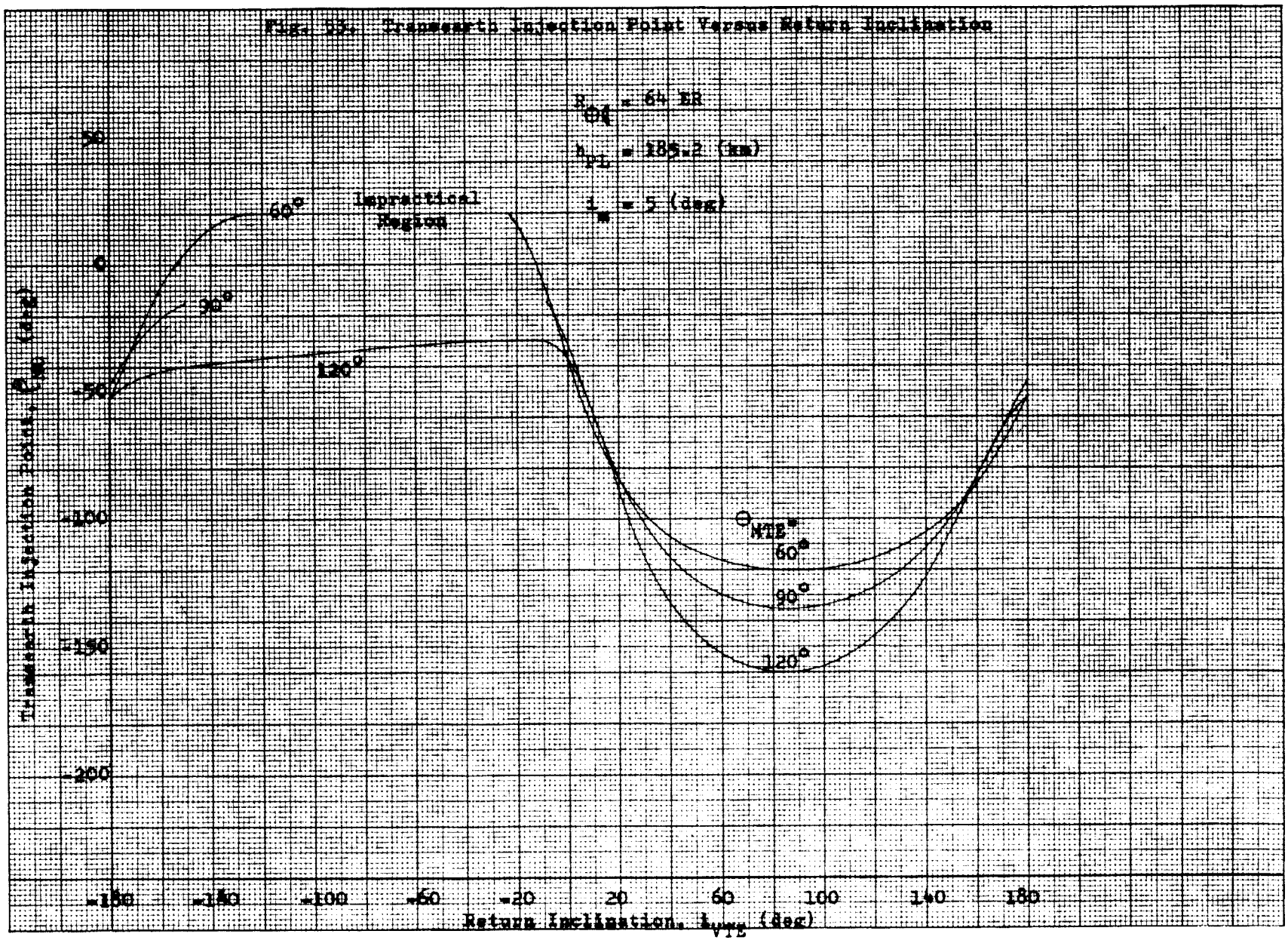

Fig. 33. Transearth Injection Point Versus Return Inclination

Fig. 54. Injection Velocity Versus Translunar Inclination

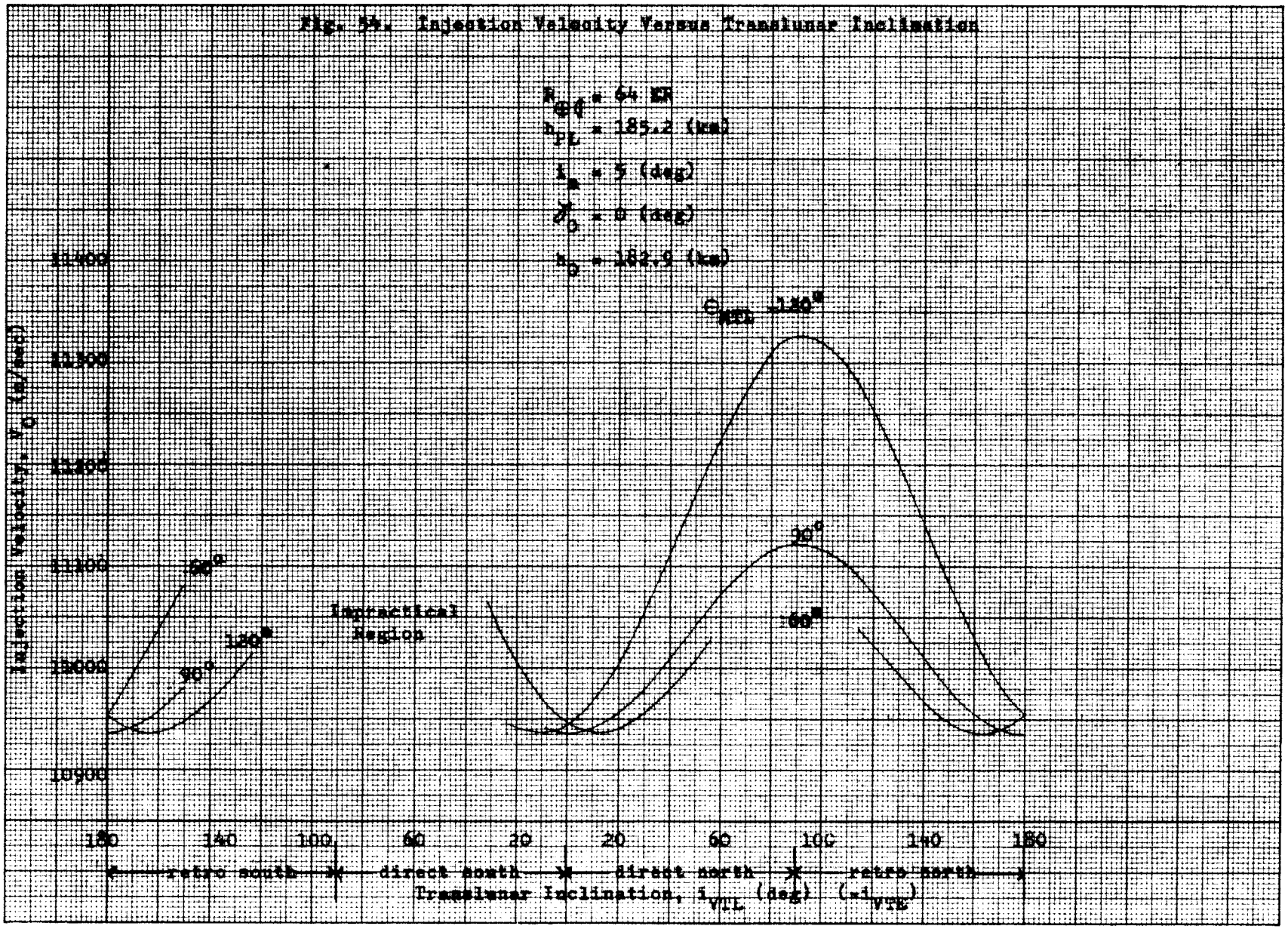

Fig. 55. Translunar Injection Position Versus Translunar Inclination

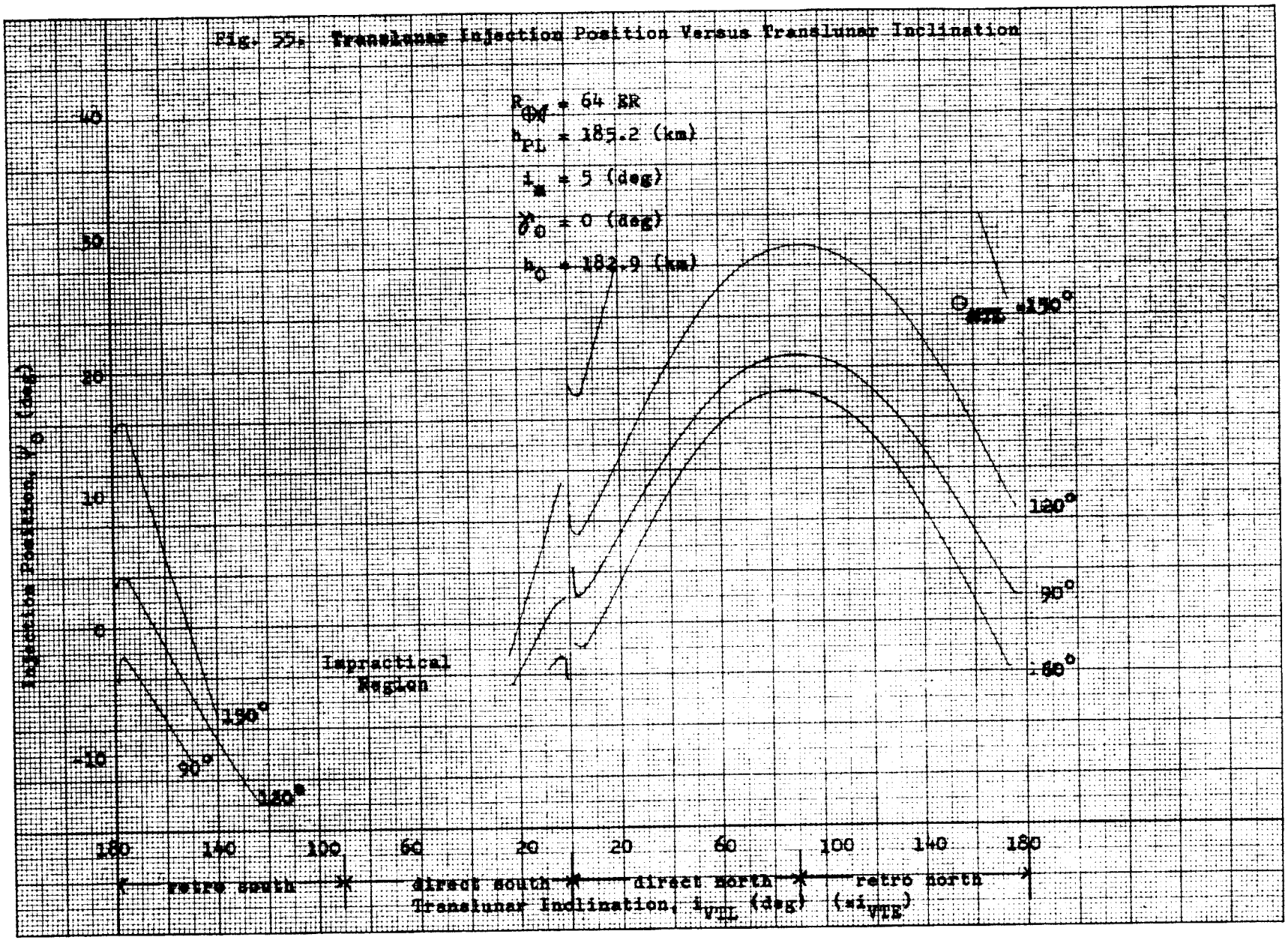

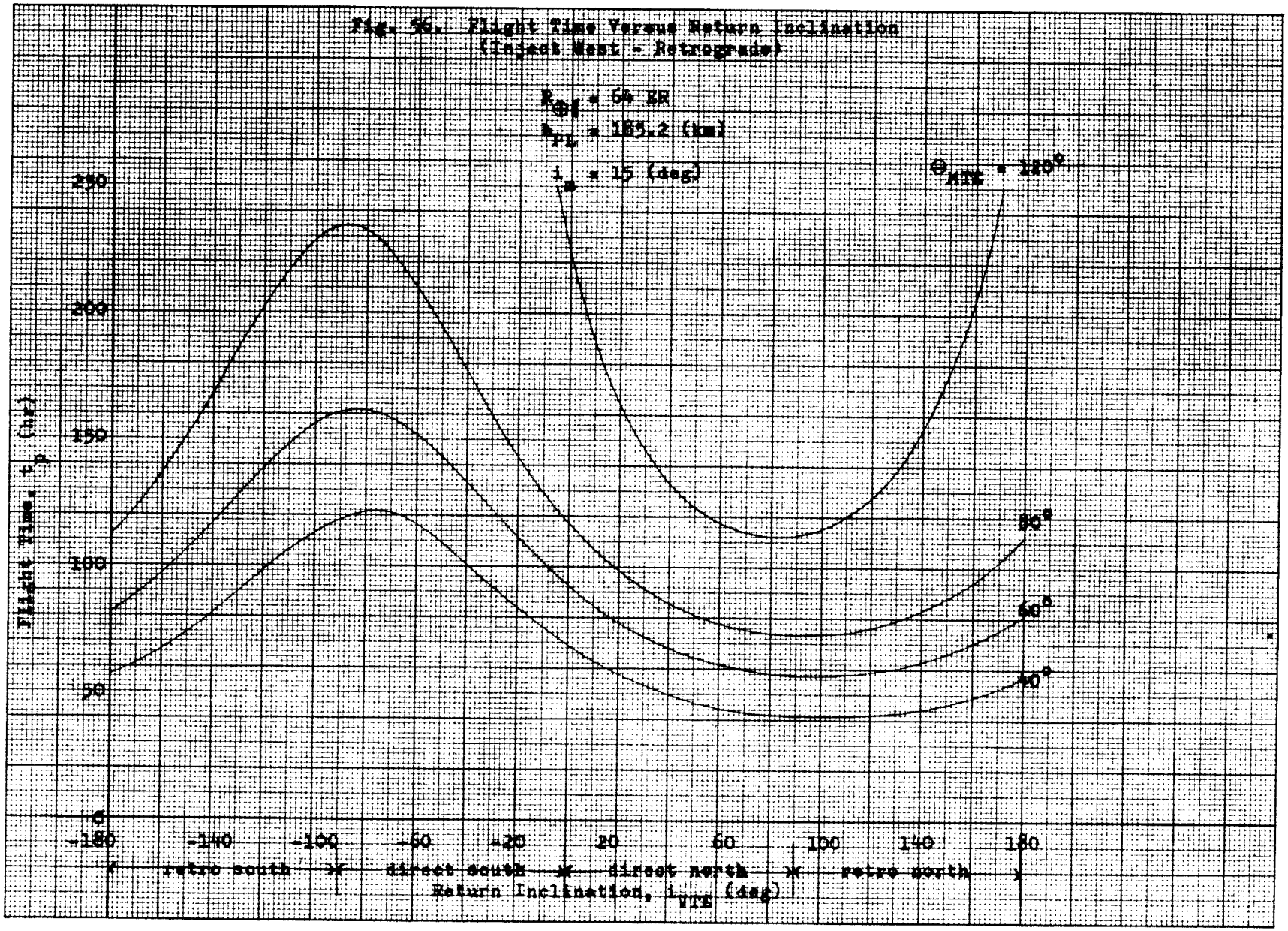

Fig. 56. Flight Time Versus Return Inclination (Inject West - Retrograde)

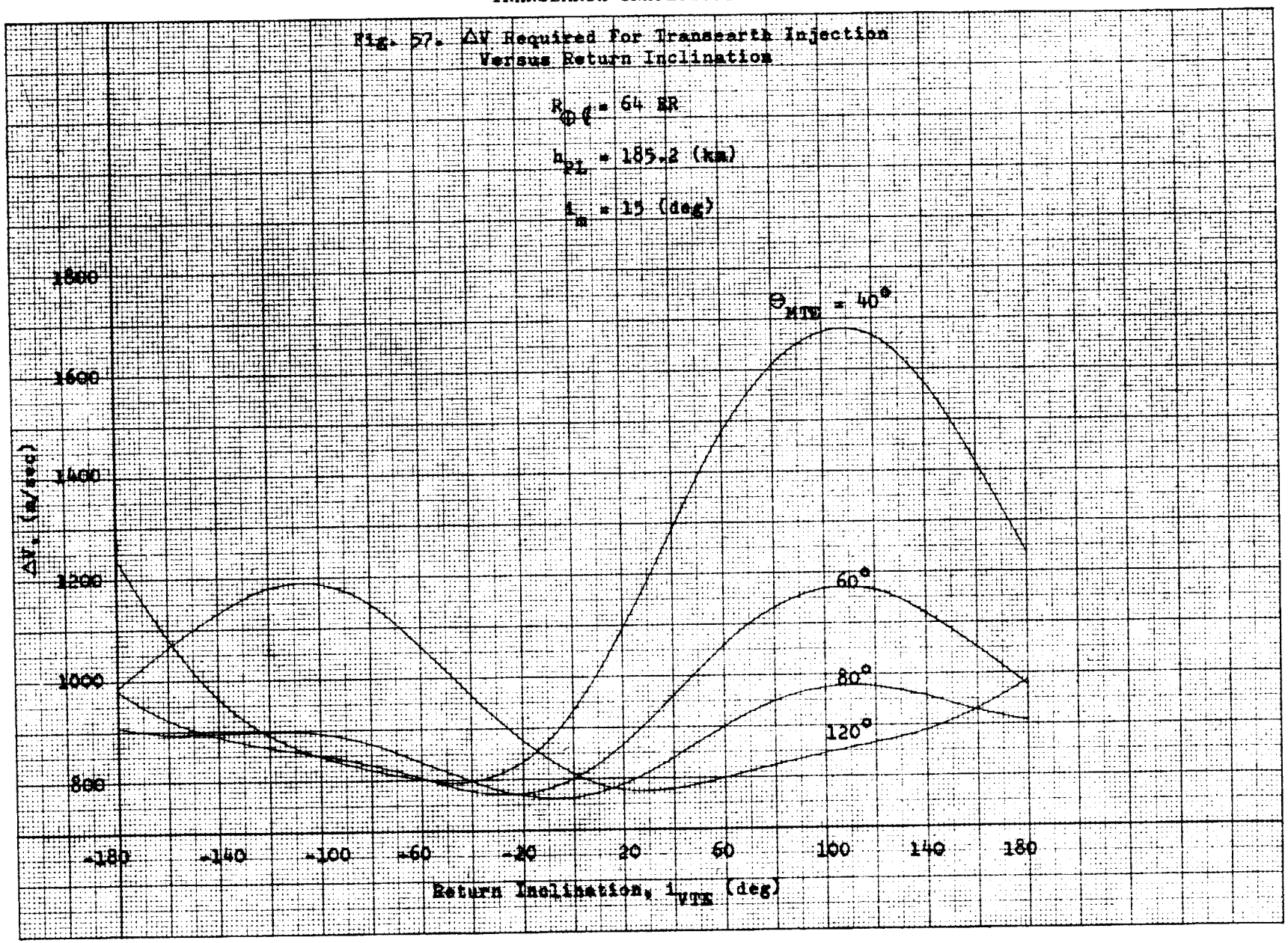

Fig. 57. ΔV Required For Transearth Injection Versus Return Inclination

Fig. 58. Transearth Injection Point Versus Return Inclination

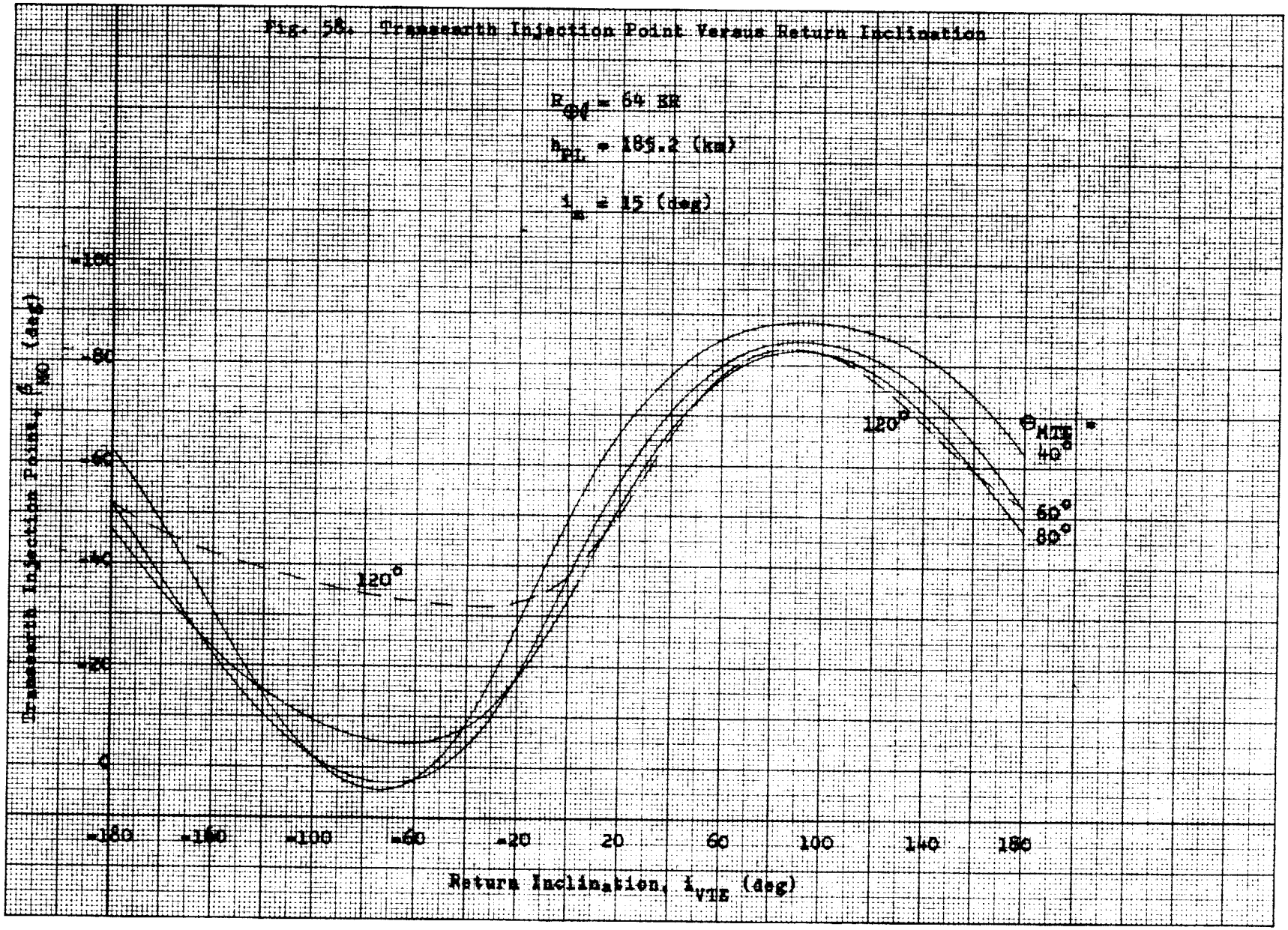

TRANSLUNAR TRAJECTORIES

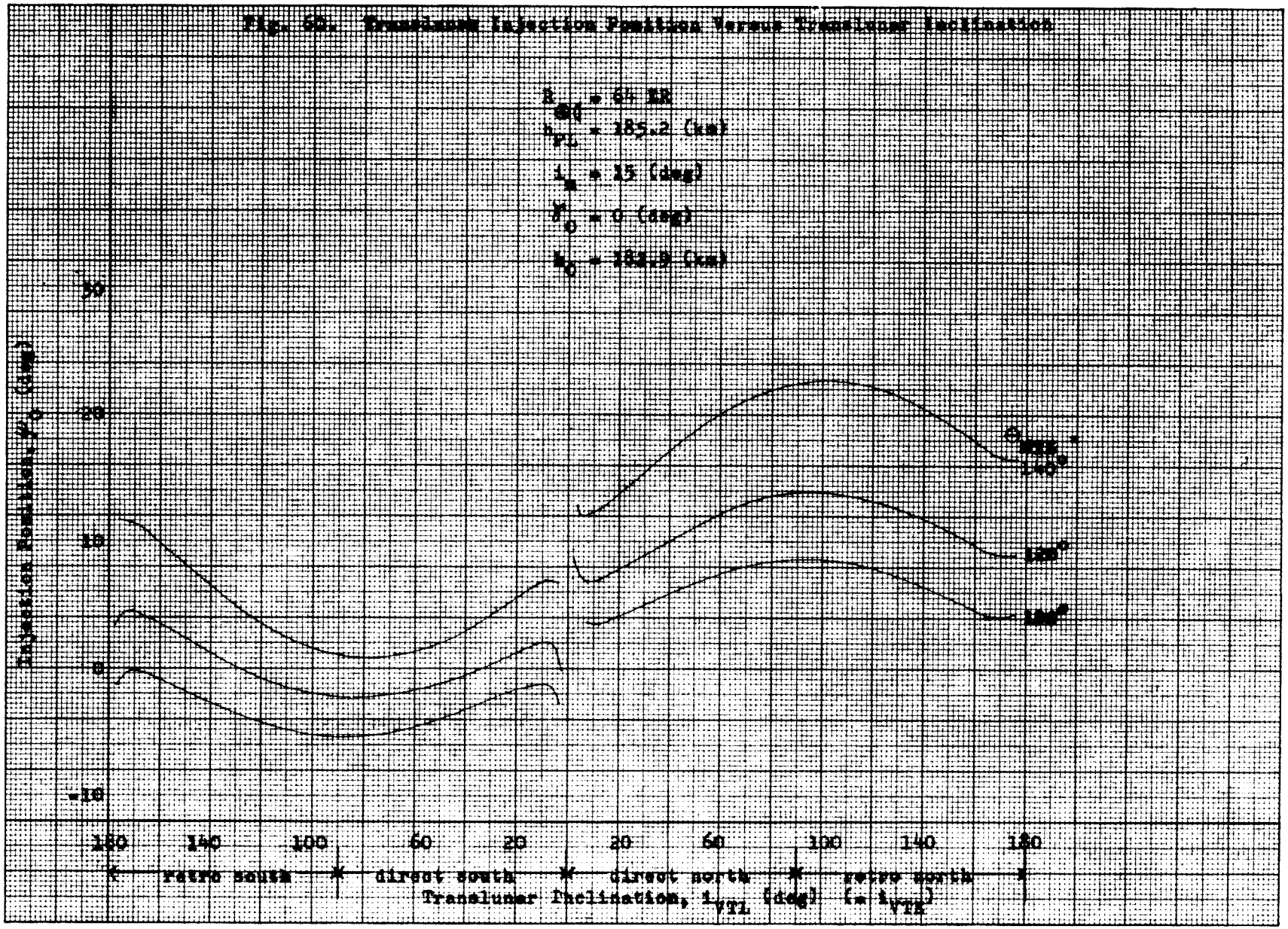
R_{SOI} = 64 ER
h_{PL} = 185.2 (km)
i_M = 15 (deg)
γ_0 = 0 (deg)
h_0 = 184.9 (km)
50
30
10
-10
Injection Position, γ_0 (deg)
180
140
100
60
20
20
60
100
140
180
retro south
direct south
direct north
retro north
Translunar Inclination, i_{VTL} [deg] (= i_{VTE})

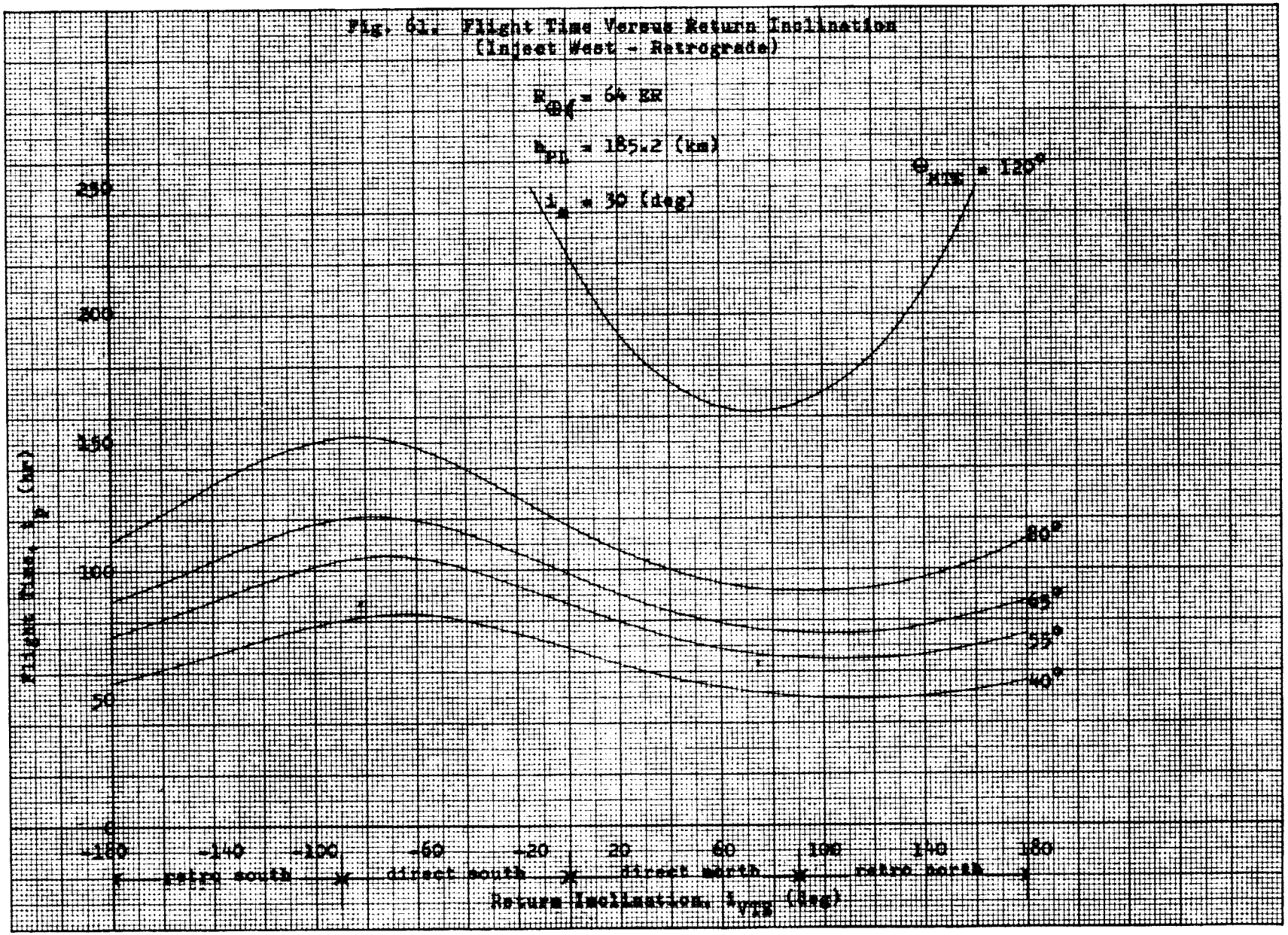

Fig. 61. Flight Time Versus Return Inclination (Inject West → Retrograde)

R_{EOI} = 64 ER

h_{PL} = 185.2 (km)

i_A = 30 (deg)

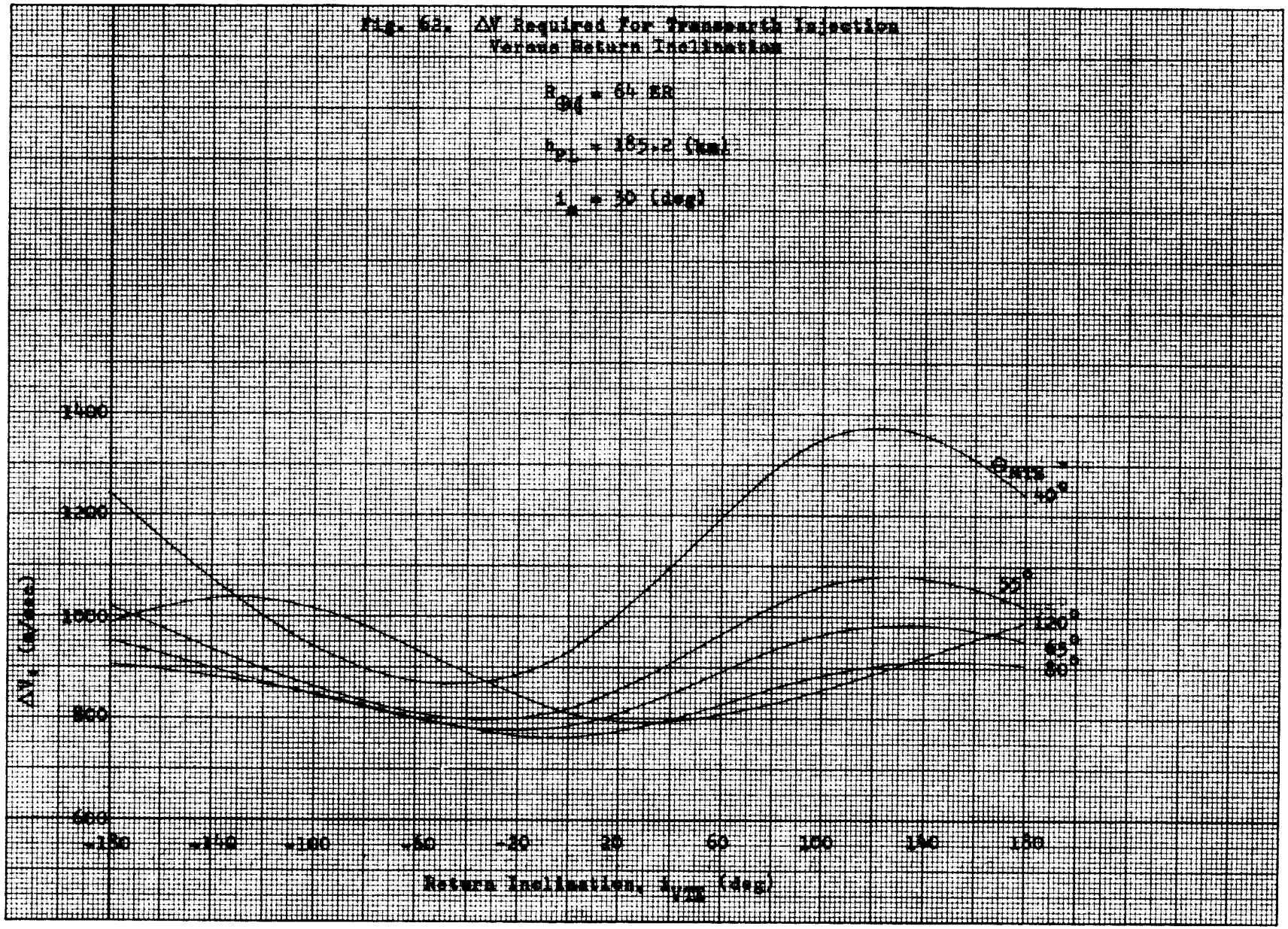

Fig. 62. ΔV Required for Transearth Injection Versus Return Inclination

Fig. 63. Transearth Injection Point Versus Return Inclination

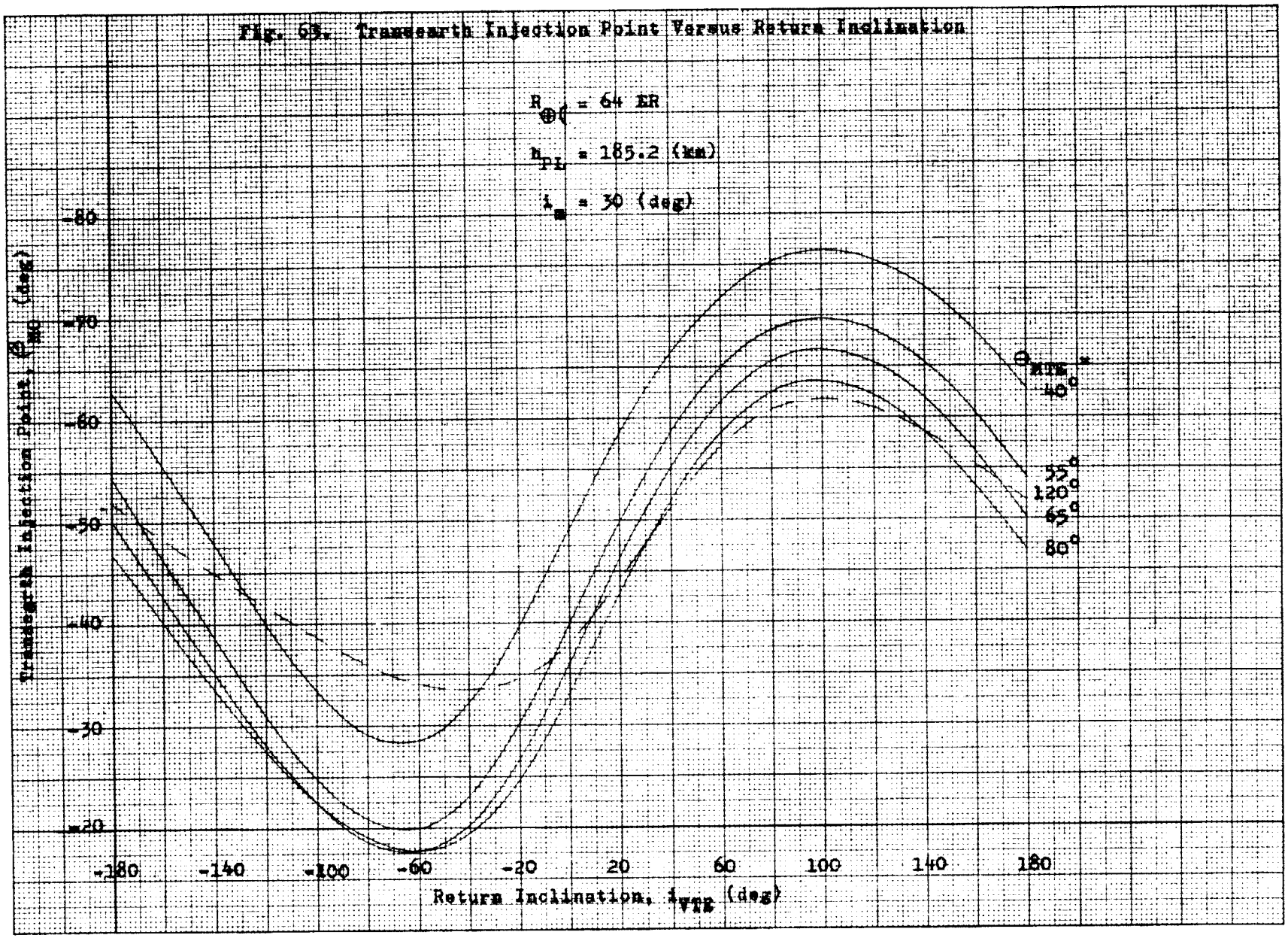

Fig. 64. Injection Velocity Versus Translunar Inclination

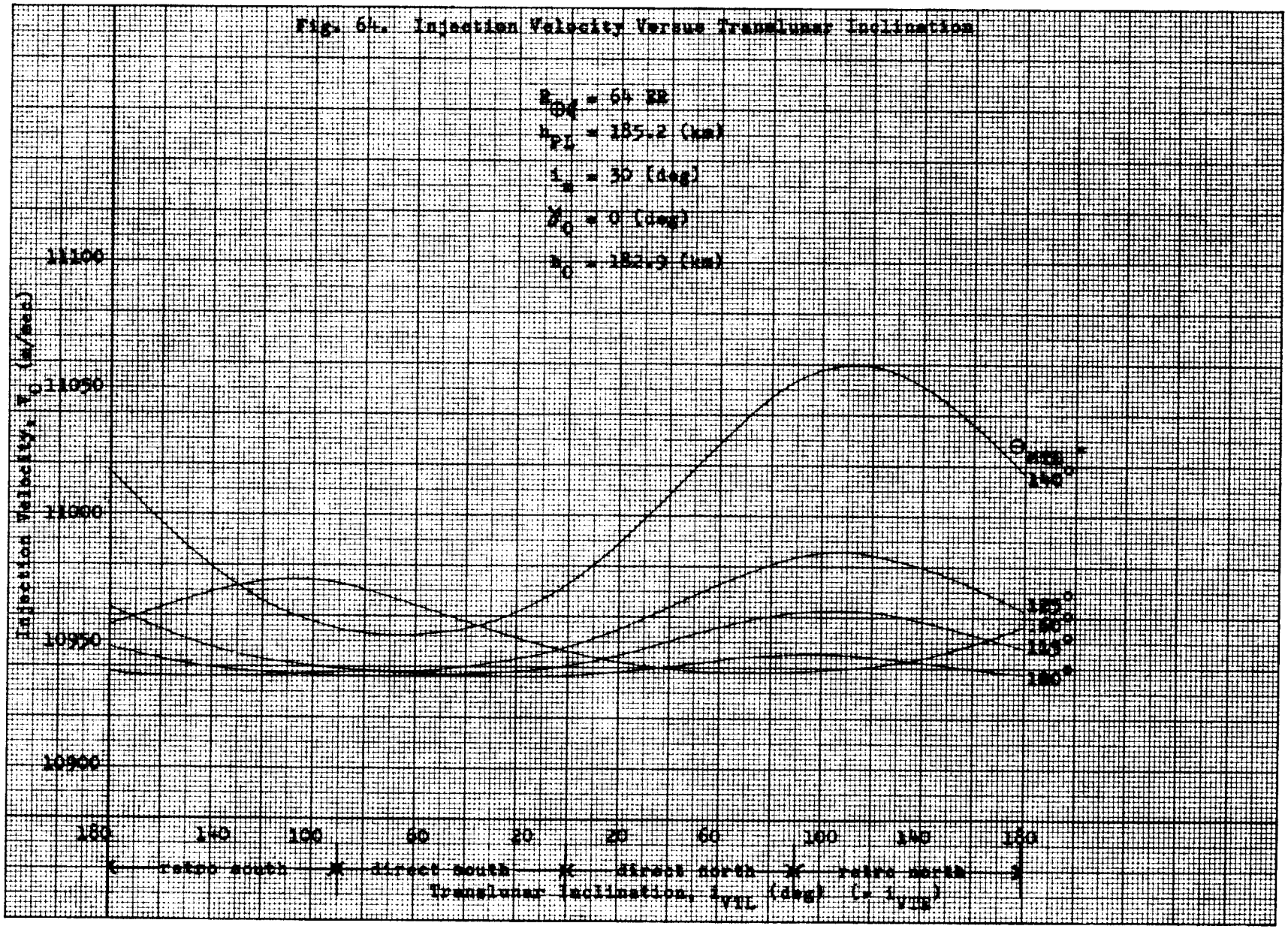

Fig. 65. Translunar Injection Position Versus Translunar Inclination

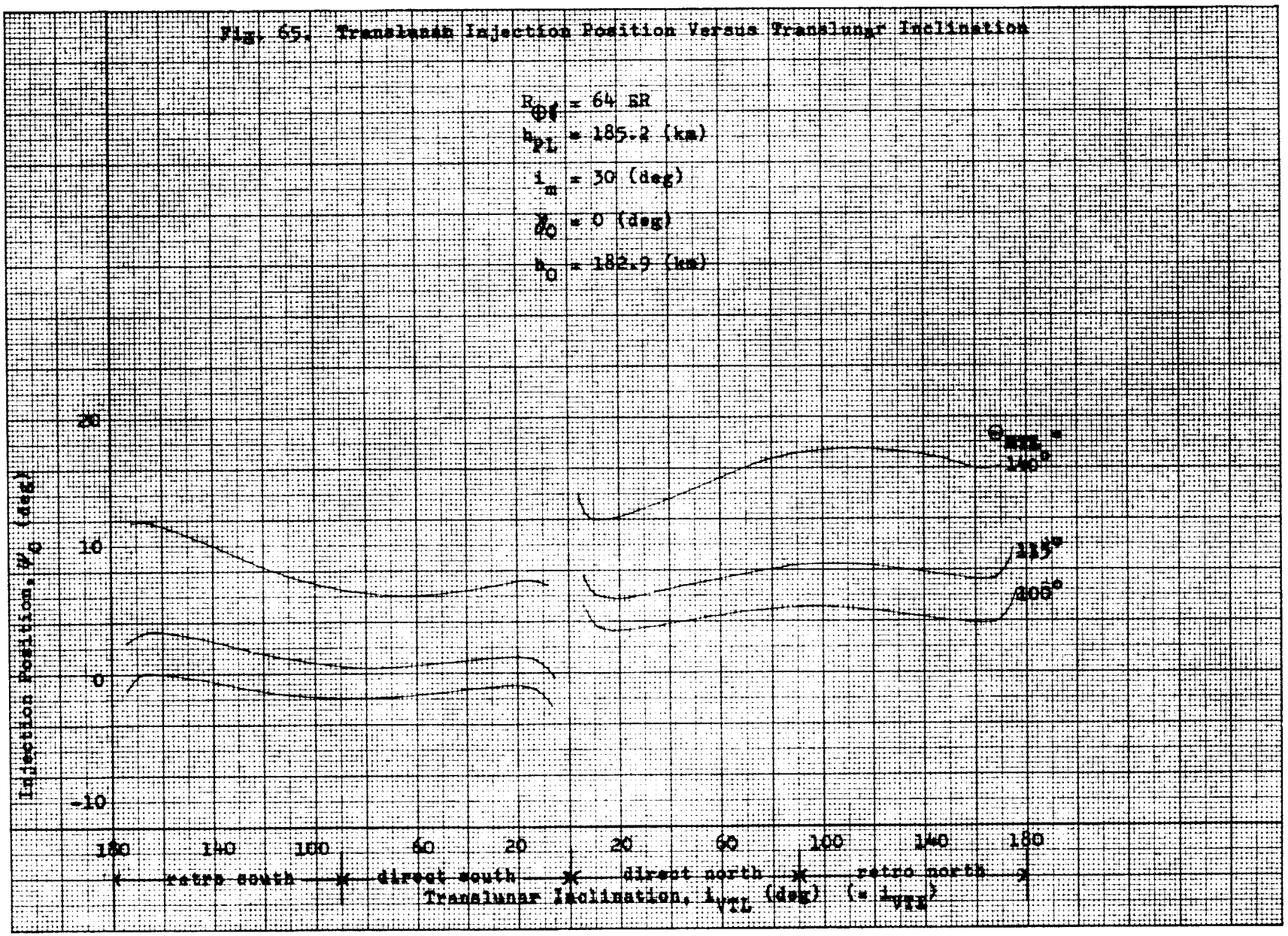

Fig. 66. Flight Time Versus Return Inclination
(Inject West = Retrograde)

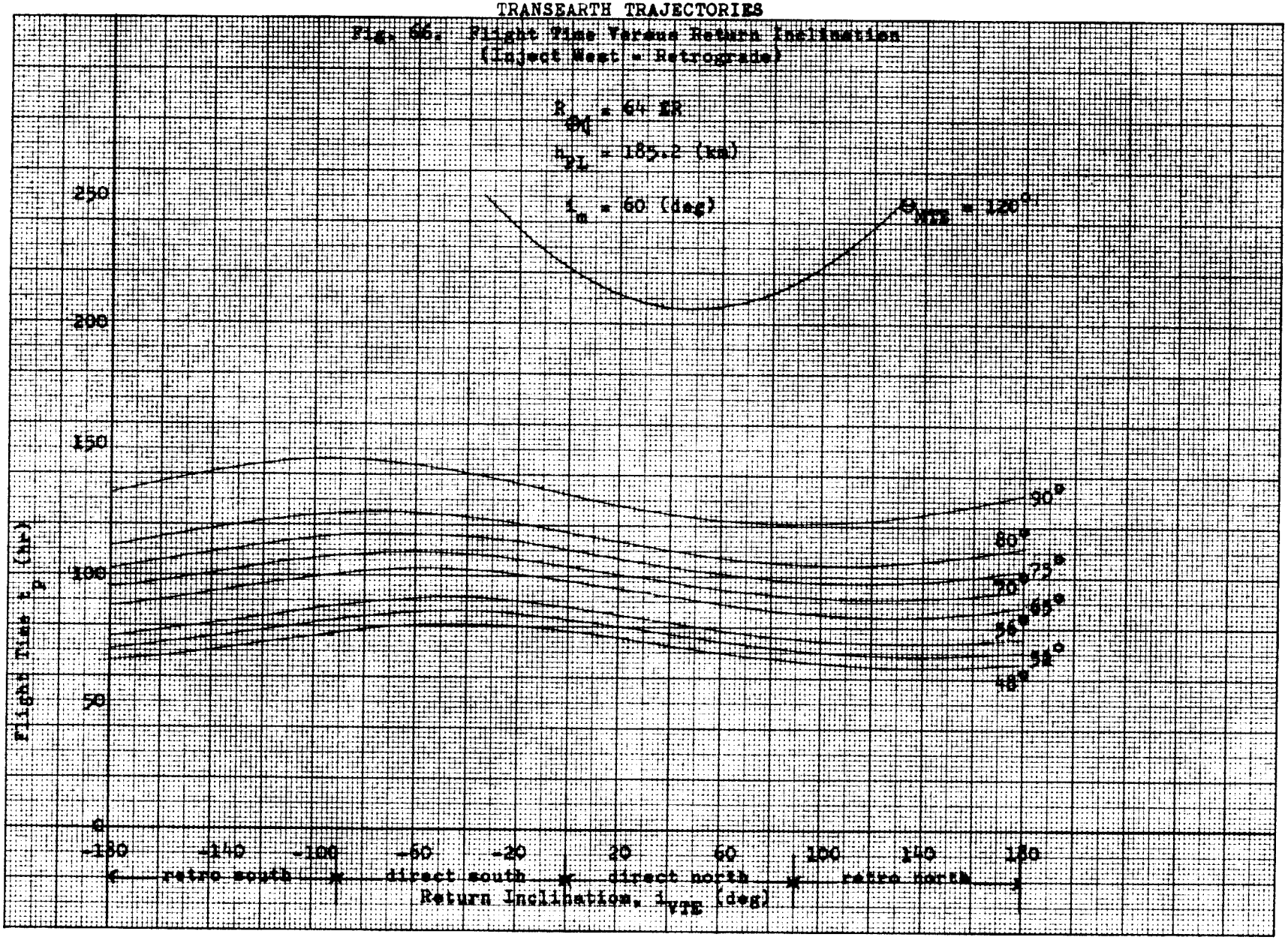

Fig. 67. ΔV Required For Transearth Injection Versus Return Inclination

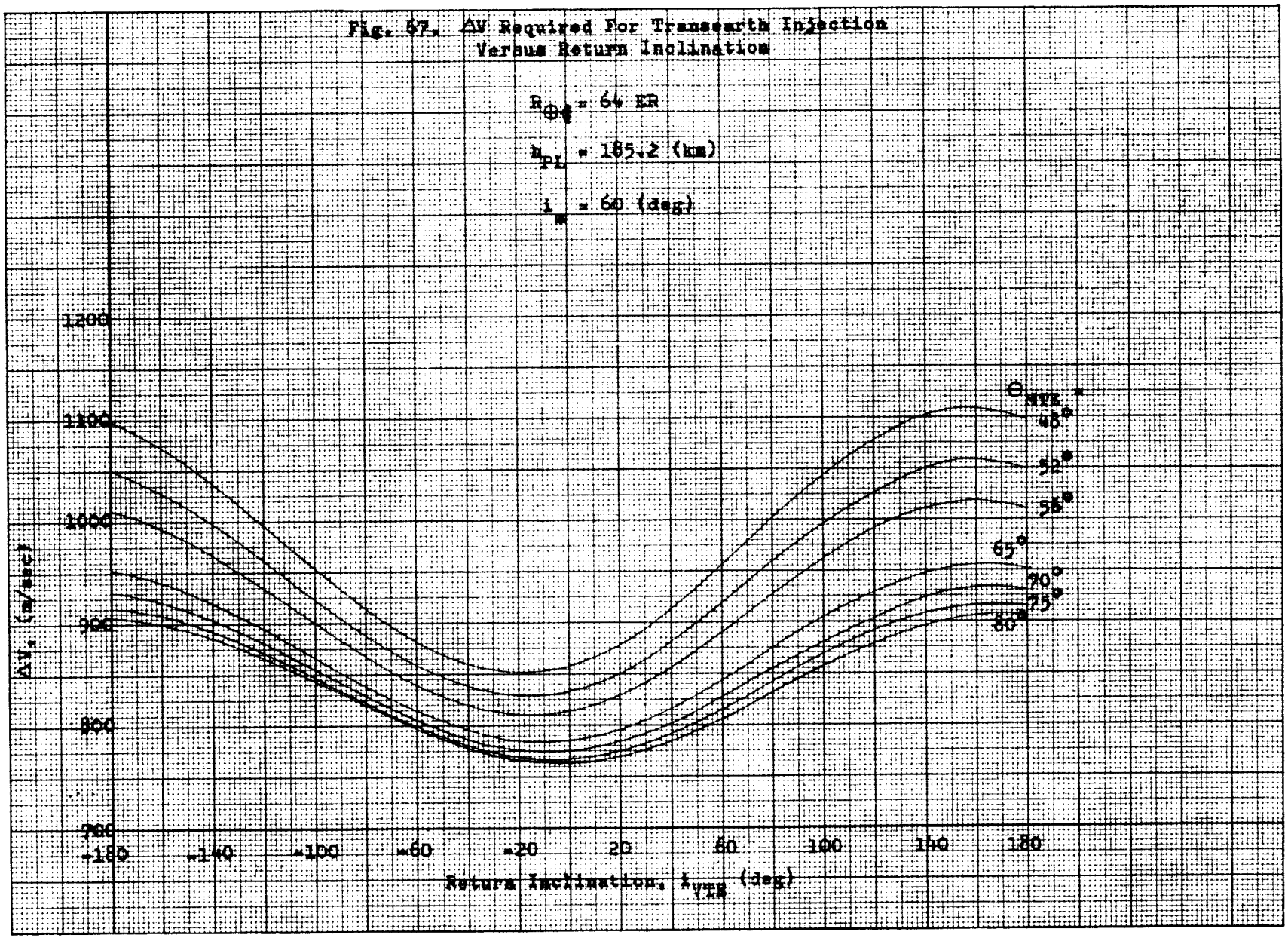

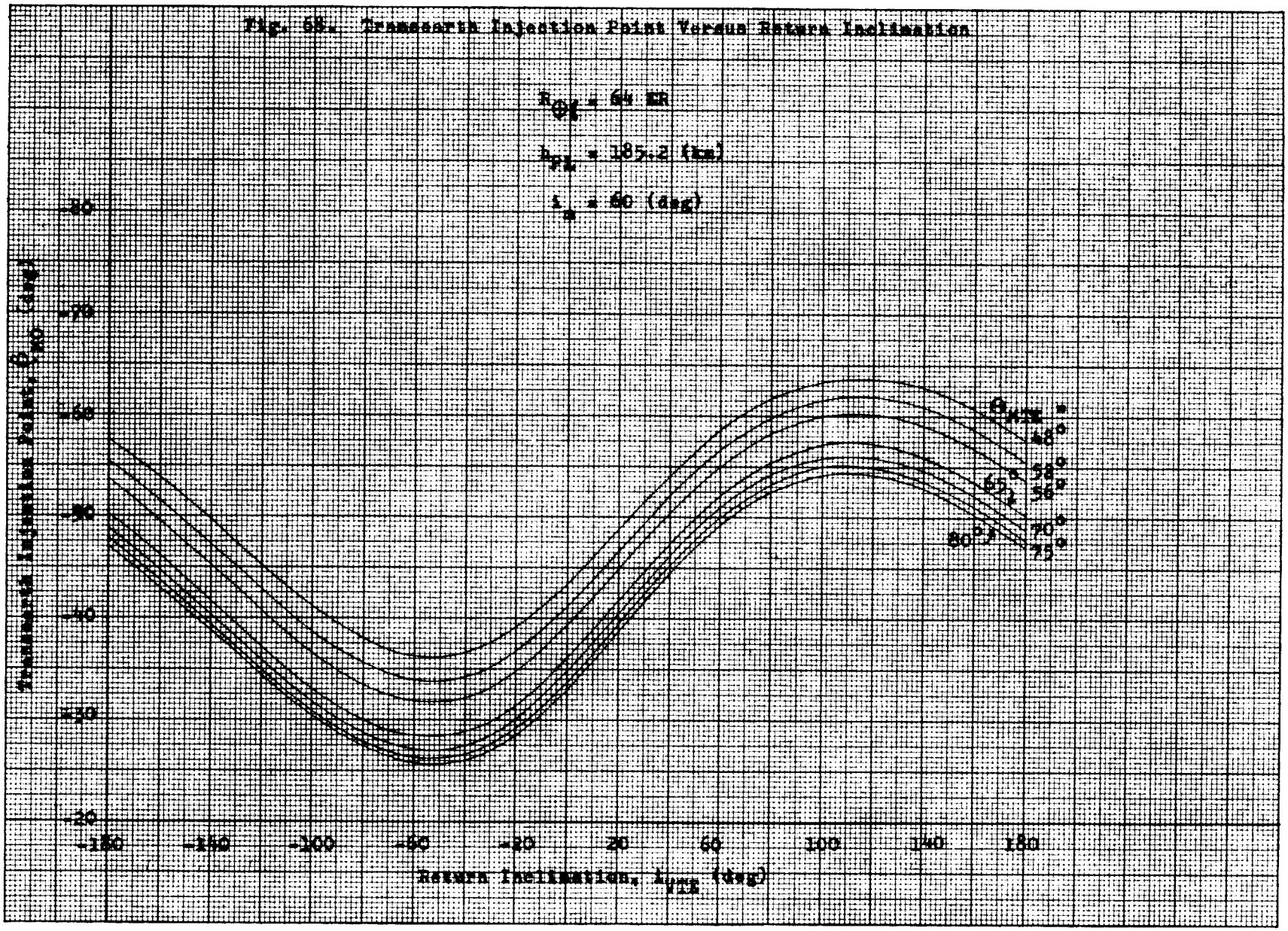

Fig. 68. Transearth Injection Point Versus Return Inclination

Fig. 69. Injection Velocity Versus Translunar Inclination
R⊕ = 64 ER
RM = 185.2 (km)
i = 60 (deg)
φ0 = 0 (deg)
h0 = 182.9 (km)
Injection Velocity, V0 (ft/sec)
Translunar Inclination, i (deg)
direct
retro
direct
retro
Ωmoon
135°
180°
225°
315°

Fig. 70. Translunar Injection Position Versus Translunar Inclination

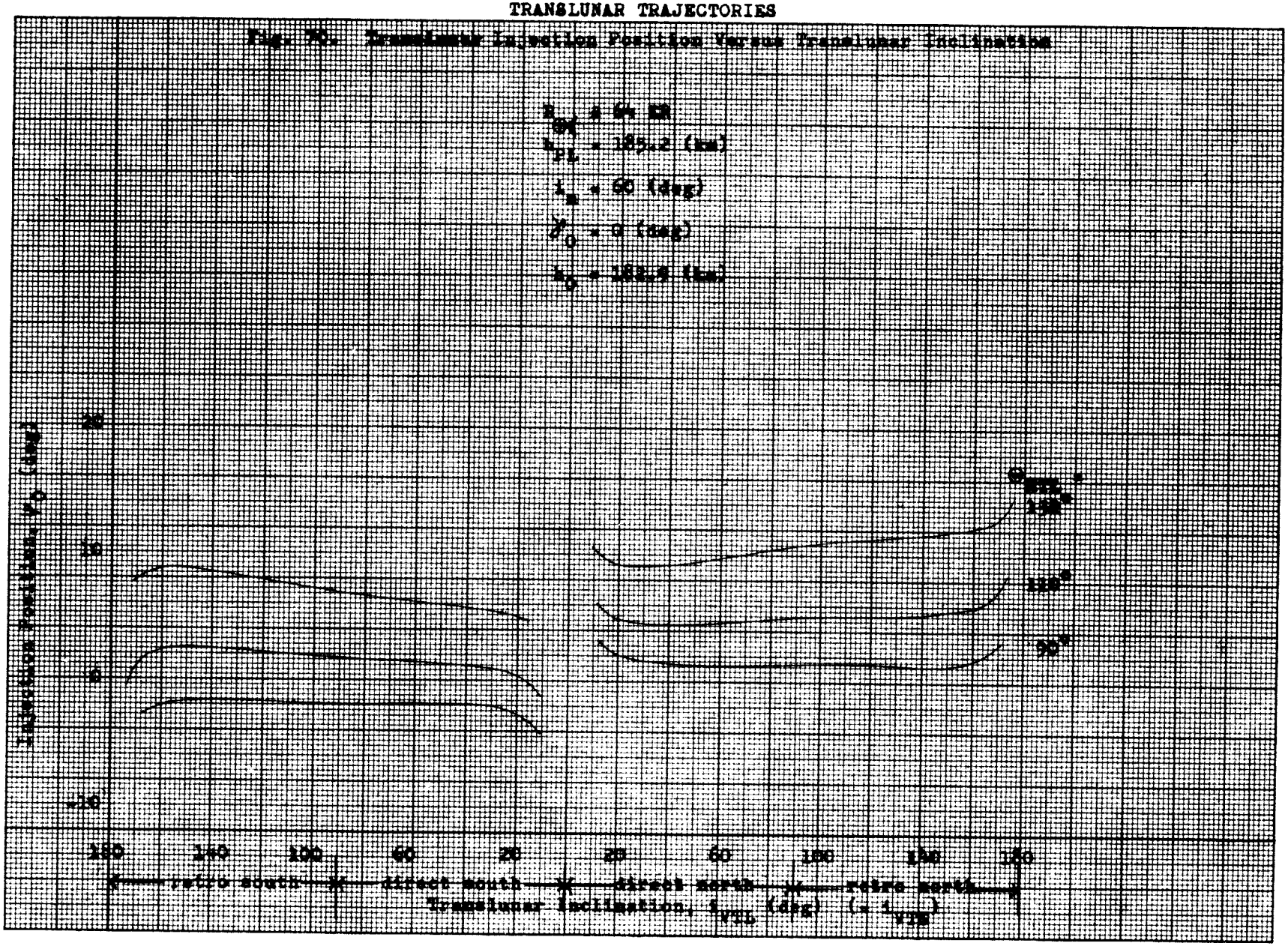

Fig. 71. Flight Time Versus Return Inclination
(Inject West - Retrograde)

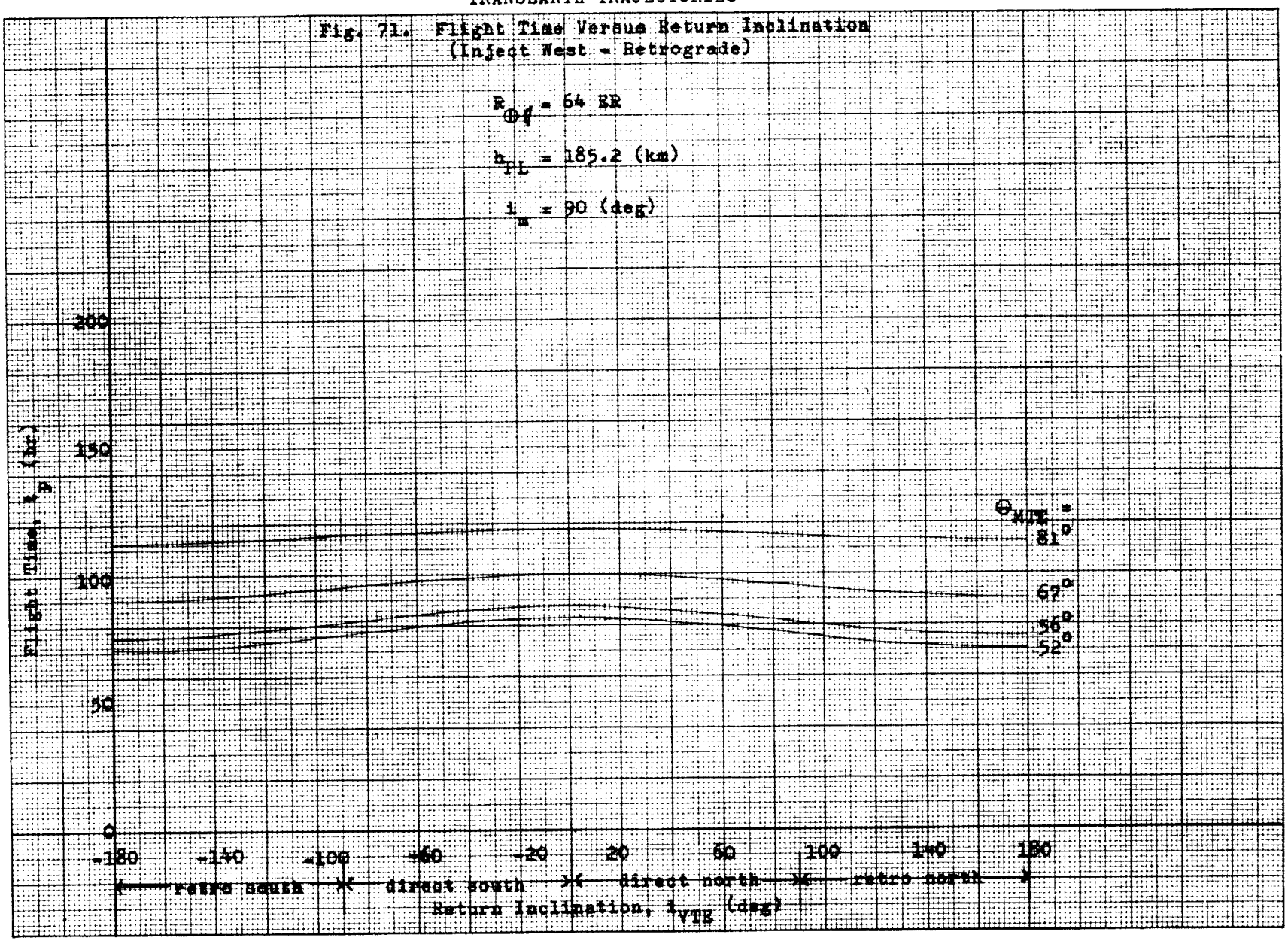

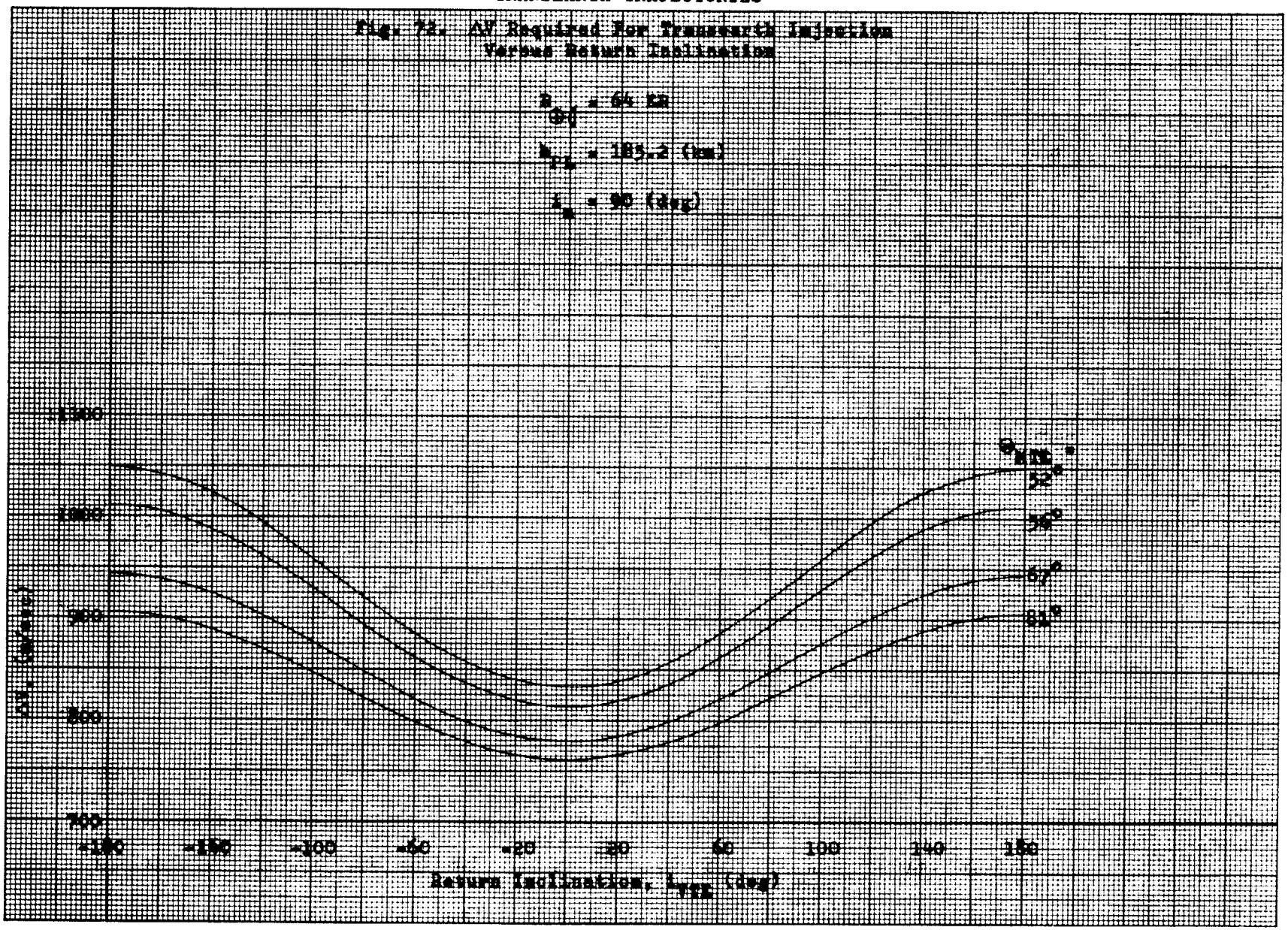
Fig. 72. ΔV Required For Transearth Injection Versus Return Inclination
R_{Pf} = 64 ER
h_{Pf} = 185.2 (km)
i_a = 90 (deg)
52°
38°
67°
81°
1400
1200
1000
800
600
-140
-100
-60
-20
20
60
100
140
150
Return Inclination, i_{TEC} (deg)

Fig. 73. Transearth Injection Point Versus Return Inclination

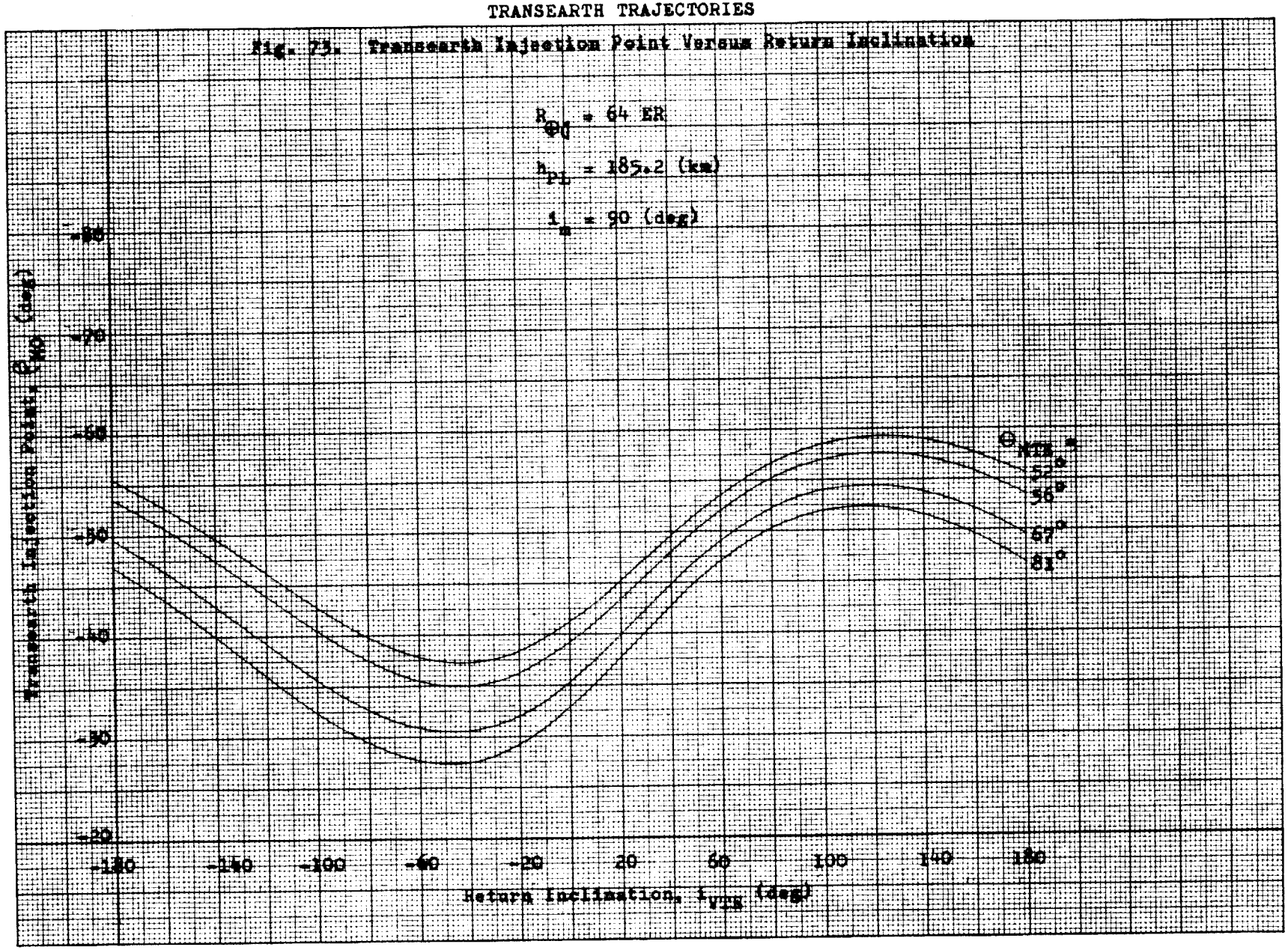

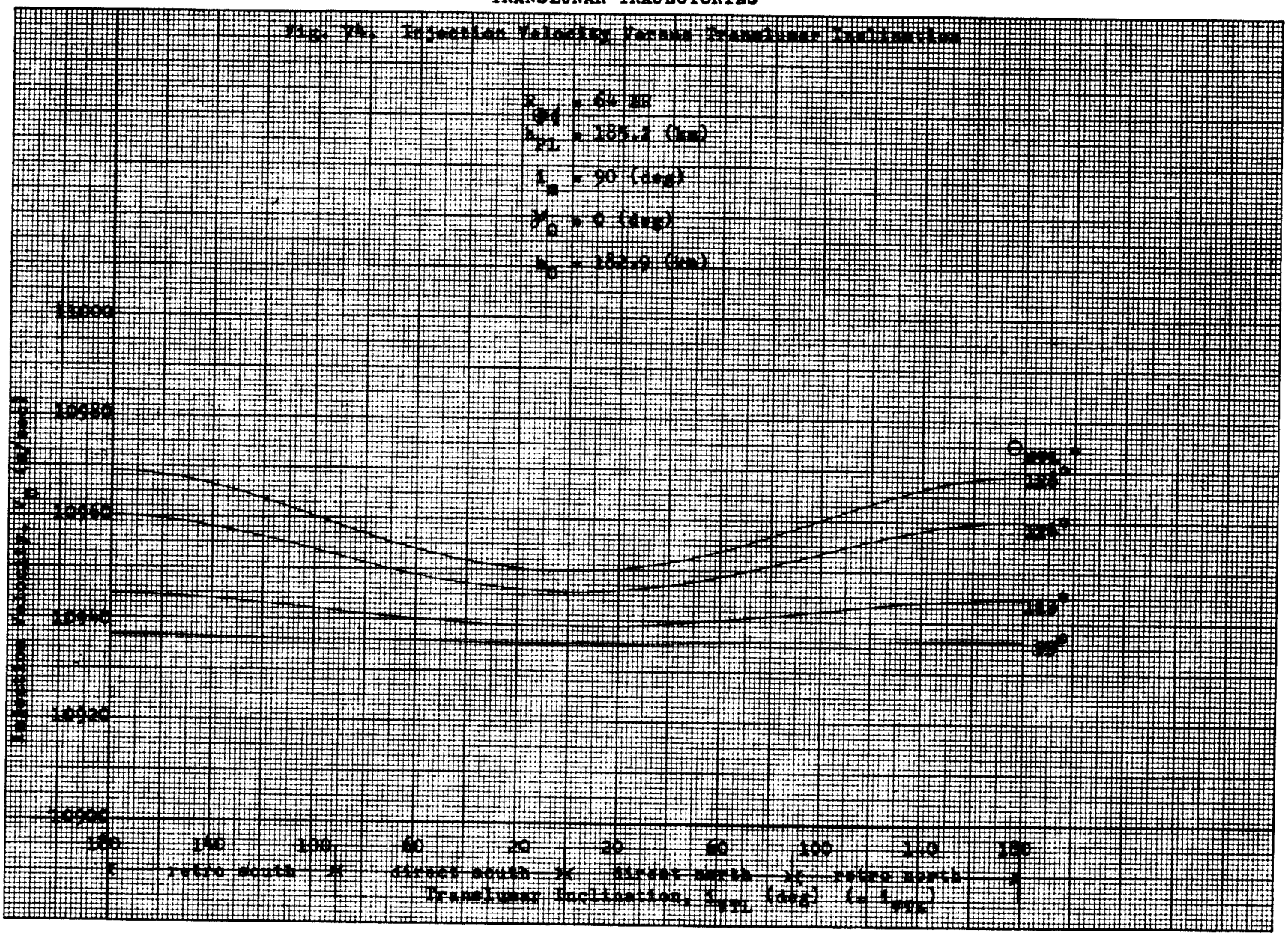

Fig. 7h. Injection Velocity Versus Translunar Inclination

TRANSLUNAR TRAJECTORIES

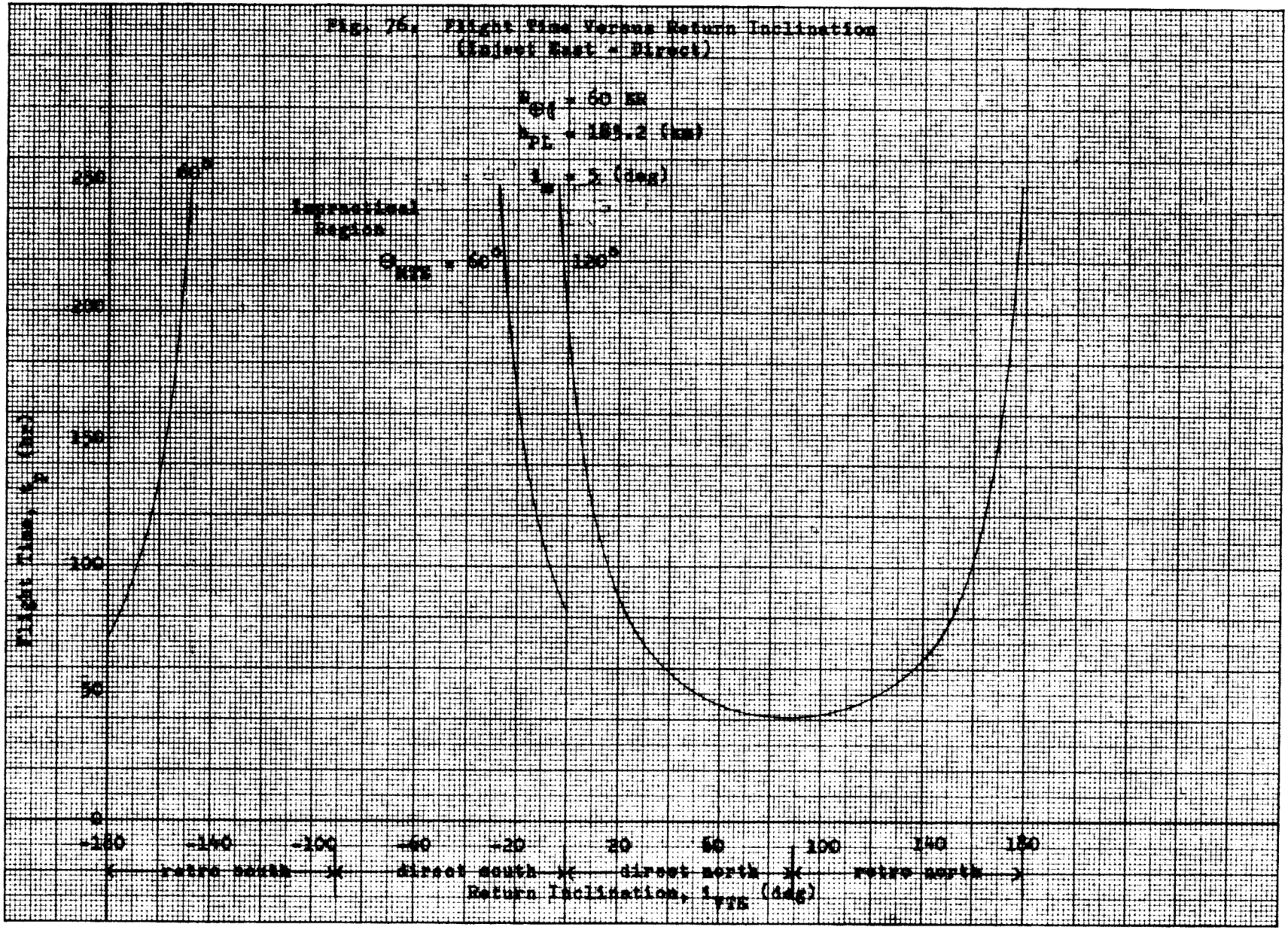

Fig. 76. Flight Time Versus Return Inclination (Inbound East - Direct)

TRANSEARTH TRAJECTORIES
Earth radius (nm)

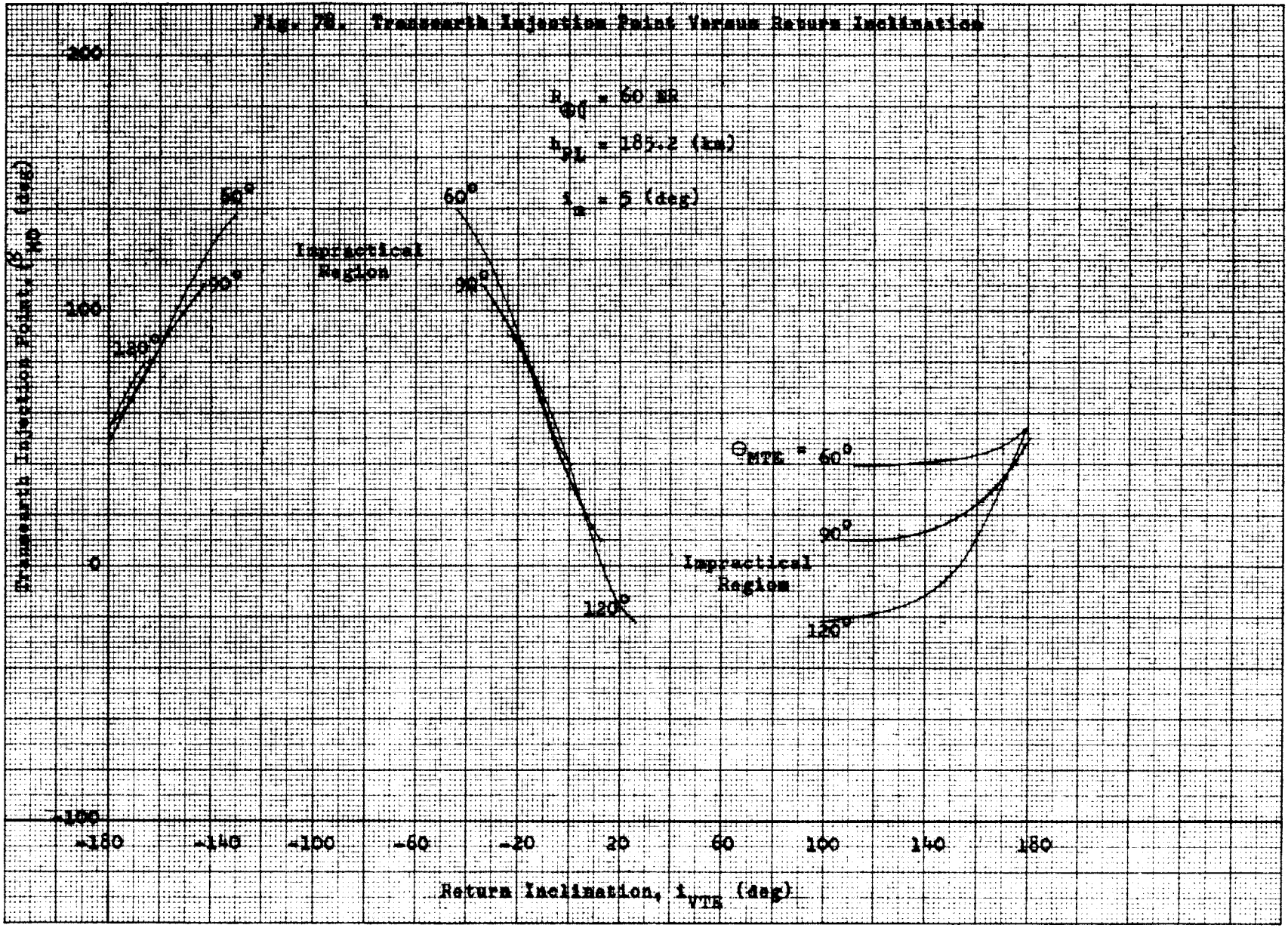

Fig. 78. Transearth Injection Point Versus Return Inclination

TRANSEARTH TRAJECTORIES
Fig. 79. Flight Time Versus Return Inclinations
(Coast, East - Direct)
120°
90°
60°
30°
0°
330°
300°
270°
240°
210°
180°
150°
50 hr
25 days
Return Inclination, i_R (deg)
Flight Time, t_F (hr)

TRANSEARTH TRAJECTORIES

TRANSEARTH TRAJECTORIES
Fig. 9A. Transearth Injection Point Versus Return Inclination
r_{pa} = 6688 km
h_{pa} = 1322 (nm)
γ_a = 13 (deg)
θ_{MIN} = 30°
60°
90°
120°
Return Inclination, i_{VIS} (deg)
Transearth Injection Radius, θ_{IN} (deg)

TRANSEARTH TRAJECTORIES

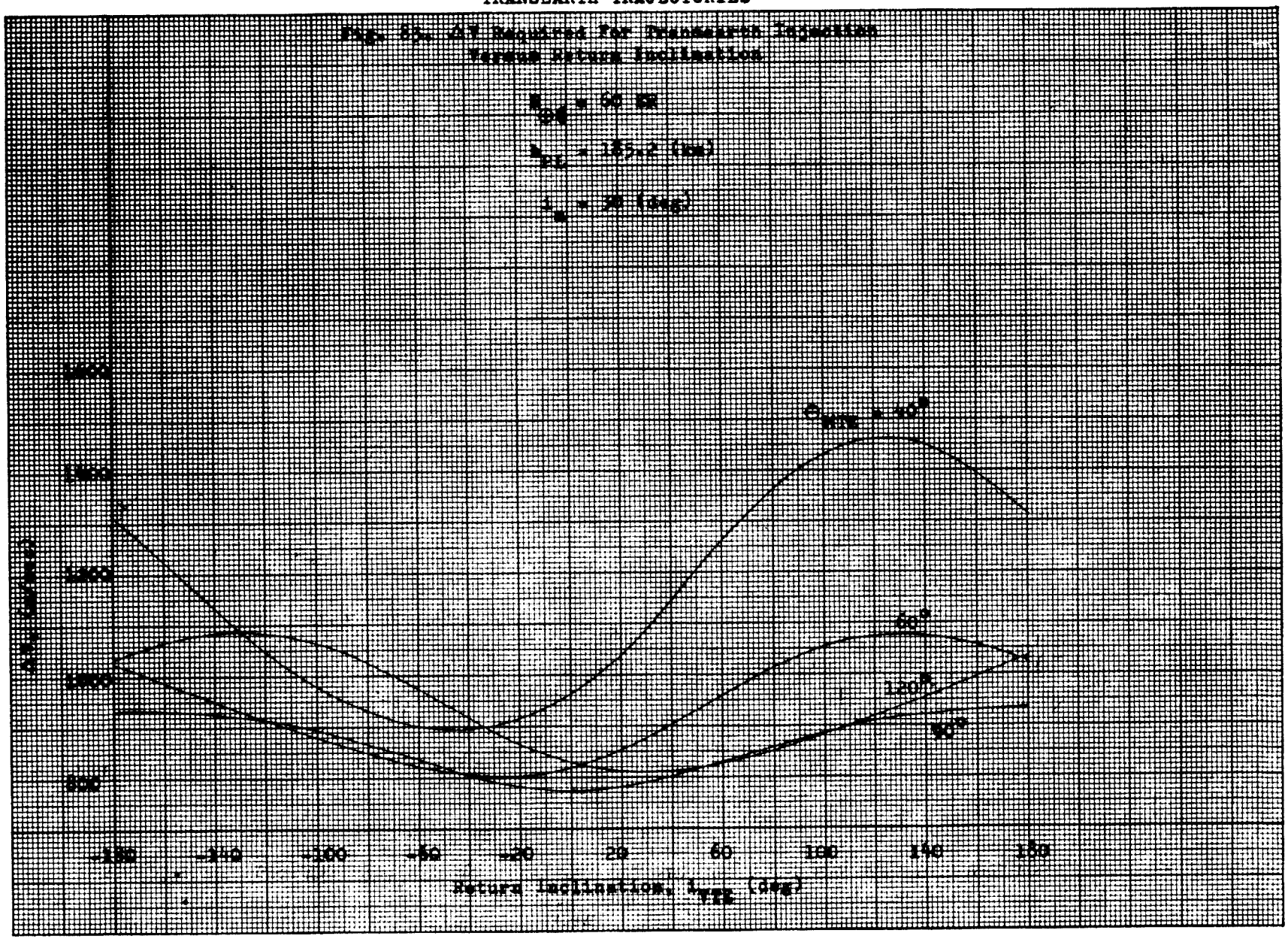
Fig. 65. ΔV Required for Transearth Injection
Versus Return Inclination
h_{pc} = 60 nm
h_{pL} = 185.2 (nm)
γ_e = 28 (deg)
Θ_{MTE} = 40°
60°
120°
90°
1600
1400
1200
800
-180
-140
-100
-60
-20
20
60
100
140
180
Return Inclination, λ_{VTE} (deg)

Fig. 8A. Transearth Injection Point Versus Return Inclination

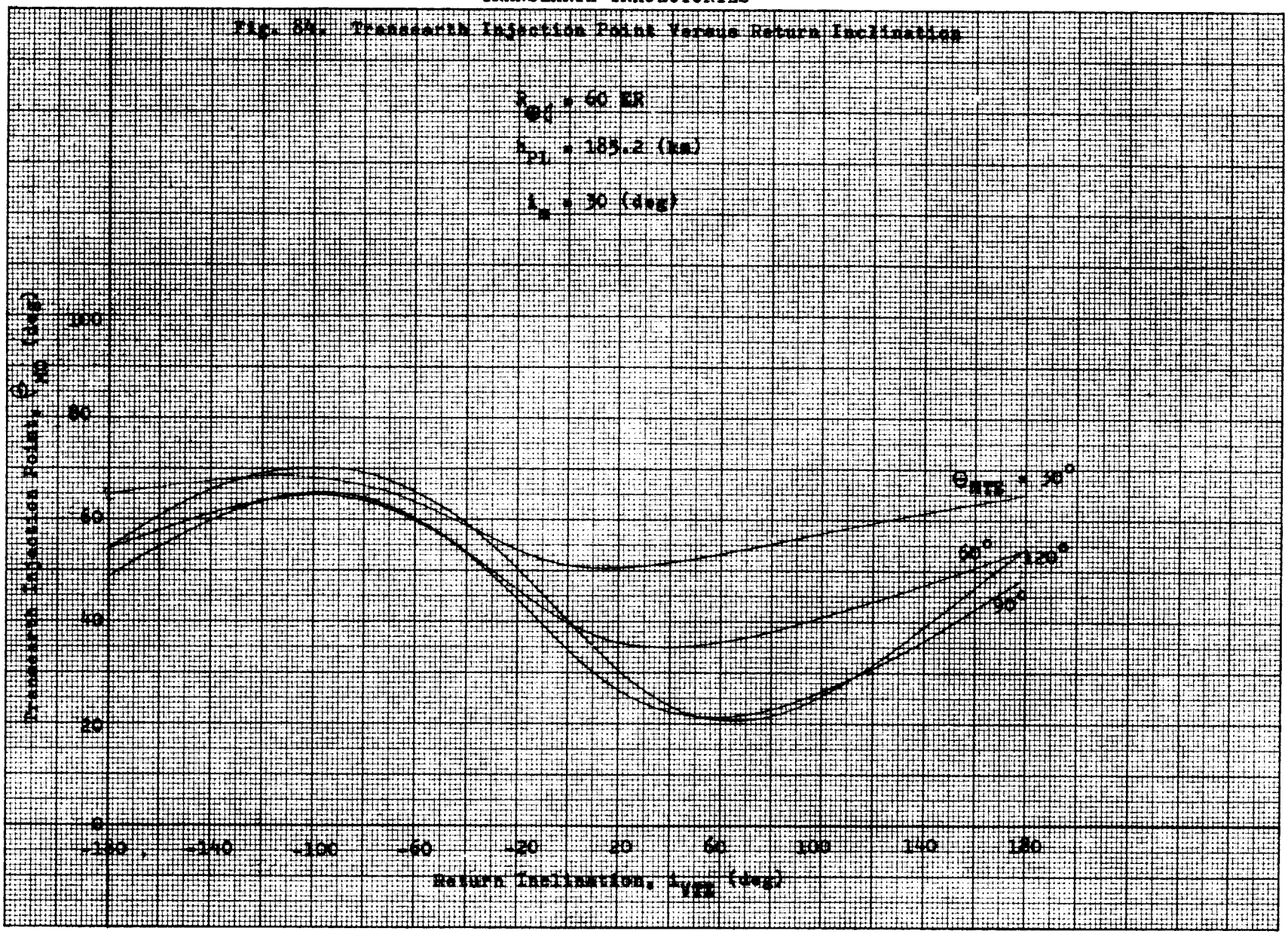

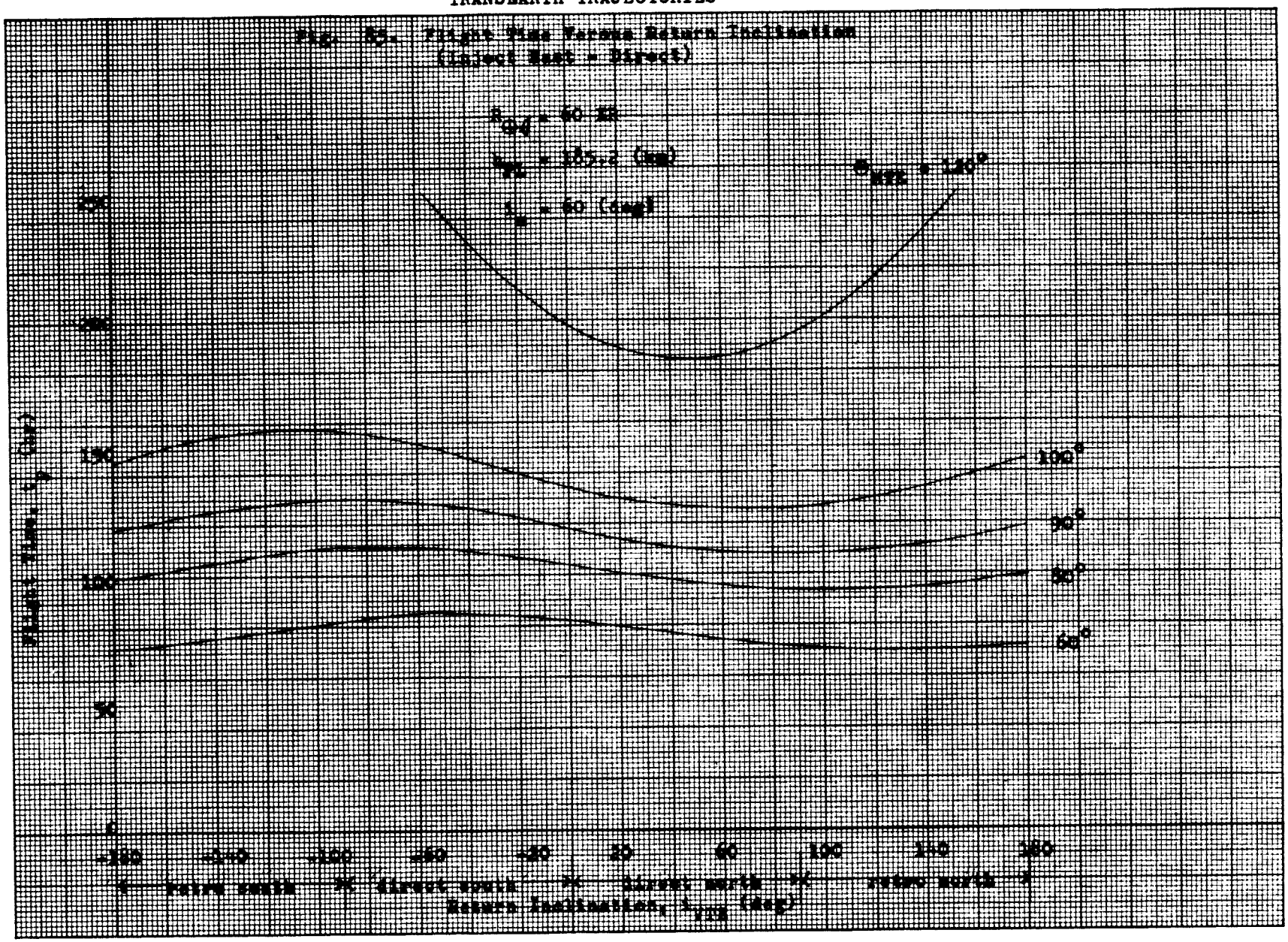
Fig. 85. Flight Time Versus Return Inclination
(Direct Exit - Direct)
R_{pA} = 60 ER
V_{∞} = 3.2 (km)
i_{∞} = 60 (deg)
θ_{max} = 140°
100°
90°
80°
60°
200
150
100
50
-180
-140
-100
-60
-20
20
60
100
140
180
retro south
direct south
direct north
retro north
Return Inclination, i_{rtn} (deg)

TRANSEARTH TRAJECTORIES

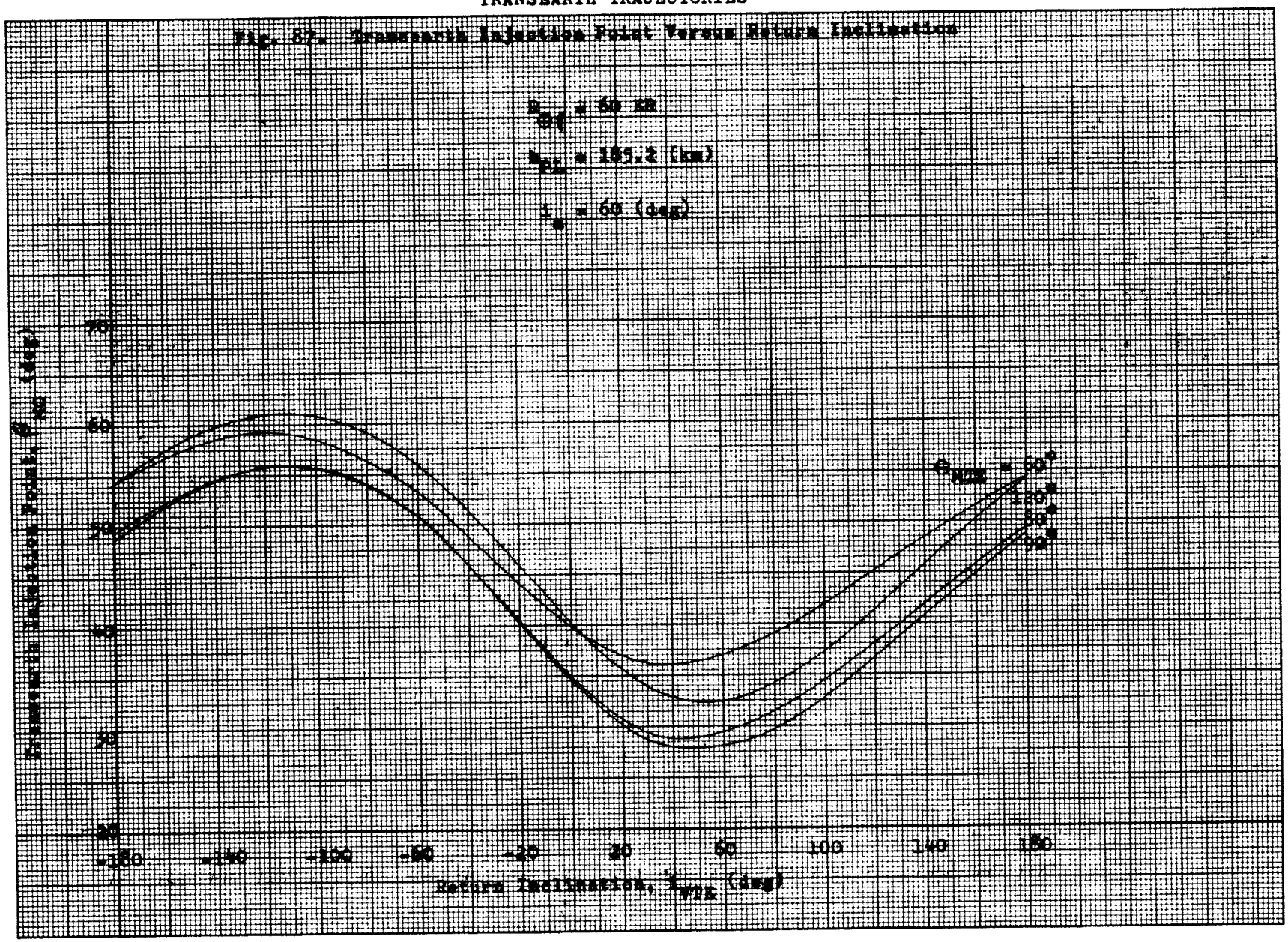

Fig. 87. Transearth Injection Point Versus Return Inclination

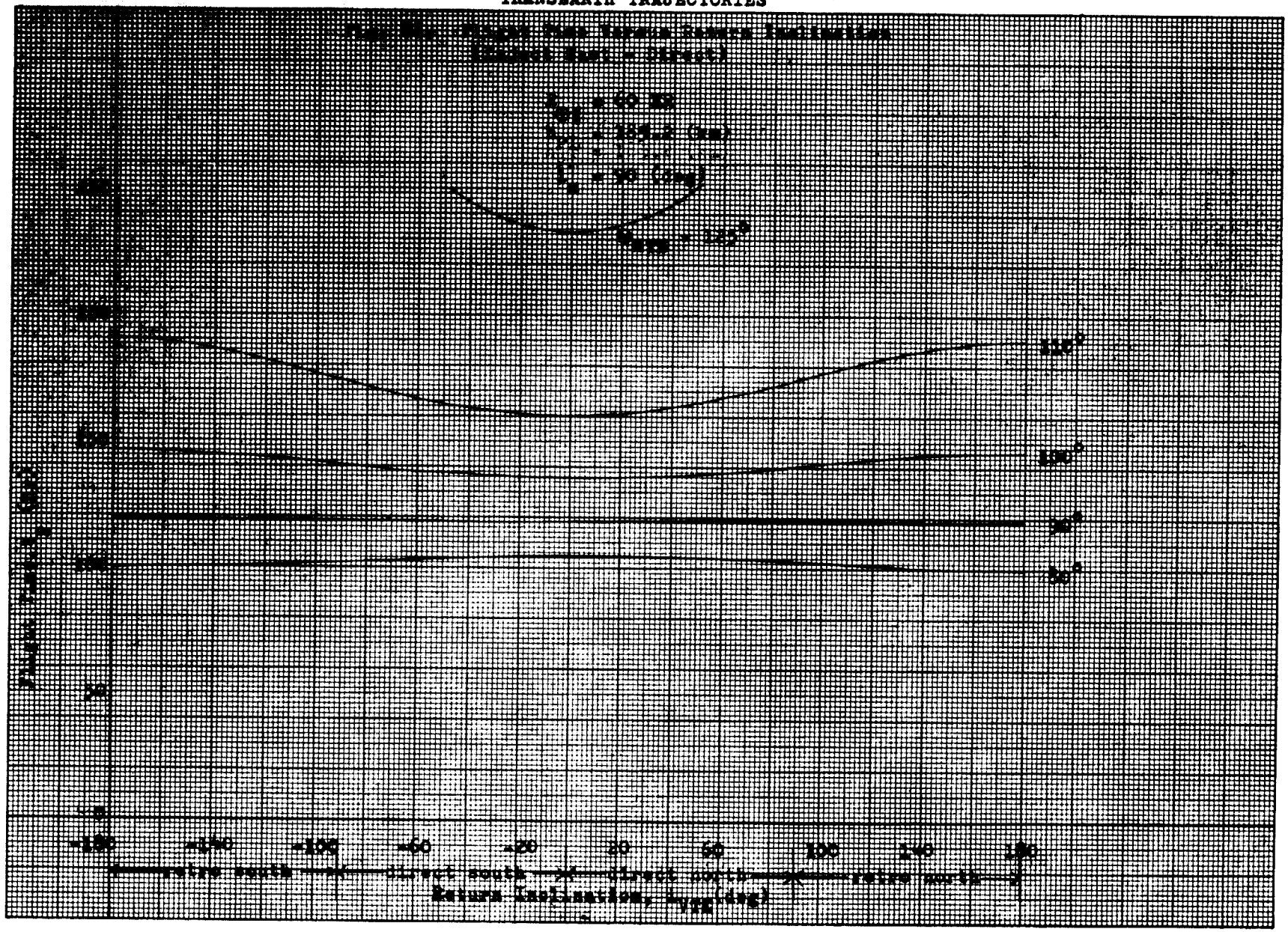
Flight Path Angle, γ_{EI} (deg)
Return Inclination, i_{RTE} (deg)
-180
-140
-100
-60
-20
20
60
100
140
180
retro south
direct south
direct north
retro north
γ_{EI} = -6.50 deg
h_{PC} = 103.2 (nm)
V_{EI} = 36 (Kfps)
ψ_{EI} = 125°
112°
100°
90°
80°

TRANSEARTH TRAJECTORIES
Return Inclination, i_RE (deg)

Fig. 50. Transearth Injection Point Versus Return Inclination

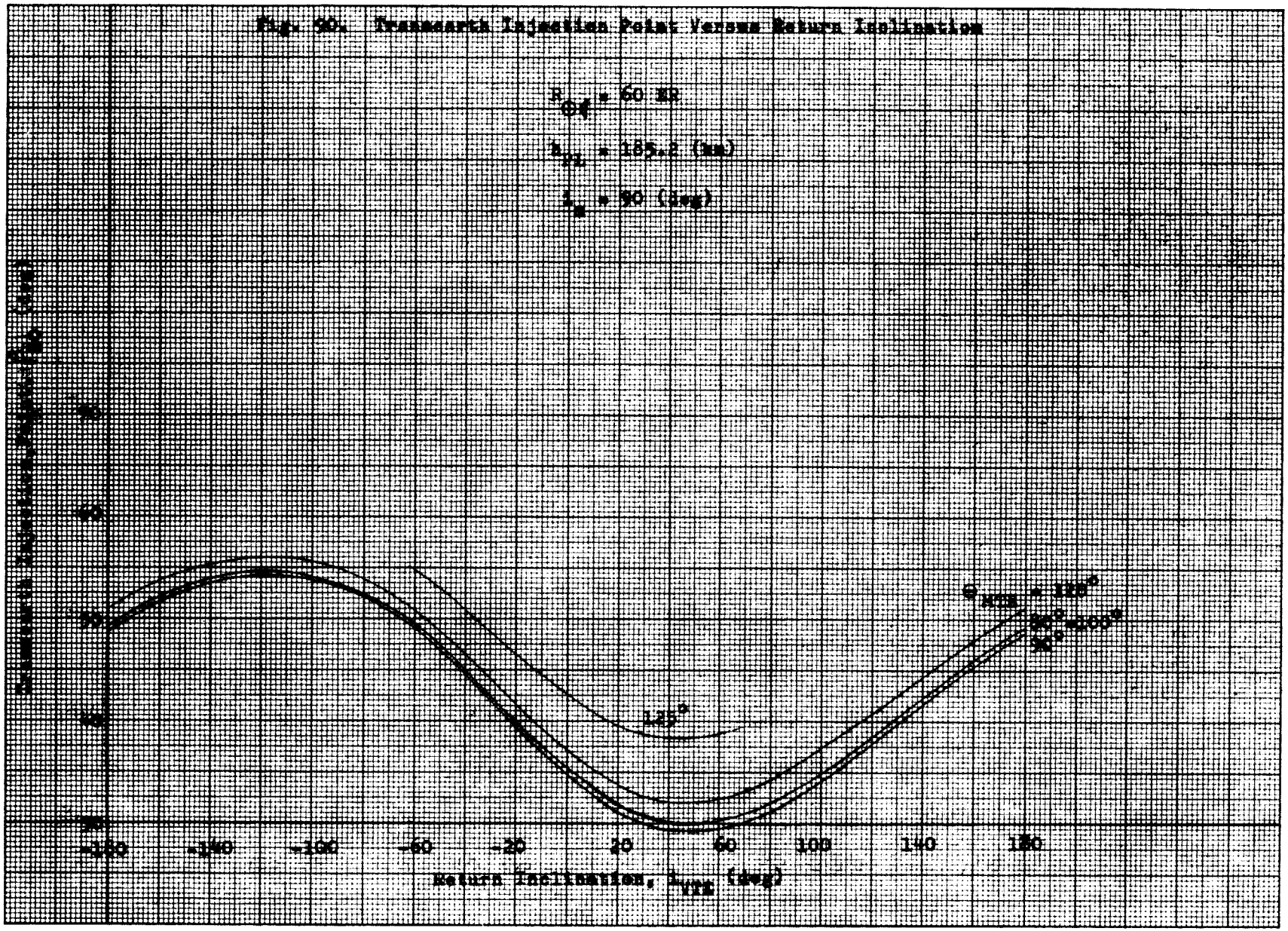

CHAPTER X

EARTH RETURN

Prepared by:

F. Santora and F. Martikan
Martin Company (Baltimore)
Aerospace Mechanics Department
March 1963

Page

A. Landing at a Specific Earth Site X-1

B. Re-Entry by Atmospheric Deceleration X-2

C. Re-Entry by Rocket Deceleration or a Combination of Atmospheric and Rocket Deceleration X-18

D. References X-24

Illustrations X-27

X. EARTH RETURN

This chapter presents the flight mechanics and guidance aspects of earth return. The material is discussed mostly in qualitative form, with the required trajectory equations and methods of solution given. For re-entry into the earth's atmosphere the limiting factors in the selection of the trajectory are not so much the ultimate aerodynamic performance of the re-entry vehicle, which could be augmented by rocket acceleration or deceleration, but the properties of the earth's atmosphere itself, which provide two design limits:

(1) Upper limit on the steepness of re-entry because of high decelerations.

(2) Lower limit on the steepness due to high aerodynamic heating or a "skipping" out of the atmosphere if insufficient dissipation of the vehicle's kinetic energy occurs.

A complete description of earth return would thus include a description of the earth's atmosphere, the aerodynamic forces and the resulting deceleration and heating of the re-entry vehicle. The properties of the earth's atmosphere have been discussed briefly in Chapter II and in more detail in Chapter II of Ref. 1. The form of the aerodynamic lift and drag terms, which become numerically very large during re-entry, has been given in Section B of Chapter IV. The present chapter discusses the techniques of re-entry, the timing of re-entry for specified lunar mission constraints, and the aerodynamic performance of and trajectory requirements for the re-entry vehicle. The aerodynamic heating aspect of re-entry (with equations for estimating convective, conductive, radiative heating in hypersonic flow and the flow field around the vehicle, thus giving the heat balance and temperature for portions of the re-entry vehicle) has been given in Chapter IX of Ref. 1, and Chapter XII of Ref. 2. Aerodynamic heating is of prime concern during a re-entry; practically all of the vehicle's kinetic energy must be dissipated in the form of heat. Most materials can only absorb a fraction of this heat energy without melting or evaporating; consequently the dissipated kinetic energy must be made to heat the gas around the body rather than the body itself.

Section A of this chapter discusses qualitatively the timing of the return and the transearth and translunar trajectory parameters which are affected by this timing if landing at a specific earth site is desired.

Section B discusses re-entry by atmospheric deceleration. In this technique a large portion of the kinetic energy of the re-entering space vehicle is converted to heat by the action of atmospheric drag until the speed of the vehicle is slow enough to permit a landing without damage to the structure and the occupants, if any. The aerodynamic maneuvering capability of the vehicle is discussed in Subsection B-4 and the techniques for guiding the re-entry vehicle to a landing in Subsection B-5.

Section C discusses earth re-entry by use of rocket and/or atmospheric deceleration to reduce the space vehicle speed from the supercircular approach speed of $\simeq 11$ km/sec to a circular orbit velocity of $\simeq 8$ km/sec. The vehicle may then remain in earth satellite orbit until such time that re-entry from orbit to a specific landing site can be accomplished. An important part of this technique, the determination of call-down frequency, has been discussed in some detail and the conditions for a recall to a specific site have been derived.

This chapter completes the discussion of the different phases of a lunar trajectory which was started with earth departure in Chapter V. The material in these chapters consisted of a discussion of techniques and requirements for each trajectory phase, as well as an attempt to catalogue all earth-to-moon trajectories of interest from Cape Canaveral and moon-to-earth trajectories from lunar satellite orbits to an arbitrary earth landing site. The task remains to combine the material on vehicle environment in Chapter II, on the geometry in Chapter III, the dynamics of Chapter IV and the detailed discussion of the trajectory phases in Chapters V to X and then to illustrate the application of this material to the preliminary design of a specific lunar mission. This task will be taken up in Chapter XI.

A. LANDING AT A SPECIFIC EARTH SITE

For manned and many unmanned lunar missions, operational concepts dictate the recovery of the spacecraft after the completion of the mission. Planning for recovery of the spacecraft will be based on landing in one of a few relatively small areas since only small areas on earth can provide adequate tracking facilities during re-entry and the recovery forces and facilities can be deployed in only a few restricted areas. In addition, the climate, the terrain and political considerations will also limit the available landing areas. Even abort trajectories can be planned to result in vehicle return to specified landing areas as discussed in Section D of Chapter VI. Only dire emergencies will require indiscriminate earth return and landing, namely when the survival of the space vehicle crew depends on it.

Once one or more landing sites have been selected, the timing of the mission must be designed to result in a landing at that site. For lunar missions the timing is a major problem and it is the first one attacked as illustrated by the two sample missions in Section G of Chapter XI. The timing problem can be solved during earth departure, at injection by choice of a suitable flight time, on the moon, or by use of parking orbits on earth return. In any case, timing depends on the particular trajectory class selected (see Chapter IV for further definition and classification of lunar trajectories).

With a circumlunar trajectory class that is designed to directly re-enter the earth's atmosphere at the end of the transearth portion of the trajectory, a major timing problem arises since

for a direct re-entry the landing will occur soon after re-entry and, therefore, will require that the landing site be close to the re-entry trajectory plane. Therefore the circumlunar mission must be planned at the time of launch (from earth) to possess a total flight time that allows the designated landing site to rotate beneath the transearth trajectory plane at re-entry or at least within the maneuvering capability of the re-entry vehicle. For a given lunar arrival date or time of the month, the earth-moon distance $R_{\oplus \mathbb{C}}$ may be assumed constant for a few hours before and after the arrival date.

The allowable i_{VTL} (Section D, Chapter XI) and the resulting i_{VTE} for a given h_{PL} also remain essentially constant. With these mission constraints, there is a corresponding total flight time, T (from launch to injection--to pericynthion--to earth re-entry). Now, if the earth landing site is not in the correct position relative to the transearth plane at re-entry (which is the general case) an adjustment in T is necessary. One way of obtaining this adjustment without the expenditure of energy is to alter h_{PL} since it is the only remaining parameter that affects T for a given arrival date. This is most clearly illustrated in Fig. 1 for two designated landing sites, namely, Australia and Edwards AFB. It is worthwhile to note here that the maximum and minimum h_{PL} required to acquire these two sites occur either at the maximum southerly or maximum northerly declination. Furthermore, note that the re-entry range required to reach the sites varies considerably.

If the mission specifically states that h_{PL} remains constant, then the adjustment in T must be achieved by means of a transearth adjustment maneuver as explained in Section E, Chapter XI. This midcourse maneuver does not alter the transearth inclination i_{VTE} but only advances or delays the time at which re-entry occurs.

An alternative to the transearth adjustment maneuver is to allow the spacecraft to arrive at earth without consideration to site location. At approximately the time of perigee, an orbital entry maneuver is executed which places the spacecraft in a close earth orbit where the spacecraft stays until the proper position of the landing site relative to the vehicle is achieved, before de-orbit, re-entry, and a landing is attempted.

The discussion thus far implicitly assumes that the acquisition of a particular lunar satellite orbit orientation defined by the $i_m - \theta_M$ relationship (see Section A of Chapter XI) is not a mission requirement. However, if the spacecraft must have a specific $i_m - \theta_M$ combination, then i_{VTE} will depend on and be in error with the desired i_{VTE}. Thus, in addition to making adjustments in total flight time to time a given landing site, it also becomes necessary to make a transearth planar change Δi_{VTE} for the three cases mentioned above. This maneuver and the corresponding energy requirements are discussed in detail in Section E of Chapter XI.

For a transearth trajectory that originates at the moon and returns a spacecraft to earth, the problem of returning to a specific earth site is not as formidable as for the circumlunar class since flight time is not constrained (see Chapters IX and XI). There are certain ramifications, however, especially if the lunar departure is conducted from a pre-established orbit resulting from lunar rendezvous or parking orbit requirements. In this case the return time can still be controlled but the return inclination i_{VTE} may have to be adjusted.

In summary, the timing problem associated with returning a spacecraft to a designated earth landing or recovery area can be solved at different times during the mission. For circumlunar trajectories the problem may be resolved at launch or in parking orbit prior to translunar injection, along the transearth trajectory, or at the completion of a mission (parking orbit at earth return). In the case of transearth trajectories established at the moon, the timing problem is resolved prior to lunar liftoff or lunar orbit departure. It must be remembered that in connection with the timing problem, it can be generally stated that a transearth midcourse correction of i_{VTE} is also required.

B. RE-ENTRY BY ATMOSPHERIC DECELERATION

A very efficient technique for recovery of lunar space vehicles after completion of the mission is to decelerate the re-entry vehicle by dissipating most of its kinetic energy in the earth's atmosphere without application of rocket thrust. For this re-entry technique there is a weight penalty in providing a heat shield, which protects the vehicle by absorbing some of the heat generated, but this weight penalty is far less than that of the fuel required to reduce the vehicle velocity by rocket deceleration. Atmospheric deceleration of a vehicle returning from a lunar mission presents a more severe problem than it does for an earth satellite. This fact is caused by the different speeds of the vehicles--11 km/sec for the lunar vehicle and 8 km/sec for the earth vehicle. However, the use of ablative heat shields in contrast to radiative and heat sink-type heat shields makes it possible to re-enter the earth's atmosphere with supercircular speeds, i.e., speeds in excess of 8 km/sec, at least from the point of view of theoretical thermodynamics. No vehicle has as yet been re-entered and recovered intact at supercircular speeds.

The re-entry portion of a trajectory is characterized by the dominance or large size of the aerodynamic forces as compared to the gravitational force on the vehicle. Since most re-entry trajectories are extremely short as compared to earth satellite orbits, for conventional lunar vehicles the presence of the atmosphere can be neglected until the vehicle altitude first drops below 122 km. Of course, just as in the case of earth satellites, the upper limit of the sensible atmosphere depends on the ballistic coefficient $B = C_D A/2M$ of the vehicle, the flight path angle γ,

and the velocity V of the vehicle. The approach trajectory above 122 km for conventional lunar vehicles and conventional return may be considered ballistic and the initial conditions of the re-entry trajectory may be characterized by the re-entry velocity V_R and the re-entry flight path angle γ_R occurring at an altitude of 122 km as illustrated in the following sketch:

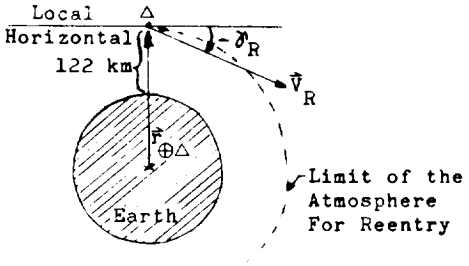

Nothing prevents the use of the equations of motion as given in Section B of Chapter IV and the initial re-entry conditions to obtain the entire trajectory by numerical integration on a digital computer. However, nonlifting vehicles with fixed aerodynamic coefficients, as well as lifting vehicles with variable aerodynamic coefficients, introduce many trajectory parameters, so that a very large number of numerically calculated trajectories must be obtained before definite trends can be established. In order to obtain an idea of re-entry trajectory characteristics, approximate analytical methods are preferable to numerical solutions just as the Voice technique enabled the determination of ballistic lunar trajectories more quickly and efficiently than numerical integration of the more complicated equations of motion. There exists no analytic solution of the full equations of motion, hence the qualifying statement that the analytic solutions are only approximate.

1. Equations of Motion for a Shallow Re-entry

Consider re-entry into the atmosphere of a spherically symmetric planet and let the atmosphere be spherically symmetric in concentric layers about the planet and be stationary with respect to the planet. Neglect lateral aerodynamic forces as well as thrust forces. The resulting descent is planar and one can introduce plane polar coordinates $r_{\oplus\Delta}$, $\theta_{\oplus\Delta} \equiv r, \theta$. The sketch below shows the components of aerodynamic lift, aerodynamic drag and velocity in this coordinate system.

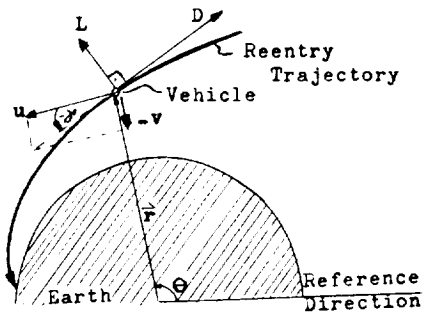

Hence the two component equations of motion in the plane polar coordinate system are as follows:

$$-\frac{dv}{dt} = g - \frac{u^2}{r} - \frac{L}{M}\cos\gamma + \frac{D}{M}\sin\gamma \qquad (1)$$

$$\frac{du}{dt} + \frac{uv}{r} = -\frac{D}{M}\left(\cos\gamma + \frac{L}{D}\sin\gamma\right) \qquad (2)$$

where

- t = time
- g = local acceleration due to gravity
- M = vehicle mass (constant)
- γ = flight path angle at any time.

In order to obtain an approximate analytical solution, Chapman (Ref. 3) introduces a Z-function.

$$Z \equiv \frac{\rho_\infty}{\alpha\left(\frac{2M}{C_D A}\right)}\sqrt{\frac{r}{\beta}}\,\bar{u} \qquad (3)$$

where

- ρ_∞ = free stream atmospheric density, $\frac{kg}{m^3}$
- C_D = drag coefficient, $C_D = \frac{D}{\frac{1}{2}\rho_\infty V^2 A}$
- $V^2 = u^2 + v^2$ = vehicle velocity squared
- A = vehicle reference area
- β = logarithmic atmospheric density gradient in units of m^{-1}

$$= -\frac{d}{dr}(\ell n\,\rho_\infty) = \frac{1}{\rho_\infty}\frac{d\rho_\infty}{dr} = \frac{\bar{M}g}{R^* T}$$

- R^* = $8.31439 \times 10^3 \frac{\text{joules}}{°K - kg}$ = gas constant
- T = local temperature of the ambient atmosphere in °K
- $\bar{M}$ = molecular weight of the atmosphere
- $\bar{u}$ = $\frac{u}{\sqrt{gr}}$ is a dimensionless horizontal velocity parameter.

Chapman (Ref. 3) then makes the assumption that the re-entry is shallow (or γ is small during entry), so that $\cos\gamma \simeq 1$, $\sin\gamma \simeq \gamma$, $V \simeq u$, $|(L/D)\tan\gamma| \ll 1$.

With the shallow re-entry consumption, the introduction of $\bar{u}$ as the independent and Z as dependent variable, the two equations of motion (1) and (2) reduce to a single ordinary nonlinear second-order differential equation. This transformed equation of motion is given here together with the physical interpretation of the terms:

$$\underbrace{\bar{u}\,Z''}_{\text{vertical acceleration}} - \underbrace{\left(Z' - \frac{Z}{\bar{u}}\right)}_{\text{vertical component of drag force}} = \underbrace{\frac{1-\bar{u}^2}{\bar{u}\,Z}\cos^4\gamma}_{\text{gravity minus centrifugal force}}$$

$$- \underbrace{\sqrt{\beta r}\,\frac{L}{D}\cos^3\gamma}_{\text{lift force}} \qquad (4)$$

with the initial conditions

$$Z(\bar{u}_i) = Z_i \quad \frac{dZ}{d\bar{u}}(\bar{u}_i) = \left(\frac{dZ}{d\bar{u}}\right)_i \qquad (4a)$$

The author then examines the structure of Eq (4) with the initial conditions representing re-entry conditions and finds that three dimensionless parameters determine the motion during shallow re-entry: the re-entry velocity parameters $(\bar{V}_R)_i = (V_R/\sqrt{gr})_i$, the lift parameter $L/D\ \sqrt{\beta r}$ and the perigee parameter

$$F_{PE} = \frac{\rho_{PE}}{2\left(\frac{2M}{C_D A}\right)}\sqrt{\frac{r_{PE}}{\beta}}, \qquad (4b)$$

where the subscript "PE" refers to vacuum perigee of the earth return trajectory.

These parameters are then utilized to find safe re-entry corridor depths (for a complete definition of re-entry corridor see Subsection B-3) that are extremely useful in comparing various re-entry vehicle configurations and trajectories. Deceleration load factors, guidance requirements, re-entry range, heating rates and L/D effects can also be accurately determined from these parameters.

Luidens (Ref. 4) presents closed form solutions of many engineering parameters of interest for specific re-entry trajectories such as constant angle of attack, constant altitude, constant net acceleration, modulated roll trajectories, etc.

Of course, attention should be given to the assumptions made in the above references to ensure applicability to re-entry trajectories in question. Only the general results obtained in Refs. 3 to 14 are discussed in this chapter and the reader is referred to these references for complete details and mathematical developments.

2. Qualitative Description of Re-entry

The equations governing re-entry as well as the results obtained from these equations by numerical or analytical methods point out the importance of the flight path angle γ_R at re-entry (h_R = 122 km for conventional vehicles). It is always negative since otherwise the vehicle could not lose altitude and re-enter.

If $|\gamma_R|$ is large, the initial approach to the earth's atmosphere is very steep and actual re-entry is accomplished in a matter of seconds. This situation is analogous to a bullet being brought to a complete stop in a very short time. The result is a tremendous deceleration that is beyond both human and structural endurance.

If $|\gamma_R|$ is very small, the approach to the earth's atmosphere is very shallow, the equation of motion, Eq (4), applies directly and this case may be likened to the ricochet of a bullet; i.e., for highly elliptic, parabolic and hyperbolic approaches the vehicle "skips" out of the atmosphere in a still highly eccentric orbit. The phenomenon of skipping out has been suggested by Chapman (Ref. 5) as a technique to re-enter the earth's atmosphere very slowly, and multiple-pass atmospheric deceleration entries are of interest for several reasons, one of which is that they provide a means of minimizing aerodynamic heating. For example, in an entry which first makes a number of supercircular passes through the outer edge of the atmosphere until the velocity is reduced to circular velocity and then completes the subcircular portion of entry with a sizable positive (see sketch) L/D, the decelerations experienced (and the rates of aerodynamic heating) can be kept relatively small.

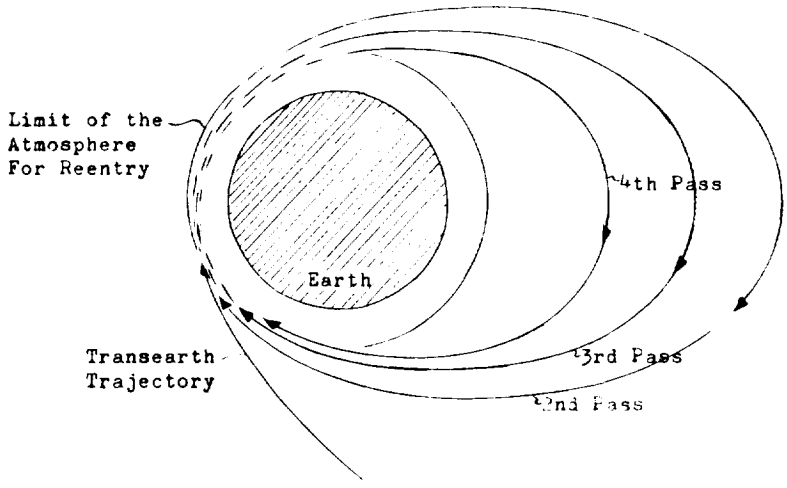

It is shown in Ref. 3 that for ballistic entries ($L/D = 0$) six supercircular passes would be required to keep the maximum heating rates about the same as those experienced during the terminal subcircular portion of entry. Since each pass is followed by a substantial period wherein the structure may cool as the vehicle orbits in preparation for a subsequent atmospheric pass, this method provides an attractive possibility for utilizing the combined heat sink and radiative capability of the structure. If the re-entry body is a lifting vehicle ($L/D \neq 0$), then it can be rolled during the atmospheric portion of the trajectory to produce a side force which changes the inclination and nodal line of the vehicle orbit in inertial space. This maneuver which does not require rocket fuel may correct any small timing and trajectory errors.

At least two important problems arise for multiple-pass atmospheric re-entries: they could require multiple passes through the Van Allen radiation belt, and they require an especially accurate re-entry guidance system (to produce the desired trajectory). For these two reasons, such a re-entry technique is considered somewhat impractical at this time.

However, there is a region of moderate values of $|\gamma_R|$ which allows the vehicle to re-enter in a single pass, provided that the heating and/or deceleration are not excessive for the returning vehicle.

The preceding qualitative discussion indicates that the direction of the re-entry velocity vector $\vec{V}_R$ must be controlled so that the penetration is neither too steep nor too shallow to assure the planned re-entry. Thus for a given type of re-entry, be it single pass or multiple pass, there exists a small region of V_R, γ_R which enables this particular type of entry. This region can be described by the concept of re-entry corridor which is defined in detail in the next subsection.

The effect of γ_R on the type of re-entry has been discussed above. As for V_R, as V_R increases the re-entry corridor becomes narrower because with increasing V_R more kinetic energy must be dissipated prior to landing; hence the heating and deceleration encountered by the vehicle become more severe. To remain in the reduced re-entry corridor, the supercircular atmospheric entry required for a direct return from the moon necessitates a much more accurate guidance system than that required for the circular entry of close earth satellites.

3. Definition of Corridor Depth

A safe re-entry corridor depth as proposed by Chapman (Ref. 5) depends on the "undershoot" and "overshoot" boundaries peculiar to the configuration of the re-entry vehicle. The undershoot boundary is defined as the steepest approach to the atmosphere that the vehicle can undertake without exceeding structural or human deceleration limits during the re-entry phase. Usually the maximum deceleration, also called the maximum load factor, of 10 g_0 is specified.

The overshoot boundary is referred to as the "shallowest" approach that can be taken with a particular vehicle to be captured by the atmosphere within one revolution around the earth, i.e., the single pass re-entry. These boundaries are illustrated in the next sketch by assuming two near-parabolic conic sections (which are representative of transearth trajectory paths prior to the re-entry phase) intersecting the earth's atmosphere. One conic section represents the undershoot boundary trajectory, and the other the overshoot boundary trajectory. If the earth and its atmosphere are ignored for the moment, then the initial conic trajectories continue to their respective vacuum perigees as shown by the dashed lines in the sketch. These conic trajectories are normally referred to as "vacuum trajectories."

Since re-entry is considered to occur at $h_R = 122$ km with a nearly constant V_R, the difference in γ_R results in vacuum perigee of the overshoot boundary which is usually higher than that of the undershoot boundary. Thus, the safe re-entry corridor can also be defined by a safe corridor depth, namely the difference in vacuum perigee altitudes $\Delta h_{PE} = h_{PE_1} - h_{PE_2}$ between the two vacuum trajectories.

The procedure that is used in obtaining the undershoot boundary is to change the configuration or to trim the lifting body re-entry vehicle close to its maximum lift-to-drag ratio $(L/D)_{max}$ at the re-entry point. This trim attitude is maintained until the maximum load factor or heating rate is encountered.

There are several methods that can be used to establish an overshoot boundary. For example, there is the "single pass overshoot," defined as the maximum vacuum perigee altitude at which the vehicle can enter at maximum negative lift coefficient ($-C_{L_{max}}$) and land within a range of one earth's circumference from the entry point. Another method uses the same technique ($-C_{L_{max}}$) but the overshoot boundary is based on an abrupt shortening in range to impact. The difference in overshoot γ_R between these two methods is approximately 0.05°, which is equivalent to approximately 1 km in corridor depth.

Still another method defines the $-C_{L_{max}}$ overshoot boundary as the maximum perigee altitude at which the vehicle can enter at $-C_{L_{max}}$ and remain within the atmosphere ($h \leq 122$ km). This boundary lies somewhere between that of the two former methods, and the major point to recognize is that the above overshoot methods have negligible effects on the corridor depths.

A final method considers the possibility of an emergency situation in which knowledge of the exact re-entry conditions is not available. Define the aerodynamic lift coefficient C_L by $C_L = \frac{L}{\frac{1}{2}\rho V^2 A}$ and denote its maximum value by $C_{L_{max}}$.

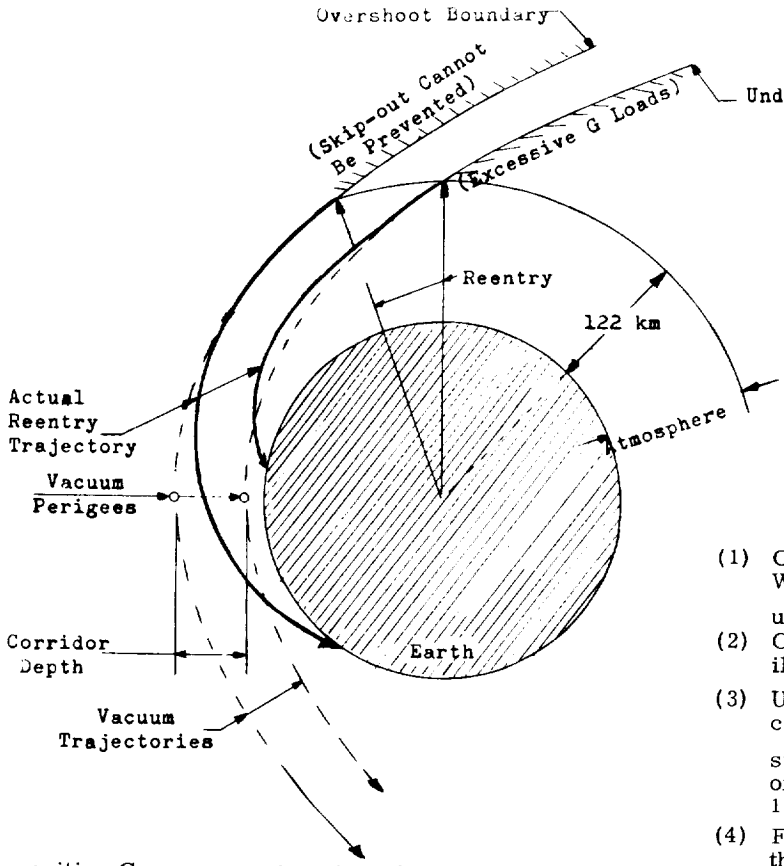

The positive $C_{L_{max}}$ overshoot boundary is defined as the maximum perigee altitude for which the vehicle can enter at positive $C_{L_{max}}$ to the point where $\gamma = 0°$ (arbitrary) at which time $-C_{L_{max}}$ is applied and the vehicle is able to remain within the atmosphere. The purpose of introducing this definition is to illustrate the reduction in corridor depth that would occur if entry into the atmosphere without precise flight path angle information were necessary. For example, in this emergency, the vehicle would have to enter at positive lift until it is determined (from a load factor time history, e.g.) that an overshoot condition exists. Once this is determined, negative lift would then be applied. This overshoot boundary is approximately 9 to 13 km below the negative $C_{L_{max}}$ boundary. From Chapman (Ref. 3), it is possible to determine undershoot and overshoot boundaries as a function of the lifting body re-entry vehicle's L/D, and ballistic parameter, $W/C_DA = g_0/2B$. Figure 2 shows both boundaries with the undershoot boundary limited to 10 g_0. It is assumed that C_L and C_D are constant, and that $V_R = 10.67$ km/sec at $h_R = 122$ km. The C_L, C_D relationships used are those presented in Ref. 5. It is further assumed that $C_{L_{max}}$ applied negatively on the overshoot boundaries and $(L/D)_{max}$ on the undershoot boundaries result in the maximum corridor depths. In Fig. 2 both boundaries are shown, thereby allowing the corridor depth to be determined directly. The associated γ_R is also included in the figure.

Although the results of such a parametric presentation are limited by the particular selection of C_L and C_D, important trends can nevertheless be established from Fig. 2:

(1) Corridor depth is independent of W/C_DA if W/C_DA is the same for undershoot and overshoot boundaries.
(2) Overshoot perigee altitude is primarily a function of W/C_LA attainable.
(3) Undershoot perigee altitude for a constant value of W/C_DA is decreased significantly by relatively low values of L/D. As L/D increases beyond 1.0, the benefits become less.
(4) For ballistic re-entry (i.e., L/D = 0), the corridor depth is only 12.8 km for a 10-g_0 maximum undershoot boundary.

The effect of V_R on corridor depth is shown in Fig. 3, which was also obtained from Ref. 5. The corridor depth variation with V_R to a 10-g_0 undershoot boundary is presented for several values of L/D.

A deceleration-limited undershoot boundary is affected not only by the maximum value of g_0 selected, but also by the particular way in which the L/D is monitored. The material presented thus far has concerned re-entry at constant lift and drag coefficients. Grant (Ref. 6) and Levy (Ref. 7) have indicated that substantial increases in corridor depth can be gained by employing variations of C_L during re-entry. Such re-entries are commonly referred to as modulated re-entries.

For a spacecraft entering the atmosphere at a given initial V_R, γ_R, W/C_DA and L/D, the deceleration varies directly as the dynamic pressure $q = \frac{1}{2}\rho_\infty V^2$ for an unmodulated re-entry. As the vehicle descends into the atmosphere, the dynamic pressure and, hence, the deceleration increase to a maximum value and then decrease. A typical deceleration time-history for an unmodulated entry is shown in the next sketch. To maintain the maximum deceleration at a value lower than the peak value of the unmodulated entry (see dashed curve in following sketch), the coefficient C_R of the resultant aerodynamic force R, $C_R = \frac{R}{\frac{1}{2}\rho_\infty V^2 A}$, is continuously decreased to compensate for the increase in dynamic pressure.

The term 'modulated re-entry' is somewhat ambiguous since it is necessary to modulate lift during almost all lifting re-entries at some time

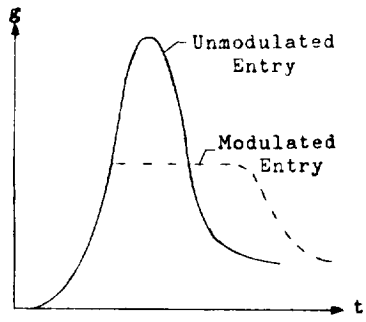

prior to landing in order to stay within the design limitations of the vehicle or to avoid atmospheric exit to extreme altitudes. Modulated re-entries, therefore, refer to re-entries in which lift and/or drag are modulated prior to the first maxima of load factor or heating rate. Constant L/D re-entries are those in which C_L and C_D are constant only until the initial maxima of load factor or heating rate are reached. Typically, a drag polar or C_L versus C_D curve for a particular vehicle takes the form shown in the sketch below.

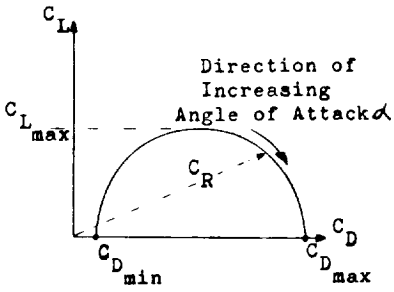

It was found by Grant that, for a given vehicle configuration entering at given values of V_R, γ_R, the lowest possible maximum deceleration can be obtained if entry is initiated at the value of C_R for $C_{L_{max}}$ and C_R is continuously decreased to the value at $C_{D_{min}}$. This result suggests the ratio C_R at $C_{D_{min}}$ to C_R at $C_{L_{max}}$ as a parameter with which to correlate the maximum reduction in peak acceleration. The ratio of minimum load factor $g_{0\ max}$ for modulated entries to $g_{0\ max}$ for unmodulated entries is shown in Fig. 4 as a function of the ratio of C_R at $C_{D_{min}}$ to C_R at $C_{L_{max}}$ for a wide range of values of V_R, γ_R, M/C_DA, and L/D_{max}. It is also interesting to show this ratio, $(g_{0\ max})_{mod}/(g_{0\ max})_{unmod}$, as a function of $(L/D)_{max}$. This is done in Fig. 5 for a typical family of vehicles that are modulated from $C_{L_{max}}$ to $C_L = 0$ and $C_{L_{max}}$ to $(L/D)_{max}$. Observe the appreciable gains up to an $(L/D)_{max}$ value of unity after which it is evident that diminishing returns occur. The data presented in Fig. 5 can then be factored with Chapman's results for constant C_L, C_D (Fig. 2) to give the 10-g_0 modulated re-entry corridors. Figure 6 presents such results for the case of modulation from $C_{L_{max}}$ to $C_L = 0$. Comparison of Figs. 2 and 6 indicates the large improvements in corridor depths that are obtained through re-entry modulation. For example, the 10-g_0 single-pass re-entry corridor for a vehicle with $L/D = 1.0$ and $W/C_DA = 4790\ \frac{nt}{m^2}$ (100 lb/ft^2) is increased from 96 km to 226 km by modulation.

The maximum load factor has been the only determining parameter of the undershoot boundary in the results presented. In some instances, aerodynamic heating may represent more severe limitation than load factor in determining the vehicle's boundary. In such cases, the heating rate-limited (q_H) or total heat-limited (Q_H) re-entry corridors would replace the overshoot corridor and possibly the undershoot corridor as well. This is based on the fact that, as the overshoot boundary is approached, the amount of total convective heat absorbed at the stagnation point increases almost exponentially for all longitudinal ranges, since the vehicle is required to spend a greater portion of the flight trajectory in the atmosphere. An increase in the total heat load would eventually result in exceeding the original heat shield material design limit, thereby restricting the allowable range as the boundary is approached. Since the amount of heat absorbed for a given γ_R varies with longitudinal range, the allowable limit is encountered at different entry angles for various values of re-entry range.

These factors led to the development of an "operational corridor" concept (Ref. 8) wherein the overshoot boundary is defined as the minimum entry angle for which the heat-load limit was not exceeded. This concept is illustrated in Fig. 7. Note that the heat-limited overshoot boundary is a function of the maximum required re-entry range. In other words, if the re-entry range required to fulfill operational considerations is large, the heat limit may define the overshoot boundary. This is altogether possible when reference is again made to Fig. 1 where required range can easily reach 16,000 km for lunar returns.

4. Re-entry Maneuvering Capability

After re-entry within the safe re-entry corridor is assured, the problem of landing at a specific site can be solved. In the case of a lifting re-entry body, the vehicle uses its aerodynamic characteristics as a means for maneuvering both longitudinally and laterally from the re-entry corridor to the site, whereas, in the case of a ballistic (nonlifting body) re-entry, either rocket burning prior to re-entry or a variable configuration can be used to obtain some maneuverability.

a. Longitudinal maneuverability

The longitudinal maneuvering capability or maneuvering in the re-entry trajectory plane is primarily a function of the vehicle's L/D_{max}. In the following sketch minimum and maximum range trajectories of a vehicle are shown entering along the undershoot and overshoot boundaries of the

re-entry corridor. The range segment marked "A" cannot be reached from any point in the corridor, whereas the segment denoted by "B" can be reached only from restricted portions of the corridor. Segment "C", entitled "Minimum Downrange Maneuvering Capability," gives the range segment that can be reached from any initial conditions within the corridor. The actual values of maximum and minimum range from overshoot and minimum range from undershoot depend strongly upon the control techniques used to obtain them. For example, the overshoot re-entries are performed initially at negative $C_{L_{max}}$. This value must be modified after single-pass entry is assured or the vehicle will experience excessive load factors. The manner in which lift is modified by the control system then determines the maneuverability that is obtained. For ranges greater than 10,000 km, the maximum altitude, h_{max}, attained with undershoot maximum range trajectories, is larger than h_R = 122 km (which results in skip re-entry trajectories); and for ranges greater than 22,000 km, penetration of the inner Van Allen radiation belt takes place since h_{max} > 740 km. Therefore, the particular control technique used to restrict h_{max} becomes the determining factor of maximum undershoot range and therefore "minimum downrange maneuvering capability" as well.

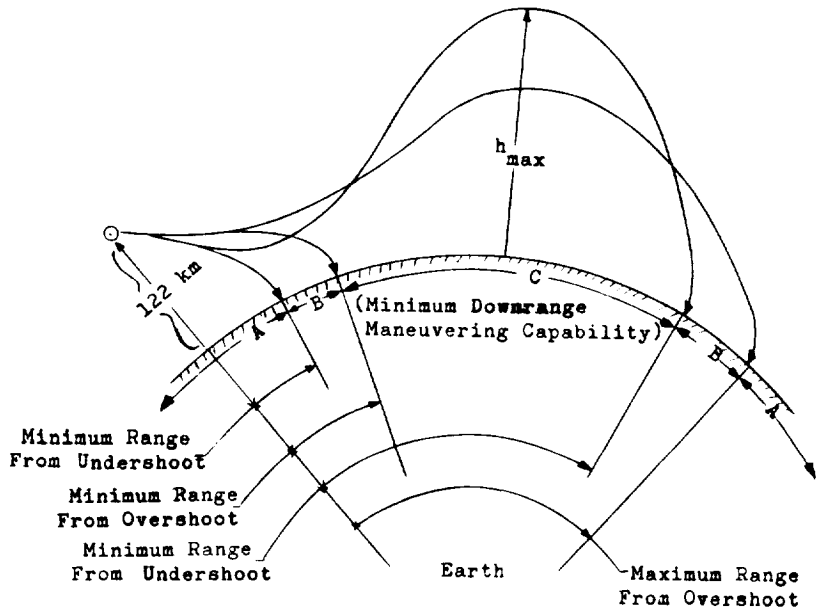

In order to gain an insight to the longitudinal re-entry range capability, Fig. 8 is presented. In this figure, longitudinal range as a function of L/D is shown for the parameter γ_R. The assumptions used in this figure are that V_R = 11 km/sec, W/C_DA = 3350 $\frac{\text{newton}}{\text{m}^2}$ (= 70 lbf/ft^2), h_R = 122 km, and L/D = constant (constant angle of attack trajectory). In addition to the range information, conditions for h_{max} = 122 km and h_{max} = 740 km are shown. It can be seen that the maximum range depends on the allowable h_{max}. Also superimposed on Fig. 8 are the 10-g_0 and 6-g_0 load factor limits which verify that the minimum range obtainable is primarily dependent on the allowable load factor.

b. Lateral maneuverability

The recovery problem implies the ability to return the vehicle to some desired point on the earth's surface. For direct entry from a lunar or deep space mission, considerable variations in re-entry point, re-entry angle, and re-entry plane must be anticipated. The re-entry vehicle must, therefore, not only possess the ability to control its longitudinal range but its lateral or cross range as well. In fact, the lateral range capability of a vehicle during entry may be more important than its longitudinal range capability. Reference 15 shows that under certain conditions a lateral range capability of ±90 km can possibly allow a variation in time of re-entry of more than three hours and variation in re-entry plane inclination i_{VE} of as much as ±13°.

Lateral range is defined as the perpendicular distance measured along the surface of the earth from the landing point to the vertical plane containing the original re-entry trajectory without lateral maneuvers (see sketch).

References 15, 16, 17 and 18 discuss the lateral maneuvering problem and resulting maneuvering envelopes also referred to as "footprints"; the reader is referred to these reports for details. However, for the purposes of this handbook, the following empirical equation is given which estimates the lateral range R_{lat} for constant L/D re-entries:

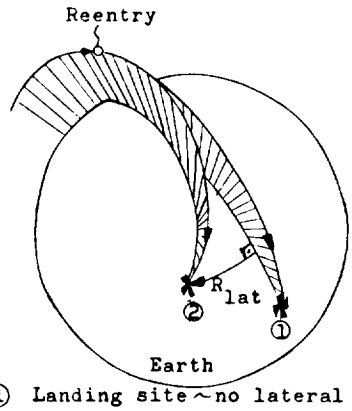

① Landing site ~ no lateral maneuvering
② Landing site ~ with lateral maneuvering
R_{lat} ~ Lateral range

$$R_{lat} = (L/D)\, \ell n\,(V_R)\, R_\oplus \sin \xi \sin \Phi_c + 1150\,(L/D)^{1.78} \sin 2\xi \text{ (km)} \qquad (5)$$

where

$R_\oplus$ = radius of the equivalent spherical earth in km

Φ_c = central angle to impact in degrees

ξ = bank angle in degrees

V_R = the re-entry speed in m/sec

Equation (5) is applicable for bank angles $\xi < 80°$.

For a first order approximation to the maximum lateral range associated with a specific vehicle, the following assumptions can be made (see Ref. 17) $\xi = 45°$, $\Phi_c = 90°$, $V_R = 11$ km/sec, $R_\oplus \simeq 6370$ km which reduces Eq (5) to the following:

$$(R_{lat})_{max} \simeq 1500\,(L/D) + 1150\,(L/D)^{1.78} \text{ (km)} \qquad (6)$$

Equation (6) is shown in Fig. 9 and, as expected, the higher the L/D, the greater the range capability.

Equation (5) can also be used to calculate approximate maneuvering envelopes, but first it is necessary to have consistent values of Φ_c and ξ. This may be achieved by making use of Fig. 8 which gives the longitudinal range capability. If the L/D values shown in Fig. 8 are considered to be the vertical component of L/D, then each of these L/D's can be related:

$$\xi = \cos^{-1} \frac{(L/D)\ \text{Fig. 8}}{(L/D)\ \text{vehicle}}$$

Thus, if a vehicle L/D is selected, Fig. 8 can be interpreted as giving range versus bank angle for various re-entry angles, i.e.,

$$\xi\,(\text{deg}) = \frac{\text{longitudinal re-entry range in km}}{111\ \text{km/deg}} \qquad (7)$$

Now if Eqs. (5), (6) and (7) are used jointly, then approximate maneuvering envelopes similar to the one shown in the next sketch can be generated. This empirical method implies that ξ is established at the time of re-entry.

Two maneuvering envelopes developed by this method are included in Figs. 10 and 11 for $\gamma_R = -5.5°$ and $\gamma_R = -7.75°$, respectively. It should be kept in mind that these envelopes are for re-entries in which bank angles, C_L and C_D, are maintained at constant values throughout the re-entry. The envelopes clearly show the effectiveness of L/D in increasing the size of the maneuvering envelope. By comparing Figs. 10 and 11, an indication of the effect of corridor depth on the envelopes can also be obtained. The lower the $(L/D)_{max}$ of a vehicle, the greater is the reduction in maximum lateral range with increasing corridor depth. This reduction in lateral range is less affected for vehicles with $(L/D)_{max} > 0.5$ (not shown).

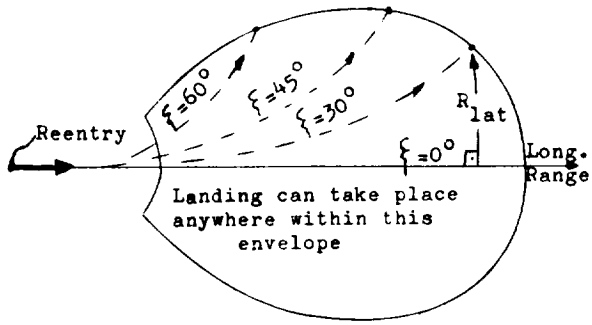

Of course, the information presented here is somewhat restrictive, but the same procedure can be followed to suit specific needs. However, when investigating vehicle capability beyond preliminary stages, it is obvious that such methods are insufficient.

In summary, the more significant factors that influence the maneuvering capability of a given vehicle of fixed $(L/D)_{max}$ are:

(1) A reduction in the maximum allowable load factor increases the minimum longitudinal range a vehicle can achieve. Since the load factor increases with bank angle due to the centrifugal force, there is a limiting bank angle for a given load factor tolerance of the vehicle. The corridor depth decreases with increasing values of the limiting bank angle but the minimum longitudinal range is relatively insensitive to it.

(2) The maximum allowable apogee altitude, h_{max}, limits the maximum range of constant L/D skip trajectories. However, if lift and drag are varied to control atmospheric exit conditions, the restriction on range becomes primarily a function of the $(L/D)_{max}$ of the vehicle. High L/D's allow more modulation or re-entry trajectory shaping than low L/D's.

(3) The minimum allowable dynamic pressure, dictated by a requirement for aerodynamic control, limits the maximum range of some classes of nonexit trajectories.

(4) The range guidance and control technique has a strong influence on the maximum longitudinal and lateral range capability and also on the minimum longitudinal range.

5. Re-entry Guidance Techniques

A vehicle directly entering the earth's atmosphere upon return from a deep space or lunar mission has an enormous amount of kinetic energy. Subsection B-4 demonstrated that during the dissipation of this energy by aerodynamic drag for lifting re-entry vehicles, a certain degree of maneuverability is available after re-entry. This section is concerned with the control of the vehicle's energy to acquire a specific landing site or recovery area without exceeding deceleration or heating limits.

There are a number of possible techniques that may be employed to guide the vehicle to a preselected landing site; they are commonly classified into (1) guidance using a nominal trajectory, implicit techniques, and (2) guidance using predictive capabilities, explicit techniques. A survey of guidance and control methods is given by Wingrove (Ref. 19). The more promising and well-known techniques are listed in the table below, and they are qualitatively discussed in order.

	Group I (implicit)	Group II (explicit)
(1) Reference trajectory techniques	✓	
(2) Linear prediction techniques	✓	
(3) Re-entry optimum trajectory steering technique	✓	
(4) Repetitive prediction steering techniques		✓
(5) Equilibrium glide steering techniques		✓

The above classification does not imply that all guidance techniques fall under only one or the other group.

Before discussing these various techniques it is desirable to understand the relationship of control and trajectory dynamics as seen on the following block diagram taken from Ref. 19. This diagram represents the equations of motion in a simplified form, illustrating the relationship of the control forces to the trajectory variables.

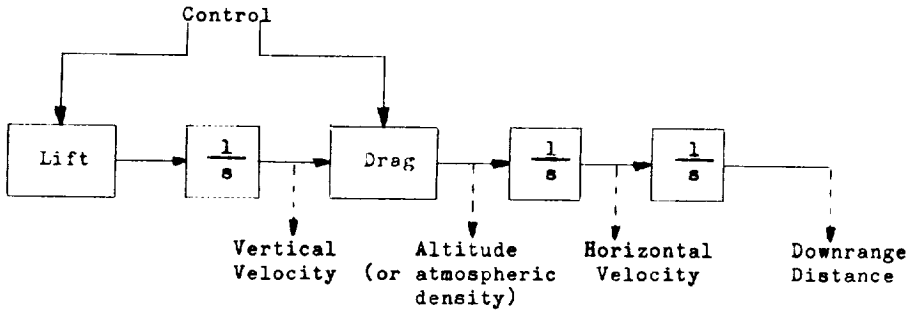

The lift force is essentially in the vertical direction, affecting the rate of change of vertical velocity. The integration 1/s of the vertical velocity gives the variation in altitude (or, what is more important, the variation in atmospheric density). This change in density affects the drag force and thus affects the rate of change of horizontal velocity. An integration of horizontal velocity gives variation in the range along the trajectory.

To control longitudinal range, the rate at which horizontal velocity is changing must be controlled; thus the drag must be controlled. Drag can be regulated principally by either changes in the configuration (i.e., by trim changes or by extending a drag brake) or by changes in atmospheric density. For example, if at any time in the trajectory the range must be extended, the lift force is increased in the vertical direction to raise the vehicle into a less dense atmosphere, thus reducing the rate of change of horizontal velocity and extending the longitudinal range.

The applicability and desirability of any guidance system or technique is weighed by the relative advantages or disadvantages with regard to (1) the ability to handle off-design re-entry conditions, (2) the on-board computer requirements, (3) the

flexibility to maintain trajectories with minimum heating or acceleration, (4) the information the guidance equation gives to the crew if manned.

a. Implicit guidance techniques

In Group I techniques, guidance by use of a nominal trajectory, the trajectory state variables (i.e., V, h, u, R) along the nominal trajectory are precomputed and stored on board. The variations in the measured variables from the stored values are used in guidance either to control the nominal trajectory (path control) or to establish a new trajectory to reach the destination (terminal control).

(1) Reference trajectory technique

This type of guidance method controls re-entry by use of stored reference trajectories. Such systems have been studied extensively for circular re-entries (Refs. 18, 20, 21 through 27) and super-circular re-entries (Refs. 28 and 29). The technique is explained with the aid of the next sketch, from Ref. 29.

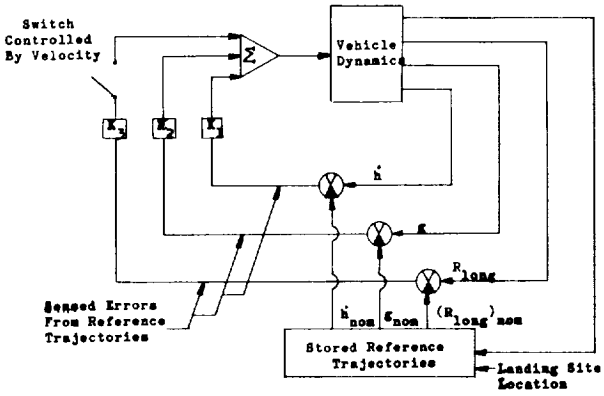

A nominal trajectory, or one in which the vehicle re-enters with the specified conditions, is selected and stored in the control system. During the actual flight, the observed or measured conditions are compared with those of the reference trajectory and the deviation of the observed from the nominal conditions, or the errors, are obtained. In the guidance system these error signals are amplified by constant-gain elements K_1, K_2, K_3 and the sum of the weighted errors is used to specify the L/D to be used to force the actual vehicle conditions to conform to those of the reference trajectory. Typically, feedbacks found to be most effective as an outer loop control were the altitude rate $\dot{h}$, deceleration g and range R.

This is essentially a third-order feedback system. Other measurements that may be used for feedback control are shown in the following chart taken from Wingrove (Ref. 19):

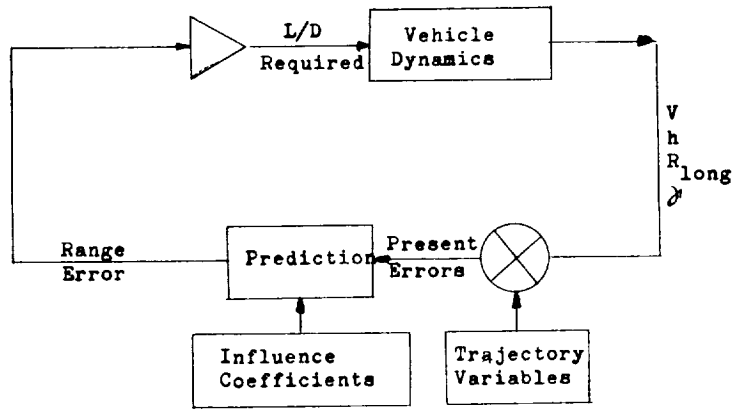

The left column of the chart shows those devices which might be used to sense the various feedback terms.

As is discussed below in Subsection b(2), damping the trajectory is especially important for those velocities greater than circular satellite velocity, where the vehicle can either skip back out of the atmosphere or exceed a given deceleration limit.

This type of guidance technique has the drawback that a large quantity of trajectory data needs to be stored in the airborne computer.

(2) Linear prediction techniques

In addition to the more simplified guidance approach taken above, prediction of critical re-entry quantities has been used (Refs. 29 through 34) to improve or augment the control logic of the reference trajectory approach. The block diagram of a typical linear prediction scheme shown below is from Foudriat (Ref. 29).

The similarity between it and the reference trajectory technique is quite evident. The stored trajectory variables are compared with the present flight conditions and the errors are obtained. However, instead of using a constant weighting function, a set of influence coefficients calculated by the adjoint technique (Ref. 31) is used to predict the effect of these present errors on the end conditions. This predicted final value in range is then used to control the L/D of the vehicle.

Thus, whereas the reference trajectory technique forces the vehicle to fly a single trajectory, the prediction technique selects one of many trajectories which terminate at the desired destination.

This guidance law is only good for the linear region near the nominal trajectory. To handle conditions far removed from the nominal, over-control is needed to assure that the landing site

Measuring Devices	First-Order Feedback	Second-Order Feedback	Third-Order Feedback	Fourth-Order Feedback
Inertial guidance unit or tracking system	Vertical velocity	Altitude	Horizontal velocity	Downrange
Accelerometer	Drag acceleration rate	Drag acceleration	Integration of drag acceleration	Second integration of drag acceleration
Temperature sensor	Atmospheric or skin temperature rate	Atmospheric or skin temperature	--	--
Pressure Sensor	Atmospheric pressure rate	Atmospheric pressure	--	--

remains within the maneuvering capability of the re-entry vehicle. Also overcontrol is needed because the prediction may be in error because of navigational errors, atmospheric density variations, aerodynamic trim variation of re-entry vehicles, and other uncertainties. The overcontrol can be achieved by multiplying the $\delta(L/D)$ determined by the sensitivity coefficients by a constant gain factor K ($K > 1$). Thus the control equation is:

$$\text{Control } (L/D) = (L/D)_{\text{nominal}} + K\ \delta(L/D) \quad (8)$$

It should be pointed out that the prediction of supercircular re-entry range suffers from a problem similar to that for the reference trajectory; that is, the control of range in the supercircular portion will cause the vehicle to skip out of the atmosphere. At present, no solution has been obtained which avoids this.

(3) Re-entry optimum trajectory steering technique

Since published work is somewhat limited in this area, only a cursory discussion is given here.

An ideal guidance scheme should determine the trajectory which minimizes the heat input to the body surface, constrain the flight path to one having acceptable acceleration limits and specified landing position and finally, provide signals to the control system to accomplish such a re-entry trajectory. This technique is similar in some respects to the linear prediction scheme given above except that the gains of the control system are optimized.

A promising technique for achieving such an optimum guidance system employs the calculus of variations. In past years, resort to variational techniques for providing guidance equations has been practically impossible due to the complicated nature of the indirect methods and their associated split boundary conditions. Tedious iteration schemes are an unfortunate necessity for obtaining extremal paths by the indirect methods of variational calculus.

Recently, several breakthroughs have occurred which show promise of applying direct methods of variational calculus to future guidance systems. Nearly simultaneously, Kelly (Refs. 35 and 36) and Bryson, et al. (Refs. 35 through 38) published methods incorporating direct variational techniques for obtaining extremal solutions with an associated reduction in computing time. Both methods make use of the system of equations adjoint to the small perturbation equations about a nominal trajectory. This adjoint system yields influence coefficients which, in turn, correct the nominal trajectory in an optimum fashion. Convergence of the method to the true optimum is accomplished by "steepest descent" methods. Other work in this area is found in Refs. 39 and 40.

These direct variational methods are actually linearized solutions to the Mayer problem of the indirect method of the calculus of variations. The approximation involves replacing the nonlinear trajectory equations of motion by a nominal trajectory and a linear, small perturbation system of equations. The adjoint of equations of the direct method corresponds to the Euler-Lagrange equations of the indirect method and the influence coefficients in the direct method correspond to the Lagrange multipliers in the indirect method. The significant advantage of the direct method is its ability to determine near optimum solutions in relatively few computer cycles.

To apply a direct variational technique to the re-entry vehicle, an on-board computer would be programmed to determine the lift commands which, in turn, would be inputs to the control system. Boundary conditions consisting of position, rate and attitude data would be provided to the computer by either on-board sensing devices or ground control links. To account for errors in the system (primarily input position and rate data), the trajectory could be continually optimized from the vehicle's present position to the desired landing site. The system would become increasingly accurate as the landing site is approached. The significant advantage of this technique lies in its ability to guide the vehicle in a manner which would optimize some pertinent trajectory parameter such as minimizing the heat input to the body, minimizing flight time, etc.

All implicit guidance techniques have the disadvantage of the limited amount of information available for pilot displays. Available pilot information depends on the particular guidance equations used, and implicit guidance techniques give information only with respect to the nominal trajectory at the particular time and not the future trajectory. This problem of pilot display can be eliminated if explicit guidance techniques are used as discussed in the next subsection, B-5b.

b. Explicit guidance techniques

Studies of guidance techniques employing fixed trajectories about which perturbations are made, have indicated that a successful landing from circular velocity can be accomplished if the deviations of the actual initial conditions of entry are close enough to the values stored in a computer memory, and if a sufficient number of perturbation variables are employed in the computation. This approach is inherently limited, however, to the variety of initial conditions and degree of trajectory diversification capable of being stored in the computer memory.

In Group II techniques, or explicit guidance techniques using predictive capabilities, a number of trajectories within the typical maneuver boundary can be chosen. From observed or measured trajectory variables the guidance system predicts continuously the trajectory by which the vehicle will reach the desired landing site without exceeding design limits and without the use of a stored nominal trajectory. An explicit guidance technique is desirable inasmuch as the re-entry guidance system will be required to handle wide variations in abort and earth return conditions and also considerable deviation from established atmospheric standards. In addition to increased flexibility, a continuous prediction system affords an advantage in its direct application to a display of predicted flight conditions and hazardous situations to the pilot in a manner in which maximum control is afforded.

The main problem with any continuous-prediction technique is the complexity of the equations employed to mechanize the prediction. To maintain accuracy and speed in spite of limited input information and restrictive amounts of computing equipment, a satisfactory compromise must be realized.

(1) Repetitive prediction steering technique

Perhaps the most feasible technique thus far proposed is the repetitive prediction steering technique studied by Foudriat (Ref. 29), Wingrove and Coate (Ref. 41), and Bryant and Frank (Ref. 8).

Additional studies of this technique may be found in Refs. 40, 42 and 43.

This technique involves, essentially, a fast solution of the simplified approximate equations of motion of the vehicle during re-entry. By inserting a desired L/D ratio and solving these equations for range, a comparison may be made between the predicted range and the actual range as determined in the guidance computer, and appropriate changes can be made in vehicle angle of attack in order to bring the predicted range in line with that desired. If this operation can be accomplished with sufficient speed, genuine closed-loop range control is possible. Studies conducted thus far indicate that such a system is feasible.

The complete equations of motion for a vehicle entering the earth's atmosphere are by nature complex and difficult to solve even with large high-speed digital computers. The feasibility of in-flight solution of these complete equations for the purpose of controlling range, deceleration and heat absorption becomes questionable because of the restrictions placed upon the size and complexity of airborne computers. It is, therefore, both mandatory and desirable to simplify the mathematical and computational requirements of the re-entry guidance and control technique.

For example, this simplification can be accomplished by Chapman's method which has reduced the equations of motion to a single, ordinary, nonlinear differential equation of second order by rejecting terms which contribute only negligibly to the solution and by the introduction of a transformation of variables (see Subsection B-1), and the method has been developed further by Bryant and Frank (Ref. 8).

Assumptions. The assumptions made in the development of the Chapman equation restrict its application to a particular range of altitudes and initial conditions which are, however, within the range of extremes predicted for lunar missions. The basic assumptions used in the development of the simplified equation of motion are repeated below:

(1) Atmosphere and planet are spherically symmetric.

(2) Variations in atmospheric temperature and molecular weight with altitude are negligible compared to any variation in density.

(3) Rotational rate of the earth and its atmosphere are negligible compared to the velocity of the vehicle.

(4) The small change in distance from the center of the earth is negligible compared to the fractional change in velocity in a given increment of time.

(5) The flight path angle γ is sufficiently small so that the component of drag is large compared to the component of lift in the horizontal direction.

Predictions of longitudinal and lateral range for flight within the atmosphere are obtained by the following equations (Ref. 8), respectively.

$$R_{long} = \frac{R_\oplus}{\sqrt{\beta r}} \int_{\bar{u}_i}^{\bar{u}_f} \frac{\cos\gamma \cos\Delta A}{Z} \, d\bar{u} \qquad (9)$$

$$R_{lat} = \frac{R_\oplus}{\sqrt{\beta r}} \int_{\bar{u}_i}^{\bar{u}_f} \frac{\cos\gamma \sin\Delta A}{Z} \, d\bar{u} \qquad (10)$$

where the symbols have been defined in Subsection B-1, and where ΔA is the change in azimuth from the initial re-entry trajectory plane

$$\Delta A = \int_{\bar{u}_i}^{\bar{u}_f} \left[\frac{C_L \sin \Phi_c}{C_D \bar{u}} + \frac{\cos\Delta A \cos\gamma \tan (R_{lat}/R_\oplus)}{Z\sqrt{\beta r}} \right] d\bar{u} \qquad (11)$$

where Φ_c is the longitudinal re-entry range (from the point of re-entry to the landing site).

Equation (10) was first used in Ref. 17 and its solution determines the range traveled over the earth's surface, measured normal to the initial re-entry trajectory plane. The load factor or deceleration in units of g_0 along the flight trajectory may be found from:

$$LF = \frac{\sqrt{\beta r}\,\bar{u}Z}{\cos\gamma} \sqrt{1 + \left(\frac{L}{D} - \tan\gamma\right)^2} \, (g_0) \qquad (12)$$

and the total time to re-enter in seconds is given by:

$$t_R = 27 \int_{\bar{u}_i}^{\bar{u}_f} \frac{-\cos\gamma}{\bar{u}Z} \, d\bar{u} \text{ (sec)} \qquad (13)$$

Finally, the total heat absorbed by the re-entry vehicle in kg-cal, measured at the stagnation point on a hemispherical heat shield, is determined by the following equation, as derived by Chapman (Ref. 5):

$$Q_{H\,(\text{convective})} = 4000\, A_H \left(\frac{M}{R_C\, A\, C_D}\right)^{1/2} \cdot \int_{\bar{u}_i}^{\bar{u}_f} \frac{(\bar{u})^{3/2}}{Z^{1/2}}\, d\bar{u} \quad \text{(kg-cal)}$$

where

M = mass of the re-entry vehicle.

A_H = aerodynamic heating reference area.

R_C = radius of curvature of the heat shield.

A = reference area for drag and lift.

This completes the list of equations necessary for that portion of the predicted trajectories that remain within the atmosphere. These equations are applicable only to atmospheric flight, because of limitations imposed by the assumption that $|\, dr/r \,| << |\, du/u \,|$ which can be shown to be equivalent to restricting the minimum value of Z in Eqs (3) and (4). This minimum value of Z is approximately 0.001, which corresponds to an altitude of from 91.44 km to 88.4 for velocities between 11 km/sec and 7.8 km/sec; in combination with a positive flight path angle, it can be used to define (the initial conditions for) a skip. If, at any time during the evaluation of Eq (4), the magnitude of Z decreases below 0.001, that part of the prediction is terminated. The prediction is completed by matching a Keplerian ellipse to the atmospheric exit conditions (γ_e, $\bar{u}_e$) calculated at $Z = Z_{min}$, which are simultaneously initial conditions for the skip portion of the trajectory.

The following Keplerian orbit equations are then used to compute the ballistic or skip portion of the trajectory:

Central angle

$$\beta_e = \tan^{-1}\left[\tan \gamma_e \left(\frac{\bar{u}_e^{\,2}}{\bar{u}_e^{\,2} - 1}\right)\right] \qquad (14)$$

Longitudinal range during ballistic flight $(R_{long})_b$

$$(R_{long})_b = 2\, R_\oplus \left[\pi - \beta_e\right] \qquad (15)$$

where β_e is measured in radians in Eq (15)

Ballistic flight lateral range $(R_{lat})_b$

$$(R_{lat})_b = R_\oplus \left\{\sin^{-1}\left[\sin i \sin(\Delta + \beta_e)\right]\right\} \qquad (16)$$

where

$$i = \cos^{-1}\left[\cos \Delta A_b \cos (R_{lat})_b / R_\oplus)\right] \qquad (17)$$

and

$$\Delta = \sin^{-1}\left[\cos (R_{lat})_b / R_\oplus) / \sin i\right] \qquad (18)$$

where ΔA_b is the change in azimuth during ballistic flight.

The apogee radius r_{max} is determined for each skip trajectory by the following Keplerian orbit expression:

$$r_{max} = R_\oplus \left\{\frac{\bar{u}_e^{\,2}}{1 - \left[1 - \bar{u}_e^{\,2}\left(2 - \frac{\bar{u}_e^{\,2}}{\cos^2 \gamma_e}\right)\right]^{1/2}}\right\} \qquad (19)$$

The solution of Eqs (14) through (19), therefore, provides the predicted values of longitudinal and lateral range for the skip or ballistic portion of the trajectory.

These values for ballistic flight are added to the range traveled up to the final conditions for the ballistic portion ($Z = Z_{min}$) to obtain a predicted range from the vehicle's present position to the point of second entry following the skip. Since the second re-entry occurs with a velocity less than circular--and at flight path angles on the order of -3° to -5°--it is relatively simple to determine the vehicle's maneuvering potential. General statements concerning vehicle performance in this part of the trajectory can be made with some confidence. For this reason, constant values of longitudinal and lateral range are added to the skip range to account for the second re-entry. These constant values can be determined so that they are approximately centrally located in the vehicle's maneuver envelope.

The total values of predicted longitudinal and lateral range are obtained by adding ranges for the atmospheric, the ballistic (if any), and the fixed second re-entry portions of the trajectory. The reader is referred to Ref. 8 for details on guidance computer mechanization.

This approach, in addition to providing a maximum allowable margin of error for the skip maneuver, greatly reduces the numerical integration load on the computer, inasmuch as integration need be provided only for a comparatively small portion of the trajectory when the point of atmospheric exit during the first re-entry is being predicted. The saving in time can be well spent in providing either more predictions per second or in decreasing the integration step size thereby increasing prediction accuracy.

The use of Chapman's equation makes the control of skip trajectories feasible, even in light of the extreme sensitivities involved in control of ballistic flight exit (or second re-entry) conditions.

Longitudinal range control can be achieved for all entries in the prescribed lunar-return guidance corridor, except along the absolute overshoot boundary, where longitudinal range is limited to 9300 km or less. In addition, accurate control of lateral range is possible with a fixed-angle-of-attack vehicle by controlling the direction of the roll angle commanded for longitudinal range control.

No knowledge of the vehicle's altitude or of the atmospheric properties is needed for accurate range control. The system has been found to operate successfully, even when comparatively large variations in atmospheric density and vehicle lifting characteristics are imposed.

The operation of such a guidance system starts with a prediction of the longitudinal range and lateral range that would be obtained if the present vehicle L/D and bank angle ξ were held constant. The location of the predicted landing site is compared with that of the desired landing site and a second prediction is made for a larger or smaller value of ξ or L/D. The bank angle and attitude commands are transmitted to the autopilot and maintained until the next prediction is made at which time the entire procedure is repeated.

(2) Equilibrium glide steering technique

When considering explicit guidance techniques for re-entry, one of the more obvious selections is based on the concept of equilibrium glide. This technique has several features which recommend its investigation:

(1) The relationship between range and velocity is simple.

(2) It has been studied extensively for subcircular re-entries.

(3) The range-velocity relationship suggests that it may be applicable to supercircular velocities.

The application of the basic equilibrium glide equation to supercircular speeds has also been studied (Ref. 44). Although it can be shown that the same equation is applicable at this speed, one must use it to steer the vehicle to a target which is associated with a velocity slightly greater than $\bar{u} = 1$. Unfortunately small perturbations away from the equilibrium glide conditions at supercircular velocity are divergent in nature rather than convergent, as in the subcircular case. This is readily seen from the equation of frequency for a perturbed trajectory $\omega_n^2 = \beta r \frac{(1 - \bar{u}^2)}{(D/W)^2}$. From the term $(1 - \bar{u}^2)$, the trajectory oscillations possess static stability below circular velocity ($\bar{u} < 1$) and are statically unstable for $\bar{u} > 1$. Stability augmentation techniques must be added to prevent this divergence. Some method of transition, such as constant altitude, from supercircular to subcircular equilibrium glide must also be provided.

The use of the equilibrium glide technique for re-entries appears feasible, but longitudinal range reduction (in comparison with those techniques which provide a skip capability) and increased total convective heat transfer are characteristics of this approach.

If the application of the equilibrium glide principle to the re-entry guidance of a lunar vehicle is considered, then several guidance laws are required, each one being applicable to a segment of the total re-entry trajectory. That portion of the trajectory when the vehicle decelerates from approximately 99.5% of circular orbital velocity to approximately Mach 5 is considered first, then the application of the equilibrium glide principle to the supercircular portion, and finally the control of the skip (if any) is considered.

Subcircular equilibrium glide. A quantitative understanding of the equilibrium glide may be gained by considering a dynamic system of the re-entry vehicle alone with the vehicle flying in such a way that the lift and the fictitious centrifugal force just balance the gravitational force. Drag is constantly reducing velocity and since both lift and centrifugal acceleration are proportional to velocity squared, they tend to decrease. Lift is also proportional to density, so that the balance can still be maintained with constant L/D if the vehicle descends into denser air as it slows down. This type of flight will be called an equilibrium glide. An equilibrium glide trajectory has the following general characteristics:

(1) Altitude is always decreasing.

(2) Flight path angle is small.

(3) The rate of descent is always increasing at a rate which is small compared to lift/mass.

(4) Lift and drag coefficients are constant.

(5) Velocity is always decreasing.

The equilibrium glide has a number of properties which make it especially attractive as a tool in re-entry guidance, namely

(1) Altitude is a function only of velocity and lift coefficient.

(2) Since the heating rate is assumed to depend only upon velocity and atmospheric density, it too is a function only of velocity and lift coefficient.

(3) The distance traveled between any two velocity states depends only upon the velocities and the lift/drag ratio.

(4) Explicit and simple expressions for the above relationships can be derived.

(5) All constant L/D trajectories (subcircular velocity) approach equilibrium glide as time progresses because of natural damping of vertical oscillations. This permits the application of the equilibrium glide expression to the latter portion of any constant L/D trajectory.

If equilibrium glide conditions exist, i.e., the lift plus centrifugal force balances the gravitational force, the atmospheric density will be a function only of velocity for any given lift coefficient. Knowing the relationship between atmospheric density and altitude, we can plot a family of altitude versus normalized velocity ($\bar{u}$) curves for various lift coefficients. A family of such curves is illustrated in the following sketch.

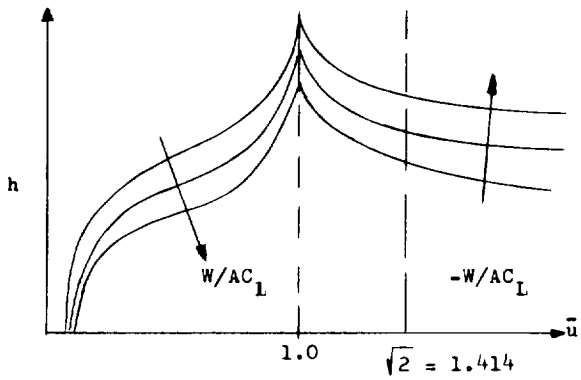

Suppose that, at a given velocity and lift coefficient, the vehicle is above the altitude shown in the sketch. Then, its lift will be less than if it were on the equilibrium curve because the density will be lower. However, the vehicle cannot remain at this altitude because gravity will reduce the altitude. Moreover, drag will be lower at the higher altitude so that velocity will drop more slowly. Hence, the slope of the altitude versus velocity curve will change in such a way as to bring the vehicle toward the equilibrium curve. This effect may be viewed as a feedback action tending to keep the vehicle on an equilibrium glide. This reasoning leads to the hypothesis that the equilibrium glide is a physically realistic as well as mathematically convenient type of trajectory.

Supercircular equilibrium glide. The equilibrium glide concept has been developed from the study of re-entry vehicle behavior at velocities less than circular orbit velocity. The possibility of extending this concept into the supercircular velocity region now suggests itself. In this region the centrifugal force exceeds the gravitational force and negative lift is needed to balance the vertical forces. Negative lift can be obtained either by flying a lifting body upside down or trimming at negative angles of attack.

As the vehicle decelerates from parabolic velocity to circular orbital velocity on such an equilibrium glide, the centrifugal acceleration drops from 2g to 1g while the lift acceleration changes from -1g to zero. Thus, to maintain the balance of forces, lift will always be numerically less than the centrifugal force. Because of this, and because both lift and centrifugal acceleration are proportional to velocity squared, altitude must increase as the vehicle decelerates. In this respect, the supercircular equilibrium glide differs from the subcircular case. As a consequence of this difference, maximum heating rate occurs at maximum velocity in the supercircular glide.

One of the most desirable properties of the subcircular equilibrium glide (the tendency of any constant L/D trajectory to approach equilibrium conditions) is absent in the supercircular region. In fact the tendency is just the opposite. This behavior is illustrated by supposing that, at a given velocity and lift coefficient, the vehicle is above the altitude shown in sketch. Then its lift will be numerically less than it would be if it were on the equilibrium curve because the density will be lower. The lift, which is negative, is then insufficient to balance the centrifugal acceleration and the vehicle rises even farther from the equilibrium curve. Thus, although the forces are in equilibrium when the vehicle is on the curve, any disturbance in the equilibrium causes the vehicle to rise or fall at an ever-increasing rate. In this sense, flight at constant negative lift coefficient is inherently unstable in altitude. The significance of these rates of divergence is that the control system must be faster than these rates if damping of the divergence is to be obtained. In other words, the guidance system must incorporate stability augmentation at supercircular velocities. In this velocity region the guidance system functions in such a way as to bring the vehicle over a specified point on earth at a specified $\bar{u}$ (which would be approximately 1.0005). The guidance system calculates the L/D command needed to do this, which together with the actual rate of climb and actual lift and drag accelerations, is incorporated into an error function which changes angle of attack in such a way as to bring the vehicle onto an equilibrium glide at the command L/D.

The equilibrium glide concept is not applicable at circular speed. Between $\bar{u} = 1.05$ and $\bar{u} = 0.995$ a different type of trajectory, possibly constant altitude, is desirable.

Skip range control. The range covered after re-entry can be substantially increased by skipping out of the atmosphere and re-entering a second time. The behavior of the vehicle outside the atmosphere can be described by the relatively simple and closed form equations of a Keplerian orbit. Thus, if the desired point of re-entry is specified, the desired path angle at exit can be calculated from the vehicle's velocity and position at exit. The atmosphere does not end abruptly, so the exact instant of exit is undefined. This difficulty is overcome by continuously maintaining the flight path angle at a value such that, if the atmosphere should disappear at that instant, the vehicle would follow the Keplerian orbit to the re-entry point. The required path angle changes with time, and aerodynamic forces are required to bring about the change. As the vehicle gains altitude, the available aerodynamic force diminishes. It should be clear that the accuracy of such a system need only be within the maneuvering capability of the vehicle from the initial conditions of the second re-entry. This is true since it is proposed that equilibrium glide control be used to control range during the second entry.

In the actual use of such a system, the range to the target, based on expected re-entry conditions, would be used to select the skip mode or supercircular equilibrium glide mode of control prior to re-entry. If the skip mode is selected, a subsequent switch to equilibrium glide must be made

prior to the second re-entry.

In addition it appears that this particular technique is easily adapted to a closed form predictive system. Instead of integration of the equations of motion, the closed-form system employs an approximate explicit solution in which all or part of the possible trajectories are considered.

The major drawback of the discussed explicit guidance techniques is the fact that the equations of motion and the equations for controlling the re-entry trajectory must be simplified considerably in order to permit closed-form solutions. Great care must be taken in not simplifying the equations too much for too large a portion of the total re-entry trajectory, so that not enough maneuverability remains to acquire the landing site with the remaining maneuverability of the vehicle during the final portion of the trajectory. The maneuverability envelope or footprint, decreases drastically with altitude and velocity as the re-entry progresses and the kinetic energy of the vehicle has been progressively diminished, and there is a constant danger of missing the desired landing site.

C. RE-ENTRY BY ROCKET DECELERATION OR A COMBINATION OF ATMOSPHERIC AND ROCKET DECELERATION

Atmospheric deceleration requires that a large portion of the kinetic energy of the vehicle be converted to heat. An alternative method that can be used is to reduce the kinetic energy of the space vehicle to that of a circular earth orbit by application of rocket thrust or a combination of atmospheric deceleration and rocket thrust. This latter method has the major disadvantage of requiring additional fuel, tankage or even extra rocket engines for the deceleration. However, its advantages include that actual earth re-entry can be performed from satellite speeds and is consequently simpler, and the lateral and longitudinal maneuverability of the vehicle can be limited if the provisions (attitude control fuel, life support equipment, etc.) allow the space vehicle to remain in earth orbit until the landing site rotates with the earth into a favorable position relative to the vehicle.

Perhaps the simplest rocket deceleration technique consists of a direct reduction of the speed of approach of the transearth trajectory to circular satellite speed. An estimate of the fuel requirements for this maneuver can be obtained by assuming the approach speed of the vehicle as parabolic and that the required velocity reduction ΔV occurs impulsively. The difference between the parabolic and circular speeds at the radius r then gives the necessary velocity reduction:

$$\Delta V = V_p - V_c = \sqrt{\frac{2\mu}{r_0}} - \sqrt{\frac{\mu}{r_0}} \simeq 0.414 \sqrt{\frac{\mu}{r_0}} \qquad (20)$$

Figure 12 gives ΔV as a function of mass ratio $\zeta = \frac{M_f}{M_0}$ where M_f is the required fuel mass, M_0 is the initial mass of the vehicle, for various orbital altitudes $h_0 = r_0 - R_\oplus$, where $R_\oplus$ is the radius of the equivalent spherical earth. The mass ratios ζ were computed from the rocket equation

$$\Delta V = g_0 I_{sp} \ln\left(\frac{\zeta}{1 - \zeta}\right) \qquad (21)$$

for fuel specific impulses I_{sp} = 300 sec and I_{sp} = 400 sec. The figure shows that the fuel expenditure for a pure rocket deceleration maneuver is very high and not too practical for the early lunar vehicles. Thus, a 22,000-newton re-entry vehicle requires approximately 11,500 newtons fuel for circularizing maneuvers with I_{sp} = 400 sec and about 12,600 newtons fuel with I_{sp} = 300 sec.

More fuel economy can be achieved if a combination of atmospheric and rocket deceleration is used to achieve the parking orbit as suggested by Sommer and Short (Ref. 9). In this combination technique, the atmosphere is re-entered briefly to take advantage of atmospheric deceleration. However, the vehicle is subsequently guided out of the atmosphere. (See sketch below.)

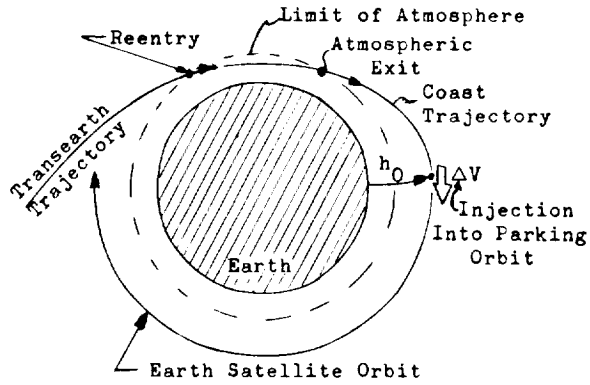

After exit with velocity, V_e, the vehicle coasts to the apogee of the Keplerian orbit, which is controlled by the exit velocity, where an accelerating velocity impulse ΔV is applied. This maneuver ensures that re-entry does not take place on the descending arm of the coast trajectory, but that the vehicle continues in the circular parking orbit until the landing site is in a favorable position with respect to the satellite.

To allow a direct comparison of the two rocket deceleration techniques, Fig. 13 gives the mass ratio ζ for circularizing the Keplerian coast trajectory for atmospheric exit velocities ranging from 7300 m/sec to 7900 m/sec for three parking orbit altitudes h_0 = 740, 555, and 370 km and for two values of specific impulse, I_{sp} = 400 sec and 300 sec. The results of the calculations shown in the figure indicate that if the vehicle is guided to exit velocities equal to or a little greater than circular satellite velocities, the fuel weight penalty is kept within practical bounds. For example, for a 22,000-newton re-entry vehicle, approximately 1500 newtons of fuel are required for the circularizing maneuver at h_0 = 740 km.

Both the technique of pure rocket deceleration and that of combined rocket and atmospheric deceleration require an additional impulse to deorbit

from the parking orbit. This impulse varies with the parking orbit altitude and the allowable dispersions from the nominal re-entry trajectory due to dispersions in atmospheric density and the variations in aerodynamic performance of the re-entry vehicle. Typically, for deorbit altitudes below 300 km, a high deorbit pulse with $\Delta V_d \simeq$ 500 m/sec will bring the vehicle in steeply and quickly with little dispersions and less maneuvering capability but higher deceleration, while a low deorbit pulse with $\Delta V_d \simeq 100$ m/sec results in a long glide with long re-entry times, large dispersions and higher heating. Any reduction in velocity below $\Delta V_d \simeq 100$ m/sec results in dispersions which may be a very significant portion of the total re-entry vehicle maneuvering capability. For deorbit altitudes above 300 km, the corresponding values of deorbit ΔV_d are probably slightly larger and the re-entry range is somewhat longer for the same limiting values of γ_R, the flight path angle at re-entry, which define the re-entry corridor.

The re-entry from the parking orbit altitude which occurs from satellite orbital velocities has been discussed fully, both from a theoretical and numerical standpoint, in Chapter IX of Ref. 1.

An important problem in maneuverable re-entry vehicle performance is the ability to recall the vehicle to a specified landing site after the vehicle has been decelerated to the circular orbit velocity. Both the orbital phase and the descent phase contribute to the determination of call-down frequency tables which may be regarded as a measure of vehicle performance. Such tables are useful for answering typical parking orbit design questions such as:

(1) What orbital characteristics are needed to have call-down on a certain revolution for a given landing site and maneuvering capability?

(2) How long is the waiting time for recall at any time during the parking orbit phase.

(3) How much do dispersions in initial conditions and orbital dispersions affect the call-down frequency?

(4) What combinations of orbital, vehicle, and landing site parameters allow vehicle recall once a day, once every three days, or some other time period?

The need to obtain call-down frequencies quickly, preferably by use of a digital computer, is obvious.

Orbital trajectory calculations can be found in Chapters III and IV of Ref. 1, while the re-entry has been discussed to some extent in the present chapter and specifically for re-entry from satellite orbital speeds in Chapter IX of Ref. 1. However, as indicated above, the design of parking orbit parameters for earth return requires the combination of the orbital and descent phases. This can be accomplished in two ways:

(1) Integrate the equations of motion numerically as was done by Rosamond (Ref. 45) for instance, who considers the touchdown accuracy of retrorocket recovered satellites (no aerodynamic maneuverability during re-entry) by minimizing the effect of rocket burnout errors, which are initial conditions in our case, through proper selection of the deorbit thrust application.

(2) Use the results of general perturbation theories during the orbit phase (Refs. 46, 47 and Chapters IV and V of Ref. 1 to give but a very few), together with re-entry results as given here in Chapter IX of Ref. 1, and by Mandell (Ref. 48)). This approach has been taken by Jensen, Townsend, et al. (Ref. 49), but these authors restrict themselves to polar orbits or arbitrarily inclined orbits with small lateral maneuverability. An improved version of this method suitable for hand calculation has been given in Chapter IX of Ref. 1.

The intent of the present discussion is to give a general method for obtaining call-down frequencies from circular orbits efficiently and quickly by use of a digital computer through introduction of the concept of ground swath to account for lateral maneuverability. The method is thus the most general; it applies for any orbital altitude, inclination, arbitrarily large lateral and longitudinal maneuverability during re-entry, as well as any launch and landing site location. The call-down equations have been programmed on the IBM 7094 at the Martin Company. Basic assumptions, derivations of the equations, as well as some results are presented below.

1. Assumptions for Computing Call-Down.

a. Initial conditions

Initial conditions, which occur at the end of the rocket burning designed to achieve the circular parking orbit, consist of the geodetic latitude, longitude, and direction of motion at the initial point. Small errors in these quantities, however, should not affect the call-down frequency significantly since the effect of these errors on the deorbit position is not cumulative.

b. Orbital conditions

The satellite is represented by a mass point in a circular orbit with a given inclination i_{VE}, $0° \leq i_{VE} \leq 180°$, and mean radius r_0. The altitude h_0 of the circular orbit is defined as its mean equatorial altitude, i.e.,

$$h_0 = r_0 - R_e, \tag{22}$$

where r_0 is the mean geocentric radius and R_e the equatorial radius of the earth. The major forces acting on the satellite are due to earth oblateness and atmospheric drag. Only secular changes in the satellite orbit will be considered important. Short and long periodic changes due to oblateness and drag as well as the effect of

other gravitational bodies, solar radiation pressure, mass irregularities in the earth, and small thrust forces have been neglected since they do not affect the call-down frequency appreciably.

The main effect of atmospheric drag is to decrease the mean orbital radius and to increase the mean motion. The radius on the j-th revolution r_j is given in terms of quantities in the (j-1)th

$$r_j = r_{j-1} - 4\pi B_{eff} \rho_{j-1} r_{j-1}^2, \qquad (23)$$

where

$$B_{eff} = F_{a0} \frac{\rho \text{ dispersed}}{\rho \text{ standard atmosphere}} \cdot \frac{C_D A}{2M}$$

is the effective ballistic coefficient, $F_{a0}(h, i_{VE})$ the atmospheric oblateness correction factor (Ref. 50), C_D the drag coefficient, A the frontal area of the satellite, M its mass, and ρ the neutral atmospheric density computed from the 1961 U.S. Standard Atmosphere (Refs. 51 and 52).

The factor $\frac{\rho \text{ dispersed}}{\rho \text{ standard atmosphere}}$ was introduced to enable simulation of constant dispersions in atmospheric density from the standard. Drag decay histories for various ballistic coefficients with the option to introduce atmospheric oblateness and dispersions in density can be obtained along with the call-down frequency. The change in period on the j-th revolution corresponding to the decrease in radius is

$$\Delta\tau_j = -\frac{12\pi^2}{\sqrt{\mu}} B_{eff} \rho_{j-1} r_{j-1}^{2.5}, \qquad (24)$$

where $\mu = GM_\oplus$ is the gravitational constant of the earth, G the universal gravitational constant and $M_\oplus$ the mass of the earth.

The secular effects of earth oblateness are summarized by the regression rate of the node,

$$\frac{d\Omega}{dt} = \dot{\Omega} = -540 J_2 \left(\frac{R_e}{r_0}\right)^2 \cos i_{VE}, \qquad (25)$$

where $J_2 = 1082.28 \times 10^{-6}$ is the constant associated with the second zonal harmonic term in the expansion of the earth's gravitational potential, and a correction to the nodal period of the satellite,

$$\Delta\tau_\beta = -\frac{3\pi}{\sqrt{\mu}} r_0^{1.5} J_2 \left(\frac{R_e}{r_0}\right)^2 \frac{7\cos^2 i_{VE} - 1}{4}, \qquad (26)$$

which can be derived from Struble (Ref. 47). The secular oblateness corrections are assumed independent of the secular drag effects, i.e., they are constant in a given parking orbit simulation on the computer.

Small dispersions from nominal in-plane orbit injection conditions can be simulated by introducing a further correction to the period, $\Delta\tau_d$, for k revolutions. These injection dispersions may be significant due to their cumulative effect on the satellite deorbit position.

c. Descent conditions

For a landing of the re-entry vehicle to be possible, the orbital plane has to be "near" the intended landing site and the satellite must be in the "correct" orbital position as given by the central angle from the ascending node. The concepts "near" and "correct" will be described quantitatively in Subsection 2.

The actual physical picture during re-entry is the following: We have a point landing site. There is a re-entry region at orbital altitude from which the re-entry vehicle may reach this point, and all possible re-entry trajectories funnel toward it. Since the earth is roughly spherical and the satellite moves in an almost central force field, the shape of this re-entry region changes considerably with orbital position as well as altitude. For call-down studies, it is much more convenient to use a maneuvering envelope which is independent of orbital position and is defined as the locus of points on earth that can be reached by aerodynamic or thrust maneuvering from a fixed deorbit position which coincides with the instantaneous satellite position. This envelope may be reduced in size by constraints of total heat, maximum heating rate, or estimated dispersions during re-entry. Each point inside and on the envelope can be defined on a nonrotating earth by a longitudinal range in the orbit plane R_{long} from deorbit, and a lateral range R_{lat} perpendicular to the orbit plane, with lateral ranges in the direction of the satellite angular velocity vector considered positive. The point on the nonrotating earth is related to one on a rotating earth by the descent time t_d and the angular velocity of the earth $\omega_\oplus$.

The assumption that the maneuvering envelope is independent of orbital position corresponds to assuming that the effect of atmospheric rotation during re-entry is negligible. We define call-down as the condition when the landing site, which is on a rotating earth, is within the maneuvering envelope of the re-entry vehicle. The altitude-dependence of the maneuvering envelope can be taken into account by introducing several envelopes for the expected deorbit altitude ranges. We assume further that each irregular maneuvering envelope is approximated by several maneuvering rectangles. Two corners of this rectangle are defined by $(R_{long})_{min}$, the corresponding $(t_d)_{min}$, and $(R_{lat})_{max}$ as well as $(R_{lat})_{min}$, respectively. Similarly, the other two corners are given by $(R_{long})_{max}$, $(t_d)_{max}$, $(R_{lat})_{max}$, and $(R_{lat})_{min}$. This definition is possible since t_d is only very weakly dependent on R_{lat}.

A measure of landing site "nearness" is $(R_{lat})_{max}$ and $(R_{lat})_{min}$ which form a ground swath around the satellite ground track. One condition for call-down is that the geocentric parallel of latitude of the landing site ϕ_f' intersect the ground swath (Figs. 14 and 15). The problem of finding this intersection is one of spherical trigonometry: Given the geocentric latitude (or declination) of the landing site ϕ_f', the orbit inclination i_{VE}, and the

lateral range R_{lat}, find the central angle β and inertial longitude λ of the intersection, as measured relative to the same ascending node. The solution of this problem is (Ref. 53, p 42):

$$\sin\beta = \frac{\sin\phi'_f - \cos i_{VE}\sin R}{\sin i_{VE}\cos R}$$

$$\sin\lambda = \frac{-\sin i_{VE}\sin R + \cos i_{VE}\cos R\sin\beta}{\cos\phi'_f}$$

$$\cos\lambda = \frac{\cos R\cos\beta}{\cos\phi'_f} \qquad (27)$$

where R_{lat} is positive in the direction of the orbital angular velocity, and

$$R = \frac{360\ R_{lat}}{2\pi R_e}\ (\text{deg}) \qquad (28)$$

Three possible cases may arise:

(1) Both $(R_{lat})_{max}$ and $(R_{lat})_{min}$ yield $|\sin\beta| > 1$. No intersection occurs and we have either a call-down on each revolution or no call-down at all. These cases can be easily distinguished by the values of ϕ'_f, i_{VE} and R_{lat}.

(2) Either $(R_{lat})_{max}$ or $(R_{lat})_{min}$ yield $|\sin\beta| > 1$. Two intersections occur near the apex, the northernmost or $|\sin\beta| > 1$. Two intersections occur near the apex, the northernmost or southernmost points of the ground track (see Fig. 15). The quadrants of β can be determined easily by the landing latitude and the relative position of the intersection with respect to the ascending node. Call the smaller value β_1, the larger value β_2, and their difference

$$\Delta\beta = \beta_2 - \beta_1 \qquad (29)$$

The quadrants of the corresponding values of λ, λ_1 and λ_2, can be determined by use of Eqs (27), and the condition that they differ at most by one from the quadrant of β. Define:

$$\Delta\lambda = \lambda_2 - \lambda_1 \text{ with } \Delta\lambda > 0 \text{ for } i_{VE} < 90°,$$

$$\Delta\lambda < 0 \text{ for } i_{VE} > 90°. \qquad (30)$$

(3) If both $(R_{lat})_{max}$ and $(R_{lat})_{min}$ yield $|\sin\beta| \leq 1$, then there are four intersections of the landing parallel of latitude with the ground swath. These intersections may be reduced to sets of two intersections by specification of a northerly or southerly approach to the landing site. Each set may now be treated separately with quadrant determination as in Case (2).

If $(R_{lat})_{max} = (R_{lat})_{min} = 0$, then the two ground swath intersections reduce to one ground track intersection which is given by letting sin R = 0 and cos R = 1 in Eqs (27):

$$\sin\beta = \frac{\sin\phi'_f}{\sin i_{VE}},$$

$$\sin\lambda = \frac{\cos i_{VE}\sin\beta}{\cos\phi'_f}, \quad \cos\lambda = \frac{\cos\beta}{\cos\phi'_f} \qquad (31)$$

The second factor in determining call-down, the "correct" orbital position, is of more importance than the correct time of deorbit, since the longitudinal range in the orbit plane imposes constraints on the location of the deorbit point. The lateral maneuverability of the re-entry vehicle offers some flexibility in the choice of deorbit point as given by $\Delta\beta = \beta_2 - \beta_1$ in Figs. 14 and 15, but in most cases this is not enough to counteract reentry atmospheric dispersions, guidance and control system errors and timing errors in the deorbit point due to density dispersions in orbit. Especially in near-polar orbits, when $\Delta\beta \to 0$, additional longitudinal range is necessary to overcome these factors and to add somewhat to the call-down frequency by imposing less severe constraints on the deorbit point location. The quantitative evaluation of the correct orbital position will be deferred until the next section.

2. Derivation of the Call-Down Conditions

There are two equations for determining call-down, one giving the position of the orbit plane with respect to the landing site and the other giving the satellite position in orbit. In each case there are conditions that have to be met for call-down to take place. The longitudinal range capability of the re-entry vehicle places constraints on the satellite position, while the lateral range capability places constraints on both orbit plane and satellite position. In the following, these equations and constraints will be derived and a method for obtaining call-down frequencies from those two equations and three constraints will be given.

Consider the angular displacement in longitude of the initial point as measured from the vernal equinox, an inertial reference direction (see Fig. 16),

$$\omega_\oplus t_0 = \Omega_0 - \lambda_0 + \lambda_1, \qquad (32)$$

where: t_0 is the initial time; λ_0 the longitude; and ϕ'_0 the geocentric latitude of the initial point; $\omega_\oplus$ the rotational rate of the earth about its axis, $\omega_\oplus = 4.178074 \times 10^{-3}$ deg/sec; Ω_0 the longitude of the ascending node at the initial time; and λ_1 the longitude of the initial site with respect to Ω_0. At landing on the m-th day, the angular displacement in longitude is given by (see Fig. 17):

$$\omega_\oplus t_f = \Omega_0 - \lambda_f + 360m + \lambda_1 + \Delta\lambda_M + n\dot{\Omega}, \qquad (33)$$

where the subscript f refers to the landing site,

m is the integral number of sidereal days (1 sidereal day = 86164.1 sec), n the number of orbital revolutions from injection to deorbit, and $\Delta\lambda_M$ the difference in longitude between λ_1 and the landing site. It can be seen from Eq (30) and Fig. 17 that one condition for call-down is

$$0 \leq \Delta\lambda_M \leq \Delta\lambda. \tag{34}$$

Equations (32) and (33) can be combined to yield

$$\omega_\oplus (t_f - t_0) = \lambda_0 - \lambda_f - \lambda_i + 360\,m + n\dot{\Omega} + \lambda_1 + \Delta\lambda_M. \tag{35}$$

The time from the initial point to landing is:

$$t_f - t_0 = n\tau_0 + \sum_{j=0}^{n} (n - j + 1)\Delta\tau_j + k\Delta\tau_d + t_d, \tag{36}$$

where τ_0 is the initial orbital period including oblateness effects and the second term gives the atmospheric drag effects on the period. Now we can solve Eqs (35) and (36) implicitly for n by elimination of $(t_f - t_0)$ between them to obtain:

$$n = \frac{\lambda_0 - \lambda_f - \lambda_i + 360\,m + \lambda_1 + \Delta\lambda_M}{\omega_\oplus (\tau_0 - \frac{\dot{\Omega}}{\omega_\oplus})} - \frac{t_d + k\Delta\tau_d}{(\tau_0 - \frac{\dot{\Omega}}{\omega_\oplus})} - \frac{\sum_{j=0}^{n} (n - j + 1)\Delta\tau_j}{(\tau_0 - \frac{\dot{\Omega}}{\omega_\oplus})}. \tag{37}$$

Another expression can be obtained for n by considering the total central angle from injection to deorbit:

$$n = \frac{\beta_i}{360} + p + \frac{\beta_1}{360} + \frac{\Delta\beta_M}{360} - \frac{R_{long}}{2\pi R_e}, \tag{38}$$

where β_i is the central angle of the initial point, p is the number of revolutions from the ascending node of β_i to the one of β_1, and $\Delta\beta_M$ is the difference in central angle between β_1 and the landing point. Equation (8) and Fig. 4 suggest the second call-down condition:

$$0 \leq \Delta\beta_M \leq \Delta\beta, \tag{39}$$

with a third condition for call-down imposed by the longitudinal maneuverability

$$(R_{long})_{min} \leq R_{long} \leq (R_{long})_{max}. \tag{40}$$

The problem of obtaining call-down frequencies for an orbiting vehicle reduces to solving for the values of n from Eqs (37) and (38) for each value of m, up to the maximum number of days in orbit, q, and subject to the constraints given by Eqs (34), (39) and (40).

However, there are several difficulties. The quantities $\Delta\lambda_M$, $\Delta\beta_M$ and $R_{long.}$ in Eqs (37) and (38) are unknown, as well as the values of n and p for each value of m. In addition, Eq (37) can be solved for n only by an approximation procedure since n occurs in the summation on the right-hand side as well as on the left-hand side.

We propose to determine the lateral maneuvering effectiveness first by considering two cases:

(1) Entry into the ground swath with $\Delta\lambda_M = 0$, $\Delta\beta_M = 0$ in Eqs (37) and (38).

(2) Exit from the ground swath with $\Delta\lambda_M = \Delta\lambda$, $\Delta\beta_M = \Delta\beta$ in the same equations.

The approximation procedure to obtain n consists of transferring the term $-\frac{t_d + k\Delta\tau_d}{(\tau_0 - \frac{\dot{\Omega}}{\omega_\oplus})}$ from Eq (37) to Eq (38), and computing

$$(n_0)_1 = \frac{\lambda_0 - \lambda_f - \lambda_i + 360\,m + \lambda_1}{\omega_\oplus (\tau_0 + \frac{\dot{\Omega}}{\omega_\oplus})} \tag{41}$$

in Case 1 as well as

$$(n_0)_2 = (n_0)_1 + \frac{\Delta\lambda}{\omega_\oplus (\tau_0 - \frac{\dot{\Omega}}{\omega_\oplus})} \tag{42}$$

in Case 2 for each value of m. Here $(n_0)_1$ and $(n_0)_2$ are the number of revolutions from the time the initial point passes through the ground track to the entry and exit of the landing point from the ground swath, respectively. The effects of drag have been neglected in Eqs (41) and (42). However, the values of $(n_0)_1$ and $(n_0)_2$ obtained from Eqs (42) and (43) for a given m permit us to calculate drag effects by replacing n by $(n_0)_1$ and $(n_0)_2$ in the drag term of Eq (37),

$$\Delta n_D = -\frac{\sum_{j=0}^{n} (n - j + 1)\Delta\tau_j}{(\tau_0 - \frac{\dot{\Omega}}{\omega_\oplus})} \tag{43}$$

Now we can compute for each day in orbit

$$(n_0 + \Delta n_D)_1 = \frac{\lambda_0 - \lambda_f - \lambda_i + 360\,m + \lambda_1}{\omega_\oplus \left(\tau_0 + \frac{\dot\Omega}{\omega_\oplus}\right)} - \frac{\sum_{j=0}^{(n_0)_1} \left[(n_0)_1 - j + 1\right] \Delta\tau_j}{\left(\tau_0 - \frac{\dot\Omega}{\omega_\oplus}\right)} \tag{44}$$

and

$$(n_0 + \Delta n_D)_2 = \frac{\lambda_0 - \lambda_f - \lambda_i + 360\,m + \lambda_i + \Delta\lambda}{\omega_\oplus \left(\tau_0 + \frac{\dot\Omega}{\omega_\oplus}\right)} - \frac{\sum_{j=0}^{(n_0)_2} \left[(n_0)_2 - j + 1\right] \Delta\tau_j}{\left(\tau_0 - \frac{\dot\Omega}{\omega_\oplus}\right)} \tag{45}$$

Denote the integral part of $(n_0 + \Delta n_D)_1$ at a given m by I_{m1} and the integral part of $(n_0 + \Delta n_D)_2$ for the same value of m by I_{m2}.

Next we determine the in-plane maneuvering effectiveness by collecting the remaining terms in the other equation. Consider entry of the landing site into the ground swath with minimum longitudinal maneuverability,

$$(n_0 + \Delta n_D)_{1\,\min} = p + \frac{\beta_i + \beta_1}{360} + \frac{(t_d)_{\min} + k\Delta\tau_d}{\left(\tau_0 - \frac{\dot\Omega}{\omega_\oplus}\right)} - \frac{(R_{long})_{\min}}{2\pi R_e}, \tag{46}$$

and its entry into the ground swath with maximum longitudinal maneuverability,

$$(n_0 + \Delta n_D)_{1\,\max} = p + \frac{\beta_i + \beta_1}{360} + \frac{(t_d)_{\max} + k\Delta\tau_d}{\left(\tau_0 - \frac{\dot\Omega}{\omega_\oplus}\right)} - \frac{(R_{long})_{\max}}{2\pi R_e} \tag{47}$$

Similarly, there are two expressions for the exit of the landing site from the ground swath which can be obtained by adding the term $\frac{\Delta\beta}{360}$ to Eqs (46) and (47), respectively. Take the smallest and largest value of the four values of $(n_0 + \Delta n_D)$ just computed and form a range

$$\text{smallest } \left[(n_0 + \Delta n_D) - p\right], \quad \text{largest } \left[(n_0 + \Delta n_D) - p\right]. \tag{48}$$

The additional assumption has been made here that atmospheric drag acts from the initial point to touchdown, i.e., during n_0 revolutions, rather than from injection to deorbit, or during n revolutions. In most practical cases R_{long} is less than one revolution and this assumption will not affect the call-down frequency appreciably. Furthermore, the drag effects on the dispersed elliptic orbit with period $\tau_j + \Delta\tau_d$ should be essentially the same as those on the nominal circular orbit with period τ_j.

The final step consists of combining lateral and in-plane maneuverability to test for call-down at a given m. Let p in Eq (48) vary between

$$(I_{m1} - 3) \le p \le (I_{m2} + 3) \tag{49}$$

and add each of these values of p to Eq (48) to form the seven ranges

$$\text{smallest } (n_0 + \Delta n_D), \quad \text{largest } (n_0 + \Delta n_D) \tag{50}$$

for each p in Eq (49).

Whenever Eq (50) and the range formed by $(n_0 + \Delta n_D)_1$ and $(n_0 + \Delta n_D)_2$ for the same m overlap, there exists a call-down on the day m. Denote each call-down day by $m = m_c$. For each value of $m = m_c$ obtain

$$n_{min} = (n_0 + \Delta n_D)_1 \text{ from Eq (44)} - \frac{(t_d)_{\max} + k\Delta\tau_d}{\left(\tau_0 - \frac{\dot\Omega}{\omega_\oplus}\right)} \tag{51}$$

$$n_{max} = (n_0 + \Delta n_D)_2 \text{ from Eq (45)} - \frac{(t_d)_{\min} + k\Delta\tau_d}{\left(\tau_0 - \frac{\dot\Omega}{\omega_\oplus}\right)} \tag{52}$$

where n is the number of revolutions from the time the injection point intersects the ground track to the time the deorbit point intersects the ground swath, and accounts essentially for lateral maneuverability. However, the controlling factor of satellite call-down is the in-plane maneuverability from deorbit to landing which places a constraint

$$\frac{\beta_1}{360} - \frac{(R_{long})_{\max}}{2\pi R_e}, \quad \frac{\beta_1 + \Delta\beta}{360} - \frac{(R_{long})_{\min}}{2\pi R_e} \tag{53}$$

on the satellite position at deorbit during any revolution. The call-down revolutions can be obtained by (1) converting the revolutions from n, which is measured from injection starting at 0, to N, the number of revolutions from the first as-

cending node, where N = 1.0 and (2) by noting for which integral number of revolutions the fractional range (Eq (53)) overlaps the range formed by N_{min} and N_{max} (Eqs (51) and (52) with n converted to N). There may be more than one call-down revolution per day if $(N_{max} - N_{min}) > 1$, which occurs for large lateral maneuverability and for small lateral maneuverability if the landing site is near the northernmost or southernmost points of the ground track. The resulting call-down table for each $m = m_c$ consists of N, the altitude, and the time in orbit for both n_{min} and n_{max}.

This discussion of call-down frequency ends the qualitative and quantitative description of re-entry which uses at least some rocket deceleration during the earth return trajectory phase. This re-entry technique reduces the demands on the heat shield materials, the guidance accuracy and the aerodynamic performance of the re-entry vehicle itself. On the other hand, a major drawback of this return technique lies in the expenditure of additional fuel and a lesser drawback in the longer time required for completion of the mission.

D. REFERENCES

1. Anon., "Orbital Flight Handbook," ER 12684, Martin Company, Space Systems Division (Baltimore) 1963.

2. Seifert, Howard S., ed., "Space Technology," John Wiley and Sons, New York, 1959. Chapter XII, "Recovery Dynamics--Heat Transfer at Hypersonic Speeds in a Planetary Atmosphere," L. Lees.

3. Chapman, Dean R., "An Approximate Analytical Method for Studying Entry into Planetary Atmospheres," NASA TR R-11, 1959 (supersedes NACA TN 4276).

4. Luidens, Roger W., "Flight-Path Characteristics for Decelerating from Supercircular Speed," NASA TN D-1091, 1961.

5. Chapman, Dean R., "An Analysis of the Corridor and Guidance Requirements for Supercircular Entry into Planetary Atmospheres," NASA TR R-55, 1959.

6. Grant, Frederick C., "Modulated Entry," NASA TN D-452, 1960.

7. Levy, Lionel, L., Jr., "Atmosphere Entries with Spacecraft Lift-Drag Ratios Modulated to Limit Decelerations," NASA TN D-1427, 1962.

8. Bryant, J. F. and Frank, M. P., "Supercircular Re-entry Guidance for a Fixed L/D Vehicle Employing a Skip for Extreme Ranges," ARS Paper 2489-62, 1962.

9. Sommer, Simon C. and Short, Barbara J., "Point Return from a Lunar Mission for a Vehicle that Maneuvers Within the Earth's Atmosphere," NASA TN D-1142, 1961.

10. Grant, Frederick C., "Importance of the Variation of Drag with Lift in Minimization of Satellite Entry Acceleration," NASA TN D-120, 1959.

11. Grant, Frederick C., "Analysis of Low-Acceleration Lifting Entry from Escape Speed," NASA TN D-249, 1960.

12. Wong, Thomas J. and Slye, Robert E., "The Effect of Lift on Entry Corridor Depth and Guidance Requirements for the Return Lunar Flight," NASA TR R-80, 1960.

13. Wang, H. E. and Chu, S. T., "Variable-Lift Re-entry at Superorbital and Orbital Speeds," Aerospace Corp Report TDR -930 (2570-20) TN-2, May 1962 (IAS Paper 62-165, 1962).

14. Galman, Barry A., "Direct Re-entry at Escape Velocity," GE-MSVD TIS R60SD357, April 1960 (AAS Preprint 60-86, August 1960).

15. Bossevain, Alfred G., "The Effect of Lateral and Longitudinal Range Control on Allowable Entry Conditions for a Point Return from Space," NASA TN D-1067, 1961.

16. Baradell, Donald L., "Lateral Range Control by Banking During Initial Phases of Supercircular Re-entries," NASA TN D-1511, 1962.

17. Slye, Robert E., "An Analytical Method for Studying the Lateral Motion of Atmosphere Entry Vehicles," NASA TN D-325, 1960.

18. Young, John W., "A Method for Longitudinal and Lateral Range Control for High-Drag Low-Lift Vehicle Entering the Atmosphere of a Rotating Earth," NASA TN D-954, 1961.

19. Wingrove, Rodney C., "A Survey of Atmosphere Re-entry Guidance and Control Methods," IAS Paper No. 63-86, 1963.

20. Reismann, H. and Pistiner, J. S., "Design and Evaluation of a Re-entry Guidance System," Astronautica Acta, Vol. VI, Fasc 2-3, July 1960, pp 79 to 114.

21. General Electric Company, "Flight Control Study of a Manned Re-entry Vehicle," WADD Technical Report 60-695, Vols. I and II, July 1960.

22. Cheatham, D. C., Young, J. W. and Eggleston, J. M., "The Variation and Control of Range Traveled in the Atmosphere by a High-Drag Variable-Lift Entry Vehicle," NASA TN D-230, 1960.

23. Teague, Roger, "Flight Mechanics of Re-entry After Flight by Means of Various Lifting Techniques," NASA MNN-M-AERO-4-60, 1960.

24. Shahan, R. L., "Re-entry Guidance for Manned Spacecraft," paper presented at

ARS-IRE, 15th Annual Technical Conference, Cincinnati, Ohio, April 1961.

25. Friedenthal, M. J., Love, J. A. and Neustadt, L. W., "Feasibility Study of an Acceleration Monitoring Guidance System for Lifting Re-entry Vehicles," STL Report 9572-0006-MU-000, October 1961.

26. Edge, C. F. and Hechtman, E. P., "Control Loop Simulation for Energy Management," Proc Aerospace Forum II Session, IAS Meeting, New York, 22 to 24 January 1962.

27. Wingrove, Rodney C. and Coate, Robert E., "Lift-Control During Atmosphere Entry from Supercircular Velocity," Proc IAS National Meeting on Manned Space Flight, St. Louis, Missouri, 30 April to 2 May 1962.

28. Wingrove, Rodney C., "A Study of Guidance to Reference Trajectories for Lifting Re-entry at Supercircular Velocity," NASA TR-151, 1963.

29. Foudriat, Edwin C., "Guidance and Control During Direct-Descent Parabolic Re-entry," NASA TN D-979, 1961.

30. Webber, A. L., "Investigation of the Instrumentation of an Atmospheric Re-entry," Report T-218, MIT Instrumentation Laboratory, September 1959.

31. Foudriat, Edwin C., "Study of the Use of a Terminal Controller Technique for Re-entry Guidance of a Capsule-Type Vehicle," NASA TN D-828, 1961.

32. Rosenbaum, Richard, "Longitudinal Range Control for a Lifting Vehicle Entering a Planetary Atmosphere," ARS Preprint 1911-61, August 1961.

33. Bryson, Arthur E., and Denham, Walter F., "A Guidance Scheme for Supercircular Re-entry of a Lifting Vehicle," ARS Preprint 2299-61 (ARS Journal, Vol. 32, June 1962. pp 894-8).

34. North, Raymond, and Speyer, Jason, "Control System for Supercircular Entry Maneuvers," IAS Paper 62-3, January 1962.

35. Kelly, H. J., Kapp, R. E., and Moyer, H., "Successive Approximation Techniques for Trajectory Optimization," IAS Symposium on Vehicle System Optimization, November 28 to 29, 1961.

36. Kelly, H. J., Gradient Theory of Optimal Flight Paths, ARS Journal Vol. 30, pp 947 to 953, October 1960.

37. Bryson, A. E., Denham, W. F., Carroll, F. J., and Mikami, Kinya, "Determination of Lift or Drag Programs to Minimize Re-entry Heating," Journal of the Aero/Space Sciences, Vol. 29, No. 4, April 1962.

38. Bryson, A. E., and Denham, W. F., "A Steepest Ascent Method of Solving Optimum Programming Problems," Raytheon Co., Missile and Space Division, Report BR-1303, August 1961.

39. Speyer, J. L., "Optimization and Control Using Perturbation Theory to Find Neighboring Optimum Paths," presented at the SIAM Symposium on Multivariable Linear Control System Theory, Boston, Mass., November 1 to 2, 1962 (to be published in series on control of the Society for Industrial and Applied Mathematics).

40. "A Study of Energy Management Techniques for a High Lift Vehicle," General Electric Company, Air Force Systems Command Technical Documentary Report ASD-TDR-62-77, Vols. 1 and 2, June 1962.

41. Wingrove, Rodney C., and Coate, Robert, E., "Piloted Simulator Tests of a Guidance System Which Can Continuously Predict Landing Point of a Low L/D Vehicle During Atmosphere Re-entry," NASA TN D-787, 1961.

42. Dow, Paul C., Jr., Fields, Donald P., and Scammell, Frank H., "Automatic Re-entry Guidance at Escape Velocity," ARS Preprint 1946-61, August 1961.

43. Lear, Inc., "A Study of Selected Control-Display Problems for Manned Aerospace Vehicles," Lear Engineering Report GR-1405, ASD Technical Report, March 1962.

44. Hildebrand, R., "Manned Re-entry at Supersatellite Speeds," IAS Paper No. 60-83, 1960.

45. Rosamond, D. L., "Satellite Recovery Techniques for Optimization of Touchdown Accuracy," Journal of the Aero/Space Sciences, Vol. 28, No. 3, March 1961.

46. Kozai, Y., "The Motion of a Close Earth Satellite," Astronomical Journal, Vol. 64, No. 9, November 1959.

47. Struble, R. A., "The Geometry of the Orbits of Artificial Satellites," Archive for Rational Mechanics and Analysis, Vol. 7, No. 2, 1961.

48. Mandell, D. S., "Maneuvering Performance of Lifting Re-Entry Vehicles," ARS Journal, Vol. 32, No. 3, March 1962.

49. Jensen, J., Townsend, G. E., Kork, J., Kraft, J. D., "Design Guide for Orbital Flight," McGraw-Hill, New York, 1962.

50. Lee, V. A., "Atmosphere-Oblateness Correction Factor for Circular Satellite Orbits," ARS Journal, Vol. 32, No. 1, January 1962.

51. Cole, A. E., Court, A., Kantor, A. J., "Standard Atmosphere Revision to 90 km," Geophysics Research Directorate, Air Force

Research and Development Command, Bedford, Mass., 28 March 1961.

52. Champion, K. S. W., and Minzner, R. A., "[illegible] Revision of United States Standard Atmosphere, 90-700 km," Geophysics Research Directorate, Air Force Research and Development Command, Bedford, Mass., 11 December 1961.

53. Chauvenet, W., "A Manual of Spherical and Practical Astronomy," Vol. 1, Dover Publications, Inc., New York, 1960.

ILLUSTRATIONS

Figure	Title	Page
1	Pericynthion Altitude & Reentry Range Versus Time of Lunar Month to Land at Australia & Edwards AFB.	X-29
2	Operational Corridor Defined	X-30
3	Effect of Entry Velocity on Corridor Depth	X-31
4	Correlation of the Maximum Reduction in Peak Deceleration with the Aerodynamic Resultant-Force Coefficient	X-32
5	Modulation Effectiveness for Lifting Vehicles	X-33
6	10-g_0 Undershoot Corridor Boundaries for an Entry Velocity of 10.7 km/sec Lift Modulated from $C_{L_{max}}$ to $C_L = 0$	X-34
7	Single Pass Overshoot and 10-g_0 Maximum Undershoot Corridor Boundaries for a Reentry Velocity of 10.7 km/sec	X-35
8	Longitudinal Range Capability	X-36
9	Estimated Maximum Lateral Range for Super-Circular Reentry	X-37
10	Maneuvering Envelope	X-38
11	Maneuvering Envelope	X-39
12	Fuel Required for Rocket Deceleration from Parabolic to Circular Velocity	X-40
13	Fuel Required to Obtain a Circular Orbit as a Function of Exit Velocity and Specific Impulse of Fuel for a Combination Rocket and Aerodynamic Deceleration.	X-41
14	Southerly Approach to a Landing (Case 3 of Descent Conditions)	X-42

ILLUSTRATIONS (continued)

Figure	Title	Page
15	Approach to a Landing Near the Northern Most Point of the Satellite Ground Track (Case 2 of Descent Conditions	X-43
16	Displacement in Longitude at the Initial Time	X-44
17	Displacement in Longitude at Landing	X-45

Fig. 1. Pericynthion Altitude & Reentry Range Versus Time Of Lunar Month To Land At Australia & Edwards AFB

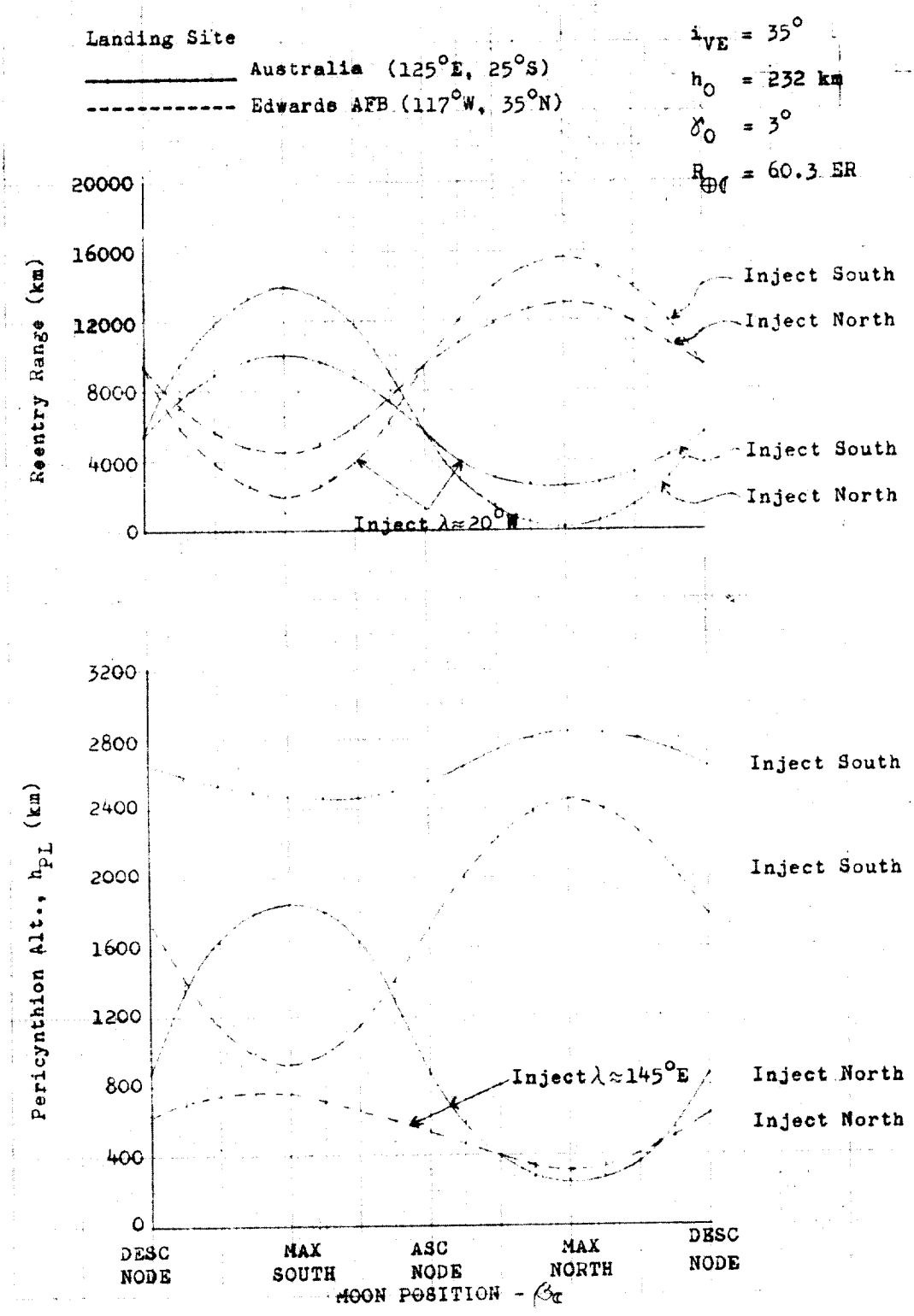

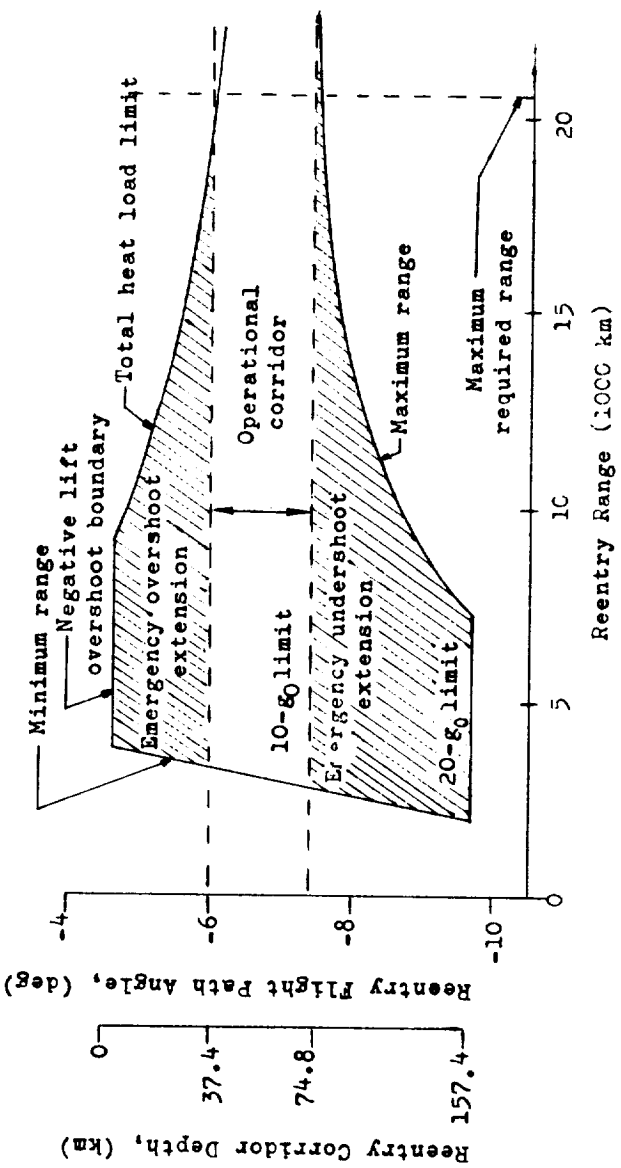

Fig. 2. Operational Corridor Defined

Fig. 3. Effect Of Entry Velocity On Corridor Depth

(10-g_0 Max. Undershoot Boundary Unmodulated)

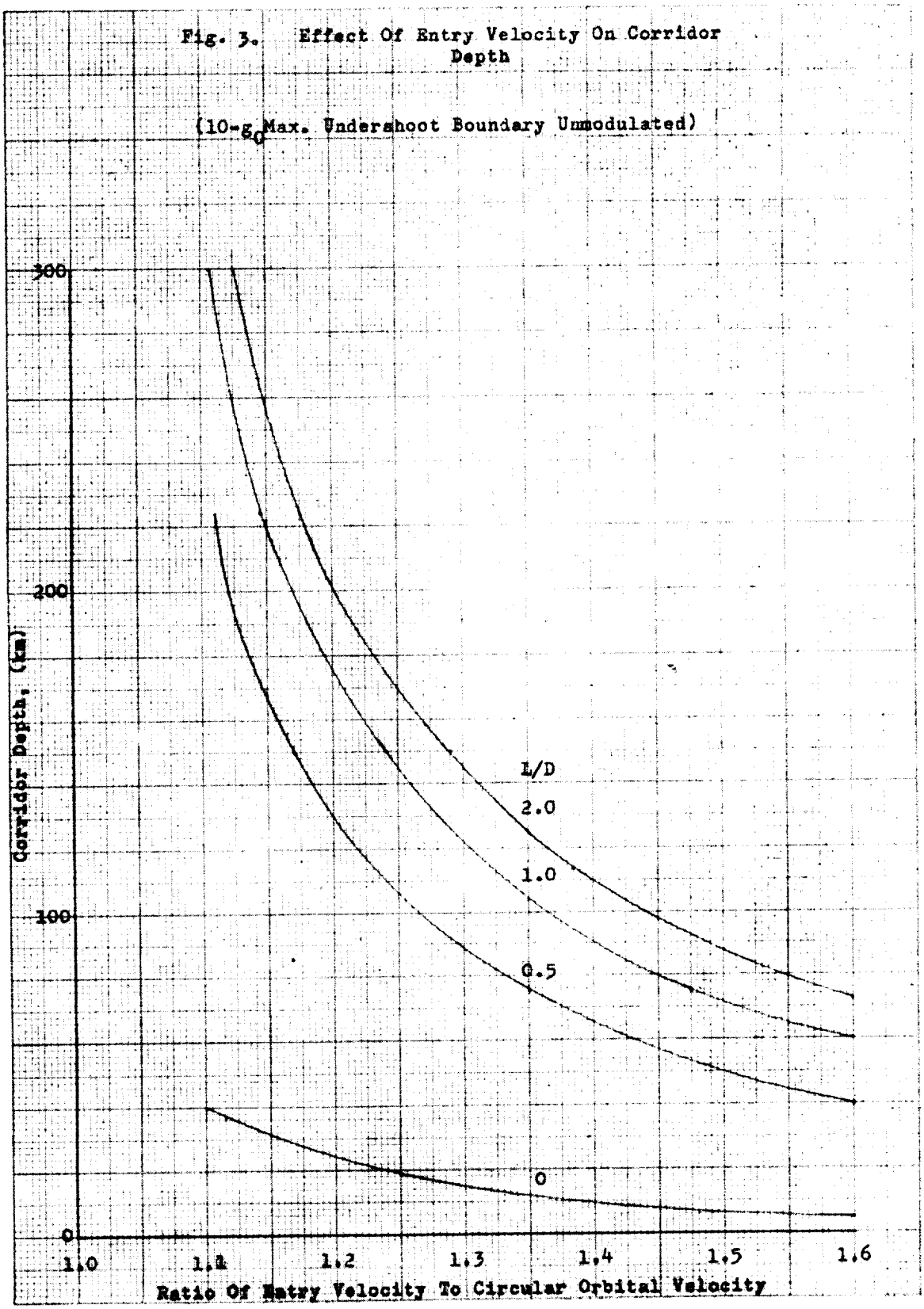

Fig. 4. Correlation Of The Maximum Reduction In Peak Deceleration With The Aerodynamic Resultant-Force Coefficient

Reentry Conditions:

h_R = 122 km

$-5.7^\circ > \gamma_R > -9.2^\circ$, $(L/D)_{unmod.} = (L/D)_{max}$, $(L/D)_{mod.}$ = L/D at $C_{L_{max}}$,

315 kg/$_{m^2}$ < M/C_DA at $(L/D)_{max}$ < 6600 kg/$_{m^2}$

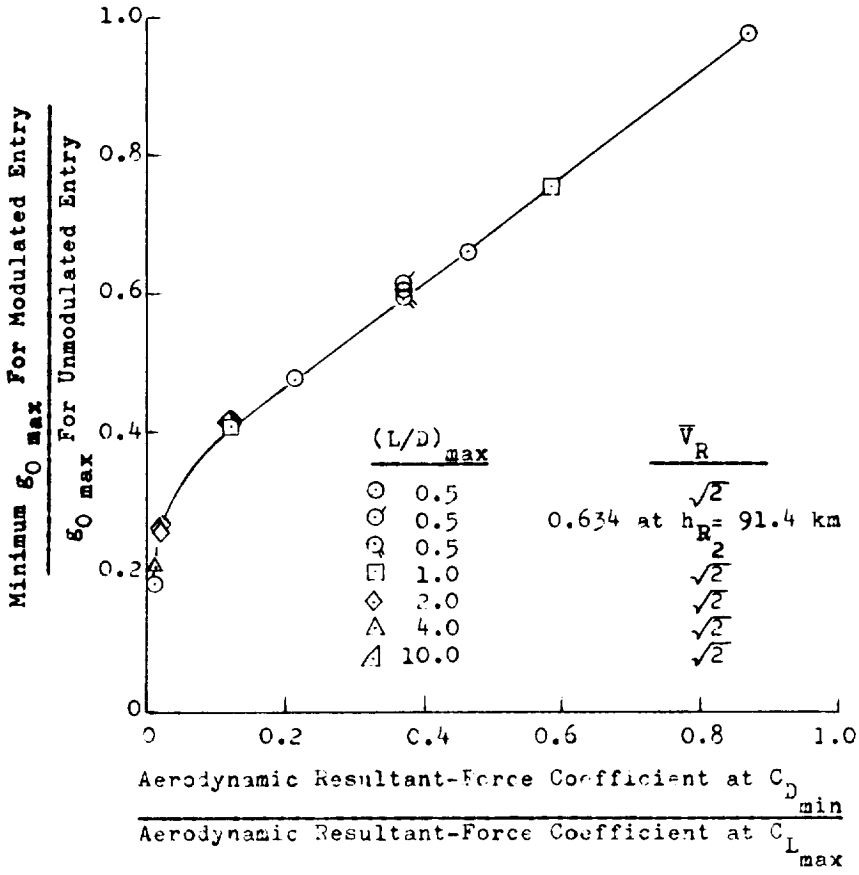

Fig. 5. Modulation Effectiveness For Lifting Vehicles

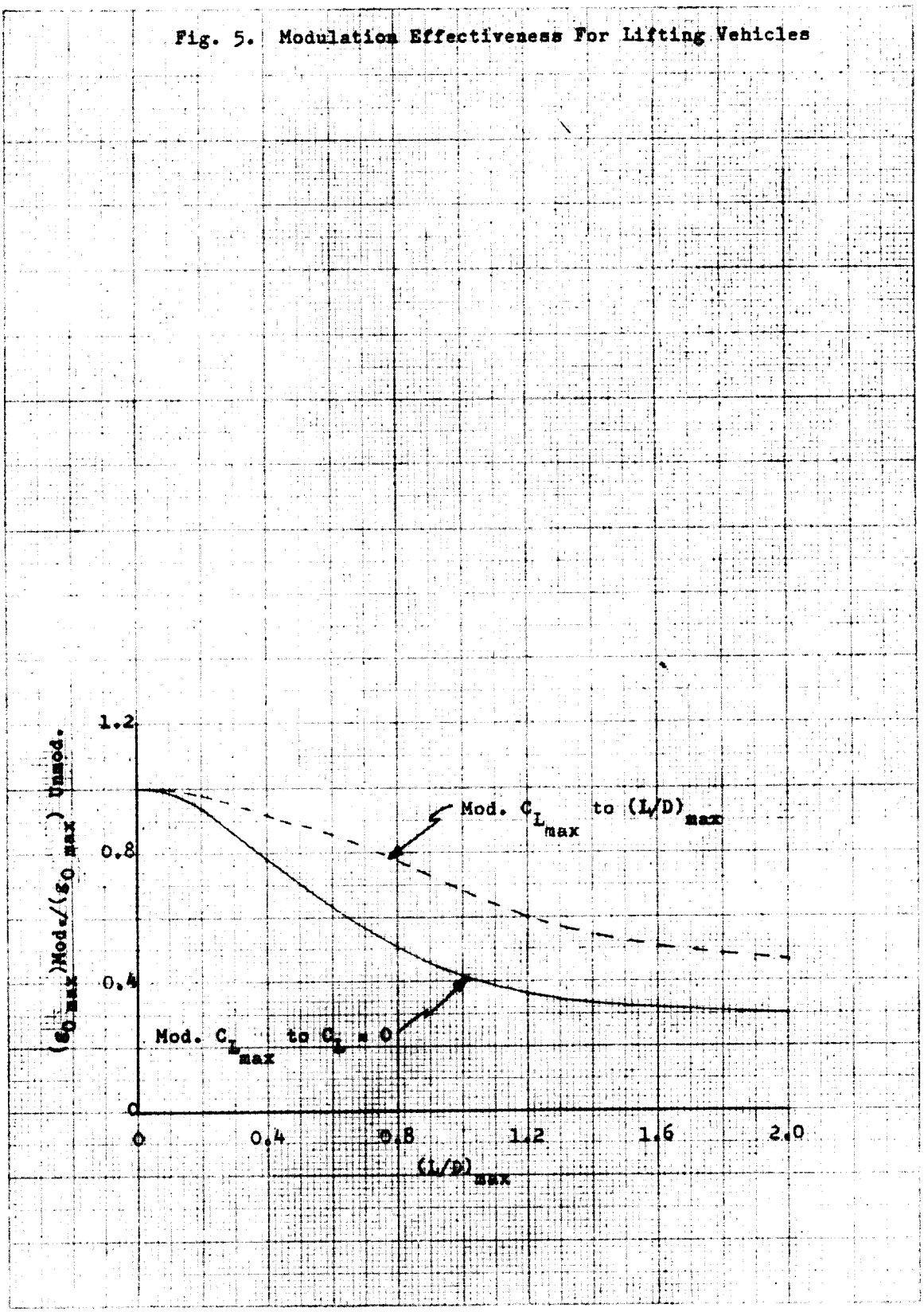

Fig. 6. Lunar Undershoot Corridor Boundaries for an Entry Velocity of 10.7 km/sec Lift Modulated From $G_{L_{max}}$ to 0
UNDERSHOOT
OVERSHOOT
VACUUM PERIGEE ALTITUDE, (KM)
FLIGHT PATH ANGLE AT 122 KM

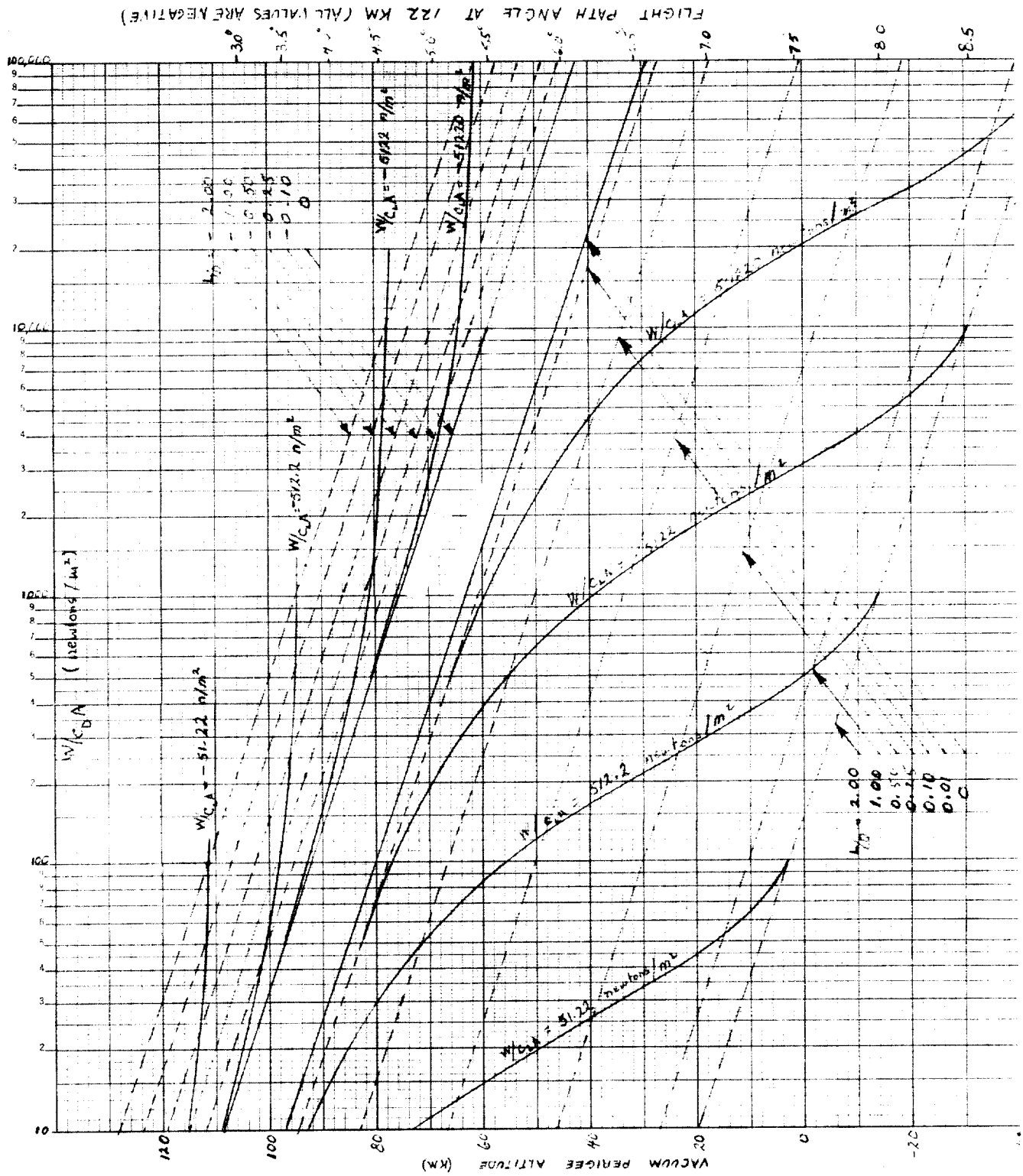

Fig. 7. Single Pass Overshoot and 10-g_0 Maximum Undershoot Corridor Boundaries For a Reentry Velocity of 10.7 km/sec

Fig. 8. Longitudinal Range Capability

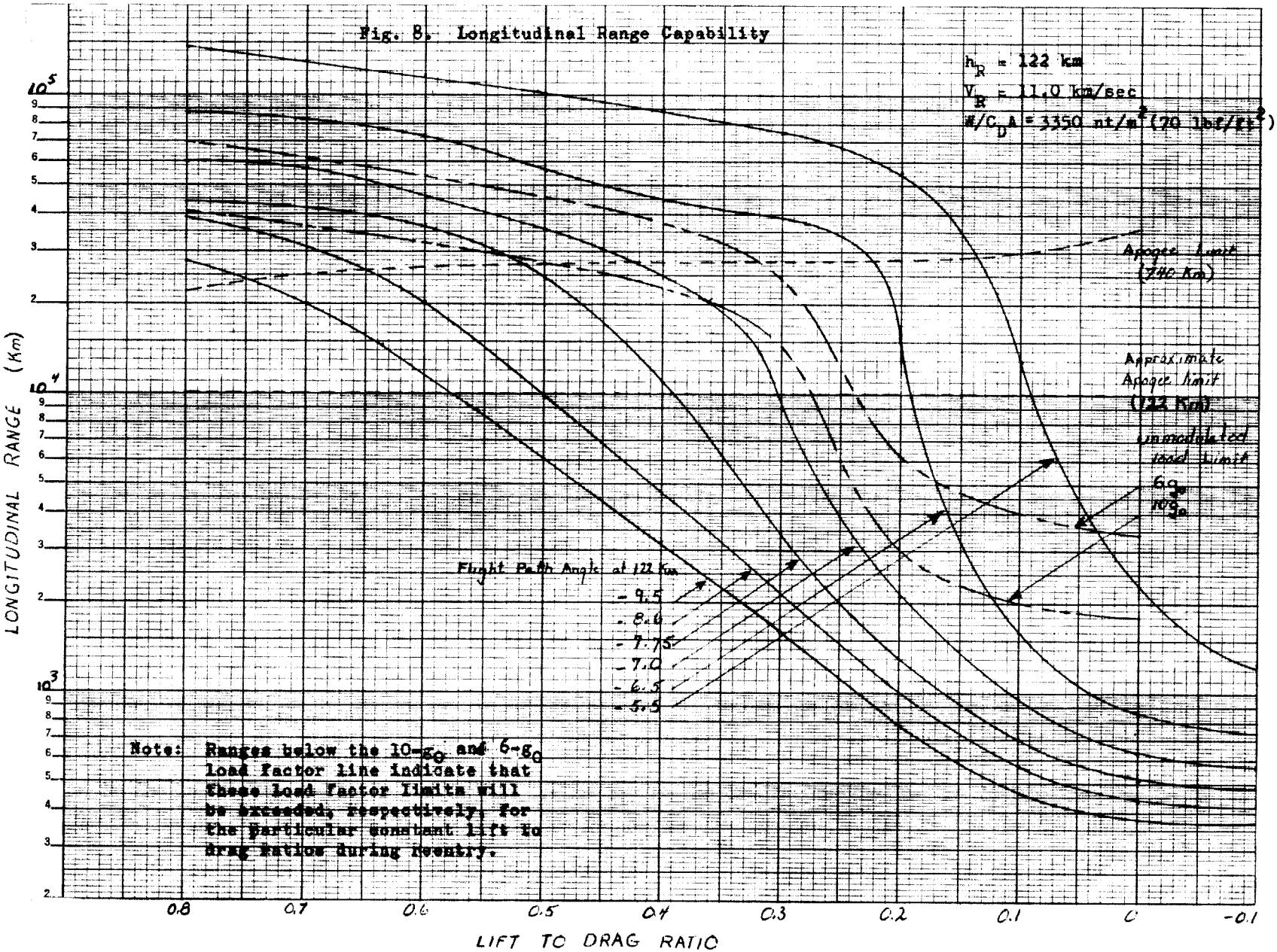

Fig. 9. Estimated Maximum Lateral Range For Super-Circular Reentry

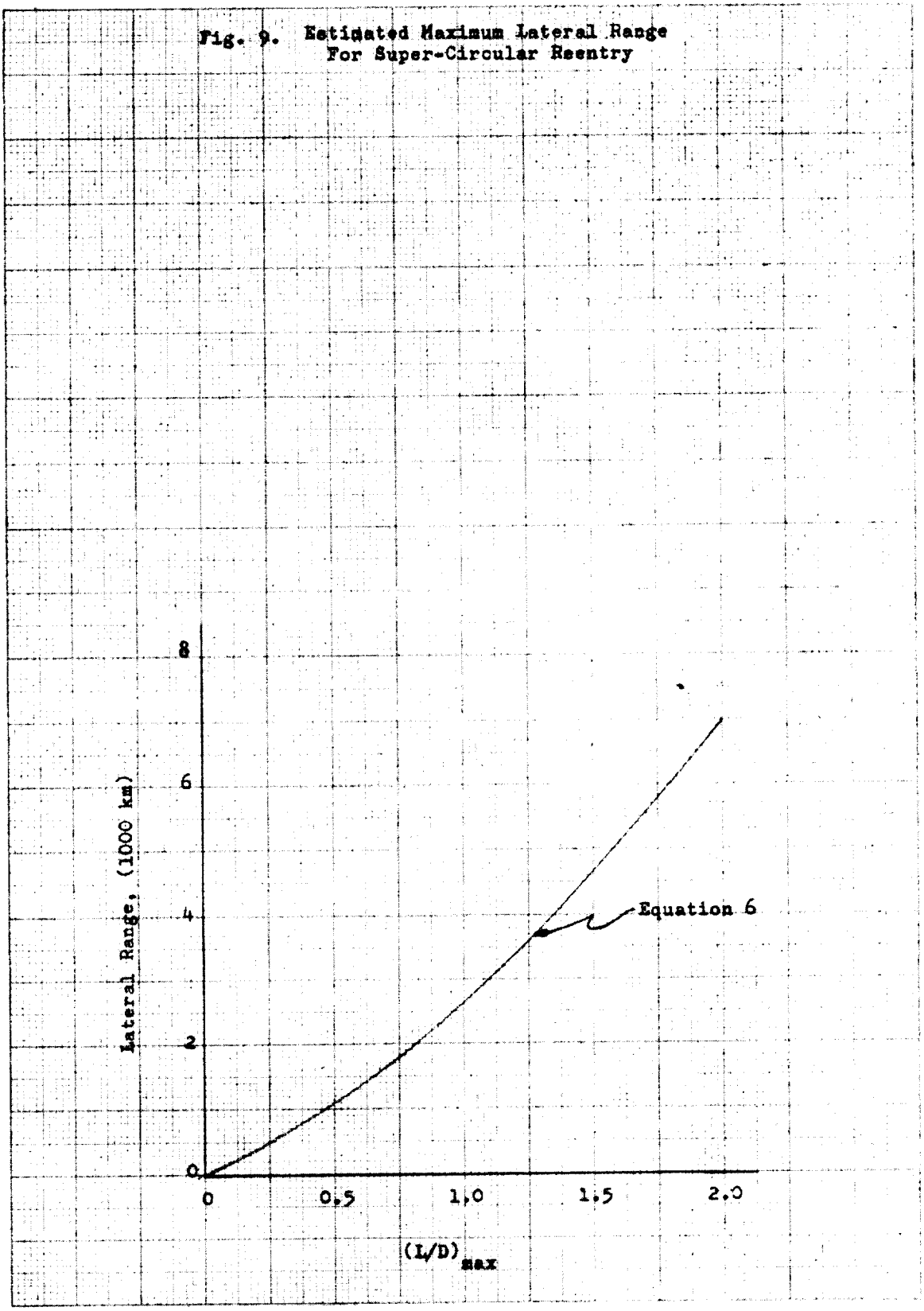

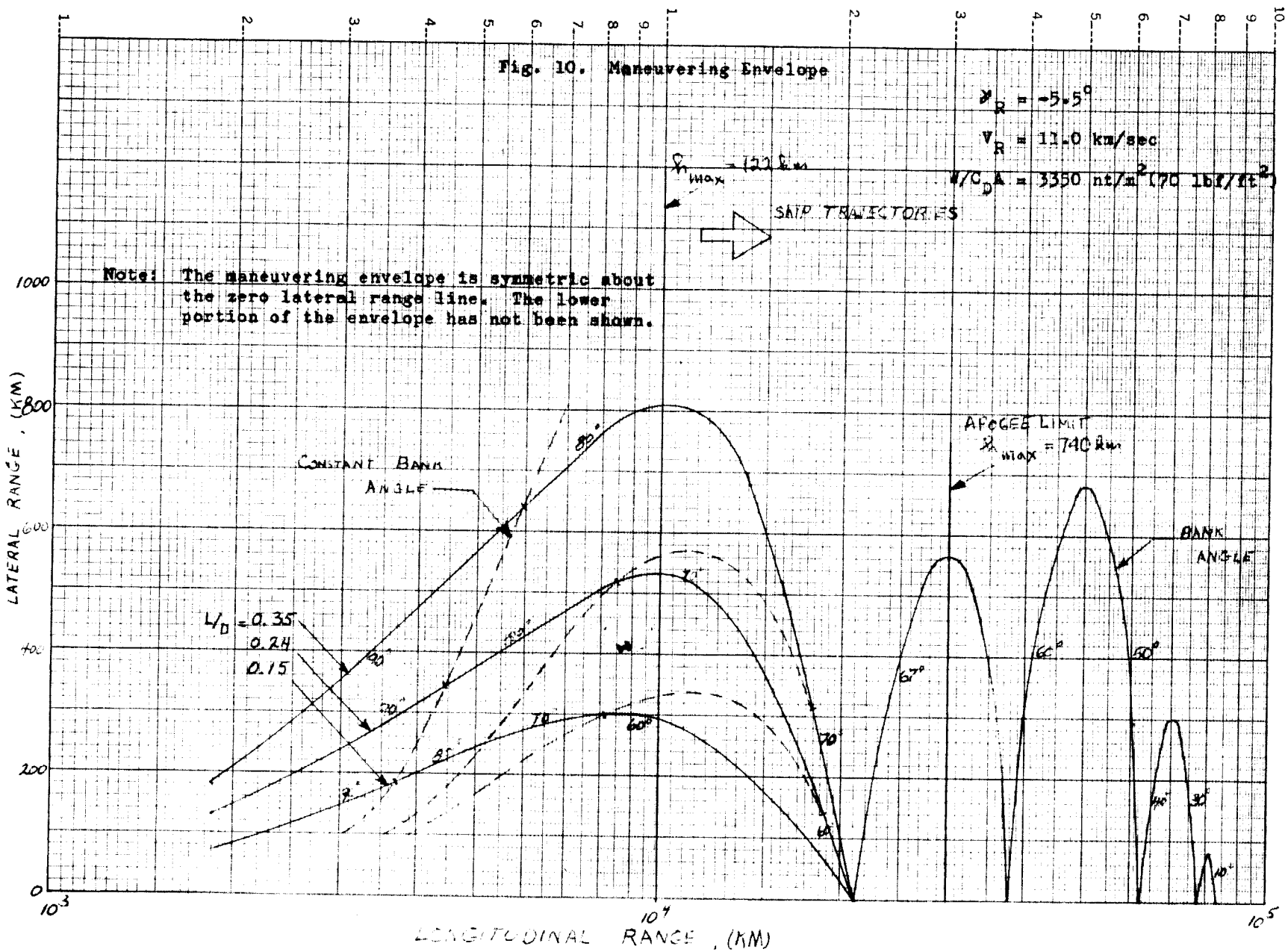
Fig. 10. Maneuvering Envelope
γ_R = -5.5°
V_R = 11.0 km/sec
χ_{max} = 122 km
W/C_DA = 3350 nt/m² (70 lbf/ft²)
SKIP TRAJECTORIES
Note: The maneuvering envelope is symmetric about the zero lateral range line. The lower portion of the envelope has not been shown.
APOGEE LIMIT
χ_{max} = 740 km
CONSTANT BANK ANGLE
BANK ANGLE
L/D = 0.35
0.24
0.15
LATERAL RANGE, (KM)
LONGITUDINAL RANGE, (KM)
0
200
400
600
800
1000
10^3
10^4
10^5

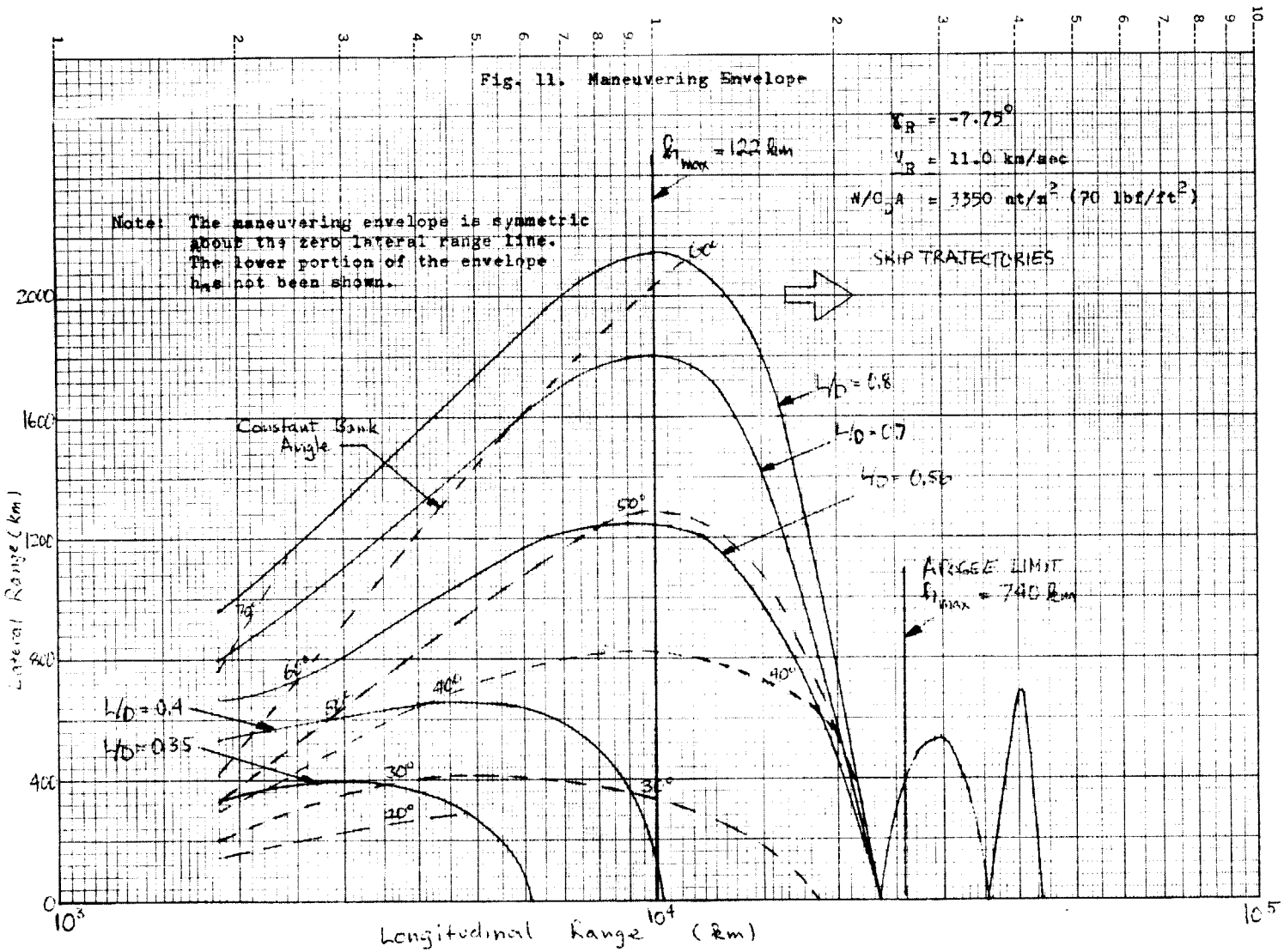
Fig. 11. Maneuvering Envelope
γ_R = -7.75°
V_R = 11.0 km/sec
W/C$_D$A = 3350 nt/m^2 (70 lbf/ft^2)
Note: The maneuvering envelope is symmetric about the zero lateral range line. The lower portion of the envelope has not been shown.
SKIP TRAJECTORIES
$\ell_{1_{max}}$ = 122 km
L/D = 0.8
L/D = 0.7
L/D = 0.56
Constant Bank Angle
ARREST LIMIT
$\ell_{1_{max}}$ = 740 km
L/D = 0.4
L/D = 0.35
Lateral Range (km)
Longitudinal Range (km)
2000
1600
1200
800
400
0
10^3
10^4
10^5

Fig. 12. Fuel Required For Rocket Deceleration From Parabolic to Circular Velocity

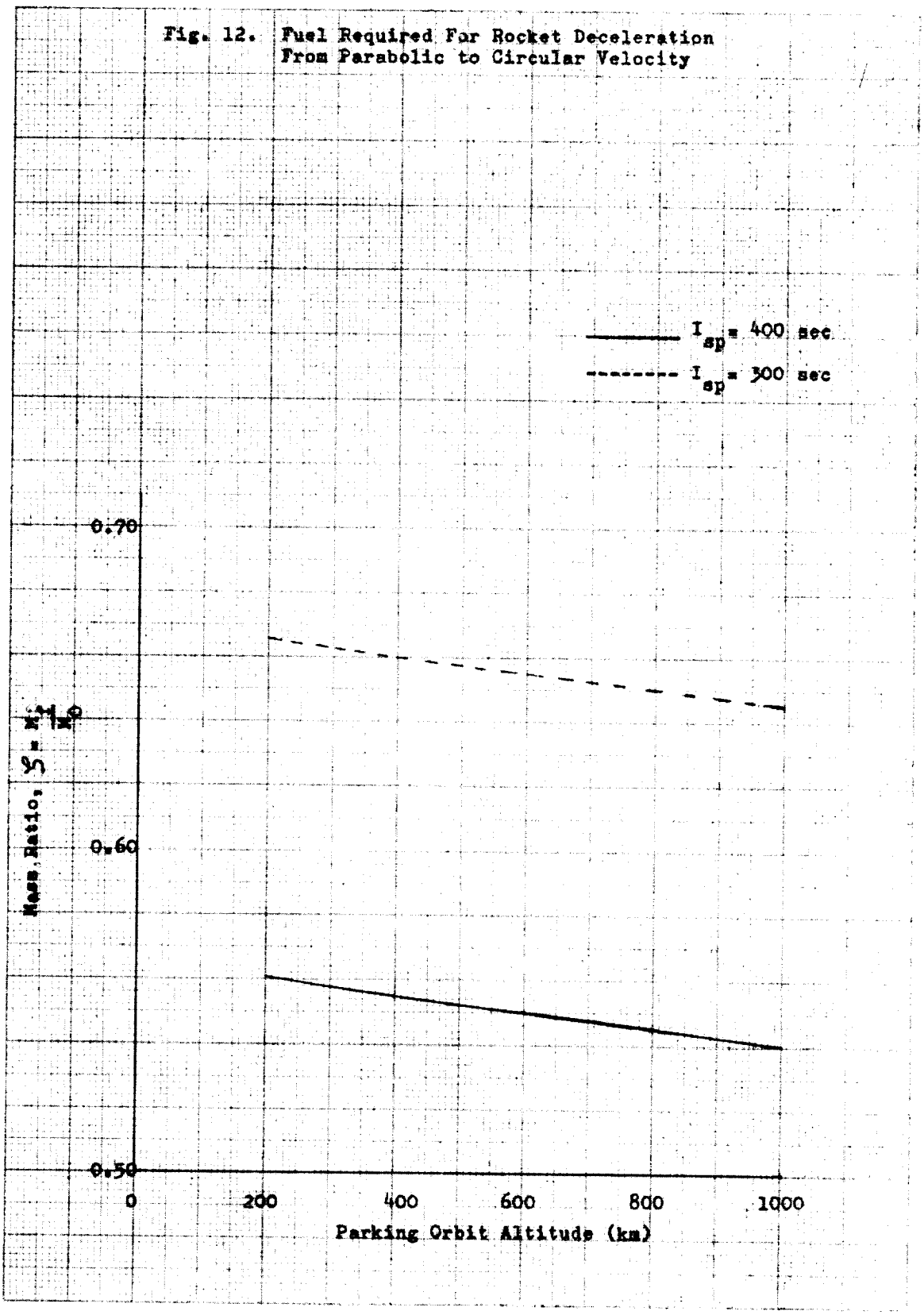

Fig. 13. Fuel Required to Obtain a Circular Orbit as a Function of Exit Velocity and Specific Impulse of Fuel for a Combination Rocket and Aerodynamic Deceleration

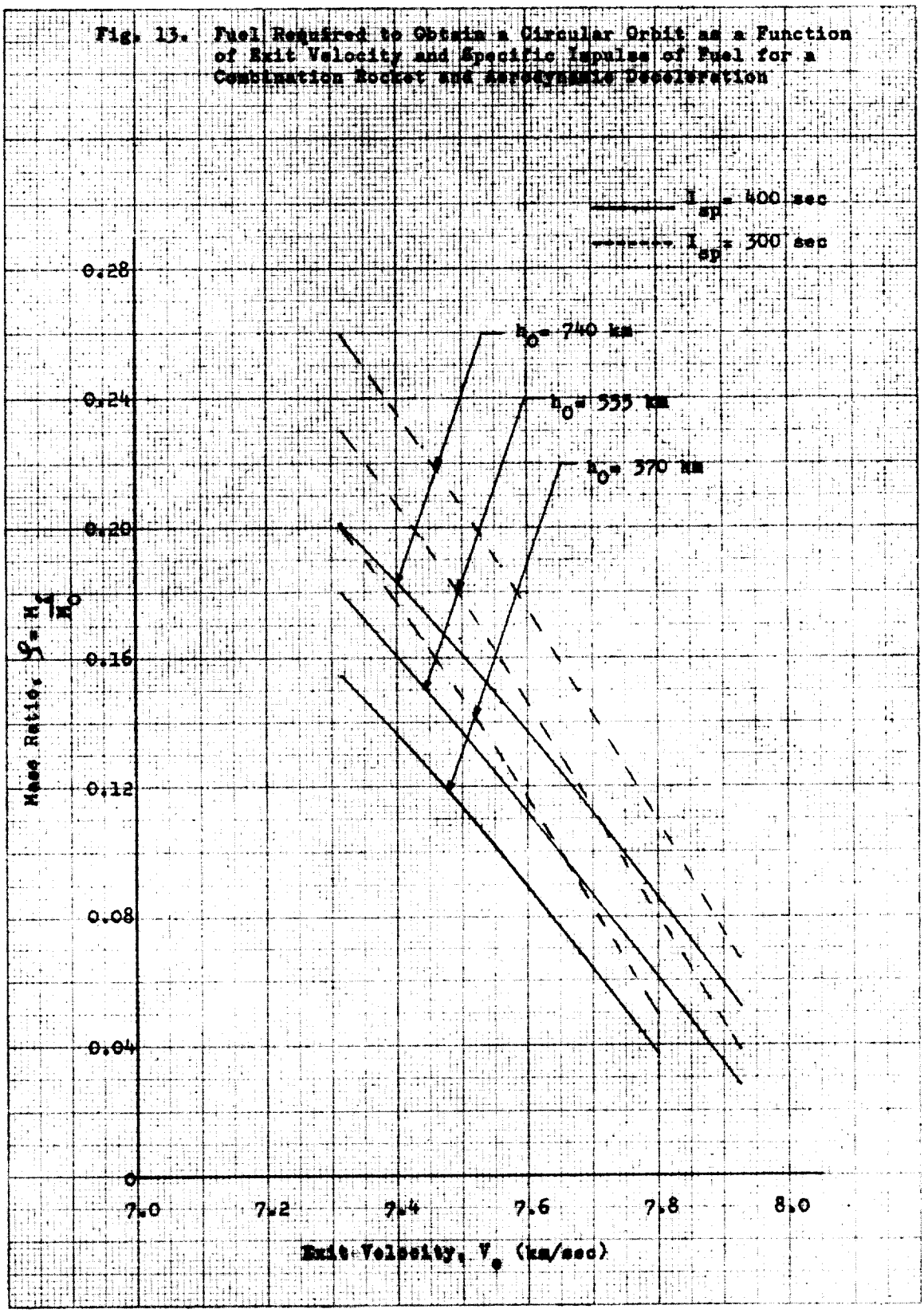

Fig. 14. Southerly Approach to a Landing
(Case 3 of Descent Conditions)

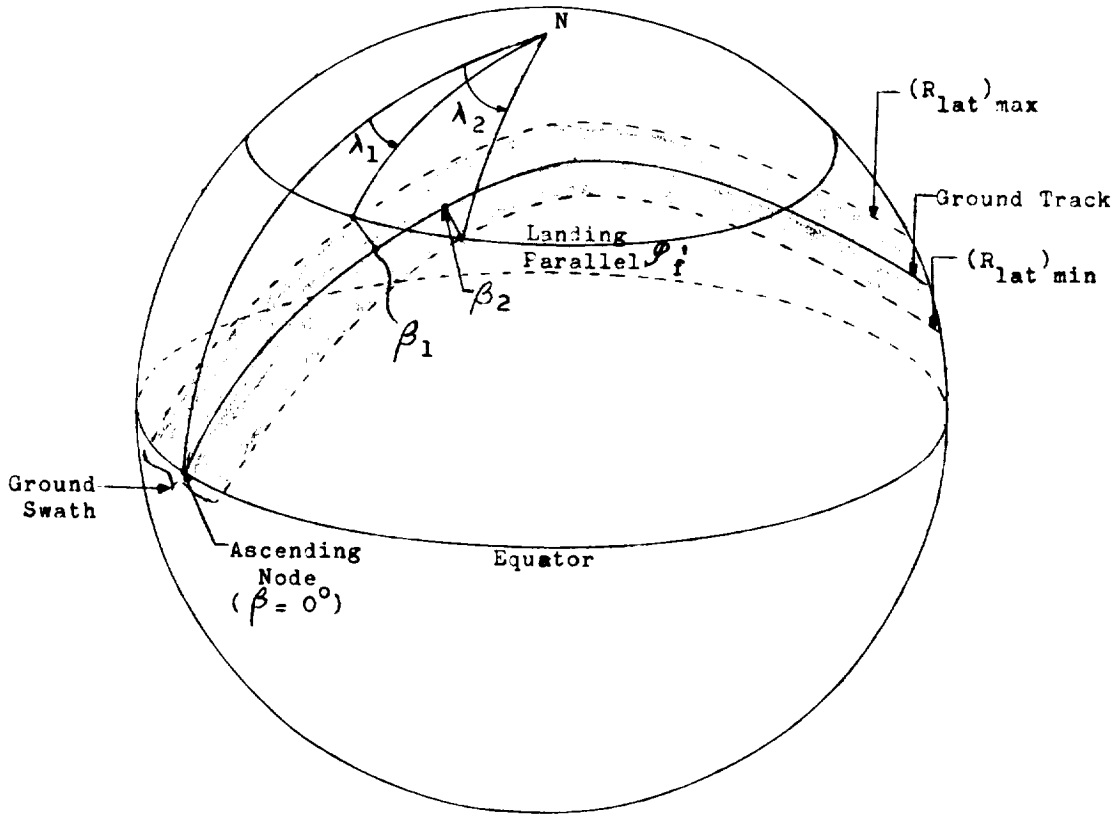

Fig. 15. Approach to a Landing Near the Northern Most Point of the Satellite Ground Track (Case 2 of Descent Conditions)

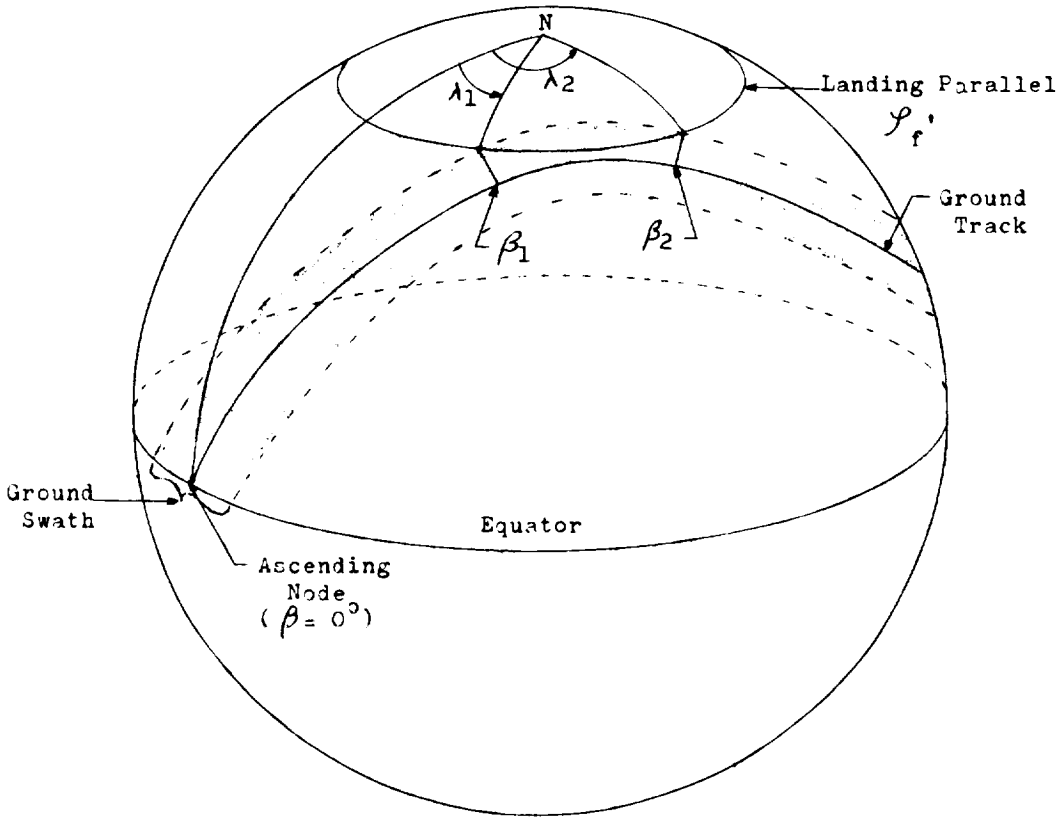

Fig. 16. Displacement in Longitude at the Initial Time

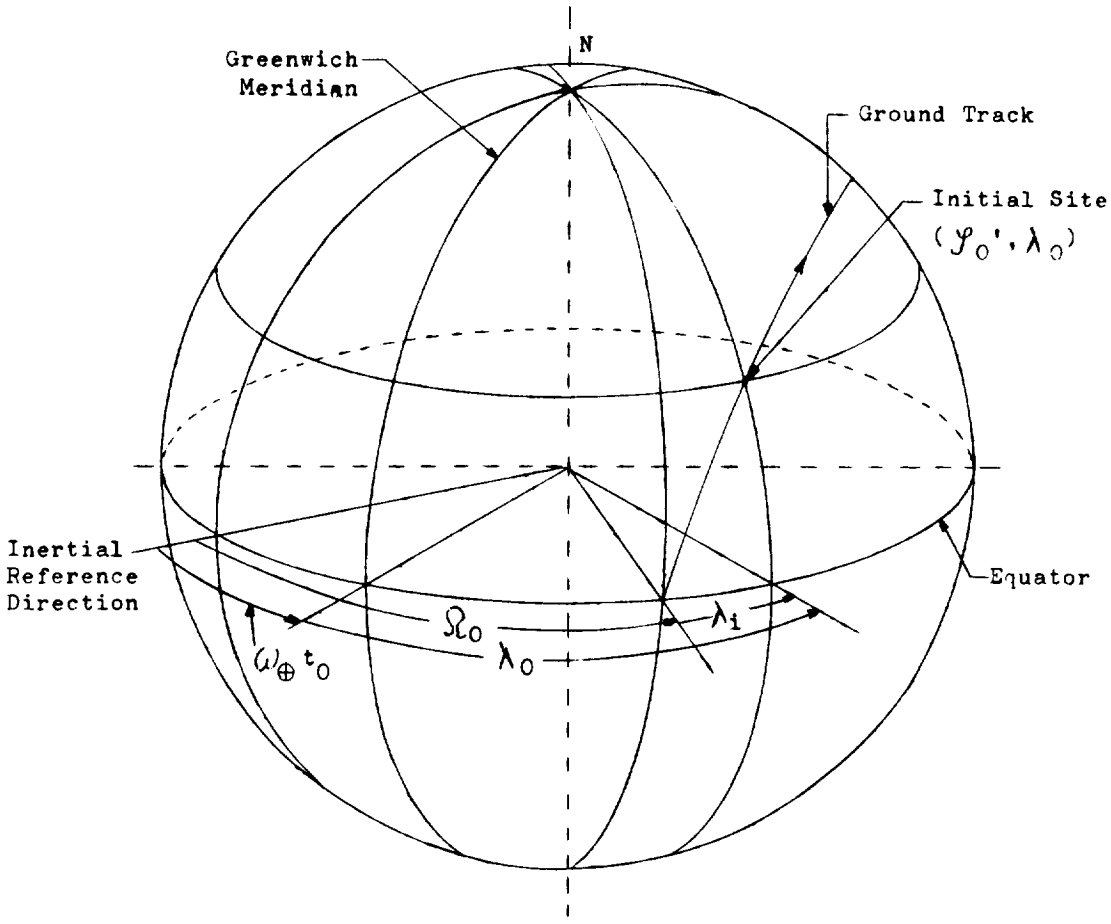

Fig. 17. Displacement in Longitude at Landing

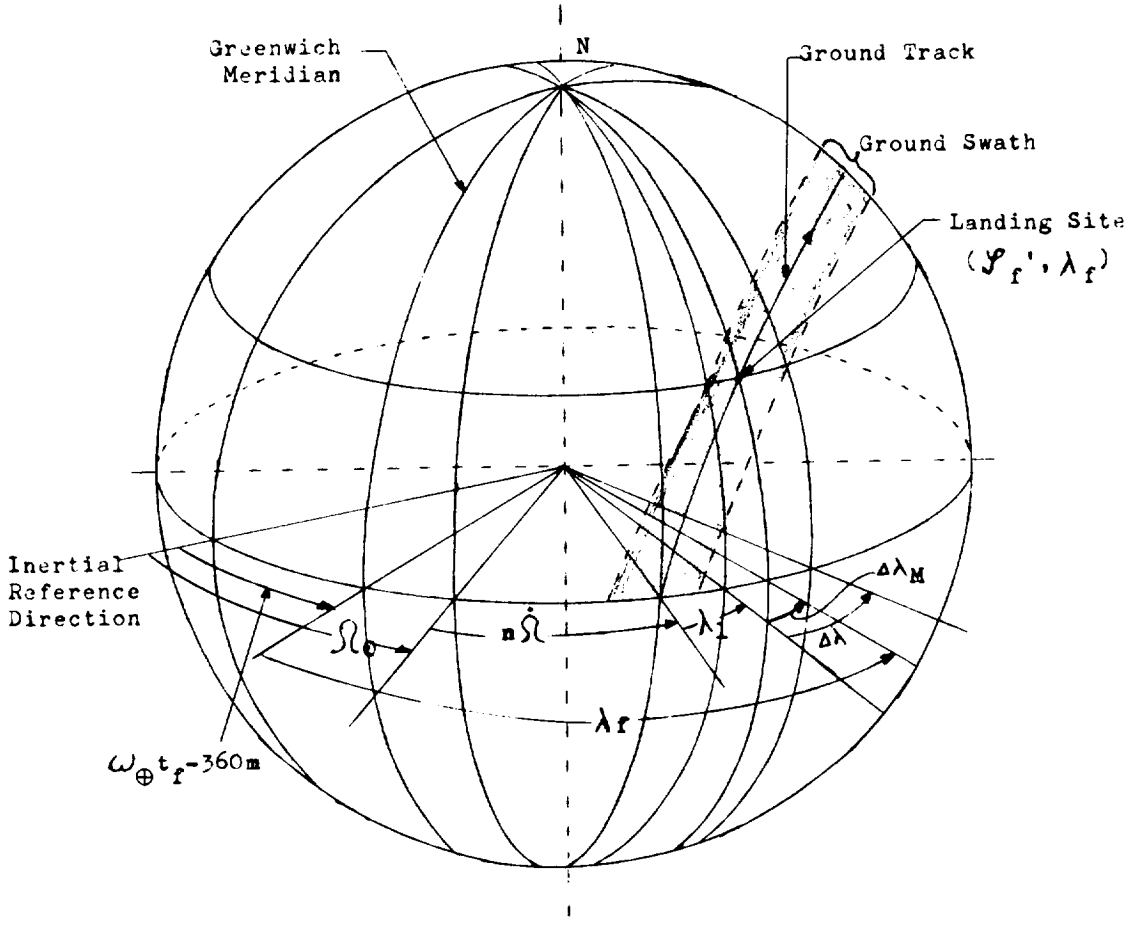

CHAPTER XI

MISSION PLANNING

Prepared by:

F. Santora and D. Kuhn
Martin Company (Baltimore)
Aerospace Mechanics Department
March 1963

		Page
A.	Required Orientation of Translunar and Transearth Trajectories Relative to the MOP	XI-1
B.	Lunar Terminator	XI-3
C.	Declination, Radial Distance, and Phases of the Moon	XI-5
D.	Conversion of General Trajectory Data to Specific Dates	XI-5
E.	Empirical Equations and Auxiliary Data for use in Mission Planning	XI-6
F.	Mission Planning Envelopes	XI-8
G.	Sample Missions	XI-9
H.	Reference	XI-29
	Tables and Illustrations	XI-31

XI. MISSION PLANNING

Chapters VI and IX have catalogued a large quantity of generalized lunar trajectory data. It is the purpose of this chapter to present the methods whereby this generalized material can be interpreted and used for specific mission dates.

Section A presents the equations for converting the selenographic coordinates of a particular lunar site or area to coordinates relative to the moon's orbital plane (MOP) and the moon-earth line ($\overrightarrow{MEL}$). In addition, the equations determine the required orientations (i_m, θ_M) of the possible circular orbits around the moon that pass over the site in question. These equations are very important and should be mechanized on a computer as soon as possible, since the $i_m - \theta_M$ relationship is essentially a boundary condition imposed by the particular mission that must be satisfied by the generalized trajectory data.

In Section B, the lunar terminator is defined and equations giving the orientation of the terminator in both the selenographic and MOP-$\overrightarrow{MEL}$ coordinate systems are presented. It is also shown how the lunar libration equations (Chapter III, Section C) are readily adapted to the calculation of the orientation of the terminator.

Section C records the declination, radial distance and phases of the moon from 1963 to 1971. This data forms the connection between the generalized material of the trajectory catalogues and specific mission dates, as will be illustrated in the sample missions, while the conversion between the two can be accomplished by means of the figures in Section D.

Section E presents empirical equations that extend the catalogued data to other injection altitudes and flight path angles (also given in Chapter VI, Section A), while still other equations are given that improve the accuracy of converting the generalized data to specific dates. This section also includes the energy requirements for controlling return flight time and changing the transearth trajectory inclination.

Section F, also used extensively for mission planning, compiles the generalized geometrical relationships (i_{VTL}, i_{VTE}, i_m, θ_M) for a given set of mission constraints ($R_{\oplus_1}$, h_{PL} or t_p) onto one chart. These summary charts are referred to as "mission planning envelopes" and are provided for both the circumlunar and approach class trajectories. These envelopes are used primarily to determine what combination of generalized trajectory parameters satisfy the boundary conditions (required $i_m - \theta_M$) generated by Section A.

Finally, Section G presents two sample missions that illustrate the procedures and steps to be followed when evaluating specific missions. The specific missions selected are a manned lunar landing and return mission and an unmanned photo-reconnaissance mission. The choice of these two missions necessitates an evaluation of material from both catalogues.

A. REQUIRED ORIENTATION OF TRANSLUNAR AND TRANSEARTH TRAJECTORIES RELATIVE TO THE MOP

In Chapters VI and IX, where translunar and transearth trajectory data were catalogued, it was seen that on arrival at the moon from a translunar trajectory, a certain trajectory orientation (i_m, θ_M) relative to the moon existed, and that the orientation varied as the mission constraints (h_{PL}, i_{VTL}, i_{VTE}, etc.) changed. In like manner, transearth trajectories departing from the moon also have an unlimited number of possible orientations. Thus, the question is, what combination of i_m, θ_M is required to orbit over, land at, or launch from a specific lunar site? In other words, trajectories arbitrarily selected will result in i_m, θ_M relationships other than the required combination, and therefore the mission specification of acquiring a specific lunar site will not be met. The required combination or relationship is easily visualized through use of the following sketch.

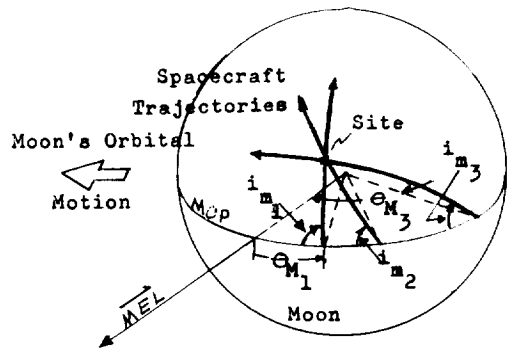

In this sketch, the moon-earth line $\overrightarrow{MEL}$ is shown at the time the spacecraft trajectory is established, which may occur at the time of pericynthion of the translunar trajectory, at lunar liftoff, or at departure from the moon. The desired landing site or reconnaissance area as indicated by the cross can be located relative to the MOP fundamental plane and the $\overrightarrow{MEL}$ direction. An unlimited number of spacecraft trajectories that acquire the site are possible; however, a unique relationship exists between the inclination i_m and orientation θ_M of which only three possibilities are shown in the sketch (i_{m_1}, θ_{M_1}; i_{m_2}, θ_{M_2}; i_{m_3}, θ_{M_3}).

Before this i_m, θ_M relationship can be determined, the position of the site relative to the $\overrightarrow{MEL}$ and MOP on the selected mission date must be determined from its location as given by its selenographic coordinates on a lunar map. The

following discussion presents a method for determining the i_m, θ_M relationship if the selenographic coordinates of the site and the mission date are known.

In Chapter III, Section C, it is pointed out how a site on the moon continually changes its position relative to the MOP because of the lunar librations. It was shown there how the total lunar librations in latitude (b) and longitude (ℓ) of the $\overrightarrow{MEL}$ may be determined by means of lunar ephemeris data. Lunar librations are measured relative to the mean center point ($\overrightarrow{MCP}$) of the moon, which is the intersection of the prime meridian and the true lunar equator as shown in the next sketch, with positive values for ℓ and b indicated:

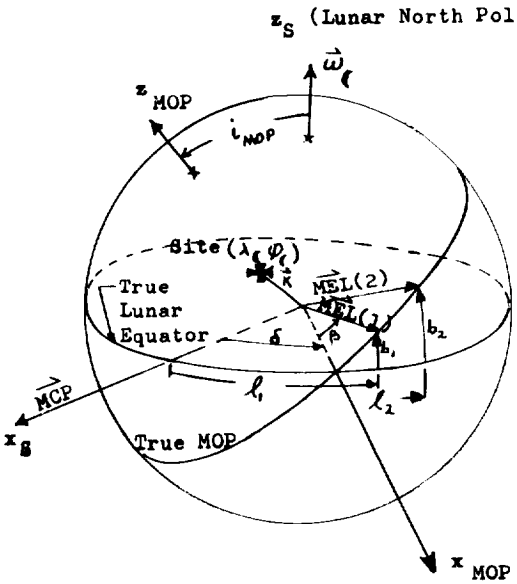

Define a coordinate system $x_{MOP}\, y_{MOP}\, z_{MOP}$, with the z_{MOP}-axis normal to the MOP in the general direction of the lunar angular velocity vector $\vec{\omega}_\ell$, the x_{MOP}-axis defining the line of intersection between the true MOP and the true lunar equator and in the general direction of the $\overrightarrow{MCP}$, and the y_{MOP}-axis completing the right-handed Cartesian coordinate system in the MOP.

In order to find the inclination of the true MOP with respect to the true lunar equator, let T be the Julian date on which the spacecraft trajectory is established, and ℓ_1 and b_1 the total librations of the $\overrightarrow{MEL}(1)$ at this date. Next, let $\overrightarrow{MEL}(2)$ be directed to the earth's position (ℓ_2, b_2) at an earlier date, but as seen from the moon at T (ℓ_2 and b_2 may be found by using the equations presented in Chapter III, Section C, for the date T but with the position coordinates of the moon $x_{\oplus\ell}$, $y_{\oplus\ell}$, $z_{\oplus\ell}$ for one-half day earlier). The two vectors $\overrightarrow{MEL}(1)$ and $\overrightarrow{MEL}(2)$ define the true earth orbital plane (EOP) about the moon. This plane may also be interpreted as the true MOP whose descending node with the true lunar equatorial plane is given by the x_{MOP}-axis.

The vector $\vec{z}_{MOP}$, which is normal to the MOP and hence identical with $\vec{z}_M$, is then defined in the selenographic coordinate system by the following determinant (see preceding sketch):

$$\vec{z}_{MOP} = \begin{vmatrix} \hat{x}_S & \hat{y}_S & \hat{z}_S \\ \cos\ell_1 \cos b_1 & \sin\ell_1 \cos b_1 & \sin b_1 \\ \cos\ell_2 \cos b_2 & \sin\ell_2 \cos b_2 & \sin b_2 \end{vmatrix} \quad (1)$$

The inclination i_{MOP} of the true MOP with respect to the true lunar equator can now be determined from Eq (1):

$$i_{MOP} = \cos^{-1}\left(\frac{\vec{z}_{MOP} \cdot \hat{z}_S}{z_{MOP}}\right) \quad (2)$$

Next, the angle δ, measured from the $\overrightarrow{MCP}$ to the x_{MOP} axis, is given by:

$$\delta = \cos^{-1}\left(\frac{\hat{z}_S \times \vec{z}_{MOP} \cdot \hat{x}_S}{\left|\hat{z}_S \times \vec{z}_{MOP}\right|}\right) \quad (3)$$

and β, measured from the x_{MOP} axis to $\overrightarrow{MEL}(1)$, by:

$$\beta = \cos^{-1}\left(\frac{\hat{z}_S \times \vec{z}_{MOP} \cdot \overrightarrow{MEL}(1)}{\left|\hat{z}_S \times \vec{z}_{MOP}\right|}\right) \quad (4)$$

By rotating the $x_S\, y_S\, z_S$ coordinate system through the three positive angles δ, i_{MOP} and β, in that order, the unit vector in the direction of a specific lunar feature, $\hat{K}$, may be found. Denote the components of $\hat{K}$ relative to the $\overrightarrow{MEL}$ and MOP coordinate system by K_1 in the $\hat{x}_{MOP}$ direction, by K_2 in the $\hat{y}_{MOP}$ direction and by K_3 in the $\hat{z}_{MOP}$ direction. The components K_1, K_2 and K_3 in terms of selenographic longitude and latitude are given by the following matrix multiplication:

$$\begin{Bmatrix} K_1 \\ K_2 \\ K_3 \end{Bmatrix} = \begin{bmatrix} \cos\beta & \sin\beta & 0 \\ -\sin\beta & \cos\beta & 0 \\ 0 & 0 & 1 \end{bmatrix} \begin{bmatrix} 1 & 0 & 0 \\ 0 & \cos i_{MOP} & \sin i_{MOP} \\ 0 & -\sin i_{MOP} & \cos i_{MOP} \end{bmatrix} \begin{bmatrix} \cos\delta & \sin\delta & 0 \\ -\sin\delta & \cos\delta & 0 \\ 0 & 0 & 1 \end{bmatrix} \begin{Bmatrix} \cos\phi_\ell \cos\lambda_\ell \\ \cos\phi_\ell \sin\lambda_\ell \\ \sin\phi_\ell \end{Bmatrix} \quad (5)$$

where:

$$\hat{K} = K_1 \hat{x}_{MOP} + K_2 \hat{y}_{MOP} + K_3 \hat{z}_{MOP}$$

and $\lambda_{\mathbb{C}}$ and $\phi_{\mathbb{C}}$ are the selenographic coordinates of the lunar site.

Define a latitude and longitude relative to the MOP as a fundamental plane and the x_{MOP}, z_{MOP} plane defining the prime meridian. In terms of:

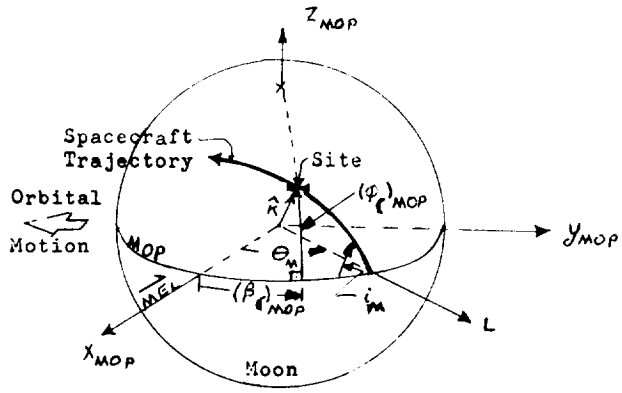

K_1, K_2, K_3, the latitude $(\phi_{\mathbb{C}})_{MOP}$ of the site relative to the $\overrightarrow{MEL}$ and MOP is given by:

$$(\phi_{\mathbb{C}})_{MOP} = 90° - \cos^{-1}(K_3), \quad -90° \leq (\phi_{\mathbb{C}})_{MOP} \leq +90° \tag{6}$$

and its longitude by

$$(\lambda_{\mathbb{C}})_{MOP} = \cos^{-1}\left(\frac{K_1^2}{K_1^2 + K_2^2}\right)^{1/2}, \quad -180° \leq (\lambda_{\mathbb{C}})_{MOP} \leq +180° \tag{7}$$

It remains to find the i_m, θ_M relationship for a given lunar site and for a given date T. First define a unit vector $\hat{L}$ in the MOP by assuming a required value of θ_M.

$$\hat{L} = \cos\theta_M \hat{x}_{MOP} + \sin\theta_M \hat{y}_{MOP} \tag{8}$$

Then the corresponding i_m required is:

$$i_m = \cos^{-1}\left(\frac{\hat{K} \times \hat{L} \cdot \hat{z}_{MOP}}{|\hat{K} \times \hat{L}|}\right)$$

Equations (8) and (9) give the desired i_m θ_M relationship.

This approach is best suited for lunar landing missions, lunar orbit missions (reconnaissance and surveillance), and lunar departure missions that do not require many lunar orbits or rendezvous with other vehicles already in lunar orbit.

For missions where lunar rendezvous is required, such as the lunar ascent phase of the "shuttle" concept (Chapter VIII) or for missions where the spacecraft spends some time in orbit around the moon prior to leaving, the approach of Eqs (8) and (9) must be modified because lunar orbits for these missions will most likely be computed in a selenocentric or selenographic coordinate system. This implies that instead of having a range of required i_m, θ_M relationships, there is only one required i_m-θ_M combination which has to be satisfied for the specific value of orbital inclination i_{VM} relative to the true lunar equator, and longitude of the ascending node Ω_{MOP} relative to the MOP in the true equatorial plane of the moon.

In order to calculate this combination, it can be assumed that the lunar site, referred to above, is a specific lunar feature that lies below the orbital path or a position calculated from the known inclination (i_{VM}) and the longitude Ω_{MOP} of the ascending node.

If Eq (4) is solved for both the calculated position and the coordinates of the ascending node (Ω_{MOP}, 0), two positions relative to the $\overrightarrow{MEL}$ and MOP are obtained, namely, $\hat{K}$ and $\hat{K}'$, as shown below.

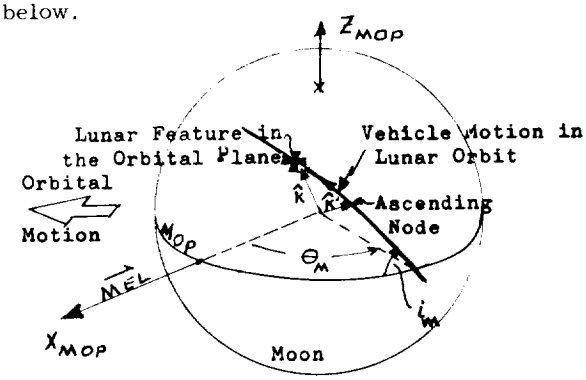

Therefore, the required i_m is:

$$i_m = \cos^{-1}\left(\frac{\hat{K} \times \hat{K}' \cdot \hat{z}_{MOP}}{|\hat{K} \times \hat{K}'|}\right)$$

and

$$\theta_M = \cos^{-1}\left(\frac{(\hat{K} \times \hat{K}') \times \hat{z}_{MOP} \cdot \hat{x}_{MOP}}{|(\hat{K} \times \hat{K}') \times \hat{z}_{MOP}|}\right)$$

It is suggested that the equations given in this section and in Section C of Chapter III be mechanized on a computer so that full usefulness of the lunar handbook can be realized. The need for mechanization will become apparent in the sample missions (Section G).

B. LUNAR TERMINATOR

In the planning of lunar missions, the lighting conditions and phases (a phase is defined as the fraction of the area of the apparent disk of the moon illuminated by the sun as observed from earth) play a major role. The importance of the lighting conditions arises from the fact that daylight is desirable for exploration and that the temperature of the lunar surface depends strongly on the orientation of the particular feature relative to the sun due to the slow rotational rate of

the moon around its axis (see Chapter II, Section B).

The lunar phase depends on a quantity defined as planetocentric elongation of the earth from the sun, and it is referred to as the "phase angle" which is denoted by i in the ephemeris and illustrated in the following sketch, where $x_\oplus$ $y_\oplus$ $z_\oplus$ is the equatorial coordinate system defined in Subsection A-1c of Chapter III.

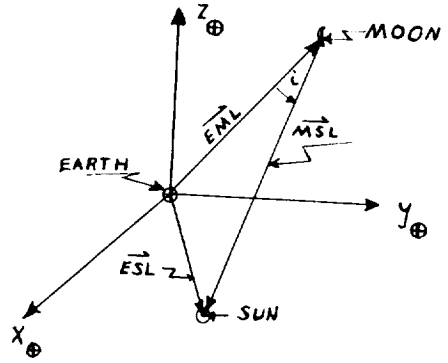

The four cardinal phases are: (1) new moon, (2) first quarter, (3) full moon, and (4) last quarter. They occur when the phase angle, i, is equal to 180°, 90°, 0° and 90°, respectively.

If the small triaxiality of the moon is neglected, the apparent lunar disk is circular. The terminator is defined as the orthogonal projection, onto a plane perpendicular to the line of sight, of the great circle that bounds the illuminated hemisphere of the moon. The terminator is therefore, in general, an ellipse, reducing to a straight line at i = 90° and becoming a circle at i = 0° or 180°. Although positions of the terminator can be obtained for this decade from the U.S. Naval Observatory, it may be desirable to produce data of this sort from a subroutine incorporated in numerically computed digital trajectory programs. Since these programs generally use stored positional data of the sun and moon in geocentric rectangular coordinates $x_\oplus$ $y_\oplus$ $z_\oplus$, the following approach can be used to determine the orientation of the lunar terminator.

In the previous sketch, the positions of the moon ($\overrightarrow{EML}$) and sun ($\overrightarrow{ESL}$) are given in geocentric mean equatorial coordinates with $x_\oplus$ in the direction of the mean equinox of date. For a given Julian date T, the moon-sun line $\overrightarrow{MSL}$ can be found through vector addition

$$\overrightarrow{MSL} = \overrightarrow{ESL} - \overrightarrow{EML} \qquad (10)$$

Now if the $\overrightarrow{MSL}$ is used in place of the $\overrightarrow{EML}$ in the libration equations in Chapter III, Section C, the selenographic position of the sun can be obtained.

This position in longitude and latitude is denoted by $\ell_\odot$ and $b_\odot$ respectively, and is shown below with positive values for $\ell_\odot$ and $b_\odot$ illustrated:

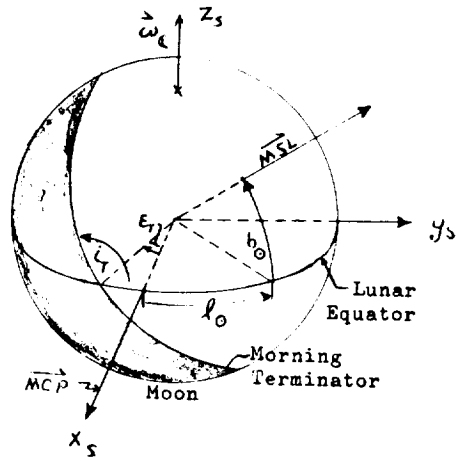

The orientation of the morning terminator, or portion of the moon just to be illuminated by the sun after the lunar night, is defined by the angles i_T and ϵ_T. These angles, illustrated above, can be found by use of Eqs (1) and (2) and noting that

$$\hat{MSL} = \cos \ell_\odot \cos b_\odot \hat{x}_S + \sin \ell_\odot \cos b_\odot \hat{y}_S + \cos b_\odot \hat{z}_S \qquad (11)$$

$$i_T = 90° + b_\odot \qquad (12)$$

where:

$$0° \le i_T \le 180°$$

$$\epsilon_T = \cos^{-1}\left(\frac{\hat{MSL} \times \hat{z}_S \cdot \hat{x}_S}{|\hat{MSL} \times \hat{z}_S|}\right) \quad 0° \le \epsilon_T \le 360° \qquad (13)$$

The orientation of the morning terminator relative to the $\overrightarrow{MEL}$ and MOP is determined by replacing the selenographic longitude and latitude of the site, λ_ℓ, ϕ_ℓ, in Eq (5) of the previous section by $\ell_\odot$ and $b_\odot$ and obtaining the unit vector $\hat{K}$, which now is the direction of the sun as seen from the center of the moon relative to the x_{MOP} y_{MOP} z_{MOP} coordinate system:

$$\hat{K} \equiv \hat{MSL} \qquad (14)$$

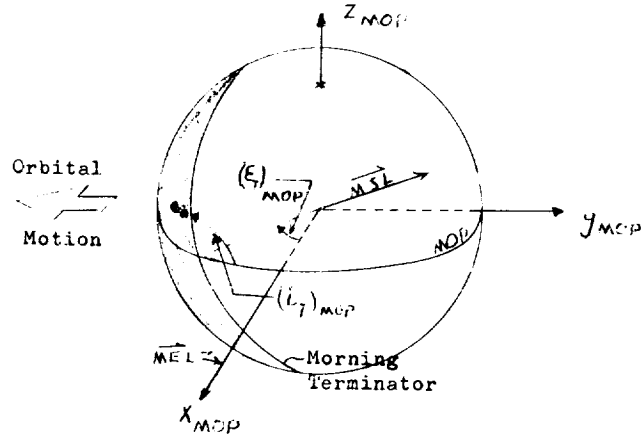

Then

$$(i_T)_{MOP} = 180 - \cos^{-1}(\hat{z}_S \cdot \hat{MSL}),$$

$$0° \leq (i_T)_{MOP} \leq 180° \qquad (15)$$

and

$$(\epsilon_T)_{MOP} = \cos^{-1}\left(\frac{\hat{MSL} \times \hat{z}_S \cdot \hat{x}_S}{|\hat{MSL} \times \hat{z}_S|}\right)$$

$$0° \leq (\epsilon_T)_{MOP} \leq 360° \qquad (16)$$

Of course, the location of the evening terminator is given by $\epsilon_T \pm 180°$ or $(\epsilon_T)_{MOP} \pm 180°$, and it is the portion of the moon just to fall into the lunar night. The inclination i_T of the evening terminator is identical to that of the morning terminator.

C. DECLINATION, RADIAL DISTANCE, AND PHASES OF THE MOON

This section presents the lunar declination δ_M, which has been denoted by $\delta_\mathbb{C}$ up to now in the handbook, the radial distance R_M, previously designated as $R_{\oplus\mathbb{C}}$, of the moon from the earth, and the phases of the moon (as previously described in Section B). The data has been taken directly from Woolston (Ref. 1), since it is in a form which permits a rapid approximate determination of the combination of declination and lighting for any calendar date for mission planning purposes.

The times of new moon, first quarter, full moon, and last quarter, as determined by the Nautical Almanac Office of the U.S. Naval Observatory are "the times at which the excess of the apparent longitude of the moon over the apparent longitude of the sun is 0°, 90°, 180°, and 270°, respectively." In the data presented herein, the determination of the phases has been approximated by comparing the geometric position of the sun with the apparent position of the moon. While reduction of the sun's geometric longitude to apparent longitude should take into account aberration and the precession and nutation in longitude, only the precession has been considered. For the period of interest, the combined contributions of nutation and aberration have been examined and it has been found that they should not exceed approximately 30" corresponding to a discrepancy in time of the moon's phase of about one minute.

A related approximation involves the use of a mean obliquity of the ecliptic at the beginning of each year rather than true obliquity in transforming from the sun's geocentric equatorial rectangular coordinates $x_{\oplus\odot}$ $y_{\oplus\odot}$ $z_{\oplus\odot}$ to the longitude. For present purposes, its effect is negligible.

Data is given in tabular and graphical form. Table 1 serves simply to identify a particular month and date with the corresponding number of the day in the year after January 0. It is intended to be used in conjunction with the plots of the declination and distance of the moon. Two forms are given: one for nonleap years, the other for leap years.

Tables 2 (a) to 2 (i) contain the calculated universal time (UT) of the phases of the moon for the years 1963 to 1971, respectively.

Figures 1 to 9 present graphs for 1963 to 1971, respectively, of the radial distance R_M (in earth radii) and declination δ_M as a function of the day of the year, numbered from January 0. Included on the graphs of the declination are symbols indicating the cardinal phases of the moon. In these tables and figures January 0, 0 hr UT corresponds to December 31, 0 hr UT of the previous year; e.g. January 9.5 is January 9, 12 hr UT.

D. CONVERSION OF GENERAL TRAJECTORY DATA TO SPECIFIC DATES

All the material in the catalogues of Chapters VI and IX is presented relative to the MOP (which, as a plane of symmetry, is independent of the orientation of the earth's equatorial plane relative to the MOP). However, for a specific date, there is a unique orientation of the equatorial plane with respect to the MOP, and the generalized trajectory data must be interpreted for that date if a mission is to be analyzed properly.

The first step is to determine the inclination of the MOP with respect to the earth's equatorial plane i_{em} and the position of the moon in its orbit. The inclination, i_{em}, can be found by means of ephemeris data, or, less accurately, by means of Figs. 1 to 9. For purposes of preliminary mission planning, the figures are adequate, and i_{em} is found by taking the maximum declination of the moon for the year and month in question ($i_{em} \equiv \delta_{\mathbb{C}\,max}$). This is shown in the following sketch of the celestial sphere.

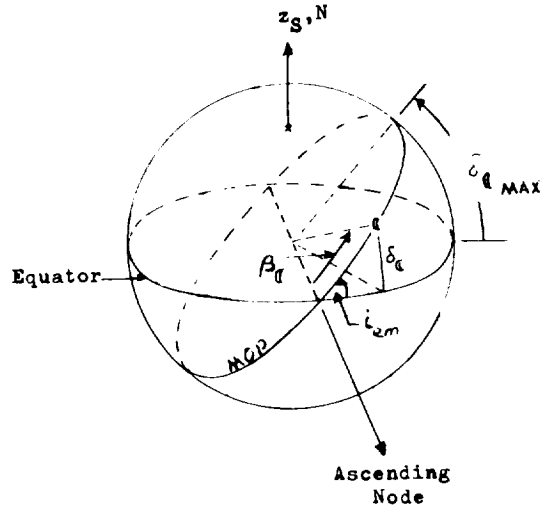

The actual declination of the moon at the date of interest is $\delta_\mathbb{C}$, and its position in orbit is given by the central angle $\beta_\mathbb{C}$ $\delta_\mathbb{C}$ is also obtained from Figs. 1 to 9, and $\beta_\mathbb{C}$ can be found in Fig. 10 or from

$$\beta_{\mathbb{C}} = \sin^{-1}\left(\frac{\sin \delta_{\mathbb{C}}}{\sin i_{em}}\right) \qquad (17)$$

In Fig. 10, $\beta_{\mathbb{C}}$ is given from 0 to 360° where 0 and 180° represent the ascending and descending nodes, respectively, and 90° and 270° the maximum northerly and southerly declinations, respectively.

As was pointed out in Chapter VI, the intersection of the translunar plane with the MOP is very nearly along the earth-moon line ($\hat{EML}$) at the date of pericynthion. Assuming, for the time being, that this intersection is identical with the $\hat{EML}$, the next sketch can be drawn.

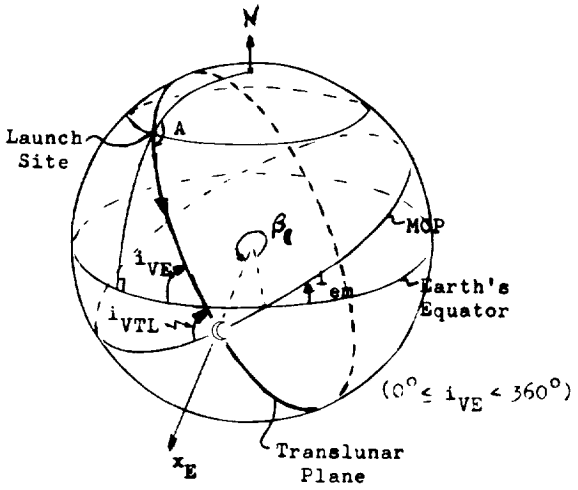

The inertial launch azimuth, A, is given by the following equation:

$$A = \sin^{-1}\left(\frac{\cos i_{VE}}{\cos \phi'_L}\right) \qquad (18)$$

ϕ'_L geocentric latitude of the earth launch site

If it is assumed that launches from Cape Canaveral are restricted in azimuth ($70° \leq A \leq 110°$), then the resulting i_{VE} will be limited to $28.5° \leq i_{VE} \leq 34.5°$. However, the inclination of the translunar plane, i_{VTL}, varies considerably depending on the time of lunar month, i.e., lunar position $\beta_{\mathbb{C}}$. Figure 11 presents the value of i_{VTL} as a function of $\beta_{\mathbb{C}}$ for $i_{VE} = 28.5°$, 31.5° and 34.5° for the years 1965 and 1966. Figure 12 shows the same information for the years 1967 to 1971. The highest i_{VTL} that can be encountered for the above azimuth restructions is 63° and the lowest is near 0°. Thus, for a given date of pericynthion the catalogue data (Chapters VI and IX) can be entered much more discriminatingly for mission analysis, as will be demonstrated in the sample missions (Section G).

In like manner, when returning to earth from a lunar mission it is highly advantageous to be able to convert i_{VTL} to the return trajectory inclination i_{VTEQ} relative to the earth's equator, or vice versa. Figures 13 and 14 present i_{VTE} as a function of $\beta_{\mathbb{C}}$ for various i_{VTEQ}.

In the above discussion, it was assumed that the intersection of the translunar and transearth planes with the MOP is coincident with the $\hat{EML}$ at the date of pericynthion or date of transearth injection from lunar orbit. This assumption is not exactly true, since, in general, the actual intersection is $(\beta_{\mathbb{C}} + \Delta\Phi)$. The next section presents empirical equations whereby $\Delta\Phi$ can be estimated. It has been found that $\Delta\Phi_{TL} < 1°$ for $|i_{VTL}| > 15°$ and $\Delta\Phi_{TE} < 2°$ for $|i_{VTE}| > 15°$.

E. EMPIRICAL EQUATIONS AND AUXILIARY DATA FOR USE IN MISSION PLANNING

1. Empirical Equations

There are four empirical equations that are used with the catalogued data of Chapters VI and IX for mission planning purposes. Two equations are utilized for extending the catalogued material to other mission constraints not given in the catalogues, and two other equations are used to increase the accuracy of analysis of specific missions.

The first two equations were previously given in Chapter VI and are repeated here for convenience.

$$\psi'_0 = \psi_0 + 2\,\Delta\gamma_0 \qquad (19)$$

Since the translunar catalogue data presented in Chapters VI and IX are given for an injection flight path angle of $\gamma_0 = 5°$ and 0°, respectively, Eq (19) is used to extend the value of γ_0 to a value γ_0'. The only trajectory variable that is significantly affected by the change in γ_0 is ψ_0, the injection position. Therefore, Eq (19) gives the new value of injection position, ψ_0', for γ_0' where $\Delta\gamma_0$ is $(\gamma_0' - \gamma_0)$.

$$V_0' = \left[V_0^2 - V_p^2\left(\frac{\Delta h_0}{r_0}\right)\right]^{\frac{1}{2}} \qquad (20)$$

It is also desirable to extend the translunar catalogue data to other injection altitudes h_0', since in Chapter VI the injection altitude, h_0, is constant (250 km), and likewise in Chapter IX, the catalogue data is presented for $h_0 = 183$ km. With a variation in h_0, the only trajectory parameter significantly affected is V_0, the injection velocity. Equation (20) gives V_0' the injection

velocity corresponding to h_0' where $\Delta h_0 = h_0' - h_0$, r_0 is the radius from the earth's center to h_0 and V_p is the 2-body parabolic speed at h_0'.

The practical limits of the above two equations are $\Delta\gamma_0 \leq \pm 20°$ and $\Delta h_0 \leq \pm 1750$ km.

The next two empirical equations allow a more accurate evaluation of the generalized catalogue material for specific dates of interest.

It was mentioned in Section D above that the intersection of the translunar or transearth plane with the MOP is adjusted by an amount $\Delta\Phi$ to be algebraically added to $\beta_{\mathbb{C}}$. This adjustment is usually ignored for $|i_{VTL}| > 15°$, $|i_{VTE}| > 15°$ but should be included for inclinations $< 15°$.

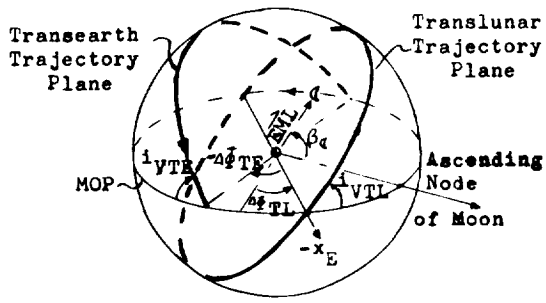

For translunar trajectories $\Delta\Phi = \Delta\Phi_{TL}$.

$$\Delta\Phi_{TL} = \pm (0.22 + 0.000156\, h_{PL})\, C_0 \sin i_{VTE} + 1.0 \qquad (21)$$

use + for inject south

use - for inject north

where

h_{PL} is measured in kilometers

C_0 is a constant determined from Fig. 15.

Therefore the intersection of the translunar plane with the MOP (which is the Voice x_E-axis) is located $\beta_{\mathbb{C}} + \Delta\Phi_{TL}$ from the ascending node of the moon's orbit around the earth.

For the case of circumlunar trajectories, the intersection of the transearth plane will not in general be coincident with the x_E-axis as shown in the above sketch, but it is located at a position $\beta_{\mathbb{C}} + \Delta\Phi_{TL} + \Delta\Phi_{TE}$, where $\Delta\Phi_{TE}$ is the adjustment required and is given by Eq (22):

$$\Delta\Phi_{TE} = \pm (0.232 + 0.0001537\, h_{PL})\, D_0 \sin i_{VTL} - E_0 \qquad (22)$$

use + for inject north

use - for inject south

$E_0 = 1.7 + 0.0375\,(R_{\oplus\mathbb{C}} - 56.0)$

$R_{\oplus\mathbb{C}}$ is measured in earth radii, h_{PL} in km

and

D_0 is obtained from Fig. 16.

Equations (21) and (22) apply only to circumlunar trajectories catalogued in Chapter VI and for $i_{VTL} \geq 2°$. For the approach class of translunar injections in Chapter IX, similar equations for $|i_{VTL}| < 15°$ are not available at this time, and the data can be used with relatively good accuracy for $|i_{VTL}| \geq 10°$ in most cases.

2. Auxiliary Data

The auxiliary data consists of the characteristic velocity impulse, ΔV, that is required to conduct certain maneuvers during transearth flight. These maneuvers may be necessary for timing the perigee, for landing site acquisition, or changing the transearth inclination for tracking purposes, or both, or they may even be interpreted as abort maneuvers.

The first maneuver involves controlling the time of arrival at vacuum perigee ($h_{PE} = 45.72$ km) without altering the transearth plane inclination. The maneuver is executed by applying a velocity impulse in a retarding direction ($-\Delta V_{TE}$) to delay the arrival or in an accelerating direction ($+\Delta V_{TE}$) to hasten the perigee arrival time. Figure 17 presents the ΔV_{TE} requirement to delay or hasten the time of perigee for a typical transearth trajectory having an eccentricity of 0.975, which is representative of the majority of lunar return trajectories. The data are presented for three different $R_{\oplus\Delta}$--namely, 20 ER, 30 ER and 40 ER--at which the maneuver is conducted. Δt in the figure represents the time difference between the nominal arrival time and the maneuver adjusted arrival time:

$$\Delta t = t_{nominal} - t_{maneuver}$$

The data was limited to eccentricities less than 1 after this maneuver.

A second maneuver that may be performed on the return flight alters the inclination of the transearth trajectory plane, i_{VTE}. In this maneuver, the time to arrive at vacuum perigee from the maneuver point is not altered. In other words, the maneuver deflects the velocity vector $\vec{V}_{\oplus\Delta}$ and does not change its magnitude or flight path angle, γ. Figure 18 shows the impulse ΔV_i required to change i_{VTE} by an amount Δi_{VTE}. Again, the eccentricity of the transearth trajectory is assumed to be 0.975, and the distances selected, at which the maneuver is conducted, are

$R_{\oplus \Delta}$ = 20, 30 and 40 ER. However, when this maneuver is performed there is a shift $\Delta\phi'_{TE}$ in the intersection of the transearth trajectory plane with the MOP. This corresponding shift with maneuver is found in Figs. 19, 20 and 21 and, thus, the position of the intersection is now $(\beta_{\oplus} + \Delta\Phi_{TL} + \Delta\Phi_{TE} + \Delta\Phi'_{TE})$.

If both a time and i_{VTE} correction are required, then the magnitude of the total velocity impulse as given by vector addition is $(\Delta V^2_{TE} + \Delta V^2_{i})^{1/2}$.

F. MISSION PLANNING ENVELOPES

The catalogued data in Chapters VI and IX refers to either geometrical or "energy" parameters; however, it is the geometric properties at given times which define its usefulness. The text below discusses the importance of displaying these geometric properties in such a manner that they lend themselves readily for mission planning.

1. Circumlunar Envelopes

For circumlunar missions, the geometric parameters involved are i_{VTL}, i_m, θ_M and i_{VTE}, which can be expressed in terms of each other by spherical trigonometry. From Section A of this chapter, it is evident that the combination of i_m and θ_M required to fulfill the mission for a certain date is a major mission constraint. With this in mind, the geometric parameters of i_{VTL}, i_m, θ_M and i_{VTE} are presented in the manner shown in the sketch below and in Figs. 22 to 31. All data has been taken from the circumlunar catalogue in Chapter VI, and it is presented with i_{VTL} as a function of θ_M for the parameter of i_{VTE} in the field of the graph. Superimposed on the figures is the remaining geometrical parameter i_m. Thus the required combination of i_m and θ_M (Section A) could be easily plotted on the same figure and the required i_{VTL} and i_{VTE} relation immediately determined. Each figure is for a specific $R_{\oplus}$ and h_{PL} and represents an inject north case. The figures can be interpreted for the inject south case by adding 180° to θ_M and letting i_{VTE} (inject south) = $-i_{VTE}$ (inject north). Notice that to the right of $i_{VTE} = 0°$, if the injection direction is north, the return direction is also north and if the injection direction is south the return direction is also south. On the left of $i_{VTE} = 0°$, the return direction is south if the injection direction is north and north if the injection direction is south. Only the direct returns are displayed on the figures.

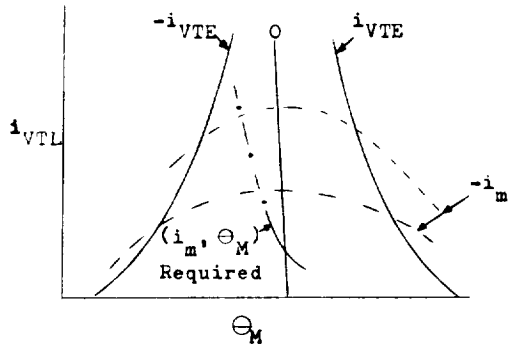

Below is a table listing the available mission planning envelopes for circumlunar trajectories.

Fig.	$R_{\oplus}$ (ER)	h_{PL} (km)
22	56	185.2
23	56	1000
24	56	5000
25	60	185.2
26	60	1000
27	60	3000
28	60	5000
29	64	185.2
30	64	1000
31	64	5000

Application of these envelopes to mission planning is clearly demonstrated in sample mission I of Section G. If desired, mission envelopes for retrograde returns can be generated from the catalogue.

2. Transearth or Translunar Envelopes

For transearth trajectories, with h_{PL} and h_{PE} constant, the geometrical parameters involved are i_m, θ_{MTE} and i_{VTE}. These parameters are plotted in envelopes which present i_{VTE} as a function of θ_{MTE} for values of i_m from 5° to 90°. The data has been obtained from the transearth trajectory catalogue of Chapter IX. For a given $R_{\oplus}$, an envelope was determined for each flight time, t_p, of 70, 90 and 110 hr and the envelopes are given in Figs. 32 to 40. They reflect data only for direct returns and the above t_p. If additional envelopes are desired for retrograde returns or other t_p, these cases can also be generated from the transearth catalogue. Listed below are the available envelopes for transearth trajectories.

Fig.	$R_{\oplus \mathbb{C}}$(ER)	t_p(hr)	
32	56	70	h_{PL} = 185.2 km
33	56	90	h_{PE} = 183 km
34	56	110	
35	60	70	(Transearth injection--west (retrograde))
36	60	90	
37	60	110	
38	64	70	
39	64	90	
40	64	110	

Figures 32 to 40 also provide scales that allow easy interpretation for translunar trajectories. The curves and scales are established through the interpretation rules given in Chapter IX, Subsection A-2. The envelopes are used in the same manner as those representing circumlunar trajectories (Figs. 22 to 31), i.e., the i_m θ_{MTE} or θ_{MTL} required to acquire a certain site or position can be directly drawn on the figures. The use of these figures is again illustrated in sample mission II of Section G.

G. SAMPLE MISSIONS

Chapter IV described various classes of lunar trajectories together with missions that might employ them. Trajectory data has been graphically catalogued for the circumlunar class in Chapter VI and for the approach and return-to-earth class in Chapter IX.

It was noted in Chapter VI that the circumlunar trajectories were restricted to passing the moon relatively close to the MOP ($i_m \lesssim \pm 15°$). If this feature is acceptable, the use of such trajectories is most desirable because of their "safe" nature, especially if the spacecraft is manned or must be recovered.

In Chapter IX it was pointed out that two types of mission parameters cannot be achieved with the circumlunar class, but an approach trajectory is required. For approach trajectories, first, the flight time from earth to the moon or from the moon to earth can be easily varied by two days, and secondly, an area or site anywhere on the lunar surface can be surveyed or explored ($0° \leq i_m \leq 180°$).

Mission planning not only involves determination of launch dates, lighting conditions, mission profiles, etc., but also includes analysis of the generalized data of the catalogues to establish various parameter trends and tradeoffs and an analysis of how these parameters form or modify the operational concept and system design. For instance, summary plots such as Figs. 7, 8, and 9 of Chapter VII can be generated to determine overall ΔV requirements to enter into a circular lunar orbit. Other summary charts dealing with flight time, injection velocity, etc., are easily obtained, and pertinent aspects of the lunar mission problem can be clearly illustrated. For example, the timing problem of returning to a specific earth site from a circumlunar trajectory, by comparing total flight times with the earth's rotation during this time, indicates that the required pericynthion altitude of the trajectory will vary throughout the lunar month. Also, when the accessibility of lunar landing sites for the approach trajectory class is considered, it can be assumed that for lunar bases at a given latitude relative to the MOP the variation in t_p and ΔV for a variation in descending node of $-30° \leq \Delta\theta_{MTL} \leq 30°$ is insignificant. This assumption is based on a comparison of t_p and ΔV necessary to land at these lunar sites. Variations in ΔV and t_p are also very small with variation in lunar latitude, and it is apparent that the higher the value of translunar trajectory inclination, i_{VTL} (which is a direct function of the day of the lunar month), the higher the value of ΔV. However, this is not necessarily true if it is acceptable to fly the mission with a different t_p.

This section illustrates that part of mission planning wherein launch and injection dates, lighting conditions as well as mission profiles and requirements are examined. To this end, two sample missions have been presented. The first mission has been chosen to illustrate the use of the circumlunar trajectory catalogue and the iterations and interpolation procedures to follow when catalogued data is not directly applicable. The first mission also illustrates the use of the transearth catalogue of Chapter IX. In the second mission, use of the translunar catalogue of Chapter IX and the empirical equations of Section E is illustrated.

The numerical procedures presented in the sample missions require only a slide rule, thereby allowing rapid evaluation of various aspects of the mission, except for the determination of the required $i_m - \theta_M$ relationship given by the equations in Section A. For this part of the mission planning phase it is again emphasized that these equations be programmed on a digital computer, if the planning of specific missions is to be done efficiently.

Although the steps outlined in the sample missions seem lengthy at times, the actual number of arithmetical steps and data manipulations is small.

1. Sample Mission I

Mission: It is desired to conduct a manned lunar mission during October 1966, for the purpose of landing and exploring the Sinus Medii region.

For purposes of visualization, a schematic of the mission is presented below.

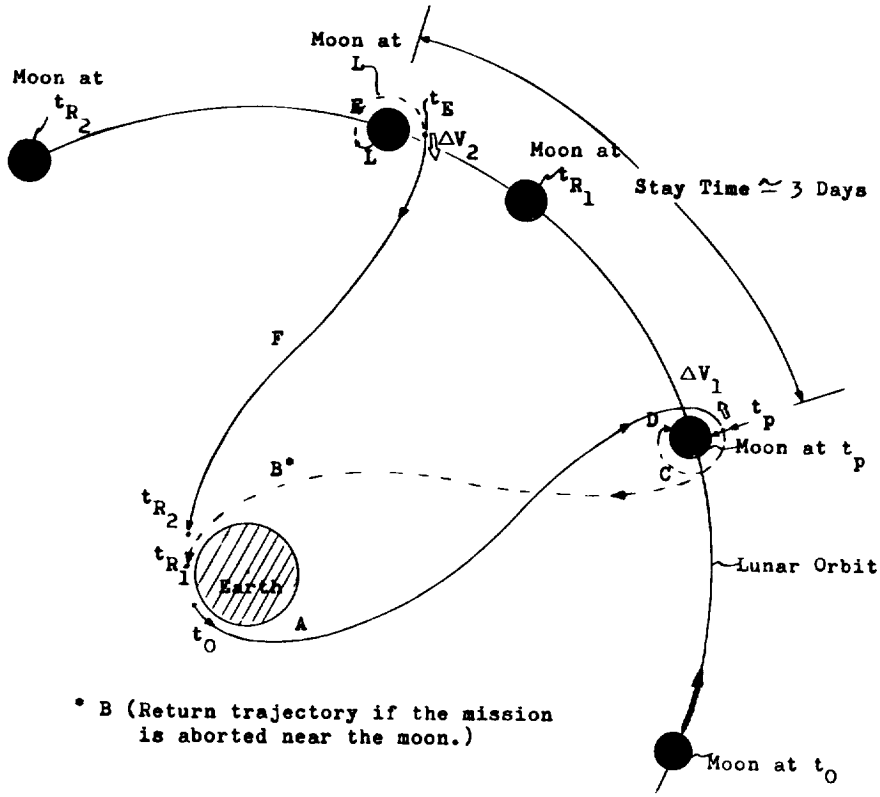

* B (Return trajectory if the mission is aborted near the moon.)

Injection into the circumlunar trajectory (A, B) takes place at time t_0. The spacecraft transfers ballistically along the nominal translunar trajectory A until pericynthion is attained at time t_p. At this time the velocity impulse ΔV_1 is applied to reduce the velocity of the spacecraft to the circular orbital velocity around the moon. The spacecraft continues in a circular lunar orbit C. At the proper point in this orbit a descent is made to the specified landing site along trajectory D. However, if for some reason the velocity impulse ΔV_1 cannot be applied, the transearth portion B of the circumlunar trajectory is designed to result in a safe re-entry at t_{R_1} of the spacecraft. (Trajectory B is referred to as the abort trajectory.) Although a safe re-entry is guaranteed in the event the mission is aborted at t_p, the geographical re-entry point may be over remote recovery areas. Therefore, a maneuver at some time on the transearth abort trajectory B should be performed to adjust the re-entry point.

If the mission is not aborted, it is assumed that the lunar landing is executed and that the crew spends approximately three days in exploration. At the end of this lunar stay period, an ascent from the lunar surface is conducted (trajectory L) and a circular parking orbit around the moon, E, established. When the proper point in the parking orbit is reached, the spacecraft is accelerated into the nominal transearth trajectory F by an impulse ΔV_2 at time t_E. The nominal transearth trajectory F allows a spacecraft to perform a re-entry at t_{R_2} along PMR (Pacific Missile Range). The detailed specifications for this mission are as follows:

Specification I. Nominal Translunar Trajectory (A)

(1) A circumlunar class translunar trajectory will be employed.

(2) The spacecraft is launched from Cape Canaveral with launch azimuth restrictions given by $70° \leq A \leq 110°$.

(3) Parking orbits are used prior to translunar injection.

(4) Injection may be either north or south relative to the MOP.

(5) Injection conditions are

$$h_0 = 250 \text{ km}$$

$$\gamma_0 = 5°$$

(6) The pericynthion altitude of the circumlunar trajectory is 185.2 km.

(7) At pericynthion, thrust is applied to decelerate the spacecraft into a circular lunar orbit.

Specification II. Abort Transearth Trajectory (B)

(8) The transearth portion of the circumlunar trajectory (if the lunar orbit is not established) must have an inclination of 31.5 ± 3° relative to the earth's equator and must return "direct."

(9) A maneuver (in order to adjust return inclination and/or time of (8)) on the transearth abort trajectory is permissible.

(10) Atmospheric re-entry at earth for the abort trajectory must be direct.

(11) Re-entry along PMR is specified and preferable, but it may occur along AMR (Atlantic Missile Range) if absolutely necessary.

(12) Vacuum perigee of the transearth trajectory is 46 km.

Specification III. Nominal Transearth Trajectory (F)

(13) The lunar landing is made in daylight and a stay time of approximately three days is desired on the lunar surface.

(14) For return, the spacecraft is launched from the lunar surface into a 185.2 km circular lunar parking orbit.

(15) The lunar launch and ascent to lunar orbit phase is to be conducted in daylight.

(16) There are no requirements for a lunar rendezvous.

(17) The spacecraft is injected from the lunar orbit into the nominal transearth trajectory that has the same specifications as given under headings 8 and 9, and the nominal re-entry occurs along the PMR.

(18) The nominal transearth injection conditions are

$$h_{PL} = 185.2 \text{ km}$$

$$\gamma_{\mathbb{C}0} = 0°$$

Step I: Choose a lunar landing site

The first step in analyzing this mission is to refer to lunar maps on which features of the lunar surface are shown. The maps that are available at present are listed and can be procured from the agencies listed in Chapter III, Subsection A-2g, and a typical lunar aeronautical chart has been reproduced in Chapter II. The objective at this time is to select the selenographic coordinates of the landing site. Although the detail required for the actual planning of missions cannot be obtained with the available maps, they nevertheless are adequate for preliminary analyses.

In the Sinus Medii region (from above referenced maps and from Fig. 1, Chapter III), it appears that a suitable landing site can be located approximately in the center of the region ($\phi_{\mathbb{C}} = 0°$, $\lambda_{\mathbb{C}} = 0°$). See Chapter III for additional explanation on selenographic coordinates $\phi_{\mathbb{C}}$, $\lambda_{\mathbb{C}}$.

Step II: Choose an arrival date

The next step is to choose an approximate pericynthion arrival date. This can be determined from Section C, which presents the approximate lighting conditions of the moon throughout this decade. From the calendar in the appendix Table 1, showing the number of days in the year after January 0, is seen that for the month of October 1966, the day of the year varies from 274 to 304. Referring next to (Figs. 4a and 4b) showing the phases of the moon for 1966, it is evident that in October 1966 there are two periods in which a daylight lunar landing can be conducted.

(1) Days 274 to 281

(2) Days 294 to 304.

The moon arrival time is arbitrarily chosen to be in the first period. Knowing that a stay time of about three days is desirable and that a launch from the lunar surface in daylight is specified (see item 15, above), an arrival time of $277^d.00$ is chosen. This time corresponds to 00:00 UT October 4, 1966. Also from Figs. 4a and 4b the declination of the moon δ_M is +20.7°, the inclination i_{em} of the MOP to the equator is 27°, and the earth-moon distance R_M is 61.9 ER. In addition, approximate lighting conditions on the arrival date can be estimated from the figures, as shown below:

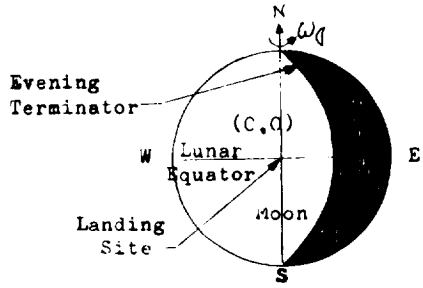

The evening terminator is approximately 45° East of the landing site. The exact lighting conditions can also be determined from Section B, if an ephemeris of the sun is available. For comparison purposes, exact lighting is presented below for the $277^d.00$:

The evening terminator is 36.5° E of the landing site and its inclination to the lunar equator is $i_T = 91°$.

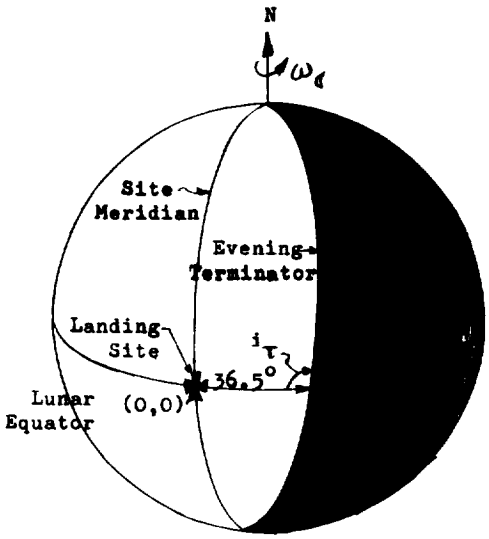

since the EML does not generally intersect the MOP due to the lunar librations (Chapter III), the flight to the landing site must be carefully planned. For a given arrival date there is a specific $\theta_M - i_m$ relationship that allows a lunar orbit to pass over a particular site (see sketch below). This facet of the problem is fully discussed in Section A.

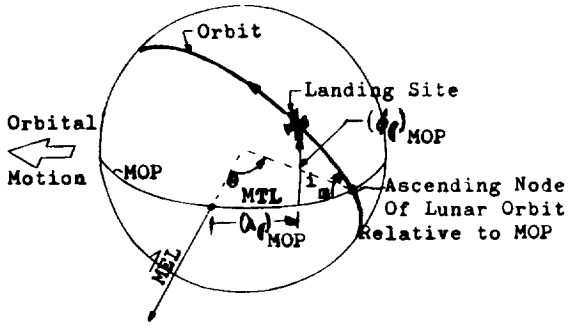

Step III: Obtain the translunar trajectory inclination limits

Referring again to Fig. 4a, $277^d.00$ is between the ascending node and maximum northerly declination of the moon $\delta_M = +20.7°$. With this in mind, and turning to Section D, the central angle, β_ℓ, measured from the ascending node to the moon, can be determined. For a $\delta_M = +20.7°$ and $\beta_\ell = 51°$ from Fig. 10. From Fig. 11, the possible ranges of i_{VTL} are found for this (see the following table).

	i_{VE} (deg)	i_{VTL} (injection north) (deg)	i_{VTL} (injection south) (deg)
Minimum	28.5	38.2	3.8
Maximum	34.5	46.0	11.7

These permissible ranges (or limits) are now superimposed on Figs. 15, 18 and 29, the mission planning envelopes for circumlunar trajectories for $h_{PL} = 185.2$ km. Each figure corresponds to a given earth moon distance; i_{VTL} is plotted against θ_M; and i_m and i_{VTE} are parameters. (see Section F for chart explanation.) For purposes of clarification, one of the charts ($R_M = 60$) is repeated at this time in Fig. 41 with the above injection limits noted on it.

Step IV: Determine required i_m, θ_M

Since the data presented on the mission planning charts is relative to the MOP and

Utilizing the equations presented in Section A, the required $\theta_M - i_m$ relationship to ensure passing over the site, after a lunar orbit has been established, is given below in the table for the selenographic landing site coordinates $\lambda_\ell = 0°$, $\phi_\ell = 0°$ at $277^d.00$. The landing site coordinates for this time relative to the $\overrightarrow{MEL}$ and MOP are $(\lambda_\ell)_{MOP} = +5.69°$ and $(\phi_\ell)_{MOP} = +1.94°$.

Required θ_M and i_m for Sample Mission I for Moon Arrival at $277^d.0$

Injection	θ_M (deg)	i_m (deg)
Direct North	10	24.23
	20	7.79
	30	4.70
	40	3.43
	50	2.77
	60	2.39
	70	2.15
	80	2.01
	90	1.95
Direct South	100	1.94
	110	2.00
	120	2.13
	130	2.35
	140	2.71
	150	3.32
	160	4.46

Direct South Injection	θ_M (deg)	i_m (deg)
↓	170	7.13
	180	18.84

The required θ_M, i_m from the above table is now superimposed on the mission planning charts. A sample of this super position is also shown in the special included envelope (Fig. 41). For the allowable i_{VTL} - range, the resulting i_{VTE} of the circumlunar trajectory can be listed as shown below:

$$\Delta\phi_{TL} = \pm(0.22 + 0.000156\, h_{PL}) \; C_0 \sin i_{VTE} + 1.0$$

where

h_{PL} = pericynthion altitude, km

C_0 = constant (from Fig. 15)

use + for inject south cases
use - for inject north cases

For $R_{\oplus\mathbb{C}}$ = 61.9 ER, and h_{PL} 185.2 km, $\Delta\phi_{TL}$ is + 1.0° for the inject north case and + 1.2° for the inject south case. Therefore, the $\beta_{\mathbb{C}}$ of 51.0°

i_{VTL} (deg)	$R_{\oplus\mathbb{C}}$ (ER)	i_{VTE} (deg)	i_m (deg)	θ_M (deg)	$R_{\oplus\mathbb{C}}$ (ER)	i_{VTE} (deg)	i_m (deg)	θ_M (deg)	$R_{\oplus\mathbb{C}}$ (ER)	i_{VTE} (deg)	i_m (deg)	θ_M (deg)
Inject North												
38.2	56	-14	5.9	25	60	-11	5.6	26	64	-12	5.8	25.5
46	↓	-19	6.9	22	↓	-15	6.6	22	↓	-14.1	6.6	22.5
Inject South												
3.8	56	+21	3.0	144	60	-21	2.5	145	64	+19	3.0	147
11.7	↓	+26	4.3	158	↓	+27	4.2	158	↓	+27	4.5	160

However, only the mission parameters associated with the highest value of i_{VTL} for each case will be selected for the remainder of this sample mission. The actual parameters occurring at $R_{\oplus\mathbb{C}}$ = 61.9 ER are obtained by cross plotting i_{VTE}, i_m, θ_M versus $R_{\oplus\mathbb{C}}$ for i_{VTL} = 46° (for inject north) and 11.7° (for inject south) with the result for the mission parameters i_{VE} = 34.5°, $R_{\oplus\mathbb{C}}$ = 61.9 ER given below:

i_{VTL} (deg)	i_{VTE} (deg)	i_m (deg)	θ_M (deg)
46.0	-14.5	6.6	22 (inject north)
11.7	+27.0	4.3	159 (inject south)

Step V: Adjusted translunar trajectory characteristics

If the $\vec{x}_E$-axis (see Chapters III and VI) were directed toward the moon at the arrival time t_p, then the above i_{VTL} is correct. However, Section E gives an empirical equation that adjusts β for a specific mission, since such alignment of $\vec{x}_E$ with lunar position at t_p does not occur in practice. The equation for $\Delta\phi_{TL}$ of Section E is repeated below:

must be adjusted by the above increments in order to determine a more accurate value of i_{VTL}. Thus, Step III is repeated by re-entering Fig. 11 with $\beta_{\mathbb{C}}$ adjusted by approximately +1.1° or $(\beta_{\mathbb{C}})_{adj}$ = 52.1°, to obtain a new value of i_{VTL} for inject north and inject south cases:

i_{VE} (deg)	i_{VTL} (inject north) (deg)	i_{VTL} (inject south) (deg)
34.5	45	12.0

Step IV is then repeated to refine the mission parameters of i_{VTE}, i_m and θ_M. The resulting adjusted parameters are:

Adjusted Parameters (i_{VE} = 34.50°, $R_{\oplus\mathbb{C}}$ = 61.9 ER)

i_{VTL} (deg)	i_{VTE} (deg)	i_m (deg)	θ_M (deg)	Case
45	-14.5	6.6	23	(inject north, return south direct)
12	+27.0	4.4	159	(inject south, return north direct)

Normally i_{VE} = 34.5° is used to evaluate the parameters. Step V can be omitted if the resulting values of i_{VTL} > 15° and the values obtained from Step IV can be used instead. However, for values of i_{VTL} < 15°, Step V must be carried through.

Step VI: Translunar flight time

To summarize steps (I) to (V), the following mission parameters have been found to acquire the landing site at $277^d.00$:

$i_{VTL} = 45°, 12.0°$

$i_{VTE} = -14.5°, +27.0°$

$h_{PL} = 185.2$ km

$R_{\oplus \mathbb{C}} = 61.9$ ER

$i_m = 6.6°, 4.4°$

$\theta_M = 23.0°, 159°$

$h_0 = 250$ km

$\gamma_0 = 5°$.

It is now desired to find the transit time t_p from the earth injection point to pericynthion. From Chapter VI, Catalogue Figs. C-5, C-29 and C-64, t_p may be obtained as a function of $R_{\mathbb{C}}$ for the above parameters. For $R_{\mathbb{C}} = 61.9$ ER $t_p = 73.0$ hr for the inject north case and 71.1 hr for the inject south case, and the time of injection onto the translunar trajectory, t_0 is given by

$$t_0 = 277^d.00 - t_p$$

Step VII: Determine launch point position on injection date

The purpose of the following several steps is to determine the adjustment in arrival and injection time such that the launch can occur from Cape Canaveral. This must be done because the arrival time chosen in Step I does not, by any means, guarantee that the translunar trajectory and parking orbit will provide an earth ground trace which passes over Cape Canaveral at liftoff.

The procedure is as follows:

Referring to Table 2, full moon occurs on September 29, 1966, at 16:48 UT and the last quarter on October 7, 1966, at 13:09 UT. These phases bracket the moon arrival time and occur on $272^d.70$ and $280^d.55$, respectively. Also from Fig. 4a, the corresponding δ_M is -0.5° and +27.0°, respectively.

From now on, only the inject north case will be considered, since the steps involving the inject south case are identical. The following sketch illustrates the hour angles of the moon and sun and the location of the Greenwich meridian and of Cape Canaveral at injection,

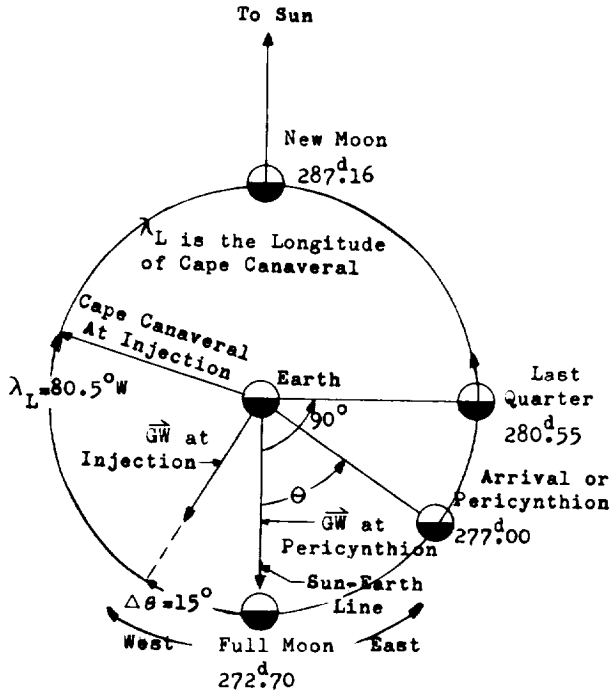

where the plane of the paper denotes the ecliptic plane. Consider the moon projected into the ecliptic plane. The average rotational rate of the moon relative to the sun-earth line in its orbit from full moon to the last quarter is given by:

$$\omega_{\oplus \mathbb{C}} = 90° / (280^d.55 - 272^d.70) = 11.47° / \text{day}$$

At arrival or pericynthion $277^d.00$, the moon is located θ degrees from the sun-earth line, where

$$\theta = (277^d.00 - 272^d.70)\,\omega_{\oplus \mathbb{C}} = 4^d.3 \times \frac{11.47°}{\text{day}} = 49.3°$$

Since pericynthion occurs at 00:00 UT, the Greenwich meridian at pericynthion, denoted by $\overrightarrow{GW}_p$ in the above sketch, is on the sun-earth line opposite to the direction to the sun. It has been determined in previous steps that injection for the inject north case takes place $73^h.0$ or $3^d.04$ earlier. Therefore, at injection the Greenwich meridian, now denoted by $\overrightarrow{GW}_0$, is located at $\Delta\theta = 15°$ where $\Delta\theta$ is positive to the west of the sun-earth line. For the inject south case $\Delta\theta = -13.5°$ (to the east of the sun-earth line) at the time of injection since the earth-moon transit time for the inject south case is $71^h.1 = 2^d.96$. The longitude of Cape Canaveral is 80.5° W; its location for the inject north case has been shown on the previous sketch. The next sketch illustrates the geometry in three dimensions for the inject north case by showing the celestial sphere centered at earth:

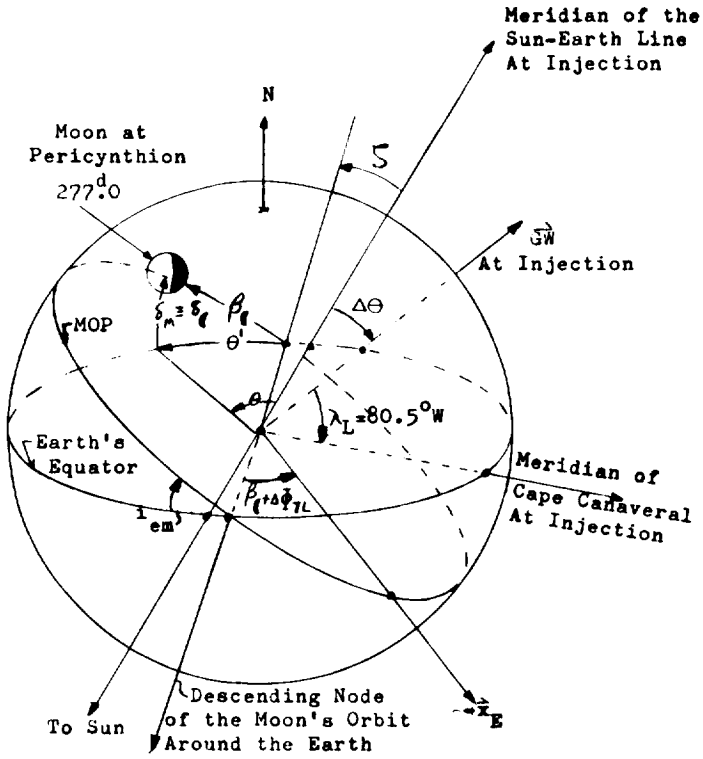

The hour angle ζ, which is measured from the midnight meridian eastward to the ascending node of the moon at injection, is given by

$$\zeta = \theta - \theta'$$

$$\theta = (273.96 - 272.7)\, 11.47 = 14.45°$$

where

$$\theta' = \theta'' \qquad 0 < \beta_{\mathbb{C}} < 180°$$

$$\theta' = 360 - \theta'' \qquad 180° < \beta_{\mathbb{C}} < 360°$$

and $\theta'' = \cos^{-1}\left(\dfrac{\cos \beta_{\mathbb{C}}}{\cos \delta_M}\right)$.

For the inject north case at injection $\beta_{\mathbb{C}} = 12°$ and $\delta_M = 5.5°$ so that

$$\theta'' = 10.3°$$

$$\theta' = 10.3°$$

$$\zeta = 14.45 - 10.3° = 4.2°$$

Therefore, the meridian of Cape Canaveral is $\lambda_L + \Delta\theta + \zeta = 80.5° + 15° + 4.2° = 99.7°$ west of the ascending node of the moon at injection ($273^d.96$).

Step VIII: Determine injection point latitude and longitude

Next the latitude and longitude of the injection point at the time of injection for the inject north case are found. From the previous sketch in step VII, the $-\vec{x}_E$-axis is located in the MOP and the included angle measured eastward from the descending node is the adjusted value of $\beta_{\mathbb{C}}$, i.e., $(\beta_{\mathbb{C}})_{adj} = \beta_{\mathbb{C}} + \Delta\Phi_{TL} = 52.1°$.

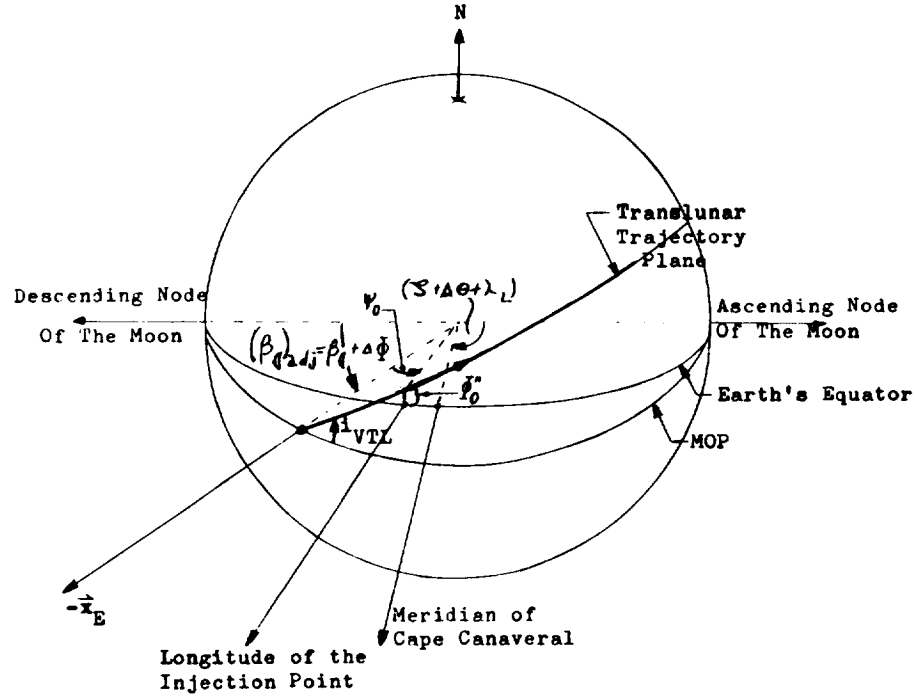

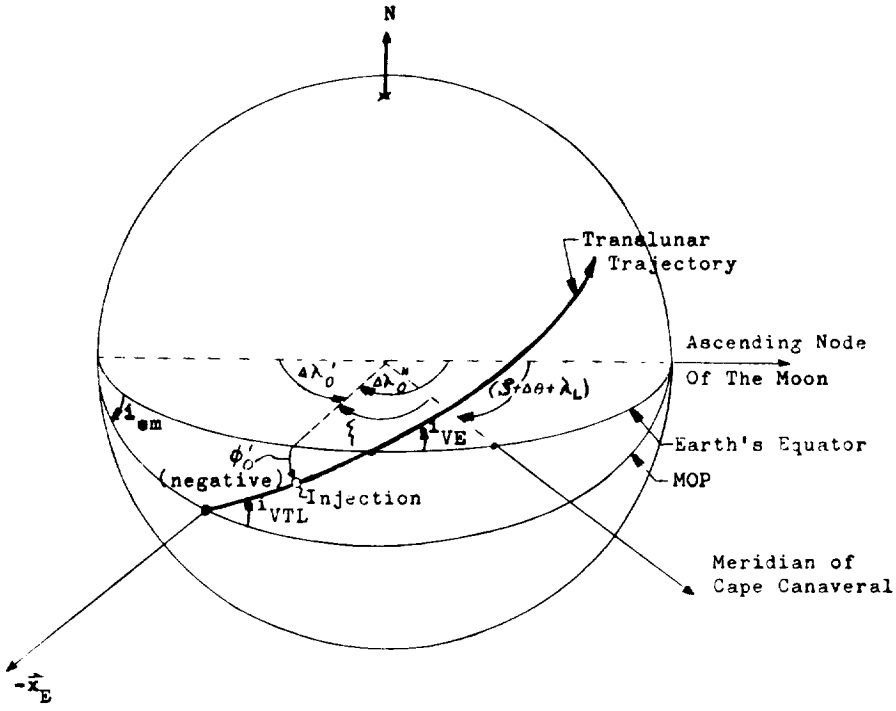

The geocentric injection latitude ϕ'_0 is given by the following equation, where ψ_0 is found in Chapter VI, Figs. C-2, C-26, C-61 for $R_{\oplus\mathbb{C}}$ = 61.9 ER, $i_{VTL} = 45°$, and $\psi_0 = 17.8°$:

$$\phi'_0 + 90° = \cos^{-1}\Big[-\sin\psi_0 \sin i_{VTL} \cdot \cos i_m + \big(\cos\psi_0 \sin(\beta_{\mathbb{C}} + \Delta\Phi_{TL}) - \sin\psi_0 \cos i_{VTL} \cdot \cos(\beta_{\mathbb{C}} + \Delta\Phi_{TL})\big)\sin i_m\Big]$$

use $-i_{VTL}$ for inject south cases

use $+i_{VTL}$ for inject north cases

where, for the present sample mission $\phi'_0 = -5°$.

The injection longitude λ_0 as illustrated in the sketch above, can be found by use of several steps:

Calculate first

$$\Delta\lambda'_0 = \cos^{-1}\left(\frac{L}{\left[L^2 + M^2\right]^{1/2}}\right)$$

where

$$L = \cos\psi_0 \cos(\beta_{\mathbb{C}} + \Delta\Phi_{TL}) - \sin\psi_0 \cos i_{VTL} \sin(\beta_{\mathbb{C}} + \Delta\Phi_{TL})$$

$$M = (\cos\psi_0 \sin(\beta_{\mathbb{C}} + \Delta\Phi_{TL}) + \sin\psi_0 \cos i_{VTL} \cos(\beta_{\mathbb{C}} + \Delta\Phi_{TL}) \cos i_m + \sin\psi_0 \sin(\pm i_{VTL}) \sin i_m$$

where the negative sign is used for inject north and the positive sign is to be used for inject south cases. If the quantity M is negative in the equation above, then $(360° - \Delta\lambda'_0)$ should be used instead of $\Delta\lambda'_0$ above. The quantity $\Delta\lambda'_0$ is the longitude increment of the injection point measured from the descending node eastward. As a second calculation, obtain $\Delta\lambda''_0$, the longitude increment of the injection point measured from the ascending node westward by use of

$0 \leq \Delta\lambda'_0 \leq 180°$ $\quad\Delta\lambda''_0 = 180° - \Delta\lambda'_0$

$180° \leq \Delta\lambda'_0 \leq 360°$ $\quad\Delta\lambda''_0 = 540° - \Delta\lambda'_0$.

For the inject north case under consideration

$\Delta\lambda'_0 = 65°$

$\Delta\lambda''_0 = 115°$.

Finally, from step VII the meridian of Cape Canaveral is 99.7° West of the ascending node of the moon at injection. Therefore the geographic injection longitude is $\lambda_0 = 80.5°$ W + $\xi = 95.8°$ W, where $\xi = \Delta\lambda''_0 - 99.7° = 15.3°$ (measured positive westward as indicated on the sketch).

Step IX: Actual launch time and pericynthion time

The ascent trajectory will be neglected for the following calculations, i.e., the lunar space vehicle

is assumed to "start out" or be launched at the parking orbit altitude h_{PL} = 185.2 km above Cape Canaveral, with the corresponding circular orbital velocity. This assumption is quite good for lunar spacecraft due to the short ascent time (on the order of 300 seconds). In any case, a further correction for launch and pericynthion time can be performed as soon as the booster for the lunar mission has been selected and ascent trajectory calculations for the booster have been performed.

With this assumption and the data generated in steps I to VIII, the next sketch can be drawn. The prime purpose of step IX is to obtain the longitude increment $\Delta\lambda$ of the parking orbit ground trace measured from the meridian of Cape Canaveral to the intersection of the latitude of Cape Canaveral by the parking orbit. Furthermore the orbital range angle Φ_{LO} from this intersection point to the translunar injection point must be determined.

Define an orbital central angle β_L from the ascending node of the parking orbit to its intersection with the launch site parallel of latitude. For i_{VE} = 34.5°, β_L becomes

$$\beta_L = \sin^{-1}\left(\frac{\sin \phi'_L}{\sin i_{VE}}\right) = \sin^{-1}\left(\frac{\sin 28.5°}{\sin 34.5°}\right) = 57.3°.$$

Define an orbital central angle from the injection point to the ascending node of the parking orbit by β'_0, where $\beta_0 = 360 - \beta'_0$, and

$$\beta'_0 = \sin^{-1}\left(\frac{\sin \phi'_0}{\sin i_{VE}}\right) = 8.9°.$$

Since these two equations are spherical trigonometry relations, the quadrant of the angles must be determined from the previous sketch. The angles β_L, β'_0 have been defined for a given hemisphere and node.

For the inject north case in question, the injection takes place in the southern hemisphere and the nearest node is the ascending node, as illustrated on the sketch.

The orbital central angle from injection to the intersection of the launch site latitude is $\beta_L + \beta'_0$ = 66.2° for this sample mission. Define the longitude increments corresponding to β_L as $\Delta\lambda_L$ and of β'_0 as $\Delta\lambda'_{PO}$ where $\Delta\lambda_L$ and $\Delta\lambda_{PO}$ are given by

$$\Delta\lambda_L = \cos^{-1}\left(\frac{\cos \beta_L}{\cos 28.5°}\right) = 52°,$$

$$\Delta\lambda_{PO} = \cos^{-1}\left(\frac{\cos \beta'_0}{\cos \phi}\right) = 6° .$$

Therefore the longitude increment from the location of Cape Canaveral to the intersection of the parking orbit with the launch parallel of latitude is

$$\Delta\lambda = \Delta\lambda_L + \Delta\lambda'_{PO} - \xi = 42.7° \text{ E}.$$

For the assumption of no ascent trajectory to the parking orbit, the spacecraft must be located either at point A or at point B at launch. Point A represents a launch azimuth A = 70°, while point B calls for A = 110°. The former point has been arbitrarily selected as the launch condition for the remainder of the sample mission. Thus, the

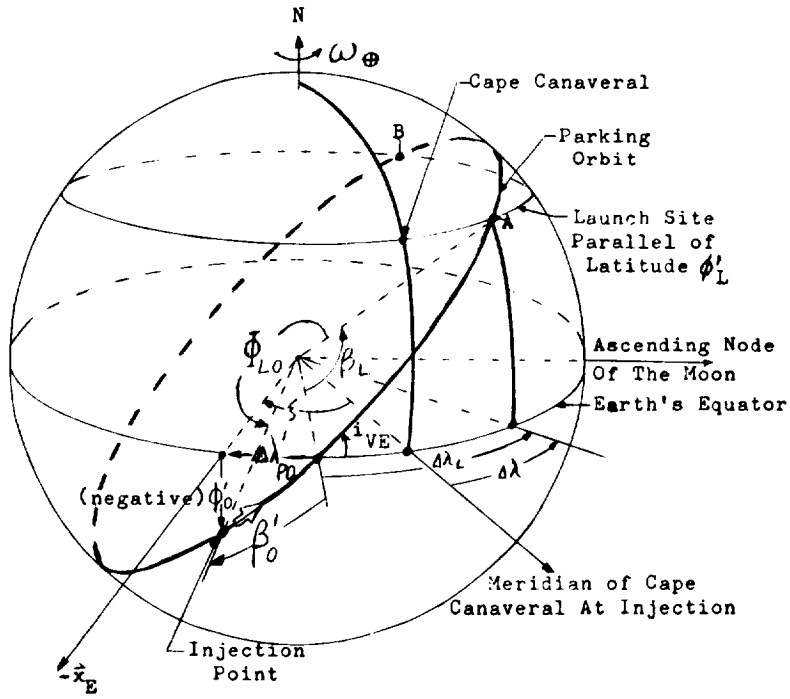

range angle Φ_{LO} from point A to the translunar injection point is

$$\Phi_{LO} = 360° - (\beta_L + \beta_0') = 297.8°.$$

Since the average angular velocity of the spacecraft in its parking orbit is 246.6 deg/hr, it must be launched from Cape Canaveral at a time equal to the injection time minus the time to travel the range angle Φ_{LO}, which is 297.8° / 246.6°/hr = 1.21 hr = 0.05 d. From step VII, translunar injection occurs on 273.96 d. Therefore the launch time is:

$$\text{launch time} = 273.96^{d} - 0.05^{d} = 273.91^{d}.$$

However, if the location of the spacecraft in the parking orbit is retraced back in time to the launch site latitude ϕ_L', Cape Canaveral itself rotates with the earth backward or westward during this interval. For an elapsed time of 1.21 hr Cape Canaveral has rotated westward by a longitude displacement equal to 1.21 hr · 15.04° / hr = 18.2°; where $\omega_\oplus$ = 15.04°/hr is the angular velocity of the earth about its axis. At launch, the actual position of Cape Canaveral is displaced from the required launch point (point A) by 42.7° + 18.2° = 60.9° toward the west as illustrated in the following sketch:

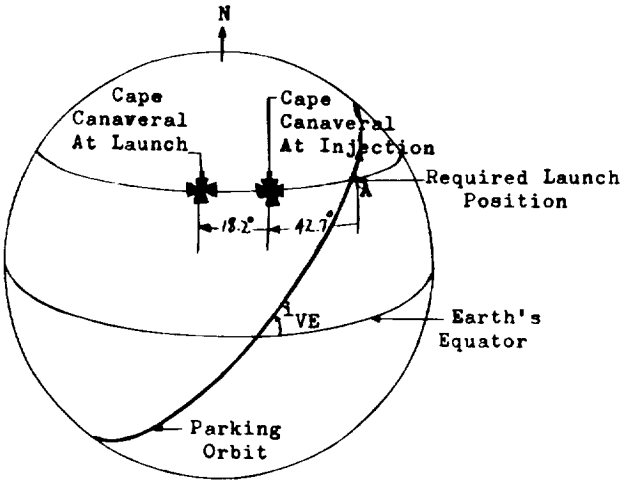

The parking orbit does not pass through Cape Canaveral at launch and the computed launch date is too early. Assuming that the flight time to the moon and all other parameters generated thus far remain unchanged by this change of launch time, then a first-order correction can be made to the launch date by conducting the launch at an interval of time Δt later, where Δt is the time required for Cape Canaveral to rotate with the earth to point A:

$$\Delta t = (18.2° + 42.7°)/15.04°/\text{hr} = 4.05 \text{ hr}.$$

Thus, the corrected launch time is:

$$\text{Launch time (corrected) } t_L = 273.96^{d} - 1.21^{h} + 4.05^{h} = 273.96^{d} + 2.84^{h} = 274.08^{d}$$

For the first-order correction, the range angle Φ_{LO} is the same for the new launch date, and the corrected injection date is

$$\text{Injection time (corrected)} = 273.96^{d} + 2.84^{h} + 1.21^{h} = 274.13^{d}$$

Similarly, the corrected arrival date is

$$\text{Moon arrival time (corrected)} = 273.96^{d} + 4.05^{h} + 73.00^{h} = 277.17^{d}$$

Step X: Iteration with improved arrival time

Steps II to IX are now repeated with the corrected moon arrival (or pericynthion) time. This is essentially the first iteration, and the steps of the first iteration are denoted by an asterisk (*). For each step, only the important parameters and their values are listed.

Step II*. The lighting conditions for the new arrival date have changed only slightly. The evening terminator is now 34.6° E of the landing site, and its inclination i_T = 91°.

Step III*. Revised values for δ_M, R_M, $\beta_{\mathbb{C}}$ and maximum i_{VTL} are δ_M = +21°, $R_{\oplus\mathbb{C}}$ = 61.8 ER, $\beta_{\mathbb{C}}$ = 52.2°, and the maximum i_{VTL} = 45° for the inject north case.

Step IV*. The required θ_M and i_m relationship for the direct inject north case are, by linear interpolation between the 277.00 d and 277.50 d:

θ_M (deg)	i_m (deg)
10	27.24
20	8.78
30	5.25
40	3.86
50	3.11
60	2.68
70	2.41
80	2.25
90	2.18

The trajectory parameters for $R_{\oplus\mathbb{C}}$ = 61.8 ER are:

i_{VTL}	i_{VTE}	i_m	θ_m	(Inject north and return south direct)
45	-12.5°	6.2°	25.2°	

Step V*. Step V* is not required, since $i_{VTL} > 15°$. However, as $\Delta\Phi_{TL}$ is approximately the same, it will be used.

Step VI*. The revised transit time is $t_p = 72.8$ hr, with injection at

$$t_0 = 277.169^{d} - 72.8^{h} = 274.136^{d}$$

Step VII*. At $t_0 = 274.136^{d}$, the angular displacement of the moon from the sun-earth line is:

$$\theta = (277.17 - 272.7)(11.47) = 51.1°$$

The Greenwich meridian is $\Delta\theta = 45.8°$ east of the sun-earth line, and the hour angle ξ remains approximately the same, i.e.,

$$\zeta = 4.2°,$$

and the meridian of Cape Canaveral is 80.5° - 45.8° + 4.2° = 38.9° W of the ascending node of the moon.

Step VIII*. The revised values for the injection parameters of step VIII become

$$(\beta_{\ell})_{adj} = 53.3$$

$$\psi_0 = 17.8°$$

$$\phi_0' = 4.4°$$

$$\Delta\lambda_0' = 63.5°$$

$$\Delta\lambda_0'' = 116.5°$$

$$\xi = 77.6°$$

$$\lambda_0 = 158.1° \text{ W}.$$

Step IX*. The revised values for the auxiliary parking orbit parameters are:

$$\beta_0' = 7.77°$$

$$\beta_L + \beta_0' = 65.07°$$

$$\Delta\lambda = 19.6° \text{ W}$$

$$\Phi_{LO} = 294.93°.$$

It takes 1.195^{h} to traverse the angle Φ_{LO} to yield

$$\text{Launch time} = 274.136^{d} - 1.195^{h} = 274.141^{d}$$

During this time, Cape Canaveral has rotated westward by a longitude increment of 18.0°.

At launch the actual longitude of Cape Canaveral is displaced from the parking orbit launch point A by 1.6° E. For this small discrepancy, the parking orbit trace, for all practical purposes, can be assumed to intersect Cape Canaveral at launch, thus satisfying the physical constraint of the mission, and eliminating the need for performing a second iteration.

However, if more accuracy is desired, the time of 0.1 hr may be subtracted from the revised launch, injection and moon arrival time to compensate for the 1.6° discrepancy mentioned above. This is also a logical point to include the ascent to parking orbit phase into the correction and to carry the calculations one decimal point further.

Step XI: Lighting conditions at earth launch time

The approximate lighting conditions may be found for the earth launch and earth injection phases with the aid of the next sketch, which shows a top view of the earth's equatorial plane.

From step VII*, $\zeta = 4.2°$, where ζ is the hour angle measured from the sun-earth line eastward to the ascending node of the moon and thus defines the location of the earth terminator as shown. Usually ζ is only accurate to within ±2°. From step VIII*, the injection meridian at the time of injection is 116.5° W of the moon's ascending node. Also from step VII*, the meridian of Cape Canaveral at injection is 38.9° W of the ascending node. Therefore the meridian of Cape Canaveral at launch is 38.9° W + 18.0° W or 56.9° W. Hence the spacecraft launch will definitely be in darkness and the injection in daylight. Launch or injection in darkness may or may not be acceptable, but for this sample mission there are no lighting restrictions for the earth-departure phase.

It should also be noted that the inject north case taken here represents the beginning of the launch tolerance for the variable translunar technique given in Chapter V. For inject north cases, launches can be made up to 4.9 hr beyond the above nominal launch time.

The same procedure can be used to determine trajectory characteristics and time of launch for the inject south case in step V.

Step XII: Aborted transearth trajectory

The next steps analyze the return-to-earth portion of the above circumlunar trajectory in the event entry into lunar orbit cannot be performed. From step IV* it was found that the return inclination i_{VTE} is -12.5° returning direct from the south. The total time of flight T (translunar injection to return vacuum perigee) is found in the same manner as the time to pericynthion t_p in steps VI and VI*. From Figs. C-6, C-30 and C-65 of the circumlunar catalogue in Chapter VI,

$$T = 143.4 \text{ hr}.$$

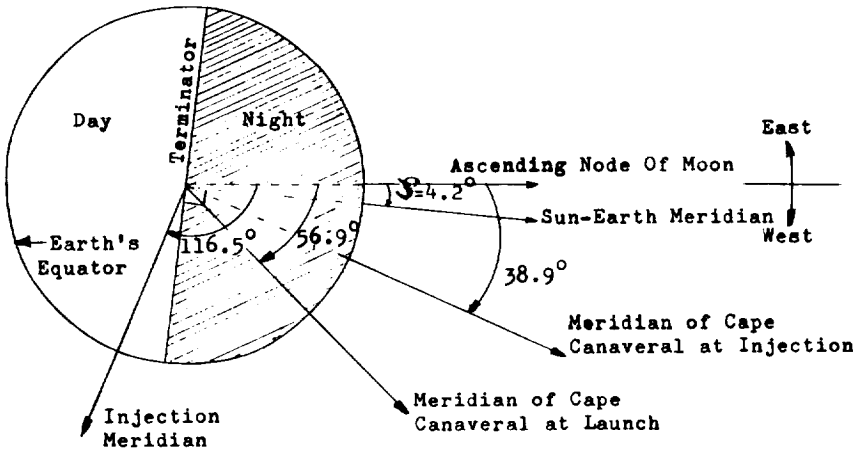

Mission specifications 8, 9 and 10 are directly related. From Chapter VI, Section A, a return inclination of $i_{VTEQ} \simeq 30°$ (relative to the equatorial plane of the earth) will place re-entry either along AMR or PMR. However, the re-entry direction must be specified relative to the equator. For re-entry along AMR, the return direction for the circumlunar trajectory is either direct from the north or retrograde from the south. Similarly, re-entry along PMR must be direct from the south or retrograde from the north. Two questions must now be resolved, namely:

(1) If the transearth trajectory does not return with the proper inclination, what is the propulsion requirement to correct the trajectory?

(2) If re-entry occurs geographically displaced from PMR, what propulsion requirement corrects the time of re-entry?

These questions will be answered in steps XIV and XV, respectively.

Step XIII: Transearth trajectory inclination (abort)

This step determines i_{VTEQ}. As was the case in steps V and V*, an empirical correction is applied to adjust the intersection of the transearth plane with the MOP. The correction factor is as follows and is discussed in Section E of this Chapter.

$$\Delta\Phi_{TE} = \pm (0.232 + 0.0001537\, h_{PL})\, D_0 \sin i_{VTE} - E_0$$

use + for inject south

use - for inject north

$$E_0 = 1.7 + 0.0375\,(R_{\oplus\mathfrak{C}} - 56)$$

where $R_{\oplus\mathfrak{C}}$ is measured in earth radii, h_{PL} in km, and D_0 is found in Fig. 16.

For the conditions:

$h_{PL} = 185.2$ km

$i_{VTE} = -12.5°$

$R_{\oplus\mathfrak{C}} = 61.8$ ER

$i_{VTL} = 45°$

$\Delta\Phi_{TE} = -1.9°$

Therefore, $(\beta_{\mathfrak{C}})_{adj} = \beta_{\mathfrak{C}} - \Delta\Phi_{TE} = 52.2°$ (step III*) $- 1.9° = 50.3°$.

Figure 13 is now entered with the above value of $(\beta_{\mathfrak{C}})_{adj}$ and $i_{VTE} = -12.5°$, yielding $i_{VTEQ} = 21°$ (direct from the north).

Step XIV: ΔV required to correct i_{VTE} (abort)

The previous step determined that the actual value of $i_{VTEQ} = 21°$. From mission specifications 8, 10 and 11, the minimum acceptable return inclination $i_{VTEQ} = -28.5°$, which is equivalent to $i_{VTEQ} = 331.5°$. (Note that this inclination is not inclination as normally defined, since it is measured from the west point on the horizon at the descending node to the branch of the trajectory in which the vehicle is approaching the node. Thus this inclination varies from 0 to 360° and carries with it the sense of vehicle motion.) Therefore, to correct the actual return inclination to the desired value, an i_{VTE} = change Δi_{VTE} of -27.5° is required, an estimate obtained also from Fig. 13. Assuming that the correction, in the form of a velocity impulse ΔV_i, is applied at a $R_{\oplus\Delta}$ of 40 ER, a first approximation of the ΔV required can be found through the use of Figs. 18 and 21. For the above conditions, $\Delta V_i = 134$ m/sec $\Delta\Phi_{TE} = +8.5°$. Re-enter Fig. 13 with $i_{VTE} = -12.5° - 27.5° = -40°$ and $(\beta'_{\mathfrak{C}})_{adj} = 53.3° + 8.5° = 61.8°$ and note that $i_{VTEQ} = 325°$. This manipulation is repeated by altering Δi_{VTE} until the desired value of i_{VTEQ} has been obtained. For this sample mission, the final values are: $\Delta V_i =$

110 m/sec, $(\beta'_{\mathbb{C}})_{adj} = 61.3°$, $\Delta\Phi_{TE} = 8°$, $i_{VTEQ} = 330°$ and $i_{VTE} = -35°$. The total time of the circumlunar trajectory remains T = 143.4 hr.

Step XV: Re-entry point position (abort)

It is assumed that the re-entry point is the vacuum perigee of the transearth trajectory, and that this point lies in the MOP. These assumptions are valid because the spacecraft's angular velocity at re-entry is much greater than the earth's rotational rate and because the actual re-entry point is but a few degrees (less than 10°) from the MOP for earth return. The following sketch illustrates re-entry:

If the ground trace of the re-entering spacecraft passes at some time through the point ($\phi' = 0°$, $\lambda = 149.5°$ E), re-entry will be along PMR (see Chapter VI, Subsection B-2). Define $\lambda = 149.5°$ E as the "acceptable longitude" meridian; it is displaced westward from the meridian of Cape Canaveral ($\lambda_L = 80.5°$ W) by 130°, and in order to satisfy the mission specifications the "acceptable longitude" meridian must pass through the ascending node of the transearth trajectory (point Q on the previous sketch). Redrawing the area of interest for the actual situation, the angle $\Delta\lambda_{PE}$ is found by spherical trigonometry.

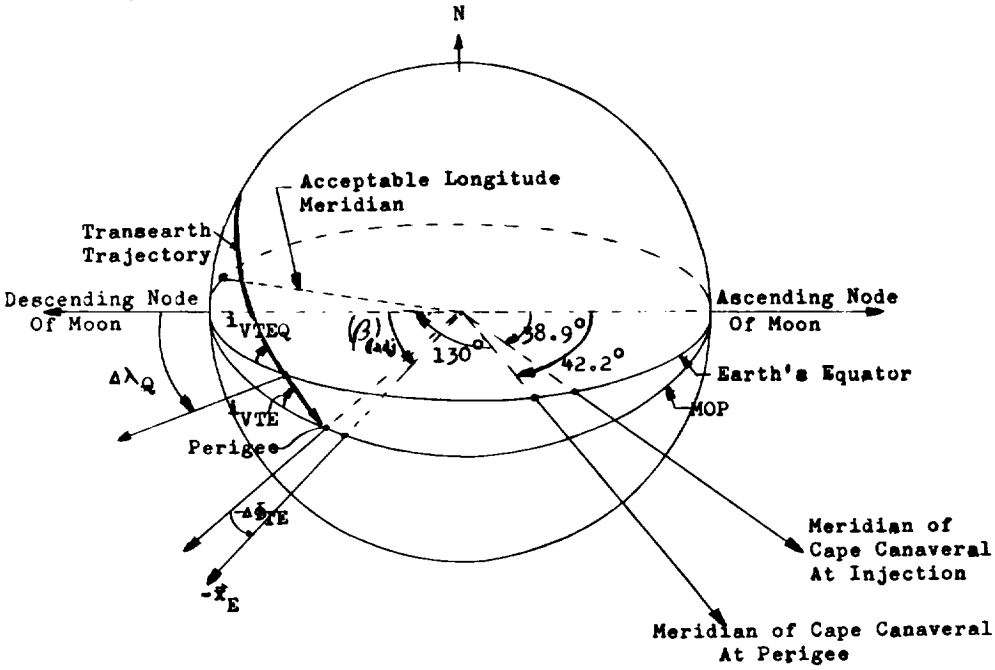

From step VII*, the meridian of Cape Canaveral is located 38.9° W of the lunar ascending node at translunar injection. During the interval from translunar injection to vacuum perigee, T = 143.4 hr, the meridian rotates with the earth at a rate of approximately 15.04 deg/hr. Therefore, at the time of perigee the position of this meridian is 42.2° W of the lunar ascending node.

where:

$$\Delta\lambda_{PE} = \tan^{-1}\left[\cos i_m \tan\left((\beta'_{\mathbb{C}})_{adj} + \Delta\Phi_{TE}\right)\right]$$

$$\delta_{PE} = \sin^{-1}\left[\sin i_m \sin\left((\beta'_{\mathbb{C}})_{adj} + \Delta\Phi_{TE}\right)\right]$$

$$\pm\lambda_{PE} = \sin^{-1}\left[\frac{\tan\delta_{PE}}{\tan i_{VTEQ}}\right]$$

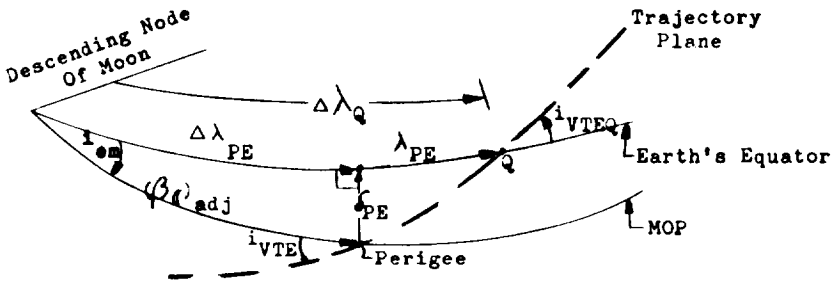

use + for + i_{VTE} (direct south return)

use - for - i_{VTE} (direct north return)

$\Delta\lambda_{PE} = 58.6°$

$\delta_{PE} = 23.4°$

$\lambda_{PE} = 30°$

$\Delta\lambda_Q = \Delta\lambda_{PE} + \lambda_{PE} = 88.6°$

Again, great care must be taken in determining the quadrants of the angles for each particular mission geometry, since spherical trigonometry has been used.

The longitude increment between Q and the meridian of Cape Canaveral at perigee is $\Delta\lambda_{LQ}$ = 180° - 88.6° - 42.2° = 47.2°. Therefore, the "acceptable longitude" meridian for PMR is located 82.8° W of Q. In order for Q to be coincident with the acceptable meridian, it becomes necessary to delay the arrival at perigee by 82.8°/15.04°/hr = 5.5 hr. From Fig. 17, if a time-delaying maneuver is conducted at $R_{\oplus\Delta}$ = 40 ER, the ΔV_t required to achieve the acceptable re-entry is 345 m/sec.

Step XVI: ΔV required to enter lunar orbit (also injection velocity)

The previous steps have analyzed the mission in the event that a circular orbit about the moon is not established, i.e., the mission is aborted. However, in the nominal case, a circular orbit is established (mission specification 7) and the energy required to accomplish this also may be found. From Chapter VI, Figs. C-4, C-28 and C-63 of the catalogue are entered with the data of step IV*, namely, $i_{VTL} = 45°$, $i_{VTE} = -12.5°$. Then for $R_{\oplus\text{☾}} = 61.8$ ER, the energy required is ΔV_1 = 905 m/sec.

The injection velocity V_0 is found in a similar manner from the catalogue (Figs. C-1, C-25 and C-60), namely, $V_0 = 10900.8$ m/sec.

Step XVII: Lighting conditions at lunar launch

Mission specification 13 on page XI-11 requires an approximate stay time on the lunar surface of 3 days. Since the arrival time at the moon is ^{d}277.16, injection into a transearth trajectory from lunar orbit is arbitrarily assumed at ^{d}280.00. Allowing time for landing, takeoff and orbit, the actual stay time on the lunar surface is approximately 2.5 days. The lighting conditions for lunar takeoff are found in the same manner as in Step II. For ^{d}280.00 the estimated (see Section C) and exact lighting agree closely; the exact conditions are shown below. The evening terminator passes through the site, and therefore, the lunar launch will take place at dusk. Launch must be westward and must occur prior to ^{d}280.00 if daylight is desired during this mission phase.

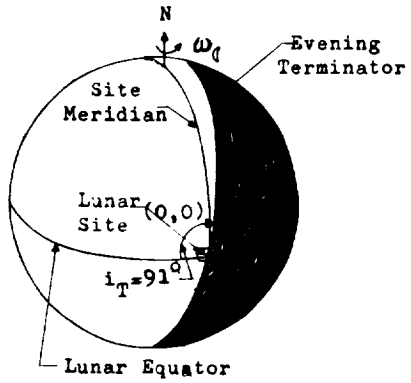

Step XVIII: Requirements for establishing the transearth trajectory

Referring to Figs. 4a and 4b the following lunar information may be obtained for ^{d}280.00:

$i_m = 27.2°$

$\delta_M = 27.2°$

$R_{\oplus\text{☾}} = 59.8$ ER

$\beta_{\text{☾}} = 90°$

(see step II for definitions).

The object of this step is to determine the required transearth trajectory inclination and time of flight from the transearth injection point to vacuum perigee on earth arrival.

At translunar injection, $t_0 = {}^d274.136$ (step VI*), the meridian of Cape Canaveral is 38.9° W of the lunar ascending node. Now the "acceptable longitude" meridian for re-entry along AMR is displaced eastward from Cape Canaveral by 55.5° (step XV), and the corresponding meridian for re-entry along the PMR is 130° W of Cape Canaveral. At ^{d}280.00, the meridian of Cape Canaveral is 81.9° W of the lunar ascending node. A first estimate for the return trip duration is exactly 3 days, and the meridian of Cape Canaveral at re-entry is 82.4° - 15.04 · (72) = 79.4° W of the lunar ascending node. The following sketch illustrates re-entry.

Returning to Fig. 10, it is noted that for $\beta_{\text{☾}}$ = 90°, i_{VTE} must equal - 15° to satisfy mission specification 17, i.e., $i_{VTEQ} = 30°$ and direct re-entry along PMR.

Before proceeding further, step IV is repeated here for the transearth injection time ^{d}280.00 and the lunar site with $\phi_{\text{☾}} = 0°$, $\lambda_{\text{☾}} = 0°$. The re-

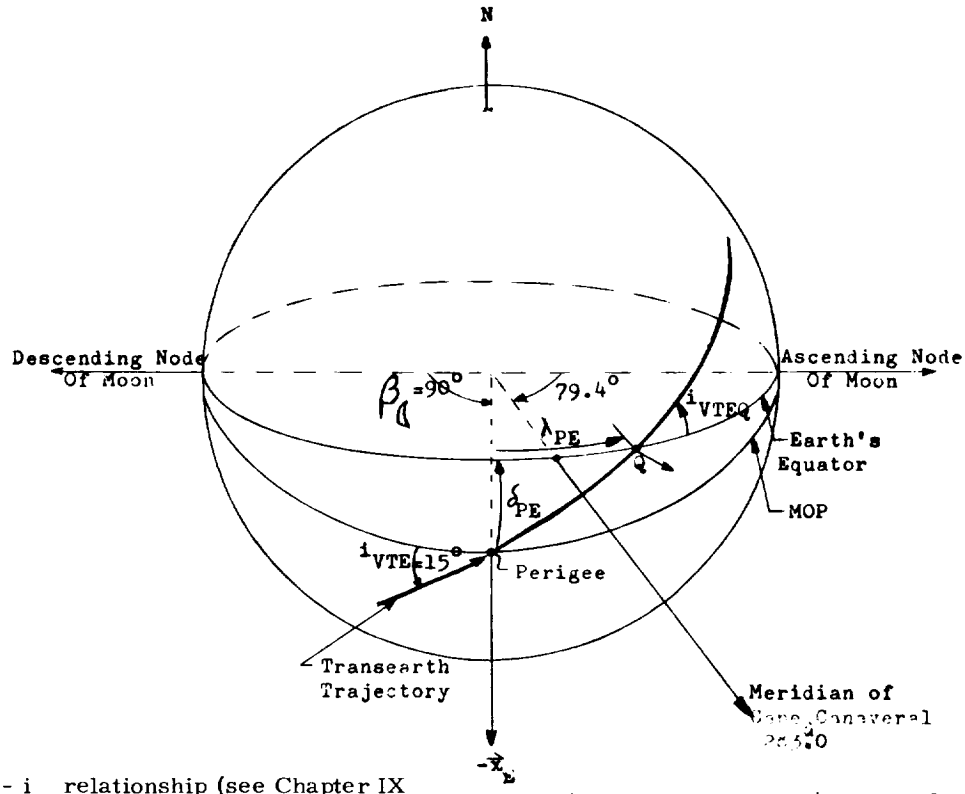

quired θ_{MTE} - i_m relationship (see Chapter IX for an explanation) is as follows:

θ_{MTE} (deg)	i_m (deg)
10	59.28
20	23.02
30	13.9
40	10.11
50	8.13
60	6.97
70	6.26
80	5.84
90	5.64
100	5.61
110	5.75
120	6.09

Since $R_{\oplus\mathbb{C}} \approx 60$ ER, the above data are superimposed on mission planning envelopes in Section F (Figs. 35, 36 and 37), a sample of which is presented in Fig. 42. These particular envelopes satisfy mission specifications 14, 17 and 18. It is confirmed that an i_{VTE} of $\pm$ 15° can be obtained for return flight times from 70 to 110 hr, and reentry may occur direct either along AMR or PMR. For this mission, nominally a direct re-entry along the PMR is specified (specification 17), implying that "direct from the south" return be made or i_{VTE} be -15°, as shown in the above sketch. Note that $\delta_M = \delta_{PE}$ for this case, and from spherical trigonometry

$$\lambda_{PE} = \sin^{-1}\left(\frac{\tan \delta_{PE}}{\tan i_{VTEQ}}\right) = 60.8°$$

The next sketch shows more clearly the geometry of timing the arrival at perigee so that it is direct along the PMR.

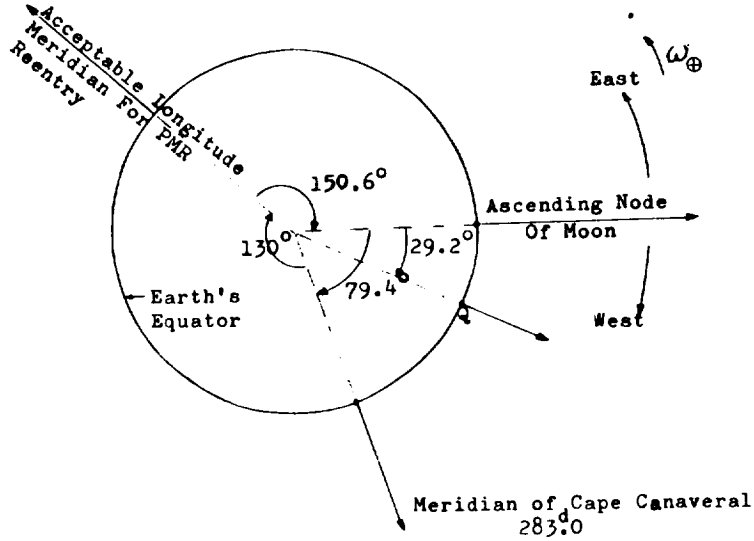

Thus, the re-entry should be timed to occur

$$\frac{130^\circ + 53.2^\circ}{15.04^\circ/\text{hr}} = 12.17 \text{ hr later, or } \left(\frac{147.6^\circ + 29.2^\circ}{15.04^\circ/\text{hr}}\right) =$$

11.73 hr earlier. The later return flight time of 72 + 12.17 = 84.17 hr will be chosen. The corresponding i_m and θ_{MTE} needed to achieve this time is obtained by cross-plotting the superimposed data of Figs. 35, 36 and 37 for an $i_{VTE} = -15.0$, and they turn out to be $i_m = 9.3^\circ$ and $\theta_{MTE} = 43.0^\circ$.

Step XIX: The transearth trajectory

Figures 26 to 50 in the catalogue of Chapter IX can be entered with these values of i_m, θ_{MTE} and the velocity impulse required to eject from lunar orbit ΔV_2, and the lunar orbit ejection position β_{M0} can be cross-plotted against i_m.

They are

$$\Delta V_2 = 840 \text{ m/sec}$$

$$\beta_{M0} = -27^\circ$$

An approximate idea of the lighting conditions at the time of transearth injection from lunar orbit is obtained by means of the following sketch, which neglects the lunar librations (see step XVII):

Transearth injection will take place in daylight, as shown, but subsequent flights will be eclipsed by the moon for a few hours.

From step XVIII, the earth arrival date is d h d
280.00 + 89.17 = 283.51. Lighting conditions at earth for re-entry may be estimated in the following manner. First, the second sketch in the previous step is partially redrawn. Secondly, repeat step VII in determining the hour angle ζ which is measured from the midnight meridian eastward to the ascending node for positive angles. Since the average rotational rate of the moon around the earth from the last quarter to new moon is $\omega_{\oplus\mathfrak{C}} = 13.6$ deg/day,

$$\zeta = 130.1^\circ - 141.6^\circ = -11.5^\circ$$

Note that the $-x_E$-axis lies in daylight, but close to the earth's terminator. Therefore, the re-entry will occur in daylight, but if the re-entry range to the required landing site is large, part of the re-entry phase and the landing will be in darkness.

2. Sample Mission II

Mission: Establish a photo-reconnaissance satellite (unmanned) around the moon to map the moon. Launch date: October 1966.

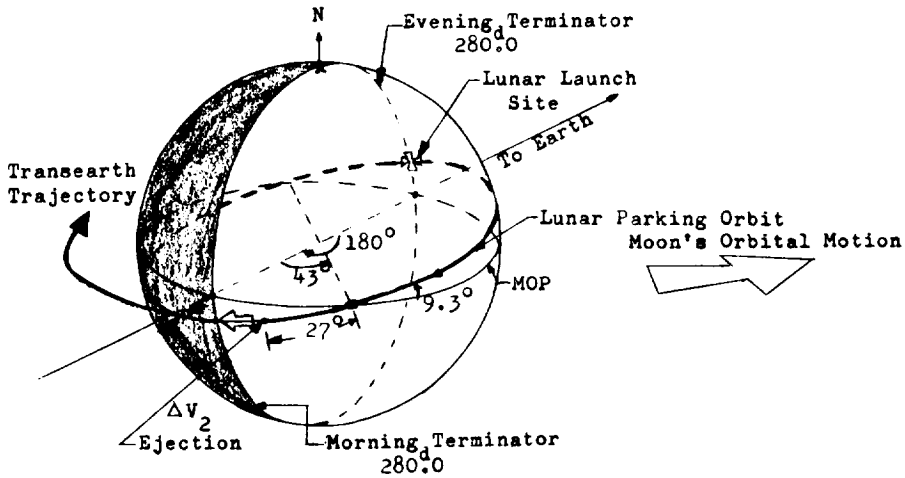

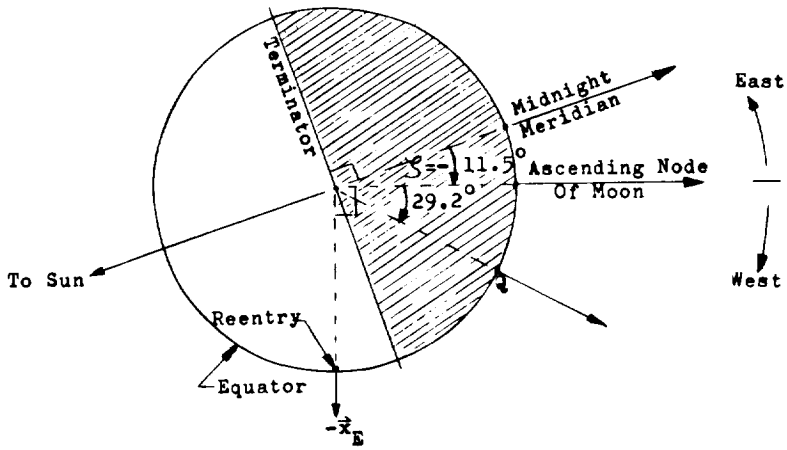

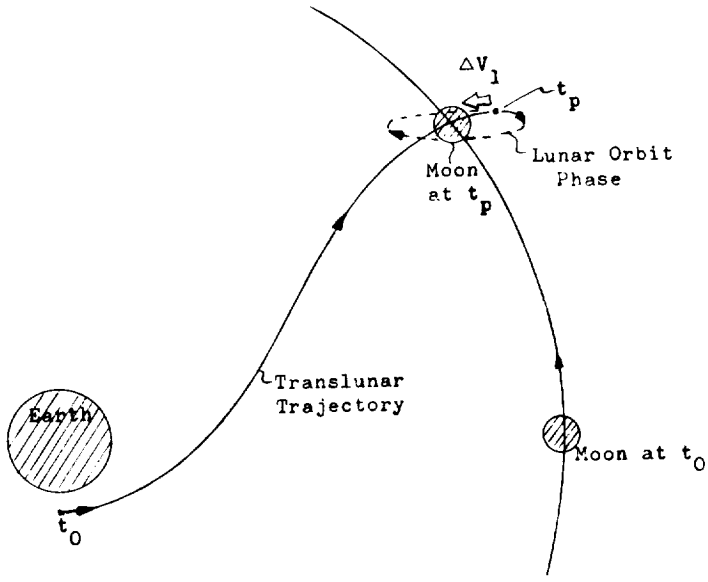

A mission schematic is shown above for clarity.

Injection into the translunar trajectory takes place at time t_0. The spacecraft then flies ballistically along the nominal trajectory until pericynthion at time t_p. At t_p, a velocity impulse ΔV_1 is applied against the direction of motion to reduce the speed of the spacecraft to the circular lunar orbit speed, from which the mission is carried out. The translunar trajectory does not necessarily have to be a portion of a circumlunar trajectory, nor is there any requirement to recover the spacecraft either nominally or in the event of a malfunction.

The detailed specifications for this mission are as follows:

Specification I. Nominal Translunar Trajectory

(1) A translunar trajectory of the approach class (Chapter IV) will be employed.

(2) The spacecraft is launched from Cape Canaveral with launch azimuth restrictions of $70° \leq A \leq 110°$.

(3) Parking orbits are used prior to translunar injection.

(4) Injection is over AMR, which implies an inject south case.

(5) Injection conditions are

$h_0 = 250$ km

$\gamma_0 = 5°$

(6) The pericynthion altitude of the circumlunar trajectory is 185.2 km.

(7) At pericynthion, thrust is applied to reduce the speed of the spacecraft to the circular lunar orbit speed.

Specification II. Lunar Satellite Orbit

(8) The orbit is to be circular with an altitude of 185.2 km above the moon.

(9) The orbit is highly inclined to the MOP to obtain nearly maximum coverage.

(10) The foremost requirement of the mission is data acquisition from the unseen side of the moon.

Step I: Determine required i_m, θ_{MTL}, and arrival time

Since there is no specific small coverage area, a particular i_m, θ_{MTL} relationship is not required. However, from mission specification 9, the lunar orbit must be highly inclined, and thus, for this mission, a polar orbit ($i_m = 90°$) is chosen. The value of θ_{MTL}, which is dependent on lighting conditions and specification 10, must still be determined. From step XVII of sample mission I, the lighting at 280.00^d, 1966 is as shown in the sketch below.

If the orientation of the lunar orbit, $\theta_{MTL} \simeq \pm 90°$ on 280.00^d, then its plane is nearly perpendicular to the terminator (also shown in the sketch). As the moon rotates about the earth to its first quarter position, it is observed from the previous sketch that the unseen face of the moon is adequately lighted and will be completely mapped in 0.5 lunar months. Thus, the foremost requirement of the mission (specification 10) is carried out as soon as possible, the entire lunar surface can be mapped in one lunar month, and any value of $\theta_{MTL} \simeq \pm 90°$ is acceptable for this mission.

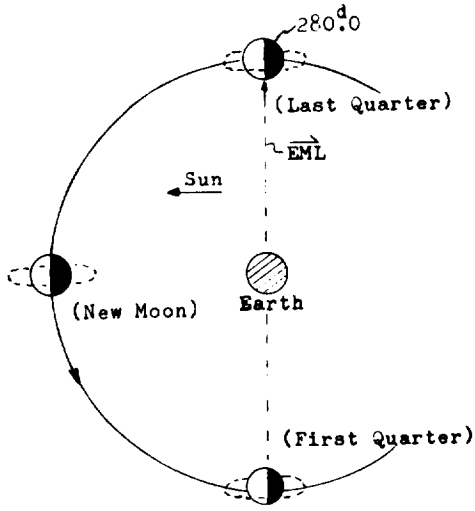

Step II: Obtain the translunar trajectory inclination

Referring to Figs. 4a and 4b, the following lunar orbit information is obtained for the $280.^d00$ day:

$i_m = 27.2°$

$\delta_M \equiv \delta_{\mathbb{C}} = 27.2°$

$R_M \equiv R_{\oplus\mathbb{C}} = 59.8$ ER

$\beta_{\mathbb{C}} = 90°$

From Fig. 11, for an $i_{VE} = 34.5°$, the i_{VTL} for the inject south case is $i_{VTL} = 23.5°$. Since $i_{VTL} > 10°$, there is no adjustment required, and, therefore, Eqs (21) and (22) of Section E are not needed.

Step III: Translunar flight time

The following required mission parameters are now known

$i_{VTL} = 23.5°$ (inject south)

$h_0 = 250$ km

$\gamma_0 = 5°$

$R_{\oplus\mathbb{C}} = 59.8$ ER ≈ 60 ER

$i_m = 90°$

$t_p = 280.00$

Referring to the transearth mission envelopes (Figs. 35, 36 and 37) for $R_{\oplus\mathbb{C}} = 60$ ER, the translunar flight time that most nearly satisfies the required i_m and θ_{MTL} is $t_p = 110$ hr. This flight time gives, for the above trajectory parameters:

$i_m = 90°$

$\theta_{MTL} = 95°$ or $-85°$

Only $\theta_{MTL} = 95°$ will be considered in the remaining discussion. Thus, the injection into the translunar trajectory occurs on

$t_0 = 280.^d00 - t_p = 275.^d416.$

Step IV: Determine launch point position at injection

This step is essentially identical to step VII of sample mission I, so only the pertinent data is given here.

Relative to the sun-earth line, the average rotation rate of the moon about the earth during the lunar phase at return is $\omega_{\oplus\mathbb{C}} = 11.47°$/day.

Thus, at t_0 the moon is located

$\theta = (275.416 - 272.7)\ 11.47 = 31.0°$

from the sun-earth line. Since the Greenwich meridian GW is coincident with the sun-earth line at $276.^d00$, at injection, GW is at $\Delta\theta = 210°$ W of the sun-earth line.

The hour angle ζ, measured from the midnight meridian eastward to the ascending node of the MOP at t_0, is:

$\zeta = \theta - \theta',$

which yields $\beta_{\mathbb{C}} = 31°$, $\delta_{\mathbb{C}} = 13.5°$, $\theta' = 28.5°$, and $\zeta = 2.5°$. Therefore, the meridian of Cape Canaveral is $(80.5° + 210° + 2.5°) = 293.0°$ W of the ascending node of the moon at t_0.

Step V: Determine injection latitude and longitude

From the last sketch in step VII of sample mission I, the $-x_E$-axis is located in the MOP, and the included angle measured eastward from the descending node is the adjusted value $(\beta_{\mathbb{C}})_{adj} = \beta_{\mathbb{C}} + \Delta\Phi_{TE}$. However, since $i_{VTL} > 10°$, $\Delta\Phi_{TE} = 0$ can be assumed, and $(\beta_{\mathbb{C}})_{adj} = 90°$ at t_p.

From Fig. 50 in the catalogue of Chapter IX, $\psi_0 = -2°$ for $i_{VTL} = 23.5°$ (inject south), $R_{\oplus\mathbb{C}} = 60$ ER, $\theta_{MTL} = 95°$, $i_m = 90°$, and $\gamma_0 = 0°$. However, mission specification 5 requires that $\gamma_0 = +5°$. Therefore, for $\gamma'_0 = 5°$ from empirical Eq (19), $\psi_0' = -2° + 10° = 8°$.

The injection latitude ϕ'_0 may now be found by the latitude equation of step VIII in sample mission I, and it is $\phi'_0 = -30°$.

The injection longitude increments $\Delta\lambda_0'$ and $\Delta\lambda_0''$ can also be found from step VIII of sample mission I, and they are $\Delta\lambda_0' = 98.5°$, $\Delta\lambda_0'' = 81.5°$.

From step IV, the meridian of Cape Canaveral is 293° W of the ascending node at injection. Hence, $\lambda_0 = 148.5°$ W.

Step VI: Determine parking orbit parameters

A sketch of the actual situation at injection is shown below. The prime purpose in this step is to determine the longitude increment of the parking orbit ground trace measured from the meridian of Cape Canaveral to the intersection of the parallel of latitude of Cape Canaveral by the parking orbit. Furthermore, the central angle from this intersection to the injection point must be determined.

The same procedure as in step IX of sample mission I is followed.

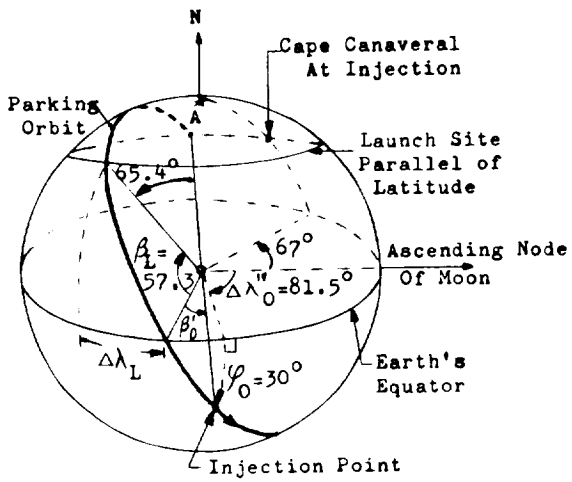

For $i_{VE} = 34.5°$, $\beta_L = 57.3°$ and $\beta'_0 = 62°$ the injection takes place in the southern hemisphere and the nearest node of the parking orbit is the descending node.

The central angle from injection to the intersection of the launch site latitude at point A (requiring a launch azimuth of A = 70°) is

$$\beta_L + \beta_0' + 65.4° = 184.7°.$$

The longitude increment of β_L is $\Delta\lambda_L$ and of β'_0 is $\Delta\lambda'_{PO}$, where $\Delta\lambda_L = 52°$ and $\Delta\lambda'_{PO} = 57.3°$. Therefore the longitude increment $\Delta\lambda$ of the intersection point A of the parking orbit with the launch site latitude from Cape Canaveral is at t_0:

$$\Delta\lambda = 180° - \Delta\lambda_L + \Delta\lambda'_{PO} + 180° - 52.0° + 57.3° + (67° + 81.5°) = 333.8° \text{ W} = 26.2° \text{ E}$$

The range angle that the spacecraft must traverse prior to reaching the injection point is $\Phi_{LO} = 184.7°$.

With the average angular velocity of the spacecraft in the parking orbit being 246.6 deg/hr, launch takes place 184.7 deg/246.6 deg/hr = 0.749 hr prior to t_0 at $t_L = 275^d.416 - 0.749$ hr $= 275^d.385$. However, at launch the actual location of Cape Canaveral is 37.5° W of point A, and, consequently, the parking orbit does not pass over the launch site. Assuming that the flight time to the moon and all other parameters generated so far are constant, a first-order correction to the launch date can be made by conducting the launch at an interval of time Δt later, which is the time required for the launch site to rotate beneath the parking orbit plane. In sample mission II

$$\Delta t = \frac{[26.2° + 15.04 \text{ deg/hr } (0.749 \text{ hr})]}{15.04 \text{ deg/hr}} = 2.49 \text{ hr}$$

and the corrected launch time is:

Launch time (corrected):

$$t_L = 275^d.416 - 0^h.749 + 2^h.49 = 275^d.489$$

Translunar injection time (corrected):

$$t_0 = 275^d.416 + 2^h.49$$

Lunar arrival time (corrected) =

$$280^d.00 + 2^h.49 = 280^d.104.$$

Step VII: Iteration with corrected arrival time

Steps II to VI are now repeated with the corrected arrival date. Each repeated step is denoted by an asterisk (*), and only the important parameters and their values are listed.

Step II*

For $t_p = 280.104^d$:

$i_m \simeq 27.2°$

$\delta_M \equiv \delta_{\mathbb{C}} \simeq 27.2°$

$R_M \equiv R_{\oplus\mathbb{C}} \simeq 59.8$ ER

$\beta_{\mathbb{C}} \simeq 90°$.

However, for this mission, from step II* it is immediately observed that insignificant changes take place in the lunar data for the corrected arrival date. In fact, very little change is detected in the following iterated steps. Therefore, it can be assumed that the translunar trajectory characteristics do not change, and, consequently, the determination of the timing and of other flight mechanics preliminary aspects is complete.

Step VIII: Lighting conditions at earth launch and injection

From step IV, $\zeta = 2.5°$, and the meridian of Cape Canaveral at launch (step VI) is 104.5° E of the ascending node of the moon. Also from step VI, the injection meridian is 81.5° W of the ascending node. The following sketch illustrates the lighting conditions.

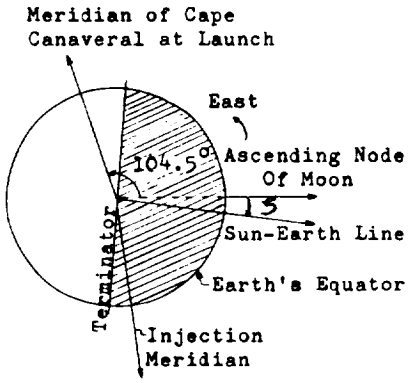

Launch takes place in the morning and in daylight. Injection takes place in the evening, mostly in darkness.

For the inject south case taken here, the launch time represents the beginning of the launch tolerance for the variable translunar technique of Chapter V. Therefore, launch is possible throughout most of the morning in daylight.

Step IX: Required injection velocity

The required injection velocity, V_0, can be obtained from Fig. 49 of the catalogue in Chapter IX for the following parameters:

$i_{VTL} = 23.5°$ (inject south)

$\theta_{MTL} = 95°$

$i_m = 90°$

$R_{\oplus\mathbb{C}} = 60$ ER

$\gamma_0 = 5°$

$h_0 = 182.9$ km

and it turns out to be

$V_0 = 10929$ m/sec.

But mission specification 5 requires that $h_0 = 250$ km; therefore, Eq (20) of Section E is used to find V_0'

$$V_0' = \left[V_0^2 - V_p^2 \left(\frac{\Delta h_0}{r_0}\right)\right]^{1/2}$$

$V_0' = 10861$ m/sec

Step X: ΔV_1 required to enter lunar orbit

The velocity impulse ΔV_1 required to reduce the vehicle speed to the value of circular lunar orbital speed at t_p is obtained from Fig. 47 of the catalogue in Chapter IX for the conditions listed in the previous step, and it is

$\Delta V_1 = 780$ m/sec.

3. Concluding Remarks

The two sample missions illustrated the application of the translunar and circumlunar trajectory catalogue, and the material in Chapters V to X as well as of Sections A to F of Chapter XI to the design of nominal lunar missions. The next step would be to lift the two major assumptions underlying the calculations for the sample missions, namely:

(1) Use a constant angular velocity $\omega_{\oplus\mathbb{C}}$ through a quarter of one revolution of the moon around the earth

(2) Neglect the ascent trajectory

and to recalculate the trajectory and lighting parameters for the nominal mission.

The second step is to calculate dispersed trajectories, i.e., to find trajectory and lighting parameters if earth launch or translunar injection or some other phase of the mission cannot occur at the nominal times and estimate navigation and guidance requirements. This is about as far as the Voice-calculated trajectories and catalogues can assist the mission designer. However, it should be noted with what ease all mission parameters can be obtained: a trajectory analyst can

obtain all necessary data for one mission in a matter of hours as compared to the days of labor required to obtain these preliminary trajectory parameters by use of numerical integration of the equations of motion. The slow and tedious preliminary design of lunar missions by numerical integration is entirely due to the high sensitivity of translunar injection parameters to lunar mission constraints and requirements as was stated in Chapters III and IV.

The third, and final step for the preliminary design of a lunar mission is the use of the parameters and initial conditions established in Step I and II for numerically integrated trajectories; the accuracy of the resulting mission timing and profile depends on the force model and the numerical integration technique used for each mission phase, as was discussed in detail in Chapter IV.

The actual mechanization of a lunar mission involves the calculation of precision trajectories as opposed to the feasibility trajectories of the three steps discussed above in the preliminary design of lunar missions. Navigation charts would have to be prepared for this, and trajectory correction points and energy requirements established for the actual mission. This would typically occur several months before the actual mission is flown to allow ample time for checking and preparation.

Throughout the mission there will be requirements for trajectory calculations in the vehicle, as well as on earth to assimilate actual position data, to predict the trajectory, and to decide on the course of action to be followed if the actual trajectory does not conform to the nominal one.

Postflight analysis will provide inputs for future improvements in procedures and trajectory simulation and calculation.

H. REFERENCES

1. Woolston, O. S., "Declination, Radial Distance, and Phases of the Moon for the Years 1961 to 1971 for Use in Trajectory Considerations," NASA TN D-911, August 1961.

TABLES AND ILLUSTRATIONS

LIST OF TABLES AND ILLUSTRATIONS

Table	Title	Page
1(a)	Calendar Showing Number of Day in Year After January 0--Nonleap Years	XI-37
1(b)	Calendar Showing Number of Day in Year After January 0--Leap Years	XI-38
2(a)	Phases of the Moon--1963	XI-39
2(b)	Phases of the Moon--1964	XI-40
2(c)	Phases of the Moon--1965	XI-41
2(d)	Phases of the Moon--1966	XI-42
2(e)	Phases of the Moon--1967	XI-43
2(f)	Phases of the Moon--1968	XI-44
2(g)	Phases of the Moon--1969	XI-45
2(h)	Phases of the Moon--1970	XI-46
2(i)	Phases of the Moon--1971	XI-47

Figure	Title	Page
1(a)	Declination and Phases of Moon for Year 1963	XI-48
1(b)	Radial Distance of Moon for Year 1963	XI-49
2(a)	Declination and Phases of Moon for Year 1964	XI-50
2(b)	Radial Distance of Moon for Year 1964	XI-51
3(a)	Declination and Phases of Moon for Year 1965	XI-52
3(b)	Radial Distance of Moon for Year 1965	XI-53
4(a)	Declination and Phases of Moon for Year 1966	XI-54
4(b)	Radial Distance of Moon for Year 1966	XI-55

LIST OF TABLES AND ILLUSTRATIONS (continued)

Figure	Title	Page
5(a)	Declination and Phases of Moon for Year 1967.	XI-56
5(b)	Radial Distance of Moon for Year 1967.	XI-57
6(a)	Declination and Phases of Moon for Year 1968.	XI-58
6(b)	Radial Distance of Moon for Year 1968.	XI-59
7(a)	Declination and Phases of Moon for Year 1969.	XI-60
7(b)	Radial Distance of Moon for Year 1969.	XI-61
8(a)	Declination and Phases of Moon for Year 1970.	XI-62
8(b)	Radial Distance of Moon for Year 1970.	XI-63
9(a)	Declination and Phases of Moon for Year 1971.	XI-64
9(b)	Radial Distance of Moon for Year 1971.	XI-65
10	Lunar Declination Versus Lunar Central Angle	XI-66
11	Required Translunar Plane Inclination (i_{VTL}) as a Function of Lunar Central Angle ($\beta_{\mathbb{C}}$)	XI-67
12	Required Translunar Plane Inclination (i_{VTL}) as a Function of Lunar Central Angle ($\beta_{\mathbb{C}}$)	XI-68
13	Relationship of Transearth Inclination to the Equator and MOP with Lunar Central Angle	XI-69
14	Relationship of Transearth Inclination to the Equator and MOP with Lunar Central Angle	XI-70
15	Constant to be Used with Empirical Equation (21). . .	XI-71
16	Constant to be Used with Empirical Equation (22). . .	XI-72
17	ΔV_{TE} Required to Control Transearth Perigee Time	XI-73
18	ΔV_i Required to Change Transearth Plan Inclination.	XI-74

LIST OF TABLES AND ILLUSTRATIONS (continued)

Figure	Title	Page
19	Angular Change ($\Delta \Phi'_{TE}$) of the Transearth Plane Intersection with the MOP Due to an Inclination Change ($\pm \Delta i_{VTE}$) Maneuver	XI-75
20	Angular Change ($\Delta \Phi'_{TE}$) of the Transearth Plane Intersection with the MOP Due to an Inclination Change ($\pm \Delta i_{VTE}$) Maneuver	XI-76
21	Angular Change ($\Delta \Phi'_{TE}$) of the Transearth Plane Intersection with the MOP Due to an Inclination Change ($\pm \Delta i_{VTE}$) Maneuver	XI-77
22	Mission Planning Envelope (Circumlunar Trajectory Class)	XI-78
23	Mission Planning Envelope (Circumlunar Trajectory Class)	XI-79
24	Mission Planning Envelope (Circumlunar Trajectory Class)	XI-80
25	Mission Planning Envelope (Circumlunar Trajectory Class)	XI-81
26	Mission Planning Envelope (Circumlunar Trajectory Class)	XI-82
27	Mission Planning Envelope (Circumlunar Trajectory Class)	XI-83
28	Mission Planning Envelope (Circumlunar Trajectory Class)	XI-84
29	Mission Planning Envelope (Circumlunar Trajectory Class)	XI-85
30	Mission Planning Envelope (Circumlunar Trajectory Class)	XI-86
31	Mission Planning Envelope (Circumlunar Trajectory Class)	XI-87

LIST OF TABLES AND ILLUSTRATIONS (continued)

Figure	Title	Page
32	Mission Planning Envelope (Approach Trajectory Class)	XI-88
33	Mission Planning Envelope (Approach Trajectory Class)	XI-89
34	Mission Planning Envelope (Approach Trajectory Class)	XI-90
35	Mission Planning Envelope (Approach Trajectory Class)	XI-91
36	Mission Planning Envelope (Approach Trajectory Class)	XI-92
37	Mission Planning Envelope (Approach Trajectory Class)	XI-93
38	Mission Planning Envelope (Approach Trajectory Class)	XI-94
39	Mission Planning Envelope (Approach Trajectory Class)	XI-95
40	Mission Planning Envelope (Approach Trajectory Class)	XI-96
41	Mission Planning Envelope (Circumlunar Trajectory Class)	XI-97
42	Mission Planning Envelope (Approach Trajectory Class	XI-98

TABLE 1.- CALENDAR SHOWING NUMBER OF DAY IN YEAR

AFTER JANUARY 0

(a) Nonleap years: 1961, 1962, 1963, 1965, 1966, 1967, 1969, 1970, and 1971

Day of month	Day of year											
	Jan.	Feb.	Mar.	Apr.	May	June	July	Aug.	Sept.	Oct.	Nov.	Dec.
1	1	32	60	91	121	152	182	213	244	274	305	335
2	2	33	61	92	122	153	183	214	245	275	306	336
3	3	34	62	93	123	154	184	215	246	276	307	337
4	4	35	63	94	124	155	185	216	247	277	308	338
5	5	36	64	95	125	156	186	217	248	278	309	339
6	6	37	65	96	126	157	187	218	249	279	310	340
7	7	38	66	97	127	158	188	219	250	280	311	341
8	8	39	67	98	128	159	189	220	251	281	312	342
9	9	40	68	99	129	160	190	221	252	282	313	343
10	10	41	69	100	130	161	191	222	253	283	314	344
11	11	42	70	101	131	162	192	223	254	284	315	345
12	12	43	71	102	132	163	193	224	255	285	316	346
13	13	44	72	103	133	164	194	225	256	286	317	347
14	14	45	73	104	134	165	195	226	257	287	318	348
15	15	46	74	105	135	166	196	227	258	288	319	349
16	16	47	75	106	136	167	197	228	259	289	320	350
17	17	48	76	107	137	168	198	229	260	290	321	351
18	18	49	77	108	138	169	199	230	261	291	322	352
19	19	50	78	109	139	170	200	231	262	292	323	353
20	20	51	79	110	140	171	201	232	263	293	324	354
21	21	52	80	111	141	172	202	233	264	294	325	355
22	22	53	81	112	142	173	203	234	265	295	326	356
23	23	54	82	113	143	174	204	235	266	296	327	357
24	24	55	83	114	144	175	205	236	267	297	328	358
25	25	56	84	115	145	176	206	237	268	298	329	359
26	26	57	85	116	146	177	207	238	269	299	330	360
27	27	58	86	117	147	178	208	239	270	300	331	361
28	28	59	87	118	148	179	209	240	271	301	332	362
29	29		88	119	149	180	210	241	272	302	333	363
30	30		89	120	150	181	211	242	273	303	334	364
31	31		90		151		212	243		304		365

TABLE 1.- CALENDAR SHOWING NUMBER OF DAY IN YEAR

AFTER JANUARY 0 - Concluded

(b) Leap years: 1964 and 1968

Day of month	Day of year											
	Jan.	Feb.	Mar.	Apr.	May	June	July	Aug.	Sept.	Oct.	Nov.	Dec.
1	1	32	61	92	122	153	183	214	245	275	306	336
2	2	33	62	93	123	154	184	215	246	276	307	337
3	3	34	63	94	124	155	185	216	247	277	308	338
4	4	35	64	95	125	156	186	217	248	278	309	339
5	5	36	65	96	126	157	187	218	249	279	310	340
6	6	37	66	97	127	158	188	219	250	280	311	341
7	7	38	67	98	128	159	189	220	251	281	312	342
8	8	39	68	99	129	160	190	221	252	282	313	343
9	9	40	69	100	130	161	191	222	253	283	314	344
10	10	41	70	101	131	162	192	223	254	284	315	345
11	11	42	71	102	132	163	193	224	255	285	316	346
12	12	43	72	103	133	164	194	225	256	286	317	347
13	13	44	73	104	134	165	195	226	257	287	318	348
14	14	45	74	105	135	166	196	227	258	288	319	349
15	15	46	75	106	136	167	197	228	259	289	320	350
16	16	47	76	107	137	168	198	229	260	290	321	351
17	17	48	77	108	138	169	199	230	261	291	322	352
18	18	49	78	109	139	170	200	231	262	292	323	353
19	19	50	79	110	140	171	201	232	263	293	324	354
20	20	51	80	111	141	172	202	233	264	294	325	355
21	21	52	81	112	142	173	203	234	265	295	326	356
22	22	53	82	113	143	174	204	235	266	296	327	357
23	23	54	83	114	144	175	205	236	267	297	328	358
24	24	55	84	115	145	176	206	237	268	298	329	359
25	25	56	85	116	146	177	207	238	269	299	330	360
26	26	57	86	117	147	178	208	239	270	300	331	361
27	27	58	87	118	148	179	209	240	271	301	332	362
28	28	59	88	119	149	180	210	241	272	302	333	363
29	29	60	89	120	150	181	211	242	273	303	334	364
30	30		90	121	151	182	212	243	274	304	335	365
31	31		91		152		213	244		305		366

TABLE 2.- PHASES OF THE MOON

[Universal time]

(a) 1963

New moon				First quarter				Full moon				Last quarter			
	d	h	m		d	h	m		d	h	m		d	h	m
				Jan.	3	1	3	Jan.	9	23	9	Jan.	17	20	35
Jan.	25	13	43	Feb.	1	8	51	Feb.	8	14	53	Feb.	16	17	40
Feb.	24	2	7	Mar.	2	17	18	Mar.	10	7	50	Mar.	18	12	9
Mar.	25	12	11	Apr.	1	3	16	Apr.	9	0	58	Apr.	17	2	54
Apr.	23	20	30	Apr.	30	15	9	May	8	17	25	May	16	13	37
May	23	4	1	May	30	4	57	June	7	8	32	June	14	20	54
June	21	11	47	June	28	20	25	July	6	21	57	July	14	1	58
July	20	20	44	July	28	13	14	Aug.	5	9	32	Aug.	12	6	22
Aug.	19	7	36	Aug.	27	6	55	Sept.	3	19	35	Sept.	10	11	43
Sept.	17	20	52	Sept.	26	0	40	Oct.	3	4	45	Oct.	9	19	28
Oct.	17	12	44	Oct.	25	17	21	Nov.	1	13	56	Nov.	8	6	38
Nov.	16	6	52	Nov.	24	7	57	Nov.	30	23	55	Dec.	7	21	35
Dec.	16	2	8	Dec.	23	19	56	Dec.	30	11	5				

TABLE 2.- PHASES OF THE MOON - Continued

[Universal time]

(b) 1964

New moon				First quarter				Full moon				Last quarter			
	d	h	m		d	h	m		d	h	m		d	h	m
												Jan.	6	15	59
Jan.	14	20	45	Jan.	22	5	30	Jan.	28	23	24	Feb.	5	12	43
Feb.	13	13	2	Feb.	20	13	25	Feb.	27	12	40	Mar.	6	10	1
Mar.	14	2	15	Mar.	20	20	40	Mar.	28	2	50	Apr.	5	5	46
Apr.	12	12	39	Apr.	19	4	10	Apr.	26	17	51	May	4	22	21
May	11	21	3	May	18	12	43	May	26	9	30	June	3	11	9
June	10	4	23	June	16	23	3	June	25	1	9	July	2	20	32
July	9	11	32	July	16	11	48	July	24	15	59	Aug.	1	3	30
Aug.	7	19	18	Aug.	15	3	21	Aug.	23	5	26	Aug.	30	9	16
Sept.	6	4	35	Sept.	13	21	25	Sept.	21	17	32	Sept.	28	15	3
Oct.	5	16	21	Oct.	13	16	58	Oct.	21	4	46	Oct.	27	22	0
Nov.	4	7	18	Nov.	12	12	21	Nov.	19	15	44	Nov.	26	7	12
Dec.	4	1	20	Dec.	12	6	3	Dec.	19	2	42	Dec.	25	19	28

TABLE 2.- PHASES OF THE MOON - Continued

[Universal time]

(c) 1965

New moon				First quarter				Full moon				Last quarter			
	d	h	m		d	h	m		d	h	m		d	h	m
Jan.	2	21	8	Jan.	10	21	1	Jan.	17	13	38	Jan.	24	11	8
Feb.	1	16	37	Feb.	9	8	54	Feb.	16	0	28	Feb.	23	5	40
Mar.	3	9	57	Mar.	10	17	53	Mar.	17	11	25	Mar.	25	1	38
Apr.	2	0	22	Apr.	9	0	41	Apr.	15	23	3	Apr.	23	21	8
May	1	11	57	May	8	6	21	May	15	11	53	May	23	14	41
May	30	21	14	June	6	12	12	June	14	2	1	June	22	5	37
June	29	4	53	July	5	19	37	July	13	17	3	July	21	17	54
July	28	11	46	Aug.	4	5	48	Aug.	12	8	23	Aug.	20	3	51
Aug.	26	18	51	Sept.	2	19	29	Sept.	10	23	33	Sept.	18	11	59
Sept.	25	3	19	Oct.	2	12	39	Oct.	10	14	15	Oct.	17	19	1
Oct.	24	14	12	Nov.	1	8	27	Nov.	9	4	16	Nov.	16	1	55
Nov.	23	4	11	Dec.	1	5	26	Dec.	8	17	22	Dec.	15	9	53
Dec.	22	21	4	Dec.	31	1	47								

TABLE 2. - PHASES OF THE MOON - Continued

[Universal time]

(d) 1966

New moon				First quarter				Full moon				Last quarter			
	d	h	m		d	h	m		d	h	m		d	h	m
								Jan.	7	5	17	Jan.	13	20	1
Jan.	21	15	47	Jan.	29	19	49	Feb.	5	15	59	Feb.	12	8	54
Feb.	20	10	50	Feb.	28	10	16	Mar.	7	1	46	Mar.	14	0	20
Mar.	22	4	47	Mar.	29	20	44	Apr.	5	11	14	Apr.	12	17	29
Apr.	20	20	36	Apr.	28	3	50	May	4	21	2	May	12	11	20
May	20	9	43	May	27	8	51	June	3	7	41	June	11	4	59
June	18	20	10	June	25	13	24	July	2	19	37	July	10	21	44
July	18	4	31	July	24	19	1	Aug.	1	9	6	Aug.	9	12	57
Aug.	16	11	49	Aug.	23	3	3	Aug.	31	0	15	Sept.	8	2	8
Sept.	14	19	14	Sept.	21	14	26	Sept.	29	16	48	Oct.	7	13	9
Oct.	14	3	53	Oct.	21	5	36	Oct.	29	10	1	Nov.	5	22	19
Nov.	12	14	27	Nov.	20	0	21	Nov.	28	2	41	Dec.	5	6	23
Dec.	12	3	14	Dec.	19	21	42	Dec.	27	17	44				

TABLE 2.- PHASES OF THE MOON - Continued

[Universal time]

(a) 1967

New moon				First quarter				Full moon				Last quarter			
	d	h	m		d	h	m		d	h	m		d	h	m
												Jan.	3	14	20
Jan.	10	18	7	Jan.	18	19	42	Jan.	26	6	41	Feb.	1	23	4
Feb.	9	10	45	Feb.	17	15	57	Feb.	24	17	44	Mar.	3	9	11
Mar.	11	4	31	Mar.	19	8	32	Mar.	26	3	22	Apr.	1	20	59
Apr.	9	22	21	Apr.	17	20	49	Apr.	24	12	4	May	1	10	34
May	9	14	56	May	17	5	19	May	23	20	23	May	31	1	53
June	8	5	15	June	15	11	13	June	22	4	58	June	29	18	40
July	7	17	1	July	14	15	54	July	21	14	40	July	29	12	15
Aug.	6	2	49	Aug.	12	20	45	Aug.	20	2	28	Aug.	28	5	36
Sept.	4	11	38	Sept.	11	3	6	Sept.	18	17	0	Sept.	26	21	45
Oct.	3	20	25	Oct.	10	12	12	Oct.	18	10	12	Oct.	26	12	5
Nov.	2	5	49	Nov.	9	1	1	Nov.	17	4	54	Nov.	25	0	24
Dec.	1	16	11	Dec.	8	17	58	Dec.	16	23	22	Dec.	24	10	49
Dec.	31	3	39												

TABLE 2.- PHASES OF THE MOON - Continued

[Universal time]

(f) 1968

New moon				First quarter				Full moon				Last quarter			
	d	h	m		d	h	m		d	h	m		d	h	m
				Jan.	7	14	24	Jan.	15	16	12	Jan.	22	19	39
Jan.	29	16	30	Feb.	6	12	21	Feb.	14	6	44	Feb.	21	3	29
Feb.	28	6	56	Mar.	7	9	21	Mar.	14	18	53	Mar.	21	11	8
Mar.	28	22	49	Apr.	6	3	28	Apr.	13	4	52	Apr.	19	19	36
Apr.	27	15	22	May	5	17	55	May	12	13	6	May	19	5	45
May	27	7	31	June	4	4	47	June	10	20	14	June	17	18	14
June	25	22	25	July	3	12	42	July	10	3	18	July	17	9	12
July	25	11	50	Aug.	1	18	35	Aug.	8	11	33	Aug.	16	2	14
Aug.	23	23	57	Aug.	30	23	35	Sept.	6	22	8	Sept.	14	20	32
Sept.	22	11	9	Sept.	29	5	7	Oct.	6	11	47	Oct.	14	15	6
Oct.	21	21	45	Oct.	28	12	40	Nov.	5	4	26	Nov.	13	8	54
Nov.	20	8	2	Nov.	26	23	31	Dec.	4	23	8	Dec.	13	0	50
Dec.	19	18	19	Dec.	26	14	15								

TABLE 2.- PHASES OF THE MOON - Continued

[Universal time]

(g) 1969

New moon				First quarter				Full moon				Last quarter			
	d	h	m		d	h	m		d	h	m		d	h	m
								Jan.	3	18	28	Jan.	11	14	1
Jan.	18	4	59	Jan.	25	8	24	Feb.	2	12	57	Feb.	10	0	9
Feb.	16	16	26	Feb.	24	4	31	Mar.	4	5	18	Mar.	11	7	45
Mar.	18	4	52	Mar.	26	0	49	Apr.	2	18	46	Apr.	9	13	59
Apr.	16	18	16	Apr.	24	19	45	May	2	5	14	May	8	20	12
May	16	8	27	May	24	12	16	May	31	13	19	June	7	3	40
June	14	23	9	June	23	1	45	June	29	20	4	July	6	13	18
July	14	14	12	July	22	12	10	July	29	2	46	Aug.	5	1	39
Aug.	13	5	17	Aug.	20	20	4	Aug.	27	10	33	Sept.	3	16	58
Sept.	11	19	56	Sept.	19	2	25	Sept.	25	20	21	Oct.	3	11	6
Oct.	11	9	40	Oct.	18	8	32	Oct.	25	8	45	Nov.	2	7	14
Nov.	9	22	12	Nov.	16	15	46	Nov.	23	23	54	Dec.	2	3	51
Dec.	9	9	42	Dec.	16	1	10	Dec.	23	17	36	Dec.	31	22	53

TABLE 2.- PHASES OF THE MOON - Continued

[Universal time]

(h) 1970

New moon				First quarter				Full moon				Last quarter			
	d	h	m		d	h	m		d	h	m		d	h	m
Jan.	7	20	36	Jan.	14	13	19	Jan.	22	12	56	Jan.	30	14	39
Feb.	6	7	13	Feb.	13	4	11	Feb.	21	8	19	Mar.	1	2	34
Mar.	7	17	43	Mar.	14	21	16	Mar.	23	1	53	Mar.	30	11	5
Apr.	6	4	10	Apr.	13	15	44	Apr.	21	16	22	Apr.	28	17	19
May	5	14	51	May	13	10	27	May	21	3	38	May	27	22	32
June	4	2	22	June	12	4	7	June	19	12	28	June	26	4	2
July	3	15	18	July	11	19	43	July	18	19	59	July	25	11	0
Aug.	2	5	59	Aug.	10	8	50	Aug.	17	3	16	Aug.	23	20	35
Aug.	31	22	2	Sept.	8	19	39	Sept.	15	11	10	Sept.	22	9	43
Sept.	30	14	32	Oct.	8	4	43	Oct.	14	20	22	Oct.	22	2	48
Oct.	30	6	28	Nov.	6	12	47	Nov.	13	7	28	Nov.	20	23	14
Nov.	28	21	15	Dec.	5	20	36	Dec.	12	21	4	Dec.	20	21	9
Dec.	28	10	43												

TABLE 2.- PHASES OF THE MOON - Concluded

[Universal time]

(i) 1971

New moon				First quarter				Full moon				Last quarter			
	d	h	m		d	h	m		d	h	m		d	h	m
				Jan.	4	4	55	Jan.	11	13	21	Jan.	19	18	9
Jan.	26	22	55	Feb.	2	14	31	Feb.	10	7	42	Feb.	18	12	14
Feb.	25	9	49	Mar.	4	2	1	Mar.	12	2	33	Mar.	20	2	30
Mar.	26	19	24	Apr.	2	15	46	Apr.	10	20	10	Apr.	18	12	58
Apr.	25	4	2	May	2	7	34	May	10	11	24	May	17	20	15
May	24	12	32	June	1	0	43	June	9	0	4	June	16	1	25
June	22	21	58	June	30	18	11	July	8	10	37	July	15	5	47
July	22	9	15	July	30	11	7	Aug.	6	19	43	Aug.	13	10	55
Aug.	20	22	54	Aug.	29	2	56	Sept.	5	4	3	Sept.	11	18	23
Sept.	19	14	43	Sept.	27	17	18	Oct.	4	12	20	Oct.	11	5	30
Oct.	19	7	59	Oct.	27	5	55	Nov.	2	21	20	Nov.	9	20	52
Nov.	18	1	46	Nov.	25	16	37	Dec.	2	7	48	Dec.	9	16	3
Dec.	17	19	3												

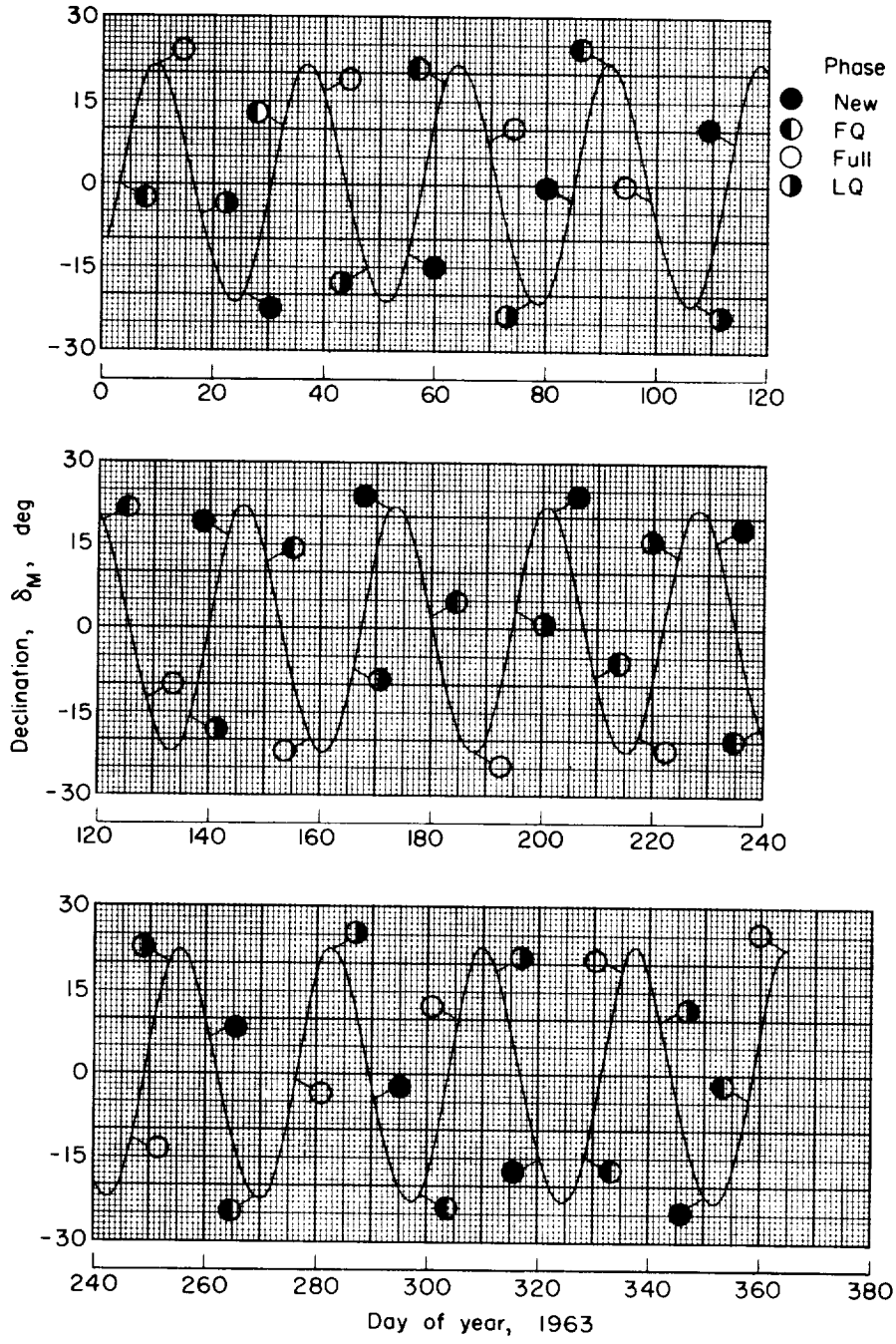

(a) Declination and phases.

Figure 1.- Declination and phases and radial distance of moon for year 1963.

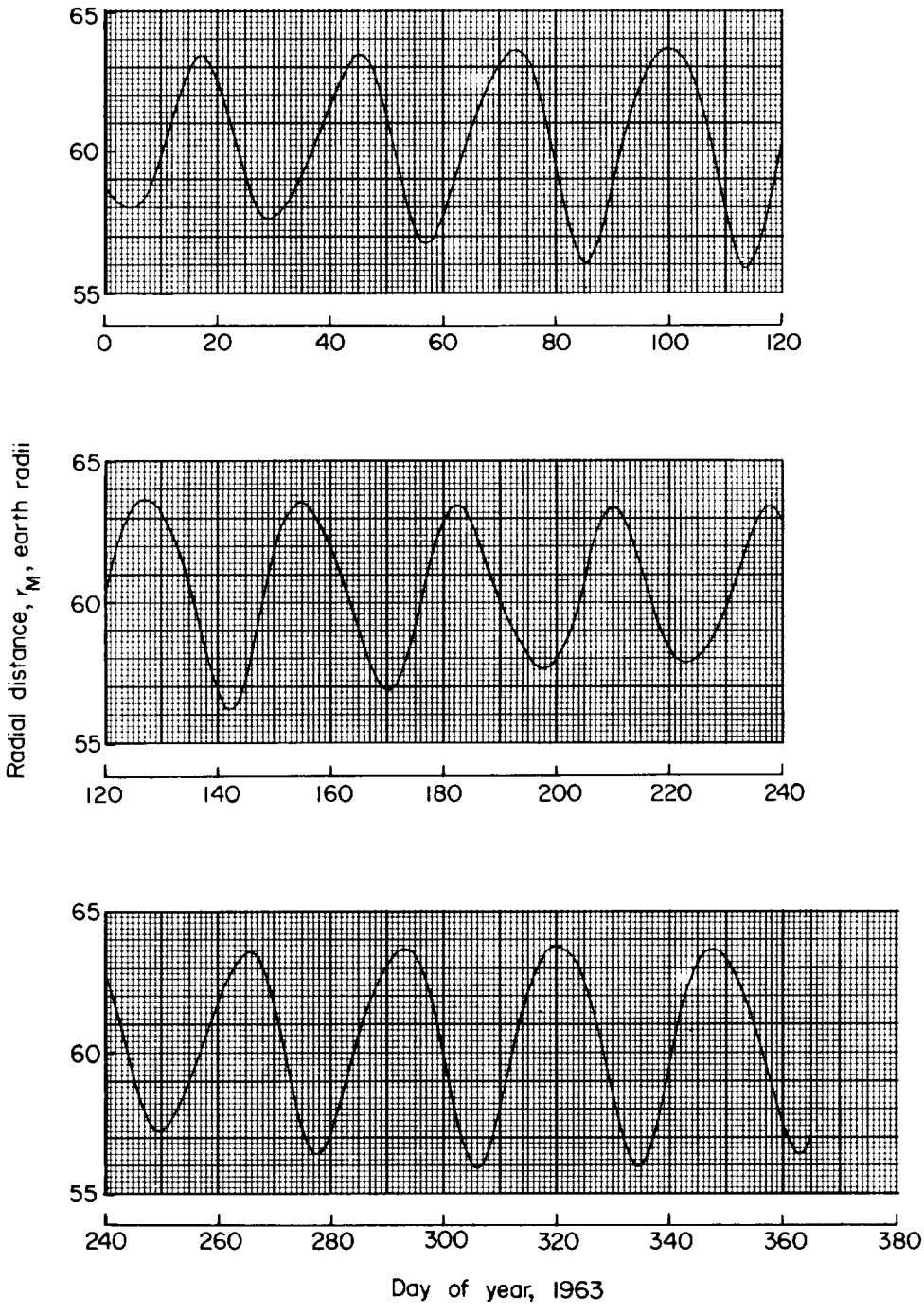

(b) Radial distance.

Figure 1. - Concluded.

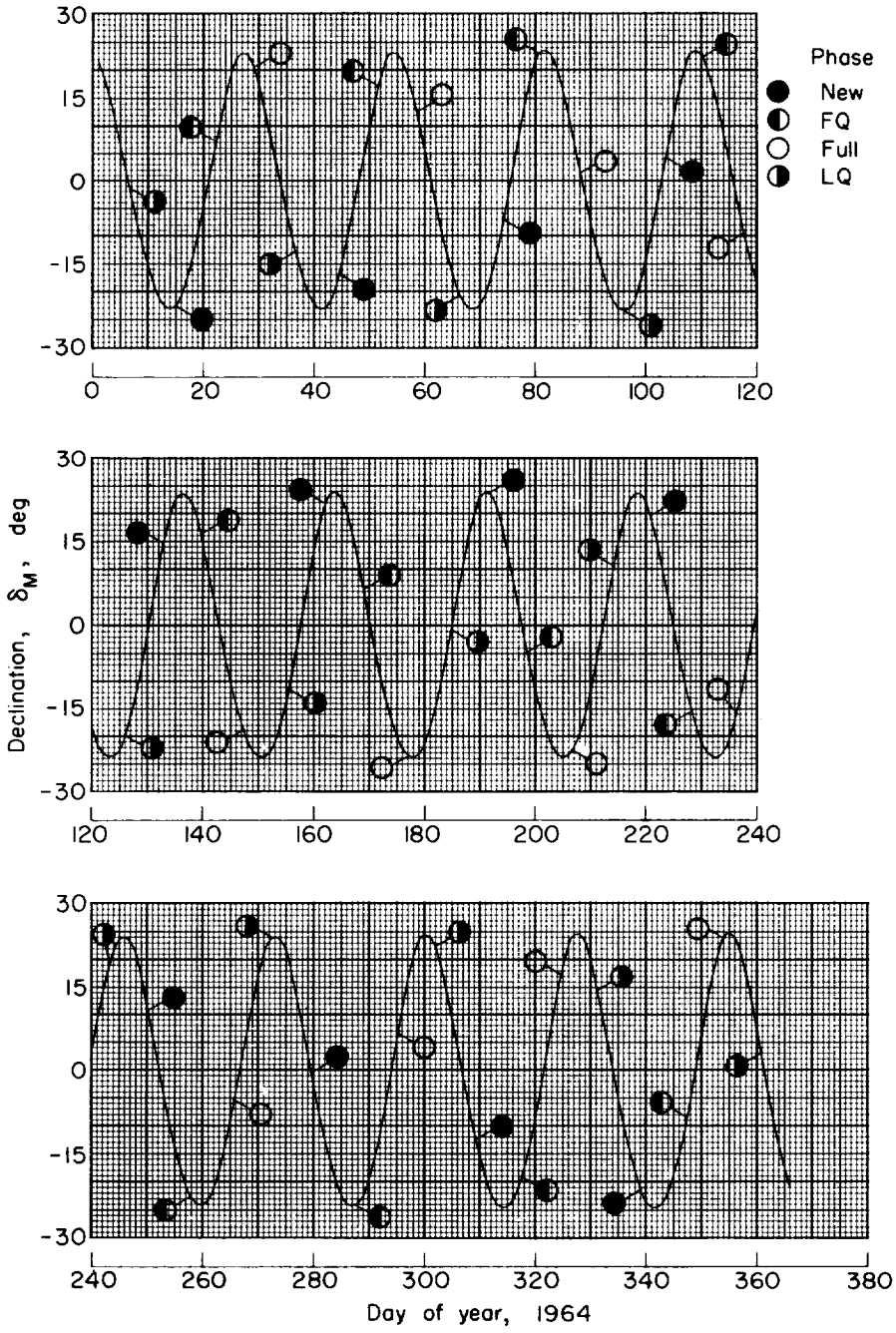

(a) Declination and phases.

Figure 2.- Declination and phases and radial distance of moon for year 1964.

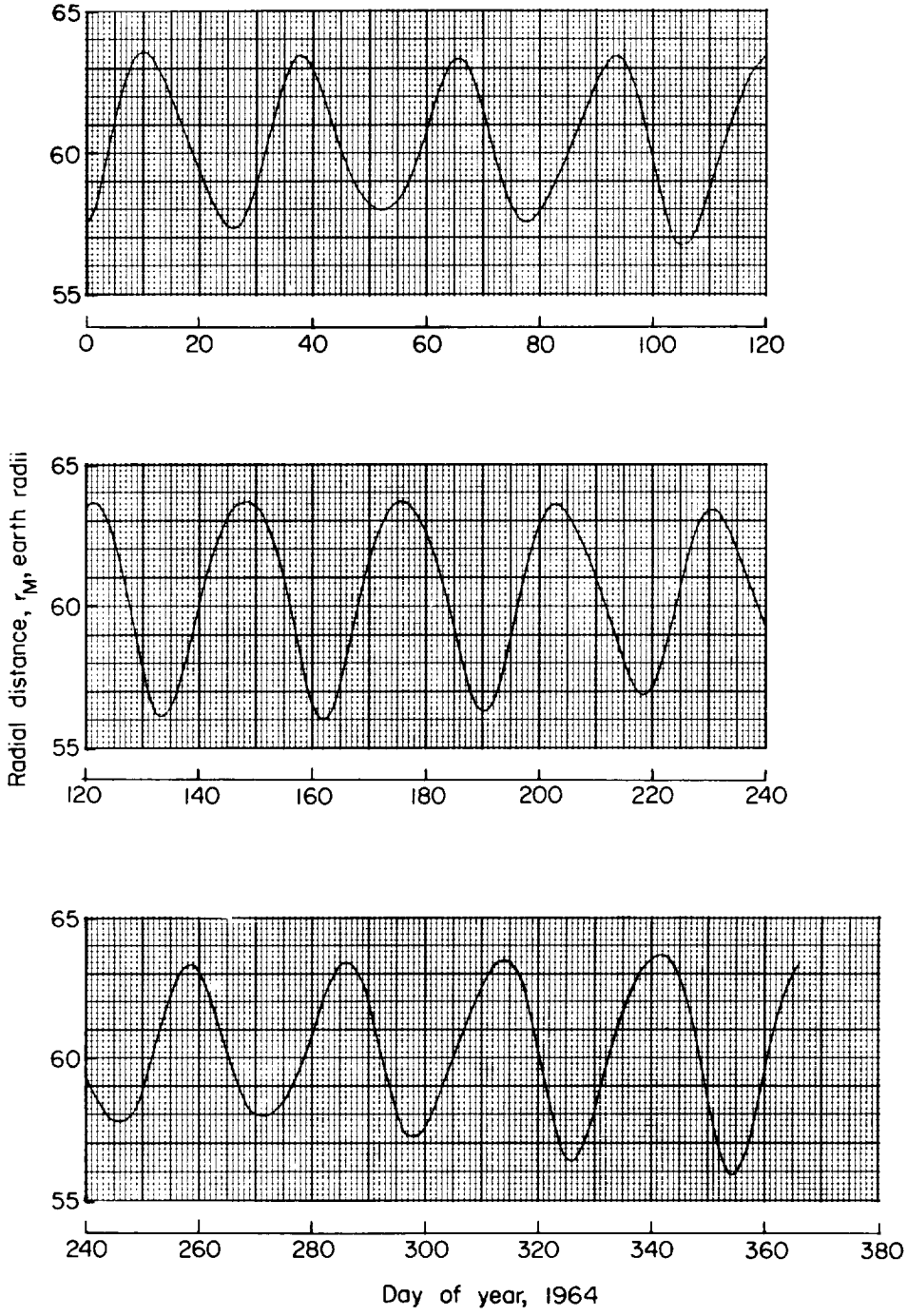

(b) Radial distance.

Figure 2.- Concluded.

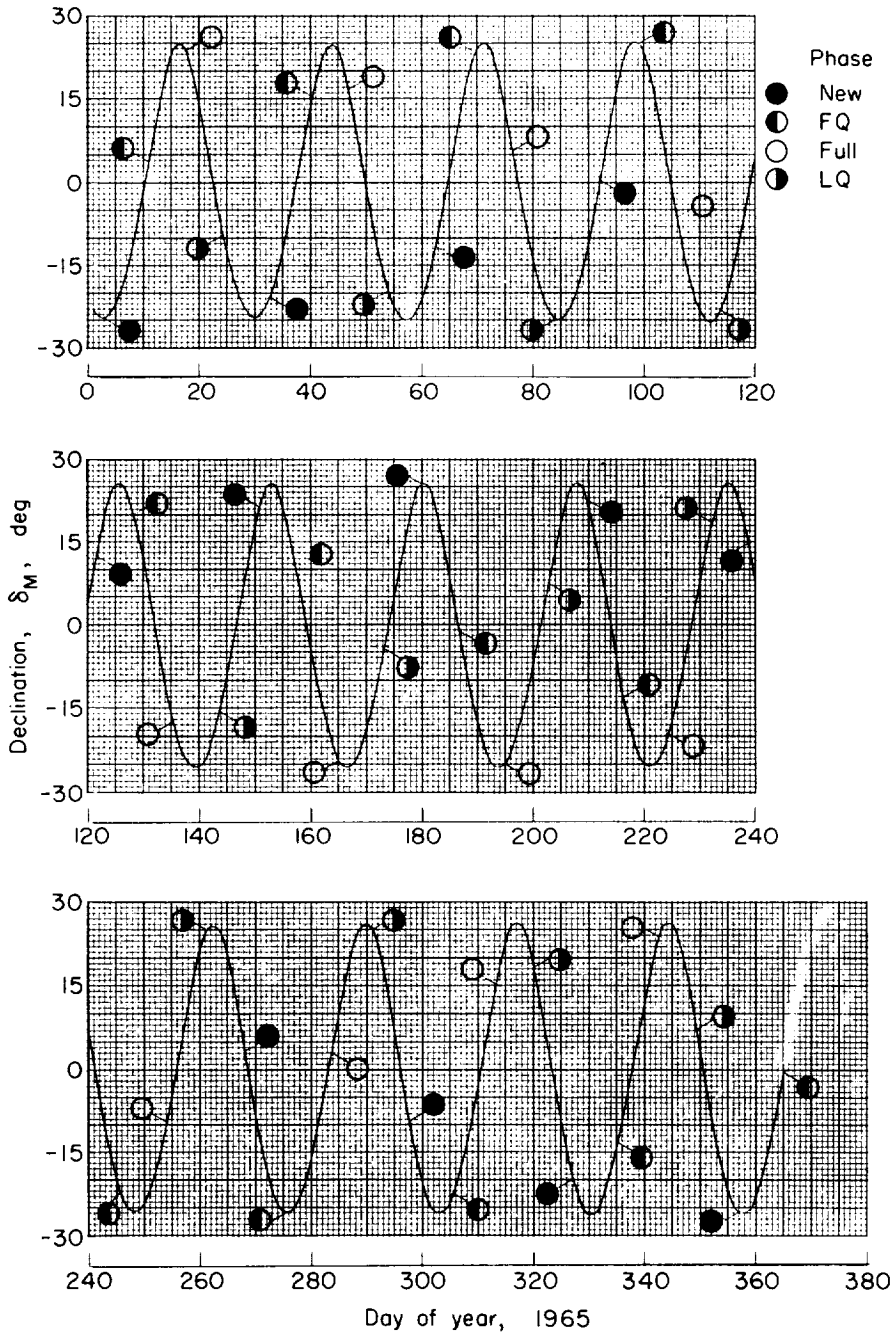

(a) Declination and phases.

Figure 3.- Declination and phases and radial distance of moon for year 1965.

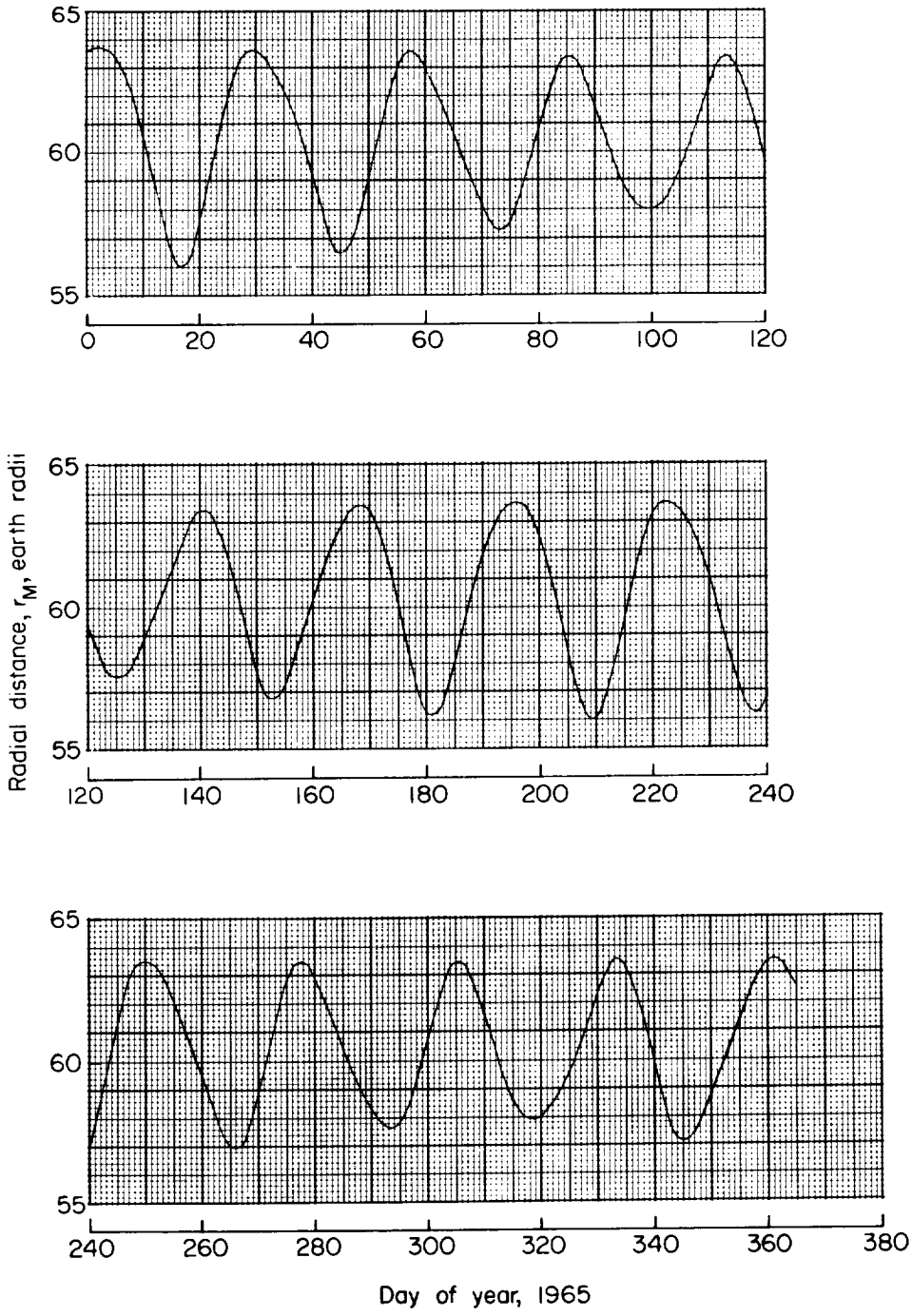

(b) Radial distance.

Figure 3.- Concluded.

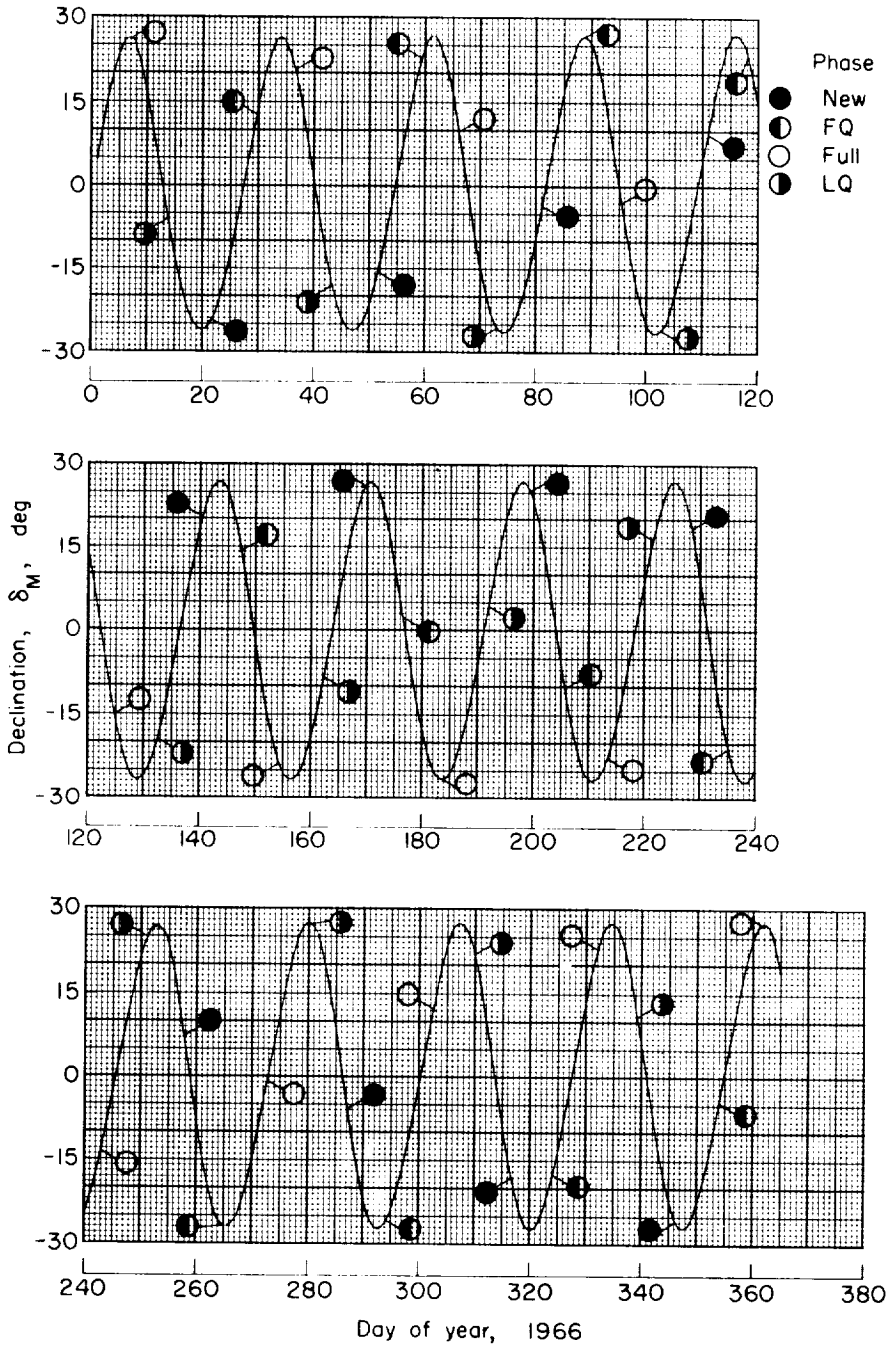

(a) Declination and phases.

Figure 4.- Declination and phases and radial distance of moon for year 1966.

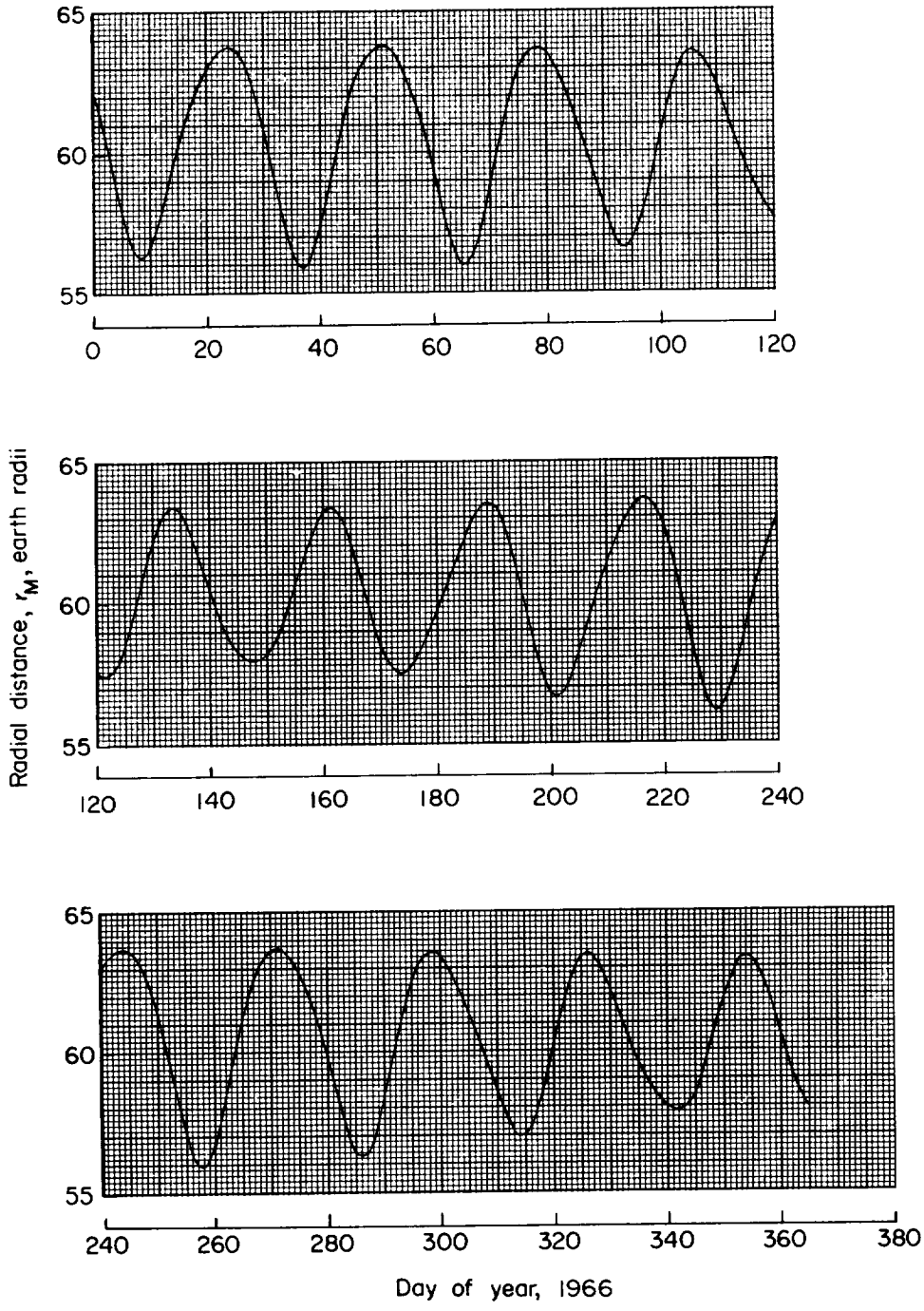

(b) Radial distance.

Figure 4. - Concluded.

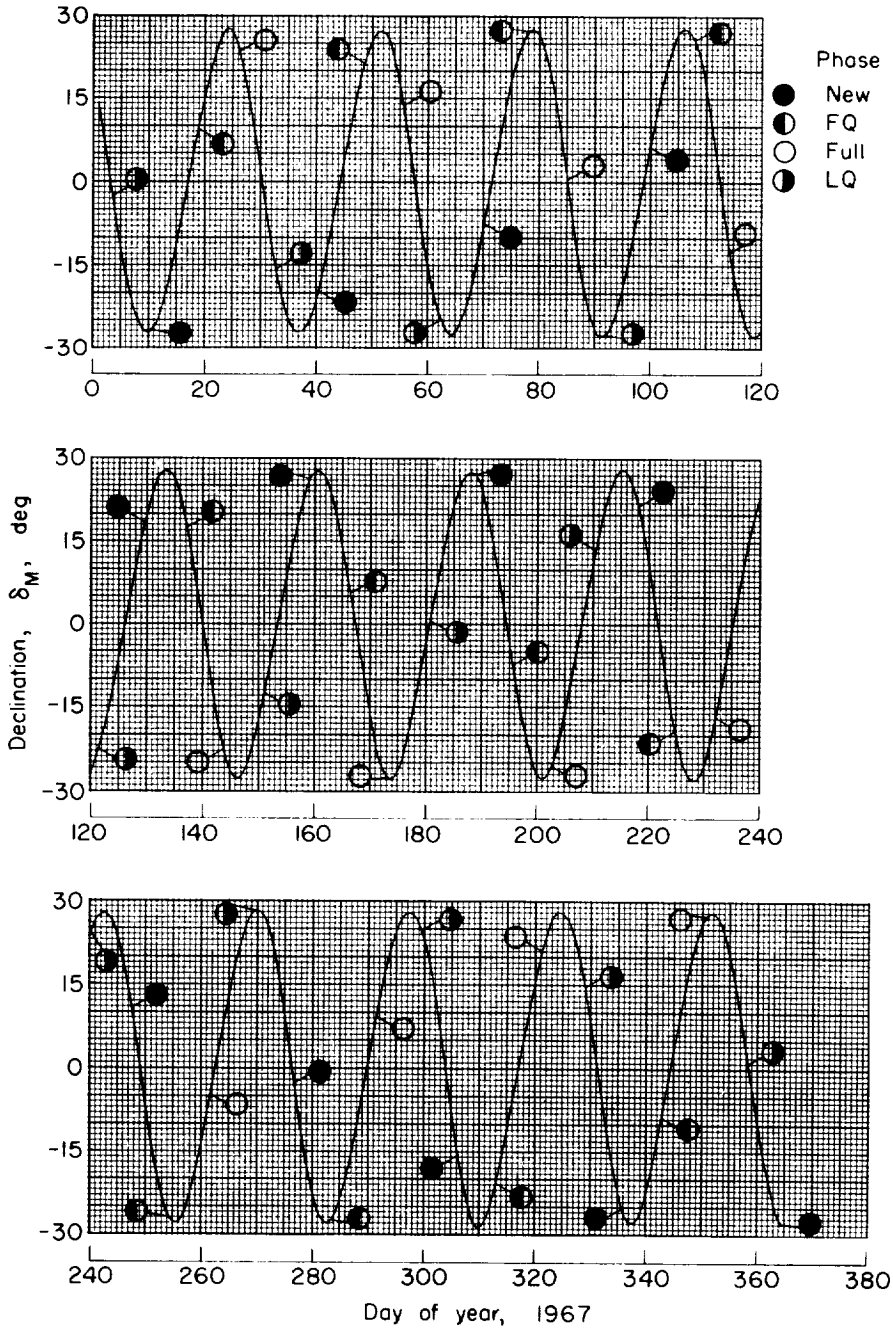

(a) Declination and phases.

Figure 5.- Declination and phases and radial distance of moon for year 1967.

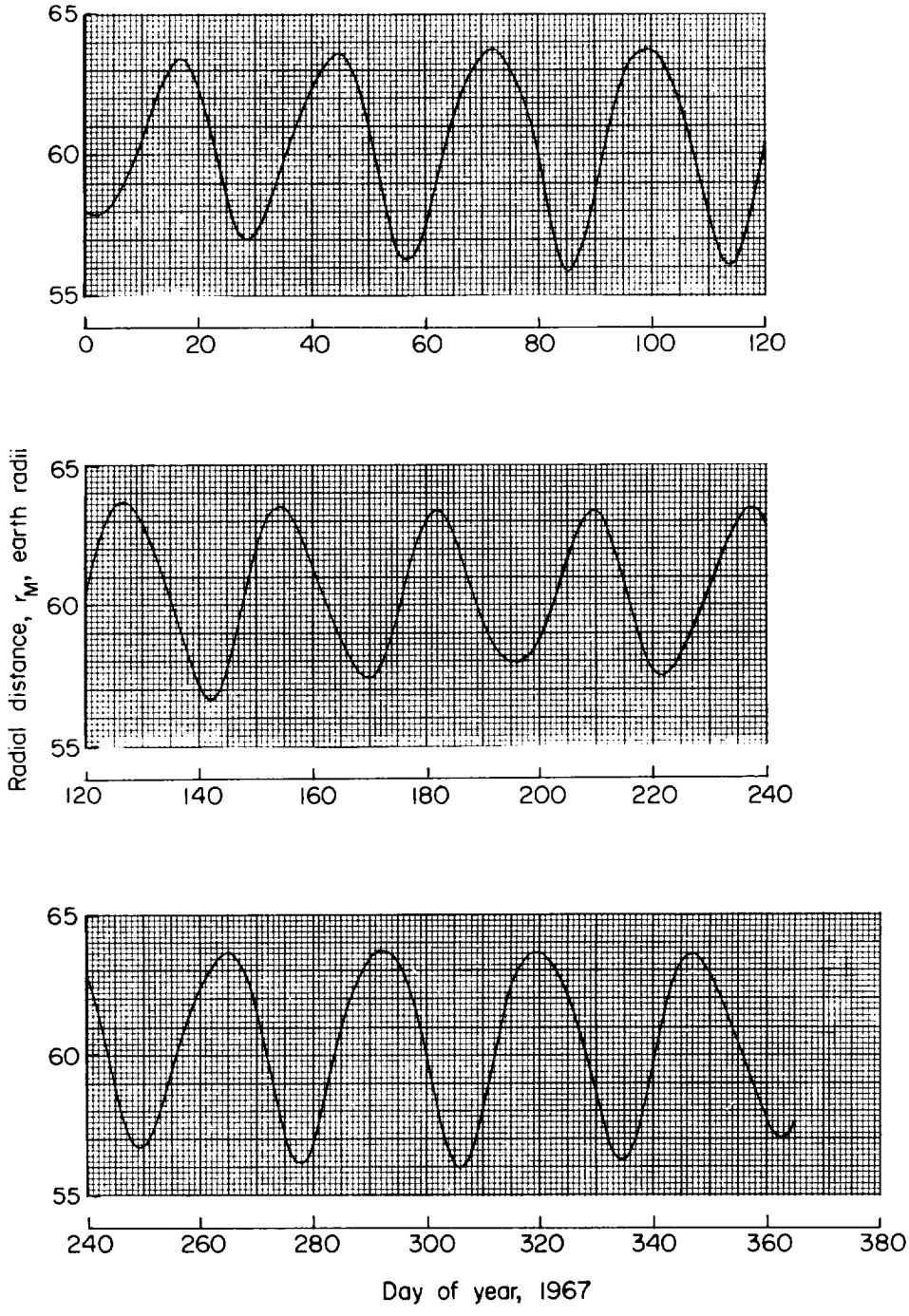

(b) Radial distance.

Figure 5.- Concluded.

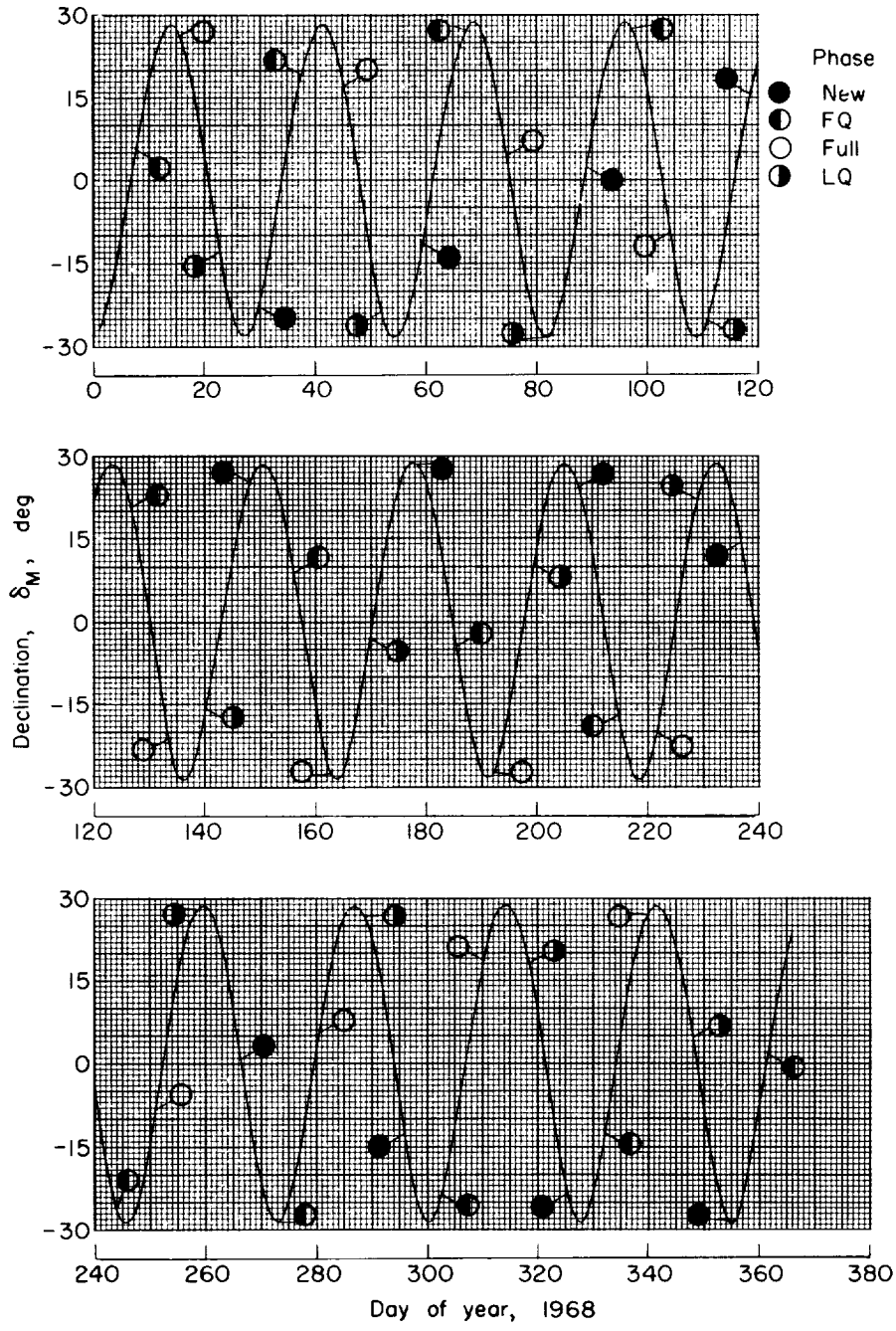

(a) Declination and phases.

Figure 6. - Declination and phases and radial distance of moon for year 1968.

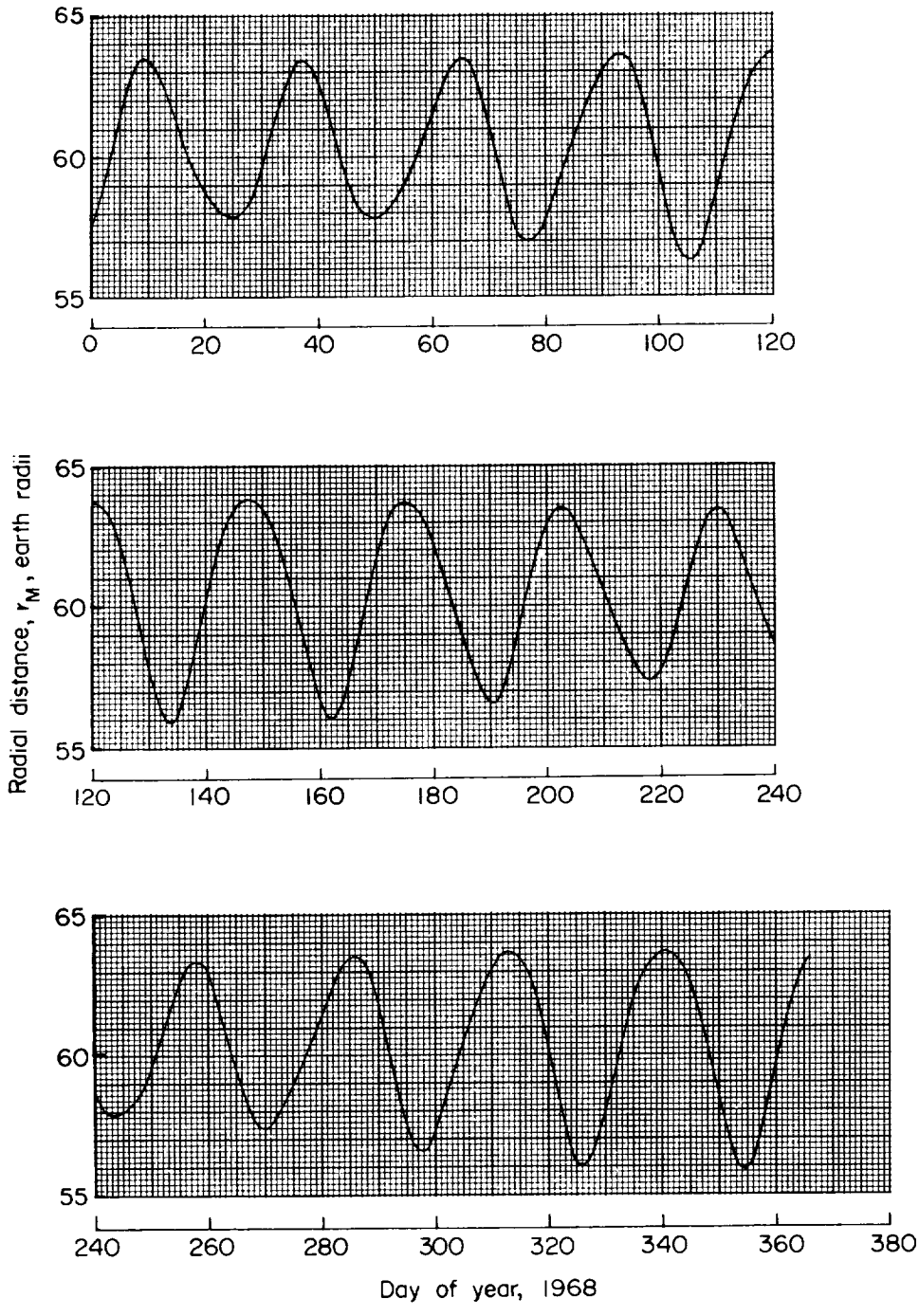

(b) Radial distance.

Figure 6.- Concluded.

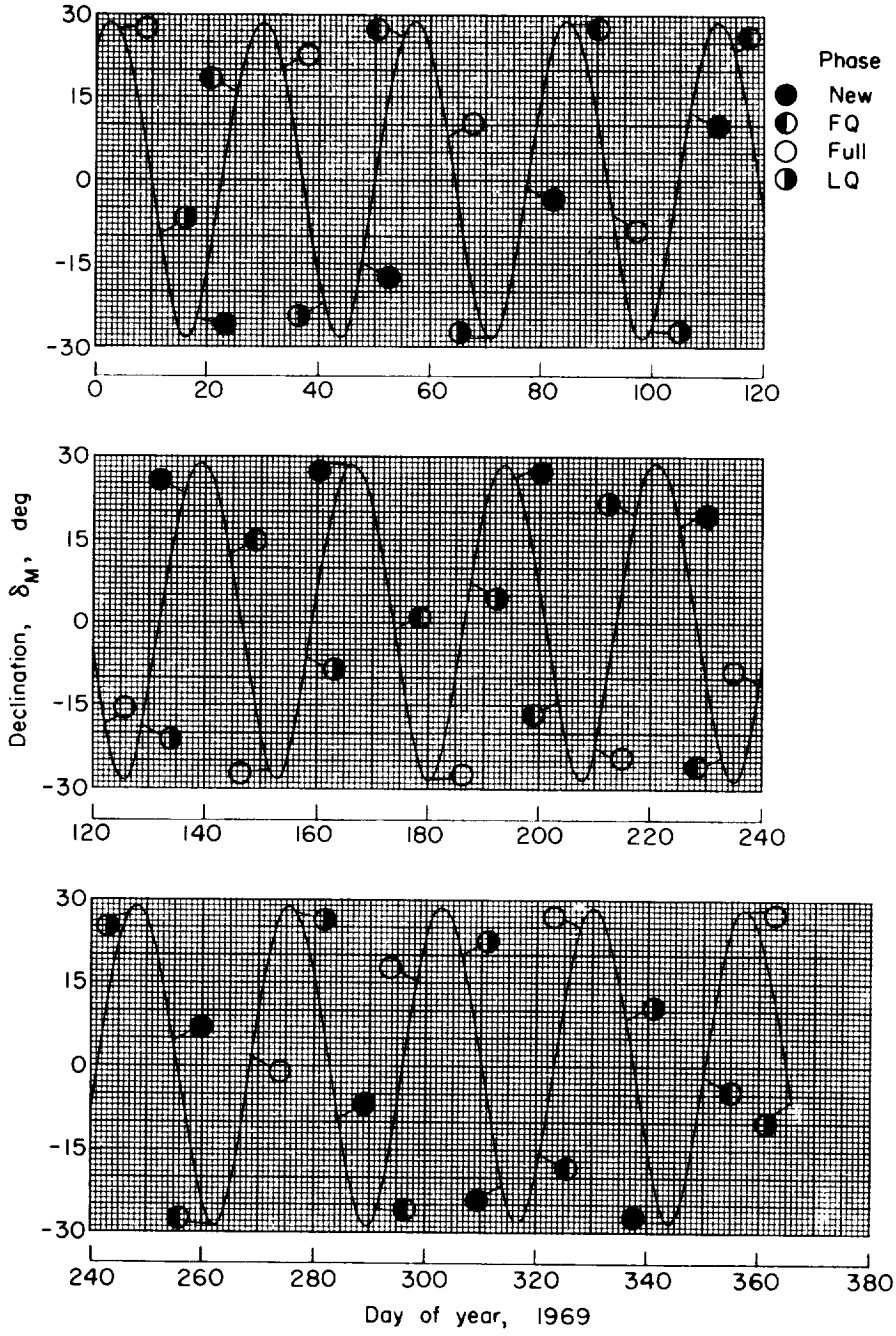

(a) Declination and phases.

Figure 7. - Declination and phases and radial distance of moon for year 1969.

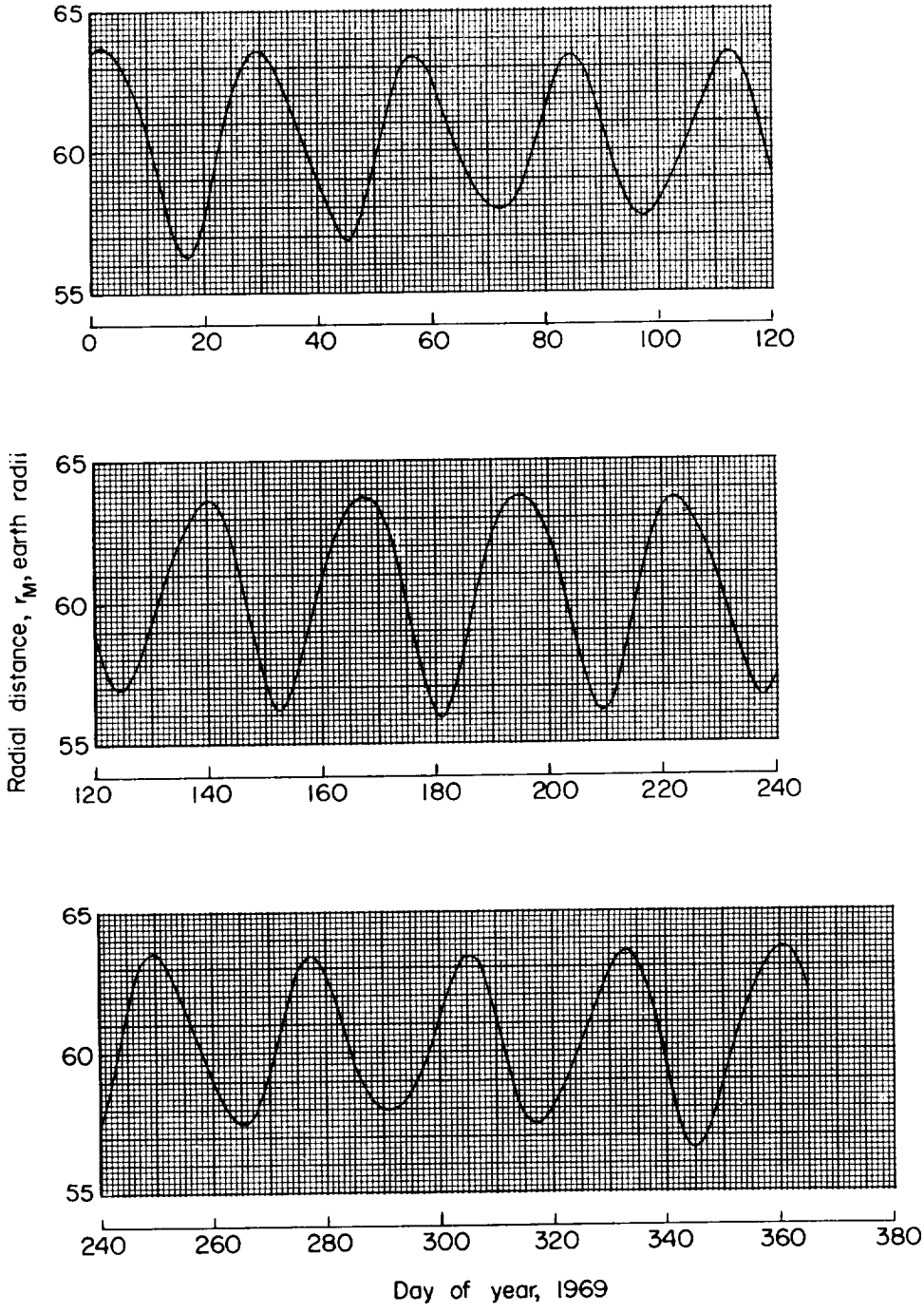

(b) Radial distance.

Figure 7. - Concluded.

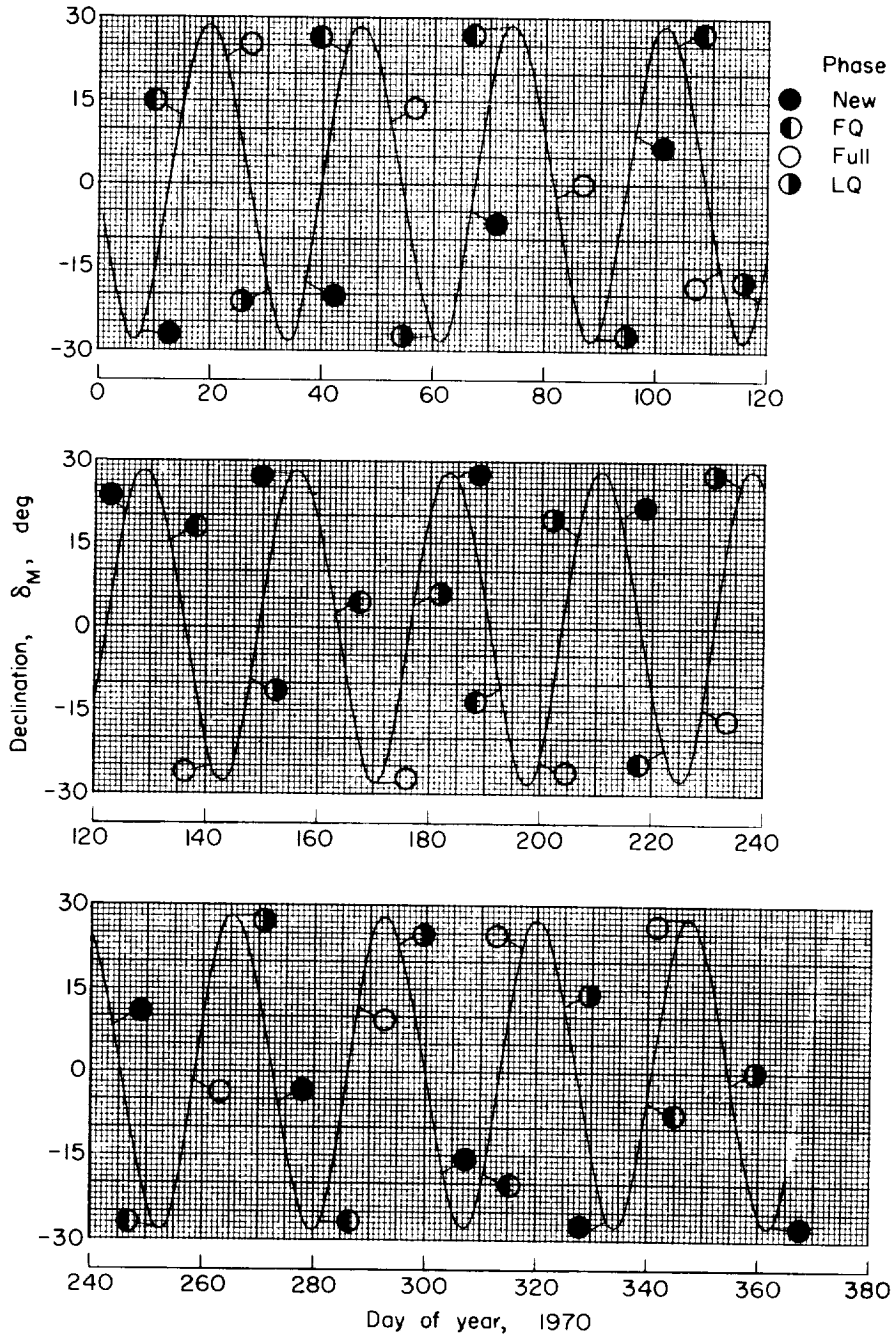

(a) Declination and phases.

Figure 8.- Declination and phases and radial distance of moon for year 1970.

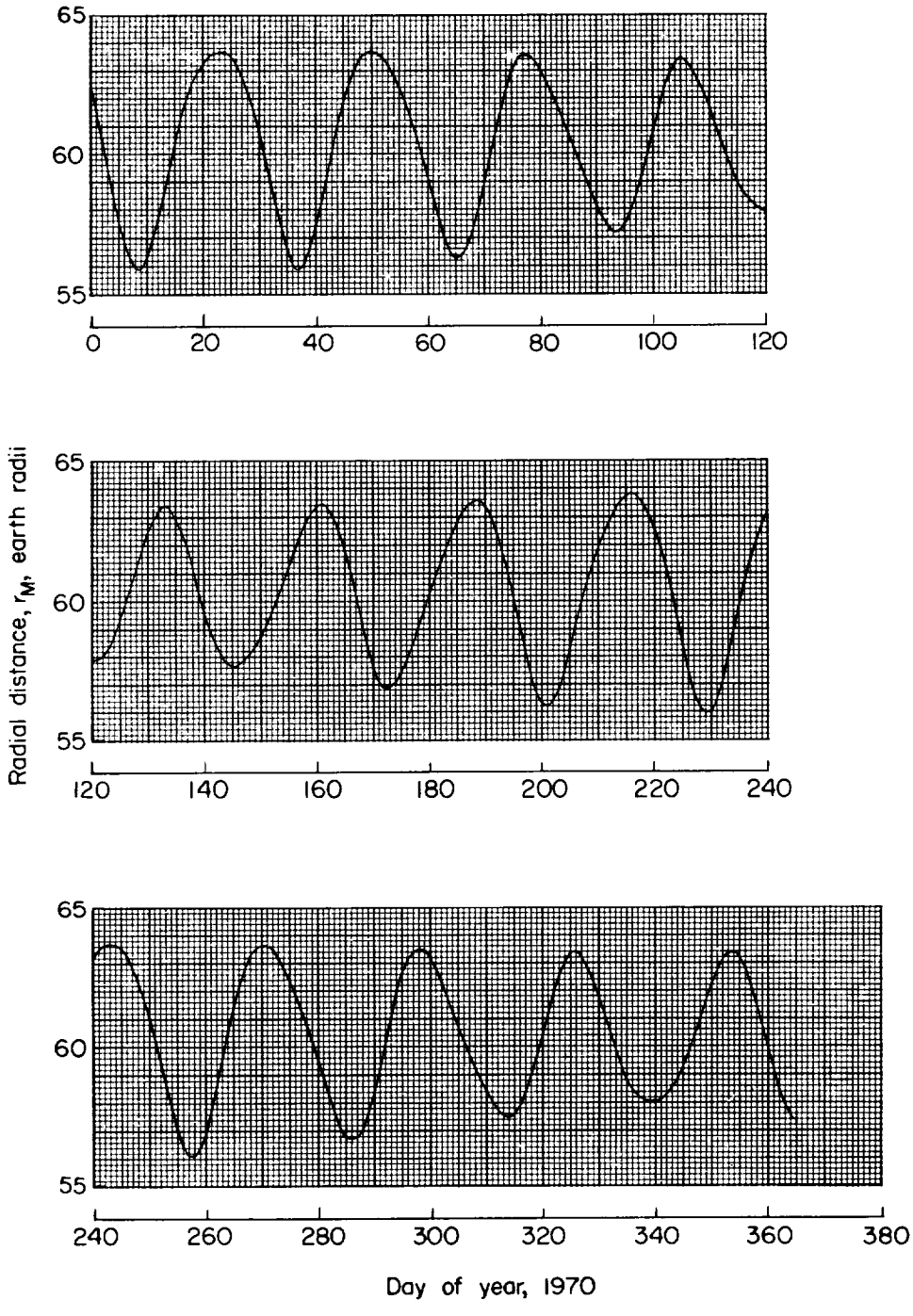

(b) Radial distance.

Figure 8. - Concluded.

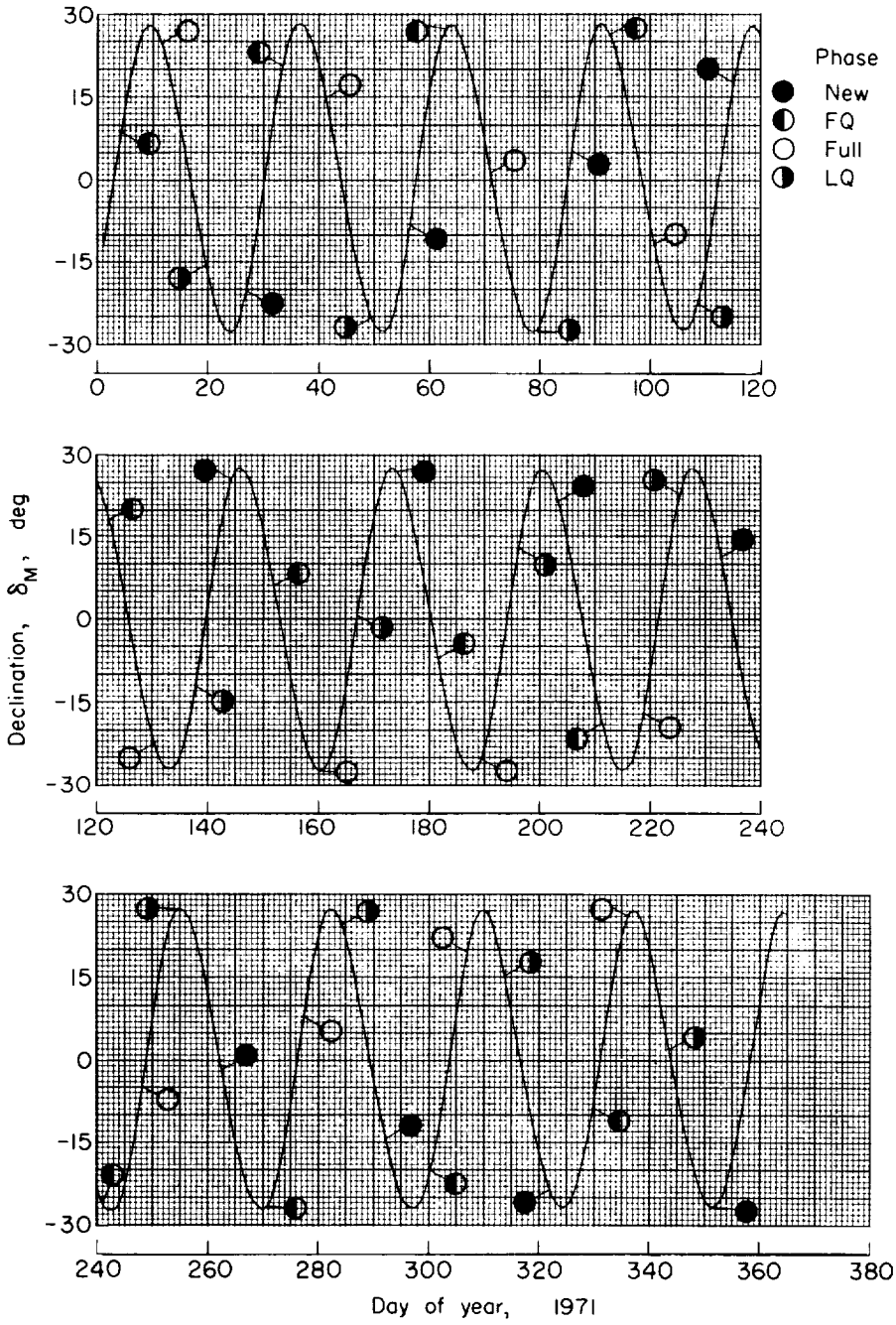

(a) Declination and phases.

Figure 9.- Declination and phases and radial distance of moon for year 1971.

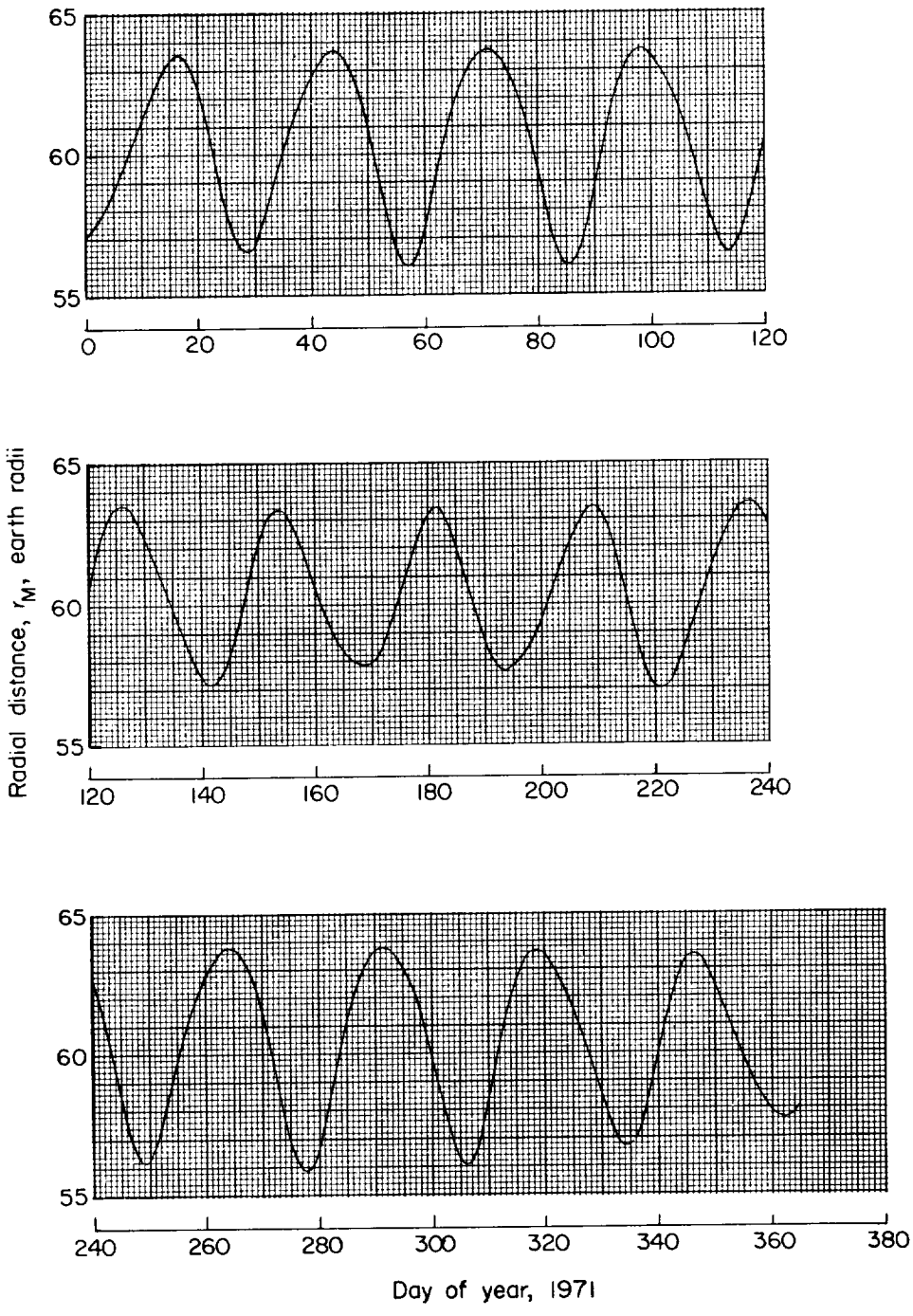

(b) Radial distance.

Figure 9. - Concluded.

NASA - Langley Field, Va L-1576

Fig. 10. Lunar Declination Versus Lunar Central Angle

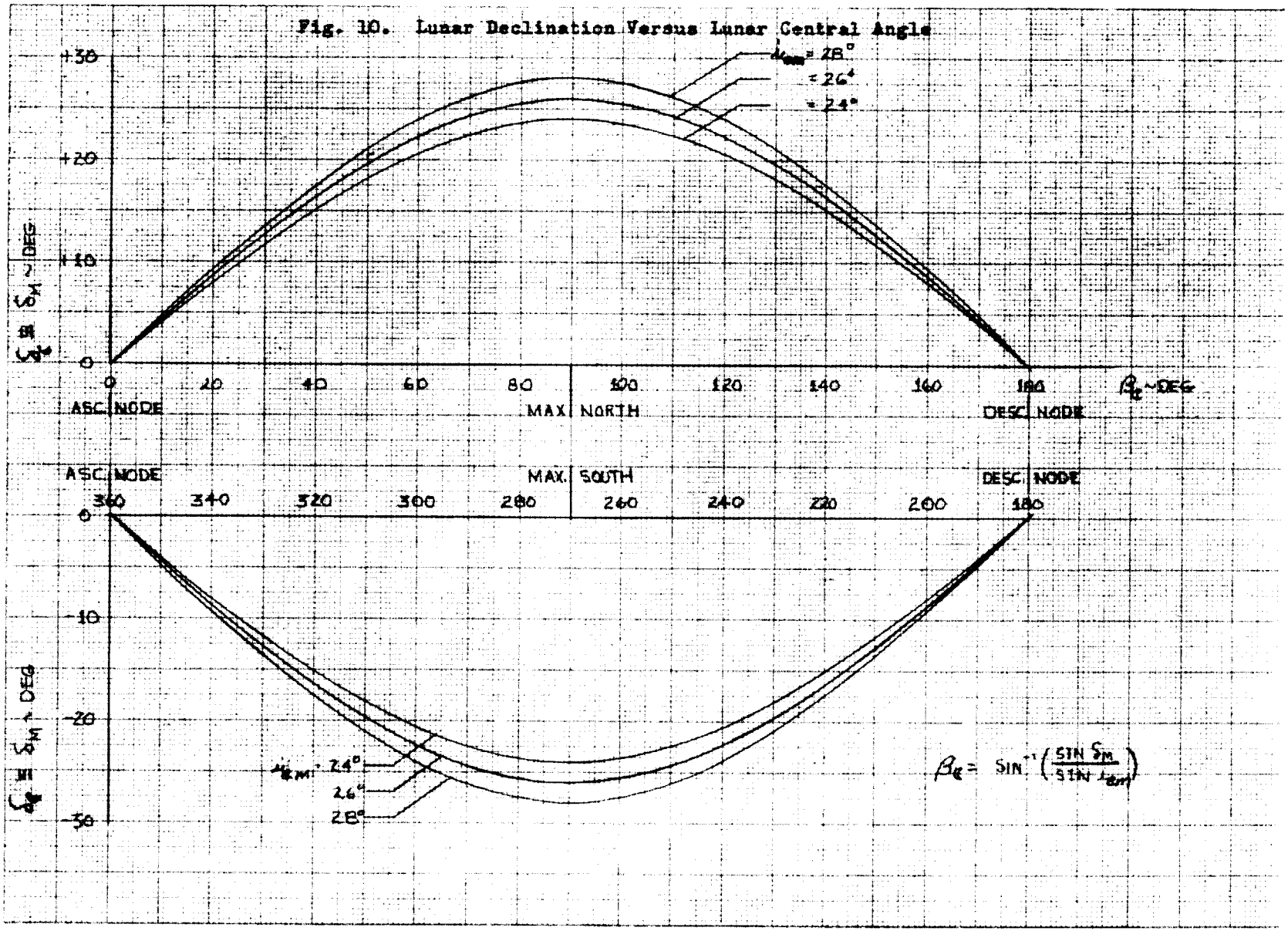

Fig. 11. Required Translunar Plane Inclination (i_{VTL}) As A Function Of Lunar Central Angle (β_ℓ)

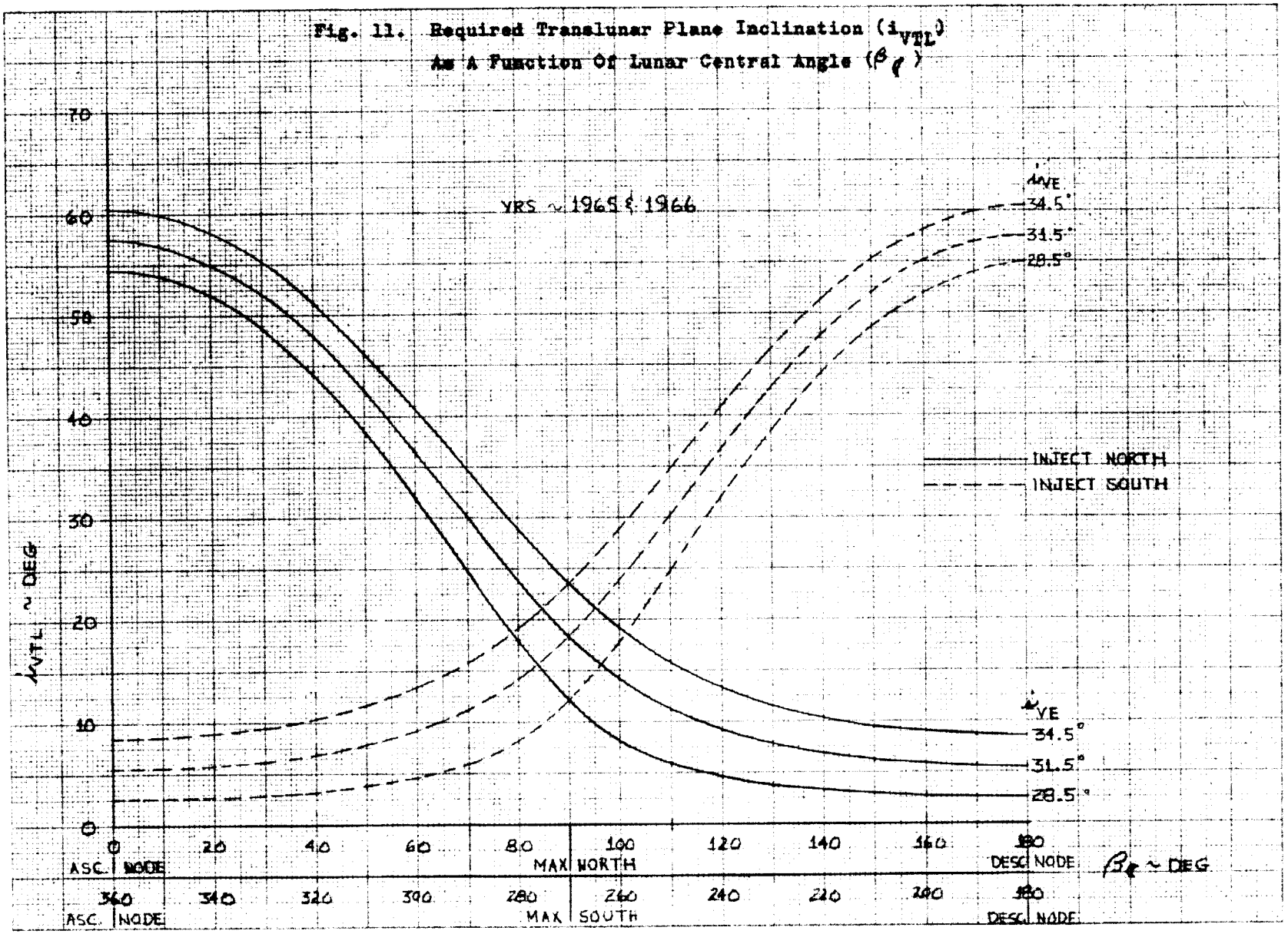

Fig. 12. Required Translunar Plane Inclination (i_{VTL}) As A Function Of Lunar Central Angle (β_ℓ)

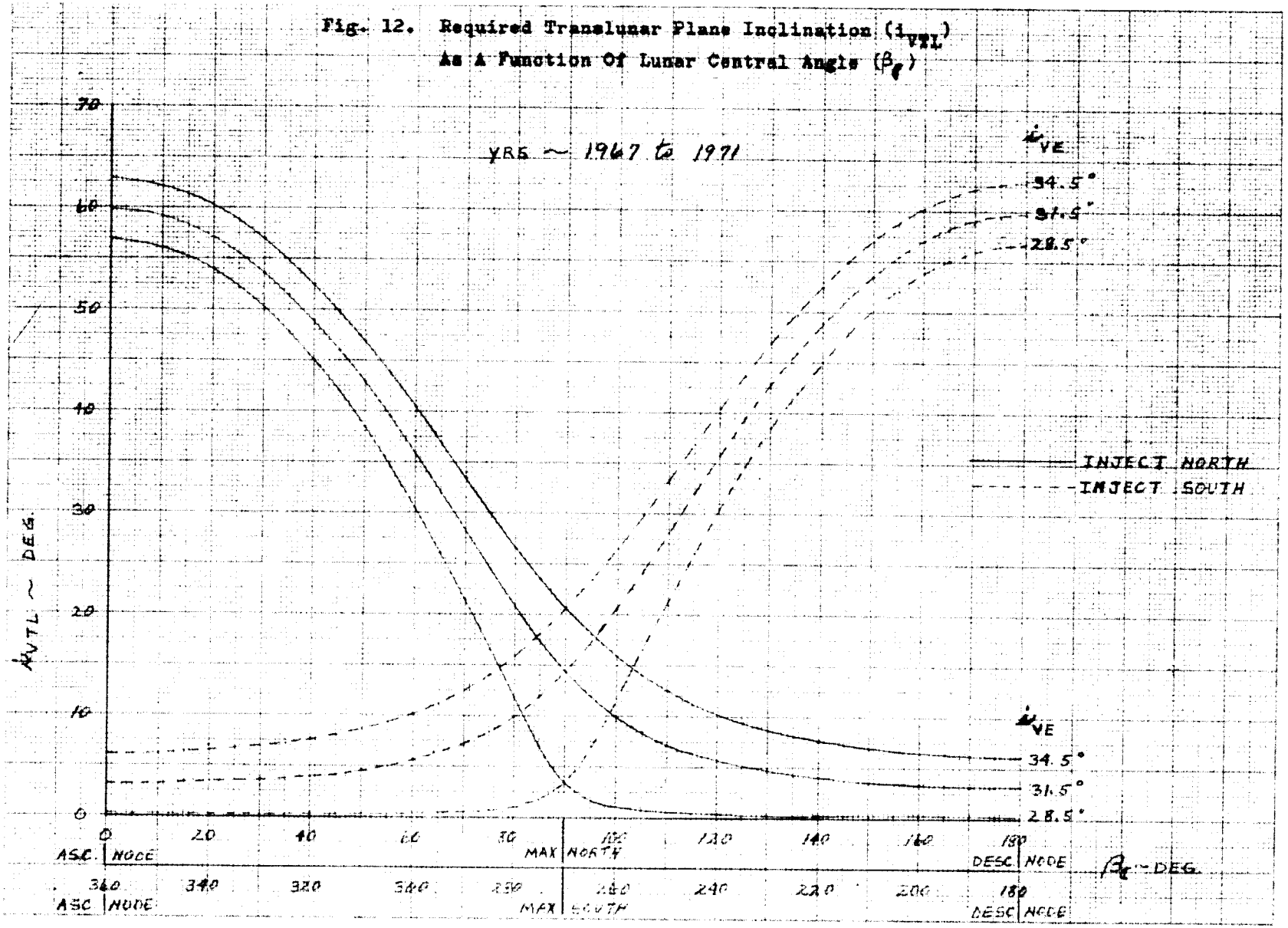

Fig. 13. Relationship Of Transearth Inclination To The Equator And MOP With Lunar Central Angle

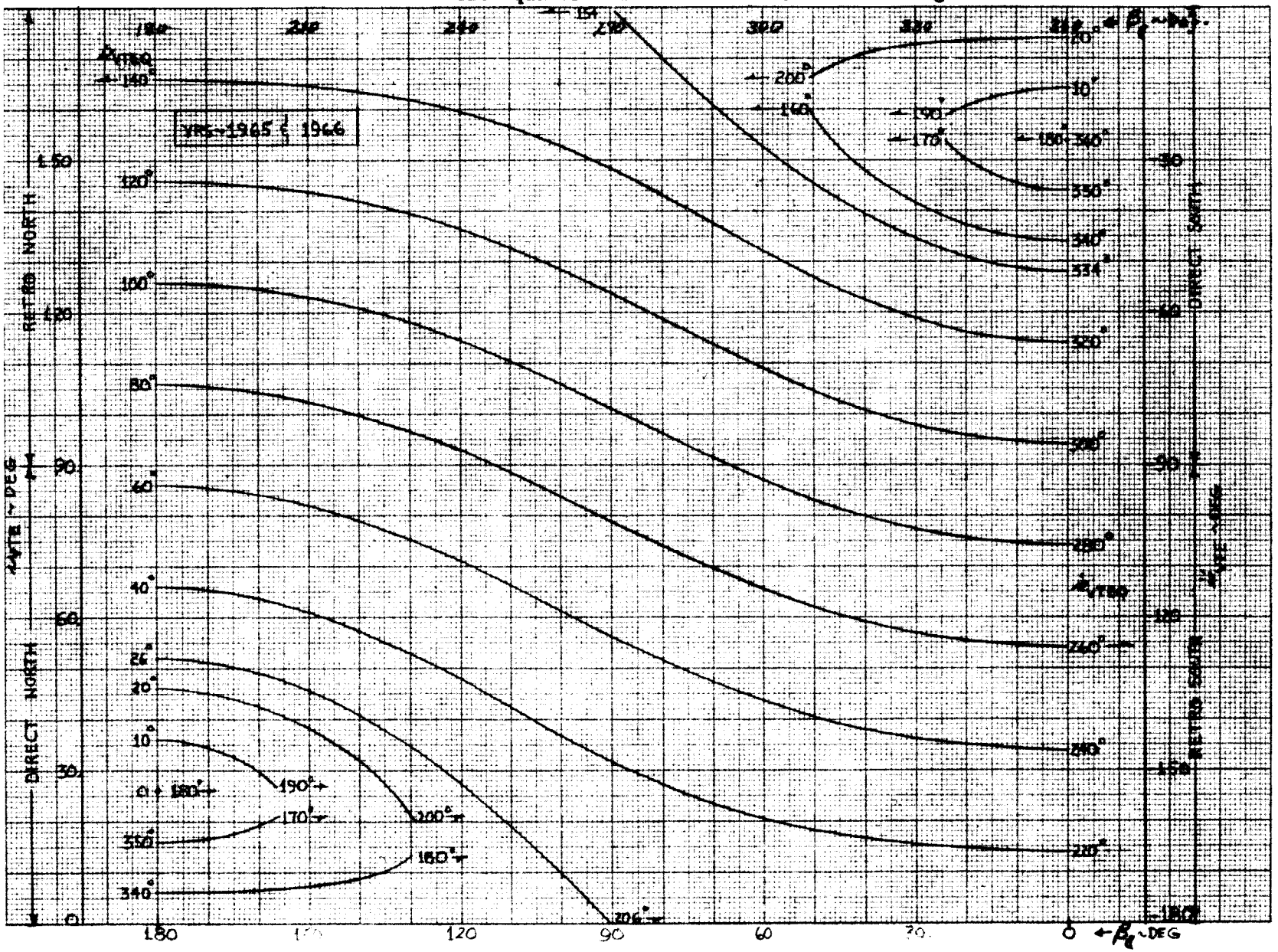

Fig. 14. Relationship Of Transearth Inclination To The Equator And MOP With Lunar Central Angle

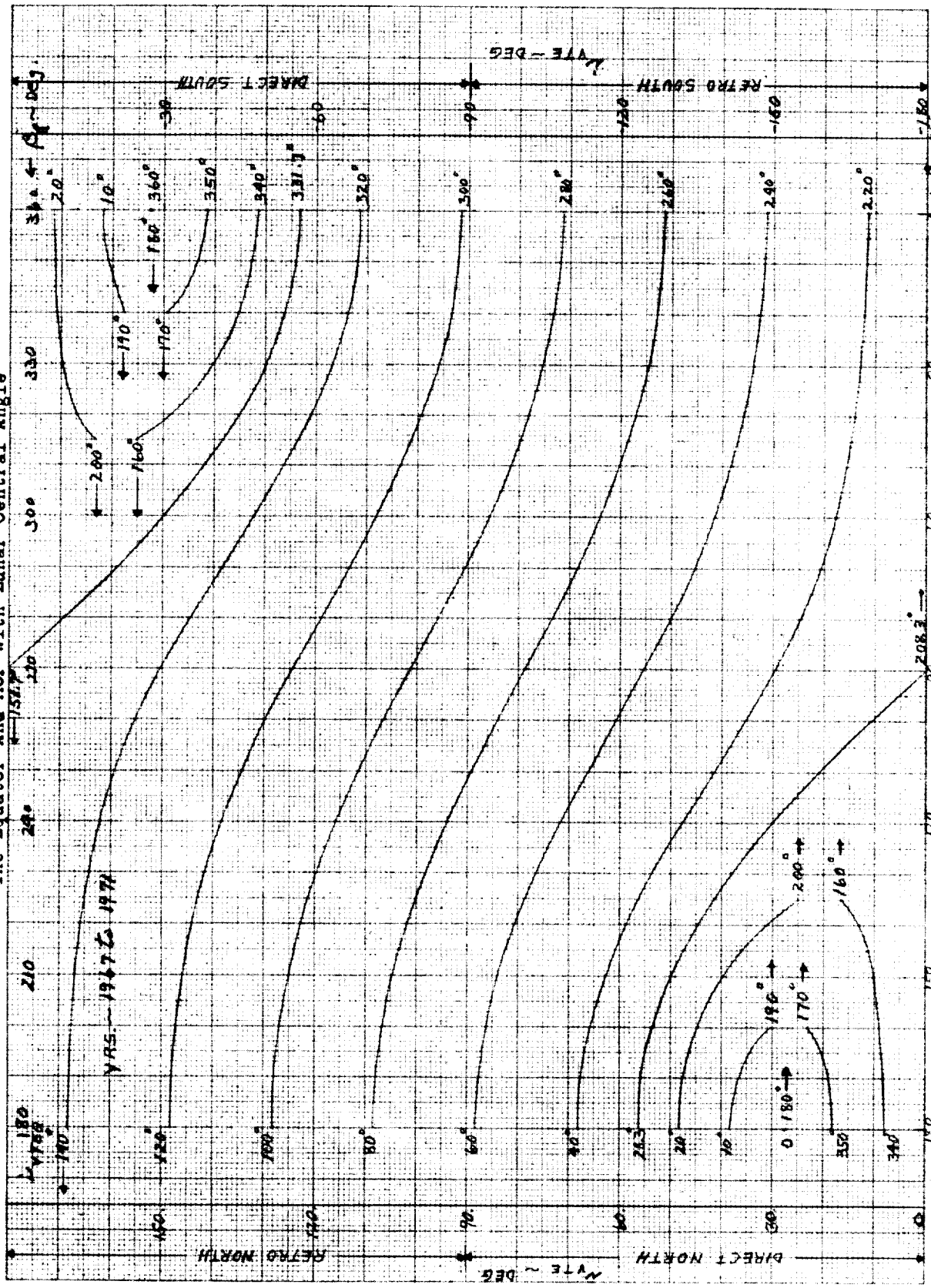

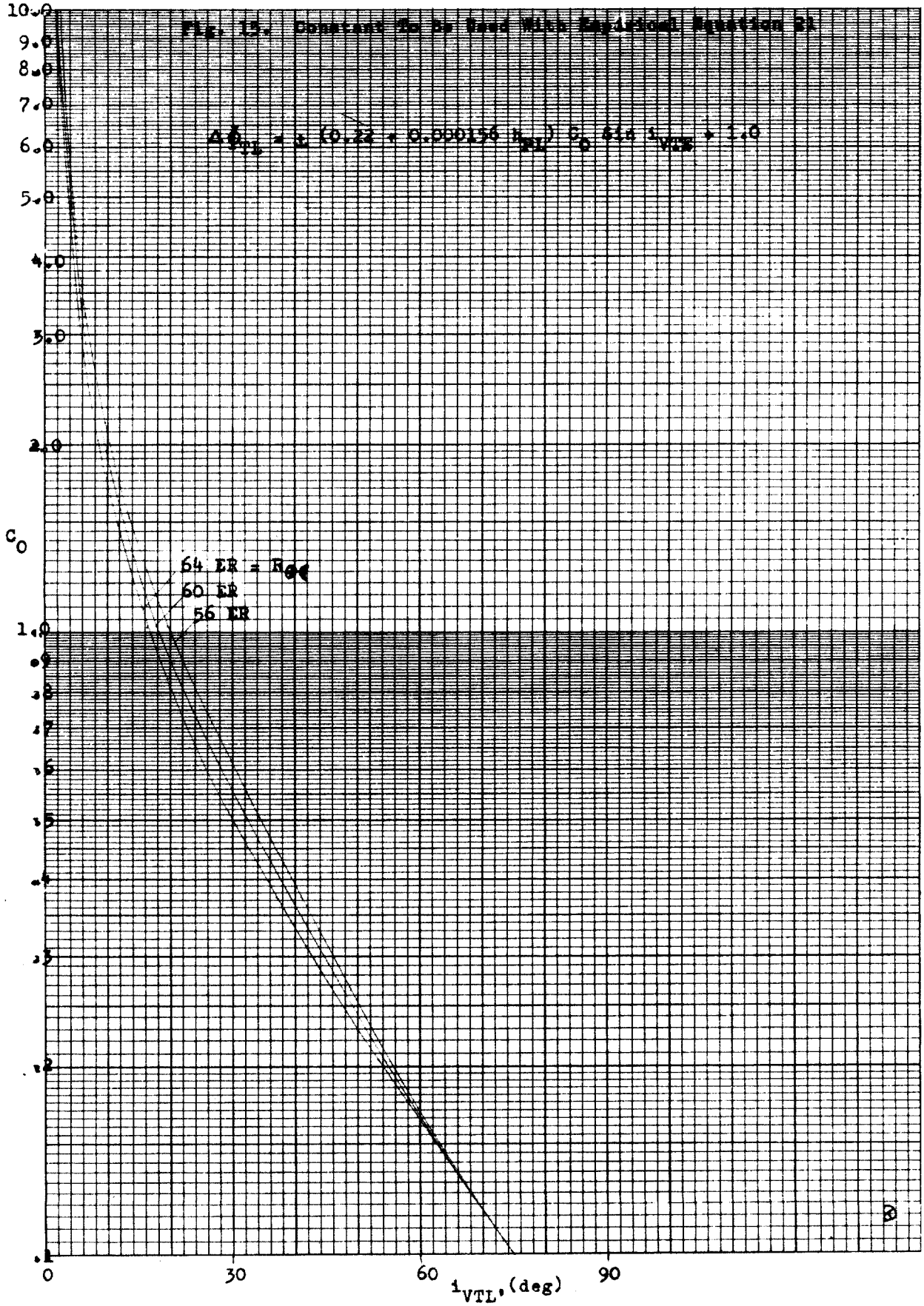
Fig. 12. Constant C_0 to be Used With Equation 21
$\Delta\phi_{VTL} = \pm (0.22 + 0.000156\ h_{RL})\ C_0\ 64.6\ i_{VTL} + 1.0$
C_0
64 ER = R_{RL}
60 ER
56 ER
10.0
9.0
8.0
7.0
6.0
5.0
4.0
3.0
2.0
1.0
0
30
60
90
i_{VTL}, (deg)

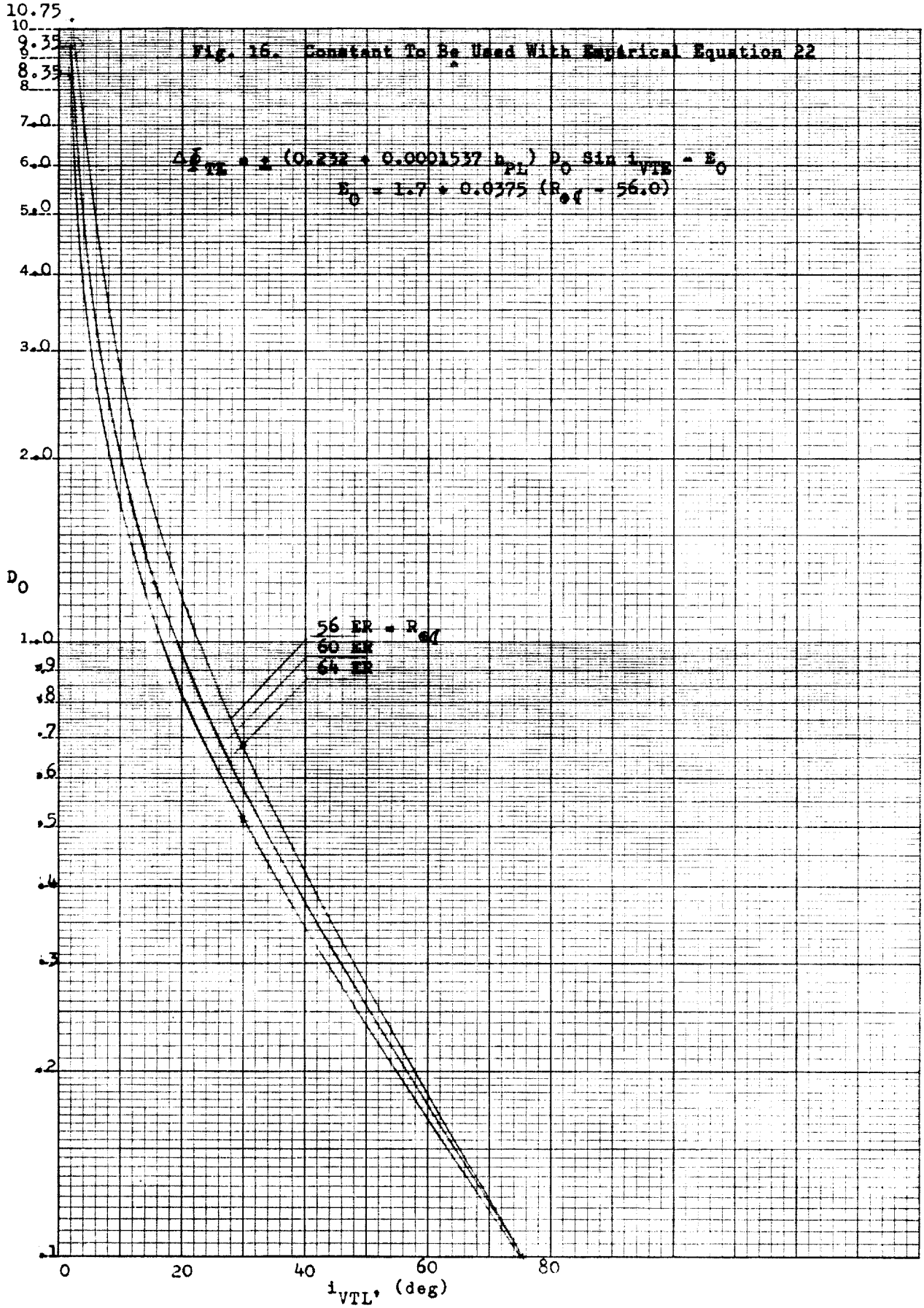
Fig. 16. Constant To Be Used With Empirical Equation 22
$\Delta\phi_{TL} = \pm (0.232 + 0.0001537\ h_{PL})\ D_0 \sin i_{VTL} - E_0$
$E_0 = 1.7 + 0.0375\ (R_{eff} - 56.0)$
56 ER = R_{eff}
60 ER
64 ER
D_0
i_{VTL}, (deg)
10.75
10
9.35
9
8.35
8
7.0
6.0
5.0
4.0
3.0
2.0
1.0
.9
.8
.7
.6
.5
.4
.3
.2
.1
0
20
40
60
80

Fig. 17. ΔV_{TE} Required To Control Transearth Perigee Time

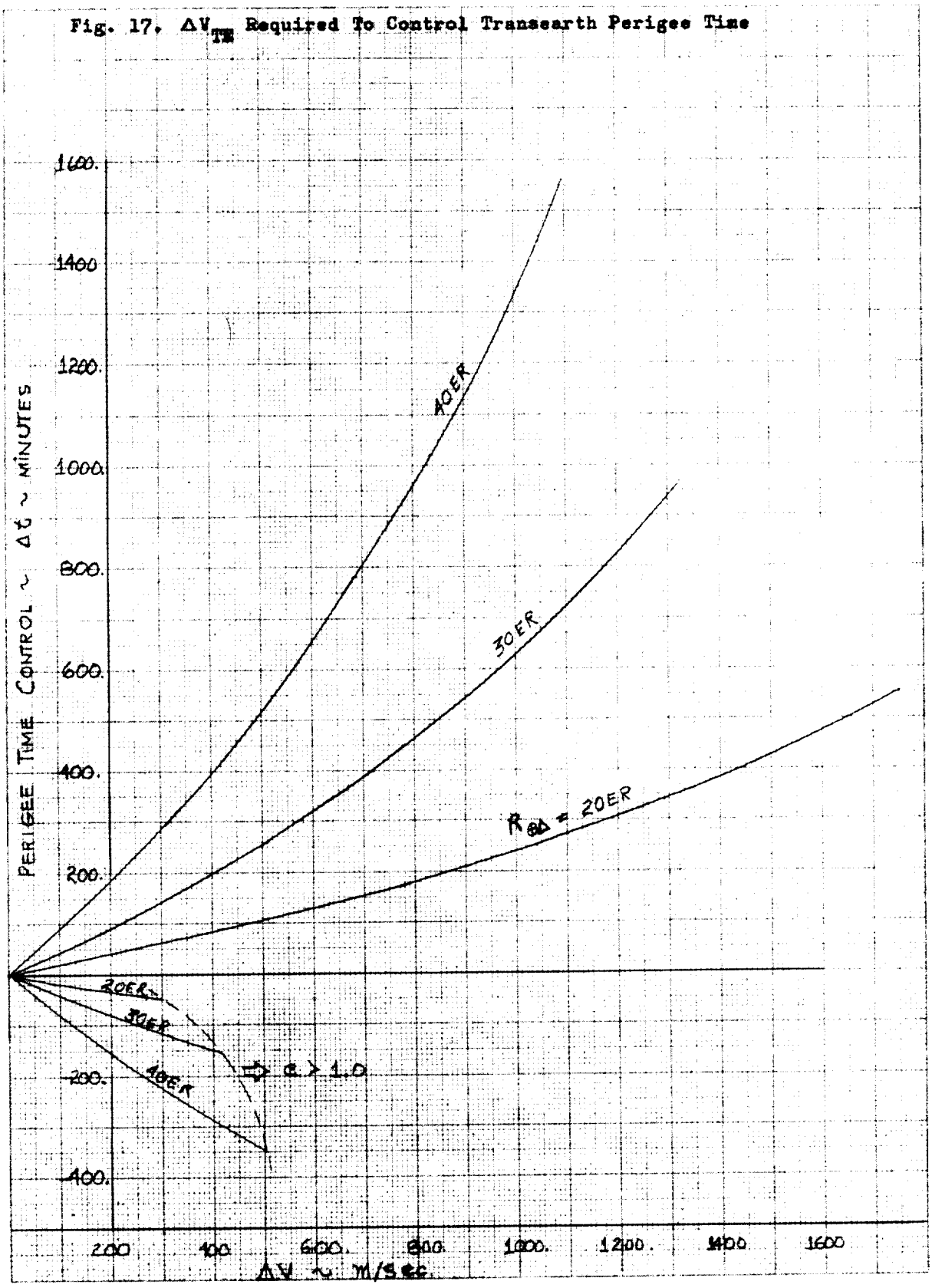

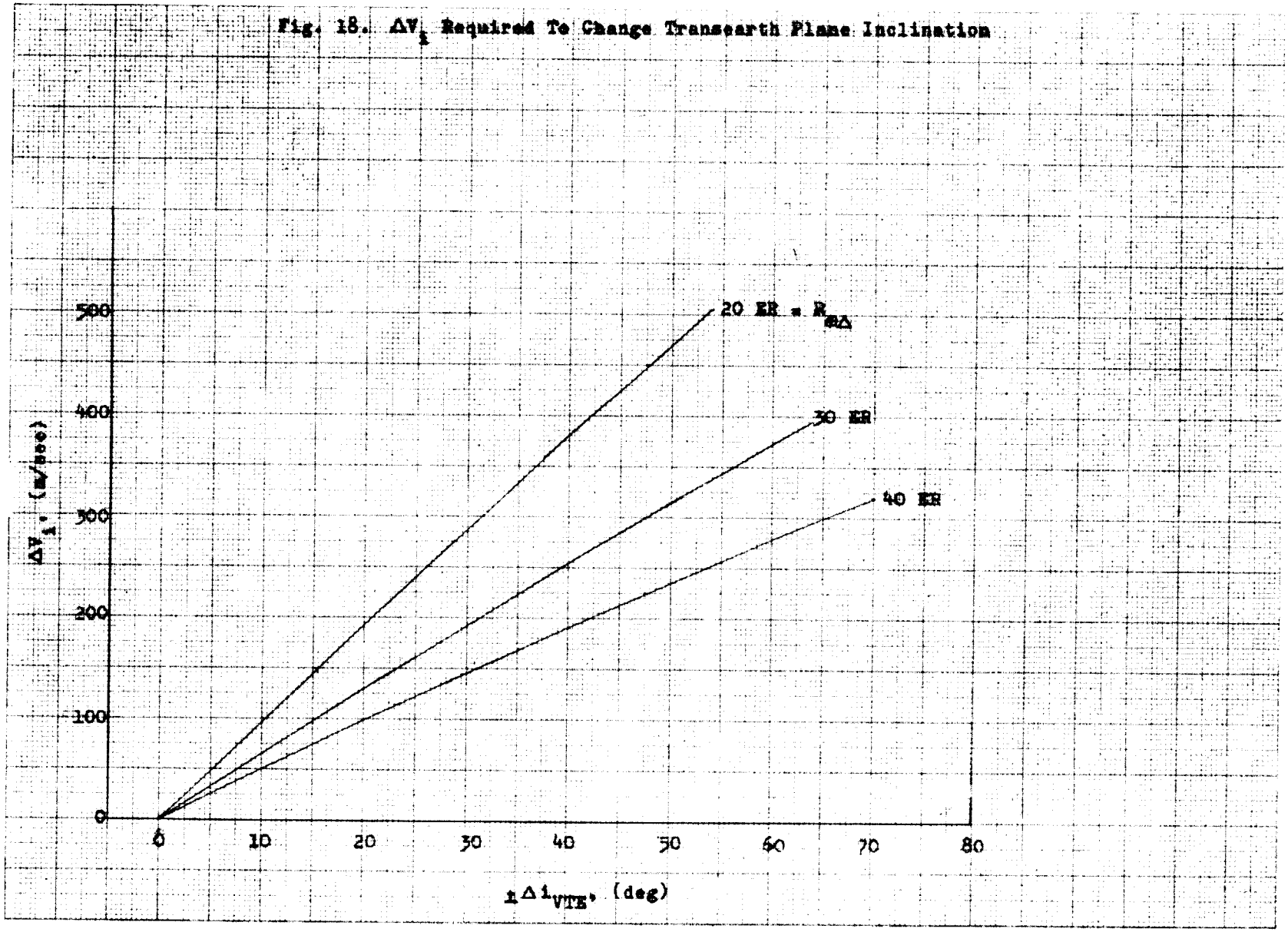

Fig. 18. ΔV_i Required To Change Transearth Plane Inclination

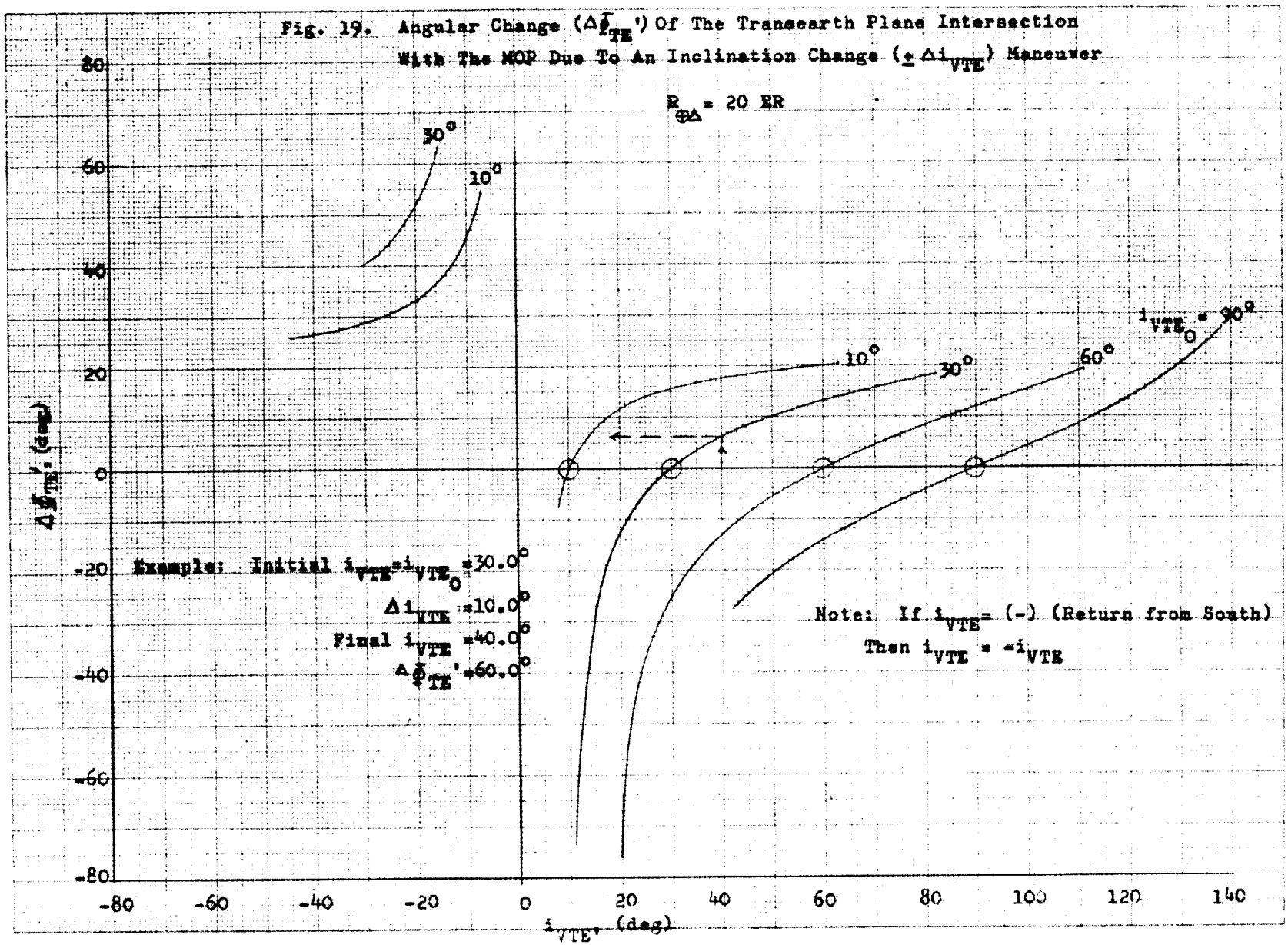
Fig. 19. Angular Change ($\Delta\phi'_{TE}$) Of The Transearth Plane Intersection With The MOP Due To An Inclination Change ($\pm\Delta i_{VTE}$) Maneuver
$R_{\oplus\Delta}$ = 20 ER
$\Delta\phi'_{TE}$, (deg)
i_{VTE}, (deg)
i_{VTE_0} = 90°
60°
30°
10°
30°
10°
Example: Initial $i_{VTE}=i_{VTE_0}$ =30.0°
Δi_{VTE} =10.0°
Final i_{VTE} =40.0°
$\Delta\phi'_{TE}$ =60.0°
Note: If i_{VTE} = (-) (Return from South)
Then i_{VTE} = $-i_{VTE}$
80
60
40
20
0
-20
-40
-60
-80
-80
-60
-40
-20
0
20
40
60
80
100
120
140

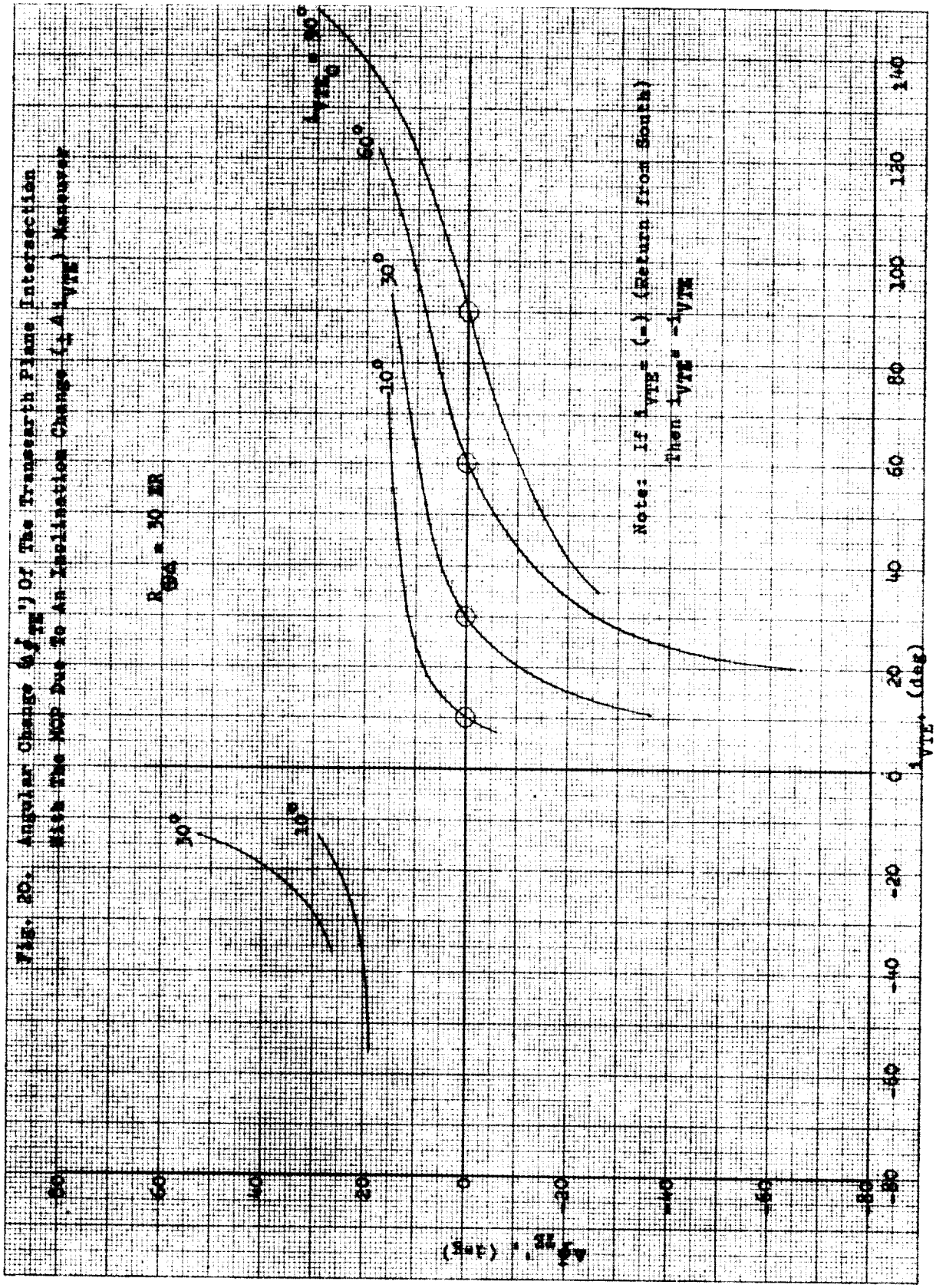
Fig. 20. Angular Change ($\Delta\gamma_{TM}$) Of The Transearth Plane Intersection With The MCP Due To An Ignition Change (Δi_{VTM}) Maneuver
R_{EM} = 30 ER
i_{VTM} = 30°
50°
30°
10°
Note: If i_{VTM} = (-) (Return from South)
Then i_{VTM} = $-i_{VTM}$
$\Delta\gamma_{TM}$ = (Set)
i_{VTM} (deg)

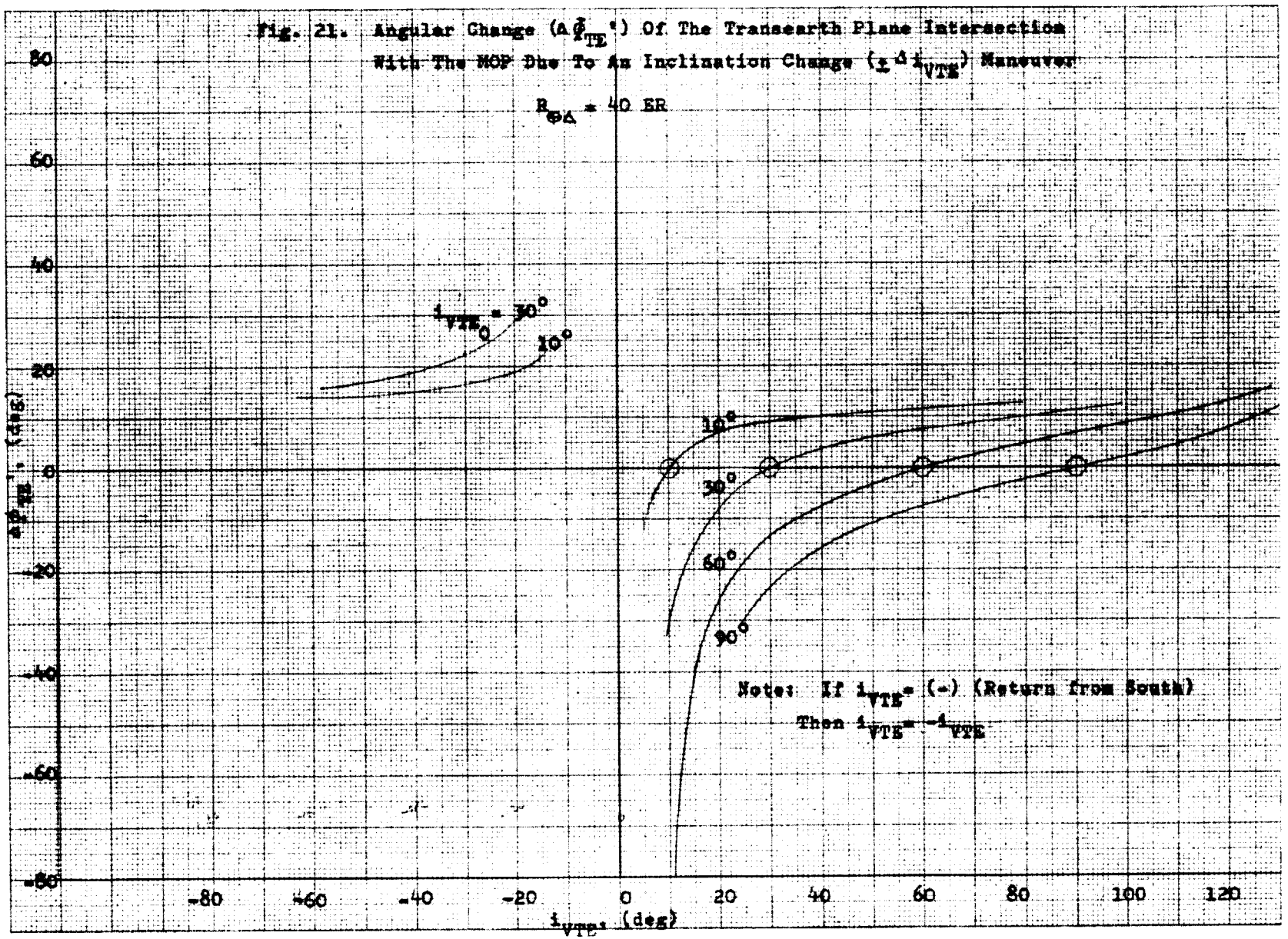
Fig. 21. Angular Change ($\Delta\phi_{TE}'$) Of The Transearth Plane Intersection With The MOP Due To An Inclination Change ($\pm\Delta i_{VTE}$) Maneuver
$R_{\Phi\Delta}$ = 40 ER
i_{VTE_0} = 30°
10°
10°
30°
60°
90°
Note: If i_{VTE} = (-) (Return from South)
Then $i_{VTE} = -i_{VTE}$
$\Delta\phi_{TE}'$ (deg)
i_{VTE} (deg)
80
60
40
20
0
-20
-40
-60
-80
-80
-60
-40
-20
0
20
40
60
80
100
120

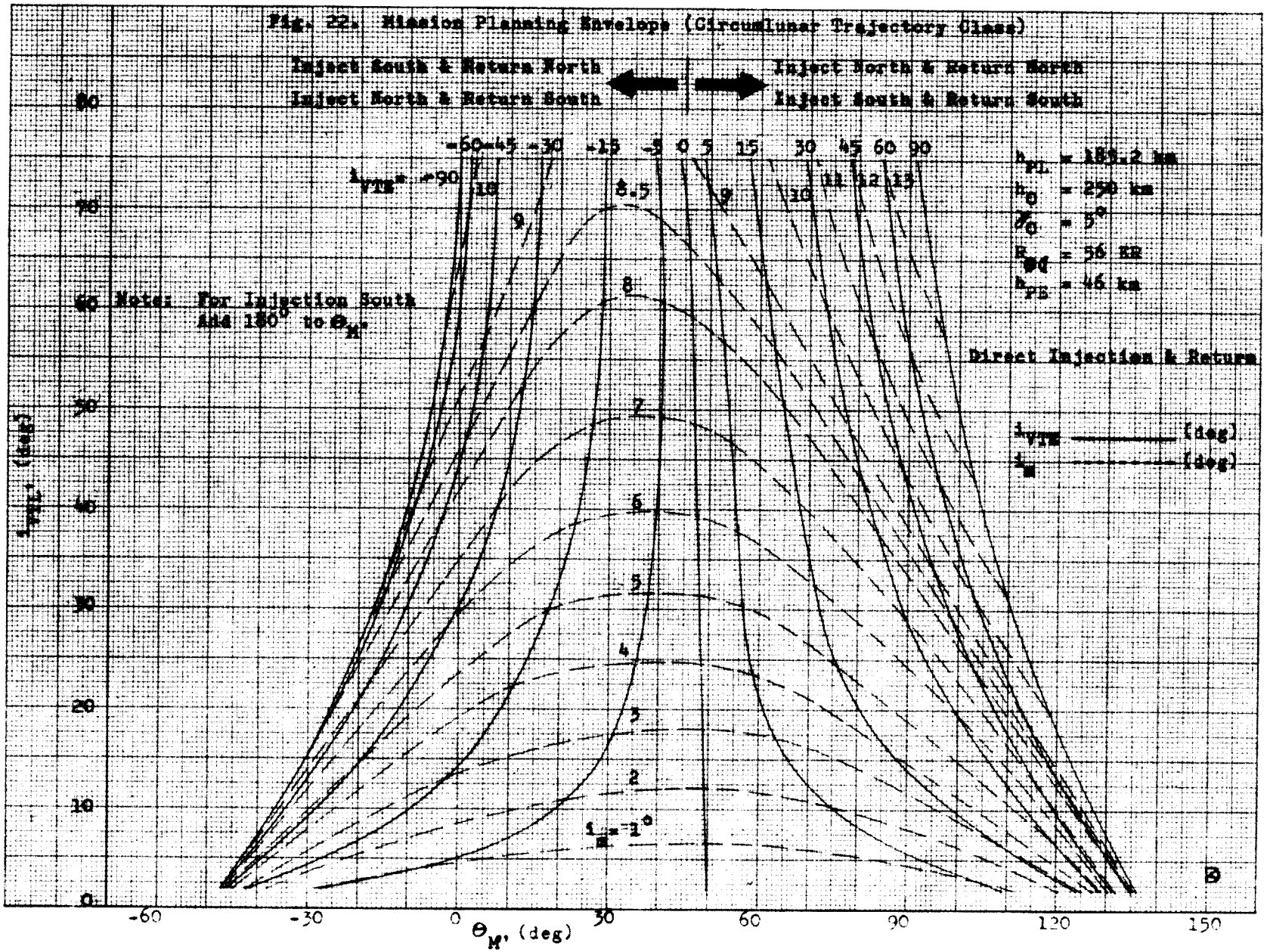

Fig. 22. Mission Planning Envelope (Circumlunar Trajectory Class)

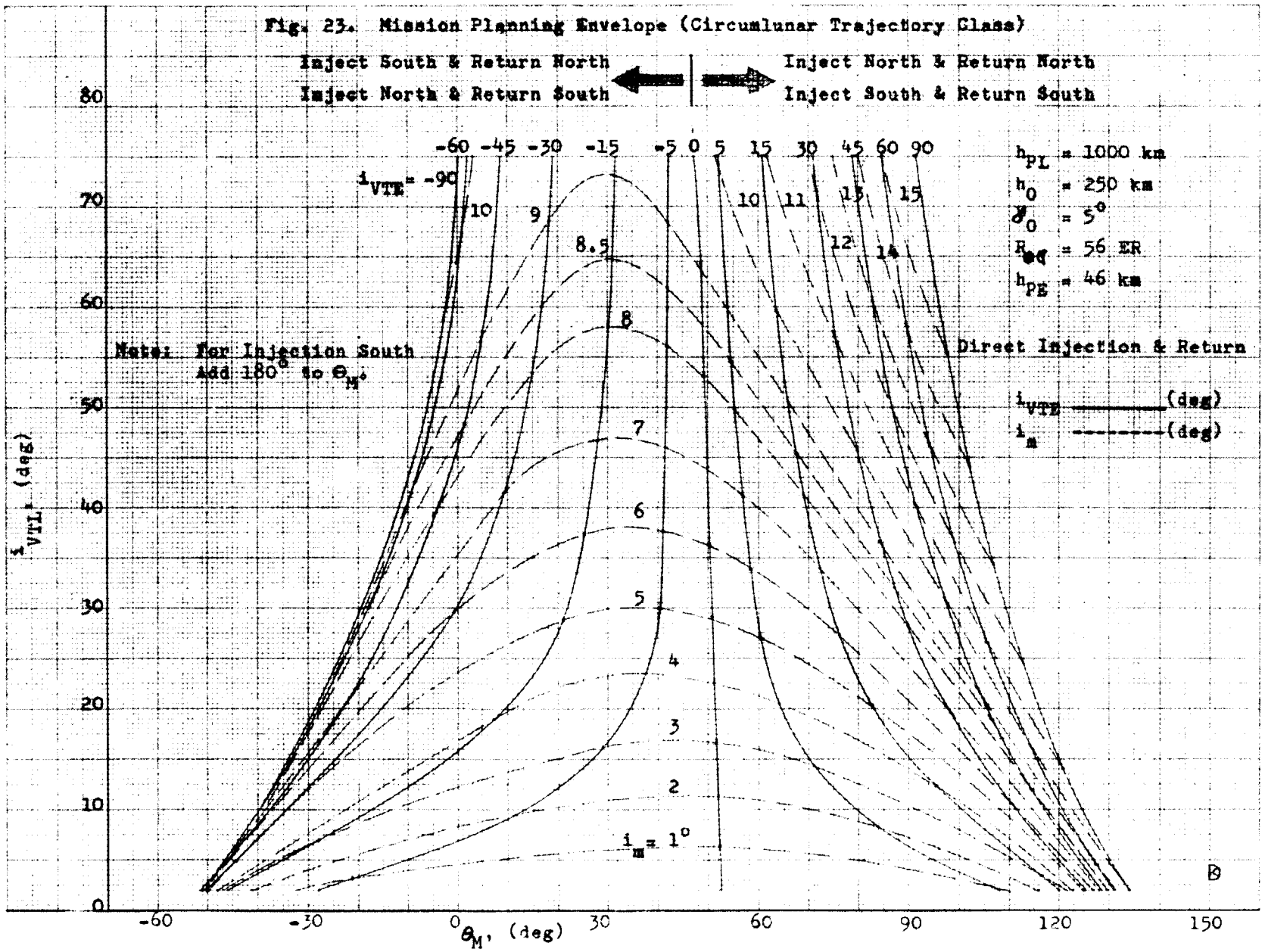
Fig. 23. Mission Planning Envelope (Circumlunar Trajectory Class)
Inject South & Return North
Inject North & Return South
Inject North & Return North
Inject South & Return South
h_{PL} = 1000 km
h_0 = 250 km
γ_0 = 5°
R_{eq} = 56 ER
h_{PE} = 46 km
Direct Injection & Return
i_{VTE} (deg)
i_m (deg)
Note: For Injection South Add 180° to θ_M
i_{VTE} (deg)
θ_M, (deg)
i_{VTE} = -90
i_m = 1°
-60 -45 -30 -15 -5 0 5 15 30 45 60 90
10 9 8.5 8 7 6 5 4 3 2
10 11 12 13 14 15
0 10 20 30 40 50 60 70 80
-60 -30 0 30 60 90 120 150
B

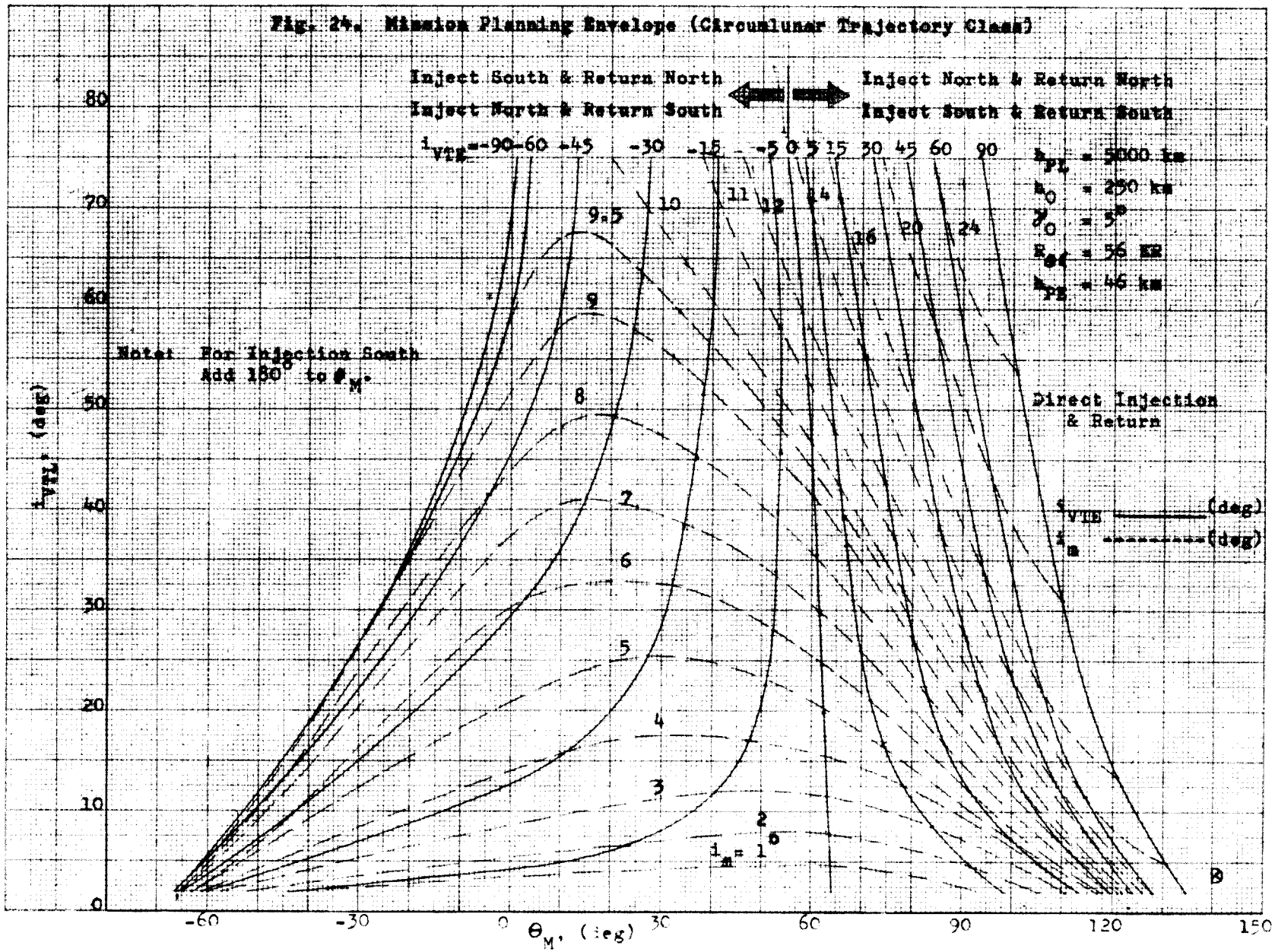

Fig. 24. Mission Planning Envelope (Circumlunar Trajectory Class)

Fig. 25. Mission Planning Envelope (Circumlunar Trajectory Class)

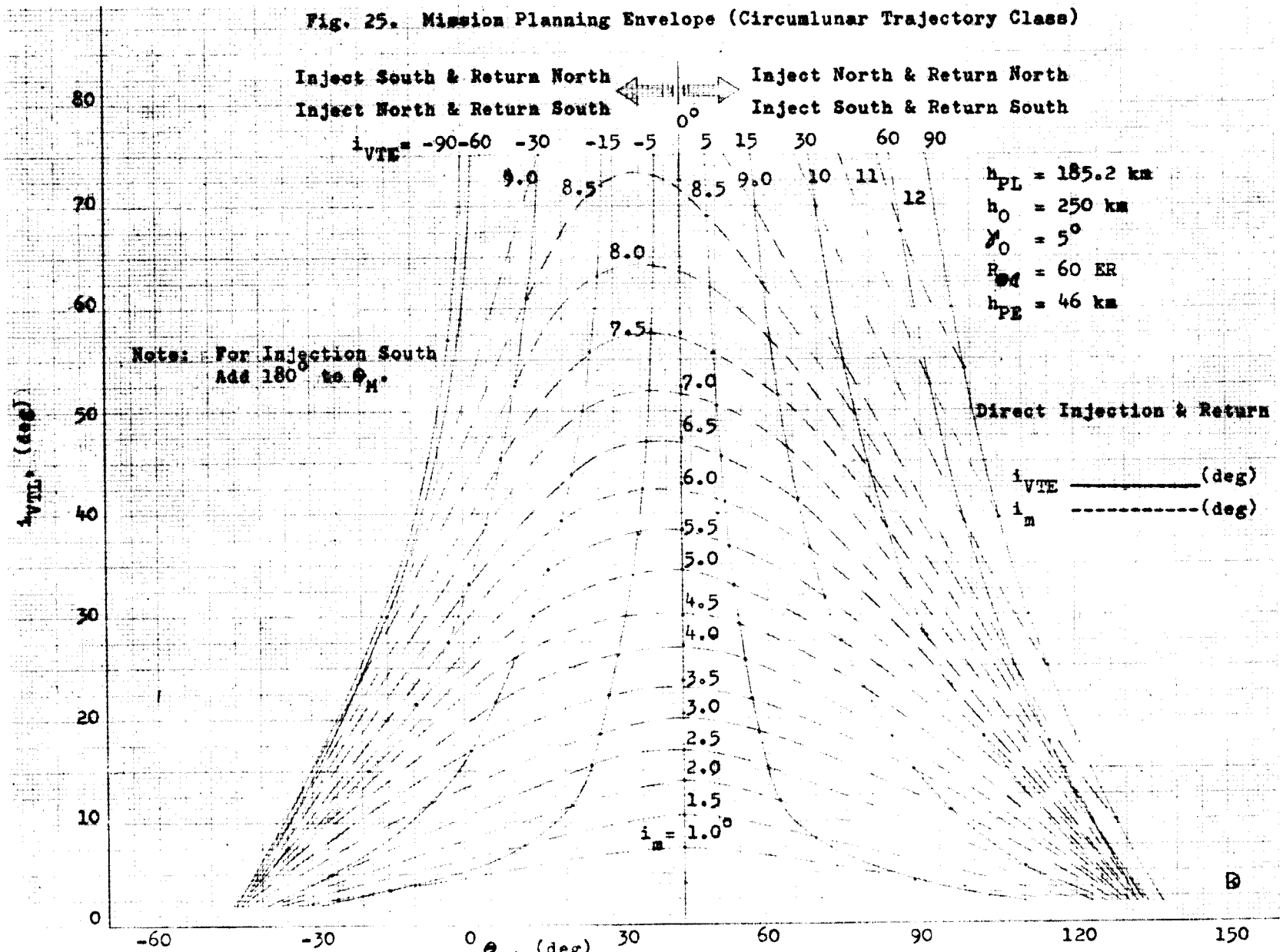

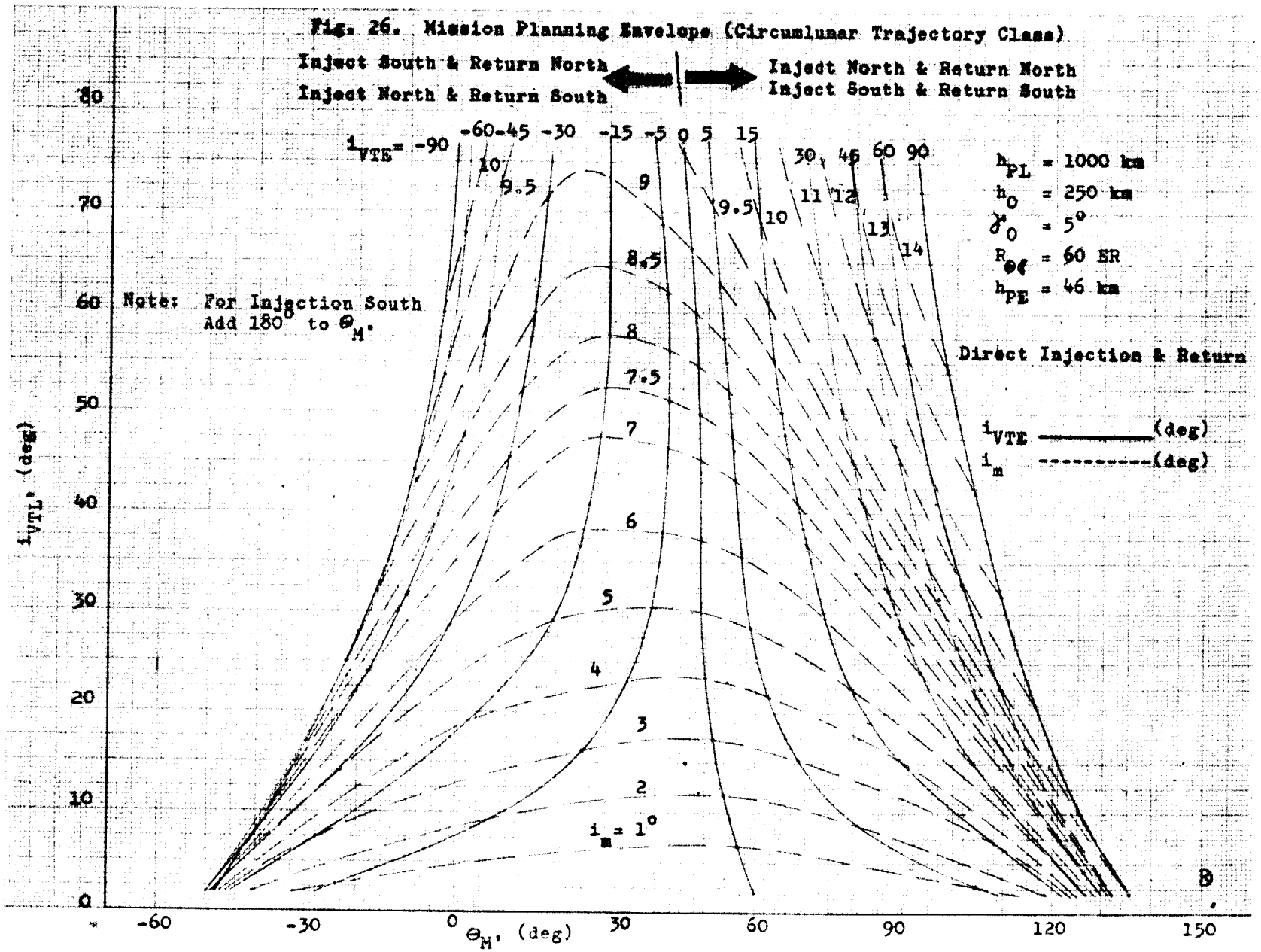
Fig. 26. Mission Planning Envelope (Circumlunar Trajectory Class)
Inject South & Return North
Inject North & Return South
Inject North & Return North
Inject South & Return South
i_{VTE} = -90
-60 -45 -30 -15 -5 0 5 15 30 45 60 90
10
9.5
9
8.5
8
7.5
7
6
5
4
3
2
i_m = 1°
9.5
10
11
12
13
14
h_{PL} = 1000 km
h_0 = 250 km
γ_0 = 5°
$R_{\oplus}$ = 60 ER
h_{PE} = 46 km
Direct Injection & Return
i_{VTE} _____(deg)
i_m ----------(deg)
Note: For Injection South Add 180° to Θ_M.
i_{VTL}, (deg)
Θ_M, (deg)
0
10
20
30
40
50
60
70
80
-60
-30
0
30
60
90
120
150
B

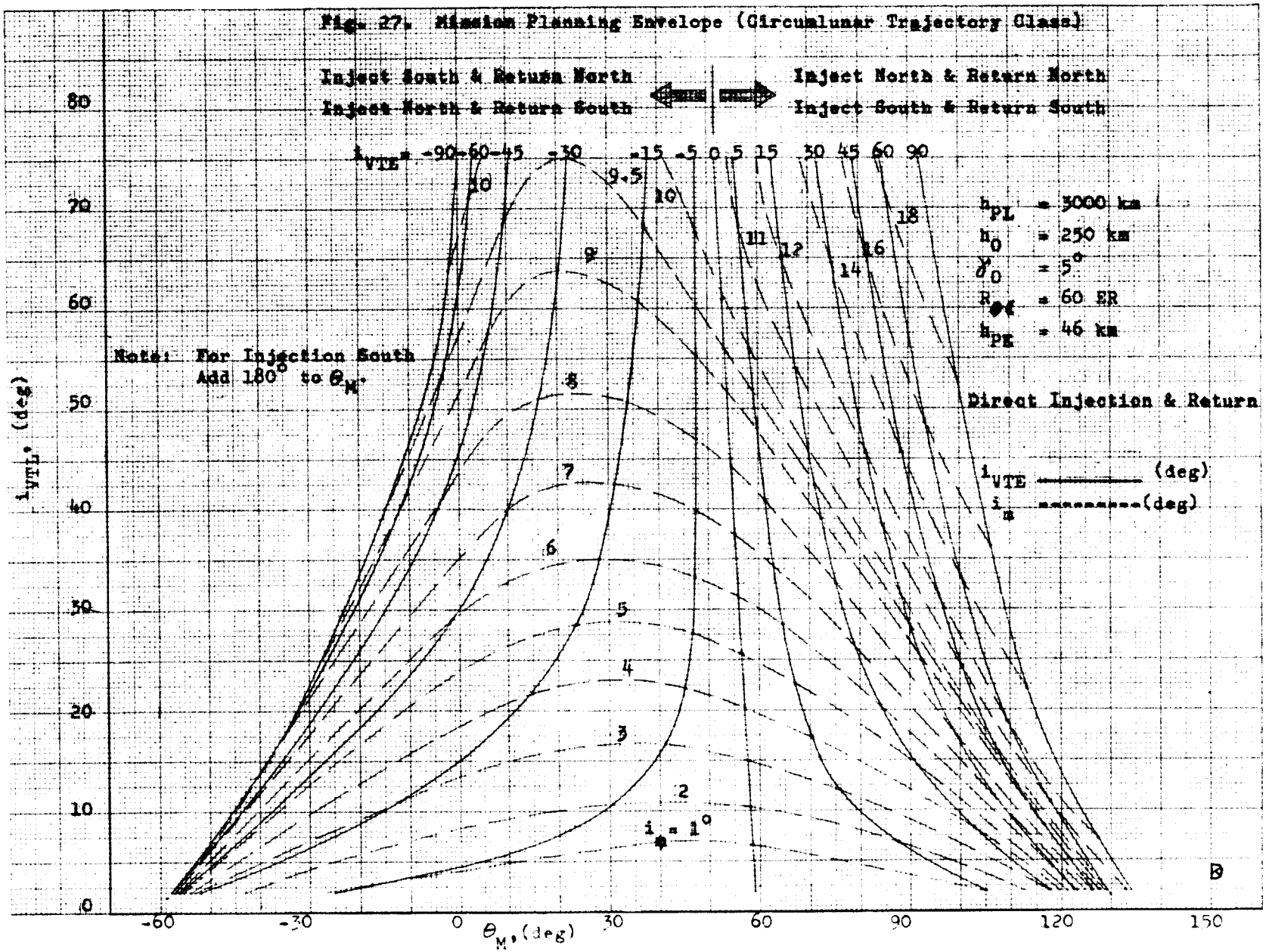
Fig. 27. Mission Planning Envelope (Circumlunar Trajectory Class)
Inject South & Return North
Inject North & Return South
Inject North & Return North
Inject South & Return South
i_{VTE} = -90 -60 -45 -30 -15 -5 0 5 15 30 45 60 90
h_{PL} = 3000 km
h_0 = 250 km
γ_0 = 5°
$R_{\oplus}$ = 60 ER
h_{PE} = 46 km
Note: For Injection South Add 180° to θ_M.
Direct Injection & Return
i_{VTE} ——— (deg)
i_m - - - - - (deg)
i_{VTL}, (deg)
θ_M, (deg)
i_m = 1°
B

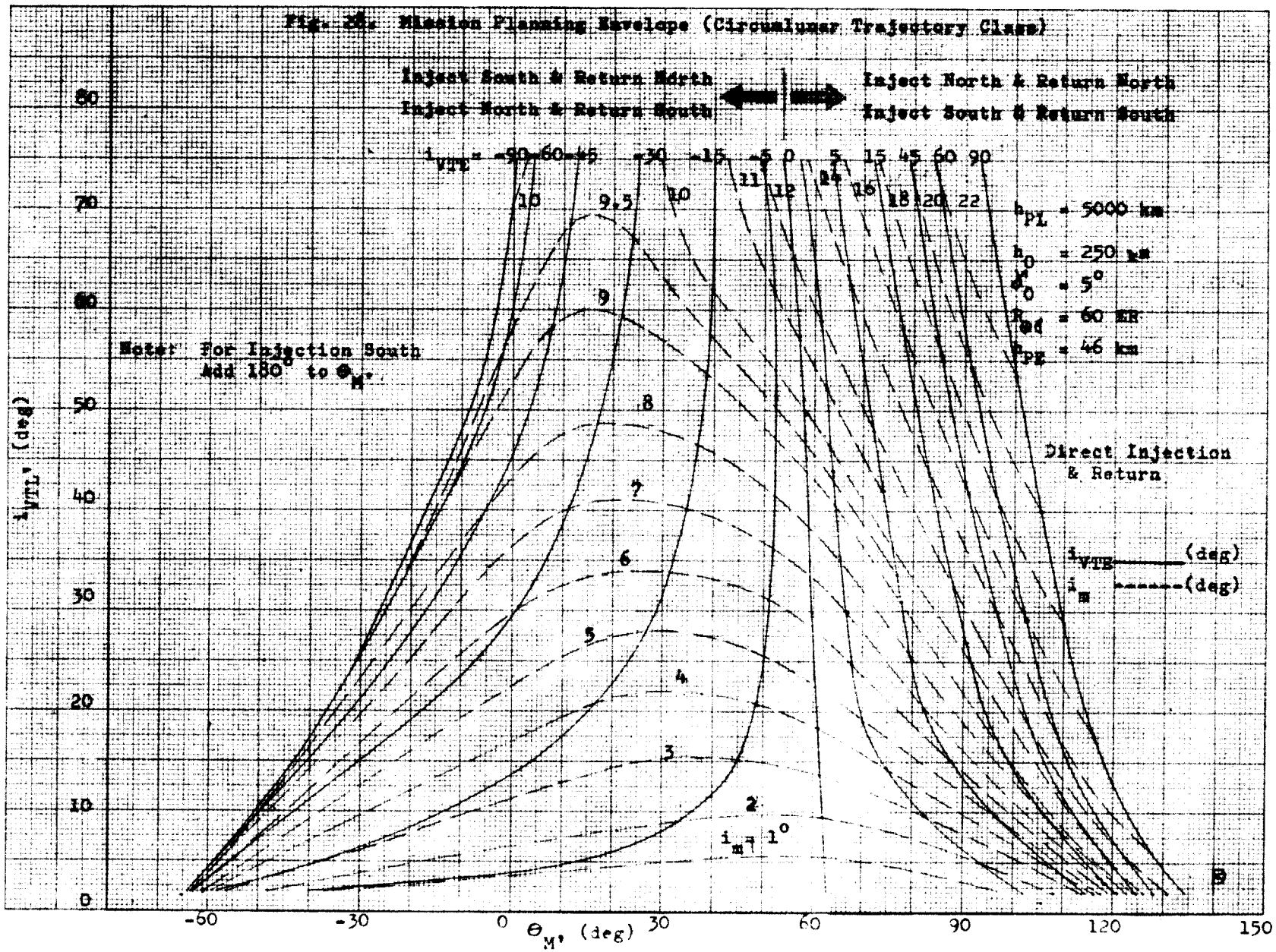

Fig. 28. Mission Planning Envelope (Circumlunar Trajectory Class)

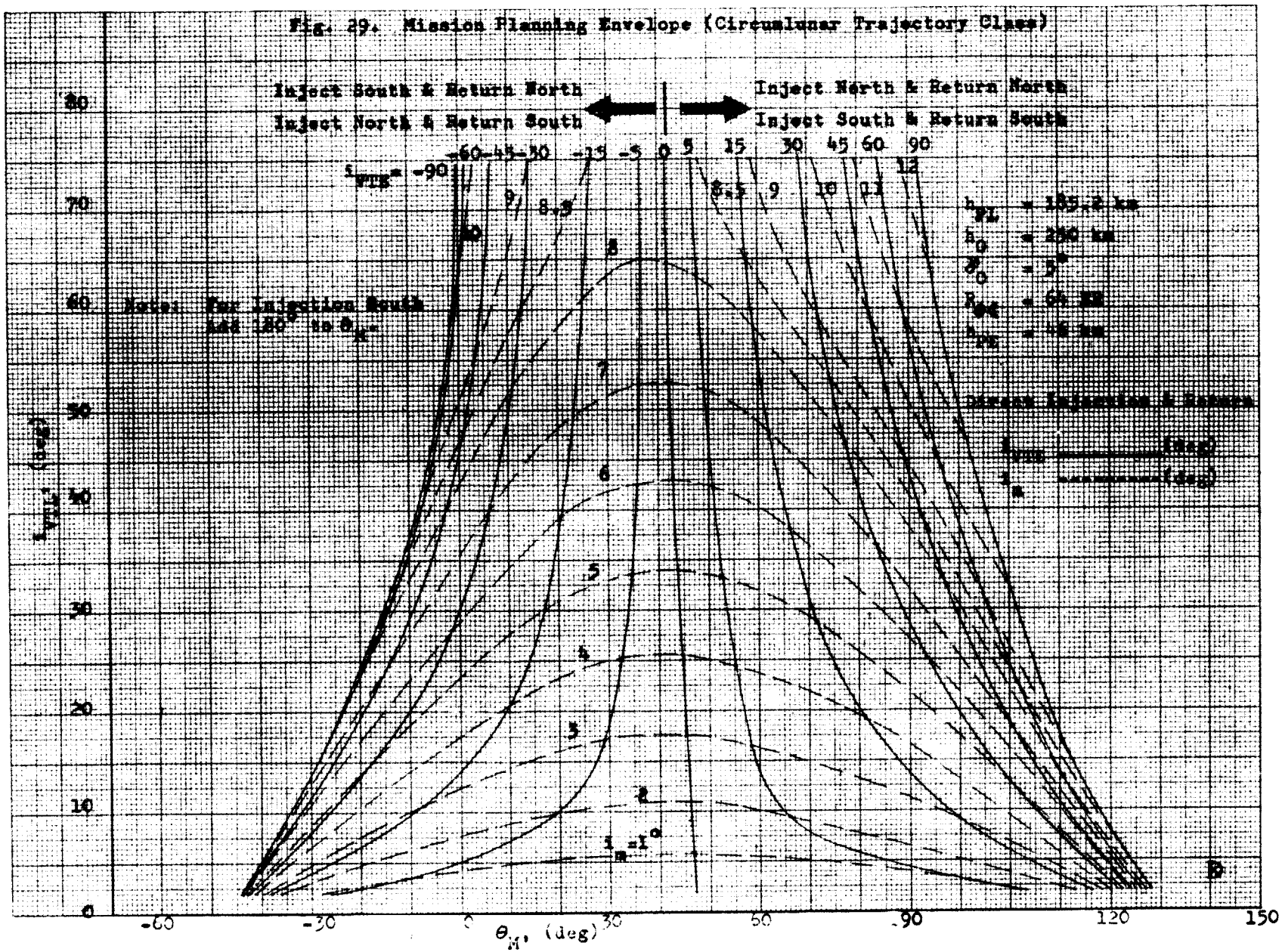

Fig. 29. Mission Planning Envelope (Circumlunar Trajectory Class)

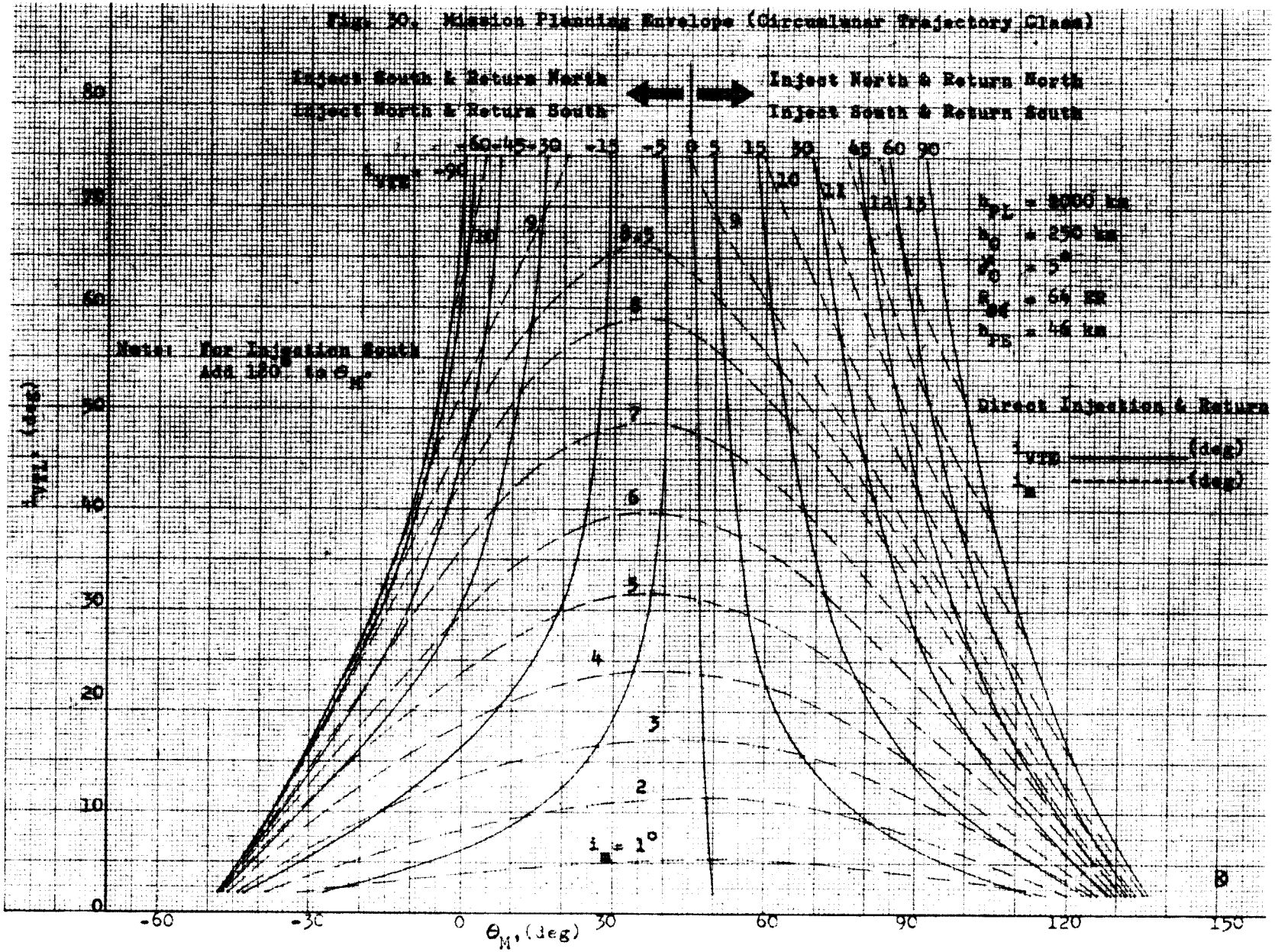

Fig. 30. Mission Planning Envelope (Circumlunar Trajectory Class)

Fig. 31. Mission Planning Envelope (Circumlunar Trajectory Class)

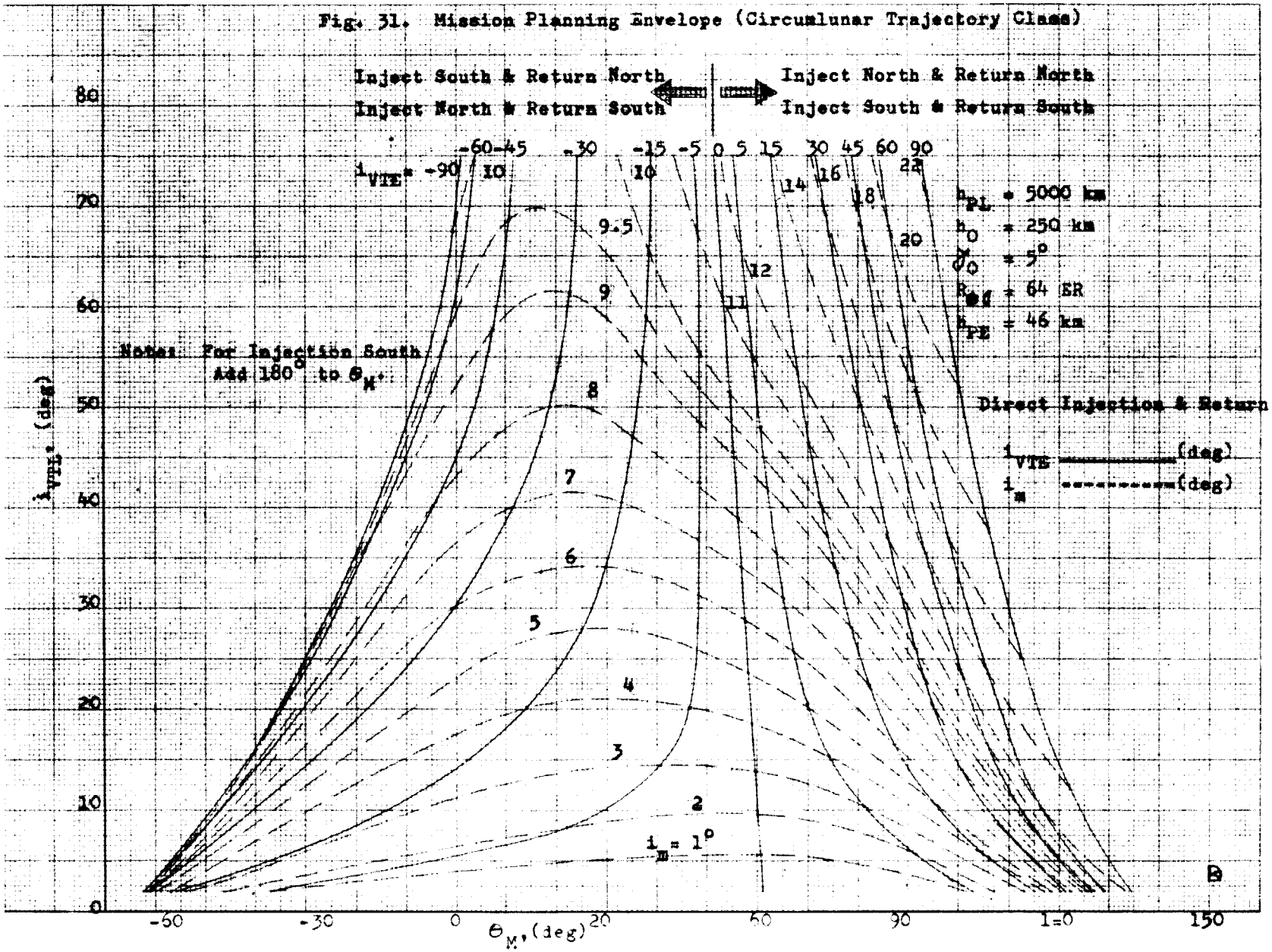

Fig. 32. Mission Planning Envelope (Approach Trajectory Class)

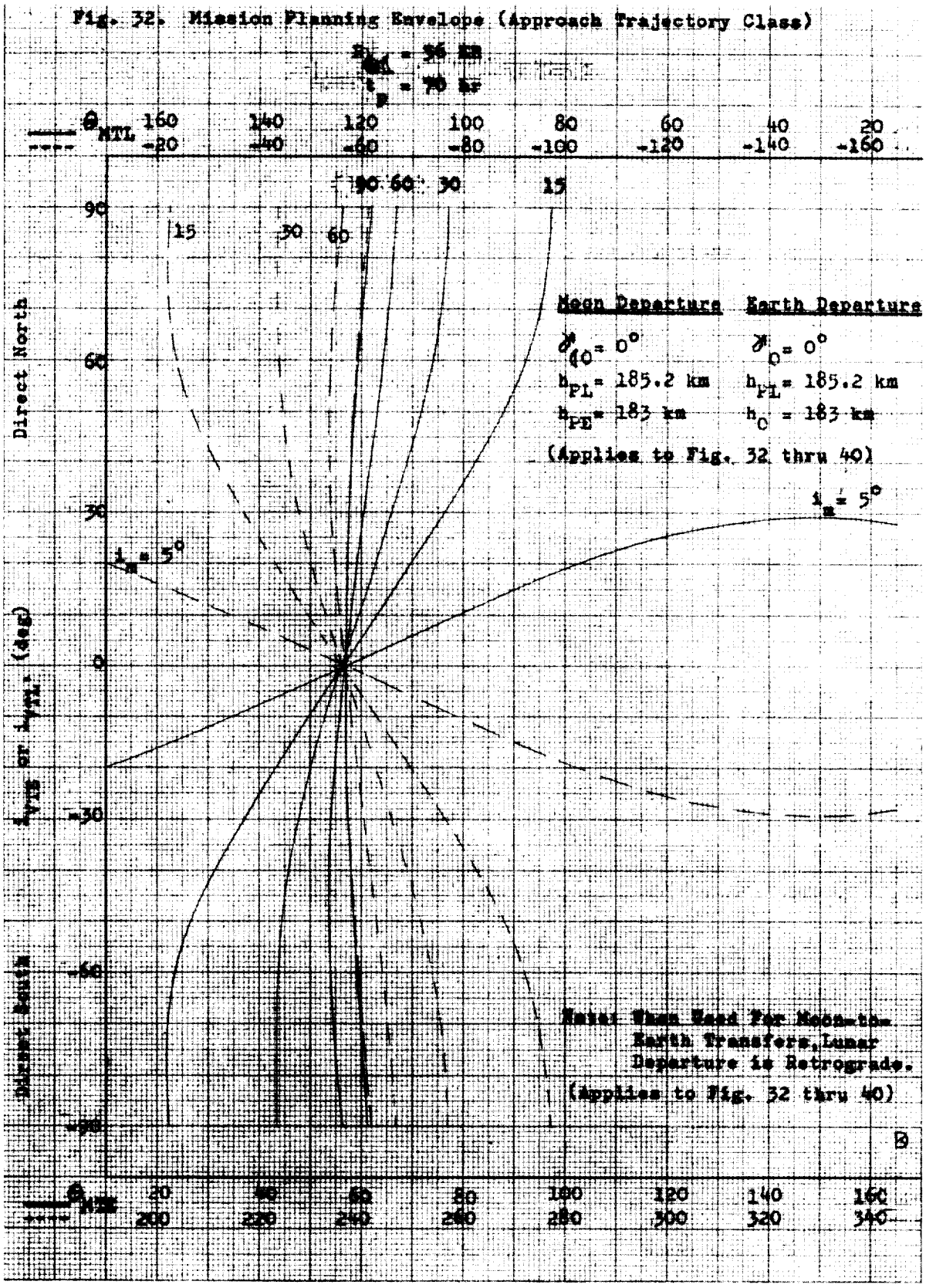

Moon Departure	Earth Departure
$\gamma_{40} = 0°$	$\gamma_0 = 0°$
$h_{PL} = 185.2$ km	$h_{PL} = 185.2$ km
$h_{PE} = 183$ km	$h_0 = 183$ km

(Applies to Fig. 32 thru 40)

Noise Term Used For Moon-to-Earth Transfers, Lunar Departure is Retrograde.

(Applies to Fig. 32 thru 40)

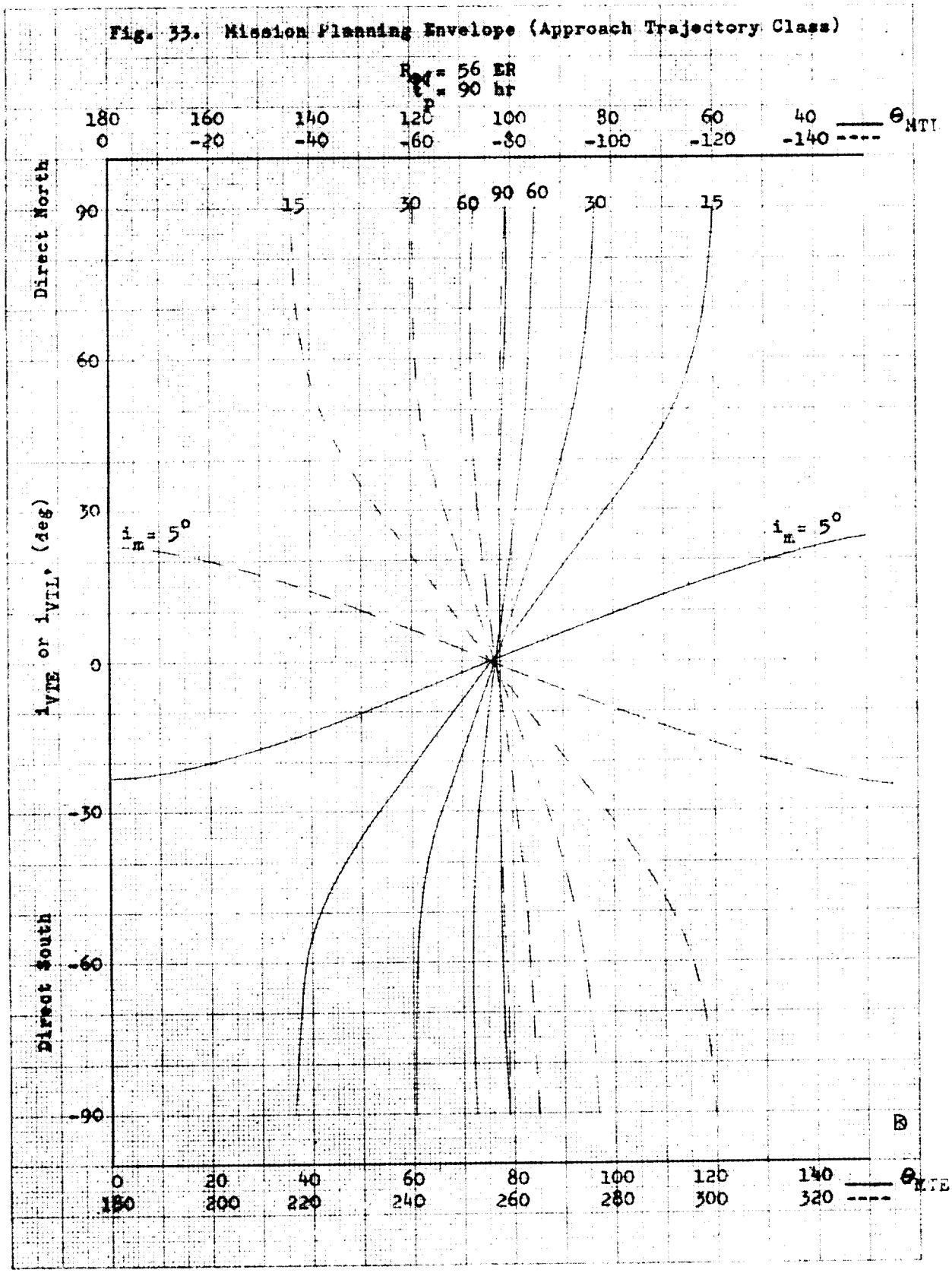

Fig. 33. Mission Planning Envelope (Approach Trajectory Class)

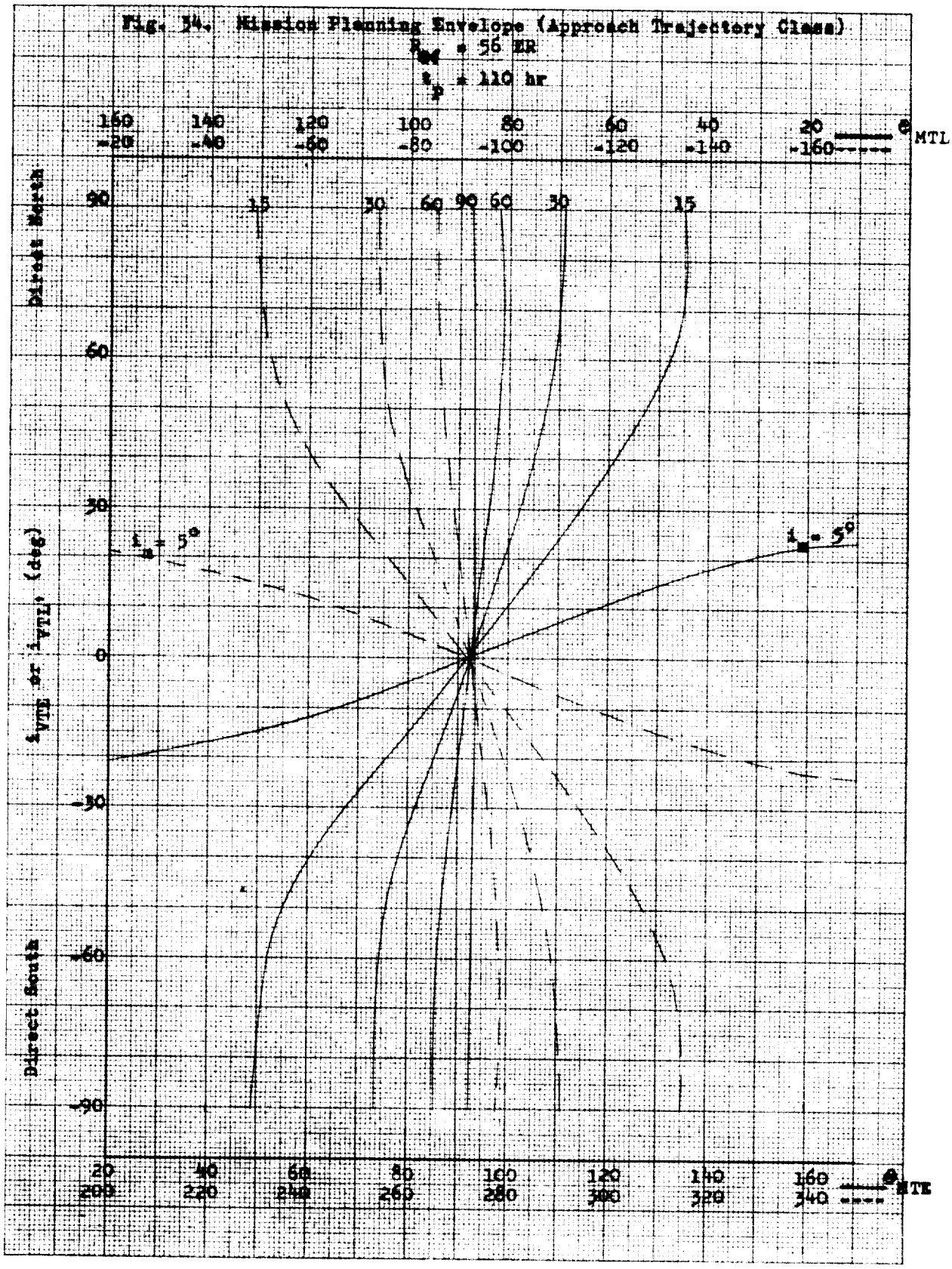

Fig. 34. Mission Planning Envelope (Approach Trajectory Clause)

Fig. 35. Mission Planning Envelope (Approach Trajectory Class)

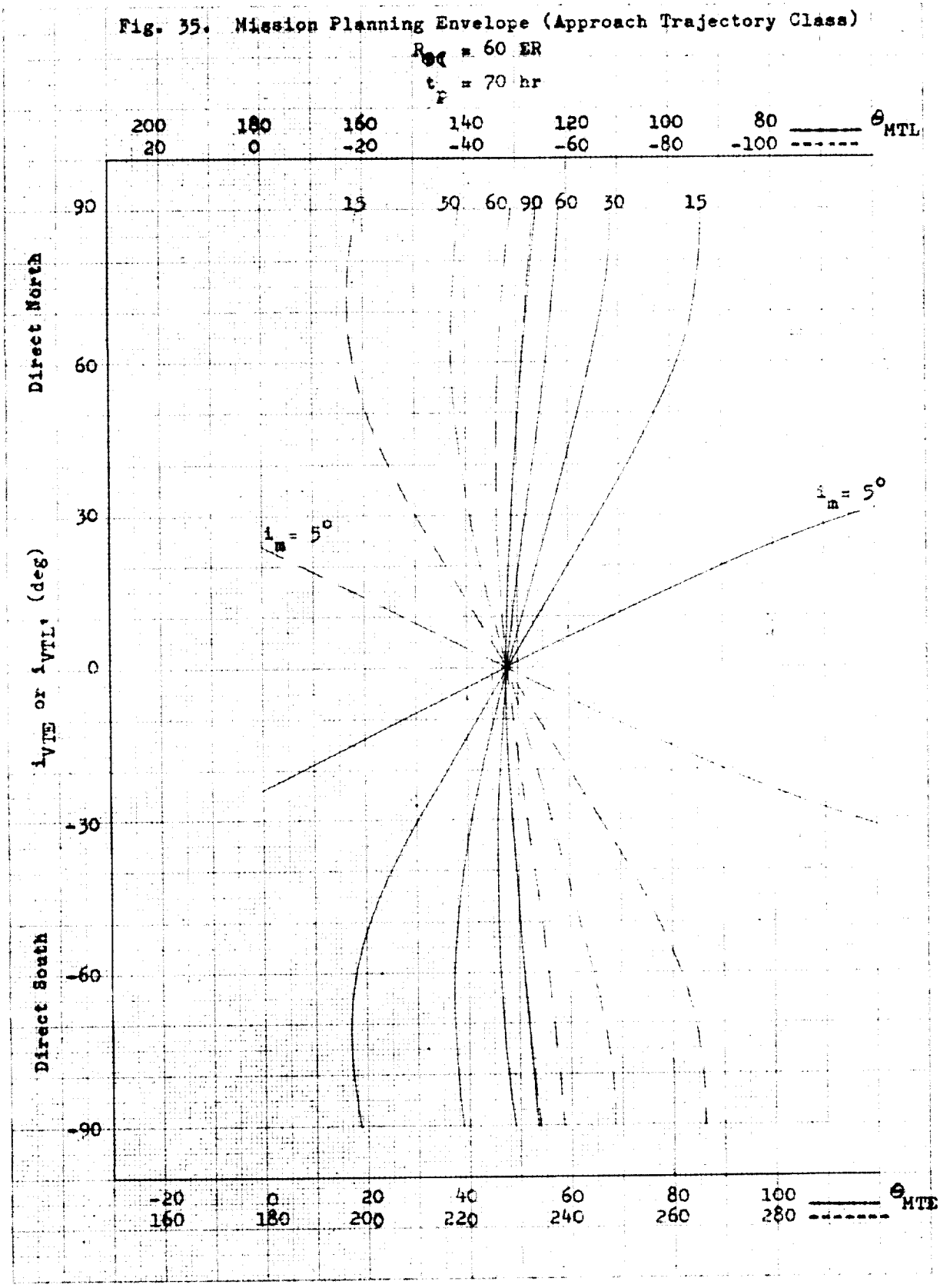

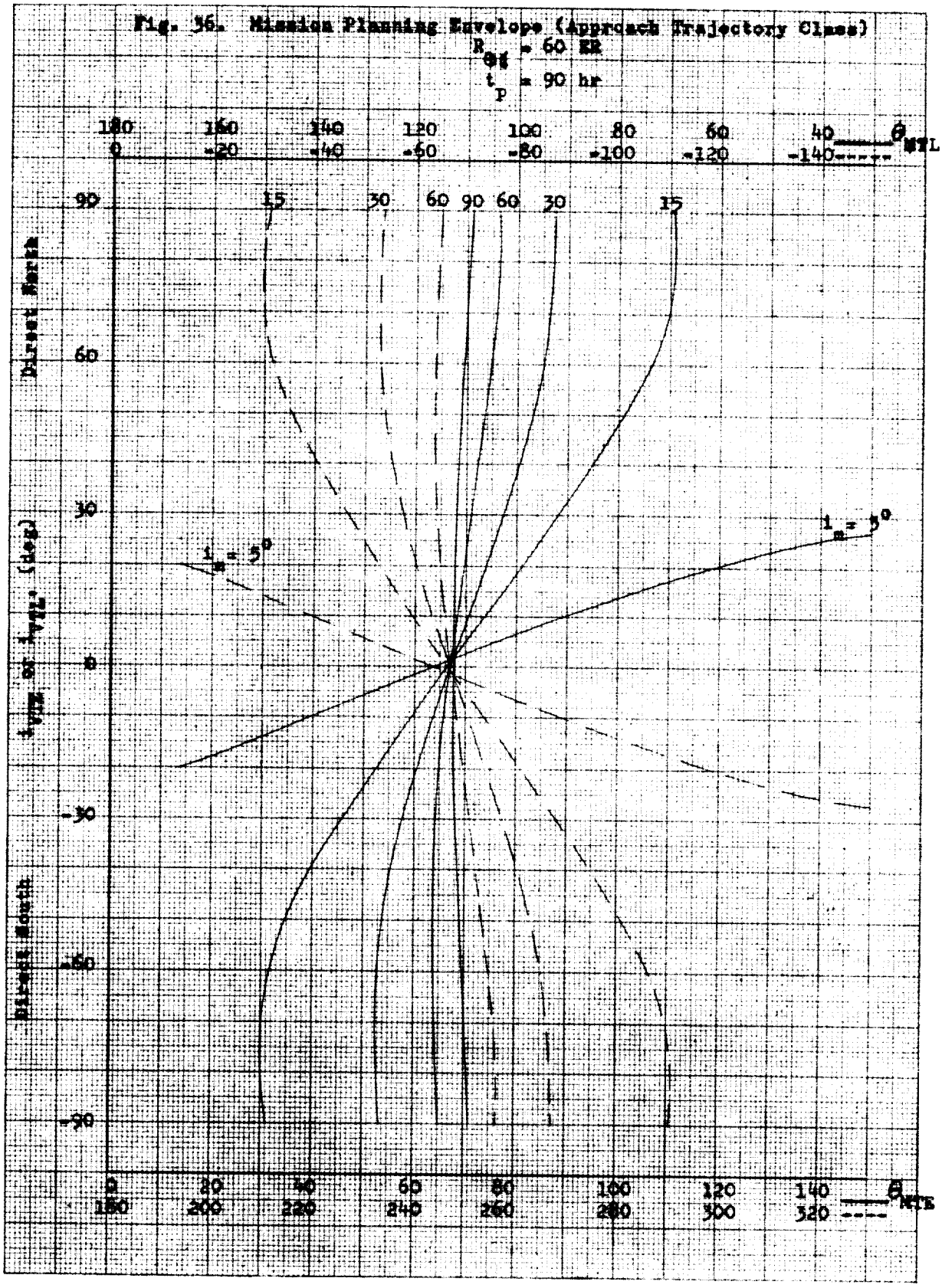
Fig. 36. Mission Planning Envelope (Approach Trajectory Clims)
R_{Bf} = 60 ER
t_p = 90 hr
θ_{MTL}
θ_{MTE}
Direct North
Direct South
i_{VTM} or i_{VTL} (deg)
$i_m = 5°$
$i_m = 5°$

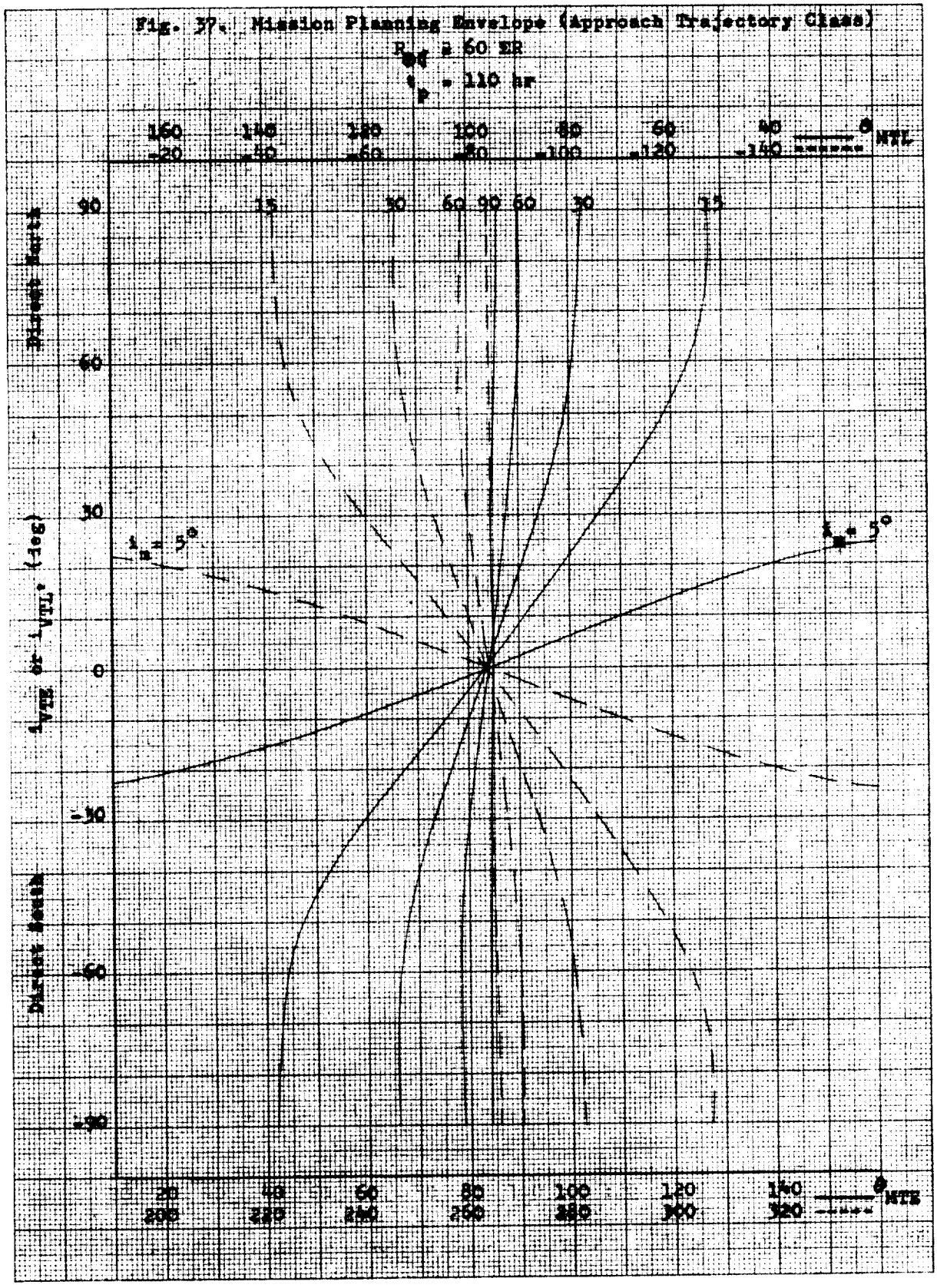
Fig. 37. Mission Planning Envelope (Approach Trajectory Class)
R_{ref} = 60 ER
t_p = 110 hr
160 140 120 100 80 60 40 0 NTL
-20 -40 -60 -80 -100 -120 -140
90 60 30 0 -30 -60 -90
15 30 60 90 60 30 15
i_m = 5°
i_m = 5°
20 40 60 80 100 120 140 NTE
200 220 240 260 280 300 320

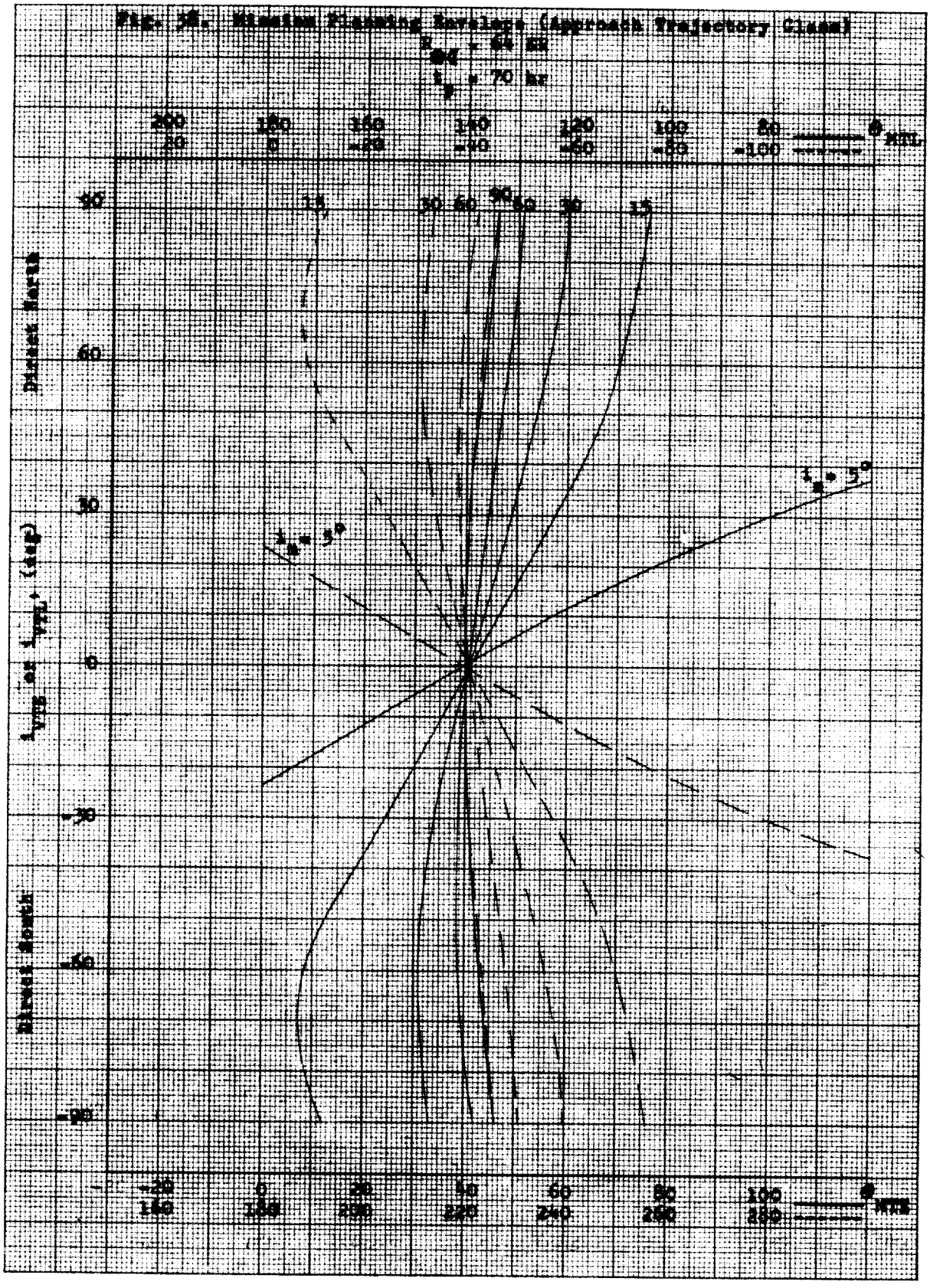
Fig. 38. Mission Planning Envelope (Approach Trajectory Diagram)
R_{EI} = 64 nm
i_E = 70 hr
Direct North
i_{VP} or i_{VP_1} (deg)
i_A = 5°
i_A = 5°
90
60
30
0
-30
-60
-90
15
30
60
90
60
30
15
200
180
160
140
120
100
80
20
0
-20
-40
-60
-80
-100
θ nm
-20
0
20
40
60
80
100
160
180
200
220
240
260
280
θ nm

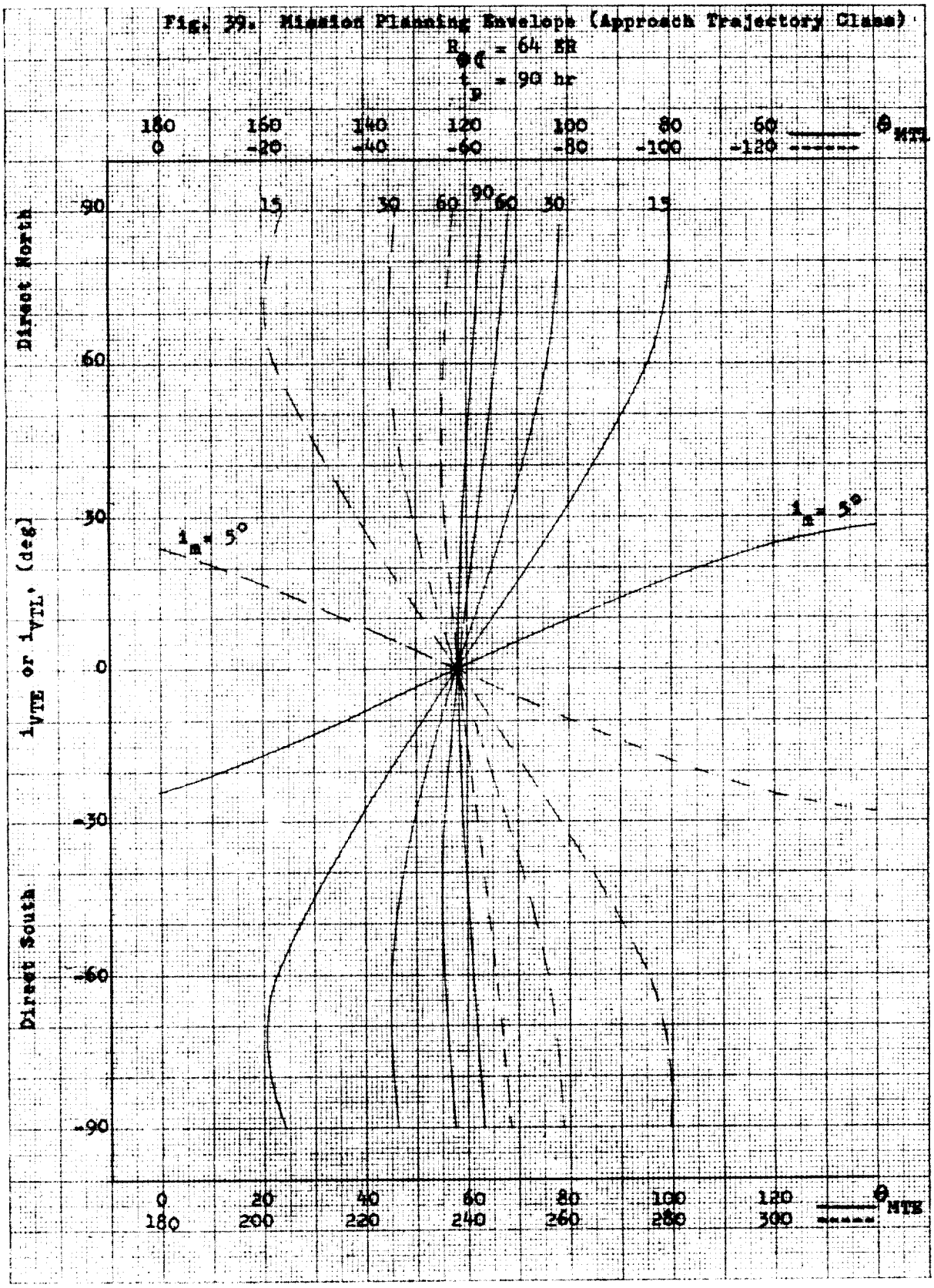
Fig. 29. Mission Planning Envelope (Approach Trajectory Class)
$R_{\oplus C}$ = 64 ER
t_p = 90 hr
180 160 140 120 100 80 60 Φ_{MTL}
0 -20 -40 -60 -80 -100 -120
90 60 30 15
Direct North
90
60
30
0
-30
-60
-90
Direct South
i_{VTE} or i_{VTL}, (deg)
i_n = 5°
i_n = 5°
0 20 40 60 80 100 120 Φ_{MTE}
180 200 220 240 260 280 300

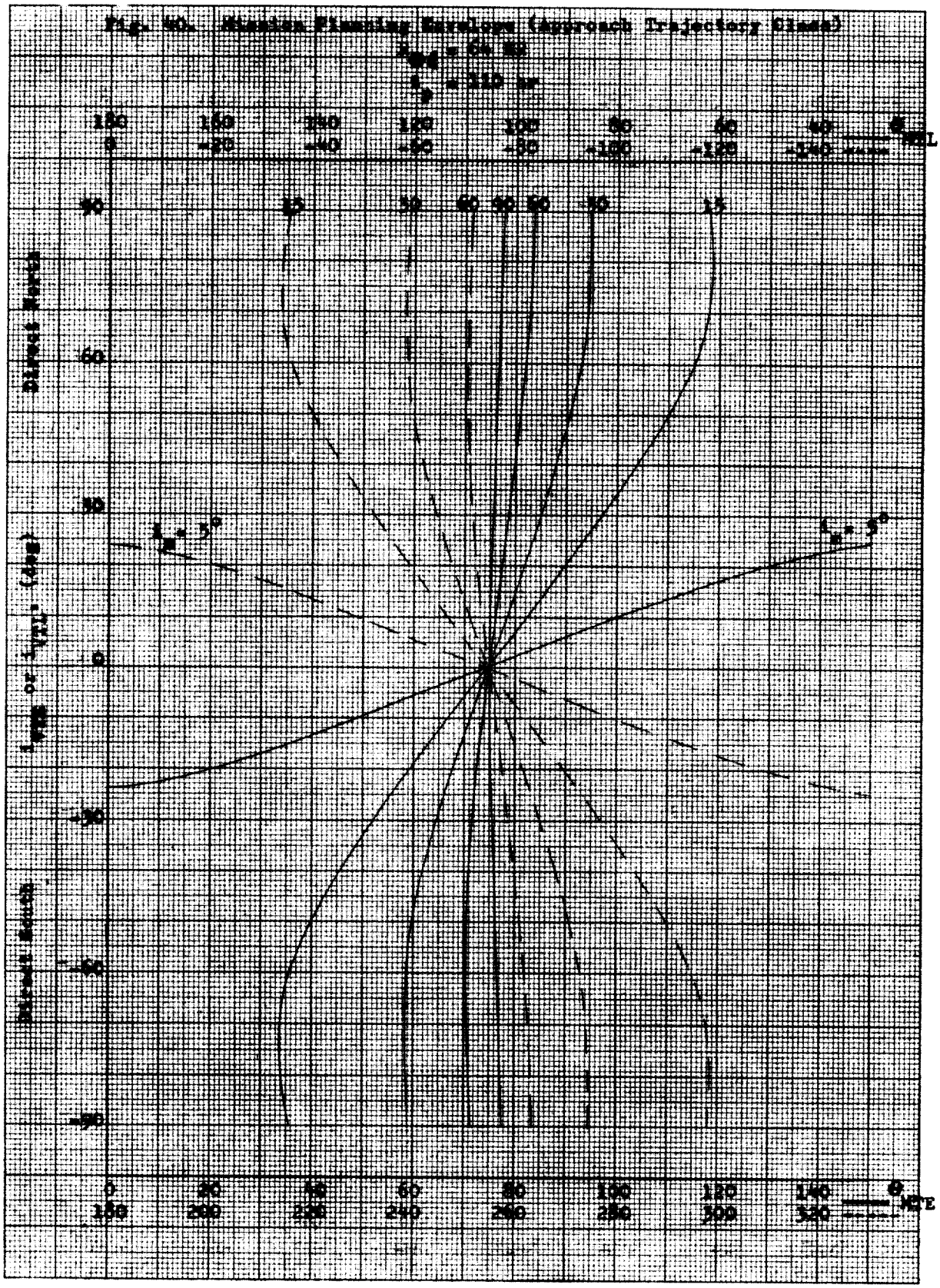
Fig. 40. Mission Planning Envelope (Approach Trajectory Plane)
Elevation Angle, degrees
Azimuth Angle, degrees
Direct Entry
Skip Entry
MCL
MCE

Fig. 41. Mission Planning Envelope (Circumlunar Trajectory Class)

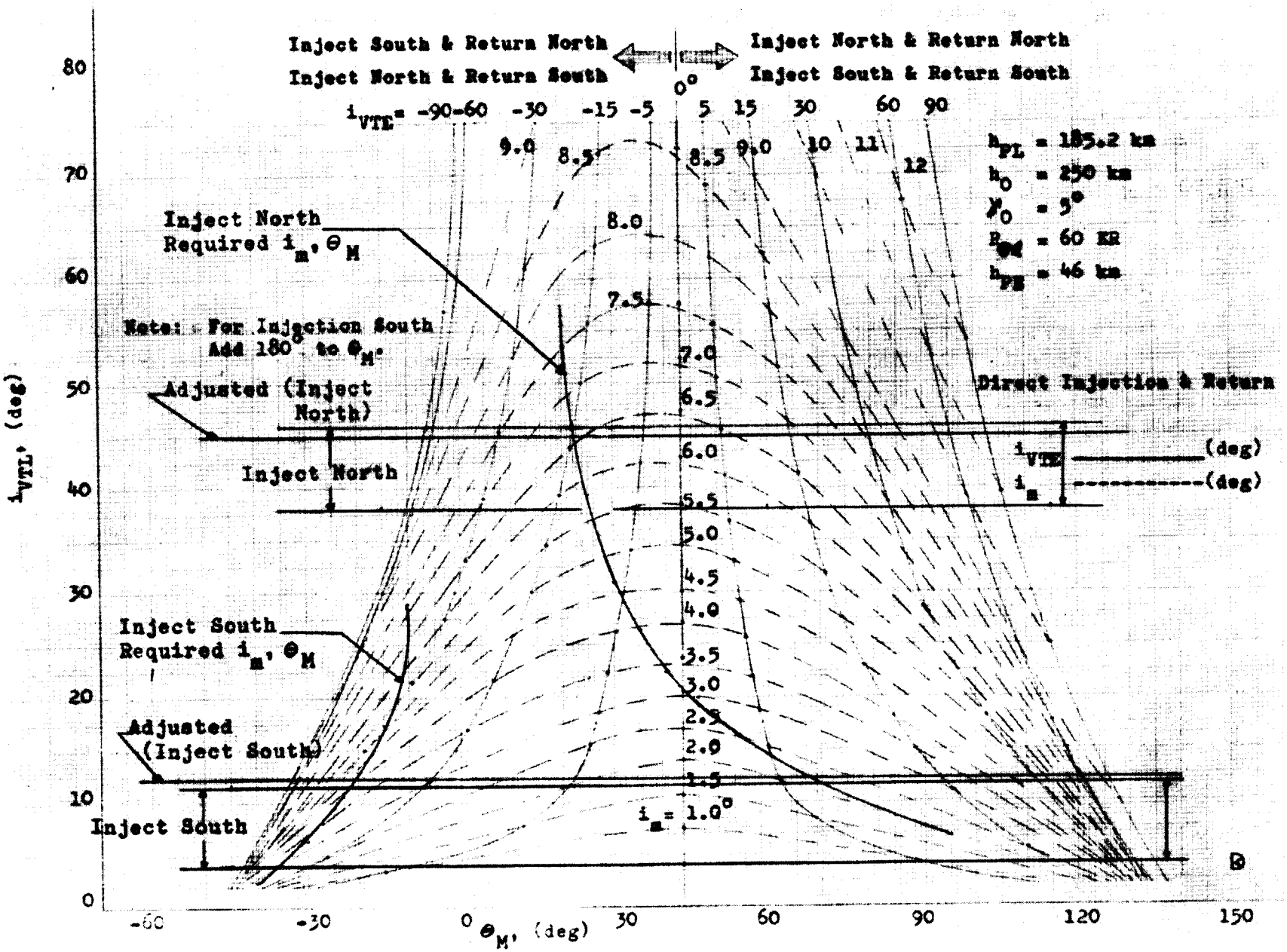

Fig. 42. Mission Planning Envelope (Approach Trajectory Clone)

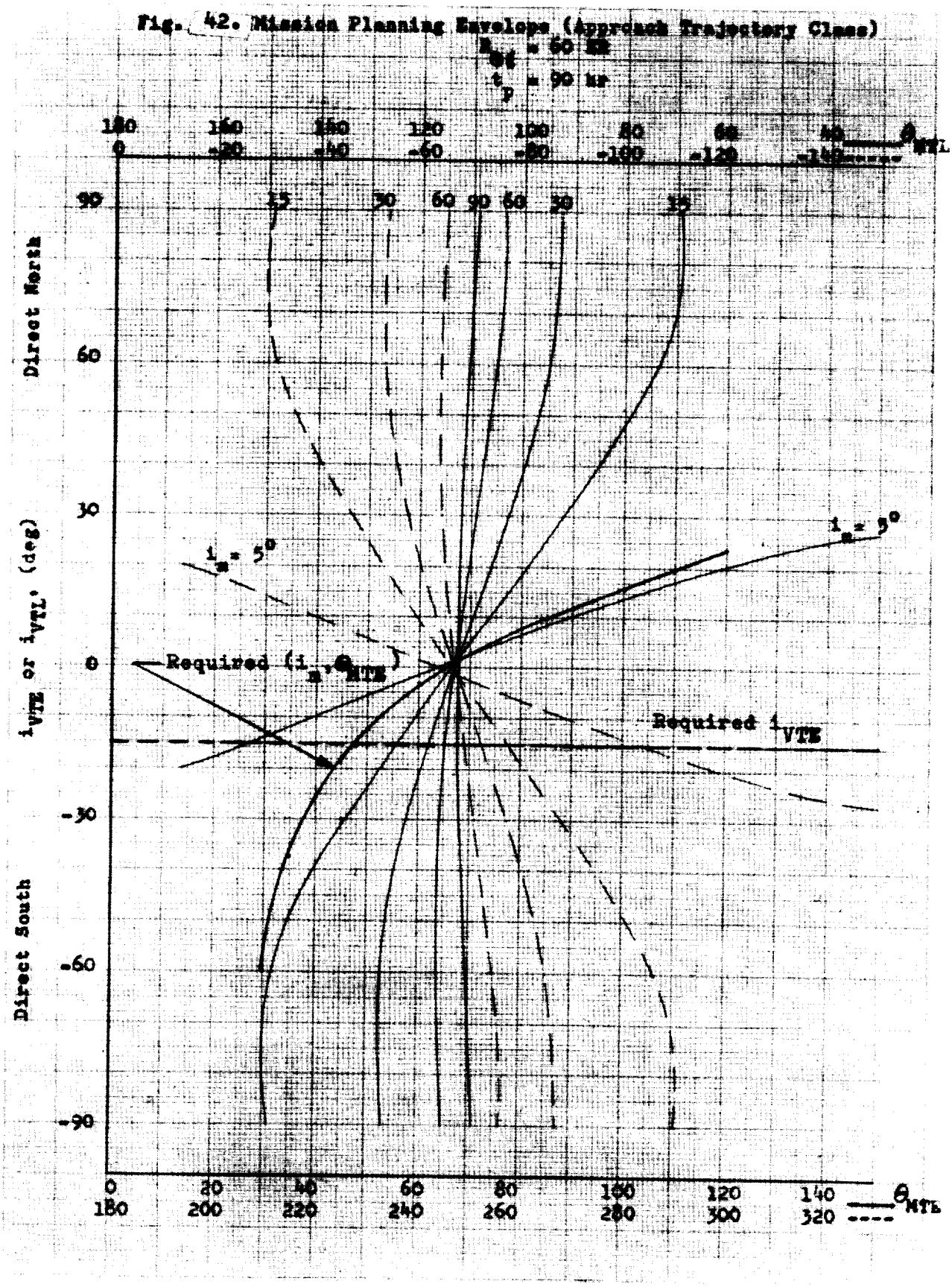

CHAPTER XII

BIBLIOGRAPHY

XII. BIBLIOGRAPHY

Any attempt to write a bibliography for lunar flight can meet with only partial success due to the vast amount of literature in this field. To be useful, the emphasis in this Bibliography has been on recent material and on material that can be obtained easily from either technical libraries or government agencies. In addition, the idea of subdividing the Bibliography by handbook chapter has been abandoned because too much material is common to several chapters.

To aid the user, this Bibliography has been subdivided into three sections. Section A lists sources that enable the engineer to keep current in the literature on lunar flight. The technical and semi-technical magazines which often contain information useful for lunar flight are given, and the ones containing proportionately the largest amount of material are emphasized by an asterisk. In addition, series of books and proceedings of meetings which are published periodically have been included.

Section B gives the bibliography of background material--essentially further references to the material of Chapters II, III and IV. Books on astronomy, space flight, and space environment, as well as reports and articles dealing with lunar flight in general and with environmental factors form the bulk of this portion of the Bibliography. For references on lunar ephemerides, the reader is referred to Subsection C-1e of Chapter III, and for references on current lunar maps to Subsection A-2g of Chapter III, since they are not repeated in the Bibliography.

Section C gives the bibliography for the various phases of lunar flight as discussed in Chapters V to X. It consists mostly of recent articles from technical journals, of NASA, ASTIA, and some company reports.

No bibliography is given for the mission analysis (Chapter XI of the Handbook), since similar material has been generated only recently, and is available in generally inaccessible internal company reports.

A. SOURCES OF FLIGHT MECHANICS MATERIAL

1. Technical Journals

Aero/Space Medicine, formerly Journal of Aviation Medicine

*American Institute of Aeronautics and Astronautics (AIAA) Journal

American Journal of Physics

*American Rocket Society (ARS) Journal, formerly Jet Propulsion

Archive for Rational Mechanics and Analysis

*Astronautica Acta

*Astronomical Journal

Astrophysical Journal

*British Interplanetary Society Journal

IRE Transactions

Journal of Applied Physics

*Journal of Astronautical Sciences

Journal of Atmospheric Sciences

Journal of Geophysical Research

*Journal of the Aero/Space Sciences, formerly Journal of the Aeronautical Sciences

Nature

Planetary and Space Sciences

Royal Aeronautical Society Journal

Soviet Astronomy

Zeitschrift für Flugwissenschaften

2. Semi-technical Journals

Aeronautics

*Aero/Space Engineering

Aero/Space Management

Air Force and Space Digest

American Geophysical Union Transactions

*Astronautical Sciences Review

*Astronautics

*Aviation Week

Canadian Aeronautics and Space Journal

Current Contents

Dissertation Abstracts

Electrical Engineering

*Missiles and Rockets

Missiles and Space

Scientific American

Space Flight

Space/Aeronautics, formerly Aviation Age

Sky and Telescope

U.S. Government Research Reports.

3. Series of Books and Proceedings of Meetings

Advances in Applied Mechanics (Academic Press)

Advances in Astronomy and Astrophysics (Academic Press)

Advances in Astronautical Sciences (Plenum Press, Mac Millan)

Advances in Geophysics (Academic Press)

Ballistic Missile and Space Technology (Academic Press)

Proceedings of the International Astronautical Congress (Springer Verlag, Vienna)

Progress in Astronautics and Rocketry(Academic Press)

Smithsonian Contributions to Astrophysics (Smithsonian Institute Astrophysics Laboratory)

Space Research (Interscience)

Vistas in Astronomy (Pergamon Press)

B. BIBLIOGRAPHY OF BACKGROUND MATERIAL

Allen, C. W., "Astrophysical Quantities," University of London, 1955.

Ackeret, J., "Zur Theorie der Rakete," Helvetica Physica Acta, Vol. 19, 1946.

Anonymous "Earth Orbital Operations Manual," ER 12684, Martin Co., Space Systems Division (Baltimore), 1963.

Baker, R. M. L., Jr., et al., "Efficient Precision Orbit Computation Techniques," ARS Journal, Vol. 30, No. 8, August 1960, pp 740 to 747.

Baker, R. M. L., Jr., "Recent Advances in Astrodynamics, 1960," ARS Journal, Vol. 30, No. 12, December 1960, pp 1127 to 1140.

Baker, R. M. L., Jr., and Makemson, M. W., "An Introduction to Astrodynamics," Academic Press (New York), 1960.

Batrakov, Yu V., "Determination of the Preliminary Orbits of Artificial Satellites from Observations with Time Approximately Known," ARS Journal, Vol. 30, No. 9, 1960, pp 859 to 864.

Birkhoff, G. D., "The Restricted Problem of Three Bodies," Collected Mathematical Papers, American Mathematical Society (New York), 1950.

Bobrovnikoff, N. T., "Natural Environment of the Moon," WADC Phase Technical Note 3, ASTIA Document No. AD 242177, Wright Air Development Center Wright-Patterson Air Force Base, Ohio, June 1959.

Brouwer, D., and Clemence, G. M., "Methods of Celestial Mechanics," Academic Press (New York), 1961.

Brown, E. W., "An Introductory Treatise on the Lunar Theory," Dover Publications (New York), 1960.

Cap, F., "Relativitatstheorie und Astronautik," Proceedings of the IXth International Astronautical Congress, Amsterdam, 1958, Springer Verlag (Vienna), 1959, pp 209 to 221.

Cole, A. E., Court, A. and Kantor, A. J., "Standard Atmosphere Revision to 90 km," Geophysics Research Directorate, Air Force Research and Development Command, Bedford, Mass., 28 March 1961.

Champion, K. S. W. and Minzner, R. A., "Proposed Revision of United States Standard Atmosphere, 90-700 km," Geophysics Research Directorate, Air Force Research and Development Command, Bedford, Mass., 11 December 1961.

Danby, J. M. A., "Fundamentals of Celestial Mechanics," MacMillan (New York), 1962.

Darwin, G. H., "Periodic Orbits," Acta Mathematica, Vol. 21, 1897.

Dubyago, A., "The Determination of Orbits," MacMillan Company (New York), 1961.

Egorov, V. A., "Certain Problems of Moon Flight Dynamics," Russian Literature of Satellites, Part 1, International Physical Index (New York), 1958.

Ehricke, K. A., "Space Flight, Vol. 1 Environment and Celestial Mechanics," D. Van Nostrand Co., Inc. (New York), 1960.

Fielder, G., "Structure of the Moon's Surface," Pergamon Press (New York), 1961.

Finlay-Freundlich, E., "Celestial Mechanics," Pergamon Press (New York), 1958.

Firsoff, V. A., "Surface of the Moon, Its Structure and Origin," Hutchinson and Co., Ltd. (London), 1961.

Grobner, W., and Cap, F., "The Three-Body Problem Earth-Moon-Spaceship," Astronautica Acta, Vol. 5, 1959, pp 287 to 312.

Heiskanen, W. A., and Vening-Meinesz, F. A., "The Earth and Its Gravity Field," McGraw-Hill (New York), 1958.

Herget, P., "The Computation of Orbits," published privately by the author, 1948.

Herrick, S., Baker, R. M. L., Jr., and Hilton, C. G., "Gravitational and Related Constants for Accurate Space Navigation," Eighth International Astronautical Congress, Barcelona, 1957 (proceedings), Springer Verlag (Vienna), 1958, pp 197 to 235.

Hill, G. W., "Researches on the Lunar Theory," Acta Mathematica, 1880, Vol. III. (Also, American Journal of Mathematics, Vol. 1, 1878-1879.)

Hohmann, W., "Die Erreichbarkeit der Himmelskörper," R. Oldenbourg (Munich), 1925.

Johnson, F. S., (editor) "Satellite Environment Handbook," Stanford Univ Press (Stanford), 1961.

Kaula, W. M., "A Geoid and World Geodetic System Based on a Combination of Gravimetric, Astrogeodetic, and Satellite Data," Journal of Geophysics, Res. Vol. 66, June 1961, pp 1799 to 1811, also NASA Technical Note TN D-702, May 1961.

Kooy, J. M. J., and Berghuis, J., "On the Numerical Computation of Free Trajectories of a Lunar Space Vehicle," Astronautica Acta, 1960, Vol. 6, Fasc 2-3, pp 115 to 143.

Kopal, Z., "The Moon, Our Nearest Celestial Neighbour," Academic Press, Inc. (New York), 1960.

Kopal, Z., (editor) "Physics and Astronomy of the Moon," Academic Press, Inc. (New York), 1962.

Krause, H. G. L., "On a Consistent Set of Astrodynamic Constants, George C. Marshall Space Flight Center Report MTP-P & VE-F 62-12 (NASA), (Huntsville, Alabama), 1963.

Krejci-Graf, K., "Der Ban der Mondoberfläche mit Vergleich der Erde, Daten and Deutung," also "Berichtigungen," Astronautica Acta, Vol. 5, 1959, pp 163 to 223 and 389.

Kuiper, G. P., (editor), "The Atmospheres of the Earth and Planets," Second Edition, Univ of Chicago Press, 1952.

Kuiper, G. P., and Middlehurst, B. M., (editors), "Planets and Satellites," Univ of Chicago Press, 1961.

Kuiper, G. P., (editor), "The Earth As a Planet," Univ of Chicago Press, 1954.

Kulikov, D. K., and Batrakov, Yu. V., "Method for Improving Orbits of Artificial Satellites of the Earth Using Observations with Approximate Values of Time," ARS Journal, Vol. 30, No. 9, 1960, pp 865 to 874.

Makemson, M. W., Baker, R. M. L., Jr., and Westrom, G. B., "Analysis and Standardization of Astrodynamic Constants," Journal of Astronautical Sciences, Vol. 8, No. 1, Spring 1961, pp 1 to 13.

Michael, W. H., "Considerations of the Motion of a Small Body in the Vicinity of the Stable Libration Points of the Earth-Moon System," NASA TR R-160, 1963.

Miele, A., "Theorem of Image Trajectories in the Earth-Moon Space," Astronautica Acta, 1960, Vol. 6, No. 5, pp 225 to 232.

Miele, A., "Flight Mechanics, Vol. 1: Theory of Flight Paths," Addison-Wesley Press (Reading, Mass.), 1962.

Moulton, F. R., "An Introduction to Celestial Mechanics," MacMillan (New York), 1914.

Oertel, G. K., and Singer, S. F., "Some Aspects of a Three-Body Problem," Astronautica Acta, Vol. 5, 1959, pp 356 to 366.

Plummer, H. C., "An Introductory Treatise on Dynamical Astronomy," Dover Publications (New York), 1960.

Poincaré, H., "La Mécanique Céleste," (three volumes) Dover Publications (New York), 1957.

Ruppe, H. O., "Minimum Energy Requirements for Space Travel," Proceedings of the Xth International Astronautical Congress, London, 1959, Springer Verlag (Vienna), 1960, pp 181 to 201.

Schindler, G. M., "Satellite Librations in the Vicinity of Equilibrium Solutions," Astronautica Acta, Vol. 6, 1960, pp 233 to 240.

Sedov, L. I., "The Orbits of Cosmic Rockets Toward the Moon," Astronautica Acta, Vol. 6, 1960, pp 16 to 31.

Seifert, H. S., (editor), "Space Technology," John Wiley and Sons (New York), 1959.

Shapiro, L., "The Prediction of Ballistic Missile Trajectories from Radar Observations," McGraw-Hill Book Company (New York), 1957.

Smart, W. M., "Celestial Mechanics," MacMillan (New York), 1914.

Subotowicz, M., "Theorie der Relativistischen n-Stufenrakete, "Proceedings of the Xth International Astronautical Congress, London, 1959, Springer Verlag (Vienna), 1960, pp 852 to 864. (Consult also references of this article.)

Tross, C., "Astronomical Constants and Their Importance in Lunar Trajectory Determination," ARS Journal, Vol. 30, No. 10, October 1960, pp 938 to 941.

Valley, S. L., (editor), "Space and Planetary Environments," Report AFCRL-62-270, Geophysics Research Directorate, January 1962.

Wilkins, H. P., "The Moon," The MacMillan Company (New York), 1955.

C. BIBLIOGRAPHY FOR THE VARIOUS PHASES OF LUNAR FLIGHT

Anonymous, "Analytical and Numerical Studies of Three-Dimensional Trajectories to the Moon," Space Technology Laboratories, Guidance and Navigation Systems Department, 10 November 1958, Report GM-TR-0165-00508.

Anonymous, "Flight Performance Handbook for Orbital Operations," Space Technology Laboratories, Inc. (Redondo Beach, California), September 1961.

Allen, N. J., and Eggers, A. J., Jr., "A Study of the Motion and Aerodynamic Heating of Missiles Entering the Earth's Atmosphere at High Supersonic Speeds, NACA TN-4047, 1957.

Battey, R. V., "Abort Considerations," NASA-Industry Apollo Technical Conference, Washington, D. C., 18 to 20 July 1961.

Battin, R. H., "A Statistical Optimizing Navigation Procedure for Space Flight," Instrumentation Laboratory, MIT (Cambridge, Mass.), May 1962.

Brown, H., and Nicoll, H. E., Jr., "Electrical Propulsion Capabilities for Lunar Exploration," AIAA Journal, Vol. 1, No. 2, February 1963, pp 314 to 319.

Brunner, M. J., "Aerodynamic and Radiant Heat Input to Space Vehicles Which Re-enter at Satellite and Escape Velocity," ARS Journal, Vol. 31, No. 8, August 1961.

Buchheim, R. W., "Motion of a Small Body in Earth-Moon Space," RM 1726, Rand Corporation, 4 June 1956.

Burns, R. E., and Singleton, L. G, "Ascent from the Lunar Surface," Report No. MTP-P & VE-F-62-7 (revised), George C. Marshall Space Flight Center (Huntsville, Alabama), 7 December 1962.

Chapman, D. R., "An Approximate Analytical Method for Studying Entry into Planetary Atmospheres," NASA TR R-11, 1959.

Chapman, D. R., "An Analysis of the Corridor and Guidance Requirements for Supercircular Entry into Planetary Atmospheres," NASA TR R-55, 1959.

Clarke, V. C., Jr., "Design of Lunar and Interplanetary Ascent Trajectories," California Institute of Technology Jet Propulsion Laboratory TR 32-30, March 1962.

Crisp, J. D. C., "The Dynamics of Supercircular Multiple-Pass Atmospheric Braking," Astronautica Acta, Vol. VIII, Fasc 1, 1962, pp 1 to 27.

Culler, G. J., and Fried, B. D., "Universal Gravity Turn Trajectories," Journal of Applied Physics, Vol. 28, No. 6, June 1957, pp 672 to 676.

Darlington, S., "Guidance and Control of Unmanned Soft Landings on the Moon," Planetary and Space Sciences, Vol. 7, July 1961, pp 70 to 75.

De Fries, P. J., "Analysis of Error Progression in Terminal Guidance for Lunar Landing," NASA TN D-605, July 1961, also Journal of Astronautical Sciences, Vol. 7, No. 4, 1961.

Duncan, R. C., "Dynamics of Atmospheric Entry," McGraw Hill (New York), 1962.

Eggers, A. J., and Wong, T. J., "Motion and Heating of Lifting Vehicles During Atmosphere Entry," ARS Journal, Vol. 31, No. 10, October 1961, pp 1364 to 1375.

Eggleston, J. M., and McGowan, W. A., "A Preliminary Study of Some Abort Trajectories Initiated During Launch of a Lunar Mission Vehicle," NASA TM X530, 1961.

Fisher, E., and Wong, C. M., "Study of a Moon Mission Utilizing a High Performance Nuclear Hydrogen Rocket," IAS Paper No. 62-60, IAS 30th Annual Meeting, January 1962.

Fosdick, G. E., and Anthony, M. L., "Three-Dimensional Pulse Optimization for Vehicles Disorbiting from Circular Orbits," Astronautica Acta, Vol. VIII, Fasc. 6, 1962, pp 343 to 375.

Fried, B. D., and Richardson, J. M., "Optimum Rocket Trajectories," Journal of Applied Physics, Vol. 27, August 1956, pp 955 to 961.

Gunkel, R. J., Shutte, R. H., "Trajectories for Direct Vehicle Transfer from Moon to Earth," Proceedings of the XIth International Astronautical Congress, Stockholm 1960, Springer Verlag (Vienna), 1961, pp 125 to 135.

Hunter, M. W., Klemperer, W. B., and Gunkel, R. J., "Impulsive Midcourse Correction of a Lunar Shot," Proceedings of the IXth International Astronautical Congress, Amsterdam 1958, Springer Verlag (Vienna), 1959, pp 626 to 638.

Huss, C. R., Hammer, H. A., and Mayer, J. P., "Parameter Study of Insertion Conditions for Lunar Missions Including Various Trajectory Considerations," NASA TR R-122.

Jensen, J., Townsend, G., Kork, J., and Kraft, D., "Design Guide to Orbital Flight," McGraw-Hill, 1962.

Kelley, H. J., "Gradient Theory of Optimal Flight Paths," ARS Journal, Vol. 30, No. 10, October 1960, pp 947 to 954.

Koelle, H. H., (editor-in-chief), "Handbook of Astronautical Engineering," McGraw-Hill (New York), 1961.

Kooy, J. M. J., "On the Orbital Computations and the Guidance Problem of a Deep Space Rocket," Proceedings of the IXth International Astronautical Congress, Amsterdam 1958, Springer Verlag (Vienna), 1959, pp 469 to 506.

Lass, H., and Solloway, C. B., "Motion of a Satellite of the Moon," ARS Journal, Vol. 31, February 1961, p 220.

Lawden, D. F., "Stationary Rocket Trajectories," Quarterly Journal of Mechanics and Applied Mathematics, Vol. 8, Part 4, December 1954, pp 488 to 504.

Lanzano, P., "Application of the Jacobi Integral of Celestial Mechanics to the Terminal Guidance of Space Probes," Proceedings of the XIth International Astronautical Congress, Stockholm 1960, Vol. 1, Springer Verlag (Vienna), 1961, pp 114 to 124.

Loh, W. H. T., "Dynamics and Thermodynamics of Re-entry," Journal of Aerospace Science, Vol. 27, No. 10, October 1960, pp 748 to 762.

McLean, J. D., Schmidt, S. F., McGee, L. A., "Optimal Filtering and Linear Prediction Applied to a Midcourse Navigation System for the Circumlunar Mission," NASA TN D-1208, March 1962.

Mickelwait, A. B., "Lunar Trajectories," ARS Journal, Vol. 29, December 1959, pp 905 to 914.

Mickelwait, A. B., and Booton, R. C., Jr., "Analytical and Numerical Studies of Three-Dimensional Trajectories to the Moon," Journal of Aerospace Sciences, Vol. 27, August 1960, pp 561 to 573.

Miele, A., and Cavoti, C. R., "Optimum Thrust Programming Along Arbitrarily Inclined Rectilinear Paths," Astronautica Acta, Vol. 4, Fasc 3, 1958, pp 167 to 181.

Porter, J. G., "Difficulties of Space Navigation," from Bates, D. R., Moore, P., eds., "Space Research and Exploration," Eyre and Spottiswoode, London, 1957, pp 151 to 164.

Rinehart, J. S., "Stresses Associated with Lunar Landings," Journal of the British Interplanetary Society, " Vol. 17, No. 12, 1960, pp 431 to 436.

Schechter, H. B., "Multibody Influence on the Least Altitude of a Lunar Satellite," ARS Journal, Vol. 32, December 1962, p 1921.

Schroeder, W., and Pittman, C. W., "A Guidance Technique for Interplanetary and Lunar Vehicles," Planetary and Space Sciences, Vol. 7, July 1961, pp 64 to 69.

Sivo, J. N., Campbell, C. E., and Hamza, V., "Analysis of Close Lunar Translation Techniques," NASA TR R-126, 1962.

Skidmore, L. J., and Penzo, P. A., "Monte Carlo Simulation of the Midcourse Guidance for Lunar Flight," IAS paper No. 62-12, IAS 30th Annual Meeting, January 1962.

Slye, R. E., "Velocity Requirements for Abort from the Boost Trajectory of a Manned Lunar Mission," NASA TN D-1038, July 1961,

Smith, G. L., Schmidt, S. F., and McGee, L. A., "Application of Statistical Filter Theory to the Optimal Estimation of Position and Velocity on Board a Circumlunar Vehicle," NASA TR R-135, 1962.

Stalony-Dobrzanski, J., "Application of Temperature Rate to Manual Flight Control of Re-entry Vehicles and Energy Management." Proc IRE National Aerospace Electronics Conference, (Dayton, Ohio), May 1962.

Stuhlinger, E., "Progress in Electric Propulsion Systems," Proceedings of the XIth International Astronautical Congress, Stockholm 1960, Vol. 1, Springer Verlag (Vienna), 1961, pp 651 to 670.

Szebehely, V. G., "Equations for Thrust Programs," Proceedings of the XIth International Astronautical Congress, Stockholm 1960, Vol. 1, Springer Verlag (Vienna), 1961, pp 431 to 443.

Tempelman, W. H., "Selected Problems in Optimum Ballistic Descent from Orbit," Astronautica Acta, Vol. VIII, Fasc 4, 1962, pp 193 to 204.

Tross, C., "Lunar Vehicle Orbit Prediction," ARS Journal, Vol. 32, No. 4, April 1962, p 582.

Weber, R. J., and Pauson, W. M., "Some Thrust and Trajectory Considerations for Lunar Landings," NASA TN D-134, 1959.

Weber, R. J., Pauson, W. M., and Burley, R. R., "Lunar Trajectories," NASA Technical Note TN D-866, August 1961.

Wong, T. J., and Slye, R. E., "Effect of Lift on Entry Corridor Depth and Guidance Requirements for the Return Lunar Flight," NASA TR R-80, ASTIA No. AD 242358, 1960.

Wong, T. J., Goodwin, G., and Slye, R. E., "Motion and Heating During Atmosphere Re-entry of Space Vehicles," NASA TN D-335, 1960.

Wrobel, J. R., et al., "Lunar Landing Vehicle Propulsion Requirements," ARS Journal, Vol. 31, No. 11, November 1961, pp 1570 to 1573.

Yashikawa, K. K., and Wick, B. H., "Radiative Heat Transfer During Atmosphere Entry at Parabolic Velocity," NASA TN D-1074, 1961.

APPENDIX A

APPENDIX A

GLOSSARY (REF. 1)

A

Aberration: apparent displacement of a body from its actual position due to the observer's motion, the object's motion and the finite speed of light.

Aberration, planetary: aberration including effects of the object's motion as well as the observer's motion during the time light travels from the object to the observer.

Aberration, stellar: aberration including only the effect of the earth's motion around the sun, mean value 29.9 km/sec.

Ablation: the gradual removal or erosion of an exposed surface of an object resulting from its high speed passage through a resistive medium.

Abort: the termination of a space mission after an emergency forces return to earth.

Albedo: fraction of total incident light reflected by a body.

Albedo, average geometric: ratio between the average brightness of the object to the brightness of a white screen of the same size normal to the incident light (lunar albedo 0.105).

Albedo, spherical: ratio of the light scattered in all directions by the object to the total incident light (lunar albedo = 0.073).

Almucantar: a parallel to the horizon.

Altitude (also elevation): a topocentric coordinate in the horizon system; the angular distance of an object above the horizon, measured on a vertical circle. Also synonymous with the height of an object above some surface.

Analytical integration: the specification of an explicit closed algebraic or series relation to represent the integral of a given function.

Angular momentum: the quantity $m\vec{r} \times \dot{\vec{r}}$ ($= r^2 \dot{\theta}$ in polar coordinates) constant for conic motion.

Anomaly: or angle; see true anomaly, mean anomaly, and eccentric anomaly.

Aphelion: the point on a heliocentric ellipse farthest from the sun.

Apocynthion (also aposelene or apolune): the point on a selenocentric elliptic orbit farthest from the moon's center.

Apofocus: the apsis on an elliptic orbit farthest from the principal focus or center of force.

Apogee: the point on a geocentric elliptical orbit farthest from the earth's center.

Apsis (plural, apsides): the point on a conic where the radius vector is a maximum or minimum. The line of apsides is the major axis extended indefinitely.

Argument of latitude: the angle in the orbit from the ascending node to the object in the direction of motion; the sum of the argument of perifocus and the true anomaly.

Argument of perifocus: the angular distance measured in the orbit plane in the direction of motion from the lines of nodes to line of apsides.

Aries: an astronomical constellation; a portion of the celestial sphere which contained the vernal equinox.

Aries, first line of: the direction of the vernal equinox (the name is a carryover from a time that the vernal equinox was in the constellation Aries).

Aspect: angular position of a body relative to its line of advance in orbit.

Astrodynamics: the engineering or practical application of celestial mechanics and other allied fields such as high altitude aerodynamics; geophysics; attitude dynamics; and electromagnetic, optimization, observation, navigation, and propulsion theory, to the contemporary problems of space vehicles. Astrodynamics is sometimes also meant to include the study of natural objects such as comets, meteorites and planets.

Astronomical unit (AU): the mean distance or semimajor axis of the orbit of a fictitious unperturbed planet having the mass (0.000,002,819 solar masses) and sidereal period (365.256,383,5 mean solar days) that Gauss adopted for the earth in his original determination of the gravitational constant K_s (= 0.017,202,089,95).

Approximately equal to 92,914,000 statute miles or 149,530,000 km.

Azimuth: a topocentric coordinate measured in the plane of the horizon from the north (or south) point on the horizon clockwise to the object.

B

Ballistic trajectory (also coast trajectory or free-flight trajectory): motion of the space vehicle without rocket burning or thrust forces.

Barker's equation: an equation that relates position to time for an object traveling in a parabolic orbit.

Barycenter: center of mass of a system of masses.

Base altitudes: reference altitudes or levels of the atmosphere between which the atmospheric temperature gradient is assumed to be a constant.

Boltzmann's constant: the ratio of the mean total energy of a molecule to its absolute temperature. Its value is 1.380×10^{-23} joule/°K.

Braking: the deceleration of a space vehicle by rocket thrust or by atmospheric drag.

Braking ellipses: a series of ellipses whose semi-major axes decrease due to the atmosphere of a planet when a vehicle attempts a landing on that planet.

Burnout: end of rocket burning for a particular rocket engine in a given stage of the rocket.

C

Call-down frequency: the frequency with which a vehicle can be recalled from orbit and landed at a specific site.

Cartesian coordinate system: a set of (usually three) mutually orthogonal straight coordinate axes which form a right-handed coordinate system.

Celestial equator: the great circle in which the plane of the terrestrial equator intersects the celestial sphere. The north celestial pole is the point of intersection of the earth's spin vector with the celestial sphere.

Celestial sphere: a hypothetical sphere of infinite dimensions, centered at the observer (or center of the earth or sun, etc.), on the inner surface of which the celestial bodies are projected and appear to move. This sphere is fixed in space, and thus, because of the earth's rotation, appears to rotate from east to west.

Centrifugal force: a fictitious position-dependent force that apparently arises when the motion of an object is observed with respect to a rotating coordinate system. The relationship yielding this "force" is $-m\vec{\omega} \times (\vec{\omega} \times \vec{r})$, where m is the mass of the object and $\vec{\omega}$ is the angular velocity vector of the rotating coordinate system.

Characteristic velocity: the sum of all absolute velocity changes required of a vehicle for a particular space flight (a measure of the total energy requirement for a flight).

Circle, galactic: fundamental plane of the galactic reference system (north pole at $12^h\ 44^m$ right ascension and +27° declination), inclined 62° to the celestial equator.

Circle, hour: secondary circles of the equatorial coordinate system, i.e., planes normal to the celestial equator.

Circle, secondary: great circles (or planes through the origin) which pass through the poles of a given coordinate system.

Circle, vertical: intersections of the celestial sphere by vertical planes in a horizontal coordinate system.

Circumlunar trajectory: a trajectory from the vicinity of the earth which passes behind the moon and returns ballistically to the vicinity of the earth.

Cislunar space: the region of space around the earth and moon, usually taken as being synonymous with the sphere of influence of the earth-moon system.

Collision parameter: the offset distance between the extension of a velocity vector of an object at a great distance from a center of attraction or repulsion and this center.

Colure, equinoctial: the plane, secondary to the equator, which passes through both the celestial poles and the equinoxes.

Colure, solstitial: the plane, secondary to the equator, which passes through both the celestial poles and the solstices.

Conjunction: a point in the orbit of a planet (or moon) where its celestial longitude equals that of the sun. If the alignment is sun-planet-earth, the planet is said to be in "inferior conjunction." This configuration is possible only with inferior planets; if it is planet-sun-earth, the planet is in "superior conjunction." Similarly, when the moon (or a superior planet) is between the earth and the sun, i.e., "new," it is said to be at conjunction.

Coordinate systems: one of a number of sets of celestial coordinate systems used in astronautics (Chapter XI).

(1) Ecliptic System uses the plane of the earth's orbit (ecliptic) as the reference. The axis of the poles of the ecliptic is at right angles to this plane. This system is most useful for intrasolar system work since all the planets move in or near the plane of the ecliptic.

(2) Equatorial System uses the celestial equator as the reference plane. The celestial equator and celestial poles coincide with extensions of the earth's equator and poles on the celestial sphere. This system is the one most commonly used in astronomy.

(3) Horizon System uses the observed horizon as the reference plane and is the common system of celestial navigation.

Coriolis force: a fictitious velocity dependent force that apparently arises when the motion of an object is reckoned with respect to a rotating coordinate system. The relationship yielding this "force" is $-2m\vec{\omega} \times \dot{\vec{r}}_r$, where m is the mass of the object, $\vec{\omega}$ is the angular velocity vector of the rotating coordinate system, and $\dot{\vec{r}}_r$ is the velocity of the object reckoned with respect to the rotating system.

Cosmic dust: fine dust particles (micrometeorites) that are concentrated in the solar system in the plane of the ecliptic (e.g., giving rise to the phenomenon of "zodiacal light") and also dispersed in a more rarefied manner in interstellar space, being more concentrated in the galactic spiral arms; also a component of comets.

Cosmic rays (direct): high-energy charged particles (e.g., with energies in excess of 100 Mev) such as protons, alpha particles and heavy nuclei which have apparently been ejected by stars and accelerated by vast magnetic fields in interstellar space.

Cosmoparticle: discrete material entities of submeteoritic mass, either in or from space. They may be "free" or individual molecules or atoms, or molecular or atomic constituents of any kind, e.g., ions, atomic nuclei, protons, neutrons, electrons, positrons, etc.

Cross product: or vector product (denoted by $\vec{A} \times \vec{B}$) of two typical vector quantities $\vec{A}$ and $\vec{B}$ can be defined either as a vector mutually perpendicular to both $\vec{A}$ and $\vec{B}$ with magnitude A B sin (A, B) or equivalently as

$$(A_yB_z - A_zB_y)\,I + (A_zB_x - A_xB_z)\,J + (A_xB_y - A_yB_x)\,K$$

where the subscripts denote the components of the vectors on the three orthogonal axes denoted by the unit vectors I, J, K.

Culmination: The time at which a heavenly body reaches the meridian of an observer. Upper culmination occurs near zenith, lower culmination near nadir.

D

Day, sidereal: the period of one rotation of the earth relative to inertial space (the stars), $23^h\ 56^m\ 04^s.090$ mean solar time.

Day, solar: the time between two successive upper (or lower) culminations of the sun, $24^h\ 03^m\ 56^s.556$ sidereal time.

Declination: the arc of an hour circle (great circles passing through the poles) intercepted between the celestial equator and the object; angular distance north or south of the celestial equator.

Definitive orbit: an orbit that is defined in a highly precise manner with due regard taken for accurate constants and observational data, and precision computational techniques including perturbations.

Differential correction: a method for finding from the observed minus computed (O - C) residuals small corrections which, when applied to the elements or constants, will reduce the deviations from the observed motion to a minimum.

Dip: the angular distance between the true horizontal and the observed horizon for an observer above ground level.

Direct motion: the term applied to eastward or counterclockwise motion of a planet or other object as seen from the North Pole (i.e., in the direction of increasing right ascension). Thus, it is motion on an orbit in which $i \leq 90$ degrees.

Diurnal: daily.

Diurnal motion: the apparent revolution of the heavenly bodies around the earth.

Dot product: or scalar product (denoted by $\vec{A} \cdot \vec{B}$) of two typical vector quantities $\vec{A}$ and $\vec{B}$ can be defined as AB cos (A, B) or equivalently as $A_xB_x + A_yB_y + A_zB_z$ where the subscripts denote the components of the vectors on three orthogonal axes.

Drag: the force occasioned by the passage of an object through a resistive medium acting in a direction opposite to that of the object's motion relative to the medium.

Drag coefficient: the total drag force acting on an object divided by one-half the local atmospheric density, the projected frontal area of the object, and the square of the magnitude of the velocity of the object relative to the resistive medium.

Drift, anomalistic: the variation or drift of a frequency source (e.g., a crystal oscillator) such that the frequency changes due to a variety of causes (e.g., temperature variation, component aging, etc.), none of which can be predicted in advance or completely controlled.

E

Eccentric anomaly: an angle at the center of an ellipse between the line of apsides and the radius of the auxiliary circle (which has radius equal to semimajor axis of ellipse and center at center of ellipse) through a point that has the same x-coordinate as a given point on the ellipse.

Eccentricity: the ratio of the radius vector through a point on a conic to the distance from the point to the directrix.

Eclipse: a name applied to cases where a nonluminous body passes into the shadow of another; eclipse of the sun means the interposition of the moon's disc between the observer and the sun.

Ecliptic: the great circle formed by the intersection of the orbital plane of the earth (the ecliptic plane) and the celestial sphere.

Ecliptic coordinate system: axes with the ecliptic as the fundamental plane and with spherical coordinates: celestial longitude and latitude.

Elements of orbit: any six independent constants defining the orbit, e.g., (1) orientation elements: Ω longitude of ascending node; i inclination of orbit plane; ω argument of perifocus; (2) dimensional elements: e eccentricity; a semimajor axis; (3) time element: T time of perifocus passage.

Elevation, angle of: the angle between the inertial velocity vector $\tilde{r}$ and the local horizontal, i.e., the plane normal to $\tilde{r}$ passing through the vehicle.

Eliminant: a determinant that is formed when n - 1 linear unknowns are eliminated from a set of n equations. The elimination of x and y, for example, from

$$a_1x + b_1y = c_1$$

$$a_2x + b_2y = c_2$$

$$a_3x + b_3y = c_3$$

yields the eliminant:

$$\begin{vmatrix} a_1 & b_1 & c_1 \\ a_2 & b_2 & c_2 \\ a_3 & b_3 & c_3 \end{vmatrix} = 0$$

Elongation, angle of: the angle between the direction to an object and to the center of the coordinate system reckoned at the observer.

Energy integral: one of the integrals of two-body motion expressing conservation of energy.

Entry angle: the angle between the velocity vector of a space vehicle relative to a resistive medium and the local horizontal.

Ephemeris (plural, ephemerdies): a table of calculated coordinates of an orbject with equidistant dates as arguments.

Ephemeris time (ET): uniform or Newtonian time, defined by mean frequency of rotation of the earth around the sun for the year 1900.

Epoch: arbitrary instant of time for which the elements of an orbit are valid (e.g., initial, injection, or correction time).

Equator, celestial: the great circle in which the plane of the terrestrial equator intersects the celestial sphere.

Equator, terrestrial: the circle in which the plane through the earth's center normal to its axis of rotation (the equatorial plane) intersects the earth's surface.

Equatorial bulge: the excess of the earth's equatorial diameter over the polar diameter (i.e., about 27 miles, 43 km); oblateness.

Equatorial satellite: a satellite whose orbit plane coincides with the earth's equatorial plane.

Equatorial system: rectangular axes referred to the equator as the fundamental plane and having spherical coordinates, right ascension and declination.

Equilateral triangle solutions: a particular solution of the three-body problem in which an object situated at one vertex of an equilateral triangle formed with the sun and a planet has a stable orbit. It was predicted by Lagrange (1772) and amply confirmed in the case of Jupiter. See Trojan asteroids.

Equinox, nutation of: arises from nutation of equator.

Equinox of date: position of equinox at epoch being used in discussion.

Equinox, precession of: arises from precession of equator.

Equinox, true: equals equinox or vernal equinox, q.v., "true" being used to emphasize distinction from mean equinox.

Equinoxes: intersections of the equator and ecliptic, the vernal equinox being the point where the sun crosses the equator going from south to north (descending node of earth's orbit).

Euler's equation: a relation in a parabolic orbit involving two radii vectors, their chord, and the time interval between them; discovered by Euler (1744).

Evection: a large perturbative term in the moon's longitude discovered by Hipparchus, amounting to 1° 15' at maximum.

F

Feasibility orbit: an orbit that can be rapidly and inexpensively computed on the basis of simplifying assumptions (e.g., two-body motion, circular orbit, three-body motion approximated by 2 two-body orbits, etc.) and yields an indication of the general feasibility of a system based upon the orbit without having to carry out a definitive orbit computation.

Free-molecule flow (or free-molecular flow): flow regime in aerodynamics in which molecules emitted from an object, as it passes through a resistive medium, do not affect the flow of oncoming molecules by scattering interactions, i.e., the mean free path of the

emitted molecules is much longer than a characteristic linear dimension of an object.

G

Galactic system: a system based on the centerline of the milky way.

Gaussian gravitational constant, K_s: factor of proportionality in Kepler's third law; the numerical value depending on the units employed. See astronautical unit.

Geocentric: referred to the center of the earth as origin.

Geocentric parallax: see parallax.

Geocentric subvehicle point: the point where the radius vector from the geocenter to a space vehicle intersects the spheroid.

Geodetic subvehicle point: the point where a line through a space vehicle normal to the spheroid intersects the spheroid.

Geoid: the mean sea-level figure of the earth.

Geoidal surface: the mean sea-level surface of the earth; surface of gravitational equipotential.

Geometric meter: the standard meter.

Geopotential meter: a unit of length employed in reckoning geopotential altitude.

Gravitational potential: at a point, the work required to remove unit mass from that point to infinity.

Greenwich meridian: the zero meridian from which geographical longitude is measured (passes through the Greenwich Observatory, England).

Ground trace: a succession of subvehicle points on earth or on any other celestial body.

Ground swath: a region around the ground trace, the boundaries of which are specified by the lateral distance from the ground trace.

Guidance and control system: a system that actively counteracts or overcomes the effects of deviations (from nominal conditions) in order to accomplish the given mission with the desired degree of exactness. Navigational inputs allow the guidance and control system to sense these deviations.

Guidance law: the equations which are mechanized in the guidance and control system.

Guidance law, explicit: the guidance computer in the vehicle predicts and the vehicle is steered along a trajectory which brings it to the desired end conditions.

Guidance law, implicit: the vehicle follows a nominal trajectory while the guidance system is active.

H

Harmonics of the earth's gravitational field: a series representing the gravitational potential of the earth whose terms form a harmonic progression, i.e., include powers of the reciprocal of distance.

Heliocentric: referred to the center of the sun as origin.

Hohmann orbit: an elliptic heliocentric trajectory for interplanetary flight, having tangency to the earth at one apsis and to another planetary orbit (e.g., that of Venus or Mars) at the opposite apsis. More generally stands for any such doubly tangent transfer ellipse.

Horizon, apparent: the horizon formed by the horizontal plane through the position of the observer.

Horizon, rational: the horizon formed by the plane through the center of the earth parallel to the observer's horizon.

Horizon coordinate system: a system of topocentric coordinates either spherical (azimuth and altitude) or rectangular, having as reference plane the celestial horizon, which is perpendicular to the direction of gravity at the observer.

Horizon scanner: an optical device that senses the radiation discontinuity between a planet or lunar surface and the stellar background of space. It can be utilized to establish a "vertical" reference based upon a "visual" horizon (which differs from both the astronomical and geodetic horizon).

Horizontal plane: that plane perpendicular to the direction of gravity at any place.

Hour angle (LHA): angle between the observer's meridian and the hour circle passing through the object, a coordinate in the rotating equator system, positive toward west, 0 to 24 hr.

Hour circle: any one of the great circles that pass through the celestial poles and, therefore, are at right angles to the equator.

I

Inclination i: angle between orbit plane and reference plane (e.g., the equator is the reference plane for geocentric orbits and the ecliptic for heliocentric orbits).

Inertial axes: axes that are not in accelerated or rotational motion.

Injection: the addition of an "instantaneous" incremental velocity vector to the satellite velocity vector at a prescribed time and place to establish a new orbit.

Injection conditions: position and velocity of rocket at the instant when the thrusting of rocket motor ends and the ballistic portion of the trajectory begins.

Intermediate orbit: an orbit tangent to the actual (or disturbed) orbit, having the same coordinates but not velocity at point of tangency.

Inversion: in this context is meant to be synonymous with the numerical solution of a set of linear algebraic equations.

Ionosphere: the ionized portion of the atmosphere above about 60 km.

Isostatic equilibrium: a situation in which the pressure under the earth's surface is the same regardless of whether it is measured under a mountain, valley or ocean, i.e., lower density strata underlie mountains while higher density strata underlie oceans.

J

Jacobi's integral: an integral of the equations of motion in a rotating coordinate system which relates the square of the velocity and the coordinates of an infinitesimal body referred to the rotating coordinate system. The constant of integration associated with Jacobi's integral is known as Jacobi's constant.

Julian date: the number of mean solar days that have elapsed since midnight, January 1, 4713 BC; e.g., the Julian date of January 1, 1960 is 2,436,934, and of February 1, 1965 is 2,438,792, etc.

K

Kepler's planetary laws: (1) every planet moves in an ellipse about the sun with the sun at one focus; (2) every planet moves in such a way that its radius vector sweeps over equal areas in equal intervals of time; (3) the squares of the periods of revolution of two planets are to each other as the cubes of their mean distances from the sun.

K_e^{-1} min: the characteristic time for geocentric orbits, i.e., the time required by hypothetical satellites to move 1 radian in a circular orbit of radius a_e (equatorial earth's radius); equal to 13,447,052 min.

K_s^{-1} day: the characteristic time for heliocentric orbits, i.e., the time required for a planet at 1 astronomical unit to move 1 radian (or 1 a.u.) along its orbit; equal to 58.132,440,87 days.

L

Lagrangian solutions: particular solutions of the three-body problem in which an infinitesimal object moves under the attraction of two finite bodies (e.g., the sun and Jupiter) which revolve in circles around their center of mass and in which the distances from the infinitesimal object to the finite bodies remain constant. See also equilateral triangle solutions and synodic satellites, i.e., the so-called straight line solutions.

Lambert's equation: an equation of the 8th degree expressing the curvature of the apparent path of a body moving around the sun, as seen from the earth: discovered by Lambert (1771).

Latitude, astronomical: the angle between the direction of gravity through a point and the equatorial plane.

Latitude, celestial: the angular distance of an object north (+) or south (-) of the ecliptic plane; a coordinate in the ecliptic system.

Latitude, geocentric: the angle between the equatorial plane and a straight line from the observer to the center of the earth. It differs from astronomical and geodetic latitudes because of the oblateness of the earth, 0° to 90° north or south.

Latitude, geodetic (or geographic latitude): the angle between the plane of the equator and a normal to a reference spheroid. Geodetic and astronomical latitudes differ only because of local deviations in the direction of gravity, 0° to 90° north or south.

Least squares inversion: a solution of a set of overdetermined linear equations such that the sum of the squares of the residuals is a minimum.

Legendre polynomials: the coefficients $P_n(c)$ in the expansion $(1 - 2ch + h^2)^{-1/2} = \sum_{n=0}^{\infty} P_x(c)\, h^n$ where $P_0(c) = 1$, $P_1(c) = 1/2\,(3c^2 - 1)$, $P_3(c) = 1/2\,(5c^3 - 3c)$, or, in general, $(n + 1)\, P_{n+1}(c) - (2n + 1)\, cP_n(c) + nP_{n-1}(c) = 0$.

Libration: (1) apparent or optical and physical tilting and side-to-side movements of the moon that render 18 percent of its surface alternately visible and invisible, (2) long-period orbital motions of the Trojan asteroids around the equilateral triangle points of the three-body Lagrangian solutions, (3) periodic perturbative oscillations in orbital elements.

Lift: the force arising from the passage of a vehicle through a resistive medium when the vehicle presents an asymmetrical form or orientation; which force acts in a direction normal to the object's motion relative to the medium.

Limb: the edge of the visible disk of the sun, moon, planet, etc.

Line of apsides: a line connecting the near to the far apsis, i.e., defines the major or transverse axis.

Line of nodes: the intersection of a reference plane and the orbit plane.

Line-of-sight: the apparent or observed direction of an object.

Longitude, celestial: the angular distance measured along the ecliptic from the vernal equinox eastward to the great circle passing through the object and normal to the ecliptic.

Longitude, ephemeris: analogous to ordinary geographic longitude, but referred to the ephemeris meridian, rather than to the Meridian of Greenwich.

Longitude, geocentric: the angular distance from the foot of the Greenwich meridian, measured along the equator, east or west, to the foot of the meridian through the place.

Longitude of ascending node: the angular distance from the vernal equinox measured eastward in the fundamental plane (ecliptic or equator) to the point of intersection with the orbit plane at the point that the object crosses from south to north.

Longitude of perifocus: sum of the angle in the fundamental plane between the vernal equinox and the line of nodes and the angle in the orbit plane between the line of nodes and the line of apsides, measured in the direction of motion.

Lunar equation: a factor required for reducing observations to the barycenter of the earth/moon system.

Lunar theory: the analytical theory of the motion of the moon. The lunar theories of Delaunay, Hansen, and Hill-Brown are used most frequently today.

Lunar unit (LU): the mean distance from the center of the earth to the center of a fictitious unperturbed moon having the mass and sidereal period of the moon. One lunar unit is approximately equal to 384,747 km or 239,122 statute miles.

Lunicentric: referred to the moon's center as origin; selenocentric.

M

Mach number: the ratio of the speed of a vehicle to the local speed of sound.

Macrometeorites: meteorites that are sufficiently massive to become fallen meteorites (and whose origin appears to be related to that of minor planets).

Magnetic storms: extensive disturbances in the earth's magnetic field.

Magnitude, stellar: a measure of the brightness of a star. A difference of five magnitudes represents a factor of 100 in brightness.

Mean anomaly: the angle through which an object would move at the uniform average angular speed n, measured from perifocus; $M = t\sqrt{\frac{\mu}{a^3}}$.

Mean center of moon (MCP): the point on the lunar surface intersected by the lunar radius that is directed toward the earth's center when the moon is at the mean ascending node and when the node coincides with the mean perigee or the mean apogee. The MCP is a specified distance from the crater Mösting A in the Sinus Medii.

Mean distance: the semimajor axis (it can be considered as an historical term).

Mean equinox of date: a fictitious equinox whose position is that of the vernal equinox at a particular date with the effect of nutation removed.

Mean free path: the path of a molecule when molecules are assumed to be smooth, rigid spheres with no external field of force acting on them; each molecule travels freely on a straight line between impacts with other molecules. The distance traversed between two successive impacts is called the free path and the average value of this distance the mean free path.

Mean solar day: the elapsed time between successive passage of the mean fictitious sun across the observer's meridian, 86,400 mean solar sec, the mean fictitious sun being a fictitious sun that moves along the celestial equator with the mean speed with which the true sun apparently moves along the ecliptic throughout the year.

Meridian: (1) Terrestrial meridians: great circles passing through North and South Poles, e.g., the observer's local meridian passes through his local zenith and the North and South Poles. (2) Celestial meridian: a great circle on the celestial sphere in the plane of the observer's terrestrial meridian.

Meridian, ephemeris: the geographical meridian which lies east of Greenwich by the amount 1.002738 times the difference (ET-UT).

Meridian passage: also called "transit" or "culmination" of a celestial object is marked by its crossing an observer's meridian.

Mesometeorites: intermediate meteorites having characteristic dimension of the order of a fraction of an inch that are stopped by the atmosphere, consumed, and are seen as common "meteors." The origin of these bodies appears to be related to that of comets

Meteor swarms: a large collection of mesometeorites (probably the remains of an "old" comet) that enters the earth's atmosphere and is seen as a swarm of meteors. The term is often applied to the actual collection of mesometeorites on heliocentric orbits in space.

Micrometeorites: very small meteorites (having a characteristic dimension of a few microns) that are stopped by the atmosphere without being consumed in flight or without producing luminous phenomena visible at the earth's surface.

Minor planets (or asteroids): small planets revolving about the sun, estimated to number more than 30,000, with diameters of more than 1 mile. The largest, Ceres, has a diameter of 488 miles.

Molecular scale temperature: the actual temperature of the atmosphere at any given height multiplied by the ratio of the mean molecular weight of the atmosphere at sea level to the mean molecular weight of the atmosphere at the given height.

Month, nodal: the time for one revolution of the moon with respect to either node.

Month, sidereal: the time between two successive arrivals of the moon at a given apparent place on the celestial sphere as indicated by the stars.

Month, synodic: the time for one revolution of the moon with respect to the apparent place of the sun, e.g., the time between conjunctions.

Moon's celestial equator: a great circle on the celestial sphere in the plane of the moon's equator, i.e., in a plane perpendicular to the moon's axis of rotation.

Moon's orbital plane (MOP): the instantaneous orbital plane of the moon around the earth, defined by the moon's geocentric radius and velocity vectors.

N

Nadir: the downward plumb-bob direction, or the point where the downward extension of the direction of a plumb-bob intersects the celestial sphere.

Navigation: the process of determining the position and velocity of a submarine, ship, airplane, or space vehicle by making observations from the vehicle of objects in the environment of the vehicle.

n-body problem: concerned with the gravitational interactions of masses m_i, m_j, i, j = 1, 2,..., n which are assumed homogeneous in spherical layers, under the Newtonian law. If n = 2, one has a two-body problem, while n = 3 is known as the three-body problem.

Newton's laws: Law of gravitation: Every particle of matter in the universe attracts every other particle with a force varying directly as the product of their masses and inversely as the square of the distance between them. Laws of motion: (1) Every particle continues in its state of rest, or of uniform motion in a straight line, unless it is compelled to change that state by a force impressed upon it. (2) The rate of change of momentum is proportional to the force impressed, and takes place in the direction of the straight line in which the force acts. (3) To every action there is an equal and opposite reaction; or the mutual actions of two bodies are always equal and oppositely directed.

Nodal passage, time of: the time T_Ω when an object passes through the node from the southern hemisphere to the northern hemisphere.

Node: the points of intersection of the great circle on the celestial sphere cut by the orbit plane and a reference plane (e.g., the ecliptic or equator reference plane).

Node, ascending: the node in the reference plane through which the body passes from South to North.

Node, descending: the node in the reference plane through which the body passes from North to South.

Node, longitude of ascending: see longitude of ascending node.

Nominal orbit: the true or ideal orbit in which space vehicle is expected to travel.

Normal places: curve formed, when several observations are available very close together in time, by smoothing observed coordinates.

Numerical differentiation: a process that allows for the numerical evaluation of the derivative of quantity, given tabular values of the quantity.

Numerical integration: a process that allows for the numerical evaluation of a definite integral.

Nutation: short period terms in the precession arising from the obliquity, the eccentricity, and the inclination of the moon's orbit and the regression of its nodes (approximately a 19-year period).

O

Obliquity of the ecliptic: the inclination of the ecliptic to the celestial equator; the angle of approximately 23° 27' between the earth's orbital plane and its equator.

Occultation: the interruption of the light from one celestial body by the intervention of another.

Opposition: the position of an object when its celestial longitude is 180° from sun, i.e., opposite to sun. (Configuration possible only with moon and superior planets.)

Orientation angles: the classical orientation elements, i.e., the inclination, longitude of the ascending node, and longitude of perifocus.

Osculating orbit: an orbit tangent to the actual or disturbed trajectory, having the same coordinates and velocity at that instant.

P

Parallactic angle: the angle between the hour circle of and the vertical circle through a body.

Parallactic inequality: a secondary effect on the solar perturbations in the moon's longitude due to the ellipticity of the earth's orbit.

Parallax: (1) Geocentric parallax: the angle at the object subtended by the earth's equatorial radius; applied to objects in the solar system. (2) Heliocentric parallax: the angle at a star, etc., subtended by the radius of the earth's orbit; applied to objects outside the solar system.

Pericynthion: the point on a selenocentric orbit nearest the moon's center.

Perifocus: the point on an orbit nearest the central force.

Perigee: the point on a geocentric orbit nearest the earth's center.

Perihelion: the point on a heliocentric orbit nearest the sun.

Period: the time required for one complete circuit of the orbit.

Period, anomalistic: interval of time from one perifocus passage to the next.

Period, nodal (also draconic): interval of time from one nodal crossing to the next.

Period, sidereal: the time required for the projection of a planet or other body to make a complete circuit of the celestial sphere. This is the true period.

Period, synodic: the time between successive oppositions of a superior planet or successive inferior conjunctions of an inferior planet.

Perturbations: deviations from exact reference motion caused by the gravitational attractions of other bodies or other forces.

General perturbations: A method of calculating the perturbative effects by expanding and integrating in series.

Special perturbations: methods of deriving the disturbed orbit by numerically integrating the rectangular coordinates or the elements.

Piecewise continuous: a function that can be divided into a finite number of pieces such that the function is continuous on the interior of each piece and such that the function approaches a finite limit at the point of connection of one piece with another. In the context of the temperature profile discussion the term is used in a more restricted sense to imply a function that is divided into a finite number or series of connected linear pieces (straight line segments).

Planetocentric: referred to the center of a planet as dynamical center or origin of coordinates.

Planets: bodies in the solar system which move in essentially elliptical paths around the sun (see Kepler's laws).

Inferior planets:	Inner, or terrestrial, planets:
Mercury	Mercury
Venus	Venus
Superior planets:	Earth
Mars	Mars
Asteroids	Asteroids, or minor planets.
Jupiter	
Saturn	
Uranus	Outer, or major, planets:
Neptune	Jupiter
Pluto	Saturn
	Uranus
	Neptune
	Pluto

Plasma: a collection of positive and negative ions that has no overall or gross charge.

Polar satellite: a satellite that passes over the north and south poles of the earth, i.e., that has an inclination of 90° with respect to the earth's equator.

Polar distance, ecliptic: complement of the celestial latitude.

Polar distance, north: complement of the declination.

Poles, celestial: the points in which the axis of rotation intersects the celestial sphere.

Poles, ecliptic: the points in which the normal to the ecliptic through the origin intersects the celestial sphere.

Poles, galactic: the points in which the fundamental galactic axis intersects the celestial sphere. The north galactic pole is at $12^h\ 44^m$ right ascension and +27° declination.

Position, apparent: coordinates of a celestial body as seen by an observer at the center of the earth referred to a coordinate system defined by the instantaneous equator, ecliptic, and equinox. The tabulated positions of the sun, moon, and planets in the American Ephemeris and Nautical Almanac are usually apparent positions.

Position, mean: coordinates of a celestial body referred to a coordinate system defined by the mean equator, ecliptic and equinox of date. This means that the periodic effects of nutation have been neglected.

Position, true: coordinates of a celestial body if corrections for planetary aberration are applied to the apparent position. A sequence of true positions as a function of time is known as a geometric ephemeris.

Potential function: see gravitational potential.

Poynting-Robertson effect: the gradual decrease in the orbital semimajor axis and eccentricity of a micrometeorite caused by the re-emission of radiant energy from the micrometeorite. The theory was first announced by Poynting and later improved and brought into conformity with the theory of relativity by Robertson.

Precession of the equinoxes: the slow, 26,000-year period westward motion of the equinoxes (and equator) along the ecliptic, arising from solar and lunar perturbations on the earth's equatorial bulge, which cause the earth's axis to precess.

Predicting a satellite's position: the six elements are the same in number as the three coordinates of position and the three components of velocity required to specify the launching conditions completely.

Primary: the body having the strongest gravitational field (most ponderous mass) in a system of bodies revolving about their common center of gravity. (Sun is the solar system's primary, earth is earth-moon system primary, etc.)

Prime meridian: the meridian defining 0° and 180° E or 180° W longitude. On earth the Greenwich meridian is the prime meridian.

R

Radiation pressure: the pressure acting on a surface exposed to incident electromagnetic radiation caused by the momentum transferred to the surface by the absorption and reflection of the radiation.

Ratios of the triangles: in the orbit determination methods of Gauss, Olbers, et al., the ratios of the triangles formed by the radii and the chords are assumed in a first approximation to be ratios of the sectors, which are the ratios of the corresponding time intervals by Kepler's second law.

Rectilinear orbit: a trajectory for which perifocus distance is zero and eccentricity is one.

Red shift, gravitational: an effect predicted by the General Theory of Relativity in which the frequency of light emitted by atoms in stellar atmospheres is decreased by a factor proportional to the (mass/radius) quotient of the star: confirmed observationally by the spectra of white dwarfs.

Re-entry: portion of a trajectory in the atmosphere of a planet; in the case of the earth it is usually taken as the portion below 400,000 ft or 122 km.

Re-entry corridor: all possible re-entry trajectories which do not produce excessive aerodynamic heating or deceleration.

Reduction to orbit: quantity added to celestial heliocentric longitude to give true longitude, q. v.

Reference ellipsoid (or spheroid): oblate spheroid closely approximating the geoid.

Reference orbit: an orbit, usually but not exclusively the best two-body orbit available, on the basis of which the perturbations are computed.

Refractive index (of a medium): the ratio of the speed of light in a vacuum to that in the medium, hence it is a measure of how greatly electromagnetic radiation rays are bent during their transit through a medium such as the earth's atmosphere.

Regression of the moon's nodes: the movement of the nodes of the moon's orbit westward along the ecliptic, due to solar perturbations, with period $\simeq$ 19 years.

Relativity effects: effects on a space vehicle trajectory and on time measurement arising by use of Einstein's special theory of relativity or of Einstein's general theory of relativity instead of the customary Newtonian mechanics for determining the trajectory. The fundamentals of these theories of relativity are discussed in Chapter IV of the Lunar Flight Handbook. Relativity effects are small in the weak gravitational field of the solar system if the space vehicle velocity is small compared to the speed of light. There are many such effects, the most prominent of which are: the time dilation predicted from the Lorentz transformation of special relativity; the time dilation, secular advance of perigee, and red-shift of spectral lines predicted by general relativity.

Rendezvous: the approach and contact of two vehicles in space.

Representation: the computation of the position of a space vehicle given the orbital elements and the time.

Residuals (O - C): differences between the observed and computed coordinates in the sense observed minus computed.

Residuals (O - 1): differences between the precomputed ideal observational data and the actual observed data on, for example, an interplanetary voyage.

Restricted n-body problem: the motion of n masses under their mutual gravitational attraction, but with one of the n masses having negligible mass and hence not influencing the motion of the other (n - 1) masses. This term is usually applied to n = 3 (see also n-body problem).

Retrograde motion: westward or clockwise motion as seen from the North Pole, i.e., motion in an orbit in which i > 90 degrees (opposite earth's rotation).

Retrorocket: a rocket attached to a space vehicle whose thrust is directed in a general direction against the inertial velocity of the space vehicle.

Reynolds number: the ratio of inertial forces to viscous forces--it is proportional to the Mach number, vehicle diameter, and the density, or, in equivalent terms, proportional to the diameter of the space vehicle in mean free paths and the vehicle speed measured in terms of the average thermal speeds of gas molecules that constitute the oncoming flow.

Right ascension: angular position of an object (e.g., star) measured eastward along the celestial equator from the vernal equinox to the great circle passing through the north celestial pole and the star (hour circle). Right ascension is often expressed in hours, minutes, and seconds ($1^h = 15°$).

S

Scale height: the distance in which an isothermal atmosphere decreases in density from 1 to 1/e.

Secular terms: expressions for perturbations that are proportional to the time.

Selenocentric: referred to the center of the moon; lunicentric.

Selenocentric equatorial coordinates: a right-handed coordinate system centered at the moon with its three axes defined by the vernal equinox, north celestial pole (of the earth), and a direction perpendicular to these two, i.e., an equatorial coordinate system translated to the moon.

Selenographic coordinates: coordinates that are rigidly attached to the moon (as geographic coordinates are attached to the earth) defined by the moon's equator and prime meridian. See mean center of moon.

Semimajor axis: the distance from the center of an ellipse to an apsis; one-half the longest diameter; one of the orbital elements.

Semiminor axis: one-half the shortest diameter of an ellipse.

Semiparameter: semilatus rectum; the perpendicular distance from the conic to the semimajor axis through either focus (not to be confused with the generic term "parameters").

Setting circles: a graduated scale that can be read visually and indicates the direction (e.g., altitude and azimuth or right ascension and declination) in which a telescope is pointed. Ordinarily they are employed to set or point a conventional astronomical telescope in the proper direction to make a given observation.

Sidereal period of a planet: see period, sidereal.

Sidereal time: the hour angle of the vernal equinox. (See Chapter II for conversion of sidereal time to mean solar time).

Sidereal year: time required by the earth to complete one revolution of its orbit; equal to 365.25636 mean solar days.

Slip flow: a flow regime in aerodynamics in which there is some departure from continuum flow and the layer of compressible fluid immediately adjacent to the surface of an object is no longer at rest but has a finite tangential "slipping" velocity.

Solar flares: short-lived areas of brilliance (covering areas of 10 million square miles or so) on the sun's chromosphere that are associated with other solar activity. Often accompanied by bursts of emitted charged corpuscles and electromagnetic radiation. They reach several times normal brightness within one or two minutes and then subside slowly over 15 to 30 minutes.

Solar parallax: the ratio of the earth's equatorial radius to its mean distance from the sun.

Solar time, mean: hour angle of fictitious mean sun increased by 12 hours. (The fictitious mean sun is a fictitious sun moving on the celestial equator with a mean motion of the real sun.) See pages 474 to 476, American Ephemeris and Nautical Almanac for conversion of mean solar time to sidereal time.

Solar wind: those low energy particles, i.e., corpuscular radiation (electrons and protons) emanating from the sun. Typical flux rates are 10^8 to 10^{10} particles per cm^2 per second, and typical energies are 1000 to 100,000 electron volts for the protons and a few electron volts for the electrons.

Solstices: the two times a year when the sun's declination is greatest north or south (about June 22 and December 22).

Space range system: a system or network of observation stations, together with their associated communication links and computational facilities, that are utilized to observe and track space vehicles, e.g., the Pacific Missile Range, the National Space Surveillance System, etc.

Specular reflection: characterized by the relation that the angle of incidence equals the angle of reflection, in contrast to diffuse reflection.

Sphere, celestial: an imaginary reference sphere; generally considered to be of infinite radius, and having its visible representation in the sky.

Spheroid: an oblate ellipsoid which closely approximates the mean sea-level figure of the earth or geoid.

Stability of a point or orbit: a point or orbit is stable if the space vehicle will remain near the point or orbit if given a small displacement and velocity. The point or orbit is unstable if the space vehicle will depart from it rapidly.

Standard atmosphere: a table of atmospheric density as a function of altitude which is accepted as a standard and used as a model to portray a typical average atmospheric density variation.

Standard deviation: the square root of the arithmetic mean of the squares of the deviations from the mean; also called root mean square error and sigma deviation.

Stationary points: points in the apparent path of a planet, etc., against the star background where the object appears to stand still because relative to the observer it is moving only in the line of sight. Such a point occurs when a planet changes its apparent motion from direct to retrograde and vice-versa.

Station error: small, usually negligible, differences between the astronomical and geodetic latitudes, due to certain anomalies (such as a mountain) in the local gravitational field.

Stratosphere: a region in which the temperature remains constant from about 18 km up to a height of 30 to 35 km.

Surface-circular satellite: a hypothetical satellite on a circular orbit about the earth having a semimajor axis equal to the earth's equatorial radius. Hence, such a satellite would "skim the surface of the earth" as it revolved on its orbit.

Synodic satellite: a hypothetical satellite, situated 0.84 of the distance to the moon on a line joining the centers of the earth and moon and having the same period of revolution as the moon, according to the Lagrangian "straight line solution" of the three-body problem.

T

Terminator: the boundary between the illuminated and dark sides of a planet or satellite. Usually one distinguishes between a morning and an evening terminator.

Three-body problem: the problem of integrating the equations of motion of three bodies (e.g., sun-moon-earth) moving under their mutual gravitational attractions: directly soluble only in particular cases. See Lagrangian solutions.

Thrust: the force exerted on a vehicle, by the discharge of a gas or propellant, in accordance with the conservation of linear momentum.

Time, ephemeris: time reckoning based upon "constant" frequency rather than frequency of earth's rotation. The current difference between ephemeris and universal time is about 35 seconds.

Time dilation: the apparent slowing-down of moving clocks. This effect arises from the special and general theory of relativity.

Time of perifocal passage: the time when a space vehicle traveling upon an orbit passes by the nearer apsis or perifocal point.

Topocentric: referred to the position of the observer on the surface of the earth, as origin.

Topocentric parallax: the difference between the geocentric and topocentric positions of a satellite.

Topocentric equatorial coordinates: a right-handed coordinate system centered at the observer with its three axes defined by the vernal equinox, north celestial pole, and a direction perpendicular to these two, i.e., an equatorial coordinate system translated to the topos.

Tracking: the process of determining the position and velocity of a celestial body by making observations from earth by optical or electromagnetic means.

Trajectory sensitivities: the partial derivatives of dependent trajectory variables with respect to independent trajectory variables.

Transitional flow: a flow regime in aerodynamics between the free-molecule flow and slip-flow regimes in which the molecules emitted from the surface of an object affect the flow of oncoming molecules, i.e., in which the mean free path of the emitted molecules becomes comparable to a characteristic linear dimension of an object.

Transearth trajectory: trajectory from the vicinity of the moon to the vicinity of the earth.

Translunar trajectory: trajectory from the vicinity of the earth to the vicinity of the moon.

Transverse axis: the distance between the apsides --identical to the semimajor axis for elliptical orbits.

Triaxial ellipsoid: a solid aspherical figure which when cut or sectioned in three (orthogonal, normal or mutually perpendicular) directions exhibits three elliptical cross sections of differing semimajor axes and eccentricities.

Tropopause: the height (varying from about 9 km over the poles to 18 km over the equator) where the gradual decrease in temperature with elevation above sea level ceases.

True anomaly: the angle about the focus between the perifocus and the radius vector in the direction of the motion.

True equinox of date: the actual position of the equinox including both precession and nutation.

Twenty-four-hour satellite: a satellite whose orbital period is approximately 24 hr. If such a satellite is on circular equatorial orbit, then it will theoretically remain fixed or "stationary" relative to the rotating earth.

Two-body orbit: the motion of a body of negligible mass around a center of attraction.

U

Umbra: the dark central portion of the shadow of a large body such as the earth or moon (used in connection with eclipses). The outer, less dark shadow is known as the penumbra.

Unit vector: a vector whose magnitude or length is unity--utilized to define directions in space.

Universal time (UT): mean solar time referred to the meridian of Greenwich, slightly non-uniform owing to the irregular rotation of the earth.

V

Van Allen radiation belt: two toroidal-shaped zones or belts of charged particles roughly situated in the plane of earth's equator. The inner belt commences at about one-fifth on an earth's radius above the equator and extends out to a little less than one earth's radius. The outer belt is located at about two-and one-half earth radii from the earth at the equator and is about one-earth radius thick. Actually the outer belt has a cross section that is shaped somewhat like a banana and extends north and south of the equatorial plane two earth radii. The northern and southern extremes of the belt's cross section (at about 45 degrees latitude) approach the earth one-half of an earth radius closer than at the equator.

Variant orbits: computed orbits in which one of the initial conditions (or parameters) is varied slightly from those of the nominal trajectory--such orbits are utilized to compute numerical partial derivatives or to determine the effects of errors in launch conditions.

Variation of latitude: small periodic changes in the position of the earth's poles due to a "wobbling" of the axis of rotation about the geometrical axis (the shortest diameter) of the earth.

Vector component: the projection of a vector on a given axis in space, e.g., if it is the X-axis then the component of the vector A on this axis is denoted by A_x.

Vector equation: an equation, whose terms include vectors, that can be resolved into component equations; e.g., $\ddot{\vec{r}} = \frac{-\mu \vec{r}}{r^3}$ actually represents the three component equations:

$$\ddot{x} = -\mu x/r^3$$

$$\ddot{y} = -\mu y/r^3$$

$$\ddot{z} = -\mu z/r^3$$

where $\ddot{\underline{r}}$ has been replaced by its three components $\ddot{x}$, $\ddot{y}$, and $\ddot{z}$ and $\underline{r}$ by its three components x, y, and z.

Velocity, circular: the magnitude of the velocity required of a body at a given point in a gravitational field which will result in the body following a circular orbital path about the center of the field.

Velocity, escape (also parabolic velocity): the minimum magnitude of the velocity required of a body at a given point in a gravitational field which will permit the body to escape from the field.

Velocity, orbital: with respect to the planets, usually the mean magnitude of the velocity in orbit--computed as the total distance traveled in one circuit divided by the period.

Vernal equinox: that point of intersection of the ecliptic and celestial equator where the sun crosses the equator from south to north in its apparent annual motion along the ecliptic.

Vis viva integral: see energy integral.

Voice trajectory program (Volume of Influence Calculated Envelopes): a patched conic lunar mission trajectory program. It uses the analytical solutions of the two-body trajectories to construct a complete trajectory from the vicinity of the earth to the moon and back.

Y

Year: the orbital period of the earth. When unqualified, it refers to the equatorial or to the calendar year, depending on its use.

Year, anomalistic: the time interval between successive passes through perihelion = 365.259,641,34 + 0.000,003,04 T days (T denotes centuries since 1900).

Year, Besselian: a time reckoning in terms of actual rather than calendar years.

Year, calendar: a variable year containing either 365 or 366 days.

Year, equatorial (also tropical or ordinary year, not calendar year): interval between transits of the sun through the moon equator 365.242, 198,79 - 0.000,006,14 T days.

Year, Julian: the year of the Julian calendar = 365.25 days.

Year, sidereal: the period of the earth relative to the stars = 365.256,360,42 + 0.000,000,11 T days.

Z

Zedir technique: the use of two cameras on a satellite whose optical axes are parallel, one of which photographs the sky (zenith) while the other simultaneously photographs the ground (nadir). Upon development and measurement, the photographs can be utilized to find the attitude of the camera's optical axis at the time of photograph.

Zenith: the point where the upward extension of the plumb-bob direction intersects the celestial sphere.

REFERENCE

1. "Flight Performance Handbook for Orbital Operations," Appendix A, Space Technology Laboratories, Inc. (Redondo Beach, California), September 1961.

APPENDIX B

COMPREHENSIVE LIST OF SYMBOLS

APPENDIX B

COMPREHENSIVE LIST OF SYMBOLS

The symbols are arranged alphabetically by chapters. Throughout the handbook a double subscript notation has been introduced to define the origin of and distances in a coordinate system. A geocentric equatorial coordinate system with origin at the center of the earth is denoted by the subscript "⊕." However, if this coordinate system is translated to the center of the moon, for instance, then two subscripts separated by a comma are used: "⊕,☾." A double subscript without a comma indicates the position of the object denoted by the second subscript relative to object denoted by the first subscript. Hence, $r_{\oplus\leftmoon}$ is the distance of the moon from the earth in any coordinate system. Sometimes it is desirable to emphasize the coordinate system in which the radius vector is measured. The radius vector of the vehicle from the center of the moon may be denoted by $\vec{r}_{\leftmoon\Delta}$, or, if the vector has components in a geocentric equatorial coordinate system, it may be denoted by $\vec{r}_{\oplus,\leftmoon\rightarrow\Delta}$.

In some chapters, it is possible to simplify this notation. Thus, in Chapter V, Earth Departure, most quantities refer to the earth, so the subscript "⊕" has been deleted when the reference to the earth is obvious. A similar statement can be made for Chapter VIII, Descent to and Ascent from the Lunar Surface, where the majority of symbols refer to the moon, and where the reference to the moon is obvious in most cases.

Vectors are denoted by an arrow and their components in a matrix equation by curly brackets, while unit vectors are denoted by carats. Hence,

$$\vec{r}_{\oplus\leftmoon} \equiv \begin{Bmatrix} x_{\oplus\leftmoon} \\ y_{\oplus\leftmoon} \\ z_{\oplus\leftmoon} \end{Bmatrix}$$

is a vector from the earth to the moon and $\hat{r}_{\oplus\leftmoon}$ is a unit vector at the center of the earth in the direction of the moon. Matrices are denoted by square brackets and determinants by straight lines, i.e.,

$$\begin{bmatrix} 1 & 0 & 0 \\ 0 & 1 & 0 \\ 0 & 0 & 1 \end{bmatrix}$$

is the unit matrix, and

$$\begin{vmatrix} 1 & 0 & 0 \\ 0 & 1 & 0 \\ 0 & 0 & 1 \end{vmatrix} \equiv 1$$

is a complex way of writing 1.

SYMBOLS

Latin Symbols

$A_{n, m}$	General spherical harmonic coefficient of order n and degree m
AU	Astronomical unit (unit of length, 1AU = 149.53 x 10^6 km)
a, b, c†	Semiaxes of the triaxially ellipsoidal moon
$B_{n, m}$	General spherical harmonic coefficient of order n and degree m
$C_{n, m}$	General spherical harmonic coefficient of order n and degree m
$C_{2, 2}$	Coefficient expressing the ellipticity of the equator
f	Flattening or oblateness of a planet
f'	Flattening of the lunar equator
f*	Flattening of the lunar prime meridian
G	Universal gravitational constant
g	Gravitational acceleration
g_o	Gravitational acceleration at the surface of the equivalent sphere
h	Altitude
I_a, I_b, I_c	Moments of inertia of the moon about the a, b, c axes, respectively
J_n	N-th order zonal harmonic coefficient in the expansion of the gravitational potential in terms of zonal harmonics, $J_n = -C_{n, 0}$
K	Thermal inertia constant $K = (\lambda \rho c)^{-1/2}$, see page II-12
$K_\odot$	Gaussian value of the solar gravitational constant in units of $AU^{3/2}$/ mean solar day
L'	Lunar inequality (see page II-4 and Table 4)
LU	Lunar unit (unit of length, 1 LU = 384747.2 km)
M	Mass
$\overline{M}$	Molecular weight of air
MSD	Mean solar day
P_n ( )	Legendre polynomial
P_n^m ( )	Associated Legendre polynomial
p	Pressure
R	Radius of the sphere of equivalent volume as the planet
R*	Universal gas constant, R* = 8.31470 x 10^3 joules/kg° K
R_e	Equatorial radius
R_p	Polar radius
R_ϕ	Radius of celestial body at latitude ϕ
$R_{\phi\lambda}$	Radius of celestial body at latitude ϕ and longitude λ
$\vec{r}$	Radius vector
r*	Radius of action of the planet
$\overline{r}_{\oplus\leftmoon}$	Mean earth-moon distance for the restricted three-body force model ($\overline{r}_{\oplus\leftmoon} \equiv 1$ LU = 384,747.2 km)
$\overline{r}_{\leftmoon}$	Mean lunar distance for the n-body force model ($\overline{r}_{\leftmoon}$ = 384,402 km)
S	Solar constant (total radiated power of the sun crossing an area of 1 $meter^2$ at a distance of 1 AU
T	Absolute temperature
T_i	Freezing point of water on the absolute temperature scale
t	Time, nonabsolute temperature (i.e., temperature measured on the Celsius or Fahrenheit scales)
t_i	Freezing point of water on the nonabsolute temperature scales
U	Gravitational potential
UT	Universal time (Greenwich mean time)
V	Velocity
V_p	Parabolic velocity (two-body escape velocity)
W	Radiated power per unit area
$x_G y_G z_G$	Geographic coordinate system

† In this list of symbols, coordinates in a given coordinate system have been listed together.

$x_S\ y_S\ z_S$	Selenographic coordinate system
$x_{\leftmoon}\ y_{\leftmoon}\ z_{\leftmoon}$	Selenocentric lunar equatorial system

Greek Symbols

$\alpha_p,\ \epsilon_p,\ i_p$	Photometric coordinates of the point P (see page II-11)
$\beta_{\leftmoon}$	Angle between the y_S axis and r_S
Λ_S	Phase angle between the $x_{\leftmoon}$ and x_S axes at time t = 0
λ	Inhomogeneity factor of the moon
$\lambda,\ \phi$	Longitude, geodetic longitude
$\lambda,\ \phi'$	Longitude, geocentric latitude
$\lambda_{\leftmoon},\ \phi_{\leftmoon}$	Selenographic longitude, latitude
μ	μ = GM: gravitational constant of the celestial body with mass M in laboratory units
ρ	Atmospheric density
ρ^*	Brightness factor used for albedo measurements
ρ_0^*	Normal albedo
σ	Standard deviation, Stefan-Boltzmann constant ($\sigma = 5.67 \times 10^{-8}$ watts/in.^{2} $(°K)^4$)
τ	Orbital period
$\omega_{\oplus\leftmoon}$	Mean angular velocity of the moon in its orbit around the earth
$\omega_{\oplus}$	Rotational rate of the earth around its axis
$\omega_{\leftmoon}$	Rotational rate of the moon around its axis

Subscripts and Superscipts

$\odot^{\dagger\dagger}$	Sun
$\oplus^{\dagger\dagger}$	Earth
$\leftmoon^{\dagger\dagger}$	Moon
$\Delta^{\dagger\dagger}$	Space vehicle
$\bar{\ }$	Mean value
d, h, m, s	Days, hours, minutes, seconds
°	Degrees (angular measure or temperature)

††These subscripts have been deleted if the reference to these bodies is obvious.

SYMBOLS

Latin symbols

A, ϵ *	Azimuth, elevation
a	Semimajor axis
C	Jacobian constant (constant of integration)
D = ☾ - L	Mean elongation of the moon from the sun
d	Number of ephemeris days from the epoch
EML	Earth-moon line
ET	Ephemeris time
e	Eccentricity
F = ☾ - Ω	Argument of lunar perigee plus mean anomaly of the moon
$\tilde{F}$	Hamiltonian of the dynamical system
f	True anomaly (central angle in an alliptic orbit measured from perifocus)
G	Universal gravitational constant
$g_\odot$, $\ell_\odot$, ℓ'**	Mean anomaly of the sun
$h_☾$	Altitude above mean lunar surface
I	Inclination of the mean lunar equator to the ecliptic
i	Inclination, $0° \leq i \leq 180°$
i_{em}	Inclination of the moon orbital plane (MOP) with respect to the earth's equatorial plane
$i_☾$	Inclination of the mean equator of the moon to the true equator or the earth
$i_{\epsilon m}$	Inclination of the moon's orbital plane with respect to the ecliptic
k	Variable introduced by Hansen's intermediate orbit
L, G, H, ℓ, g, h	Canonical orbital elements (Delaunay variables) defined in Subsection C-1
L	Mean longitude of the sun
ℓ	Mean anomaly (of the moon), which is simultaneously a Delaunay variable
ℓ, b	Selenographic coordinates of the earth: (total librations of the moon in longitude and latitude, respectively)
ℓ', b'	Optical librations of the moon in longitude and latitude
$\delta\ell$, δb	Physical librations of the moon in longitude and latitude
$\hat{L}$	Unit vector along the moon-earth line (MEL)
M	Mass
MCP	Mean center point of the moon
MEL	Moon-earth line
MOP	Lunar orbital plane
MST	Mean solar time
m	Parameter introduced by Hill in his lunar theory
n	Mean motion or mean angular velocity in the orbit
P_n ( )	Legendre polynomial of order n in ( )
q	Perifocus distance
R	Disturbing function
R_e	Equatorial radius of the earth
$R_☾$	Mean radius of the moon
R_ϕ	Local radius of the earth
$r_\oplus$	Distance from the center of the earth
$r_☾$	Distance from the center of the moon
$\bar{r}_{\oplus☾}$	Mean distance between the center of the earth and center of the moon
r	Orbital radius (with respect to any reference body)
S	Angle between the earth-moon and earth-sun lines at earth
ST	Sidereal time
T	Number of Julian centuries (36,525 ephemeris days) from the epoch 1900 Jan 0.5 ET
T_ω	Time of perifocal passage
T_Ω	Time of ascending nodal crossing

*In this list of symbols coordinates in a given coordinate system have been listed together.

**All three symbols have been used to denote the mean anomaly of the sun in various parts of this chapter since all three are used frequently.

t	Time
t_0	Time of epoch, which is any time reference
U	Gravitational potential, work function, or negative of the gravitational potential energy. The symbol U is also used for gravitational field strength or potential per unit mass
UT	Universal time
V	Velocity (magnitude of)
W	Total energy
$\tilde{W}$	Function introduced by Hansen (Subsection C-1)
$x_b\ y_b\ z_b$	Body axis system
$x_e\ y_e\ z_e$	Inertial orbit plane coordinate system with origin at earth
$x_G\ y_G\ z_G$	Rectangular geographic coordinate system
$x_h\ y_h\ z_h$	Topocentric horizon system
$x_m\ y_m\ z_m$	Inertial orbit plane coordinate system with origin at moon
$x_0\ y_0\ z_0$	Inertial orbit plane coordinate system with origin at barycenter of the earth-moon system
$x'_0\ y'_0\ z'_0$	Inertial orbit plane coordinate system with origin at barycenter of the earth-moon-sun system
$x_P\ y_P\ z_P$	General fixed orbit plane system
$x_R\ y_R\ z_R$	Rotating orbit plane system--general rotating coordinate system
$x_{R_{\mathbb{C}}}\ y_{R_{\mathbb{C}}}\ z_{R_{\mathbb{C}}}$	Rotating orbit plane system--coordinate system rotating with mean motion of the sun
$x_S,\ y_S,\ z_S$	Rectangular selenographic system
$x_\epsilon\ y_\epsilon\ z_\epsilon$	Geocentric ecliptic coordinates
$x_\Omega\ y_\Omega\ z_\Omega$	Fixed orbit plane system with x-axis directed to the ascending node
$x'_\oplus\ y'_\oplus\ z'_\oplus$	Geocentric equatorial system with $x'_\oplus$ directed toward true vernal equinox
$x_\omega\ y_\omega\ z_\omega$	Fixed orbit plane system with x-axis directed to perifocus
$x_\oplus\ y_\oplus\ z_\oplus$	Geocentric equatorial system with $x_\oplus$ directed toward mean vernal equinox of a specified epoch
$x_{\mathbb{C}},\ y_{\mathbb{C}},\ z_{\mathbb{C}}$	Selenocentric lunar equatorial system
$x_{\mathbb{C},\Omega}\ y_{\mathbb{C},\Omega}\ z_{\mathbb{C},\Omega}$	Selenocentric lunar equatorial system with $x_{\mathbb{C},\Omega}$ in the direction of the ascending node on ecliptic
y	Variable introduced in Hansen's intermediate orbit
z	Variable introduced in Hansen's intermediate orbit

Greek symbols

α	Constant of sine parallax of the moon
$\alpha,\ \delta$	Right ascension, declination
$\beta = \omega + f$	Angle between the mean ascending node and the instantaneous position of the vehicle
γ	Constant of inclination of the moon's orbit
Γ	Mean longitude of solar perigee in the orbit of the sun around the earth, i.e., angle in the ecliptic from the mean equinox of date to solar perigee
Γ'	Mean longitude of lunar perigee, i.e., angle in the ecliptic from the mean equinox of date to the mean ascending node of the lunar orbit and then to lunar perigee along the orbit
Δ	Angle along the mean equator of the moon from its ascending node on the true equator of the earth to its ascending node on the ecliptic of date
ϵ	Mean obliquity of the ecliptic
$\epsilon_0 = \tilde{\omega} + \ell_0$	Mean longitude at epoch t_0
θ	Orbital central angle of the moon after time t
$\theta' = \omega_{\mathbb{C}}\, t$	Angle of rotation of the moon in in time t
Λ_G	Angle between the x_e and x_G axes at t = 0
Λ_M	Angle in the moon's equatorial plane from the ascending node to the lunar prime meridian
Λ_S	Angle between the $x_{\mathbb{C}}$ and x_S axes at t = 0
$\lambda,\ \phi'$	Longitude, geocentric latitude
$\lambda,\ \phi$	Longitude, geodetic latitude

λ, ϕ^*	Longitude, astronomical latitude
λ_ϵ, β_ϵ	Celestial longitude, celestial latitude
$\lambda_{\mathbb{C}}$, $\phi_{\mathbb{C}}$	Selenographic longitude, latitude
$\lambda'_{\mathbb{C}}$	Selenographic colongitude
$\mu = GM_\oplus$	Gravitational constant of the earth
$\nu = \frac{M_{\mathbb{C}}}{M_\oplus + M_{\mathbb{C}}}$	Ratio of the mass of the moon to the total mass of the earth and moon
$\pi_{\mathbb{C}}$	Horizontal parallax of the moon
ρ	Change in I due to the physical librations of the moon
σ	Change in Ω due to the physical librations of the moon
Φ	Angle between the x_0 and x_R axes at time t = 0
ψ	Angle between the $x_{\mathbb{C}}$, Ω axis and $z_{\mathbb{C}}$, Ωx ($\overrightarrow{MEL}$ x $z_{\mathbb{C}}$, Ω)
Ω	Longitude of the mean ascending node (of the moon) measured from the mean equinox of date.
Ω'	Longitude of the mean ascending node (of the moon) measured from the true equinox
$\Omega_{\mathbb{C}}$	Right ascension of the ascending node of the mean lunar equator measured from true equinox of date along the true celestial (earth) equatorial plane
ω	Argument of perifocus, angle in the orbit plane between the ascending node and perigee
$\tilde{\omega} = \Omega + \omega$	Longitude of perifocus
ω_R	Angular velocity of the rotating orbit plane coordinate system
$\omega_\oplus$	Angular velocity of the earth about its axis
$\omega_{\mathbb{C}}$	Angular velocity of the moon about its axis
$\omega_{\oplus\mathbb{C}}$	Angular velocity of the earth-moon system about the barycenter
$\mathbb{C} = \Omega' + \omega + \ell$	Mean orbital longitude of the moon (referred to true equinox)

Subscripts and Superscripts

$\odot$	Sun
$\oplus$	Earth
$\mathbb{C}$	Moon
Δ	Vehicle
0	Initial conditions (also barycentric inertial coordinates)
h, m, s	Hours, minutes of time, seconds of time
r, °, ', "	Revolutions, degrees, minutes of arc, seconds of arc
~	Hansen's intermediate orbit

SYMBOLS

Latin symbols

A_{ref}	Constant reference area characterizing the space vehicle
A_s	Area of the vehicle perpendicular to the earth-sun line
A	Area
A_a	Area of the space vehicle perpendicular to $\vec{V}_a$
A_e	Azimuth on earth
A_Δ	Vehicle surface area
$A_\odot$	Surface area of the sun
a, b, c	Principal axes of inertia of the moon
B	Ballistic coefficient $B = \frac{C_D A_a}{2M_\Delta}$
b_m	Lunar trajectory impact parameter, or the distance between the asymptote of the hyperbolic circumlunar orbit and the center of the moon
C_D	Drag coefficient
C_i	i-th value of the Jacobi constant (restricted three-body problem)
C_L	Lift coefficient
C_x, C_y, C_z	Aerodynamic coefficients in body axes x_b, y_b, z_b, respectively
c	Speed of light, c = 299,792.5 km/sec
$\vec{D}$	Atmospheric drag force
$\vec{D}_E$	Electromagnetic (drag) forces
$\vec{D}_M$	Meteoritic drag force
$\vec{D}_S$	Force due to solar radiation pressure
E	Energy per unit mass
E_P	Energy of a photon
$\overrightarrow{EML}$	Earth-moon line
$e_\mathbb{C}$	Eccentricity of the lunar orbit
$e_{m\Delta}$	Eccentricity of the space vehicle orbit around the moon
f	Dimensionless quantity defined by Eq (69)
$\vec{f}$	Acceleration (force per unit mass)
$\vec{f}_i$	Acceleration of the space vehicle due to oblateness of the i-th celestial body
G	Universal gravitational constant
$\vec{g}$	Gravitational acceleration
h	Planck's constant, $h = 6.625 \times 10^{-34}$ joule/sec
$\vec{h}$	Angular momentum per unit mass
h_e	Altitude above the earth
h_{PE}	Return vacuum perigee altitude
h_{PL}	Pericynthion altitude
$h_\oplus$	Altitude above earth's equator
I_a, I_b, I_c	Lunar moments of inertia about the three principal axes of inertia a, b, c
i_m	Inclination of the trajectory to the moon's orbital plane
i_{em}	Inclination of the lunar orbit to the earth's equatorial plane
i_{VE}	Inclination of the vehicle with respect to the earth's equatorial plane $0 \le i_{VE} \le 180°$
i_{VTE}	Inclination of the transearth trajectory to MOP
i_{VTL}	Inclination of the translunar plane to the MOP at the time of injection
i_{VTEQ}	Inclination of the transearth trajectory to the earth's equator
J_n	Expansion coefficients in the expansion of the earth's gravitational potential (empirical constants determined by measurements)
k	Boltzmann constant $k = 1.380 \times 10^{-23}$ joule/°K
k_v	Constant of proportionality relating the gravisphere to the volume of influence
L	Aerodynamic lift force
LOR	Lunar orbit rendezvous mission (a landing technique)
LU	Lunar unit ($\equiv \bar{r}_{\oplus\mathbb{C}}$)
l, m, n*	Direction cosines
M	Mass
M_M	Total mass of meteorites striking the space vehicle from a given direction
MOP	Moon's orbital plane (x_E y_E plane)

*In this list of symbols the coordinates in a given coordinate system have been listed together.

m	Equivalent mass of a photon, also mass of molecule
N	Number of photon collisions per unit time per unit area
N_0	Number of molecules per unit volume
$\vec{n}_\Delta$	Nongravitational forces per unit mass acting on the space vehicle
$\vec{P}$	Momentum of a photon
$P_n(\ )$	Legendre polynomial of n-th order in ( )
p_s	Solar radiation pressure (force per unit area)
p_{s0}	Solar radiation pressure constant defined by Eq (81)
q	Dimensionless quantity defined by Eq (66)
q_e	Charge of an electron, $q_e = 1.602 \times 10^{-19}$ coulomb
q_s	Factor indicating the type of collision of the photon with the vehicle
R_e	Equatorial radius of the earth
R_{rel}	Relativistic corrections to the equations of motion
r, θ	Plane polar coordinates
$\vec{r}$	Radius vector
r_g	Radius of the lunar gravisphere
r_v	Radius of the lunar volume of influence
$\bar{r}_{\oplus \mathbb{(}}$	Lunar unit or earth-moon distance used in the restricted three-body problem, $\bar{r}_{\oplus \mathbb{(}} = 384747.2$ km
S, S'	Inertial coordinate systems, coordinate systems in general
T	Absolute temperature (°K)
$\vec{T}$	Rocket thrust force
$T(\ )$	Rotation matrix with angle of rotation ( )
t	Time, also total transit time to the moon
t_d	Time of departure from lunar orbit
t_e	Time of entry into lunar orbit
t_i	Impact time
t_p	Time of pericynthion (closest approach to moon)
U	Gravitational potential
U_i	Expansion terms in the earth's gravitational potential
$U_{\mathbb{(}i}$	Expansion terms in the lunar gravitational potential
$\vec{V}$	Velocity
$\vec{V}_a$	Vehicle velocity relative to the atmosphere
$\vec{V}_{\oplus a}$	Velocity of the atmosphere in the geocentric equatorial coordinate system
$V_{\oplus M}$	Average speed of the meteorites hitting the vehicle
$\bar{V}_{e\mathbb{(}}$	Average thermal speed of an electron
$(V_{e\Delta})_{max}$	Maximum restricted three-body escape speed from earth
$(V_{e\Delta})_{min}$	Minimum restricted three-body escape speed from earth
V_{ep}	Two-body escape speed from earth or parabolic velocity of the earth
V_p	Space vehicle speed relative to the plasma
Voice	Volume of influence calculated envelopes trajectory computation technique
$W_\odot$	Total radiated power by the sun
W_Δ	Radiated power per unit area arriving at the space vehicle
$x_b\ y_b\ z_b$	Body axis coordinate system with origin at the vehicle center of gravity
$x_E\ y_E\ z_E$	Trajectory coordinates with origin at the center of the earth and the x_E-axis along the intersection of the translunar trajectory plane with the MOP and in the general direction of the moon (see Fig. 4 of Chapter IV)
$x_e\ y_e\ z_e$	Trajectory coordinates with origin at the center of the earth and axes parallel to the inertial barycentric coordinate system
$x_M\ y_M\ z_M$	Selenocentric trajectory coordinate system with the y_M-axis defined by the intersection of the $x_M\ y_M$ with the $x_E\ y_E$ planes
$x_m\ y_m\ z_m$	Trajectory coordinates with origin at the center of the moon and axes parallel to the inertial barycentric coordinates
$x_0\ y_0\ z_0$	Inertial coordinate system with origin at the earth-moon system barycenter
$x_R\ y_R\ z_R$	Rotating coordinates with origin at the barycenter and the x_R-axis along the earth-moon line

$x_S\ y_S\ z_S$ Selenographic coordinate system

$x_v\ y_v\ z_v$ Vehicle-centered coordinate system with the z_v-axis in the direction of the radius vector, x_v-axis in the general direction of motion

$x_w\ y_w\ z_w$ Wind axes with origin at the center of gravity (or, alternately, the center of pressure) of the vehicle, with the x_w-axis in the direction of $\vec{V}_a$

$x_\oplus\ y_\oplus\ z_\oplus$ Geocentric equatorial coordinate system with $x_\oplus$ axis directed toward the mean equinox

$x_{\oplus 0}\ y_{\oplus 0}\ z_{\oplus 0}$ Inertial equatorial coordinate system with origin at the barycenter of the physical model chosen and $x_{\oplus 0}$ axis directed toward the mean equinox

$x_{\oplus u}\ y_{\oplus u}\ z_{\oplus u}$ Geocentric equatorial coordinates of the space vehicle in a Keplerian (unperturbed) orbit

Greek symbols

α Angle of attack

$\alpha,\ \delta$ Right ascension, declination

α_e The angle between the x_e-axis and the x_R-axis

β Relativistic correction factor (see table on p IV-37), $\beta = 1/\left(1 - \frac{V^2}{c^2}\right)^{1/2}$

β Yaw angle

$\beta_{\leftmoon}$ Angle between the y axis and $\vec{r}_{\leftmoon\Delta}$ (see sketch on p IV-24)

β_{M0} Orbital central angle of the ejection point from lunar orbit

γ_e Inertial flight path angle with respect to earth, or angle between $r_{e\Delta}$ and $\vec{V}_{e\Delta}$ minus 90°

γ_M Inertial flight path angle with respect to the moon

Δi_{VTL} Change in i_{VTL} due to lunar gravitational attraction or drift characteristic of the trajectory

Δr_g Distance from the center of the moon to the center of the lunar gravisphere

Δr_v Distance from the center of the moon to the center of the spherical lunar volume of influence

ΔV Characteristic velocity of the thrust maneuver

$\Delta V_{e\Delta 0}$ Correction to the injection velocity

ΔV_g Change in velocity due to the gravitational attraction of the moon (see sketch on p IV-12)

$\Delta\lambda_{0\leftmoon}$ Longitude difference between the injection point and the moon at impact or when $r_{e\Delta} = \bar{r}_{\oplus\leftmoon}$

ϵ Emissivity of the sun

η_e Angle between x_R and $\vec{r}_{e\Delta 0}$

η_m Angle between the moon-earth line and $r_{\leftmoon\Delta}$

$\theta,\ \phi,\ \psi$ Rotation angles from body axes to vehicle-centered equatorial coordinate axes

$\theta_{0\leftmoon}$ Total in-plane angle from injection to the lunar orbit

θ_M Angle between $(-\overrightarrow{EML})$ and the y_M axis

μ GM, gravitational constant of body with mass M

ν The reduced mass of the earth moon system; i.e., the ratio of the lunar mass to the sun of the lunar mass and earth mass $\nu = \frac{M_{\leftmoon}}{M_\oplus + M_{\leftmoon}}$

ν_p Frequency of the radiation

ξ Bank angle

$\xi_1,\ \xi_2$ Auxiliary angles defined on the sketch on page IV-18 and Eq (41)

$\xi,\ \eta,\ \zeta$ Differences between perturbed and unperturbed vehicle coordinates, i.e., $\xi_{\oplus\Delta} = x_{\oplus\Delta} - x_{\oplus u}$, etc.

ρ Atmospheric density

ρ_M Average density of meteoritic material in space

σ Stefan-Boltzmann constant, $\sigma = 5.67 \times 10^{-8} \frac{\text{watts}}{m^2\ (°K)^4}$

$\tau_{\oplus\leftmoon}$ Period of rotation of the earth-moon system

Φ The initial angle between the inertial and rotating coordinate systems, i.e., the x_0 and x_R coordinate axes, also planar angle from injection to the position of the moon at injection

Φ_Δ Electrostatic potential of the vehicle

Φ^*	Lead angle of the moon (angle from the x_E-axis to the position of the moon at injection)
ϕ'	Geocentric latitude
$\phi_{\leftmoon}$	Selenocentric latitude (see sketch on p IV-24)
ψ_0	Angle measured from the intersection of the translunar plane with the moon's orbital plane (negative $\vec{x}_E$ axis) to the injection point
Ω	Right ascension of the ascending node
$\omega_{\oplus\leftmoon}$	The rotational rate of the earth-moon line around the barycenter, $\omega_{\oplus\leftmoon} = 2.661669484 \times 10^{-6}$ rad/sec
$\omega_\oplus$	Rotational rate of the earth about its axis $\omega_\oplus = 7.292115 \times 10^{-5}$ rad/sec

Subscripts and superscripts

$\odot$	Sun
$\oplus$	Earth
$\leftmoon$	Moon
$\triangle$	Vehicle
0	Injection conditions
u	Unperturbed (Keplerian) conditions
M	Meteoritic, pertaining to meteorites

SYMBOLS*

Latin Symbols

A	Inertial launch azimuth (great circle course on a nonrotating earth) measured clockwise from geographic north
h	Altitude
h_{BO}	Booster burnout altitude (launch phase)
I_{sp}	Specific impulse
i_{em}	Inclination of the MOP (moon's orbital plane) to the earth's equator
i_{VE}	Inclination of the translunar trajectory plane (or parking orbit plane, which is assumed the same) to the earth's equator
i_{VTE}	Inclination of the transearth trajectory plane to the MOP
i_{VTL}	Inclination of the translunar trajectory plane to the MOP
L/D	Lift-to-drag ratio
MOP	Lunar orbital plane
n	Number of satellite revolutions in parking orbit to achieve the correct phase relationship to rendezvous
r	Radius
T	Thrust (earth sea level force)
t	Time
t_a	Time of ascent to parking orbit
t_{aN}	Nominal ascent time
t_N	Nominal time of arrival at apogee
t_p	Time of pericynthion (closest approach to the moon)
t_{tr}	Transfer time from the intermediate orbit to the parking orbit
V	Velocity relative to an earth
V_{req}	Required velocity
W_0	Weight of the spacecraft at the start of rocket burning (earth sea level weight)
W_f	Weight of the propellant (earth sea level weight)
$\vec{x}_E$	Vector along the intersection between the translunar trajectory plane and the MOP in the general direction opposite to the lunar position

Greek Symbols

α	Inclination of the great circle course between the ascending node of the parking orbit and the launch site
ß	Orbital central angle to be "gained" or "lost" by the spacecraft in the parking orbit
$ß_{req}$	Required central angle of the "phantom" satellite to effect rendezvous
$ß_T$	Orbital central angle of the rendezvous point
$ß_{TL}$	Angle between the ascending node of the MOP to the intersection of the translunar trajectory with the MOP
γ	Local flight path angle measured from the local horizontal to the velocity vector
Δ	Increment (in general)
ΔA	Change in azimuth, which is the turn angle of the spacecraft's velocity vector
Δt_L	Launch time tolerance
ΔV	Characteristic velocity of the maneuver
ΔV_{cap}	Characteristic velocity of the total maneuvering capability of the spacecraft
$\Delta ß'$	Central angle between the spacecraft and the phantom satellite
$\Delta ß'_{req}$	Required central angle (or phase angle) for a Hohmann transfer to a parking orbit for rendezvous
$\Delta \lambda$	Longitude increment through which the launch site moves due to the earth's rotation
$\Delta \Phi$	Required shift in the x_E-direction due to a missed injection
$\Delta \Phi'$	Range extension increment
$\Delta \psi_0$	Increment in injection position angle (measured from the $-x_E$-axis) traversed during the injection phase

*Since the spacecraft and earth are the only celestial bodies considered and all parameters are referred to earth, the subscripts "$\oplus$" and "Δ" have been deleted for conciseness; i.e., $\vec{V}_{\oplus\Delta 0}$, the injection velocity of the vehicle relative to earth becomes V_0.

δ	Central angle along the great circle course between the ascending node of the parking orbit and the launch site
ϵ	Thrust angle, measured from the velocity vector to the thrust vector
ζ	Mass ratio, $\zeta = \frac{W_f}{W_0}$
λ	Longitude
λ_{NL}	Inertial longitude of the launch site measured from the ascending node of the parking orbit
τ	Orbital period
Φ	Range angle (general)
Φ_a	Ascent range angle (from launch to injection into the parking orbit)
Φ^*	Lunar lead angle (measured from the x_E-axis to the lunar position at injection
ψ_0	Position angle at the completion of injection, measured from the $-x_E$-axis to the injection point, $\psi_0 = \psi_0' + \Delta\psi_0$
ψ_0'	Position angle at the start of injection, measured from the $-x_E$-axis to the injection initiation point
ω	Rotational rate of a satellite in circular orbit

Subscripts and Superscripts

A	Abort conditions
a	Ascent trajectory (from launch to injection into parking orbit)
i	Intermediate or waiting orbit
j	Conditions at a point during the injection burning phase
L	Launch
N	Nominal conditions
0	Injection conditions
P	Parking orbit
R	Re-entry conditions

SYMBOLS

Latin Symbols

A	Angle at the space vehicle between the radius to earth to the radius to the moon
A_e	Inertial launch azimuth on earth
A^*	Angle between the edge of the lunar disc and a star
a	Semimajor axis
c	Velocity of light in vacuo, c = 299,792.5 km/sec
D	Apparent diameter of the moon
$\overrightarrow{EML}$	Earth-moon line
ER	Earth radius, unit of length with 1 ER = 6378.163 km
e	Eccentricity
h	Altitude
h_{PE}	Return vacuum perigee altitude
h_{PL}	Pericynthion altitude (altitude above the lunar surface at the point of closest approach to the moon)
i_m	Inclination of the vehicle orbit around the moon to the MOP
i_{VE}	Inclination of the translunar trajectory and earth parking orbit to the earth's equatorial plane
i_{VTE}	Inclination of the transearth trajectory plane to the MOP
i_{VTEQ}	Inclination of the transearth trajectory plane to the earth's equatorial plane
i_{VTL}	Inclination of the translunar trajectory plane to the moon's orbital plane
$\overrightarrow{MEL}$	Moon-earth line
MOP	Moon's orbital plane
$\hat{m}$	Unit vector from the space vehicle toward the earth
n	Number of the abort way-station, which is equivalent to the number of sidereal days or complete earth rotations
$\hat{n}$	Unit vector from the space vehicle toward a star
$\hat{n}'$	Unit vector from the space vehicle toward the moon
R	Radius in units of ER
$R_\oplus$	Radius of the equivalent spherical earth, $R_\oplus$ = 6371.02 km
$R_\leftmoon$	Radius of the equivalent spherical moon, $R_\leftmoon$ = 1738.16 km
$R_{\oplus\leftmoon}$	Earth-moon distance in units of ER
$\vec{r}$	Radius vector (from the center of the earth)
$\hat{s}_1$, $\hat{s}_2$	Unit vectors from the space vehicle in the direction of stars 1 and 2, respectively
T	Total flight time in a circumlunar trajectory, measured from injection to return vacuum perigee
t	Time
t_p	Flight time to pericynthion
t_R	Time from the decision to abort the mission to re-entry
V	Velocity
V_p	Parabolic velocity (two-body earth escape speed)
$x_E\ y_E\ z_E$ †	Geocentric nonrotating Voice coordinate system
$x_P\ y_P\ z_P$	Orbit plane coordinate system illustrated in the sketch on p VI-12
$x_R\ y_R\ z_R$	Rotating rectangular coordinate system of the restricted three-body problem discussed in Subsection B-2 of Chapter III
$x_v\ y_v\ z_v$	Vehicle-centered coordinate system, with the z_v-axis in the direction of the local vertical, the x_v-axis along the local horizontal in the flight direction; the y_v-axis completes the right-handed Catesian system by defininin a lateral direction.

Greek Symbols

β_M	Orbital central angle of the pericynthion point, measured positively toward the north from the descending node of the orbit relative to the MOP

†In this list of symbols the coordinates of a particular coordinate system have been listed together.

γ	Apparent angular diameter of the moon
γ_0	Flight path angle at translunar injection (angle between the local horizontal and the velocity vector)
ΔA	Change in azimuth during the abort maneuver
ΔP	Angular error in the line of position, which is the radius vector from the prime body to the space vehicle
Δt	Time increments for timing abort defined on p VI-26
ΔV	Equivalent velocity impulse to enter a circular orbit around the moon from the circumlunar trajectory
ΔV_A	Equivalent velocity impulse of the abort maneuver
ΔV_p	Midcourse guidance correction required to correct the position of the pericynthion point
ΔV_{TOT}	Total midcourse guidance correction
ΔV_v	Midcourse guidance correction required to reorient the velocity vector at pericynthion
$\Delta \Phi_R$	Range angle of the required longitudinal maneuverability from reentry
ϵ	Angle between the vehicle velocity vector before and after the abort maneuver
θ_M	Angle between the $\overrightarrow{EML}$ and the descending node of the lunar orbit with respect to the MOP
$\lambda_{\leftmoon}, \phi_{\leftmoon}$	Selenographic longitude, latitude
$\hat{\rho}$	Unit vector perpendicular to $\hat{n}$
σ_1, σ_2	Angle between $\vec{r}_{\oplus\Delta}$ and stars 1 and 2, respectively
σ_s	Angle between $\hat{s}_1$ and $\hat{s}_2$
Φ^*	Moon lead angle (angle from the lunar position to the x_E-axis measured in the MOP at the time of translunar injection)
Φ_A, Φ_R, Φ_0	Range angles for timing abort, defined on p VI-27
ψ_0	Angle between the $-x_E$-axis and the injection point measured in the translunar trajectory plane

Subscripts and Superscripts

A	Abort trajectory and maneuver conditions
0	Injection conditions
T	Translunar trajectory conditions prior to the abort maneuver
TE	Transearth trajectory conditions
TL	Translunar trajectory conditions
'	Denotes desired conditions (i.e., other than catalogued conditions)
$\oplus$ ††	Earth
$\leftmoon$ ††	Moon
Δ ††	Space vehicle

††These subscripts have been omitted when reference to the respective body is obvious

SYMBOLS*

Latin Symbols

a	Semimajor axis
$C_{2,2}$	Second-order, second degree harmonic coefficient in the expansion of the gravitation potential U in terms of spherical harmonics
C_2	A particular value of the Jacobi constant (see also Chapter III)
$\vec{D}$	Atmospheric drag force
ER	Earth radii (unit of length, 1 ER = 6378.163 km)
e	Eccentricity
$\vec{F}$	Gravitational force
f	True anomaly
G	Universal gravitational constant
$g_{\oplus 0}$	Average acceleration due to gravity at earth sea level (conversion factor from absolute to gravitational units)
$g_{\leftmoon}$	Acceleration due to moon's gravity
h	Altitude
h_{PL}	Pericynthion altitude
I_{sp}	Specific impulse
i**	Orbital inclination (general)
i_m	Inclination of lunar orbit with respect to the MOP
i_{VTE}	Inclination of the transearth trajectory to the MOP
i_{VTL}	Inclination of the translunar trajectory to the MOP
J_2	Second-order zonal harmonic coefficient in the expansion of the gravitational potential U in terms of spherical harmonics
LR	Lunar radii (unit of length, 1 LR = 1738.16 km)
ℓ	Mean anomaly
M	Mass
M_0	Initial space vehicle mass
M_e	Final space vehicle mass
MOP	Moon's orbital plane
m	$m = \frac{2\pi/\tau_0}{\omega_{\leftmoon}}$, ratio of the angular velocity of the lunar satellite in its orbit to the rotational rate of the moon about its axis
p	Semi-latus rectum
$R_{\oplus\leftmoon}$	Earth-moon distance in units of ER
$R_{\leftmoon}$	Radius or the equivalent spherical moon, $R_{\leftmoon}$ = 1738.16 km
R	Radius of moon in direction of earth
$\vec{r}$	Radius vector
r_0	Average orbital radius for unperturbed orbits, equivalent to the semi-latus rectum of the unperturbed orbit
$\bar{r}_0$	Average orbital radius if oblateness effects are taken into account
r_{PL}	Pericynthion radius (the pericynthion is the point of closest approach to the moon)
r_S	Distance from the origin in the selenographic coordinate system
$r_{\leftmoon}$	Distance from the origin in the selenocentric coordinate system
T	Thrust
t	Time
t_b	Total rocket burning time
U	Gravitational potential
$V_{\leftmoon c}$	Circular orbit velocity for an orbit around the moon
W_0	Initial space vehicle weight
$\dot{W}_f$	Propellant weight flow rate
x_S, y_S, z_S***	Coordinates in selenographic coordinate system
$x_{\leftmoon}, y_{\leftmoon}, z_{\leftmoon}$***	Coordinates in selenocentric coordinate system

*The moon symbol "☾" has been deleted in many cases where the reference to the moon of that particular quantity is obvious.

**In this chapter i refers primarily to the orbital inclination with respect to the lunar equator.

***In this list of symbols the coordinates in a given coordinate system have been listed together.

Greek Symbols

β	Orbital central angle measured along the orbit from the ascending node, $0° \leq \beta < 360°$
γ	Flight path angle with respect to the lunar local horizontal
$\Delta r_{\leftmoon}$	$\Delta r_{\leftmoon} = r_{\leftmoon} - r_{\leftmoon 0}$, difference in radius between a perturbed and a Keplerian orbit
ΔV	Equivalent velocity increment of the orbit entry or departure maneuver
$\Delta\lambda_{N\Delta}$	Longitude of the subsatellite point relative to the ascending node
$\Delta\lambda_{\leftmoon}$	Longitudinal shift between two successive satellite ground tracks
$\Delta\tau_\beta$	$\Delta\tau_\beta = \tau_\beta - \tau_0$, difference between the nodal and Keplerian periods
δ_S	Declination of the subsatellite point
θ_{MTL}	Angle between the earth-moon line and the line toward the descending node of the lunar orbit
Λ_S	Angle between the $x_{\leftmoon}$ and x_S axes at time t = 0
λ_{AN}	Selenographic longitude of the ascending node
$\lambda_{\leftmoon}, \phi$	Selenographic longitude, latitude
μ	$\mu = GM$, gravitational constant of the celestial body with mass M
$\rho_{\leftmoon SL}$	Atmospheric density at the surface of the moon
$\rho_{\oplus SL}$	Earth sea level atmospheric density
σ_c	Predicted instrument reading
σ_R	Instrument reading
τ	Orbital period
τ_0	Keplerian orbital period
τ_r	Anomalistic period for a perturbed orbit
τ_β	Nodal period for a perturbed orbit
$\Phi_{\leftmoon}$	$\Phi_{\leftmoon} = U_{\leftmoon} - \frac{\mu_{\leftmoon}}{r_{\leftmoon}}$, potential of the perturbating gravitational force; perturbation potential; perturbing function
Ω	Longitude of the mean ascending node
Ω'	Longitude of the instantaneous ascending node
ω	Argument of perifocus (angle in the orbital plane from the ascending node to the perifocus)
$\omega_{\leftmoon}$	Rotational rate of the moon about its axis $\omega_{\leftmoon} = 2.661699484 \times 10^{-6}$ rad/sec

Subscripts and Superscripts

0	Denotes value for unperturbed (Keplerian) orbit
$\odot$	Sun
$\oplus$	Earth
$\leftmoon$	Moon
Δ	Space vehicle
$\bar{\ }$	Average value of a quantity if oblateness effects are taken into account

SYMBOLS*

Latin Symbols

a	Acceleration
f_0	Thrust acceleration or thrust-to-mass ratio $f_0 = \frac{T}{M_0}$
F_τ, F_σ	Tangential forces, normal forces in a two-dimensional trajectory
$g_{\oplus 0}$	Acceleration due to earth gravity at sea level
$g_\mathbb{C}$	Acceleration due to lunar gravity
$\bar{g}_\mathbb{C}$	Average value of $g_\mathbb{C}$
$g_{\mathbb{C}0}$	Acceleration due to lunar gravity at the surface of the moon
H	Hamiltonian function
h	Altitude above the lunar surface
h_A	Abort altitude
h_{AL}	Apocynthion altitude (farthest departure from the moon)
h_{PL}	Pericynthion altitude (closest approach to the moon)
h_{BO}	Burnout altitude (on a lunar ascent trajectory)
I_{sp}	Specific impulse (earth sea level value)
LM	Landing module (entire translunar space vehicle lands on the lunar surface, sometimes also applied to the shuttle)
M	Instantaneous total mass of the vehicle
M_f	Fuel mass
M_0	Initial total mass of the vehicle
M_p	Total propulsion system mass (less fuel mass)
$\dot{M}$	Mass flow rate, or rate of fuel expenditure by rocket engine
MOM	Lunar orbital module
MOP	Moon's orbital plane
p	Maximum resistive pressure at impact
P	Maximum penetration depth of a hard impact spike
$\vec{r}$	Radius vector
$R_\mathbb{C}$	Lunar radius
t	Time
t_b	Burning time
t_t	Tilt time
$\vec{T}$	Thrust vector (earth sea level force)
$\vec{u}$	Control vector with control variables as components
V	Velocity in a nonrotating coordinate system
V_{ex}	Rocket exhaust velocity
V_i	Impact velocity
W	Vehicle weight (earth sea level weight)
W_0	Vehicle weight at initiation of burning (earth sea level weight)
W_f	Weight of propellant expended (earth sea level weight)
x_ℓ, y_ℓ **	Trajectory coordinate system with origin at the subsatellite point on the lunar surface
x, z	Trajectory coordinate system defined in Subsection B-2e
$x_t y_t$	Inertial two-dimensional trajectory coordinate system with origin at the center of the moon with x_t in the lunar equatorial plane and y_t toward the northernmost point of the descent plane
$x_{\ell t}$	Total horizontal distance of translation
x_t, y_t, z_t	Inertial three-dimensional trajectory coordinate system with unspecified rotation
$\vec{X}$	State vector describing the behavior of the system

*In most cases the subscript "$\mathbb{C}$" has been deleted since the symbols are referred to the moon, i.e., $\gamma_\mathbb{C}$, the flight path angle with respect to the local horizontal at the moon is denoted by γ, $h_{\mathbb{C}\,BO}$, the burnout altitude on the moon is denoted by h_{BO}, etc.

***In this list of symbols, coordinates in a given coordinate system have been listed together.

Greek Symbols

α	Orbital central angle describing a safe abort window
β	Orbital central angle
γ	Flight path angle with respect to local horizontal
γ_t	Flight path angle with respect to inertial axes
ΔV	Characteristic velocity of the maneuver $\Delta V = -V_{ex} \ell n\,(1-\zeta)$
ΔV_A	Characteristic velocity of the abort maneuver
ΔV_c	Characteristic velocity of the circularizing maneuver in the abort trajectory
ζ	Mass ratio $\zeta = \frac{W_f}{W_o}$
Θ	Orbit departure angle (angle from deorbit to pericynthion of the descent trajectory)
θ	Thrust vector angle with respect to local horizontal (also referred to as pitch angle)
$\bar{\theta}$	Thrust vector angle with respect to the inertial $(-x_t)$-axis, $\bar{\theta} = 180° - \theta_t$
θ_t	Thrust vector angle with respect to inertial x_t - axis (also referred to as inertial pitch angle)
$\mu_{\mathbb{C}}$	$\mu_{\mathbb{C}} = GM_{\mathbb{C}}$ the gravitational constant of the moon
ξ	Separation angle (orbital central angle between the LM and the MOM)
τ	Orbital period (Keplerian orbit), also used to denote final time
Φ	Range angle in the trajectory plane
Φ_b	Range angle from the end of ascent burning to orbit injection
Φ_0	Range angle from lunar lift-off to lunar orbit injection
Φ_d	Range angle from lunar deorbit to initiation of the braking maneuver
ϕ_t	Roll angle
ψ_t	Yaw angle
ω	Trajectory constant $\omega = \left[\mu_{\mathbb{C}} / R_{\mathbb{C}}^3\right]^{1/2}$
ω_{vc}	Command pitch rate
ω_{wc}	Command yaw rate

Subscripts and Superscripts

A	Abort
c	Command
f	End conditions (sometimes used for denoting propellant)
j	j^{-th} rocket burning phase during descent
nom	Nominal conditions
t	Total, or referring to the inertial $x_t y_t z_t$ coordinate system
0	Initial conditions
$\mathbb{C}$	Moon (when the reference to the moon is obvious this symbol will be deleted)
Δ	Vehicle (when the reference to the vehicle is obvious this symbol will be deleted)

CHAPTER IX

SYMBOLS

Latin Symbols

$\overrightarrow{EML}$	Earth-moon line
ER	Earth radii (unit of length, 1 ER = 6378.163 km)
h_0*	Translunar injection altitude (relative to earth)
h_{PE}	Vacuum perigee altitude of the transearth trajectory
h_{PL}	Pericynthion altitude, also transearth injection altitude
i_m	Inclination of the vehicle orbit to the MOP
i_{VTE}	Inclination of the transearth trajectory plane to the MOP, $-180° \leq i_{VTE} \leq 180°$
i_{VTL}	Inclination of the translunar trajectory plane to the MOP $-180° \leq i_{VTL} \leq 180°$
$\overrightarrow{MEL}$	Moon-earth line
MOP	Lunar orbital plane
$R_{\leftmoon}$	Radius of the moon (the radius of the equivalent spherical moon)
$R_{\oplus\leftmoon}$	Earth-moon distance measured in units of earth radii (ER)
$r_{\leftmoon\Delta}$	Orbital radius of the circular lunar orbit
t	Time
t_p	Flight time from transearth injection near the moon to vacuum perigee
V_0	Translunar injection velocity (relative to a nonrotating geocentric coordinate system)
$V_{\leftmoon 0}$	Injection velocity into the transearth trajectory
$V_{\leftmoon c}$	Velocity of the vehicle in the circular lunar orbit
$V_{\leftmoon\Delta}$	Vehicle selenocentric velocity (nonrotating coordinate system)
$V_{\oplus\Delta}$	Vehicle geocentric velocity
$V_{\oplus\leftmoon}$	Geocentric velocity of the moon
x_v, y_v, z_v**	Vehicle-centered coordinate system defined in Subsection B-2
$x_{\leftmoon}, y_{\leftmoon}, z_{\leftmoon}$	Selenocentric (nonrotating) coordinate system

*The earth symbol has been omitted from the translunar injection conditions.

Greek Symbols

β_M	Orbital central angle of the vehicle in lunar orbit $-180° \leq \beta_M \leq 180°$, measured positively toward north from the descending node
$\gamma_{\leftmoon}$	Flight path angle with respect to the lunar local horizontal
γ_0	Translunar injection flight path angle with respect to the local horizontal on earth
ΔV	Equivalent velocity impulse of the transearth injection maneuver
ΔV_p	Midcourse guidance velocity correction for future position changes
ΔV_{TOT}	Total midcourse guidance velocity correction
ΔV_v	Midcourse guidance velocity correction
θ_M	Angle in the MOP between the $\overrightarrow{EML}$ and the line toward the descending node $-180° \leq \theta_M \leq +180°$ measured positively toward the east. This angle is similar to the orbital element "longitude of the ascending node"
ψ_0	Translunar injection position measured in the translunar trajectory plane from its intersection with the MOP to the injection position

Subscripts and Superscripts

0	Injection conditions
TE	Transearth
TL	Translunar

**In this list of symbols coordinates in a given coordinate system have been listed together.

SYMBOLS

Latin Symbols

A	Aerodynamic reference area of the vehicle
A_H	Aerodynamic heating reference area
B	Ballistic coefficient, $B = \frac{C_D A}{2M}$
B_{eff}	Effective ballistic coefficient (i.e., if the oblateness and dispersions of the atmosphere is absorbed in the ballistic coefficient
C_D	Drag coefficient
C_L	Lift coefficient
C_R	Resultant aerodynamic force coefficient
D	Drag
F_{PE}	Perigee parameter defined by Eq (4b)
g	Local acceleration due to gravity
g_0	Acceleration due to gravity at sea level (conversion factor from mass to weight in a gravitational system)
h	Altitude
h_{max}	Apogee altitude of the skip trajectory
h_{PE}	Vacuum perigee altitude
h_{PL}	Pericynthion altitude (closest approach to the moon)
I_{sp}	Specific impulse of fuel
i_m	Inclination of the vehicle orbit to the MOP
i_{VE}	Inclination of the vehicle orbit to the earth's equator
i_{VTE}	Inclination of the transearth trajectory plane to the MOP
i_{VTL}	Inclination of the translunar trajectory plane to the MOP
J_2	Second-order zonal harmonic coefficient in the expansion of the earth's gravitational potential in terms of zonal harmonics
k	Number of satellite revolutions during which satellite period dispersions occur
L	Lift
L/D	Lift-to-drag ratio
M	Mass
$\overline{M}$	Molecular weight of the atmosphere
MOP	Moon's orbital plane
m	Number of days
N	Number of satellite revolutions with N = 1.0 at the first ascending node
n	Number of satellite revolutions
p	Integral number of satellite revolutions
Q_H	Total heat transfer to the vehicle
q	Dynamic pressure, $q = \frac{1}{2}\rho_\infty V^2$
q_H	Heating rate of the vehicle
$\vec{R}$	Resultant aerodynamic force $\vec{R} = \vec{L} + \vec{D}$
R^*	Gas constant, $R^* = 8.31439 \times 10^3$ joules/°K - kg
$R_\oplus$	Radius of the equivalent spherical earth
R_e	Equatorial radius of the earth
R_{lat}	Lateral range (measured perpendicular to the re-entry trajectory)
R_{long}	Longitudinal range
r	Radius
T	Total flight time for a circumlunar trajectory (time from translunar injection to earth-return vacuum perigee); also, temperature measured in degrees Kelvin
t	Time
t_d	Descent time (time from deorbit to landing)
t_R	Total time to re-enter (time from re-entry to landing)
u, v	Horizontal and vertical velocity components (see sketch on page X-3)
$\bar{u}$	Independent variable introduced by Chapman which has the physical meaning of a dimensionless horizontal velocity parameter which gives horizontal velocity as a fraction of circular satellite velocity, $\bar{u} = \frac{u}{\sqrt{gr}} = \frac{u}{V_c}$

V	Velocity
V_c	Circular velocity
V_p	Parabolic velocity
$(\overline{V}_R)_i$	Re-entry velocity parameter $(\overline{V}_R)_i = \left(\frac{V_R}{\sqrt{gr}}\right)_i = \left(\frac{V_R}{V_c}\right)_i$
W	Weight
Z	Dependent variable introduced by Chapman and defined by Eq (3)

Greek Symbols

β	Logarithmic density gradient of the atmosphere $\beta = -\frac{d}{dr}(\ell n \rho_\infty)$
β_e	Orbital central angle during ballistic flight
γ	Flight path angle (angle between the local horizontal and the velocity vector)
ΔA	Change in azimuth
ΔV	Equivalent velocity impulse of the maneuver
ΔV_d	Equivalent velocity impulse of the deorbit maneuver
$\Delta \tau_d$	Dispersions in the orbital period
ζ	Mass ratio $\zeta = \frac{M_f}{M_0}$
θ_M	Angle between the earth-moon line and the descending node of the lunar orbit on the MOP
λ, ϕ'	Longitude, geocentric latitude
μ	Gravitational constant of the earth
ξ	Bank angle
ρ, ρ_∞	Atmospheric density; also referred to as free-stream density
τ_β	Nodal period (time from one ascending nodal crossing to the next)
Φ_c	Central angle from re-entry to landing
$\dot{\Omega}$	Regression rate of the ascending node
$\omega_\oplus$	Rotational rate of the earth around its axis

Subscripts and Superscripts

b	Ballistic flight conditions
e	Atmospheric exit conditions for a skip re-entry
f	Landing site conditions
PE	Vacuum perigee conditions
R	Re-entry conditions
0	Initial conditions in the parking orbit on earth return
$\oplus$ †	Earth

†The earth symbol has been deleted in the cases when the reference to earth is obvious.

SYMBOLS

Latin Symbols

A	Inertial azimuth on earth, $0° \leq A < 360°$, measured from geographic north
C_0, D_0, E_0	Constants appearing in empirical Eqs (21) and (22)
$\overrightarrow{EML}$	Earth-moon line
EOP	Earth's orbital plane
ER	Earth radii (a unit of length, 1 ER = 6378.163 km)
$\overrightarrow{ESL}$	Earth-sun line
$\overrightarrow{GW}$	Vector from the center of the earth to the intersection of the Greenwich meridian with the earth's equator (or the MOP or the ecliptic)
h	Altitude
h_{PE}	Vacuum perigee altitude
h_{PL}	Pericynthion altitude (pericynthion = point of closest approach to the moon)
i	Phase angle (see Section B)
i_{em}	Inclination of the MOP relative to the earth's equatorial plane
i_{MOP}	Inclination of the true lunar orbital plane (MOP) with respect to the true lunar equator
i_m	Inclination of the vehicle in lunar orbit to the MOP
$(i_T)_{MOP}$	Inclination of the morning terminator relative to the MOP
i_T	Inclination of the morning terminator relative to the lunar equator
i_{VE}	Inclination of the vehicle relative to the earth's equator
i_{VM}	Inclination of the vehicle in lunar orbit relative to the true lunar equator
i_{VTE}	Inclination of the transearth trajectory to the MOP
i_{VTEQ}	Inclination of the transearth trajectory to the earth's equator
i_{VTL}	Inclination of the translunar trajectory to the MOP
$\hat{K}(K_1, K_2, K_3)$	Unit vector from the center of the moon to a specific lunar feature, with components K_1, K_2, K_3 in the x_{MOP}, y_{MOP}, z_{MOP} directions, respectively
$\hat{L}$	Unit vector in the MOP defining the required value of θ_M
ℓ, b	Lunar librations in longitude and latitude (selenographic coordinates of the earth)
$\ell_\odot$, $b_\odot$	Selenographic coordinates of the sun
$\overrightarrow{MCP}$	Mean center point (vector from the center of the moon in the direction of the mean center point)
$\overrightarrow{MEL}$	Moon-earth line (vector from the center of the moon to the center of the earth)
MOP	Moon's orbital plane
$\overrightarrow{MSL}$	Moon-sun line (vector from the center of the moon to the center of the sun)
R	Radius measured in units of ER
$R_M \equiv R_{\oplus\leftmoon}$	Earth-moon distance in units of ER
r	Radius
T	Julian date; also, total flight time for a circumlunar trajectory (time from translunar injection to return vacuum perigee)
t	Time
t_E	Time of transearth injection
t_p	Flight time to pericynthion from translunar injection
t_R	Time at re-entry
UT	Universal time
V	Velocity
V_p	Parabolic or two-body earth escape velocity
x_M, y_M, z_M*	Selenocentric trajectory coordinate system (see Chapter IV, Section C)
x_{MOP}, y_{MOP}, z_{MOP}	Selenocentric nonrotating coordinate system with the x_{MOP}-axis defining the intersection of the true MOP with the true lunar equator

* In this list of symbols, coordinates in a given coordinate system have been listed together.

x_S, y_S, z_S	Selenographic coordinate system
$x_\oplus, y_\oplus, z_\oplus$	Geocentric equatorial (nonrotating) coordinate system
$x_{\oplus\leftmoon}, y_{\oplus\leftmoon}, z_{\oplus\leftmoon}$	Geocentric equatorial position of the moon
$x_{\oplus\odot}, y_{\oplus\odot}, z_{\oplus\odot}$	Geocentric equatorial position of the sun

Greek Symbols

β	Angle measured from the x_{MOP}- axis to the $\overrightarrow{MEL}$
β_L	Orbital central angle of the launch site measured positively northward from the ascending node
β_{M0}	Transearth injection position from lunar orbit, or orbital central angle of the vehicle in the lunar orbit, measured positively toward north from the ascending node
β_0'	Orbital central angle of the translunar injection point, measured positively northward from the ascending node
$\beta_\leftmoon$	Orbital central angle of the moon, measured from the ascending node of the lunar orbit around earth, $0° \leq \beta_\leftmoon < 360°$
γ	Flight path angle relative to the local horizontal on earth
ΔV	Equivalent velocity impulse to decelerate into or accelerate from lunar orbit
ΔV_i	Equivalent velocity impulse to change i_{VTE} by Δi_{VTE}
ΔV_{TE}	Equivalent velocity impulse to change the time of arrival at vacuum perigee by Δt
$\Delta\lambda$	Longitude increment, $\Delta\lambda$ with various subscripts and their interpretations given in the text and sketches of Section G
$\Delta\phi$	Required shift in the x_E- direction (which defines the intersection of the translunar or transearth trajectory plane with the MOP)
δ	Angle measured from the $\overrightarrow{MCP}$ to the x_{MOP}- axis
$\delta_M \equiv \delta_\leftmoon$	Declination of the moon
ϵ_T	Selenographic longitude of the morning terminator, measured positive to the west
$(\epsilon_T)_{MOP}$	Longitude of the morning terminator, measured in the MOP from the $\overrightarrow{MEL}$
ζ	Hour angle, measured in the earth's equatorial plane westward from the midnight meridian to the ascending node of the lunar orbit around the earth
θ	Angle from the sun-earth line to the instantaneous position of the moon, projected into the ecliptic plane
θ_M	Angle in the MOP between the $\overrightarrow{EML}$ and the line toward the descending node, measured positively to the east
λ, ϕ'	Longitude, geocentric latitude
$\lambda_{MOP}, \phi_{MOP}$	Lunar longitude, latitude defined with respect to the $\overrightarrow{MEL}$ and the MOP
$\lambda_\leftmoon, \phi_\leftmoon$	Selenographic longitude, latitude
ξ	Auxiliary angle defined in Section G
Φ_{LO}	Range angle from launch to injection in the earth parking orbit
ψ_0	Angle measured from the intersection of the translunar trajectory plane with the MOP to the injection point
Ω_{MOP}	Longitude of the ascending node relative to the MOP, or angle in the true lunar equator, measured from the intersection with the MOP to the ascending node of the orbit
$\omega_\leftmoon$	Rotational rate of the moon about its axis
$\omega_{\oplus\leftmoon}$	Angular velocity of the moon in its orbit around earth

Subscripts and Superscripts

adj	adjusted
d, h, m, s	days, hours, minutes of time, seconds of time
L	Launch
0	Injection
PE	Return vacuum perigee
TE	Transearth
TL	Translunar
$\odot$	Sun

⊕ Earth

☾ Moon

△ Space vehicle

INDEX

(A)

	Page
Abort, lunar landing,	VIII-25-32
to preselected landing site,	VI-24
translunar,	VI-22-27
in translunar injection,	V-19-21
to the vicinity of the moon,	VI-22
way-stations,	VI-25
Allunar trajectories,	IV-7-9
Approach trajectories,	IV-6-7
Ascent to and descent from the lunar surface,	VIII-1-34
abort, lunar landing,	VIII-25-32
ascent from lunar surface,	VIII-18-21
descent to the lunar surface,	VIII-1-18
direct,	VIII-1-10
indirect,	VIII-10-18
guidance laws,	VIII-9, 12
hovering,	VIII-21-25
optimization, trajectory,	VIII-8, 15
references,	VIII-32
translation,	VIII-2-25
Astronautical constants,	II-1-10

(B)

Bibliography (Chapter 12)

Braking for re-entry, (sec re-entry)

(C)

Call down, assumptions,	X-19
equations,	X-21
Catalogue, generalization of circumlunar data,	VI-4
injection conditions, and accuracy,	VI-5

Page

Circumlunar envelopes, ... XI-8
Circumlunar trajectories, ... IV-7-9
Circumlunar trajectory catalogue, ... VI-1
Constants, astronautic, ... II-1-10
Conversion data, ... II-20-27
Conversion of trajectory data, ... XI-5
Coordinate systems, ... III-1-13
Corridor, reentry, ... X-5

(D)

Declaration of the moon, ... XI-5
Delauney lunar theory, ... III-22
Departure, earth, ... V-1-21
  abort, in translunar injection, ... V-19-21
  injection, abort, ... V-19-21
    propulsion system requirements, ... V-13-19
    translunar, ... V-14-21
    tolerance, ... V-15
  launch tolerance, direct ascent, ... V-2-6
    indirect ascent, ... V-7-12, 14
  trajectory, translunar, fixed technique, ... V-2-12
    variable technique, ... V-12-14
Departure from lunar orbit, ... VII-9-11
Descent to lunar surface, ... VIII-1-18
  direct, ... VIII-1-10
  indirect, ... VIII-10-18
Determining lunar orbits, ... VII-11-12

(E)

Earth centered coordinates, ... III-1-2
Earth departure, ... V-1-21

Page

Earth-moon system, ... III-1-35
coordinate systems, ... III-1-13
earth centered, ... III-1-2
ecliptic, ... III-3
equatorial, ... III-2
geographic, ... III-1
selenographic, ... III-3-10
topocentric, ... III-2
trajectory-based, ... III-10
vehicle-centered, ... III-13
Voice, ... III-12
geometry of earth-moon system, ... III-1-13
lunar, theory, ... III-22-30
maps, lunar, ... III-12
moon, librations of, ... III-30-34
motion of, ... III-22-34
motion in earth-moon space, ... III-14-22
references, ... III-34-35
three-body problem, ... III-14-17
restricted, ... III-17-22
Earth return (see return, earth),
Ecliptic coordinates, ... III-3
Entry into lunar orbit, ... VII-9-11
Environmental data, ... II-10-20
Equatorial coordinates, ... III-2

(F)

Force models for trajectory computation, ... IV-13-39

(G)

Geographic coordinates, ... III-1
Geometry of earth-moon system, ... III-1-13

Page

Ground traces of lunar orbits, ... VII-7
Guidance concepts, earth-moon transfer, ... VI-18
Guidance laws, ascent and descent, ... VIII-18-21

(H)

Hansen lunar theory, ... III-25
Hill-Brown lunar theory, ... III-26
Hovering, ... VIII-21-25

(I)

Impact trajectories, ... IV-7
Injection, translunar, ... V-14-21
  tolerance, ... V-15
  propulsion system requirements, ... V-18-19
  abort, ... V-19-21
Injection requirements for lunar trajectories, ... VI-1-7

(L)

Landing, soft, ... VIII-1
Landing at a specific earth site, ... X-1-2
Landing missions, ... IV-9-11
Launch tolerance, direct ascent, ... V-2-6, 12-14
  indirect ascent, ... V-7-12, 14
Librations, ... III-30-34
Lunar exploration programs, ... II-27-32
Lunar orbit, ... VII-1-13
  characteristics, ... VII-1-9
  determination, ... VII-11-12
  entry and departure maneuvers, ... VII-9-11
  ground traces, ... VII-7
  missions, ... VII-1
  perturbations, ... VII-2
  stability, ... VII-7

Page

Lunar orbit missions, ... IV-9
Lunar passage and escape, ... IV-11
Lunar probes, ... IV-2-7
Lunar terminator, ... XI-3-5
Lunar theory, ... III-22-30

(M)

Many body trajectories, ... IV-21-29
Maps, lunar, ... III-10
Midcourse, guidance and energy requirements, ... VI-15-22
  methods for determining correction, ... VI-16
Mission planning, ... XI-1-29
  auxiliary data for use in mission planning, ... XI-7
  circumlunar envelopes, ... XI-8
  conversion of general trajectory data to specific dates, ... XI-5
  declination, radial distance, and phases of the moon, . . XI-5
  empirical equations for use in mission planning, ... XI-6
  lunar terminator, ... XI-3-5
  mission planning envelopes, ... XI-8-9
  references, ... XI-29
  required orientation of translunar and transearth trajectories relative to the MOP, ... XI-1-3
  sample missions, ... XI-9-29
    lunar reconnaissance mission, ... XI-24-29
    manned lunar mission, ... XI-9-24
  transearth or translunar envelopes, ... XI-8
Moon-to-earth transfer, ... IX-1-9
Moon, librations of, ... III-30-34
  motion of, ... III-22-34
Motion in earth-moon space, ... III-14-22
Motion, equations of, ... III-17

(N)

	Page
Navigation, techniques,	VI-7-13
observational considerations,	VI-7
Navigational and trajectory requirements,	VI-7-13
Nomenclature for circumlunar trajectories,	IV-11-13
Non-gravitational forces,	IV-29-38

(O)

Optimization, trajectory,	VIII-8, 15

(P)

Perturbations of lunar orbits,	VII-2
Phases of the moon,	XI-5
Physical data,	II-1-42
astronautical constants,	II-1-10
adopted constants,	II-10
geocentric constants,	II-4-5
heliocentric constants,	II-1-10
planetocentric constants,	II-2-4
selenocentric constants,	II-5-10
environmental data,	II-10-20
cislunar space,	II-15-20
near earth,	II-11-15
references,	II-33-34
summary of lunar exploration programs,	II-27-32
systems of units and conversion tables,	II-20-27
Probe, lunar,	VIII-2

(R)

Radial distance of the moon,	XI-5
Re-entry,	
corridor,	X-5
equations of motion,	X-3

Page

guidance techniques, ... X-10
maneuverability, ... X-7
qualitative description, ... X-4
by rocket, ... X-18-24
References and bibliography,
bibliography, (Chapter 12)
descent to lunar surface, ... VIII-32
earth departure, ... V-21
earth-moon system, ... III-34-35
earth to moon transfer, ... VI-27
earth return, ... X-24-25
lunar orbit, ... VII-12-13
mission planning, ... XI-29
physical data, ... II-33-34
trajectories in the earth-moon system, ... IV-43-44
Return, earth, ... X-1-25
assumptions for computing call-down, ... X-19
definition of corridor depth, ... X-5
derivation of the call-down conditions, ... X-21
equations of motion for a shallow re-entry X-3
landing at a specific earth site, ... X-1-2
qualitative description of re-entry, ... X-4
re-entry by atmospheric deceleration, ... X-2-18
re-entry by rocket deceleration, ... X-18-24

(S)

Selenographic coordinates, ... III-3-10
Stability of lunar orbits, ... VII-7

(T)

Time, mean solar, ... III-1
universal, ... III-1

Page

Three-body problem, general, ... III-14-17
restricted, ... III-17-22
Topocentric coordinates, ... III-2
Tracking and communication, ... VI-14
Trajectory-based coordinates, ... III-10
Trajectories in the earth-moon system, ... IV-1-44
accuracy of trajectories, ... IV-38-39
additional class of circumlunar orbits, ... IV-42
approach trajectories, ... IV-6-7
circumlunar and allunar missions, ... IV-7-9
classification and nomenclature, ... IV-1
force models, ... IV-13-39
impact trajectories, ... IV-7
landing missions, ... IV-9-11
lunar orbit missions, ... IV-9
lunar passages and escape, ... IV-11
lunar probes, ... IV-2-7
many body trajectories, ... IV-21-29
nomenclature and characteristics of a circumlunar trajectory, ... IV-11-13
nongravitational forces, ... IV-29-38
planar dynamics of earth's field, ... IV-13-14
planar dynamics of lunar field, ... IV-18
references, ... IV-43-44
restricted 3-body trajectories, ... IV-20-21
space stations, ... IV-11
succession of 2-body trajectories, ... IV-13-20
transition from earth-to-moon influence, ... IV-14-18
Voice technique, ... IV-39-42
Transearth or translunar envelopes, ... XI-8-9
Transfer, earth-to-moon, ... VI-1-27
abort to preselected landing sites, ... VI-24

Page

abort to the vicinity of earth, ... VI-22
abort way-stations, ... VI-25
catalogue, generalization of circumlunar trajectory data, ... VI-4
injection conditions and trajectory data, ... VI-5
guidance concepts, earth-to-moon transfer, ... VI-18
injection requirements for lunar trajectories, ... VI-1-7
methods for determining midcourse corrections, ... VI-16
midcourse guidance and energy requirements, ... VI-15-22
navigation and tracking requirements, ... VI-7-15
navigational techniques, ... VI-7-13
observational considerations, ... VI-7
references, ... VI-27
tracking and communications for lunar missions, ... VI-14
translunar abort, ... VI-22-27
Transfer, moon-to-earth IX-1-9
injection, requirements for, ... IX-1-7
midcourse guidance and energy, ... IX-7-9
transearth trajectory, ... IX-1-5
energy requirements, ... IX-7-8
guidance, ... IX-8
Translunar injection, ... V-14-21
Translunar trajectory, fixed, ... V-2-12
variable, ... V-12-14

(V)

Vehicle-centered coordinates, ... III-13
Voice coordinate system, ... III-12
Voice, description of, ... IV-39-42